frontiers
RESEARCH TOPICS

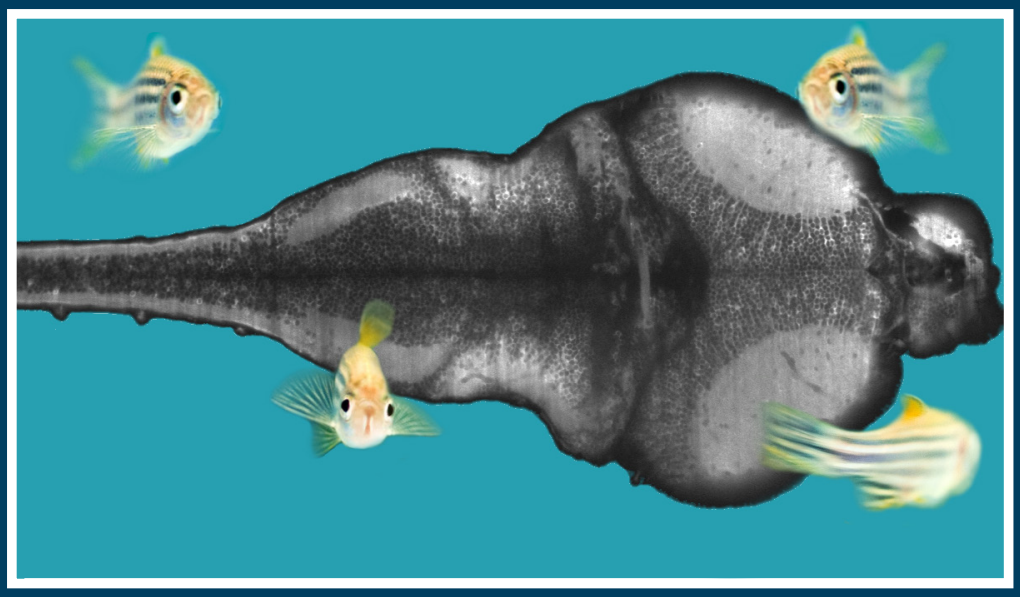

THE WORLD ACCORDING TO ZEBRAFISH: HOW NEURAL CIRCUITS GENERATE BEHAVIOUR

Topic Editors
Germán Sumbre and Gonzalo G. de Polavieja

frontiers in
NEURAL CIRCUITS

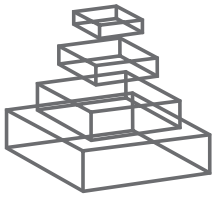

frontiers

ISSN 1664-8714
ISBN 978-2-88919-328-8
DOI 10.3389/978-2-88919-328-8

ABOUT FRONTIERS

Frontiers is more than just an open-access publisher of scholarly articles: it is a pioneering approach to the world of academia, radically improving the way scholarly research is managed. The grand vision of Frontiers is a world where all people have an equal opportunity to seek, share and generate knowledge. Frontiers provides immediate and permanent online open access to all its publications, but this alone is not enough to realize our grand goals.

FRONTIERS JOURNAL SERIES

The Frontiers Journal Series is a multi-tier and interdisciplinary set of open-access, online journals, promising a paradigm shift from the current review, selection and dissemination processes in academic publishing.
All Frontiers journals are driven by researchers for researchers; therefore, they constitute a service to the scholarly community. At the same time, the Frontiers Journal Series operates on a revolutionary invention, the tiered publishing system, initially addressing specific communities of scholars, and gradually climbing up to broader public understanding, thus serving the interests of the lay society, too.

DEDICATION TO QUALITY

Each Frontiers article is a landmark of the highest quality, thanks to genuinely collaborative interactions between authors and review editors, who include some of the world's best academicians. Research must be certified by peers before entering a stream of knowledge that may eventually reach the public - and shape society; therefore, Frontiers only applies the most rigorous and unbiased reviews.
Frontiers revolutionizes research publishing by freely delivering the most outstanding research, evaluated with no bias from both the academic and social point of view.
By applying the most advanced information technologies, Frontiers is catapulting scholarly publishing into a new generation.

WHAT ARE FRONTIERS RESEARCH TOPICS?

Frontiers Research Topics are very popular trademarks of the Frontiers Journals Series: they are collections of at least ten articles, all centered on a particular subject. With their unique mix of varied contributions from Original Research to Review Articles, Frontiers Research Topics unify the most influential researchers, the latest key findings and historical advances in a hot research area!
Find out more on how to host your own Frontiers Research Topic or contribute to one as an author by contacting the Frontiers Editorial Office: researchtopics@frontiersin.org

THE WORLD ACCORDING TO ZEBRAFISH: HOW NEURAL CIRCUITS GENERATE BEHAVIOUR

Topic Editors:
Germán Sumbre, Ecole Normale Supérieure, France
Gonzalo G. de Polavieja, Instituto Cajal, CSIC, Spain; Champalimaud Neuroscience Programme, Champalimaud Center for the Unknown, Lisbon, Portugal

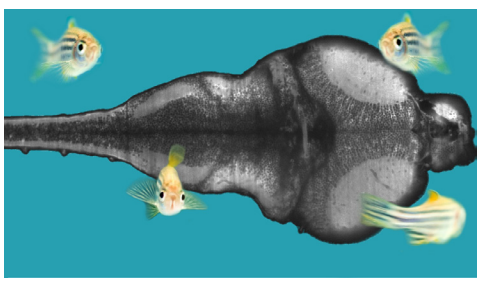

The cover picture shows a photomontage of the brain of a transgenic zebrafish larva expressing GCaMP3 in the entire neuronal population, imaged using SPIM (Panier et al. 2013), and adult zebrafish swimming around it. The cover represents the spirit of this special topic aiming to the understanding of how neural circuits generate behaviour.

Adult zebrafish picture taken by Olga Simón. Brain image taken by Thomas Panier and Raphaël Candelier. Photomontage performed by Ori Di Vincenzo.

Understanding how the brain functions is one of the most ambitious current scientific goals. This challenge will only be accomplish by a multidisciplinary approach involving genetics, molecular biology, optics, ethology, neurobiology and mathematics and using tractable model systems.

The zebrafish larva is a transparent genetically tractable small vertebrate, ideal for the combination state-of-the-art imaging techniques (e.g. two-photon scanning microscopy, single-plane illumination microscopy, spatial light modulator microscopy and lightfield microscopy), bioluminiscence and optogenetics to monitor and manipulate neuronal activity from single specific neurons up to the entire brain, in an intact behaving organism.

Furthermore, the zebrafish model offers large and increasing collection of mutant and transgenic lines modelling human brain diseases.

With these advantages in hand, the zebrafish larva became in the recent years, a novel animal model to study neuronal circuits and behaviour, taking us closer than ever before to understand how the brain controls behaviour.

Table of Contents

BEHAVIOUR

NEUROANATOMY

DISEASE MODELS & ADDICTION

frontiers in
NEURAL CIRCUITS

EDITORIAL
published: 30 July 2014
doi: 10.3389/fncir.2014.00091

The world according to zebrafish: how neural circuits generate behavior

Germán Sumbre[1,2,3]* and Gonzalo G. de Polavieja[4,5]*

[1] *Ecole Normale Supérieure, Institut de Biologie de l'ENS, Paris, France*
[2] *Inserm, U1024, Paris, France*
[3] *CNRS, UMR 8197, Paris, France*
[4] *Instituto Cajal, Consejo Superior de Investigaciones Científicas, Madrid, Spain*
[5] *Champalimaud Neuroscience Programme, Champalimaud Center for the Unknown, Lisbon, Portugal*
**Correspondence: sumbre@biologie.ens.fr; gonzalo.polavieja@neuro.fchampalimaud.org*

Edited and reviewed by:
Florian Engert, Harvard University, USA

Keywords: zebrafish, behavior, neuronal circuit dynamics, neuroanatomy, Models of human brain disorders

Understanding how the brain controls motor behavior and generates cognitive functions still remains one of the most challenging goals in science and neuroscience in particular.

Toward this goal it is important to use a multidisciplinary approach involving genetics, molecular biology, optics, ethology, neurobiology, and mathematical modeling. This strategy is most efficient when using animal models with relatively simple nervous systems still capable of producing complex motor behaviors. Genetically tractable models enable labeling specific neurons and monitoring and manipulating neuronal activity of single cells or entire circuits via optogenetics (Fenno et al., 2011; Akerboom et al., 2013; Aston-Jones and Deisseroth, 2013; Chen et al., 2013; Marvin et al., 2013).

The zebrafish *Danio rerio* is a small shoaling tropical freshwater fish native to rivers of south Asia. It is a member of the teleostei infraclass, a monophyletic group that emerged ∼340 million years ago (Amores et al., 2011). Compared to other vertebrate species, teleost fish underwent an additional round of whole-genome duplication (Meyer and Schartl, 1999).

Zebrafish has been used for developmental and genetic studies since the late 1950s. By the 1980s, zebrafish was already used as a genetically tractable organism. In 2001 the zebrafish genome-sequencing project was launched and recently its protein-coding genes were compared to those of humans (Friedrich et al., 2010; Howe et al., 2013). This large-scale project showed that zebrafish have 26,206 protein-coding genes (Collins et al., 2012), with ∼70% of human genes having at least one obvious zebrafish ortholog (Howe et al., 2013).

The combination of high-throughput mutagenesis and TILLING (Wienholds et al., 2003) or specifically targeted DNA sequence mutations [Zinc-finger nucleases (Doyon et al., 2008), TALENS (Sander et al., 2011) and CRISPR (Hwang et al., 2013)], enable DNA precise editing and thus the generation of transgenic and/or specific mutant zebrafish lines. Among this increasing collection of available mutants, several were identified as vertebrate models of certain human neurodevelopmental, neurological, and neurodegenerative syndromes and diseases [e.g., Parkinson's (Lam et al., 2005; Flinn et al., 2008), Alzheimer's (Newman et al., 2007, 2011), Rett's syndrome (Pietri et al., 2013), ALS (Gibbs et al., 1976; Burrill and Easter, 1994; Da Costa et al., 2014), tinnitus (Wu et al., 2014), psychiatric disorders (Norton, 2013), Huntington's disease (Schiffer et al., 2007), Lowe's syndrome (Ramirez et al., 2012), and more (Sager et al., 2010)].

Furthermore, large-scale enhancer-trap screens in combination with DNA insertion methods (e.g., Tol2, Kawakami and Shima, 1999), bioinformatics and the Gal4/UAS system generated a vast collection of transgenic fish and a large database of tissue/cell-type specific promoters (Scott et al., 2007; Asakawa et al., 2008).

An additional advantage of the zebrafish larva model is its transparent skin, small size and the fact that it mainly uses cutaneous breathing (up to ∼14 days post-fertilization, dpf). These three characteristics make possible to restrain larvae in a drop of low-melting agarose without the use of any paralyzers or anesthetics, in intact conditions, without the use of surgical procedures to expose and image the brain.

With the development of recent state-of-the-art optical techniques including two-photon scanning microscopy (Ahrens et al., 2012; Portugues et al., 2014), Single plain illumination microscopy (Ahrens et al., 2013b; Panier et al., 2013), lightfield microscopy (Broxton et al., 2013), and Spatial light modulator microscopy (Quirin et al., 2013), the entire brain can be now simultaneously imaged and its activity monitored with single or near single-cell resolution. On the other hand, fiber optics (Miri et al., 2011; Kubo et al., 2014), Digital micromirror devices (Wyart et al., 2009), and holographic pattern illumination (Vaziri and Emiliani, 2012) can be used to stimulate optogenetic tools in single cells or large neuronal circuits.

The combination of all these techniques together with the larva's small size and skin transparency enable monitoring in toto brain dynamics and manipulate its activity in an intact, non-anesthetized, non-paralyzed vertebrate (Ahrens et al., 2013b; Panier et al., 2013; Portugues et al., 2014).

From a behavioral point of view, upon hatching the larva needs to immediately catch prey and avoid predators in order to survive. This strong evolutionary pressure leads to a rapid development of functional sensory systems in general, and vision in particular,

creating a reach repertoire of visuo-motor behaviors (Fleisch and Neuhauss, 2006; Portugues and Engert, 2009). For example, the startle escape response [a flash of light induces a directional swimming behavior (Burgess and Granato, 2007)], optokinetic response [OKR, compensatory eye saccades evoked by coherent field motion (Rinner et al., 2005; Mueller and Neuhauss, 2010)], optomotor response [OMR, compensatory tail movements evoked by coherent field motion (Orger et al., 2000)], dorsal-light response (DLR, Neuhauss, 2003), feeding behavior (Budick and O'Malley, 2000), and eye lateralization [preferential use of one eye over the other depending on the type of visual stimulus (Miklósi and Andrew, 2006)]. Furthermore, they also show rheotaxis (Olszewski et al., 2012), odor and gustatory-induced behaviors (Mathuru et al., 2012; Boyer et al., 2013), learning and memory (Aizenberg and Schuman, 2011; Valente et al., 2012; Roberts et al., 2013), and circadian rhythms and sleep (Naumann et al., 2010; Chiu and Prober, 2013; Elbaz et al., 2013), among others.

At the juvenile and adult stages, zebrafish develop more complex behaviors such as social learning, shoaling, group decision making and learning, courtship, territoriality, and hierarchy (Arganda et al., 2012; Oliveira, 2013).

With all these multidisciplinary advantages in hand and a relative simple nervous system [∼100,000 neurons at 7 dpf (Hill et al., 2003; Naumann et al., 2010)], still with a well-conserved vertebrate structure, the zebrafish is becoming an emerging experimental model in neurosciences and neuroethology (Friedrich et al., 2010).

Recent studies have shown that it is also possible to monitor and/or manipulate neuronal dynamics in partially agarose-restrained behaving intact larvae and therefore correlate neuronal activity and motor behavior. Moreover, close-loop visual virtual reality can be used so larvae can get visual feedback of their own acts despite being immobilized (Ahrens et al., 2012, 2013a).

Alternatively, although lacking cellular resolution, using transgenic larvae expressing a bioluminescence protein such as GFP-Aequorin expressed in specific cell populations, it is possible to monitor brain activities in unrestrained freely behaving animals (Naumann et al., 2010).

Furthermore, due to the zebrafish ex-uterus development all embryonic and larval developmental stages following fecundation are accessible for imaging.

The combination of the genetic and optical state-of-the-art techniques with the zebrafish experimental model is yielding high-dimensional large data sets pushing the limits of current data analysis standards, forcing for the development of new methodologies and novel theoretical models.

A future challenge in the field will be monitoring whole-brain activity with near single-neuron resolution from multiple freely behaving and socially interacting individuals.

In this topic we have gathered a collection of original articles, reviews, and opinions covering a wide-spectrum of topics from behavior up to whole-brain activity recordings, both in wild type and in neurological human-syndrome models, providing an overview of current state and future directions of zebrafish circuits neuroscience and behavior research field.

We have organized this eBook in 4 different chapters:

1. Neuroanatomy
2. Neuronal circuit dynamics
3. Behavior
4. Models of brain disorders and addiction

The zebrafish model in combination with recently developed imaging techniques, optogenetics, and sophisticated mathematical methods for analysis of the acquired large data sets is bringing us closer than ever before to the understanding of how brain dynamics relates to behavior.

REFERENCES

Ahrens, M. B., Huang, K. H., Narayan, S., Mensh, B. D., and Engert, F. (2013a). Two-photon calcium imaging during fictive navigation in virtual environments. *Front. Neural Circuits* 7:104. doi: 10.3389/fncir.2013.00104

Ahrens, M. B., Li, J. M., Orger, M. B., Robson, D. N., Schier, A. F., Engert, F., et al. (2012). Brain-wide neuronal dynamics during motor adaptation in zebrafish. *Nature* 485, 471–477. doi: 10.1038/nature11057

Ahrens, M. B., Orger, M. B., Robson, D. N., Li, J. M., and Keller, P. J. (2013b). Whole-brain functional imaging at cellular resolution using light-sheet microscopy. *Nat. Methods* 10, 413–420. doi: 10.1038/nmeth.2434

Aizenberg, M., and Schuman, E. M. (2011). Cerebellar-dependent learning in larval zebrafish. *J. Neurosci.* 31, 8708–8712. doi: 10.1523/JNEUROSCI.6565-10.2011

Akerboom, J., Carreras Calderón, N., Tian, L., Wabnig, S., Prigge, M., Tolö, J., et al. (2013). Genetically encoded calcium indicators for multi-color neural activity imaging and combination with optogenetics. *Front. Mol. Neurosci.* 6:2. doi: 10.3389/fnmol.2013.00002

Amores, A., Catchen, J., Ferrara, A., Fontenot, Q., and Postlethwait, J. H. (2011). Genome evolution and meiotic maps by massively parallel DNA sequencing: spotted gar, an outgroup for the teleost genome duplication. *Genetics* 188, 799–808. doi: 10.1534/genetics.111.127324

Arganda, S., Pérez-Escudero, A., and de Polavieja, G. G. (2012). A common rule for decision making in animal collectives across species. *Proc. Natl. Acad. Sci. U.S.A.* 109, 20508–20513. doi: 10.1073/pnas.1210664109

Asakawa, K., Suster, M. L., Mizusawa, K., Nagayoshi, S., Kotani, T., Urasaki, A., et al. (2008). Genetic dissection of neural circuits by Tol2 transposon-mediated Gal4 gene and enhancer trapping in zebrafish. *Proc. Natl. Acad. Sci. U.S.A.* 105, 1255–1260. doi: 10.1073/pnas.0704963105

Aston-Jones, G., and Deisseroth, K. (2013). Recent advances in optogenetics and pharmacogenetics. *Brain Res.* 1511, 1–5. doi: 10.1016/j.brainres.2013.01.026

Boyer, B., Ernest, S., and Rosa, F. (2013). Egr-1 induction provides a genetic response to food aversion in zebrafish. *Front. Behav. Neurosci.* 7:51. doi: 10.3389/fnbeh.2013.00051

Broxton, M., Grosenick, L., Yang, S., Cohen, N., Andalman, A., Deisseroth, K., et al. (2013). Wave optics theory and 3-D deconvolution for the light field microscope. *Opt. Express* 21, 25418–25439. doi: 10.1364/OE.21.025418

Budick, S. A., and O'Malley, D. M. (2000). Locomotor repertoire of the larval zebrafish: swimming, turning and prey capture. *J. Exp. Biol.* 203, 2565–2579.

Burgess, H. A., and Granato, M. (2007). Modulation of locomotor activity in larval zebrafish during light adaptation. *J. Exp. Biol.* 210, 2526–2539. doi: 10.1242/jeb.003939

Burrill, J. D., and Easter, S. S. (1994). Development of the retinofugal projections in the embryonic and larval zebrafish (*Brachydanio rerio*). *J. Comp. Neurol.* 346, 583–600. doi: 10.1002/cne.903460410

Chen, T.-W., Wardill, T. J., Sun, Y., Pulver, S. R., Renninger, S. L., Baohan, A., et al. (2013). Ultrasensitive fluorescent proteins for imaging neuronal activity. *Nature* 499, 295–300. doi: 10.1038/nature12354

Chiu, C. N., and Prober, D. A. (2013). Regulation of zebrafish sleep and arousal states: current and prospective approaches. *Front. Neural Circuits* 7:58. doi: 10.3389/fncir.2013.00058

Collins, J. E., White, S., Searle, S. M. J., and Stemple, D. L. (2012). Incorporating RNA-seq data into the zebrafish Ensembl genebuild. *Genome Res.* 22, 2067–2078. doi: 10.1101/gr.137901.112

Da Costa, M. M. J., Allen, C. E., Higginbottom, A., Ramesh, T., Shaw, P. J., and McDermott, C. J. (2014). A new zebrafish model produced by TILLING of SOD1-related amyotrophic lateral sclerosis replicates key features of the disease and represents a tool for *in vivo* therapeutic screening. *Dis. Model. Mech.* 7, 73–81. doi: 10.1242/dmm.012013

Doyon, Y., McCammon, J. M., Miller, J. C., Faraji, F., Ngo, C., Katibah, G. E., et al. (2008). Heritable targeted gene disruption in zebrafish using designed zinc-finger nucleases. *Nat. Biotechnol.* 26, 702–708. doi: 10.1038/nbt1409

Elbaz, I., Foulkes, N. S., Gothilf, Y., and Appelbaum, L. (2013). Circadian clocks, rhythmic synaptic plasticity and the sleep-wake cycle in zebrafish. *Front. Neural Circuits* 7:9. doi: 10.3389/fncir.2013.00009

Fenno, L., Yizhar, O., and Deisseroth, K. (2011). The development and application of optogenetics. *Annu. Rev. Neurosci.* 34, 389–412. doi: 10.1146/annurev-neuro-061010-113817

Fleisch, V. C., and Neuhauss, S. C. F. (2006). Visual behavior in zebrafish. *Zebrafish* 3, 191–201. doi: 10.1089/zeb.2006.3.191

Flinn, L., Bretaud, S., Lo, C., Ingham, P. W., and Bandmann, O. (2008). Zebrafish as a new animal model for movement disorders. *J. Neurochem.* 106, 1991–1997. doi: 10.1111/j.1471-4159.2008.05463.x

Friedrich, R. W., Jacobson, G. A., and Zhu, P. (2010). Circuit neuroscience in zebrafish. *Curr. Biol.* 20, R371–R381. doi: 10.1016/j.cub.2010.02.039

Gibbs, H., McCall, S., and Venkatesan, T. (1976). Differential gain and bistability using a sodium-filled fabry-perot interferometer. *Phys. Rev. Lett.* 36, 1135–1138. doi: 10.1103/PhysRevLett.36.1135

Hill, A., Howard, C. V., Strahle, U., and Cossins, A. (2003). Neurodevelopmental defects in zebrafish (*Danio rerio*) at environmentally relevant dioxin (TCDD) concentrations. *Toxicol. Sci.* 76, 392–399. doi: 10.1093/toxsci/kfg241

Howe, K., Clark, M. D., Torroja, C. F., Torrance, J., Berthelot, C., Muffato, M., et al. (2013). The zebrafish reference genome sequence and its relationship to the human genome. *Nature* 496, 498–503. doi: 10.1038/nature12111

Hwang, W. Y., Fu, Y., Reyon, D., Maeder, M. L., Tsai, S. Q., Sander, J. D., et al. (2013). Efficient genome editing in zebrafish using a CRISPR-Cas system. *Nat. Biotechnol.* 31, 227–229. doi: 10.1038/nbt.2501

Kawakami, K., and Shima, A. (1999). Identification of the Tol2 transposase of the medaka fish Oryzias latipes that catalyzes excision of a nonautonomous Tol2 element in zebrafish *Danio rerio*. *Gene* 240, 239–244.

Kubo, F., Hablitzel, B., Dal Maschio, M., Driever, W., Baier, H., and Arrenberg, A. B. (2014). Functional architecture of an optic flow-responsive area that drives horizontal eye movements in zebrafish. *Neuron* 81, 1344–1359. doi: 10.1016/j.neuron.2014.02.043

Lam, C. S., Korzh, V., and Strahle, U. (2005). Zebrafish embryos are susceptible to the dopaminergic neurotoxin MPTP. *Eur. J. Neurosci.* 21, 1758–1762. doi: 10.1111/j.1460-9568.2005.03988.x

Marvin, J. S., Borghuis, B. G., Tian, L., Cichon, J., Harnett, M. T., Akerboom, J., et al. (2013). An optimized fluorescent probe for visualizing glutamate neurotransmission. *Nat. Methods* 10, 162–170. doi: 10.1038/nmeth.2333

Mathuru, A. S., Kibat, C., Cheong, W. F., Shui, G., Wenk, M. R., Friedrich, R. W., et al. (2012). Chondroitin fragments are odorants that trigger fear behavior in fish. *Curr. Biol.* 22, 538–544. doi: 10.1016/j.cub.2012.01.061

Meyer, A., and Schartl, M. (1999). Gene and genome duplications in vertebrates: the one-to-four (-to-eight in fish) rule and the evolution of novel gene functions. *Curr. Opin. Cell Biol.* 11, 699–704.

Miklósi, A., and Andrew, R. J. (2006). The zebrafish as a model for behavioral studies. *Zebrafish* 3, 227–234. doi: 10.1089/zeb.2006.3.227

Miri, A., Daie, K., Arrenberg, A. B., Baier, H., Aksay, E., and Tank, D. W. (2011). Spatial gradients and multidimensional dynamics in a neural integrator circuit. *Nat. Neurosci.* 14, 1150–1159. doi: 10.1038/nn.2888

Mueller, K. P., and Neuhauss, S. C. F. (2010). Quantitative measurements of the optokinetic response in adult fish. *J. Neurosci. Methods* 186, 29–34. doi: 10.1016/j.jneumeth.2009.10.020

Naumann, E. A., Kampff, A. R., Prober, D. A., Schier, A. F., and Engert, F. (2010). Monitoring neural activity with bioluminescence during natural behavior. *Nat. Neurosci.* 13, 513–520. doi: 10.1038/nn.2518

Neuhauss, S. C. F. (2003). Behavioral genetic approaches to visual system development and function in zebrafish. *J. Neurobiol.* 54, 148–160. doi: 10.1002/neu.10165

Newman, M., Musgrave, I. F., Musgrave, F. I., and Lardelli, M. (2007). Alzheimer disease: amyloidogenesis, the presenilins and animal models. *Biochim. Biophys. Acta* 1772, 285–297. doi: 10.1016/j.bbadis.2006.12.001

Newman, M., Verdile, G., Martins, R. N., and Lardelli, M. (2011). Zebrafish as a tool in Alzheimer's disease research. *Biochim. Biophys. Acta* 1812, 346–352. doi: 10.1016/j.bbadis.2010.09.012

Norton, W. H. J. (2013). Toward developmental models of psychiatric disorders in zebrafish. *Front. Neural Circuits* 7:79. doi: 10.3389/fncir.2013.00079

Oliveira, R. F. (2013). Mind the fish: zebrafish as a model in cognitive social neuroscience. *Front. Neural Circuits* 7:131. doi: 10.3389/fncir.2013.00131

Olszewski, J., Haehnel, M., Taguchi, M., and Liao, J. C. (2012). Zebrafish larvae exhibit rheotaxis and can escape a continuous suction source using their lateral line. *PLoS ONE* 7:e36661. doi: 10.1371/journal.pone.0036661

Orger, M. B., Smear, M. C., Anstis, S. M., and Baier, H. (2000). Perception of Fourier and non-Fourier motion by larval zebrafish. *Nat. Neurosci.* 3, 1128–1133. doi: 10.1038/80649

Panier, T., Romano, S. A., Olive, R., Pietri, T., Sumbre, G., Candelier, R., et al. (2013). Fast functional imaging of multiple brain regions in intact zebrafish larvae using selective plane illumination microscopy. *Front. Neural Circuits* 7:65. doi: 10.3389/fncir.2013.00065

Pietri, T., Roman, A.-C., Guyon, N., Romano, S. A., Washbourne, P., Moens, C. B., et al. (2013). The first mecp2-null zebrafish model shows altered motor behaviors. *Front. Neural Circuits* 7:118. doi: 10.3389/fncir.2013.00118

Portugues, R., and Engert, F. (2009). The neural basis of visual behaviors in the larval zebrafish. *Curr. Opin. Neurobiol.* 19, 644–647. doi: 10.1016/j.conb.2009.10.007

Portugues, R., Feierstein, C. E., Engert, F., and Orger, M. B. (2014). Whole-brain activity maps reveal stereotyped, distributed networks for visuomotor behavior. *Neuron* 81, 1328–1343. doi: 10.1016/j.neuron.2014.01.019

Quirin, S., Peterka, D. S., and Yuste, R. (2013). Instantaneous three-dimensional sensing using spatial light modulator illumination with extended depth of field imaging. *Opt. Express* 21, 16007–16021. doi : 10.1364/OE.21.016007

Ramirez, I. B.-R., Pietka, G., Jones, D. R., Divecha, N., Alia, A., Baraban, S. C., et al. (2012). Impaired neural development in a zebrafish model for Lowe syndrome. *Hum. Mol. Genet.* 21, 1744–1759. doi: 10.1093/hmg/ddr608

Rinner, O., Rick, J. M., and Neuhauss, S. C. F. (2005). Contrast sensitivity, spatial and temporal tuning of the larval zebrafish optokinetic response. *Invest. Ophthalmol. Vis. Sci.* 46, 137–142. doi: 10.1167/iovs.04-0682

Roberts, A. C., Bill, B. R., and Glanzman, D. L. (2013). Learning and memory in zebrafish larvae. *Front. Neural Circuits* 7:126. doi: 10.3389/fncir.2013.00126

Sager, J. J., Bai, Q., and Burton, E. A. (2010). Transgenic zebrafish models of neurodegenerative diseases. *Brain Struct. Funct.* 214, 285–302. doi: 10.1007/s00429-009-0237-1

Sander, J. D., Cade, L., Khayter, C., Reyon, D., Peterson, R. T., Joung, J. K., et al. (2011). Targeted gene disruption in somatic zebrafish cells using engineered TALENs. *Nat. Biotechnol.* 29, 697–698. doi: 10.1038/nbt.1934

Schiffer, N. W., Broadley, S. A., Hirschberger, T., Tavan, P., Kretzschmar, H. A., Giese, A., et al. (2007). Identification of anti-prion compounds as efficient inhibitors of polyglutamine protein aggregation in a zebrafish model. *J. Biol. Chem.* 282, 9195–9203. doi: 10.1074/jbc.M607865200

Scott, E. K., Mason, L., Arrenberg, A. B., Ziv, L., Gosse, N. J., Xiao, T., et al. (2007). Targeting neural circuitry in zebrafish using GAL4 enhancer trapping. *Nat. Methods* 4, 323–326. doi: 10.1038/nmeth1033

Valente, A., Huang, K.-H., Portugues, R., and Engert, F. (2012). Ontogeny of classical and operant learning behaviors in zebrafish. *Learn. Mem.* 19, 170–177. doi: 10.1101/lm.025668.112

Vaziri, A., and Emiliani, V. (2012). Reshaping the optical dimension in optogenetics. *Curr. Opin. Neurobiol.* 22, 128–137. doi: 10.1016/j.conb.2011.11.011

Wienholds, E., van Eeden, F., Kosters, M., Mudde, J., Plasterk, R. H. A., and Cuppen, E. (2003). Efficient target-selected mutagenesis in zebrafish. *Genome Res.* 13, 2700–2707. doi: 10.1101/gr.1725103

Wu, C., Sharma, K., Laster, K., Hersi, M., Torres, C., Lukas, T. J., et al. (2014). Kcnq1-5 (Kv7.1-5) potassium channel expression in the adult zebrafish. *BMC Physiol.* 14:1. doi: 10.1186/1472-6793-14-1

Wyart, C., Del Bene, F., Warp, E., Scott, E. K., Trauner, D., Baier, H., et al. (2009). Optogenetic dissection of a behavioural module in the vertebrate spinal cord. *Nature* 461, 407–410. doi: 10.1038/nature 08323

Conflict of Interest Statement: The authors declare that the research was conducted in the absence of any commercial or financial relationships that could be construed as a potential conflict of interest.

Received: 07 April 2014; accepted: 11 July 2014; published online: 30 July 2014.
Citation: Sumbre G and de Polavieja GG (2014) The world according to zebrafish: how neural circuits generate behavior. Front. Neural Circuits ***8****:91. doi: 10.3389/fncir. 2014.00091*
This article was submitted to the journal Frontiers in Neural Circuits.

frontiers in
NEURAL CIRCUITS

MINI REVIEW ARTICLE
published: 25 January 2013
doi: 10.3389/fncir.2012.00125

Fish in the matrix: motor learning in a virtual world

Florian Engert*

Harvard University, Cambridge, MA, USA

Edited by:
German Sumbre, Ecole Normale Superieure, France

Reviewed by:
David Parker, Cambridge University, UK
Emre Yaksi, Vlaams Instituut voor Biotechnologie, Belgium

****Correspondence:***
Florian Engert, Biological Laboratories 2073, 16 Divinity Avenue, Cambridge, MA 02138, USA.
e-mail: florian@mcb.harvard.edu

One of the large remaining challenges in the field of zebrafish neuroscience is the establishment of techniques and preparations that permit the recording and perturbation of neural activity in animals that can interact meaningfully with the environment. Since it is very difficult to do this in freely behaving zebrafish, I describe here two alternative approaches that meet this goal via tethered preparations. The first uses head-fixation in agarose in combination with online imaging and analysis of tail motion. In the second method, paralyzed fish are suspended with suction pipettes in mid-water and nerve root recordings serve as indicators for intended locomotion. In both cases, fish can be immersed into a virtual environment and allowed to interact with this virtual world via real or fictive tail motions. The specific examples given in this review focus primarily on the role of visual feedback – but the general principles certainly extend to other modalities, including proprioception, hearing, balance, and somatosensation.

Keywords: fictive locomotion, virtual environments, zebrafish, bioluminescence imaging, closed-loop system

There are two fundamentally different forms of sensory information that are being processed by the brain. The form that is more commonly studied – also the form that neuroscientists mostly worry about – is the kind that informs the brain about what is happening in the outside world. This kind of information is represented by neural activity that is evoked by changes in the environment due to all possible kinds of physical or biological events. We live, after all, in a constantly changing world and it clearly helps to be informed speedily of these changes. A large part of neuroscience is involved with the study of how this kind of sensory evoked activity is represented at different stages of processing in the brain and how it gets filtered for optimal extraction of the information that is most relevant for the generation of adaptive behaviors.

The zebrafish is a good model system to address these kinds of questions, since its translucence and small size makes it ideally suited for monitoring neural activity throughout the brain with modern optical methods. This striking advantage features prominently in other articles in this special issue and there are multiple examples across many modalities where such studies have added to our understanding of how sensory information is represented in the brain (Niell and Smith, 2005; Ramdya and Engert, 2008; Sumbre et al., 2008; Del Bene et al., 2010; Blumhagen et al., 2011; Grama and Engert, 2012) and how this neural activity ultimately leads to the generation of specific behaviors. Thus, fish have been shown to turn in specific directions with specific turn amplitudes (Orger et al., 2008), to modulate their swim speed according to sensory input (McLean et al., 2008), and to change the threshold for escape turns according to situational context (Mu et al., 2012).

The topic of this review is not related to this kind of question at all. Rather, it addresses the issue of how the second form of sensory information gets processed, namely the kind of sensory activity that results from the motion of the animal itself. Such self-generated sensory stimuli are termed reafference and they occur across many modalities whenever any movement is executed. When walking forward we experience reverse optic flow, that is, we perceive the world to be moving in the opposite direction. We also experience pressure on the bottom of our feet and air might flow over our skin. Whenever we vocalize we experience a very distinct auditory reafference, namely the sound of our own voice which, of course, needs to get processed quite differently than somebody else's utterance and such reafference clearly is a useful thing to pay attention to when we learn to sing or speak. I'm sure we can, with some creative thinking, even come up with good examples of olfactory reafference.

The main difference between this reafferent signal and the initially mentioned form of sensory input, commonly known as the exafference, is that it does not inform us about what effect the world has on us, but rather tells us what effect we have on the world. As such it informs the brain about the success and accuracy of ongoing movements and is immensely useful for – and most likely central to – all forms of motor learning and motor adaptation. The easiest way one can imagine such a learning process to take place, is that the reafference gets compared, somewhere in the brain, to an expected value, most likely represented by an efference copy, that is, a copy of the motor-command that is usually available in many brain regions. As soon as a difference is detected between expected outcome and actual reafference, plasticity mechanisms need to kick in, in order to adjust future motor-commands.

It is clear that such motor learning phenomena cannot be studied in paralyzed – and much less in anesthetized – animals, since here the actual execution of a behavior is the origin and cause of sensory stimulation.

If the goal is then to study the neural dynamics underlying these reafferent signals, a way has to be found that allows the monitoring of neural activity, ideally at cellular resolution and throughout the whole brain, while the animal is interacting with its environment. An additional requirement for such an experimental set-up is that it ought to allow control over the reafferent signal. In order

to do this, an explicit decoupling of the motor action from the resulting sensory feedback is required such that the feedback link can now be programed in under complete experimental control. In such a setting, the subject can be rendered stronger or weaker than in real life by modifying the gain of the motor to sensory transformation. This is a feature that usually comes for free in all virtual environments where the simulated speed and strength of the operator/subject can be dialed in at will.

Such virtual environments usually require the tethering of the animal – and elegant implementations of this approach, where the tethering of the animal has been made compatible with 2-photon imaging, have been described for fruitflies suspended in midair in flight-simulators (Maimon et al., 2010; Tang et al., 2004) or walking on two dimensional treadmills (Seelig and Jayaraman, 2011) and in rodents running in place on floating styrofoam balls (Dombeck et al., 2007; Harvey et al., 2009) (**Figures 1A,B**). A major challenge in zebrafish research has long been to design a similar paradigm around a small animal wriggling in water.

The first step to implement such a paradigm is to establish technology that allows the readout of behavior in immobilized or at least head-fixed preparations, and this has been solved in various ways in the past. One, reasonably straightforward, route is first to embed the fish in low-melting-point agarose (low-melting-point such as not to boil the animal when immersing it into the still liquid medium), then to free the tail once the agarose has set and subsequently observe tail motion with a high-speed camera to obtain a proxy of intended locomotion (**Figure 1C**). This approach has been used in a number of imaging – as well as perturbation studies in the zebrafish larva (O'Malley et al., 1996, 2004; Ritter et al., 2001; Szobota et al., 2007; Sumbre et al., 2008; Wyart et al., 2009). An alternative approach is to paralyze the animal with a toxin that specifically blocks the neuromuscular junction (substances like curare or bungarotoxin are commonly used), then suspend it in mid-water with several suction pipette and have two or more of the pipettes double as recording electrodes to measure nerve root activity through the skin on both sides of the body (**Figure 1D**). These nerve recordings have been used extensively in lamprey as a readout for fictive swimming (Fagerstedt et al., 2001) and have also lead to exciting findings on midbrain circuitry in goldfish (Fetcho and Svoboda, 1993) and zebrafish (Masino and Fetcho, 2005). Such recordings provide very similar information to tail motion monitored with a camera and provide the additional benefit of removing all possible motion artifacts. One residual, but significant concern associated with these paralytica is of course that they might also interfere with processing at the level of the CNS. As such it is recommended to bolster all experiments that involve fictive swim recordings with thorough controls that ensure that central processing is not compromised by the neurotoxins. One possible way to do this is to perform comparable experiments in non-paralyzed preparations – head-fixed, but tail-free for example – and deal with the resulting motion artifacts through enhanced image analysis (Dombeck et al., 2007).

To make the leap from providing a simple read-out of behavior, be it fictive or physical, to a set-up where the animal actually interacts meaningfully with the environment, another essential step is necessary: the behavior needs to be analyzed in real time and fed back into a computer system that updates the environment (usually a virtual one) according to the recorded locomotor events. This classic approach using virtual environments is well known to all users of flight simulators and all players of first person video games such as Quake or Doom. In the absence of a closed-feedback loop, the delivery of sensory information to the animal is decoupled from the behavior and analysis of true interaction or navigation is not possible. The active player of a video game would then become a passive watcher of television.

Probably the first implementations of such closed-loop systems are described by Bernhard Hassenstein and Werner Reichardt in the 1950s (Hassenstein and Reichardt, 1956), where a rüsselkäfer (*Chlorophanus viridis*) walks interactively on a spangenglobus (**Figure 2**), an ultra lightweight globe made of bamboo twigs (Hassenstein, 1991). This closed-loop preparation was famously used to generate the still valid Hassenstein–Reichardt model for the fundamental computations underlying direction selective responses in the visual system.

In order to apply such a closed-loop system to the larval zebrafish, locomotor events need to be analyzed online and the computed locomotion must then be used to update a virtual environment displayed on computer screens placed either below or around the animal. Importantly, the gain in this virtual navigation setting can be dialed in by the experimenter. A given locomotor readout can be translated into a large or small distance covered in the virtual world and thus the animal can be equipped with virtual superpower or virtual feebleness at the dial of a button. Both ways of implementing swimming in a virtual world, fictive swims as well as actual tail motion in a head-fixed preparation, have been used recently in two articles that described the ability of larval zebrafish to adapt to these gain changes. In both studies larval zebrafish were immersed into virtual environments and the fictive strength of the fish – represented by the feedback gain of the closed-loop system – was changed periodically between high and low settings. In both cases it was found that fish indeed change their swimming behavior in response to such changes in the biophysics of the virtual environment (Portugues and Engert, 2011; Ahrens et al., 2012).

One of the main contributions that these studies provided was the development of efficient algorithms that allow the translation of locomotor activity into intended movement of the animal and subsequently the real time update of a virtual environment that was represented by computer monitors surrounding the fish. Particularly in the case where motor nerve recordings serve as the exclusive source of behavioral output, analogies to the movie "The Matrix" are obvious: the feature film describes a world in the distant future where the heroes interact with an entirely virtual world simply by virtue of activity in their brains.

It should be noted that in most of the preparations described in this mini-review, closed-loop feedback has been restricted to vision. In principle it is possible to add other modalities and immerse the animal into a more complete virtual world. The inner ear or the neuromasts of the lateral line could be stimulated whenever a swim event occurs to mimic locomotor-feedback in the form of acceleration or water flow; the tail could be moved passively to provide proprioceptive feedback and one could also change the cues related to temperature and/or chemo-sensation in correlation with the position of the animal in the virtual world. An interesting observation is that in most cases such a complete representation of

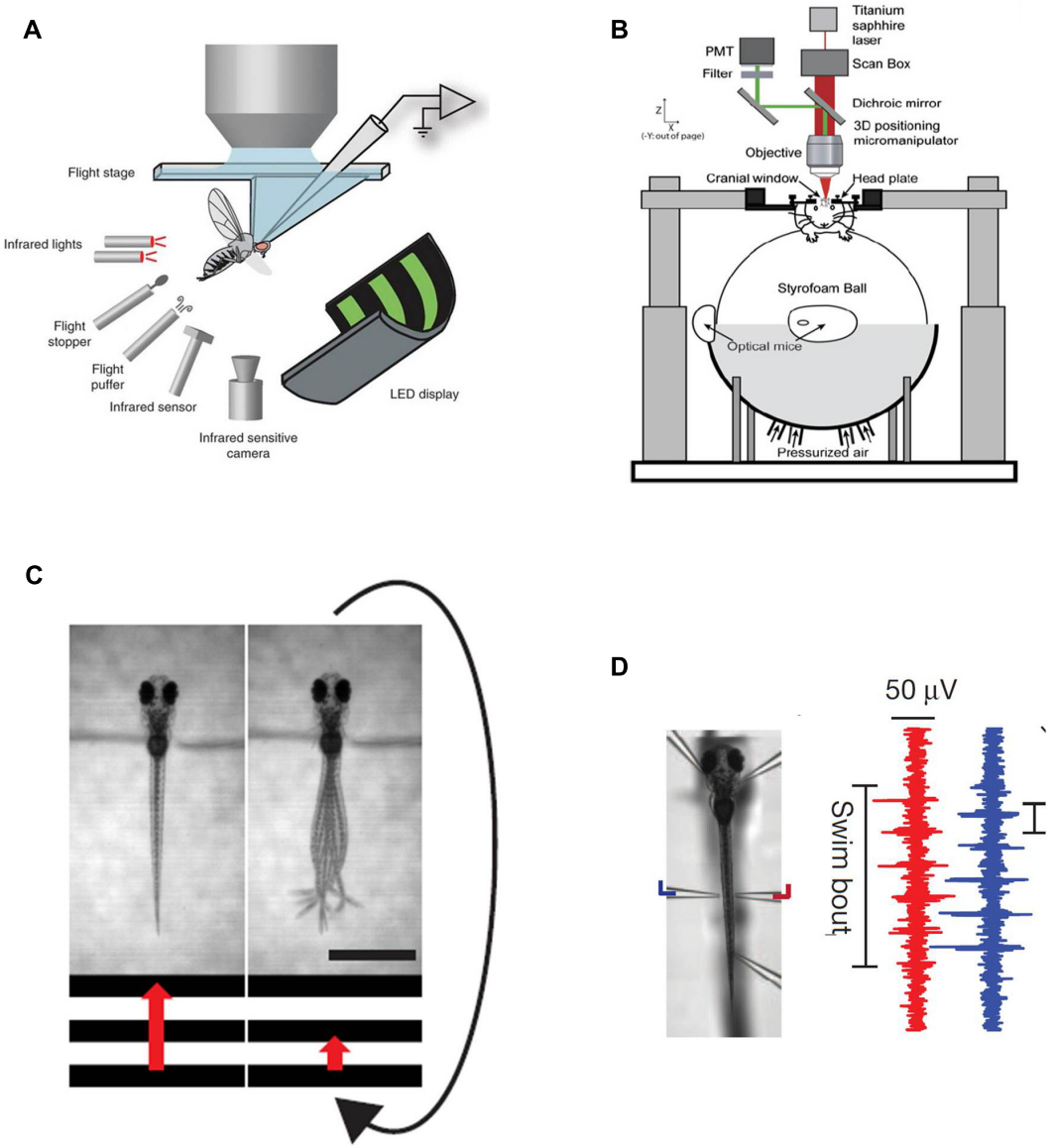

FIGURE 1 | Existing methods for simultaneous behavior and neural recording. (A) a fly in a flight arena while whole-cell recordings are made from VS cells (from the Dickinson lab, Maimon et al., 2010, reproduced with permission). **(B)** A mouse walking on a suspended ball through a virtual reality environment while its brain is two-photon scanned (from the Tank lab, Dombeck et al., 2007, reproduced with permission; Harvey et al., 2009). **(C)** Diagram illustrating the closed-loop experimental setup in a larval zebrafish. A moving grating is shown to a head-restrained larva (the grating speed is represented by the red arrow) and its behavior is monitored with a high-speed camera. When the fish swims the stimulus slows down such that the relative motion between the larva and the moving grating resembles freely swimming conditions. The scale bar at the bottom right is 1 mm. **(D)** *Left*: Photomicrograph of a fish suspended in mid-water from five pipettes, two of which double as recording electrodes. *Right*: Example of a two-channel recording of a fictive swim. The left (blue) and right (red) signals are out of phase, as in earlier fictive swimming publications such as Masino and Fetcho (2005).

reafference is not necessary for appropriate and meaningful behavior in a virtual world. Often it is sufficient to provide meaningful and consistent feedback to a single modality and then the absence of feedback in remaining input channels gets quickly ignored.

Good examples for such phenomena are found in current attempts to develop brain machine interfaces that allow monkeys as well as human subjects to move cursors over computer screens, or operate machinery simply by thinking about it. These serve probably as the best examples for the necessary plasticity in such closed systems since here the brain has very little a priory information of how activity in specific neuronal ensembles leads to changes in the environment via the motor systems that connect the two.

As such it is obvious that the brain needs to learn how to control the environment through these novel means, presumably via established algorithms of motor learning.

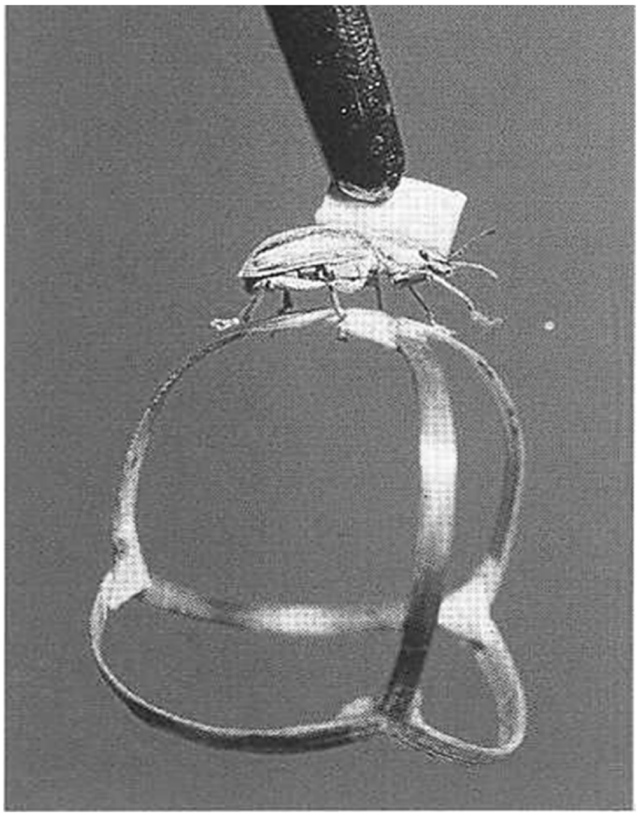

FIGURE 2 | Tethered *Chlorophanus* walking on a Y-maze globe.

An intriguing finding in the zebrafish studies – as well as the preceding experiments on flies – was that animals are able to adapt their behavior to different conditions of the virtual environment with surprising speed. Very similar adjustments to artificially induced changes in reafference were found in a series of landmark studies in the weakly electric fish. Here changes in the reafference of the animal's electric discharge was found to be canceled precisely by a negative image presynaptic to secondary sensory neurons – and this cancellation adapted quickly when the strength of the reafference was artificially manipulated (Bell, 1981; Bell et al., 1997). Furthermore, this adjustable subtraction of an expected value from the actual reafference was not limited to weakly electric fish; similar adaptations were found in many ray finned fishes that are equipped with sensitive electro receptive organs where reafferent signals are generated by various forms of rhythmic muscle activity like breathing or swimming (Bodznick et al., 1999; Zhang and Bodznick, 2008).

Analogously, in a swimming zebrafish a change in the "strength" of the virtual fish, e.g., a scenario where the fish suddenly found itself with much more – or much less – power than expected, the animals responded within a few seconds by adapting their behavior: a "weak" fish, for instance, increased its swim vigor to compensate for the decrease in strength of the visual feedback, whereas a "strong" fish did the opposite. Interestingly, the animals also "remembered" these changes in behavior for some time.

Since fish are readily amenable to whole brain calcium imaging – as is made clear in several other articles in this issue – it was straightforward to isolate several different types of neural activity that occurred during this behavior (Ahrens et al., 2012). Some neurons increased their activity when the fish swam harder, others when the fish swam more gently. Yet other groups, arguably the most interesting ones, were specifically active during the period when reafferent feedback was changed to render the animal unexpectedly weak or powerful. These "error" or "surprise" neurons are good candidates for the sites in the fish's brain where an efference copy gets compared to the reafference and they were found in many different brain areas, including the inferior olive and the cerebellum, both areas known to be involved in motor control in mammals. While it is still unclear how far the similarities between larval zebrafish's and mammalian brains extend in terms of anatomy and neuronal cell-types, it is clear that the general principles are pretty much conserved. Essential elements, like the inferior olive, the different nuclei of the cerebellum as well as individual neuronal types such as Purkinje and granule cells are certainly present in both species.

As such these studies open the field for a whole array of experiments that hopefully will shed light on the neural basis of motor learning in the vertebrate brain.

To summarize, these closed-loop implementations of fish behavior in virtual environments allow first forays into the study of entire neural ensembles, spanning from sensory input all the way to motor output, in a behaving animal that is flexibly adjusting its behavior in responses to changes in the feedback it receives from the environment. It thus opens the way for many similar experiments in which we can exhaustively study neural activity during true interactive behavior in a vertebrate model organism. Hopefully, this will serve to illuminate how large populations of neurons, across many brain areas, work together to generate flexible behavior.

REFERENCES

Ahrens, M. B., Li, J. M., Orger, M. B., Robson, D. N., Schier, A. F., Engert, F., et al. (2012). Brain-wide neuronal dynamics during motor adaptation in zebrafish. *Nature* 485, 471–477.

Bell, C. C. (1981). An efference copy which is modified by reafferent input. *Science* 214, 450–453.

Bell, C. C., Han, V. Z., Sugawara, Y., and Grant, K. (1997). Synaptic plasticity in a cerebellum-like structure depends on temporal order. *Nature* 387, 278–281.

Blumhagen, F., Zhu, P., Shum, J., Scharer, Y. P., Yaksi, E., Deisseroth, K., et al. (2011). Neuronal filtering of multiplexed odour representations. *Nature* 479, 493–498.

Bodznick, D., Montgomery, J. C., and Carey, M. (1999). Adaptive mechanisms in the elasmobranch hindbrain. *J. Exp. Biol.* 202, 1357–1364.

Del Bene, F., Wyart, C., Robles, E., Tran, A., Looger, L., Scott, E. K., et al. (2010). Filtering of visual information in the tectum by an identified neural circuit. *Science* 330, 669–673.

Dombeck, D. A., Khabbaz, A. N., Collman, F., Adelman, T. L., and Tank, D. W. (2007). Imaging large-scale neural activity with cellular resolution in awake, mobile mice. *Neuron* 56, 43–57.

Fagerstedt, P., Orlovsky, G. N., Deliagina, T. G., Grillner, S., and Ullen, F. (2001). Lateral turns in the Lamprey. II. Activity of reticulospinal neurons during the generation of fictive turns. *J. Neurophysiol.* 86, 2257–2265.

Fetcho, J. R., and Svoboda, K. R. (1993). Fictive swimming elicited by electrical stimulation of the midbrain in goldfish. *J. Neurophysiol.* 70, 765–780.

Grama, A., and Engert, F. (2012). Direction selectivity in the larval zebrafish tectum is mediated by asymmetric inhibition. *Front. Neural Circuits* 6:59. doi: 10.3389/fncir.2012.00059

Harvey, C. D., Collman, F., Dombeck, D. A., and Tank, D. W. (2009). Intracellular dynamics of hippocampal place cells during virtual navigation. *Nature* 461, 941–946.

Hassenstein, B. (1991). "Der Biologe Bernhard Hassenstein," in *Freiburger Universitätsblätter*, Vol. 114 (Freiburg: Rombach-Verlag), 85–112.

Hassenstein, B., and Reichardt, W. (1956). Wie sehen Insekten Bewegung? *Z. Naturforsch.* 11b, 513–524.

Maimon, G., Straw, A. D., and Dickinson, M. H. (2010). Active flight increases the gain of visual motion processing in *Drosophila*. *Nat. Neurosci.* 13, 393–399.

Masino, M. A., and Fetcho, J. R. (2005). Fictive swimming motor patterns in wild type and mutant larval zebrafish. *J. Neurophysiol.* 93, 3177–3188.

McLean, D. L., Masino, M. A., Koh, I. Y., Lindquist, W. B., and Fetcho, J. R. (2008). Continuous shifts in the active set of spinal interneurons during changes in locomotor speed. *Nat. Neurosci.* 11, 1419–1429.

Mu, Y., Li, X. Q., Zhang, B., and Du, J. L. (2012). Visual input modulates audiomotor function via hypothalamic dopaminergic neurons through a cooperative mechanism. *Neuron* 75, 688–699.

Niell, C. M., and Smith, S. J. (2005). Functional imaging reveals rapid development of visual response properties in the zebrafish tectum. *Neuron* 45, 941–951.

O'Malley, D. M., Kao, Y. H., and Fetcho, J. R. (1996). Imaging the functional organization of zebrafish hindbrain segments during escape behaviors. *Neuron* 17, 1145–1155.

O'Malley, D. M., Sankrithi, N. S., Borla, M. A., Parker, S., Banden, S., Gahtan, E., et al. (2004). Optical physiology and locomotor behaviors of wild-type and nacre zebrafish. *Methods Cell Biol.* 76, 261–284.

Orger, M. B., Kampff, A. R., Severi, K. E., Bollmann, J. H., and Engert, F. (2008). Control of visually guided behavior by distinct populations of spinal projection neurons. *Nat. Neurosci.* 11, 327–333.

Portugues, R., and Engert, F. (2011). Adaptive locomotor behavior in larval zebrafish. *Front. Syst. Neurosci.* 5:72. doi: 10.3389/fnsys.2011.00072

Ramdya, P., and Engert, F. (2008). Emergence of binocular functional properties in a monocular neural circuit. *Nat. Neurosci.* 11, 1083–1090.

Ritter, D. A., Bhatt, D. H., and Fetcho, J. R. (2001). In vivo imaging of zebrafish reveals differences in the spinal networks for escape and swimming movements. *J. Neurosci.* 21, 8956–8965.

Seelig, J. D., and Jayaraman, V. (2011). Studying sensorimotor processing with physiology in behaving *Drosophila*. *Int. Rev. Neurobiol.* 99, 169–189.

Sumbre, G., Muto, A., Baier, H., and Poo, M. M. (2008). Entrained rhythmic activities of neuronal ensembles as perceptual memory of time interval. *Nature* 456, 102–106.

Szobota, S., Gorostiza, P., Del Bene, F., Wyart, C., Fortin, D. L., Kolstad, K. D., et al. (2007). Remote control of neuronal activity with a light-gated glutamate receptor. *Neuron* 54, 535–545.

Tang, S., Wolf, R., Xu, S., and Heisenberg, M. (2004). Visual pattern recognition in *Drosophila* is invariant for retinal position. *Science* 305, 1020–1022.

Wyart, C., Del Bene, F., Warp, E., Scott, E. K., Trauner, D., Baier, H., et al. (2009). Optogenetic dissection of a behavioural module in the vertebrate spinal cord. *Nature* 461, 407–410.

Zhang, Z., and Bodznick, D. (2008). Plasticity in a cerebellar-like structure: suppressing reafference during episodic behaviors. *J. Exp. Biol.* 211, 3720–3728.

Conflict of Interest Statement: The author declares that the research was conducted in the absence of any commercial or financial relationships that could be construed as a potential conflict of interest.

Received: 15 November 2012; paper pending published: 04 December 2012; accepted: 26 December 2012; published online: 25 January 2013.

*Citation: Engert F (2013) Fish in the matrix: motor learning in a virtual world. Front. Neural Circuits **6**:125. doi: 10.3389/fncir.2012.00125*

frontiers in
NEURAL CIRCUITS

REVIEW ARTICLE
published: 23 April 2013
doi: 10.3389/fncir.2013.00071

Analyzing the structure and function of neuronal circuits in zebrafish

Rainer W. Friedrich*, Christel Genoud and Adrian A. Wanner

Friedrich Miescher Institute for Biomedical Research, Basel, Switzerland

Edited by:
German Sumbre, Ecole Normale Superieure, France

Reviewed by:
Florian Engert, Harvard University, USA
Misha B. Ahrens, Howard Hughes Medical Institute, USA

****Correspondence:***
Rainer W. Friedrich, Friedrich Miescher Institute for Biomedical Research, Maulbeerstrasse 66, 4058 Basel, Switzerland.
e-mail: rainer.friedrich@fmi.ch

The clever choice of animal models has been instrumental for many breakthrough discoveries in life sciences. One of the outstanding challenges in neuroscience is the in-depth analysis of neuronal circuits to understand how interactions between large numbers of neurons give rise to the computational power of the brain. A promising model organism to address this challenge is the zebrafish, not only because it is cheap, transparent and accessible to sophisticated genetic manipulations but also because it offers unique advantages for quantitative analyses of circuit structure and function. One of the most important advantages of zebrafish is its small brain size, both at larval and adult stages. Small brains enable exhaustive measurements of neuronal activity patterns by optical imaging and facilitate large-scale reconstructions of wiring diagrams by electron microscopic approaches. Such information is important, and probably essential, to obtain mechanistic insights into neuronal computations underlying higher brain functions and dysfunctions. This review provides a brief overview over current methods and motivations for dense reconstructions of neuronal activity and connectivity patterns. It then discusses selective advantages of zebrafish and provides examples how these advantages are exploited to study neuronal computations in the olfactory bulb.

Keywords: zebrafish, neuronal circuit, reconstruction, activity pattern, olfactory system

During the last century, a series of seminal discoveries demonstrated that brains are constructed modularly from distinct types of neurons, that information is transmitted by discrete action potentials, that electrical signals are generated and shaped by a plethora of ion channels, and that signals are passed and modulated through synapses (Albright et al., 2000). Many of these phenomena are now understood, in principle, at the molecular and biophysical level. Additional results provided detailed anatomical descriptions of the brain, uncovered mechanisms governing brain development, and revealed the engagement of defined brain regions in perceptual and cognitive tasks. Nevertheless, for many brain functions it is still unclear how they emerge from the biophysical properties of neurons and their interactions. Important elementary computations underlying higher brain functions are performed by subsets of neurons – neuronal circuits – that are typically defined as anatomically distinct networks of 10^2 – 10^7 neurons in vertebrates. Because circuit-level computations depend on dynamic interactions between large numbers of neurons, they cannot be fully analyzed by studying one neuron at a time. Rather, understanding neuronal circuit function also requires quantitative analyses of activity patterns across neuronal populations and rigorous analyses of network connectivity. Since neuronal circuits are stunningly complex even in comparison to other biological systems, a profound understanding of neuronal circuits is an enormous task. However, without such an understanding, key aspects of the brain remain elusive, and the rational design of treatments for psychiatric and neurological disorders is severely hampered. Quantitative analyses of neuronal circuit structure and function therefore present an outstanding scientific challenge, not only for neuroscience but also for other fields such as engineering and theoretical disciplines.

ANALYSIS OF NEURONAL CIRCUITS: METHODS AND MODEL SYSTEMS

Over the last decade, technological developments have opened fundamentally new opportunities to study neuronal circuits. These include sophisticated molecular approaches to identify, label and manipulate specific types of neurons in the brain, quantitative paradigms to study behavior, advances in extracellular recording techniques to measure action potential firing of multiple neurons in behaving animals, and important developments in intracellular recording methods (Luo et al., 2008; Scanziani and Hausser, 2009). In addition, three technologies are currently changing the landscape of neuroscience research. First, multiphoton calcium imaging can visualize activity patterns across large numbers of neurons with single-neuron spatial resolution and a temporal resolution between a few milliseconds and approximately a second (Denk and Svoboda, 1997; Kerr and Denk, 2008). Although multiphoton microscopy was first described more than 20 years ago (Denk et al., 1990), the technique became widely used only recently, partly because optical know-how has spread within the neuroscience community and because microscopes with good performance can now be obtained commercially. In parallel, genetically encoded calcium indicators were optimized to the point that they reliably report the occurrence of one or a few action potentials with sufficient signal-to-noise ratio (Akerboom et al., 2012; Looger and Griesbeck, 2012). As a consequence, multiphoton calcium imaging is now used in many laboratories to measure

neuronal activity across populations of neurons, providing direct insights into the function of neuronal circuits.

Second, opto- or pharmacogenetic tools have been developed to depolarize or hyperpolarize defined neurons by light or by specific chemical compounds, respectively. Neuronal activity can now be manipulated with unprecedented spatial, temporal and cell type specificity through the intersection of genetic targeting and optical stimulation (Bamann et al., 2010; Mattis et al., 2011; Yizhar et al., 2011; Zhang et al., 2011). When applied in behaving animals, opto- and pharmacogenetic manipulations can uncover causal relationships between the activity of identified neurons and behavioral outputs. Furthermore, opto- or pharmacogenetic tools can be used to perturb activity patterns within an active circuit, to impose specific neuronal activity patterns onto a population, and to up- or downregulate the activity of specific cell types. These approaches are extremely valuable for systematic analyses of functional circuit properties *in vitro* and *in vivo*.

Third, novel methods have been developed to analyze the connectivity between neurons in a circuit. Genetic labeling with combinations of fluorescent proteins permits light-microscopic tracing of multiple neurons within a tissue (Livet et al., 2007; Lichtman and Denk, 2011), and transsynaptic viral tracers can visualize neurons that are monosynaptically connected to one or a few target neurons (Wickersham et al., 2007; Luo et al., 2008). These approaches cannot, however, reconstruct the complete set of neuronal connections in most circuits. Currently, dense circuit reconstructions rely on morphological tracing of neurons and on the identification of their synaptic connections in image stacks. This approach requires high spatial resolution ($\sim$25 nm or better) throughout large volumes (often $>$100 μm in each dimension; Lichtman and Denk, 2011). In small volumes, nanometer resolution has been achieved by imaging of serial ultrathin sections in a transmission electron microscope (Harris et al., 2006) but this approach cannot easily be scaled up because it depends heavily on manual labor. Recently, methods for efficient ultrastructural imaging of large volumes have been developed that are based on the automated sectioning of a tissue block (Denk and Horstmann, 2004; Hayworth et al., 2006; Kasthuri et al., 2007; Helmstaedter et al., 2008; Knott et al., 2008; Briggman and Bock, 2012; Denk et al., 2012). In one approach, an automated tape-collecting ultramicrotome (ATUM) is used to cut sections at a thickness of $<$30 nm and collect them on a carbon-coated tape (Hayworth et al., 2006; Kasthuri et al., 2007; Tapia et al., 2012). Sections are then imaged in a scanning electron microscope (SEM). Other approaches section the tissue block inside the vacuum chamber of an SEM and take images of the block face, rather than the section, after each cut. Sections can be either cut by a diamond knife (SBEM), which achieves thicknesses $<$25 nm and offers a large field of view ($>$1 mm), or milled by a focused ion beam (FIB-SEM), which achieves thicknesses down to 5 nm but in a smaller field of view ($<$80 μm; Denk and Horstmann, 2004; Helmstaedter et al., 2008; Knott et al., 2008; Briggman and Bock, 2012). An advantage of the ATUM approach is that sections are preserved, allowing for post-staining, repeated imaging, and parallel imaging in multiple microscopes. Block face methods discard sections but minimize image registration problems, achieve thinner cutting, and have been reported repeatedly to cut thousands of sections without a single loss (Denk and Horstmann, 2004; Briggman et al., 2011). Although 3D electron microscopy and the associated sample preparation methods are demanding, the rate-limiting step for the reconstruction of entire circuits is usually data analysis, i.e., the tracing of neurons and the identification of synapses in stacks of EM images (Helmstaedter et al., 2008). The current gold standard for the reliable reconstruction of neurons is manual tracing (Helmstaedter et al., 2011), making the dense reconstruction of large circuits an enormous task. However, as connectivity imposes hard constraints on the exchange of information between neurons, solid and comprehensive information about a circuit's wiring diagram is highly valuable and, in many cases, likely to be necessary to understand how a circuit computes (Briggman and Bock, 2012; Denk et al., 2012). Reconstructing wiring diagrams of neuronal circuits is therefore a critical challenge in systems neuroscience.

To exploit the full potential of novel methods it is important to apply them in appropriate model systems. History shows that the selection of animal models such as *Drosophila*, mice, *C. elegans* or *Aplysia* has been critical for breakthrough discoveries, much like the development of novel technologies. Because many approaches to neuronal circuits rely on genetically encoded probes there is a strong incentive to choose a species for which advanced molecular and transgenic methods are established. Among invertebrates, obvious candidates are *C. elegans* and *Drosophila*. Some principles of information processing in other species can, however, not be addressed in *C. elegans*. Moreover, electrophysiological recordings are difficult, and the behavioral repertoire is limited. Many results obtained in *Drosophila* have been instructive and can be generalized to vertebrates. Interesting insights into general computational principles are likely to emerge from comparative studies of neuronal circuits that evolved independently but perform similar tasks in invertebrates and vertebrates. Some brain functions, however, are likely to differ between insects and vertebrates, as suggested by obvious differences in general brain anatomy and many other observations. It is thus desired to complement insect model systems with vertebrate models that offer similar experimental advantages.

The main genetic model systems among vertebrates are the mouse and the zebrafish. Driven by advances in genetic methods, the mouse has become popular in neuroscience and many important techniques were established for experiments *in vitro* and *in vivo*. However, detailed analyses of neuronal circuit structure and function are still presenting a major challenge. An important limitation of mice is often that only a small fraction of the neurons involved in a given computation can be recorded, reconstructed or manipulated experimentally. Zebrafish have less of a history in neuroscience although they have no obvious principal limitations. In fact, recent studies demonstrated that key approaches such as whole-cell recordings, multiphoton calcium imaging, and quantitative behavioral analyses can be applied very efficiently. Moreover, the spectrum of methods for genetic manipulations has been extended significantly, for example by introducing two-component expression systems such as the Gal4- and the Tet-systems, and by establishing approaches for the targeted mutation of genes (Scott et al., 2007; Zhu et al., 2009; Huang et al., 2011; Bedell et al., 2012). Importantly, valuable resources have been created within the

growing community of zebrafish neuroscientists, including large collections of Gal4 driver lines to target genetically encoded probes to specific types of neurons (Scott et al., 2007; Baier and Scott, 2009; Kawakami et al., 2010). An ongoing effort at the Sanger Center is creating mutations in every gene within the next few years (http://www.sanger.ac.uk/Projects/D_rerio/zmp/). As a consequence, zebrafish now offer a broad spectrum of opportunities for neurophysiological and molecular experiments that shows no obvious shortcomings compared to mice. Currently, the main limitation of zebrafish may be the availability of quantitative assays for complex behaviors. This situation is unlikely to reflect a limited behavioral repertoire of zebrafish but may simply be due to the fact that zebrafish neuroethology is still at an early stage. Indeed, various studies have demonstrated that zebrafish and closely related species display complex behaviors including schoaling, territorial behavior, kin recognition, associative learning including trace conditioning, place preference learning, spatial navigation, and others (Prober et al., 2006; Rodriguez et al., 2006; Gerlach et al., 2008; Saverino and Gerlai, 2008; Agetsuma et al., 2010; Norton and Bally-Cuif, 2010; Arganda et al., 2012; Karnik and Gerlai, 2012). It is therefore likely that advanced and quantitative behavioral assays for zebrafish can and will be developed in the future to study higher brain functions. A main difference between zebrafish and mice is their brain size. The zebrafish brain is substantially smaller both in terms of physical size and in terms of the number of neurons. Since small brain size provides clear advantages for quantitative analyses of neuronal activity and connectivity patterns, zebrafish offer the possibility to study features of neuronal circuits that cannot easily be studied in mice, as discussed below. The zebrafish therefore offers unique advantages for quantitative studies of neuronal circuit structure and function.

ZEBRAFISH AS A MODEL IN SYSTEMS NEUROSCIENCE: SIZE MATTERS

Originally, the zebrafish has been chosen as a model system for genetics and developmental biology. Based on pioneering work by Streisinger et al. (1981), a group of researches including Christiane Nüsslein-Volhard, Monte Westerfield, and many others established important resources and used zebrafish to analyze vertebrate development by large-scale mutagenesis screens (see issue 123 of Development, 1996). Some advantages of zebrafish for developmental genetics, such as their transparency at early developmental stages and their low cost, are also useful for systems neuroscience. Nevertheless, neurophysiology remained an exotic area of research in zebrafish for many years. Recently, however, zebrafish neuroscience started to boom, which may be due to two major reasons. First, pioneering studies demonstrated that advanced methods including electrophysiology, imaging of genetically encoded probes, and optogenetics, can be used and combined very efficiently in larval and adult zebrafish. Second, as quantitative analyses of neuronal circuits moved into the focus of neuroscience, a growing community of scientists becomes interested in projects that appear feasible in zebrafish but daunting in larger species. As a consequence, zebrafish neuroscience has attracted scientists with diverse backgrounds and has become a highly dynamic and stimulating field.

Some advantages of zebrafish for neuroscience are "convenient" rather than "essential." For example, the transparency of zebrafish larvae is often considered an advantage because it allows for calcium imaging of neuronal activity patterns and for optogenetic manipulations of neurons without the need for surgical procedures (O'Malley et al., 1996; Baier and Scott, 2009; Wyart et al., 2009; Blumhagen et al., 2011; Ahrens et al., 2012; del Bene and Wyart, 2012; Ahrens and Keller, 2013; Portugues et al., 2013). In some cases, however, surgical procedures are no principal barrier to reach the scientific goal. Neuronal population activity in some brain areas of behaving rodents can, for example, be measured by multiphoton calcium imaging using head-fixation and a virtual environment (Dombeck et al., 2007) or using head-mounted miniature microscopes (Sawinski et al., 2009; Ghosh et al., 2011). Likewise, optogenetic manipulations can be performed without dramatic experimental limitations using implanted optical fibers (Yizhar et al., 2011). Transparency is therefore essential only under specific experimental constraints, for example when optical access is needed simultaneously at different locations or from different directions (Ahrens et al., 2012; Tomer et al., 2012; Ahrens and Keller, 2013).

Other advantages of zebrafish are more fundamental because they enable experiments that cannot be performed in other organisms using available technology. Often, these advantages are related to the small size of the zebrafish brain. Size is a basic, yet very important, property of a model organism because key steps in the analysis of neuronal circuits have size constraints. These are particularly obvious for the exhaustive measurements of neuronal activity patterns by multiphoton calcium imaging and for the reconstruction of wiring diagrams by 3D-EM. The zebrafish brain is only <0.5 mm thick and 1.5 mm long in larvae, and between 0.4 and 2 mm thick and about 4.5 mm long in adults (Wullimann et al., 1996). The total number of neurons is on the order of 10^5 in larvae and 10^7 in adults (Hill et al., 2003; Hinsch and Zupanc, 2007).

The small physical size of the zebrafish brain obviously facilitates optical access for measurements of neuronal activity patterns by multiphoton calcium imaging. However, physical brain size is not always a principal limitation for imaging neuronal activity patterns because gradient index lenses or other technical solutions can now provide access even to deep neurons in the rodent brain (Ghosh et al., 2011). Rather, the primary constraint on measurements of neuronal activity patterns is often the absolute number of neurons that can be sampled during the time available for an experiment. Many experiments, particularly those that involve behavior, cannot be extended beyond a few hours and require the repeated application of multiple stimuli, separated by resting periods. As a consequence, the number of neurons whose activity can be sampled is typically not larger than a few thousand, and often much smaller. This number may be increased by future developments of technologies such as selective plane illumination microscopy (Tomer et al., 2012; Ahrens and Keller, 2013). However, solutions for exhaustive sampling of circuits that contain millions of neurons will likely remain difficult or impossible in the near future. In zebrafish, however, homologous circuits usually consist of much fewer neurons than in mice. The olfactory bulb (OB), for example, contains only ∼500 neurons in larval zebrafish and 20000 –

30000 neurons in adults (Mack-Bucher et al., 2007; Wiechert et al., 2010), as compared to $\sim 10^6 - 10^7$ neurons in adult mice. Zebrafish therefore allow for the sampling of neuronal activity across a large fraction of neurons in many brain areas.

Why is exhaustive sampling of neuronal activity patterns important? Some computations of neuronal circuits can indeed be studied by sparse sampling. In particular, sparse sampling is sufficient when responses are dense and when a computation can be explained by simple statistical properties of neuronal activity patterns. For example, responses of individual neurons in sensory brain areas are often scaled as a function of the mean input by an operation termed "normalization" (Carandini and Heeger, 2011). This operation has been studied in detail in the retina and primary visual cortex for responses to well-defined stimuli such as gratings of different orientation. Under these conditions, normalization can be analyzed by measuring a neuron's orientation tuning and estimating the mean population activity from a small number of recordings. This is possible because the computation does not depend on the precise structure of the population activity but only on its mean. Other functions of neuronal circuits, however, cannot be analyzed rigorously by sparse sampling. Dense sampling can, for example, be required to define the state of a network, particularly when these states are not triggered by an external event but occur spontaneously. Generally, dense sampling becomes important when neuronal activity itself is sparse and when information processing depends on specific subsets of neurons. In higher visual areas, for example, some neurons respond selectively to objects such as specific faces. For many stimuli, salient responses that contain much of the information about an object will therefore be missed when the population is sampled sparsely. Furthermore, many computations in the brain cannot be uncovered by measuring only first-order statistical properties of neuronal activity or connectivity patterns. For example, it is assumed that information is stored in memory networks by strengthening and weakening of specific synapses, resulting in the stabilization of specific neuronal ensemble responses during memory recall (Marr, 1970, 1971; McNaughton and Morris, 1987). In theory, such a stabilization of neuronal ensembles can occur without a major change in the mean activity across the population. For example, it is possible that the activity of some neurons increases while the activity of other neurons decreases so that activity patterns are reorganized, rather than enhanced or suppressed as a whole. It may be expected that such a reorganization affects specific, presumably sparse, subsets of neurons while the activity of many other neurons is not strongly altered. Moreover, it is possible that changes in synaptic coupling manifest themselves in the correlation between the activity of multiple neurons. In these cases, global statistical properties of activity patterns are insufficient to fully understand the computation. Dense measurements and detailed neuron-by-neuron analyses of activity patterns may therefore be required for rigorous insights into some important neuronal computations. Circuits whose function depends on sparse activity and on the specific structure of activity patterns are probably common in vertebrates, e.g., in the cortex and cerebellum.

Small brain size also has obvious advantages for the reconstruction of wiring diagrams by 3D-EM. One reason why small tissue samples are desired is that the acquisition of EM image stacks is slow. This is, however, not a hard limitation because sectioning and imaging of relatively large samples (millimeters) is technically feasible and because faster imaging is likely to become possible in the future (Denk et al., 2012). Moreover, since many questions about circuit connectivity can be addressed by analyzing a small number of specimens, imaging times on the order of weeks, months or even years may be tolerated. The main size constraint on circuit reconstruction comes from the fact that the analysis of the data is extremely laborious. So far, the reconstruction of neurons has been performed manually by humans. The first, and so far the only, circuit for which an almost complete wiring diagram has been published is the nervous system of *C. elegans*, which consists of only 302 neurons (White et al., 1986; Chen et al., 2006; Varshney et al., 2011). Nevertheless, the reconstruction involved the labor of many humans over many years. More recently, large numbers of neurons in the mammalian retina have been reconstructed by humans who traced center lines (skeletons) of neurites using specialized, user-friendly software (Briggman et al., 2011; Helmstaedter et al., 2011). The tracing speeds obtained by this approach were on the order of 5–6 h/mm path length, not including error correction and synapse identification (Helmstaedter et al., 2011). The dense reconstruction of large circuits is therefore an enormous task considering that a cubic millimeter of cortical tissue contains approximately 4.5 km of neurites (Braitenberg and Schüz, 1998). Large-scale tracing of neurites is currently addressed by recruiting large cohorts of human tracers ("crowd-sourcing") and by the development of automated reconstruction methods (Turaga et al., 2010; Ciresan et al., 2012). It is, however, likely that the exhaustive reconstruction of large circuits will remain a massive task for a considerable future. Without automated procedures that increase reconstruction speed by orders of magnitude it is expected that the sheer bulk of the task will make the reconstruction of many circuits impossible in practice. A small model system such as zebrafish can therefore provide major advantages.

Some of the reasons why dense reconstructions of wiring diagrams are important are closely related to the reasons why dense measurements of neuronal activity patterns are important. Sparse sampling of connections may be sufficient to understand neuronal computations that depend only on simple statistical features of the connectivity matrix. For example, to normalize the output of individual neurons as a function of the mean population activity, neurons have to receive a signal reflecting the mean population activity. This signal does not require specific connectivity between individual neurons but can be extracted by neurons receiving stochastic, and sufficiently dense, input from the network. The statistical properties of connectivity required to understand the essence of this computation – averaging – can thus be obtained by sparse probing of connections. Other computations, however, require more detailed knowledge of wiring diagrams. A recent study in the retina revealed that direction-selectivity of ganglion cells depends on synaptic input from specific subsets of starburst amacrine cells, which was revealed by reconstructions of multiple neurons within the same retinal tissue block (Briggman et al., 2011). Precise knowledge of connectivity is therefore important to understand the mechanistic basis of some computations even in the retina, where cell types and mean connectivity have been analyzed in more detail than in most other brain areas. Detailed and exhaustive

analyses of neuron-by-neuron connectivity should be particularly important for neuronal circuits whose functions are shaped by experience. For example, it is assumed that the storage of information is accomplished by the strengthening or weakening of specific synaptic connections and, on longer timescales, by the elimination and formation of synaptic connections in a network. The reconstruction of the precise synaptic connectivity between many neurons would therefore provide a direct approach to analyze information storage by networks of neurons (Seung, 2009).

Dense reconstructions of wiring diagrams will immediately provide novel information about topological features of neuronal circuits such as reciprocal or circular connectivity, cliques of interconnected neurons and other structural "motifs." This information is of central importance for computational modeling and theoretical approaches to neuronal circuit function. Obviously, wiring diagrams provide hard constraints for circuit models but, by themselves, are most likely insufficient to explain and predict the function of many circuits. Detailed wiring diagrams may therefore be necessary, but not necessarily sufficient, to understand how a circuit computes (Briggman and Bock, 2012; Denk et al., 2012). An important goal in the field is therefore to combine the reconstruction of wiring diagrams with functional studies of neurons or neuronal ensembles, an approach that was, for example, used to analyze direction-selective circuits in the retina (Briggman et al., 2011).

The small brain of zebrafish provides essential advantages for exhaustive measurements of neuronal activity patterns and the underlying connectivity. Below, we will briefly review recent studies from our own group that have exploited these advantages to study the structure and function of neuronal circuits in the OB, the first olfactory processing center in the brain.

FUNCTIONAL AND STRUCTURAL ANALYSIS OF NEURONAL CIRCUITS IN THE OLFACTORY BULB OF ZEBRAFISH

The OB receives direct input from sensory neurons in the nose through an array of discrete neuropil structures, the glomeruli. Each glomerulus receives input from sensory neurons expressing the same odorant receptor. Individual odorant receptors can be activated by a spectrum of ligands, and each odorant activates a specific combination of odorant receptors. In the input layer of the OB, odors are therefore represented by a specific pattern of afferent activity across the array of glomeruli. In zebrafish, these odor-evoked input activity patterns have been visualized by voltage- or calcium-sensitive dye imaging of sensory axons (Friedrich and Korsching, 1997, 1998). Glomerular activity patterns are processed by a distributed network consisting of principal neurons, the mitral cells (MCs), and various types of local interneurons including granule cells, periglomerular cells and short axon cells. OB output is then conveyed by MCs to multiple higher brain areas.

Calcium imaging demonstrated that chemically similar amino acids, which are natural odorants for teleosts, activate specific, yet highly overlapping, combinations of glomeruli (Friedrich and Korsching, 1997). Activity patterns evoked by the same stimuli across MCs become more distinct during an odor response, as revealed by electrophysiological recordings and multiphoton calcium imaging (Friedrich and Laurent, 2001; Friedrich et al., 2004; Yaksi and Friedrich, 2006; Yaksi et al., 2007). Hence, neuronal circuits in the OB perform a pattern decorrelation, an elementary computation that can facilitate odor discrimination and autoassociative memory storage. This decorrelation was observed when responses from a substantial fraction of MCs were recorded. If the number of MCs in the analysis is reduced by removing MCs from the sample, pattern decorrelation became increasingly more difficult to detect. Hence, a sufficient density of sampling is required to observe this computation. This density has been achieved in the OB of adult zebrafish, which contains approximately 1500 MCs (Yaksi et al., 2007), but may be difficult to achieve in the OB of mice, which contains approximately 50000 MCs, distributed throughout a large volume.

A decorrelation of activity patterns appears useful when overlapping patterns represent different information but is counterproductive when overlapping patterns are noisy representations of the same stimulus. This conflict could be resolved if MC activity patterns are stable against small differences in the input but become decorrelated when differences exceed a certain range. To test this possibility, we "morphed" one odorant into a similar one through a series of intermediate mixtures with different concentration ratios and measured activity across large numbers of MCs by multiphoton calcium imaging. Morphing of the odor stimulus resulted in MC activity patterns that remained similar within certain ranges of the morphing series but became suddenly decorrelated at the transition between these stability ranges (Niessing and Friedrich, 2010). Hence, decorrelation divides the coding space of MCs into discrete, relatively stable regions that are separated by instable transition regions. This discontinuous decorrelation can act as a sensory filter and results in a discrete classification of odor representations. The potential number of stable regions is very large, implying that discretized MC activity patterns represent the stimulus space at high resolution. Further analysis showed that the decorrelation at transition points was mediated by coordinated response changes among small ensembles of MCs, rather than by shifts in the global network state (Niessing and Friedrich, 2010). Decorrelation is therefore mediated by distinct, small subsets of MCs, which explains why it is difficult to observe when only few neurons are analyzed. Hence, a detailed study of pattern decorrelation in the OB requires sufficiently dense sampling because the computation depends on sparse and specific subsets of neurons.

Computational modeling and theoretical analyses revealed that pattern decorrelation can emerge from thresholding, a generic operation performed by spiking neurons, and from sparse recurrent connectivity within the circuit (Wiechert et al., 2010). Abrupt transitions between output patterns might be created by connectivity among specific ensembles of neurons, although other mechanisms are also conceivable. A thorough analysis of the connectivity underlying pattern decorrelation may therefore require dense reconstruction of the circuit. Detailed knowledge of the wiring diagram is also expected to reveal other important structural features of the circuit. We therefore started to reconstruct neurons in the OB and their connections by SBEM and manual tracing. Because this is a considerable task we are currently applying this approach to the OB of larvae, rather than adult fish (Miyasaka et al., 2012).

In larvae expressing a genetically encoded calcium indicator in almost all neurons, we first measure responses of up to 50 % of all

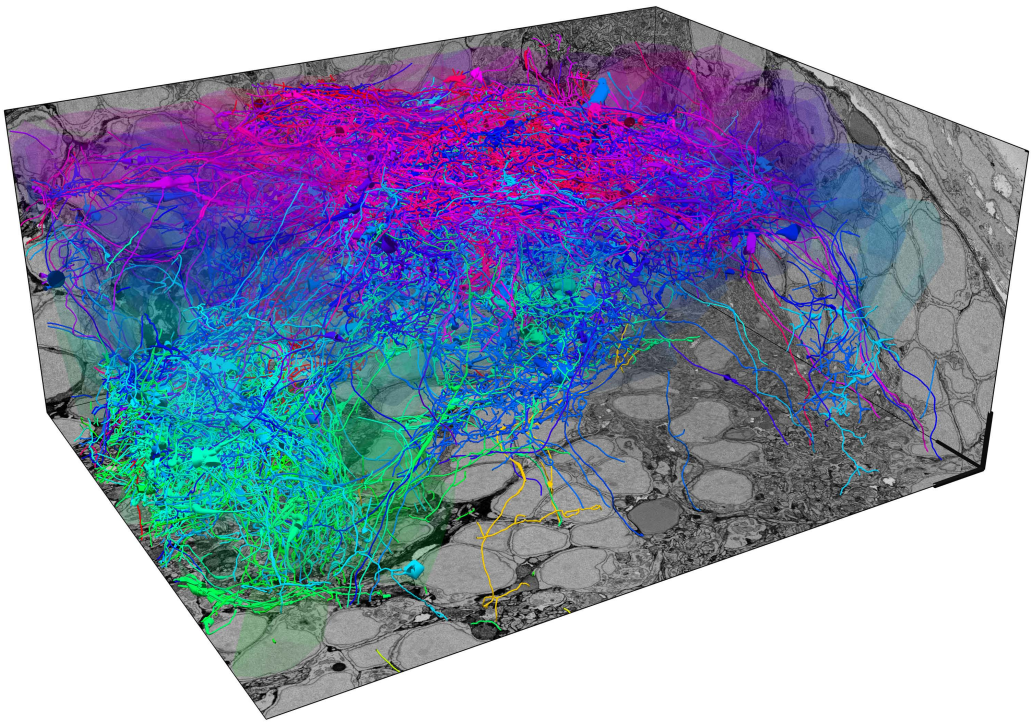

FIGURE 1 | Exhaustive reconstruction of neurons in the olfactory bulb of a zebrafish larva by serial block face scanning EM (SBEM). Shown are skeleton reconstructions of 137 neurons associated with different developing glomeruli (protoglomeruli) in the OB of a zebrafish larva (four days post-fertilization). Somata are transparent to enhance visibility of neurites. Each neuron has been manually reconstructed by three human tracers. Skeletons represent the consensus of the three reconstructions for each neuron. The diameter of skeletons represents the variation in the redundant reconstructions, providing a rough estimate of the neurite's diameter. Neurons are color-coded according to their soma location along the z-axis. Scale bars: 5 μm.

neurons in one OB to different odors by multiphoton microscopy. After fixation, staining and embedding of the sample, a stack of EM images covering the same OB is then acquired by SBEM with a voxel size of approximately 10 nm^3 × 10 nm^3 × 25 nm^3. Image acquisition takes 2–3 weeks and the total volume of the stack is approximately 90 μm^3 × 120 μm^3 × 70 μm^3. However, the subvolume that is filled by neurites and presents the major challenge for reconstruction is substantially smaller because a large fraction of the total volume is occupied by somata. In one OB, we have so far manually reconstructed skeletons of approximately 75% of all neurons with the help of external tracers (**Figure 1**). Each neuron has been reconstructed multiple times by different individuals to detect, analyze and correct tracing errors. Although the quantitative evaluation is still ongoing, preliminary results indicate that the reliability of reconstructions is high. Most discrepancies between different tracings of the same neurons appear to be due to individual mistakes, for example when a tracer missed a branch point. Such errors are easy to detect and correct. Disagreement originating from ambiguities in the data, which may be caused by insufficient resolution or contrast, appears to be very rare. Since the staining methods used in this study generate contrast of extra- and intracellular membranes, synapses can be identified visually in the EM images. Quantitative comparisons with EM images obtained at higher resolution are underway to determine the reliability of synapse identification in stacks obtained by SBEM. Although the manual reconstruction of an entire OB is a substantial task, it can be accomplished with the help of a limited number of external tracers (<50) within a reasonable time frame (<1 year). Assuming that reconstruction time scales with volume, the reconstruction of all neurons in the OB of a mouse by the same approach would take many kiloyears.

The goal of this study is to reconstruct all neurons within the OB, identify most of their synaptic connections, and relate the resulting connectivity matrix to the functional response properties of neurons measured by multiphoton calcium imaging. Such a dense reconstruction of activity and connectivity patterns in a complete circuit is expected to provide novel insights into circuit function that may be difficult, or even impossible, to obtain by other approaches.

CONCLUDING REMARKS

The zebrafish is becoming a popular model for studying the structure and function of neuronal circuits because it presents a variety of advantages over other animal models. Some of these advantages are useful, although not essential, while others enable experiments that are difficult or impossible to perform in other genetic model organisms. A key advantage of zebrafish, both at larval and adult stages, is its small size. Small brains are particularly useful and,

in some cases, essential for quantitative and exhaustive studies of neuronal activity and connectivity patterns. As such analyses are a major bottleneck in the mechanistic analysis of many neuronal computations, zebrafish have the potential to promote true breakthrough discoveries in systems neuroscience. Moreover, ongoing efforts are establishing zebrafish models for various neurological, psychiatric and other diseases. Zebrafish also offer the opportunity to perform large-scale screens not only of mutant phenotypes, but also of small molecule effects on behavior and potentially other phenomena (Kokel et al., 2010, 2013; Rihel et al., 2010). It may therefore be expected that zebrafish will also become an interesting model system to take studies of neuronal circuits into the domain of translational research.

ACKNOWLEDGMENTS

We thank members of the Friedrich lab and many other friends and colleagues for stimulating discussions. Work in the laboratory is supported by the Novartis Research Foundation, the Swiss Nationalfonds (SNF), the Human Frontiers Science Program (HFSP), the European Union (EU), the Deutsche Forschungsgemeinschaft (DFG) and the European Molecular Biology Organization (EMBO).

REFERENCES

Agetsuma, M., Aizawa, H., Aoki, T., Nakayama, R., Takahoko, M., Goto, M., et al. (2010). The habenula is crucial for experience-dependent modification of fear responses in zebrafish. *Nat. Neurosci.* 13, 1354–1356.

Ahrens, M. B., and Keller, P. J. (2013). Whole-brain functional imaging at cellular resolution using light-sheet microscopy. *Nat. Methods* doi: 10.1038/nmeth.2434 [Epub ahead of print].

Ahrens, M. B., Li, J. M., Orger, M. B., Robson, D. N., Schier, A. F., Engert, F., et al. (2012). Brain-wide neuronal dynamics during motor adaptation in zebrafish. *Nature* 485, 471–477.

Akerboom, J., Chen, T. W., Wardill, T. J., Tian, L., Marvin, J. S., Mutlu, S., et al. (2012). Optimization of a GCaMP calcium indicator for neural activity imaging. *J. Neurosci.* 32, 13819–13840.

Albright, T. D., Jessell, T. M., Kandel, E. R., and Posner, M. I. (2000). Neural science: a century of progress and the mysteries that remain. *Neuron* 25(Suppl.), S1–S55.

Arganda, S., Perez-Escudero, A., and De Polavieja, G. G. (2012). A common rule for decision making in animal collectives across species. *Proc. Natl. Acad. Sci. U.S.A.* 109, 20508–20513.

Baier, H., and Scott, E. K. (2009). Genetic and optical targeting of neural circuits and behavior-zebrafish in the spotlight. *Curr. Opin. Neurobiol.* 19, 553–560.

Bamann, C., Nagel, G., and Bamberg, E. (2010). Microbial rhodopsins in the spotlight. *Curr. Opin. Neurobiol.* 20, 610–616.

Bedell, V. M., Wang, Y., Campbell, J. M., Poshusta, T. L., Starker, C. G., Krug, R. G. II, et al. (2012). In vivo genome editing using a high-efficiency TALEN system. *Nature* 491, 114–118.

Blumhagen, F., Zhu, P., Shum, J., Zhang Schärer, Y.-P., Yaksi, E., Deisseroth, K., et al. (2011). Neuronal filtering of multiplexed odour representations. *Nature* 479, 493–498.

Braitenberg, V., and Schüz, A. (1998). *Cortex: Statistics and Geometry of Neuronal Connectivity*. Berlin: Springer.

Briggman, K. L., and Bock, D. D. (2012). Volume electron microscopy for neuronal circuit reconstruction. *Curr. Opin. Neurobiol.* 22, 154–161.

Briggman, K. L., Helmstaedter, M., and Denk, W. (2011). Wiring specificity in the direction-selectivity circuit of the retina. *Nature* 471, 183–188.

Carandini, M., and Heeger, D. J. (2011). Normalization as a canonical neural computation. *Nat. Rev. Neurosci.* 13, 51–62.

Chen, B. L., Hall, D. H., and Chklovskii, D. B. (2006). Wiring optimization can relate neuronal structure and function. *Proc. Natl. Acad. Sci. U.S.A.* 103, 4723–4728.

Ciresan, D. C., Giusti, A., Gambardella, L. M., and Schmidhuber, J. (2012). "Deep neural networks segment neuronal membranes in electron microscopy images," in *Advances in Neural Information Processing Systems (NIPS) 25*, eds P. Bartlett, F. C. N. Pereira, C. J. C. Burges, L. Bottou, and K. Q. Weinberger (Cambridge, MA: MIT Press).

del Bene, F., and Wyart, C. (2012). Optogenetics: a new enlightenment age for zebrafish neurobiology. *Dev. Neurobiol.* 72, 404–414.

Denk, W., Briggman, K. L., and Helmstaedter, M. (2012). Structural neurobiology: missing link to a mechanistic understanding of neural computation. *Nat. Rev. Neurosci.* 13, 351–358.

Denk, W., and Horstmann, H. (2004). Serial block-face scanning electron microscopy to reconstruct three-dimensional tissue nanostructure. *PLoS Biol.* 2:e329. doi: 10.1371/journal.pbio.0020329

Denk, W., Strickler, J. H., and Webb, W. W. (1990). Two-photon laser scanning fluorescence microscopy. *Science* 248, 73–76.

Denk, W., and Svoboda, K. (1997). Photon upmanship: why multiphoton imaging is more than a gimmick. *Neuron* 18, 351–357.

Dombeck, D. A., Khabbaz, A. N., Collman, F., Adelman, T. L., and Tank, D. W. (2007). Imaging large-scale neural activity with cellular resolution in awake, mobile mice. *Neuron* 56, 43–57.

Friedrich, R. W., Habermann, C. J., and Laurent, G. (2004). Multiplexing using synchrony in the zebrafish olfactory bulb. *Nat. Neurosci.* 7, 862–871.

Friedrich, R. W., and Korsching, S. I. (1997). Combinatorial and chemotopic odorant coding in the zebrafish olfactory bulb visualized by optical imaging. *Neuron* 18, 737–752.

Friedrich, R. W., and Korsching, S. I. (1998). Chemotopic, combinatorial and noncombinatorial odorant representations in the olfactory bulb revealed using a voltage-sensitive axon tracer. *J. Neurosci.* 18, 9977–9988.

Friedrich, R. W., and Laurent, G. (2001). Dynamic optimization of odor representations in the olfactory bulb by slow temporal patterning of mitral cell activity. *Science* 291, 889–894.

Gerlach, G., Hodgins-Davis, A., Avolio, C., and Schunter, C. (2008). Kin recognition in zebrafish: a 24-hour window for olfactory imprinting. *Proc. Biol. Sci.* 275, 2165–2170.

Ghosh, K. K., Burns, L. D., Cocker, E. D., Nimmerjahn, A., Ziv, Y., Gamal, A. E., et al. (2011). Miniaturized integration of a fluorescence microscope. *Nat. Methods* 8, 871–878.

Harris, K. M., Perry, E., Bourne, J., Feinberg, M., Ostroff, L., and Hurlburt, J. (2006). Uniform serial sectioning for transmission electron microscopy. *J. Neurosci.* 26, 12101–12103.

Hayworth, K. J., Kasthuri, N., Schalek, R., and Lichtman, J. W. (2006). Automating the collection of ultrathin serial sections for large volume TEM reconstructions. *Microsc. Microanal.* 12, 86–87.

Helmstaedter, M., Briggman, K. L., and Denk, W. (2008). 3D structural imaging of the brain with photons and electrons. *Curr. Opin. Neurobiol* 18, 633–641.

Helmstaedter, M., Briggman, K. L., and Denk, W. (2011). High-accuracy neurite reconstruction for high-throughput neuroanatomy. *Nat. Neurosci.* 14, 1081–1088.

Hill, A., Howard, C. V., Strahle, U., and Cossins, A. (2003). Neurodevelopmental defects in zebrafish (*Danio rerio*) at environmentally relevant dioxin (TCDD) concentrations. *Toxicol. Sci.* 76, 392–399.

Hinsch, K., and Zupanc, G. K. (2007). Generation and long-term persistence of new neurons in the adult zebrafish brain: a quantitative analysis. *Neuroscience* 146, 679–696.

Huang, P., Xiao, A., Zhou, M., Zhu, Z., Lin, S., and Zhang, B. (2011). Heritable gene targeting in zebrafish using customized TALENs. *Nat. Biotechnol.* 29, 699–700.

Karnik, I., and Gerlai, R. (2012). Can zebrafish learn spatial tasks? An empirical analysis of place and single CS-US associative learning. *Behav. Brain Res.* 233, 415–421.

Kasthuri, N., Hayworth, K., Lichtman, J., Erdman, N., and Ackerley, C. A. (2007). New technique for ultrathin serial brain section imaging using scanning electron microscopy. *Microsc. Microanal.* 13(Suppl. 2), 26–27.

Kawakami, K., Abe, G., Asada, T., Asakawa, K., Fukuda, R., Ito, A., et al. (2010). zTrap: zebrafish gene trap and enhancer trap database. *BMC Dev. Biol.* 10:105. doi: 10.1186/1471-213X-10-105

Kerr, J. N., and Denk, W. (2008). Imaging in vivo: watching the brain in action. *Nat. Rev. Neurosci.* 9, 195–205.

Knott, G., Marchman, H., Wall, D., and Lich, B. (2008). Serial section scanning electron microscopy of adult brain tissue using focused ion beam milling. *J. Neurosci.* 28, 2959–2964.

Kokel, D., Bryan, J., Laggner, C., White, R., Cheung, C. Y., Mateus, R., et al. (2010). Rapid behavior-based identification of neuroactive small molecules in the zebrafish. *Nat. Chem. Biol.* 6, 231–237.

Kokel, D., Cheung, C. Y., Mills, R., Coutinho-Budd, J., Huang, L., Setola, V., et al. (2013). Photochemical activation of TRPA1 channels in neurons and animals. *Nat. Chem. Biol.* 9, 257–263.

Lichtman, J. W., and Denk, W. (2011). The big and the small: challenges of imaging the brain's circuits. *Science* 334, 618–623.

Livet, J., Weissman, T. A., Kang, H., Draft, R. W., Lu, J., Bennis, R. A., et al. (2007). Transgenic strategies for combinatorial expression of fluorescent proteins in the nervous system. *Nature* 450, 56–62.

Looger, L. L., and Griesbeck, O. (2012). Genetically encoded neural activity indicators. *Curr. Opin. Neurobiol.* 22, 18–23.

Luo, L., Callaway, E. M., and Svoboda, K. (2008). Genetic dissection of neural circuits. *Neuron* 57, 634–660.

Mack-Bucher, J. A., Li, J., and Friedrich, R. W. (2007). Early functional development of interneurons in the zebrafish olfactory bulb. *Eur. J. Neurosci.* 25, 460–470.

Marr, D. (1970). A theory for cerebral neocortex. *Proc. R. Soc. Lond. B Biol. Sci.* 176, 161–234.

Marr, D. (1971). Simple memory: a theory for archicortex. *Philos. Trans. R. Soc. Lond. B Biol. Sci.* 262, 23–81.

Mattis, J., Tye, K. M., Ferenczi, E. A., Ramakrishnan, C., O'shea, D. J., Prakash, R., et al. (2011). Principles for applying optogenetic tools derived from direct comparative analysis of microbial opsins. *Nat. Methods* 9, 159–172.

McNaughton, B. L., and Morris, R. G. M. (1987). Hippocampal synaptic enhancement and information storage within a distributed memory system. *Trends Neurosci.* 10, 408–415.

Miyasaka, N., Wanner, A. A., Li, J., Mack-Bucher, J., Genoud, C., Yoshihara, Y., et al. (2012). Functional development of the olfactory system in zebrafish. *Mech. Dev.* doi: 10.1016/j.mod.2012.09.001 [Epub ahead of print].

Niessing, J., and Friedrich, R. W. (2010). Olfactory pattern classification by discrete neuronal network states. *Nature* 465, 47–52.

Norton, W., and Bally-Cuif, L. (2010). Adult zebrafish as a model organism for behavioural genetics. *BMC Neurosci.* 11:90. doi: 10.1186/1471-2202-11-90

O'Malley, D. M., Kao, Y. H., and Fetcho, J. R. (1996). Imaging the functional organization of zebrafish hindbrain segments during escape behaviors. *Neuron* 17, 1145–1155.

Portugues, R., Severi, K. E., Wyart, C., and Ahrens, M. B. (2013). Optogenetics in a transparent animal: circuit function in the larval zebrafish. *Curr. Opin. Neurobiol.* 23, 119–126.

Prober, D. A., Rihel, J., Onah, A. A., Sung, R. J., and Schier, A. F. (2006). Hypocretin/orexin overexpression induces an insomnia-like phenotype in zebrafish. *J. Neurosci.* 26, 13400–13410.

Rihel, J., Prober, D. A., Arvanites, A., Lam, K., Zimmerman, S., Jang, S., et al. (2010). Zebrafish behavioral profiling links drugs to biological targets and rest/wake regulation. *Science* 327, 348–351.

Rodriguez, F., Broglio, C., Duran, E., Gomez, A., and Salas, C. (2006). "Neural mechanisms of learning in teleost fish," in *Fish Cognition and Behavior*, eds C. Brown, K. Laland, and J. Krause (Oxford: Blackwell publishing).

Saverino, C., and Gerlai, R. (2008). The social zebrafish: behavioral responses to conspecific, heterospecific, and computer animated fish. *Behav. Brain. Res.* 191, 77–87.

Sawinski, J., Wallace, D. J., Greenberg, D. S., Grossmann, S., Denk, W., and Kerr, J. N. (2009). Visually evoked activity in cortical cells imaged in freely moving animals. *Proc. Natl. Acad. Sci. U.S.A.* 106, 19557–19562.

Scanziani, M., and Hausser, M. (2009). Electrophysiology in the age of light. *Nature* 461, 930–939.

Scott, E. K., Mason, L., Arrenberg, A. B., Ziv, L., Gosse, N. J., Xiao, T., et al. (2007). Targeting neural circuitry in zebrafish using GAL4 enhancer trapping. *Nat. Methods* 4, 323–326.

Seung, H. S. (2009). Reading the book of memory: sparse sampling versus dense mapping of connectomes. *Neuron* 62, 17–29.

Streisinger, G., Walker, C., Dower, N., Knauber, D., and Singer, F. (1981). Production of clones of homozygous diploid zebra fish (*Brachydanio rerio*). *Nature* 291, 293–296.

Tapia, J. C., Kasthuri, N., Hayworth, K. J., Schalek, R., Lichtman, J. W., Smith, S. J., et al. (2012). High-contrast en bloc staining of neuronal tissue for field emission scanning electron microscopy. *Nat. Protoc.* 7, 193–206.

Tomer, R., Khairy, K., Amat, F., and Keller, P. J. (2012). Quantitative high-speed imaging of entire developing embryos with simultaneous multi-view light-sheet microscopy. *Nat. Methods* 9, 755–763.

Turaga, S. C., Murray, J. F., Jain, V., Roth, F., Helmstaedter, M., Briggman, K., et al. (2010). Convolutional networks can learn to generate affinity graphs for image segmentation. *Neural Comput.* 22, 511–538.

Varshney, L. R., Chen, B. L., Paniagua, E., Hall, D. H., and Chklovskii, D. B. (2011). Structural properties of the *Caenorhabditis elegans* neuronal network. *PLoS Comput. Biol.* 7:e1001066. doi: 10.1371/journal.pcbi.1001066

White, J. G., Southgate, E., Thomson, J. N., and Brenner, S. (1986). The structure of the nervous system of the nematode *Caenorhabditis elegans*. *Philos. Trans. R. Soc. Lond. B Biol. Sci.* 314, 1–340.

Wickersham, I. R., Lyon, D. C., Barnard, R. J., Mori, T., Finke, S., Conzelmann, K. K., et al. (2007). Monosynaptic restriction of transsynaptic tracing from single, genetically targeted neurons. *Neuron* 53, 639–647.

Wiechert, M. T., Judkewitz, B., Riecke, H., and Friedrich, R. W. (2010). Mechanisms of pattern decorrelation by recurrent neuronal circuits. *Nat. Neurosci.* 13, 1003–1010.

Wullimann, M. F., Rupp, B., and Reichert, H. (1996). *Neuroanatomy of the Zebrafish Brain: a Topological Atlas*. Basel: Birkhäuser.

Wyart, C., Del Bene, F., Warp, E., Scott, E. K., Trauner, D., Baier, H., et al. (2009). Optogenetic dissection of a behavioural module in the vertebrate spinal cord. *Nature* 461, 407–410.

Yaksi, E., and Friedrich, R. W. (2006). Reconstruction of firing rate changes across neuronal populations by temporally deconvolved Ca2+ imaging. *Nat. Methods* 3, 377–383.

Yaksi, E., Judkewitz, B., and Friedrich, R. W. (2007). Topological reorganization of odor representations in the olfactory bulb. *PLoS Biol.* 5:e178. doi: 10.1371/journal.pbio.0050178

Yizhar, O., Fenno, L. E., Davidson, T. J., Mogri, M., and Deisseroth, K. (2011). Optogenetics in neural systems. *Neuron* 71, 9–34.

Zhang, F., Vierock, J., Yizhar, O., Fenno, L. E., Tsunoda, S., Kianianmomeni, A., et al. (2011). The microbial opsin family of optogenetic tools. *Cell* 147, 1446–1457.

Zhu, P., Narita, Y., Bundschuh, S. T., Fajardo, O., Zhang Scharer, Y. P., Chattopadhyaya, B., et al. (2009). Optogenetic dissection of neuronal circuits in zebrafish using viral gene transfer and the Tet system. *Front. Neural Circuits* 3:21. doi: 10.3389/neuro.04.021.2009

Conflict of Interest Statement: The authors declare that the research was conducted in the absence of any commercial or financial relationships that could be construed as a potential conflict of interest.

Received: 30 January 2013; paper pending published: 01 March 2013; accepted: 03 April 2013; published online: 23 April 2013.

Citation: Friedrich RW, Genoud C and Wanner AA (2013) Analyzing the structure and function of neuronal circuits in zebrafish. Front. Neural Circuits ***7****:71. doi: 10.3389/fncir.2013.00071*

frontiers in
NEURAL CIRCUITS

PERSPECTIVE ARTICLE
published: 10 May 2013
doi: 10.3389/fncir.2013.00089

SINs and SOMs: neural microcircuits for size tuning in the zebrafish and mouse visual pathway

Alison J. Barker[1,2] and Herwig Baier[1]*

[1] *Department Genes-Circuits-Behavior, Max Planck Institute of Neurobiology, Martinsried, Germany*
[2] *Neuroscience Graduate Program, University of California San Francisco, San Francisco, CA, USA*

Edited by:
Gonzalo G. De Polavieja, Instituto Cajal – Consejo Superior de Investigaciones Científicas, Spain

Reviewed by:
Iris Salecker, MRC National Institute for Medical Research, UK
Koichi Kawakami, National Institute of Genetics, Japan

***Correspondence:**
Herwig Baier, Department Genes-Circuits-Behavior, Max Planck Institute of Neurobiology, Am Klopferspitz 18, 82152 Martinsried, Germany.
e-mail: hbaier@neuro.mpg.de

In many animals, a fast and reliable circuit for discriminating between predator-sized objects and edible (prey-sized) objects is necessary for survival. How are receptive fields (RFs) in visual brain areas organized to extract information about size? Recent studies from the zebrafish optic tectum and the mouse visual cortex suggest *de novo* shaping of RFs by subtypes of inhibitory neurons. Del Bene et al. (2010) describe a population of GABAergic neurons in the zebrafish optic tectum (superficial interneurons, SINs) that are necessary for size filtering during prey capture. Adesnik et al. (2012) describe a somatostatin-expressing interneuron population (SOMs) that confers surround suppression on layer II/III pyramidal cells in mouse V1. Strikingly both the SINs and the SOMs, display size-dependent response properties. Increasing visual stimulus size increases excitatory input to these neurons. Dampening SIN or SOM activity alters tuning of neighboring circuits such that they lose preference for small objects. Both results provide exciting evidence for mechanisms of size filtering in visual circuits. Here we review the roles of the SINs and the SOMs and speculate on the similarity of such spatial filters across species.

Keywords: optic tectum, visual cortex, zebrafish (*Danio rerio*), size discrimination, inhibitory interneurons

THE SINs

The pursuit and capture of small prey (e.g., *paramecia*) by the zebrafish larva require that information about the size and motion of the prey object be continually tracked. Larvae with laser ablations of the optic tectum are unable to perform this behavior (Gahtan et al., 2005), and several studies have identified neurons in the tectum with preferential size tuning to prey-sized objects (Sajovic and Levinthal, 1982a,b; Niell and Smith, 2005; Muto et al., 2013). Del Bene et al. (2010) searched for the locus of small object tuning in the tectum. Retinal ganglion cell axons enter the tectum largely in its superficial layers (Robles et al., 2013). Visual information is then transmitted through synaptic circuitry to the deeper layers of the tectal neuropil, from where it is carried on to the motor centers of the midbrain and hindbrain. The resident neurons in the deep layers of the tectum are the periventricular neurons (PVNs). They comprise two main classes: periventricular interneurons (PVINs) make only local connections in the tectum, whereas the periventricular projection neurons (PVPNs) receive inputs from PVIN axons in the deeper layers and send efferent axons to premotor and motor areas (Nevin et al., 2010). Only some classes of PVINs send dendrites to the superficial, retinorecipient layers.

By selectively expressing genetically encoded calcium indicators (GCaMP1.6 and 3) in retinal ganglion cell axons, Del Bene and colleagues (2010) found that retinal afferents displayed uniform activity regardless of stimulus size. On the other hand, dendrites of PVNs (presumably a mix of PVINs and PVPNs) stratifying within the deep layers of the tectal neuropil were preferentially tuned to small moving bars, whereas many PVIN dendrites in the superficial neuropil were responsive to both full-field visual stimuli (here a full screen flash) and small moving bars. The characteristic tuning to small moving objects of less than 10° was observed in many single PVNs and across populations of PVNs (**Figures 1A,A′**). Dampening GABAergic tone through local application of bicuculline increased Ca^{2+} responses to large objects, suggesting that GABAergic control normally sieves information by size as it trickles down to the deep layers. How is this achieved?

Del Bene et al. (2010) identified a population of GABAergic interneurons, the superficial interneurons (SINs), positioned in the superficial tectum. Using a transgenic Gal4 line that allowed them to target these cells – they showed that SINs are preferentially tuned to wide-field visual stimuli (**Figures 1A,A′**). When presented with a moving bar of increasing width, SINs expressing GCaMP displayed increasing Ca^{+2} responses as the size of the bar increased. Selectively ablating the SINs by photoactivation of KillerRed protein resulted in a loss of small object preference in the deep tectal layers. Importantly, the KillerRed experiments demonstrate that size tuning in the tectum is not inherited solely (if at all) from the retina. Rather intratectal circuits substantially contribute to size tuning. In addition, synaptically silencing SINs through genetically targeted expression of tetanus toxin decreased performance of larvae in a prey capture assay, providing a link between the size tuning for small objects in the deep neuropil and size-discrimination behavior. The optomotor response (OMR) requires the detection of large-field motion and is not dependent on an intact tectum (Roeser and Baier, 2003). As expected silencing of the SINs had no measurable effect on the OMR (Del Bene et al., 2010).

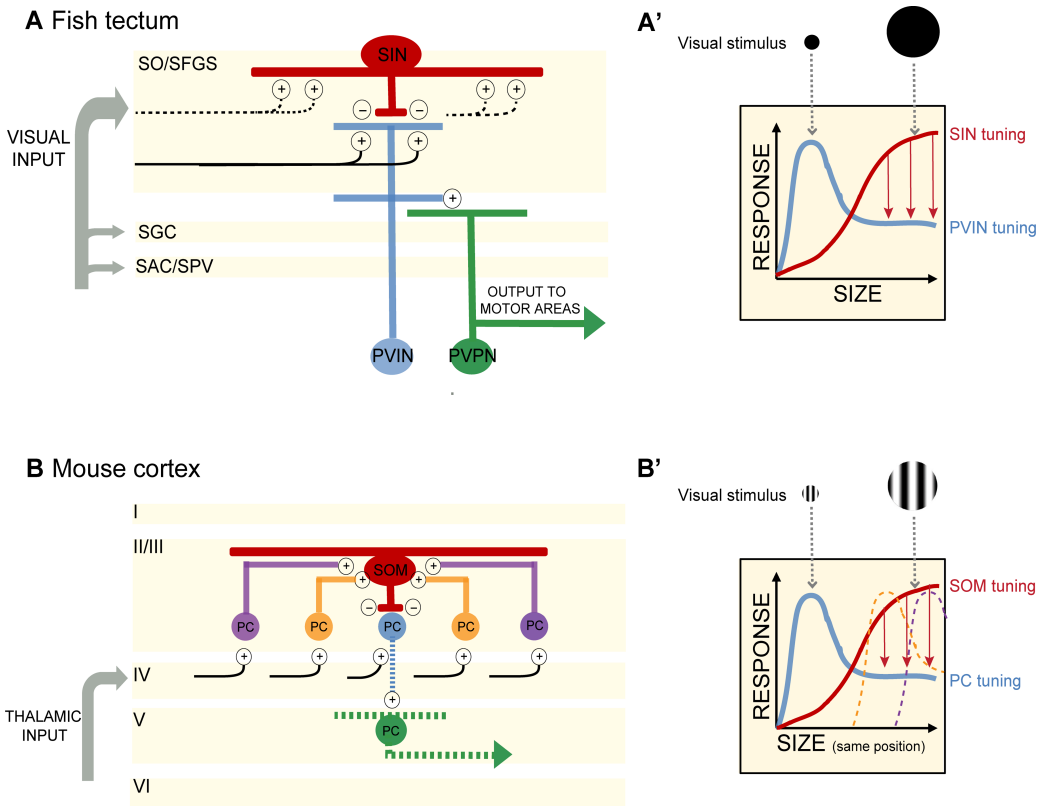

FIGURE 1 | (A) In the optic tectum of the zebrafish larva, superficial interneurons (SINs) are preferentially tuned to large objects in the visual field. Periventricular neurons (PVNs) with dendrites stratifying in the deep neuropil are preferentially tuned to small objects. PVINs denote periventricular interneurons, PVPNs, periventricular projection neurons. Retinal inputs distribute among four main layers of the tectum (SO, stratum opticum; SFGS, stratum fibrosum et griseum superficiale; SGC, stratum griseum centrale; SAC/SPV, stratum album centrale/stratum periventriculare). SIN cell bodies are located in the SO and extend dendritic and axonal arbors throughout the SFGS. SINs may receive excitatory synaptic input directly from retinal ganglion cell axons or from PVINs or both. Plus and negative signs denote excitatory and inhibitory connections, respectively. Blue and red indicate excitatory and inhibitory interneurons, respectively. Projection neurons are colored in green. Black lines depict retinal ganglion cell axons. Dashed lines indicate predicted, but not yet demonstrated synaptic connections. **(A′)** Schematic of SIN filtering in the optic tectum. As the size of the visual stimulus increases, SINs become activated and provide inhibitory input to sharpen the tuning of PVIN receptive fields. Size-tuning curves for SINs and PVINs are depicted by red and blue curves, respectively. Red arrows denote inhibition acting to sharpen tuning. **(B)** In the mouse visual cortex, somatostatin-expressing interneurons (SOMs) are preferentially tuned to large objects in the visual field and display no surround suppression. SOMs are positioned in layer II/III and receive lateral excitatory inputs from pyramidal cells (PCs) in layer II/III. SOMs provide inhibition to neighboring layer II/III PCs, resulting in surround suppression and PC preferential tuning to smaller objects. Cortical layers I to VI are denoted. Plus and negative signs denote excitatory and inhibitory connections, respectively. Red denotes inhibitory interneurons. Excitatory PCs in layer II/III are colored in blue, orange, and purple (corresponding to their relative distance from the SOM). The central PC (shown in blue) receives surround suppression from the SOM. PCs in layer V are colored in green. For simplicity in this schematic, only connections pertaining to size filtering circuitry are shown. Projections of layer II/III PCs are not shown. Black lines depict input from the thalamus. Dashed lines indicate predicted, but not yet demonstrated synaptic connections. **(B′)**Schematic of SOM filtering in the visual cortex. Here the visual stimulus is a drifting grating (within a circular aperture) of increasing size. Size tuning of the central PC shown in (**B**; blue) is depicted here with a blue size-tuning curve. As the stimulus size increases beyond the size of the blue PC's receptive field, the receptive fields of neighboring PCs are activated. The large visual stimulus occupies the same position in the visual field as the small stimulus, but increases in diameter thus encompassing multiple PC receptive fields (depicted here by the orange and purple size-tuning curves). These PCs provide excitatory drive to a SOM. SOM activation in turn provides surround suppression to the blue PC. The size-tuning curve of the SOM is depicted in red. Red arrows denote inhibition acting to sharpen tuning.

Already in 1982, Sajovic and Levinthal observed that tectal neurons can be optimally tuned to objects much smaller than their receptive fields (RFs), and smaller even than the RFs of retinal ganglion cells providing visual input. Sajovic and Levinthal (1982a,b) suggested that inhibition was responsible for this size tuning, but the exact nature of the inhibitory mechanism remained elusive. A piece of this puzzle has been resolved in the identification of the SINs, but it is likely that there are additional sources of inhibition acting in the tectum. Conversely, it is possible that the SINs have additional functions in filtering incoming visual inputs.

THE SOMs

A key feature of visual cortical neurons is their selective tuning to both the size and orientation of objects in the visual field (Angelucci and Bressloff, 2006). Adesnik et al. (2012) investigated the contribution of surround suppression to size tuning in the mouse visual cortex (V1). In awake behaving mice, drifting

gratings were presented in a circular aperture of increasing size to determine the preferred stimulus size for pyramidal cells (PCs) and two populations of inhibitory neurons in layer II/III in V1. PC size tuning was determined through extracellular recordings of single units, while loose patch recordings were employed to determine size tuning in parvalbumin-expressing neurons (PVs) and somatostatin-expressing neurons (SOMs). PCs displayed preferred tuning to relatively small apertures (around 22°), while PVs and SOMs preferred tuning was for larger apertures (**Figures 1B,B′**). Both PCs and PVs exhibited surround suppression (as the stimulus size increased outside the RF of the neuron, firing rate decreased). Significantly, in addition to having larger RFs than PCs and PVs, the SOMs exhibited no surround suppression.

How are inputs to SOMs structured to generate large RFs lacking surround suppression? Adesnik et al. (2012) determined that SOMs sum excitation across visual space through lateral excitation from PCs in layer II/III. While recording from SOMs and directly activating layer IV PCs expressing channelrhodopsin (ChR2) little excitation in the SOMs was observed. In contrast, ChR2-mediated activation of layer II/III PCs resulted in large increases in excitatory drive to SOMs. By simultaneously recording from PCs in layer II/III, the authors were able to make comparisons between SOM activity and PC activity while stimulating each layer. Unlike the lateral excitatory drive onto SOMs, PVs appeared to receive the majority of their excitatory input from layer IV PCs.

In electrophysiology experiments performed while expressing halorhodopsin (NpHR) in SOMs and ChR2 in layer II/III PCs, the authors confirmed that layer II/III PC activation resulted in increased excitatory input and spiking in SOMs with the opposite effect on non-ChR2 expressing PCs – increased inhibitory postsynaptic currents (IPSCs) and decreased spiking. When SOMs were silenced with NpHR activation during these dual recordings from SOMs and neighboring PCs, SOM spiking was reduced and inhibition of PCs was lost (measured by decreased IPSCs). These experiments suggested that SOMs are responsible for the PC inhibition observed during the presentation of a large visual stimulus (**Figure 1B′**). The results of Adesnik et al. (2012) are similar to the findings of Del Bene et al. (2010) in demonstrating that (1) there is an anatomically identifiable microcircuit for size filtering and (2) size filtering is not solely transmitted by input from earlier stages of visual processing, but can be computed directly in visual brain regions.

SOMe SINsible OPEN QUESTIONS

Some details of SIN and SOM circuitry remain obscure. How are inputs to SOMs and SINs organized? Adesnik et al. (2012) demonstrate direct synaptic connections between SOMs and neighboring PCs in layer II/III, yet the lateral extent of SOM inhibition across layer II/III is unknown. For example, how many PCs send input to a single SOM? Similarly, how many PCs receive inhibition from a single SOM? It is also unclear how SOM inhibition shapes the output of the system. Are RFs in layer V neurons (the site of projection neurons to other brain regions) also changed when SOMs are silenced? SINs have a direct effect on size-dependent behavioral responses in the zebrafish. How might eliminating SOMs affect visually mediated behaviors in the mouse?

The local circuitry of the SINs in the fish tectum is even less well understood. To what cells are the SINs synaptically connected? Taking a note from the SOMs, one might predict that SINs receive input from PVNs mapping adjacent areas of visual space and provide feedback inhibition onto PVNs to modulate PVN firing for a maximum response to small objects. More likely, SINs receive direct retinal input and provide feedforward inhibition to PVNs, restricting their size tuning (see **Figure 1A**). Detailed electrophysiology experiments as performed by Adesnik et al. (2012), are needed in this system.

LOOKING FORWARD

One interesting question is how other inhibitory populations contribute to shape size tuning. Might multiple filters for small-sized objects exist? Or filters for large or medium-sized objects? Additional interneuron populations have been described in the visual cortex and tectum (e.g., Kerlin et al., 2010; Robles et al., 2011). It will also be worthwhile to explore if SIN and SOM mechanisms for size filtering are employed by other visual brain areas. In the mouse, retinal input is not exclusively channeled to the cortex. Substantial retinal input arrives in the superior colliculus (SC). Evidence of surround suppression has been reported in the superficial layers of mouse SC, where the majority of cells are optimally tuned to small objects (6°–10°) and display decreased responsiveness at larger stimulus sizes (Wang et al., 2010). Further characterization of GABAergic populations in the mouse SC will be necessary to determine if SIN/SOM-like mechanisms are at work in this visual brain region.

One behavioral implication of size-filtering circuitry is the ability to recognize edible objects during prey capture. This behavior is impaired when SIN function is perturbed (Del Bene et al., 2010). Predator avoidance, the recognition and avoidance of large objects, is equally important for an organism's survival. Avoidance behavior in many species can be elicited through the presentation of a looming stimulus, a two-dimensional representation of an object on a collision course. For looming objects it is not just the size of the object that is important rather its rate of expansion, taking into account the size and speed of the approaching object (Fotowat and Gabbiani, 2011). Loom-sensitive neurons have been detected in the mouse retina (Münch et al., 2009). Might the SINs or SOMs be part of a loom-detecting circuit? Additional studies to probe speed and size tuning of SINs and SOMs may provide valuable insights into their potential role in avoidance behaviors.

Despite differences in methodology and model organisms, a unifying principle emerges from these studies: size tuning relies on local inhibition to reshape RFs and filter out wide-field visual inputs. While the tectum is homologous to the mammalian SC it is striking that mechanisms for size filtering are similar between species and across visual brain areas. It is therefore tempting to extend these findings to other sensory systems where the role of local inhibition may act to refine and reshape RFs. This may be necessary to ensure the fidelity of synaptic transmission, increase single-to-noise ratios or allow for greater flexibility in extracting relevant information from raw sensory input. The results in mouse visual cortex demonstrate how local inhibition can shape RFs in visual brain regions. The zebrafish tectum findings provide

a clear link between inhibition-modulated size tuning in visual brain regions and behavior that relies on size discrimination. This work provides one final lesson – that these small vertebrates have a lot to tell us about neural circuits and perception.

ACKNOWLEDGMENTS

The authors would like to thank members of the Baier Lab for critical comments and review. This work was supported by an NSF graduate research fellowship (Alison J. Barker) and the Max Planck Society.

REFERENCES

Adesnik, H., Bruns, W., Taniguchi, H., Huang, Z. J., and Scanziani, M. (2012). A neural circuit for spatial summation in visual cortex. *Nature* 490, 226–231.

Angelucci, A., and Bressloff, P. C. (2006). Contribution of feedforward, lateral and feedback connections to the classical receptive field center and extra-classical receptive field surround of primate V1 neurons. *Prog. Brain Res.* 154, 93–120.

Del Bene, F., Wyart, C., Robles, E., Tran, A., Looger, L., Scott, E. K., et al. (2010). Filtering of visual information in the tectum by an identified neural circuit. *Science* 330, 669–673.

Fotowat, H., and Gabbiani, F. (2011). Collision detection as a model for sensory-motor integration. *Annu. Rev. Neurosci.* 34, 1–19.

Gahtan, E., Tanger, P., and Baier, H. (2005). Visual prey capture in larval zebrafish is controlled by identified reticulospinal neurons downstream of the tectum. *J. Neurosci.* 25, 9294–9303.

Kerlin, A. M., Andermann, M. L., Berezovskii, V. K., and Reid, R. C. (2010). Broadly tuned response properties of diverse inhibitory neuron subtypes in mouse visual cortex. *Neuron* 67, 858–871.

Münch, T. A., da Silveira, R. A., Siegert, S., Viney, T. J., Awatramani, G. B., and Roska, B. (2009). Approach sensitivity in the retina processed by a multifunctional neural circuit. *Nat. Neurosci.* 12, 1308–1316.

Muto, A., Ohkura, M., Abe, G., Nakai, J., and Kawakami, K. (2013). Real-time visualization of neuronal activity during perception. *Curr. Biol.* 23, 307–311.

Nevin, L. M., Robles, E., Baier, H., and Scott, E. K. (2010). Focusing on optic tectum circuitry through the lens of genetics. *BMC Biol.* 8:126. doi: 10.1186/1741-7007-8-126

Niell, C. M., and Smith, S. J. (2005). Functional imaging reveals rapid development of visual response properties in the zebrafish tectum. *Neuron* 45, 941–951.

Robles, E., Smith, S. J., and Baier, H. (2011). Characterization of genetically targeted neuron types in the zebrafish optic tectum. *Front. Neural Circuits* 5:1. doi: 10.3389/fncir.2011.00001

Robles, E., Filosa, A., and Baier, H. (2013). Precise lamination of retinal axons generates multiple parallel input pathways in the tectum. *J. Neurosci.* 33, 5027–5039.

Roeser, T., and Baier, H. (2003). Visuomotor behaviors in larval zebrafish after GFP-guided laser ablation of the optic tectum. *J. Neurosci.* 23, 3726–3734.

Sajovic, P., and Levinthal, C. (1982a). Visual cells of zebrafish optic tectum: mapping with small spots. *Neuroscience* 7, 2407–2426.

Sajovic, P., and Levinthal, C. (1982b). Visual response properties of zebrafish tectal cells. *Neuroscience* 7, 2427–2440.

Wang, L., Sarnaik, R., Rangarajan, K., Liu, X., and Cang, J. (2010). Visual receptive field properties of neurons in the superficial superior colliculus of the mouse. *J. Neurosci.* 30, 16573–16584.

Conflict of Interest Statement: The authors declare that the research was conducted in the absence of any commercial or financial relationships that could be construed as a potential conflict of interest.

Received: 14 February 2013; accepted: 21 April 2013; published online: 10 May 2013.

Citation: Barker AJ and Baier H (2013) SINs and SOMs: neural microcircuits for size tuning in the zebrafish and mouse visual pathway. Front. Neural Circuits 7:89. doi: 10.3389/fncir.2013.00089

frontiers in
NEURAL CIRCUITS

MINI REVIEW ARTICLE
published: 18 June 2013
doi: 10.3389/fncir.2013.00111

Direction selectivity in the visual system of the zebrafish larva

Christoph Gebhardt*[1,2,3], *Herwig Baier*[4] *and Filippo Del Bene*[1,2,3]

[1] *Institut Curie, Centre de Recherche, Paris, France*
[2] *CNRS UMR 3215, Paris, France*
[3] *INSERM U934, Paris, France*
[4] *Department Genes – Circuits – Behavior, Max Planck Institute of Neurobiology, Martinsried, Germany*

Edited by:
German Sumbre, Ecole Normale Superieure, France

Reviewed by:
Carlos D. Aizenman, Brown University, USA
Klaus-Peter Hoffmann, University Bochum, Germany

***Correspondence:**
Filippo Del Bene, Institut Curie, Centre de Recherche, Batiment. BDD, 11-13 Rue Pierre et Marie Curie, 75005 Paris, France
e-mail: filippo.del-bene@curie.fr

Neural circuits in the vertebrate retina extract the direction of object motion from visual scenes and convey this information to sensory brain areas, including the optic tectum. It is unclear how computational layers beyond the retina process directional inputs. Recent developmental and functional studies in the zebrafish larva, using minimally invasive optical imaging techniques, indicate that direction selectivity might be a genetically hardwired property of the zebrafish brain. Axons from specific direction-selective (DS) retinal ganglion cells appear to converge on distinct laminae in the superficial tectal neuropil where they serve as inputs to DS postsynaptic neurons of matching specificity. In addition, inhibitory recurrent circuits in the tectum might strengthen the DS response of tectal output neurons. Here we review these recent findings and discuss some controversies with a particular focus on the zebrafish tectum's role in extracting directional features from moving visual scenes.

Keywords: visual system, direction selectivity, zebrafish, optic tectum, neural circuits

INTRODUCTION

Extracting motion information from a visual scene is a key ability of most visual systems throughout the animal kingdom. Moving objects change their position over time in reference to the animal and thus project onto the retina as both spatial and temporal patterns of varying light intensities. With regard to motion detection, an important parameter that can be extracted from these patterns is the direction of a moving stimulus. This information is of vital importance for specific behaviors such as prey capture, collision avoidance, or escape from a predator.

Detailed information has been gathered in insects and mammals about motion processing, but studies were mostly restricted to the computations performed by the sensory surface, i.e., small retinal circuits (Elstrott and Feller, 2009; Borst and Euler, 2011; Wei and Feller, 2011). How direction-selective (DS) is attained and processed by higher brain areas is less evident. Studies addressing this question in the mammalian visual cortex have often investigated either single neurons by electrophysiology or columns of many hundred or thousand of cells by optical imaging, thus lacking the resolution necessary to ask circuit-level questions (Bonhoeffer and Grinvald, 1991; Chapman et al., 1996; Priebe et al., 2010).

The optic tectum of larval zebrafish is an excellent brain structure to study motion processing at a higher circuit-level. The tectum is the main retinorecipient brain region and homologous to the superior colliculus in mammals. Sitting at the surface of the brain, it is easily accessible to a wide variety of techniques, including electrophysiology, laser ablations, optogenetics, and optical imaging. In addition to receiving a majority of retinal afferents, the tectum is an integrator of sensory information from multiple modalities (Meek, 1983; Vanegas and Ito, 1983). Main areas of the tectum can be histologically distinguished. The *stratum periventriculare* (SPV) contains the cell bodies of most tectal neurons (periventricular neurons, PVNs) whereas the synaptic neuropil area contains the PVNs' dendrites and axons as well as the axons of retinal ganglion cells (RGCs). The tectal neuropil is a precisely laminated structure within which the RGC axons mostly target the superficial layers (Xiao et al., 2005): the *stratum opticum* (SO), right beneath the basement membrane, and the *stratum fibrosum et griseum superficiale* (SFGS). Classical Golgi studies in adult goldfish and genetic single-cell labeling in larval zebrafish revealed that the PVNs have a single dendritic shaft that extends into the tectal neuropil, often crossing multiple layers (Vanegas et al., 1974; Meek and Schellart, 1978; Scott and Baier, 2009; Nevin et al., 2010; Robles et al., 2011).

Importantly, zebrafish are also genetically accessible rendering them well suited for functional studies of the visual system that require targeting of protein-based indicators to genetically identified subpopulations of neurons. This opens up the exciting possibility of studying DS processing across specific neuronal populations, often with single-cell resolution.

DEVELOPMENT OF DS IN THE OPTIC TECTUM APPEARS TO BE GENETICALLY HARDWIRED

The anatomical and morphological development of the zebrafish larval visual system has been investigated in great detail (e.g., Stuermer, 1988). Between 34 and 48 hours post fertilization (hpf) retinal axons leave the retina and start invading the tectal neuropil. By 72 hpf, retinal axons have sparsely innervated the entire tectum and begin to form terminations at their topographically correct targets. At around the same time, the lens has developed to produce a focused image within the photoreceptor layer of the retina

(Easter and Nicola, 1996). After tectal coverage is achieved, dendritic arbors undergo remodeling until a relatively stable state is reached around 7 days post fertilization (dpf). The laminar development of retinotectal wiring seems to be largely independent of externally evoked visual activity. Activity-dependent mechanisms, however, influence the refinement of the RGC arbors that form the visuotopic map (Stuermer et al., 1990; Gnuegge et al., 2001; Hua et al., 2005; Smear et al., 2007; Nevin et al., 2008; Fredj et al., 2010).

Extraction of directional information from a visual scene requires that DS neurons exhibit an asymmetric response to visual stimuli that move in the preferred vs. the opposite (null) direction. This functional asymmetry must ultimately be a consequence of an asymmetry in wiring, regulation of synaptic strengths, or dendritic conductance. How does this asymmetry come about during development? Several possibilities have been proposed. For one, it could be that this asymmetry of DS circuits is genetically hardwired, for instance by cell-surface molecular cues that act upon dendrite or synapse distribution and are expressed very early in visual system development. It is also possible that DS circuits show initially non-asymmetric responses and are subsequently biased in one direction by activity-dependent mechanisms. Of course, genetic hardwiring and activity-based mechanisms might also act in concert to shape the final DS response of neurons of the visual system.

In a landmark study, Niell and Smith (2005) used *in vivo* Ca^{2+} imaging with the synthetic Ca^{2+} indicator OGB1-AM for an initial functional description of the entire tectal cell population during development. Among other visual parameters, the authors also examined DS in the tectum. They reported that a large proportion of tectal cells were already DS as early as 72 hpf and DS reached nearly mature levels after 78 hpf. This is perhaps surprising considering that during that time window the very first retinal axons have barely reached their termination zones in the tectum and retinotectal circuits are still undergoing thorough refinement. Furthermore, zebrafish larvae that were reared completely in the dark showed normal DS responses, which were indistinguishable from larvae reared under default light–dark cycle conditions.

The latter finding is not consistent with a study in *Xenopus* tadpoles (Engert et al., 2002). This paper reported that DS of tectal cells was not apparent at early developmental stages but extensive training with a moving stimulus was able to induce DS responses in a few recorded tectal neurons, suggesting an experience-dependent mode of DS development. This discrepancy between zebrafish and *Xenopus* could be due to a true species difference as others (Podgorski et al., 2012) have also found DS plasticity after visual training in tadpoles. However, it might also be possible that in tadpoles, DS of tectal cells is present at early stages and repeated training generated short-lasting single neuron and/or network connectivity changes that obscured the initially hardwired tuning of the recorded tectal cells.

Niell and Smith's findings were, however, largely confirmed and extended, by a later study (Ramdya and Engert, 2008). Normally, retinal projections to the tectum are completely crossed, i.e., tectal neurons are monocular. By surgically removing a single tectal lobe the authors partially re-routed the retinal projection to the ipsilateral tectum, thereby generating a few binocularly innervated tectal cells (i.e., neurons that responded to inputs from both eyes). They found that these binocular cells showed the same DS response to moving stimuli when these were presented to either eye. Furthermore, depriving the animals from any externally evoked visual activity by rearing them in the dark, showed again no difference in the development of the observed binocular DS compared to light-reared larvae. This is in agreement with the experience-independent DS development observed earlier by Niell and Smith (2005). Furthermore, since it is also unlikely that correlated intrinsic activities between the two eyes occur, this might indicate that the development of direction selectivity in zebrafish is, in addition to being experience-independent, also independent of spontaneously generated retinal waves (Wong et al., 1993).

Taken together the available evidence suggests that, at least in zebrafish, direction selectivity is established at the earliest stage measurable and develops independently of activity in the visual system.

TECTUM-INTRINSIC COMPUTATION OF DIRECTION SELECTIVITY

Functional models of DS differ mainly in how excitatory or inhibitory input currents are tuned (i.e., to the preferred vs. the null-direction) and then integrated in time to finally give rise to tectal DS outputs. In the zebrafish, there is evidence for two different DS mechanisms being implemented. For one, DS could be predominantly computed by retinal circuits, which then would drive postsynaptic DS neurons directly via direction-tuned excitatory inputs. Alternatively, excitatory retinal input might show rather weak DS and subsequent tectal recurrent inhibition, tuned to the null-direction, might shape the final PVN response in the preferred direction of the stimulus. Both of these mechanisms are not mutually exclusive and might be implemented in a complementary fashion in retina and tectum (**Figure 1**).

In the above-mentioned study, Ramdya and Engert (2008) found evidence for a null-inhibition mechanism in the zebrafish tectum. By using the surgically induced binocular retinotectal circuit they addressed if direction selectivity is computed in the retina and then projected into pre-specified tectal modules or if, alternatively, tectal inhibitory circuits perform this computation. Two lines of evidence suggested that the latter mechanism is at work. First, the authors performed an experiment in which they displayed a visual stimulus consisting of two stationary spots separated in time and jumping between different visual field positions of one eye. These two stationary spots are seen as apparent motion and elicit a DS response in a subset of the recorded tectal neurons. Showing these two spots with a slight delay to the left and right eye of fish with binocular input to the tectum, should not elicit any DS response if direction selectivity relies purely on retinal computation. However, the authors observed that some binocular tectal cells were showing a response to an apparent-motion stimulus that was comparable to the stimulus applied to the contralateral eye alone. Second, a pharmacological block of tectal inhibition by injection of bicuculline in the tectum led to a loss of DS in most of the tectal neurons under normal conditions. This was due to the response to the null-direction being strongly increased after drug injection.

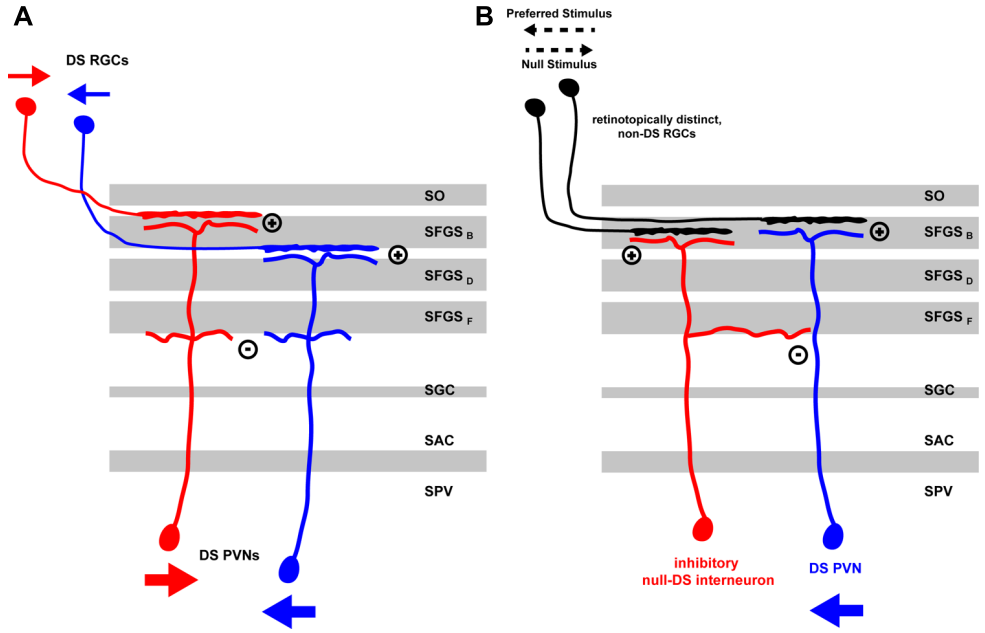

FIGURE 1 | Mechanisms for direction selectivity computation in the zebrafish larva tectum. (A) Direction information from a moving stimulus is extracted by retinal circuits and transferred by RGC axons, which are specific for the stimulus direction (small red or blue arrows), to distinct laminae in the tectal neuropil. The retinal arbors are then targeted by the distal arbors of PVNs in their respective laminae thus acquiring direction specificity themselves. Heterotypic connections between proximal PVN arbors might lead to reciprocal inhibition thus sharpening DS PVN response to a moving stimulus in a specific direction (large red or blue arrows). **(B)** A DS PVN (blue) receives excitatory inputs from one or more non-DS RGCs in the tectal neuropil. In addition, it receives intratectal inhibitory input from an interneuron (red) that is retinotopically positioned on the side of the DS PVN facing the preferred stimulus direction. Thus, a moving stimulus in the preferred direction (black pointed arrow) elicits excitatory currents in the retina that excite DS PVNs. Currents from the inhibitory interneurons arrive later and do not interfere with the PVNs activity state. Moving stimuli in the null-direction, however, elicit inhibitory currents in the tectal interneuron, which arrive first at the DS PVN thus blocking any subsequent excitatory currents the DS PVN might receive from the retina. DS, direction-selective; RGC, retinal ganglion cell; PVN, periventricular neuron; SAC, stratum album centrale; SFGS (B-F), sublaminae of stratum fibrosum et griseum superficiale; SGC, stratum griseum centrale; SO, stratum opticum; SPV, stratum periventriculare.

Taken together, these results provided evidence for a tectal DS computing mechanism involving strong recurrent inhibition tuned to the null-direction rather than direct retinal excitatory currents. It is unclear, however, if the artificially altered circuit is indeed indicative of how direction selectivity is computed under normal, unaltered conditions or if the apparent-motion stimulus is at all suited for investigating feature extraction from a moving visual scene. For instance, if the retinal inputs to the recorded tectal cells are already DS, then activation by the apparent-motion stimulus, even though it may not be the optimal stimulus, will elicit a DS response in the postsynaptic cell. This response can look deceptively similar to a tectum-intrinsic, *de novo* DS computation.

In a follow-up paper, Grama and Engert (2012) analyzed the contribution of excitatory and inhibitory currents to tectal DS in more detail. By patching a random set of tectal neurons in the SPV, they found that excitatory input currents, supposedly originating from the retina, were correlated but not tuned to the direction of the stimulus motion, as measured by counting the spikes evoked by a moving bar. However, inhibitory currents, presumably coming from tectal inhibitory interneurons, were inversely correlated with the direction of motion, i.e., they were biased for the null-direction. Furthermore, the authors observed latencies in the millisecond range between excitatory and inhibitory currents. Inhibitory currents preceded the excitatory ones in the null-direction (median = 39 ms) and vice versa in the preferred direction (median = 157 ms). Based on this evidence, the authors suggested a model in which tectal DS responses are computed from non-DS retinal inputs by tectal recurrent inhibition. For such a mechanism to work, they postulated the existence of a special type of tectal interneuron, which, similar to the starburst amacrine cell in the retina (Fried et al., 2002), is responding to moving stimuli in the null-direction and is asymmetrically connected to DS tectal output neurons (**Figure 1**). This interneuron type should be positioned on the side of the DS cell that represents the preferred direction along the corresponding axis of the retinotopic map. In this configuration, stimuli coming from the null-direction will selectively suppress the response of the output cell. While plausible, there is currently no evidence for the existence of such an asymmetrically organized circuit in the zebrafish tectum.

TECTAL PROCESSING OF DIRECTION-SELECTIVE RETINAL INPUTS

Differing from an exclusively tectum-intrinsic mechanism for direction computation, two recent studies showed that RGC inputs are already tuned to stimulus direction when they reach the tectum. In the first study, Meyer and colleagues expressed the genetically encoded Ca^{2+}indicator SypGCaMP3, driven by

the *isl2b* promoter, in almost all retinal synapses terminating in the retinorecipient layers of the tectum (Nikolaou et al., 2012). By statistical analysis of activity distribution maps from stacks of several animals over several experimental trials, they found three major RGC DS input clusters in the tectal neuropil, one caudal-to-rostral and two different rostral-to-caudal directed clusters with a down-up or up-down DS component respectively. These DS clusters match the response tuning profiles of the previously reported DS-RGCs in goldfish (Maximov et al., 2005). In the tectum, these inputs were segregated superficially in two discrete layers of the SFGS. Caudal-to-rostral-tuned inputs were distributed more superficially in the tectal neuropil than inputs of the other directions. Notably, these layers are preferentially innervated by RGCs that have bistratified dendrites in the ON and OFF sublayers of the inner plexiform layer of the retina (Robles et al., 2013). RGCs of this class have been shown to be DS in several other vertebrates, including birds, mammals, and fish.

Furthermore, Nikolaou et al. (2012) reported that retinal synaptic inputs responding to caudal-to-rostral motion predominated quantitatively over those responding to rostral-to-caudal motion, which is consistent with previous studies (Maximov et al., 2005; Niell and Smith, 2005). Moreover, the authors found two clusters of orientation-selective (OS) presynaptic inputs (horizontal and vertical motion in both directions) that spanned several laminae in the middle layers of the neuropil and were well separated from DS inputs in the superficial neuropil. Surprisingly, they observed also a retinotopic bias of the observed DS and OS clusters. The DS inputs were mostly confined to the posterior half of the tectum while the two OS clusters were distributed anteriorly and posteriorly, respectively. It is currently unclear if these distributions reflect the existence of topographically restricted RGC populations, retinotopic differences in the retinal circuits or presynaptic modulation within the tectum. Considering that these cumulative imaging data were highly processed and thresholded, it is also possible that synapse density of DS cells and thus SypGCaMP3 expression accounted for the observed topographic differences.

The most comprehensive study of DS in the zebrafish retinotectal system so far was recently presented by Bollmann and colleagues (Gabriel et al., 2012). From an enhancer-trap screen, they identified two Gal4-VP16 transgenic lines that labeled subsets of DS interneurons in the tectum. *Tg(Oh:G3)* drives expression of UAS (upstream activation sequence)-linked reporter genes mostly in rostral-to-caudal-tuned cells, whereas *Tg(Oh:G4)* labels caudal-to-rostral-tuned cells. In addition to differences in DS, these two subsets of tectal neurons also differ morphologically. While both are bistratified, they have their distal dendritic arbor in different layers of the tectal neuropil.

Similar to Nikolaou et al. (2012), Gabriel et al. (2012) reported three main types of presynaptic DS inputs (one caudal-to-rostral cluster and two rostral-to-caudal ones) and observed that each targets one specific lamina in the tectal neuropil. In a series of elegant experiments, Gabriel et al. (2012) showed that functionally identified postsynaptic neurons had their dendritic arbors specifically in the very same laminae in the neuropil as the matching DS RGC inputs, lending further weight to their mapping of DS retinal inputs.

While the two studies by Nikolaou et al. (2012) and Gabriel et al. (2012) converge on the same broad conclusions they differ in important details, which appear irreconcilable at first glance. Gabriel et al. (2012) observed one rostral-to-caudal-tuned cluster (with both up-down and down-up DS component) that was situated more superficially in the tectal neuropil than the caudal-to-rostral-tuned cluster. This is the inverse of what Nikolaou and colleagues reported. How can this apparent discrepancy be explained? The precise layout of the laminar distribution of retinal inputs in the tectal neuropil might offer a solution. In a parallel set of studies, utilizing brain bow labeling of RGC axons, Robles et al. (2013) reported that the zebrafish retinotectal neuropil is composed of at least ten laminae. The SO is subdivided into two layers, SO1 and SO2, while the SFGS contains six distinct layers, SFGS1 through SFGS6. Each of the retinotectal layers harbors a complete retinotopic map and is innervated by a distinct combination of RGC types (Robles et al., 2013). In this new scheme, Gabriel et al.'s DS inputs might, for instance, be localized to SO2, SFGS1 and maybe SFGS2, while Nikolaou et al.'s might be in SFGS1 and SFGS2. The two studies would then unequivocally agree that one of the ten layers, most likely SFGS1, is sensitive to caudal-to-rostral direction.

The reason for the differences in both studies could be that weak rostral-to-caudal oriented signals (i.e. rostral-to-caudal signals found in SO2 and SFGS2, respectively) might have been difficult to record: In order to isolate the presynaptic activity in the tectum, Gabriel et al. (2012) used pan-neuronal GCaMP3-expression and subsequent pharmacological blockage of glutamatergic transmission in tectal cells. This approach could have lead to a high intensity background impeding the detection of weak clusters. By contrast, the genetic targeting and/or expression levels of SypGCaMP3 in the study by Nikolaou et al. (2012) might not have been sufficient to reveal all existing retinal laminae. Furthermore, the threshold for identifying DS input signals were set differently in the two studies. This choice might also have contributed to the observed differences.

In summary, a scheme that assumes the existence of three presynaptic layers in the superficial third of the neuropil with alternating DS, a caudal-to-rostral lamina sandwiched between two rostral-to-caudal oriented ones (possibly each of the latter containing two distinct sub-clusters with a down-up or up-down DS component, respectively), might explain the available data.

Furthermore, Gabriel et al. (2012) reported that excitatory inputs, likely from RGCs, determine the DSof at least some tectal cell types. This is in agreement with Nikolaou et al. (2012), but appears to contradict the conclusions of Grama and Engert (2012) who did not find DS-tuned excitatory inputs but emphasized rather the importance of inversely DS-tuned inhibitory intra-tectal currents. Gabriel et al. (2012) also report that the two different types of bistratified DS tectal neurons are GABAergic, inhibitory interneurons. Thus, they suggest that a feed-forward, null-direction inhibition via the proximal dendritic arbors of the cells might serve as a means to fine-tune the tectum's output. It is still possible that some types of tectal cells are mainly driven by DS excitatory input, whereas others are controlled by DS-tuned inhibitory inputs.

CONCLUSION AND DIRECTIONS FOR FUTURE RESEARCH

DS neurons are found in several regions along the visual pathway, including retina, tectum, and cortex. It is important to understand how neurons acquire DS characteristics at each of these stages. Studies in zebrafish have revealed that DS is hardwired and can develop independently of patterns of activity. In the tectum, DS retinal inputs terminate in the tectal neuropil in specific laminae, where they form connections with the lamina-restricted dendrites of tectal interneurons. This feed-forward mode of DS wiring is reminiscent of the so-called "labeled lines" that are found in other sensory systems (Kauer and White, 2001). Evidence for the contribution of tectal recurrent connections, especially inhibitory ones, is less clear. If it exists, it might contribute to sharpening the response of DS output neurons.

In conclusion, it seems to us that, for a complete understanding of DS computation, additional genetic markers for functionally identified types of DS neurons are needed, not only in the tectum but also in the retina (Huberman et al., 2009; Gabriel et al., 2012). It will be productive to trace the connections of the different types of DS-RGCs from the retina to the tectal layers and identify their postsynaptic partners. Future research should also elucidate how DS computation is used in behavioral contexts, i.e., how DS information is transferred to motor centers and used to generate oriented behavior toward prey or away from predators. The zebrafish tectum, as a prominent center for sensorimotor transformation in an optically and genetically accessible organism, will be an excellent place to investigate these fundamental questions of systems neuroscience.

ACKNOWLEDGMENTS

We like to thank Johann Bollmann, Thomas Auer and Alessandro Filosa for their comments on the manuscript. Michael Orger provided valuable insight and advice on imaging.

REFERENCES

Bonhoeffer, T., and Grinvald, A. (1991). Iso-orientation domains in cat visual cortex are arranged in pinwheel-like patterns. *Nature* 353, 429–431. doi: 10.1038/353429a0

Borst, A., and Euler, T. (2011). Seeing things in motion: models, circuits, and mechanisms. *Neuron* 71, 974–994. doi: 10.1016/j.neuron.2011.08.031

Chapman, B., Stryker, M. P., and Bonhoeffer, T. (1996). Development of orientation preference maps in ferret primary visual cortex. *J. Neurosci.* 16, 6443–6453.

Easter, J., and Nicola, G. N. (1996). The development of vision in the zebrafish (*Danio rerio*). *Dev. Biol.* 180, 646–663. doi: 10.1006/dbio.1996.0335

Elstrott, J., and Feller, M. B. (2009). Vision and the establishment of direction-selectivity: a tale of two circuits. *Curr. Opin. Neurobiol.* 19, 293–297. doi: 10.1016/j.conb.2009.03.004

Engert, F., Tao, H. W., Zhang, L. I., and Poo, M. (2002). Moving visual stimuli rapidly induce direction sensitivity of developing tectal neurons. *Nature* 419, 470–475. doi: 10.1038/nature00988

Fredj, N. B., Hammond, S., Otsuna, H., Chien, C.-B., Burrone, J., and Meyer, M. P. (2010). Synaptic activity and activity-dependent competition regulates axon arbor maturation, growth arrest, and territory in the retinotectal projection. *J. Neurosci.* 30, 10939–10951. doi: 10.1523/JNEUROSCI.1556-10.2010

Fried, S. I., Münch, T. A., and Werblin, F. S. (2002). Mechanisms and circuitry underlying directional selectivity in the retina. *Nature* 420, 411–414. doi: 10.1038/nature01179

Gabriel, J. P., Trivedi, C. A., Maurer, C. M., Ryu, S., and Bollmann, J. H. (2012). Layer-specific targeting of direction-selective neurons in the zebrafish optic tectum. *Neuron* 76, 1147–1160. doi: 10.1016/j.neuron.2012.12.003

Gnuegge, L., Schmid, S., and Neuhauss, S. C. F. (2001). Analysis of the activity-deprived zebrafish mutant macho reveals an essential requirement of neuronal activity for the development of a fine-grained visuotopic map. *J. Neurosci.* 21, 3542–3548.

Grama, A., and Engert, F. (2012). Direction selectivity in the larval zebrafish tectum is mediated by asymmetric inhibition. *Front. Neural Circuits* 6:59. doi: 10.3389/fncir.2012.00059

Hua, J. Y., Smear, M. C., Baier, H., and Smith, S. J. (2005). Regulation of axon growth in vivo by activity-based competition. *Nature* 434, 1022–1026. doi: 10.1038/nature03409

Huberman, A. D., Wei, W., Elstrott, J., Stafford, B. K., Feller, M. B., and Barres, B. A. (2009). Genetic identification of an On-Off direction- selective retinal ganglion cell subtype reveals a layer-specific subcortical map of posterior motion. *Neuron* 62, 327–334. doi: 10.1016/j.neuron.2009.04.014

Kauer, J. S., and White, J. (2001). Imaging and coding in the olfactory system. *Ann. Rev. Neurosci.* 24, 963–979. doi: 10.1146/annurev.neuro.24.1.963

Maximov, V., Maximova, E., and Maximov, P. (2005). Direction selectivity in the goldfish tectum revisited. *Ann. N. Y. Acad. Sci.* 1048, 198–205. doi: 10.1196/annals.1342.018

Meek, J. (1983). Functional anatomy of the tectum mesencephali of the goldfish. An explorative analysis of the functional implications of the laminar structural organization of the tectum. *Brain Res.* 287, 247–297.

Meek, J., and Schellart, N. A. (1978). A Golgi study of goldfish optic tectum. *J. Comp. Neurol.* 182, 89–122. doi: 10.1002/cne.901820107

Nevin, L. M., Robles, E., Baier, H., and Scott, E. K. (2010). Focusing on optic tectum circuitry through the lens of genetics. *BMC Biol.* 8:126. doi: 10.1186/1741-7007-8-126

Nevin, L. M., Taylor, M. R., and Baier, H. (2008). Hardwiring of fine synaptic layers in the zebrafish visual pathway. *Neural Dev.* 3, 36. doi: 10.1186/1749-8104-3-36

Niell, C. M., and Smith, S. J. (2005). Functional imaging reveals rapid development of visual response properties in the zebrafish tectum. *Neuron* 45, 941–951. doi: 10.1016/j.neuron.2005.01.047

Nikolaou, N., Lowe, A. S., Walker, A. S., Abbas, F., Hunter, P. R., Thompson, I. D., et al. (2012). Parametric functional maps of visual inputs to the tectum. *Neuron* 76, 317–324. doi: 10.1016/j.neuron.2012.08.040

Podgorski, K., Dunfield, D., and Haas, K. (2012). Functional clustering drives encoding improvement in a developing brain network during awake visual learning. *PLoS Biol.* 10:e1001236. doi: 10.1371/journal.pbio.1001236

Priebe, N. J., Lampl, I., and Ferster, D. (2010). Mechanisms of direction selectivity in cat primary visual cortex as revealed by visual adaptation. *J. Neurophysiol.* 104, 2615–2623. doi: 10.1152/jn.00241.2010

Ramdya, P., and Engert, F. (2008). Emergence of binocular functional properties in a monocular neural circuit. *Nat. Neurosci.* 11, 1083–1090. doi: 10.1038/nn.2166

Robles, E., Filosa, A., and Baier, H. (2013). Precise lamination of retinal axons generates multiple parallel input pathways in the tectum. *J. Neurosci.* 33, 5027–5039. doi: 10.1523/JNEUROSCI.4990-12.2013

Robles, E., Smith, S. J., and Baier, H. (2011). Characterization of genetically targeted neuron types in the zebrafish optic tectum. *Front. Neural Circuits* 5:1. doi: 10.3389/fncir.2011.00001

Scott, E. K., and Baier, H. (2009). The cellular architecture of the larval zebrafish tectum, as revealed by Gal4 enhancer trap lines. *Front. Neural Circuits* 3:13. doi: 10.3389/neuro.04.013.2009

Smear, M. C., Tao, H. W., Staub, W., Orger, M. B., Gosse, N. J., Liu, Y., et al. (2007). Vesicular glutamate transport at a central synapse limits the acuity of visual perception in zebrafish. *Neuron* 53, 65–77. doi: 10.1016/j.neuron.2006.12.013

Stuermer, C. A. (1988). Retinotopic organization of the developing retinotectal projection in the zebrafish embryo. *J. Neurosci.* 8, 4513–4530.

Stuermer, C. A., Rohrer, B., and Münz, H. (1990). Development of the retinotectal projection in zebrafish embryos under TTX-induced neural-impulse blockade. *J. Neurosci.* 10, 3615–3626.

Vanegas, H., and Ito, H. (1983). Morphological aspects of the teleostean visual system: a review. *Brain Res.* 287, 117–137. doi: 10.1016/0165-0173(83)90036-X

Vanegas, H., Laufer, M., and Amat, J. (1974). The optic tectum of a perciform teleost I. General configuration and cytoarchitecture. *J.*

Comp. Neurol. 154, 43–60. doi: 10.1002/cne.901540104

Wei, W., and Feller, M. B. (2011). Organization and development of direction-selective circuits in the retina. *Trends Neurosci.* 34, 638–645. doi: 10.1016/j.tins.2011.08.002

Wong, R. O. L., Meister, M., and Shatz, C. J. (1993). Transient period of correlated bursting activity during development of the mammalian retina. *Neuron* 11, 923–938. doi: 10.1016/0896-6273(93)90122-8

Xiao, T., Roeser, T., Staub, W., and Baier, H. (2005). A GFP-based genetic screen reveals mutations that disrupt the architecture of the zebrafish retinotectal projection. *Development* 132, 2955–2967. doi: 10.1242/dev.01861

Conflict of Interest Statement: The authors declare that the research was conducted in the absence of any commercial or financial relationships that could be construed as a potential conflict of interest.

Received: 08 March 2013; paper pending published: 05 April 2013; accepted: 28 May 2013; published online: 18 June 2013.

Citation: Gebhardt C, Baier H and Del Bene F (2013) Direction selectivity in the visual system of the zebrafish larva. Front. Neural Circuits 7:111. doi: 10.3389/fncir.2013.00111

frontiers in
NEURAL CIRCUITS

PERSPECTIVE ARTICLE
published: 11 June 2013
doi: 10.3389/fncir.2013.00110

Prey capture in zebrafish larvae serves as a model to study cognitive functions

Akira Muto*[1,2]* *and Koichi Kawakami*[1,2]

[1] *Division of Molecular and Developmental Biology, National Institute of Genetics, Mishima, Shizuoka, Japan*
[2] *Department of Genetics, The Graduate University for Advanced Studies (SOKENDAI), Mishima, Shizuoka, Japan*

Edited by:
German Sumbre, École Normale Supérieure, France

Reviewed by:
German Sumbre, École Normale Supérieure, France
Filippo Del Bene, Institut Curie, France
Isaac Henry Bianco, Harvard University, USA

***Correspondence:**
Akira Muto and Koichi Kawakami, Division of Molecular and Developmental Biology, National Institute of Genetics, Yata 1111, Mishima, Shizuoka 411-8540, Japan
e-mail: akimuto@nig.ac.jp; kokawaka@nig.ac.jp

Prey capture in zebrafish larvae is an innate behavior which can be observed as early as 4 days postfertilization, the day when they start to swim. This simple behavior apparently involves several neural processes including visual perception, recognition, decision-making, and motor control, and, therefore, serves as a good model system to study cognitive functions underlying natural behaviors in vertebrates. Recent progresses in imaging techniques provided us with a unique opportunity to image neuronal activity in the brain of an intact fish in real-time while the fish perceives a natural prey, paramecium. By expanding this approach, it would be possible to image entire brain areas at a single-cell resolution in real-time during prey capture, and identify neuronal circuits important for cognitive functions. Further, activation or inhibition of those neuronal circuits with recently developed optogenetic tools or neurotoxins should shed light on their roles. Thus, we will be able to explore the prey capture in zebrafish larvae more thoroughly at cellular levels, which should establish a basis of understanding of the cognitive function in vertebrates.

Keywords: zebrafish, prey capture, calcium imaging, GCaMP, visual perception

WHAT CAN WE LEARN FROM THE PREY-CAPTURE BEHAVIOR?

Animal behavior should be adaptive to ever-changing environments, which is essential for survival. This behavioral flexibility is achieved by the cognitive faculty of the brain. In order to study the neural mechanisms underlying cognition and behavior, it is desirable to analyze the activity of individual neurons throughout the brain. Even though the ultimate goal is to understand the human brain, because of the overwhelming number of the neurons (10^{12} neurons) and their connections, reductionist approaches with animal models should be employed to investigate principles of neural functions. A zebrafish larva has approximately 78,000 neurons in a small, transparent brain (Hill et al., 2003), which allows us to observe a wide area of the brain in a single microscopic field and to visualize and manipulate neuronal activity during a behavioral task.

The zebrafish is a diurnal animal equipped with a highly developed visual system (Branchek, 1984; Branchek and Bremiller, 1984; Easter and Nicola, 1996). Four days after fertilization, zebrafish larvae start swimming and feeding, and capture any potential food. We found that a zebrafish larva shows stereotyped processes of the prey-capture behavior against a small air bubble (**Figure 1**). When a larva perceives the air bubble (**Figure 1A**), the larva initiates the prey-capture behavior; namely, orients itself and exhibits eye convergence (**Figure 1B**). During this orienting behavior, the larva often performs J-turn, bending a far caudal part of the tail to one-side, to fine-tune its position and angle (**Figure 1B**; McElligott and O'Malley, 2005). Then the larva approaches the air bubble as keeping their eyes converged (**Figure 1C**; Bianco et al., 2011), and it captures it (**Figure 1D**). After a successful capture, the larva assesses if it is food or not. If it was not food, the larva spits it out (**Figure 1E**) and swims away from it (**Figure 1F**). In this behavior, there seem to be a couple of decision-making steps: the first step is whether to change its orientation toward the air bubble or to ignore it (**Figures 1A,B**). The final decision is whether to perform the action of catching or to abort the sequence of behaviors (**Figures 1C,D**). The transition from one step to the next step looks probabilistic.

What factors are essential for the larvae to recognize the potential food and making the decision to initiate the prey-capture behavior? How are these decision-making processes modulated by internal states such as hunger or past experience? Through answering these questions, we will be able to get more insights into cognitive functions in the vertebrate brain.

GCaMP: A SENSITIVE PROBE FOR CALCIUM IMAGING

To identify neurons that are responsible for the cognitive tasks in the brain, we need a sensitive probe that can report activity in individual neurons *in vivo*. Calcium-sensitive fluorescence probes can measure calcium influx which occurs upon voltage changes in the neurons. Genetically encoded calcium indicators (GECIs) are particularly useful because they can be introduced into neurons of interest using a proper promoter that drives specific expression. GCaMP is a GECI, that consists of circularly permutated enhanced green fluorescent protein (EGFP), calmodulin, and calmodulin-binding peptide M13, and has been widely used for imaging (Nakai et al., 2001). Previously, we generated transgenic zebrafish expressing GCaMP-HS, a modified version of the original GCaMP, and visualized activity of spinal motoneurons during a coiling behavior of an embryo (Muto et al., 2011). However, GCaMP-HS was not sensitive enough to report signals from individual neurons in the optic tectum (Muto, unpublished observation). Therefore,

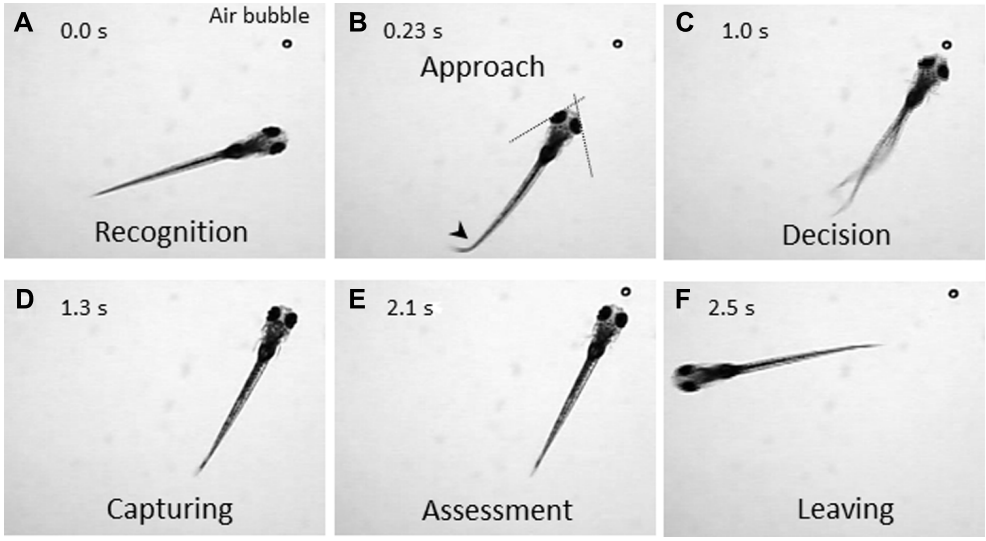

FIGURE 1 | Prey-capture behavior can be divided into multiple steps of actions. A 7-day postfertilization (dpf) larva reacts to an air bubble. A possible cognitive or motor process is assigned to each action. **(A)** *Recognition*: An object (an air bubble) comes into sight of a larva and recognized. **(B)** *Approach*: The larva orients its body toward the object with eye convergence (indicated by two crossed dotted lines). An arrowhead indicates J-turn. **(C)** *Decision-making*: The larva makes the final decision to catch the object or abort the behavior. **(D)** *Capturing*: The larva successfully captures the object and put it into the mouth. **(E)** *Assessment*: The larva spits the air bubble out because it is not food. **(F)** *Leaving*: The larva leaves the air bubble to explore other areas.

we generated a more sensitive GCaMP, GCaMP7a. Fluorescence changes detected with GCaMP7a during spontaneous neuronal activity in the tectal neuropil, were approximately threefold greater than those detected with GCaMP-HS. By using GCaMP7a, we could visualize neuronal activity in the tectum while the zebrafish larva perceived a paramecium (**Figure 2A**; Muto et al., 2013).

The efforts to improve the signal amplitude and the calcium sensitivity of GCaMP are currently ongoing in several laboratories (Akerboom et al., 2012; Ohkura et al., 2012b; Hoi et al., 2013). The sensitivity of the latest GCaMPs can detect single action potentials *in vivo*. Yet, they may still be less sensitive in comparison to the chemical probe, Oregon Green BAPTA-1 (OGB-1; Akerboom et al., 2012).

HOW TO IMAGE? FREE-SWIMMING LARVA vs. IMMOBILIZED LARVA

During prey capture against an air bubble or a paramecium, the zebrafish larva exhibits a sequence of discrete motor patterns. So, how can we image the moving brain? It is, in general, very difficult to detect fluorescence intensity changes of moving objects. In the previous study, we successfully detected neuronal activity in a free-swimming larva, mapped locations of the calcium signal in the brain and of the paramecia at the same time, and revealed that activation of the anterior optic tectum is likely to evoke prey-capture behavior (Muto et al., 2013). In this case, we imaged neuronal activity between bouts of swimming activity, that is, when the larva did not move (Muto et al., 2013). It is difficult to image the brain activity of zebrafish larvae in motion. With currently available GCaMPs, the duration of the exposure time required for image acquisition is typically in the order of tens to hundreds of milliseconds. This exposure time gives only blurred image when the object is moving. To image a moving larva, much brighter fluorescence probes and more sensitive cameras are required.

An alternative approach to image the brain activity is the use of a partially restrained larva; namely, its head and trunk are fixed in agarose while its eyes and tail are free. In this condition, two defining features of prey capture, eye convergence and J-turns, can be observed (Bianco et al., 2011). The merit of this setup is that, one can present any visual stimuli on a liquid-crystal display (LCD) screen that may mimic an air bubble or a paramecium. Because motionless objects are not perceived in the visual system of a larva (Muto et al., 2013), the stimulus to be presented should contain a motion component, which maybe direct (e.g., a moving spot which mimics a paramecium) or relative (e.g., a stationary spot on a moving background, which mimics an air bubble). As shown in **Figure 2**, a moving spot could evoke both neuronal activity in the tectum and the eye convergence in the partially restrained larva. The eye convergence is an initial step of the sequential behaviors (**Figure 1B**). The succeeding steps of prey capture can also be investigated in a closed-loop virtual reality setup (Trivedi and Bollmann, 2013). Thus, we can study multiple steps of prey capture in a partially restrained larva. What visual cues are more likely to evoke prey recognition? Which neurons are activated during the prey recognition? How will these neuronal activities be changed before and after the larva learned that the air bubble was not food?

Pioneering ethological study by Ewert (1980) showed that, in prey catching behavior, toads preferred visual stimuli that resembled a shape and moving pattern of a worm, in contrast to the same shape rotated by 90°. In zebrafish, preference for size and speed of a moving spot in prey-capture behavior has been reported (Bianco

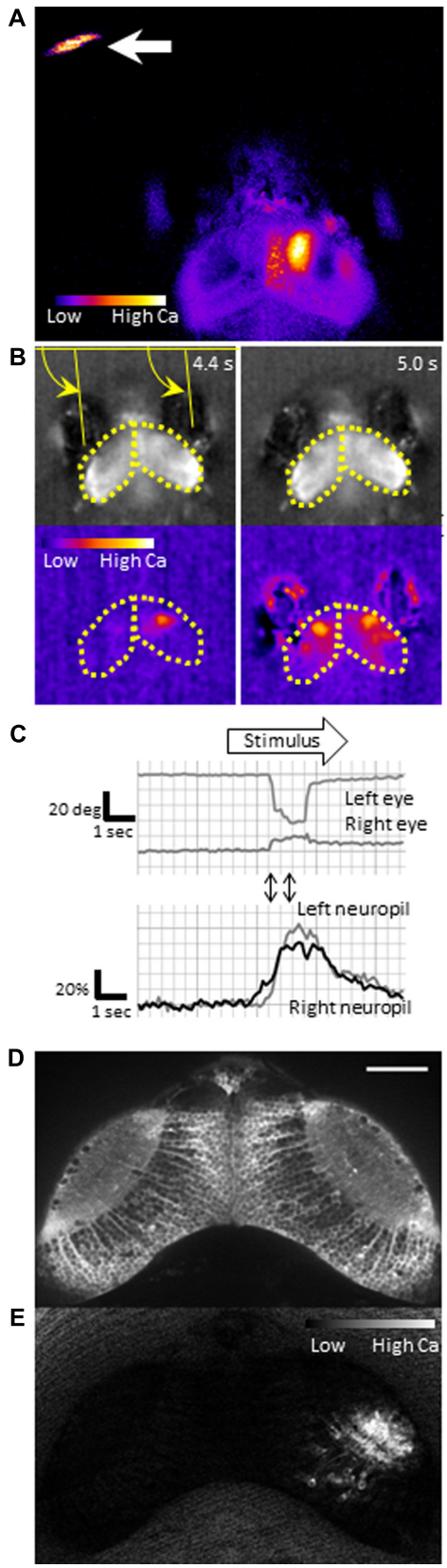

FIGURE 2 | Continued

FIGURE 2 | Continued
Functional imaging of the zebrafish larval brain. GCaMP7a is expressed in the optic tectum of a 7-dpf zebrafish larva embedded in agarose. **(A)** Tectal responses during perception of a swimming paramecium (arrow). Calcium signals are observed in both cell bodies and the neuropil on the right tectum when a paramecium is in the left hemifield. Ratio image was created and pseudo-colored to show fluorescence changes. **(B)** Tectal responses during perception of a moving spot. A small LCD screen is placed in front of the larva and a moving spot is presented (from left to the right). *Top*: Raw images to show eye positions. *Bottom*: Pseudo-colored images to show fluorescence changes. Yellow arrows indicate eye positions (angles). Yellow dotted lines delineate the optic tectum. **(C)** Eye positions (*top*) and GCaMP7a fluorescence intensity changes (*bottom*) during experiment **(B)**. A moving spot was presented during the time shown as an open arrow. Two-way arrows indicate the time points of 4.4 and 5.0 s shown in **(B)**. The eye convergence (inward movement of both left and right eyes) was evoked by the moving spot. **(D)** Neuronal activity in the optic tectum of a 4-dpf zebrafish larva. A spinning disk confocal microscope (CSU-W1, Yokogawa Electric Corporation, Tokyo, Japan) was used for recording. Scale bar: 50 μm. **(E)** The ratiometric image of **(D)** to reveal the fluorescence change. Small populations of neurons in the right tectum are temporally activated.

et al., 2011). In medaka fish, a moving object with pink noise component was more potent to evoke feeding behavior (Matsunaga and Watanabe, 2012). These findings should be taken account into the parameters to create a "virtual paramecia" on the LCD screen.

TOWARD ELUCIDATION OF THE ENTIRE FUNCTIONAL NEURAL CIRCUITS FOR PREY CAPTURE

The optic tectum has a laminar structure; superficial layers that receive sensory input and deeper layers that are involved in motor output (Salas et al., 1997). Visual information processing for prey recognition starts at the most superficial layer, the stratum opticum (SO) in the tectum. Del Bene et al. (2010) discovered that a subclass of GABAergic interneurons located in the SO responded preferentially to visual stimuli with larger spatial frequency, and was indispensable for recognition of small objects and paramecia. We predicted functional connections between the anterior tectum area and the motor pathway that generates approach swimming (Muto et al., 2013). Identification of the neural pathway(s) that follows the initial stages of visual perception is the target of the future study. Gahtan et al. (2005) found that a pair of reticulospinal neurons, namely, MeLc (caudal medial–lateral) and MeLr (rostral medial–lateral) in the nucleus of the medial longitudinal fasciculus of the midbrain tegmentum is essential for prey capture, specifically orienting behavior. These reticulospinal neurons extend their dendrites toward the ventral tectum, which suggests that they convey the output from the tectum to the motor system (Gahtan et al., 2005). It is unclear whether these identified pathways play a role in prey recognition itself (e.g., pattern recognition of food) or in up- or downstream of it (e.g., specifying the range of possible food size, or relaying the motor command for prey capture). The neural pathway(s) that follows the initial stages of visual perception will be identified by examining neuronal activity of the entire brain using pan-neuronal GCaMP expression (Ahrens et al., 2012) and also investigating specific populations of neurons in which the GCaMP is expressed via Gal4-UAS system (Kawakami et al., 2010).

TECHNICAL REQUIREMENTS FOR THE FUTURE STUDY

To explore neuronal activity in wide areas of the brain by calcium imaging, it is necessary to achieve single-cell resolution deep in the brain with high acquisition rates. Fulfilling this requirement is still a technical challenge. Fluorescent compound microscopy can generate real-time images (typically, ∼10 fps in our recording set up), but only detect calcium signals near the surface of the tectum from a dorsal side (**Figures 2A,B**). It does not give enough resolution along the *z*-axis to separate signals from overlapping neurons. Two-photon scanning microscopy gives much deeper light penetration with excellent image quality. The drawback is a slow frame acquisition rate due to the slow laser scanning (a few frames per second; Ahrens et al., 2012). A spinning-disk confocal microscope can achieve a higher temporal resolution, and onset of the calcium rise could be determined with a precision of up to several milliseconds (Takahashi et al., 2007). We could detect neuronal activity at a single-cell resolution in the optic tectum (**Figures 2D,E**). The use of light sheet microscopy may solve both penetration and temporal resolution problems, and has been applied to the entire brain imaging (Huisken, 2012; Ahrens et al., 2013). Another critical issue in calcium imaging of the visual system is how to minimize undesirable retinal stimulation by the excitation light. *nacre* mutants have been commonly used because the lack of melanophores in this mutant allows light penetration which is necessary for brain imaging, whereas the intact retinal pigment epithelia block the scattered excitation light coming from the back of the retina (Sumbre et al., 2008; Muto et al., 2013). The amount of excitation light should be minimized so that it does not interfere with the visual stimulus.

Once we identify neuronal circuits activated during a prey-capture behavior, we need to manipulate their activity to prove necessity and sufficiency. Necessity can be tested by blocking neuronal activity with a neurotoxin (Asakawa et al., 2008) or optogenetic tools such as halorhodopsin (Arrenberg et al., 2010). Sufficiency can be tested by optical activation of the identified neurons with light-gated glutamate receptors or channelrhodopsin-2 (Douglass et al., 2008; Wyart et al., 2009; Arrenberg et al., 2010). These effectors can be genetically expressed using a tissue-specific promoter (Faraco et al., 2006), the regulatory elements located on a bacterial artificial chromosome (BAC; Suster et al., 2011), or Gal4 driver lines in combination with UAS constructs (Asakawa et al., 2008). A possible limitation is that expression of effector genes may not be restricted to specific neuronal circuits, rather, they are often expressed in multiple regions. To achieve specific expression of effectors that inhibit neuronal activity, it will be necessary to combine two expression systems, e.g., Cre/loxP and Gal4-UAS (Sato et al., 2007). Specificity in the optogenetic activation can also be achieved by spatially restricted illuminations. Fiber optics can be used to illuminate a small area by choosing an appropriate fiber size (Arrenberg et al., 2009). Spatially patterned illumination can be achieved with a digital micromirror device (DMD; Zhu et al., 2012) or by digital holography (Oron et al., 2012).

The effect of neuronal activation by channelrhodopsin-2 or inhibition by halorhodopsin should be confirmed by calcium imaging, which requires the simultaneous use of an optogenetic tool and a calcium probe. Both GCaMP and channelrhodopsin-2 require blue light, and therefore cannot be used at the same time. Color-shifted GCaMPs have been developed (Zhao et al., 2011; Ohkura et al., 2012a; Walker et al., 2013), and their usefulness *in vivo* in transgenic animals should be investigated and demonstrated.

In conclusion, prey capture in a zebrafish larva involves cognitive processes and, therefore, serves as an excellent model to visualize higher brain functions at a cellular level. As a first step, we visualized neuronal activity at the initial step of the prey-capture behavior, prey perception (Muto et al., 2013). Further imaging studies will reveal the entire functional neuronal circuits that are activated during this behavior. In combination with recent technology advances including optogenetic tools, we will obtain more insights into basic principles of computational and cognitive properties of the brain.

REFERENCES

Ahrens, M. B., Li, J. M., Orger, M. B., Robson, D. N., Schier, A. F., Engert, F., et al. (2012). Brain-wide neuronal dynamics during motor adaptation in zebrafish. *Nature* 485, 471–477. doi: 10.1038/nature11057

Ahrens, M. B., Orger, M. B., Robson, D. N., Li, J. M., and Keller, P. J. (2013). Whole-brain functional imaging at cellular resolution using light-sheet microscopy. *Nat. Methods* 10, 413–420. doi: 10.1038/nmeth.2434

Akerboom, J., Chen, T. W., Wardill, T. J., Tian, L., Marvin, J. S., Mutlu, S., et al. (2012). Optimization of a GCaMP calcium indicator for neural activity imaging. *J. Neurosci.* 32, 13819–13840. doi: 10.1523/JNEUROSCI.2601-12.2012

Arrenberg, A. B., Del Bene, F., and Baier, H. (2009). Optical control of zebrafish behavior with halorhodopsin. *Proc. Natl. Acad. Sci. U.S.A.* 106, 17968–17973. doi: 10.1073/pnas.0906252106

Arrenberg, A. B., Stainier, D. Y., Baier, H., and Huisken, J. (2010). Optogenetic control of cardiac function. *Science* 330, 971–974. doi: 10.1126/science.1195929

Asakawa, K., Suster, M. L., Mizusawa, K., Nagayoshi, S., Kotani, T., Urasaki, A., et al. (2008). Genetic dissection of neural circuits by Tol2 transposon-mediated Gal4 gene and enhancer trapping in zebrafish. *Proc. Natl. Acad. Sci. U.S.A.* 105, 1255–1260. doi: 10.1073/pnas.0704963105

Bianco, I. H., Kampff, A. R., and Engert, F. (2011). Prey capture behavior evoked by simple visual stimuli in larval zebrafish. *Front Syst. Neurosci.* 5:101. doi: 10.3389/fnsys.2011.00101

Branchek, T. (1984). The development of photoreceptors in the zebrafish, *Brachydanio rerio*. II. Function. *J. Comp. Neurol.* 224, 116–122. doi: 10.1002/cne.902240110

Branchek, T., and Bremiller, R. (1984). The development of photoreceptors in the zebrafish, *Brachydanio rerio*. I. Structure. *J. Comp. Neurol.* 224, 107–115. doi: 10.1002/cne.902240109

Del Bene, F., Wyart, C., Robles, E., Tran, A., Looger, L., Scott, E. K., et al. (2010). Filtering of visual information in the tectum by an identified neural circuit. *Science* 330, 669–673. doi: 10.1126/science.1192949

Douglass, A. D., Kraves, S., Deisseroth, K., Schier, A. F., and Engert, F. (2008). Escape behavior elicited by single, channelrhodopsin-2-evoked spikes in zebrafish somatosensory neurons. *Curr. Biol.* 18, 1133–1137. doi: 10.1016/j.cub.2008.06.077

Easter, S. S. Jr., and Nicola, G. N. (1996). The development of vision in the zebrafish (*Danio rerio*). *Dev. Biol.* 180, 646–663. doi: 10.1006/dbio.1996.0335

Ewert, J. P. (1980). *Neuroethology*. Berlin: Springer-Verlag. doi: 10.1007/978-3-642-67500-3

Faraco, J. H., Appelbaum, L., Marin, W., Gaus, S. E., Mourrain, P., and Mignot, E. (2006). Regulation of hypocretin (orexin) expression in embryonic zebrafish. *J. Biol. Chem.* 281, 29753–29761. doi: 10.1074/jbc.M605811200

Gahtan, E., Tanger, P., and Baier, H. (2005). Visual prey capture in larval zebrafish is controlled by identified reticulospinal neurons downstream

of the tectum. *J. Neurosci.* 25, 9294–9303. doi: 10.1523/JNEUROSCI.2678-05.2005

Hill, A., Howard, C. V., Strahle, U., and Cossins, A. (2003). Neurodevelopmental defects in zebrafish (*Danio rerio*) at environmentally relevant dioxin (TCDD) concentrations. *Toxicol. Sci.* 76, 392–399. doi: 10.1093/toxsci/kfg241

Hoi, H., Matsuda, T., Nagai, T., and Campbell, R. E. (2013). Highlightable Ca(2+) indicators for live cell imaging. *J. Am. Chem. Soc.* 135, 46–49. doi: 10.1021/ja310184a

Huisken, J. (2012). Slicing embryos gently with laser light sheets. *Bioessays* 34, 406–411. doi: 10.1002/bies.201100120

Kawakami, K., Abe, G., Asada, T., Asakawa, K., Fukuda, R., Ito, A., et al. (2010). zTrap: zebrafish gene trap and enhancer trap database. *BMC Dev. Biol.* 10:105. doi: 10.1186/1471-213X-10-105

Matsunaga, W., and Watanabe, E. (2012). Visual motion with pink noise induces predation behaviour. *Sci. Rep.* 2, 219. doi: 10.1038/srep00219

McElligott, M. B., and O'Malley, D. M. (2005). Prey tracking by larval zebrafish: axial kinematics and visual control. *Brain Behav. Evol.* 66, 177–196. doi: 10.1159/000087158

Muto, A., Ohkura, M., Abe, G., Nakai, J., and Kawakami, K. (2013). Real-time visualization of neuronal activity during perception. *Curr. Biol.* 23, 307–311. doi: 10.1016/j.cub.2012.12.040

Muto, A., Ohkura, M., Kotani, T., Higashijima, S., Nakai, J., and Kawakami, K. (2011). Genetic visualization with an improved GCaMP calcium indicator reveals spatiotemporal activation of the spinal motor neurons in zebrafish. *Proc. Natl. Acad. Sci. U.S.A.* 108, 5425–5430. doi: 10.1073/pnas.1000887108

Nakai, J., Ohkura, M., and Imoto, K. (2001). A high signal-to-noise Ca(2+) probe composed of a single green fluorescent protein. *Nat. Biotechnol.* 19, 137–141. doi: 10.1038/84397

Ohkura, M., Sasaki, T., Kobayashi, C., Ikegaya, Y., and Nakai, J. (2012a). An improved genetically encoded red fluorescent Ca^{2+} indicator for detecting optically evoked action potentials. *PLoS ONE* 7:e39933. doi: 10.1371/journal.pone.0039933

Ohkura, M., Sasaki, T., Sadakari, J., Gengyo-Ando, K., Kagawa-Nagamura, Y., Kobayashi, C., et al. (2012b). Genetically encoded green fluorescent Ca^{2+} indicators with improved detectability for neuronal Ca^{2+} signals. *PLoS ONE* 7:e51286. doi: 10.1371/journal.pone.0051286

Oron, D., Papagiakoumou, E., Anselmi, F., and Emiliani, V. (2012). Two-photon optogenetics. *Prog. Brain Res.* 196, 119–143. doi: 10.1016/B978-0-444-59426-6.00007-0

Salas, C., Herrero, L., Rodriguez, F., and Torres, B. (1997). Tectal codification of eye movements in goldfish studied by electrical microstimulation. f. *Neuroscience* 78, 271–288. doi: 10.1016/S0306-4522(97)83048-5

Sato, T., Hamaoka, T., Aizawa, H., Hosoya, T., and Okamoto, H. (2007). Genetic single-cell mosaic analysis implicates ephrinB2 reverse signaling in projections from the posterior tectum to the hindbrain in zebrafish. *J. Neurosci.* 27, 5271–5279. doi: 10.1523/JNEUROSCI.0883-07.2007

Sumbre, G., Muto, A., Baier, H., and Poo, M. M. (2008). Entrained rhythmic activities of neuronal ensembles as perceptual memory of time interval. *Nature* 456, 102–106. doi: 10.1038/nature07351

Suster, M. L., Abe, G., Schouw, A., and Kawakami, K. (2011). Transposon-mediated BAC transgenesis in zebrafish. *Nat. Protoc.* 6, 1998–2021. doi: 10.1038/nprot.2011.416

Takahashi, N., Sasaki, T., Usami, A., Matsuki, N., and Ikegaya, Y. (2007). Watching neuronal circuit dynamics through functional multineuron calcium imaging (fMCI). *Neurosci. Res.* 58, 219–225. doi: 10.1016/j.neures.2007.03.001

Trivedi, C. A., and Bollmann, J. H. (2013). Visually driven chaining of elementary swim patterns into a goal-directed motor sequence: a virtual reality study of zebrafish prey capture. *Front. Neural Circuits* 7:86. doi: 10.3389/fncir.2013.00086

Walker, A. S., Burrone, J., and Meyer, M. P. (2013). Functional imaging in the zebrafish retinotectal system using RGECO. *Front Neural Circuits* 7:34. doi: 10.3389/fncir.2013.00034

Wyart, C., Del Bene, F., Warp, E., Scott, E. K., Trauner, D., Baier, H., et al. (2009). Optogenetic dissection of a behavioural module in the vertebrate spinal cord. *Nature* 461, 407–410. doi: 10.1038/nature08323

Zhao, Y., Araki, S., Wu, J., Teramoto, T., Chang, Y. F., Nakano, M., et al. (2011). An expanded palette of genetically encoded Ca(2)(+) indicators. *Science* 333, 1888–1891. doi: 10.1126/science.1208592

Zhu, P., Fajardo, O., Shum, J., Zhang Scharer, Y. P., and Friedrich, R. W. (2012). High-resolution optical control of spatiotemporal neuronal activity patterns in zebrafish using a digital micromirror device. *Nat. Protoc.* 7, 1410–1425. doi: 10.1038/nprot.2012.072

Conflict of Interest Statement: The authors declare that the research was conducted in the absence of any commercial or financial relationships that could be construed as a potential conflict of interest.

Received: 01 April 2013; paper pending published: 02 May 2013; accepted: 26 May 2013; published online: 11 June 2013.

Citation: Muto A and Kawakami K (2013) Prey capture in zebrafish larvae serves as a model to study cognitive functions. Front. Neural Circuits 7:110. doi: 10.3389/fncir.2013.00110

frontiers in
NEURAL CIRCUITS

ORIGINAL RESEARCH ARTICLE
published: 10 May 2013
doi: 10.3389/fncir.2013.00086

Visually driven chaining of elementary swim patterns into a goal-directed motor sequence: a virtual reality study of zebrafish prey capture

Chintan A. Trivedi* and Johann H. Bollmann*

Neural Circuits and Behavior Group, Department of Biomedical Optics, Max Planck Institute for Medical Research, Heidelberg, Germany

Edited by:
Gonzalo G. De Polavieja, Instituto Cajal - CSIC, Spain

Reviewed by:
Martin Meyer, King's College London, UK
Claire Wyart, Brain and Spinal cord Institute (ICM), France

****Correspondence:***
Chintan A. Trivedi and Johann H. Bollmann, Neural Circuits and Behavior Group, Department of Biomedical Optics, Max Planck Institute for Medical Research, Jahnstrasse 29, 69120 Heidelberg, Germany.
e-mail: chintan.trivedi@mpimf-heidelberg.mpg.de; johann.bollmann@mpimf-heidelberg.mpg.de

Prey capture behavior critically depends on rapid processing of sensory input in order to track, approach, and catch the target. When using vision, the nervous system faces the problem of extracting relevant information from a continuous stream of input in order to detect and categorize visible objects as potential prey and to select appropriate motor patterns for approach. For prey capture, many vertebrates exhibit intermittent locomotion, in which discrete motor patterns are chained into a sequence, interrupted by short periods of rest. Here, using high-speed recordings of full-length prey capture sequences performed by freely swimming zebrafish larvae in the presence of a single paramecium, we provide a detailed kinematic analysis of first and subsequent swim bouts during prey capture. Using Fourier analysis, we show that individual swim bouts represent an elementary motor pattern. Changes in orientation are directed toward the target on a graded scale and are implemented by an asymmetric tail bend component superimposed on this basic motor pattern. To further investigate the role of visual feedback on the efficiency and speed of this complex behavior, we developed a closed-loop virtual reality setup in which minimally restrained larvae recapitulated interconnected swim patterns closely resembling those observed during prey capture in freely moving fish. Systematic variation of stimulus properties showed that prey capture is initiated within a narrow range of stimulus size and velocity. Furthermore, variations in the delay and location of swim triggered visual feedback showed that the reaction time of secondary and later swims is shorter for stimuli that appear within a narrow spatio-temporal window following a swim. This suggests that the larva may generate an expectation of stimulus position, which enables accelerated motor sequencing if the expectation is met by appropriate visual feedback.

Keywords: zebrafish, prey capture, virtual reality, goal-directed behavior, intermittent locomotion, double-step saccade, motor sequence, saccadic suppression

INTRODUCTION

Goal-directed behaviors consist of sequenced movements that bring the organism closer to a desired object, location or insight, typically associated with reward. The properties of the target, the sensory processing capabilities, and the architecture of the motor system determine whether the execution of movement steps is continuous or discrete in time. For instance reaching and smooth pursuit eye movements are classic examples when movement steps are combined fluently to generate a smooth trajectory (Wolpert and Ghahramani, 2000; Lisberger, 2010). On the other end of the spectrum, the class of chained, interrupted motor sequences is epitomized by saccadic eye movements (Land, 1999; Schall and Thompson, 1999), which steer our gaze during tasks such as visual search or reading a text.

A well-studied and paramount type of goal-directed motion is visually guided prey capture behavior, which involves the tracking and pursuit of a target typically moving in an unpredictable fashion. Thus, a substantial part of the visuomotor circuitry must be geared toward the efficient control of this behavior, which comprises the detection and classification of objects and the selection of appropriate motor patterns to approach and capture the prey (Ewert et al., 2001). In visually guided prey capture, the animal must solve the problem of reducing the angle between the target and its own heading direction while simultaneously approaching the target. Individual movement steps may be pre-programmed and executed ballistically; alternatively, continuous target tracking and pursuit movements may be adjusted in real time according to the changing trajectory of the prey. In both cases, visual feedback is essential for generating subsequent motor commands in order to correct for target displacement and motor errors.

A quantitative analysis of how the spatio-temporal properties of the stimulus impact such complex motor sequences can provide information about the underlying neural mechanisms, (e.g., Schlegel and Schuster, 2008). Approaches in which a restrained animal is presented with artificial stimuli in a closed-loop configuration have been developed in order to mimic the effect of the animal's own movement responses on sensory input ["virtual

reality," reviewed by Dombeck and Reiser (2012)]. These techniques enable the experimenter to sample the visuomotor system using precisely controlled stimulus sequences with expected or unexpected visual feedback, and also to measure underlying neural activity using opto- and electrophysiological techniques (Harvey et al., 2009; Dombeck et al., 2010; Seelig et al., 2010; Ahrens et al., 2012).

Larval zebrafish exhibit visually guided motor-behaviors beginning at 4 days post fertilization, including robust optomotor and optokinetic responses (reviewed in Neuhauss, 2003; Portugues and Engert, 2009; Fero et al., 2011). Notably, zebrafish also engage in prey capture behavior beginning around 5 days post fertilization. When hunting prey, the fish performs a number of approaching swimming maneuvers, interrupted by brief pauses (McElligott and O'Malley, 2005), characteristic of intermittent locomotion (Kramer and McLaughlin, 2001). When the prey is in striking distance, the fish performs a capture swim (Borla et al., 2002), which terminates the sequence. Fin-tail co-ordination during prey capture (McClenahan et al., 2012) as well as individual examples of these bout-like swim patterns have been described kinematically and subjected to a categorical description (Borla et al., 2002; McElligott and O'Malley, 2005; Bianco et al., 2011). Furthermore, prey capture behavior depends on vision, and ablation of the tectum and of tegmental projection neurons in the nucleus of the medial longitudinal fasciculus (nMLF) suggested that these anatomical structures are likely to be serial components in the visuomotor pathway mediating this behavior (Gahtan et al., 2005).

While individual swims during prey capture were observed to represent slow forward swims and unique low-angle turns exclusively performed during this behavior ("J-turns," McElligott and O'Malley, 2005), less is known about how the entire motor sequence is assembled in time from individual swim patterns. For instance, it is unclear whether swim bouts occurring early and late during the prey capture sequence may represent a single class of elementary motor pattern that could be modulated on a continuous scale to cover a large range of turning angles. Furthermore, although single swims could be evoked in an open-loop assay using artificial stimuli (Bianco et al., 2011), it is unknown how visual feedback controls the timing of individual swim bouts within such a sequence, which requires closed-loop visual stimulation techniques not yet developed in this model system.

To address these questions, we used high-speed video to record prey capture sequences of freely moving larvae, which yielded a comprehensive overview of motor patterns used in this behavior. Importantly, we recorded full-length prey capture sequences in the presence of only one paramecium at a time, which allowed us to observe target-directed turning patterns in a large angular range in the absence of stimulus competition. A quantitative analysis of visual properties of the prey during this naturally occurring behavior was used to design a set of virtual prey stimuli that were able to trigger target-directed sequences in minimally restrained larvae in a closed-loop assay. Also, by introducing small perturbations of motor-induced visual feedback at high temporal and spatial resolution, we observed that the timing of motor output was dependent on the location and timing of visual feedback. Parts of this work have been reported in abstract form (Trivedi et al., 2011).

RESULTS

SWIM SEQUENCES DURING PREY-CAPTURE BEHAVIOR

When swimming freely in a small arena to which a paramecium is added, larval zebrafish quickly engage in prey capture behavior. The larva performs several swim bouts within a few 100s of milliseconds, during which the larva successively minimizes the angle and distance between its body axis and the prey, stepwise approaching the prey until it is close enough to capture the object with high probability (**Figure 1A**) (McElligott and O'Malley, 2005).

Here, we use high-speed video recordings of zebrafish larvae performing full-length prey capture sequences in a small arena in the presence of single paramecia under ambient white light illumination (**Figure 1B**; **Movies S1, S2**). These movies were recorded using infrared dark-field illumination, which allowed us to record eye and tail movements and to measure the geometric relationships between hunter and prey in detail (**Figures 1A,C**). Prey capture sequences are interspersed with spontaneous swims at irregular intervals. We observed that the first prey-directed swims were accompanied by near maximal convergence of the eye contralateral to the prey, while the ipsilateral eye converged partially. Only the second swim brought both eyes into a maximally converged configuration (**Figure 1D**), which the fish maintained until after it had attempted a capture swim against the prey. We chose this characteristic two-step eye convergence pattern as a criterion to define the start of a prey capture sequence (Trivedi et al., 2011) (**Figure 1C**) in order to investigate the spatio-temporal dynamics of subsequent swims of this multistep motor behavior. Following the first swim in a sequence, the larva performed prey-directed swims in rapid succession. We analyzed 30 high-speed movies, in each of which an entire sequence from first swim to the final prey capture swim was recorded. These sequences had a mean duration of 1.23 ± 0.13 s (mean $\pm$ sem), and consisted of 4.4 ± 0.28 individual swim bouts (excluding the capture swim, $n = 30$ sequences). The inter-bout-interval (IBI) between swims decreased from 324 ± 54 ms after the first swim, to a minimum IBI of 124 ± 27 ms after the 4th swim ($n = 30$ sequences) (**Figure 1E**). The fish-object distance decreased monotonically (**Figure 1F**). Because only a single paramecium was present at all times, we could unambiguously determine the salient geometric features of the prey at the beginning and throughout the prey capture sequence. From measurements in single video frames immediately before and after a swim, we determined the angular size and angular velocity of the targeted paramecium relative to the midpoint between the eyes (**Figures 1G,H**). As expected from elementary geometry, average angular size, and velocity increased as the fish approached the prey.

SINGLE SWIMS COVER A LARGE ANGULAR RANGE, CONTROLLED BY TARGET POSITION

Next, we analyzed the kinematics of individual swims during the prey capture sequence in order to relate swim output to visual input during individual steps of the motor sequence. Zebrafish larvae at this stage use tail beat frequencies between 20 and 80 Hz

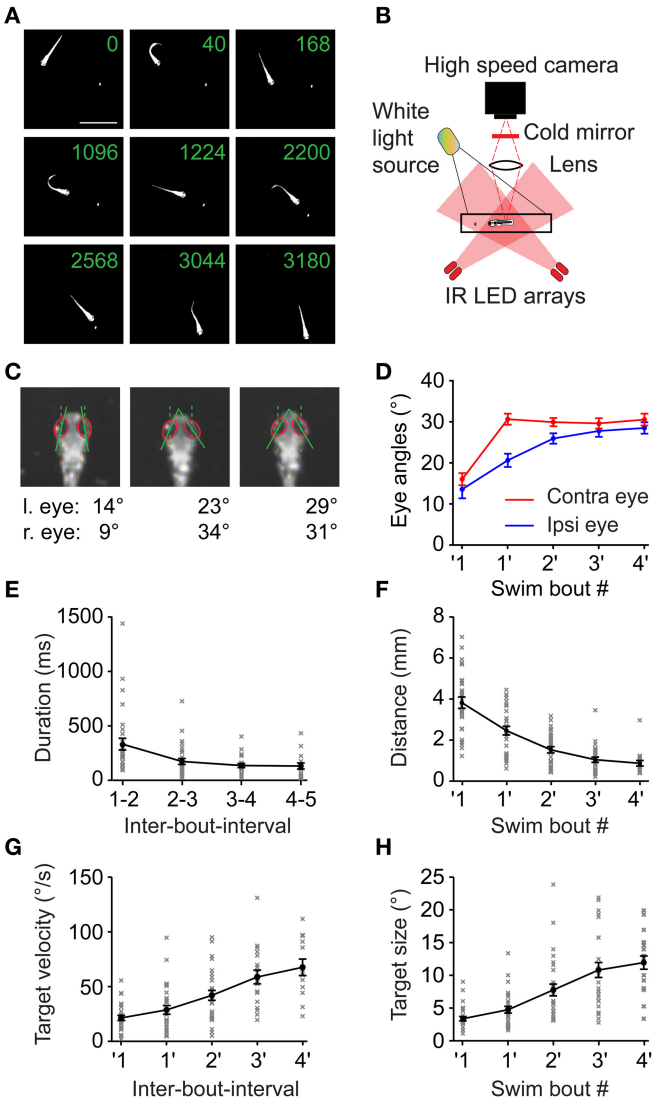

FIGURE 1 | Swim sequences during prey capture behavior. (A) Selected frames of a 6 dpf larva performing a prey capture sequence recorded at 250 frames/s showing swim and rest episodes. Same field of view for all 9 frames (scale bar: 4 mm). Only one paramecium present (elongated white object, highlighted by local contrast enhancement). Numbers in each frame indicate time in milliseconds. Frames 2, 4, 6, and 8 show the 1st, 2nd, 4th and the capture swim in the sequence, respectively. **(B)** Experimental setup to record high speed movies of freely moving larva capturing prey. **(C)** Ipsilateral and contralateral eye angle measurements before 1st, after 1st and after 2nd swim. Magnified view of larval head, rotated to an upright position for clarity. Red ellipses: outline of the eyes, solid lines: major axis of ellipses; dashed lines: fish heading direction. **(D)** Ipsilateral and contralateral eye angles during the prey capture sequence (mean ± sem; $n = 30$ sequences). Note: eyes are specified as ipsilateral or contralateral based on the location of the prey target before the first swim of the sequence. This assignment was maintained for eye angle measurements made throughout the sequence irrespective of the location of the target in successive swims. **(E)** The interval between two successive swim bouts (IBI) decreased monotonically as the sequence progressed ($n = 30$ sequences). **(F)** Distance between the larva and the prey decreased monotonically with each swim from 3.8 ± 0.27 mm before first swim to 0.89 ± 0.13 mm after 4th swim. **(G)** Angular velocity of the prey measured between two swims increased monotonically from 21.1°/s ± 2.3°/s before first swim to 67°/s ± 7.5°/s after 4th swim. **(H)** Angular size of the prey increased from 3.2° ± 0.3° before first swim to 11.9° ± 1° after 4th swim. In **(D), (F), (G),** and **(H),** ′1 indicates measurements immediately before the first swim of a sequence, while 1′ indicates measurements immediately after the first swim and so on.

(Budick and O'Malley, 2000; McLean et al., 2008), which makes it difficult to measure tail kinematics and the relative timing of eye and tail movements with high precision when using frame rates ≤ 100 Hz (Bianco et al., 2011). Therefore, we used recordings at 250 or 500 Hz to measure tail and eye movements as a basis for kinematic analysis. Video records were analyzed automatically using a machine vision algorithm that determined the midline of the larva in each frame after binary operations and distance map conversion (Materials and Methods). The midline was then divided into six line segments consisting of the head segment, representing the body axis, and five tail segments (**Figure 2A**). The angular deviations $\gamma_1(t), \ldots, \gamma_5(t)$ of tail segments were

automatically measured against the body axis. Furthermore, the angle $\phi(t)$ between the position of the prey with respect to the body axis and its distance $d(t)$ with respect to the midpoint between the eyes were extracted automatically. Thus, the temporal evolution of the prey capture sequence was parameterized using a set of 8 observables (d, ϕ, θ, $\gamma_1, \ldots, \gamma_5$) (**Figures 2A,B**).

Swim bouts during prey capture exhibited one-sided, asymmetric tail bending on a graded scale, which led to different degrees of turning, as shown in three examples in **Figure 2C** (**i–iii**). Among these swim bouts, we observed small angle turns that were not observed during spontaneous swimming, consistent with earlier results (McElligott and O'Malley, 2005). When comparing the change in orientation ($\Delta\theta$) with the fish-target angle immediately before the swim (ϕ_{pre}), a high correlation was observed ($r_{Pearson} = 0.97$, $p < 10^{-10}$), which suggests that the fish can orient toward the prey on a fine graded scale (**Figure 2D**). The distribution of turning angles ($\Delta\theta$) across all swims varied smoothly and corresponded well to the distribution of fish-target angles (ϕ_{pre}) up to angles of ∼60° (**Figure 2E**). When the distribution of turning angles ($\Delta\theta$) was normalized to the occurrence of fish-target angles, turning angles were distributed uniformly within this range (**Figure 2F**). Apparently, the fish attempts to minimize the angle between its body axis and the location of the prey within one swim, and it does so with a precision of $|\phi_{post}| = 8.06° \pm 1.7°$ when the fish-target angle is in the range $0° < \phi_{pre} < 60°$ (**Figure 2G**). In general, we observed more undershoot in turning (64%, 69 out of 107 swims) than overshoot (36%, 38 out of 107 swims). Note that large-angle turns preferentially occurred at early stages of the sequence compared to small-angle turns (see color-coded order of swims in **Figures 2D,G,H**). Noteworthy, the number of tail beat cycles per swim was not significantly different (One-Way ANOVA, $p = 0.32$, $n = 107$) for large and small angle turns (mean number of tail beat cycles per swim for 1st, 2nd, 3rd, and 4th swim was 2.92 ± 0.08, 3.02 ± 0.1, 2.88 ± 0.09, and 2.74 ± 0.1, respectively). We observed that the duration of the individual swim bout decreased slightly during the progression of the sequence: the mean duration of 1st, 2nd, 3rd, and 4th swim was 141 ± 2.8, 136 ± 4.5, 124 ± 3.4, and 116 ± 4.9 ms, respectively. This temporal compression is explained by the observation that the duration of the first tail beat cycle varied with the change in orientation ($\Delta\theta$) in a graded fashion (**Figure 2H**), and larger changes predominantly occurred during the first and second swim.

This suggests that the larva controls the degree of turning smoothly by an asymmetric bend component of the tail, which prolongs the duration of the first tail beat cycle. More generally, the prey capture sequence appears to be composed of an elementary swim pattern, or motor primitive (Grillner, 1981; Bizzi et al., 2000), whose angular bias is modulated on a graded scale by the fish-target angle ϕ_{pre} preceding the swim by some 10s of milliseconds. The beginning of a sequence is effectively triggered by small objects subtending <5° visual angle moving at speeds of ∼20°/s (**Figures 1G,H**). This may represent a trigger feature for prey capture behavior in larval zebrafish. Since in 30 sequences, fish engaged in prey capture at initial fish-target angles of $20° < \phi_{pre} < 105°$, i.e., when the prey was invisible to the contralateral eye, the sequence seems to be preferentially initiated in a monocular sub-circuit of the visuo motor pathway.

LOW FREQUENCY CONTENT OF INDIVIDUAL SWIM BOUTS PREDICTS THE CHANGE IN ORIENTATION

Next, we sought to predict the change in orientation ($\Delta\theta$) of this elementary swim pattern from measurements of tail angle kinematics. The waveforms of the tail angles $\gamma_1, \ldots, \gamma_5$ were extracted from the recorded swim patterns and were analyzed to further characterize individual motor patterns. We calculated the spectral composition of swim bouts during prey capture using discrete Fourier analysis. Single-sided amplitude spectra were computed for each tail segment waveform individually and subsequently summed (**Figure 3A**, and Materials and Methods). This analysis was applied to all swim bouts comprising varying degrees of turning (**Figure 3B,i–iii**, left panels, and **3C**).

Notably, swim bouts during prey capture exhibited a peak in the sum spectrum at a low frequency between 3 and 5 Hz (**Figure 3C**, left arrow), whose peak amplitude ("LF amplitude_{rms}") showed a strong correlation with the change in orientation $\Delta\theta$ ($r_{Pearson} = 0.97$, $p < 10^{-10}$; **Figure 3D**) and with the fish-target angle ϕ_{pre} ($r_{Pearson} = 0.9$, $p < 10^{-10}$; **Figure 3E**). Furthermore, the location of the LF peak was constant and did not vary with the change in orientation $\Delta\theta$ (slope = 0.02, $r_{pearson} = 0.38$, $p = 0.03$, **Figure 3F**, circles). The peak at 3–5 Hz was also present in the spectra of the individual tail segment waveforms (**Figure 3A**, right panel). The slope of the linear fit between the LF amplitude_{rms} and the fish-target angle (ϕ_{pre}) was lower for first swims (slope = 0.62) than for subsequent swims (slope = 0.95; **Figure 3E**). This can be attributed to the observation that the fraction of turns that undershot the target was larger for first swims, when the fish-target angles ϕ_{pre} tend to be large (**Figure 2G**). Furthermore, the graded relationship between the low frequency component and the turning angle becomes apparent when the tail segment waveforms are filtered at low and high band-pass settings. While the high-frequency components of the tail segment angles oscillate symmetrically around 0, the low frequency components reflect the amount of turning on a continuous scale (**Figure 3B**, right panels).

Second, we found that all swims had a pronounced peak at higher frequencies in the sum spectrum at 28.2 ± 0.56 Hz (range: 20–35 Hz, $n = 107$ swims; **Figure 3C**, right arrow), which corresponds to the time-averaged tail beat frequency during a swim. The location of the high frequency peak varied mildly with the change in orientation $\Delta\theta$ during the swim (slope = −0.11, $r_{Pearson} = 0.64$, $p < 10^{-10}$, **Figure 3F**; crosses), but never exceeded 35 Hz. This is much lower than the maximal tail-beat frequency larvae at this stage can employ during other behaviors, e.g., escape [up to ∼80 Hz; (McLean et al., 2008)]. We also noted that the larva approached the prey within a swim by variable amounts, ranging between 0 and 3 mm, with larger distances covered at earlier stages of the sequence (**Figure 3G**). While the tail beat frequency, the number of cycles per swim and the swim duration were relatively constant across all swims, we observed that the HF amplitude_{rms} was strongly correlated with the distance traveled during a swim ($r_{Pearson} = 0.82$, $p < 10^{-10}$;

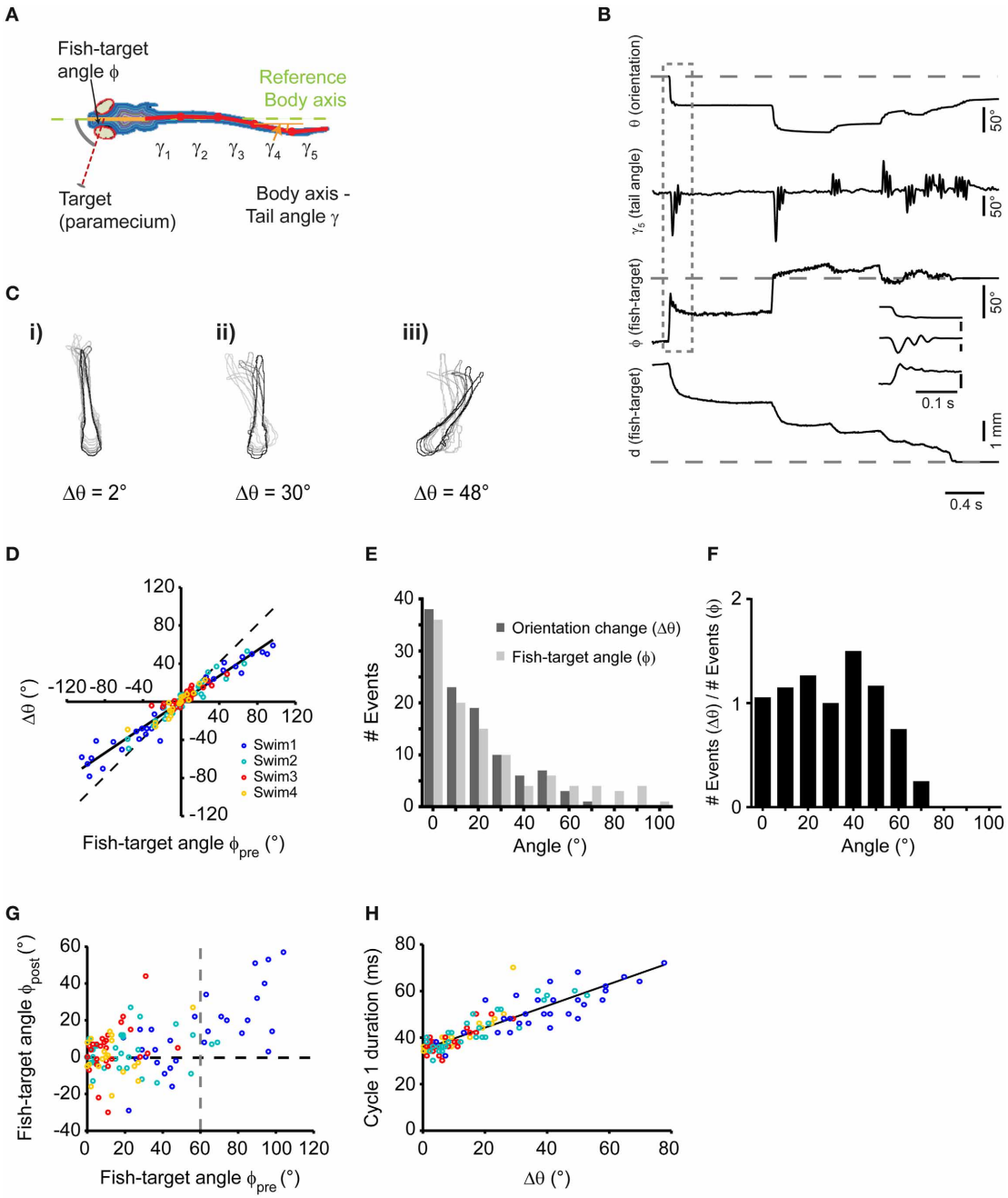

FIGURE 2 | Single swims cover a large angular range, controlled by target position. (A) Illustration depicting automated image processing and parameter extraction from an individual frame. Colored contour lines represent distance map of the fish body. Six segments were used to fit the midline (Solid orange line: head segment; solid red lines: the tail split into five equidistant segments). Broken green line represents body axis with reference to which the deviations of the tail segments ($\gamma_1, \ldots, \gamma_5$) were measured. **(B)** Time course of analyzed parameters for the sequence shown in **Figure 1A** on a frame-by-frame basis. Inset shows a blow up of the first swim bout of the sequence (dashed box). **(C)** Three examples (**i,ii,** and **iii**) of swims associated with change in orientation of 2, 30, and 48°, respectively. Every 10th frame (frame rate: 500/s) of the fish contour is overlaid. Light to dark contours indicate the progress of the swim bout from beginning to end. **(D)** Scatter plot of the change in body orientation ($\Delta\theta$) generated by a swim bout vs. fish-target angle (ϕ_{pre}) preceding the swim. Broken line: unity line; Solid line: straight line fit. **(E)** Histogram of fish-target angle (ϕ_{pre}) and change in orientation ($\Delta\theta$) from the data shown in **(D)**. Data were grouped into 10°-bins (1st bin contains angles from −5 to 5°, 2nd bin contains angles from −5 to −15° and from 5 to 15°, and so on). **(F)** Histogram of the orientation change ($\Delta\theta$), normalized to the occurrence of fish-target angles (ϕ_{pre}) for the data shown in **(D)**. Bin width as in **(E)**. **(G)** Scatter plot of fish-target angle after each swim (ϕ_{post}) vs. fish-target angle before the swim (ϕ_{pre}). Data points with negative fish-target angles (corresponding to prey on left side) were point-reflected about the origin. **(H)** Scatter plot of duration of first cycle in a swim bout vs. the resulting change in orientation. Data points with negative changes in orientation (corresponding to swims toward the left) were mirror-reflected about the y-axis. In **(D), (G),** and **(H)**, data points are color-coded to show the 1st, 2nd, 3rd, and 4th swims during a sequence.

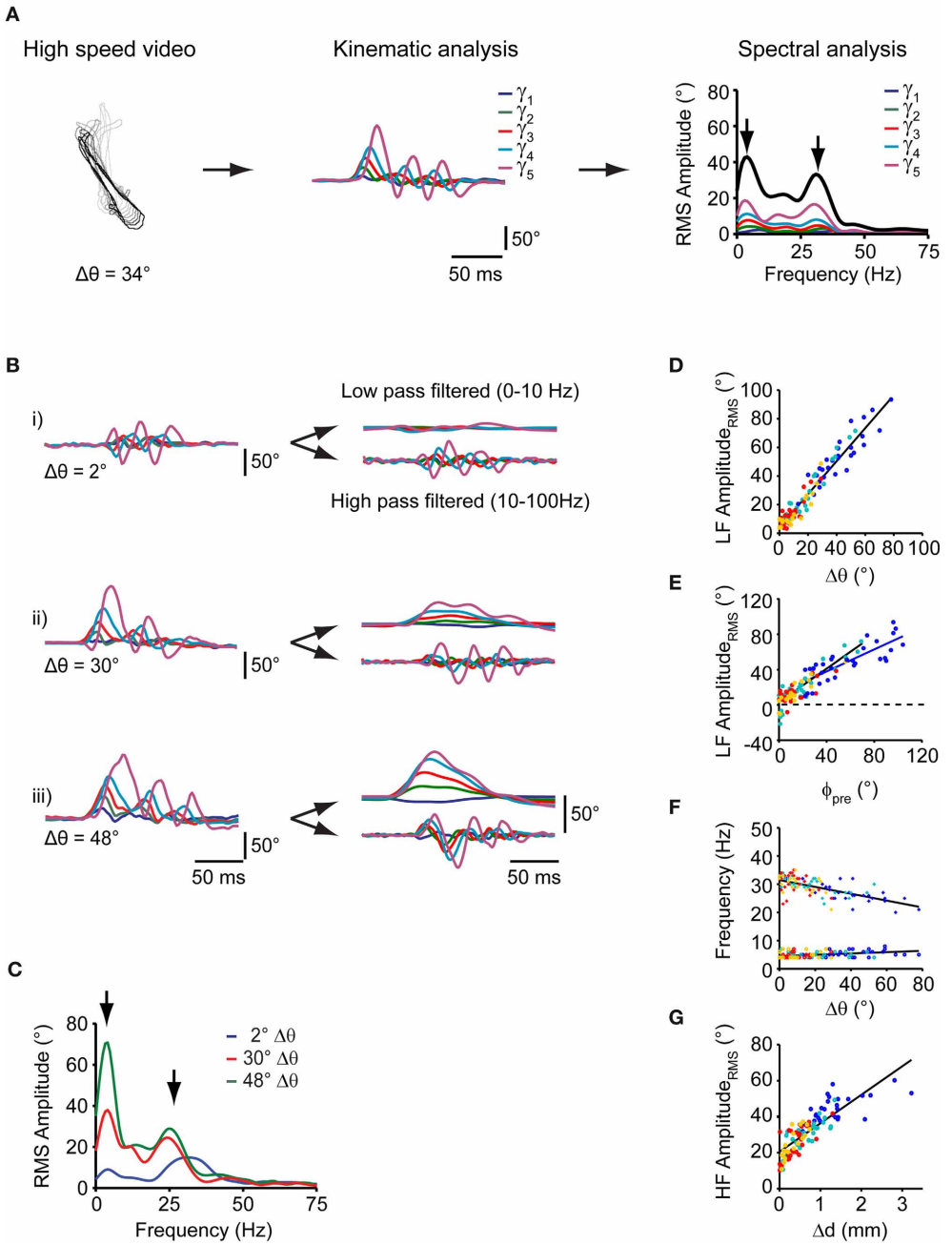

FIGURE 3 | Spectral analysis of individual swim bouts of the freely moving larva during prey capture. (A) Schematic representation of spectral analysis of single swim bouts. Left: fish contours of a swim bout. Center: time course of tail angles ($\gamma_1, \ldots, \gamma_5$) obtained from automated tail angle measurement. Right: Fourier transform of each of the tail angle traces ($\gamma_1, \ldots, \gamma_5$) results in individual RMS amplitude spectra shown in the corresponding color. Sum of these individual spectra is shown as bold black curve. Note two peaks in the spectra (arrows). **(B)** Left: time course of tail angles ($\gamma_1, \ldots, \gamma_5$) for the three swim examples shown in **Figure 2C**. Right: time course of tail angles after low- and high-band-pass filtering. **(C)** Summed RMS amplitude spectra for the three swim bouts shown in **(B)**. Note two peaks in the amplitude spectra (arrows) at frequencies similar to those in (**A**, right panel). The peak at lower frequencies (~4 Hz) scales with change in orientation ($\Delta\theta$). **(D)** Scatter plot of the low-frequency (LF) peak amplitude from spectral analysis vs. change in orientation ($\Delta\theta$). Colors indicate swim bout number (as in **Figure 2**). **(E)** Scatter plot of the low-frequency peak amplitude from spectral analysis vs. fish-target angle (ϕ_{pre}) preceding the swim. Solid lines: straight line fits to the data pairs from first swims (blue) and subsequent swims (black) during a sequence. Note shallower slope for first swims. Same color code as in **(D)**. **(F)** Scatter plot of the location of the high frequency peak (crosses) and low frequency peak (circles) vs. the change in orientation after each swim ($\Delta\theta$). Lines are straight line fits to the data. Same color code as in **(D)**. **(G)** Scatter plot of high-frequency (HF) peak amplitude vs. change in fish-target distance (Δd) after the swim bout. Same color code as in **(D)**.

Figure 3G). This indicates that the fish regulates its forward drive by amplitude modulation during prey capture behavior. Taken together, the relatively constant peaks in the frequency spectrum, the smooth distribution of changes in orientation covering a large range of angles, and the constant number of tail beat cycles suggests that an elementary motor pattern is employed at all stages of the prey capture sequence (other than the capture swim).

VISUALLY EVOKED SWIMS IN RESTRAINED LARVAE MIMIC MOTOR PATTERNS OF THE PREY CAPTURE SEQUENCE

Detailed analysis of prey capture behavior showed that freely moving larvae use an elementary, directionally graded motor pattern that is chained into a sequence in order to approach and catch prey. Next, we tested whether this swim pattern can be evoked in minimally restrained larvae using artificial stimuli in a virtual environment. To create a virtual reality, we positioned the larva with the head in the center of a quartz glass chamber, held in place by a thin collar of agarose at the level of the ear that allowed the larva to move its eyes and tail freely. Using a DLP projector, computer-generated stimuli were projected onto a screen that subtended a horizontal visual angle of $\sim$110° centered around the heading direction of the fish. Visual targets consisted of small white rectangles of various sizes moving with different velocities against a dark structured background. The motor behavior of the fish was recorded using infrared darkfield illumination and high speed video recordings (**Figure 4A**).

First, we sought to identify stimulus conditions that could serve as a trigger to initiate the first swim of a prey capture sequence. We found that small moving rectangles readily evoked short directed swim patterns similar to those observed in the freely moving larva during prey capture (**Figure 4B**). Specifically, we observed both directed swims toward the moving target with small target size as well as avoidance swims directed away from it when the size and velocity of the stimulus were increased, consistent with earlier results in freely moving larvae (Bianco et al., 2011). Notably, target-directed swims were accompanied by contralateral eye convergence, which was a hallmark of first swims in our recordings of prey capture sequences. By contrast, we observed contralateral eye divergence during avoidance swims (**Figure 4C**, left vs. right panel).

Using automatic image analysis, we quantified tail and eye angles in the high-speed video recordings to determine the dependence of motor output on target size and velocity (**Figure 4C**). Summed, single-sided amplitude spectra were computed from tail angles $\gamma_1, \ldots, \gamma_5$ as described above, which showed a low frequency peak at 3.63 ± 0.07 Hz, and a high frequency peak at 26.3 ± 0.26 Hz ($n = 75$ swims), similar to motor patterns during free swimming, for both target-directed and avoidance swims (**Figure 4D**, left vs. right). A direction index (DI) was assigned to each swim, which was the low frequency peak of the amplitude spectrum, multiplied by the sign of the average tail angle integral, so that target-directed and avoidance swims had a positive and negative DI, respectively (Materials and Methods).

During free prey capture, the fish encounters prey objects of different angular sizes and velocities at early and late stages of the sequence (**Figures 1G,H**). We tested 16 pairs of target size and velocity that can occur under realistic conditions of the prey capture sequence (**Figure 4E**). Stimuli were most effective in triggering a first swim in a 60 s stimulus trial when they were small and moved at moderate to high velocity (**Figure 4E,i**, upper left corner), whereas the probability of evoking a swim declined with larger target sizes and lower velocities. Target-directed swims preferentially occurred when the stimulus was small (positive DI; **Figure 4E,ii**, left half), and were accompanied by convergence of the contralateral eye (**Figure 4E,iv**), which supports the notion that first swims of a prey capture sequence were evoked. By contrast, avoidance swims were evoked preferentially by larger targets moving at high velocities (negative DI; **Figure 4E,ii**, upper right corner) and were accompanied by contralateral eye divergence (**Figure 4E,iv**). In both cases the ipsilateral eye exhibited smaller positional changes (**Figure 4E,iii**).

Next, in order to test whether the asymmetric bend component of the tail varied with the fish-target angle in a graded way, we used targets that moved unilaterally in a wider range of [0°, 90°] in one half of the visual field (**Figure 4F**, inset). From single-sided amplitude spectra (not shown), we observed that the spectral amplitude at 4 Hz covaried with the fish-target angle ϕ_{pre}. The slope of a linear fit was 0.5 and the y-intercept was 9.8° (**Figure 4F**, blue straight line), similar to the slope and y-intercept of the same relationship during first swims in freely moving larvae (**Figure 4F**, gray straight line, slope = 0.62, y-intercept = 13.1°). Slope and y-intercept were not statistically different in the two conditions (ANCOVA, $p = 0.45$ and $p = 0.62$ for slope and y-intercept, respectively). This suggests that the fish performed graded, target-directed swims similar to first swims that define the start of prey capture sequences in freely moving animals. On visual inspection, the LF amplitude$_{rms}$ tended to be somewhat smaller in the restrained case, which reflects an overall reduction of tail segment angles during intended turning, and is probably caused by a larger drag force on the tail when the larva's head is held in a fixed position. Finally, the number of tail beat cycles in these swims was 5.82 ± 0.18 and the mean swim duration was 287 ± 9 ms ($n = 39$ swims). This increase in swim duration in the restrained larva is consistent with a prolonged duration of swim bouts observed in the fictive swim preparation (Buss and Drapeau, 2001) and may be caused by the altered sensory (e.g., visual, vestibular, somatosensory) feedback when the larva is partially restrained in agarose. However, it should be noted that the location of the low and high frequency components in the swim spectra of restrained larvae (**Figure 4D**) were very similar to those in the freely moving case, suggesting that the motor patterns observed in the restrained experiments were comparable and also elementary in nature.

VIRTUAL PREY CAPTURE IN A CLOSED-LOOP PROJECTION SYSTEM

Restrained fish performed first swims in response to small projected targets moving at a realistic speed. Next, we intended to close the loop of the virtual reality system to generate an update of the visual world similar to what the fish would experience when orienting during natural prey capture (**Figures 5A,B**). During orienting swims, the change in orientation is accomplished within 1–2 cycles of the tail beat, i.e., in <100 ms (compare **Figure 2B**, inset). Therefore, to implement an update of the visual world

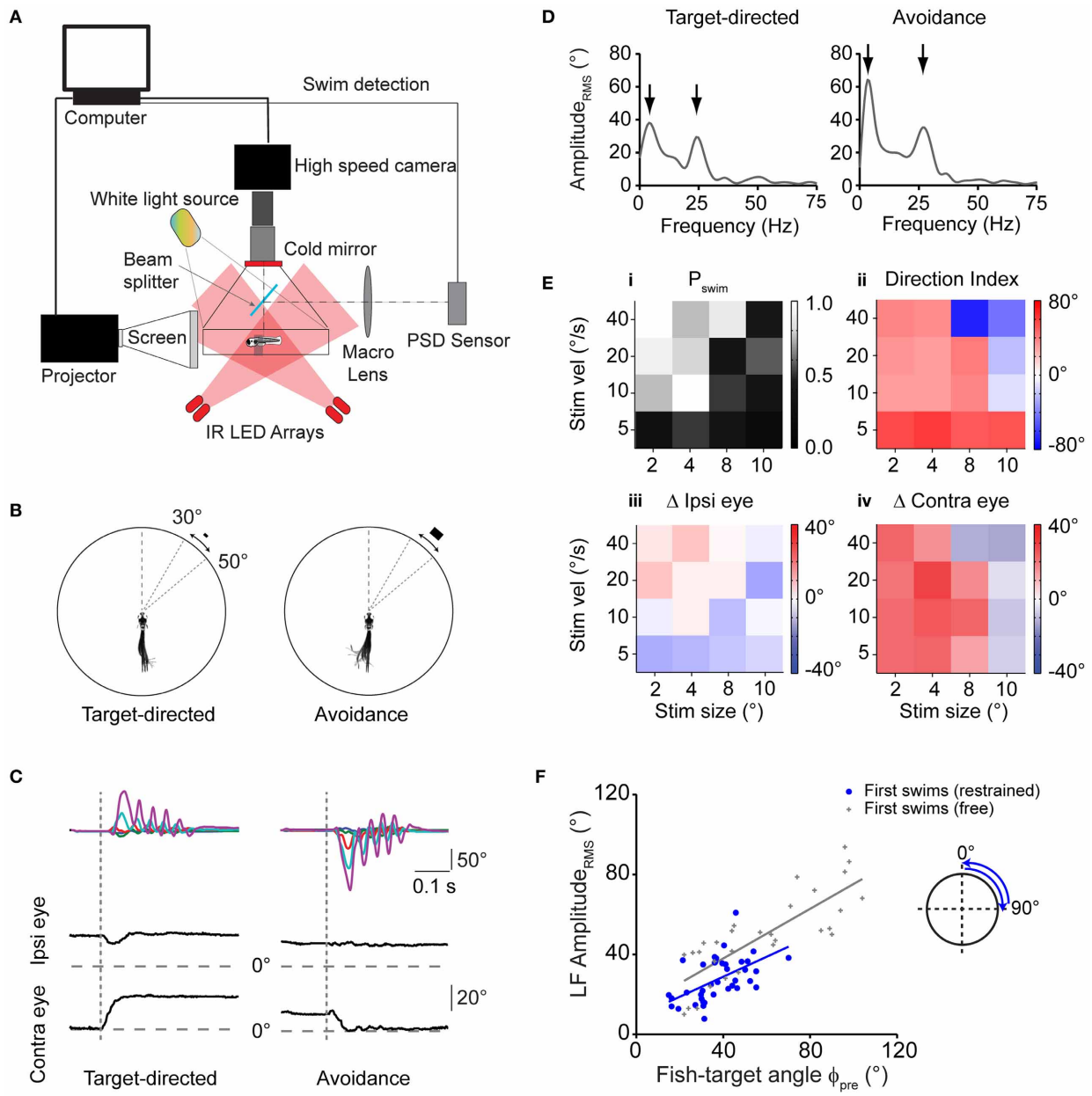

FIGURE 4 | Virtual prey-like stimuli evoke swims similar to motor patterns during prey capture. (A) Illustration depicting the setup used to record swim bouts in response to visual stimuli presented to minimally restrained larvae. A position-sensitive device (PSD, right) is used to detect swims and update the visual stimulus at high speed. **(B)** Left: swim bout toward a rectangular stimulus (width × height: 2 × 1°), moving at 20°/s peripherally between 30 and 50°. Right: swim bout toward the opposite direction of a rectangular stimulus (8 × 4°) moving at 40°/s. Every 10th frame of the high speed movies during the swim bout is overlaid. Angular dimensions drawn to scale. Fish and chamber dimensions not drawn to scale. **(C)** Time course of tail angles and ipsilateral and contralateral eye angles for the examples shown in **(B)** obtained using automated image analysis. Same color code as in **Figure 3A**. Note: high spatial resolution during imaging of restrained larvae allowed automated eye angle analysis. **(D)** Summed RMS amplitude spectra obtained from traces in **(C)** for the target-directed (left) and avoidance swim bout (right). Note two peaks in the spectra (arrows), similar to spectra measured in freely moving larvae during prey capture. **(E)** Summary of motor output in response to 16 different combinations of size and velocity of a moving stimulus. Panel **(i)**: probability of observing a swim bout during a 60 s interval of stimulus presentation. Panel **(ii)**: direction index calculated from LF peaks in the amplitude spectrum, showing target-directed, and avoidance turns (red and blue squares, respectively). Panel **(iii)**: change in position of ipsilateral eye. Positive values indicate rotation to more nasal position. Panel **(iv)**: same as panel **(iii)**, but for contralateral eye. Positive values indicate rotation to more nasal position. In panels **(ii–iv)**, colors indicate mean values ($n = 6$–12 trials for each stimulus parameter pair). Note: for each panel, the value of the target size denotes the width of the stimulus and width:height ratio is always 2:1. **(F)** Scatter plot of the LF peak $\text{amplitude}_{\text{rms}}$ from spectral analysis vs. fish-target angle (ϕ_{pre}) immediately preceding the swim. A trial consisted of the stimulus moving from center to periphery (rostro-caudal) or periphery to center (caudo-rostral), where it disappeared. Stimulus size and velocity 2° and 20°/s, respectively. Blue solid line: straight line fit. Also shown are data pairs (LF peak $\text{amplitude}_{\text{rms}}$; ϕ_{pre}) and straight line fit from first swims in freely moving larvae (gray symbols; same data as in **Figure 3E**).

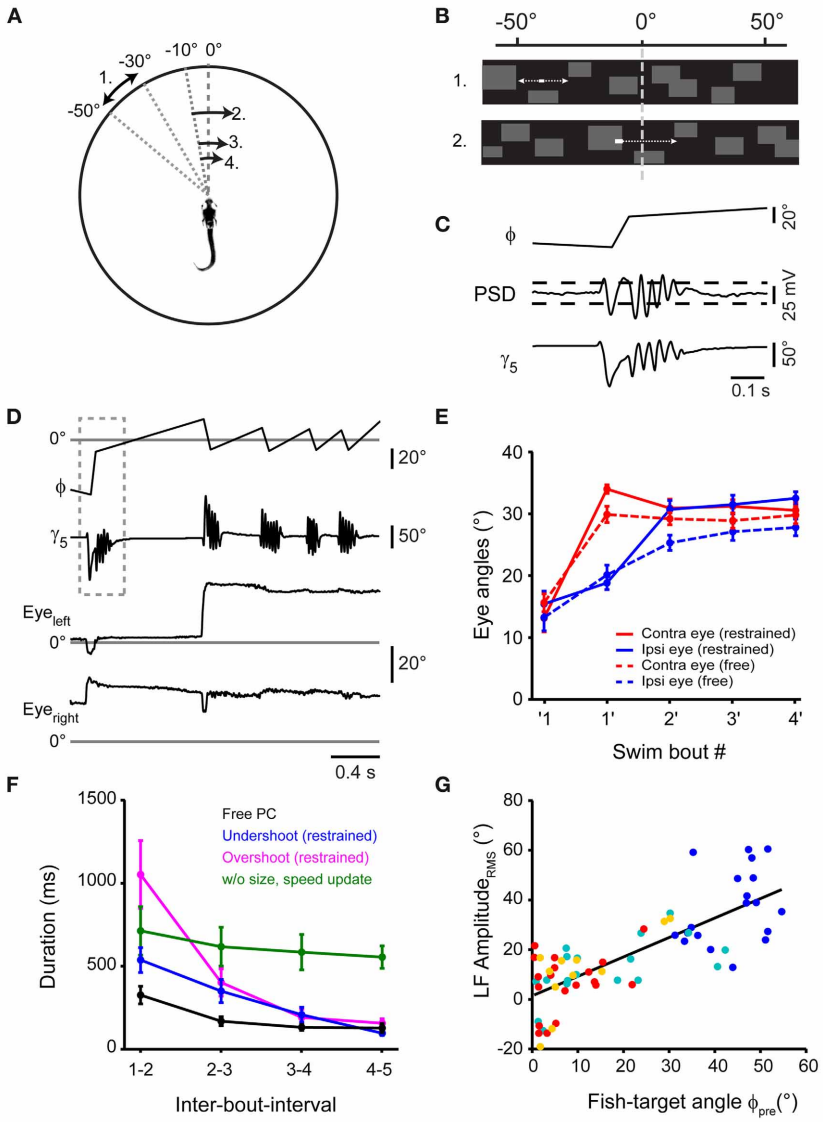

FIGURE 5 | Virtual prey capture behavior in a closed-loop system. **(A)** Illustration depicting the stimulus update paradigm used to evoke prey capture-like swim sequences in minimally restrained larvae. Numbers indicate order of appearance of moving stimulus, arrows indicate direction. Here, following detection of a swim, the stimulus was translated to $-10°$, from where it moved across the midline into the contralateral visual hemifield. Target size and velocity were increased following each swim, emulating an approach of the larva toward the target. This is illustrated by reducing the distance of arrows in the diagram. **(B)** Representation of the stimulus from the perspective of the larva. Initially, a rectangular target moves in the periphery against a background of low spatial frequency content (upper panel). At the onset of a swim bout, target and background translate smoothly toward the visual field center (within $\pm 10°$, update velocity $\sim 400°/s$), emulating a change in orientation of the fish toward the target. Subsequently, the target continues to move against the background (lower panel). **(C)** Detection of swim bouts. Bottom: time course of caudal tail angle γ_5, during a target-directed swim bout. Center: time course of PSD voltage during the swim. Top: fish-target angle (ϕ) before, during, and after the swim bout. Target and background rotation were triggered in real-time by threshold-crossing of the PSD signal (indicated by dashed horizontal lines). **(D)** A swim sequence resembling prey capture sequences in freely moving larvae, recorded in a minimally restrained larva. Top: time course of fish-target angle ϕ. Second from top: caudal tail angle γ_5. Dashed box indicates temporal window shown in **(C)** on an expanded scale. Bottom two traces: left and right eye angle traces. **(E)** Comparison of ipsilateral eye angles ($15.4 \pm 2.1°$ before first swim; $32.5 \pm 1.1°$ after 4th swim) and contralateral eye angles ($13.1 \pm 2.2°$ before first swim; $30.6 \pm 1.3°$ after 4th swim) during sequences in restrained larvae (solid line; $n = 19$ sequences) to eye angles in freely moving larvae (broken line; $n = 30$ sequences). **(F)** Comparison of inter-bout-intervals (IBIs) for different stimulus conditions. Black line: IBIs during prey capture sequences in freely moving larvae ($n = 30$ sequences). Blue line: IBIs during sequences of restrained larvae, where target is translated to $-10°$ during the first swim, representing undershoot ($n = 11$ sequences). Magenta line: IBIs during sequences of restrained larvae, where target is translated to $+10°$ during the first swim, representing overshoot ($n = 8$ sequences). Green line: IBIs during sequences of restrained larvae, where target is translated to $-10°$ during the first swim, representing undershoot, but without increases in stimulus size and velocity throughout the sequence ($n = 6$ sequences). **(G)** Scatter plot of the LF peak amplitude from spectral analysis vs. fish-target angle (ϕ_{pre}) immediately preceding the swim ($n = 19$ sequences). Same color code as in **Figure 2**.

with sufficiently small delays, we equipped the virtual reality setup with a fast, position-sensitive device (PSD) in parallel to the high-speed camera (**Figure 4A**, right arm). Thus, deviations of the tail position during swimming were detected in real time. Threshold-crossing of the PSD signal was used to trigger an update of the visual stimulus in <60 milliseconds following the onset of a swim bout (**Figures 5B,C**). The update consisted of a translation of the visual stimulus and background within 80 ms to a position within ±10° from the central position of the screen, from where the stimulus continued to move toward the periphery against a stationary background (**Figures 5B,C**). The fish often responded to the updated stimulus with a second target-directed swim, which triggered a second stimulus update to ±10° from the center. Typically, three or more swim bouts could be evoked this way in rapid succession, very much resembling prey capture sequences in freely moving larvae (**Figure 5D**; **Movies S3, S4**). Importantly, these evoked sequences were accompanied by a two-step eye convergence pattern during the first and second swim (**Figure 5E**), similar to the natural pattern during free hunting (**Figure 1D**). In order to present realistic stimulus cues, we updated the stimulus size and velocity according to the measured values observed during free prey capture behavior, which could serve as distance cues to the animal. Notably, the IBIs between evoked swims decreased rapidly during the virtual prey capture sequence, similar to the rapid shortening of IBIs during free prey capture sequences (**Figure 5F**). It should be noted that IBIs also depended on the update position after the first swim. When an undershoot in turning was simulated by updating the stimulus to a position of −10° from where it moved across the midline into the hemifield of the contralateral eye (**Figure 5F**, blue line), IBIs were systematically faster than when an overshoot in turning was simulated by updating the stimulus beyond the midline to +10° after the detection of the first swim (**Figure 5F**, magenta line). This indicates that the fish is sensitive to small changes in update location, with a significant slowing of reaction times when the fish virtually overshoots the target. Furthermore, when the size and velocity of the updated moving target were kept constant during a virtual prey capture sequence, resembling a distant moving prey without approach, the fish still performed multiple target-directed swims, albeit with negligible reduction in IBIs (**Figure 5F**, green line). Together, these findings suggest that once the prey capture sequence has started, the stepwise increases of stimulus size and velocity serve as features of a visual feedback signal that may accelerate the programming and execution of subsequent swim bouts.

Finally, we also analyzed the relation between the DI of each swim and the instantaneous fish-target angle ϕ_{pre} before the swim (**Figure 5G**). The DI was correlated with ϕ_{pre} for early and late swims in the evoked swim sequence ($r_{Pearson} = 0.77$, $p < 10^{-10}$), similar to sequences in freely moving larvae. After 4–5 swims, the fish typically stopped responding or performed a long-duration (>500 ms) struggle swim. This suggests that the visual feedback late in the sequence had become inappropriate, which led to a departure from the normal behavioral trajectory. In conclusion, these data show that the classical sequential prey capture behavior can be evoked in a closed-loop virtual environment with fast visual feedback and realistic update of visual target properties.

TIMING OF SEQUENCED SWIMS DEPENDS ON TARGET UPDATE LOCATION

To further delineate the influence of single stimulus properties on the IBIs of second swims, we systematically varied the update location after the first swim in a narrow range around the center of the visual field while keeping update size and velocity constant, (**Figures 6A–C**). The PSD-detected onset of a first swim triggered a translation of the visual target and background to near center positions. The target was maintained at this pre-specified position until the end of the first swim (as estimated from the PSD signal in real time), after which it continued to move into the contralateral field. We observed that small changes in the updated stimulus location had a significant effect on the IBI (**Figure 6D**, One-Way ANOVA for means, $p = 0.0003$). A minimal IBI of 442 ± 33 ms ($n = 6$) was observed when the target was updated to 0°, simulating a perfectly aligned orientation at the end of the first swim. Small deviations in update position ranging between ±10° resulted in significantly longer IBIs (two sample t-test, $p = 0.0055$ and $p = 0.0015$ for 10° undershoot and overshoot, respectively). Based on this observation, we analyzed whether the IBIs between first and second swims during prey capture in freely moving larvae showed a similar dependence on target position after the first swim. In 18 sequences, in which the fish-target angle after the first swim was between −15° and +15°, minimal IBIs were observed for post-swim fish-target angles near 0°, in good agreement with the data from the virtual reality experiment (**Figure 6E**). This suggests that the larva's visual system is remarkably sensitive to the perceived error in turning and can trigger second swims more rapidly when the target is at a central position. Furthermore, the deviation of the target from central position may generate a corrective signal that is used for computing asymmetric turning bias for a second swim, which may require additional processing time.

TIMING OF SEQUENCED SWIMS DEPENDS ON UPDATE DELAYS

The previous experiment showed that the larva proceeds rapidly in the motor sequence when the first swim brings the target into a central position. This could mean that a window of expectation is opened, which enables the larva to perform accelerated swims if expected and true target position overlap. To measure the time course of this window, we programmed the stimulus to appear at the optimal target position of 0°, but varied the update to occur with a delay between 100 and 500 ms after the onset of the first swim (**Figures 7A–D**). This stimulus paradigm resulted in sweeps in which the stimulus reappeared and moved either shortly before or after the end of the swim, resulting in negative or positive delay values (Δt), respectively. Notably, we observed that the IBIs were minimal when the stimulus reappeared around the end of the swim (**Figures 7C,E**). By contrast, when the stimulus returned earlier or later, longer IBIs were observed (**Figures 7B,D,E**). We also determined the reaction time, which exhibited a minimum for delay values around the end of the swim as well (**Figure 7F**). Notably, when comparing trials in which $\Delta t < -50$ ms, the reaction time was significantly longer than in those trials where the stimulus appeared at the end of the swim (within Δt ±50 ms, two-sample t-test, $p < 10^{-5}$). This suggests that the larva is less sensitive to visual

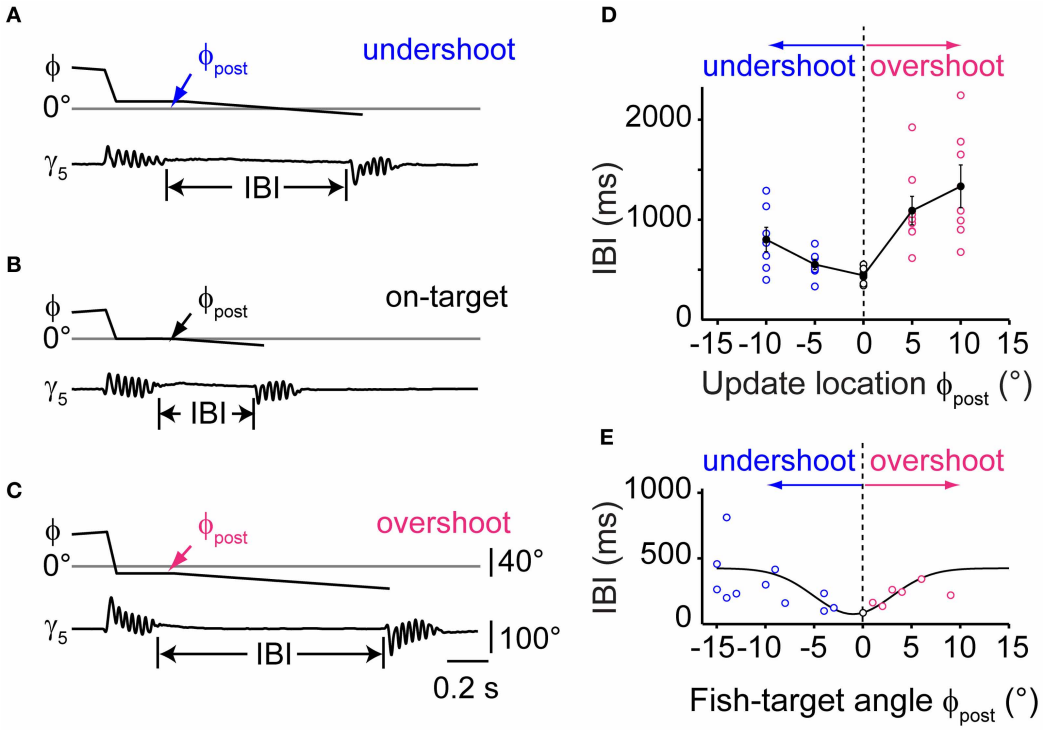

FIGURE 6 | Timing of sequenced swim bouts depends on updated stimulus location. (A) Time course of fish-target angle ϕ and caudal tail angle γ_5 during a pair of swim bouts evoked by a moving target in a restrained larva. First swim was directed toward a stimulus moving in the periphery (35–55°). Onset of the first swim triggered a translation of stimulus/background stopping short 10° from the midline, simulating an undershoot in turning. The end of the first swim triggered stimulus motion at constant velocity toward the contralateral hemifield, evoking a second, target-directed swim. Inter-bout-interval (IBI) indicated by vertical lines. **(B)** Same as in panel **(A)**, but with the stimulus/background translated to the center of the visual field (0°) during the first swim, simulating exact alignment of the larva with the location of prey ("on-target"). Note that the IBI is considerably shorter. **(C)** Same as in panel **(A)**, but with the stimulus/background translated beyond the center of the visual field by 10° during the first swim, simulating an overshoot in turning. **(D)** Dependence of IBIs on the update location of the stimulus during the first swim bout. Trials with initial stimulus position on the left or right side were interspersed and pooled. Negative values of update location represent an undershoot; positive values an overshoot during the first swim. Data from $n = 6$ fish. **(E)** Data from recordings of freely moving larvae performing prey capture sequences. Scatter plot of IBIs between first and second swim bout in which the fish-target angle ϕ_{post} (measured at the end of the first swim) varied between ±15°. Negative values correspond to an undershoot, positive values to an overshoot in turning. Note the minimum in IBIs for small turning error near $\phi_{post} = 0°$. Solid line is a Gaussian fit curve.

feedback while swimming. Similarly, when the second stimulus was presented only ~100 ms after the end of the first swim (**Figures 7D–F**), reaction times increased again, indicating that the window of expected stimulus processing closes shortly after the swim.

We also tested whether increasing the size and velocity of the second stimulus could further reduce this minimal reaction time. With a second stimulus of larger size and velocity (3°, 30°/s), we observed second responses with a reaction time of 318 ± 47 ms ($n = 14$ trials; **Figure 7G**). This was significantly faster than the reaction time observed with second stimuli at unchanged size and velocity (622 ± 60 ms; two sample t-test, $p = 0.0006$, averaged for trials with Δt within ±100 ms). The duration of the first swims for the two differing update conditions was not significantly different (two sample t-test, $p = 0.21$). Hence, the shortening in reaction time can be attributed to the change in size and velocity of the stimulus. In conclusion, larval zebrafish showed variable IBIs and reaction times between the first and second swim of a virtual prey capture sequence, with a minimal IBI when the stimulus reappeared after a simulated turn near 0° at the end of the first swim. This lends support to the notion that during hunting, the larva uses visual feedback in-between swims to compare the observed location with an expected target position, which enables the larvae to perform more rapidly if predicted and observed target positions agree in space and time.

DISCUSSION

Here, we present a quantitative description of prey capture behavior with respect to several visual stimulus parameters and behavioral output. Quantitative analysis of fish-target angles preceding a swim bout and change in orientation after the swim bout showed that there is a graded relationship between visual input and motor output (**Figure 2**). We further quantified the kinematics of each of these bouts using spectral analysis to show that a graded continuum of seemingly different swim patterns can be produced by modulating one elementary motor pattern. In order to test the boundary conditions for input space under which prey capture sequences are observed, we developed a closed-loop

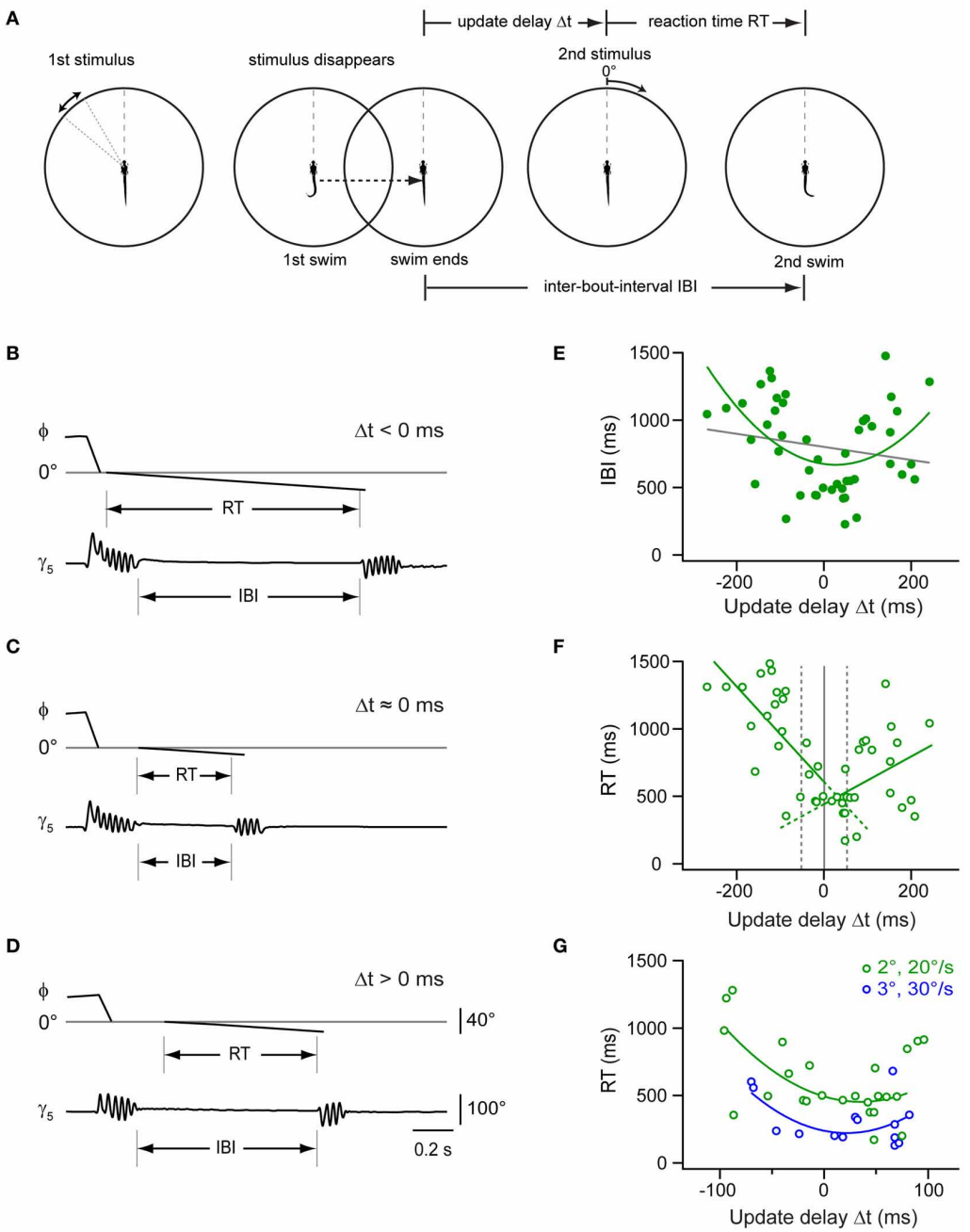

FIGURE 7 | Impact of stimulus timing on inter-bout-intervals and reaction times in a two-step stimulus paradigm. (A) Schematic of a two-step stimulus paradigm with variable delay. First stimulus is a target moving in the periphery (35–55°; left panel), which eventually triggers a target-directed swim (second panel). Stimulus and background translate to center (0°), and the stimulus disappears. After a variable delay, the target reappears at the center and moves toward the periphery at constant size and speed (2°; 20°/s; 3rd panel), until the larva performs a second directed swim, which ends the trial (right panel). Update delays (Δt) and inter-bout-intervals (IBI) are measured relative to the end of the first swim, reaction time (RT) is measured from onset of second stimulus. **(B)** Time course of fish-target angle ϕ and caudal tail angle γ_5 during paired swim bouts evoked by the two-step stimulus paradigm. The second stimulus appeared before the end of the first swim, corresponding to a $\Delta t < 0$ ms. Note long IBI. **(C)** Same as in **(B)**, but with second stimulus appearing near end of first swim ($\Delta t \approx 0$ ms). Note short IBI. **(D)** Same as in **(B)**, but with second stimulus appearing after end of first swim ($\Delta t > 0$ ms). Note longer IBI. Scale bars apply to panel **(B–D)**. **(E)** Scatter plot of IBIs vs. update delay (Δt). Gray line: straight line fit ($r_{Pearson} = 0.18$). Green curve: second order polynomial fit to the data ($r = 0.46$). Note minimum near $\Delta t \approx 0$ ms ($n = 47$ trials from 13 fish). **(F)** Scatter plot of reaction times (RT) vs. update delays (Δt). Green lines: straight line fits to data points with negative and positive update delays (Δt), respectively ($n = 47$ trials from 13 fish). Broken gray lines represent three different delay groups i.e., $\Delta t < -50$ ms, -50 ms $< \Delta t <$ 50ms, and $\Delta t >$ 50 ms. **(G)** Scatter plot of RT values vs. update delays (Δt) on an expanded time scale (–100 to 100 ms). Reaction times are shorter when the second stimulus is larger and faster (3°; 30°/s; $n = 14$ trials from 5 fish; blue symbols) than under control conditions [2°; 20°/s; green symbols, same as in panel **(F)**]. Blue and green curves are second order polynomial fits to data points measured under the two conditions, respectively.

visual environment that is feedback driven by the larval motor output. By deriving a combination of stimulus parameters from naturally occurring prey capture, we elicited behavioral sequences in restrained larvae using virtual prey stimuli. Such visually guided behavioral sequences were very similar to prey capture in freely moving larvae with respect to spectral components of individual swim bouts as well as in the monotonically decreasing inter-bout intervals. By taking advantage of the precise control over stimulus parameters and visual feedback, we manipulated the timing, location, size, and velocity of the stimulus following the detection of a swim bout. This allowed us to probe how visual feedback could influence the timing between two swims.

ELEMENTARY MOTOR PATTERN DURING PREY CAPTURE SEQUENCES

The discrete swim bouts during prey capture sequences (except for the final capture swim) appear to be versions of an elementary motor pattern, modulated on a graded scale by an asymmetric turning component. The notion that only one basic motor pattern is modulated and chained into a sequence is supported by our observation that early and late swim bouts in the sequence employed a rather constant tail beat frequency of ∼30 Hz, which did not appreciably vary with change in orientation. Also, swim bouts at all turning angles exhibited a constant number of cycles per swim. Finally, we observed that this basic swim pattern enabled the larva to turn on a graded scale within a range between 0° and ∼60°, and that turning angles were distributed continuously within this range (**Figures 2D–F**). This may represent a departure from the notion that larval zebrafish use different classes of motor patterns during prey capture, such as "slow swims" for forward swimming and "J-turns" for orienting swims (McElligott and O'Malley, 2005; Bianco et al., 2011). Instead, the motor pattern may consist of a basic burst-like tail beat component, symmetrically oscillating at ∼30 Hz and terminated after ∼150 ms. Onto this basic pattern, a slower, asymmetric turning component may be superimposed, which biases the bending of the tail toward the desired side of turning. The turning component appears to be freely adjustable within a large angular range, and controlled by the angular position of the prey (**Figures 2D** and **3E**).

What could be the organization of the neural commands underlying such a directionally graded, but temporally rather uniform motor pattern during prey capture? Based on the stereotypical dynamics of the basic motor pattern, we hypothesize that a symmetric command component (S) from a subset of descending reticulospinal (RS) neurons serves as a trigger to initiate a swim bout, whose frequency is set by the characteristic frequency of pattern generator modules in the spinal cord (Grillner et al., 1991; Wiggin et al., 2012). This signal may be symmetrically distributed about the midline of the RS system; currently, it is unclear which RS cells in the zebrafish hindbrain may be involved in carrying such a bilateral signal. By contrast, a second command component (A) may be asymmetrically distributed in descending RS neurons, which could evoke more tonic muscle recruitment on the turning side to drive unilateral tail displacement. It is unclear whether this asymmetric component (A) is carried by the same descending RS neurons that also mediate the swim initiation command (S) or by different RS neurons. It has been shown that activity in specific RS cell types, such as MiV cells, correlates with change in orientation during the optomotor response (Orger et al., 2008). This, together with the large number of descending RS neurons suggests that the S-component and the A-component could be assigned to different RS cell types also during prey capture. Furthermore, it is not known whether this elementary swim pattern is actively terminated or whether its duration reflects the intrinsic decay of activity in a damped oscillator circuit (Wyart et al., 2009). We observed that swim bouts in restrained larvae were longer than those observed during freely moving behavior. This suggests that the duration of elementary swim patterns may be controlled by the duration of descending command signals, which has been observed for longer swim episodes in lamprey (Deliagina et al., 2000). The duration of such descending "gate" signals that drive swimming, or alternatively, the timing of a descending "stop" signal that could terminate a swim (Roberts et al., 2008), may in turn be controlled by visual or non-visual sensory feedback due to the self-motion during the swim, which is lacking in the restrained larva, and could therefore explain the difference in swim duration.

Looking upstream, we may ask what neural mechanisms may generate the trigger/gating component (S) and the position component (A) of the command signals for this elementary motor pattern. Earlier loss-of-function experiments using laser ablation have shown that the tectum is essential for directed turning and successful prey capture in larval zebrafish (Gahtan et al., 2005). Furthermore, bulk-loading and stochastic single-cell labeling techniques demonstrated the presence of direct ipsi- and contralateral projections from the tectum to the ventral neuropil of the hindbrain, where descending RS neurons could receive direct synaptic input via their ventral dendrites (Metcalfe et al., 1986; Sato et al., 2007; Robles et al., 2011). On a functional level, Ca^{2+} imaging in the tectum demonstrated a retinotopic map of visual space onto the tectal cell population both for artificial stimuli and for natural prey objects (Niell and Smith, 2005; Muto et al., 2013). Taken together, these findings corroborate the notion that the angular position of the targeted prey is encoded in the location of activity in the retinorecipient layers of the tectal neuropil. Tectal location of activity, in turn, is thought to be transformed into a rate-coded motor command signal at the level of brainstem command neurons (Scudder et al., 2002). Experiments using electrical stimulation of the tectum in goldfish showed that stimulus location correlates with the evoked tail bend amplitude, consistent with this model (Herrero et al., 1998). It has been suggested that projection neurons from rostral and caudal regions of the tectum may form synapses onto command neurons in the reticular formation with increasing synaptic weights, which could explain this transformation of location of activity into firing rate (Moschovakis et al., 1998; Groh, 2001). To test this model in zebrafish, it will be important to investigate whether projection neurons from rostral and caudal regions of the tectum drive activity in the same set of RS neurons with different synaptic efficacies.

MULTISTEP SEQUENCES AND VISUAL FEEDBACK

In freely moving larvae, we observed a characteristic two-step eye convergence pattern during the first two directed swims toward

the prey. This two-step convergence pattern was also observed during closed-loop visual stimulation in our virtual reality prey capture assay. While this is generally consistent with the recent proposal that eye convergence is associated with the first swim bout of the capture sequence, we did not observe that convergence movements rotate both eyes symmetrically to the nasal limit of the oculomotor range within a single swim (Bianco et al., 2011). Rather, the ipsilateral eye converged only partially during the first swim, with weaker convergence typically occurring during large angle turns. This suggests that convergence of the two eyes can be controlled independently. During the first swim, the ipsilateral eye position may depend on the combination of a divergence signal, which scales with the asymmetric turning command component, and a competing convergence signal, which drives the eye toward its nasal limit. A possible reason for the different observations in eye convergence may lie in the different experimental conditions, e.g. the high density of paramecia used in the earlier assay (>200 paramecia per dish, Bianco et al., 2011), compared to a single paramecium in our assay. This can also explain the different average distances of targeted prey at the onset of the sequence (3.8 mm in our assay vs. 1.55 mm in the earlier study). In a high density assay, the larva is likely to simultaneously encounter multiple prey objects within its visual range and may tend to perform low-angle swims to the target nearest to its heading direction.

The prominent burst-and-pause swim pattern employed by the larva during prey capture falls into the class of intermittent locomotor behaviors. This sample/move strategy is employed during pursuit behavior by various species such as flies (Boeddeker and Egelhaaf, 2005), lizards (Avery et al., 1987), and toads (Lock and Collett, 1979; Ewert, 1987) and can be compared to saccadic eye movements during visual search in the primate (Land, 1992, 1999; Schall and Thompson, 1999). It has been generally reasoned that this mode of locomotion may be ecologically advantageous to enable short-lasting states of intermittent rest, during which prey or predatory objects may be detected more reliably due to the lack of sensory input generated by self-motion [reviewed in Kramer and McLaughlin (2001)]. We observed that prey capture sequences performed by larval zebrafish consisted of an elementary swim pattern, separated by IBIs of decreasing duration (**Figure 1**). This is consistent with the relatively short interval observed between individual prey capture-related swim bouts (McElligott and O'Malley, 2005), and contrasts with the relatively long IBIs between routine swims in the absence of prey (Fuiman and Webb, 1988). Importantly, closed-loop experiments in which the larva was challenged with variable stimulus properties in between swims showed that the IBIs, and therefore reaction times, critically depended on position, size, and velocity of the updated target (**Figures 5**, **6**). When approach was simulated by successively increasing target size and velocity after each swim [e.g. to (8°, 50°/s) after the 3rd swim], IBIs monotonically decreased between target-directed swims. By contrast, stimuli of comparable size and velocity (e.g., 8°, 40°/s) in isolation evoked avoidance swims directed away from the target when the larva was not in "prey capture mode" as judged by an unconverged eye position (**Figure 4E**). This suggests that the visuomotor system may transition into an internal state that facilitates prey capture behavior, during which visual feedback guides the sequence of target-directed motor patterns in rapid succession.

When is this visual feedback used to program the next discrete motor pattern in a sequence? Variable delay experiments in which the reappearance of the visual stimulus was timed to occur before, near or after the end of a swim revealed that the larva responded most rapidly to stimuli coinciding with swim termination. Notably, stimuli appearing before the end of the swim evoked a second swim with longer latencies, suggesting that the visuomotor system is less sensitive to visual feedback during execution of a swim bout. This could represent a form of movement-induced suppression of input processing, which has been observed in prey capture behavior, e.g., in the toad (Lock and Collett, 1979). In the primate visuomotor system, eye movement-induced "saccadic suppression" has been explained with a combination of corollary discharge and a forward visual masking mechanism (Wurtz, 2008). Functional experiments in the zebrafish may help to elucidate the neural substrates and mechanisms of a possible swim-induced suppression of visual processing during intermittent prey capture behavior.

Finally, we also observed that not only the timing of the visual feedback, but also its position had a significant effect on reaction times. A minimum of latencies was observed when the updated stimulus position was "head-on," simulating a perfect alignment of the larva with the prey (**Figure 6D**). A qualitatively similar minimum of IBIs was also observed in the freely moving larvae (**Figure 6E**). This suggests that the larva is able to execute components of the prey capture sequence more rapidly when expected and perceived target positions overlap. Because this target-aligned configuration only occurs after the prey capture sequence has been initiated, when the target is centered in the binocular field of view, we speculate that a specific bilateral distribution of activity exists in the anterior-most region of the two tectal hemispheres that may trigger forward swims with minimal delay. By contrast, off-axis alignment of the prey during the sequence may require more processing time to program an asymmetric command component (A) in addition to the symmetric forward component (S) before the next swim is generated. The virtual reality techniques developed here may enable experiments using functional Ca^{2+} imaging and multiphoton-targeted patch-clamp recordings (Gabriel et al., 2012) to investigate the spatio-temporal distribution of activity underlying this complex form of visually guided behavior.

MATERIALS AND METHODS

ZEBRAFISH MAINTENANCE

Zebrafish maintenance and breedings were carried out under standard conditions (Westerfield, 2007). Fertilized eggs were raised in embryo medium at 27°C under a 14/10 h light/dark cycle. Wildtype zebrafish larvae (ABTL) and *nacre* mutants (Lister et al., 1999) (6–8 days post-fertilization, dpf) were used. All procedures were performed according to the guidelines of the German animal welfare law and approved by the local administration.

FREELY MOVING LARVAE

Larvae were pre-selected based on whether they successfully performed prey capture sequences in the presence of paramecia during a ∼5 min observation period under the dissection microscope. Selected larvae were transferred to a small arena (diameter 16 mm, height 5 mm) with opaque walls and a transparent bottom, filled with embryo medium to a height of 3–4 mm, to which a single paramecium was added. The chamber was illuminated from the top with white light using a goose neck lamp. Three arrays of infra-red LEDs (Kingbright, BLO-106) were mounted at a 45°-angle underneath the chamber to enable recording of the fish and paramecium under dark-field illumination. Prey capture sequences were recorded using a high-speed camera (AOS Imaging Systems, Model S-PRI 1039). A cold mirror was used to block visible light from the camera. Sequences were recorded at 250 or 500 frames/s. Recordings in which the larva or the prey touched the wall immediately before, during or after a prey capture sequence were discarded. All experiments were performed at room temperature, and bath temperature was observed to increase by no more than 2.5°C within 2 h.

PARTIALLY RESTRAINED LARVAE

Larvae were preselected as described above. Selected larvae were anesthetized using 0.02% MS-222 in embryo medium for 5 min. The anesthetized larva was embedded in low-melting point agarose (4%) dorsal side up in the center of a quartz glass chamber (diameter 40 mm, height 25 mm, Hilgenberg, Germany), filled with a Sylgard base (∼15 mm in height). After the agarose had set, the chamber was filled with embryo medium. Agarose around the head and tail was carefully removed using a scalpel, leaving only a thin collar surrounding the ear and the swim bladder. This allowed the larva to perform eye and tail movements. A diffusive material (E-color #216, Rosco, CA, USA) was attached to the outer wall of the chamber as a projection screen. Larvae were allowed to adapt to ambient light and embedding conditions for 15–30 min. After this period, the animal was monitored for spontaneous saccades and swim activity. Also, moving dot stimuli were shown to test the responsiveness of the animal. Larvae that did not respond with occasional directed swims or showed struggling behavior repeatedly in a ∼30 min period were not used further. All recordings of motor activity in restrained larvae were performed at 500 frames/s.

VISUAL STIMULATION

Visual stimuli were generated using custom-written programs in the Python based OpenGL VisionEgg software (Straw, 2008). Stimuli were projected onto the screen using a microprojector (Optoma Pico PK-102) at a refresh rate of 60 Hz. The visual scene consisted of a low spatial frequency surround of randomly positioned gray rectangles against a black background (nominal contrast ratio 16%). Small, rectangular targets (aspect ratio 2:1) moved against this stationary background at maximal contrast ("white"; gray level 255). Following swim detection (see below), the target and background moved synchronously at a pre-specified angular velocity (∼400°/s) to a new angular position, to emulate retinal slip and the rotation of visual surround during an orienting turn of the larva. Subsequently the target resumed movement against the stationary background, depending on stimulus paradigm (see below).

Swimming and eye movements were recorded continuously at 500 frames/s during presentation of the moving target ("stimulus trial"), which was aborted after 56 s, if no response was observed. In order to control the stimulus in real time, the tail of the larva was projected onto a PSD (SiTek, 2L4-CP5) through a biconvex lens ($f = 70$ mm) via a 50/50 beam splitter in the acquisition path. Tail movement generated an oscillating signal in the PSD, which was sampled at 1 kHz (PCI-6259 board, National Instruments) and analyzed in real-time to detect the beginning and end of a swim bout. Threshold-crossing of the PSD-signal triggered the translation of the target and background to a prespecified update location within ±10° of the visual field center. Stimulus presentation, high-speed video recording and acquisition of the PSD signal were synchronized using a common trigger signal. Using this system, updates of target and background could be implemented with an intrinsic delay of ∼30–50 ms after the detection of a swim bout. Data acquisition and real-time updates of visual stimuli were controlled automatically by custom-written programs in LabVIEW.

STIMULUS PARADIGMS

Optimization of prey-like stimulus

To test the effectiveness of small moving targets in triggering directed swims, we varied the size and velocity of the rectangular target, moving peripherally in the 30–50° range. Sixteen pairs of target size and velocity were chosen in the range 2–10° and 5–40°/s, respectively, similar to values measured during free prey capture sequences. Stimulus targets were shown randomly on the left or right side of the larva. During the experiment, the fish was observed to assume apparently different states. A state of prolonged rest was often followed by a state during which the larva performed periodic spontaneous saccades. Also, in some cases, struggle movements were observed that were followed by a prolonged resting state, lasting several minutes. Target-directed swim bouts were rarely observed following struggle swims or during the resting state. Therefore, trials were initiated during the state of spontaneous saccadic activity. A trial ended when the fish performed a swim bout or after 56 s, if no swim occurred. The response probability for different stimulus sizes and velocities was calculated for trials initiated under these conditions (**Figure 4E**).

Sequences of prey-like stimuli

To elicit motor sequences, first swims were evoked using a prey-like stimulus (2°; 20°/s) moving in the monocular visual field either between 30° and 50° or between 35° and 55° (interspersed trials on left or right side). Closed-loop visual feedback was implemented by translating the stimulus and background rapidly triggered by the detection of a swim bout. After stimulus/background translation, the stimulus resumed movement at a prespecified size and velocity toward the contralateral side of the visual field, which typically evoked another directed swim bout and eye convergence. Sequences of up to 6 target-directed swim bouts could be evoked by this method.

Kinematic analysis from high-speed video recordings

Automated image analysis of high speed movies was performed using custom written algorithms in LabVIEW and manual measurements on frames were performed in ImageJ.

Image analysis (Free larvae)

High-speed recordings of freely moving larvae were saved as 8-bit grayscale movies and processed *post-hoc* to extract parametric information. First, a background image was subtracted from the movie, which highlighted the larva and the paramecium. Next, the 8-bit frames were scaled by histogram-equalization and converted to binary images using thresholding. Subsequently, binary morphological operations were performed that rejected small objects or those that touched the border of the image, and filled holes in binary objects. As a result, only the larva was visible as a binary object in each frame. Next, movie frames were automatically rotated such that the long axis of the larval binary object was aligned with the initial heading of the fish. Then, the binary object was converted to a distance map using the Danielsson distance mapping algorithm to reconstruct the midline of the larva. The distance map shows the distance of each pixel in a binary object to the nearest background pixel. The midline was reconstructed starting from the maximum pixel in the distance map, which is located near the center of the head. The positions of the maximum pixel in each image column were located iteratively toward the snout and tail and connected to obtain the midline of the larva. Next, the midline shape was approximated using a fit of six connected straight lines. The first segment was fit to the midline of the head (which was measured between the snout and the swim bladder). The remaining midline was fit using five line segments of equal length. Orientation of the fish (θ) was measured as the angle of the head segment of the midline in a global reference frame. Tail movement during swim bouts was quantified as the angle ($\gamma_1, \ldots, \gamma_5$) between the individual tail segments and the body axis (defined as the heading direction of the first segment).

To track the position of the paramecium, the same morphological operations were performed on the binary movie, but with a processing step that rejected large objects, leaving the paramecium as the only object. After manual selection of the paramecium in the first frame, the algorithm tracked its trajectory automatically for all subsequent frames. Furthermore, the fish-target angle (ϕ) and the fish-target distance (d) (i.e., the distance between the center of the head segment and the centroid of the paramecium) were measured on a frame-by-frame basis in which the binary images of the fish and the paramecium were overlaid. The distance traveled during a swim bout was calculated as the difference between the fish-target distance before and after the swim.

High-speed recordings of freely moving larvae covered a larger field of view, which precluded an automatic analysis of kinematic parameters of small details. Therefore, we manually measured ipsilateral and contralateral eye angles with respect to the body axis in individual frames before and after a swim bout. Also, angular size and angular velocity of the prey in the interval between two swims were manually determined by measurements in individual frames. We also manually measured fish-target angle in the frames before and after a swim bout as well as change in orientation to corroborate our automated analysis.

Image analysis (Restrained larvae)

For minimally restrained larvae, we could use the image analysis algorithm designed for freely moving larva after minor modifications. Since there was no reference frame for background subtraction, we used a linear remapping of the histogram to reduce background pixel values and increase fish pixel values. The linear remapping factor was adjusted empirically for each experiment. Subsequently, the gray scale image was binarized using fixed threshold values. Binary morphological operations identical to the ones mentioned earlier were performed to ensure that the image consisted of one object i.e., the larva. Distance mapping and midline extraction procedures were also the same as described above.

In addition to the tail segment angles ($\gamma_1, \ldots, \gamma_5$), the algorithm also measured ipsilateral and contralateral eye angles automatically for restrained larvae. The algorithm prompted the user to draw a region of interest around the head which included both eyes. This region of interest was then extracted and an adaptive negative thresholding subroutine was used to detect the two eyes. Subsequently, binary morphological operations were performed and two binary objects were obtained. Each eye was fitted with an ellipse and the angle between the major axis of the ellipse and the body axis of the fish was recorded as the eye angle.

Fourier analysis of swim bouts

In order to investigate the frequency composition for each swim bout, we performed discrete Fourier analysis using a temporal window around the swim traces. The length of this window was set to 150 ms for freely moving larva and 300 ms for restrained larva. A Bessel band-pass filter was then applied to the extracted individual waveforms, each containing deviations of one of the five tail segments with respect to the body axis ($\gamma_1, \ldots, \gamma_5$). The low cut-off frequency of the filter was set to 0.5 Hz to eliminate the effect of a slow drift in the tail that is often observed following swim bouts. The high cut-off frequency of the filter was set to 100 Hz to eliminate high frequency noise that may result from frame-to-frame jitter in tail angle measurements. A discrete Fourier transform (DFT) was then applied to these filtered waveforms. A DFT operation on a time series resulted in a two-sided complex spectrum. This spectrum was then converted to a two-sided amplitude spectrum.

$$X_k = \sum_{n=0}^{N-1} x_n \cdot e^{-i2\pi n \frac{k}{N}}, \text{ where } k = 0, 1, 2, \ldots, N-1$$

(Discrete Fourier Transform)

$$A_k = \frac{X_k}{N}, \text{ where } k = 0, 1, 2, \ldots, N-1$$

(Two-sided complex spectrum)

Since the DFT spectrum is conjugate symmetric, this two-sided spectrum was then converted to a single-sided spectrum by using the first ($N/2$–1) components.

$B_k = A_0$, for $k = 0$ else,

$$B_k = \sqrt{2} \cdot A_k, \text{ for } k = 1, 2, \ldots N/2 - 1$$
(Single-sided RMS spectrum)

The magnitude of this complex single-sided RMS spectrum was used to obtain an RMS amplitude spectrum.

$$B_{mag} = |B_k|, \text{(Magnitude for the RMS spectrum)}$$

This resulted in a single-sided amplitude spectrum for each individual tail segment. Subsequently, we summed these individual spectra to obtain one spectrum for each swim. Since the frequency resolution for a spectrum is limited by the sampling frequency and the Nyquist criterion, we used a spline interpolation algorithm to improve our estimate of the magnitude at different frequencies in the spectrum. Further, to assign directionality to each swim, the temporal traces of all five tail angles $\gamma_1, \ldots, \gamma_5$ were averaged and subsequently integrated. The sign of this integral was subsequently multiplied with the amplitude of the low frequency peak in the sum spectrum to obtain a "DI" for each swim.

$DI = sign\left[\int_0^t dt \frac{1}{5}\sum_{i=1}^{5}\gamma_i(t)\right] \times \frac{1}{3}\sum_{k=3}^{5} B_{mag_k}$, where γ_i is the angle for ith tail segment and B_{mag} is the value of the sum spectrum at kth frequency, here yielding an average peak amplitude between 3 and 5 Hz. Spectral analysis and the computation of directional index was performed using Labview8.6 (National Instruments).

ACKNOWLEDGMENTS

We are grateful to W. Denk for generous support and helpful discussions. We thank S. Ryu, J. Gabriel, F. Svara, R. De Marco, S. Preuß, and M. Rüppell for helpful discussions. We are grateful to A. Schaefer, R. De Marco, S. Preuß, F. Svara, and J. Kornfeld for comments on an earlier version of the manuscript. We thank N. Neef and M. Lukat for expert help with mechanical design, J. Tritthardt, C. Kieser, and R. Rödel for expert help with electronic design, M. Kaiser and A. Scherbarth for technical assistance, and K. Bauer, M. Hilpert, C. Kasamasch, M. Müller, K. Rohm, C. Roome for IT assistance. Johann H. Bollmann is a member of the Interdisciplinary Centre for Neurosciences (IZN) and the Excellence Cluster *CellNetworks/EcTop "From synapse to disease"* at Heidelberg University. This work was supported by the Max Planck Society and the Deutsche Forschungsgemeinschaft (DFG, BO3746/1-1).

SUPPLEMENTARY MATERIAL

The Supplementary Material for this article can be found online at: http://www.frontiersin.org/NeuralCircuits/10.3389/fncir.2013.00086/abstract

Movie S1 | Movie of a sequence of swim bouts performed by a 6 dpf larval zebrafish during prey capture. Movie recorded at 250 frames/s and played back in real time.

Movie S2 | Same movie as in S1, played back at 30 frames/s.

Movie S3 | Movie of a restrained larval zebrafish responding to a stimulus sequence with directed swim bouts and eye convergence. Movie recorded at 500 frames/s and played back in real time. The stimulus frames were generated and recorded using VisionEgg software and overlaid with the movie in LabVIEW.

Movie S4 | Same movie as in S3, played back at 60 frames/s.

REFERENCES

Ahrens, M. B., Li, J. M., Orger, M. B., Robson, D. N., Schier, A. F., Engert, F., et al. (2012). Brain-wide neuronal dynamics during motor adaptation in zebrafish. *Nature* 485, 471–477.

Avery, R., Mueller, C., Smith, J., and Bond, D. (1987). The movement patterns of lacertid lizards: speed, gait and pauses in *Lacerta vivipara*. *J. Zool.* 211, 47–63.

Bianco, I. H., Kampff, A. R., and Engert, F. (2011). Prey capture behavior evoked by simple visual stimuli in larval zebrafish. *Front. Syst. Neurosci.* 5:101. doi: 10.3389/fnsys.2011.00101

Bizzi, E., Tresch, M. C., Saltiel, P., and d'Avella, A. (2000). New perspectives on spinal motor systems. *Nat. Rev. Neurosci.* 1, 101–108.

Boeddeker, N., and Egelhaaf, M. (2005). A single control system for smooth and saccade-like pursuit in blowflies. *J. Exp. Biol.* 208, 1563–1572.

Borla, M. A., Palecek, B., Budick, S., and O'Malley, D. M. (2002). Prey capture by larval zebrafish: evidence for fine axial motor control. *Brain Behav. Evol.* 60, 207–229.

Budick, S. A., and O'Malley, D. M. (2000). Locomotor repertoire of the larval zebrafish: swimming, turning and prey capture. *J. Exp. Biol.* 203, 2565–2579.

Buss, R. R., and Drapeau, P. (2001). Synaptic drive to motoneurons during fictive swimming in the developing zebrafish. *J. Neurophysiol.* 86, 197–210.

Deliagina, T., Zelenin, P., Fagerstedt, P., Grillner, S., and Orlovsky, G. (2000). Activity of reticulospinal neurons during locomotion in the freely behaving lamprey. *J. Neurophysiol.* 83, 853–863.

Dombeck, D. A., Harvey, C. D., Tian, L., Looger, L. L., and Tank, D. W. (2010). Functional imaging of hippocampal place cells at cellular resolution during virtual navigation. *Nat. Neurosci.* 13, 1433–1440.

Dombeck, D. A., and Reiser, M. B. (2012). Real neuroscience in virtual worlds. *Curr. Opin. Neurobiol.* 22, 3–10.

Ewert, J. P. (1987). Neuroethology of releasing mechanisms: prey-catching in toads. *Behav. Brain Sci.* 10, 337–368.

Ewert, J. P., Buxbaum-Conradi, H., Dreisvogt, F., Glagow, M., Merkel-Harff, C., Röttgen, A., et al. (2001). Neural modulation of visuomotor functions underlying prey-catching behaviour in anurans: perception, attention, motor performance, learning. *Comp. Biochem. Physiol. A Mol. Integr. Physiol.* 128, 417–460.

Fero, K., Yokogawa, T., and Burgess, H. A. (2011). The behavioral repertoire of larval zebrafish. *Neuromethods* 52, 249–291.

Fuiman, L. A., and Webb, P. W. (1988). Ontogeny of routine swimming activity and performance in zebra danios (Teleostei: Cyprinidae). *Anim. Behav.* 36, 250–261.

Gabriel, J. P., Trivedi, C. A., Maurer, C. M., Ryu, S., and Bollmann, J. H. (2012). Layer-specific targeting of direction-selective neurons in the zebrafish optic tectum. *Neuron* 76, 1147–1160.

Gahtan, E., Tanger, P., and Baier, H. (2005). Visual prey capture in larval zebrafish is controlled by identified reticulospinal neurons downstream of the tectum. *J. Neurosci.* 25, 9294–9303.

Grillner, S. (1981). "Control of locomotion in bipeds, tetrapods and fish," in *Handbook of Physiology, Section 1. The Nervous System II. Motor Control*, ed V. B. Brooks (Maryland, DC: American Physiology Society Waverly Press), 1179–1236.

Grillner, S., Wallen, P., Brodin, L., and Lansner, A. (1991). Neuronal network generating locomotor behavior in lamprey: circuitry, transmitters, membrane properties, and simulation. *Annu. Rev. Neurosci.* 14, 169–199.

Groh, J. M. (2001). Converting neural signals from place codes to rate codes. *Biol. Cybern.* 85, 159–165.

Harvey, C. D., Collman, F., Dombeck, D. A., and Tank, D. W. (2009). Intracellular dynamics of hippocampal place cells during virtual navigation. *Nature* 461, 941–946.

Herrero, L., Rodriguez, F., Salas, C., and Torres, B. (1998). Tail and eye movements evoked by electrical

microstimulation of the optic tectum in goldfish. *Exp. Brain Res.* 120, 291–305.

Kramer, D. L., and McLaughlin, R. L. (2001). The behavioral ecology of intermittent locomotion. *Am. Zool.* 41, 137–153.

Land, M. F. (1992). Visual tracking and pursuit: humans and arthropods compared. *J. Insect Physiol.* 38, 939–951.

Land, M. F. (1999). Motion and vision: why animals move their eyes. *J. Comp. Physiol. A* 185, 341–352.

Lisberger, S. G. (2010). Visual guidance of smooth-pursuit eye movements: sensation, action, and what happens in between. *Neuron* 66, 477–491.

Lister, J. A., Robertson, C. P., Lepage, T., Johnson, S. L., and Raible, D. W. (1999). Nacre encodes a zebrafish microphthalmia-related protein that regulates neural-crest-derived pigment cell fate. *Development* 126, 3757–3767.

Lock, A., and Collett, T. (1979). A toad's devious approach to its prey: a study of some complex uses of depth vision. *J. Comp. Physiol. A* 131, 179–189.

McClenahan, P., Troup, M., and Scott, E. K. (2012). Fin-tail coordination during escape and predatory behavior in larval zebrafish. *PloS one* 7:e32295. doi: 10.1371/journal.pone.0032295

McElligott, M. B., and O'Malley, D. M. (2005). Prey tracking by larval zebrafish: axial kinematics and visual control. *Brain Behav. Evol.* 66, 177–196.

McLean, D. L., Masino, M. A., Koh, I. Y. Y., Lindquist, W. B., and Fetcho, J. R. (2008). Continuous shifts in the active set of spinal interneurons during changes in locomotor speed. *Nat. Neurosci.* 11, 1419–1429.

Metcalfe, W. K., Mendelson, B., and Kimmel, C. B. (1986). Segmental homologies among reticulospinal neurons in the hindbrain of the zebrafish larva. *J. Comp. Neurol.* 251, 147–159.

Moschovakis, A., Kitama, T., Dalezios, Y., Petit, J., Brandi, A., and Grantyn, A. (1998). An anatomical substrate for the spatiotemporal transformation. *J. Neurosci.* 18, 10219–10229.

Muto, A., Ohkura, M., Abe, G., Nakai, J., and Kawakami, K. (2013). Real-time visualization of neuronal activity during perception. *Curr. Biol.* 23, 307–311.

Neuhauss, S. C. F. (2003). Behavioral genetic approaches to visual system development and function in zebrafish. *J. Neurobiol.* 54, 148–160.

Niell, C. M., and Smith, S. J. (2005). Functional imaging reveals rapid development of visual response properties in the zebrafish tectum. *Neuron* 45, 941–951.

Orger, M. B., Kampff, A. R., Severi, K. E., Bollmann, J. H., and Engert, F. (2008). Control of visually guided behavior by distinct populations of spinal projection neurons. *Nat. Neurosci.* 11, 327–333.

Portugues, R., and Engert, F. (2009). The neural basis of visual behaviors in the larval zebrafish. *Curr. Opin. Neurobiol.* 19, 644–647.

Roberts, A., Li, W. C., and Soffe, S. R. (2008). Roles for inhibition: studies on networks controlling swimming in young frog tadpoles. *J. Comp. Physiol. A* 194, 185–193.

Robles, E., Smith, S. J., and Baier, H. (2011). Characterization of genetically targeted neuron types in the zebrafish optic tectum. *Front. Neural Circuits* 5:1. doi: 10.3389/fncir.2011.00001

Sato, T., Hamaoka, T., Aizawa, H., Hosoya, T., and Okamoto, H. (2007). Genetic single-cell mosaic analysis implicates ephrinB2 reverse signaling in projections from the posterior tectum to the hindbrain in zebrafish. *J. Neurosci.* 27, 5271–5279.

Schall, J. D., and Thompson, K. G. (1999). Neural selection and control of visually guided eye movements. *Annu. Rev. Neurosci.* 22, 241–259.

Schlegel, T., and Schuster, S. (2008). Small circuits for large tasks: high-speed decision-making in archerfish. *Science* 319, 104–106.

Scudder, C. A., Kaneko, C. R. S., and Fuchs, A. F. (2002). The brainstem burst generator for saccadic eye movements—a modern synthesis. *Exp. Brain Res.* 142, 439–462.

Seelig, J. D., Chiappe, M. E., Lott, G. K., Dutta, A., Osborne, J. E., Reiser, M. B., et al. (2010). Two-photon calcium imaging from head-fixed Drosophila during optomotor walking behavior. *Nat. Methods* 7, 535–540.

Straw, A. D. (2008). Vision egg: an open-source library for realtime visual stimulus generation. *Front. Neuroinform.* 2:4. doi: 10.3389/neuro.11.004.2008

Trivedi, C. A., Gabriel, J. P., and Bollmann, J. H. (2011). "A closed-loop visual environment to elicit behavioral sequences for understanding visuo-motor transformation in larval zebrafish," in *Society for Neuroscience Abstract Viewer and Itinerary Planner* (Washington, DC), 41.

Westerfield, M. (2007). *The Zebrafish Book: A Guide for the Laboratory Use of Zebrafish (Danio Rerio)*. Eugene, OR: University of Oregon Press.

Wiggin, T. D., Anderson, T. M., Eian, J., Peck, J. H., and Masino, M. A. (2012). Episodic swimming in the larval zebrafish is generated by a spatially distributed spinal network with modular functional organization. *J. Neurophysiol.* 108, 925–934.

Wolpert, D. M., and Ghahramani, Z. (2000). Computational principles of movement neuroscience. *Nat. Neurosci.* 3, 1212–1217.

Wurtz, R. H. (2008). Neuronal mechanisms of visual stability. *Vis. Res.* 48, 2070.

Wyart, C., Del Bene, F., Warp, E., Scott, E. K., Trauner, D., Baier, H., et al. (2009). Optogenetic dissection of a behavioural module in the vertebrate spinal cord. *Nature* 461, 407–410.

Conflict of Interest Statement: The authors declare that the research was conducted in the absence of any commercial or financial relationships that could be construed as a potential conflict of interest.

Received: 15 February 2013; paper pending published: 22 March 2013; accepted: 17 April 2013; published online: 10 May 2013.

Citation: Trivedi CA and Bollmann JH (2013) Visually driven chaining of elementary swim patterns into a goal-directed motor sequence: a virtual reality study of zebrafish prey capture. Front. Neural Circuits 7:86. doi: 10.3389/fncir.2013.00086

frontiers in
NEURAL CIRCUITS

ORIGINAL RESEARCH ARTICLE
published: 06 March 2013
doi: 10.3389/fncir.2013.00034

Functional imaging in the zebrafish retinotectal system using RGECO

Alison S. Walker , Juan Burrone and Martin P. Meyer*

MRC Centre for Developmental Neurobiology, King's College London, London, UK

Edited by:
German Sumbre, École Normale Supérieure, France

Reviewed by:
Leon Lagnado, MRC Laboratory of Molecular Biology, UK
Filippo Del Bene, Institut Curie, France

***Correspondence:**
Martin P. Meyer, MRC Centre for Developmental Neurobiology, King's College London, New Hunt's House, Guy's Campus, London SE1 1UL, UK.
e-mail: martin.meyer@kcl.ac.uk

Genetically encoded calcium indicators (GECIs) allow repeated, non-invasive measurements of neural activity in defined populations of neurons, but until recently GECIs based on single fluorescent proteins have been limited to the green region of the color spectrum. Recent efforts in protein engineering have expanded the color palette of GECIs. One of these new GECIs, the red RGECO, is spectrally separate from the traditional GFP-based sensors such as GCaMP, and therefore opens the way for simultaneous, multicolor imaging of neural activity. While RGECO has been shown to report spontaneous calcium fluctuations in neurons, the precise relationship of RGECO signal to evoked-neural activity is not known. Measurements of neural activity using RGECO *in vivo* have also not been reported. Using dissociated hippocampal neurons we performed a systematic analysis of two forms of RGECO- a cytosolic form and a presynaptically localized form generated by fusion of RGECO to the presynaptic protein, synaptophysin (SyRGECO). We find that RGECO and GCaMP3 are comparable in terms of dynamic range, signal-to-noise ratios and kinetics but that RGECO is a more reliable reporter of single action potentials. In terms of performance SyGCaMP3 and SyRGECO are comparable, and both are more sensitive reporters of activity than the cytosolic form of each probe. Using the zebrafish retinotectal system we show that SyRGECO and RGECO are can report neural activity *in vivo* and that RGECO expression permits detailed structural analysis of neuronal arbors. We have exploited these attributes to provide a morphological and functional description of tectal cells selective for motion along the vertical axis. These results open up the possibility of using zebrafish to functionally image genetically defined pre- and postsynaptic circuit components, separable by color, which will be a powerful approach to studying neural interactions in the brain.

Keywords: calcium indicator, RGECO, SyRGECO, zebrafish, *in vivo* imaging, direction selectivity, orientation selectivity

INTRODUCTION

Genetically encoded calcium indicators (GECIs) permit repeated, non-invasive measurements of neural activity in defined populations of neurons *in vivo* (e.g., Mank et al., 2008; Tian et al., 2009; Lutcke et al., 2010; Nikolaou et al., 2012). They are therefore invaluable for studying long-term changes in neuronal activity associated with development, experience, and disease. The potential for GECIs to address long-standing questions in the field of neuroscience has certainly been a major driving force behind the development of GECIs with faster kinetics, increased sensitivity, dynamic range, and signal-to-noise ratios—attributes that are particularly desirable for studying neuronal function. Protein engineering of the GCaMP family of GECIs for example, has resulted in incremental improvements in some of these attributes so that a recent generation GCaMP, GCaMP3, is now widely used to study neural activity in a number of different model systems (Tian et al., 2009; Huber et al., 2012; Nikolaou et al., 2012). Despite these improvements in probe performance GECIs based on single fluorescent proteins have, until recently, been limited to the green region of the color spectrum. The color palette of available single wavelength GECIs has recently been expanded, however, and now includes a red-shifted indicator (R-GECO1; hereafter simply referred to as RGECO) based on a circularly-permuted mApple fluorophore (Zhao et al., 2011b). RGECO displays very little spectral overlap with GFP-based indicators such as the GCaMPs and this offers the potential for simultaneous, multicolor imaging of neural activity. While it has been demonstrated that RGECO is capable of reporting spontaneous calcium oscillations and large calcium transients triggered by chemically-induced depolarization, the precise relationship between RGECO responses and the number of action potentials (APs) is not known (Zhao et al., 2011b). As a result, thorough comparison of RGECO with existing probes is difficult. Furthermore, the use of RGECO to report neural activity *in vivo* has not been demonstrated. Here, we characterized RGECO response properties in neurons *in vitro* and *in vivo*, and further describe a presynaptically targeted form called synaptophysin-RGECO (SyRGECO). *In vitro* experiments performed in dissociated hippocampal neurons directly compared the response properties of both these probes with the existing green indicator GCaMP3 and its presynaptic targeted version, SyGCaMP3. We find that RGECO and GCaMP3 are comparable in terms of dynamic range, signal-to-noise ratios and kinetics but

that RGECO is a more reliable reporter of single APs. We also provide evidence that the method of illumination can profoundly influence RGECO performance, and that this may underlie the discrepancy between our findings and those of a previous study (Yamada and Mikoshiba, 2012). We also show that the expression of RGECO and SyRGECO in the retinotectal system of the larval zebrafish can be used to report neuronal activation *in vivo*. Single tectal neurons expressing RGECO, or retinal ganglion cell (RGC) axons expressing SyRGECO responded to visual stimulation paradigms and allowed reliable and robust measurements of orientation- and direction-selectivity. These results suggest that RGECO is a viable reporter of neural activity that could be used in combination with established, GFP-based indicators such as the GCaMP family for two-color functional imaging *in vivo*.

MATERIALS AND METHODS

GENERATION OF PLASMID CONSTRUCTS

For *in vitro* studies, we used the cytomegalovirus (CMV) promoter to drive GECI expression. For *in vivo* studies, we made use of the Gal4:UAS system (Koster and Fraser, 2001). CMV:RGECO was obtained from Addgene (Addgene plasmid 32444). To generate CMV:SyRGECO and UAS:SyRGECO, RGECO was amplified with primers to introduce *SmaI* and *ClaI* sites and subcloned into the pCRBlunt II-TOPO shuttle vector (Invitrogen). The amplified RGECO gene was cut from the shuttle vector with *SmaI* and *ClaI* and directionally cloned into either the CMV:SyGCaMP3 or UAS:SyGCaMP3 vectors (Nikolaou et al., 2012), replacing GCaMP3 in each case. CMV:GCaMP3 was generated by PCR amplifying GCaMP3 with *BamHI* and *NotI* sites and directionally cloning the product into the *BamHI/NotI* sites of pEGFP-N2 (Clontech Laboratories) thus replacing the *EGFP* sequence. To generate the Huc:Gal4:UAS:RGECO plasmid the HuC promoter was excised from a HuC:GFP plasmid (gift of James Jontes, OHSU, USA) with *SacII* and *NotI* which was subsequently blunted by Klenow treatment. Gal4FF was excised from an ath5:Gal4 plasmid (Gift of Steve Wilson, UCL, UK) using *NotI* and *NcoI* which was also blunted with Klenow. The HuC and Gal4FF fragments were then triple ligated with a pEGFP-N2 plasmid (Clontech), which had been cut with *SacII* and *NotI*. The Huc-Gal4-Sv40 fragment was excised from the resulting plasmid using *SacII* and *AflII*, which was blunted with Klenow, and subcloned in pBS SK (+) which had been cut with *SacII* and *NotI* (blunted) to generate HuC-Gal4FF pBS SK. The UAS:RGECO fragment was subcloned as an *AflII-AseI* fragment (both ends blunted by klenow treatment) into the *EcoRV* site of HuC:Gal4FF pBS SK to generate HuC:Gal4:UAS:RGECO.

CHARACTERISATION OF RGECO AND SyRGECO IN DISSOCIATED HIPPOCAMPAL NEURON CULTURES

Dissociated hippocampal cultures were prepared as described previously (Nikolaou et al., 2012). Plasmids coding for either GCaMP3, RGECO, SyGCaMP3, or SyRGECO, under the control of the CMV promoter, were co- or singly transfected at day 7 *in vitro* using Lipofectamine 2000 (Invitrogen). All experiments were performed on >14 days *in vitro* neurons. For extracellular field stimulation coverslips, on which neurons were cultured, were mounted in a custom-made chamber fitted with a pair of parallel platinum electrodes, 5 mm apart. During imaging and stimulation, neurons were incubated in HEPES-buffered saline (HBS; 139 mM NaCl, 2.5 mM KCl, 10 mM HEPES, 10 mM D-glucose, 2 mM $CaCl_2$ and 1.3 mM $MgCl_2$; pH 7.3 and 290 mOsmol) containing 0.025 mM amino-5-phosphonovaleric acid (APV) and 0.02 mM 6-cyano-7-nitroquinoxaline-2,3-dione (CNQX) at room temperature. Neurons were stimulated by delivering 1–2 ms, 80 V voltage pulses at 20 Hz, where each pulse approximates a single action potential (AP) (Zhao et al., 2011a). Single, 2, 5, 10, 20, 40, and 60 pulse stimulations were delivered, with multiple 10 AP stimulations interleaved during the time course of each experiment. One to twenty AP stimuli were pseudo-randomized, however, 40 and 60 AP stimuli were always delivered at the end of the stimulus sets to prevent possible activity-induced plasticity or rundown of responses. RGECO and GCaMP3 fluorescence signals from co-transfected neurons were recorded sequentially to avoid spectral cross–talk. Confocal imaging of hippocampal neurons was performed using an Olympus FV1000 confocal microscope equipped with a 40×/0.8 NA water-immersion objective (Olympus). Functional time-series were acquired at a rate of approximately 6 Hz and 0.2 × 0.2 μm resolution. RGECO was excited with a 543 nm laser line, with emission collected via a 560–660 nm band pass emission filter, whereas GCaMP3 was excited with a 488 nm laser line, with emission collected via a 505–525 nm band pass emission filter. Widefield images were obtained using an Olympus IX71 inverted microscope with a CCD camera (Coolsnap HQ) controlled by Slidebook software (Intelligent Imaging Innovations), equipped with a 40×/1.0 NA oil-immersion objective (Olympus). Functional time-series were acquired at a rate of approximately 6 Hz and with approximately 0.25 × 0.25 μm resolution. The excitation light source was a xenon-arc lamp (Lambda LS; Sutter Instruments), in which light exposure was regulated by a rapid shutter (smartShutter; Sutter Instruments) controlled by a Sutter Instruments lambda 10–3 controller, fitted with 470 ± 20 nm and 565 ± 22 nm band pass excitation, 515 ± 20 nm band pass and 590-nm long pass dichroic and 510 ± 15 nm band pass and 650 ± 36 nm band pass emission filters (Chroma Technology Corporation) for GCaMP3 and RGECO, respectively. Hippocampal data were analysed using custom written Matlab codes (Mathworks). Normalized signal intensity changes (ΔF/F) were calculated on time-series for each voxel. The maximum ΔF/F during the stimulus period for each voxel was used to generate summary images. For RGECO and GCaMP3, the mean of a square (10 × 10 voxels) region of interest (ROI) applied to summary images gave the peak response. As RGECO, but not GCaMP3, was expressed in the nucleus, ROIs were selected within the cytoplasmic region of the cell body. For SyGCaMP3 and SyRGECO-expressing neurons, ROIs were defined by an empirically derived threshold based on the summary images for the first 10 AP stimulation. Once defined these ROIs were applied to all other stimulations. In cases where rundown was observed, normalization was performed to generate stimulus-response curves based on the exponential regression of multiple 10 AP stimulations interspersed within each experiment. This enabled a correction factor to be applied to each stimulus timepoint. RGECO and GCaMP3 detection thresholds for single-APs were calculated as

ΔF/F responses greater than three standard deviations of baseline noise. Rise and decay kinetics were calculated for 10 AP stimulations using semi-automated spike analysis software (Synaptosoft Inc.). In experiments where rundown occurred, kinetics were calculated from solely the first 10 AP stimulation to prevent bias from rundown. To determine the degree of co-localization of SyGCaMP3 and SyRGECO, puncta intensities of both probes were calculated within 7 × 7 voxel ROIs. To determine the degree of co-localization that arises through chance, analysis was also performed on datasets in which the SyGCaMP3 image was flipped vertically relative to the SyRGECO image.

MICROINJECTION AND IMAGING OF ZEBRAFISH LARVAE AND NEURITE TRACING

All *in vivo* experiments were performed in the pigmentation mutant, nacre which lacks all neural crest derived melanophores (Lister et al., 1999). On occasion, microinjections were performed on Tg(Isl2b:Gal4; UAS:SyGCaMP3) embryos. This transgenic line of zebrafish expresses SyGCaMP3 in RGCs. To generate transient and mosaic expression of RGECO in tectal cells a HuC:Gal4:5UAS:RGECO plasmid (50 ng/μl) in Danieau solution [1 M NaCl, 0.25 M HEPES, 30 mM $Ca(NO_3)_2$, 20 mM $MgSO_4$] was microinjected into embryos at the 1–4 cell stage. This single plasmid contained the pan-neuronal promoter, HuC driving expression of the yeast transcriptional activator protein Gal4 directly upstream of the Gal4 DNA binding motif, the Upstream Activation Sequence (UAS) in frame with RGECO. In order to generate mosaic expression of SyRGECO in RGCs an activator plasmid containing Gal4 driven by an upstream HuC promoter (HuC:Gal4) was co-injected with an effector plasmid, where SyRGECO expression is driven by a UAS motif in frame with SyRGECO (UAS:SyRGECO). The effector and activator plasmids were both injected at a concentration of 25 ng/μl in Danieau solution. Plasmid DNA was prepared using miniprep kits (Qiagen). Zebrafish were maintained at 28.5°C on a 14 h ON/10 h OFF light cycle. Confocal imaging of visually-evoked RGECO and SyRGECO responses was performed using an LSM 710 confocal microscope equipped with a spectral detection scan head and a 20×/1.0 NA water-immersion objective (Carl Zeiss). Excitation was provided by a 543 nm laser line. Functional time-series were acquired at a rate of 6.5 Hz and 0.208 × 0.208 μm voxel resolution (256 × 256 voxels) and <2.1 AU pinhole aperture. Optical sections were obtained at <1.6 μm intervals and maximum intensity projections of RGECO and SyRGECO-expressing neurons were generated using NIH ImageJ. The Simple Neurite Tracer in FIJI (a processing package based on ImageJ released under the General Public License) was used to perform semi-automated tracing of z-stacks for 3D reconstruction of arbors and calculation of total branch lengths.

VISUAL STIMULATION AND ANALYSIS OF ORIENTATION- AND DIRECTION-SELECTIVITY

Visual stimulation and confocal imaging of zebrafish larvae *in vivo* were as described previously (Nikolaou et al., 2012). Briefly, larvae with mosaic expression of RGECO in tectal cells, and SyRGECO in retinal ganglion cells (RGCs) were restrained in 2% low melting point agarose, mounted dorsally onto a customized glass platform. The agarose was sufficient to restrain the larvae so that anesthesia was not required. Agarose was removed from in front of one eye, and the larva positioned with this eye facing a screen onto which visual stimuli were projected, while time-series were simultaneously captured from the contralateral tectum. The projected image filled a visual field of approximately 97° by 63°. Visual stimuli consisted of dark bars (8 cd/m^2) (25% of mean) on a mean gray background (32 cd/m^2). Each bar was 10° in width moving at 20°/s and separated from the preceding bar by 30°—enabling more than one bar on the screen at any one time. The long axis of the bar was orthogonal to the direction of motion. Bars were presented at 12 different directions evenly spaced across 360° and displayed in a pseudorandom order. A blank screen null condition of 2 s was also interleaved. Each inter-epoch interval was 8 s to enable the RGECO and SyRGECO signals to return baseline. Visual experiments were generated and controlled using custom written Labview and Matlab code (MathWorks) implemented on a ViSaGe stimulus presenter (Cambridge Research Systems, UK) and delivered via a DLP pico projector (Optoma). *In vivo* functional data were analysed as previously described (Nikolaou et al., 2012), excepting that median filtering was not performed in the image processing of this data.

WHOLE-MOUNT IMMUNOLABELING OF LARVAL ZEBRAFISH WITH SINGLE CELL EXPRESSION OF RGECO AND SyRGECO

Larval zebrafish were fixed with 2% paraformaldehyde (PFA) in phosphate-buffered saline (PBS) for 2 h at room temperature, and then treated with 0.25% Trypsin in PBS on ice for 20 min. The samples were blocked in 0.4% Blocking Reagent (Roche, Nutley, NJ) in PBS-T (1% Triton) for 2 h before incubating with primary antibodies (diluted 1:500 in 0.4% Blocking Reagent in PBS-T) for 2 days at 4°C. RGECO and SyRGECO were labeled by a rabbit polyclonal antibody which recognizes DsRed (Clonetech-632496). On experiments performed in the Tg(Isl2b:Gal4; UAS:SyGCaMP3) zebrafish larvae, SyGCaMP3 expression was amplified using a chicken polyclonal antibody which recognizes GFP (abcam-13970). Larvae were incubated for 1 day at 4°C in secondary antibodies Alexa Fluor 488 goat anti-chicken, 546 and anti-rabbit, and the nuclear stain TO-PRO-3 (Invitrogen-T3605) all diluted 1:500 in 0.4% Blocking Reagent in PBST. Labeled larvae were imaged as described above.

ANIMALS

All work in this study was approved by the local Animal Care and Use Committee (King's College London), and was carried out in accordance with the Animals (Experimental Procedures) Act, 1986, under license from the United Kingdom Home Office.

RESULTS

In vitro CHARACTERISATION OF RGECO

In order to directly compare the performance of RGECO with GCaMP3 both probes were co-transfected into dissociated hippocampal neurons. mApple, the fluorescent protein on which RGECO is based, exhibits a ∼270-fold increase in bleaching rate under arc lamp illumination compared to the scanned laser illumination used in confocal imaging (Shaner et al., 2008).

To examine whether the form of illumination influences the performance of RGECO, characterization was performed using both widefield fluorescence and confocal imaging. Expression of GCaMP3 and RGECO permitted visualization of neuronal morphology and, as previously reported (Yamada and Mikoshiba, 2012), GCaMP3 is excluded from the nucleus while RGECO is not (**Figures 1A,B**, top panels). Normalized changes in fluorescence ($\Delta F/F$) were measured in response to varying numbers of APs delivered via extracellular field stimulation (1–2 ms, 80 V, 20 Hz). Typical peak $\Delta F/F$ response images are illustrated in the bottom panels of **Figures 1A(i,ii)**, and concatenated fluorescence traces obtained from somatic ROIs in response to a typical stimulus set are shown in **Figure 1B**. To examine whether probe performance was stable over time, responses to a 10 AP test stimulus were measured at regular intervals during each experiment. Under widefield illumination RGECO responses to these test stimuli showed an exponential decrease in amplitude, a trend not shown by GCaMP3 expressed in the same neuron [**Figures 1B,D(i)**]. This progressive decrease in RGECO signal, which we will refer to as rundown, is also clearly evident in the mean RGECO traces to 40 and 60 APs which are delivered toward the end of the stimulus set, and have lower peak values than responses recorded for fewer numbers of APs delivered earlier in the stimulus set [**Figure 1C(i)**]. This contrasts with GCaMP3 where the peaks of the mean response traces increase steadily with stimulus strength until they plateau at approximately 40 APs [**Figures 1C(i),E(i)**]. By applying a correction factor derived from the exponential rundown of RGECO to the RGECO responses (see section "Materials and Methods") we were able to generate a stimulus-response curve for this probe that mirrored that of GCaMP3 in terms of dynamic range [**Figure 1 E(i)**]. When identical experiments were performed using confocal microscopy we did not observe any rundown in RGECO responses over time [**Figure 1D(ii)**]. As a result no correction of the data was required, and the responses of RGECO to varying numbers of APs display a dynamic range highly similar to that of GCaMP3 [**Figures 1C(ii),E(ii)**]. In addition, RGECO proved to be a more robust reporter of single APs than GCaMP3 [**Figure 1E** (insets)]. Responses to single spikes measured using confocal microscopy (which does not suffer from potential correction-based errors) showed that RGECO detects 1 AP in 88% of trials, compared to only 38% for GCaMP3 (see section "Materials and Methods"). Furthermore, the kinetics of RGECO and GCaMP3 to 10 AP stimuli were very similar (½t rise: GCaMP3, 566 ± 39 ms and RGECO, 511 ± 26 ms; ½t decay: GCaMP3, 1020 ± 51 ms and RGECO, 1039 ± 60 ms). Lastly, we performed these experiments on neurons transfected with either RGECO or GCaMP3 alone. In singly transfected neurons the response magnitudes, sensitivity, and dynamic range of GCaMP3 and RGECO were similar to those measured in co-transfected neurons [**Figures 1F(i,ii)**]. As with co-transfected neurons, RGECO exhibited rundown in singly transfected cells imaged with widefield microscopy (**Figure 1G**).

These results suggest that the prolonged and continuous excitation of RGECO under widefield fluorescence imaging severely compromises its ability to faithfully report levels of neuronal activity. However, when using confocal imaging and scanned excitation RGECO does not show the rundown seen with widefield imaging, and performs as well as GCaMP3 at reporting stronger stimuli while demonstrating greater sensitivity to single APs.

In vitro CHARACTERISATION OF SyRGECO

One of the strengths of using GECIs is the ability to target their expression to specific subcellular compartments. Here, we have used a previously described strategy (Dreosti et al., 2009) to restrict probe expression to presynaptic terminals through fusion of GCaMP3 and RGECO to synaptophysin, a synaptic vesicle protein. Targeting GECIs to synaptic boutons allows recording of calcium transients which specifically trigger neurotransmitter release. Synaptophysin-GCaMP3 (SyGCaMP3) has been previously characterized using widefield fluorescence microscopy (Nikolaou et al., 2012), while synaptophysin-RGECO (SyRGECO) is a newly generated probe. Using widefield fluorescence imaging we found that the rundown of SyRGECO responses was so rapid that we were unable to characterize the probe using this form of microscopy. Instead, SyGCaMP3 and SyRGECO were characterized side-by-side in co-transfected dissociated hippocampal neurons using confocal microscopy. In these neurons both probes exhibited a punctate pattern of expression (**Figure 2A**), with 97% of SyRGECO puncta co-localizing with SyGCaMP3 (157 puncta from 4 cells; data not shown), which has previously been shown to be localized to presynaptic terminals *in vitro* (Nikolaou et al., 2012). When stimulated, the peak response ($\Delta F/F$) is mainly localized to presynaptic boutons with much lower signals produced in the adjoining axon (see insets in **Figure 2A**). Using the same stimulation paradigms used to characterize cytosolic RGECO we found that responses of both SyGCaMP3 and SyRGECO were not stable over time, with both exhibiting an approximately 40% rundown in response to 10 AP test stimulations interspersed throughout the experiment (**Figure 2B**). Application of a correction factor derived from the slope of the rundown led to the generation of stimulus-response curves. We found that SyGCaMP3 and SyRGECO exhibited very similar responses at all stimulus strengths both in terms of response magnitude (**Figure 2C**) and kinetics to 10 AP stimuli (½t rise: SyGCaMP3, 409 ± 50 ms and SyRGECO 401 ± 46 ms; ½t decay: SyGCaMP3, 901 ± 96 ms and SyRGECO, 951 ± 105). In comparison to the cytosolic forms, we find that SyGCaMP3 exhibits greater sensitivity to low numbers of APs (1–5 APs) compared to GCaMP3. While SyRGECO is more sensitive to single spikes than cytosolic RGECO, the stimulus-response curve of SyRGECO more closely resembles that of cytosolic RGECO (**Figure 2D**). These results demonstrate that RGECO, when targeted to presynaptic terminals, retains its high sensitivity and large dynamic range.

CHARACTERISATION OF SINGLE ORIENTATION-SELECTIVE TECTAL CELLS *In vivo* USING RGECO

In order to characterize RGECO *in vivo* we labeled single tectal neurons in the larval zebrafish using mosaic labeling techniques and imaged calcium signals in response to visual stimulation. As well as reporting visually evoked activity, RGECO expression also permitted analysis of tectal cell morphology (**Figure 3A**). Furthermore, RGECO fluorescence could be amplified by *post-hoc* immunostaining with a DsRed antibody to provide detailed

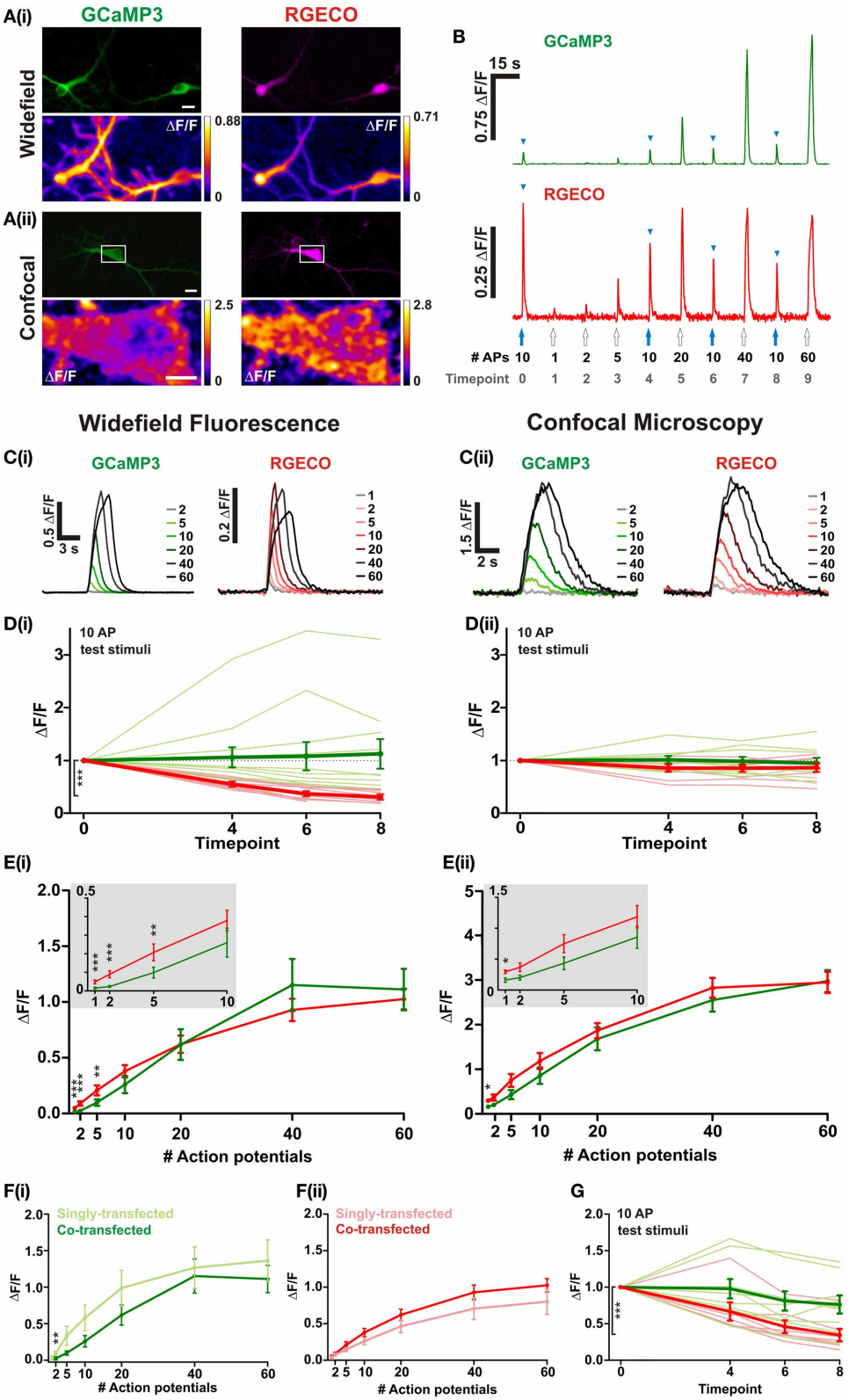

FIGURE 1 | Characterisation of RGECO and GCaMP3 expressed in hippocampal neurons. For **(A–E)** neurons were co-transfected with RGECO and GCaMP3 to allow side-by-side characterization in the same neuron. **(A)** Images obtained using widefield **(i)** and confocal **(ii)** microscopy. Top panels show fluorescence images of GCaMP3 (green) and RGECO (magenta) co-transfected neurons; bottom panels show peak ΔF/F response summary images to 10 APs. Voxels are color-coded according to the maximum

(Continued)

FIGURE 1 | Continued
recorded ΔF/F (scale to the right). White boxes in top panel of **(ii)** indicate the area used for functional imaging in the bottom panel. Top panels scale bars = 10 μm; For **(ii)** bottom panel scale bar =5 μm. **(B)** Responses of RGECO and GCaMP3 from the same cell using widefield fluorescence to a typical experimental stimulation paradigm. The number of APs is indicated and blue arrowheads mark responses to interspersed repeats of 10 APs. **(C–E)** Characterisation of GCaMP3 and RGECO using widefield fluorescence **(i)** and confocal microscopy **(ii)**. **(C)** Mean responses of GCaMP3 and RGECO to a range of APs delivered at 20 Hz (widefield $n = 8$ cells; confocal $n = 7$). **(D)** Peak ΔF/F responses of RGECO and GCaMP3 to interspersed 10 AP test stimuli over the time course of the experiment (widefield $n = 12$ cells; confocal $n = 7$ cells). Mean responses and responses of individual cells are shown in bold and faint lines, respectively. For **(i)** note the significant rundown of RGECO responses (red traces) using widefield fluorescence, which is not seen with GCaMP3 (green traces), nor when using confocal microscopy **(ii)**. Kruskal-Wallis one-way ANOVA followed by Dunn's post-test. **(E)** Peak ΔF/F over AP number for RGECO and GCaMP3 (widefield $n = 12$ cells; confocal $n = 7$ cells). RGECO responses measured using widefield imaging are corrected for rundown (see section "Materials and Methods"). Insets show magnified region (1–10 APs) of plots and demonstrate that RGECO is better at reporting low spiking activity than GCAMP3. Wilcoxon signed rank tests. **(F)** Peak ΔF/F over AP number for GCaMP3 **(i)** and RGECO **(ii)** measured in single- and co-transfected neurons using widefield microscopy (single-transfected: GCaMP3 $n = 7$, RGECO $n = 6$; co-transfected: $n = 12$). Responses of RGECO were corrected for rundown (see section "Materials and Methods"). Mann Whitney test. **(G)** Mean peak ΔF/F responses of neurons singly-transfected with either GCaMP3 or RGECO (bold green and red, respectively) to interspersed 10 AP test stimuli over the timecourse of the experiment (GCaMP3 $n = 7$ cells; RGECO $n = 6$ cells). Responses of individual cells are denoted by thin green (GCaMP3) and red (RGECO) lines, respectively. Kruskal-Wallis One-Way ANOVA followed by Dunn's post-test. **(B–G)** GCaMP3-green traces; RGECO-red traces. Significance: * < 0.05, ** < 0.01, *** < 0.0001.

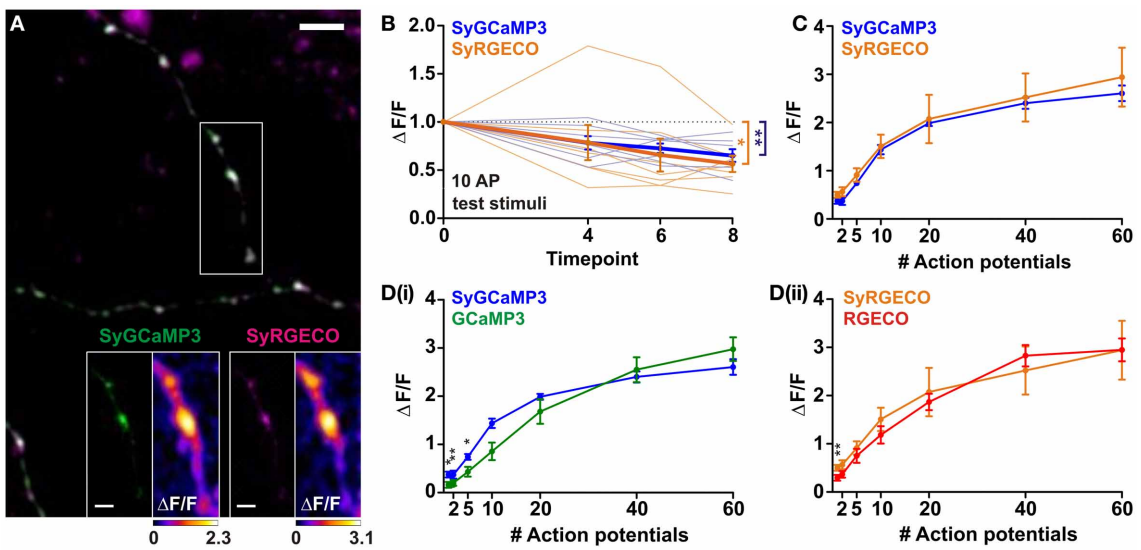

FIGURE 2 | Characterisation of SyGCaMP3 and SyRGECO in hippocampal neurons. (A) Dissociated hippocampal neurons co-expressing SyGCaMP3 (green) and SyRGECO (magenta). Scale bar = 5 μm. White box indicates area used for functional imaging in SyGCaMP3 and SyRGECO insets. Right hand panels of insets show peak ΔF/F response summary images to 10 APs. Voxels are color-coded according to the maximum recorded ΔF/F (scales below). Scale bars for insets = 2 μm. **(B)** Peak ΔF/F responses for SyGCaMP3 and SyRGECO to interspersed 10 APs test stimuli throughout the experiment. Mean responses and individual cell responses are shown in bold and faint lines, respectively ($n = 7$ cells). Kruskall-Wallis One-Way ANOVA followed by Dunn's post-test. **(C)** Peak ΔF/F over AP number for SyGCaMP3 and SyRGECO ($n = 7$ cells). Responses are corrected for rundown (see section "Materials and Methods"). **(D)** Comparison of the peak ΔF/F over AP number for SyGCaMP3 and cytosolic GCaMP3 **(i)**; and for SyRGECO and RGECO **(ii)** using confocal microscopy (SyGCaMP3 $n = 7$; GCaMP3 $n = 12$, SyRGECO $n = 7$; RGECO $n = 12$). SyGCaMP3 and SyRGECO were both corrected for rundown (see section "Materials and Methods"), as cytosolic GCaMP3 and RGECO did not exhibit rundown using confocal microscopy (see **Figure 1**) they were not corrected. Mann whitney tests. Significance: * < 0.05, ** < 0.01.

structural analysis. This also allowed for co-labeling of tectal landmarks such as RGC axons and tectal cell nuclei so that cell body and dendritic arbor positions of single RGECO expressing neurons could be analysed (**Figure 3B**). For functional imaging, zebrafish larvae were restrained in agarose with one eye facing a screen onto which dark bars were projected that moved across the visual field in 12 different directions (**Figure 3C**). The long axis of the bar was orthogonal to the direction of motion. Tectal soma responses to visual stimulation were captured by confocal imaging of the contralateral tectum. **Figure 3D** shows a montage of a tuning experiment performed on a single neuron (Cell 1) in which each voxel is color-coded according to the integral response at each stimulus direction. **Figure 3E** shows a representative ΔF/F trace of a single voxel from Cell 1 during a tuning experiment. For the example shown, RGECO reported selective fluorescent increases for motion along the vertical axis (**Figure 3D**). This was measured explicitly for each responding voxel using two measures of orientation-tuning: 1-circular variance and the mean orientation-selective index (OSI), with the complex angle providing the preferred angle for orientation-selective responses.

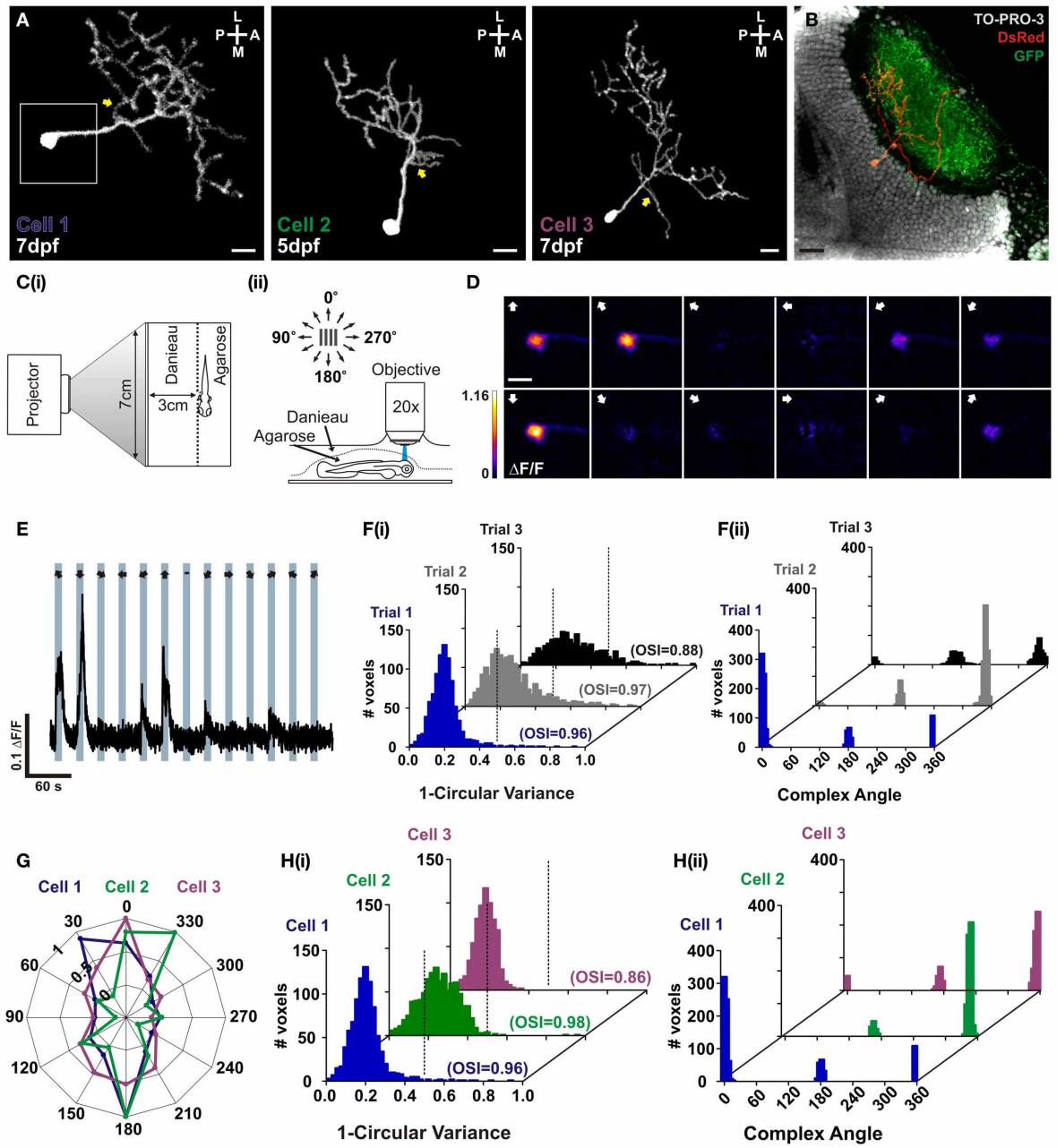

FIGURE 3 | *In vivo* characterization of orientation-selective tectal neurons expressing RGECO. (A) Dorsal view of three example volumetric fills (see section "Materials and Methods") of tectal neurons expressing RGECO at either 5- or 7- days post fertilization (dpf), as labeled. Image orientation is shown top right (L, lateral; M, medial; A, anterior; P, posterior). Yellow arrows indicate short proximal branches emanating from primary dendrites. Scale bars = 10 μm. White box indicates the area imaged for **(D)**. **(B)** *Post-hoc* immunostaining of a Tg(Isl2b:gal4:UAS:SyGCaMP3) zebrafish in which retinal ganglion cells express SyGCaMP3, with RGECO expression in a single tectal cell (Cell 3). Scale bar = 20 μm. **(C)** Schematic detailing the experimental set-up. **(i)** Larvae are immobilized in agarose, with one eye viewing a projection screen. **(ii)** Visually evoked responses are recorded in the contralateral tectum. **(D)** Montage of summary integral ΔF/F response images to a bar drifting in 12 different directions. The direction of motion is indicated by arrows in the top left of each panel. Voxels are color-coded to the maximum recorded integral ΔF/F (scale to the left). Scale bar = 10 μm. **(E)** Representative ΔF/F trace of a single voxel during a tuning experiment for Cell 1. Stimulus epochs are shown in blue with the direction of motion indicated by arrows (dash indicates the "blank" epoch). **(F)** Quantative voxel-wise analysis of the orientation-selectivity of Cell 1 across repeated trials. **(i)** Distribution of 1-circular variance for responsive voxels for each trial, as labeled. Voxels with values less than 0.5 (dotted line) are considered orientation-selective. Mean orientation-selective index (OSI) values are shown bottom left of each example histogram. **(ii)** Distribution of the complex (preferred) angle of all voxels in **(i)**. **(G)** Representative color-coded polar plots of single voxel integral responses of example cells (Cells 1–3). **(H)** Quantative voxel-wise analysis of orientation-selectivity for example tectal cells. **(i)** Distribution of 1-circular variance for responsive voxels for example cells [color-coding as in **(E)**]. Mean OSI values are shown bottom left of each example histogram. **(ii)** Distribution of the complex (preferred) angles of all voxels in **(i)**.

Both measures revealed Cell 1 to be highly selective (1-circular variance< 0.5, OSI> 0.5) for motion along the vertical axis (**Figure 3F**). To examine whether rundown of RGECO occurred during *in vivo* imaging we performed three consecutive tuning experiments. We reasoned that significant rundown of RGECO during the course of an experiment could cause trial-to-trial differences in tuning curves because the direction of motion is randomized for each trial, meaning that any rundown could artificially boost the response amplitude to the first presented direction relative to the last. However, we find that all three trials revealed cell 1 to be highly orientation-selective with an invariant complex angle showing selectivity for motion along the vertical axis (**Figure 3F**).

We found that our expression strategy often labels tectal cells that are orientation-selective for motion along the vertical axis (**Figures 3G,H**). We were interested in whether these functionally similar cell types also shared morphological traits. For all 3 cells studied here, we found a small proximal branch that extends from the primary dendrite (**Figure 3A** yellow arrows) and an asymmetrical elaboration of the dendritic tree in the posterolateral quadrant. These dendrites were found in the deeper portion of the stratum fibrosum et griseum superficiale (SFGS) of the tectal neuropil but were not strictly laminar in structure. In addition, the two age-matched examples, cell 1 and cell 3, showed comparatively large dendritic trees extending 95.23 μm and 91.81 μm respectively across the anterior–posterior axis of the tectum, and total branch lengths of 854 μm and 884 μm respectively.

These results demonstrate that RGECO can be used to report neuronal morphology and function *in vivo*. We have exploited these attributes to provide the first morphological and functional description of orientation-selective tectal cells in the zebrafish optic tectum.

SyRGECO REPORTS THE DIRECTION-SELECTIVITY OF A SINGLE RGC

In vivo

In order to test the performance of SyRGECO *in vivo*, calcium transients in the axon arbor of a singly-labeled RGC expressing SyRGECO were measured in response to visual stimulation. The labeled axon showed a punctate distribution of SyRGECO, consistent with a presynaptic localization and the axon arbor showed a classic planar morphology (**Figure 4A**). On presentation of a moving bar, stimulus-locked selective fluorescence increases were recorded (**Figure 4C**) which were confined to the regions of SyRGECO expression (**Figure 4B**). A montage of a tuning experiment in which each voxel is color-coded according to the integral response at each stimulus direction suggests selectivity for anterior (tail-to-head) motion (**Figure 4B**). This was examined closer by calculating the vector magnitude of each responding voxel with application of an empirically derived vector sum magnitude threshold (>0.001) to distinguish direction-selective from non-direction-selective voxels. For the cell shown, the majority of voxels are suprathreshold [**Figure 4D(i)**] with a mean summed vector angle of 280° [**Figure 4D(ii)**], which demonstrates selectivity for anterior motion. These results demonstrate that when fused to synaptophysin, RGECO (SyRGECO) can be used *in vivo* to report presynaptic activity in response to physiologically relevant stimuli.

DISCUSSION

The purpose of this study was to characterize the newly engineered red-shifted GECI RGECO in response to different numbers of APs *in vitro*, to generate a red-shifted synaptically-targeted GECI based on RGECO, and to determine whether RGECO is a useful reporter of neural activity *in vivo*, which has previously not been demonstrated.

In terms of performance *in vitro* we found that RGECO was comparable to the GFP-based GECI, GCaMP3, when imaged using confocal microscopy. Dynamic range, response magnitude and kinetics were not significantly different between RGECO and GCaMP3 when co-expressed in the same cells. Furthermore, co-expression did not alter the performance of either probe relative to cultures transfected with a single probe. This suggests that RGECO is not only useful for reporting a range of activity patterns but that it can also be used in combination with the more traditional GFP-based reporters of neural activity such as GCaMP family members (Tian et al., 2009; Muto et al., 2011; Akerboom et al., 2012) and synaptopHluorins (Miesenbock et al., 1998). Indeed, RGECO showed a greater sensitivity than GCaMP3 for detecting single spikes, an important advantage as this metric, in addition to linearity, is essential for the deconvolution of complex calcium signals into spikes (Yaksi and Friedrich, 2006; Dreosti et al., 2009). Furthermore, we found that RGECO, when fused to synaptophysin, acted as a good reporter of calcium influx at synaptic boutons with a similar dynamic range, magnitude of response and kinetics as SyGCaMP3.

Our findings contrast with those of a previous study in which RGECO was found to perform poorly in comparison to GCaMP3 (Yamada and Mikoshiba, 2012). During the course of our investigation we have discovered that differences in methods of RGECO excitation could provide a likely explanation for this discrepancy. We consistently observed light-dependent rundown in RGECO responses under widefield excitation, where under prolonged periods of widefield illumination RGECO becomes increasingly unreliable in reporting neural activity. Because these experiments were performed on neurons also expressing GCaMP3, which did not display rundown, we can rule out neuron ill-health or activity-induced plasticity as the cause of reduced RGECO responses. RGECO rundown was not observed when using the scanned illumination used in confocal microscopy, suggesting that either the method or degree of illumination can influence the response properties of RGECO. The confocal frame scan rate used in our study was fairly modest (6 Hz) and was targeted to the cell soma. Yamada and Mikoshiba (2012) characterized RGECO using rapid (200 Hz) 2-photon line-scanning over a region of apical dendrite. The RGECO excitation-emission cycling rates are therefore likely to be far higher in the Yamada study than in ours. In general, RGECO rundown is also likely to be exacerbated by imaging in low volume regions such as dendritic and axonal processes where there is less naïve probe available to replenish the light-depleted pool. This may underlie the rundown observed here of SyGCaMP3 and SyRGECO which are confined to the presynaptic terminal. Tethering these probes to synaptic vesicles will also limit probe motility and hence recovery from the rundown by probe turnover.

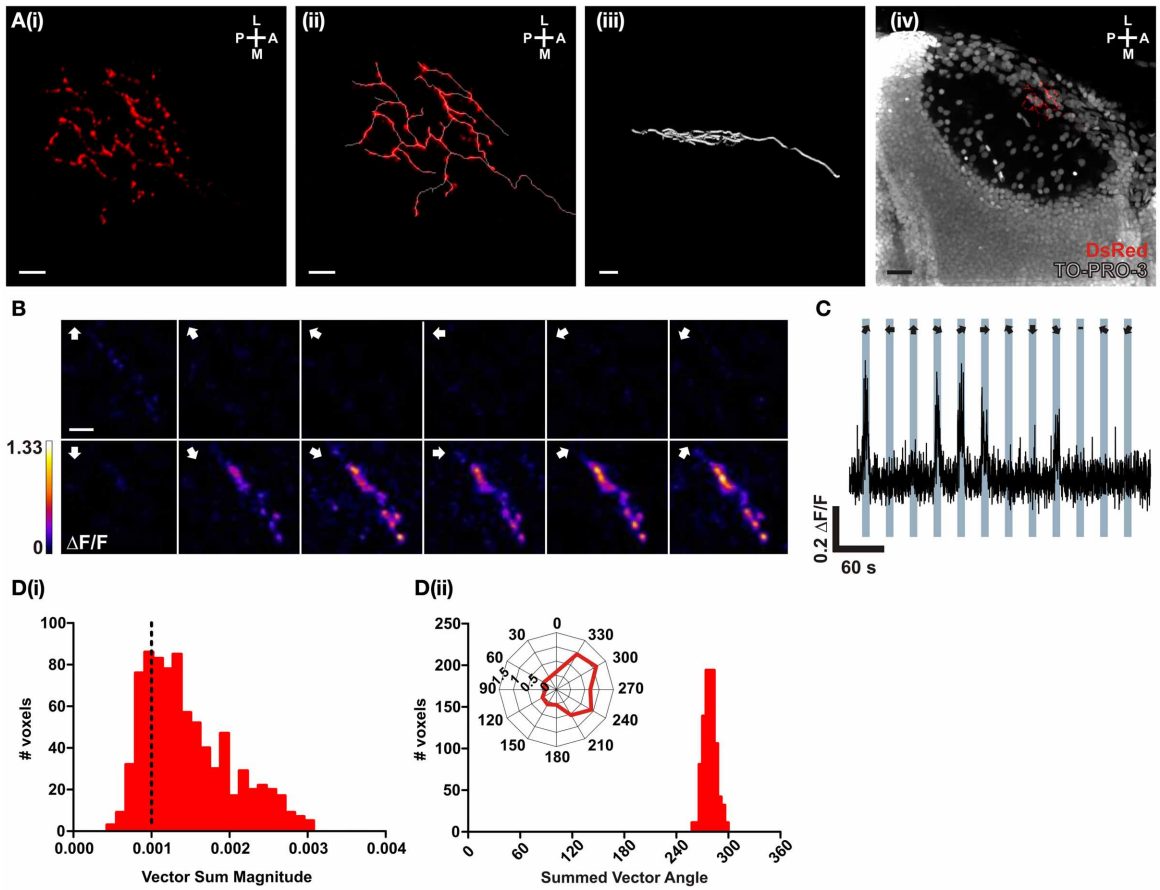

FIGURE 4 | *In vivo* characterization of a direction-selective RGC expressing SyRGECO. (A) A typical RGC axon expressing SyRGECO arborizing in the tectum at 6 dpf; **(i)** SyRGECO immunolabeled with an anti-DsRed antibody, **(ii)** immunolabeled RGECO overlaid with a trace for arbor morphology, **(iii)** side-on view of laminar arbor organization, **(iv)** nuclear staining with TOPRO-3 reveals relative RGC arbor position within the tectum. Image orientation is shown in top right for (L, lateral; M, medial; A, anterior; P, posterior). For **(i–iii)** scale bar = 5 μm; **(iv)** scale bar = 20 μm. **(B)** Montage showing typical integral ΔF/F responses of all voxels in the imaging region. Direction of motion is indicated by arrows in the top left of each panel. Voxels are color-coded to the maximum recorded integral ΔF/F (scale to the left). Scale bar = 3 μm. **(C)** Representative ΔF/F trace of a single voxel during a tuning experiment. Stimulus epochs are shown in blue with the direction of motion indicated by arrows (dash indicates the "blank" epoch). **(D)** Quantative voxel-wise analysis of direction-selectivity. **(i)** Distribution of vector sum for responsive voxels. Voxels larger than 0.001 (dotted line) are considered direction-selective. **(ii)** Distribution of the preferred angle of all suprathreshold direction-selective voxels in **(i)**. Representative polar plot shows the integral responses of a single voxel to the labeled directions of motion.

The basis for the light-induced rundown of RGECO responses is not clear. mApple, the fluorophore on which RGECO is based, bleaches far more quickly under widefield illumination than under confocal scanning (Shaner et al., 2008) indicating sensitivity to the method of illumination. However, photobleaching cannot fully explain RGECO rundown as we did not see significant bleaching of RGECO in our experiments and our response metric (ΔF/F) specifically normalizes for baseline fluorescence. This suggests that rundown may instead be due to a light-induced change in either the ability to bind calcium or to exhibit calcium-dependent increases in fluorescence. Whatever its underlying causes, the light-dependent rundown of RGECO means that this probe should be used with caution and with the appropriate controls.

To examine the performance of RGECO *in vivo* we used the retinotectal projection of zebrafish as a model system. While the broad function of the tectum is known: it converts a visuotopic map into motor commands that orient the head and body toward or away from a visual stimulus (for review see Nevin et al., 2010), the specific computations performed by local tectal circuits are not well understood. This is due to our relatively poor understanding of the essential circuit components: the various tectal cell types, their morphologies, functional properties and how cell types interact with one another (but see Robles et al., 2011; Gabriel et al., 2012 for examples). Expression of GECIs in single, identifiable cell types are well suited to addressing these gaps in our knowledge. In zebrafish it is also relatively straightforward to label and image single neurons and to provide visual stimuli to probe the functional properties of labeled cells (Dreosti et al., 2009; Gabriel et al., 2012; Nikolaou et al., 2012). Here we expressed SyRGECO in single RGCs and cytosolic RGECO in single tectal cells in larval zebrafish and used

a drifting bar stimulus to functionally image two cell types: a direction-selective RGC with preference for tail-to-head motion, and orientation-selective tectal cells with a preference for motion along the vertical axis. In three successive tuning experiments performed on the same RGECO expressing tectal cell we saw that three measures of orientation tuning: 1-circular variance, orientation-selective index and complex angle were relatively invariant suggesting that RGECO rundown was not significantly altering the ability to measure tuning profiles *in vivo*. In order to classify neurons they must be defined using multiple criteria including morphology, molecular markers, patterns of connectivity and function. Our results suggest that RGECO and SyRGECO may be used to define two of these criteria; morphology and function, simultaneously. The direction-selective RGC that we describe here is located within the superficial tectal neuropil which matches the location of anterior-selective RGC axons described in a functional population study of RGC inputs to the tectum (Nikolaou et al., 2012). SyRGECO expression allowed for reconstruction of axonal arbor morphology, identification of putative presynaptic terminals and placement of the axon arbor within the tectal neuropil. The RGECO expressing tectal cells presented here demonstrate strikingly similar functional properties but also have morphological features in common. The somata of the orientation-selective tectal cells we have imaged are located quite superficially in stratum periventriculare with dendritic arbors that, although not strictly laminar, target the deeper layers of SFGS—a position that matches the location of vertically tuned orientation-selective RGC inputs into the tectum (Nikolaou et al., 2012). This suggests that excitatory, vertically-tuned RGC inputs may be the major determinant of axis-selectivity for these tectal cells. Indeed, a major advance afforded by the development of RGECO is using two color functional imaging to test hypotheses such as this. Expression of RGECO in single tectal neurons in a background of SyGCaMP3-expressing RGC axons (Nikolaou et al., 2012) will allow for direct correlative studies of pre- and postsynaptic tuning properties. For circuit neuroscience in general, functionally imaging genetically defined pre- and postsynaptic circuit components, separable by color, promises to be a powerful approach to studying neural interactions in the brain.

ACKNOWLEDGMENTS

Many thanks to: Mideia Kotsogianni for preparation of dissociated hippocampal cultures; Andrew Lowe for software design and valuable instruction; Paul Hunter, Nikolas Nikolaou, and Fatima Abbas for practical help, advice, and for comments on the manuscript; James Jontes (HuC:GFP) and Steve Wilson (ath5:Gal4) for DNA constructs and Robert E. Campbell for RGECO cDNA (Addgene plasmid 32444). Funding: This work was supported by an MRC 4 years Ph.D. studentship (Alison S. Walker), MRC project grants (Martin P. Meyer and Juan Burrone) and a Wellcome Trust Investigator Award and Lister Prize fellowship to Juan Burrone.

REFERENCES

Akerboom, J., Chen, T. W., Wardill, T. J., Tian, L., Marvin, J. S., Mutlu, S., et al. (2012). Optimization of a GCaMP calcium indicator for neural activity imaging. *J. Neurosci.* 32, 13819–13840.

Dreosti, E., Odermatt, B., Dorostkar, M. M., and Lagnado, L. (2009). A genetically encoded reporter of synaptic activity *in vivo*. *Nat. Methods* 6, 883–889.

Gabriel, J. P., Trivedi, C. A., Maurer, C. M., Ryu, S., and Bollmann, J. H. (2012). Layer-specific targeting of direction-selective neurons in the zebrafish optic tectum. *Neuron* 76, 1147–1160.

Huber, D., Gutnisky, D. A., Peron, S., O'Connor, D. H., Wiegert, J. S., Tian, L., et al. (2012). Multiple dynamic representations in the motor cortex during sensorimotor learning. *Nature* 484, 473–478.

Koster, R. W., and Fraser, S. E. (2001). Tracing transgene expression in living zebrafish embryos. *Dev. Biol.* 233, 329–346.

Lister, J. A., Robertson, C. P., Lepage, T., Johnson, S. L., and Raible, D. W. (1999). nacre encodes a zebrafish microphthalmia-related protein that regulates neural-crest-derived pigment cell fate. *Development* 126, 3757–3767.

Lutcke, H., Murayama, M., Hahn, T., Margolis, D. J., Astori, S., Zum Alten Borgloh, S. M., et al. (2010). Optical recording of neuronal activity with a genetically-encoded calcium indicator in anesthetized and freely moving mice. *Front. Neural Circuits* 4:9. doi: 10.3389/fncir.2010.00009

Mank, M., Santos, A. F., Direnberger, S., Mrsic-Flogel, T. D., Hofer, S. B., Stein, V., et al. (2008). A genetically encoded calcium indicator for chronic *in vivo* two-photon imaging. *Nat. Methods* 5, 805–811.

Miesenbock, G., De Angelis, D. A., and Rothman, J. E. (1998). Visualizing secretion and synaptic transmission with pH-sensitive green fluorescent proteins. *Nature* 394, 192–195.

Muto, A., Ohkura, M., Kotani, T., Higashijima, S., Nakai, J., and Kawakami, K. (2011). Genetic visualization with an improved GCaMP calcium indicator reveals spatiotemporal activation of the spinal motor neurons in zebrafish. *Proc. Natl. Acad. Sci. U.S.A.* 108, 5425–5430.

Nevin, L. M., Robles, E., Baier, H., and Scott, E. K. (2010). Focusing on optic tectum circuitry through the lens of genetics. *BMC Biol.* 8:126. doi: 10.1186/1741-7007-8-126

Nikolaou, N., Lowe, A. S., Walker, A. S., Abbas, F., Hunter, P. R., Thompson, I. D., et al. (2012). Parametric functional maps of visual inputs to the tectum. *Neuron* 76, 317–324.

Robles, E., Smith, S. J., and Baier, H. (2011). Characterization of genetically targeted neuron types in the zebrafish optic tectum. *Front. Neural Circuits* 5:1. doi: 10.3389/fncir.2011.00001

Shaner, N. C., Lin, M. Z., McKeown, M. R., Steinbach, P. A., Hazelwood, K. L., Davidson, M. W., et al. (2008). Improving the photostability of bright monomeric orange and red fluorescent proteins. *Nat. Methods* 5, 545–551.

Tian, L., Hires, S. A., Mao, T., Huber, D., Chiappe, M. E., Chalasani, S. H., et al. (2009). Imaging neural activity in worms, flies and mice with improved GCaMP calcium indicators. *Nat. Methods* 6, 875–881.

Yaksi, E., and Friedrich, R. W. (2006). Reconstruction of firing rate changes across neuronal populations by temporally deconvolved Ca^{2+} imaging. *Nat. Methods* 3, 377–383.

Yamada, Y., and Mikoshiba, K. (2012). Quantitative comparison of novel GCaMP-type genetically encoded Ca(2+) indicators in mammalian neurons. *Front. Cell Neurosci.* 6:41. doi: 10.3389/fncel.2012.00041

Zhao, C., Dreosti, E., and Lagnado, L. (2011a). Homeostatic synaptic plasticity through changes in presynaptic calcium influx. *J. Neurosci.* 31, 7492–7496.

Zhao, Y., Araki, S., Wu, J., Teramoto, T., Chang, Y. F., Nakano, M., et al. (2011b). An expanded palette of genetically encoded Ca(2)(+) indicators. *Science* 333, 1888–1891.

Conflict of Interest Statement: The authors declare that the research was conducted in the absence of any commercial or financial relationships that could be construed as a potential conflict of interest.

Received: 17 January 2013; paper pending published: 09 February 2013; accepted: 15 February 2013; published online: 06 March 2013.

Citation: Walker AS, Burrone J and Meyer MP (2013) Functional imaging in the zebrafish retinotectal system using RGECO. Front. Neural Circuits 7:34. doi: 10.3389/fncir.2013.00034

frontiers in
NEURAL CIRCUITS

ORIGINAL RESEARCH ARTICLE
published: 17 April 2013
doi: 10.3389/fncir.2013.00067

Control of a specific motor program by a small brain area in zebrafish

Otto Fajardo*, Peixin Zhu and Rainer W. Friedrich*

Friedrich Miescher Institute for Biomedical Research, Basel, Switzerland

Edited by:
German Sumbre, Ecole Normale Superieure, France

Reviewed by:
David McLean, Northwestern University, USA
Donald O'Malley, Northeastern University, USA

****Correspondence:***
Otto Fajardo and Rainer W. Friedrich, Friedrich Miescher Institute for Biomedical Research, Maulbeerstrasse 66, 4058 Basel, Switzerland.
e-mail: otto.fajardo@fmi.ch; rainer.friedrich@fmi.ch

Complex motor behaviors are thought to be coordinated by networks of brain nuclei that may control different elementary motor programs. Transparent zebrafish larvae offer the opportunity to analyze the functional organization of motor control networks by optical manipulations of neuronal activity during behavior. We examined motor behavior in transgenic larvae expressing channelrhodopsin-2 throughout many neurons in the brain. Wide-field optical stimulation triggered backward and rotating movements caused by the repeated execution of J-turns, a specific motor program that normally occurs during prey capture. Although optically-evoked activity was widespread, behavioral responses were highly coordinated and lateralized. 3-D mapping of behavioral responses to local optical stimuli revealed that J-turns can be triggered specifically in the anterior-ventral optic tectum (avOT) and/or the adjacent pretectum. These results suggest that the execution of J-turns is controlled by a small group of neurons in the midbrain that may act as a command center. The identification of a brain area controlling a defined motor program involved in prey capture is a step toward a comprehensive analysis of neuronal circuits mediating sensorimotor behaviors of zebrafish.

Keywords: zebrafish, optogenetics, motor control, prey capture, J-turn

INTRODUCTION

The brain adjusts behavioral actions to events in the environment by transforming sensory input into specific motor output. Even seemingly simple sensory-motor transformations comprise multiple components such as a quantitative evaluation of specific sensory information, sometimes a binary decision, and the computation of appropriate motor commands. A fundamental goal of neuroscience is to understand how each of these tasks are performed by ensembles of neurons, and how these ensembles interact to produce a coherent behavioral response to sensory input (Grillner et al., 2008). An important first step toward this goal is the decomposition of sensory processing and behavioral output into distinct components and the identification of brain areas that control these components. An attractive animal model for systematic analyses of sensory-motor transformations is the larval zebrafish because it is small, transparent, and amenable to sophisticated genetic manipulations (Friedrich et al., 2010). As a consequence, it is possible to activate or silence genetically or spatially defined subsets of neurons by optogenetic approaches and analyze their functions in the context of specific behaviors (Arrenberg et al., 2009; Wyart et al., 2009; del Bene and Wyart, 2012).

Zebrafish larvae have been used to explore the neural basis of simple visual behaviors such as the optokinetic and optomotor responses (Liu and Fetcho, 1999; Neuhauss et al., 1999; Orger et al., 2000, 2008; Orger and Baier, 2005; Huang et al., 2006; Emran et al., 2007; Schoonheim et al., 2010). Visual information is first processed in the retina and then conveyed by retinal ganglion cells to 10 different target areas, the largest of which is the optic tectum (Burrill and Easter, 1994). Optokinetic and optomotor responses are driven by coherent visual motion, which is processed in extra-tectal target areas of retinal ganglion cells (Roeser and Baier, 2003; Gahtan et al., 2005). For the optomotor response, changes in swimming speed and direction were found to be controlled by descending command neurons in the brainstem (Orger et al., 2008). A more complex behavior involving multiple components is prey capture, which emerges ∼5 days post fertilization (dpf) when larvae start to feed. This behavior is operant in nature, is induced by small visual stimuli, and consists of a sequence of motor actions that mediate the approach and finally the catch of the prey (Borla et al., 2002; McElligott and O'Malley, 2005; Portugues and Engert, 2009).

Prey capture of zebrafish larvae is strongly reduced in the dark or in blind fish, as measured by the ability to consume Paramecia in a Petri dish (Gahtan et al., 2005; McElligott and O'Malley, 2005). Unlike optokinetic or optomotor reflexes, prey capture is impaired by ablation of the optic tectum (Roeser and Baier, 2003; Gahtan et al., 2005). Tectal output relevant for prey capture may be conveyed to motor nuclei in the hindbrain and spinal cord via the nucleus of the medial longitudinal fascicle (Gahtan et al., 2005) and the reticular formation (Sato et al., 2007). However, the precise set of nuclei involved in prey capture, and the flow of information between these nuclei, has not been established. As prey capture involves a sequence of distinct motor actions, different components of the behavior may be controlled by distinct ensembles of neurons, which could interact serially or in parallel.

Motor behavior leading to prey capture has been decomposed into three phases: orientation toward the prey, approach, and strike (Budick and O'Malley, 2000). During orientation, the fish turns to orient its anterior-posterior body axis toward the

prey. This is achieved by a distinctive motor pattern known as J-turn that consists of repetitive unilateral bends of the caudal tail, often accompanied by parallel movements of the pectoral fins (McElligott and O'Malley, 2005). J-turns rotate the body axis of the fish and sometimes result in a slow backward movement (McElligott and O'Malley, 2005). In addition, J-turns are accompanied by convergent eye movements that increase the frontal field of binocular vision, possibly to facilitate stereoscopic estimates of the distance to the prey (Ewert et al., 2001; Bianco et al., 2011). Under laboratory conditions, J-turns including convergent eye movements can be evoked by small moving dots in the frontal visual field (Bianco et al., 2011). These J-turns rotate the fish toward the stimulus, presumably because the stimulus mimics prey. Larger visual stimuli, in contrast, evoke turns in the opposite direction (Bianco et al., 2011). J-turns are therefore a distinct motor program in a sequence of swimming maneuvers during prey capture. However, the brain areas involved in the neural control of J-turns remain unknown. Ablations of the optic tectum in zebrafish larvae reduced small-angle turning movements in the presence of prey (Gahtan et al., 2005), and the tectum contains neurons that are tuned to small moving stimuli (Niell and Smith, 2005; Del Bene et al., 2010). One candidate area that may control J-turns is therefore the optic tectum.

We previously generated transgenic fish expressing channelrhodopsin-2 fused to yellow fluorescent protein (ChR2YFP) under the control of the HuC promoter and the Tet system. Illumination of these larvae with blue light-evoked slow backward movements, a behavior that does not occur spontaneously (Zhu et al., 2009). In this study, we found that this behavior is not caused by uncoordinated muscle movements but by the repeated execution of J-turns. Calcium imaging showed that blue light stimulation evoked widespread neuronal activity in multiple brain regions. However, fiber-optic mapping of behavioral responses revealed that J-turns are specifically triggered by optical stimulation of the anterior-ventral tectum and possibly the underlying pretectum. Focal optical stimulation of this area evoked all characteristics of J-turns in a lateralized fashion. Our experiments therefore identified a small circumscribed brain area that exerts specific control over a defined motor program. These results provide insights into a distinct component of the sensory-motor transformations involved in prey capture.

MATERIALS AND METHODS

ANIMALS

Adult fish were maintained at 25°C on a 14/10 h on/off light cycle. HuC:itTA/Ptet:ChR2YFP (lines 2 and 3), Dlx4/6:itTA/Ptet:ChR2YFP (Zhu et al., 2009), and OMP:ChR2YFP (Blumhagen et al., 2011) were outcrossed to wild-type fish (strain AbTÜ/tl) to obtain offspring expressing ChR2YFP and ChR2YFP-negative siblings as controls ("wt"). HuC:itTA/Ptet:ChR2YFP fish were also crossed to nacre(−/−) fish and the F1 generation was incrossed to obtain ChR2YFP-positive fish in the nacre background. Eggs were collected and maintained in E3 medium containing (in mM) 5 NaCl, 0.17 KCl, 0.33 $CaCl_2$, and 0.33 $MgSO_4$. After sorting at 4–6 dpf, larvae were maintained in standard fish water from the facility and fed powdered fish food. Fish were used between 13 and 25 dpf unless stated otherwise. All experimental protocols were approved by the Veterinary Department of the Canton Basel-Stadt (Switzerland).

BEHAVIORAL ANALYSIS OF FREELY SWIMMING LARVAE

Low-zoom videos from individual zebrafish larvae were collected in a 35 mm Petri dish at a rate of 30 frames per second (fps) using a video tracking system (Zebralab, Viewpoint, France). One light-emitting diode (LED; Luxeon V-Star; 470 nm and 590 nm) equipped with a collimator was placed next to the Petri dish at a distance of ∼5 cm and an angle of ∼45°. The LED produced ∼0.35 mW/mm^2 at the location of the dish. For experiments testing the effect of light intensity, multiple LEDs (Luxeon Rebel; 470 nm) were arranged around the Petri dish in a circle. Behavioral responses of each larva were tested only once after acclimation of the larvae to the Petri dish for 2–3 min. A trial consisted of three 20 s periods. Blue light was off during the first and the third period and on during the second period. Swimming trajectories were extracted using Viewpoint software and further analyzed in Matlab (Mathworks). Swimming speed was quantified as the mean displacement between adjacent frames, divided by the frame time, and binned into 1 s bins. The "visuomotor on response" was quantified as the mean change in swimming speed during 2 s after light onset, relative to a 10 s baseline period before light onset. The steady state light response was quantified as the mean change in swimming speed during the last 10 s during illumination relative to baseline. The off-response was quantified as the mean change in swimming speed during 20 s after light offset relative to the last 10 s during illumination. Behaviors were visually classified as J-turning when fish moved backwards and the caudal part of the tail was bent repeatedly to one side.

To obtain high-resolution videos, individual zebrafish larvae were placed in a circular arena of 15 mm diameter under a dissecting microscope (SZX 16 with 1xPF Plapo Objective; Olympus) and filmed at a rate of 60 fps using a Grasshopper GRAS-03K2M-C (Point Grey) camera and mot-mot software (Straw and Dickinson, 2009). Fish were illuminated by a blue LED (Luxeon V-Star; 470 nm) placed next to the arena as described above. Blue light was turned on manually when the fish entered the center of the arena. Behaviors were classified by visual inspection of video sequences into one of four categories: "J-turn," "escape," "stop," or "no response." "J-turn" was scored as described above. "Escape" was defined as an abrupt episode of fast swimming within the first frame after light onset. A more precise analysis of this behavior was not possible because it is too fast to resolve in detail at 60 fps (Liu and Fetcho, 1999). "Stop" was defined as an abrupt cessation of swimming for at least 200 ms after light onset. "No response" was scored when no obvious change in swimming speed and direction were detected relative to a period of ∼5 s before light onset.

HEAD-FIXED BEHAVIOR

HuC:itTA/Ptet:ChR2YFP larvae used in experiments with head fixation were pre-selected for backward-swimming responses under the conditions described above. Fish were anesthetized in tricaine methanesulfonate (MS-222; 0.1 mg/ml, Sigma-Aldrich) and embedded in 1.5% type VII agarose (low gelling temperature, Sigma-Aldrich) within a 35 mm petri dish. Agarose around

the tail and pectoral fins was removed and MS-222 was washed out with fresh fish water to let the fish recover from anesthesia. Wide-field optical stimulation was performed for 3 s with an LED as described above (∼0.35 mW/mm^2). Spatially restricted optical stimulation was performed through the objective of a custom microscope (Euler et al., 2009; Zhu et al., 2012) or using an optical fiber. The microscope was equipped with a 20× objective (Zeiss, NA 1.0), a blue excitation filter (460/50 nm), and a 300 W Xe lamp (LB-LS/30, Sutter Instrument Co.). The mean light intensity in the specimen plane was ∼3 mW/mm^2. However, illumination intensity was not uniform throughout the field of view but substantially higher in the center. For fiber-optic stimulation, optical fibers of 50 or 200 μm diameter (Thorlabs, M14L05 or BFL22-200, respectively) were coupled to a blue laser (CNI; MBL-F-457 nm-500 mW) as described (Zhu et al., 2012). Fibers were held by a hollow metallic rod that was fixed to a rotating mount. The rod was bent by 90° so that the bare end of the fiber was perpendicular to the surface of the fish and could be rotated about the anterior-posterior axis. The rotating mount was held by a motorized manipulator to change fiber position and place the fiber tip close to the fish at each position. The mean light power at the end of the fiber was 110 ± 17 mW/mm^2 (average over all experiments). To examine the intensity-dependence of behavioral responses, light intensity was varied between 0 and 800 mW/mm^2. Larvae were filmed at a rate of 60 fps (LED stimulation) or 200 fps (fiber-optic stimulation) using a Grasshoper GRAS-03K2M-C (Point Grey) camera mounted on a dissecting microscope (SZX 16 with 1xPF Plapo Objective; Olympus). In experiments using optical stimulation through an objective, larvae were filmed using the same camera through the condensor of the microscope at 25 fps. Image acquisition was controlled by mot-mot software (Straw and Dickinson, 2009).

Blue light illumination was synchronized to video acquisition by a TTL signal. For coarse behavioral analyses, videos were analyzed visually to classify tail motion as "J-turn," "forward swimming," "C-bend," "escape/struggling," or "no movement." "J-turn" was defined as in freely swimming fish as repetitive low-amplitude unilateral bends of the caudal part of the tail (McElligott and O'Malley, 2005). "Forward swimming" was defined as repetitive low amplitude bilateral undulations of the tail (Wyart et al., 2009). "C-bend" was defined as a single large amplitude unilateral bend of the tail, as described previously (Liu and Fetcho, 1999; Sankrithi and O'Malley, 2010). "Escape/struggling" was defined as multiple large-amplitude bilateral bends of the tail (Liu and Fetcho, 1999; Sankrithi and O'Malley, 2010). "No movement" was scored if no tail movements occurred during light stimulation.

For more detailed quantitative analyses of tail movements, videos acquired at 200 fps were analyzed to extract the curvature of the tail in each frame by custom software written in Python. The curvature of the tail was measured using methods similar to those used in a previous study (Bianco et al., 2011). We computed the skeleton of the tail at each frame, divided it in 10 segments, calculated the nine angles between segments and summed over all angles. Resulting traces representing tail bend angle as a function of time were filtered with a low-pass butterworth filter. Anti-clockwise bends are represented by positive angles and clock-wise bends are represented by negative angles. To calculate the asymmetry coefficient from the trace representing tail angle as a function of time, the sign of the absolute tail angle (positive or negative) was determined at each peak of the trace. The asymmetry coefficient was then calculated as the number of peaks with positive sign minus the number of peaks with sign, divided by the total number of peaks. Values close to 0 thus reflect symmetric tail movements while numbers close to one represent highly asymmetric tail movements. Cumulative amplitudes of tail bends were calculated as the sum of the differences between successive peaks and therefore reflect the total amount of tail movement during the behavior. To evaluate eye movements, we fit an ellipse to each eye and extracted the angle of the longer axis relative to the midline of the fish. Resulting traces representing eye angle as a function of time were filtered with a low-pass butterworth filter. Positive changes in angle correspond to eye movements in clockwise direction. Vergence angle was defined as the difference between the angles of the left and right eyes. Rotation toward the midline of either eye results in an increase in vergence angle.

CONFOCAL IMAGING

Fish were anesthetized with MS222 (0.1 mg/ml, Sigma-Aldrich) and decapitated. The preparation was glued to the lid of a 35 mm petri dish with tissue adhesive (Vetbond, 3M) and the skin over the brain was removed with a 0.125 mm tungsten dissection probe (WPI). Confocal imaging was then performed using an Olympus Fluoview microscope with a 488 nm excitation laser and an emission filter for eGFP/YFP (505/50 nm).

KAEDE PHOTOCONVERTION

HuC:kaede transgenic fish (Sato et al., 2006) were anesthetized with MS222 (0.1 mg/ml), embedded in agarose and placed under a dissection microscope (SZX 16 with 1x PF Plapo Objective; Olympus). An optic fiber (50 μm diameter) was coupled to a 405 nm laser (CNI; MDL-III-405nm-250mW) and positioned at the target site using the same procedure as for blue light stimulation. Fish were illuminated for 5 min. Kaede fluorescence was then imaged using a customized two-photon microscope equipped with a 20× water immersion objective (NA 1.0; Zeiss), a Ti:Sapphire laser (SpectraPhysics, Mountain View, CA, USA) at 860 nm, and a photomultiplier-based whole-field detector with emission filters 535/50 nm (green/yellow) and 640/75 nm (red). Data acquisition was controlled by ScanImage and Ephus software (Pologruto et al., 2003; Suter et al., 2010).

ANALYSIS OF MELANOPHORES

Fish were anesthetized in MS-222 (0.1 mg/ml, Sigma-Aldrich), embedded in type VII agarose (low gelling temperature, Sigma-Aldrich) and placed under a dissecting microscope (SZX 16 with 1x PF Plapo Objective; Olympus), A picture of the head was taken using a camera attached to the microscope (F-view system; Olympus) while the fish was illuminated from below with an LED lamp integrated into the microscope stand. Images were taken after several minutes of illumination to ensure that melanophores were in the light-adapted state. Using Matlab (Mathworks), pictures were binarized by thresholding, registered by landmarks

(snout, eyes, and ears) and summed into a single image. A mask was then drawn over the region over the brain, excluding the eyes and ears. Pixel values represent the number of fish in which the given pixel was covered by a melanophore.

CALCIUM IMAGING

Fish were anesthetized and paralyzed with MS-222 (0.1 mg/ml, Sigma-Aldrich) and Mivacron (0.5 mg/ml, GlaxoSmithKline), respectively, and decapitated. The preparation was glued to a small plastic slide using tissue glue (Vetbond; 3M). Fish water was replaced by cold teleost ACSF (131 mM NaCl, 2 mM KCl, 1.25 mM KH2PO4, 2 mM MgSO4, 10 mM glucose, 2.5 mM CaCl2, and 20 mM NaHCO3) (Mathieson and Maler, 1988) and drugs were washed out. The skin and skull over the brain were removed with a 0.125 mm tungsten dissection probe. The preparation was then incubated at room temperature with rhod-2-AM (6.25 μg in 2 μl DMSO/pluronic F-127 80/20; Invitrogen) for 45 min in ACSF that was continuously bubbled with 95% O2/5% CO2. The preparation was viewed under a custom microscope equipped with a 20× objective (N.A. 1.0; Zeiss) (Euler et al., 2009; Zhu et al., 2012). An optic fiber (200 μm diameter) coupled to a blue laser was placed close to the preparation at an angle of ∼30° so that the light beam was directed approximately to the anterior tectum on one side of the brain. Conventional epifluorescence imaging was performed using a Xe arc lamp (Sutter Instrument Co. LB-LS/30, 300 W), a 545/25 excitation filter, a 605/70 emission filter, and a CCD camera (CoolSnap; Photometrics). Data was acquired using custom software written in Igor (Wavemetrics) and analyzed using custom software written in Python. Fluorescence signals were expressed as relative changes in fluorescence intensity (ΔF/F) in each pixel with respect to a pre-stimulus baseline.

STATISTICAL ANALYSIS

All summary data are presented as mean ± s.e.m unless noted otherwise. Age of fish in days is reported with the standard deviation (SD). Statistical tests used are stated in the Results.

RESULTS

OPTICAL STIMULATION OF MOTOR BEHAVIOR IN ZEBRAFISH LARVAE EXPRESSING CHANNELRHODOPSIN-2

In a previous study, multiple lines of HuC:itTA/Ptet:ChR2YFP transgenic zebrafish were created that express two transgenes: (1) the Tet activator, itTA, under the control of the HuC promoter, and (2) channelrhodopsin-2 (ChR2) fused to yellow fluorescent protein (YFP; Chr2YFP) under the control of Ptet, a Tet responder element (Zhu et al., 2009). As a result, Chr2YFP is expressed in many, though not all, neurons at larval stages (**Figure 1A**). In some of these lines, exposure to blue light triggered slow backward movement of larvae. However, because motor behavior was analyzed at low resolution, it remained unclear whether backward movements were generated by a coordinated motor program, or whether they were caused by uncoordinated muscle contractions (Zhu et al., 2009).

To address this question we illuminated freely swimming zebrafish larvae between 13 and 24 dpf (mean ± SD: 16 ± 3 dpf) with a blue LED for 20 s and monitored motor behavior by video imaging at high magnification. The light intensity at the specimen was ∼0.35 mW/mm^2. Under baseline conditions, larvae showed normal swimming behavior, consisting of bouts separated by periods of little or no movement. Light onset triggered different motor behaviors that were classified as "backward movement," "visuomotor on response," "stop," "escape," and "no response." "Backward movement consisted of a slow backward displacement, often associated with lateral excursions or rotations. This behavior was never observed spontaneously in clean water. The "visuomotor on response" is a well-described transient increase in mean swimming speed after a change in ambient light levels, mainly due to an increase in bout frequency, that is mediated by the visual system (Burgess and Granato, 2007). "Escape" was defined as a sudden episode of high-speed swimming after light onset. "Stop" was defined as a cessation of swimming, and "no response" was scored when no obvious change in swimming behavior was observed.

Among HuC:itTA/Ptet:ChR2YFP larvae ($n = 47$; one trial per fish), 43% responded to blue light stimulation with backward movement, 23% showed a visuomotor on response, 6% stopped swimming, 15% escaped, and 13% showed no response. In wt siblings that did not express ChR2 ($n = 12$), backward movement was never observed but 50% showed visuomotor on responses, 17% stopped swimming, 8% escaped, and 25% showed no response (**Figure 1B**). In addition, we selected three HuC:itTA/Ptet:ChR2YFP larvae that swam backwards during blue light illumination and tested their response to illumination with an amber LED (590 nm, ∼0.35 mW/mm^2). All of these fish showed a strong visuomotor on response to amber light but no backward motion. These results confirm that backward movement is triggered by activation of ChR2. The observed frequency of backward movement was somewhat lower than in a previous study (43% vs. ∼80%) (Zhu et al., 2009), possibly because the expression levels of ChR2YFP decreased slightly over successive generations.

High-magnification videos showed that fish performed slow, repeated, unilateral tail bends during backward movement episodes. These bends were usually limited to the caudal part of the tail while the proximal trunk appeared stiff (**Figure 1C**). This motor behavior resulted in a net backward motion and often also rotated the fish (**Figure 1C, overlay**). Within a trial, tail bends were usually exclusively to one side (45% to the right, 50% to the left; 5% both sides). This behavior closely resembles J-turns, a motor pattern displayed during prey capture (McElligott and O'Malley, 2005; Bianco et al., 2011). The latency (time from blue light onset to the beginning of tail movement) and the duration of this behavior were 186 ± 50 ms and 1038 ± 50 ms, respectively.

To characterize the motor behavior underlying optically-evoked backward movement in more detail we immobilized larvae by embedding the head in agarose and filmed motor behavior at 60 Hz. The tail and pectoral fins were free [age of fish: 17.5 ± 4 dpf (mean ± SD); range: 13–24 dpf]. Tail movements evoked by a 3 s illumination with a blue LED (∼0.35 mW/mm^2) were classified into motor patterns that have been associated with different swimming patterns: J-turning, forward swimming, C-bends, escape/struggling, and no movement (**Figure 1D**). J-turning was defined as repeated unilateral bends of the caudal tail. Forward

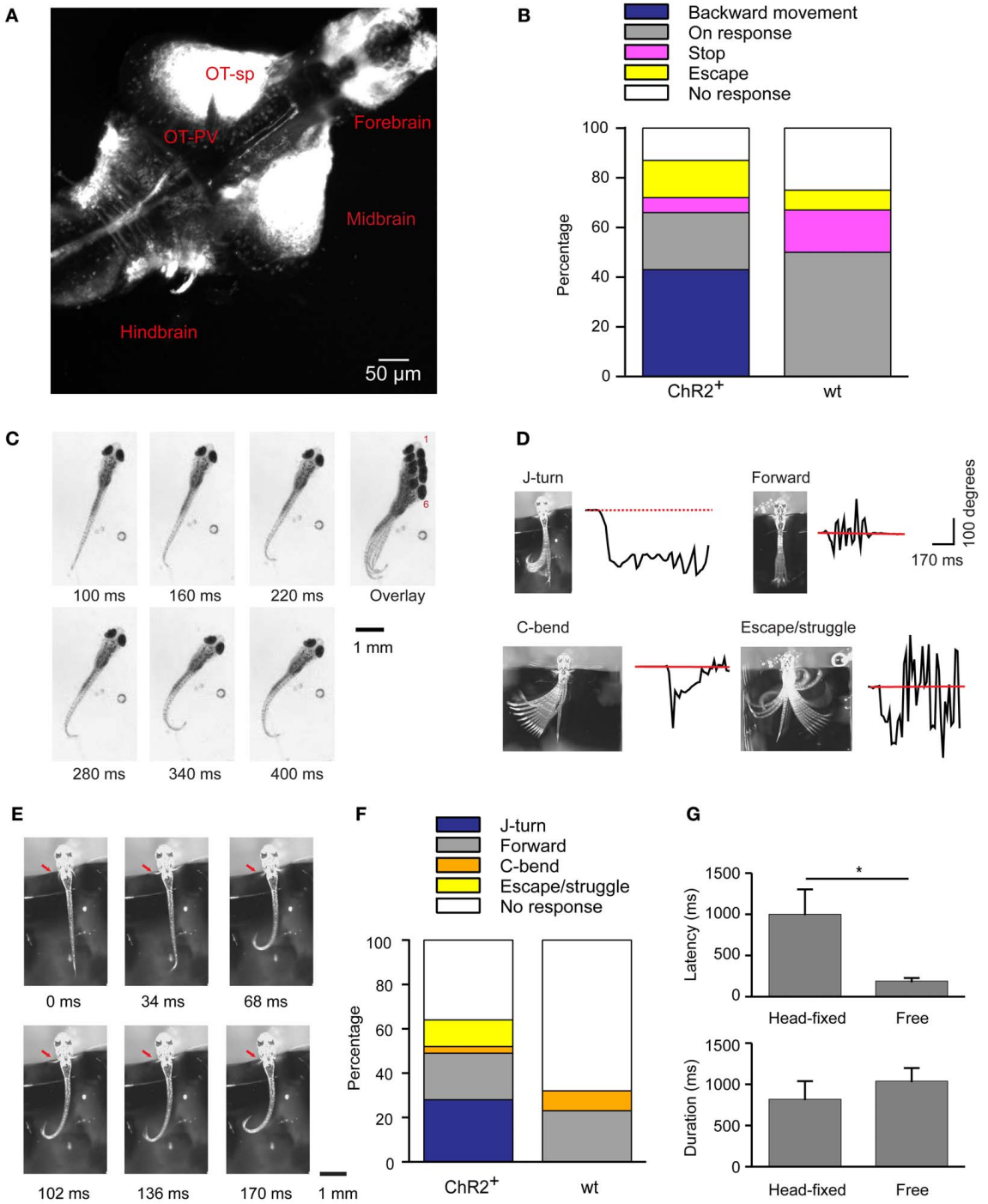

FIGURE 1 | Optical stimulation evokes J-turn in HuC:itTA/Ptet:ChR2YFP zebrafish larvae. (A) Pattern of ChR2YFP expression in the brain of a HuC:itTA/Ptet:ChR2YFP larva (17 dpf; z-projection of a confocal stack). OT-sp, Optic tectum-superficial layers; OT-PV, Optic tectum-periventricular layer. **(B)** Classification of behavioral responses to blue light stimulation in freely swimming zebrafish larvae. Backward movement was the dominant response in HuC:itTA/Ptet:ChR2YFP transgenics (ChR2$^+$; $n = 47$ fish; one trial per fish) but never occurred in wt siblings (wt; $n = 12$). **(C)** Video sequence of a freely swimming HuC:itTA/Ptet:ChR2YFP larvae during an episode of backward movement. Note unilateral bends of the caudal tail, a characteristic of J-turns. Overlay illustrates net backward movement and rotation. **(D)** Examples of four different behaviors observed in head-fixed fish. Black traces show the curvature of the tail as a function of time. Red line represents the resting angle (straight tail). **(E)** Video sequence of a J-turn response in a head-fixed larva. Note unilateral bends of the caudal tail and symmetric movement of the pectoral fins (red arrow). **(F)** Classification of behavioral responses to blue light stimulation in head-fixed larvae. J-turns were frequently observed in HuC:itTA/Ptet:ChR2YFP (95 trials in 17 fish) but never in wt siblings (44 trials in 8 fish). **(G)** Latency (time from blue light onset to the initiation of motor response) and duration of J-turns evoked by blue light stimulation in freely swimming ($n = 12$) and head-fixed ($n = 15$) HuC:itTA/Ptet:ChR2YFP larvae (mean ± s.e.m.). *$p = 0.019$, Student's t-test.

swimming was defined as continuous and symmetric undulations of the entire tail with intermediate amplitude and frequency. C-bends were defined as single, fast unilateral bends of the tail. This well-characterized motor program orients the fish away from an aversive stimulus during an escape response (Liu and Fetcho, 1999). Escape swimming/struggling was defined as high-amplitude, bilateral tail movements more vigorous than forward swimming. No response was scored when no obvious movements were observed. Head-fixed HuC:itTA/Ptet:ChR2YFP fish responded to light with J-turns (**Figure 1E**; **Movie S1**), although with lower probability than under free-swimming conditions ($n = 95$ trials in 17 fish, **Figure 1F**), indicating that head-fixation increased behavioral thresholds. Wt siblings never performed J-turns and usually showed no response ($n = 44$ trials in 8 fish, **Figure 1F**). The latency of optically-evoked J-turns in HuC:itTA/Ptet:ChR2YFP fish (1001 ± 302 ms; $n = 15$ fish) was longer than in freely swimming animals (Student's t-test, $p = 0.019$) but the duration was similar (819 ± 200 ms, $n = 15$ fish; Student's t-test, $p > 0.05$, **Figure 1G**).

In zebrafish hunting real or virtual prey, J-turns often involve simultaneous forward and backward swings of both pectoral fins ("in-phase fin movements"). During forward swimming, in contrast, pectoral fins are moved in anti-phase or held still (Thorsen et al., 2004). Moreover, J-turns are often associated with convergent eye movements (Borla et al., 2002; McElligott and O'Malley, 2005; Bianco et al., 2011). We found that unilateral tail movements evoked by optical stimulation of head-fixed HuC:itTA/Ptet:ChR2YFP larvae were accompanied by in-phase movements of both pectoral fins in almost all trials (95%) (**Figure 1E, arrow**; **Movie S1**). During behavior classified as forward swimming, in-phase movements of the pectoral fins occurred in only 10% of trials while anti-phase movements were frequently observed. Moreover, optical stimulation that evoked J-turning often also evoked convergent eye movements (**Figure 2A**; **Movie S1**). To quantify eye movements we measured the angular difference in the orientation of the two eyes (vergence angle) before and during exposure to blue light. This difference was clearly positive in HuC:itTA/Ptet:ChR2YFP larvae, indicating convergence of the eyes, but near 0 in wt siblings [150 trials in ChR2 positive fish and 44 trials in WT fish, Student's t-test, $p < 0.001$; age of fish: 18 ± 3.4 dpf (mean ± SD), range: 13–22 dpf; **Figure 2B**]. In HuC:itTA/Ptet:ChR2YFP fish, convergent eye movements occurred in the majority of trials that evoked unilateral tail movements ($n = 65$) but were virtually absent when optical stimulation failed to evoke tail movements ($n = 49$). No convergent eye movements were observed in wt fish ($n = 32$; **Figure 2C**). Hence, optical stimulation evoked a coordinated motor program with all characteristics of J-turns. We therefore refer to the motor behavior during optically-evoked backward movements as J-turning.

During prey capture, J-turns orient the fish toward the prey before the strike (McElligott and O'Malley, 2005). J-turns do therefore not normally occur in isolation but are embedded in a sequence of other motor programs (McElligott and O'Malley, 2005). Moreover, episodes of J-turning are brief, which explains why J-turning is not always associated with a net backward movement during prey capture. Optogenetic stimulation of HuC:itTA/Ptet:ChR2YFP larvae therefore triggered the repeated execution of an isolated motor pattern.

FURTHER CHARACTERIZATION OF OPTICALLY-EVOKED J-TURNS

To further quantify motor behavior in head-fixed fish we selectively illuminated the midbrain with a laser through an optic fiber (diameter, 200 or 50 μm; light intensity 110 ± 17 mW/mm^2), filmed motor behavior at 200 Hz, and quantified the curvature of the tail [18 ± 3.6 dpf (mean ± SD), range: 13–24 dpf]. We restricted our analysis to J-turns and forward swimming because C-bends and escape/struggling swimming were too fast to track even at 200 Hz. Forward swimming was characterized by bilateral low amplitude tail bends, while J-turns were characterized by repetitive unilateral bends of the caudal tail (**Figure 3A**). To quantify the frequency of tail bends in these two behaviors we analyzed tail curvature as a function of time (**Figure 3A**), computed power spectra of each trial, and averaged power spectra over trials. Power spectra of J-turns had a peak at low frequency (<5 Hz) reflecting the unilateral excursion of the tail, and another, broad peak between 15 and 20 Hz that reflects repetitive bending of the caudal tail. This frequency is similar to the tail bend frequency during naturally occurring J-turns or slightly lower (McElligott and O'Malley, 2005; Bianco et al., 2011). Small differences between optically-evoked and naturally occurring behaviors may be due to head fixation or differences in age. Power spectra of forward swims showed one or multiple peaks between 15 and 20 Hz (**Figure 3B**).

Asymmetry of tail movements to the left and right sides was quantified by a coefficient that varies between 0 (completely symmetric tail movements) and 1 (tail bent to only one side). This analysis confirmed that tail movements were highly asymmetric during J-turns but nearly symmetric during forward swims (J-turns: 0.88 ± 0.01, $n = 138$ trials in 12 fish; forward swims: 0.12 ± 0.02, $n = 35$ trials in 9 fish; $p < 0.001$, Student's t-test; **Figures 3A,C**). The latency of J-turns and forward swims was not significantly different (J-turns: 736 ± 50 ms; forward swimming: 870 ± 131 ms; $p > 0.05$, Student's t-test; **Figure 3D**). The duration of the behavior was determined as the period during light stimulation when obvious tail movements occurred. During this period, fish sometimes showed multiple episodes of tail movements, separated by short episodes of low activity. On average, the duration of J-turn behavior (1115 ± 61 ms) was significantly lower than the duration of forward swims (1542 ± 172 ms; $p = 0.004$, Student's t-test, **Figure 3E**). Nevertheless, the mean duration of J-turn behavior appeared substantially longer than episodes of J-turning during prey capture (Borla et al., 2002; McElligott and O'Malley, 2005; Bianco et al., 2011). J-turns usually ceased before the end of the 3 s light stimulation. This observation is consistent with transient J-turn responses to stimulation with virtual prey (Bianco et al., 2011) and may reflect fatigue, inactivation of ChR2, or adaptation. The mean frequency of tail beats, averaged over the duration of the behavior, was significantly lower during J-turning than during forward swimming (12 ± 0.5 vs. 15 ± 0.9 Hz; $p = 0.005$, Student's t-test, **Figure 3F**). The cumulative amplitude of tail beats (sum of absolute amplitude peaks) was also significantly lower during J-turns (613 ± 34° vs. 1997 ± 293°; $p < 0.001$, Student's t-test,

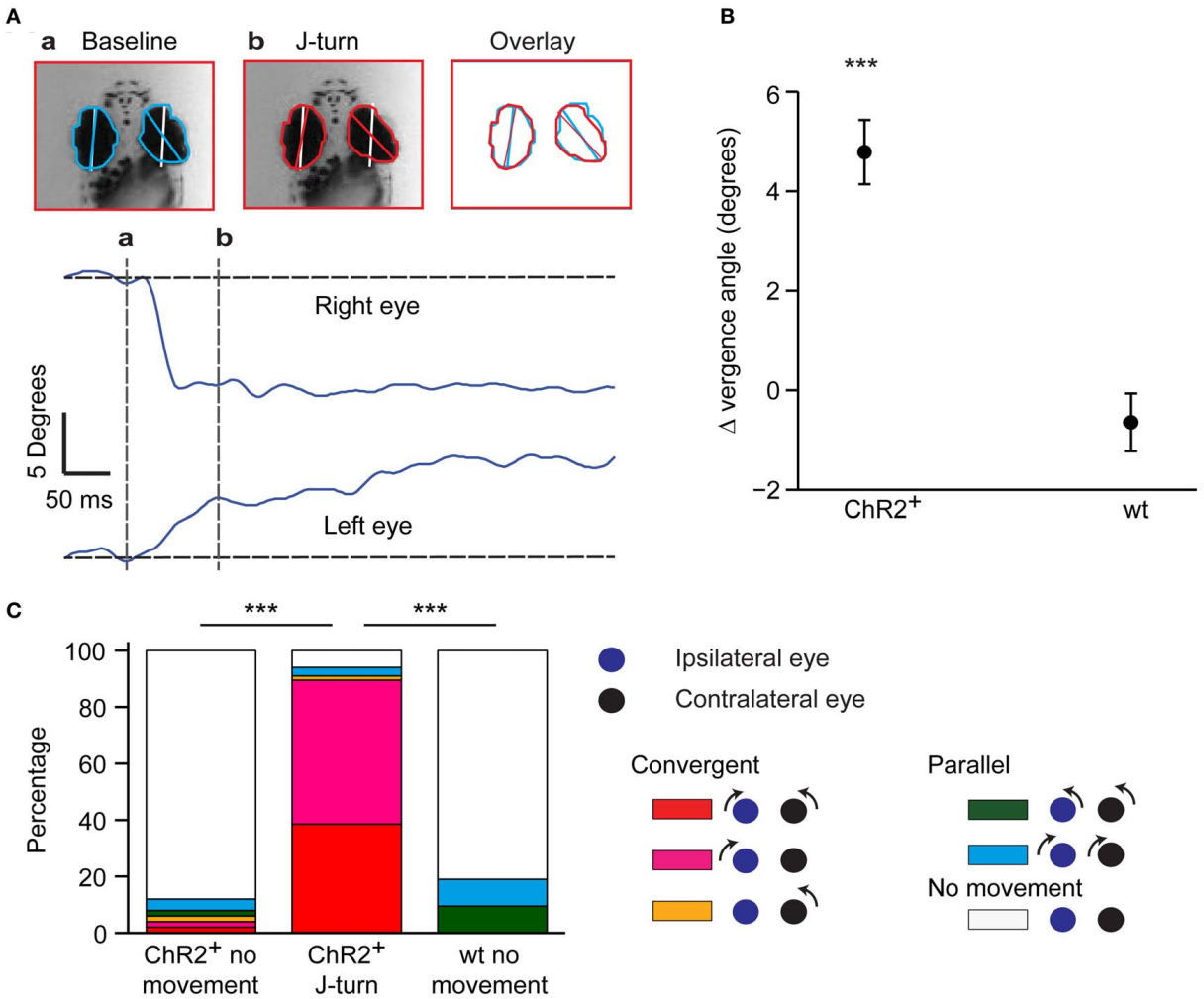

FIGURE 2 | Convergent eye movements during optically-evoked J-turns. (A) Eye position before (a) and during (b) a J-turn evoked by optical stimulation in a HuC:itTA/Ptet:ChR2YFP larva. White lines show orientation of anterior-posterior axis; colored lines show angle of the eye. Overlay shows convergence of eyes during J-turn. Traces show angular changes in eye position as a function of time. **(B)** Mean change in eye vergence angle (±s.e.m.) evoked by blue light stimulation in HuC:itTA/Ptet:ChR2YFP larvae (ChR2$^+$) and wt siblings. Positive change indicates convergence of eyes. $^{***}p < 0.001$, Student's *t*-test. **(C)** Classification of eye movements in HuC:itTA/Ptet:ChR2YFP larvae that did not respond to blue light ($n = 49$), in HuC:itTA/Ptet:ChR2YFP larvae responding with J-turns ($n = 65$), and in wt siblings, which never responded with J-turns ($n = 32$). An eye movement was defined as an angular change in eye position >2°. Convergent eye movements were closely associated with J-turns. $^{***}p < 0.001$, Chi-square test for comparison of the frequency of convergent eye movements.

Figure 3G), consistent with the lower duration and tail beat frequency. Increasing the intensity of the light stimulus dramatically reduced the latency of J-turn responses but did not affect tail beat frequency (**Figures 3H,I**). These results further support the conclusion that optical stimulation triggered the execution of a stereotyped motor program.

Using optical stimulation with a 200 μm fiber, the intensity threshold for evoking J-turn in HuC:itTA/Ptet:ChR2YFP larvae was 32 ± 8.5 mW/mm^2 (mean threshold in 10 larvae). For light intensities up to ∼600 mW/mm^2, J-turns were the behavioral response that was most frequently observed (**Figure 3I**). Beyond ∼600 mW/mm^2, J-turn responses were mixed with escape or struggling-like responses, presumably because the light stimulus produced noxious heat. In wt fish, no behavioral response was observed for light intensities below 217 ± 16 mW/mm^2 (mean threshold in 8 larvae). Higher intensities sometimes produced forward swimming, which may reflect a visuomotor response to the light. Above ∼600 mW/mm^2, light stimulation occasionally produced escape or struggle responses, as observed in HuC:itTA/Ptet:ChR2YFP larvae (**Figure 3J**). These results confirm that J-turning is a distinct motor program that is evoked by optical stimulation of neurons and overrides other motor behaviors.

We next examined the age-dependence of J-turn responses in freely swimming HuC:itTA/Ptet:ChR2YFP fish stimulated with a blue LED (∼0.35 mW/mm^2). The probability of triggering J-turns increased abruptly after 11 dpf and decreased somewhat after 21 dpf (**Figure 3K**). The reason for this age-dependence

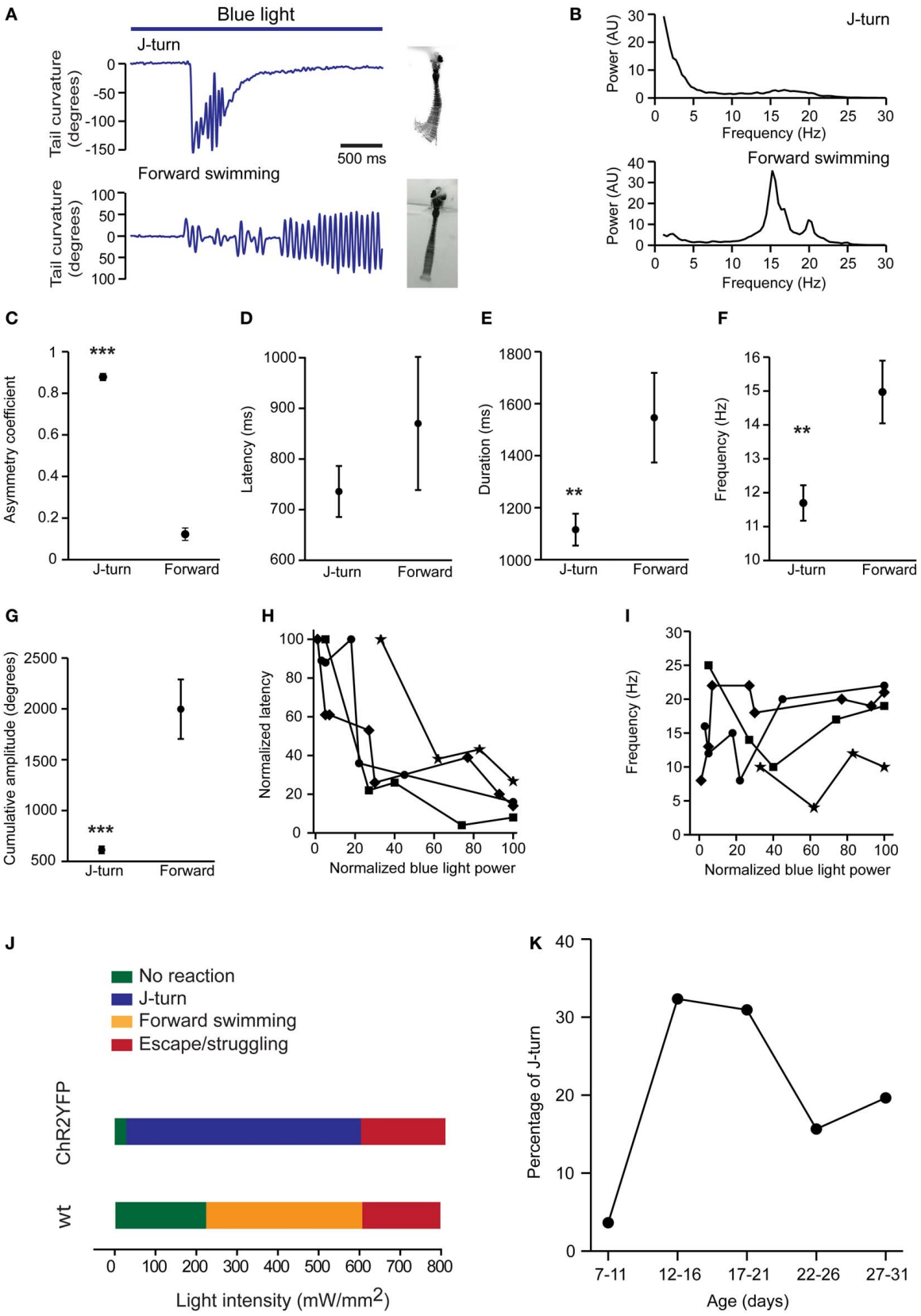

FIGURE 3 | Continued

FIGURE 3 | Quantitative comparison of J-turns and forward swimming. **(A)** Examples of tail curvature as a function of time during episodes of forward swimming and J-turning. Fish were stimulated with blue light starting at the onset of the trace. **(B)** Power spectral analysis of tail curvature during forward swimming and J-turns (average over all trials). **(C–G)** Asymmetry of tail movements, latency of motor response, duration of motor behavior, mean frequency of tail beats, and cumulative amplitude of tail beats for optically-evoked J-turns ($n = 138$ trials in 12 larvae; mean ± s.e.m.) and forward swims ($n = 35$ trials in 9 larvae). Mean frequency and cumulative amplitude were calculated over the total duration of the behavior, including short periods of inactivity. $^{**}p < 0.01$; $^{***}p < 0.001$; Student's *t*-test. **(H,I)** Latency and frequency of J-turns as a function of light intensity in four HuC:itTA/Ptet:ChR2YFP larvae. Because behavioral thresholds varied between individuals, data for each larvae were normalized to the maximum intensity used for each larva. Latencies were normalized to the maximum latency observed in each larva. **(J)** Dependence of behavioral response on intensity of blue light stimulation. Colored bars indicate the most frequently observed response as a function of light intensity in HuC:itTA/Ptet:ChR2YFP larvae ($n = 10$ fish) and wt siblings ($n = 8$). **(K)** Probability of J-turn responses as a function of age.

remains unclear. A possible reason for the relatively late onset is that the motor programs mediating J-turns or the upstream command centers are not fully developed before 11 dpf. However, J-turns occur during prey capture already at 5 dpf and can be evoked by virtual prey at the same age (Budick and O'Malley, 2000; Bianco et al., 2011). Alternatively, optical stimulation may be inefficient at early stages because neuronal response thresholds are higher. The decline in the probability of J-turning after 21 dpf could be due to decreased penetration of the light into the brain because skin and bones become less transparent. Alternatively, fish may use motor programs others than J-turns for prey capture at later stages. Moreover, it is possible that expression of ChR2YFP in neurons involved in J-turns is downregulated at later developmental stages. However, no obvious change in expression pattern was observed around 21 dpf (see below), although expression eventually becomes restricted to defined types of neurons in adult fish (Zhu et al., 2009).

To explore whether J-turns are triggered by the activation of specific subsets of neurons we first examined the effect of blue light exposure on freely swimming larvae of two other ChR2-expressing lines, Dlx4/6:itTA/Ptet:ChR2YFP (Zhu et al., 2009) and OMP:ChR2YFP (Blumhagen et al., 2011). Dlx4/6:itTA/Ptet:ChR2YFP transgenic fish express ChR2 in a large number of GABAergic interneurons (Zerucha et al., 2000; Zhu et al., 2009), while OMP:ChR2YFP transgenics express ChR2 in a subset of olfactory sensory neurons (Sato et al., 2005). Larvae of these lines, as well as HuC:itTA/Ptet:ChR2YFP and wt larvae, were exposed to blue light for 20 s while swimming speed was measured continuously (**Figure 4A**). Changes in swimming speed relative to a baseline, measured over 10 s before light onset, were then quantified in three time windows: 0–2 s after light onset, 10–20 s after light onset, and 0–20 s after light offset. The first time window (0–2 s after onset) captures the visuomotor on response, a well-described transient increase in swimming speed evoked by a sudden change in ambient light levels (Easter and Nicola, 1996; Burgess and Granato, 2007). The second time window (10–20 s after onset) was chosen to quantify steady-state effects of blue light, while the third time window (0–20 s after offset) was chosen to quantify after-effects of light exposure ("off-response"). Results were averaged in two age groups (7–13 and 14–20 dpf).

A clear visuomotor on response after light onset was observed in all lines except HuC:itTA/Ptet:ChR2YFP (**Figure 4B**). Moreover, HuC:itTA/Ptet:ChR2YFP, but not other lines, showed pronounced negative changes in swimming speed during the steady-state light response (**Figure 4C**). These effects were observed as a trend in young larvae (7–13 dpf) and statistically significant for the second age group (14–20 dpf). No significant differences were observed between off-responses of different lines in any age group (**Figure 4D**). Previous observations indicated that an obvious visuomotor on response is rare in HuC:itTA/Ptet:ChR2YFP larvae because they swim backwards instead (Zhu et al., 2009). Consistent with this conclusion, J-turns were observed in ∼30% of the trials with HuC:itTA/Ptet:ChR2YFP but never in larvae of other lines (**Figure 4E**). These results confirm that J-turns are not evoked by non-specific optical stimulation of neurons or by visual input. Rather, the optical stimulation of J-turns appears to require a particular pattern of ChR2 expression, suggesting that J-turns were triggered by the stimulation of specific neurons.

OPTICAL STIMULATION EVOKED BROADLY DISTRIBUTED NEURONAL ACTIVITY

To examine the distribution of activity in the brain evoked by optical stimulation in HuC:itTA/Ptet:ChR2YFP larvae [19 ± 3.2 dpf (mean ± SD), range: 14–23 dpf] we exposed the brain from the dorsal side in an *ex-vivo* preparation of the head and loaded neurons with the calcium-sensitive dye rhod-2-AM by bath incubation. Light pulses from a blue laser (duration, 500 ms) were directed at the midbrain through an optical fiber (diameter, 200 μm) from one side. Calcium signals were measured by wide-field epifluorescence imaging with a CCD camera. Because optical stimulation interfered with quantitative fluorescence imaging, changes in indicator fluorescence were measured immediately after the optical stimulus.

In HuC:itTA/Ptet:ChR2YFP fish, optical stimulation at two different intensities (7 mW/mm^2 and 40 mW/mm^2) evoked calcium signals in various brain areas including the tectum, torus longitudinalis, and cerebellum. This response is expected to contain different components evoked by activation of ChR2 and by visual stimulation through the eyes. Consistent with this assumption, optical stimulation of wt siblings evoked smaller calcium signals (**Figures 5A,B**) that were almost completely abolished after surgical removal of the eyes (**Figures 5C,D**). In HuC:itTA/Ptet:ChR2YFP fish, in contrast, a substantial signal remained after removal of the eyes, confirming that optical stimulation can directly stimulate neurons in the brain by activation of ChR2. This residual response was widespread, which could be due to the broad expression of ChR2, the propagation of locally evoked activity, or both. The distribution of light-evoked activity does therefore not provide specific information about the brain areas controlling J-turns.

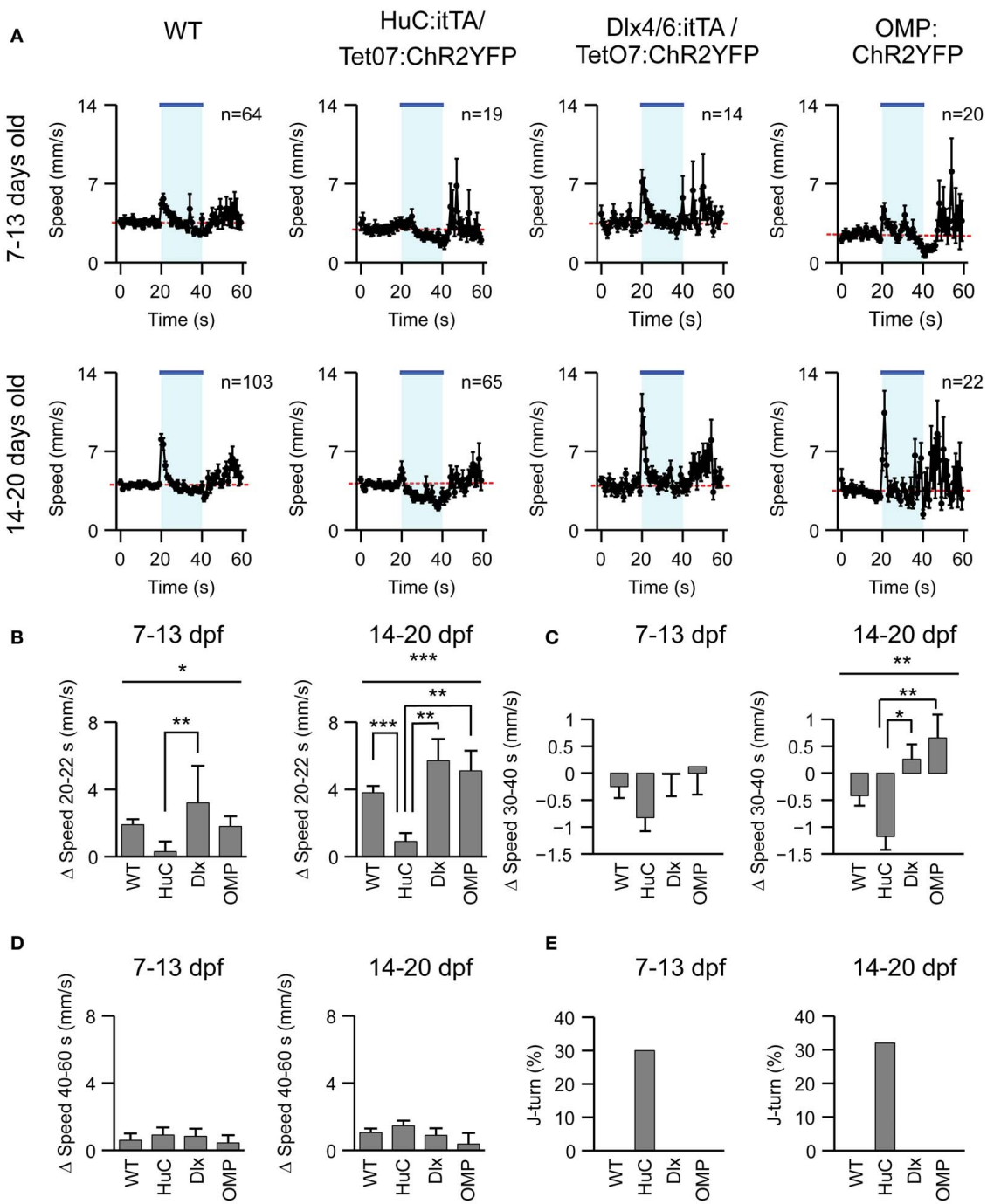

FIGURE 4 | Effects of optical stimulation in different transgenic fish lines. (A) Swimming speed as a function of time (1 s bins) in four different zebrafish lines and two different age groups before, during and after a 20 s exposure to blue light (bar; LED). *n*, number of fish. **(B–D)** Mean change in swimming speed during a 2 s period after light onset (20–22 s), a 10 s period before light offset (30–40 s) and a 20 s period after light offset (40–60 s). **(E)** Percentage of J-turn responses evoked by blue light stimulation in different fish lines. Error bars show s.e.m. $^{*}p < 0.05$; $^{**}p < 0.01$; $^{***}p < 0.001$; ANOVA and Bonferroni *post-hoc* test.

J-TURNING DEPENDS ON LIGHT INTENSITY

To explore which brain areas are involved in optically-evoked J-turns we first correlated the occurrence of J-turns to the expression pattern of ChR2YFP. Although the HuC promoter can drive expression in most or all neurons, expression of ChR2YFP in HuC:itTA/Ptet:ChR2YFP fish was not pan-neuronal because it was controlled by the Tet system, which often restricts expression to specific subsets of the neurons that are normally targeted by

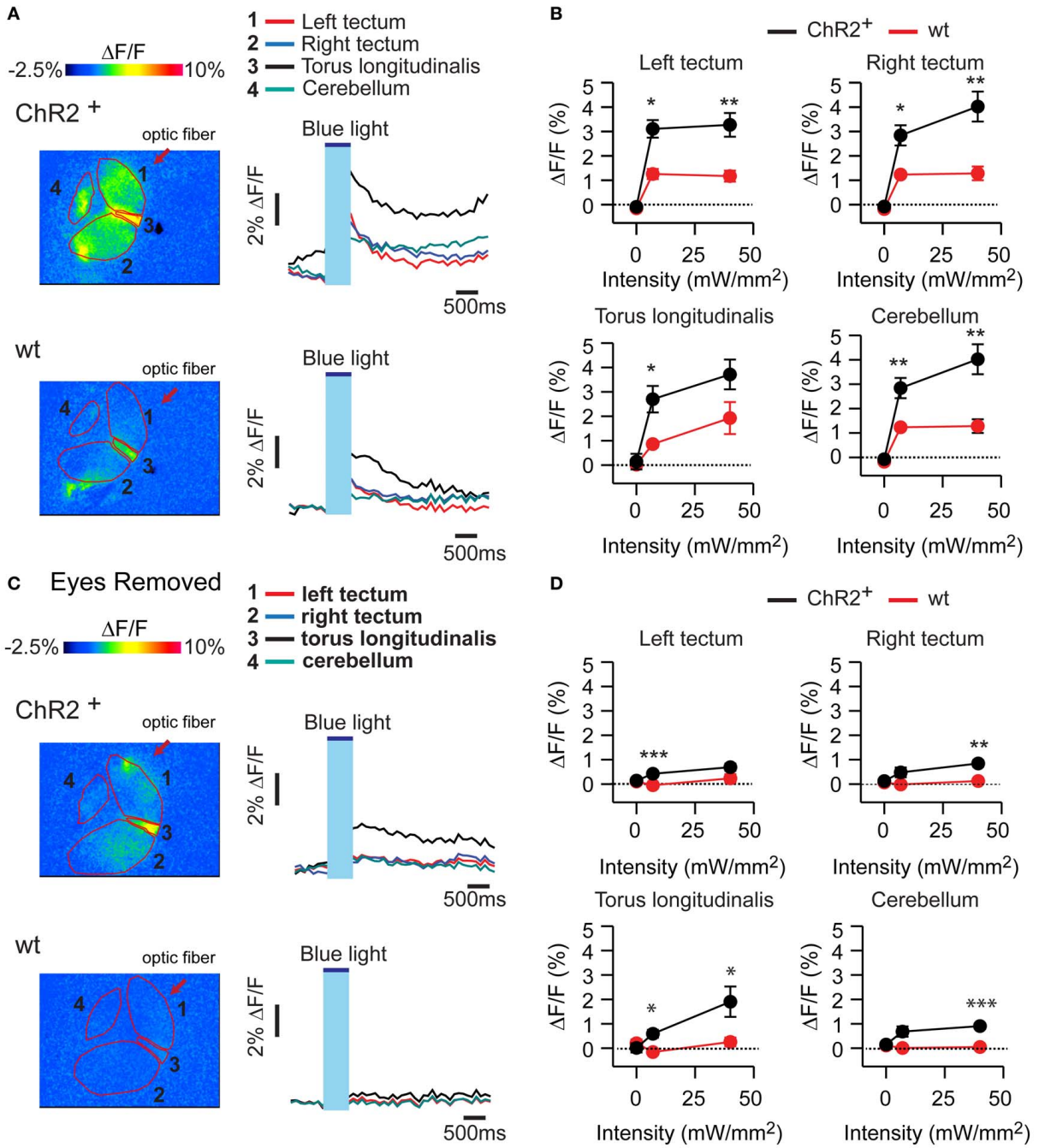

FIGURE 5 | Calcium signals evoked by optical stimulation. **(A)** Changes in fluorescence intensity of the calcium indicator rhod-2 in an *ex-vivo* preparation of the larval head after optical stimulation with blue light. Top: HuC:itTA/Ptet:ChR2YFP; bottom: wt. Four different brain areas are outlined (left optic tectum, right optic tectum, torus longitudinalis, cerebellum). **(B)** Mean changes in fluorescence intensity in these brain areas evoked by stimuli of two different intensities. Error bars show s.e.m. **(C,D)** Same experiments performed in preparations without eyes. Error bars show s.e.m. $^{*}p < 0.05$; $^{**}p < 0.01$; $^{***}p < 0.001$; Student's *t*-test.

the promoter driving itTA expression. This "sparsening" appears to depend on the integration site of one or both of the transgenes (HuC:itTA and Ptet:ChR2YFP) and therefore results in expression differences between founder lines (Zhu et al., 2009). Individual larvae from more than one founder were exposed to three blue light stimulations (LED, 3 s; ~0.35 mW/mm^2). Eight larvae were then selected that responded with J-turn to all three stimulations, as well as four larvae that did not respond to light [19 ± 3.2 dpf (mean ± SD), range: 15–22 dpf]. In each of these larvae, ChR2YFP expression was analyzed by confocal microscopy.

As expected, the expression of ChR2YFP showed distinct differences between individuals in some brain areas (**Figure 6A**). For example, the tecto-toral pathway (**Figure 6A**, red arrow) or a prominent group of reticular neurons (**Figure 6A**, yellow arrow) expressed ChR2YFP in some fish but not in others. However, none of the observed expression differences correlated with the occurrence of J-turns (**Figure 6A**). We noticed, however, that the expression of ChR2YFP was stronger in larvae that performed J-turns, particularly in the optic tectum (**Figure 6A**, ligh blue arrow). These results suggest that J-turns are initiated by neurons that express Chr2YFP in most or all founder lines such as the optic tectum, and that other factors, such as expression levels, are responsible for the behavioral variations between individuals.

The observed correlation between expression levels and J-turn responses raises the possibility that some fish failed to respond to optical stimulation because the effective stimulation intensity was too low. In live fish, the effective stimulation intensity is expected to depend on pigmentation because access of blue

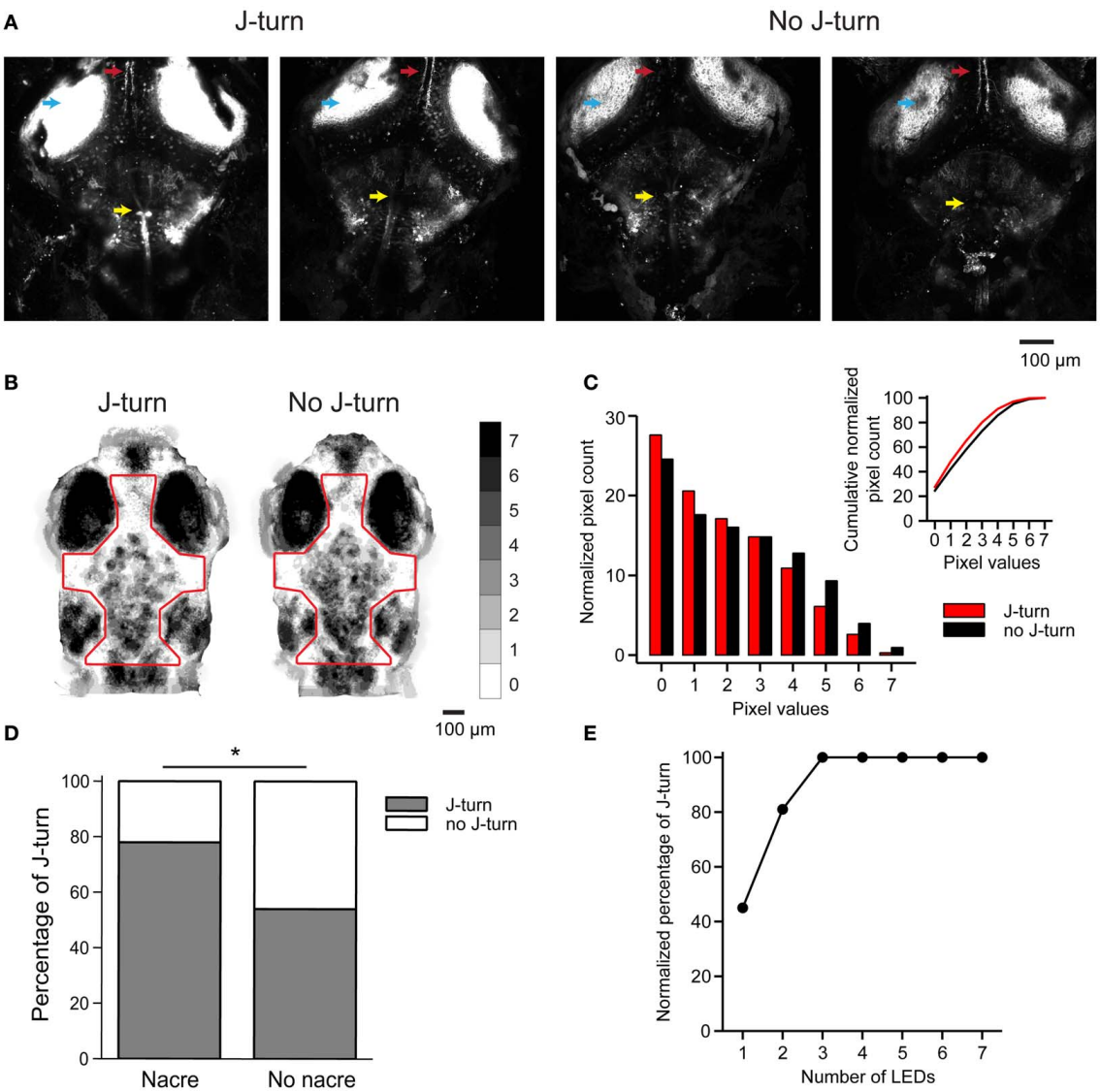

FIGURE 6 | J-turn responses depend on efficiency of optical stimulation. **(A)** ChR2YFP expression in two HuC:itTA/Ptet:ChR2YFP larvae that responded to blue light stimulation with J-turns (left) and two siblings that did not respond (right). Arrowheads depict the optic tectum, the tecto-toral pathway, and a prominent group of hindbrain neurons. Images are z-projections of confocal stacks acquired using the same settings. **(B)** Sum of binarized and registered images of seven HuC:itTA/Ptet:ChR2YFP larvae that responded to blue light stimulation with J-turns and seven siblings that did not respond. Gray levels indicate the number of larvae in which each pixel was covered by pigment. Pigmentation was then quantified within the outlined area. **(C)** Distribution of pixel counts in the images in **(B)**. The distribution is shifted to the left for images from larvae that responded with J-turns, indicating less pigmentation (Kolmogorov-Smirnov test, $p < 0.001$). Insert shows cumulative distributions of pixel counts. **(D)** Probability of J-turning in HUC:itTA/Ptet:ChR2YFP fish in the nacre background and in pigmented siblings. $*p = 0.021$, Chi-square test. **(E)** Normalized probability of J-turn responses in pigmented HuC:itTA/Ptet:ChR2YFP larvae ($n = 20$) as a function of light intensity (number of LEDs).

light to the brain is blocked by melanophores. The pattern of melanophores differs between individuals but is usually more similar between siblings than between larvae from different lines (Engeszer et al., 2008). We therefore analyzed melanophore patterns in seven HuC:itTA/Ptet:ChR2YFP larvae that responded to blue light LED stimulation with J-turn and compared them to melanophore patterns of seven HuC:itTA/Ptet:ChR2YFP fish that failed to respond [18 ± 4.8 dpf (mean ± SD), range: 13–25 dpf]. Images of the head were binarized by thresholding to extract melanophores, registered by landmarks (snout, eyes, and ears), and summed for each group (**Figure 6B**). The value of each pixel therefore represents the number of fish in which the corresponding location was covered by a melanophore. We found no consistent difference in the spatial pattern of melanophores between the two groups. However, the mean coverage of the head by melanophores, as evaluated from the distributions of pixel values, was significantly higher in fish that did not respond to optical stimulation ($p < 0.001$, Komogorov-Smirnov test; **Figure 6C**). It is therefore possible that individual fish failed to respond to light stimulation because melanophores reduced the effective stimulus intenstity.

To test whether a difference in the effective optical stimulation intensity can account for inter-individual variations in behavioral responses we outcrossed HuC:itTA and Ptet:ChR2YFP to the nacre mutant, which lacks melanophores. Because nacre is recessive, siblings with and without melanophores could then be obtained from the same crossings. The probability of J-turn responses to light stimulation was significantly higher in fish with the nacre phenotype than in pigmented siblings (78% of 41 nacre fish vs. 54% of 62 wt siblings; $p = 0.021$, Chi-square test, age = 15 dpf; **Figure 6D**). Moreover, when light intensity was increased by additional LEDs the probability of J-turning increased until it reached a saturating level ($n = 20$ fish, age = 14 dpf, **Figure 6E**). These results indicate that inter-individual variations in J-turn responses were, at least in part, due to differences in the effectiveness of light stimulation.

SPATIAL MAPPING OF BRAIN AREAS CONTROLLING J-TURNS

To identify brain areas involved in J-turning we mapped behavioral responses of head-fixed HuC:itTA/Ptet:ChR2YFP larvae to focal optical stimulation at different sites. Coarse mapping was performed by illuminating circular areas ∼400 μm in diameter using a microscope equipped with a 20× objective, a blue excitation filter (460/50 nm), and an epifluorescence lamp (LB-LS/30, 300W, Sutter Instrument Co.). Tail movements were filmed through the condenser. We illuminated four regions in the midline over the forebrain, midbrain, hindbrain, and rostral spinal cord and found the probability of evoking J-turns to be maximal in the midbrain [$p = 0.62$, 24 trials in 8 fish, 19 ± 2.9 dpf (mean ± SD), range: 16–23 dpf; **Figure 7A**]. Optical stimulation in all other regions, as well as broad illumination of the tail (not shown), evoked little or no J-turning. Finer mapping with smaller light stimuli (∼150 μm in diameter) in the same fish confirmed that J-turn responses were triggered selectively in the midbrain ($p = 0.4$ in a central area; 15 trials in 5 fish at each position, **Figure 7B**). Wt siblings showed no response to illumination of any region [15 trials in 5 fish at each position, 19 ± 3.1 dpf (mean ± SD), range: 16–23 dpf; **Figures 7A,B**).

To map behavioral responses more precisely we used a blue laser coupled to an optical fiber. This method produces slightly divergent cones of light with relatively sharp edges whose diameter depends on the diameter of the optical fiber (Arrenberg et al., 2009; Zhu et al., 2012). Using a relatively large fiber (200 μm diameter) oriented perpendicularly to the brain surface and an average light intensity of 110 ± 17 mW/mm^2, J-turns could again be evoked in the midbrain but not in adjacent brain regions of HuC:itTA/Ptet:ChR2YFP larvae ($p = 0.5$ in the midbrain; 24 trials in 8 fish at each position; age: 18 ± 3.4 dpf (mean ± SD), range: 13–21 dpf] while wt fish did not respond [21 trials in 7 fish at each position; age: 18 ± 3.6 dpf (mean ± SD), range: 13–21 dpf; **Figure 7C**]. Finer mapping with a 50 μm fiber perpendicular to the dorsal brain surface revealed two regions in the anterior midbrain where J-turns could be triggered in each trial. These regions were ∼65 μm lateral to the midline and bilaterally symmetric. As the fiber was moved away from these regions, the probability of evoking J-turns decreased sharply [$n = 8$ fish; multiple trials at each position; age: 17 ± 4 dpf (mean ± SD), range: 13–22 dpf; **Figure 7D**]. J-turns can therefore be triggered specifically by stimulation of a small, circumscribed region in the anterior midbrain.

We further observed that the side of stimulation determined the direction of tail movements: illumination on the right side evoked tail bends exclusively to the left and vice versa ($n = 26$ trials with 200 μm fiber; $n = 35$ trials with 50 μm fiber; **Figure 7E**). Furthermore, when optical stimulation on one side evoked convergent eye movements ($n = 25$ trials in 4 fish), the magnitude and speed of eye movements were significantly larger on the ipsilateral side (paired student t-test, $p < 0.001$, **Figures 7F,G**). The latency of the ipsilateral eye movement was significantly shorter than the response latency of the contralateral eye (paired student t-test, $p = 0.047$, **Figure 7H**). Moreover, the response latency of the ipsilateral eye was significantly shorter than the latency of the tail movement (paired student t-test, $p = 0.02$, **Figure 7H**) whereas the latency of the contralateral eye movement was significantly longer. Convergent eye movements always included the ipsilateral eye, but not always the contralateral eye (**Figure 2C**). Eye movement is therefore asymmetric and, on average, initiated before tail movement, consistent with results obtained by visual stimulation with virtual prey (Bianco et al., 2011). These results show that J-turn behavior is strongly lateralized.

LOCALIZATION OF A BRAIN AREA THAT CONTROLS J-TURNS

Mapping with a vertical fiber identified the x–y coordinates of a brain area triggering J-turns but cannot identify its location in the third dimension because the light is not focused. We therefore rotated the 50 μm optic fiber by 45° and re-mapped tail movements evoked by optical stimulation at different positions in the anterior midbrain. When the fiber came in from the left, tail movements in a specific direction were evoked at distinct sites (**Figure 8A, top**) that were displaced leftwards compared to the locations where equivalent tail movements were

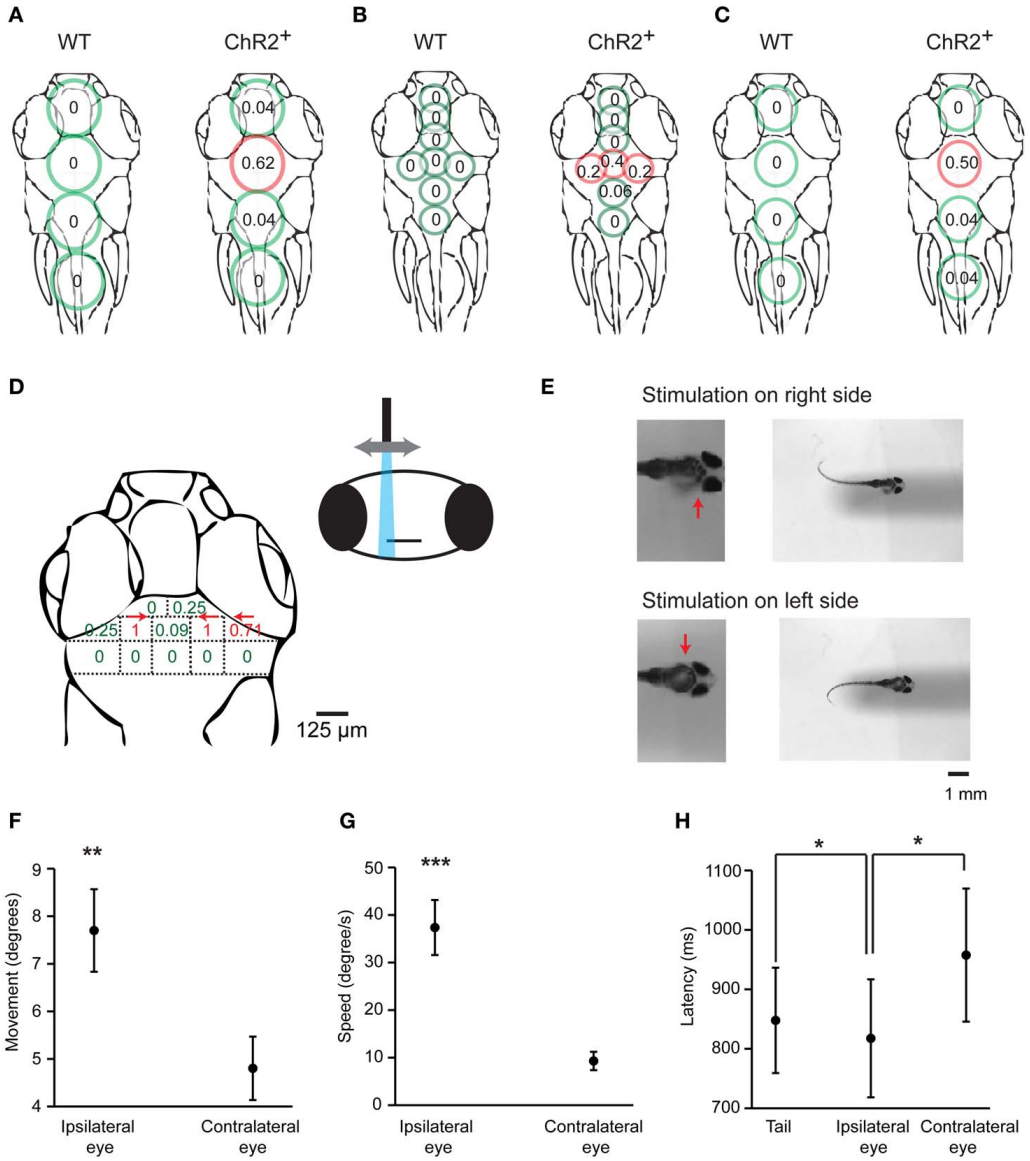

FIGURE 7 | Mapping of J-turn responses by local optical stimulation. **(A)** Approximate regions illuminated with blue light from an epifluorescence lamp (circles) superimposed on an outline of the zebrafish head (dorsal view). Numbers within circles show the probability of J-turn responses to optical stimulation in each location in HuC:itTA/Ptet:ChR2YFP larvae (ChR2$^+$; $n = 8$ fish, 3 trials at each position) and wt siblings ($n = 5$ fish, 3 trials at each position). **(B)** Same with more restricted blue light illumination (field aperture closed; $n = 5$ fish, 3 trials at each position for ChR2$^+$ and wt siblings). **(C)** Mapping of J-turn responses to blue light stimulation through a vertical optic fiber (diameter, 200 µm; $n = 8$ fish for ChR2$^+$ and $n = 7$ fish for wt; 3 trials at each position). **(D)** Mapping of J-turn responses to optical stimulation in the midbrain using a vertical optical fiber with 50 µm diameter. Numbers indicate the probability of J-turn responses at the corresponding positions ($n = 4$ fish, between 3 and 13 trials each position). Arrows indicate the direction of tail bends when the probability of J-turning was >0.25. **(E)** Images showing tail bends evoked by optical stimulation in the anterior tectum with a small optical fiber (50 µm) on different sides. Arrows show the side of the brain that was stimulated. **(F,G)** Mean angular movement and movement speed of the ipsilateral and contralateral eyes evoked by stimulation with an optical fiber (50 µm) above the anterior tectum on one side. **(H)** Mean latency of eye movements and tail movements. All error bars show s.e.m. $^*p < 0.05$; $^{**}p < 0.01$; $^{***}p < 0.001$; Student's *t*-test.

evoked by vertical fiber stimulation (**Figure 7D**). Likewise, stimulation sites producing equivalent tail movements were displaced rightwards when the fiber came in from right (**Figure 8A, bottom**). The depth of the region activated during J-turn can be thus be estimated by triangulation (see schematic illustration in **Figure 8B**). This procedure indicates that the brain region triggering J-turns is situated in the anterior tectum or the underying pretectum, approximately 80–150 µm below the brain surface.

To anatomically localize the brain area activated by optical stimulation we traced the stimulation light in fish expressing the photoswitchable protein kaede under the control of the

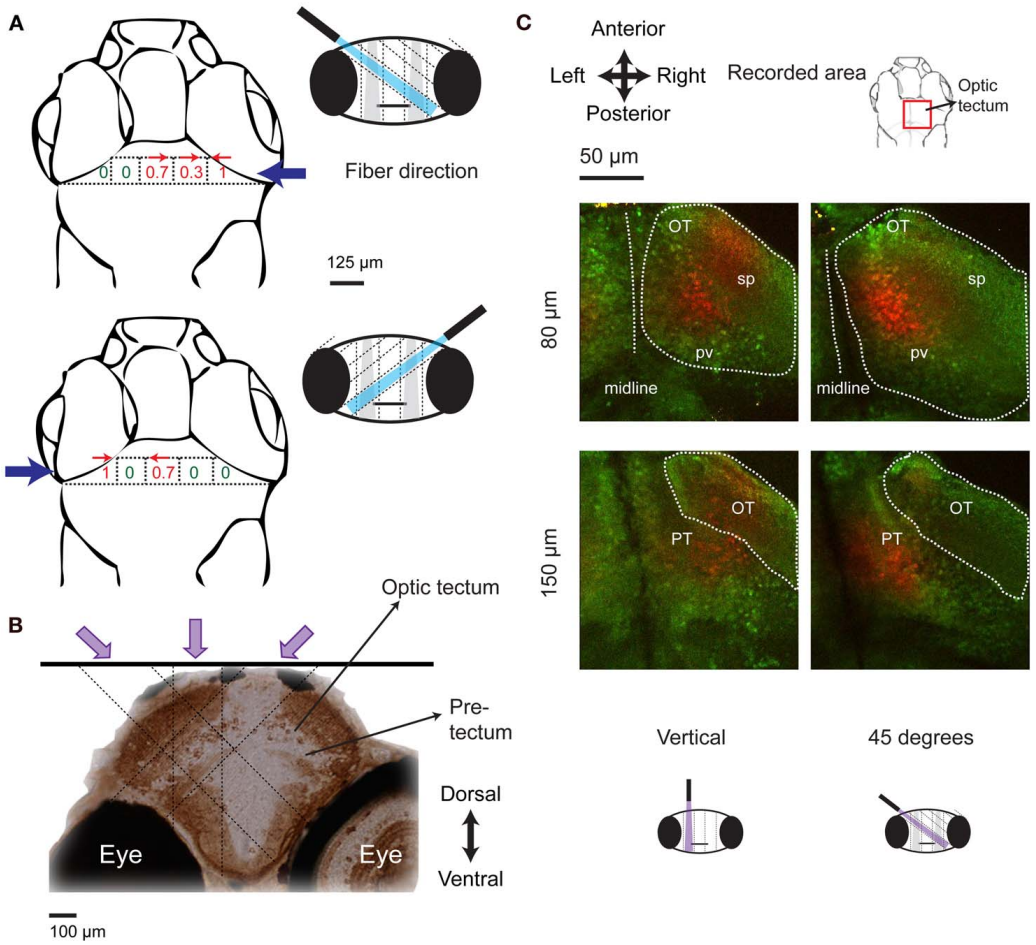

FIGURE 8 | Localization of the brain area triggering J-turns in 3-D. **(A)** Probabilities of evoking J-turns in the midbrain of HuC:itTA/Ptet:ChR2YFP larvae with a 50 µm optical fiber tilted by 45° to the left or to the right. Numbers indicate the probability of J-turn responses at the corresponding positions ($n = 3$ fish, 3 trials at each position). Arrows indicate the direction of evoked tail bends when the probability of J-turning was >0.25. **(B)** Schematic illustration of the localization of the brain area triggering J-turns by triangulation. Image shows a coronal section of the zebrafish brain stained with anti-GFP, approximately at the rostro-caudal position where J-turns were evoked with highest probability (level of anterior tectum). Dashed lines indicate the light paths of optical stimuli (vertical and 45°) that produced J-turns with maximal probability. Light paths intersect in a region containing the anterior-ventral optic tectum (avOT) and part of the pretectum. **(C)** Photoconversion of kaede after illumination with UV light through an optic fiber (50 µm) oriented vertically or at 45°. The fiber was positioned at sites that produced maximal probabilities of J-turn. Images (z-projections of small multiphoton stacks) are shown at two depths for two fish illuminated at different angles. Most photoconverted neurons (red) were found in the avOT. OT, optic tectum; pv, periventricular layer; sp, superficial layers; PT, pretectum.

HuC promoter (HuC:kaede) (Sato et al., 2006; Arrenberg et al., 2009). When illuminated with violet light, fluorescence emission of kaede changes from green to red (Sato et al., 2006). A 50 µm optical fiber oriented vertically or at 45° was placed at the positions where the probability of evoking J-turns by blue light was maximal in HuC:itTA/Ptet:ChR2YFP fish. Fish were then illuminated through the fiber with light from a violet laser (405 nm) for 5 min. Red and green fluorescence of Kaede was examined in a volume around the stimulation site by multiphoton microscopy. Photoconverted kaede protein was detected in columns of ~50 µm diameter along the projected paths of the violet light ($n = 8$ in 4 fish for vertical illumination and $n = 3$ in 3 fish for 45°, age: 15–16 dpf; **Figure 8C**). Columns produced by stimulation at different angles (vertical or 45°) overlapped mainly in the ventral part of the anterior optic tectum. This area includes fibers coming from the retina and cell bodies in the periventricular layer of the tectum (Meek and Schellart, 1978; Scott and Baier, 2009; Robles et al., 2011). Some cells in a structure ventral to the optic tectum, presumably the pretectum, were also photoconverted (**Figure 8C**). The identity of this area could not be determined unequivocally because precise anatomical atlases at the developmental stages examined here are not available. Comparisons with anatomical data from earlier stages suggest that this area may be located between structures identified as the pretectum and the early migrated pretectum (M1) (Mueller and Wullimann, 2002), or coincide with terminal field AF-9, which may differentiate into the nucleus pretectalis pars dorsalis and/or pars

ventralis during development (Burrill and Easter, 1994). These results demonstrate that J-turns were triggered by stimulating the anterior-ventral optic tectum (avOT) and/or an adjacent pretectal nucleus.

DISCUSSION

Optogenetic mapping of behavioral responses in transgenic zebrafish expressing ChR2 revealed that the activation of avOT or the adjacent pretectum evokes J-turns, a well-defined motor program involved in prey capture. J-turns consisted of highly coordinated motor components and could not be evoked elsewhere in the brain, suggesting that the anterior-ventral tectum acts as a command center controlling a defined motor program. These findings provide insights into senorimotor transformations underlying a complex behavior that is critical for the survival of zebrafish larvae.

MAPPING OF A DEFINED MOTOR BEHAVIOR IN ZEBRAFISH

A previous study reported that larval HuC:itTA/Ptet:ChR2YFP zebrafish respond to wide-field optical stimulation with slow backward movements and rotations (Zhu et al., 2009). High-resolution video analysis in freely swimming and head-fixed larvae revealed that this behavior is not due to uncoordinated muscle contractions but produced by the repeated execution of J-turns. J-turns must involve the coordinated control of multiple muscle groups in different body parts to achieve unilateral caudal tail bends, parallel movements of pectoral fins, and convergent eye movements. Quantitative behavioral analyses showed that these motor components co-varied in different trials, exhibited a high degree of temporal coherence, and were strongly lateralized. Optical stimulation did therefore not activate different muscle groups independently but triggered the execution of a coordinated motor program, indicating that optical stimulation activated a command center upstream of local motor control.

Optical stimulation evoked calcium signals throughout multiple brain areas, consistent with the widespread expression of ChR2. These results indicate that optical stimulation was not restricted to specific subsets of neurons but activated multiple types of neurons throughout the brain. Motor output, however, was distinct, highly coordinated and reproducible. The most likely explanation for this unexpected finding is that the motor program for J-turns is activated at low threshold and suppresses other behavioral reactions. Consistent with this assumption, HuC:itTA/Ptet:ChR2YFP larvae exposed to amber (590 nm) instead of blue light produced visuomotor on responses, the typical visual response of wt larvae, rather than J-turns. Likewise, blue light stimulation under head-fixed conditions triggered J-turns in HuC:itTA/Ptet:ChR2YFP larvae but forward swimming in wt larvae throughout a broad intensity range. Hence, optically-evoked J-turns appear to override visuomotor on responses. These results suggest that different motor programs are controlled in a competitive fashion such that the execution of one motor program suppresses the execution of others. Well-defined, stereotyped motor programs may therefore be controlled by different command centers that inhibit each other (Ewert et al., 2001; Humphries et al., 2007; Orger et al., 2008). Obviously, such a competitive and modular organization of motor control can establish coherent behavioral outputs by avoiding interference between conflicting motor programs.

Observations in zebrafish and many other species suggest that neuronal circuits controlling stereotyped motor programs are, at least in some cases, spatially localized in the brain (Ewert, 1967; Schaefer, 1970; Syka and Radil-Weiss, 1971; Stein and Clamann, 1981; McHaffie and Stein, 1982; Al-Akel et al., 1986; Salas et al., 1997; Herrero et al., 1998; Valentine et al., 2002; Gahtan et al., 2005; Saitoh et al., 2007; Schoonheim et al., 2010; Miri et al., 2011). Consistent with this notion, we found that J-turns can be triggered efficiently and specifically by optical stimulation within a small volume ($<100\,\mu m$ in diameter) containing avOT and a small part of an adjacent pretectal area. This volume was localized with high precision in three dimensions by optical stimulation with a thin fiber at different angles. The volume is relatively deep and contained neurons that expressed ChR2YFP at similar levels as neurons in other tectal areas. It is therefore unlikely that behavioral responses were triggered specifically in this area because optical stimulation was more efficient than in other regions. Rather, our results suggest that this area is functionally specialized to control J-turns.

Experiments using electrical stimulation in different vertebrate species indicate that the optic tectum or its homolog, the superior colliculus, is involved in orienting movements of the eyes, pinnae, head, and body toward a target (Ewert, 1967; Schaefer, 1970; Syka and Radil-Weiss, 1971; Stein and Clamann, 1981; McHaffie and Stein, 1982; du Lac and Knudsen, 1990; Herrero et al., 1998; Valentine et al., 2002; Saitoh et al., 2007). As J-turns orient zebrafish toward small, prey-like objects, our results are consistent with this general notion. Moreover, we found that optical stimulation in avOT also produced coordinated eye movements, which may be another motor behavior involved in orientation (Bianco et al., 2011). The precise mechanisms by which tectal circuits convert sensory inputs into motor commands are, however, poorly understood. The zebrafish may therefore provide an excellent experimental model to study these sensorimotor transformations. Experiments in various species also demonstrated that electrical stimulation in other brain areas such as the brainstem can produce coordinated motor output, presumably by activation of command neurons (Sterman and Fairchild, 1966; Grillner and Shik, 1973; Grillner et al., 2008). As the brainstem contains various nuclei that transmit information to the spinal cord, it is likely to further process motor signals before relaying them to central pattern generators in the spinal cord (Grillner et al., 2008). The functions and interactions of brain stem nuclei are, however, not well-understood. As shown by this study and others (Arrenberg et al., 2009; Scott and Baier, 2009; Schoonheim et al., 2010), optogenetic mapping in zebrafish is a promising approach to address these questions.

TECTAL CONTROL OF MOTOR OUTPUT

The volume where optical stimulation evoked J-turns coincided mostly with avOT. This tectal subregion encompasses ~15% of the total tectal volume and is not delineated from other parts of the tectum by obvious anatomical boundaries. Since photoconversion of kaede was observed also in an adjacent pretectal

area it cannot be excluded that J-turns were elicited by stimulation of this pretectal area, or by simultaneous stimulation of the pretectum and avOT. However, the number of photoconverted neurons in the pretectum was low. Moreover, optical stimulation at angles and positions that should have favored stimulation of the pretectal area did not efficiently trigger J-turns. We therefore conclude that J-turns were probably evoked by stimulation of avOT.

J-turns can be evoked by small moving objects ("virtual prey") in a subregion of the visual field (Bianco et al., 2011). One possibility is that avOT receives retinal input from this subregion. If so, the optical stimulation used in our experiments may have evoked J-turns by creating a "neural illusion" of a small moving object in the appropriate visual subfield. Such an illusion could be evoked if optical stimulation produced specific responses of the corresponding retinal axons. However, this is highly unlikely because optical stimuli were stationary and J-turns could be evoked by wide-field illumination with blue light. J-turns were therefore likely triggered by stimulation of tectal neurons. Unlike retinal afferents, many tectal neurons responded more efficiently to small moving bars than to large moving bars (Del Bene et al., 2010). A "neural illusion" of a small moving object may therefore be created by direct stimulation of these neurons.

Wide-field stimulation would be expected to create conflicting "neural illusions" simultaneously in many virtual positions in the visual field. Moreover, neurons responding to small bars are not restricted to avOT but distributed throughout the optic tectum (Niell and Smith, 2005; Del Bene et al., 2010). Activation of tectal neurons tuned to small objects can therefore not explain the observed J-turn responses without additional assumptions. One possibility is that avOT contains a larger number or a higher density of neurons responding to small objects than other tectal regions. Widespread optical stimulation may therefore evoke strong activity in avOT, which may trigger J-turns and suppress other behavioral responses. Alternatively, avOT may be functionally different from other tectal areas and specialized for the control of J-turns. One possible specialization of avOT could be projections to specific motor nuclei. It may therefore be hypothesized that the tectal output to motor areas controlling J-turns arises specifically in avOT. Targets in more lateral or caudal directions should therefore not evoke J-turns but possibly trigger other motor behaviors. Consistent with this hypothesis, J-turns during prey capture correlate with activity in a tectal area consistent with avOT, as revealed by calcium imaging in freely swimming larvae (Muto et al., 2013).

The finding that J-turns could be evoked specifically in avOT but not in other tectal areas raises the possibility that the tectum is not a homogeneous structure but contains functionally specialized subregions. Consistent with this hypothesis, electrical stimulation in different regions of the tectum elicited different motor reactions in goldfish (Salas et al., 1997; Herrero et al., 1998). As input from retinal ganglion cells to the optic tectum appears to be topographic and continuous (Xiao et al., 2005; Gosse et al., 2008), functional specializations of tectal subregions may be established by region-specific neuronal circuits within the tectum, or by specific projections from tectal subregions to other brain areas. This hypothesis could be tested experimentally by tracing tectal outputs from avOT and other tectal subregions to downstream brain areas such as the reticular formation (Sato et al., 2007). A spatial patterning of tectal outputs would appear useful if stimuli in different regions of the visual field convey information that is relevant for the control of different behaviors. Alternatively, output from the tectum may be homogeneous, and different behavioral responses to activity in specific tectal areas may be generated by downstream target areas that analyze tectal output. Various results indicate that the optical tectum is not a purely sensory area for processing of visual information but also involved in other functions including motor control (Meek and Schellart, 1978; Goodale, 1996; Gandhi and Katnani, 2011). This notion is reinforced by the finding that specific optical stimulation of the avOT produces a distinct motor output.

Previous studies demonstrated that ablation of the optic tectum impairs prey capture in zebrafish (Gahtan et al., 2005) and goldfish (Springer et al., 1977). This impairment was associated with a reduction in small-angle turns, possibly J-turns (Gahtan et al., 2005). AvOT may therefore be both sufficient and necessary to evoke J-turns, although this hypothesis remains to be tested by additional experiments. Even if avOT is a hub for the control of J-turns, other brain areas are also likely to be involved in this behavior. For example, the work by Ewert and colleagues in toads indicates that visual stimuli signaling prey and predators stimulate neurons in the optic tectum and in the pretectum, respectively, that interact when both types of stimuli are presented simultaneously (Ewert et al., 2001). Prey capture by zebrafish involves a sequence of behavioral components that need to be coordinated by interactions between specific groups of neurons, presumably across brain areas. The identification of avOT as an area that can trigger J-turns is a step toward the functional understanding of this network.

ACKNOWLEDGMENTS

The authors thank Paul Argast for help with mechanics, Sebastian Bundschuh and Peter Buchmann for help with construction of LED devices and Laure Bally-Cuif for HuC:kaede fish. This work was supported by the Novartis Research Foundation, a Marie Curie Fellowship of the European Union to Otto Fajardo, the Swiss Nationalfonds (SNF), and the Human Frontiers Science Program (HFSP).

SUPPLEMENTARY MATERIAL

The Supplementary Material for this article can be found online at http://www.frontiersin.org/Neural_Circuits/10.3389/fncir.2013.00067/abstract

Movie S1 | Light-evoked J-turns and convergent eye movements in a head-fixed HuC:itTA/Ptet:ChR2YFP fish. The optic tectum was illuminated with blue light through an optical fiber (200 μm diameter) for the duration of the movie. Light onset was at the first frame. The original frame rate was 200 Hz; the movie is slowed down by a factor of four.

REFERENCES

Al-Akel, A. S., Guthrie, D. M., and Banks, J. R. (1986). Motor responses to localized electrical stimulation of the tectum in the freshwater perch (*Perca fluviatilis*). *Neuroscience* 19, 1381–1391.

Arrenberg, A. B., Del Bene, F., and Baier, H. (2009). Optical control of zebrafish behavior with halorhodopsin. *Proc. Natl. Acad. Sci. U.S.A.* 106, 17968–17973.

Bianco, I. H., Kampff, A. R., and Engert, F. (2011). Prey capture behavior evoked by simple visual stimuli in larval zebrafish. *Front. Syst. Neurosci.* 5:101. doi: 10.3389/fnsys.2011.00101

Blumhagen, F., Zhu, P., Shum, J., Scharer, Y. P., Yaksi, E., Deisseroth, K., et al. (2011). Neuronal filtering of multiplexed odour representations. *Nature* 479, 493–498.

Borla, M. A., Palecek, B., Budick, S., and O'Malley, D. M. (2002). Prey capture by larval zebrafish: evidence for fine axial motor control. *Brain Behav. Evol.* 60, 207–229.

Budick, S. A., and O'Malley, D. M. (2000). Locomotor repertoire of the larval zebrafish: swimming, turning and prey capture. *J. Exp. Biol.* 203, 2565–2579.

Burgess, H. A., and Granato, M. (2007). Modulation of locomotor activity in larval zebrafish during light adaptation. *J. Exp. Biol.* 210, 2526–2539.

Burrill, J. D., and Easter, S. S. Jr. (1994). Development of the retinofugal projections in the embryonic and larval zebrafish (*Brachydanio rerio*). *J. Comp. Neurol.* 346, 583–600.

del Bene, F., and Wyart, C. (2012). Optogenetics: a new enlightenment age for zebrafish neurobiology. *Dev. Neurobiol.* 72, 404–414.

Del Bene, F., Wyart, C., Robles, E., Tran, A., Looger, L., Scott, E. K., et al. (2010). Filtering of visual information in the tectum by an identified neural circuit. *Science* 330, 669–673.

du Lac, S., and Knudsen, E. I. (1990). Neural maps of head movement vector and speed in the optic tectum of the barn owl. *J. Neurophysiol.* 63, 131–146.

Easter, S. S. Jr., and Nicola, G. N. (1996). The development of vision in the zebrafish (*Danio rerio*). *Dev. Biol.* 180, 646–663.

Emran, F., Rihel, J., Adolph, A. R., Wong, K. Y., Kraves, S., and Dowling, J. E. (2007). OFF ganglion cells cannot drive the optokinetic reflex in zebrafish. *Proc. Natl. Acad. Sci. U.S.A.* 104, 19126–19131.

Engeszer, R. E., Wang, G., Ryan, M. J., and Parichy, D. M. (2008). Sex-specific perceptual spaces for a vertebrate basal social aggregative behavior. *Proc. Natl. Acad. Sci. U.S.A.* 105, 929–933.

Euler, T., Hausselt, S. E., Margolis, D. J., Breuninger, T., Castell, X., Detwiler, P. B., et al. (2009). Eyecup scope–optical recordings of light stimulus-evoked fluorescence signals in the retina. *Pflugers Arch.* 457, 1393–1414.

Ewert, J. P. (1967). [Electric stimulation of the retinal projection field in the midbrain of the terrestrial toad (*Bufo bufo* L.)]. *Pflugers Arch. Gesamte Physiol. Menschen Tiere* 295, 90–98.

Ewert, J. P., Buxbaum-Conradi, H., Dreisvogt, F., Glagow, M., Merkel-Harff, C., Rottgen, A., et al. (2001). Neural modulation of visuomotor functions underlying prey-catching behaviour in anurans: perception, attention, motor performance, learning. *Comp. Biochem. Physiol. A Mol. Integr. Physiol.* 128, 417–461.

Friedrich, R. W., Jacobson, G. A., and Zhu, P. (2010). Circuit neuroscience in zebrafish. *Curr. Biol.* 20, R371–R381.

Gahtan, E., Tanger, P., and Baier, H. (2005). Visual prey capture in larval zebrafish is controlled by identified reticulospinal neurons downstream of the tectum. *J. Neurosci.* 25, 9294–9303.

Gandhi, N. J., and Katnani, H. A. (2011). Motor functions of the superior colliculus. *Annu. Rev. Neurosci.* 34, 205–231.

Goodale, M. A. (1996). Visuomotor modules in the vertebrate brain. *Can. J. Physiol. Pharmacol.* 74, 390–400.

Gosse, N. J., Nevin, L. M., and Baier, H. (2008). Retinotopic order in the absence of axon competition. *Nature* 452, 892–895.

Grillner, S., and Shik, M. L. (1973). On the descending control of the lumbosacral spinal cord from the "mesencephalic locomotor region". *Acta Physiol. Scand.* 87, 320–333.

Grillner, S., Wallen, P., Saitoh, K., Kozlov, A., and Robertson, B. (2008). Neural bases of goal-directed locomotion in vertebrates–an overview. *Brain Res. Rev.* 57, 2–12.

Herrero, L., Rodriguez, F., Salas, C., and Torres, B. (1998). Tail and eye movements evoked by electrical microstimulation of the optic tectum in goldfish. *Exp. Brain Res.* 120, 291–305.

Huang, Y. Y., Rinner, O., Hedinger, P., Liu, S. C., and Neuhauss, S. C. (2006). Oculomotor instabilities in zebrafish mutant belladonna: a behavioral model for congenital nystagmus caused by axonal misrouting. *J. Neurosci.* 26, 9873–9880.

Humphries, M. D., Gurney, K., and Prescott, T. J. (2007). Is there a brainstem substrate for action selection? *Philos. Trans. R. Soc. Lond. B Biol. Sci.* 362, 1627–1639.

Liu, K. S., and Fetcho, J. R. (1999). Laser ablations reveal functional relationships of segmental hindbrain neurons in zebrafish. *Neuron* 23, 325–335.

Mathieson, W. B., and Maler, L. (1988). Morphological and electrophysiological properties of a novel *in vitro* preparation: the electrosensory lateral line lobe brain slice. *J. Comp. Physiol. A* 163, 489–506.

McElligott, M. B., and O'Malley, D. M. (2005). Prey tracking by larval zebrafish: axial kinematics and visual control. *Brain Behav. Evol.* 66, 177–196.

McHaffie, J. G., and Stein, B. E. (1982). Eye movements evoked by electrical stimulation in the superior colliculus of rats and hamsters. *Brain Res.* 247, 243–253.

Meek, J., and Schellart, N. A. (1978). A Golgi study of goldfish optic tectum. *J. Comp. Neurol.* 182, 89–122.

Miri, A., Daie, K., Burdine, R. D., Aksay, E., and Tank, D. W. (2011). Regression-based identification of behavior-encoding neurons during large-scale optical imaging of neural activity at cellular resolution. *J. Neurophysiol.* 105, 964–980.

Mueller, T., and Wullimann, M. F. (2002). BrdU-, neuroD (nrd)- and Hu-studies reveal unusual non-ventricular neurogenesis in the postembryonic zebrafish forebrain. *Mech. Dev.* 117, 123–135.

Muto, A., Ohkura, M., Abe, G., Nakai, J., and Kawakami, K. (2013). Real-time visualization of neuronal activity during perception. *Curr. Biol.* 23, 307–311.

Neuhauss, S. C., Biehlmaier, O., Seeliger, M. W., Das, T., Kohler, K., Harris, W. A., et al. (1999). Genetic disorders of vision revealed by a behavioral screen of 400 essential loci in zebrafish. *J. Neurosci.* 19, 8603–8615.

Niell, C. M., and Smith, S. J. (2005). Functional imaging reveals rapid development of visual response properties in the zebrafish tectum. *Neuron* 45, 941–951.

Orger, M. B., and Baier, H. (2005). Channeling of red and green cone inputs to the zebrafish optomotor response. *Vis. Neurosci.* 22, 275–281.

Orger, M. B., Kampff, A. R., Severi, K. E., Bollmann, J. H., and Engert, F. (2008). Control of visually guided behavior by distinct populations of spinal projection neurons. *Nat. Neurosci.* 11, 327–333.

Orger, M. B., Smear, M. C., Anstis, S. M., and Baier, H. (2000). Perception of Fourier and non-Fourier motion by larval zebrafish. *Nat. Neurosci.* 3, 1128–1133.

Pologruto, T. A., Sabatini, B. L., and Svoboda, K. (2003). ScanImage: flexible software for operating laser scanning microscopes. *Biomed. Eng. Online* 2, 13.

Portugues, R., and Engert, F. (2009). The neural basis of visual behaviors in the larval zebrafish. *Curr. Opin. Neurobiol.* 19, 644–647.

Robles, E., Smith, S. J., and Baier, H. (2011). Characterization of genetically targeted neuron types in the zebrafish optic tectum. *Front. Neural Circuits* 5:1. doi: 10.3389/fncir.2011.00001

Roeser, T., and Baier, H. (2003). Visuomotor behaviors in larval zebrafish after GFP-guided laser ablation of the optic tectum. *J. Neurosci.* 23, 3726–3734.

Saitoh, K., Menard, A., and Grillner, S. (2007). Tectal control of locomotion, steering, and eye movements in lamprey. *J. Neurophysiol.* 97, 3093–3108.

Salas, C., Herrero, L., Rodriguez, F., and Torres, B. (1997). Tectal codification of eye movements in goldfish studied by electrical microstimulation. f. *Neuroscience* 78, 271–288.

Sankrithi, N. S., and O'Malley, D. M. (2010). Activation of a multisensory, multifunctional nucleus in the zebrafish midbrain during diverse locomotor behaviors. *Neuroscience* 166, 970–993.

Sato, T., Hamaoka, T., Aizawa, H., Hosoya, T., and Okamoto, H. (2007). Genetic single-cell mosaic analysis implicates ephrinB2 reverse signaling in projections from the posterior tectum to the hindbrain in zebrafish. *J. Neurosci.* 27, 5271–5279.

Sato, T., Takahoko, M., and Okamoto, H. (2006). HuC:Kaede, a useful tool to label neural morphologies in networks *in vivo*. *Genesis* 44, 136–142.

Sato, Y., Miyasaka, N., and Yoshihara, Y. (2005). Mutually exclusive glomerular innervation by two distinct types of olfactory sensory neurons revealed in transgenic zebrafish. *J. Neurosci.* 25, 4889–4897.

Schaefer, K. P. (1970). Unit analysis and electrical stimulation in the optic tectum of rabbits and cats. *Brain Behav. Evol.* 3, 222–240.

Schoonheim, P. J., Arrenberg, A. B., Del Bene, F., and Baier, H. (2010). Optogenetic localization and genetic perturbation

of saccade-generating neurons in zebrafish. *J. Neurosci.* 30, 7111–7120.

Scott, E. K., and Baier, H. (2009). The cellular architecture of the larval zebrafish tectum, as revealed by gal4 enhancer trap lines. *Front. Neural Circuits* 3:13. doi: 10.3389/neuro.04.013.2009

Springer, A. D., Easter, S. S. Jr., and Agranoff, B. W. (1977). The role of the optic tectum in various visually mediated behaviors of goldfish. *Brain Res.* 128, 393–404.

Stein, B. E., and Clamann, H. P. (1981). Control of pinna movements and sensorimotor register in cat superior colliculus. *Brain Behav. Evol.* 19, 180–192.

Sterman, M. B., and Fairchild, M. D. (1966). Modification of locomotor performance by reticular formation and basal forebrain stimulation in the cat: evidence for reciprocal systems. *Brain Res.* 2, 205–217.

Straw, A. D., and Dickinson, M. H. (2009). Motmot, an open-source toolkit for realtime video acquisition and analysis. *Source Code Biol. Med.* 4, 5.

Suter, B. A., O'Connor, T., Iyer, V., Petreanu, L. T., Hooks, B. M., Kiritani, T., et al. (2010). Ephus: multipurpose data acquisition software for neuroscience experiments. *Front. Neural Circuits* 4:100. doi: 10.3389/fncir.2010.00100

Syka, J., and Radil-Weiss, T. (1971). Electrical stimulation of the tectum in freely moving cats. *Brain Res.* 28, 567–572.

Thorsen, D. H., Cassidy, J. J., and Hale, M. E. (2004). Swimming of larval zebrafish: fin-axis coordination and implications for function and neural control. *J. Exp. Biol.* 207, 4175–4183.

Valentine, D. E., Sinha, S. R., and Moss, C. F. (2002). Orienting responses and vocalizations produced by microstimulation in the superior colliculus of the echolocating bat, *Eptesicus fuscus*. *J. Comp. Physiol. A Neuroethol. Sens. Neural Behav. Physiol.* 188, 89–108.

Wyart, C., Del Bene, F., Warp, E., Scott, E. K., Trauner, D., Baier, H., et al. (2009). Optogenetic dissection of a behavioural module in the vertebrate spinal cord. *Nature* 461, 407–410.

Xiao, T., Roeser, T., Staub, W., and Baier, H. (2005). A GFP-based genetic screen reveals mutations that disrupt the architecture of the zebrafish retinotectal projection. *Development* 132, 2955–2967.

Zerucha, T., Stuhmer, T., Hatch, G., Park, B. K., Long, Q., Yu, G., et al. (2000). A highly conserved enhancer in the Dlx5/Dlx6 intergenic region is the site of cross-regulatory interactions between Dlx genes in the embryonic forebrain. *J. Neurosci.* 20, 709–721.

Zhu, P., Fajardo, O., Shum, J., Zhang Scharer, Y. P., and Friedrich, R. W. (2012). High-resolution optical control of spatiotemporal neuronal activity patterns in zebrafish using a digital micromirror device. *Nat. Protoc.* 7, 1410–1425.

Zhu, P., Narita, Y., Bundschuh, S. T., Fajardo, O., Scharer, Y. P., Chattopadhyaya, B., et al. (2009). Optogenetic dissection of neuronal circuits in zebrafish using viral gene transfer and the tet system. *Front. Neural Circuits* 3:21. doi: 10.3389/neuro.04.021.2009

Conflict of Interest Statement: The authors declare that the research was conducted in the absence of any commercial or financial relationships that could be construed as a potential conflict of interest.

Received: 31 January 2013; paper pending published: 12 February 2013; accepted: 30 March 2013; published online: 17 April 2013.

Citation: Fajardo O, Zhu P and Friedrich RW (2013) Control of a specific motor program by a small brain area in zebrafish. Front. Neural Circuits 7:67. doi: 10.3389/fncir.2013.00067

frontiers in
NEURAL CIRCUITS

ORIGINAL RESEARCH ARTICLE
published: 28 May 2013
doi: 10.3389/fncir.2013.00103

KCC2-dependent subcellular E_{Cl} difference of ON-OFF retinal ganglion cells in larval zebrafish

Rong-wei Zhang *, Shu-yi Zhang and Jiu-lin Du *

Institute of Neuroscience and State Key Laboratory of Neuroscience, Shanghai Institutes for Biological Sciences, Chinese Academy of Sciences, Shanghai, China

Edited by:
German Sumbre, Ecole Normale Superieure, France

Reviewed by:
Filippo Del Bene, Institut Curie, France
Laura Cancedda, Istituto Italiano di Tecnologia, Italy

****Correspondence:***
Rong-wei Zhang, Associate Investigator, Institute of Neuroscience and State Key Laboratory of Neuroscience, Shanghai Institutes for Biological Sciences, Chinese Academy of Sciences, 320 Yue-yang Road, Shanghai 200031, China.
e-mail: zhangrw@ion.ac.cn;

Jiu-lin Du, Principal Investigator, Institute of Neuroscience and State Key Laboratory of Neuroscience, Shanghai Institutes for Biological Sciences, Chinese Academy of Sciences, 320 Yue-yang Road, Shanghai 200031, China.
e-mail: forestdu@ion.ac.cn

Subcellular difference in the reversal potential of Cl^- (E_{Cl}) has been found in many types of neurons. As local E_{Cl} largely determines the action of nearby GABAergic/glycinergic synapses, subcellular E_{Cl} difference can effectively regulate neuronal computation. The ON-OFF retinal ganglion cell (RGC) processes both ON and OFF visual signals via its ON and OFF dendrites, respectively. It is thus interesting to investigate whether the ON and OFF dendrites of single RGCs exhibit different local E_{Cl}. Here, using *in vivo* gramicidin-perforated patch recording in larval zebrafish ON-OFF RGCs, we examine local E_{Cl} at the ON and OFF dendrites, and soma through measuring light-evoked ON and OFF inhibitory responses, and GABA-induced response at the soma, respectively. We find there are subcellular E_{Cl} differences between the soma and dendrite, as well as between the ON and OFF dendrites of single RGCs. These somato-dendritic and inter-dendritic E_{Cl} differences are dependent on the Cl^- extruder, K^+/Cl^- co-transporter (KCC2), because they are largely diminished by down-regulating *kcc2* expression with morpholino oligonucleotides (MOs) or by blocking KCC2 function with furosemide. Thus, our findings indicate that there exists KCC2-dependent E_{Cl} difference between the ON and OFF dendrites of individual ON-OFF RGCs that may differentially affect visual processing in the ON and OFF pathways.

Keywords: Cl^- reversal potential, GABA, KCC2, subcellular, retinal ganglion cells, *in vivo* whole-cell recording, zebrafish

INTRODUCTION

Intracellular Cl^- homeostasis is involved in the regulation of many cellular functions, including cell volume and membrane excitability (Blaesse et al., 2009). In the neurons of neonatal brains, developmental up-regulation of the Cl^- extruder K^+/Cl^- co-transporter (KCC2) and down-regulation of the Cl^- importer $Na^+/K^+/Cl^-$ (NKCC) cause progressive reduction of intracellular chloride concentration ($[Cl^-]_i$), resulting in a hyperpolarization shift of the Cl^- reversal potential (E_{Cl}) and a switch of gamma aminobutyric acid (GABA) action from excitation to inhibition (Wang and Kriegstein, 2009; Ben-Ari et al., 2012).

In individual neurons, differential subcellular distribution of KCC2 and/or NKCC can generate an uneven $[Cl^-]_i$ gradient along neuronal processes, leading to different GABA actions on the same neuron (Vardi et al., 2000; Khirug et al., 2005; Duebel et al., 2006; Gavrikov et al., 2006). In starburst amacrine cells of rabbit retinae, KCC2 and NKCC2 are preferentially located at distal and proximal dendrites, respectively, resulting in GABA-evoked hyperpolarization at distal dendrites and depolarization at proximal dendrites. This inter-dendritic difference in the GABA action contributes to direction-selective light responses of those cells (Gavrikov et al., 2003, 2006). Similarly, the dendrite and axon of ON bipolar cells preferentially express NKCC and KCC2, respectively (Vardi et al., 2000; Duebel et al., 2006), resulting in a depolarization action of synaptic inputs from horizontal cells to BC dendrites and a hyperpolarization action of synaptic inputs from amacrine cells to BC axons. Therefore, non-uniform subcellular distribution of KCC2 and/or NKCC in retinal cells can regulate visual information processing.

The ON-OFF retinal ganglion cell (RGC) extends multi-stratified dendrites into both the sublamina *a* and *b* of the inner plexiform layer, where it receives visual information from OFF and ON bipolar cells, respectively. Moreover, both light-evoked ON and OFF responses of those cells can be modulated by inhibitory synaptic inputs originated from GABAergic and glycinergic amacrine cells. It is thus of interest to examine whether the action of GABAergic/glycinergic inhibition is different between the ON and OFF dendrites of ON-OFF RGCs. To address this question, we performed gramicidin-perforated patch recording in intact larval zebrafish, and examined Cl^- reversal potential (E_{Cl}) at the soma, and ON and OFF dendrites of ON-OFF RGCs during 2.5–6 days post-fertilization (dpf). We found that there are subcellular E_{Cl} differences between the soma and dendrite (somato-dendritic), and between the ON and OFF dendrites (inter-dendritic). The E_{Cl} difference is largely dependent on KCC2 function because it was diminished by genetic knockdown or pharmacological blockade of KCC2.

MATERIALS AND METHODS

ZEBRAFISH PREPARATION

Wild-type AB adult zebrafish (*Danio rerio*) were maintained in the National Zebrafish Resources of China (Shanghai, China) with an automatic fish-housing system (ESEN, China) at 28°C. Embryos and larvae were raised on a 14–10 h light-dark cycle in 10% Hank's solution, which consists of (in mM) 140 NaCl, 5.4 KCl, 0.25 Na_2HPO_4, 0.44 KH_2PO_4, 1.3 $CaCl_2$, 1.0 $MgSO_4$, and 4.2 $NaHCO_3$ (pH 7.2) (Westerfield, 1995). Electrophysiological recordings were performed on 2.5- to 6-dpf larval zebrafish at room temperature (22–26°C). All zebrafish handling procedures followed the guideline of Institute of Neuroscience, Chinese Academy of Sciences.

ELECTROPHYSIOLOGICAL RECORDING

In vivo whole-cell recordings were made from the cells at the ganglion cell layer of the retina according to our previous experimental procedure (Zhang et al., 2010). Based on previous reports (Kay et al., 2001; Wei et al., 2012), displaced amacrine cells are rarely observed in zebrafish larvae and the majority of cells at the ganglion cell layer are RGCs. After dissection, the larval preparation was continuously perfused with external solution, which consists of (in mM) 134 NaCl, 2.9 KCl, 2.1 $CaCl_2$, 1.2 $MgCl_2$, 10 HEPES and 10 glucose (290 mOsm/L, pH 7.8). Recording micropipettes were made from borosilicate capillaries (BF 120-69-15, Sutter Instrument), and had a resistance in the range of 10–15 MΩ. In order to measure physiological E_{Cl} of zebrafish RGCs, we performed gramicidin-perforated patch recording, with which intracellular Cl^- homeostasis was not disturbed (Kyrozis and Reichling, 1995). The pipette was tip-filled with gramicidin-free internal solution and then back-filled with internal solution containing 10 μg/ml gramicidin. For gramicidin recordings (**Figures 2–5**), we used internal solution with high Cl^- concentration that contains (in mM) 110 KCl, 6 NaCl, 2 $CaCl_2$, 2 $MgCl_2$, 10 HEPES, and 10 EGTA (260 mOsm/L, pH 7.4). For calibrating dendritic E_{Cl} measurement (**Figure 1**), we performed conventional whole-cell recordings with low Cl^- concentration-containing internal solution. The recording was made with an EPC-10 amplifier (Heka, Germany), and signals were filtered at 2.9 kHz and sampled at 10 kHz. Data were discarded if the series resistance varied >20% during recordings. To evoke light responses of RGCs, 2-s whole-field light flash was given via a cooled light source controlled by an electrical shutter (LS6Z2, Uniblitz). All drugs were purchased from Sigma (St. Louis).

KNOCKDOWN OF ZEBRAFISH *kcc2*

Morpholino oligonucleotides (MOs) were used to down-regulate the expression of zebrafish *kcc2* gene. The *kcc2* MO (TGGATGTTGCATCTCCTGTGAACAT) and a standard control MO (CCTCCTACCTCAGTTACAATTTATA) were produced by Gene Tools (Philomath, OR), and used in our previous study (Zhang et al., 2010). A dose of 8-ng MO was pressure-injected into the animal pole of zebrafish embryos at 1-cell stage. Since the MOs were tagged with the fluorophore lissamine at the 3′ terminal, the distribution of MOs in zebrafish RGCs could be visualized by fluorescent signal.

STATISTICAL ANALYSIS

Lillie test was first performed to examine the normality assumption of data. For normal data, paired or unpaired student's *t*-test was used for statistical significance analysis between two groups. For data which was not normal, Wilcoxen sign-rank test was then used for significance analysis. For testing the significance of the differences in the cumulative distribution of E_{Cl}, the non-parametric Kolmogorov–Smirnov test was used (**Figures 4**, **5**). The *P*-value <0.05 was considered to be statistically significant. All results were represented as mean ± SEM.

RESULTS

MEASUREMENT OF RGC DENDRITIC E_{Cl}

Under infra-red visual guidance, RGCs in intact zebrafish larvae aged from 2.5 to 6 dpf were recorded, and their light responses

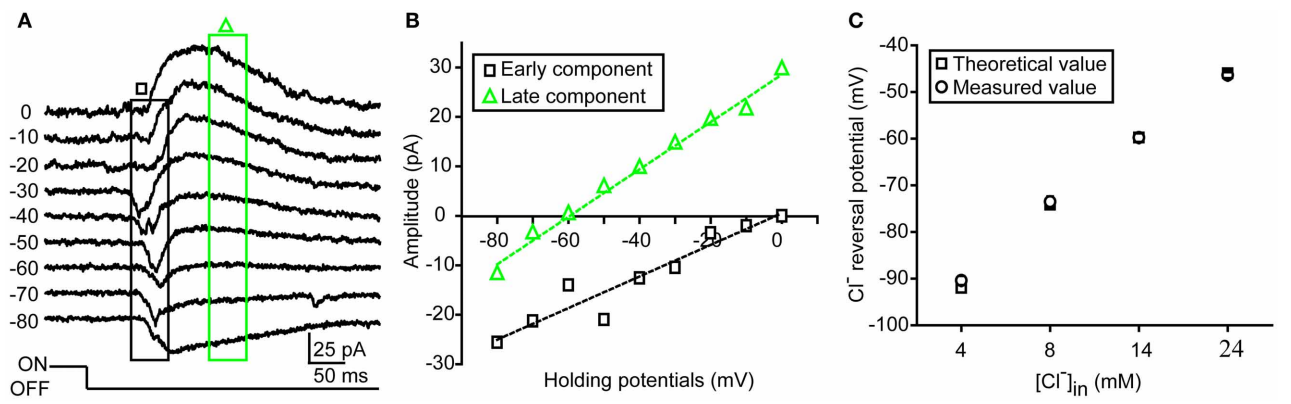

FIGURE 1 | Measurement of dendritic E_{Cl} in zebrafish RGCs. (A) An example showing light-evoked OFF synaptic responses recorded at different holding potentials from −80 to 0 mV when the ON-OFF RGC was loaded with 14 mM Cl^- internal solution under conventional whole-cell recording mode. **(B)** I–V curves of early (black square) and late (green triangle) components of light-evoked responses. Dendritic E_{Cl}, calculated by fitting the I–V curve of the late-phase component with linear regression, is about −60 mV, close to the Cl^- equilibrium potential (−59.8 mV). **(C)** Theoretical (square) and measured (circle) dendritic E_{Cl} when the RGCs was loaded with internal solution with different Cl^- concentration (4, 8, 14, or 24 mM). The data were obtained from 10 cells at each data point. The values are represented as mean ± SEM.

were evoked by the application of 2-s whole-field light flashes. In the present study, ON-OFF RGCs, which responded to both the onset and offset of light stimuli, were selected for investigation. Most of those cells exhibited small bi-stratified or diffuse dendritic fields (Zhang et al., 2010). Similar to other species (Gao and Wu, 1998; Pang et al., 2003), light-evoked responses (LERs) of zebrafish ON-OFF RGCs could be temporally divided into two synaptic components after the onset of the responses (**Figure 1**). In order to confirm the measurement of dendritic E_{Cl} based on light-evoked inhibitory component, we firstly performed conventional whole-cell recording on RGC soma with internal solution containing low Cl^- concentration (14 mM) (**Figures 1A,B**). The early component of OFF LER (0–50 ms after the LER onset) was reversed at ~0 mV (**Figures 1A,B**), which is believed to be mediated by glutamatergic inputs from bipolar cells. Meanwhile, the late component (150–200 ms after the LER onset) was reversed around −60 mV, similar to the theoretical E_{Cl} according to the Nernst equation (**Figure 1B**), supporting the notion that this component was mediated by GABAergic/glycinergic inputs from amacrine cells.

As inhibitory synapses are mainly formed at RGC dendrites, the reversal potential of the late-phase ON and OFF light responses can reflect the local E_{Cl} of ON and OFF dendrites of RGCs, respectively. To further confirm this point, we loaded ON-OFF RGCs with internal solution containing different Cl^- concentration (4, 8, 14, or 24 mM) under conventional whole-cell recording mode. We found that the average reversal potential of late-phase LERs was almost the same as the theoretical E_{Cl}: at 4 mM, −90.4 ± 1.0 vs. −92.0 mV; at 8 mM, −73.6 ± 1.1 vs. −74.2 mV; at 14 mM, −59.8 ± 0.9 vs. −59.8 mV; at 24 mM, −46.4 ± 0.6 vs −46 mV (**Figure 1C**).

SOMATO-DENDRITIC AND INTER-DENDRITIC E_{Cl} DIFFERENCES

In order to examine physiological E_{Cl} of ON-OFF RGCs, we performed gramicidin-perforated recordings in all following experiments. Besides dendritic E_{Cl} measurement based on light-evoked inhibitory responses, we also examined somatic E_{Cl} through puffing GABA solution (50 μM) onto RGC soma via a glass micropipette (**Figure 2A**) (Zhang et al., 2010). The peak amplitude of GABA-induced currents was measured when the ON-OFF RGC was held at different potentials (square, **Figure 2B**). Interestingly, there were obvious differences between somatic and dendritic E_{Cl} in single RGCs (**Figures 2B,C**). Somatic E_{Cl} was more negative than both ON and OFF dendritic

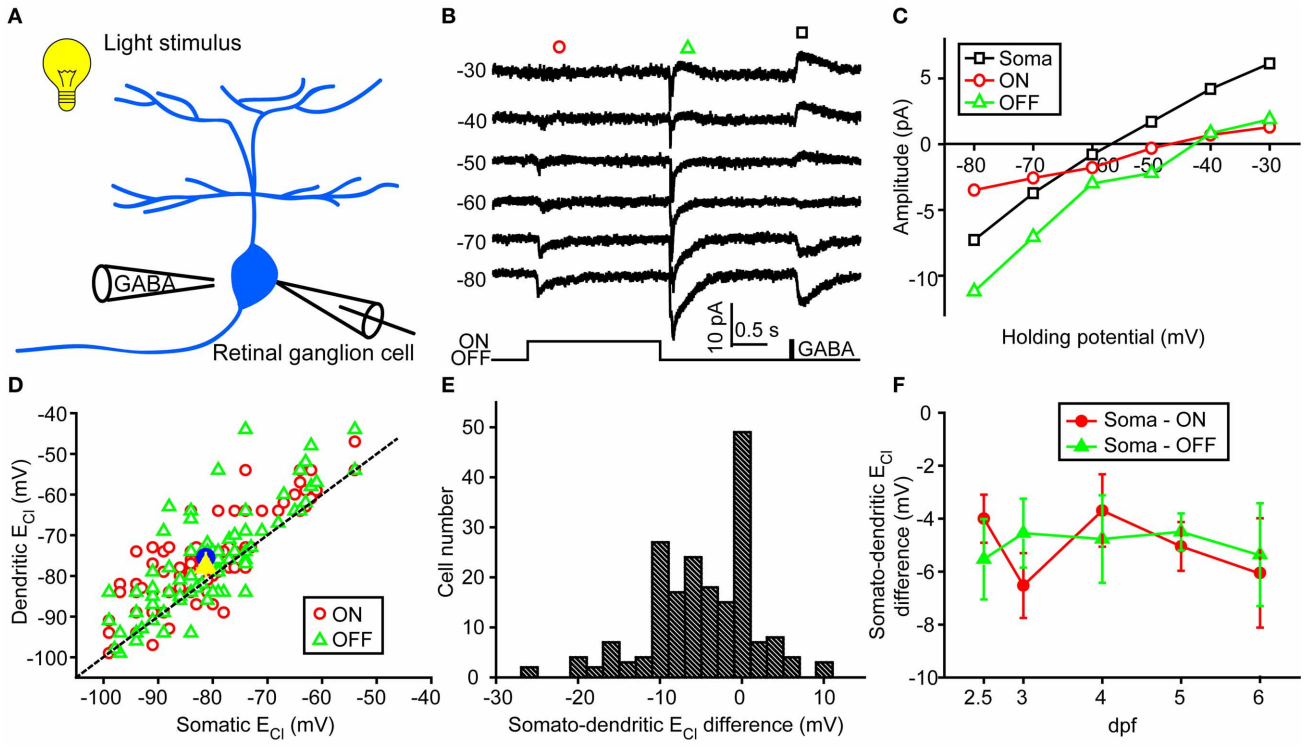

FIGURE 2 | Somato-dendritic E_{Cl} difference of zebrafish ON-OFF RGCs. **(A)** A schematic showing the experimental procedure. **(B)** Light-evoked ON (red circle) and OFF (green triangle) synaptic responses and GABA-induced currents (black square) were simultaneously recorded at different holding potentials from an ON-OFF RGC under gramicidin-perforated patch recording mode. **(C)** I–V curves of GABA-induced current at the RGC soma (black square), and the late-phase components of ON (red circle) and OFF (green triangle) light-evoked responses. The data were obtained from the same cell with **(B)**. **(D)** Plots of dendritic E_{Cl} against somatic E_{Cl}. The dotted line represents the orthogonal, and the blue circle and yellow triangle represent the mean E_{Cl} of ON and OFF responses, respectively. The data were obtained from 98 ON-OFF RGCs. **(E)** Distribution of somato-dendritic E_{Cl} difference. **(F)** Mean E_{Cl} differences between soma and ON or OFF dendrites of ON-OFF RGCs from 2.5 to 6 dpf. At each data points, the cell number is more than 13. The values are represented as mean ± SEM.

E_{Cl} (soma vs. ON dendrite, -81.3 ± 1.1 vs. -76.1 ± 1.1 mV, $n = 98$, $P < 0.0001$; soma vs. OFF dendrite, -81.3 ± 1.1 vs. -77.1 ± 1.3 mV, $n = 98$, $P < 0.0001$, paired student's t-test; **Figure 2D**), and the somato-dendritic E_{Cl} difference varied in individual cells (**Figure 2E**). During 2.5–6 dpf, the average E_{Cl} difference between the soma and ON or OFF dendrite remained relatively consistent (**Figure 2F**). Furthermore, there was also a difference between ON and OFF dendritic E_{Cl} in individual RGCs (**Figure 3**). In 53 out of 152 ON-OFF RGCs, ON dendritic E_{Cl} was more negative than OFF dendrite E_{Cl} (**Figures 3A,C**), whereas the situation was reversal in other 60 cells (**Figures 3B,C**). In total, the absolute difference between ON and OFF dendritic E_{Cl} ranged from 4.6 to 8.2 mV during 2.5–6 dpf (**Figure 3D**), and exhibited a significant increase from 2.5 to 3 dpf ($P < 0.05$), implying a developmental change of subcellular Cl^- homeostasis between ON and OFF dendrites during this stage. Taken together, there is a Cl^- gradient within subcellular compartments of larval zebrafish ON-OFF RGCs.

Kcc2 REGULATES SUBCELLULAR E_{Cl} DIFFERENCES

Since intracellular Cl^- homeostasis is maintained by the action of cation/Cl^- co-transporters (CCCs) (Blaesse et al., 2009), the difference between somatic and dendritic E_{Cl} in zebrafish ON-OFF RGCs implies differential distribution of CCCs, e.g., KCC2, at different subcellular regions of these cells. To examine this point, we micro-injected morpholino oligos (MOs) into zebrafish embryos at 1-cell stage to down-regulate *kcc2* expression (see Materials and Methods). Knockdown of zebrafish *kcc2* resulted in a shift of both the dendritic and somatic E_{Cl} in ON-OFF RGCs toward a depolarization level (**Figures 4A,B**), indicating the effectiveness of *kcc2* MO (Zhang et al., 2010). Importantly, the absolute value of inter-dendritic E_{Cl} difference between ON and OFF dendrites of RGCs was significantly reduced in *kcc2* morphants in comparison to the control group (*kcc2* MO, 2.8 ± 0.9 mV; control MO, 8.7 ± 1.6 mV; $P < 0.01$, Kolmogorov–Smirnov test; **Figures 4C–E**). Similar reduction was observed in somato-dendritic E_{Cl} difference (*kcc2* MO, -1.8 ± 0.9 mV; control MO, -7.4 ± 1.3 mV; $P < 0.01$, Kolmogorov–Smirnov test; **Figure 4F**).

To further confirm the role of KCC2 in the subcellular difference of E_{Cl}, we then applied furosemide (50 μM), a broad-spectrum inhibitor of CCCs (Payne et al., 2003), to suppress KCC2 function. Similar to KCC2 knockdown experiments, bath application of furosemide significantly reduced inter-dendritic E_{Cl} difference from 7.2 ± 1.4 to 1.6 ± 0.6 mV ($P < 0.01$, Kolmogorov–Smirnov test; **Figure 5A**) and somato-dendritic E_{Cl} difference from -4.8 ± 0.8 to -1.5 ± 0.5 mV ($P < 0.01$, Kolmogorov–Smirnov test; **Figure 5B**). Taken together, these results indicate that KCC2 plays an important role in the establishment of the subcellular difference of E_{Cl} in zebrafish ON-OFF RGCs.

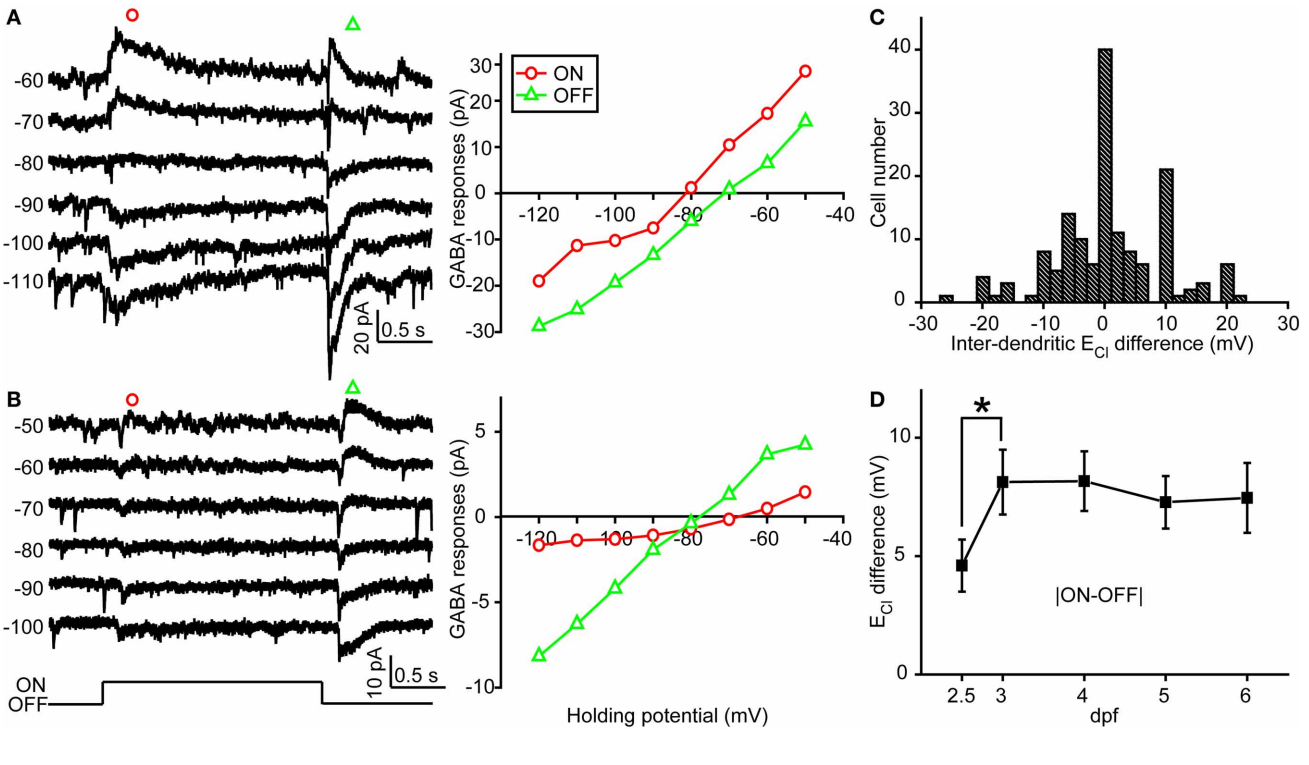

FIGURE 3 | Inter-dendritic E_{Cl} difference between ON and OFF dendrites of zebrafish ON-OFF RGCs. (A,B) Left, light-evoked ON and OFF synaptic responses recorded at different holding potentials from two ON-OFF RGCs under gramicidin-perforated patch recording mode. Right, I–V curves of the late-phase components of light-evoked ON (red circle) and OFF (green triangle) responses. **(C)** Distribution of the inter-dendritic E_{Cl} difference from 152 cells. **(D)** Mean absolute values of inter-dendritic E_{Cl} difference from 2.5 to 6 dpf. At each data points, the cell number is more than 15. $^*P < 0.05$, unpaired Student's t-test. The values are represented as mean ± SEM.

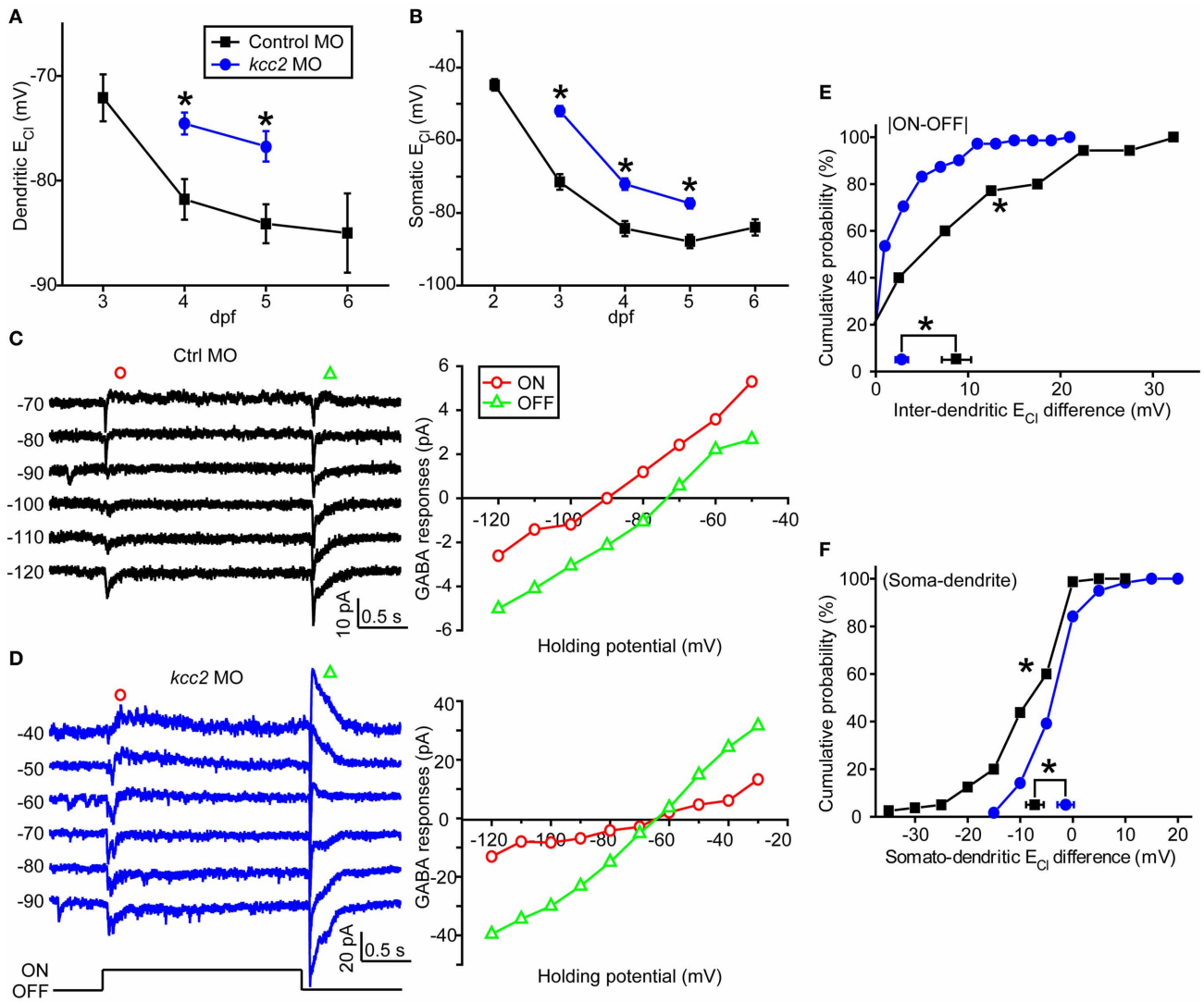

FIGURE 4 | Knockdown of zebrafish *kcc2* diminishes subcellular E_{Cl} difference. **(A,B)** Mean dendritic **(A)** and somatic **(B)** E_{Cl} of control (black square) and *kcc2* morphants (blue circle). At each data points, the cell number is more than 8. **(C,D)** Left, Light-evoked ON and OFF responses of RGCs from a control **(C)** and *kcc2* morphants **(D)** under gramicidin-perforated patch recording mode. Right, I–V curves of the late-phase components of light responses. **(E,F)** Cumulative probability of inter-dendritic **(E)** and somato-dendritic **(F)** E_{Cl} differences in control ($n = 35$ cells) and *kcc2* morphants ($n = 71$ cells). The symbols near the X-axis represent the mean E_{Cl} differences. $^*P < 0.01$, Kolmogorov–Smirnov test. The values are represented as mean ± SEM.

DISCUSSION

In the present study, we performed *in vivo* gramicidin-perforated recordings in developing zebrafish ON-OFF RGCs, and found somato-dendritic and inter-dendritic E_{Cl} differences (**Figure 6**), which were largely dependent on KCC2 function. Our findings indicate that KCC2 plays an important role in the establishment of subcellular E_{Cl} differences in RGCs.

Spatial distribution of KCC2 and/or NKCC1 produces subcellular $[Cl^-]_i$ gradient along different parts of individual neurons. In hippocampal principal cells, KCC2 is primarily expressed at dendritic spines, but rarely at soma and dendritic shafts (Gulyas et al., 2001), causing a somato-dendritic $[Cl^-]_i$ gradient (Khirug et al., 2005). In the retina, KCC2 and NKCC1 are preferentially expressed at the axon terminals and dendrites of ON bipolar cells, respectively (Vardi et al., 2000), implying the existence of subcellular $[Cl^-]_i$ gradient in bipolar cells. Consistently, it is found that the soma of ON bipolar cells exhibits more negative E_{Cl} than their dendrites (Duebel et al., 2006). Therefore, ON bipolar cells may receive depolarizing GABAergic actions from horizontal cells at their dendrites, but receive hyperpolarizing GABAergic inputs from amacrine cells at their axon terminals.

In zebrafish larvae, the expression of *kcc2* is first detected at 2 dpf, and increased in following days (Reynolds et al., 2008), leading to an excitation-to-inhibition switch of GABAergic action

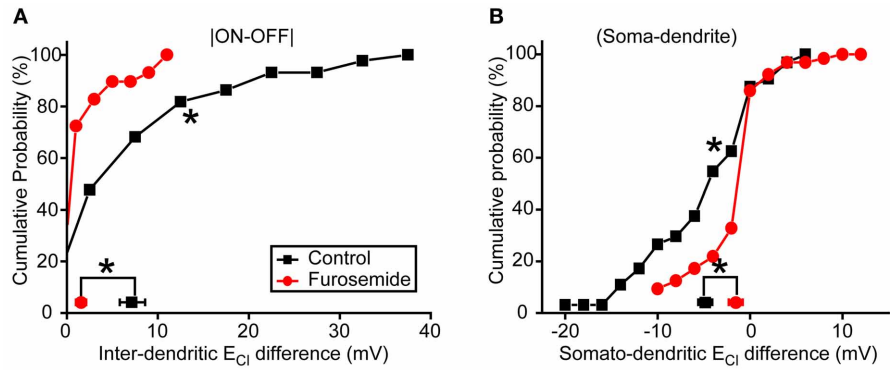

FIGURE 5 | Blockade of KCC2 reduces subcellular E_{Cl} difference. (A,B) Cumulative probability of inter-dendritic **(A)** and somato-dendritic **(B)** E_{Cl} difference in control ($n = 44$ cells) and furosemide-treated ($n = 29$ cells) animals. The symbols near the X-axis represent the mean E_{Cl} differences. $^*P < 0.01$, Kolmogorov–Smirnov test. The values are represented as mean ± SEM.

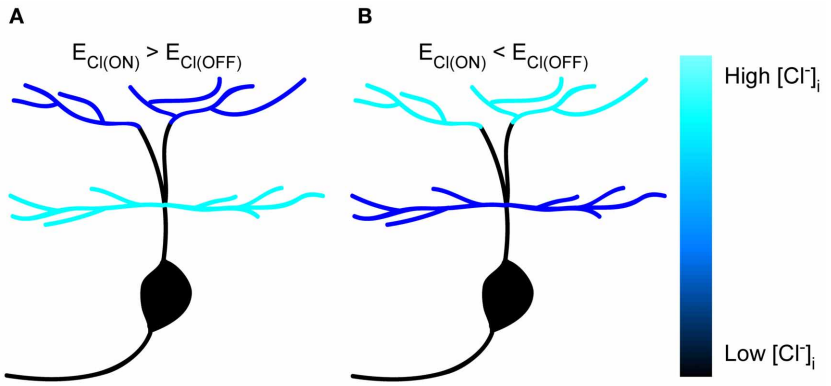

FIGURE 6 | Schematic of subcellular E_{Cl} differences within single zebrafish RGCs. (A,B) Cartoon showing subcellular E_{Cl} differences between soma, ON and OFF dendrites in zebrafish ON-OFF RGCs. The $[Cl^-]_i$ is color-coded.

in RGCs at 2.5 dpf (Zhang et al., 2010). Our data show that somato-dendritic and inter-dendritic $[Cl^-]_i$ gradients already exist even at 2.5 dpf (**Figures 2F**, **3D**), a time point when zebrafish RGCs begin to exhibit LERs (Zhang et al., 2010). This suggests that the initial establishment of subcellular $[Cl^-]_i$ gradient is intrinsic and not dependent on visual experience. Notably, the increase of inter-dendritic E_{Cl} difference occurs between 2.5 and 3 dpf, time points when the level of *kcc2* expression is elevated (Reynolds et al., 2008; Zhang et al., 2010). Moreover, our findings that knockdown of *kcc2* expression or pharmacological blockade of KCC2 function largely diminished inter-dendritic $[Cl^-]_i$ gradients imply differential KCC2 distribution between ON and OFF dendrites, perhaps due to sequential formation of RGC dendrites. Mumm and colleagues performed *in vivo* time-lapse imaging in developing zebrafish RGCs, and found that the inner dendritic arbor of some RGCs first formed, following by the addition of dendritic strata in the outer sublamina of the inner plexiform layer, *vice versa* in other RGCs examined (Mumm et al., 2006). This sequential growth of multi-stratified dendrites may cause differential KCC2 expression between ON and OFF dendrites, leading to inter-dendritic E_{Cl} difference in developing zebrafish RGCs. However, due to the lack of specific antibodies for zebrafish KCC2, we cannot examine the subcellular distribution of KCC2 within an individual RGC. Despite the lack of *kcc2* zebrafish antibodies, a genetic approach could be used. For example, generating a transgenic line expressing *kcc2*-GFP and/or NKCC1-RFP will be helpful for us to correlate electrophysiology directly with the *kcc2*/NKCC1 ratio at different subcellular compartments. Furthermore, we could combine voltage-sensitive and chloride-sensitive dyes to confirm whether different *kcc2*/NKCC1 ratios may change ECl at different cellular regions, leading to differential GABA-induced actions. In the future, KCC2 immunostaining and intracellular Cl^- imaging in zebrafish RGCs may help us understand the mechanism underlying the formation of subcellular $[Cl^-]_i$ gradient.

As local E_{Cl} can determine the strength or even polarity of GABAergic/glycinergic synaptic inputs, the inter-dendritic E_{Cl} difference in ON-OFF RGCs may lead to a differential extent of inhibition at ON and OFF dendrites, and

cause asymmetric light-evoked spiking activity between ON and OFF visual pathways (Joselevitch and Kamermans, 2009; Zhang and McCall, 2012). Therefore, subcellular E_{Cl} differences in zebrafish RGCs can play a role in visual information processing.

ACKNOWLEDGMENTS

This work was supported by grants to Jiu-lin Du from 973 Program (2011CBA00400, 2012CB945101), the Strategic Priority Research Program (XDB02040300) and the Hundred Talents Program from the Chinese Academy of Sciences.

REFERENCES

Ben-Ari, Y., Woodin, M. A., Sernagor, E., Cancedda, L., Vinay, L., Rivera, C., et al. (2012). Refuting the challenges of the developmental shift of polarity of GABA actions: GABA more exciting than ever! *Front. Cell. Neurosci.* 6:35. doi: 10.3389/fncel.2012.00035

Blaesse, P., Airaksinen, M. S., Rivera, C., and Kaila, K. (2009). Cation-chloride cotransporters and neuronal function. *Neuron* 61, 820–838. doi: 10.1016/j.neuron.2009.03.003

Duebel, J., Haverkamp, S., Schleich, W., Feng, G., Augustine, G. J., Kuner, T., and Euler, T. (2006). Two-photon imaging reveals somatodendritic chloride gradient in retinal ON-type bipolar cells expressing the biosensor Clomeleon. *Neuron* 49, 81–94. doi: 10.1016/j.neuron.2005.10.035

Gao, F., and Wu, S. M. (1998). Characterization of spontaneous inhibitory synaptic currents in salamander retinal ganglion cells. *J. Neurophysiol.* 80, 1752–1764.

Gavrikov, K. E., Dmitriev, A. V., Keyser, K. T., and Mangel, S. C. (2003). Cation–chloride cotransporters mediate neural computation in the retina. *Proc. Natl. Acad. Sci. U.S.A.* 100, 16047–16052. doi: 10.1073/pnas.2637041100

Gavrikov, K. E., Nilson, J. E., Dmitriev, A. V., Zucker, C. L., and Mangel, S. C. (2006). Dendritic compartmentalization of chloride cotransporters underlies directional responses of starburst amacrine cells in retina. *Proc. Natl. Acad. Sci. U.S.A.* 103, 18793–18798. doi: 10.1073/pnas.0604551103

Gulyas, A. I., Sik, A., Payne, J. A., Kaila, K., and Freund, T. F. (2001). The KCl cotransporter, KCC2, is highly expressed in the vicinity of excitatory synapses in the rat hippocampus. *Eur. J. Neurosci.* 13, 2205–2217.

Joselevitch, C., and Kamermans, M. (2009). Retinal parallel pathways: seeing with our inner fish. *Vision Res.* 49, 943–959. doi: 10.1016/j.visres.2008.07.019

Kay, J. N., Finger-Baier, K. C., Roeser, T., Staub, W., and Baier, H. (2001). Retinal ganglion cell genesis requires lakritz, a Zebrafish atonal Homolog. *Neuron* 30, 725–736. doi: 10.1016/S0896-6273(01)00312-9

Khirug, S., Huttu, K., Ludwig, A., Smirnov, S., Voipio, J., Rivera, C., et al. (2005). Distinct properties of functional KCC2 expression in immature mouse hippocampal neurons in culture and in acute slices. *Eur. J. Neurosci.* 21, 899–904. doi: 10.1111/j.1460-9568.2005.03886.x

Kyrozis, A., and Reichling, D. B. (1995). Perforated-patch recording with gramicidin avoids artifactual changes in intracellular chloride concentration. *J. Neurosci. Methods* 57, 27–35. doi: 10.1016/0165-0270(94)00116-X

Mumm, J. S., Williams, P. R., Godinho, L., Koerber, A., Pittman, A. J., Roeser, T., Chien, C. B., Baier, H., and Wong, R. O. (2006). *In vivo* imaging reveals dendritic targeting of laminated afferents by zebrafish retinal ganglion cells. *Neuron* 52, 609–621. doi: 10.1016/j.neuron.2006.10.004

Pang, J. J., Gao, F., and Wu, S. M. (2003). Light-evoked excitatory and inhibitory synaptic inputs to ON and OFF alpha ganglion cells in the mouse retina. *J. Neurosci.* 23, 6063–6073.

Payne, J. A., Rivera, C., Voipio, J., and Kaila, K. (2003). Cation-chloride co-transporters in neuronal communication, development and trauma. *Trends Neurosci.* 26, 199–206. doi: 10.1016/S0166-2236(03)00068-7

Reynolds, A., Brustein, E., Liao, M., Mercado, A., Babilonia, E., Mount, D. B., et al. (2008). Neurogenic role of the depolarizing chloride gradient revealed by global overexpression of KCC2 from the onset of development. *J. Neurosci.* 28, 1588–1597. doi: 10.1523/JNEUROSCI.3791-07.2008

Vardi, N., Zhang, L. L., Payne, J. A., and Sterling, P. (2000). Evidence that different cation chloride cotransporters in retinal neurons allow opposite responses to GABA. *J. Neurosci.* 20, 7657–7663.

Wang, D. D., and Kriegstein, A. R. (2009). Defining the role of GABA in cortical development. *J. Physiol.* 587, 1873–1879. doi: 10.1113/jphysiol.2008.167635

Wei, H. P., Yao, Y. Y., Zhang, R. W., Zhao, X. F., and Du, J. L. (2012). Activity-induced long-term potentiation of excitatory synapses in developing zebrafish retina *in vivo*. *Neuron* 75, 479–489. doi: 10.1016/j.neuron.2012.05.031

Westerfield, M. (1995). *The Zebrafish Book: A Guide for the Laboratory Use of Zebrafish (Danio rerio)*. Eugene, OR: University of Oregon Press.

Zhang, C., and McCall, M. A. (2012). Receptor targets of amacrine cells. *Vis. Neurosci.* 29, 11–29. doi: 10.1017/S0952523812000028

Zhang, R. W., Wei, H. P., Xia, Y. M., and Du, J. L. (2010). Development of light response and GABAergic excitation-to-inhibition switch in zebrafish retinal ganglion cells. *J. Physiol.* 588, 2557–2569. doi: 10.1113/jphysiol.2010.187088

Conflict of Interest Statement: The authors declare that the research was conducted in the absence of any commercial or financial relationships that could be construed as a potential conflict of interest.

Received: 18 February 2013; paper pending published: 18 March 2013; accepted: 11 May 2013; published online: 28 May 2013.

Citation: Zhang R-W, Zhang S-Y and Du J-L (2013) KCC2-dependent subcellular E_{Cl} difference of ON-OFF retinal ganglion cells in larval zebrafish. Front. Neural Circuits 7:103. doi: 10.3389/fncir.2013.00103

frontiers in
NEURAL CIRCUITS

REVIEW ARTICLE
published: 11 April 2013
doi: 10.3389/fncir.2013.00062

Neural circuits mediating olfactory-driven behavior in fish

Florence Kermen[1,2†], *Luis M. Franco*[1,2,3†], *Cameron Wyatt*[1,2] *and Emre Yaksi*[1,2,3*]

[1] Neuroelectronics Research Flanders, Leuven, Belgium
[2] Vlaams Instituut voor Biotechnologie, Leuven, Belgium
[3] KU Leuven, Leuven, Belgium

Edited by:
German Sumbre, Ecole Normal Supérieure, France

Reviewed by:
Peter Brunjes, University of Virginia, USA
Suresh Jesuthasan, Duke/NUS Graduate Medical School, Singapore

***Correspondence:**
Emre Yaksi, Neuroelectronics Research Flanders, Imec Campus, Kapeldreef 75, Leuven, Belgium.
e-mail: emre.Yaksi@nerf.be

† Florence Kermen and Luis M. Franco have contributed equally to this work.

The fish olfactory system processes odor signals and mediates behaviors that are crucial for survival such as foraging, courtship, and alarm response. Although the upstream olfactory brain areas (olfactory epithelium and olfactory bulb) are well-studied, less is known about their target brain areas and the role they play in generating odor-driven behaviors. Here we review a broad range of literature on the anatomy, physiology, and behavioral output of the olfactory system and its target areas in a wide range of teleost fish. Additionally, we discuss how applying recent technological advancements to the zebrafish (*Danio rerio*) could help in understanding the function of these target areas. We hope to provide a framework for elucidating the neural circuit computations underlying the odor-driven behaviors in this small, transparent, and genetically amenable vertebrate.

Keywords: teleost, zebrafish, anatomy and physiology, behavior, olfactory bulb, olfactory epithelium, habenula, hypothalamus

INTRODUCTION

Teleosts, the infraclass to which zebrafish belong, account for nearly half of all extant vertebrate species. The diversity of forms in these closely related species provide opportunities to study similar but distinct brain organizations and behavioral programs. Due to this, there already exists a wealth of literature on the teleost olfactory system, pre-dating many genetic and optical techniques, in such members as goldfish and catfish. Despite these variations, the architecture of the zebrafish olfactory system is fundamentally similar to that of other vertebrates. On the molecular level, families of receptor proteins expressed by the olfactory sensory neurons are comparable within most vertebrates, with zebrafish possessing a modest repertoire several times smaller than that of mammals (Alioto and Ngai, 2005).

The olfactory system is of particular relevance to systems neuroscience due to the large variety of stimuli that need to be encoded as well as the simple but interesting computations it performs, such as gain control, pattern decorrelation, categorization, and detecting weak stimuli despite highly dynamic background "noise." Furthermore, olfactory stimuli can trigger a wide range of behaviors related to reproduction, appetite, fear, and anxiety, which allow the study of the brain circuits that are involved in generating these essential behaviors. Finally, the activity patterns evoked by these odors can be readily recorded in highly conserved structures of the olfactory system, i.e., the olfactory epithelium, the olfactory bulb, and olfactory telencephalic and diencephalic centers, owing to the accessibility of these brain regions in zebrafish.

Over the past decade, the zebrafish (*Danio rerio*) has become increasingly popular in systems neuroscience. The success of this model organism is mainly due to its small brain that is amenable to functional imaging and genetic manipulations. The extensive genetic toolbox of the zebrafish can readily be combined with optical and electrophysiological techniques and quantitative behavioral assays to perform experiments that were impossible only a few years ago. Here we review a wide range of literature on the anatomy and the function of the olfactory system in zebrafish and other teleosts and discuss how the novel experimental tools of the zebrafish can and will transform this field. We hope to provide a framework for elucidating the neural circuit computations underlying the odor-driven behaviors in this small, transparent, and genetically amenable vertebrate.

ODORANTS SENSED BY FISH

The fish olfactory system can detect a wide range of water soluble compounds which elicit, or contribute to, behaviors crucial for survival such as feeding, reproduction, social interaction, and avoiding predation. Amino acids and nucleotides indicate the presence of food. Nucleotides, such as adenosine-5′-triphosphate (ATP), indicate food freshness in carp (Hara and Zielinski, 2007). Amino acids induce appetitive swimming behavior characterized by increased number of turns and swimming speed in zebrafish (Lindsay and Vogt, 2004). Steroids and prostaglandin F2α, which are hormones produced in the gonads and released in urine, were shown to trigger species and sex specific reproductive behaviors in a variety of teleosts (Hurk and Lambert, 1983; Stacey and Kyle, 1983). Bile acids are steroids secreted by the liver and released in urine, which have been implicated in migration to spawning sites in lampreys (Sorensen et al., 2005). While bile acids are agreed upon as one of the main classes of odorant in fish, their putative role as social pheromones, indicating the presence of other fish, is not yet conclusively proven in teleosts (Doving et al., 1980). Compounds released from the skin of injured fish have long been known to elicit a vigorous, stereotyped alarm response from many species of fish (von Frisch, 1941). This alarm response is characterized by darting followed by slow swimming or freezing (Speedie and Gerlai, 2008; Doving and Lastein, 2009).

OLFACTORY EPITHELIUM

Odorants are detected upon interaction with olfactory receptors (ORs) in the nose. Teleosts have two nasal cavities, one on each side of the head at the extremity of the snout (Hansen and Zielinski, 2005). Unlike in mammals, there is no sniffing in teleost fish. Each nasal cavity is composed of an anterior nostril, through which water enters the nose, and a posterior nostril, through which water exits the nose. The olfactory epithelium lies between these two nostrils (Hara and Zielinski, 2007). In zebrafish, it is multilamellar and rosette-shaped. Zebrafish olfactory sensory neurons are comprised of three morphologically distinct types of cells: (1) ciliated cells, with long dendrites and few cilia, (2) microvillous sensory neurons, with shorter dendrites and microvilli, (3) crypt cells, pear-shaped cells specific to fish, with microvilli and few cilia (Hansen and Zielinski, 2005). While ciliated and microvillous cells are present in higher vertebrates, crypt cells have only been found in fish (Hansen et al., 1999; Schmachtenberg, 2006; Vielma et al., 2008). The soma of olfactory sensory neurons are located at different depths in the olfactory epithelium: ciliated cells are situated in the deep layer, microvillous cells are located in the intermediate layer and mature crypt cells are located in the most superficial layer, forming the pseudo-stratified structure of the olfactory epithelium. Scattered amongst the olfactory sensory neurons are ciliated non-sensory cells, which help to move the mucus covering the olfactory epithelium (Zeiske et al., 1992). Crypt, microvillous, and ciliated cells are dispersed throughout the epithelium. They represent respectively 2, 8, and 90% of the total olfactory sensory neuron population, in trout and mackerel (Sato and Suzuki, 2001; Schmachtenberg, 2006). Olfactory sensory neurons are constantly renewed throughout adult life or following chemical lesion of the epithelium (Cancalon, 1982; Julliard et al., 1996; Bettini et al., 2006). This regeneration is mediated by the division of basal cells located in the deepest layer of the olfactory epithelium (Cancalon, 1982).

In fish, as in mammals, the detection of odorants by olfactory sensory neurons is mediated by different families of G-protein-coupled receptors. The zebrafish genome contains 143 OR genes, 56 vomeronasal receptor (VR) genes, and 109 trace amine-associated receptor (TAAR) genes (Alioto and Ngai, 2005; Hashiguchi and Nishida, 2006, 2007; Saraiva and Korsching, 2007). Ciliated cells express ORs whereas microvillous cells express VRs (Yoshihara, 2009). The precise identity of the receptor mediating the odor response in crypt cells is not known. However, a recent study found that crypt cells express a member of the VR family in zebrafish (Oka et al., 2012). Subsets of zebrafish olfactory sensory neurons express members of the TAAR gene family (Hussain et al., 2009).

As in other vertebrates, most olfactory sensory neurons express only one receptor (Sato et al., 2007). As a consequence, the response profile of a given neuron is constrained by the receptive field of the receptor it expresses. Patch clamp recordings of neurons isolated from fish olfactory epithelium provided insights into the repertoire of ligands that bind to ORs and VRs. In channel catfish, both ciliated and microvillous cells respond to amino acids (Sato and Suzuki, 2001; Hansen et al., 2003; Schmachtenberg and Bacigalupo, 2004). Ciliated cells also respond to urine extracts containing bile acids and might be involved in alarm substance detection (Sato and Suzuki, 2001; Doving and Lastein, 2009). Nucleotides activate microvillous cells (Hansen et al., 2003). However, the ligands of crypt cells have proven more elusive. Since their discovery, crypt cells have been hypothesized to participate in reproductive pheromone detection. Their density and depth in the olfactory epithelium was shown to vary depending on the seasons in sexually mature carp (Hamdani el et al., 2008). Moreover crypt cell density is sex-dependent in certain fish species (Bettini et al., 2012). A large majority of crypt cells respond to only one category of odorants. Intracellular recordings and calcium imaging studies carried out on mackerel and juvenile trout showed that different subsets of crypt cells respond either to amino acids, bile acids, or reproductive pheromones (Schmachtenberg, 2006; Vielma et al., 2008; Bazaes and Schmachtenberg, 2012). However, in mature trout, the majority of crypt cells respond to reproductive pheromones of the opposite sex and not to the other categories, indicating a change in the response profile of crypt cells during life, depending on sexual maturity and sex of the fish (Bazaes and Schmachtenberg, 2012).

As in other vertebrates, zebrafish olfactory sensory neurons expressing the same receptor are dispersed throughout the epithelium (Baier et al., 1994; Weth et al., 1996). They project their axons via the olfactory nerve to the same glomerulus in the ipsilateral olfactory bulb (Hansen and Zielinski, 2005; Sato et al., 2007). Moreover, the bulbar projection pattern of the three types of olfactory sensory neurons shows a coarse spatial organization. Using a double transgenic zebrafish line labeling ciliated and microvillous cells with different fluorophores, studies have shown that ciliated cells mainly project to the dorsal and medial olfactory bulb, whereas microvillous cells project to the lateral olfactory bulb (Sato et al., 2005, 2007). Retrograde labeling of the olfactory epithelium following lipophilic tracer application to different bulbar domains showed that crypt cells project to the ventral olfactory bulb in carp and to the dorsomedial olfactory bulb in zebrafish (Hamdani el and Doving, 2006; Gayoso et al., 2012). This projection pattern, shown in **Figure 1**, is well-conserved between the two bulbs of the same zebrafish, as well as among individual zebrafish (Baier and Korsching, 1994; Braubach et al., 2012).

Additionally, a subset of fibers originating from the nose reach the telencephalon without contacting the olfactory bulb in several teleosts (Honkanen and Ekstrom, 1990; Riddle and Oakley, 1992; Gayoso et al., 2011). Extrabulbar primary olfactory projections to telencephalic centers have also been described in amphibians but not in mammals (Pinelli et al., 2004). In white sturgeon, these fibers terminate in the posterior tubercle, a diencephalic region (Northcutt, 2011). In trout, these fibers innervate the ventral nucleus of the ventral telencephalon (Vv) and the dorsal telencephalon, as well as the preoptic area and the hypothalamus (Becerra et al., 1994; Anadon et al., 1995). In zebrafish, lipophilic tracer application in the Vv retrogradely labels a few bipolar olfactory sensory neurons in the olfactory epithelium, indicating that ciliated and/or microvillous cells send direct projections to Vv (Gayoso et al., 2011). Nevertheless, the functional role of these extrabulbar primary connections remains unknown.

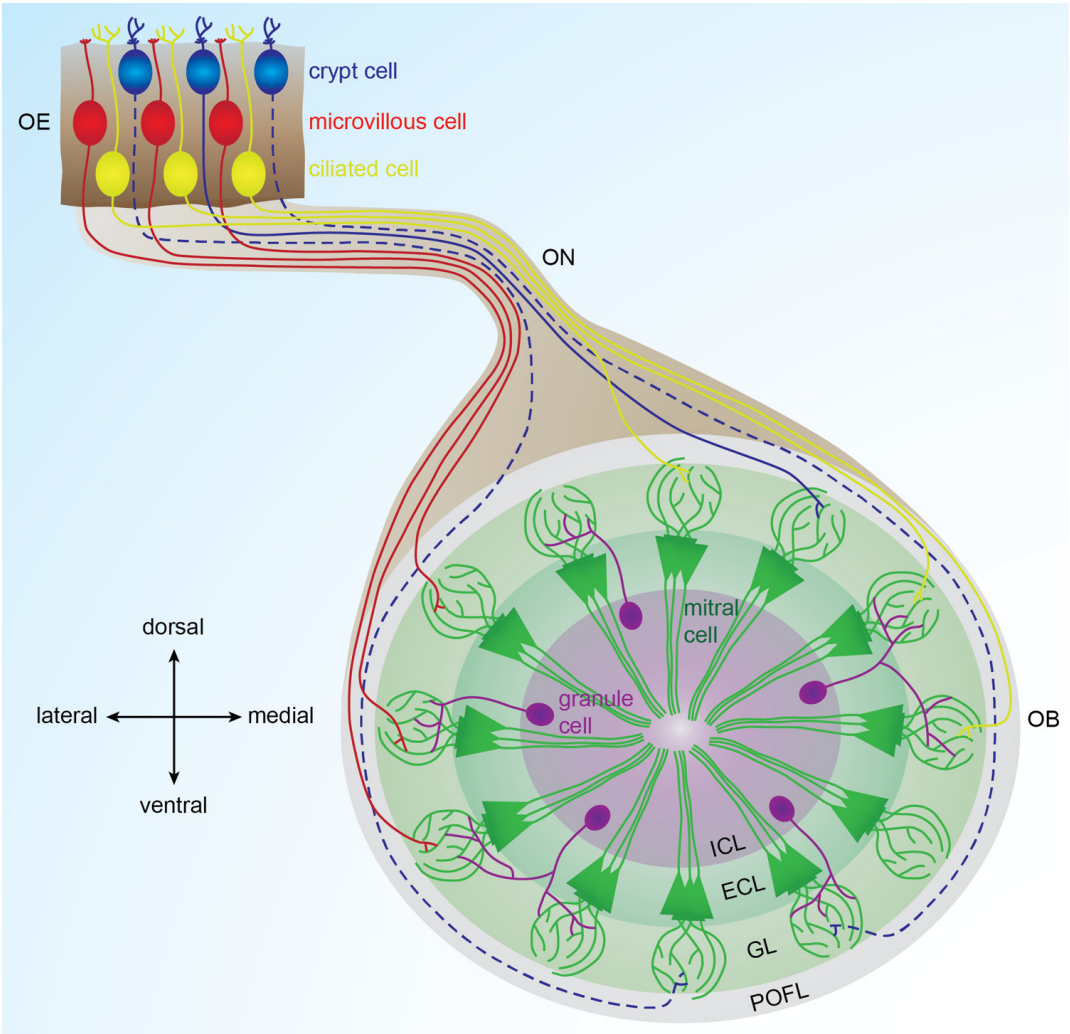

FIGURE 1 | Organization of the olfactory bulb network. Odorants are detected in the olfactory epithelium by three types of sensory neurons (microvillous, ciliated, and crypt cells) that project to different glomeruli located in different areas of the olfactory bulb. Ciliated cells mainly project to the dorsal and medial olfactory bulb; microvillous cells project to the lateral olfactory bulb (Sato et al., 2005, 2007). Crypt cells project to a dorsomedial domain in zebrafish and to a ventral domain in carp (Hamdani el and Doving, 2006; Gayoso et al., 2012). In each glomerulus, olfactory sensory neuron axons contact dendrites of mitral cells, the output cells of the olfactory bulb. Inhibitory interneurons called granules cells are located in the deepest layer of the bulb and modulate the activity of mitral cells. Solid lines represent connections described in zebrafish. Dotted lines represent connections described in other fish species. OE: olfactory epithelium, OB: olfactory bulb, ON: olfactory nerve, POFL: primary olfactory fiber layer, GL: glomerular layer, ECL: external cell layer, ICL: internal cell layer.

THE OLFACTORY BULB: PRIMARY PROCESSING OF ODOR INFORMATION

The olfactory bulb is the vertebrate brain structure that receives the large majority of olfactory sensory neuron inputs through the olfactory nerve. Understanding the neurophysiological mechanisms governing odor processing in the olfactory bulb requires a profound comprehension of its neuronal connectivity and physiological properties. In zebrafish, the olfactory bulb is comprised of approximately 20,000 neurons (Friedrich et al., 2009) organized in four concentric layers (**Figure 1**). From superficial to deep, these are: (1) primary olfactory fiber layer, formed by olfactory sensory neuron axons (Sato et al., 2007); (2) glomerular layer, containing approximately ≈140 spherical modules of neuropil named glomeruli (Braubach et al., 2012); (3) external cell layer, consisting of mitral and ruffed cell somas (Fuller and Byrd, 2005; Fuller et al., 2006); and (4) internal cell layer, containing cell bodies of different interneurons, namely juxtaglomerular, periglomerular, and granular cells (Edwards and Michel, 2002; Bundschuh et al., 2012).

Glutamatergic mitral and ruffed cells are the principal cells of the olfactory bulb in fish (Edwards and Michel, 2002). In zebrafish, apical dendrites of mitral cells receive direct synaptic inputs from olfactory sensory neurons in glomeruli and project to the telencephalon and diencephalon (Fuller et al., 2006; Miyasaka et al., 2009). Teleost ruffed cells are not innervated by olfactory sensory neurons. Nevertheless, ruffed cells receive synaptic contacts from

mitral cells and bulbar interneurons (Kosaka and Hama, 1979, 1981, 1982; Kosaka, 1980).

Interneurons are localized deeper in the olfactory bulb. They mediate lateral interactions within bulbar neurons. The ratio of interneurons to mitral cells is 10:1 in zebrafish (Wiechert et al., 2010), whereas in mammals it is 100:1 (Rosselli-Austin and Altman, 1979). In zebrafish, GABAergic granule cells, which lack axons, are located in the inner layer of the olfactory bulb and extend their processes to make dendrodendritic synaptic connections with principal cells. Juxtaglomerular and periglomerular cells are apposed to glomeruli and express glutamate and dopamine, respectively, in addition to GABA (Byrd and Brunjes, 1995; Edwards and Michel, 2002).

ODOR CODING IN THE OLFACTORY BULB

Each glomerulus receives convergent input from olfactory sensory neurons expressing the same odorant receptor (Sato et al., 2005, 2007). Individual odorant receptors respond to different odors and a given odor generally activates several odorant receptors. As a consequence, odor stimulation in zebrafish and goldfish activates spatially distributed ensembles of glomeruli (Friedrich and Korsching, 1997, 1998; Speca et al., 1999; Fuss and Korsching, 2001). Glomeruli responding to similar molecular features are organized into defined zones within the olfactory bulb, forming chemotopic maps. Yet, odorants frequently activate glomeruli beyond their chemotopical domain. As a consequence, odorants are represented as fractured maps in the olfactory bulb (Friedrich and Korsching, 1997, 1998). In zebrafish, first-order chemical features, such as molecular categories, are encoded by large glomerular domains. Second-order features, such as carbon chain length or branching, are encoded by local differences of glomerular activity patterns within chemotopical domains (Friedrich and Korsching, 1997, 1998; Fuss and Korsching, 2001; Korsching, 2001). Chemotopic maps are therefore hierarchically organized such that fine maps of secondary features are nested within coarse maps of primary features (Friedrich and Korsching, 1997, 1998).

In zebrafish, the lateral subregion of the olfactory bulb responds preferentially to amino acids and to nucleotides, whereas the medial subregion responds to bile acids (Friedrich and Korsching, 1997, 1998; Koide et al., 2009). Genetic ablation of subsets of synaptic inputs to the olfactory bulb from the olfactory epithelium has revealed that the lateral glomerular cluster is responsible for feeding behavior evoked by amino acids (Koide et al., 2009). Fish skin extract is a mixture of several compounds that trigger alarm responses in zebrafish and one of its components is shown to activate mediodorsal posterior and anterolateral olfactory glomeruli (Mathuru et al., 2012). In addition, a group of ventral glomeruli responds to prostaglandin (Friedrich and Korsching, 1998). Amino acids, bile acids, and nucleotides evoke combinatorial glomerular activity patterns that overlap but are sufficiently complex so that even very similar odorants can be discriminated. In contrast, pheromones are represented in a non-combinatorial fashion, suggesting a direct relay to brain structures controlling sex behavior and endocrine states (Friedrich and Korsching, 1997, 1998).

In goldfish, ruffed cells are spontaneously active, and are inhibited by granule cells which are activated by mitral cells (Zippel et al., 1999). Upon odor stimulation, mitral cells respond with high frequency burst-like firing rates triggered by olfactory sensory neuron activity, whereas ruffed cell firing rates are low. Moreover, mitral and ruffed cells frequently respond with contrasting activity patterns. Excitation of mitral cells drives ruffed cell inactivation via granule cells, and inhibition of mitral cells releases ruffed cells from inactivation (Zippel et al., 1999).

In zebrafish, mitral cell activity patterns are dynamically reorganized during the initial phase (∼400 ms) of an odor response before they reach a steady state (Friedrich and Laurent, 2001, 2004). Mitral cell activity patterns evoked by similar odorants overlap during the early phase of the odor response but subsequently diverge. Hence initially overlapping odor responses decorrelate over time (Friedrich and Laurent, 2001, 2004). It has been suggested that mitral cell firing patterns convey multiplexed information about odors simultaneously (Friedrich et al., 2004). This study proposed that the mitral cell action potentials, which are phase-locked to the local field potential oscillations, carry information about the odor category and the remaining mitral cell activity informs about precise odorant identity. Thus, multiplexed mitral cell activity patterns simultaneously convey information about complementary odorant features (Friedrich et al., 2004). Although glomerular responses to different odors are highly variable, total mitral cell firing remains within a relatively narrow range, suggesting a gain control, probably through inhibitory circuits (Friedrich and Laurent, 2004; Friedrich et al., 2009).

SYNAPTIC INPUTS TO THE OLFACTORY BULB FROM HIGHER BRAIN AREAS

In zebrafish, the olfactory bulb receives serotonergic inputs from raphe nuclei (Lillesaar et al., 2009) and cholinergic inputs through the terminal nerve ganglion (Edwards et al., 2007). In rodents, serotonin and acetylcholine increase the activity of interneurons while reducing the excitability of principal cells (Castillo et al., 1999; Ghatpande et al., 2006; Pressler et al., 2007; Petzold et al., 2009; Liu et al., 2012). In carp, noradrenaline enhances postsynaptic long term potentiation evoked by tetanic stimulation of mitral cell–granule cell synapses (Satou et al., 2006). In addition, centrifugal fibers originating from the telencephalon terminate in the olfactory bulb internal cell layer of teleosts, probably making synaptic contact with granule cells, raising the possibility that cortical feedback modulates the bulbar network (Munz et al., 1982; Stell et al., 1984; Zucker and Dowling, 1987). Nevertheless, further studies are needed in order to elucidate the physiological role of these neuromodulators onto bulbar neural circuits in fish.

ORGANIZATION OF OLFACTORY BULB PROJECTIONS

Mitral cells extend their axons through the medial and lateral olfactory tracts to different higher brain centers (**Figure 2**). In carp and zebrafish, the lateral olfactory tract contains mainly fibers originating in the lateral olfactory bulb, whereas the medial olfactory tract contains mainly fibers originating from the medial olfactory bulb (Sheldon, 1912). Anatomical tracing studies have shown that the teleost medial olfactory tract is subdivided into medial and lateral regions (Sheldon, 1912; Finger, 1975; Bass, 1981; von Bartheld et al., 1984). The lateral part of the medial olfactory tract is comprised largely of centrifugal fibers projecting to the olfactory

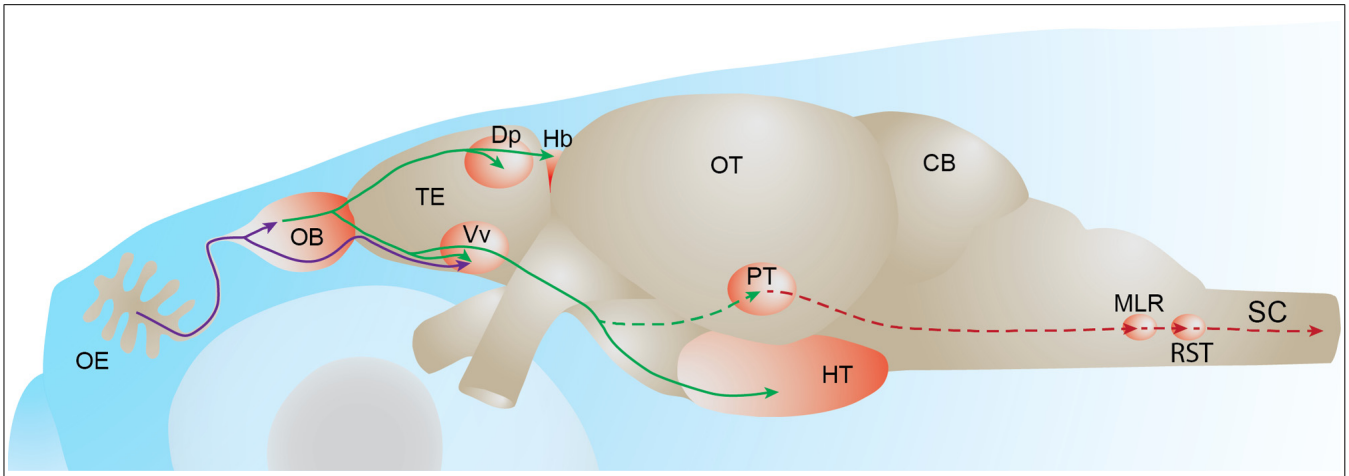

FIGURE 2 | Fish olfactory system. Primary projections from olfactory sensory neurons to the olfactory bulb or telencephalon are depicted in purple. Secondary olfactory projections from the olfactory bulb to the telencephalon and diencephalon are depicted in green. A putative olfacto-motor pathway connecting the posterior tubercle to executive motor centers in the mesencephalon, described in lampreys, is depicted in red. Solid lines represent connections described in zebrafish. Dotted lines represent connections described in other fish species. OE: olfactory epithelium, OB: olfactory bulb, TE: telencephalon, Dp: dorsal-posterior part of the telencephalon, Hb: habenula, Vv: ventral nucleus of the ventral telencephalon, OT: optic tectum, PT: posterior tubercle, HT: hypothalamus, CB: cerebellum, MLR: mesencephalic locomotor region; RST: reticulo-spinal tract, SC: spinal cord.

bulb whereas the medial part of the medial olfactory tract as well as the lateral olfactory tract contain mitral cell axons projecting to telencephalic and diencephalic areas (von Bartheld et al., 1984). In addition, the medial part of the medial olfactory tract carries mitral cell axons that project to the contralateral olfactory bulb (von Bartheld et al., 1984).

The medial and lateral olfactory tracts are separate, anatomically well-defined axon bundles, which enables the study of their physiological function by several experimental manipulations across different fish species (Stacey and Kyle, 1983; Hamdani et al., 2000, 2001). It was shown that the electrical stimulation of the medial olfactory tract induces alarm reaction or reproductive behavior, while lateral olfactory tract stimulation induces feeding behaviors in cod (Doving and Selset, 1980). These different functions could arise from different projection profiles of these two tracts to higher brain centers. In the goldfish, fibers carried by the medial and lateral olfactory tracts reach target areas in the telencephalon and the posterior tubercle of the diencephalon (von Bartheld et al., 1984). This study also showed that the lateral olfactory tract specifically innervates the habenula while the medial olfactory tract also sends projections to the Vv. These projection patterns have been confirmed by anatomical tracing studies in other fish species (Huesa et al., 2000; Folgueira et al., 2004; Northcutt, 2011). In zebrafish, the mitral cells are shown to project to Vv and the dorsal-posterior part of the telencephalon (Dp) and to the right habenula and the hypothalamus in the diencephalon (Rink and Wullimann, 2004; Miyasaka et al., 2009; Gayoso et al., 2011).

OLFACTORY BULB TARGETS

TELENCEPHALON

Dp in teleosts corresponds to the mammalian primary olfactory (piriform) cortex, whereas teleost Vv is the homolog of the septal area, a part of the limbic system, in mammals. Whether the chemotopic odor maps in the olfactory bulb are maintained in Dp and Vv in fishes remains a subject of debate. Recording of single neurons in the channel catfish pallium showed a spatial segregation of neurons preferentially responding to odorants belonging to the same biological categories (Nikonov et al., 2005). This study showed that bile acids preferentially activate the medial pallium whereas amino acids and nucleotides preferentially activate the lateral pallium (comprising Dp), indicating a gross chemotopical organization in the telencephalic targets of the olfactory bulb. However, a recent functional imaging study suggested that the spatial segregation of odor responses was not prominent in Vv and Dp neurons of zebrafish (Yaksi et al., 2009). This study showed that Vv and Dp display overlapping and distributed activity in response to various odor categories (bile acids, amino acids, nucleotides). Hence odor representations in the telencephalon do not display strong chemotopy (although slight differences between the distribution of amino acid and bile acid-evoked activity can be observed in the Dp). This is in accordance with work in rodents, where optical imaging in the mouse primary olfactory cortex shows that odor-evoked activity is not spatially segregated in the main bulbar target (Stettler and Axel, 2009).

Vv and Dp neurons were shown to have different response properties. Vv neurons are broadly tuned resulting in overlapping representation of odor categories, whereas Dp neurons respond to odors more specifically (Yaksi et al., 2009). The activity of mitral cell ensembles was shown to carry multiplexed information about stimulus features such as category and identity (Friedrich et al., 2004). How is the multiplexed output provided by the olfactory bulb decrypted in the telencephalic targets? Dp cells were shown to be relatively insensitive to oscillatory mitral cell activity, which informs about odor categories (Blumhagen et al., 2011). This study suggests that Dp establishes

specific and decorrelated odor representations. However a previous study suggests that the pattern correlation in Dp neurons is not significantly different from the pattern correlation in mitral cells (Yaksi et al., 2009). Further studies are needed to examine whether the multiplexed olfactory bulb output is read and used by its targets.

Importantly, Vv and Dp receive substantial neuromodulatory inputs which could participate in odor response refinement in these areas. In zebrafish, the pallium (comprising Dp) and the subpallium (comprising Vv) share inputs from locus coeruleus (noradrenergic), raphe nuclei (serotoninergic), and posterior tubercle (dopaminergic; Rink and Wullimann, 2004; Scharer et al., 2012). The subpallium additionally receives inputs from the cholinergic superior reticular nucleus and the histaminergic caudal hypothalamus (Rink and Wullimann, 2004). It was shown that dopamine selectively decreases inhibitory but not excitatory odor responses in the Dp (Scharer et al., 2012). Calcium imaging further showed that the amplitude of odor responses was increased in the presence of dopamine, without affecting the spatial response pattern. Therefore, dopamine mediated increase of odor response gain might mediate changes in odor saliency during learning.

DIENCEPHALON

Habenula

The habenula is a highly conserved brain region that connects the forebrain to brainstem nuclei such as the interpeduncular nucleus, the serotonergic raphe nuclei and the ventral tegmental area containing dopaminergic neurons (Tomizawa et al., 2001; Hikosaka, 2010). The habenula is divided into two parts based on connectivity and functional heterogeneity: the medial and lateral mammalian habenulae, which are homologous to the dorsal and ventral fish habenulae, respectively (Amo et al., 2010). It was shown in several teleost species that mitral cells project to the habenula (Wedgwood, 1974; von Bartheld et al., 1984; Miyasaka et al., 2009; Northcutt, 2011). In zebrafish, bulbar projections to the habenula are asymmetric. Indeed, it has been shown that mitral cells located in both olfactory bulbs send axons that terminate in the medial compartment of the right habenula (Miyasaka et al., 2009).

The mammalian homolog of the fish ventral habenula has been proposed to participate in the control of motor behaviors depending on stimulus values by influencing the activity of dopaminergic neurons (Hikosaka, 2010). Moreover, two recent studies showed that when the dorsal habenula is genetically inactivated, zebrafish display altered responses to conditioned fear stimuli (Agetsuma et al., 2010; Lee et al., 2010). These studies indicate a role for the habenula in experience-dependent modulation of fear responses. The role of habenula in odor processing and the functional architecture of its circuitry remain to be uncovered.

Posterior tubercle

The posterior tubercle is a ventral region of the posterior diencephalon. Because the posterior tubercle contains dopaminergic cells, it has been proposed to be functionally similar to the mammalian mesolimbic dopaminergic system (Rink and Wullimann, 2001). Bulbar efferents have been shown to terminate in the posterior tubercle of several teleost fish (Matz, 1995; Von Bartheld, 2004; Derjean et al., 2010; Northcutt, 2011; Northcutt and Rink, 2012). However, it is currently not known whether this projection also exists in zebrafish.

A recent work suggested that the projections from the olfactory bulb to the posterior tubercle play a role in the generation of olfactory-driven locomotor activity in the sea lamprey (Derjean et al., 2010). This study showed that stimulation of the medial olfactory bulb by glutamate injection generated rhythmical electrical activity in reticulospinal cells and in the ventral root of the spinal cord, which resembles fictive locomotion. The proposed olfacto-motor pathway is comprised of a medial glomerulus projecting to the posterior tubercle, which would then transmit the olfactory input to the mesencephalic locomotor region that in turn excites reticulospinal cells which are command neurons responsible for the activation of spinal locomotor networks. This study is the first demonstration of a functional connection between the olfactory system and the spinal locomotor network in vertebrates.

Hypothalamus

In mammals, the hypothalamic nuclei, located in the ventral diencephalon, play a pivotal role in the regulation of a number of vital physiological functions via direct synaptic stimulation of a wide range of targets or the secretion of various neuropeptides (Machluf et al., 2011). Homologs of diverse hypothalamic cell types secreting oxytocin, gonadotropin-releasing hormone, neuropeptide Y, and hypocretin have been identified in teleosts (Machluf et al., 2011). Hence it is likely that the zebrafish and terrestrial vertebrates have similar hypothalamic functions such as regulation of sleep, blood pressure, temperature, thirst and satiety, stress, reproduction, and social behavior. Mitral cells send direct projections to the hypothalamic area in fish but the exact localization of mitral cell terminals in hypothalamic nuclei and the functional significance of these projections remain unknown. In rodents, a ventral glomerulus projects to vasopressin or oxytocin secreting hypothalamic neurons (Hatton and Yang, 1989; Smithson et al., 1992; Bader et al., 2012). Vasopressin and oxytocin are known to modulate social behaviors in rodents as well as in fish (Godwin and Thompson, 2012). Olfactory cues are very important in signaling the presence of food or sexual partners in fish. The monosynaptic bulbo-hypothalamic projection in fish is therefore probably involved in the modulation of feeding and reproductive behaviors.

CONCLUSION

Olfactory computations performed by the upstream olfactory brain areas in relation to behavior are well-documented in teleosts. Despite minor anatomical differences, the general principles and computations performed by the fish olfactory system are highly similar to what is described in terrestrial vertebrates. Odors are detected in a combinatorial manner by receptors expressed in olfactory sensory neurons. Olfactory sensory neurons expressing the same receptor are dispersed in the olfactory epithelium and project to one spatially confined glomerulus. Hence, the shuffled peripheral epithelial activation is reorganized into odor specific glomerular maps in the olfactory bulb. Odor-evoked activity patterns among mitral cell ensembles become less correlated with

time, potentially helping discrimination of similar odorants. Ethologically relevant classes of odors tend to activate specific bulbar domains, resulting in a coarse topographic organization of different odor categories. Odor responses in the telencephalon do not seem to be topologically organized and the precise circuit mechanisms underlying the transformations of olfactory information in telencephalic targets still remain to be discovered. Odor responses in diencephalic areas such as the hypothalamus and habenula are currently not documented. Zebrafish lines that express calcium indicators in these areas are already available, which should allow the function of these areas to be revealed in the near future.

Currently, the neural pathways connecting the olfactory system to brain regions involved in the execution of different behaviors are not known in zebrafish. However, new techniques are rapidly being adopted which allow the tracing of functional connectivity in the olfacto-motor pathway. For example, the green fluorescent protein reconstitution across synaptic partners (GRASP) method, where non-fluorescent green fluorescent protein fragments expressed in two different neurons assemble to form the fluorophore at the synapse, is mainly used in invertebrates but is being adapted for vertebrates (Yamagata and Sanes, 2012). Additionally, links must be established between neural activity in olfactory bulb targets and relevant behavioral outputs. In this regard, the possibility of activating and deactivating genetically targeted neural populations offers new perspectives to understand how circuits elicit or modulate behavior. For example, the precise and non-invasive optogenetic stimulation of olfactory sensory neuron subsets already enables specific swimming patterns to be elicited in freely behaving zebrafish larvae (Zhu et al., 2009). In summary, thanks to its innate properties and a timely convergence of new techniques, the zebrafish olfactory system is an increasingly attractive model to understand the function of neural circuits involved in olfactory processing.

ACKNOWLEDGMENT

This work was supported by Fyssens post-doctoral fellowship to Florence Kermen, VIB-PhD program funding to Luis M.Franco, AXA research post-doctoral fellowship to Cameron Wyatt and NERF funding to Emre Yaksi.

REFERENCES

Agetsuma, M., Aizawa, H., Aoki, T., Nakayama, R., Takahoko, M., Goto, M., et al. (2010). The habenula is crucial for experience-dependent modification of fear responses in zebrafish. *Nat. Neurosci.* 13, 1354–1356.

Alioto, T. S., and Ngai, J. (2005). The odorant receptor repertoire of teleost fish. *BMC Genomics* 6:173. doi: 10.1186/1471-2164-6-173

Amo, R., Aizawa, H., Takahoko, M., Kobayashi, M., Takahashi, R., Aoki, T., et al. (2010). Identification of the zebrafish ventral habenula as a homolog of the mammalian lateral habenula. *J. Neurosci.* 30, 1566–1574.

Anadon, R., Manso, M. J., Rodriguez-Moldes, I., and Becerra, M. (1995). Neurons of the olfactory organ projecting to the caudal telencephalon and hypothalamus: a carbocyanine-dye labelling study in the brown trout (Teleostei). *Neurosci. Lett.* 191, 157–160.

Bader, A., Klein, B., Breer, H., and Strotmann, J. (2012). Connectivity from OR37 expressing olfactory sensory neurons to distinct cell types in the hypothalamus. *Front. Neural Circuits* 6:84. doi: 10.3389/fncir.2012.00084

Baier, H., and Korsching, S. (1994). Olfactory glomeruli in the zebrafish form an invariant pattern and are identifiable across animals. *J. Neurosci.* 14, 219–230.

Baier, H., Rotter, S., and Korsching, S. (1994). Connectional topography in the zebrafish olfactory system: random positions but regular spacing of sensory neurons projecting to an individual glomerulus. *Proc. Natl. Acad. Sci. U.S.A.* 91, 11646–11650.

Bass, A. H. (1981). Telencephalic efferents in channel catfish, *Ictalurus punctatus*: projections to the olfactory bulb and optic tectum. *Brain Behav. Evol.* 19, 1–16.

Bazaes, A., and Schmachtenberg, O. (2012). Odorant tuning of olfactory crypt cells from juvenile and adult rainbow trout. *J. Exp. Biol.* 215, 1740–1748.

Becerra, M., Manso, M. J., Rodriguez-Moldes, I., and Anadon, R. (1994). Primary olfactory fibres project to the ventral telencephalon and preoptic region in trout (*Salmo trutta*): a developmental immunocytochemical study. *J. Comp. Neurol.* 342, 131–143.

Bettini, S., Ciani, F., and Franceschini, V. (2006). Recovery of the olfactory receptor neurons in the African *Tilapia mariae* following exposure to low copper level. *Aquat. Toxicol.* 76, 321–328.

Bettini, S., Lazzari, M., and Franceschini, V. (2012). Quantitative analysis of crypt cell population during postnatal development of the olfactory organ of the guppy, *Poecilia reticulata* (Teleostei, Poecilidae), from birth to sexual maturity. *J. Exp. Biol.* 215, 2711–2715.

Blumhagen, F., Zhu, P., Shum, J., Scharer, Y. P., Yaksi, E., Deisseroth, K., et al. (2011). Neuronal filtering of multiplexed odour representations. *Nature* 479, 493–498.

Braubach, O. R., Fine, A., and Croll, R. P. (2012). Distribution and functional organization of glomeruli in the olfactory bulbs of zebrafish (*Danio rerio*). *J. Comp. Neurol.* 520, 2317–2339.

Bundschuh, S. T., Zhu, P., Scharer, Y. P., and Friedrich, R. W. (2012). Dopaminergic modulation of mitral cells and odor responses in the zebrafish olfactory bulb. *J. Neurosci.* 32, 6830–6840.

Byrd, C. A., and Brunjes, P. C. (1995). Organization of the olfactory system in the adult zebrafish: histological, immunohistochemical, and quantitative analysis. *J. Comp. Neurol.* 358, 247–259.

Cancalon, P. (1982). Degeneration and regeneration of olfactory cells induced by ZnSO4 and other chemicals. *Tissue Cell* 14, 717–733.

Castillo, P. E., Carleton, A., Vincent, J. D., and Lledo, P. M. (1999). Multiple and opposing roles of cholinergic transmission in the main olfactory bulb. *J. Neurosci.* 19, 9180–9191.

Derjean, D., Moussaddy, A., Atallah, E., St-Pierre, M., Auclair, F., Chang, S., et al. (2010). A novel neural substrate for the transformation of olfactory inputs into motor output. *PLoS Biol.* 8:e1000567. doi: 10.1371/journal.pbio.1000567

Doving, K. B., and Lastein, S. (2009). The alarm reaction in fishes–odorants, modulations of responses, neural pathways. *Ann. N. Y. Acad. Sci.* 1170, 413–423.

Doving, K. B., and Selset, R. (1980). Behavior patterns in cod released by electrical stimulation of olfactory tract bundlets. *Science* 207, 559–560.

Doving, K. B., Selset, R., and Thommesen, G. (1980). Olfactory sensitivity to bile acids in salmonid fishes. *Acta Physiol. Scand.* 108, 123–131.

Edwards, J. G., Greig, A., Sakata, Y., Elkin, D., and Michel, W. C. (2007). Cholinergic innervation of the zebrafish olfactory bulb. *J. Comp. Neurol.* 504, 631–645.

Edwards, J. G., and Michel, W. C. (2002). Odor-stimulated glutamatergic neurotransmission in the zebrafish olfactory bulb. *J. Comp. Neurol.* 454, 294–309.

Finger, T. E. (1975). The distribution of the olfactory tracts in the bullhead catfish, *Ictalurus nebulosus*. *J. Comp. Neurol.* 161, 125–141.

Folgueira, M., Anadon, R., and Yanez, J. (2004). An experimental study of the connections of the telencephalon in the rainbow trout (*Oncorhynchus mykiss*). I: olfactory bulb and ventral area. *J. Comp. Neurol.* 480, 180–203.

Friedrich, R. W., Habermann, C. J., and Laurent, G. (2004). Multiplexing using synchrony in the zebrafish olfactory bulb. *Nat. Neurosci.* 7, 862–871.

Friedrich, R. W., and Korsching, S. I. (1997). Combinatorial and chemotopic odorant coding in the zebrafish olfactory bulb visualized by optical imaging. *Neuron* 18, 737–752.

Friedrich, R. W., and Korsching, S. I. (1998). Chemotopic, combinatorial, and noncombinatorial odorant representations in the olfactory bulb revealed using a voltage-sensitive axon tracer. *J. Neurosci.* 18, 9977–9988.

Friedrich, R. W., and Laurent, G. (2001). Dynamic optimization of odor representations by slow temporal patterning of mitral cell activity. *Science* 291, 889–894.

Friedrich, R. W., and Laurent, G. (2004). Dynamics of olfactory bulb input and output activity during odor stimulation in zebrafish. *J. Neurophysiol.* 91, 2658–2669.

Friedrich, R. W., Yaksi, E., Judkewitz, B., and Wiechert, M. T. (2009). Processing of odor representations by neuronal circuits in the olfactory bulb. *Ann. N. Y. Acad. Sci.* 1170, 293–297.

Fuller, C. L., and Byrd, C. A. (2005). Ruffed cells identified in the adult zebrafish olfactory bulb. *Neurosci. Lett.* 379, 190–194.

Fuller, C. L., Yettaw, H. K., and Byrd, C. A. (2006). Mitral cells in the olfactory bulb of adult zebrafish (*Danio rerio*): morphology and distribution. *J. Comp. Neurol.* 499, 218–230.

Fuss, S. H., and Korsching, S. I. (2001). Odorant feature detection: activity mapping of structure response relationships in the zebrafish olfactory bulb. *J. Neurosci.* 21, 8396–8407.

Gayoso, J., Castro, A., Anadon, R., and Manso, M. J. (2012). Crypt cells of the zebrafish *Danio rerio* mainly project to the dorsomedial glomerular field of the olfactory bulb. *Chem. Senses* 37, 357–369.

Gayoso, J. A., Castro, A., Anadon, R., and Manso, M. J. (2011). Differential bulbar and extrabulbar projections of diverse olfactory receptor neuron populations in the adult zebrafish (*Danio rerio*). *J. Comp. Neurol.* 519, 247–276.

Ghatpande, A. S., Sivaraaman, K., and Vijayaraghavan, S. (2006). Store calcium mediates cholinergic effects on mIPSCs in the rat main olfactory bulb. *J. Neurophysiol.* 95, 1345–1355.

Godwin, J., and Thompson, R. (2012). Nonapeptides and social behavior in fishes. *Horm. Behav.* 61, 230–238.

Hamdani, E. H., Kasumyan, A., and Doving, K. B. (2001). Is feeding behaviour in crucian carp mediated by the lateral olfactory tract? *Chem. Senses* 26, 1133–1138.

Hamdani, E. H., Stabell, O. B., Alexander, G., and Doving, K. B. (2000). Alarm reaction in the crucian carp is mediated by the medial bundle of the medial olfactory tract. *Chem. Senses* 25, 103–109.

Hamdani el, H., and Doving, K. B. (2006). Specific projection of the sensory crypt cells in the olfactory system in crucian carp, *Carassius carassius*. *Chem. Senses* 31, 63–67.

Hamdani el, H., Lastein, S., Gregersen, F., and Doving, K. B. (2008). Seasonal variations in olfactory sensory neurons–fish sensitivity to sex pheromones explained? *Chem. Senses* 33, 119–123.

Hansen, A., Rolen, S. H., Anderson, K., Morita, Y., Caprio, J., and Finger, T. E. (2003). Correlation between olfactory receptor cell type and function in the channel catfish. *J. Neurosci.* 23, 9328–9339.

Hansen, A., and Zielinski, B. S. (2005). Diversity in the olfactory epithelium of bony fishes: development, lamellar arrangement, sensory neuron cell types and transduction components. *J. Neurocytol.* 34, 183–208.

Hansen, A., Zippel, H. P., Sorensen, P. W., and Caprio, J. (1999). Ultrastructure of the olfactory epithelium in intact, axotomized, and bulbectomized goldfish, *Carassius auratus*. *Microsc. Res. Tech.* 45, 325–338.

Hara, T. J., and Zielinski, B. (2007). "Olfaction," in *Sensory Systems Neuroscience* (Oxford: Elsevier Academic Press), 1–43.

Hashiguchi, Y., and Nishida, M. (2006). Evolution and origin of vomeronasal-type odorant receptor gene repertoire in fishes. *BMC Evol. Biol.* 6:76. doi: 10.1186/1471-2148-6-76

Hashiguchi, Y., and Nishida, M. (2007). Evolution of trace amine associated receptor (TAAR) gene family in vertebrates: lineage-specific expansions and degradations of a second class of vertebrate chemosensory receptors expressed in the olfactory epithelium. *Mol. Biol. Evol.* 24, 2099–2107.

Hatton, G. I., and Yang, Q. Z. (1989). Supraoptic nucleus afferents from the main olfactory bulb–II. Intracellularly recorded responses to lateral olfactory tract stimulation in rat brain slices. *Neuroscience* 31, 289–297.

Hikosaka, O. (2010). The habenula: from stress evasion to value-based decision-making. *Nat. Rev. Neurosci.* 11, 503–513.

Honkanen, T., and Ekstrom, P. (1990). An immunocytochemical study of the olfactory projections in the three-spined stickleback, *Gasterosteus aculeatus*, L. *J. Comp. Neurol.* 292, 65–72.

Huesa, G., Anadon, R., and Yanez, J. (2000). Olfactory projections in a chondrostean fish, *Acipenser baeri*: an experimental study. *J. Comp. Neurol.* 428, 145–158.

Hurk, R. V. D., and Lambert, J. G. D. (1983). Ovarian steroid glucuronides function as sex pheromones for male zebrafish, *Brachydanio rerio*. *Can. J. Zool.* 61, 2381–2387.

Hussain, A., Saraiva, L. R., and Korsching, S. I. (2009). Positive Darwinian selection and the birth of an olfactory receptor clade in teleosts. *Proc. Natl. Acad. Sci. U.S.A.* 106, 4313–4318.

Julliard, A. K., Saucier, D., and Astic, L. (1996). Time-course of apoptosis in the olfactory epithelium of rainbow trout exposed to a low copper level. *Tissue Cell* 28, 367–377.

Koide, T., Miyasaka, N., Morimoto, K., Asakawa, K., Urasaki, A., Kawakami, K., et al. (2009). Olfactory neural circuitry for attraction to amino acids revealed by transposon-mediated gene trap approach in zebrafish. *Proc. Natl. Acad. Sci. U.S.A.* 106, 9884–9889.

Korsching, S. I. (2001). Odor maps in the brain: spatial aspects of odor representation in sensory surface and olfactory bulb. *Cell. Mol. Life. Sci.* 58, 520–530.

Kosaka, T. (1980). Ruffed cell: a new type of neuron with a distinctive initial unmyelinated portion of the axon in the olfactory bulb of the goldfish (*Carassius auratus*): II. Fine structure of the ruffed cell. *J. Comp. Neurol.* 193, 119–145.

Kosaka, T., and Hama, K. (1979). Ruffed cell: a new type of neuron with a distinctive initial unmyelinated portion of the axon in the olfactory bulb of the goldfish (*Carassius auratus*) I. Golgi impregnation and serial thin sectioning studies. *J. Comp. Neurol.* 186, 301–319.

Kosaka, T., and Hama, K. (1981). Ruffed cell: a new type of neuron with a distinctive initial unmyelinated portion of the axon in the olfactory bulb of the goldfish (*Carassius auratus*). III. Three-dimensional structure of the ruffed cell dendrite. *J. Comp. Neurol.* 201, 571–587.

Kosaka, T., and Hama, K. (1982). Synaptic organization in the teleost olfactory bulb. *J. Physiol. (Paris)* 78, 707–719.

Lee, A., Mathuru, A. S., Teh, C., Kibat, C., Korzh, V., Penney, T. B., et al. (2010). The habenula prevents helpless behavior in larval zebrafish. *Curr. Biol.* 20, 2211–2216.

Lillesaar, C., Stigloher, C., Tannhauser, B., Wullimann, M. F., and Bally-Cuif, L. (2009). Axonal projections originating from raphe serotonergic neurons in the developing and adult zebrafish, *Danio rerio*, using transgenics to visualize raphe-specific pet1 expression. *J. Comp. Neurol.* 512, 158–182.

Lindsay, S. M., and Vogt, R. G. (2004). Behavioral responses of newly hatched zebrafish (*Danio rerio*) to amino acid chemostimulants. *Chem. Senses* 29, 93–100.

Liu, S., Aungst, J. L., Puche, A. C., and Shipley, M. T. (2012). Serotonin modulates the population activity profile of olfactory bulb external tufted cells. *J. Neurophysiol.* 107, 473–483.

Machluf, Y., Gutnick, A., and Levkowitz, G. (2011). Development of the zebrafish hypothalamus. *Ann. N. Y. Acad. Sci.* 1220, 93–105.

Mathuru, A. S., Kibat, C., Cheong, W. F., Shui, G., Wenk, M. R., Friedrich, R. W., et al. (2012). Chondroitin fragments are odorants that trigger fear behavior in fish. *Curr. Biol.* 22, 538–544.

Matz, S. P. (1995). Connections of the olfactory bulb in the chinook salmon (*Oncorhynchus tshawytscha*). *Brain Behav. Evol.* 46, 108–120.

Miyasaka, N., Morimoto, K., Tsubokawa, T., Higashijima, S., Okamoto, H., and Yoshihara, Y. (2009). From the olfactory bulb to higher brain centers: genetic visualization of secondary olfactory pathways in zebrafish. *J. Neurosci.* 29, 4756–4767.

Munz, H., Claas, B., Stumpf, W. E., and Jennes, L. (1982). Centrifugal innervation of the retina by luteinizing hormone releasing hormone (LHRH)-immunoreactive telencephalic neurons in teleostean fishes. *Cell Tissue Res.* 222, 313–323.

Nikonov, A. A., Finger, T. E., and Caprio, J. (2005). Beyond the olfactory bulb: an odotopic map in the forebrain. *Proc. Natl. Acad. Sci. U.S.A.* 102, 18688–18693.

Northcutt, R. G. (2011). Olfactory projections in the white sturgeon, *Acipenser transmontanus*: an experimental study. *J. Comp. Neurol.* 519, 1999–2022.

Northcutt, R. G., and Rink, E. (2012). Olfactory projections in the lepidosirenid lungfishes. *Brain Behav. Evol.* 79, 4–25.

Oka, Y., Saraiva, L. R., and Korsching, S. I. (2012). Crypt neurons express a single V1R-related ora gene. *Chem. Senses* 37, 219–227.

Petzold, G. C., Hagiwara, A., and Murthy, V. N. (2009). Serotonergic modulation of odor input to the mammalian olfactory bulb. *Nat. Neurosci.* 12, 784–791.

Pinelli, C., D'aniello, B., Polese, G., and Rastogi, R. K. (2004). Extrabulbar olfactory system and nervus terminalis FMRFamide immunoreactive components in *Xenopus laevis* ontogenesis. *J. Chem. Neuroanat.* 28, 37–46.

Pressler, R. T., Inoue, T., and Strowbridge, B. W. (2007). Muscarinic receptor activation modulates granule cell excitability and potentiates inhibition onto mitral cells in the rat olfactory bulb. *J. Neurosci.* 27, 10969–10981.

Riddle, D. R., and Oakley, B. (1992). Immunocytochemical identification of primary olfactory afferents in rainbow trout. *J. Comp. Neurol.* 324, 575–589.

Rink, E., and Wullimann, M. F. (2001). The teleostean (zebrafish) dopaminergic system ascending to the subpallium (striatum) is located in the basal diencephalon (posterior tuberculum). *Brain Res.* 889, 316–330.

Rink, E., and Wullimann, M. F. (2004). Connections of the ventral telencephalon (subpallium) in the zebrafish (*Danio rerio*). *Brain Res.* 1011, 206–220.

Rosselli-Austin, L., and Altman, J. (1979). The postnatal development of the main olfactory bulb of the rat. *J. Dev. Physiol.* 1, 295–313.

Saraiva, L. R., and Korsching, S. I. (2007). A novel olfactory receptor gene family in teleost fish. *Genome Res.* 17, 1448–1457.

Sato, K., and Suzuki, N. (2001). Whole-cell response characteristics of ciliated and microvillous olfactory receptor neurons to amino acids, pheromone candidates and urine in rainbow trout. *Chem. Senses* 26, 1145–1156.

Sato, Y., Miyasaka, N., and Yoshihara, Y. (2005). Mutually exclusive glomerular innervation by two distinct types of olfactory sensory neurons revealed in transgenic zebrafish. *J. Neurosci.* 25, 4889–4897.

Sato, Y., Miyasaka, N., and Yoshihara, Y. (2007). Hierarchical regulation of odorant receptor gene choice and subsequent axonal projection of olfactory sensory neurons in zebrafish. *J. Neurosci.* 27, 1606–1615.

Satou, M., Hoshikawa, R., Sato, Y., and Okawa, K. (2006). An in vitro study of long-term potentiation in the carp (*Cyprinus carpio* L.) olfactory bulb. *J. Comp. Physiol. A Neuroethol. Sens. Neural Behav. Physiol.* 192, 135–150.

Scharer, Y. P., Shum, J., Moressis, A., and Friedrich, R. W. (2012). Dopaminergic modulation of synaptic transmission and neuronal activity patterns in the zebrafish homolog of olfactory cortex. *Front. Neural Circuits* 6:76. doi: 10.3389/fncir.2012.00076

Schmachtenberg, O. (2006). Histological and electrophysiological properties of crypt cells from the olfactory epithelium of the marine teleost *Trachurus symmetricus*. *J. Comp. Neurol.* 495, 113–121.

Schmachtenberg, O., and Bacigalupo, J. (2004). Olfactory transduction in ciliated receptor neurons of the Cabinza grunt, *Isacia conceptionis* (Teleostei: Haemulidae). *Eur. J. Neurosci.* 20, 3378–3386.

Sheldon, R. E. (1912). The olfactory tracts and centers in teleosts. *J. Comp. Neurol.* 22, 177–339.

Smithson, K. G., Weiss, M. L., and Hatton, G. I. (1992). Supraoptic nucleus afferents from the accessory olfactory bulb: evidence from anterograde and retrograde tract tracing in the rat. *Brain Res. Bull.* 29, 209–220.

Sorensen, P. W., Fine, J. M., Dvornikovs, V., Jeffrey, C. S., Shao, F., Wang, J., et al. (2005). Mixture of new sulfated steroids functions as a migratory pheromone in the sea lamprey. *Nat. Chem. Biol.* 1, 324–328.

Speca, D. J., Lin, D. M., Sorensen, P. W., Isacoff, E. Y., Ngai, J., and Dittman, A. H. (1999). Functional identification of a goldfish odorant receptor. *Neuron* 23, 487–498.

Speedie, N., and Gerlai, R. (2008). Alarm substance induced behavioral responses in zebrafish (*Danio rerio*). *Behav. Brain Res.* 188, 168–177.

Stacey, N. E., and Kyle, A. L. (1983). Effects of olfactory tract lesions on sexual and feeding behavior in the goldfish. *Physiol. Behav.* 30, 621–628.

Stell, W. K., Walker, S. E., Chohan, K. S., and Ball, A. K. (1984). The goldfish nervus terminalis: a luteinizing hormone-releasing hormone and molluscan cardioexcitatory peptide immunoreactive olfactoretinal pathway. *Proc. Natl. Acad. Sci. U.S.A.* 81, 940–944.

Stettler, D. D., and Axel, R. (2009). Representations of odor in the piriform cortex. *Neuron* 63, 854–864.

Tomizawa, K., Katayama, H., and Nakayasu, H. (2001). A novel monoclonal antibody recognizes a previously unknown subdivision of the habenulo-interpeduncular system in zebrafish. *Brain Res.* 901, 117–127.

Vielma, A., Ardiles, A., Delgado, L., and Schmachtenberg, O. (2008). The elusive crypt olfactory receptor neuron: evidence for its stimulation by amino acids and cAMP pathway agonists. *J. Exp. Biol.* 211, 2417–2422.

Von Bartheld, C. S. (2004). The terminal nerve and its relation with extrabulbar "olfactory" projections: lessons from lampreys and lungfishes. *Microsc. Res. Tech.* 65, 13–24.

von Bartheld, C. S., Meyer, D. L., Fiebig, E., and Ebbesson, S. O. (1984). Central connections of the olfactory bulb in the goldfish, *Carassius auratus*. *Cell Tissue Res.* 238, 475–487.

von Frisch, K. (1941). Über einen Schreckstoff der Fischhaut und seine biologische Bedeutung. *Z. Vgl. Physiol.* 29, 46–145.

Wedgwood, M. (1974). Proceedings: Connections between the olfactory bulb and the habenula and dorsomedial thalamic nuclei. *J. Physiol.* 239, 88P–89P.

Weth, F., Nadler, W., and Korsching, S. (1996). Nested expression domains for odorant receptors in zebrafish olfactory epithelium. *Proc. Natl. Acad. Sci. U.S.A.* 93, 13321–13326.

Wiechert, M. T., Judkewitz, B., Riecke, H., and Friedrich, R. W. (2010). Mechanisms of pattern decorrelation by recurrent neuronal circuits. *Nat. Neurosci.* 13, 1003–1010.

Yaksi, E., Von Saint Paul, F., Niessing, J., Bundschuh, S. T., and Friedrich, R. W. (2009). Transformation of odor representations in target areas of the olfactory bulb. *Nat. Neurosci.* 12, 474–482.

Yamagata, M., and Sanes, J. R. (2012). Transgenic strategy for identifying synaptic connections in mice by fluorescence complementation (GRASP). *Front. Mol. Neurosci.* 5:18. doi: 10.3389/fnmol.2012.00018

Yoshihara, Y. (2009). Molecular genetic dissection of the zebrafish olfactory system. *Results Probl. Cell Differ.* 47, 97–120.

Zeiske, E., Theisen, B., and Breucker, H. (1992). "Structure, development and evolutionary aspects of the peripheral olfactory system," in *Fish Chemoreception* (London: Chapman and Hall), 13–39.

Zhu, P., Narita, Y., Bundschuh, S. T., Fajardo, O., Scharer, Y. P., Chattopadhyaya, B., et al. (2009). Optogenetic dissection of neuronal circuits in Zebrafish using viral gene transfer and the tet system. *Front. Neural Circuits* 3:21. doi: 10.3389/neuro.04.021

Zippel, H. P., Reschke, C., and Korff, V. (1999). Simultaneous recordings from two physiologically different types of relay neurons, mitral cells and ruffed cells, in the olfactory bulb of goldfish. *Cell. Mol. Biol. (Noisy-le-grand)* 45, 327–337.

Zucker, C. L., and Dowling, J. E. (1987). Centrifugal fibres synapse on dopaminergic interplexiform cells in the teleost retina. *Nature* 330, 166–168.

Conflict of Interest Statement: The authors declare that the research was conducted in the absence of any commercial or financial relationships that could be construed as a potential conflict of interest.

Received: 31 January 2013; paper pending published: 19 February 2013; accepted: 18 March 2013; published online: 11 April 2013.

Citation: Kermen F, Franco LM, Wyatt C and Yaksi E (2013) Neural circuits mediating olfactory-driven behavior in fish. Front. Neural Circuits ***7****:62. doi: 10.3389/fncir.2013.00062*

frontiers in
NEURAL CIRCUITS

ORIGINAL RESEARCH ARTICLE
published: 21 May 2013
doi: 10.3389/fncir.2013.00098

Aversive cues fail to activate *fos* expression in the asymmetric olfactory-habenula pathway of zebrafish

Tagide N. deCarvalho[1]*, Courtney M. Akitake[1], Christine Thisse[2], Bernard Thisse[2] and Marnie E. Halpern[1]*

[1] Department of Embryology, Carnegie Institution for Science, Baltimore, MD, USA
[2] Department of Cell Biology, Health Science Center, University of Virginia, Charlottesville, VA, USA

Edited by:
German Sumbre, Ecole Normale Superieure, France

Reviewed by:
Minmin Luo, National Institute of Biological Sciences, China
Suresh Jesuthasan, Duke/NUS Graduate Medical School, Singapore

***Correspondence:**
Tagide N. deCarvalho and Marnie E. Halpern, Department of Embryology, Carnegie Institution for Science, 3520 San Martin Drive, Baltimore, MD 21218, USA.
e-mail: decarvalho@ciwemb.edu; halpern@ciwemb.edu

The dorsal habenular nuclei of the zebrafish epithalamus have become a valuable model for studying the development of left-right (L-R) asymmetry and its function in the vertebrate brain. The bilaterally paired dorsal habenulae exhibit striking differences in size, neuroanatomical organization, and molecular properties. They also display differences in their efferent connections with the interpeduncular nucleus (IPN) and in their afferent input, with a subset of mitral cells distributed on both sides of the olfactory bulb innervating only the right habenula. Previous studies have implicated the dorsal habenulae in modulating fear/anxiety responses in juvenile and adult zebrafish. It has been suggested that the asymmetric olfactory-habenula pathway (OB-Ha), revealed by selective labeling from an *lhx2a:YFP* transgene, mediates fear behaviors elicited by alarm pheromone. Here we show that expression of the *fam84b* gene demarcates a unique region of the right habenula that is the site of innervation by *lhx2a:YFP*-labeled olfactory axons. Upon ablation of the parapineal, which normally promotes left habenular identity; the *fam84b* domain is present in both dorsal habenulae and *lhx2a:YFP*-labeled olfactory bulb neurons form synapses on the left and the right side. To explore the relevance of the asymmetric olfactory projection and how it might influence habenular function, we tested activation of this pathway using odorants known to evoke behaviors. We find that alarm substance or other aversive odors, and attractive cues, activate *fos* expression in subsets of cells in the olfactory bulb but not in the *lhx2a:YFP* expressing population. Moreover, neither alarm pheromone nor chondroitin sulfate elicited *fos* activation in the dorsal habenulae. The results indicate that L-R asymmetry of the epithalamus sets the directionality of olfactory innervation, however, the *lhx2a:YFP* OB-Ha pathway does not appear to mediate fear responses to aversive odorants.

Keywords: behavior, asymmetry, alarm pheromone, *fos*, *fam84b*

INTRODUCTION

The epithalamus of the teleost brain shows a high degree of left-right (L-R) asymmetry (Concha and Wilson, 2001; Kuan et al., 2007a; Signore et al., 2009); however, the functional significance of this specialization is unknown. In zebrafish, the pineal stalk emerges just to the left of the midline and the accessory parapineal is located to its left (Concha et al., 2000; Liang et al., 2000; Gamse et al., 2002). The adjacent paired habenular nuclei are comprised of dorsal and ventral nuclei, which correspond to the mammalian medial and lateral nuclei, respectively (Amo et al., 2010). The dorsal nuclei can be further divided into asymmetric subnuclei based on their distinct molecular properties (Gamse et al., 2003; Aizawa et al., 2005; Gamse et al., 2005) and the region of the interpeduncular nucleus (IPN) that they innervate (Agetsuma et al., 2010). Thus, the dorsal habenulae display striking differences in size, neuroanatomy, molecular properties, and connectivity.

The asymmetric properties of the zebrafish larval epithalamus arise in a step-wise manner, with Nodal signaling setting the directionality of the pineal complex (Concha et al., 2000; Liang et al., 2000) and the parapineal, which emerges on the left side, providing cues that differentiate the left dorsal habenula from the right (Concha et al., 2003; Gamse et al., 2003; Snelson et al., 2008; Regan et al., 2009). The dorsal habenular nuclei are part of an evolutionarily conserved conduction system between the limbic forebrain and the midbrain via efferent connections to the IPN (Herrick, 1948; Sutherland, 1982; Hikosaka et al., 2008; Bianco and Wilson, 2009). However, in zebrafish, habenular connections to the IPN do not show mirror image symmetry as in mammals (Ramón y Cajal, 1995). Instead, efferents from the left habenula project to the dorsal, intermediate, and ventral regions of the IPN, and the right habenula innervates only the ventral region (Gamse et al., 2005). Further supporting dorsoventral differences at the target, neurons in the dorsal IPN project to the griseum centrale, a region thought to be equivalent to the mammalian periaqueductal gray, whereas those in the ventral IPN innervate the median raphe nucleus (Agetsuma et al., 2010). L-R differences in habenular connectivity thus result in distinct limbic to midbrain pathways on each side of the brain.

In mammals, the habenular region has been implicated in a wide range of behaviors including fear, sex, and feeding (Sutherland, 1982; Bianco and Wilson, 2009; Hikosaka, 2010; Okamoto et al., 2012). The role of the lateral/ventral habenular nuclei in the modulation of emotional behaviors has been intensively studied in rhesus monkey and humans [refer to Hikosaka (2010)]. The function of the medial/dorsal habenula is less well-understood; however, there is evidence that aversive stimuli or stress induce behavioral, biochemical and immunological responses (Silver et al., 1996; Carboni et al., 1998; Cirulli et al., 1998; Sugama et al., 2002; Wilhelm, 2011; Kobayashi et al., 2013).

Recent studies on zebrafish demonstrate that the dorsal habenulae regulate fear-related behaviors. Juveniles with the dorsal habenulae (and other structures) genetically ablated did not learn to avoid an aversive stimulus when paired with a conditional one (Lee et al., 2010). Inactivation of an asymmetric dorsal habenular subnucleus resulted in increased freezing behavior in adult zebrafish in response to a conditioned aversive stimulus (Agetsuma et al., 2010). These studies suggest that the dorsal habenula is an experience-dependent modulator of anxiety and fear-related decision-making (Okamoto et al., 2012).

A known stimulus that elicits fear in fish is "Schreckstoff" or fear substance, an array of chemicals exuded from injured skin, which functions as a predation signal for nearby individuals (Pfeiffer, 1977). Perception of such alarm pheromones in zebrafish provokes rapid darting or freezing, alternative behaviors in response to fear (Waldman, 1982; Speedie and Gerlai, 2008). Because of the dorsal habenula's involvement in modulating fear responses, it has been proposed that alarm pheromone may be the odorant cue for the asymmetrically projecting olfactory-habenula (OB-Ha) pathway (Concha et al., 2012). Furthermore, whole skin extract or glycosaminoglycan chondroitin, results in increased calcium signaling in the medio-dorsal portion of the posterior olfactory bulb (Mathuru et al., 2012), where *lhx2a:YFP* labeled mitral cells are located.

In the present study, we describe a unique domain in the right dorsal habenula characterized by expression of the *fam84b* gene and associated with a discrete neuropil density that corresponds to the site of innervating *lhx2a:YFP* positive olfactory mitral cells. Expression of *fam84b* and the synaptic terminals of the *lhx2a:YFP* neurons are always found in the dorsal habenula that is contralateral to the parapineal. Following removal of the parapineal, *fam84b* expression appears in the left and the right dorsal habenulae and both receive innervation from the olfactory neurons, indicating that directional asymmetry of the epithalamus is sufficient to influence pre-synaptic input. To examine the function of the asymmetric OB-Ha pathway, induction of *fos* expression was used as a measure of neuronal activation in response to a variety of odorants. We find that adult zebrafish exposed to alarm substance extracted from skin, or to the purified component chondroitin sulfate, show robust *fos* activation in the olfactory bulb, but not in the *lhx2a:YFP* subpopulation or in the dorsal habenulae. The results show that the epithalamus directs the formation of an asymmetric telencephalic connection; however, substances that provoke fearful behaviors do not appear to activate this unique OB-HA pathway.

MATERIALS AND METHODS

ZEBRAFISH

Zebrafish were housed at 27°C on a 14:10 h light:dark cycle. Zebrafish used in this study were the wild-type AB strain (Walker, 1999) and the transgenic lines *Tg(-10lhx2a:GAP-EYFP)*^{zf177} [formerly called *Tg(lhx2a:gap-YFP)*] and *Tg(-10lhx2a:SYP-GFP)*^{zf186} [formerly called *Tg(lhx2a:Syp-GFP)*; Miyasaka et al., 2009] and *Tg(foxd3*:GFP)^{fkg17} (Gilmour et al., 2002). To visualize the dorsal habenular nuclei, a transgenic reporter, *TgBAC(gng8:Eco.NfsB-2A-CAAX-GFP)* (DKEY-18313 BAC; Genbank accession number CR450711) that is habenula-specific at 4–5 days post-fertilization (dpf) (Akitake and Halpern, unpublished observations) was also employed. Maintenance of zebrafish and experimental procedures were carried out in accordance with the protocol approved by Institutional Animal Care and Use Committee. Naming of transgenic lines and zebrafish genes (see below) follow the nomenclature guidelines provided by the Zebrafish Model Organism Database (ZFIN).

RNA *in situ* HYBRIDIZATION AND IMMUNOFLUORESCENCE

The *family with sequence similarity 84, member B* (*fam84b)* gene was identified in an *in situ* hybridization screen of zebrafish cDNAs for their tissue-specific patterns of expression (Thisse and Thisse, 2004). The *fam84b* clone came from a cDNA library prepared from adult zebrafish kidney. Digoxigenin-(DIG) and fluorescein (FITC)-labeled RNA probes were synthesized using reagents from Roche Molecular Biochemical. The *fam84b* plasmid was linearized with NotI and transcribed with SP6 RNA polymerase. A clone of the *v-fos FBJ murine osteosarcoma viral oncogene homolog* gene *(fos*, formerly referred to as *c-fos*) was generated by amplifying a 602 base pair fragment from cDNA prepared from RNA of 3 dpf larvae using forward and reverse primers (TCTCCTCTGTGGCGCCCTCC and GTCTGGAACCGAGCGAGCCG) and subcloning into the pCRII-TOPO vector (Invitrogen). For probe synthesis, the *fos* plasmid was linearized with BamHI and transcribed with T7 RNA polymerase. The *orthodenticle homolog 5* (*otx5*) and *potassium channel tetramerization domain containing 12.1* (*kctd12.1*, formerly called *leftover*) probes were prepared as described (Gamse et al., 2002, 2003). A probe for the *early growth response 1* (*egr1*) gene was synthesized as in Close et al. (2002).

Single and double label colorimetric RNA *in situ* hybridization experiments were performed as previously described for larvae (Gamse et al., 2002) and adult brain tissue (Gorelick et al., 2008). To enhance signal intensity, 5% dextran sulfate (Millipore) was added to the hybridization buffer as in Lauter et al. (2011). Following the colorimetric reaction, adult brains were embedded in 4% low melting point agarose (SeaPlaque, Lonza) and 50 μm coronal sections were collected using a vibratome (Leica VT1000S).

For fluorescent *in situ* hybridization alone or coupled with immunolabeling for yellow fluorescent protein (YFP)/green fluorescent protein (GFP) YFP/GFP, we followed the protocol described in Gamse et al. (2002) until the anti-DIG antibody-blocking step. Samples were placed in maleic acid buffer (MAB) with 2% blocking reagent (Roche) for 1 h according to Lauter et al. (2011). Anti-DIG-antibody conjugated with horseradish

peroxidase (Roche) alone or together with anti-GFP rabbit antibody (Torrey Pines TP401) was diluted 1:500 in blocking solution and incubated at 4°C overnight. Probes were visualized by tyramide signal amplification (TSA) reagents that were prepared as described (Vize et al., 2009). Anti-GFP antibody cross-reacts with YFP. Reaction buffer contained 4-iodophenol (Sigma-Aldrich) and 2% dextran sulfate. Tyramide-Cy5 was used for the first *in situ* hybridization probe. For double in *situ* hybridization, reacted samples were incubated in blocking solution for 1 h and then at 4°C overnight in diluted (1:500) anti-FITC-antibody conjugated with horseradish peroxidase (Roche). Tyramide-Cy3 was used for the second *in situ* hybridization probe. Adult brains were embedded in 4% low melting point agarose and 50 μm coronal vibratome sections were collected prior to the TSA detection step. The sections were mounted in Prolong Gold or *Slowfade* Gold (Invitrogen) antifade mounting media. For immunolabeling following fluorescent *in situ* hybridization, reacted samples were placed in blocking solution (0.1% Triton PBS with 10% sheep serum) for 1 h and then in diluted (1:500) goat anti-rabbit-Cy3 antibody (Jackson ImmunoResearch) at 4°C overnight.

ODOR ASSAYS

Alarm substance (hereinafter referred to as skin extract) was freshly prepared on the day of testing. Adult fish were immersed in an ice water slurry and decapitated. To prepare skin extract solution, the body was placed in 10 mL distilled water, the skin was abraded with 250 grit sandpaper and 15 shallow cuts were made using a protocol modified from Speedie and Gerlai (2008). Extracts were collected and pooled from 5 male and 5 female individuals (100 mL total) and filtered under vacuum using a 0.2 μm filter (Nalgene).

Adult zebrafish (3–6 months) of both sexes were placed in 1 L breeding tanks (Aquatic Habitats) containing system water and acclimated for 1 h prior to odorant exposure. All experiments were performed with adults because larval zebrafish do not respond to alarm pheromone (Waldman, 1982). For alarm pheromone assays, single fish were placed in tanks separated by black paper. Solutions were delivered via a 5/32 × 9/32 mm diameter tygon tube (Pennplex) entering below the water line. A 10 mL syringe filled with 2.5 mL of the skin extract or chondroitin sulfate solution was connected to the other end of the plastic tubing and the contents slowly injected into each tank for a final concentration of 0.2% skin extract or 1 μg/ml shark chondroitin sulfate (Sigma-Aldrich). Other ecologically and behaviorally relevant odors were tested in a similar manner; however, groups of 5 fish were placed in one tank for each odorant. Test chemicals were purchased through Sigma-Aldrich and used at a final concentration of 400 μM for L-cysteine and putrescine and 40 μM for cadaverine and trimethylamine. Ground fish flakes (100 mg/L; Tetramin Tropical Flakes), 0.1% bile obtained from freshly killed tilapia (*Orechromis mossambicus*) and 0.25% of a conspecific extract, which was obtained by grinding and straining 10 freshly sacrificed adult zebrafish of both sexes into a 10 ml of distilled water were also tested. Control individuals received only distilled water. Following odorant exposure, fish were held in the experimental tanks for 30 min, then immersed in an ice water slurry and decapitated. Brains were immediately dissected in cold PBS and fixed in 4% paraformaldehyde at 4°C overnight.

As a positive control, the glutamate receptor agonist, kainic acid, was used to elicit *fos* expression in *lhx2a:YFP* labeled mitral cells. Primary sensory neurons excite mitral cells through AMPA and kainic ionotropic glutamate receptors (Tabor and Friedrich, 2008); therefore, treatment with kainic acid is expected to induce neural activity in the olfactory bulb. Adult fish were anesthetized with 4% tricaine (ethyl 3-aminobenzoate methanesulfonate solution; Sigma-Aldrich; Westerfield, 2000) and placed on a damp sponge. Kainic acid (Tocris Bioscience) was injected into the peritoneal cavity via a syringe (28G, Beckton Dickinson) at 10 mg per kg body mass in phosphate buffered saline (PBS). Control fish were injected with PBS only. The injected fish were placed in a recovery tank for 30 min and treated as above.

PARAPINEAL ABLATION

Parapineal ablation was performed on *Tg*(*foxd3*:*GFP*)^{fkg17}, *Tg*(*foxd3*:*GFP*)^{fkg17}; *Tg*(*-10lhx2a:GAP-EYFP*)^{zf177} or *Tg*(*foxd3*:*GFP*)^{fkg17}; *Tg*(*-10lhx2a:SYP-GFP*)^{zf186} embryos at 2 or 3 dpf. Embryos were anesthetized with 0.04% tricaine (ethyl 3-aminobenzoate methanesulfonate solution; Sigma-Aldrich; Westerfield, 2000) and positioned dorsal side up in 1.2% low melting-temperature agarose under a 40 × water immersion lens. A scanning beam (885 nm excitation) from a multiphoton Ti:Sapphire laser (MaiTai HP, Spectra-Physics) mounted on a Leica SP5 confocal microscope was focused on the parapineal. Cell ablation was achieved by scanning with a 30–40% filter wheel (power) setting for 1 to 3 two-second passes. The extent of ablation was monitored with a 10% filter wheel setting after each scan pass until GFP was no longer detected. Successful ablation of the parapineal was re-evaluated by fluorescence microscopy prior to live imaging or fixation. In control larvae, cells in the brain were ablated on the opposite side of the pineal or adjacent to the parapineal.

IMAGING

Bright-field images were collected using an Axiocam HRc digital camera mounted on an Axioskop (Carl Zeiss). Fluorescent images were captured using a Zeiss Imager.Z1 microscope equipped with an AxioCam MRm digital camera or with a Leica SP5 confocal microscope. Images were pseudocolored and three-dimensional projections were generated using Imaris (Bitplane) or Axiovision (Carl Zeiss) software.

RESULTS

lhx2a:*YFP* OLFACTORY NEURONS PROJECT TO A *fam84b*-EXPRESSING SUBREGION OF THE RIGHT DORSAL HABENULA

The dorsal habenular nuclei exhibit L-R differences in gene expression and in the extent of dense neuropil (Concha et al., 2000; Gamse et al., 2003, 2005), while the ventral nuclei are bilaterally symmetrical (Amo et al., 2010). The *fam84b* gene, which encodes a breast cancer membrane-associated protein (Adam et al., 2003) is transcribed bilaterally in the ventral habenulae, but is also expressed in an unusual pattern in only the right dorsal habenula (**Figures 1A** and **2A**). The *fam84b* domain is within the lateral subnucleus of the right dorsal habenula (**Figure 1B**), defined by expression of the *kctd12.1* gene (Aizawa et al., 2005; Gamse et al., 2005). The medio-lateral designation of habenular subnuclei is based on their position in the adult brain, which

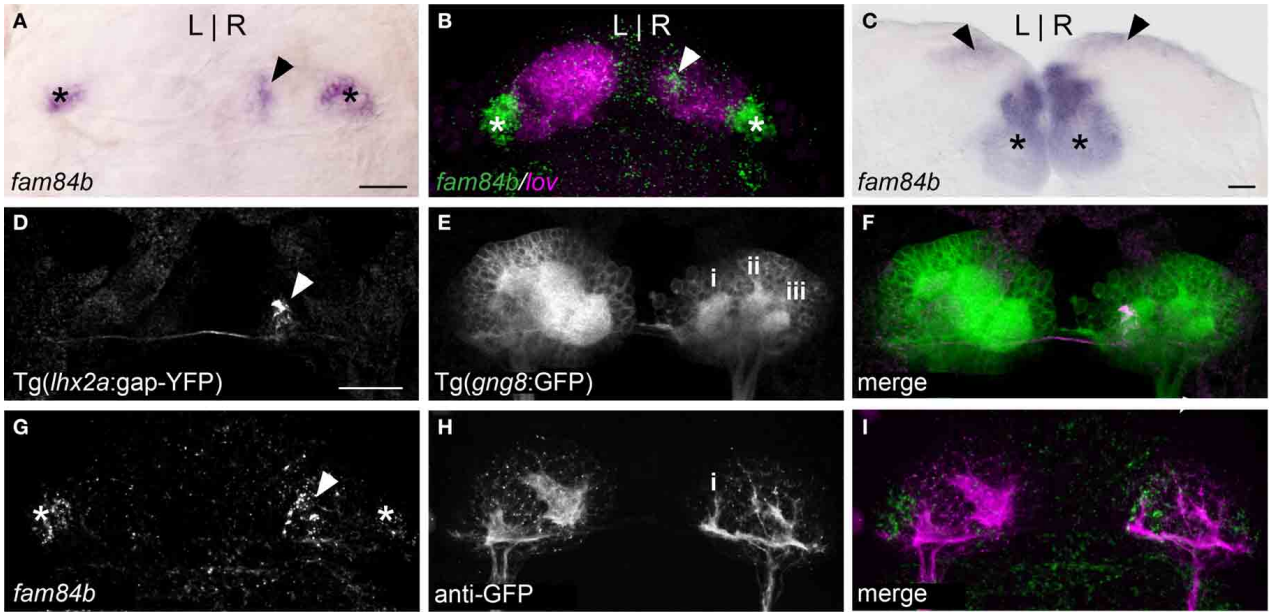

FIGURE 1 | A unique subnucleus in the right dorsal habenula of larval zebrafish. (A) The *fam84b* gene is expressed in a medial domain in the right dorsal habenula (black arrowhead) and bilaterally in the ventral habenulae (asterisks in **A–C,G**). **(B)** The right-only *fam84b* domain (white arrowhead) is located within the *kctd 12.1* (lov)-expressing subnucleus, as demonstrated by fluorescent *in situ* hybridization. **(C)** *fam84b* is expressed bilaterally in the adult dorsal habenulae (black arrowheads). **(D–F)** Live imaging of *Tg*(*gng8:nfsB-CAAX-GFP*)^{c375} larva reveals that axons of *lhx2a:YFP* labeled olfactory mitral cells (white arrowhead in **D**) terminate at the medial neuropil (i in **E**) of the right habenula. More lateral neuropil clusters are indicated (ii,iii). **(G–I)** The medial neuropil cluster (i) visualized by anti-GFP immunofluorescence in *Tg*(*gng8:nfsB-CAAX-GFP*)^{c375} larva is closely associated with the *fam84b* expression domain (white arrowhead in **G**) revealed by fluorescent *in situ* hybridization. All larvae 4 dpf; scale bars = 50 μm.

differs from the larva due to extensive reorganization that occurs during development (Amo et al., 2009). Expression of *fam84b* is bilateral in the adult, but remains more extensive in the right dorsal habenula (**Figure 1C**).

Accumulations of neuropil differ between the left and right dorsal habenulae of larval zebrafish, as visualized by immunolabeling with antibodies against acetylated α-Tubulin (Concha et al., 2000; Taylor et al., 2011) or Synaptic Vesicle Protein 2 (SV2) (Hendricks and Jesuthasan, 2007; Miyasaka et al., 2009), and by labeling of membrane-tagged GFP in live *Tg*(*gng8:nfsB-CAAX-GFP*)^{c375} larvae. The left side has an expanded neuropil that extends the width of the dorsal habenula, while the right dorsal habenula has three more distinct, small clusters (**Figure 1E**). The most medial cluster corresponds to the site of innervation of *lhx2a*:YFP labeled axons from the olfactory bulb (**Figures 1D–F**) and overlaps with the *fam84b*-expressing cells (**Figures 1G–I**). The convergence of asymmetric pre-synaptic olfactory input, a discrete neuropil cluster and restricted *fam84b* expression suggests that the right dorsal habenula contains a functionally unique subnucleus.

DIRECTIONALITY OF OLFACTORY INNERVATION IS DETERMINED BY L-R ASYMMETRY OF THE EPITHALAMUS

Parapineal cells originate from the pineal anlage at 28 h post-fertilization (hpf) and migrate to the left side of the brain in >95% of embryos (Concha et al., 2003; Gamse et al., 2003). By 40 hpf, *kctd12.1* is strongly expressed in the presumptive left habenula and to a far lesser extent in the right. However, when the parapineal is found on the right side of the brain, either spontaneously (<5%) or following perturbation of Nodal-related signaling (Facchin et al., 2009), the asymmetric *kctd12.1* expression pattern is L-R reversed. Loss of the parapineal, either by laser-mediated cell ablation (Concha et al., 2003; Gamse et al., 2003) or the consequence of mutation (Snelson et al., 2008; Regan et al., 2009) results in symmetric development of the habenulae, with both the left and right nuclei exhibiting properties of the right habenula. Accordingly, when the parapineal is situated on the right side of the brain, *fam84b* is expressed in the left dorsal habenula ($n = 3$, **Figure 2B**) and, following ablation of the parapineal, *fam84b* domains are found bilaterally in both dorsal habenulae (control $n = 4$, **Figures 3A,B**; ablated $n = 5$, **Figures 3C,D**).

We examined whether altered directional asymmetry of the epithalamus also influences the connectivity of *lhx2a:YFP* labeled mitral cells. L-R reversal of parapineal position correlated with the olfactory bulb mitral cells innervating the left habenula rather than the right (**Figures 2C,D**). Compared to control ablated larvae with unilateral input to the right habenula (**Figures 3E–G**), lhx2a:YFP efferents innervate both dorsal habenulae in larvae with an ablated parapineal ($n = 14$, **Figures 3H–J**). These results indicate that L-R asymmetry of the epithalamic region directs olfactory connectivity. The bilateral projections likely form functional synapses, as evidenced by the localization of synaptic vesicles using *Tg*(*-10lhx2a:SYP-GFP*)^{zf186}, in which a synaptophysin-YFP fusion protein is expressed under the control of the *lhx2a* cis-regulatory elements (Miyasaka et al., 2009).

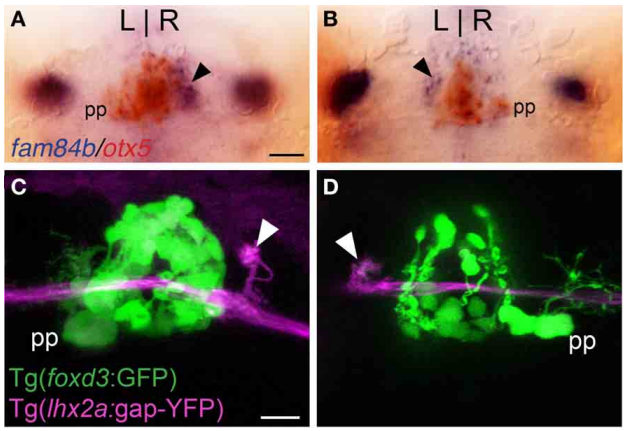

FIGURE 2 | Asymmetric olfactory input is contralateral to the parapineal. (A,B) Larvae with the parapineal (pp) on the left of the pineal anlage exhibit *fam84b* expression (blue) in the right dorsal habenula (black arrow). Conversely, spontaneous L-R reversal of parapineal position corresponds with *fam84b* expression on the left. The pineal complex expresses the *otx5* gene (red), revealed by double label *in situ* hybridization methods. **(C,D)** Live imaging of *Tg(foxd3:GFP)*^{fkg17}; *Tg(-10lhx2a:GAP-EYFP)*^{zf177} larvae. When the parapineal is on the left, *lhx2a:YFP* labeled terminals (white arrowhead) are found in the right dorsal habenula. With L-R reversal of epithalamic asymmetry, olfactory axons terminate in the left dorsal habenula. All larvae 4 dpf. Scale bars = 50 μm for **(A,B)** and 25 μm for **(C,D)**.

Clusters of synaptic vesicles were found in axon terminals at both dorsal habenulae ($n = 3$, **Figures 3N,O**). Ablation of the parapineal at a later developmental stage (77–80 hpf), following the establishment of the *lhx2a:YFP* olfactory-right habenula projection, also resulted in innervation of both dorsal habenulae ($n = 13$, **Figures 3K–M**). This reveals that the parapineal is required for the maintenance of dorsal habenular L-R identity, and that the OB-Ha pathway is highly plastic.

ALARM PHEROMONE DOES NOT STIMULATE THE OB-Ha PATHWAY

The dorsal habenulae have been implicated in modulating fear responses. Therefore, we examined whether substances known to provoke anxious behaviors in fish activate the asymmetric OB-Ha pathway in adult zebrafish. We used induction of *fos* expression as an indirect read-out of neural activity. This approach has been successfully applied in mammals to map the habenular response to a variety of stimuli (e.g., Kazi et al., 2004; Zhang et al., 2005; Paul et al., 2011) and the response to odorants in the olfactory bulb (e.g., Guthrie et al., 1993; Sallaz and Jourdan, 1993; Guthrie and Gall, 1995). We also examined expression of *egr1* but it was less robust than *fos* and was not detected in the olfactory bulb in response to chondroitin sulfate ($n = 9$, data not shown) or vehicle control ($n = 5$).

Exposure to skin extract ($n = 11$, **Figure 4A**) or purified shark chondroitin sulfate ($n = 4$, **Figure 4C**) did not elicit higher *fos* expression in the right dorsal habenula above control levels ($n = 5$, **Figure 4B** and $n = 6$, **Figure 4D**). In both treatment groups, a few *fos* positive neurons were found in the right habenula, but comparable expression was also observed in controls, suggesting that baseline *fos* induction is due to stimulus-unrelated activity caused by the experimental paradigm.

We also examined the response to chondroitin sulfate in the olfactory bulb. The olfactory bulb is comprised of several layers and, in zebrafish, mitral cell bodies reside within the glomerular and superficial inner cell layers while the interneuronal granule cells are found in a deeper position (Fuller et al., 2006). We observed that chondroitan sulfate treated individuals exhibited higher levels of *fos* expression in all regions ($n = 4$, **Figure 4E**) compared to controls ($n = 6$, **Figure 4F**). However, *fos* transcripts were never detected in *lhx2a:YFP* labeled mitral cells (chondroitin sulfate $n = 8$, control $= 3$, **Figures 4G,H**). In contrast, many olfactory bulb neurons including the *lhx2a*:YFP mitral cell subpopulation were activated with the glutamate receptor agonist kainic acid (**Figures 4I–L**). The centrally located fos positive cells are granule cells, whereas those found in the same layer or directly adjacent to *lhx2a*-expressing neurons are most likely mitral cells.

ECOLOGICALLY RELEVANT ODORS STIMULATE NON-*lhx2a:YFP* OLFACTORY BULB NEURONS

All odorant treatments elicited a qualitatively higher *fos* response above negative control throughout the olfactory bulb region but not in *lhx2a:YFP* labeled mitral cells (data not shown, putrescine $n = 4$, cadaverine $n = 3$, trimethylamine $n = 3$, L-cysteine $n = 4$, fish flakes $n = 5$, conspecific extract $n = 3$, Tilapia bile $n = 4$).

DISCUSSION

The connection from primary sensory neurons in the olfactory epithelium to secondary mitral cells in the olfactory bulb that project directly to the right habenula provides a defined pathway to study the establishment and behavioral significance of L-R asymmetry in the vertebrate brain.

Previous studies demonstrated that the parapineal influences the identity of the adjacent dorsal habenula. When the parapineal is located to the right of the pineal, rather than at its typical left-sided position, the directionality of habenular L-R asymmetry is reversed. In the absence of the parapineal, the left and right dorsal habenular nuclei develop similarly, with gene expression patterns, neuroanatomical organization, and restricted efferent connections to the IPN characteristic of the right nucleus. Accordingly, we find that the parapineal also affects the formation of a subnucleus in the right habenula, defined by expression of *fam84b* and the absence of the olfactory cell adhesion molecule (OCAM; Miyasaka et al., 2009). This subnucleus is found within a region designated as the lateral subnucleus of the dorsal habenula (Aizawa et al., 2005). It also corresponds with the location of a coherent neuropil cluster and the site of axon terminals of *lhx2a:YFP* olfactory mitral cells. With a L-R reversal in parapineal position, this subnucleus is now found in the left dorsal habenula. Following ablation of the parapineal, *fam84b* expression is present bilaterally and both the left and right habenular nuclei are innervated by the *lhx2a:YFP* neuronal population. These findings indicate that L-R asymmetry of the epithalamic region is sufficient to direct telencephalic input. Thus, a small difference in one region of the brain (e.g., the parapineal) not only influences the development of neighboring structures (e.g., the

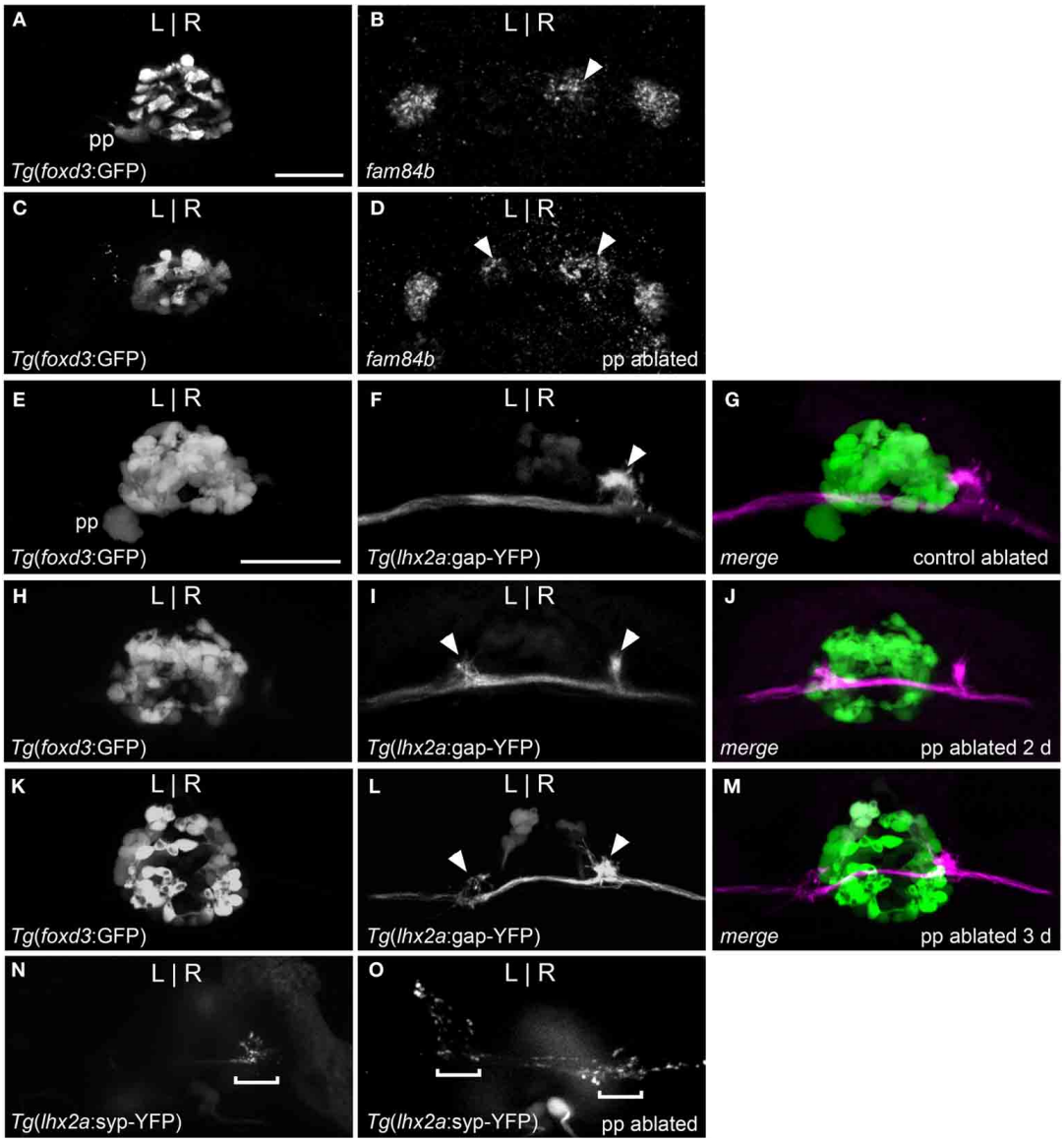

FIGURE 3 | Parapineal ablation results in symmetric OB-Ha pathway. **(A)** Live imaging of *Tg*(*foxd3*:GFP)^{fkg17} larva, with parapineal (pp) situated to the left of the pineal. **(B)** Fluorescent *in situ* hybridization reveals *fam84b* transcripts in the right dorsal habenula (white arrow) and bilaterally in the ventral habenulae at 4 dpf. **(C)** Parapineal ablation at 2 dpf results in **(D)** bilateral *fam84b* domains (white arrowheads) in the dorsal habenulae. **(E–G)** *lhx2a:YFP* mitral cells (white arrowhead) innervate the right habenula of control-ablated larvae, but **(H)** in the absence of the parapineal, they terminate **(I,J)** at both habenulae (white arrowheads in **I**). **(K–M)** Parapineal ablation at 3 dpf also results in bilateral *lhx2a:YFP* projections (white arrowheads in **L**). **(N)** Region of synaptic vesicle density (demarcated by bracket) in the right dorsal habenula of *Tg*(*-10lhx2a:SYP-GFP*)^{zf186} larva is found **(O)** bilaterally following parapineal ablation. All images, except for **(B,D)** are of live larvae at 4 dpf, 5 dpf **(K–M)** and 6 dpf **(N,O)**. Scale bars = 40 μm.

dorsal habenulae), but also has farther-reaching consequences on pre-synaptic as well as post-synaptic neurons.

The molecular mechanisms that direct the asymmetric connection between *lhx2a:YFP* mitral cells and the right habenula have yet to be determined. One possibility is unilateral expression of an axon guidance molecule. The *neuropilin receptor 1a* (*nrp1a*) gene, for example, is expressed only by neurons in the left dorsal habenula (Kuan et al., 2007b). Its ligand, Sema3D, is produced in the midline rostral to the IPN and is important for guiding left habenula neurons to the dorsal region of the IPN (Kuan et al., 2007b). Innervation of the right dorsal habenula by *lhx2a:YFP* mitral cells is unaltered following depletion of Nrp1a (deCarvalho and Halpern, unpublished observations), suggesting that formation of the asymmetric OB-Ha pathway does not rely on repulsive Sema3D-Nrp1 signaling. An alternative hypothesis is that the *fam84b*-expressing cells provide an attractive signal to guide *lhx2a:YFP* axons to or stabilize their synapses at the right habenula. Fam84b (also known as breast cancer membrane protein 101 and NSE2) encodes a protein of unknown function that interacts with α1-Catenin and is localized to the

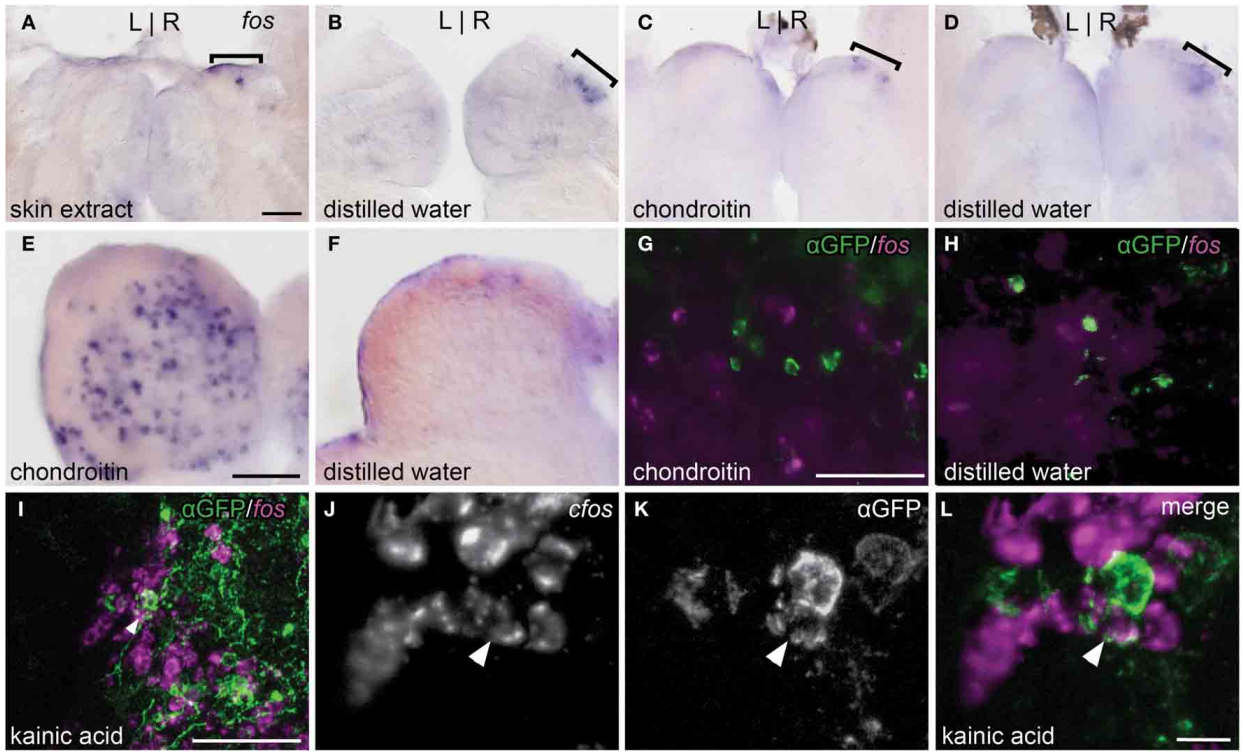

FIGURE 4 | Alarm substances do not stimulate the asymmetric OB-Ha pathway. (A,B) Skin extract does not elicit higher *fos* expression (brackets) than controls in the dorsal habenula. **(C,D)** Chondroitin sulfate also does not activate *fos* expression above controls in the dorsal habenula. **(E,F)** Robust induction of *fos* expression in the olfactory bulb is observed following chondroitin sulfate exposure. **(G,H)** *fos* transcripts revealed by fluorescent *in situ* hybridization do not colocalize with immunolabeled *lhx2a:YFP* neurons in the olfactory bulb. **(I)** Kainic acid induces *fos* expression in a subset of *lhx2a:YFP* labeled olfactory neurons. **(J–L)** Higher magnification of **(I)**, with double labeled neuron indicated (white arrowhead). Coronal sections (50 μm) of adult brains. Scale bars = 40 μm for **(A–D)**, **(E,F)**, **(G,H),** and **(J–L)**, and 10 μm for **(I)**.

membrane in regions of cell-cell contact (Adam et al., 2003). However, Fam84b itself is unlikely to be the guidance cue for innervating *lhx2a:YFP* axons as the appearance of *fam84b* transcripts follows rather than precedes olfactory axon outgrowth to the right habenula (deCarvalho and Halpern, unpublished observations). Although the cues that establish the asymmetric OB-Ha projection are unknown, localization of synaptic vesicles in axonal terminals at the right habenula strongly suggest that this is a functional connection. Confirmation of laterality in neuronal activity will come from transgenic approaches, such as selective optogenetic activation of the lhx2a-expressing subpopulation with expression of the calcium indicator GCaMP (e.g. Muto et al., 2011; Ahrens et al., 2012; Akerboom et al., 2012).

The identity of the *lhx2a:YFP*-expressing olfactory neurons does not lend much insight as to the odorant cues that stimulate this pathway. The *lhx2a:YFP* labeled primary sensory neurons are a subpopulation of crypt cells, one of three types of olfactory sensory neurons (OSNs) defined by their morphology in fish (Hansen and Zeiske, 1998). Crypt cells are relatively sparse compared to other OSNs (Hansen and Finger, 2000; Schmachtenberg, 2006) and, in zebrafish, appear to be nearly homogenous in their expression of the olfactory receptor gene, *ora4* (Oka et al., 2012). Ligands for the Ora4 receptor are unknown, although there is evidence in the trout that crypt cells are most sensitive to sexual pheromones (Vielma et al., 2008; Bazaes and Schmachtenberg, 2012). The restricted expression of *lhx2a* coupled with the fact that ∼10% of OSNs are *ora4* negative, suggests that crypt cells are a diverse population and that the Ob-Ha pathway may sense a distinct odorant cue.

Because the *lhx2a:YFP* olfactory projections are located in an region of the OB responsive to the alarm pheromone component, chondroitin sulfate (Mathuru et al., 2012), and the dorsal habenulae have been implicated in the modulation of fear (Agetsuma et al., 2010; Lee et al., 2010), it was proposed that the asymmetric OB-Ha pathway in zebrafish mediates avoidance behavior elicited by alarm substances (Concha et al., 2012). To test this hypothesis, we measured *fos* expression in the olfactory bulb and dorsal habenulae following exposure to a variety of odorant cues. Induction of immediate early gene expression, such as *fos*, has been widely used as a read-out of olfactory stimulation in rodents (e.g., Guthrie et al., 1993; Sallaz and Jourdan, 1993; Guthrie and Gall, 1995; Okuyama et al., 2011; Bepari et al., 2012). In zebrafish, *fos* expression was an effective measure of neural activity upon light avoidance; (Lau et al., 2011) and in pharmacologically induced seizures (Baraban et al., 2005).

We found that a variety of complex and purified odorants produced robust *fos* expression in the olfactory bulb of adult

zebrafish, supporting the validity of the assay. However, contrary to their proposed role, neither alarm pheromone nor chondroitin sulfate alone elicited *fos* activation in the *lhx2a:YFP* OB-Ha pathway. We did not detect colocalization of *fos* transcripts in *lhx2a:YFP* labeled mitral cells nor did we observe *fos* activation in the right habenula above control levels. We tested other odors known to be aversive or attractive cues, including polyamines that have been shown to elicit olfactory responses in fish (Friedrich and Korsching, 1998; Michel et al., 2003; Rolen et al., 2003) and may serve as feeding cues (Rolen et al., 2003). Additional attractive odors tested were food, conspecifics and bile, which is a social cue (Doving et al., 1980; Polkinghorne et al., 2001). We also examined the response to L-cysteine because zebrafish show strong avoidance to this odor (Vitebsky et al., 2005) and relatively high sensitivity compared to other amino acids (Michel and Lubomudrov, 1995). In all cases, *fos* expression was observed in cells in the OB but not in the *lhx2a:YFP* subpopulation. Thus, the *lhx2a:YFP* labeled pathway appears to be unresponsive to ecologically relevant odor cues known to elicit behavior in fish. Consistent with these findings, we also did not detect *fos* expression in the right dorsal habenula above baseline levels. Curiously, *fos* expression was frequently observed in the right habenula of controls as well as individuals exposed to odorants, suggesting that this activity was caused by some aspect of the experimental set-up or handling of the adult fish.

The most likely explanation for the absence of *fos* activation in *lhx2a-YFP* olfactory neurons is that a relevant odor was not tested. However, it is also possible that subcomponents of complex odorants such as fish flakes or conspecific extract masked or antagonized an activating cue (e.g., specific amino acids). Purified amino acids and specific components of sexual pheromones have been shown to elicit responses in the crypt cells of other fish species (Vielma et al., 2008; Bazaes and Schmachtenberg, 2012).

Alternatively, although the glutamate agonist kainic acid induced *fos* expression in *lhx2a:YFP* mitral cells, the *fos* response to odorants may be less robust in these neurons. Several functional mapping studies of the olfactory bulb in other species have demonstrated that mitral cells are competent to activate transcription of *fos* or other immediate early genes; however, expression is often reduced and less extensive than in the granule cell interneurons (e.g., Guthrie et al., 1993; Sallaz and Jourdan, 1993; Guthrie and Gall, 1995). Transcriptional activation is also known to differ in sensitivity among immediate early genes (Isogai et al., 2011; Bepari et al., 2012). For this reason, we examined expression of another immediate early gene, *egr1*, but in contrast to *fos*, *egr1* transcripts were not detected in the olfactory bulb following exposure to chondroitin sulfate. An alternative method may be required to assay neuronal activity in the asymmetrically projecting mitral cells, such as the use of genetically-encoded Ca^{2+} indicators.

It is also possible that the *lhx2a-YFP* labeled mitral cells consist of two distinct subpopulations, those that either express *fos* in response to kainic acid or do not. Neuroanatomical tracing of individual *lhx2a-YFP* mitral cells indicates that a fraction may terminate in the telencephalon (Miyasaka et al., 2009), whereas the majority projects to the right habenula. Whether these alternative projection patterns correspond to neurons with different sensitivities to *fos* activation remains to be determined.

Lateralization of olfactory systems is prevalent in invertebrates and appears to function either as a means to enhance odor discrimination or facilitate olfactory learning. For example, in *Caenorhabditis elegans,* bilaterally-paired sensory neurons express different olfactory receptors on the left and right side of the head (Wes and Bargmann, 2001). Asymmetry at the molecular level allows the worm to sense multiple odors using a limited number of OSNs. In the honeybee, individuals trained with their right antenna perform better on olfactory memory tasks than those trained with the left antenna (Letzkus et al., 2006). The right antenna seems to mediate short-term olfactory memory while the left is specialized for long-term memory retention (Rogers and Vallortigara, 2008). The higher number of sensilla on the right antennae compared to the left may account for lateralized olfaction in honeybees (Frasnelli et al., 2010). A recent study in *Drosophila* demonstrates that L-R differences may be quite subtle, in that differential neurotransmitter release between the ipsilateral and contralateral projections of single OSNs enables directional sensing of localized odorants (Gaudry et al., 2013).

Although the significance of asymmetry in zebrafish olfactory projections remains to be demonstrated, it may facilitate differential processing of stimuli as in invertebrate models. Several teleost species are known to exhibit L-R differences in their olfactory system. In flatfish such as the winter flounder, the upward facing right olfactory pathway from the olfactory epithelium through the telencephalon is significantly larger in volume (Prasada Rao and Finger, 1984) and L-R glomerular organization of the olfactory bulb is highly asymmetric in the turbot (Doldan et al., 2011). Studies of olfactory sensitivity in the Senegalese sole demonstrate tuning between the left and right olfactory epithelia to several different odorants (Velez et al., 2005, 2007).

The discovery of a specialized subnucleus in the right dorsal habenula of the zebrafish larva that is the site of olfactory innervation could provide important clues as to the downstream circuitry that mediates a lateralized response to environmental cues. The finding that directional asymmetry of the developing epithalamus guides the formation of this subnucleus reveals an unsuspected plasticity in olfactory connectivity and suggests that local L-R differences may have widespread consequences on neural pathways throughout the brain.

ACKNOWLEDGMENTS

We thank Ana Quintanal and Lindsey Knapp for technical assistance, Yi-Lin Yan and John Postlethwait for providing the *egr1* plasmid, Philippe Mourrain for *fos* primers, and Erik Duboué for helpful comments on the manuscript. Tagide N. deCarvalho is a recipient of a Ruth L. Kirschstein National Research Service Award (F32MH091980). This study was supported by funds to Christine Thisse and Bernard Thisse from the University of Virginia and by a grant to Marnie E. Halpern from the National Institutes of Health (2R01HD042215).

REFERENCES

Adam, P. J., Boyd, R., Tyson, K. L., Fletcher, G. C., Stamps, A., Hudson, L., et al. (2003). Comprehensive proteomic analysis of breast cancer cell membranes reveals unique proteins with potential roles in clinical cancer. *J. Biol. Chem.* 278, 6482–6489.

Agetsuma, M., Aizawa, H., Aoki, T., Nakayama, R., Takahoko, M., Goto, M., et al. (2010). The habenula is crucial for experience-dependent modification of fear responses in zebrafish. *Nat. Neurosci.* 13, 1354–1356.

Ahrens, M. B., Li, J. M., Orger, M. B., Robson, D. N., Schier, A. F., Engert, F., et al. (2012). Brain-wide neuronal dynamics during motor adaptation in zebrafish. *Nature* 485, 471–477.

Aizawa, H., Bianco, I. H., Hamaoka, T., Miyashita, T., Uemura, O., Concha, M. L., et al. (2005). Laterotopic representation of left-right information onto the dorso-ventral axis of a zebrafish midbrain target nucleus. *Curr. Biol.* 15, 238–243.

Akerboom, J., Chen, T. W., Wardill, T. J., Tian, L., Marvin, J. S., Mutlu, S., et al. (2012). Optimization of a GCaMP calcium indicator for neural activity imaging. *J. Neurosci.* 32, 13819–13840.

Amo, R., Aizawa, H., Takahashi, R., Kobayashi, M., Takahoko, M., Aoki, T., et al. (2009). Identification of the zebrafish ventral habenula as a homologue of the mammalian lateral habenula. *Neurosci. Res.* 65, S227.

Amo, R., Aizawa, H., Takahoko, M., Kobayashi, M., Takahashi, R., Aoki, T., et al. (2010). Identification of the zebrafish ventral habenula as a homolog of the mammalian lateral habenula. *J. Neurosci.* 30, 1566–1574.

Baraban, S. C., Taylor, M. R., Castro, P. A., and Baier, H. (2005). Pentylenetetrazole induced changes in zebrafish behavior, neural activity and c-fos expression. *Neuroscience* 131, 759–768.

Bazaes, A., and Schmachtenberg, O. (2012). Odorant tuning of olfactory crypt cells from juvenile and adult rainbow trout. *J. Exp. Biol.* 215, 1740–1748.

Bepari, A. K., Watanabe, K., Yamaguchi, M., Tamamaki, N., and Hirohide, T. (2012). Visualization of odor-induced neuronal activity by immediate early gene expression. *BMC Neurosci.* 13:140. doi: 10.1186/1471-2202-13-140

Bianco, I. H., and Wilson, S. W. (2009). The habenular nuclei: a conserved asymmetric relay station in the vertebrate brain. *Philos. Trans. R. Soc. Lond. B Biol. Sci.* 364, 1005–1020.

Carboni, L., Carletti, R., Tacconi, S., Corti, C., and Ferraguti, F. (1998). Differential expression of SAPK isoforms in the rat brain. An *in situ* hybridisation study in the adult rat brain and during post-natal development. *Mol. Brain Res.* 60, 57–68.

Cirulli, F., Pistillo, L., De Acetis, L., Alleva, E., and Aloe, L. (1998). Increased number of mast cells in the central nervous system of adult male mice following chronic subordination stress. *Brain Behav. Immun.* 12, 123–133.

Close, R., Toro, S., Martial, J. A., and Muller, M. (2002). Expression of the zinc finger Egr1 gene during zebrafish embryonic development. *Mech. Dev.* 118, 269–272.

Concha, M. L., Bianco, I. H., and Wilson, S. W. (2012). Encoding asymmetry within neural circuits. *Nat. Rev. Neurosci.* 13, 832–843.

Concha, M. L., Burdine, R. D., Russell, C., Schier, A. F., and Wilson, S. W. (2000). A nodal signaling pathway regulates the laterality of neuroanatomical asymmetries in the zebrafish forebrain. *Neuron* 28, 399–409.

Concha, M. L., Russell, C., Regan, J. C., Tawk, M., Sidi, S., Gilmour, D. T., et al. (2003). Local tissue interactions across the dorsal midline of the forebrain establish CNS laterality. *Neuron* 39, 423–438.

Concha, M. L., and Wilson, S. W. (2001). Asymmetry in the epithalamus of vertebrates. *J. Anat.* 199, 63–84.

Doldan, M. J., Cid, P., Mantilla, L., and De Miguel Villegas, E. (2011). Development of the olfactory system in turbot (Psetta maxima L.). *J. Chem. Neuroanat.* 41, 148–157.

Doving, K. B., Selset, R., and Thommesen, G. (1980). Olfactory sensitivity to bile acids in salmonid fishes. *Acta Physiol. Scand.* 108, 123–131.

Facchin, L., Burgess, H. A., Siddiqi, M., Granato, M., and Halpern, M. E. (2009). Determining the function of zebrafish epithalamic asymmetry. *Philos. Trans. R. Soc. Lond. B Biol. Sci.* 364, 1021–1032.

Frasnelli, E., Anfora, G., Trona, F., Tessarolo, F., and Vallortigara, G. (2010). Morpho-functional asymmetry of the olfactory receptors of the honeybee (*Apis mellifera*). *Behav. Brain Res.* 209, 221–225.

Friedrich, R. W., and Korsching, S. I. (1998). Chemotopic, combinatorial, and noncombinatorial odorant representations in the olfactory bulb revealed using a voltage-sensitive axon tracer. *J. Neurosci.* 18, 9977–9988.

Fuller, C. L., Yettaw, H. K., and Byrd, C. A. (2006). Mitral cells in the olfactory bulb of adult zebrafish (Danio rerio): morphology and distribution. *J. Comp. Neurol.* 499, 218–230.

Gamse, J. T., Kuan, Y. S., Macurak, M., Brosamle, C., Thisse, B., Thisse, C., et al. (2005). Directional asymmetry of the zebrafish epithalamus guides dorsoventral innervation of the midbrain target. *Development* 132, 4869–4881.

Gamse, J. T., Shen, Y. C., Thisse, C., Thisse, B., Raymond, P. A., Halpern, M. E., et al. (2002). Otx5 regulates genes that show circadian expression in the zebrafish pineal complex. *Nat. Genet.* 30, 117–121.

Gamse, J. T., Thisse, C., Thisse, B., and Halpern, M. E. (2003). The parapineal mediates left-right asymmetry in the zebrafish diencephalon. *Development* 130, 1059–1068.

Gaudry, Q., Hong, E. J., Kain, J., De Bivort, B. L., and Wilson, R. I. (2013). Asymmetric neurotransmitter release enables rapid odour lateralization in Drosophila. *Nature* 493, 424–428.

Gilmour, D. T., Maischein, H. M., and Nusslein-Volhard, C. (2002). Migration and function of a glial subtype in the vertebrate peripheral nervous system. *Neuron* 34, 577–588.

Gorelick, D. A., Watson, W., and Halpern, M. E. (2008). Androgen receptor gene expression in the developing and adult zebrafish brain. *Dev. Dyn.* 237, 2987–2995.

Guthrie, K. M., Anderson, A. J., Leon, M., and Gall, C. (1993). Odor-induced increases in c-fos mRNA expression reveal an anatomical "unit" for odor processing in olfactory bulb. *Proc. Natl. Acad. Sci. U.S.A.* 90, 3329–3333.

Guthrie, K. M., and Gall, C. M. (1995). Functional mapping of odor-activated neurons in the olfactory bulb. *Chem. Senses* 20, 271–282.

Hansen, A., and Finger, T. E. (2000). Phyletic distribution of crypt-type olfactory receptor neurons in fishes. *Brain Behav. Evol.* 55, 100–110.

Hansen, A., and Zeiske, E. (1998). The peripheral olfactory organ of the zebrafish, *Danio rerio*: an ultrastructural study. *Chem. Senses* 23, 39–48.

Hendricks, M., and Jesuthasan, S. (2007). Asymmetric innervation of the habenula in zebrafish. *J. Comp. Neurol.* 502, 611–619.

Herrick, J. C. (1948). *The Brain of the Tiger Salamander, Ambystoma tigrinum.* Chicago, IL: University of Chicago Press.

Hikosaka, O. (2010). The habenula: from stress evasion to value-based decision-making. *Nat. Rev. Neurosci.* 11, 503–513.

Hikosaka, O., Sesack, S. R., Lecourtier, L., and Shepard, P. D. (2008). Habenula: crossroad between the basal ganglia and the limbic system. *J. Neurosci.* 28, 11825–11829.

Isogai, Y., Si, S., Pont-Lezica, L., Tan, T., Kapoor, V., Murthy, V. N., et al. (2011). Molecular organization of vomeronasal chemoreception. *Nature* 478, 241–245.

Kazi, J., Shiro, M., Kuchiiwa, S., and Nakagawa, S. (2004). Prolonged expression of c-Fos protein in the lateral habenular nucleus of the japanese monkey (Macaca fuscata) after eye enucleation. *Neurosignals* 13, 130–133.

Kobayashi, Y., Sano, Y., Vannoni, E., Goto, H., Suzuki, H., Oba, A., et al. (2013). Genetic dissection of medial habenula-interpeduncular nucleus pathway function in mice. *Front. Behav. Neurosci.* 7:17. doi: 10.3389/fnbeh.2013.00017

Kuan, Y. S., Gamse, J. T., Schreiber, A. M., and Halpern, M. E. (2007a). Selective asymmetry in a conserved forebrain to midbrain projection. *J. Exp. Zool.* 308B, 669–678.

Kuan, Y. S., Yu, H. H., Moens, C. B., and Halpern, M. E. (2007b). Neuropilin asymmetry mediates a left-right difference in habenular connectivity. *Development* 134, 857–865.

Lau, B. Y., Mathur, P., Gould, G. G., and Guo, S. (2011). Identification of a brain center whose activity discriminates a choice behavior in zebrafish. *Proc. Natl. Acad. Sci. U.S.A.* 108, 2581–2586.

Lauter, G., Soll, I., and Hauptmann, G. (2011). Multicolor fluorescent in situ hybridization to define abutting and overlapping gene expression in the embryonic zebrafish brain. *Neural Dev.* 6:10. doi: 10.1186/1749-8104-6-10

Lee, A., Mathuru, A. S., Teh, C., Kibat, C., Korzh, V., Penney, T. B., et al. (2010). The habenula prevents helpless behavior in larval zebrafish. *Curr. Biol.* 20, 2211–2216.

Letzkus, P., Ribi, W. A., Wood, J. T., Zhu, H., Zhang, S. W., and Srinivasan, M. V. (2006). Lateralization of olfaction in the honeybee *Apis mellifera*. *Curr. Biol.* 16, 1471–1476.

Liang, J. O., Etheridge, A., Hantsoo, L., Rubinstein, A. L., Nowak, S. J., Belmonte, J. C. I., et al. (2000).

Asymmetric nodal signaling in the zebrafish diencephalon positions the pineal organ. *Development* 127, 5101–5112.

Mathuru, A. S., Kibat, C., Cheong, W. F., Shui, G., Wenk, M. R., Friedrich, R. W., et al. (2012). Chondroitin fragments are odorants that trigger fear behavior in fish. *Curr. Biol.* 22, 538–544.

Michel, W. C., and Lubomudrov, L. M. (1995). Specificity and sensitivity of the olfactory organ of the zebrafis, Danio rerio. *J. Comp. Physiol. A* 177, 191–199.

Michel, W. C., Sanderson, M. J., Olson, J. K., and Lipschitz, D. L. (2003). Evidence of a novel transduction pathway mediating detection of polyamines by the zebrafish olfactory system. *J. Exp. Biol.* 206, 1697–1706.

Miyasaka, N., Morimoto, K., Tsubokawa, T., Higashijima, S., Okamoto, H., and Yoshihara, Y. (2009). From the olfactory bulb to higher brain centers: genetic visualization of secondary olfactory pathways in zebrafish. *J. Neurosci.* 29, 4756–4767.

Muto, A., Ohkura, M., Kotani, T., Higashijima, S., Nakai, J., and Kawakami, K. (2011). Genetic visualization with an improved GCaMP calcium indicator reveals spatiotemporal activation of the spinal motor neurons in zebrafish. *Proc. Natl. Acad. Sci. U.S.A.* 108, 5425–5430.

Oka, Y., Saraiva, L. R., and Korsching, S. I. (2012). Crypt neurons express a single V1R-related ora gene. *Chem. Senses* 37, 219–227.

Okamoto, H., Agetsuma, M., and Aizawa, H. (2012). Genetic dissection of the zebrafish habenula, a possible switching board for selection of behavioral strategy to cope with fear and anxiety. *Dev. Neurobiol.* 72, 386–394.

Okuyama, T., Suehiro, Y., Imada, H., Shimada, A., Naruse, K., Takeda, H., et al. (2011). Induction of c-fos transcription in the medaka brain (Oryzias latipes) in response to mating stimuli. *Biochem. Biophys. Res. Commun.* 404, 453–457.

Paul, M. J., Indic, P., and Schwartz, W. J. (2011). A role for the habenula in the regulation of locomotor activity cycles. *Eur. J. Neurosci.* 34, 478–488.

Pfeiffer, W. (1977). The distribution of fright reaction and alarm substance cells in fishes. *Copeia* 4, 653–665.

Polkinghorne, C. N., Olson, J. M., Gallaher, D. G., and Sorensen, P. W. (2001). Larval sea lamprey release two unique bile acids to the water at a rate sufficient to produce detectable riverine pheromone plumes. *Fish Physiol. Biochem.* 24, 15–30.

Prasada Rao, P. D., and Finger, T. E. (1984). Asymmetry of the olfactory system in the brain of the winter flounder, Pseudopleuronectes americanus. *J. Comp. Neurol.* 225, 492–510.

Ramón y Cajal, S. (1995). *Histology of the Nervous System of Man and Vertebrates*. Translated from the French by N. Swanson and L. W. Swanson. New York, NY: Oxford University Press.

Regan, J. C., Concha, M. L., Roussigne, M., Russell, C., and Wilson, S. W. (2009). An Fgf8-dependent bistable cell migratory event establishes CNS asymmetry. *Neuron* 61, 27–34.

Rogers, L. J., and Vallortigara, G. (2008). From antenna to antenna: lateral shift of olfactory memory recall by honeybees. *PLoS ONE* 3:e2340. doi: 10.1371/journal.pone.0002340

Rolen, S. H., Sorensen, P. W., Mattson, D., and Caprio, J. (2003). Polyamines as olfactory stimuli in the goldfish Carassius auratus. *J. Exp. Biol.* 206, 1683–1696.

Sallaz, M., and Jourdan, F. (1993). C-fos expression and 2-deoxyglucose uptake in the olfactory bulb of odour-stimulated awake rats. *Neuroreport* 4, 55–58.

Schmachtenberg, O. (2006). Histological and electrophysiological properties of crypt cells from the olfactory epithelium of the marine teleost *Trachurus symmetricus*. *J. Comp. Neurol.* 495, 113–121.

Signore, I. A., Guerrero, N., Loosli, F., Colombo, A., Villalon, A., Wittbrodt, J., et al. (2009). Zebrafish and medaka: model organisms for a comparative developmental approach of brain asymmetry. *Philos. Trans. R. Soc. Lond. B Biol. Sci.* 364, 991–1003.

Silver, R., Silverman, A. J., Vitkovic, L., and Lederhendler, I. I. (1996). Mast cells in the brain: evidence and functional significance. *Trends Neurosci.* 19, 25–31.

Snelson, C. D., Santhakumar, K., Halpern, M. E., and Gamse, J. T. (2008). Tbx2b is required for the development of the parapineal organ. *Development* 135, 1693–1702.

Speedie, N., and Gerlai, R. (2008). Alarm substance induced behavioral responses in zebrafish (Danio rerio). *Behav. Brain Res.* 188, 168–177.

Sugama, S., Cho, B. P., Baker, H., Joh, T. H., Lucero, J., and Conti, B. (2002). Neurons of the superior nucleus of the medial habenula and ependymal cells express IL-18 in rat CNS. *Brain Res.* 958, 1–9.

Sutherland, R. J. (1982). The dorsal diencephalic conduction system – a review of the anatomy and functions of the habenular complex. *Neurosci. Biobehav. Rev.* 6, 1–13.

Tabor, R., and Friedrich, R. W. (2008). Pharmacological analysis of ionotropic glutamate receptor function in neuronal circuits of the zebrafish olfactory bulb. *PLoS ONE* 3:e1416. doi: 10.1371/journal.pone.0001416

Taylor, R. W., Qi, J. Y., Talaga, A. K., Ma, T. P., Pan, L., Bartholomew, C. R., et al. (2011). Asymmetric inhibition of Ulk2 causes left-right differences in habenular neuropil formation. *J. Neurosci.* 31, 9869–9878.

Thisse, B., Thisse, C. (2004). *Fast Release Clones: A High Throughput Expression Analysis*. ZFIN Direct Data Submission (http://zfin.org). Available online at: http://zfin.org/cgi-bin/webdriver?MIval=aa-pubview2.apg&OID=ZDB-PUB-040907-1

Velez, Z., Hubbard, C. A., Barata, E. N., and Canario, A. V. M. (2005). Evidence for functional asymmetry in the olfactory system of the senegalese sole (*Solea senegalensis*). *Physiol. Biochem. Zool.* 78, 756–765.

Velez, Z., Hubbard, P. C., Barata, E. N., and Canario, A. V. M. (2007). Differential detection of conspecific-derived odorants by the two olfactory epithelia of the Senegalese sole (*Solea senegalensis*). *Gen. Comp. Endocrinol.* 153, 418–425.

Vielma, A., Ardiles, A., Delgado, L., and Schmachtenberg, O. (2008). The elusive crypt olfactory receptor neuron: evidence for its stimulation by amino acids and cAMP pathway agonists. *J. Exp. Biol.* 211, 2417–2422.

Vitebsky, A., Reyes, R., Sanderson, M. J., Michel, W. C., and Whitlock, K. E. (2005). Isolation and characterization of the laure olfactory behavioral mutant in the zebrafish, *Danio rerio*. *Dev. Dyn.* 234, 229–242.

Vize, P. D., Mccoy, K. E., and Zhou, X. (2009). Multichannel wholemount fluorescent and fluorescent/chromogenic *in situ* hybridization in *Xenopus* embryos. *Nat. Protoc.* 4, 975–983.

Waldman, B. (1982). Quantitative and developmental analyses of the alarm reaction in the Zebra Danio, Brachydanio rerio. *Copeia* 1, 1–9.

Walker, C. (1999). Haploid screens and gamma-ray mutagenesis. *Methods Cell Biol.* 60, 43–70.

Wes, P. D., and Bargmann, C. I. (2001). C. elegans odour discrimination requires asymmetric diversity in olfactory neurons. *Nature* 410, 698–701.

Westerfield, M. (2000). *The Zebrafish Book*. Eugene, OR: University of Oregon Press.

Wilhelm, M. (2011). Neuro-immune interactions in the dove brain. *Gen. Comp. Endocrinol.* 172, 173–180.

Zhang, F. Q., Zhou, W. H., Liu, H. F., Zhu, H. Q., Tang, S., Lai, M. J., et al. (2005). Increased c-Fos expression in the medial part of the lateral habenula during cue-evoked heroin-seeking in rats. *Neurosci. Lett.* 386, 133–137.

Conflict of Interest Statement: The authors declare that the research was conducted in the absence of any commercial or financial relationships that could be construed as a potential conflict of interest.

Received: 16 February 2013; paper pending published: 06 March 2013; accepted: 02 May 2013; published online: 21 May 2013.

Citation: deCarvalho TN, Akitake CM, Thisse C, Thisse B and Halpern ME (2013) Aversive cues fail to activate fos expression in the asymmetric olfactory-habenula pathway of zebrafish. Front. Neural Circuits 7:98. doi: 10.3389/fncir.2013.00098

frontiers in
NEURAL CIRCUITS

ORIGINAL RESEARCH ARTICLE
published: 28 February 2014
doi: 10.3389/fncir.2014.00010

Optogenetic perturbations reveal the dynamics of an oculomotor integrator

***Pedro J. Gonçalves*[1,2,3†], *Aristides B. Arrenberg*[4,5*†], *Bastian Hablitzel*[5], *Herwig Baier*[4,6] and *Christian K. Machens*[1,2*]**

[1] Group for Neural Theory, Departement d'Etudes Cognitives, INSERM U960, École Normale Supérieure, Paris, France
[2] Champalimaud Neuroscience Program, Centro Champalimaud – Champalimaud Centre for the Unknown, Lisbon, Portugal
[3] Gatsby Computational Neuroscience Unit, University College London, London, UK
[4] Neuroscience Program, Department of Physiology, University of California San Francisco, San Francisco, CA, USA
[5] Faculty of Biology, Center for Biological Signaling Studies, University of Freiburg, Freiburg, Germany
[6] Max Planck Institute of Neurobiology, Martinsried, Germany

Edited by:
German Sumbre, École Normale Supérieure, France

Reviewed by:
Yoram Burak, Hebrew University, Israel
Yonatan Loewenstein, Hebrew University, Israel

****Correspondence:***
Aristides B. Arrenberg, Department of Developmental Biology, Faculty of Biology, Center for Biological Signaling Studies, Institute Biology 1, University of Freiburg, Hauptstrasse 1, D-79104 Freiburg, Germany
e-mail: aristides.arrenberg@biologie.uni-freiburg.de;
Christian K. Machens, Champalimaud Neuroscience Program, Centro Champalimaud – Champalimaud Centre for the Unknown, Neurociências (26.34), Av. Brasília, Doca de Pedrouços, 1400-038 Lisbon, Portugal
e-mail: christian.machens@neuro.fchampalimaud.org

† These authors have contributed equally to this work.

Many neural systems can store short-term information in persistently firing neurons. Such persistent activity is believed to be maintained by recurrent feedback among neurons. This hypothesis has been fleshed out in detail for the oculomotor integrator (OI) for which the so-called "line attractor" network model can explain a large set of observations. Here we show that there is a plethora of such models, distinguished by the relative strength of recurrent excitation and inhibition. In each model, the firing rates of the neurons relax toward the persistent activity states. The dynamics of relaxation can be quite different, however, and depend on the levels of recurrent excitation and inhibition. To identify the correct model, we directly measure these relaxation dynamics by performing optogenetic perturbations in the OI of zebrafish expressing halorhodopsin or channelrhodopsin. We show that instantaneous, inhibitory stimulations of the OI lead to persistent, centripetal eye position changes ipsilateral to the stimulation. Excitatory stimulations similarly cause centripetal eye position changes, yet only contralateral to the stimulation. These results show that the dynamics of the OI are organized around a central attractor state—the null position of the eyes—which stabilizes the system against random perturbations. Our results pose new constraints on the circuit connectivity of the system and provide new insights into the mechanisms underlying persistent activity.

Keywords: neural integrator, optogenetics, model, zebrafish, oculomotor system, network dynamics

INTRODUCTION

Neural activity deep within the nervous system or close to the motor periphery is largely driven by a combination of intrinsic neuronal properties and recurrent feedback among neurons. Such activity is almost always dynamic, changing either fast, as in central pattern or sequence generators (Marder and Bucher, 2001; Hahnloser et al., 2002), or slowly, as in the neural integrators that have been found at many levels of the nervous system (Robinson, 1968; Pastor et al., 1994; Gold and Shadlen, 2001; Wong et al., 2007; Goldman et al., 2009). A key question in neuroscience is how neural systems generate and control these internal dynamics through links between individual neurons.

One of the simplest and best-studied systems to address this question is the oculomotor integrator (OI) for horizontal eye movements. Neurons in the OI are persistently active with a discharge rate that is directly proportional to the horizontal eye position (Lopez-Barneo et al., 1982; Delgado-García et al., 1989; Fukushima et al., 1992; McFarland and Fuchs, 1992; Aksay et al., 2000). This graded persistent activity typifies a simple form of short-term memory and shares many similarities with the persistent activity found in higher-order brain areas during working memory (Brody et al., 2003; Major and Tank, 2004; Goldman et al., 2009). Several theoretical studies have shown how the persistent activity in the OI can be generated through precise recurrent synaptic feedback among neurons (Cannon et al., 1983; Cannon and Robinson, 1985; Seung, 1996; Seung et al., 2000; Aksay et al., 2007). This body of work has led to a network model of the OI that can essentially reproduce all experimentally measured features in the goldfish, such as the distribution of tuning curves (Seung et al., 2000; Aksay et al., 2007), the correlations between simultaneously recorded neurons, the generation of saccades, or the system's response to unilateral silencing (Aksay et al., 2007). Moreover, several candidate mechanisms were pointed out

to explain the remarkable robustness of the system (Koulakov et al., 2002; Goldman et al., 2003; Moreau and Sontag, 2003).

Here, we show that this network model can be understood as a particular instantiation of a class of models, all of which can explain the shared experimental features across animals. The models are only distinguished by the specific ratio of excitatory and inhibitory inputs to the neurons. Each network model fully specifies the dynamics of the OI. While the dynamics are similar in the system's normal operating regime, they are distinct outside of this regime. Specifically, different network models relax differently toward the persistent activity states. Consequently, different instantiations of the network models make different predictions on how the OI will react to perturbations. These predictions can be tested with the recent advances of optogenetic tools which allow us to manipulate systems with high spatio-temporal precision (Nagel et al., 2003; Boyden et al., 2005; Lima and Miesenböck, 2005; Han and Boyden, 2007; Zhang et al., 2007a,b; Douglass et al., 2008; Huber et al., 2008; Arrenberg et al., 2009; Schoonheim et al., 2010; Fenno et al., 2011).

In systems that are strongly driven by their own internal dynamics, the outcome of a perturbation depends on a combination of the externally applied stimulation and the intrinsic network dynamics. In many instances, neural systems are not sufficiently well known to disentangle the two and make precise and quantitative predictions. The modeling approach we pursue here, however, provides the opportunity to predict the influence of these two competing effects, and by comparison with experimental data, adjust the model, and further our understanding of the system.

Here, we test these model predictions using transgenic zebrafish expressing either halorhodopsin (NpHR), a light-driven chloride pump, or channelrhodospin (ChR2), a light-activated cation channel (Zhang et al., 2007a,b; Arrenberg et al., 2009; Fenno et al., 2011). We show that these instantaneous and small perturbations of the OI network yield crucial insights into the dynamics around the system's normal operating regime. We show that only one of the network models can explain all the data. This model suggests a dominance of unilateral self-excitation, concurrent with a weak coupling between OI cells in the left and right hemisphere. While the stable states still form a line attractor in our new model, the dynamics around the line attractor differ from those of previously proposed models. Specifically, the dynamics are organized around the center of the line attractor which corresponds to the null position of the eyes. This network arrangement could be preferable for the animal, since any perturbations due to noise or synaptic mistuning will cause drifts toward the resting state, instead of drifting toward extreme population activities and eye positions.

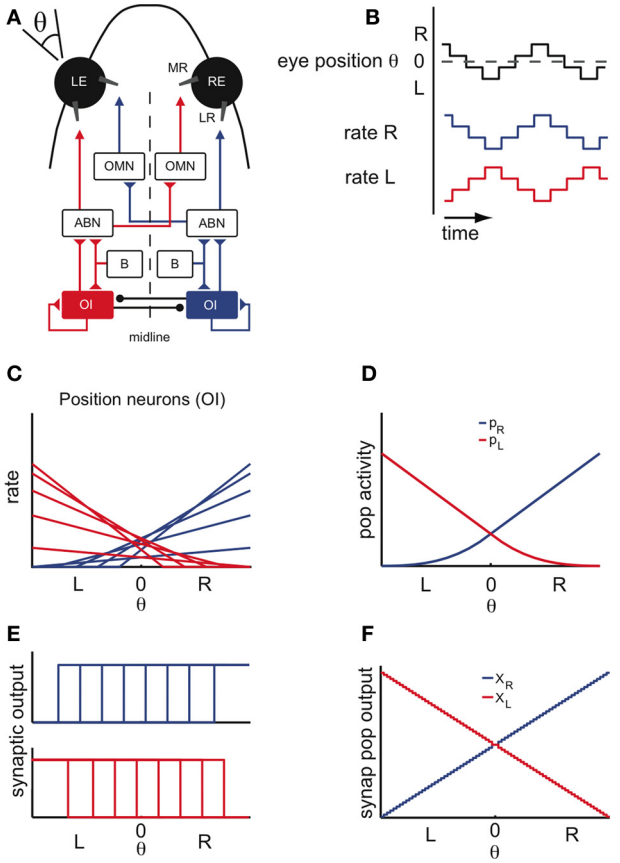

FIGURE 1 | Properties of the oculomotor integrator (OI). (A) Schematic of the oculomotor system for horizontal eye movements. The neurons carrying a position signal are located in the oculomotor integrator (OI) and are thought to integrate (in the sense of calculus) the velocity signal from the burst nucleus (B). Studies of pairwise neural correlations suggest recurrent excitatory connections within each side of the OI and mutual-inhibition between opposite sides. The burst nucleus (B) generates the saccadic eye movements. Position and velocity signals are provided to the muscles (LR: lateral rectus; MR: medial rectus) via excitation of the motoneurons in the abducens nucleus (ABN) and the contralateral oculomotor nucleus (OMN). **(B)** Idealized eye position trace and concurrent position cell activity. In the absence of external visual feedback, the fish moves its eyes spontaneously in scanning cycles, side to side (left side L; right side R; central position 0), alternating stable fixations with saccades. Stable firing rates of the position cells are linearly related to eye position during behavior. **(C)** Tuning curves of right (blue) and left (red) position cells. **(D)** Overall population activity of the left (p_L) and right side (p_R), defined as the sum over the activity of all individual cells. **(E)** Single-cell synaptic tuning curves for right (top) and left (bottom) position cells, with thresholds assumed to span the whole motor range. **(F)** Synaptic population activities of right (X_R) and left (X_L) half of the integrator as a function of eye position. Note the staircase shape of the curves, a consequence of the saturation of the single-cell synaptic activity curves.

RESULTS

NETWORK MODELS OF THE OCULOMOTOR INTEGRATOR

The main anatomical and physiological features of the OI are summarized in **Figures 1A–C**. The OI is located in the hindbrain and composed of two bilaterally symmetric neuronal nuclei (**Figure 1A**). In goldfish, these nuclei consist of around $N = 40$ neurons (Pastor et al., 1994; Aksay et al., 2000), and are referred to as Area I. Quick horizontal eye movements (saccades) are generated by motoneurons in the abducens and oculomotor cranial nuclei (ABN, OMN, **Figure 1A**), which receive a velocity command from excitatory burst cells. The OI receives a collateral of the velocity signal and integrates it in the mathematical sense to create a position signal. The firing rates of the OI neurons are therefore linearly related to eye position (**Figures 1B,C**). The slope of their tuning curves is higher for neurons with more central eye position firing thresholds and lower for neurons with

contraversive, peripheral eye position thresholds (Aksay et al., 2000), a property that has been called "recruitment order" (see Materials and Methods). Neurons from the same side are usually positively correlated, whereas neurons from opposite sides are negatively correlated, suggesting that the two sides are coupled by mutual inhibition and self-excitation (Aksay et al., 2003) as shown in **Figure 1A**. The firing rates of these "position" neurons remain stable in the absence of visual feedback and provide the signal that controls fixation of the horizontal eye position (Mensh et al., 2004).

These observations indicate that the network of position neurons can maintain a continuum of persistent firing rates over several seconds, i.e., the time scale of a typical eye fixation. Since only these persistent firing patterns are observed, the population activity of the two sides must be highly constrained. We use these constraints to reduce the network dynamics to the dynamics of the two interacting populations, which we describe by their summed activity (**Figures 1D,F** – see also **Figures A1D–F**). We will write X_L and X_R for the left- and right-side population output, measured as the resulting post-synaptic conductances (**Figures 1E,F**) and will refer to this population output as "population activity."

As further discussed below, our modeling framework requires that the synaptic currents saturate to balance the progressive recruitment of neurons. Although such synaptic non-linearities are yet to be found in the OI, we here assume their presence. As discussed in the Materials and Methods, we choose step input-output functions to simplify the model tuning but can relax that assumption by using smoother sigmoidal functions (see Appendix). Given this choice, the synaptic output tuning curves are idealized, saturated versions of the firing rate tuning curves (**Figures 1C,E**). For simplicity of the model tuning, we also assume that the single-cell synaptic outputs have thresholds spanning the whole eye position range. This assumption can be reconciled with the data if the synaptic currents have different thresholds (Aksay et al., 2007). In consequence, the left- and right-side synaptic population outputs X_L and X_R resemble a staircase function where each step is caused by the synaptic input-output function of a single neuron (**Figures 1E,F**—see also Materials and Methods). Since there are many neurons involved, these population outputs approximate linear functions of the eye position.

The essence of our network models is shown in **Figure 2** (see also Materials and Methods; a Matlab-based implementation of the models is available in the online supplementary information). In **Figure 2A**, we plot the population activities of **Figure 1F** against each other. Given the staircase shape of the population outputs, the resulting relationship is composed of multiple points on a line, which we here approximate by the red-blue line. This line illustrates the persistent firing states of the system, which range from virtual silence on the right and strong activity on the left side ($X_R = 0$, X_L large, red color) to virtual silence on the left and strong activity on the right (X_R large, $X_L = 0$, blue color). Different eye positions correspond to different points on this line (**Figure 2B**; see also below), and each point corresponds to a stable mode of firing for the network. The line is therefore often called a "line attractor" (Seung, 1996).

In the absence of synaptic input, neurons cease to fire given the neuronal leak. Therefore, for neural activities to be stable in a network in the absence of an external input, the recurrent network input to each neuron has to exactly match the neuronal leak (see Materials and Methods). An imbalance between those would cause either runaway excitation or inhibition. As the eye position moves from left to right, this balance of inputs and neuronal leaks needs to be maintained despite the non-linear distortions (such as thresholds or saturations) introduced by the biophysics of neurons and synapses. The resulting distortions can be compensated by the successive recruitment of neurons from one side and the suppression of neurons from the opposite side, as prescribed by the recruitment order (**Figure 1C**, see Materials and Methods, for details) (Seung, 1996; Seung et al., 2000; Aksay et al., 2007). It is important to note however that to obtain a line attractor in our network models, fine-tuning of the parameters is necessary, since changes in the parameters as small as 1% disrupt the line attractor dynamics.

Given the connectivity of the two sides of the system, the response of a neuron (on the right) is modeled as $x_R = H(aX_R - cX_L + h)$, where parameter "a" determines the weight of the excitatory input from the right population X_R, parameter "c" determines the weight of the inhibitory input from the left population X_L, and parameter "h" models constant external inputs to the network. The function $H(.)$ models the neuron's input-output function, and is either a threshold-linear function (in the case of a firing rate response) or a Heaviside function (in the case of a synaptic output response). The threshold of this input–output function corresponds to the set of points for which $aX_R - cX_L + h = 0$ (orange threshold line, **Figure 2A**). Any (X_R, X_L) combination that is below the orange line will make the right side neuron shown in **Figure 2A** fire.

The recruitment order fixes the thresholds of the neurons on the red-blue line as illustrated by the blue circles for a few example neurons (**Figure 2A**). However, the data do not specify how a neuron would respond to population activities X_R and X_L outside of this line, leaving a degree of freedom that is related to the relative strength of the self-excitatory input "a" and cross-inhibitory input "c" into each neuron (**Figure 2A**). Depending on how this threshold line is chosen for each neuron, the dynamics of the population activities outside of the line attractor change accordingly.

The dynamics of four exemplary models are illustrated in **Figures 2C–F**. Here, the arrows point in the direction in which the population activities evolve from different starting points. In **Figure 2C**, the line attractor is generated through mutual inhibition of the two sides. This configuration corresponds to one of the oldest models proposed for the OI (Cannon et al., 1983). In **Figure 2D**, the external excitatory connections are weakened, yet the resulting detrimental effect is compensated by weak self-excitation. This model was tested by Aksay et al. (2007), and is an extrapolation from the model in Seung et al. (2000): the authors here included mutual inhibition, while keeping orthogonal relaxation dynamics to the line attractor. We note that for both the mutual inhibition model and the weak self-excitation model,

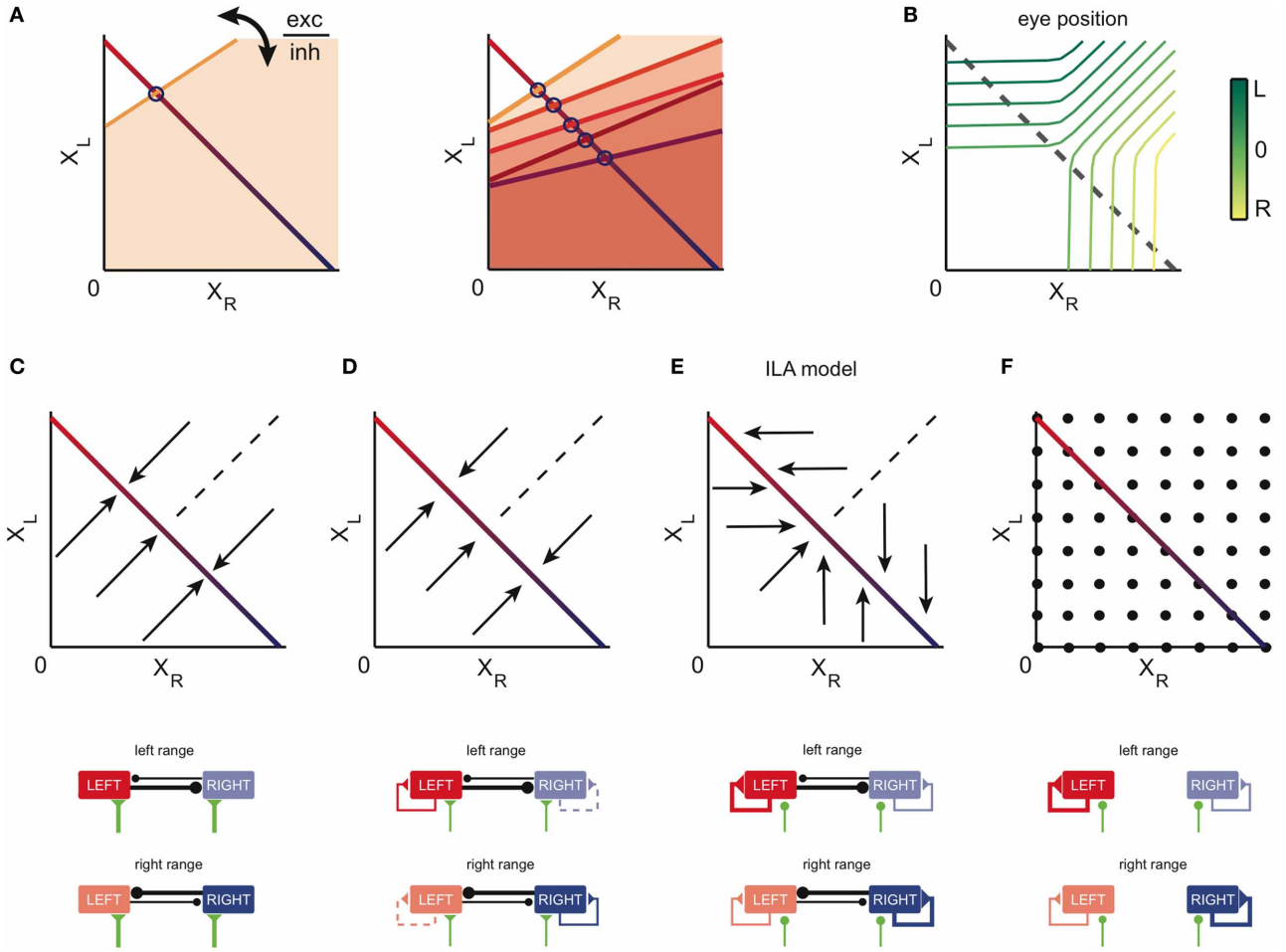

FIGURE 2 | Network models of the OI: construction and dynamics. **(A)** State space of the network model. We assume that the state is uniquely described by the value of the left and right population activities, X_L and X_R. The red-blue colored line corresponds to the stable equilibrium points (line attractor) of the system. Left eye positions are on the red part of the line, right eye positions on its blue part. Blue circles indicate the eye position thresholds of the tuning curves of neurons from the right population along the line attractor. Orange lines correspond to the thresholds of firing for other states of the system (orange shaded areas indicate the corresponding regions above the threshold). Left: the respective slopes are given by the relative strength of the (self-) excitatory and (cross-) inhibitory input into each neuron. Right: as the eyes move from left to right, more and more neurons from the right population get recruited (compare **Figure 1C**). **(B)** Mapping of position population activities onto eye position. The colored iso-lines correspond to different eye positions θ in the (X_R, X_L) space. The gray dashed line indicates the line attractor and thereby the stable equilibrium states of the system. **(C–F)** Example models generated within our theoretical framework. Top: state space of the example models. Arrows indicate the direction of the dynamics. Points indicate stationary states. Bottom: connectivity. Thick, thin, and dashed connectivity lines correspond to strong, weak, and very weak neural connections. The thickness of these connections corresponds to the absolute of the sum of the excitatory post-synaptic potentials (EPSP) and inhibitory post-synaptic potentials (IPSP) of the neurons post-synaptic to the connection. The green lines depict external (e.g., vestibular) inputs to the integrator areas. **(C)** A model in which neural activity is kept persistent due to mutual inhibition between the sides. **(D)** A model in which both mutual inhibition and self-excitation provide the stability of the persistent states. **(E)** The ILA model, which can reproduce the goldfish inactivation results (Aksay et al., 2007). Here, the dynamics are mostly unidirectional and involve only one population on each side (arrows are horizontal or vertical). In the left motor range (bottom panel, top), the left network sustains its firing through self-excitation, whereas the right network is passive, given the weakness of the recurrent inputs. Therefore, the dynamics are dominated by the left network. In the right range (bottom panel, bottom), the inputs and dynamics are reversed. **(F)** A model in which persistent activity is generated through self-excitation only. Here, both sides are completely independent, and every combination of population activities is stable.

the dynamics outside of the attractor are orthogonal to the line, although the mutual inhibition model suggests faster dynamics (as indicated by the longer arrows).

The population dynamics of the model in **Figure 2E** were introduced by Aksay et al. (2007) to account for unilateral inactivation experiments in the goldfish. To obtain such dynamics in our modeling framework, the inhibitory and excitatory connections are set up so that each half of the oculomotor range is stabilized by an independent line attractor (ILA model). As a consequence, the population with the high activity (e.g., X_R) does not change its activity when the other side's population activity (X_L) is reduced. This situation is given when the left half of the system is silenced, which is equivalent to setting $X_L = 0$. Although the dynamics above the line attractor are unconstrained

by experimental data, this model proposes that the dynamics above and below the line attractor are antiparallel to each other. We note that the ILA model captures the same population state space dynamics as the model suggested in Aksay et al. (2007), although the detailed implementation differs from the one in Aksay et al. (2007): the model does not incorporate input-output functions with high synaptic thresholds and uses a different distribution of tuning curves and cross-inhibition (see Materials and Methods).

A last example model is shown in **Figure 2F**. Here, the line attractor is stabilized through self-excitation only, and the inhibitory connections are non-existent. We note that this model is an extension of the model in Seung et al. (2000) from one population to two populations of excitatory neurons. In this case, any point outside of the line will be a potential stable fixed point as well. The system may still be confined to the line in practice, if the burst input during saccades always moves the population activities back onto the line.

UNILATERAL INSTANTANEOUS PERTURBATIONS: MODEL PREDICTIONS

The network models allow us to predict precisely how a perturbation would affect the system. Most importantly, these perturbations can be observed at the level of the eye position which makes the predictions experimentally accessible. To link the population activities to the eye position, we note that the iso-eye-position curves are likely passing through a non-linear transform introduced in the abducens nucleus (**Figure 2B**; discrepancy of position cell and motoneuron tuning curves—for details see **Figure A3** and Materials and Methods). This bending of the curves also provides a simple explanation for the results of unilateral silencing of the OI in which the stabilization of eye position remains functional in only half the motor range and for roughly half the range of population activities (Aksay et al., 2007).

We can then simulate the response of the models to unilateral instantaneous inhibition and excitation, mimicking optogenetic stimulations with NpHR and ChR2, respectively. This idea is illustrated in **Figure 3**, where we focus on one of the network models, the ILA model (**Figure 2E**).

Figures 3A–D shows the effect of inhibiting the left half of the OI in the ILA model. Due to the extra inhibition, the left population activity X_L decreases immediately, as indicated by the arrows in **Figure 3A**. If the eye position before stimulation (initial eye position) is in the left range (black point), the inhibition causes the system state to cross θ isolines transversely so that the eye makes large movements to the right (orange point). If the initial eye position is in the right range, the system state shifts mostly in parallel to θ isolines, and the eye movements are small or null. After switching-off the inhibition stimulus, the system relaxes back to the line according to the dynamics of the intact system (**Figure 3B**). We note that if the initial eye position is in the left range, X_R increases, thereby moving the eye further to the midline. If the initial position is in the right range, X_L increases and X_R does not change after the stimulation is turned-off, so that the system returns to its initial state and the net eye movement is null (**Figures 3A,B**). We can extend this perturbation analysis to all initial eye positions, i.e., all points on the line attractor. Naturally, the results will depend on both the length and intensity of the stimulation. We used a brief stimulation (200 ms) and varying stimulation intensities. The net eye movement resulting from the combination of stimulation and relaxation was measured as the difference $\Delta\theta$ in eye positions just before the stimulation and 1 s after the stimulation (see simulations in **Figure 3C**). Large $\Delta\theta$ are observed when the initial eye position is in the left range, and negligible $\Delta\theta$ when the initial position is in the right range, (**Figure 3D**).

With similar reasoning, we can explore the system's response to excitatory perturbations (**Figures 3E–H**). During left excitation of the ILA model (**Figure 3E**), the left population activity, X_L, increases. After the stimulation, the system state relaxes back to the line attractor with the dynamics of the intact system (**Figure 3F**). If the initial eye position is in the left range, the value of X_L stays constant, and the right population activity, X_R, decreases (**Figures 3F,G**). Altogether, the eye makes therefore large movements to the left. If the initial position is in the right range, the system state moves mostly in parallel to θ isolines and the eye movements are small or null. Consequently, the perturbations $\Delta\theta$ of eye position occur mostly on the ipsilateral side to the stimulation, similar to the inhibitory perturbations, but with opposite sign (**Figures 3G,H**).

In both cases, the perturbations $\Delta\theta$ reflect the relaxation dynamics of the system, i.e., the dynamics of the intact system. By measuring these simulated perturbations for the full range of initial eye positions, we can cover all points of the line attractor. While we have illustrated these perturbations for the ILA model, we can perform similar predictions for the whole range of models. Conversely, we can measure the system's response to perturbations in optogenetic experiments, and then simply infer the dynamics of the system around the line attractor that are consistent with the experiments.

We note that we here modeled NpHR stimulations as divisive and ChR2 stimulations as additive. This distinction is based on electrophysiological recordings from the caudal zebrafish hindbrain (not limited to OI cells) which showed that NpHR stimulations induce a change in firing rate that is dependent on the initial firing rate, while for ChR2 stimulations no such effect was observed in the (small) range of firing rates tested (**Figure A9**). Therefore, for simplicity, we modeled the effect of ChR2 stimulation as being additive. However, assuming a subtractive influence of NpHR on population activity, or a multiplicative influence of ChR2 yields qualitatively the same results (Gonçalves, 2012) (simulation data not shown), and does not impede our ability to infer the overall dynamics from measurements.

UNILATERAL OPTOGENETIC PERTURBATIONS: RESULTS OF NpHR EXPERIMENTS

To measure the effects of such instantaneous perturbations, and in turn infer the dynamics around the line attractor, we used fiber optic stimulations (Arrenberg et al., 2009) in behaving transgenic zebrafish (**Figures 4A,B**, **Figure A7**). Zebrafish are likely to have the same basic oculomotor circuit architecture and physiology as adult goldfish. The zebrafish larvae (5–8 days post-fertilization, dpf) were immobilized in agarose, and the agarose surrounding

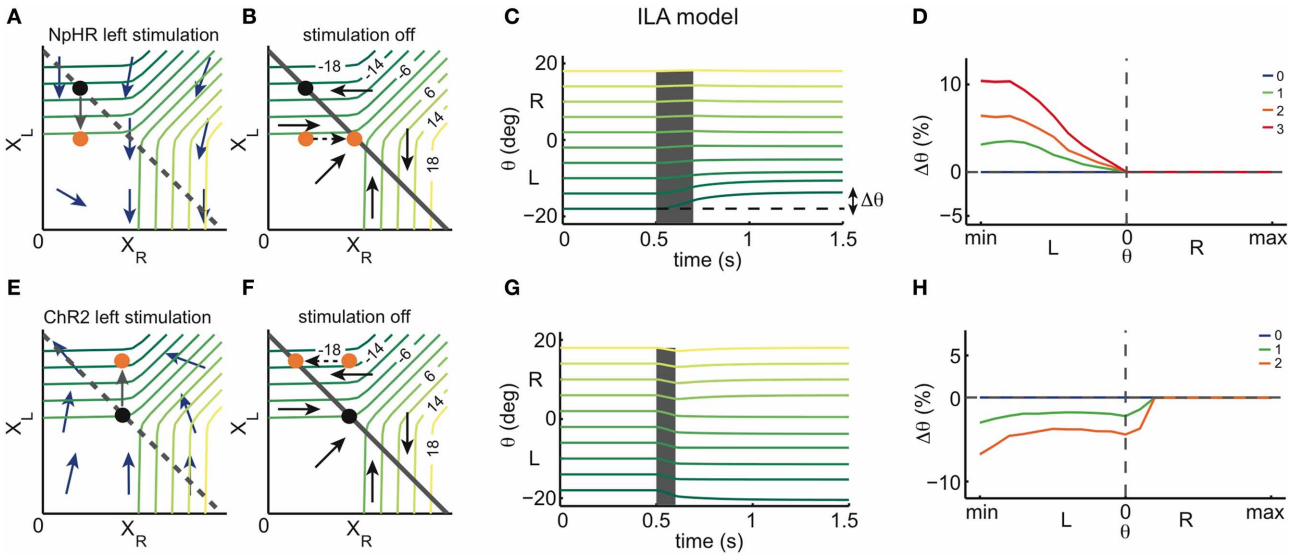

FIGURE 3 | Instantaneous perturbations of the left OI: simulations. **(A)** State space of the ILA model during left inhibitory stimulation. The blue arrows correspond to the dynamics of the model during a stimulation and show that the left population activity is driven toward lower values, while the right population activity is largely unaffected. The black dot represents one example eye position and population activity (X_R, X_L) before stimulation. The orange dot represents the population activity and eye position after stimulation. The gray arrow corresponds to the movement from the initial to the final position. We note that the arrows are enlarged to clarify the direction of the movement, and do not correspond to the magnitude of the movements observed in simulations in **(C)**. The gray dashed line corresponds to the line attractor (which is overridden by the stimulation). **(B)** State space of the ILA network model after stimulation offset. Population activities relax back to the line attractor according to the dynamics of the intact system, given by the arrows. The colored iso-lines are annotated with the corresponding eye positions θ. The gray line corresponds to the line attractor. **(C)** Simulated eye position traces during left stimulation (gray shaded period) for the ILA model. Colors indicate the initial eye position (before the stimulation). The deflections of the eye position depend on the initial eye position. Only initial eye positions in the left half of the motor range can be affected by the stimulation. **(D)** ILA model predictions for the eye position changes, Δθ, as a function of the initial eye position, θ. Color indicates the intensity of stimulation. Positive Δθ correspond to changes toward the right, and negative Δθ correspond to changes toward the left. Eye position changes are measured as a proportion of the whole motor range, and "min" and "max" are the minimum and maximum eye positions of the motor range. For each intensity of stimulation, the respective plot corresponds to averages over 4000 stimulations in each of 21 eye positions. **(E)** State space of the ILA model during left excitatory stimulation. As can be seen by the dynamics, the left population activity increases, while the right population activity is largely unaffected. **(F)** Relaxation to the line attractor after stimulation. **(G)** Simulated eye position traces during left stimulation (gray shaded period). Same format as panel **(C)**. Only initial eye positions in the left half of the motor range can be affected by the stimulation. **(H)** ILA model predictions for the eye position changes, Δθ, as a function of the initial eye position, θ. Simulations were performed as in panel **(D)**.

the eyes was removed. An optic fiber was positioned above the hindbrain to stimulate halorhodopsin (NpHR) or channelrhodopsin (ChR2). The transgenes *Tg(UAS:ChR2(H134R)-mCherry)s1986t* or *Tg(UAS:NpHR-mCherry)s1989t* were driven by the enhancer trap line *Et(E1b:Gal4)s1101t*, resulting in broad expression of ChR2 or NpHR in neurons (Scott et al., 2007; Arrenberg et al., 2009). To localize the zebrafish OI (Miri et al., 2011a) we performed unilateral light stimulations on different rostro-caudal positions of the hindbrain and measured the resulting eye drift magnitudes (**Figures 4B–D**). We chose short 200 ms stimulations to use the same time scale as burst signals which the position neurons typically integrate and to allow the NpHR-induced hyperpolarization to saturate. Two previous reports (Miri et al., 2011a,b) localized the integrator neurons in rhombomere 7 and 8 of the larval zebrafish, based on the corresponding location in the goldfish, two-photon laser ablations and on optogenetic loss-of-function experiments. In these laser ablation and optogenetic experiments, a single location was tested (rhombomere 7 and 8) and found to have an effect on the integrator performance. Here, we used small diameter optic fiber stimulations (50 μm) to test multiple positions (**Figure 4C**). The photoactivated volumes were columns of tissue approximately 10–15 cells wide and protruding through the entire dorsoventral extent of the hindbrain, as judged by Kaede photoconversion experiments (**Figure A7**). The maximal effect was observed around 50–150 μm caudal of the Mauthner cells, somewhat more rostral (rhombomere 5, 6, and 7) than in the previous reports (Miri et al., 2011a,b) (**Figure 4D**, Supplementary Movie 1).

We first focused on inhibitory (NpHR) perturbations. Unilateral stimulations about 100 μm caudal of the Mauthner cells (rhombomere 7 and 6) resulted in a drift of the eye position following a saccade (**Figure 4E**). As in the numerical simulations protocol, we computed the changes Δθ in eye position from just before the stimulation to 1 s after the stimulation. For simplicity, all unilateral stimulation results are plotted as left stimulations. **Figures 5A,B** show the results for a single fish: the eye positions are perturbed strongly in the left range and only weakly in the right range. In the left range, the more eccentric the initial eye position, the higher the elicited change in the eye position toward the right, as indicated by the positive Δθ. Additionally, the

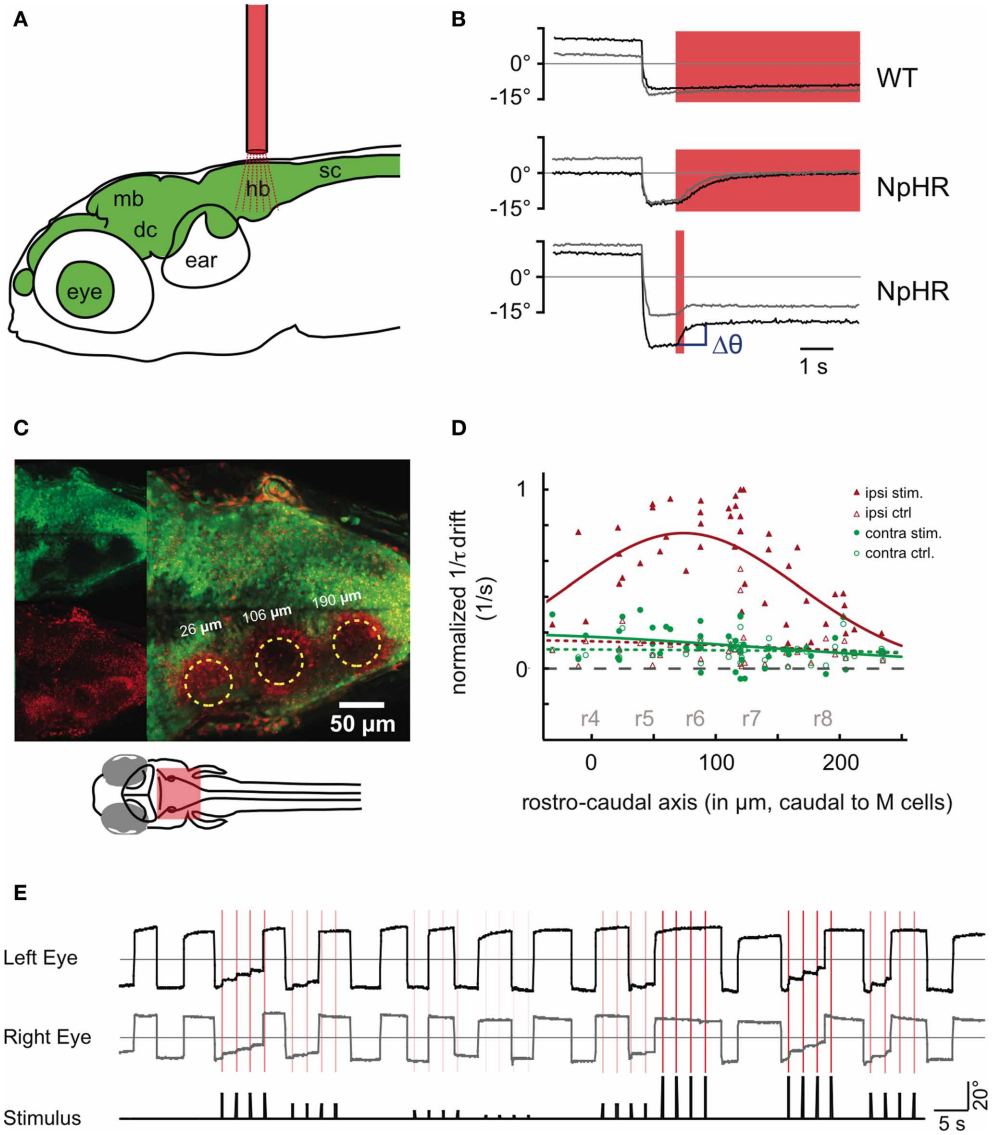

FIGURE 4 | Halorhodopsin (NpHR) stimulation in the hindbrain induces drifts in the eye position. (A) An optic fiber (red) is placed above the zebrafish head (6 dpf) to perturb neuronal activity in the brain (green). hb, hidbrain; sc, spinal cord; mb, midbrain; dc, diencephalon. **(B)** Bilateral NpHR stimulation in the hindbrain induces eye drifts toward the null position. Saccades to the left side are shown for both the left eye (black trace) and the right eye (gray trace). The red shade indicates the stimulation period (6 s or 200 ms). Top: Wildtype animal. Middle: NpHR expressing animal, 6 s stimulation. Bottom: NpHR expressor, 200 ms stimulation. $\Delta\theta$ (blue) is the change in eye position from before the stimulation to 1 s after the stimulation. **(C,D)** An optic fiber (50 µm diameter) was placed at different rostro-caudal positions of the hindbrain and the resulting eye drift magnitudes during unilateral stimulation were measured. **(C)** A 5 dpf hindbrain transgenic for *Et(E1b:Gal4-VP16)s1101t*, *Tg(UAS:NpHR-mCherry)s1989t*, and *Tg(UAS:Kaede)s1999t*. The green channel contains non-converted Kaede signal (upper left), while the red channel contains converted Kaede and mCherry fluorescence. Kaede was photoconverted from green to red at three fiber positions (yellow circles). A maximum projection of selected optical slices is shown. Note: The broadly distributed red speckles are NpHR-mCherry fluorescent protein aggregates. **(D)** Inverse of the time constants of drift τ (in (1/s), see Materials and Methods—Data Analysis) induced by NpHR stimulations at different rostro-caudal levels, relative to the Mauthner cell position ($n = 7$ animals). The data is split according to the eye position before stimulation. Eye positions (averaged across the two eyes) on the same side as the stimulation (left) are plotted in red (ipsiversive) and eye positions on the opposite side (contraversive) are plotted in green. Control trials (open symbols, no light stimulation) are included. The data points are fitted by Gaussian curves. Approximate locations of rhombomeres r4–r8 are indicated in gray. **(E)** Two minutes of recording in a fish with frequent spontaneous eye movements. In this experiment, NpHR was stimulated four times on the left side after the fish made a saccade. Each stimulation is marked as a vertical red line in the recording and the red color intensity of the line corresponds to the light power used for the stimulation. The relative stimulation intensity (black line) is plotted in addition below the eye traces. Panel **(A)** is modified from Figure 4 of Baier and Scott (2009).

magnitude of this change increased with the stimulation intensity. These results become more distinct when averaging over all fish ($n = 24$) (see **Figure 5C**).

The results of the halorhodopsin activation experiments therefore agree with the ILA model that we used as an example network model in **Figures 3A–D**. We note two small differences to the predictions of the ILA model. First, even in the absence of NpHR stimulation, the eyes move slowly toward the null position from the whole motor range. Accordingly, the zebrafish eyes are slightly mistuned, whereas the ILA model is not. Second, the eyes show positive perturbation $\Delta\theta$ at the null position, unlike the model predictions (with $\Delta\theta = 0$ for $\theta = 0$). This difference could be due to uncertainties in the eye position: since the model only predicts positive perturbations, $\Delta\theta \geq 0$, any ambiguity in eye position, be it due to uncertainty of the null position (see Materials and Methods), measurement errors, or hysteresis in the system itself, will shift the average perturbation at $\theta = 0$ to a positive value. Altogether, the dynamics of the OI below the line attractor are therefore well-captured by the ILA model (compare **Figure 2E**). The halorhodopsin inactivation experiments thereby confirm the pharmacological inactivation experiments of Aksay et al. (2007).

UNILATERAL OPTOGENETIC PERTURBATIONS: RESULTS OF ChR2 EXPERIMENTS

Following the same protocol as in the NpHR experiments, we next performed unilateral instantaneous stimulations (100 ms) in animals expressing ChR2 so that one side of the OI was excited (**Figures 5D–F**). Again, all unilateral stimulations were pooled and plotted as left stimulations. When the initial eye position was in the right range, the perturbations generally caused an eye movement toward the left, i.e., toward the null position, as indicated by the negative $\Delta\theta$. In this case, we furthermore observed that more eccentric initial eye positions or higher intensity stimulations induced stronger changes in the eye position. On the other hand, when the initial eye position was in the left range, stimulations elicited very small or no changes toward the right after 1 s, when compared to the control case (**Figures 5D–F**).

For very high ChR2 stimulation intensities, we additionally noted eye movements toward the null position when the initial eye position was on the same side as the stimulation (ipsiversive eye positions; **Figure A6**). Since we are interested in inferring the dynamics in the immediate vicinity of the line attractor, we linearly regressed the magnitude of the drift at very low

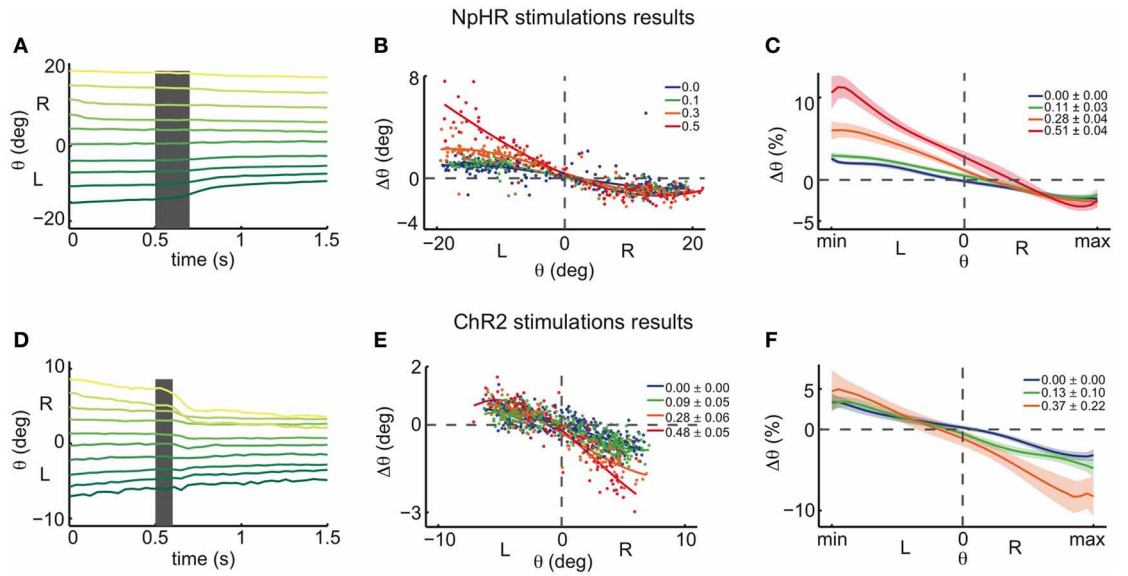

FIGURE 5 | Halorhodopsin and channelrhodopsin instantaneous stimulations of the left OI: experimental results. (A) Experimentally recorded eye position traces, averaged across eyes, during NpHR stimulation (0.5 mW). Averages over 96 eye traces (for each eye) of 1.5 s each, distributed across 10 initial eye position bins, in one fish. Same format as in **Figure 3C**. Stimulation of the left OI elicited movements toward the right in the left range, and small or no movements toward the left in the right range, in agreement with the ILA model predictions from **Figure 3C**. **(B)** Experimentally recorded eye position changes, $\Delta\theta$, as a function of initial eye position, θ, averaged across both eyes (see **Figure A6**, for individual eyes). Data are from the same single fish recording as in **(A)** (for each eye, 372 stimulations, 258 control points, 4 intensity bins, over the course of 3 h). Same format as in **Figure 3D**. The stimulations were binned and colored according to the average stimulation light power in mW for each bin. Spline fits were performed on the binned data to highlight the data trend. **(C)** Spline fit averages across all tested fish ($n = 24$ recordings), same format as in **Figure 3D**. The motor ranges of all fish were normalized before averaging, and the y-axis indicates the eye position changes $\Delta\theta$ as a proportion of the motor range. Legends indicate the light power averages in mW for each bin and respective standard errors across recordings. The shaded envelopes indicate standard errors. **(D)** Experimentally recorded eye position traces during ChR2 stimulation (between 0.37 and 0.56 mW). Averages over 76 stimulations in one fish. Same format as in **Figure 3C**. The stimulation elicited movements toward the left in the right range, and small or no movements toward the right in the left range, in contrast with ILA model predictions from **Figure 3C**. **(E)** Experimentally recorded eye position changes, $\Delta\theta$, as a function of initial eye position, θ, averaged across both eyes (see **Figure A6** for individual eyes). Data are from the same single fish recording as in **(D)** (for each eye, 523 stimulations, 382 control points, over the course of 3 h). Same format and analysis protocol as in panel **(B)**. **(F)** Spline fit averages across all tested fish ($n = 19$ recordings), same format and analysis protocol as in panel **(C)**.

stimulation intensities (**Figure 6A**). In agreement with the data for medium intensities (**Figure 5F**), low intensity stimulation induces eye movements mostly during contraversive eye positions (when the initial eye position is on the other side as the stimulation; **Figures 6B,C**).

The results of the channelrhodopsin activation experiments therefore invalidate the ILA model, as we find that weak excitatory unilateral perturbations of the left OI induce centripetal (toward the null position) and not centrifugal eye movements. Furthermore, we find the strongest effect on the side contralateral to the perturbation, and almost no effect on the ipsilateral side. We note that the perturbations resulting from experimental excitation and inhibition are approximately point-symmetric with respect to the central eye position, ($\theta = 0$, $\Delta\theta = 0$), and not reflection-symmetric with respect to $\Delta\theta = 0$, as proposed by the ILA model.

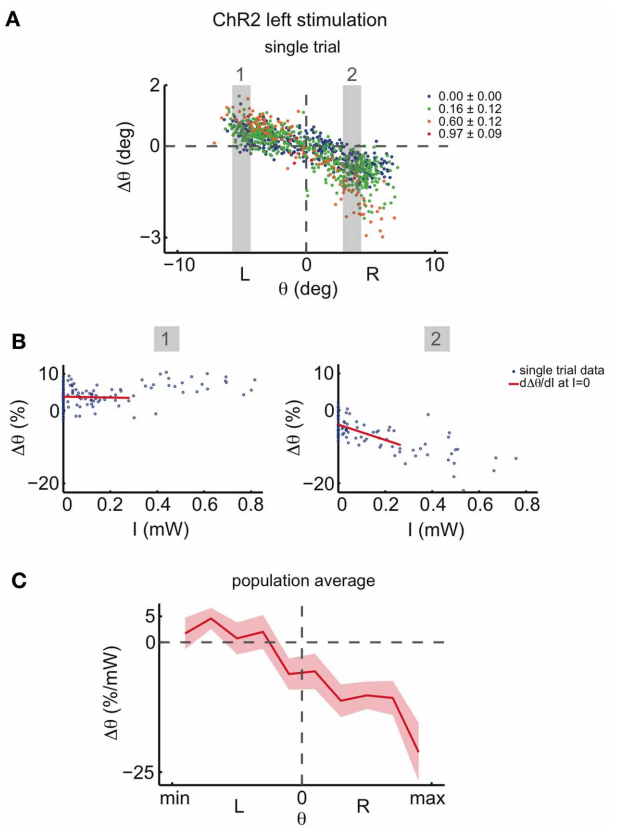

FIGURE 6 | Effect of ChR2 stimulations at very low light intensities. (A) Eye position changes $\Delta\theta$ caused by left side ChR2 stimulation vs. eye position previous to stimulation, for one recording, averaged across both eyes. Data were binned and colored according to light power. Legends indicate the stimulation light power average in mW for each bin. The two gray shaded areas highlight the ranges of initial eye positions θ for which the function between $\Delta\theta$ and intensity of stimulation, I, is analyzed in **(B)**. **(B)** $\Delta\theta$ vs. intensity of stimulation, I, for the two highlighted eye position ranges in **(A)**. In blue are the data points, and in red a linear regression fit for the data in the range $0\,\text{mW} < I < 0.28\,\text{mW}$. The derivative of the function between $\Delta\theta$ and I at $I = 0$ is assumed to be the slope of this linear regression fit. **(C)** Averages of the derivatives $d\Delta\theta/dI$ ($I = 0$) vs. eye position previous to stimulation across all tested fish ($n = 19$ recordings). The plot envelopes indicate standard errors.

THE OI DYNAMICS AROUND THE LINE ATTRACTOR

The results from the NpHR and ChR2 experiments provide us with the means to infer the OI dynamics around the line attractor. Since the inhibitory stimulations yield results similar to those predicted by the ILA model (compare **Figure 3D** and **Figure 5C**), we conclude that the dynamics below the line attractor are similar to those of the ILA model (**Figure 2E**). To obtain the observed point-symmetry of the perturbations (**Figures 5C,F**), however, we need to assume that the dynamics above the line attractor are roughly orthogonal to the dynamics below. Consequently, our experimental results suggest a model with dynamics as shown in **Figure 7A**. Here, the dynamics outside the line attractor are organized around a central point, corresponding to the null position of the eyes (the "null position" or NP model). Although **Figure 7A** illustrates the overall flow of the trajectories toward the line, we note that our line attractors are composed of individual fixed points, such that the fine-scale dynamics change in the vicinity of the line (see **Figure A4C**). Although the fine-scale dynamics predict small changes toward the left in the left range after ChR2 stimulation, these small changes do not appear in the predictions if we assume that the system is noisy.

These conclusions are further supported when we analyze the transient dynamics of the experimental eye movements around the NpHR or ChR2 stimulation period (**Figures 7C–F**). If the initial eye positions are in the left range, the NpHR stimulation generates monotonic eye movements toward the right, as indicated by the transient, positive derivatives of the eye movements (green traces in **Figure 7C**). If the initial eye positions are in the right range, the NpHR stimulation leaves them essentially unaffected. This contrasts with the ChR2 stimulations which transiently affect all eye positions. For initial eye positions in the left range, the stimulation causes transiently biphasic eye movements, as indicated by the negative, then positive derivatives of the eye movements (green traces in **Figure 7E**). In other words, the eye is briefly moved to a more eccentric position, before relaxing back to its original position. For initial eye positions in the right range, we observe an overall negative derivative of the eye movement, generating a centripetal eye position drift (yellow traces in **Figure 7E**).

These transient dynamics match with the population activity dynamics predicted by the NP model (**Figures 7D,F**). Let us focus on the excitatory perturbations. When the left OI is excited, the left population activity X_L increases in the whole motor range (**Figure 7F**). In the relaxation phase, if the initial eye position is in the left range, the system counterbalances the left stimulation by decreasing X_L without changing X_R. Accordingly, eye movements are biphasic and altogether eye position changes only marginally. In the right motor range, the right population activity decreases in the relaxation phase, while the left population activity stays intact, thus causing centripetal (to the null position) eye movements (**Figure 7F**).

Besides explaining the perturbation data well (**Figures 7G,H**), the resulting NP model is also in better agreement with the natural leakiness of the OI, i.e., the slow drift in eye positions that

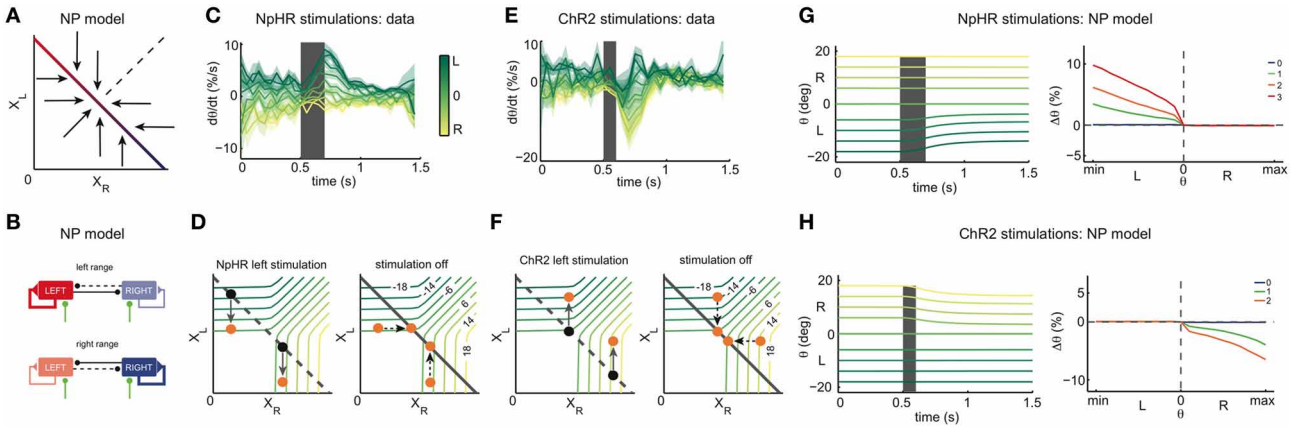

FIGURE 7 | Inference of the OI dynamics. (A) State space of the model inferred from the NpHR and ChR2 instantaneous stimulations: the NP model. In the NP model, the dynamics below the line attractor are orthogonal to the dynamics above the line attractor. **(B)** Effective connectivity of the NP model. In the left range (top), the left network receives stronger self-excitatory and weaker cross-inhibitory inputs than the right network. For low activity of the right network, the left network sustains its firing, whereas for high activity of the right network, the activity of the left network is decreased. In the right range (bottom), the inputs and dynamics are reversed. Overall, cross-inhibition is very weak. **(C)** Average across all experimental recordings of the derivatives of the eye position traces during left side NpHR stimulation (light power between 0 and 0.8 mW). Eye position derivatives are measured as a proportion of the motor range. Colors indicate the initial eye position (before the stimulation). The shaded envelopes indicate standard errors. For initial eye positions in the right half of the motor range (yellow traces), the left side stimulation leads to either small positive deflections of the eye position (i.e., toward the right), or null deflections. In contrast, for initial eye positions in the left half of the motor range (green traces), the left stimulation leads to positive derivatives, i.e., strong rightward eye movements. **(D)** State space interpretation of the transient dynamics in **(C)**. Left: dynamics during left inhibitory stimulation. The left population activity decreases, while the right population activity is largely unaffected. Right: relaxation to line attractor after stimulation. In the right range, the system relaxes to positions close to the position previous to stimulation. **(E)** Average across all ChR2 trials (light power between 0 and 0.28 mW) of the derivatives of the eye traces. For initial eye positions in the right half of the motor range (yellow traces), the left stimulation leads to negative deflections of the eye position, i.e., toward the left. In contrast, for initial eye positions in the left half of the motor range (green traces), the left stimulation leads to biphasic eye movements, first negative derivatives (i.e., leftwards) then positive derivatives (i.e., rightwards). **(F)** State space interpretation of the transient dynamics in **(E)**. Left: dynamics during left excitatory stimulation. The left population activity increases, while the right population activity is largely unaffected. Right: relaxation to line attractor after stimulation. **(G)** NpHR stimulation of the NP model. Left: simulated eye position traces during left stimulation (gray shaded period), with same format as **Figure 5A**. Only initial eye positions in the left half of the motor range are affected by the stimulation. Right: NP model predictions for the eye position changes, $\Delta\theta$, as a function of the initial eye position, θ. **(H)** ChR2 stimulation of the NP model. Left: simulated eye position traces during left stimulation (gray shaded period), with same format as **Figure 5D**. Stimulation causes eye position changes only in the right half of the motor range. Right: NP model predictions for the eye position changes, $\Delta\theta$, as a function of the initial eye position, θ. In the right panels of **(G,H)**, averages were computed over 4000 stimulations in each of 21 eye positions, for each intensity of stimulation.

we observe even in the absence of perturbations (**Figures 5C,F**). First, we note that many (random) mistunings of the synaptic parameters will automatically lead to leaky eye positions. Second, even in the perfectly tuned NP model, the slow centripetal drift will emerge due to the presence of noise in the neuron's firing. Since any internally generated noise in the OI will have similar (if smaller) effects than our perturbations, such noise will cause slow centripetal, and thereby leaky eye movements (see **Figure A4D**).

STIMULATION OF AFFERENTS TO THE INTEGRATOR

While the dynamics that we inferred through the experiments seem perfectly reasonable, the applicability of the NP model to the OI hinges on the correctness of our experiments. One particular concern is that the limits of the integrator cells in the larval zebrafish are not well-established. Hence, we cannot rule out that we may be stimulating efferent motor neurons or afferent inputs (for instance, vestibular neurons) to the integrator. Since stimulation of motor neurons should not lead to persistent eye position changes, we ignore the potential stimulation of those neurons. However, stimulating afferent inputs to the integrator, in addition to the integrator cells remains a possibility. Using the modeling framework, we show below that accidental stimulation of these afferent inputs does not invalidate our conclusions.

We distinguish four possible scenarios for afferent stimulation (**Figure 8A**): in the first two scenarios, afferent stimulation leads to either ipsilateral excitation or inhibition of the integrator cells (violet and green arrows), and in that case our overall stimulation direction does not change in the synaptic population output space. In the other two scenarios, the afferent stimulation leads to either contralateral excitation or inhibition of integrator cells (red and blue arrows), therefore introducing a component to the stimulation which is orthogonal to the pure integrator stimulation.

For a cross-inhibitory architecture, the dynamics above the line attractor are either as in the ILA model (**Figure 2E**), as in the NP model (**Figure 7A**), or somewhere in between (in that case, the dynamics are roughly perpendicular to the line attractor, as in **Figure 2D**). We simulated all four afferent stimulation scenarios for each of the three models, and assumed that afferent stimulation has half the magnitude of the direct

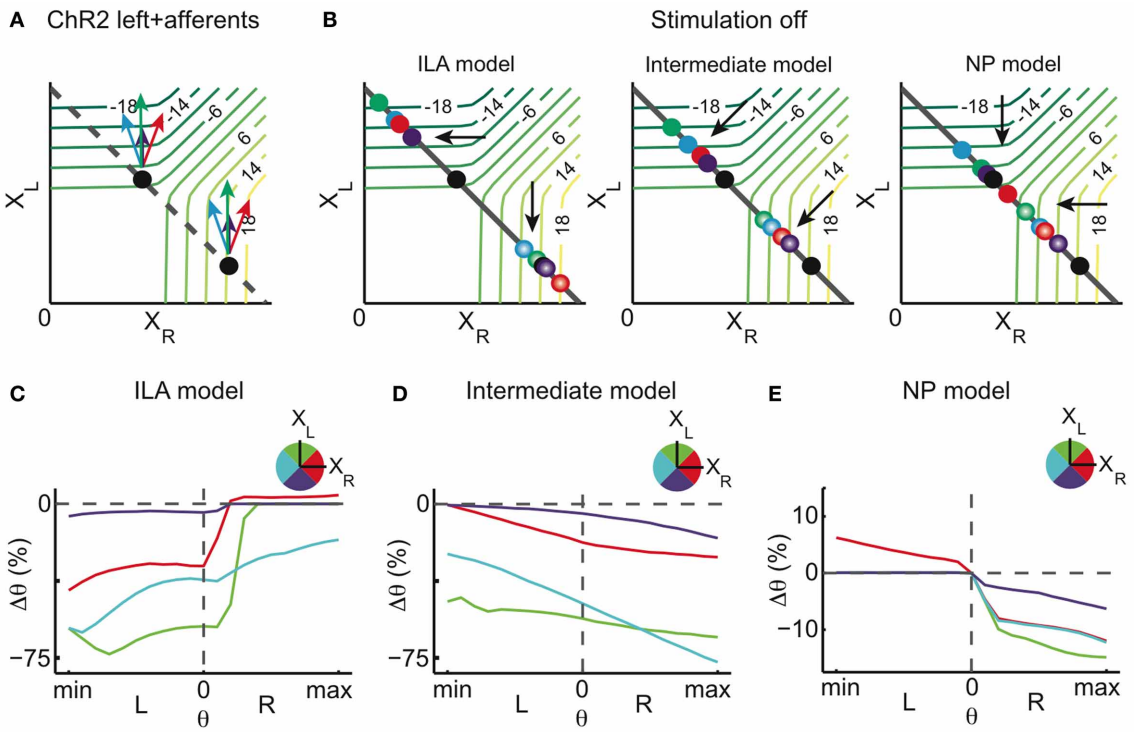

FIGURE 8 | Stimulation of afferents to the integrator (model). Potential ChR2 stimulation of afferents to the left and right half of the integrator in addition to direct ChR2 stimulation of the left OI. **(A)** Stimulation of afferents to the left OI changes the overall magnitude of the stimulation. When affecting excitatory afferent neurons, the stimulation magnitude is increased (green arrows), when affecting inhibitory afferent neurons, it is decreased (violet arrows). When afferents to the right OI are stimulated, an orthogonal component is added to the overall stimulation effect. Additional stimulation of inhibitory afferent neurons pulls the perturbation to smaller values of X_R (blue arrow) whereas additional stimulation of excitatory afferent neurons increases the right population activity (red arrow). **(B)** Relaxation after stimulation for three different models: ILA model, intermediate model, and NP model. The final state of the system is represented by dots, colored according to the respective afferent stimulation. **(C–E)** Eye position changes $\Delta\theta$ caused by direct and afferent stimulation (afferent stimulation has half the magnitude of the direct integrator stimulation) vs. eye position previous to stimulation for the three different models, where color indicates the direction of afferent stimulation in the state space. Neither the ILA model nor the intermediate model lead to results similar to the data: the ILA model mainly leads to centrifugal movements on the ipsiversive side regardless of the type of afferent stimulation; the intermediate model leads to changes toward the left in most of the motor range, for all afferent stimulations. Only the NP model leads to results similar to the data, and especially so when the net afferent stimulation leads to contralateral excitation (red curve). For each intensity of stimulation, the respective plot corresponds to averages over 4000 stimulations in each of 21 eye positions.

integrator stimulation. As can be seen in **Figures 8B–E**, neither the ILA model nor the intermediate model produce results similar to the data (regardless of the type of afferent stimulation). Only the NP model leads to the results observed in the data.

Furthermore, the NP model provides an explanation for the effect of the high intensity stimulation mentioned earlier (compare **Figure A6**): if at high intensity, unilateral ChR2 stimulation also excited the contralateral side via light scattering, then the NP model would indeed predict centripetal eye drifts on the ipsilateral side (**Figure 8E**, red curve).

CONNECTIVITY IN THE INTEGRATOR

In conclusion, the NP model is the only candidate model within our theoretical framework that agrees with all aspects of the data. Most importantly, these dynamics suggest a different connectivity than implied by the previously proposed models. The respective, effective connectivities for the NP model are shown in **Figure 7B**. The dynamics are mediated by weak mutual inhibition and a self-excitation whose effective strength depends on eye position, suggesting that both sides are almost, albeit not completely, decoupled, in line with previous findings in the goldfish (Debowy and Baker, 2011). To keep the self-excitation in check, external (e.g. vestibular) inputs to this model are inhibitory. A detailed description of the implementation of the network models can be found in the Materials and Methods.

DISCUSSION

SUMMARY

We showed that a whole range of network models could account for the set of electrophysiological features that have been measured in OIs across animals of different species. These models differ from each other by the relative strength of self-excitation and mutual inhibition, and the respective dynamics prevailing in the population activity state space outside of the line attractor. To test these models and experimentally unveil the dynamics of the OI, we performed optogenetic perturbations in the larval zebrafish. Using the silencer NpHR, we found that unilateral

light stimulation induced eye movements back to the midpoint, if the eye position prior to the stimulation was on the same side as the stimulation. The experimental results for NpHR in larval zebrafish were in accordance with results from goldfish using inactivation with lidocaine (Aksay et al., 2007), therefore corroborating the previously proposed ILA population dynamics. However, we found that unilateral ChR2 stimulations did not have the opposite effect to NpHR stimulations predicted by the ILA dynamics, i.e., centrifugal (away from the null position) eye movements on the stimulation side (ipsiversive eye positions). Instead, ChR2 stimulations had a centripetal (toward the null positions) effect on eye positions on the side opposite to the stimulation (contraversive eye positions).

Hence, perturbations always tend to drive the eye positions toward the midpoint, indicating that this point is the focus of the OI dynamics. Consequently, we inferred the dynamics around the line attractor from these experiments, and named the resulting model the null-position or NP model. This model suggests an OI architecture with strong self-excitation and weak cross-inhibition. Only a specific combination of excitation on one side and inhibition on the other will lead to actual changes in the position signal as required in saccadic eye movements (e.g., movements from one range to the opposite range) (Gonçalves, 2012). Interestingly, our results can at least in part explain the findings in pharmacological experiments where glutamate or GABA agonists were injected in the OI. Both an increase in excitation as well as an increase in inhibition resulted in centripetal eye movements, much as in our experiments (Arnold et al., 1999).

EXPERIMENTAL FEATURES AND LIMITATIONS

In the presented study we show how optogenetic experiments can be combined with modeling to infer the dynamics of a neural circuit module for integration. In the last few years, the field of optogenetics has provided a powerful set of techniques to perform gain- and loss-of-function experiments (reviewed in Zhang et al., 2007a; Luo et al., 2008; Fenno et al., 2011) and has been applied to zebrafish (Szobota et al., 2007; Douglass et al., 2008; Arrenberg et al., 2009; Baier and Scott, 2009; Zhu et al., 2009; Schoonheim et al., 2010). A fundamental problem in interpreting the effects of optogenetic stimulations is that a system's response is a combination of the stimulation magnitude and the intrinsic network dynamics. Indeed, the eye movements induced through the optogenetic perturbations depended on both the light-intensity, i.e., the strength of stimulation, and on the eye position, i.e., the internal state of the system prior to stimulation. To understand these interdependencies, we relied on network modeling (Seung, 1996; Seung et al., 2000; Goldman et al., 2003; Eliasmith, 2005; Aksay et al., 2007). In turn, the mismatches between the model predictions and the experimental results allowed us to constrain the class of feasible network models and thereby improve our understanding of the OI. This general approach illustrates the importance of the internal state of a system during a perturbation. Wherever this internal state is at least partially known, optogenetic perturbations can provide useful clues toward the underlying network dynamics.

In our experiments we made use of a Gal4 driver line that drove strong expression broadly in neurons. While local stimulation in this line led to marked behavioral changes, the manipulation was not specific to the neural integrator. The neural integrator in larval zebrafish is distributed across approximately 150 μm in the hindbrain of the larval zebrafish (Miri et al., 2011a), with non-integrator neurons interspersed between the cells with position signals. However, our results are not easily explained by a stimulation of these non-integrator neurons. First, both NpHR and ChR2 stimulation induce stable and persistent changes in eye position. This persistent change makes an influence of the motoneurons that lie in close rostral proximity to the integrator unlikely. Exclusive motoneuron stimulation should cause the eyes to move back to the original position immediately after stimulation offset, an effect we did not observe. Second, we may have stimulated cells which project to the integrator such as the saccade-generating neurons. However, saccade generating neurons are only active during saccades and unilateral stimulation is therefore expected to only change the saccade frequency (Schoonheim et al., 2010) and have no effect in-between saccades. Nevertheless, a low level stimulation of the saccade-generating neurons could have occurred without the generation of a measurable saccade: in that case, given that saccade-generating neurons excite the ipsilateral OI and inhibit the contralateral OI, a perturbation of these neurons would cause an indirect stimulation of the integrator neurons roughly in the same direction as the direct integrator stimulation, therefore not invalidating the interpretation of our results. Third, we may have affected some of the vestibular inputs to the OI. However, even in this scenario, our conclusions about the integrator dynamics hold up. Since vestibular inputs are included in the network models, we can simply simulate their accidental stimulation. As shown in **Figure 8**, accidental stimulation offsets the magnitude of induced eye drifts, but overall does not alter their eye position dependence. Within the range of models considered, the data can therefore only be explained by the NP model, but not by the other models.

We have stimulated excitatory and inhibitory integrator cells at the same time, which could potentially lead to unexpected network effects, e.g., due to induced imbalances of excitation and inhibition within the network. However, several observations support our interpretation of the data. First, electrophysiological recordings in the hindbrain of the same zebrafish lines used in this study suggest that more than 80% of NpHR expressing cells were significantly silenced during illumination and more than 90% of ChR2 expressing cells showed an increase in firing rate upon illumination (Arrenberg et al., 2009). Second, NpHR stimulation results are in agreement with the pharmacological inactivations in the goldfish integrator (Aksay et al., 2007), therefore confirming the inhibitory nature of the NpHR stimulations on the integrator. Third, ChR2 stimulation leads to different results than NpHR stimulation, which is proper inhibition. Fourth, both ChR2 and NpHR experiments were performed with the same Gal4 driver line. Therefore, if ChR2 stimulation led to net inhibition of the integrator, then NpHR stimulation would lead to excitation of the integrator which is ruled out based on the second observation. While these results suggest that optogenetic manipulations of the neural integrator changed the network activity in the expected direction, future zebrafish lines, e.g., with specificity for excitatory or inhibitory neurons, will facilitate the dissection of this circuit.

One could hypothesize that the effect of ChR2 stimulation saturates or reverses (depolarization block, Kleinlogel et al., 2011) with increasing stimulation intensities or for highly active cells. Our previous electrophysiological recordings provided no evidence for such an effect (Arrenberg et al., 2009, **Figure A9**). More importantly, this possibility is not supported by the eye movement data in the range of intensities analyzed, since the eye movements scale linearly with the stimulation light intensity (**Figure 6B**). Also, the effect does not reverse at high light intensities (**Figure A6**). As a final note, the modeling framework already assumes that the synapses of highly active neurons are saturated, so that, at least within the model, ChR2 stimulation does not affect these neurons.

In this study, we deliberately focused on the dynamics in the neighborhood of the stable eye position states. Consequently, our analysis was restricted to stimulation with low or medium light intensities. The NP model, however, makes predictions for any stimulation intensity, opening the question of what happens when the stimulation intensity is increased. As shown in the **Figure A6**, for high NpHR stimulation intensities, we additionally found small centripetal movements when the eye position was on the side opposite to the stimulation. For high ChR2 stimulations, we found centripetal eye movements when the eyes were on the same side as the stimulation. In the NP model, this would require a change in the dynamics far away from the line attractor, requiring the arrows to bend further toward the midline. While it seems unlikely that the effects at higher light intensities can be explained through scattering of light into the other hemisphere (data not shown), the effect could potentially be explained through strong stimulation of vestibular inputs. Furthermore, we notice that strong ChR2 stimulation could synchronize the activities of cells, which may have a range of effects, including complete shutting down of persistent activity (Dipoppa, 2012). We therefore refrained from including these observations in the model.

MODEL FEATURES, LIMITATIONS, AND PREDICTIONS

Integrators are ubiquitous in the brain and are involved in several important computations. For instance, in decision-making tasks requiring sensory integrations, neurons in the lateral intraparietal cortex behave similar to integrators (Gold and Shadlen, 2001; Wong et al., 2007). In working memory tasks, neurons in the prefrontal cortex exhibit almost linear dynamics during the times in which an animal needs to remember a stimulus, similar to integrators operating in several dimensions (Singh and Eliasmith, 2006; Machens et al., 2010). In the head direction system, a head velocity signal is integrated into head position (Zhang, 1996).

In previous line attractor models, it has generally been assumed that noise causes random drift along the line (Seung, 1996). While this is true in models with orthogonal dynamics around the line (such as the model illustrated in **Figure 2D**), in the case of the NP model the relaxation to the line has a preferred direction, therefore causing a systematic drift toward the null position. The term "line attractor" for the NP model is therefore strictly only valid in the limit of vanishing noise. For large noise levels, the model shows flow toward the central eye position with equivalent speed from every point in the state space. Hence, one could interpret the NP model as suggesting that the OI operates like a single fixed point, and not a line attractor, as extensively suggested in previous literature. However, for large noise levels, we can re-tune the NP model to recover the NP dynamics in the proximity to the line by implementing stronger cross-inhibition (simulations not shown). In any case, random perturbations of the NP model (such as noise) are unlikely to cause a centrifugal drift of the eye position.

Given the centripetal drift suggested by the NP model, we hypothesize that the OI features dynamics with a higher degree of built-in "safety" than previously thought. The OI has been observed to be leaky on longer time scales, both in goldfish and zebrafish (Mensh et al., 2004; Miri et al., 2011a). This leakiness may be a behaviorally advantageous feature, since, by bringing the system to the central position by default, it enables the relaxation of the eye muscles. Yet even higher brain systems may rely on such a built-in leakiness. In working memory tasks that employ graded persistent activity (Machens et al., 2005), for instance, a tendency to drift toward the central point while memorizing a sensory stimulus could explain the psychophysical errors that are known as contraction bias (Ashourian and Loewenstein, 2011).

While this built-in "safety" may help against noise in the system, it does not solve the fine-tuning problem, i.e., the instability of the line attractor against perturbations in the synaptic weights in the network. Indeed, this fine-tuning problem is a separate problem, somewhat orthogonal to the problems that we have investigated here, for which several solutions have been proposed (Koulakov et al., 2002; Goldman et al., 2003; Moreau and Sontag, 2003).

While we here have assumed that neural integration in the oculomotor system is generated through precise recurrent feedback in a neural circuit, in previous literature single-cell mechanisms have been put forward to explain neural integration observed in multiple areas in the brain. In particular, following an experimental demonstration of integration in individual cells from the entorhinal cortex (Egorov et al., 2002), a body of theoretical work has proposed several biophysical mechanisms which could underlie single cell integration, dispensing synaptic feedback (Loewenstein and Sompolinsky, 2003; Fransén et al., 2006). In the OI, unilateral disruption of the connectivity leads to neural activity drifts with time constants which are typically above 1 s (Pastor et al., 1994; Aksay et al., 2007), suggesting that single-cell mechanisms possibly play a role in the process of integration. However, single-cell mechanisms remain largely uncharacterized in the integrator, and therefore we here have followed the network mechanisms hypothesis as in previous studies of this system (Seung, 1996; Aksay et al., 2007). The contribution of single-cell mechanisms to the slow dynamics in the integrator is a challenge for future research.

We also note that our network model is a rate-model, in which the activities of individual cells are described by rates rather than precise spike times. Although we lose biophysical realism with this type of model, we gain analytical tractability, a very useful asset in interpreting experimental results within a theoretical framework, and in constructing models in accordance with data. Since the position cells exhibit persistent activity with regular firing (Aksay et al., 2003), temporal averages of spiking events are a good

qualitative description of the system. Nevertheless, an equivalent model with spiking neurons could be built as shown in Seung et al. (2000), Eliasmith (2005).

Given the weak mutual-inhibition, the NP model behaves close to a system with a plane of stable fixed points (see **Figure 2F**), and shows slow dynamics around the line. We note that the relaxation of the eye positions after stimulation is indeed slow (on the order of 200 ms). However, these slow dynamics could be reflecting the dynamics of the muscle physics rather than the slow dynamics of the integrator. Future work should show whether such slow dynamics can indeed be observed.

Our network model features multiple stable fixed points, which suggests that the eye positions corresponding to these fixed points should be held comparatively longer than eye positions in-between the fixed points. However, in our data, the system seems to visit a range of eye positions in a homogeneous way (both during NpHR stimulation and during spontaneous, slow eye position decay), which contrasts with the prediction of our model. Such homogeneity could be due to external factors to the integrator, such as small saccadic commands causing smooth eye movement fluctuations, or the dynamics of the motor neurons and muscles. Nevertheless, the homogeneity found in the data challenges our hypothesis of discrete fixed points in the integrator and suggests further studies to elucidate this question.

Our modeling framework assumes a specific mapping from network activity to eye position, based on the difference between the tuning curves of position neurons and motor neurons (see Materials and Methods). Although this assumption is essential in our framework to account for the unilateral inactivation results in Aksay et al. (2007), one could relax it and assume linearity between population synaptic outputs and eye position by introducing high synaptic thresholds in the same fashion as in Aksay et al. (2007). However, we believe that the non-linear mapping is most likely present in the system and should be included in future modeling studies of the oculomotor system.

In a recent study (Miri et al., 2011a), zebrafish position neurons were shown to have variable timescales of integration, so that the associated relaxation time constants varied across neurons over one order of magnitude. This suggests that the dynamics of the OI could be high-dimensional (on the order of the number of neurons), in contrast with our line attractor model, which is implemented with homogeneous time constants across neurons and has low (2D) dimensional dynamics. Given that in this study we are interested in the dynamics of the population activities, the details of single-cell time constants do not affect our conclusions. In the future, it will be interesting to perform optogenetic stimulations and at the same time measure the activities of the position cells to explore the full state space, and realize the dimensionality of the system's dynamics.

Our models belong to a series of works suggesting that the OI builds up a line attractor by a balance between neural saturation and progressive recruitment of neurons to compensate such saturation (Seung, 1996; Seung et al., 2000; Aksay et al., 2007). Future work should specifically target the validity of this assumption as it is crucial for the whole modeling framework. Specifically, this assumption predicts that neurons have no responsibility or influence on eye positions that are below their firing threshold or that are sufficiently above that threshold (when they run into saturation). This prediction could e.g., be tested with single-cell ChR2 stimulation. Excitatory stimulation of different cells would then lead to movements in different eye ranges, enhancing the fact that different neurons are responsible for different stable activities on the motor range (Gonçalves, 2012). Consequently, combining single-cell optogenetics with the framework here designed has the potential to provide even deeper insights into the detailed structure of the OI in the future.

MATERIALS AND METHODS

EXPERIMENTS

Animals

For all experiments, we used zebrafish larvae between the age of 5 and 8 dpf. Animals were transgenic for a combination of the following transgenes: *Et(E1b:Gal4)s1101t*, *Tg(UAS:NpHR-mCherry)s1989t*, *Tg(UAS:Kaede)s1999t*, *Tg(UAS:ChR2-mCherry)s1986t*. In addition, the larvae were mutant for the *mitfa*/*nacre* gene (*mitfa*^{s170}, *mitfa*^{s184}, or *mitfa*^{b692} alleles), which rendered the skin transparent and facilitated fiber optic stimulation as well as eye position detection. Siblings that did not express NpHR or ChR2 served as control groups and are labeled wt here. Adult fish were either transgenic for *Et(E1b:Gal4)s1101t* or for the optogenetic responders, since keeping optogenetic expressors in the s1101t line would have resulted in variegation of the expression. Embryos/larvae were raised in the dark and not fed. For each experiment, about 4 clutches were screened and the strongest expressors were kept.

Many Gal4s1101t/UAS:NpHR expressing larvae had non-inflated swim bladders or showed only infrequent eye movements. For this reason, each mounted larva was observed for 1 min under a stereoscope and only larvae that showed saccades in both directions and good peripheral eye fixations were used for the experiments. This way, only the best behaving 20% of the mounted larvae were used. Control larvae were screened the same way, although a higher percentage of larvae could be used for experiments. The screened NpHR expressing and non-expressing larvae had similar eye drift rates in the absence of stimulation (see Figure 4 in Miri et al., 2011a). The magnitudes of the induced eye position drifts were somewhat variable between animals stimulated at the same position, which we attribute to the expression level/variegation variability between animals. For example, in one animal in **Figure A8**, we noted a patch of cells in which NpHR expression was absent, which resulted in a much reduced effect on eye position (see points [0.08, 86 μm] and [0.15, 86 μm] for the left and the right eye in the ipsi stim. condition). We excluded 5 animals from the analysis in **Figure 5F**, since the induced eye position changes were much smaller than in the majority of animals.

Mounting

Larvae were mounted in a drop of low-melting agarose (1.6%) in a petri dish (35 mm diameter). A platinum wire (100 μm in diameter) glued to a pasteur pipette was used to flatten the liquid agarose drop by moving the wire at the perimeter of the drop and thus increasing the agarose-covered area in the dish, so that the height of the liquid approximately matched the height of the

larva. This step took 10 s and ensured that the optic fiber could be placed close to the skin in the experiment. Next, we used the wire to position the larva dorsal side up. The agarose solidified for 5–10 min and egg water was added. A second platinum wire (100 μm) that was flattened at the tip and bend 70° about 2 mm from the tip was used to make agarose incisions, moving the platinum wire sideways so that the flattened part acted like a knife. Sometimes the agarose would lose its adhesion and we found that using a fresh petri dish for every fish ameliorated this problem. Also, the fish sometimes managed to escape and we found that inserting the platinum wire directly at the eye and moving it outwards worked better than the other way round. Two blocks surrounding the eyes were cut and the flat side of the platinum wire was now used to scoop the blocks out. The stereoscope backlight was set at an angle (dark field) to visualize the cut agarose and make sure that the agarose surrounding the eyes was completely removed. After 3 min of rest, the frequency of eye movements was observed (see Animals). To minimize water evaporation, a dish lid was placed on the petri dish in some of the recordings. The dish lid had a 1 cm diameter hole to allow for the placement of the optic fiber.

Laser stimulation

For laser stimulations, we used an AOTF to couple lasers of three different wavelengths (633, 561, 488 nm) into a multimode optic fiber. We made use of the laser system of a disassembled confocal microscope. For UV photoconversions, we manually switched the stimulation fiber to a fiber coupled UV laser (355 nm). Fiber preparations were described previously (Arrenberg et al., 2009). The AOTF was used to modulate the laser intensity by providing an analog voltage from the DAQ device connected to the computer. For some experiments we used a multi-laser system from Ikecool (Anaheim, CA), however the analog modulation was not good enough to precisely control light intensity on a millisecond-basis (significant baseline light at 0 Volts and the intensity was not stable enough after a switch from 0 Volts to almost full power). We recommend the inclined scientist to rather buy a system from Toptica (Munich, Germany) or Omicron (Rodgau-Dudenhofen, Germany). The optic fiber (including Thorlabs' FT030 protective tubing) was placed in a glass pipette with an angled tip. The pipette was mounted on a fine micromanipulator and the fiber was positioned over the hindbrain. While x-y position could be judged easily by looking through the stereoscope, the z-positioning was more difficult. In cases in which the z-position was unclear, we used the fine micro-manipulation to lower the fiber tip slowly until (a) the mechanic strain on the agarose moved the skin of the fish slightly or (b) until the fish startled. We then moved the fiber back up by a small distance (≈20 μm).

Experimental setup

The larva was placed under a stereoscope and a custom-built LED array was used as a backlight. White LED light was used to position the animals and IR LED light (850 nm) to image the head with a CCD camera (up to 60 Hz, TheImagingSource, Bremen, Germany). During the experiment, dim room lights were kept on and sometimes a weak white backlight was used in addition so that the experiments were performed under low light intensity and low contrast conditions. We did not record in the dark, because wildtype animals showed a behavioral response to the stimulation light in the dark, which was much reduced or absent in the presence of the backlight (Miri et al., 2011a) (the larvae probably see some of the scattered stimulation light). We note that larval post-saccadic eye fixations were somewhat leakier in the dark (when compared to low light conditions), suggesting that larvae were using visual feedback to improve ocular stability. However, this effect was small in comparison to eye position changes induced by medium light intensities, so that we are confident to be measuring the integrator performance in our experiments. A custom-written LabVIEW program (National Instruments, Austin, TX) was used to image, record angular eye positions, and to trigger stimulations via a NI USB DAQ box. Images were acquired at 30–45 Hz and particle analysis (NI Vision) was used to detect eye positions and write them to a text file (together with the stimulation time points) for later analysis. Eye positions were measured and plotted in real time and fiber optic stimulations were triggered based on them. In most experiments a single 200 ms stimulation of constant intensity was delivered automatically 1 s after the eyes had made a saccade. In some experiments four consecutive stimulations were delivered for each saccade (1, 3, 5, and 7 s after the saccade). The stimulation intensities were chosen randomly: we either used five fixed intensities or the computer picked values from an exponential distribution of intensities that biased toward smaller intensities. No stimulation was applied after every third saccade, and these periods served as our control trials. Recordings typically lasted for at least 30 min and up to 12 h. The LabVIEW program can be requested from the authors.

DATA ANALYSIS

The files containing eye position trace and stimulation data were analyzed with custom algorithms using MATLAB. We only analyzed the first 3 h of each experiment, since in some recordings (without dish lid) water evaporation affected the camera focus and thereby the correct detection of eye position angles. The induced eye movements were measured as the change in eye position from stimulation start to 1 s after stimulation start. Most induced eye movements consisted of a single monotonic drift that was completed within 400 ms after stimulation. However, a 1 s interval was chosen to account for potential variations of the duration of the post-stimulation drift. The eye position change, averaged across left and right eye, was then plotted against the initial eye position, averaged across eyes. The results from each fish were fitted by a cubic smoothing spline with boundary second derivatives equal to zero, using the spline fit-package developed for MATLAB by Jonas Lundgren. This fitting procedure was repeated for several stimulation intensity bins. A population plot was generated by averaging the spline fits of all fish, for each intensity bin. We observed some variability of motor ranges across fish, especially in animals expressing ChR2, which tended to have a smaller motor range (average motor range and respective standard deviations in NpHR animals: [−20.0° ± 5°; 18.7° ± 4.4°]; in ChR2 animals [−13.7° ± 3.9°; 13° ± 3.5°]). Therefore, before averaging across animals, we normalized all motor ranges to generate a smooth population plot. In some fish, there was an undersampling of events at the eccentric eye positions, and therefore we removed the 5% most eccentric events on the right

side and on the left side before averaging across animals. In several fish, some intensity bins did not span the full motor range, and we extrapolated the corresponding splines. To account for the uncertainty of the extrapolation, we performed a weighted average over fish for eccentric eye positions, with weights that decreased as the extrapolation distance increased.

The null-position of the eyes was defined as the average of the extreme eye positions. Note that this definition only works well for eyes which explore eye positions in both directions equally well, which was not the case for every fish. However, in our hands this was the best definition since other definitions (median, average, fixed at $+8°/-8°$) were more subjective or decreased the across-fish consistency of the results. An animal's distribution of post-saccadic eye positions was often bimodal, since the animal explored the peripheral positions more frequently. In some experiments, we stimulated multiple times (1, 3, 5, and 7 s) after a single post-saccadic fixation in order to access the full scope of eye positions.

The location of stimulation was in caudal proximity to the previously identified region containing saccade generating neurons (Schoonheim et al., 2010), and in a fraction of the events, the stimulation induced a saccade (more frequently for ChR2 stimulations than for NpHR). Since this study focuses on the performance of the integrator, we did not include these events in our analysis. In **Figure 5**, these were excluded by a velocity threshold ($>20°$/s). In **Figure 4D**, the data points result from eye velocity vs. eye position fits (linear regression through the origin, see **Figure A8**), and correspond to the inverse of the eye position drift time constant at a specific hindbrain location. For each fit, only the middle 70% of the eye velocity/eye position data points were fitted, thereby excluding outliers caused by saccades. For each eye, the eye drift was normalized across hindbrain positions. Each data point in **Figure 4D** corresponds to one fish (average of the normalized left and right eye, for individual eyes see **Figure A8**) and hindbrain position. The data points for **Figure 4D** (eye drift vs. hindbrain position) were then fitted by gaussian functions. For the Gaussian fit functions in **Figure 4D**, the mean was restricted to the interval [0; 200]. This modification was made because for approximately flat distributions (control data points ipsi ctrl, contra stim, contra ctrl) peripheral data points sometimes caused Gaussian fits with means far away from the tested hindbrain region.

THEORETICAL FRAMEWORK: NETWORK MODEL

In previous work (Gonçalves, 2012), we show how to build a line attractor model accounting for the main findings in the oculomotor integrator, using basic design principles that have previously been suggested in the literature (Seung, 1996; Eliasmith, 2005; Machens and Brody, 2008). We use these principles to clarify how the network connectivity is related to the tuning curve properties. Here, we summarize the main features of the model developed in Gonçalves (2012).

We start by describing the assumptions and simplifications underlying the network model. Most of these assumptions are adapted from the previous literature and are based either on arguments of plausibility and simplicity or on observations about the oculomotor integrator (Seung, 1996; Aksay et al., 2000; Seung et al., 2000; Aksay et al., 2007; Machens and Brody, 2008).

Assumption 1 (Two opposing populations). We assume that the dynamics are controlled by two population variables, X_R and X_L, one for each side. These variables shall represent the effect one population has on the postsynaptic currents of neurons in the other population; a specific definition will follow below. We assume that in its normal working regime, these two "synaptic" population activities oppose each other, so that, as the activity in one population grows, that of the other drops. For simplicity we therefore assume that

$$\beta = X_R + X_L \tag{1}$$

where β is a constant value.

Assumption 2 (Eye position). We furthermore assume that within this working regime (but not outside of it) the eye position can be read out as

$$\theta = X_R - X_L \tag{2}$$

where right range positions are defined as positive eye positions, and left range positions as negative.

Assumption 3 (Firing rates). We furthermore assume that each neuron's firing rate in the stationary state is determined by its excitatory input from the same population, scaled by a weight a_i, the inhibitory input from the opposite population, scaled by a weight c_i, and some external (e.g., vestibular) input, h_i, so that

$$r_{R,i} = [a_i X_R - c_i X_L + h_i]_+ \tag{3}$$

$$r_{L,i} = [a_i X_L - c_i X_R + h_i]_+ \tag{4}$$

where $i = 1, \ldots, n$ indexes the neuron, and $[\cdot]_+$ is a threshold-linear function (**Figure A1A**). For simplicity, we assume complete symmetry of the two systems, so that neurons in the two populations have exactly the same set of parameters values.

Tuning curve constraints

Using the (abstract) threshold-linear tuning curves, we can describe the firing rates of the right and left position neurons, $r_{R,i}$ and $r_{L,i}$, as a function of the eye position θ (see **Figure 1C**), so that (for $i = 1, \ldots, n$)

$$r_{R,i} = [s_i(\theta - t_i)]_+ \tag{5}$$

$$r_{L,i} = [-s_i(\theta - t_i)]_+ \tag{6}$$

where s_i and t_i are the tuning curves' slope and threshold, which are assumed to obey the recruitment order (Aksay et al., 2000) (see **Figure A2**). Since the parameters s_i and t_i are given by the data, they constrain the possible choices of a_i, c_i, h_i from Equations (3,4). More specifically, on the curve defined by Equation (1), the following relations need to hold:

$$s_i = \frac{a_i + c_i}{2} \tag{7}$$

$$t_i = -\frac{(a_i - c_i)\beta + 2h_i}{a_i + c_i}. \tag{8}$$

To obtain the constraints on the excitatory and inhibitory inputs, a_i and c_i, as well as the external inputs, h_i, we need to invert

this relationship. Since there are three parameters on one side (a_i, c_i, h_i) and two on the other (s_i, t_i), this inversion is not unique. We therefore introduce a free parameter λ_i to obtain

$$a_i = 2\lambda_i s_i \tag{9}$$

$$c_i = 2(1 - \lambda_i)\, s_i \tag{10}$$

$$h_i = s_i(1 - 2\lambda_i)\,\beta - s_i t_i. \tag{11}$$

The free parameter $\lambda_i \in [0, 1]$ controls the relative role of self-excitation and mutual inhibition. For $\lambda_i = 0$, a neuron receives only inhibitory inputs from the other side, and for $\lambda_i = 1$, it receives only excitatory inputs from the same side. No matter how λ_i is chosen, as long as a_i, c_i, and h_i follow the above equations, the measured recruitment order will be obeyed (see **Figure A2**).

Stationarity constraints

Next, we need to make sure that the firing rates of the neurons are in a stationary state during fixations of the eye. To do so, we have to define how the individual neural firing rates combine to give rise to the synaptic population activities X_L and X_R.

Assumption 4 (Synaptic Population Activity). We assume that the synaptic population activities are generated through a linear combination of the individual neural activities such that (for the right population)

$$X_R = \sum_{i=1}^{n} b_i g\big(r_{R,i}\big) \tag{12}$$

where b_i is a weighting factor, that determines the contribution of the i-th neuron to the synaptic population activity and $g(\cdot)$ is a sigmoidal function that captures possible non-linearities. These non-linearities can capture saturations in the contribution of individual neural firing rates to the synaptic population activity.

Plugging Equations (2,5) into the above equation, and using the relation $X_L = \beta - X_R$, we obtain the following condition for stationarity:

$$X_R = \sum_{i=1}^{n} b_i H(s_i\,(2X_R - \beta - t_i)) \quad \text{with} \quad H(\cdot) = g\left([\cdot]_+\right) \tag{13}$$

Here, $H(\cdot)$ is a neural input-output function that combines the effect of the neuron's threshold-linear tuning curves and other non-linearities modeled through the sigmoidal function $g(\cdot)$, such as synaptic saturation (see **Figure A1B**). For instance, $H(\cdot)$ could be a function similar to the one shown in **Figure A1C**. To obtain a continuum of stationary solutions, i.e., solutions to the above equation for many values of X_R, the parameters b_i can be fit so that the above relation holds approximately (see **Figures A1G,H**) (Seung, 1996; Eliasmith, 2005; Machens and Brody, 2008). Since the input-output functions $H(\cdot)$ are shifted with respect to the X_R-axis due to the differently distributed threshold values t_i, a workable solution usually exists. We note that with this fitting, we recover the desired line of synaptic population activities in the normal working regime (see Equation (1) and **Figure A1I**).

Input-output functions

Before fitting the parameters b_i, we need to make a specific choice for the input-output function $H(\cdot)$. Our choice will be driven by a quest for simplicity:

Assumption 5 (Input-output function). We assume that the possible synaptic saturation can be modeled by a heaviside function so that

$$H(x) = \begin{matrix} 0 \text{ if } x \le 0 \\ 1 \text{ if } x > 0 \end{matrix} \tag{14}$$

In this case, the summation of a set of Heaviside functions $H(\cdot)$ in Equation (13) results in a function that resembles a staircase (see **Figure A1H**). In turn, a particularly simple solution is given if we assume that all $b_i = b$ are the same, and that the t_i are equally spaced across the whole range of eye positions. In this case, the staircase approximates a linear function whose slope is determined by b, and we only need to set this single parameter to its proper value. This solution assumes, though, that the thresholds t_i extend over the whole eye position range which has not been observed experimentally. Rather, the thresholds cluster in only half the eye position range (as indicated in **Figure 1C**). However, the framework can easily incorporate this constraint by making the assumption that a) $H(\cdot)$ does not saturate completely and is a concave function for large inputs, and b) $H(\cdot)$ features high-synaptic thresholds. This has indeed been the assumption in the past (Aksay et al., 2007). In this case, the parameters b_i have to be fit by linear regression. Use of the Heaviside function, however, simplifies the mathematics and makes the underlying architecture more transparent (Machens and Brody, 2008).

Dynamics of the network

To develop a dynamical equation for the network and clarify the network connectivity, we define the effective (or synaptic) output of a neuron as

$$x_{R,i} = g\big(r_{R,i}\big) \tag{15}$$

so that Equation (12) becomes

$$X_R = \sum_i b_i x_{R,i}. \tag{16}$$

Identical equations hold for the left population. Using Equations (3,4), we can now reformulate the stationarity condition on the level of single cells, using the effective outputs of the neurons,

$$x_{R,i} = H\left(a_i X_R - c_i X_L + h_i\right) \tag{17}$$

$$= H\left(\sum_{j=1}^{n} a_i b_j x_{R,j} - \sum_{j=1}^{n} c_i b_j x_{L,j} + h_i\right). \tag{18}$$

Just as the population equations, these equations have solutions for a continuum of values of $x_{R,i}$ as long as the parameters b_i are fitted as described above. To equip the network with dynamics,

we need to assume how the neural activities relax to this stationary state once the system is perturbed. Let us define the following abbreviations,

$$w_{ij,E} = a_i b_j, \tag{19}$$

$$w_{ij,I} = c_i b_j, \tag{20}$$

where $w_{ij,E}$ denotes the weight of an excitatory connection from neuron j to neuron i and $w_{ij,I}$ denotes the weight of an inhibitory connection from neuron j to neuron i.

Assumption 6 (Exponential relaxation). We assume that the neural activities relax exponentially to the stationary state. This leads to a network with standard Wilson-Cowan dynamics (Dayan and Abbott, 2001),

$$\tau \dot{x}_{R,i}(t) = -x_{R,i}(t) + H\left(\sum_{j=1}^{n} w_{ij,E} x_{R,j} - \sum_{j=1}^{n} w_{ij,I} x_{L,j} + h_i\right) \tag{21}$$

where now each neuron i receives excitatory and inhibitory inputs from the two populations. An identical equation holds for the neurons in the left population and is obtained by switching the L and R subscripts.

Firing rate dynamics are assumed to be very fast as compared to synaptic dynamics, and are therefore always in equilibrium:

$$r_{R,i} = \left[\sum_{j=1}^{n} w_{ij,E} x_{R,j} - \sum_{j=1}^{n} w_{ij,I} x_{L,j} + h_i\right]_+ \tag{22}$$

As previously, an identical equation holds for the neurons in the left population and is obtained by switching the L and R subscripts.

In this model, neurons are excitatory to their own population and inhibitory to the opposing population. However, we can build equivalent models obeying Dale's law, i.e., where neurons are either excitatory or inhibitory, but not both at the same time (unpublished results). A systematic way of mapping networks with mixed excitatory and inhibitory neurons to networks that obey Dale's law was recently proposed in Parisien et al. (2008).

As can be seen in Equations (19,20), we here assume low-rank connectivity. This connectivity has been a standard assumption of all previously proposed models of the oculomotor integrator (Seung, 1996; Aksay et al., 2007) for two reasons: (1) the experimentally observed stable activities across cells in the integrator along the eye position range suggest that the system has low dimensional dynamics, characteristic of a low-rank connectivity system; (2) this assumption simplifies the theoretical treatment of the problem. However, the assumed connectivity should only be viewed as an effective connectivity rather than a direct mapping onto biophysical synapses. Mathematically, one can relax the low-rank assumption: the connectivity matrix can be expanded into "modes" (using singular value decomposition, e.g.), and the dynamics of the oculomotor integrator are simply governed by the first and strongest mode which governs the dynamics in the plane of population activities. However, one could add many more weaker (and orthogonal) modes that would only impact the transient dynamics of single neurons, while leaving the dynamics of the summed population intact. These weaker modes can change the (biophysical) connectivity in many ways, while leaving the effective connectivity the same.

THEORETICAL FRAMEWORK: FROM NETWORK ACTIVITY TO EYE POSITIONS

Neural integrator mapping to eye positions

Oculomotor plant dynamics are the result of the innervation of two antagonist muscles (medial rectus and lateral rectus) by motor neurons delivering the position signal (**Figure 1A**). Consequently, we assume that the eye position θ is related to the difference between right and left motor population activities, making the function f_x between synaptic population activities (X_R, X_L) and eye position non-linear (see Appendix for details).

Oculomotor plant dynamics

To model the observed inertia or sluggishness of the whole system in response to the perturbations (most likely a consequence of muscle inertia and eye dynamics) we implemented a simple exponential decay toward the network stable activities with a time constant τ_θ, so that

$$\tau_\theta \dot{\theta} = -\theta + f_x(X_R, X_L)\,. \tag{23}$$

By visual inspection of zebrafish eye traces, we chose $\tau_\theta = 200$ ms.

UNILATERAL INACTIVATION

Now that we have fully determined the relationship between the integrator neural activities and the eye position, we can appropriately interpret the pharmacological inactivation results of (Aksay et al., 2007). After unilateral silencing of the oculomotor integrator, the animals manage to fixate the eyes on the contralateral half of the motor range, and the activities of the intact neurons remain stable within this range. In our framework, this suggests a range of stable points on the upper half of the activity axis X_R and X_L. These stable ranges provide an important constraint for the ILA and NP models, limiting the possible choices of λ_i that we can make in Equations (9–11).

PARAMETER TUNING OF NETWORK MODELS

We have clarified the dynamics along the axes required by the pharmacological inactivation results of Aksay et al. (2007), so that we can proceed to the final tuning of the network model.

Independent of the choice of λ_i, the proposed network connectivities feature a line attractor in the (X_R, X_L) space that agrees with the recruitment order. However, the desired dynamics outside of the attractor, e.g., the dynamics along the axes required by the pharmacological inactivation results, further constrain the tuning of the parameter λ_i. Given the low number of neurons and simplicity of the tuning, we manually tuned this parameter to change the dynamics around the line attractor. However, a least squares optimization procedure could also be built to solve the problem.

In **Figure A4**, we present two model solutions presented in the main section, the independent line attractor model (ILA model)

and the null position model (NP model) (see Appendix for the detailed parameter tuning procedure). In general, the nullcline of each half OI is the set of points in space where the dynamics in the corresponding direction are zero. In both ILA and NP models, we tuned the nullclines of either side to consist of densely arranged parallel lines, such that the vectors in the flow field are bound to be either horizontal or vertical. For instance, in the NP model, left range, vertical nullclines of the right side (in blue) ensure that the system has weak dynamics on the horizontal direction, and therefore the dynamics are mostly on the vertical direction.

We note that in the NP model, we have tuned the nullclines to end close to the line of fixed points, to ensure that each piece of nullcline intersects only one piece of the opposite nullcline and therefore obtain a line of fixed points (**Figure A4B**, left). If we relax that assumption and allow for a band attractor for instance, then the nullclines do not have to end as close to the diagonal.

ILA MODEL DYNAMICS

The ILA model with 36 neurons on each half of the integrator is illustrated in **Figure A4A**. As can be seen, the nullclines resulting from the summation of the input-output functions H(.) of the individual neurons intersect in a line of stable points (**Figure A4A**, left). Furthermore, after complete left inactivation, the system is able to maintain stable positions in the right range (results not shown), as obtained in the pharmacological experiments (Aksay et al., 2007). Finally, this model shows the experimentally observed recruitment order feature, i.e., the higher the threshold the higher the slope of the tuning curves (**Figure A2**), since it was imposed into the model. The dynamics of the ILA model are qualitatively similar to the dynamics of the model developed in Aksay et al. (2007) (see **Figure A4A**, right). The respective network parameters are listed in **Table A1**.

NP MODEL DYNAMICS

In **Figure A4B**, we illustrate the NP model. Just as the ILA model, the system is able to maintain stable eye positions in half the original range after unilateral silencing. The model differs from the ILA model in one important aspect, however. The upper half of the nullcline (**Figure A4B**, left) is now maintained largely by self-excitation. In fact, the two halves of the oculomotor integrator are almost independent, and the threshold of the neurons is mostly determined by the self-excitatory inputs. However, due to the weak, mutual cross-inhibition, this independence is slightly disturbed, leading to the dynamics shown in **Figure A4B**, right. Altogether, the NP model has qualitatively the same dynamics below the line attractor as the ILA model but different dynamics above the line attractor. However, the NP model dynamics are slower than the ILA model dynamics in the whole state space, given the low inter-dependence of the two areas in the NP model (the arrow lengths in **Figure A4A**, right panel, and **Figure A4B**, right panel, are in different scales). The respective network parameters are listed in **Table A1**.

Despite the connectivity differences between ILA model and NP model, since these models share the same qualitative dynamics below the line attractor, NpHR left stimulation leads to very similar results in both models, with minor differences (results not shown).

Due to the use of Heaviside input-output functions and the resulting staircase character of the nullclines, the network implementation of the NP model features additional fine-scale dynamics that are not illustrated in **Figures 7A**, **A4B** (see detail of the dynamics in **Figure A4C**). These dynamics do not affect the trajectories in the noise-less case, and disappear when more realistic (e.g., sigmoidal) input-output functions are used for tuning the model (simulations not shown).

THEORETICAL FRAMEWORK: INSTANTANEOUS PERTURBATIONS

As shown in the results section, we experimentally test the range of models by performing instantaneous perturbations with optogenetic tools: inactivation with halorhodopsin (NpHR) and excitation with channelrhodopsin (ChR2). To model the perturbations, it is crucial to understand the effects of optogenetic tools in the activities of stimulated cells.

It has previously been shown (Arrenberg et al., 2009) that inactivation by NpHR stimulation leads to stronger inactivation of high activity cells than low activity cells, so the inactivation effects are approximately divisive. ChR2 stimulation, on the other hand, causes an increase in activity independent of the original activities (Arrenberg et al., 2009). To incorporate optogenetic stimulations in our dynamical systems model, we take these experimental observations into account.

Perturbations with halorhodopsin (NpHR)

Given the divisive nature of the inhibitory perturbations, we model these as multiplicative interactions of the input-output function. Assume that a neuron is perturbed with a brief stimulation of magnitude α_i ($0 < \alpha_i < 1$) and duration T. We simulate the synaptic output of such a perturbed neuron (from the left) as

$$\tau \dot{x}_{L,i}(t) = -x_{L,i}(t) + (1 - \alpha_i D(t))\, H(a_i X_L(t) - c_i X_R(t) + h_i)\,, \quad i = 1, \ldots, n \tag{24}$$

where $D(t) = H(t - t_0)H(t_0 + T - t)$ is a unit perturbation pulse, starting at time t_0, and lasting for T seconds. Consequently, at the population level, the system is described by the following population equations during an inactivation of the left half of the integrator:

$$\tau \dot{X}_R(t) = -X_R(t) + \sum_{i=1}^{n} H(a_i X_R(t) - c_i X_L(t) + h_i) \tag{25}$$

$$\tau \dot{X}_L(t) = -X_L(t) + \sum_{i=1}^{n} (1 - \alpha_i D(t))\, H(a_i X_L(t) - c_i X_R(t) + h_i) \tag{26}$$

The parameters α_i are chosen at random from a Gaussian distribution whose mean μ is equal across neurons, but grows linearly with the stimulation intensity. The standard deviation of the distribution of α_i was given as $\sigma = \mu_{\min}/2$ where $\mu_{\min}$ indicates the smallest perturbation intensity tested. To ensure that the stimulation strength is always positive, negative α_i were rectified. Since

the mapping of the physical stimulation intensities (in mW) onto the network was unknown, we hand-tuned the mean stimulation effect μ to give results in a reasonable range for the ILA and NP models.

Perturbations with channelrhodopsin (ChR2)

Given the assumed additive nature of the excitatory perturbations, we model these as external excitatory inputs into the cells:

$$\tau\dot{X}_R(t) = -X_R(t) + \sum_{i=1}^{n} H(a_i X_R(t) - c_i X_L(t) + h_i) \quad (27)$$

$$\tau\dot{X}_L(t) = -X_L(t) + \sum_{i=1}^{n} H(a_i X_L(t) - c_i X_R(t) + h_i + \alpha_i D(t)) \quad (28)$$

where $D(t) = H(t - t_0)H(t_0 + T - t)$ is once more a unit perturbation pulse, starting at time t_0, and lasting for T seconds. The parameters α_i are chosen from Gaussian distributions, as above, with mean μ and fixed standard deviation, equivalent to one half of the mean of the smallest tested intensity, $\sigma = \mu/2$. As above, the range of intensities tested was hand-tuned for both models, to fall in the experimentally observed range.

Perturbations protocol

To simulate the perturbations, we roughly follow the outline of the experimental perturbations. The model is simulated numerically in MATLAB, using the Euler method. Each trial lasts 1.5 s, and is initialized at one stable eye position, and after 0.5 s, is provided a perturbation of the same duration as in experiments (200 and 100 ms for NpHR and ChR2 trials, respectively). This procedure is repeated for perturbations of different stimulation intensities, and several eye positions across the motor range, and typically 4000 times for each condition (initial eye position, perturbation intensity). The population activities in the network are simulated according to Equation (25) and Equation (26) for the NpHR and Equation (27) and Equation (28) for the ChR2 perturbations. Eye positions are assigned to the resulting population activities according to the mappings outlined in Appendix. Just as for the experimental data, we measure the resulting changes in eye position, $\Delta\theta$, as a function of the eye position θ just before perturbation. For each perturbation intensity, all neurons are assumed to receive a perturbation magnitude taken from a normal distribution, as explained above.

MATLAB PACKAGE

A Matlab package in which the ILA model and the NP model are implemented is provided in the online supplementary information.

AUTHOR CONTRIBUTIONS

Pedro J. Gonçalves and Christian K. Machens designed the model. Pedro J. Gonçalves performed the simulations. Aristides B. Arrenberg and Herwig Baier conceived the experiments. Aristides B. Arrenberg and Bastian Hablitzel performed the experiments. Pedro J. Gonçalves, Aristides B. Arrenberg, Bastian Hablitzel, and Christian K. Machens analyzed the data. Pedro J. Gonçalves, Aristides B. Arrenberg, Herwig Baier, and Christian K. Machens wrote the paper. Pedro J. Gonçalves and Aristides B. Arrenberg contributed equally to this work.

ACKNOWLEDGMENTS

Pedro J. Gonçalves was part of the PhD Program in Computational Biology of Instituto Gulbenkian de Ciência, supported by Fundação Calouste Gulbenkian, Siemens SA and Fundação para a Ciência e Tecnologia (Portugal) through grant SFRH/BD/33210/2007. Aristides B. Arrenberg was supported by a Krevans fellowship and Aristides B. Arrenberg and Bastian Hablitzel are supported by the Excellence Initiative of the German Federal and State Governments (Centre for Biological Signaling Studies EXC 294-B5-Driever). Herwig Baier was funded by NIH R01 NS053358, the NIH Nanomedicine Development Center "Optical Control of Biological Functions" and the Max Planck Society. Christian K. Machens was funded by a "Chaire d'excellence" of the French Research Agency (ANR), a "Chaire d'excellence" of INSERM and the Emmy-Noether Program of the German Research Foundation. We thank Jan Huisken for his help regarding the laser setup.

SUPPLEMENTARY MATERIAL

The Supplementary Material for this article can be found online at: http://www.frontiersin.org/journal/10.3389/fncir.2014.00010/abstract

REFERENCES

Aksay, E., Baker, R., Seung, H. S., and Tank, D. W. (2000). Anatomy and discharge properties of pre-motor neurons in the goldfish medulla that have eye-position signals during fixations. *J. Neurophysiol.* 84, 1035–1049.

Aksay, E., Baker, R., Seung, H. S., and Tank, D. W. (2003). Correlated discharge among cell pairs within the oculomotor horizontal velocity-to-position integrator. *J. Neurosci.* 23, 10852–10858.

Aksay, E., Olasagasti, I., Mensh, B. D., Baker, R., Goldman, M. S., and Tank, D. W. (2007). Functional dissection of circuitry in a neural integrator. *Nat. Neurosci.* 10, 494–504. doi: 10.1038/nn1877

Arnold, D. B., Robinson, D. A., and Leigh, R. J. (1999). Nystagmus induced by pharmacological inactivation of the brainstem ocular motor integrator in monkey. *Vision Res* 39, 4286–4295. doi: 10.1016/S0042-6989(99)00142-X

Arrenberg, A. B., Del Bene, F., and Baier, H. (2009). Optical control of zebrafish behavior with halorhodopsin. *Proc. Natl. Acad. Sci. U.S.A.* 106, 17968–17973. doi: 10.1073/pnas.0906252106

Ashourian, P. and Loewenstein, Y. (2011). Bayesian inference underlies the contraction bias in delayed comparison tasks. *PLoS ONE* 6:e19551. doi: 10.1371/journal.pone.0019551

Baier, H. and Scott, E. K. (2009). Genetic and optical targeting of neural circuits and behavior–zebrafish in the spotlight. *Curr. Opin. Neurobiol.* 19, 553–560. doi: 10.1016/j.conb.2009.08.001

Boyden, E. S., Zhang, F., Bamberg, E., Nagel, G., and Deisseroth, K. (2005). Millisecond-timescale, genetically targeted optical control of neural activity. *Nat. Neurosci.* 8, 1263–1268. doi: 10.1038/nn1525

Brody, C. D., Romo, R., and Kepecs, A. (2003). Basic mechanisms for graded persistent activity: discrete attractors, continuous attractors, and dynamic representations. *Curr. Opin. Neurobiol.* 13, 204–211. doi: 10.1016/S0959-4388(03)00050-3

Cannon, S. C., and Robinson, D. A. (1985). An improved neural-network model for the neural integrator of the oculomotor system: more realistic neuron behavior. *Biol. Cybern.* 53, 93–108. doi: 10.1007/BF00337026

Cannon, S. C., Robinson, D. A., and Shamma, S. (1983). A proposed neural network for the integrator of the oculomotor system. *Biol. Cybern.* 49, 127–136. doi: 10.1007/BF00320393

Dayan, P., and Abbott, L. (2001). *Theoretical Neuroscience: Computational and Mathematical Modeling of Neural Systems, 1st Edn*. Cambridge, MA: The MIT Press.

Debowy, O., and Baker, R. (2011). Encoding of eye position in the goldfish horizontal oculomotor neural integrator. *J. Neurophysiol.* 105, 896–909. doi: 10.1152/jn.00313.2010

Delgado-García, J. M., Vidal, P. P., Gómez, C., and Berthoz, A. (1989). A neurophysiological study of prepositus hypoglossi neurons projecting to oculomotor and preoculomotor nuclei in the alert cat. *Neuroscience* 29, 291–307. doi: 10.1016/0306-4522(89)90058-4

Dipoppa, M. (2012). *The Role of Correlations and Oscillations as a Unified Mechanism Controlling Persistent Neural Activity and Working Memory*. PhD thesis, Universite Pierre et Marie Curie.

Douglass, A. D., Kraves, S., Deisseroth, K., Schier, A. F., and Engert, F. (2008). Escape behavior elicited by single, channelrhodopsin-2-evoked spikes in zebrafish somatosensory neurons. *Curr. Biol.* 18, 1133–1137. doi: 10.1016/j.cub.2008.06.077

Egorov, A. V., Hamam, B. N., Fransen, E., Hasselmo, M. E., and Alonso, A. A. (2002). Graded persistent activity in entorhinal cortex neurons. *Nature* 420, 173–178. doi: 10.1038/nature01171

Eliasmith, C. (2005). A unified approach to building and controlling spiking attractor networks. *Neural Comput.* 17, 1276–1314. doi: 10.1162/0899766053630332

Fenno, L., Yizhar, O., and Deisseroth, K. (2011). The development and application of optogenetics. *Annu. Rev. Neurosci.* 34, 389–412. doi: 10.1146/annurev-neuro-061010-113817

Fransén, E., Tahvildari, B., Egorov, A. V., Hasselmo, M. E., and Alonso, A. A. (2006). Mechanism of graded persistent cellular activity of entorhinal cortex layer v neurons. *Neuron* 49, 735–746. doi: 10.1016/j.neuron.2006.01.036

Fukushima, K., Kaneko, C. R., and Fuchs, A. F. (1992). The neuronal substrate of integration in the oculomotor system. *Prog. Neurobiol.* 39, 609–639. doi: 10.1016/0301-0082(92)90016-8

Gold, J. I. and Shadlen, M. N. (2001). Neural computations that underlie decisions about sensory stimuli. *Trends Cogn. Sci.* 5, 10–16. doi: 10.1016/S1364-6613(00)01567-9

Goldman, M., Compte, A., and Wang, X. (2009). "Neural integrator models," in *Encyclopedia of Neuroscience,* Vol. 6, ed L. R. Squire (Oxford: Academic Press). 165–178.

Goldman, M. S., Levine, J. H., Major, G., Tank, D. W., and Seung, H. S. (2003). Robust persistent neural activity in a model integrator with multiple hysteretic dendrites per neuron. *Cereb. Cortex* 13, 1185–1195. doi: 10.1093/cercor/bhg095

Gonçalves, P. J. (2012). *A Neural Circuit Model of the Oculomotor Integrator: Theory for Optogenetic Dissection*. PhD thesis, Universite Pierre et Marie Curie.

Hahnloser, R. H. R., Kozhevnikov, A. A., and Fee, M. S. (2002). An ultra-sparse code underlies the generation of neural sequences in a songbird. *Nature* 419, 65–70. doi: 10.1038/nature00974

Han, X., and Boyden, E. S. (2007). Multiple-color optical activation, silencing, and desynchronization of neural activity, with single-spike temporal resolution. *PLoS ONE* 2:e299. doi: 10.1371/journal.pone.0000299

Huber, D., Petreanu, L., Ghitani, N., Ranade, S., Hromádka, T., Mainen, Z., et al. (2008). Sparse optical microstimulation in barrel cortex drives learned behaviour in freely moving mice. *Nature* 451, 61–64. doi: 10.1038/nature06445

Kleinlogel, S., Feldbauer, K., Dempski, R. E., Fotis, H., Wood, P. G., Bamann, C., et al. (2011). Ultra light-sensitive and fast neuronal activation with the Ca^{2+}-permeable channelrhodopsin catch. *Nat. Neurosci.* 14, 513–518. doi: 10.1038/nn.2776

Koulakov, A. A., Raghavachari, S., Kepecs, A., and Lisman, J. E. (2002). Model for a robust neural integrator. *Nat. Neurosci.* 5, 775–782. doi: 10.1038/nn893

Lima, S. Q., and Miesenböck, G. (2005). Remote control of behavior through genetically targeted photostimulation of neurons. *Cell* 121, 141–152. doi: 10.1016/j.cell.2005.02.004

Loewenstein, Y., and Sompolinsky, H. (2003). Temporal integration by calcium dynamics in a model neuron. *Nat. Neurosci.* 6, 961–967. doi: 10.1038/nn1109

Lopez-Barneo, J., Darlot, C., Berthoz, A., and Baker, R. (1982). Neuronal activity in prepositus nucleus correlated with eye movement in the alert cat. *J. Neurophysiol.* 47, 329–352.

Luo, L., Callaway, E. M., and Svoboda, K. (2008). Genetic dissection of neural circuits. *Neuron* 57, 634–660. doi: 10.1016/j.neuron.2008.01.002

Machens, C. K., and Brody, C. D. (2008). Design of continuous attractor networks with monotonic tuning using a symmetry principle. *Neural Comput.* 20, 452–485. doi: 10.1162/neco.2007.07-06-297

Machens, C. K., Romo, R., and Brody, C. D. (2005). Flexible control of mutual inhibition: a neural model of two-interval discrimination. *Science* 307, 1121–1124. doi: 10.1126/science.1104171

Machens, C. K., Romo, R., and Brody, C. D. (2010). Functional, but not anatomical, separation of "what" and "when" in prefrontal cortex. *J. Neurosci.* 30, 350–360. doi: 10.1523/JNEUROSCI.3276-09.2010

Major, G., and Tank, D. (2004). Persistent neural activity: prevalence and mechanisms. *Curr. Opin. Neurobiol.* 14, 675–684. doi: 10.1016/j.conb.2004.10.017

Marder, E., and Bucher, D. (2001). Central pattern generators and the control of rhythmic movements. *Curr. Biol.* 11, R986–R996. doi: 10.1016/S0960-9822(01)00581-4

McFarland, J. L., and Fuchs, A. F. (1992). Discharge patterns in nucleus prepositus hypoglossi and adjacent medial vestibular nucleus during horizontal eye movement in behaving macaques. *J. Neurophysiol.* 68, 319–332.

Mensh, B. D., Aksay, E., Lee, D. D., Seung, H. S., and Tank, D. W. (2004). Spontaneous eye movements in goldfish: oculomotor integrator performance, plasticity, and dependence on visual feedback. *Vision Res.* 44, 711–726. doi: 10.1016/j.visres.2003.10.015

Miri, A., Daie, K., Arrenberg, A. B., Baier, H., Aksay, E., and Tank, D. W. (2011a). Spatial gradients and multidimensional dynamics in a neural integrator circuit. *Nat. Neurosci.* 14, 1150–1159. doi: 10.1038/nn.2888

Miri, A., Daie, K., Burdine, R. D., Aksay, E., and Tank, D. W. (2011b). Regression-based identification of behavior-encoding neurons during large-scale optical imaging of neural activity at cellular resolution. *J. Neurophysiol.* 105, 964–980. doi: 10.1152/jn.00702.2010

Moreau, L., and Sontag, E. (2003). Balancing at the border of instability. *Phys. Rev. E Stat. Nonlin. Soft Matter Phys.* 68:020901. doi: 10.1103/PhysRevE.68.020901

Nagel, G., Szellas, T., Huhn, W., Kateriya, S., Adeishvili, N., Berthold, P., et al. (2003). Channelrhodopsin-2, a directly light-gated cation-selective membrane channel. *Proc. Natl. Acad. Sci. U.S.A.* 100, 13940–13945. doi: 10.1073/pnas.1936192100

Parisien, C., Anderson, C. H., and Eliasmith, C. (2008). Solving the problem of negative synaptic weights in cortical models. *Neural Comput.* 20, 1473–1494. doi: 10.1162/neco.2008.07-06-295

Pastor, A. M., la Cruz, R. R. D., and Baker, R. (1994). Eye position and eye velocity integrators reside in separate brainstem nuclei. *Proc. Natl. Acad. Sci. U.S.A.* 91, 807–811. doi: 10.1073/pnas.91.2.807

Robinson, D. A. (1968). Eye movement control in primates. the oculomotor system contains specialized subsystems for acquiring and tracking visual targets. *Science* 161, 1219–1224. doi: 10.1126/science.161.3847.1219

Schoonheim, P. J., Arrenberg, A. B., Del Bene, F., and Baier, H. (2010). Optogenetic localization and genetic perturbation of saccade-generating neurons in zebrafish. *J. Neurosci.* 30, 7111–7120. doi: 10.1523/JNEUROSCI.5193-09.2010

Scott, E. K., Mason, L., Arrenberg, A. B., Ziv, L., Gosse, N. J., Xiao, T., et al. (2007). Targeting neural circuitry in zebrafish using gal4 enhancer trapping. *Nat. Methods* 4, 323–326. doi: 10.1038/nmeth1033

Seung, H. S. (1996). How the brain keeps the eyes still. *Proc. Natl. Acad. Sci. U.S.A.* 93, 13339–13344. doi: 10.1073/pnas.93.23.13339

Seung, H. S., Lee, D. D., Reis, B. Y., and Tank, D. W. (2000). Stability of the memory of eye position in a recurrent network of conductance-based model neurons. *Neuron* 26, 259–271. doi: 10.1016/S0896-6273(00)81155-1

Singh, R., and Eliasmith, C. (2006). Higher-dimensional neurons explain the tuning and dynamics of working memory cells. *J. Neurosci.* 26, 3667–3678. doi: 10.1523/JNEUROSCI.4864-05.2006

Szobota, S., Gorostiza, P., Del Bene, F., Wyart, C., Fortin, D. L., Kolstad, K. D., et al. (2007). Remote control of neuronal activity with a light-gated glutamate receptor. *Neuron* 54, 535–545. doi: 10.1016/j.neuron.2007.05.010

Wong, K.-F., Huk, A. C., Shadlen, M. N., and Wang, X.-J. (2007). Neural circuit dynamics underlying accumulation of time-varying evidence during perceptual decision making. *Front. Comput. Neurosci.* 1:6. doi: 10.3389/neuro.10.006.2007

Zhang, F., Aravanis, A. M., Adamantidis, A., de Lecea, L., and Deisseroth, K. (2007a). Circuit-breakers: optical technologies for probing neural signals and systems. *Nat. Rev. Neurosci.* 8, 577–581. doi: 10.1038/nrn2192

Zhang, F., Wang, L.-P., Brauner, M., Liewald, J. F., Kay, K., Watzke, N., et al. (2007b). Multimodal fast optical interrogation of neural circuitry. *Nature* 446, 633–639. doi: 10.1038/nature05744

Zhang, K. (1996). Representation of spatial orientation by the intrinsic dynamics of the head-direction cell ensemble: a theory. *J. Neurosci.* 16, 2112–2126.

Zhu, P., Narita, Y., Bundschuh, S. T., Fajardo, O., Schärer, Y.-P. Z., Chattopadhyaya, B., et al. (2009). Optogenetic dissection of neuronal circuits in zebrafish using viral gene transfer and the tet system. *Front. Neural Circuits* 3:21. doi: 10.3389/neuro.04.021.2009

Conflict of Interest Statement: The authors declare that the research was conducted in the absence of any commercial or financial relationships that could be construed as a potential conflict of interest.

Received: 26 February 2013; accepted: 30 January 2014; published online: 28 February 2014.

Citation: Gonçalves PJ, Arrenberg AB, Hablitzel B, Baier H and Machens CK (2014) Optogenetic perturbations reveal the dynamics of an oculomotor integrator. Front. Neural Circuits ***8****:10. doi: 10.3389/fncir.2014.00010*

This article was submitted to the journal Frontiers in Neural Circuits.

frontiers in
NEURAL CIRCUITS

METHODS ARTICLE
published: 09 April 2013
doi: 10.3389/fncir.2013.00065

Fast functional imaging of multiple brain regions in intact zebrafish larvae using Selective Plane Illumination Microscopy

Thomas Panier[1], Sebastián A. Romano[2,3,4], Raphaël Olive[1], Thomas Pietri[2,3,4], Germán Sumbre[2,3,4], Raphaël Candelier[1] and Georges Debrégeas[1]*

[1] *CNRS/UPMC Laboratoire Jean Perrin, Université Paris 6, Paris, France*
[2] *Ecole Normale Supérieure, Institut de Biologie de l'ENS, IBENS, Paris, France*
[3] *Inserm, U1024, Paris, France*
[4] *CNRS, UMR 8197, Paris, France*

Edited by:
Gonzalo G. De Polavieja, Instituto Cajal. CSIC, Spain

Reviewed by:
Rainer W. Friedrich, Friedrich Miescher Institute for Biomedical Research, Switzerland
Johann Bollmann, Max Planck Institute for Medical Research, Germany

****Correspondence:***
Georges Debrégeas, CNRS/UPMC Laboratoire Jean Perrin, Université Paris 6, FRE 3231, 4 place Jussieu, 75005 Paris, France.
e-mail: georges.debregeas@upmc.fr

The optical transparency and the small dimensions of zebrafish at the larval stage make it a vertebrate model of choice for brain-wide *in-vivo* functional imaging. However, current point-scanning imaging techniques, such as two-photon or confocal microscopy, impose a strong limit on acquisition speed which in turn sets the number of neurons that can be simultaneously recorded. At 5 Hz, this number is of the order of one thousand, i.e., approximately 1–2% of the brain. Here we demonstrate that this limitation can be greatly overcome by using Selective-plane Illumination Microscopy (SPIM). Zebrafish larvae expressing the genetically encoded calcium indicator GCaMP3 were illuminated with a scanned laser sheet and imaged with a camera whose optical axis was oriented orthogonally to the illumination plane. This optical sectioning approach was shown to permit functional imaging of a very large fraction of the brain volume of 5–9-day-old larvae with single- or near single-cell resolution. The spontaneous activity of up to 5,000 neurons was recorded at 20 Hz for 20–60 min. By rapidly scanning the specimen in the axial direction, the activity of 25,000 individual neurons from 5 different z-planes (approximately 30% of the entire brain) could be simultaneously monitored at 4 Hz. Compared to point-scanning techniques, this imaging strategy thus yields a ≃20-fold increase in data throughput (number of recorded neurons times acquisition rate) without compromising the signal-to-noise ratio (SNR). The extended field of view offered by the SPIM method allowed us to directly identify large scale ensembles of neurons, spanning several brain regions, that displayed correlated activity and were thus likely to participate in common neural processes. The benefits and limitations of SPIM for functional imaging in zebrafish as well as future developments are briefly discussed.

Keywords: zebrafish model system, spontaneous activity, correlation analysis, neuroimaging, imaging, three-dimensional, light-sheet imaging

INTRODUCTION

Cognitive processes generally implicate extended neural networks spanning several areas of the brain. In order to shed light on the neural basis of these processes, it is thus necessary to simultaneously monitor the dynamics of multiple brain regions with single-cell resolution (Alivisatos et al., 2012). In striking contrast with this requirement, current experimental methods sample a small number of neurons located in a single brain area. Silicon-based nanoprobes allow electrophysiologists to simultaneously record up to a few hundred neurons (Du et al., 2011; Stevenson and Kording, 2011). Their future development is however limited by the intrinsically invasive nature of the technique. In the last two decades, functional imaging approaches, in which the neurons' spiking dynamics is monitored *via* the increase in fluorescence of calcium-binding reporters, have allowed to partially circumvent this limitation (Grienberger and Konnerth, 2012). Further assets of neuro-imaging, with respect to electrophysiology, include the accurate localization of the monitored neurons, the possibility to distinguish cell identity using specific markers and the precise manipulation of neural activity using optogenetic methods (Wyart et al., 2009).

Imaging of three-dimensional fluorescent tissues requires optical sectioning, which is generally obtained by using confocal or two-photon microscopy (Denk et al., 1990; Yuste and Denk, 1995; Bollmann and Engert, 2009). These point-scanning microscopy (PSM) approaches in turn impose a drastic limit in recording speed: in order to collect a significant number of photons in a given voxel, a minimum laser dwelling time of the order of 1 µs is needed (Holekamp et al., 2008). This yields a bound of roughly 10^6 voxels per second in acquisition rate, which, even with optimized scanning trajectories (Salomé et al., 2006; Lillis et al., 2008; Grewe et al., 2010; Katona et al., 2012), limits the number of neurons that can be dynamically recorded.

In recent years, selective-plane illumination microscopy (SPIM) has been rediscovered in the context of embryo development (Mertz, 2011; Tomer et al., 2011; Weber and Huisken, 2011)

and physiology (Huisken et al., 2004; Verveer et al., 2007; Keller and Dodt, 2012). In this imaging configuration, optical sectioning is performed through side-on illumination of the sample by a thin (micrometer-thick) laser sheet, whereas fluorescence photons are collected by a camera whose optical axis is orthogonal to the illumination plane. One of the significant assets of this approach, compared to PSM, lies in the fact that different regions in the focal plane are simultaneously illuminated and are thus exposed for a much longer time in average. As a result, the data throughput is in practice limited by the camera transfer rate, which is currently of the order of a few hundreds of Mpixels per second for highly sensitive sensors.

The strongest limitation of light-sheet microscopy compared to epifluoresence methods lies in the need to access the sample from two orthogonal axis. This is a severe constraint when dealing with large organs such as mammalian brain (Engelbrecht et al., 2010), which may explain why this method has not yet received a lot of attention from neurophysiologists. The only functional imaging experiments using SPIM that have been reported so far were performed on excised mice's vomeronasal organs (Holekamp et al., 2008; Turaga and Holy, 2012). Although the effective penetration depth was quite modest (of the order of 150 μm), this experiment did prove to produce simultaneous recordings of an unprecedented number of neurons with single-cell resolution.

Zebrafish is an ideal candidate for the use of SPIM-based *in vivo* functional imaging. At the larval stage, its brain is transparent and relatively small (typically $200 \times 500 \times 1000\,\mu$m) which makes it fully amenable for PSM-based calcium imaging (Higashijima et al., 2003; Niell and Smith, 2005; Ramdya and Engert, 2008; Sumbre et al., 2008; McLean and Fetcho, 2009; Del Bene et al., 2010; Aizenberg and Schuman, 2011; Ahrens et al., 2012). Here we demonstrate that SPIM can be used as an alternative optical method for functional imaging in zebrafish, as it also provides single- or near single-cell resolution of a very large fraction of the brain volume of larvae aged 5–9 dpf. We show that this technique further yields a $\simeq$20-fold increase in acquisition speed (number of recorded neurons times acquisition rate) compared to point-scanning techniques without compromising the signal-to-noise ratio (SNR). We illustrate the potential of this approach by using the extended FOV provided by the SPIM technique to identify multiple brain regions exhibiting correlated spontaneous activity, and thus likely to participate in common neural processes. Since zebrafish larvae's brains are relatively small and compact (almost no extra-cellular space), we show that the *simultaneous* recording of the whole brain activity at several Hertz with single-cell resolution is within reach.

MATERIALS AND METHODS

GENERATION OF TRANSGENIC FISH

The tol2 HuC:GCaMP3 vector was built by successive ligations of a 3.2 kb fragment of the zebrafish HuC (elav3) promoter (gift from HC Park, Kyungpook National University, Korea. Park et al., 2000), then GCaMP3 calcium probe (gift from L. Looger, Howard Hughes Medical Institute, Ashburn, Virginia, USA Tian et al., 2012) into pT2KXIG in (from K. Kawakami, National Institute of Genetics, Shizuoka, Japan). HuC promoter drives the expression of a RNA-binding protein and has been involved in neuronal differentiation. In zebrafish, the 3.2 kb proximal region encompassing 2771 base pairs of the 5′-upstream sequence up to the translation start site in +383/+385, has been shown to be sufficient to target specifically and efficiently all differentiated neurons (Park et al., 2000).

One cell stage Nacre zebrafish embryos (Lister et al., 1999) (mitfa−/−) were injected with 20 ng of the plasmid DNA and 25 ng of transposase RNA (generated from pCS-TP plasmid, K. Kawakami). Injected embryos were raised to adulthood and crossed individually with Nacre fish to obtain F1 embryos. These embryos were then screened and selected according to their level of transgene expression. The embryos with the strongest expression were raised to adulthood and incrossed to obtain the homozygous HuC:GCaMP3^{GS5} line. The HuC:GCaMP3^{GS5} embryos were collected and raised at 28.5°C in E3 embryo medium. The larvae were kept under 14/10 h on/off light cycles and fed after 6 dpf. All experiments were approved by *Le Comité d'Éthique pour l'Expérimentation Animale Charles Darwin* (Ce5/2009/027).

LARVAE PREPARATION

Zebrafish larvae aged 5–9 dpf were embedded in a low-melting-temperature agarose solution at a concentration of 1.8% in embryo medium. In order to minimize movement artifacts, the solution contained 0.3 mg/ml of Pancuronium bromide, a paralyzing agent. The fish was introduced into a glass capillary tube of internal diameter 1.5 mm. The tube was then inserted inside a PMMA square chamber filled with embryo medium and the fish was partially extruded using a piece of plastic tubing inserted in the capillary tube (**Figure 1C**). Both sides of the specimen chamber along the illumination path consisted of glass coverslips. The larva dorsoventral axis was aligned vertically by rotation of the agarose cylinder. The chamber was then positioned in the SPIM set-up on a 3-axis manual positioning stage. A piezo-positioner (piezosystem jena PZ 400 OEM) further allowed sub-micrometric vertical displacement of the chamber.

OPTICAL SET-UP

The light sheet was obtained by rapidly scanning a focused laser beam through the specimen (**Figure 1A**). A 488 nm Coherent Sapphire laser beam of power 2 mW and $1/e^2$ diameter of 0.7 mm was projected onto a galvanometric scanning mirror (Century Sunny TSH8203) driven sinusoidally at 200–400 Hz over an angular range of 9°. A scanning lens (30 mm focal length—Thorlabs AC254-030-A), placed in front of the scanning mirror, transformed the angular deflection into a horizontal displacement of the incident light. The beam was then refocused by a tube lens (200 mm focal length - Thorlabs AC508-200-A) onto the entrance pupil of a low-NA (0.16) 5x objective lens (Zeiss EC Plan-Neofluar) facing the specimen chamber. The association of the scanning and the tube lenses extended the beam to a diameter of 4.6 mm at the entrance of the illumination objective. This optical configuration yielded a 2 mm-wide illumination sheet. Its thickness profile was characterized by imaging 100 nm in diameter fluorescent beads embedded in an agarose gel cylinder as

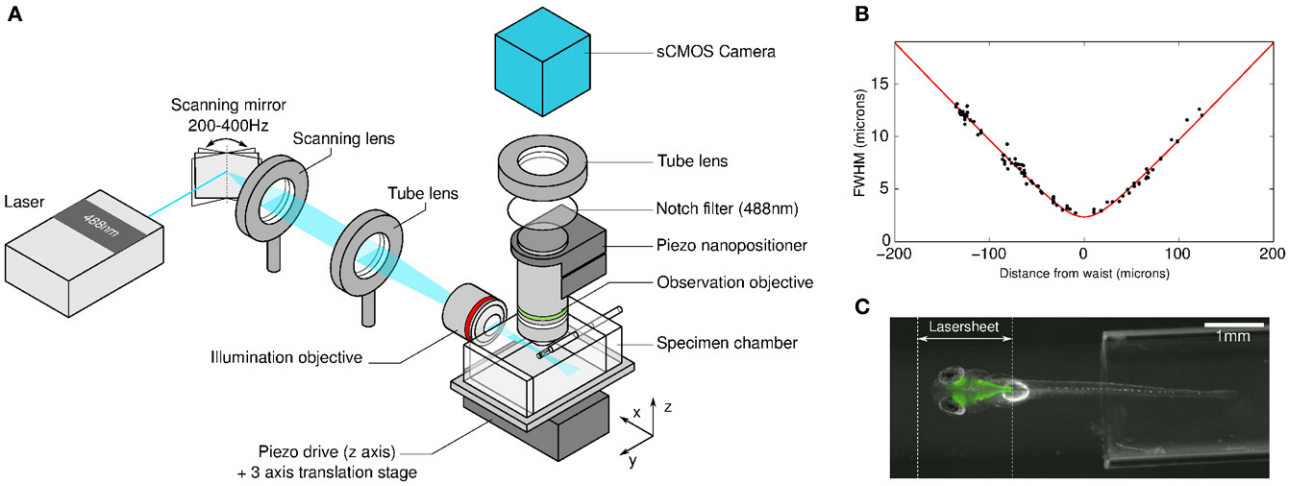

FIGURE 1 | SPIM-based functional imaging. (A) Sketch of the optical set-up. **(B)** Laser sheet thickness profile (FWHM) along the light propagation axis. Each data point corresponds to a measurement obtained with one fluorescent bead. The red curve is the best fit of the data with the theoretical profile of a Gaussian focused beam (see Truong et al., 2011) from which the value of the waist's FWHM = 2.3 μm is deduced. **(C)** Low magnification image of the larva embedded in the agarose gel cylinder and illuminated by the light sheet.

they were scanned vertically across the laser sheet. The recorded intensity signal of each bead exhibited a Gaussian profile from which the local laser-sheet full width at half maximum (FWHM) was extracted. The sheet profile was found invariant along the scanning direction, as shown by the small dispersion obtained when plotting the measured FWHM values against the beads' distance to the waist (**Figure 1B**). The profile along the propagation axis was found consistent with that expected for a Gaussian beam.

The detection objective consisted of a high-NA (1.0) 20x water-immersion objective (Olympus XLUM-PLFLN) mounted vertically onto a piezo nanopositioner (piezosystem jena MIPOS 500), allowing precise adjustment of the focus plane with the light sheet. The fluorescence light was collected by a tube lens (150 mm focal length -Thorlabs AC254-150-A) and passed through a notch filter (Thorlabs NF488-15) in order to eliminate 488 nm photons. The image was then formed onto a sCMOS sensor (PCOedge). Full 16-bit images (2560 × 2160 pixels) could be recorded at a maximum rate of 100 Hz directly onto RAID-0 hard drives. The 20x magnification yielded a field of view of $1 \times 0.8\,mm^2$, with a pixel area of $0.4 \times 0.4\,\mu m^2$. In standard experiments, images were recorded at 10–20 Hz for 20–60 min and then converted into 16-bit TIFF files.

3D RECORDINGS

3D recordings were obtained by sequentially imaging 5 distinct z-planes separated by a distance of 8 μm (total range of 32 μm). Every 50 ms, the specimen chamber was rapidly moved to a next position using the piezo-positioner. The sequence of the successive positions was interlaced in order to minimize the maximum step size and thus limit the acceleration imposed on the fish. The camera was asynchronously triggered 10 ms after each vertical displacement, and each frame was acquired for an exposure time of 40 ms. The 10 ms delay was necessary to allow for the agar cylinder to come to rest and prevent vibration-induced blurring of the images. At the end of the run, the frames were sorted to produce 5 separate stacks corresponding to each z-plane. Each stack was analyzed independently using the same algorithm as in single z-plane recordings.

AUTOMATIC IMAGE SEGMENTATION

A segmentation routine written in Matlab was developed in order to automatically identify the regions of interest (ROIs) corresponding to individual somata and neuropil regions (the Matlab code is provided as a Supplementary Material). The brain contour was first manually outlined on the first image. A highly contrasted image was then obtained by time-averaging the complete images stack. Small XY drifts were corrected by registering each image of the stack with respect to the first one by extracting the displacement vector that provided the maximum correlation. The typical maximum excursion measured over an experimental run was of the order of a few microns. However small, if not corrected, this drift was found to significantly blur the time-averaged image and hamper the proper identification of individual somata. The drift displacement sequence was also used to identify periods of strong motor behaviors. As they induced significant artifacts in the fluorescence signals, the corresponding time-periods were eliminated from the analysis.

The segmentation procedure consisted of several steps. First, the image was smoothed by running a Gaussian filter with a width equal to half the typical soma diameter (5 pixels). Local contrast stretching was applied at the scale of individual neurons. A watershed algorithm was implemented on the resulting smoothed gray-scale image, returning a collection of adjacent regions associated with putative individual somata (regions of neuropil of similar area were also retained for further analysis). A few regions were then automatically eliminated based on morphological constraints (retained ROIs had a total area between

40 and 400 pixels and an equivalent ellipse eccentricity less than 0.85). The program allowed further visualization of the resulting segmentation and manual elimination of incorrectly identified neurons. Typically, a few tens of regions, essentially located at the border of the brain, were manually discarded. Given the large FOV offered by the visualization technique, up to 5,000 somata were typically imaged and their individual ROI automatically detected within a single z-plane. This segmentation procedure took approximately 1 h per 10,000 frames, with a few minutes of user time.

SIGNAL EXTRACTION AND BASELINE NOISE ESTIMATION

The fluorescence time signal $F(t)$ for each neuron was extracted by evaluating the mean intensity across the pixels within each ROI, in each motion-corrected image. After subtraction of the background, estimated from the average intensity of pixels outside the brain, a baseline fluorescence signal was estimated for each neuron by the running average of the 8th percentile of the raw data in sliding windows of 30 s length (Dombeck et al., 2007). The resulting smooth curve b_{slow} locally approximated the baseline level and reflected slow fluctuations unrelated to the fast calcium transients evoked by spiking activity. The relative variation of fluorescence intensity, dF/F, was calculated as $dF/F = (F(t) - b_{\text{slow}})/b_{\text{slow}}$.

The standard deviation σ_{noise} of each neuron's baseline fluctuations was extracted from the distribution of neuronal dF/F values. These distributions are skewed toward positive values reflecting the presence of activity-evoked positive transients in the fluorescence signal. In contrast, negative data points are unlikely to be related to neuronal firing. The standard deviation of the baseline noise was thus estimated by postulating that these negative fluctuations were part of a Gaussian stochastic process. Consistently, the corresponding region of the distribution could be accurately fitted with a Gaussian function ($r^2 = 0.997 \pm 0.002$ for a representative dataset) from which the standard deviation σ_{noise} was extracted for each neuron's fluorescence time-series.

2P-PSM EXPERIMENTS

In order to provide a comparison between SPIM and 2P-PSM approaches, neural recordings of spontaneous activity in the tectum were performed on similar GCaMP3-expressing larvae using a MOM-sutter system. Its main components consisted of a 25x NA1.05 Olympus objective and a Mai Tai DeepSee Ti:sapphire laser used at 920 nm with an output power of less than 3 mW after the objective. The filters consisted of a FF705 dichroic, a AFF01-680 short path (IR Blocker) and a FF01520/70 band-pass filter, all from Semrock. The PMT was a H1070 (GaAsP) from Hamamatsu. Images of 256 x 256 pixels were acquired at 4 Hz.

ANALYSIS OF NEURONAL ACTIVITY CORRELATIONS

For this analysis, we only considered fluorescence transients inferred to result from neuronal firing by imposing a threshold on each individual time-series. Any dF/F value below $3\,\sigma_{\text{noise}}$ was set to 0. For each dataset, 100 independent runs of the K-means algorithm with squared Euclidean distance and random seeds were performed (MacQueen, 1967). Only the run with minimal total sum of distances was retained. In order to determine the total number K of clusters in the segmentation, a sweep in K space between 1 and 20 was performed, and the results were inspected with silhouette plots. For example, when analyzing the data displayed in **Figure 5**, $K = 12$ was found to be the best solution. Importantly, the neuronal clusters shown in this figure, which are the most compact, proved robust with respect to changes in K between 10 and 20.

RESULTS

Our main objective was to establish the advantages and limitations of SPIM for *in-vivo* functional imaging in zebrafish. Spontaneous activity was recorded in 5–9-day-old HuC:GCaMP3 zebrafish larvae. First, we characterized the volume of the brain accessible to single-cell calcium imaging using SPIM. Second, we estimated the gain in the number of neurons that could be simultaneously sampled, and in the maximum accessible acquisition rate, that this imaging strategy provides compared to standard 2P-PSM experiments. Finally, we showed how the extended FOV provided by SPIM allows one to probe correlations in spontaneous activity among multiple brain regions as an indication of inter-regional brain connectivity.

OPTICAL SECTIONING EFFICIENCY OF THE SPIM SET-UP

In SPIM, the efficiency of the optical sectioning is set by the thickness of the illumination sheet. As expected for scanned illumination with a Gaussian beam, the laser sheet profile was found to be invariant along the scanning axis and to display a hyperbolic profile along the light propagation axis, with a diffraction-limited minimum thickness of 2.3 μm located at the focal plane of the illumination objective (see **Figure 1B**). This value was found to increase to 7 μm at a distance of 80 μm from the waist. Given the characteristic inter-neuron distance (of the order of 7 μm), the method thus yields single neuron resolution over a FOV of $\simeq 160 \times 1000\,\mu$m around the midline of the larva, a region which contains the majority of the somata. In the most distal regions of the zebrafish brain, the illumination sheet spans 1–2 neuron diameter such that SPIM does not provide single-cell resolution.

Despite this limited axial resolution, the images appeared highly contrasted in most of the brain volume, allowing for the implementation of an automatic segmentation algorithm in order to identify ROIs associated with each neuron. This aspect of the method is illustrated in **Figure 2**. Images were taken at successive z-positions with 0.4 μm intervals across the brain over a total vertical distance of 220 μm (see Supplementary Movie 1). The exposure time was set to 100 ms such that the complete stack was acquired in less than 1 min. We were able to automatically identify virtually all the somata throughout the brain volume except for small telencephalic regions located in the shadow of the eye and in the neuropil regions.

The robustness of the automatic segmentation procedure is illustrated in **Figure 2B** for different brain areas at a depth of 104 μm, which corresponded to the middle of the preceding stack. The segmentation was performed on the image obtained by time-averaging 18, 000 frames acquired at 10 Hz over 30 min, which corresponds to a typical neural recording configuration. The possibility to automatically identify somata's ROIs is a crucial

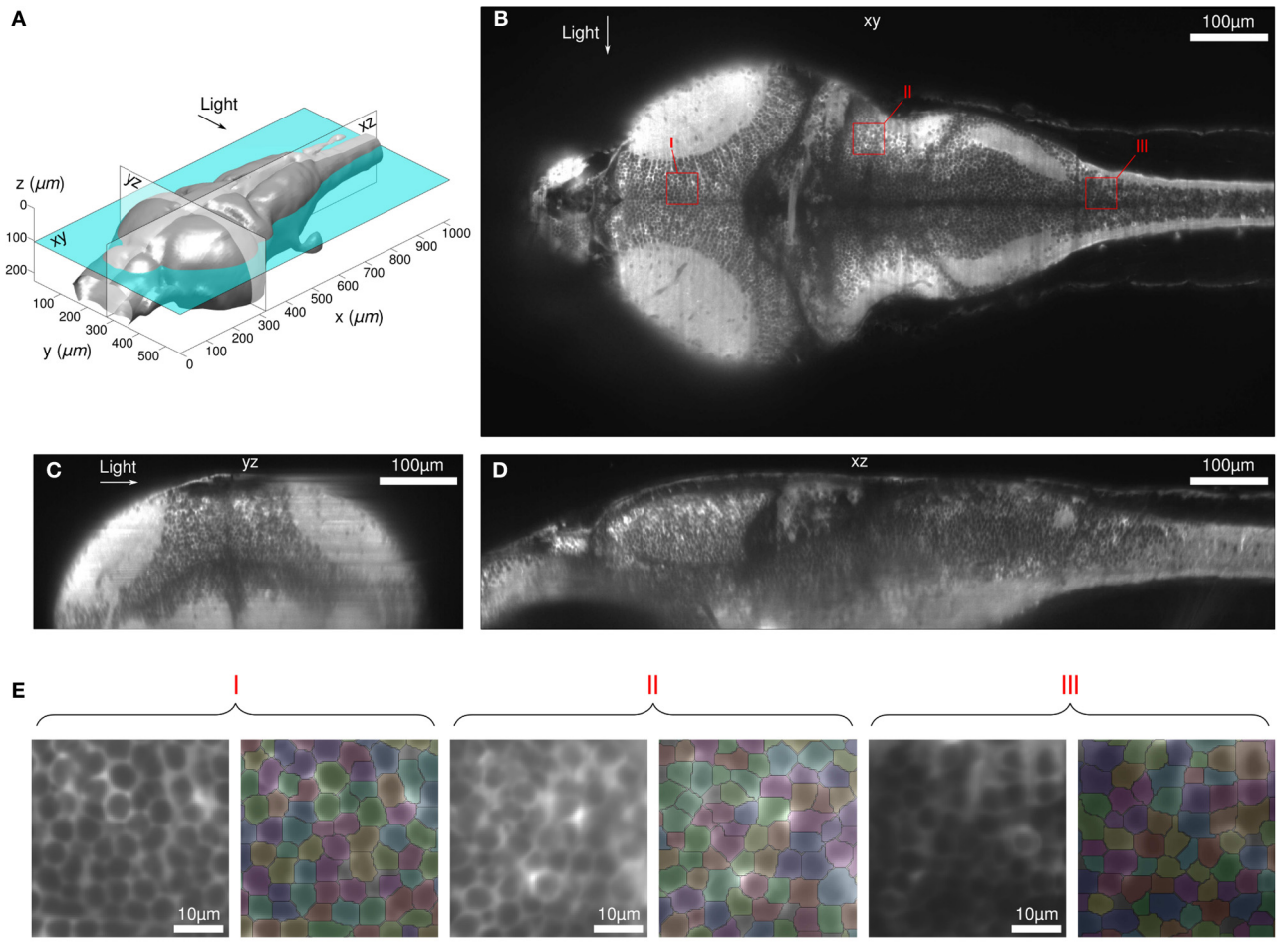

FIGURE 2 | Stack and segmentation. (A–D) Multi-view sections of the brain-volume reconstructed from a complete 3D stack (no filtering). The voxel volume is $0.4 \times 0.4 \times 0.4\,\mu m^3$. See Supplementary Movie 1 for a complete visualization of the brain. **(E)** Result of the segmentation algorithm for 3 different sub-regions shown in **(B)** with red-squares.

aspect of the present approach, since the manual outlining of ≃5,000 neurons per plane would otherwise impose a severe practical limit on the method.

One should be aware that the light sheet thickness measurement described in Materials and Methods provides an upper bound for the axial resolution in the actual experiment. When imaging the brain volume, the scattering of the illumination beam tends to reduce the effective axial resolution. Similarly, the x-y resolution is expected to be degraded by the scattering of the fluorescence photons. The magnitude of these effects was estimated by computing the cellular-scale contrast, defined as the difference in intensity between the brightest and dimmest pixels (second and 98th percentile) over areas slightly larger than the somata characteristic ROIs. As anticipated, the contrast was found to be maximum in the most dorsal region of the fish, where the distances traveled by the illumination and fluorescent photons were both minimum. The contrast then decreased continuously with the depth of observation, but with a moderate decay rate of $40 \pm 5\%$ per $100\,\mu m$.

FAST, BRAIN-WIDE CALCIUM IMAGING

Images of a single z-plane were acquired at 10–20 Hz (50–100 ms exposure time) over periods of 20–60 min (a short excerpt of a 10 Hz recording is provided in supplementary Movie 2). In the majority of the experiments, the plane of observation was chosen to encompass a large number of neurons from all major brain regions (spinal cord, hindbrain, midbrain, and forebrain). After automatic segmentation, the relative fluorescence time series dF/F was extracted for each individual soma and for neuropil regions of similar area (**Figure 3**).

As no external stimulation was applied, the recorded fluorescence dynamics reflected spontaneous neural activity. Strictly speaking, the illumination wavelength (488 nm) being within the fish visual spectrum, the larva was submitted to a visual stimulation. However, owing to the rapid scanning rate (>200 Hz), such a stimulation can be considered physiologically time-invariant and the fish is expected to habituate rapidly. Consistently, we did not observe any systematic change in the level of neural activity over the duration of the experiments. This was

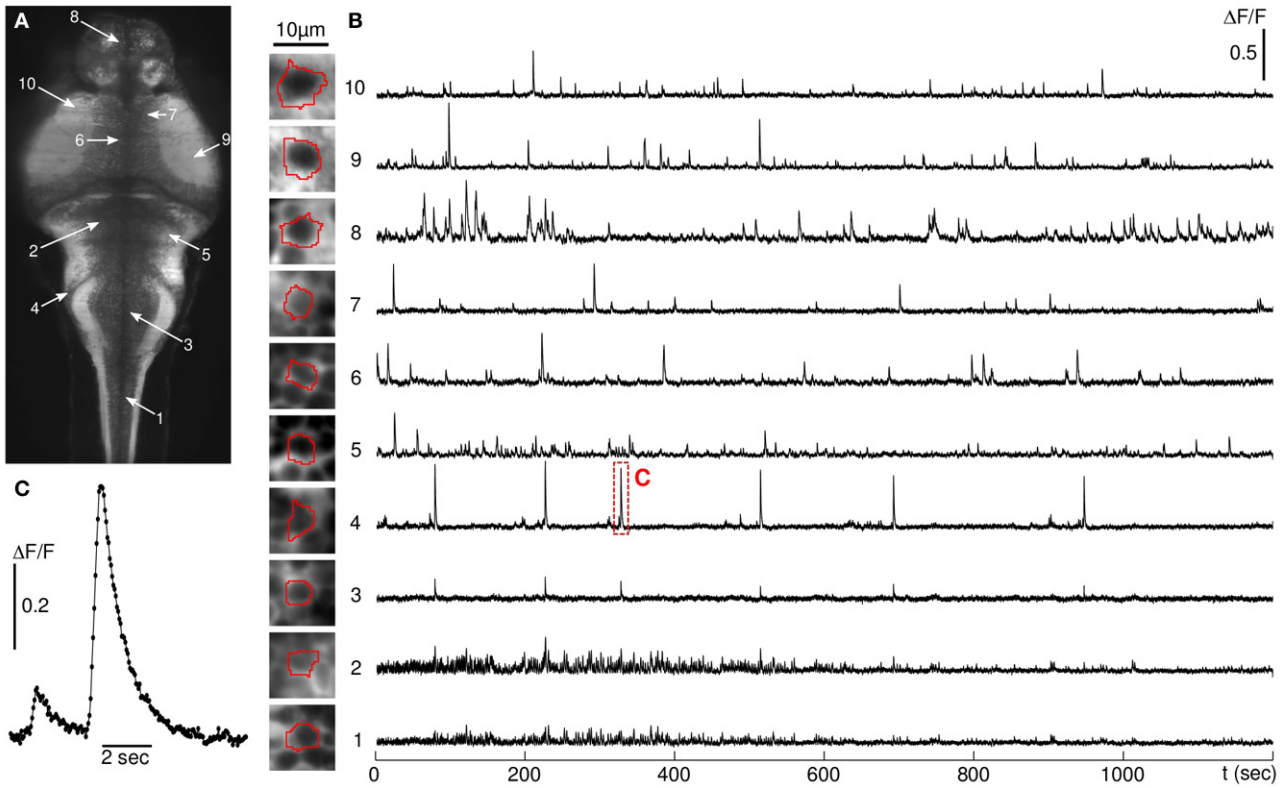

FIGURE 3 | Fluorescence signals. (A) Time-averaged image of a brain slice of a 6 dpf larva. **(B)** Individual traces of 10 neurons whose locations are indicated in red on the image, recorded at 20 Hz acquisition rate. the thumbnails display each neuron's ROI. **(C)** Blow-up view of a typical activity-related fluorescence event indicated by a red rectangle in **(B)**.

checked by computing the mean of the activity-related transients in the first and second half of the runs. The difference between both measurements was not found to be statistically significant.

In all runs, the laser intensity was set to 2 mW. At this power, the fluorescence baseline did not display any noticeable decay over the duration of the experimental runs, which indicated the absence of significant photo-bleaching. Furthermore, as already mentioned, the level of activity showed no systematic change. Both observations provided a solid indication that phototoxicity effects should be rather limited at this level of illumination. At 6 mW, although the level of photo-bleaching was still relatively modest (≈10% baseline intensity decay in 20 min), the activity-related signal from somata in all regions of the brain tended to vanish. This effect was reversible, i.e. the original fluorescence transient level could be recovered by setting the power back to 2 mW. The most plausible interpretation of this set of observations is that before phototoxicity effects become significant, the calcium-bound fluorophores, which have a much higher quantum yield that the unbound species, reached their photo-emission saturation rate resulting in a significant reduction in amplitude of the fluorescence transients.

In some experiments, streaking artifacts were observed in the form of rapid correlated fluctuations of intensity along narrow bands oriented parallel to the illumination axis. These flickering regions resulted from the motion of light absorbing objects (probably the hemoglobin within blood cells) circulating along the exposed face of the animal. As they crossed the light sheet, they projected a thin shadow along the illumination path. When too intense, these fluctuations biased the analysis of the fluorescence signals, so that the corresponding neurons had to be manually eliminated from the analysis.

THREE-DIMENSIONAL CALCIUM-IMAGING

The high data throughput provided by SPIM can be used to obtain dynamic 3D brain-wide recordings of neural activity at a lower acquisition rate. As a proof of concept, we recorded 5 different z-planes, separated by 8 µm, a distance which guaranteed that neurons from different slices were distinct. Axial scanning was obtained by sequentially moving the specimen at the successive z-positions (**Figure 4A**). This approach allowed for the simultaneous recording of over 25,000 individual neurons (and large neuropil regions) at 4 Hz. **Figures 4B,C** shows the location of the centers of mass of the sampled ROIs and the associated dF/F traces for a few neurons, located in different regions of the brain.

EVALUATING THE SIGNAL-TO-NOISE RATIO (SNR)

In order to evaluate the sensitivity of the method, a statistical comparison was made between spontaneous activity recordings

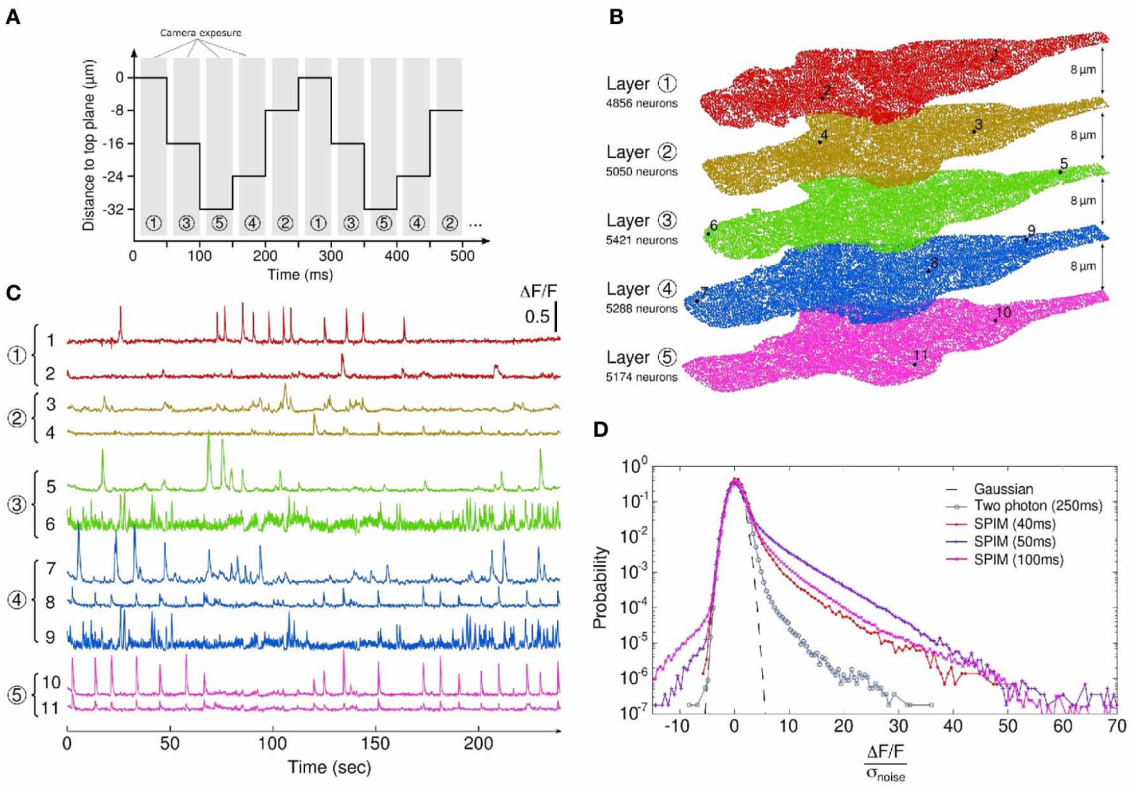

FIGURE 4 | 3D calcium-imaging. (A) Interlaced sequence of acquisition of 5 z-planes separated by 8 µm intervals. Exposure time is 40 ms and each plane is recorded at a rate of 4 Hz. **(B)** Localization of the monitored ROIs (somas and neuropil regions) obtained through automatic segmentation on the 5 different planes. The number of actual somas is given for each z-plane, yielding a total of 25789 simultaneously recorded neurons (see Supplementary Movie 3 for the 5 z-frames fluorescence dynamics). **(C)** Characteristic signals from neurons within the stack. **(D)** Comparison of the noise-normalized fluorescence signal distributions for SPIM-based experiments (colored) and a 2P-PSM experiment (gray). For each experiment, the exposure time is indicated. The 40 ms-exposure SPIM experiment is the 3D imaging run (5 z-planes, 4 Hz effective recording rate).

obtained using SPIM and 2P-PSM in the tectal region under comparable experimental conditions (see Materials and Methods, all statistics were computed from three independent runs for each set-up). At 10 Hz acquisition rate, the standard deviation σ_{noise} of the baseline fluorescence signal (extracted for each neuron, see Materials and Methods) using SPIM was found to be of order 1% ($\sigma_{noise} = 0.008 \pm 0.002$). This quantity was measured at 0.13 ± 0.04 in 2P-PSM at 4 Hz acquisition rate. The relatively low noise level observed in SPIM is a consequence of the larger photon count provided by the method. A significant fraction of these photons, however, originates from regions outside the in-focus ROIs, owing to the less efficient sectioning and the wide-field nature of this optical method. This in turn increases the background signal, thus limiting the amplitude of the dF/F transients. For comparable configurations, 2P-PSM recordings actually displayed statistically higher dF/F peak signals: the average of the dF/F values within the highest percentile was found to be 0.11 and 0.55 in SPIM and 2P-PSM, respectively.

To provide a fair SNR comparison between both methods, each neuronal dF/F distribution was thus normalized by its baseline noise standard deviation σ_{noise}. The resulting noise-normalized fluorescence distributions are shown in **Figure 4D** for three experimental SPIM runs (single z-plane recordings at acquisition rates 10 and 20 Hz, 5 z-planes 3D recording at 4 Hz) and for a typical run performed at 4 Hz using 2P-PSM. Although the SPIM experiments used lower exposure times (40–100 ms instead of 250 ms), the corresponding distributions appeared to be more significantly skewed toward large positive values as compared to 2P-PSM, which indicated that the SNR was improved. Across all experiments, the skewness of the noise-normalized distribution was found to be 3.70 ± 0.78 in SPIM as compared to 0.54 ± 0.11 in 2P-PSM. Although this difference is statistically significant, one should consider such a determination of the relative SNR as a rough estimate since the level of spontaneous activity in the tectum may vary significantly between runs.

IDENTIFYING BRAIN-WIDE HIGHLY CORRELATED NEURONAL CLUSTERS

One of the important assets of the SPIM method, with respect to PSM approaches, lies in the possibility of simultaneously recording neural activity in distinct brain regions. This in turn enables the identification of ensembles of neurons spanning

different regions of the brain that exhibit correlated activity and are thus likely to be interconnected or activated by a common source. Here we illustrate this possibility by using a 60 min long single plane recording of multiple brain regions at 10 Hz acquisition rate. The fluorescence time-series of each neuron was first thresholded in order to extract activity-related events (see Materials and Methods). The rest of the data points was set to zero. This thresholding was necessary to eliminate coherent baseline noise, induced by minute laser intensity fluctuations, which would have otherwise biased the correlation analysis.

The distribution of pair-wise correlations showed a heavy-tail of fairly large values, suggesting the presence of significantly correlated activity (**Figure 5A**). As a first attempt to identify the optimal clustering of the neural activity time-series, the K-means algorithm was implemented (see Materials and Methods). An example of the computed partitionings is shown in **Figure 5B**, where a reasonable clusterization of highly correlated neuronal groups with moderate cross-talk can be observed. Three of these clusters topographical layouts are shown in **Figures 5C–G**, together with excerpts of (unfiltered) fluorescence traces of 3 neurons within each cluster.

The first cluster revealed significant correlations among neighboring neurons in the optic tectum (**Figure 5C**). Notice that the mean pair-wise correlation was found to continuously decay from a confined region located at the border of the neuropil. The second cluster consisted of neurons mostly located in the spinal cord (**Figure 5E**). In the first 10 min of the run, these neurons exhibited characteristic rhythmic synchronous activity at a typical frequency of 0.2 Hz (see **Figure 5F**). In the paralyzed preparation, these bouts of spinal cord activity are likely to be associated with fictive swimming events. The large FOV allowed us to further identify a sub-population of distant neurons located in two bilaterally symmetric confined regions, which probably correspond to the medial octavolateralis nucleus. A similar cluster of correlated neurons was observed in another animal exhibiting fictive swimming. Finally, stripes of neurons located in the vagal lobe, a brain structure implicated in the processing of gustatory stimuli, were found to be correlated with distant bilaterally symmetric neuronal clusters probably located at the secondary gustatory nuclei (SGN), in the isthmus ventrally to the cerebellum (**Figure 5G**). It should be noticed that these three functional clusters, associated with three distinct modalities (visual, motor, and gustatory), were identified from a single 60 min long recording of a single z-plane.

DISCUSSION

In PSM-based calcium-imaging, neurons are probed sequentially, which imposes a trade-off between the number of sampled neurons N_{cells} and the acquisition rate f_{acq} (Lütcke and Helmchen, 2011). In order to increase the maximum of the product $N_{\text{cells}}f_{\text{acq}}$, AOM-based random scanning approaches have been developed, which aimed at minimizing the time wasted in acquiring regions outside the neurons volume. Notice that this issue is almost irrelevant in zebrafish, since most of the brain consists of tightly packed somata (almost no extra-cellular space). A fundamental limit in data throughput is, however, set by the minimum dwelling time of the laser at each voxel required to record a significant number of photons.

Scanned laser sheet imaging also relies on sequential recording of neurons, but those within a given line are illuminated and recorded in parallel. As established in the present experiment, this yields a $\simeq 20-$fold increase in the accessible $N_{\text{cells}}f_{\text{acq}}$ product for similar experimental conditions. Hence, while current PSM-based calcium-imaging set-ups in zebrafish allow monitoring $\simeq$1000 neurons at 5 Hz, SPIM allows monitoring up to 5,000 neurons from a single z-plane at 20 Hz, and over 25,000 neurons from 5 different z-planes at 4 Hz, with similar or better SNR. This large increase in data throughput offered by SPIM-based calcium imaging opens new opportunities for studying various aspects of neural processes.

TOWARD *in toto* DYNAMIC NEURAL RECORDING OF A VERTEBRATE BRAIN

Larval zebrafish constitutes a unique vertebrate system to study the activity of brain-wide neural circuits and help decipher the way information is processed across different brain regions. This possibility was illustrated in a recent paper by Ahrens et al. (2012). By recording calcium activity in an animal that interacted fictively with a virtual environment, the authors were able to identify neural populations spanning multiple brain areas that were activated during specific phases of adaptive locomotion. Owing to the limited number of neurons sampled during a single recording, different experiments and animals had to be fused in order to produce a complete physiological map of the associated neural networks. This approach was not only time-consuming but also implicitly assumed that the recruited neuronal population was invariant from run to run and animal to animal. In order to overcome these limitations, one would need to *simultaneously* record the complete brain. This would allow for the gathering of similar data on a single-trial basis, and thus permit one to probe the variability in the spatial pattern of the recruited neural population.

In its current configuration, our SPIM set-up allows one to simultaneously sample $\simeq$30% of the total number of neurons (Hill et al., 2003) at 4 Hz. Given the decay time of GCaMP3 (of the order of 0.5 s), this acquisition rate guarantees that any calcium transient for a given neuron within this volume is detected. This result was shown as a proof-of-concept and further refinements are needed. In particular, axial scanning was obtained by continuously moving the sample across the light-sheet. This approach presents two major drawbacks. First, it submits the larva to an oscillatory acceleration of maximum amplitude of order $0.1\,\text{ms}^{-2} = 10^{-2}\,g$ where g is the gravitational acceleration. Although relatively low, this inertial stimulation may trigger responses from the fish's vestibular system. Second, the softness of the agar gel limits the rate at which successive z-positions can be imaged, since a significant time is needed for the cylinder to come to rest. Both issues could be addressed by maintaining the specimen fixed while synchronously moving the laser sheet (using a second galvanometric mirror) and the observation objective. Higher z-scanning rates could also be obtained by using tunable optical components (Grewe et al., 2011). Given the constant progress in GECI sensitivity (Akerboom et al., 2012) and sCMOS

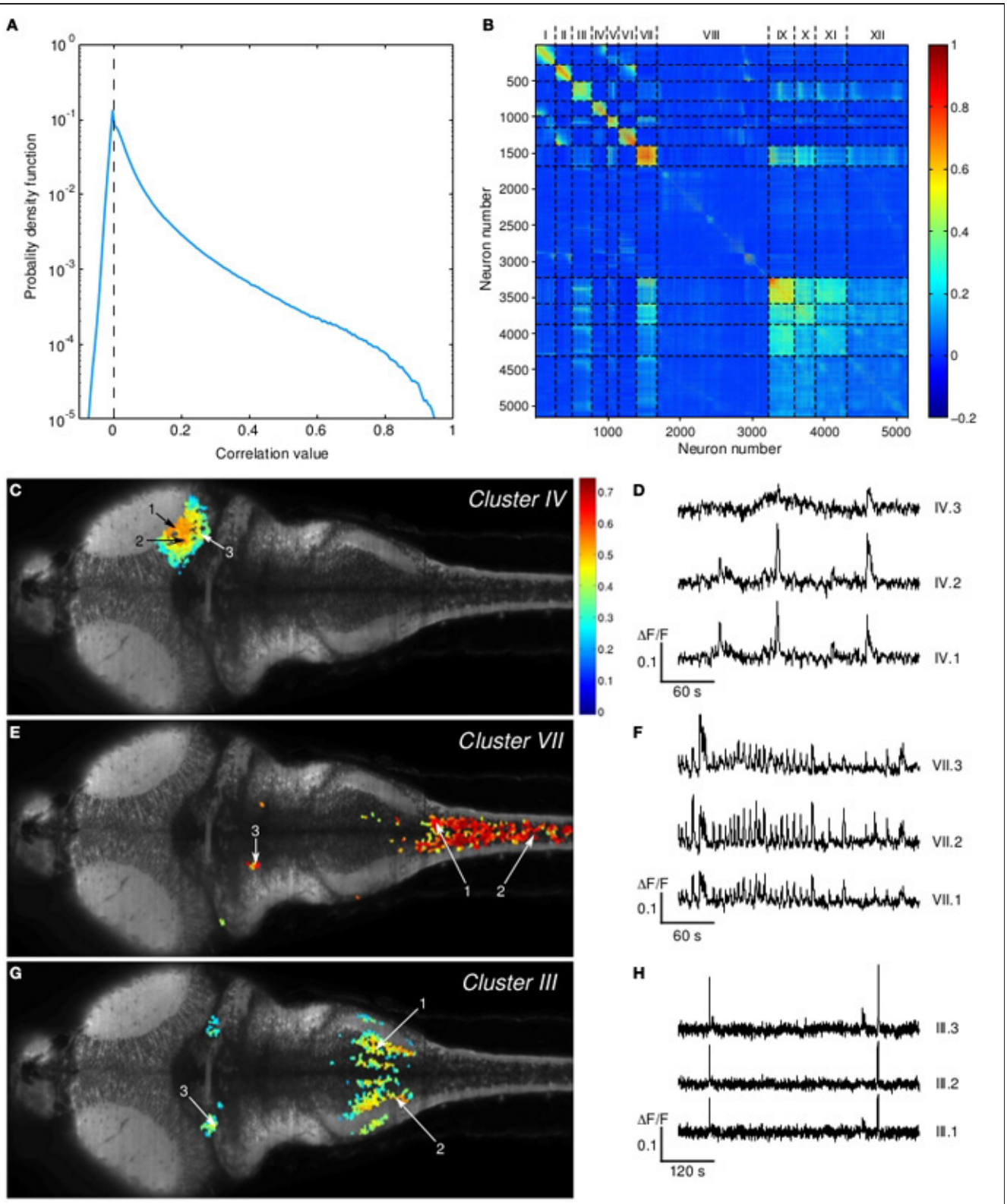

FIGURE 5 | Activity-correlated neuronal clusters. (A) Distribution of pair-wise correlations. The data were obtained from a 10 Hz, 60 min long experiment on a 6 dpf larva. **(B)** Correlation matrix sorted using the K-means algorithm with associated cluster partitioning. **(C–G)** Topographical layouts of clusters IV-VII-III. The color code corresponds to the mean pair-wise correlation value with the neurons from the cluster. For each cluster, 3 short excerpts of fluorescence traces exhibiting clear activity correlation are shown **(D–H)**.

sensors, SPIM-based calcium imaging should provide virtually full brain simultaneous recording at several Hertz in the near future.

PROBING THE TIME-STRUCTURE OF BRAIN-WIDE NEURAL ACTIVITY PATTERNS

Calcium-imaging was originally seen as a way to overcome the limitation in the number of neurons that could be recorded using electrophysiological approaches. For a long time, it was believed that an inevitable corollary of this method was to sacrifice temporal information as the calcium signals were typically probed at a few Hertz, far below physiological timescales. In recent years, several fast imaging experiments proved this assumption wrong. Recently, Grewe *et al.* demonstrated a $\simeq$10 ms resolution on the firing dynamics of individual neurons based on calcium-imaging performed at hundreds of Hertz (Grewe et al., 2010). This time-resolution was actually set by the intrinsic dynamics of the fluorescent calcium indicator (Oregon Green BAPTA-1). This achievement demonstrated that calcium-imaging could constitute a suitable method for probing neural networks dynamics with near-millisecond resolution, and thus could serve to explore how spike-timing may play a role in neural processes. However, this exciting result was obtained at the cost of the number of probed neurons, of the order of a few tens *i.e.* close to that currently recorded using silicon-based nanoprobes. Fast *in vivo* neural recordings are thus currently restricted to spatially confined micro-circuits. In contrast, SPIM should allow reaching high acquisition rates while still probing a large number of neurons. In the present experiments, the acquisition rate was limited to 20 Hz since the relatively slow GCaMP3 rising time (of the order of 100 ms) sets the bandwidth within which spiking dynamics can be efficiently probed. Increasing the acquisition rate would only degrade SNR without enhancing the time-resolution. With sufficiently rapid and sensitive calcium reporters—such as the synthetic sensors used by Grewe et al. (2010)—it should be possible to record up to 1000 neurons with near-millisecond resolution.

Several limitations of this method still need to be addressed. First, the optical sectioning only guarantees single-cell resolution in the most proximal part of the brain. Different methods could be implemented to increase the axial resolution, such as structured illumination (Keller et al., 2010) or confocal light-sheet imaging (Silvestri et al., 2012). A second issue is related to the use of visible light illumination (488 nm), which currently hampers the proper stimulation of the fish visual system. This limitation could be circumvented by using two photon fluorescence excitation with the same SPIM geometry (Palero et al., 2010; Truong et al., 2011). This would in turn opens the possibility to implement Bessel-beam illumination. Beyond the expected gain in optical sectioning efficiency provided by this method (Planchon et al., 2011), the self-healing property of Bessel beams may permit to mitigate the problems of streaking.

In the present article, we have demonstrated how the extended FOV provided by this alternative imaging strategy allows one to identify brain-wide functional neuronal circuits by straightforward correlation analysis of the spontaneous activity pattern. Overall, the combination of SPIM-based functional imaging, transgenic larvae and methods for statistical data analysis will lead to the generation of a whole brain atlas of functional neuronal connectivity, either by monitoring spontaneous or sensory-evoked activity, or through localized channelrhodopsin-2 stimulation.

ACKNOWLEDGMENTS

We are grateful to Laurent Bourdieu and Jean-François Leger for constant support and numerous advices throughout the assembly of the SPIM set-up. This work was supported in part by EraSysBio+ ZeBrain and ERC stg 243106.

SUPPLEMENTARY MATERIAL

The Supplementary Material for this article can be found online at: http://www.frontiersin.org/Neural_Circuits/10.3389/fncir.2013.00065/abstract

REFERENCES

Ahrens, M. B., Li, J. M., Orger, M. B., Robson, D. N., Schier, A. F., Engert, F., et al. (2012). Brain-wide neuronal dynamics during motor adaptation in zebrafish. *Nature* 485, 471–477.

Aizenberg, M., and Schuman, E. M. (2011). Cerebellar-dependent learning in larval zebrafish. *J. Neurosci.* 31, 8708–8712.

Akerboom, J., Chen, T.-W., Wardill, T. J., Tian, L., Marvin, J. S., Mutlu, S., et al. (2012). Optimization of a GCaMP calcium indicator for neural activity imaging. *J. Neurosci.* 32, 13819–13840.

Alivisatos, A., Chun, M., Church, G. M., Greenspan, R. J., Roukes, M. L., and Yuste, R. (2012). The brain activity map project and the challenge of functional connectomics. *Neuron* 74, 970–974.

Bollmann, J. H., and Engert, F. (2009). Subcellular topography of visually driven dendritic activity in the vertebrate visual system. *Neuron* 61, 895–905.

Del Bene, F., Wyart, C., Robles, E., Tran, A., Looger, L., Scott, E. K., et al. (2010). Filtering of visual information in the tectum by an identified neural circuit. *Science* 330, 669–673.

Denk, W., Strickler, J., and Webb, W. (1990). Two-photon laser scanning fluorescence microscopy. *Science* 248, 73–76.

Dombeck, D. A., Khabbaz, A. N., Collman, F., Adelman, T. L., and Tank, D. W. (2007). Imaging large-scale neural activity with cellular resolution in awake, mobile mice. *Neuron* 56, 43–57.

Du, J., Blanche, T. J., Harrison, R. R., Lester, H. A., and Masmanidis, S. C. (2011). Multiplexed, high density electrophysiology with nanofabricated neural probes. *PLoS ONE* 6:e26204. doi: 10.1371/journal.pone.0026204

Engelbrecht, C. J., Voigt, F., and Helmchen, F. (2010). Miniaturized selective plane illumination microscopy for high-contrast *in vivo* fluorescence imaging. *Opt. Lett.* 35, 1413–1415.

Grewe, B. F., Langer, D., Kasper, H., Kampa, B. M., and Helmchen, F. (2010). High-speed *in vivo* calcium imaging reveals neuronal network activity with near-millisecond precision. *Nat. Methods* 7, 399–405.

Grewe, B. F., Voigt, F. F., van't Hoff, M., and Helmchen, F. (2011). Fast two-layer two-photon imaging of neuronal cell populations using an electrically tunable lens. *Biomed. Opt. Express* 2, 2035–2046.

Grienberger, C., and Konnerth, A. (2012). Imaging calcium in neurons. *Neuron* 73, 862–885.

Higashijima, S.-I., Masino, M. A., Mandel, G., and Fetcho, J. R. (2003). Imaging neuronal activity during zebrafish behavior with a genetically encoded calcium indicator. *J. Neurophysiol.* 90, 3986–3997.

Hill, A., Howard, C. V., Strahle, U., and Cossins, A. (2003). Neurodevelopmental defects in zebrafish (*Danio rerio*) at environmentally relevant dioxin (TCDD) concentrations. *Toxicol. Sci.* 76, 392–399.

Holekamp, T. F., Turaga, D., and Holy, T. E. (2008). Fast three-dimensional fluorescence imaging of activity in neural populations by objective-coupled planar illumination microscopy. *Neuron* 57, 661–672.

Huisken, J., Swoger, J., Del Bene, F., Wittbrodt, J., and Stelzer, E. H. K. (2004). Optical sectioning deep inside live embryos by selective plane illumination microscopy. *Science* 305, 1007–1009.

Katona, G., Szalay, G., Maak, P., Kaszas, A., Veress, M., Hillier, D., et al. (2012). Fast two-photon *in vivo* imaging with three-dimensional random-access scanning in large tissue volumes. *Nat. Methods* 9, 201–208.

Keller, P. J., and Dodt, H.-U. (2012). Light sheet microscopy of living or cleared specimens. *Curr. Opin. Neurobiol.* 22, 138–143.

Keller, P. J., Schmidt, A. D., Santella, A., Khairy, K., Bao, Z., Wittbrodt, J., et al. (2010). Fast, high-contrast imaging of animal development with scanned light sheet-based structured-illumination microscopy. *Nat. Methods* 7, 637–642.

Lillis, K. P., Eng, A., White, J. A., and Mertz, J. (2008). Two-photon imaging of spatially extended neuronal network dynamics with high temporal resolution. *J. Neurosci. Methods* 172, 178–184.

Lister, J. A., Robertson, C. P., Lepage, T., Johnson, S. L., and Raible, D. W. (1999). Nacre encodes a zebrafish microphthalmia-related protein that regulates neural-crest-derived pigment cell fate. *Development* 126, 3757–3767.

Lütcke, H., and Helmchen, F. (2011). Two-photon imaging and analysis of neural network dynamics. *Rep. Prog. Phys.* 74:086602. doi: 10.1088/0034-4885/74/8/086602

MacQueen, J. (1967). "Some methods for classification and analysis of multivariate observations," in *Proceedings of 5-th Berkeley Symposium on Mathematical Statistics and Probability,* Vol. 1, (Berkeley, CA: University of California Press), 281–297.

McLean, D. L., and Fetcho, J. R. (2009). Spinal interneurons differentiate sequentially from those driving the fastest swimming movements in larval zebrafish to those driving the slowest ones. *J. Neurosci.* 29, 13566–13577.

Mertz, J. (2011). Optical sectioning microscopy with planar or structured illumination. *Nat. Methods* 8, 811–819.

Niell, C. M., and Smith, S. J. (2005). Functional imaging reveals rapid development of visual response properties in the zebrafish tectum. *Neuron* 45, 941–951.

Palero, J., Santos, S. I. C. O., Artigas, D., and Loza-Alvarez, P. (2010). A simple scanless two-photon fluorescence microscope using selective plane illumination. *Opt. Express* 18, 8491–8498.

Park, H. C., Kim, C. H., Bae, Y. K., Yeo, S. Y., Kim, S. H., Hong, S. K., et al. (2000). Analysis of upstream elements in the HuC promoter leads to the establishment of transgenic zebrafish with fluorescent neurons. *Dev. Biol.* 227, 279–293.

Planchon, T. A., Gao, L., Milkie, D. E., Davidson, M. W., Galbraith, J. A., Galbraith, C. G., et al. (2011). Rapid three-dimensional isotropic imaging of living cells using Bessel beam plane illumination. *Nat. Methods* 8, 417–423.

Ramdya, P., and Engert, F. (2008). Emergence of binocular functional properties in a monocular neural circuit. *Nat. Neurosci.* 11, 1083–1090.

Salomé, R., Kremer, Y., Dieudonné, S., Léger, J.-F., Krichevsky, O., Wyart, C., et al. (2006). Ultrafast random-access scanning in two-photon microscopy using acousto-optic deflectors. *J. Neurosci. Methods* 154, 161–174.

Silvestri, L., Bria, A., Sacconi, L., Iannello, G., and Pavone, F. S. (2012). Confocal light sheet microscopy: micron-scale neuroanatomy of the entire mouse brain. *Opt. Express* 20, 20582–20598.

Stevenson, I. H., and Kording, K. P. (2011). How advances in neural recording affect data analysis. *Nat. Neurosci.* 14, 139–142.

Sumbre, G., Muto, A., Baier, H., and Poo, M.-M. (2008). Entrained rhythmic activities of neuronal ensembles as perceptual memory of time interval. *Nature* 456, 102–106.

Tian, L., Hires, S. A., and Looger, L. L. (2012). Imaging neuronal activity with genetically encoded calcium indicators. *Cold Spring Harb. Protoc.* 2012, 647–656.

Tomer, R., Khairy, K., and Keller, P. J. (2011). Shedding light on the system: studying embryonic development with light sheet microscopy. *Curr. Opin. Genet. Dev.* 21, 558–565.

Truong, T. V., Supatto, W., Koos, D. S., Choi, J. M., and Fraser, S. E. (2011). Deep and fast live imaging with two-photon scanned light-sheet microscopy. *Nat. Methods* 8, 757–760.

Turaga, D., and Holy, T. E. (2012). Organization of vomeronasal sensory coding revealed by fast volumetric calcium imaging. *J. Neurosci.* 32, 1612–1621.

Verveer, P. J., Swoger, J., Pampaloni, F., Greger, K., Marcello, M., and Stelzer, E. H. K. (2007). High-resolution three-dimensional imaging of large specimens with light sheet-based microscopy. *Nat. Methods* 4, 311–313.

Weber, M., and Huisken, J. (2011). Light sheet microscopy for real-time developmental biology. *Curr. Opin. Genet. Dev.* 21, 566–572.

Wyart, C., Del Bene, F., Warp, E., Scott, E. K., Trauner, D., Baier, H., et al. (2009). Optogenetic dissection of a behavioural module in the vertebrate spinal cord. *Nature* 461, 407–410.

Yuste, R., and Denk, W. (1995). Dendritic spines as basic functional units of neuronal integration. *Nature* 375, 682–684.

Conflict of Interest Statement: The authors declare that the research was conducted in the absence of any commercial or financial relationships that could be construed as a potential conflict of interest.

Received: 08 February 2013; accepted: 25 March 2013; published online: 09 April 2013.

Citation: Panier T, Romano SA, Olive R, Pietri T, Sumbre G, Candelier R and Debrégeas G (2013) Fast functional imaging of multiple brain regions in intact zebrafish larvae using Selective Plane Illumination Microscopy. Front. Neural Circuits 7:65. doi: 10.3389/fncir.2013.00065

frontiers in
NEURAL CIRCUITS

ORIGINAL RESEARCH ARTICLE
published: 07 June 2013
doi: 10.3389/fncir.2013.00108

Fusion of locomotor maneuvers, and improving sensory capabilities, give rise to the flexible homing strikes of juvenile zebrafish

Rebecca E. Westphal [1] ***and Donald M. O'Malley*** [2] *******

[1] *Department of Natural Sciences, North Shore Community College, Lynn, MA, USA*
[2] *Department of Biology, Northeastern University, Boston, MA, USA*

Edited by:
German Sumbre, Ecole Normale Superieure, France

Reviewed by:
Matthew McHenry, University of California, Irvine, USA
Ethan Gahtan, Humboldt State University, USA
Mark A. Masino, University of Minnesota, USA

****Correspondence:***
Donald M. O'Malley, Department of Biology, Northeastern University, 134 Mugar Hall, Boston, MA 02115, USA
e-mail: d.omalley@neu.edu

At 5 days post-fertilization and 4 mm in length, zebrafish larvae are successful predators of mobile prey items. The tracking and capture of 200 μm long *Paramecia* requires efficient sensorimotor transformations and precise neural controls that activate axial musculature for orientation and propulsion, while coordinating jaw muscle activity to engulf them. Using high-speed imaging, we report striking changes across ontogeny in the kinematics, structure and efficacy of zebrafish feeding episodes. Most notably, the discrete tracking maneuvers used by larval fish (turns, forward swims) become fused with prey capture swims to form the continuous, fluid homing strikes of juvenile and adult zebrafish. Across this same developmental time frame, the duration of feeding episodes become much shorter, with strikes occurring at broader angles and from much greater distances than seen with larval zebrafish. Moreover, juveniles use a surprisingly diverse array of motor patterns that constitute a flexible predatory strategy. This enhances the ability of zebrafish to capture more mobile prey items such as *Artemia*. Visually-guided tracking is complemented by the mechanosensory lateral line system. Neomycin ablation of lateral line hair cells reduced the accuracy of strikes and overall feeding rates, especially when neomycin-treated larvae and juveniles were placed in the dark. Darkness by itself reduced the distance from which strikes were launched, as visualized by infrared imaging. Rapid growth and changing morphology, including ossification of skeletal elements and differentiation of control musculature, present challenges for sustaining and enhancing predatory capabilities. The concurrent expansion of the cerebellum and subpallium (an ancestral basal ganglia) may contribute to the emergence of juvenile homing strikes, whose ontogeny possibly mirrors a phylogenetic expansion of motor capabilities.

Keywords: zebrafish, prey capture, ontogeny, lateral line, motor learning, evolution, imaging, vision

INTRODUCTION

Vertebrate animals begin life with only rudimentary motor skills, but these skills progress enormously over ontogenetic time. Predation is a particularly valuable skill and many predatory mammals have an extensive epoch of "play" where such skills are learned and honed. Fishes, however, must generally fend for themselves and so must continuously and effectively perform this behavior while undergoing rapid growth and changing ecological circumstances. Zebrafish commence exogenous feeding at about 5 days post fertilization (dpf). At this early developmental stage, zebrafish have an estimated 300 descending neurons that project from the brainstem to the spinal cord (Kimmel, 1982; Kimmel et al., 1982, 1985; Metcalfe et al., 1986; Gahtan et al., 2002; summarized in O'Malley et al., 2003). Over the course of about 90 days, zebrafish progress through the early larval, late larval and juvenile ontogenetic stages before reaching adulthood (Parichy et al., 2009). Effective prey capture is ongoing throughout this time, but how this capability is maintained and advanced is not known.

Many physiological, morphological and behavioral changes occur throughout zebrafish ontogenesis (see e.g., Nüsslein-Volhard and Dahm, 2002; Webb and Shirey, 2003; Ghysen and Dambly-Chaudière, 2004; Hernández et al., 2005; Larson et al., 2006; Bae et al., 2009; Valente et al., 2012), with especially substantial growth from the age of first predation (about 5 dpf) to the late juvenile stage (summarized in **Figure 1**). One of the most conspicuous morphological developments is differentiation of the fins. Larval fish hatch with a single primordial fin fold which is eventually replaced by the caudal, dorsal, and anal fins (Nüsslein-Volhard and Dahm, 2002; McHenry and Lauder, 2006; Danos and Lauder, 2007). Concurrently, the paired pectoral fins develop from a simple endoskeletal disc to a more complex fin, including twelve actinotrichia (fin rays) in each of the bilateral pectoral fins. This is accompanied by the differentiation of pectoral fin-associated muscles and neurons (Thorsen and Hale, 2005, 2007; Green and Hale, 2012). In addition to these changes in the appendicular skeleton and associated musculature, the jaw is also gaining new function: premaxillary

protrusion is facilitated by the ossification of the kinethmoid bone during late larval developmental (Hernández, 2000; Hernández et al., 2002; Staab and Hernández, 2010). Moreover, the body form is becoming more streamlined (McHenry and Lauder, 2006).

KINEMATIC DETAILS

While few data are available for later life stages, the kinematics of early-larval zebrafish preying upon *Paramecium multinucleatum* have been described in some detail. Predation on these small, 200–300 μm long prey items was described using high-speed imaging. Prey tracking, at this stage, consists of a variable number and combination of orienting turns and forward swims that serve to better align the fish to its prey by decreasing its angular deviation and distance (McElligott and O'Malley, 2005; McClenahan et al., 2012; Patterson et al., 2013). The orienting turns are kinematically distinct from previously described larval turns (routine and escape) and were called "J-turns" because of their rhythmic J-bends that are unilateral, far caudal (85.5% body length) and of high amplitude (bend angles >90°). The forward swim bouts observed during tracking are indistinguishable from previously described slow swims (Budick and O'Malley, 2000). These slow swims involve rhythmic tail beats that propel the fish forward, closer to the prey. In addition, there are a variety of fin movements associated with swimming and predatory behaviors (Thorsen et al., 2004; Danos and Lauder, 2007; McClenahan et al., 2012).

The consummatory phase of larval feeding, termed a capture swim, consists of a distinctive maneuver in which "fine axial motor control" generates rapid, precise acceleration through the prey item's location (Borla et al., 2002). The capture swim is initiated only when the larva is within a 3–7° heading of the *Paramecium* and is associated with a peak in the instantaneous tail beat frequency and velocity, and concomitant propulsion of the fish forward to capture the *Paramecium*. It appears to be facilitated by vergence eye movements (Bianco et al., 2011; Patterson et al., 2013). Peak velocity during this capture event is around 30 μm/ms compared to the ubiquitous "slow swims," which have comparably slower linear velocities of about 15 μm/ms. Predation by larvae thus consists of a series of discrete locomotor maneuvers and is innate in that successful strikes are seen from the first feeding episodes. For juveniles and adults, there are so far only preliminary reports about prey tracking and strike kinematics (Bonaiuto et al., 2007; Westphal and O'Malley, 2010).

SENSORY CONTROL OF PREY CAPTURE

In regards to sensory mechanisms of predation, there is accumulating data specifically for larval sensory controls. Larval zebrafish are known to dramatically reduce prey consumption when placed in the dark and do not appear to exhibit the distinct tracking and capture maneuvers used in the light (McElligott and O'Malley, 2005). However, the precise relationship between visual signals and the distinct motor elements of larval prey tracking and capture remain undefined. Gahtan et al. (2005) investigated the role of the optic tectum, (homologous to the mammalian superior colliculus) in the guidance of zebrafish feeding episodes. Bilateral tectal ablations were shown to decrease, but not eliminate, feeding in larval zebrafish (also see Burrill and Easter, 1994, regarding other retinorecipient areas). *Lakritz* mutants, which lack retinal ganglion cells, also show a deficit in feeding rate (Gahtan et al., 2005). More recent data has defined key criteria of the visual stimulus (Bianco et al., 2011; Patterson et al., 2013) and suggested a role for binocular visual information. These data notwithstanding, feeding is *not* abolished in the dark and other sensory modalities may contribute.

The mechanosensory lateral line (Münz, 1989) is a plausible candidate for guiding zebrafish prey capture in the dark, and might also provide short range sensory information to aid predation in circumstances where visual information is readily available. The lateral line is found in fishes and aquatic amphibians and contributes to a variety of behaviors including rheotaxis (Montgomery et al., 1997), eddy chemotaxis (Gardiner and Atema, 2007), station holding (Montgomery et al., 2003), hydrodynamic imaging (Hassan, 1989; Windsor et al., 2008) and predator avoidance (McHenry et al., 2009; Stewart et al., 2013). Of note here is the possible role for lateral line in prey capture (New et al., 2001; Pohlmann et al., 2004), that may derive from its specialized structures. The posterior lateral line consists of an array of neuromasts running along the lateral surfaces of the fish's trunk. This is complemented by an anterior lateral line system comprised of clusters of neuromasts located around the head region.

The further specialization of the lateral line into canal and superficial systems of neuromasts might also facilitate prey detection and tracking. Superficial neuromasts contribute to the detection of water currents moving over the surface of the fish and facilitate the rheotaxic behavioral response (Montgomery et al., 1997; Olszewski et al., 2012). The amplitude of cupula displacement is proportional to the velocity of water flow which enables water velocity to be encoded by the afferent firing rate (Münz, 1989). In contrast, canal neuromasts are located in ossified canals between two pores. When there is a pressure difference at the surface, water flows through the pores, deflecting the neuromast. The canal neuromasts are likely responsible for detection of water vibrations created by a predator (McHenry et al., 2009) or prey item (Montgomery, 1989; Janssen and Corcoran, 1993; Montgomery et al., 2002, 2003; Pohlmann et al., 2004; Bassett et al., 2007). The lateral line (perhaps the anterior neuromasts) was suggested as a possible releaser of the capture swim, but at present there are only preliminary reports on the contribution of lateral line to predation by larval and juvenile zebrafish (Bonaiuto et al., 2007; Westphal and O'Malley, 2010).

ONTOGENY OF ADVANCED PREDATORY CAPABILITIES

To better understand the ontogeny and neural control of zebrafish predation, more information is needed about the changing kinematics and strategy of predation, as well as the sensory controls that enable this critical behavior. Using high-speed behavioral imaging, we document a rapid increase in the sophistication and efficacy of predatory episodes that is highlighted by (1) a fusion of basic motor maneuvers into seamless "homing strikes" and (2) a surprisingly flexible array of motor patterns (including bend sequences) that allows juvenile fish to effectively strike throughout much of the imaging arena. In addition, we provide evidence

Early Larval Stage (3 dpf, 4 mm TL)

Changes in Morphology/Physiology

- Fins comprised of a single primordial fin-fold and paired pectoral fins.
- Cerebellar/ forebrain development throughout larval period (Bae et al., 2009).

Structure of Feeding Episodes

- Feeding episodes composed of multiple discrete maneuvers, separated by pauses.
- The final "close-in" on prey is accomplished with a distinct capture swim.

Late Larval Stage (14 dpf, 6 mm TL)

Changes in Morphology/Physiology

- Ossification of kinethmoid bone, facilitating jaw-protrusion (Hernandez et al., 2002).

Structure of Feeding Episodes

- Partial fusion of feeding episodes is seen, with shorter duration episodes.
- Fewer maneuvers seen in a single episode.

Juvenile Stage (30 dpf, 10 mm TL)

Changes in Morphology/Physiology

- Fin Musculature Reaches adult-like morphology (Thorsen & Hale, 2005).
- Ossification of lateral line canals (Webb & Shirey, 2003).
- Emergence of social behaviors (Larson et al., 2006).

Structure of Feeding Episodes

- Complete fusion of most feeding episodes is evident.
- Strikes are possible from farther distances and greater offset angles, compared to larval stages.

Adult Stage (90 dpf, 20 mm TL)

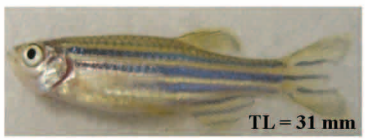

Changes in Morphology/Physiology

- Tertiary reticulospinal neurons present (neurogenesis occurs at an unknown developmental time point between larval and adult stages; Lee & Eaton, 1991).

Structure of Feeding Episodes

- Complete fusion of all feeding maneuvers is evident.

FIGURE 1 | Changes in zebrafish morphology and predatory behavior across ontogeny. Four developmental stages (early larval, late larval, juvenile, and adult) are defined based upon total length, which defines the start of each stage. Each stage is accompanied by a representative image of a fish and the typical age at which it begins. Zebrafish develop gradually, i.e., without a distinct metamorphosis, but major changes in body form occur throughout these stages, including changes to fins, bones and body form. Morphological change is accompanied by behavioral changes, which are summarized. The early larval micrograph is courtesy of Dr. Edward Devlin.

that the lateral line system contributes to predatory success across ontogenetic stages.

METHODS

All protocols and experiments were approved by the Northeastern University Institutional Animal Care and Use Committee.

ZEBRAFISH HUSBANDRY

Broodstock

Zebrafish adults were maintained at 28–29°C on a light cycle of 14 h light: 10 h dark (lights on at 7 am; lights off at 9 pm). Fish were fed "Omega-One" flake food and *Artemia salina*, each twice per day. Water parameters including temperature, pH, and conductivity were monitored daily. Twenty percent water changes were performed weekly.

Larvae

Zebrafish larvae were maintained in an incubator at 28.5°C on the same 14:10 light cycle as adults. Waste was removed and 60–90% of the water was changed daily. Zebrafish were fed *Paramecium multinucleatum* (approximately 200 μm in size) starting at 5 days post fertilization (dpf). *P. multinucleatum* were cultured off site, fresh cultures were delivered weekly. Starting at 10 dpf zebrafish were fed newly-hatched *Artemia salina* nauplii (approximately 450 μm). *A. salina* were cultured daily from cysts (Brine Shrimp Direct). *Paramecium* was continued after the start of *Artemia* until all fish in the clutch displayed a "pink" abdomen, indicating that they were successfully feeding on *Artemia*. All zebrafish used in this study were wild type, of the EKW strain (Ekkwill Water Life Resources, FL).

RECORDING OF FEEDING EPISODES

Stages

Because larvae in a given clutch develop at varying rates, total length is a preferred metric to define developmental age (Parichy et al., 2009). Zebrafish were grouped according to total length (TL, in mm), which was used to define the start of successive ontogenetic stages (**Figure 1**). Fish between 4.0 and 6.0 mm in total length were categorized as early larvae. Fish with a total length between 6.0 mm and 10.0 mm are of the late larval stage. Juvenile fish are between 10.0 mm and 20.0 mm in total length, while fish greater than 20.0 mm in total length are considered adults.

Most feeding videos were acquired at 500 frames/second with a Redlake MotionScope charge coupled device (CCD) camera fitted with a macro zoom lens. Some videos were acquired with a EG&G Reticon high speed camera. To ensure that fish were not satiated prior to observation, food was withheld for approximately 24 h. Larval fish were carefully transferred to a Petri dish with an internal diameter of 34 mm. Juvenile and adult fish were placed in a cylindrical glass bowl with an internal diameter of 102 mm. To minimize movement of the fish within the water column, containers were only filled to about two to three times the height of the fish. During real-time observations, the running 2048-frame buffer of the Redlake camera was manually stopped after feeding was observed and the preceding relevant frames were selected and manually saved for later analysis. A single calibration image of a ruler was taken at the same magnification and saved along with the feeding videos as a calibration frame. This calibration image was used to set the scale (pixels/cm) for all distance measurements.

Definitions

The term "feeding episode" is used to describe each entire feeding event and may include both tracking and strike components. It may be one continuous locomotor bout, or may be divided up into "maneuvers" and "pauses." The "strike" is the last continuous maneuver of a feeding episode, and typically culminates in capture of the prey item.

KINEMATIC AND BEHAVIORAL MEASUREMENTS

Videos were viewed frame-by-frame using NIH *Image J*. The following measurements and calculations were made.

Statistical analyses

All error bars in the figures represent standard deviation, while the *p*-values in the paper are based upon *t*-tests, including the Welch-Satterthwaite *t*-test, which allows for both unequal sample sizes and unequal variances.

Total length of fish (mm)

The length from the tip of the snout to the end of the caudal fin.

Duration of feeding episodes (ms)

This was measured from the onset of a feeding episode, i.e., the initial movement towards a prey item, to the moment of capture or contact with the prey item. During visual monitoring of behavior, zebrafish have quiescent periods that are long in relationship to the duration of feeding episodes. To more precisely define the onset of an episode, any active movement that occurs with a gap of 1 s or more earlier than any tracking or strike maneuver leading to prey capture is not considered part of the episode (coasting is considered part of the quiescent periods by this definition). Single maneuver episodes (including adult and most juvenile strikes) occur when there is no active movement within the 1 s window preceding the strike movement bout.

Duration of strike (ms)

The strike is the last maneuver of a feeding episode. The start of the strike is marked by the frame preceding the first movement of the final maneuver and terminates when the fish makes contact with the prey item. When the feeding episode is a single, continuous movement bout, that entire movement bout is considered the strike.

Distance to prey (mm)

The distance from the tip of the snout to the prey item, measured at any time during the feeding episode.

Offset angle (°)

This is the angular deviation between the fish and prey item, measured at any time during the feeding episode. This angle is defined by two lines. The first is a line extended from the midline of the fish at the rostral-caudal location of pectoral fin attachment to the

midpoint between the two eyes. The second line is measured from the same midline location of pectoral fin attachment and extends to the center of the prey item.

Pause time (ms)

The time during which no axial or pectoral fin movement is observed. The number of pause frames is counted and converted to milliseconds.

Cumulative pause time (ms)

The sum of all the individual pause intervals in a single feeding episode.

Episode velocity (μm/ms)

This is the straight-line velocity for each complete feeding episode. The distance (in μm) is measured from the fish's starting position to its final position at the end of the episode (point of contact with the prey item); the distance is divided by the elapsed time (in ms), yielding episode velocity in microns per millisecond.

Normalized episode velocity (BL/s)

The normalized velocity is calculated by dividing the episode velocity by the total length of the fish, yielding a velocity measured in body lengths per second.

Instantaneous and peak velocity (μm/ms)

Custom MATLAB code was used to track the center of mass of a fish over the entire feeding episode. Videos were first imported into Image J where the threshold function was used to create a black (fish) on a white (background). This was done to minimizes background noise in the frame. The feeding episode was then saved as an image sequence and imported into MATLAB. Once the video was imported, a minimum size threshold was set (70 pixels). This eliminated any background items smaller than the fish. A series of "dilate" commands, followed by a series of "erode" commands were then executed to help ensure continuity of the shape. The series of dilate and erode commands sharpen the borders so that the fish can be tracked. Dilate commands replace the pixel with the darkest neighboring value and erode commands replace the pixel with the lightest neighboring pixel. When performed iteratively it sharpens the edges of the image. The "centroid" command was then used. This command is designed to find the center of area of a 2D shape and so served as a good approximation of the center of mass of the fish. MATLAB then ran through the series of images (.jpg files), recording the *xy* coordinates of the centroid for each frame. These *xy* coordinates and the time elapsed between frames was used to calculate the velocity of the fish. A sliding-window filter averaging $n = 5$ frames was applied. This smoothing function helped to remove any background noise due to slight error inherent in the automated tracking. Manual velocity calculations were also done and these values compared well with those computed in MATLAB. The maximum instantaneous velocity in each episode was recorded as the peak velocity for that episode and these peak values were averaged to determine the mean peak velocity for each group of zebrafish.

Normalized peak velocity (BLs/s)

Velocities obtained were normalized to body length by dividing the peak velocity (mm/s) by the total length of the fish (mm). This value is the normalized peak velocity in units of "body lengths per second" (BL/s).

Instantaneous tail beat frequency, iTBF

The tail-beat-frequency of forward swimming is normally calculated as the reciprocal of the duration of one cycle of axial bending. The iTBF value is calculated based upon the half-cycle duration. One half cycle starts with a maximum tail bend to one side and ends at the maximum tail bend to the opposite side. The value of 1/(2× half-cycle duration) is equal to the iTBF.

SENSORY MANIPULATIONS AND RELATED ANALYSES

Paramecia and *Artemia* were filmed at 250 frames per second for 4 s. Subsequently, videos were analyzed using Image J to determine velocity. Distance traveled between successive frames was divided by the time elapsed to generate instantaneous velocities (μm/ms). The peak instantaneous velocities recorded from 5 individuals were averaged to determine the peak velocity for each species. Average instantaneous velocities were also determined for each individual and averaged over 5 individuals to determine the average velocity for each species.

Deprivation of visual information

Sensory information to the visual system was blocked by placing the fish in a light-tight box.

Lateral line lesion

By immersing fish in 250 μM neomycin, the lateral line sensory system was disabled (protocol from Owens et al., 2009). Fish were treated for 30 min and then allowed to recover for 1–2 h before experiments were conducted. Behavioral studies were always performed the same day as the neomycin lesion.

DASPEI staining

Hair cells were labeled by bath application of the fluorescent mitochondrial dye DASPEI (2-(4-(dimethylamino)styryl)-N-ethylpyridinium iodide) (λ excitation = 461 nm; λ emission = 489 nm) at 0.001% bath concentration for 15 min. Fish were subsequently embedded in 1.2% low melt agarose or 3% methylcellulose and imaged on a BioRad MRC 600 confocal microscope. Successful lesioning of neuromasts after neomycin treatment was confirmed by periodic inspection to observe elimination of the DASPEI labeling. Intact neuromasts appeared as bright, punctate spots on the fish.

Feeding success

Ten fish were selected from each of three age groups (8, 24, and 180 dpf) and the percentage of successful strikes recorded. A total of 5 control feeding episodes were collected from each fish. Once control feeding episodes were collected fish were subjected to the lateral line lesioning protocol. After a 1 h recovery period, 5 additional feeding episodes were collected from the same fish. Only those fish with a total of 10 recorded feeding episodes (5 control, 5 neomycin treated) were used in the subsequent analysis.

Feeding rates

Zebrafish were individually placed in cylindrical glass bowls (internal diameter of 102 mm, water depth ≈20 mm). *Artemia* were individually counted and added to each dish (30 *Artemia* per dish). Fish were placed into one of four treatment groups: I. Light, lateral line intact; II. Light, lateral line lesioned; III. Dark, lateral line intact; IV. Dark, lateral line lesioned. Fish were allowed to feed for 2 h at which point they were removed and the remaining *Artemia* were counted. The number of *Artemia* consumed in 2 h was used to calculate feeding rate (*Artemia*/hour).

Recording of dark feeding episodes

A group of seven 39-dpf zebrafish were placed together in a cylindrical glass bowl (internal diameter = 102 mm) above an infrared light inside a light-tight, dark enclosure. A tube of dark cloth was wrapped around the bowl and extended up to the camera lens providing a second light barrier within the recording box. Videos were collected at 250 frames per second. All events were saved, including both successful and unsuccessful events. At this point, the enclosure was opened and the fabric tube was removed from the dish. An additional recording session yielded 10 control (light) feeding events, including both successful and unsuccessful episodes. Distance at initiation of feeding episodes was measured for both the light and dark conditions.

RESULTS

Zebrafish do not undergo discrete metamorphic changes, but develop gradually into adult-like form, over a period of several months. To illustrate maturation of form and predatory performance, four successive stages of development were evaluated, namely: early larval, late larval, juvenile and adult. Over the first 30 days, in the progression from early larval into juvenile form, there is a near tripling in length with stream-lining of the body and radical change in fin structure, approaching the adult's caudal fin form. **Figure 1** summarizes these changes, showing the typical age at which each stage begins (as defined by starting length). Provided below for these stages are details of strike kinematics, measures of predatory performance, and sensory system contributions.

While early larval predatory episodes were comprised of discrete tracking maneuvers and a brief capture swim as previously reported, variations were noticed. A minority of strikes exhibited especially pronounced bending of the caudal trunk (**Figure 2A**), while subtler bending was more typical (**Figure 2B**). The greater bending was associated with faster velocity and a slightly higher tail beat frequency (**Figure 2C**), leading to more abrupt acceleration through the prey item. These episodes all fell, nonetheless, within the general locomotor pattern previously described for early larval capture swims. Young larval zebrafish sometimes consume prey by stationary suction feeding (Budick and O'Malley, 2000), which continues at later developmental stages, but most predatory episodes observed in these experiments involved substantial locomotion. Because locomotor aspects of predation were of interest, the data below concern only feeding episodes with a significant locomotor component.

Trajectories are presented for zebrafish stages along with montages of kinematic features of the final strike (**Figure 3**); all times shown are in relation to initiation of a feeding episode (at 0 ms). Early larvae (**Figure 3A**) initiate feeding episodes at a relatively short distance from the target prey item (a *Paramecium*), typically

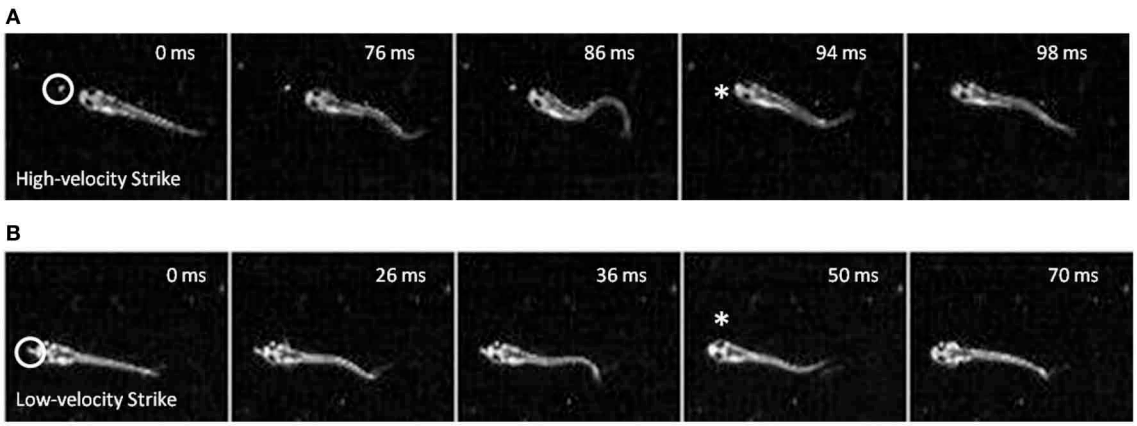

C

	High-Velocity Strike	Low-Velocity Strike	P value
Percent of Strikes	27% (8/30)	73% (22/30)	n/a
Peak TBF	50.36 ± 14.83 Hz	39.17 ± 6.15 Hz	0.0727
Peak Velocity	14.52 ± 1.55 BL/s	6.88 ± 2.2 BL/s	< 0.0005

FIGURE 2 | Early larval prey strikes vary in locomotor speed. In **(A)** there is pronounced bending of the caudal trunk which results in abrupt acceleration through the prey item. The *Paramecium* is circled in the first frame, while the asterisk marks the moment of capture. **(B)** Also shows a caudal bend and acceleration, but not to the same degree as **(A)**. In early larvae, these strikes (capture swims) typically follow a series of tracking maneuvers that align the larva with the *Paramecium*. Larvae shown in **(A)** and **(B)** are 4.1 mm in length. **(C)** Summarizes the peak tail-beat frequency and velocity values of the low and high velocity strikes.

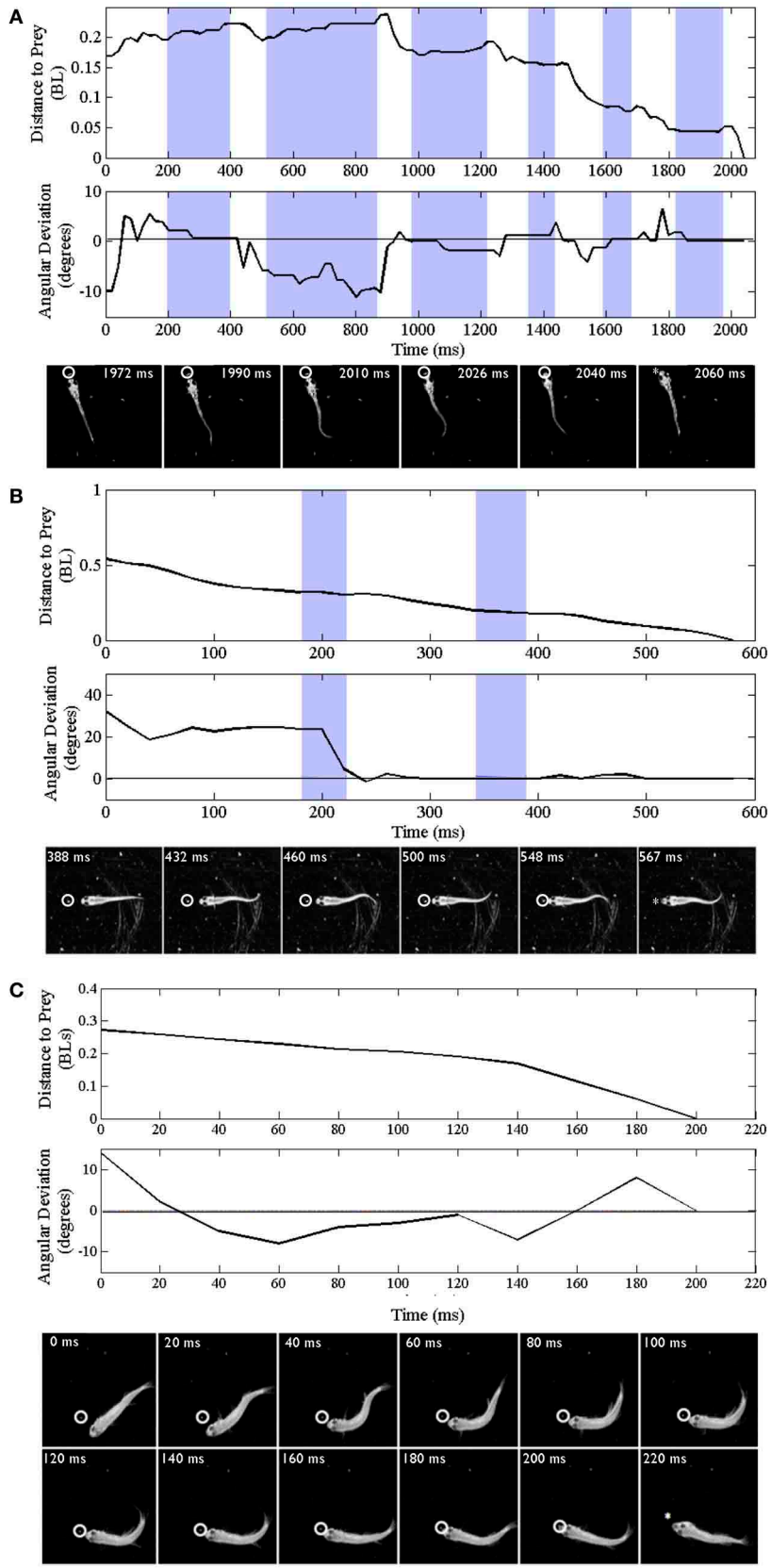

FIGURE 3 | Continued

FIGURE 3 | Trajectories of early larval, late larval and juvenile feeding episodes. Three representative episodes are illustrated via plots of distance to the prey item (upper plots) and changes in offset angle (in degrees), between the fish and prey item (lower plots). The montages of frames from the high-speed videos illustrate locomotor components of just the final strike; all times are in relation to the initial movement towards the prey item ($t = 0$). Shaded portions of the plots represent pauses in locomotor movements, whereas non-shaded areas represent active swimming or turning. The final capture swim or strike occurs in the last non-shaded segment of each plot. **(A–C)** Represent early larval, late larval and juvenile episodes respectively. **(A)** Representative episode of an early larval zebrafish (3.8 mm in length) feeding on a *Paramecium*; total episode duration was 2024 ms. In this episode the tracking phase includes one J-turn (the first non-shaded area) and five forward swimming maneuvers. This is followed by the final maneuver, a strike (capture swim) as illustrated in the montage. **(B)** Feeding episode of a representative late larval zebrafish (9.2 mm) was 576 ms in duration. It included two tracking maneuvers, two pauses (shaded areas), with the final strike consisting of rhythmic trunk bending as seen in the montage. **(C)** Example juvenile feeding episode has no pauses and shows continuous closing and aligning to the prey before the final strike, which occurred 200 ms after the initial turn towards the *Artemia*.

less than one half the fish's own body length. The tracking phase consists of distinct J-turns and forward slow swims, separated by brief pauses, and is followed by a distinct capture swim bout. In a subsequent, transitional phase, the late larval stage, predatory episodes are varied in nature, but often comprised of multiple movements. The example in **Figure 3B** has two pauses and just two tracking maneuvers that align the larva with the *Artemia*; it is also shorter in duration. The segregation of function into distinct kinds of tracking maneuvers becomes blurred, in this transition, as does the distinction between tracking and strike maneuvers. While some elements of early larval tracking are retained by the late larvae, more complex maneuvers are frequently observed in which forward propulsive and turning movements are conjoined, resulting in distinct trunk kinematics.

FUSION OF LOCOMOTOR ELEMENTS

In the example juvenile feeding episode shown (**Figure 3C**), the juvenile moves continuously from episode initiation through to striking the *Artemia*. Absent pauses, the total elapsed times of juvenile feeding episodes can be much smaller (note the different time scales in **Figures 3A–C**). Also, the example of **Figure 3C** has no substantive "forward swimming" component or rhythmic trunk bending. Instead, after a caudal kink in the trunk at 20 ms, there is a pronounced bend to the right that helps propel the juvenile through the *Artemia*'*s* location. This is but one example and juvenile strike patterns are quite varied as described below.

Replay of high-speed video of prey capture episodes allowed them to be classified as single maneuver, or multi-maneuver (using discrete movement bouts separated by pauses). For instance, a 5-day-old larval episode might consist of: J-turn – pause – slow swim – pause – capture swim. As zebrafish mature, the discrete tracking and strike maneuvers used by early larvae disappear. Most juvenile and all adult zebrafish instead display a single, continuous (and often complex) feeding maneuver where orientation and approach to a prey item are merged together. Because these fluid maneuvers often cover significant distance and/or show substantial direction change, they are referred to here as "homing strikes." In quantitative terms, all early larval feeding episodes ($n = 43$) contain multiple movement bouts, while 73% of late larval feeding episodes ($n = 37$) used two or more maneuvers and only 24% of juvenile episodes ($n = 34$) were multi-maneuver. Thus, the large majority of juvenile and all adult locomotor-driven feeding episodes ($n = 38$) were single maneuver episodes, i.e., homing strikes.

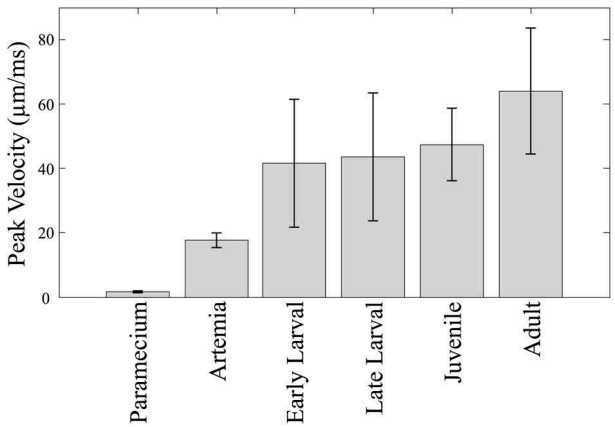

FIGURE 4 | Predator vs. prey velocities. The mean peak velocity of different prey items are shown along with velocities of zebrafish at different stages. The mean peak velocities of the zebrafish increase over time, but not dramatically so. Zebrafish of all ages are much faster than *Paramecia* and *Artemia*.

PREDATOR vs. PREY

Relative swim velocity is important in that faster velocities may enable capture of faster prey. **Figure 4** summarizes mean peak velocity (in μm/ms) of the main prey items studied here, *Paramecia* and *Artemia*, along with the zebrafish mean peak velocities which, at all stages, are higher than the prey items consumed during those stages. Early larvae show peak velocities ranging from 22 to 79 μm/ms, much faster than *Paramecia* which swim at an average velocity of 0.61 ± 0.1 μm/ms s.d., and a peak velocity of 1.72 ± 0.3 μm/ms, s.d. *Artemia* swim at an average velocity of 5.19 ± 0.7 μm/ms s.d., and a peak velocity of 17.6 ± 2.3 μm/ms, s.d. *Artemia* are preyed upon by late larval and juvenile zebrafish, which have peak velocities ranging from 21 to 89 μm/ms and 32 to 94 μm/ms, respectively. Zebrafish can thus attain peak velocities that are much faster than these laboratory prey items.

MEASURES RELATED TO PREDATORY CAPABILITY

The total duration of individual feeding episodes (which includes tracking and capture components) decreases over ontogeny (**Figure 5A**). Early larval feeding episodes are the longest, and duration falls dramatically by the juvenile and adult stages. The early and late larval episodes were significantly longer than

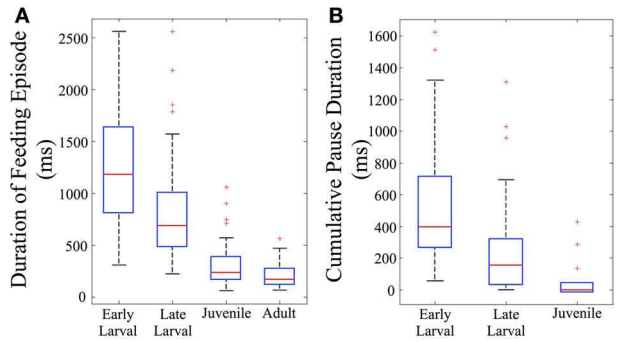

FIGURE 5 | Feeding episodes become shorter and pause time decreases across ontogeny. Feeding episodes were binned according to ontogenetic stages (based on total length) and the durations and total pause time determined. In the box plots used to represent these data, the central red line indicates the median value of each data bin, while the 25th and 75th quartiles are enclosed inside the box profiles. Note that mean values in the Results are higher than the median values due to the effect of one-sided, high numerical value outlier data points, shown as red crosses. **(A)** The duration of feeding episodes (including pauses and maneuvers) falls across ontogeny ($n = 156$). **(B)** The summed duration of the individual pauses between discrete motor elements also falls across ontogeny ($n = 82$). By definition, only multi-maneuver feeding episodes include pauses; there are no pause data for adult fish which were always "single-maneuver."

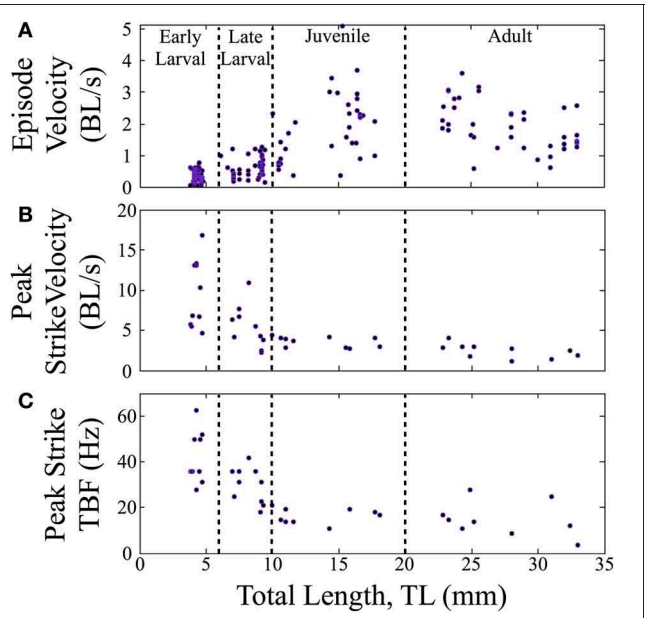

FIGURE 6 | Normalized feeding velocities and tail beat frequency change across ontogeny. Scatter plots are shown with the successive stages separated by vertical lines. **(A)** The normalized episode velocity (in body lengths/s) of feeding episodes increases over time, which is due at least in part to decreasing pause time. **(B)** Early larvae show the highest peak velocities, which occur at the end of the capture swim bout. Peak velocity then declines as zebrafish transition through the late larval stage and become juveniles; any further decline is slight. For early larvae, the strike is a tiny fraction of the feeding episodes, hence the large peak values in **(B)**, but low episode velocities in **(A)**. **(C)** Early larvae also show a high peak tail-beat frequency, which then declines across subsequent stages in a pattern mirroring the decline in peak strike velocity.

juvenile and adult feeding episodes ($p < 0.005$), demonstrating that older fish are able to capture prey items more quickly (at least within the constraints of our feeding arena). Also calculated was cumulative pause time for all episodes that included multiple maneuvers ($n = 82$). This fell sharply with development (**Figure 5B**). The early larval cumulative pause durations (mean $= 534 \pm 402$ ms, s.d.), were much longer than those of both late larval (326 ± 329 ms, s.d.) and juvenile (115 ± 146 ms, s.d.) fish. Because adults were never observed to pause during individual feeding episodes, they are not represented in **Figure 5B**.

In terms of swimming speed, both peak strike velocity and episode velocity (average speed across an entire episode) were measured. Normalized episode velocity, which includes any pause time, increased over ontogeny ($n = 157$, **Figure 6A**), primarily in the late larval to juvenile transition. The data points for early larvae (4 to 6 mm TL) are fairly clustered, in contrast to the broader distributions for older fish. A subset of feeding episodes ($n = 40$), of sufficient quality for automated analysis, was further analyzed to determine the normalized peak velocity and peak tail beat frequency for feeding strikes. An exponential decrease in normalized peak velocity (BL/s) is seen as fish mature (**Figure 6B**). Concurrently, there is a sharp decline in peak tail beat frequency (measured in Hz; **Figure 6C**), indicating a change in the operation of neural oscillators in spinal cord.

When measured in absolute terms (μm/ms), early larvae were (somewhat unexpectedly) seen to exhibit absolute peak swimming velocities roughly comparable to those of juvenile and even adult zebrafish (**Figure 7**), although adults showed the highest recorded velocities. In contrast, the overall episode velocity increased dramatically, especially across the larval to juvenile transition. These results are explained by the pronounced but brief burst of acceleration seen in early larval capture swims which yield high peak velocities, whereas episode velocities are low due to the frequent pauses. The differences between episode vs. peak velocity are statistically significant for both early and late larvae ($p < 0.0005$).

The angles and distances from which feeding episodes are launched are another measure of predatory capability. **Figure 8A** shows the offset angles from which both episodes (E) and final strikes (S) are launched ($n = 157$). Offset is the angle between the zebrafish's orientation and the direction to the prey item, so that a 90° offset angle would require a net right or left turn to approach the prey. The strike offset angle is miniscule for early larvae, but increases markedly across development. In contrast, episode offset angles begin large and increase further. For both early and late larvae, the offset angles are significantly smaller for strikes than episodes ($p < 0.005$). By the adult stage, all feeding episodes are comprised of single movement bouts and so the episode and strike offset angles are essentially the same and represent an ability to strike throughout much of the feeding arena. As the box plots indicate, zebrafish of all ages tend to initiate predatory episodes within ±60° of their heading. In regards to strike distance, **Figure 8B** shows that strikes (S) are launched from very

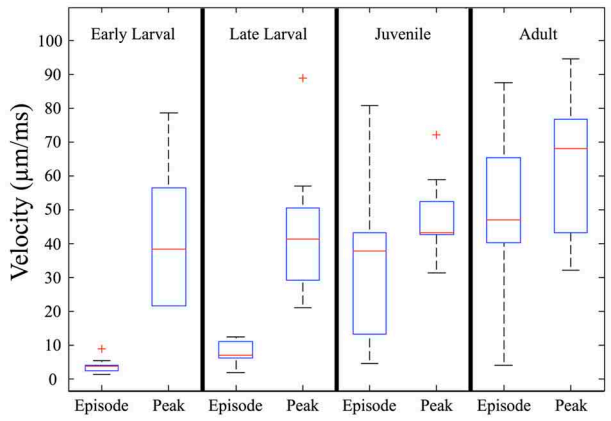

FIGURE 7 | Episode velocity increases across the larval to juvenile transition. The episode velocity (average velocity across each feeding episode) increases markedly from the larval to juvenile stages. In contrast, the peak absolute velocity does not change greatly, but trends larger for adults. The differences between peak and episode velocity are significant for both early larvae and late larvae ($p < 0.0005$), which is explained by an abrupt peak occurring during capture swims. Because the juveniles and adults mostly lack pauses, their episode and peak velocities are more similar, yet still show transient peaks during their predatory maneuvers. In addition, the larval episode values are tightly clustered, but become highly variable in the juvenile and adult stages, reflecting more diverse predatory behaviors. Red crosses represent outlier data points.

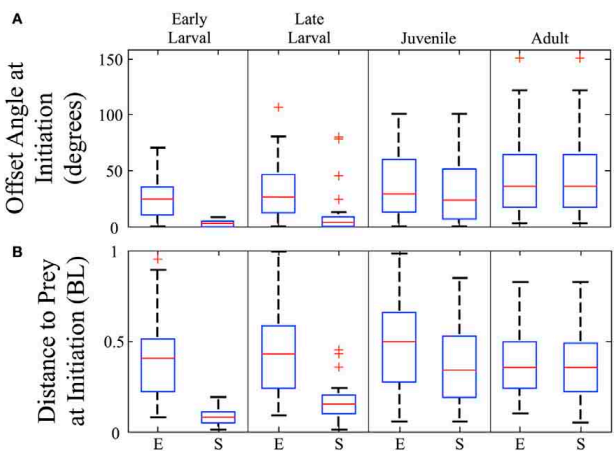

FIGURE 8 | Strike offset angle and distance increase sharply across development. Box plots are shown for each ontogenetic stage providing the offset angle **(A)** and the normalized distance **(B)**, in body lengths (BL) at the initiation of both the feeding episode (E) and the final strikes (S). The strike offset angles and strike distances show substantial increases, particularly at the larval to juvenile transition. In contrast, the overall (episode) angle from which predation is launched increases only modestly, while the normalized overall (episode) distance does not show a consistent trend. Red crosses represent outlier data points.

close distances in early larvae, but this rises many fold in juveniles and adults, even as normalized to body length. Feeding episodes (E), however, are launched at similar (normalized) distances across age groups.

DIVERSITY OF JUVENILE HOMING STRIKES

Figure 9 illustrates the diversity of strike patterns used by juvenile zebrafish. These early data were collected in a smaller, relatively confined feeding arena that may have imposed greater demands in terms of striking at prey items. The three exemplar strikes all consist of a single bout of continuous trunk movement, with precise orienting turns and propulsion executed in close coordination with jaw protrusions (arrows), hence the term "homing strikes." The first example (**Figure 9A**) consists of a single large but slow bend that precisely orients the juvenile towards the *Artemia* (inside circle). There are no subsequent bends, so this strike lacks the rhythmic component of escape and slow swimming behaviors. In contrast, the homing strike in **Figure 9B** consists of an initial turn followed by five cycles of slow swimming, after which the larva coasts directly through the *Artemia*'s location.

The last example (**Figure 9C**) documents more flexible regulation of axial musculature. This homing strike consists of three bends in total beginning with a large, sustained and rostral bend (turn) that orients the rostral trunk towards the *Artemia*. Two smaller, caudal bends are superimposed upon the rostral bend and seem to propel the well-oriented rostral trunk directly towards the *Artemia*. This particular strategy seems related to the close proximity of the Artemia which could be seen swimming near the right eye of the juvenile, eventually reaching a suitable position for a strike to be launched (black circles indicate *Artemia*'s location at different times). Jaw protrusions and *Artemia* are more readily observed when viewing movies, versus still photos, but the jaw protrusion (arrow) in the last frame of **Figure 9C** is evident and emerges at the proper time for efficient prey capture. The kinematic features of these exemplar homing strikes differ sufficiently from one another as to be considered distinct predatory strategies.

CONTRIBUTIONS AND MATURATION OF SENSORY SYSTEMS

In some first feeding episodes, young larvae oriented and moved towards a nearby prey item, but did not consume it. Failed episodes resulted from both misses and, more frequently, aborted episodes, where items were tracked and approached, but no strike was launched. In comparing successful and aborted episodes (**Figure 10**), both showed larvae orienting via J-turns towards a *Paramecium* and approaching it, but in the aborted case (lower row), the larva abruptly turned away terminating the feeding episode. **Table 1** provides a comparison of 19 successful and 19 aborted feeding episodes.

The decision of early larval fish to abort a feeding episode did not correlate with either prey velocity or distance to prey at strike initiation/abort (in the aborted trials, the prey were slightly closer). Aborted efforts had only modestly longer episode durations, but the final pause duration, after which the larva either strikes at the *Paramecia* or turns away, showed a large difference: the final pause of aborted episodes was 8-fold longer than those seen in successful episodes. The cause of aborted episodes is unknown, but may have to do with the sensory detection of prey items, as considered next.

While zebrafish are primarily visual predators, they do feed in the dark, albeit at lower rates. Using infrared (IR) illumination,

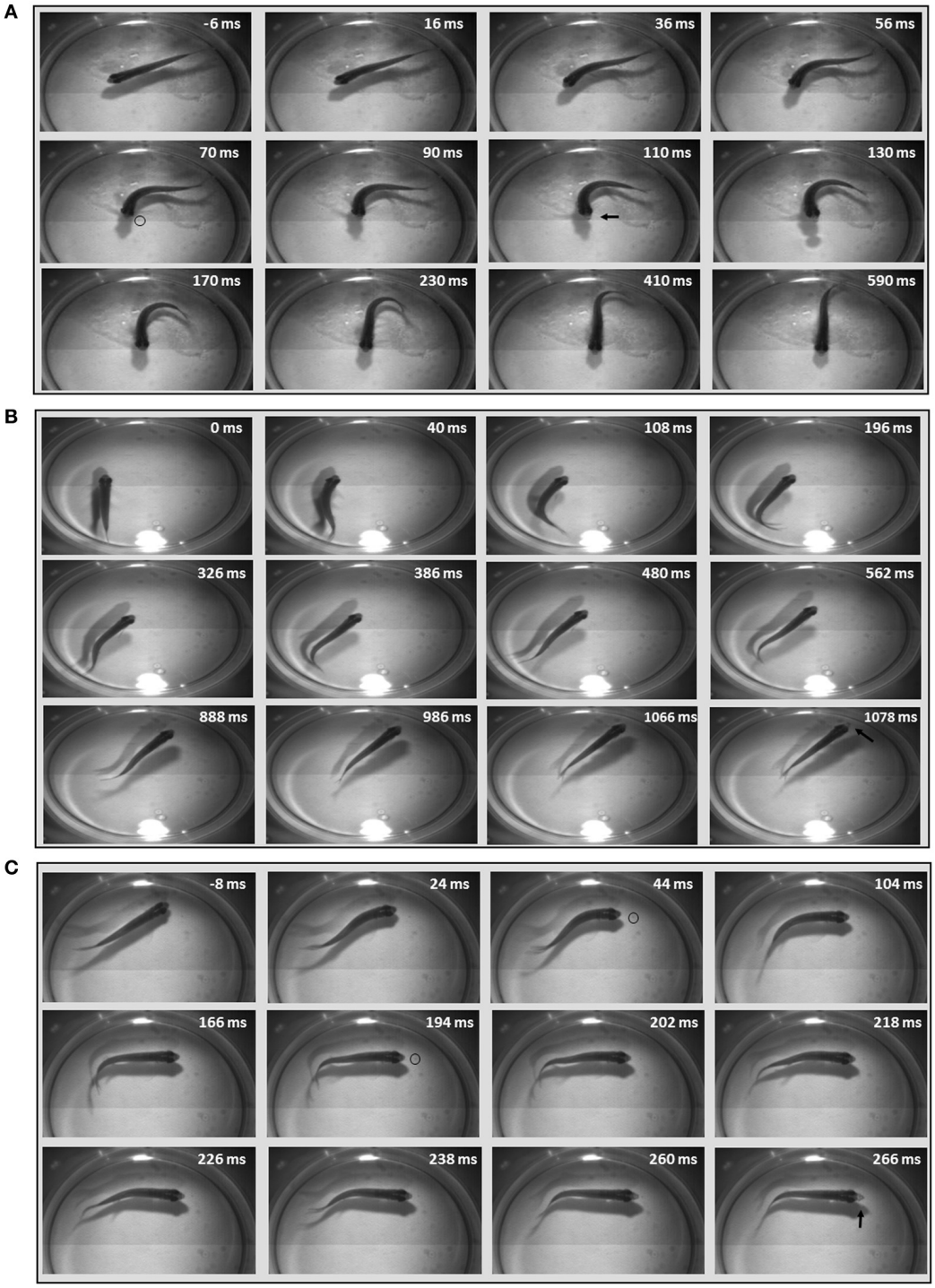

FIGURE 9 | Diversity of juvenile homing strikes. Three example homing strikes were chosen to represent the diversity of kinematic patterns and motor commands used in juvenile strikes. Select frames are shown with elapsed time after initiation of episode given in milliseconds; negative numbers denote resting frames before the strike. The first strike example **(A)** shows a single large bend, with prey capture occurring as the head swings to the *Artemia*. *Artemia* are easier to see in movies than still images, but the small dot (inside black circle) is an *Artemia* nearing the juvenile's mouth, at 70 ms. It is evident in the next frame at 90 ms, but is obscured (or gone) in the next frame, where the lightly colored jaw is protruding (indicated by arrow) at 110 ms. **(B)** Shows rhythmic, slow forward swimming after an initial turn. Bending movements stop near the end of the episode, before the juvenile coasts through the *Artemia's* location (which is very faint). Jaw protrusion can be seen in the last frame (arrow). **(C)** Shows a more elaborate maneuver, with details on the bend sequence described in the text. The location of the *Artemia* is slightly more visible in these still images and is marked at several time points by black circles. Jaw protrusion is most pronounced in the final frame (arrow).

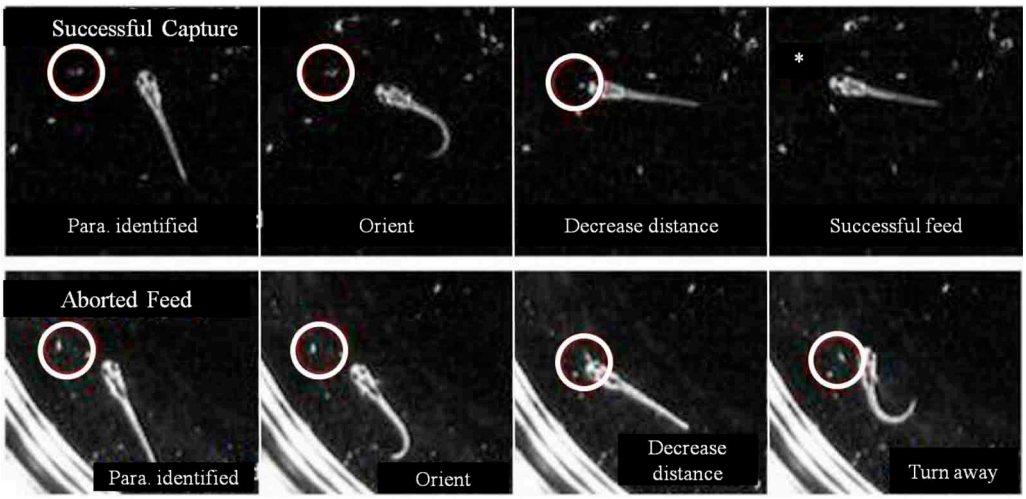

FIGURE 10 | Aborted vs. successful feeding episodes of larval zebrafish. Tracking maneuvers appear similar between successful feeding episodes (**upper panel**) and aborted feeding episodes (**lower panel**). Both panels show the onset of tracking, orientation to the prey and a closing maneuver to the point where the larvae are very close and well oriented towards the *Paramecium*. While the larva successfully engulfs the *Paramecium* using a capture swim in the upper sequence, the aborted episode in the lower sequence shows a distinct turn that produces a large offset angle away from the prey item, ending the episode (the edge of the Petri dish is seen in the **lower panel**).

Table 1 | Completed vs. Aborted feeding episodes.

	Completed feeding episode	Aborted feeding episode	*p*-value
Episode duration	1138 ± 567 ms	1684 ± 780 ms	0.0149
Cumulative pause time, %	39 ± 16	55 ± 22	0.0142
Average prey velocity	0.94 ± 0.48 mm/s	0.87 ± 0.6 mm/s	0.2672
Distance at start of episode	1.73 ± 0.93 mm	1.37 ± 0.78 mm	0.113
Distance, final pause onset	0.57 ± 0.53 mm	0.36 ± 0.22 mm	0.17
Duration of final pause	58.42 ± 51.11 ms	494.38 ± 313.87 ms	<0.0005
Prey movement, final pause	0.05 ± 0.05 mm	0.34 ± 0.36 mm	<0.0005
Prey velocity, final pause	0.74 ± 1.2 mm/s	0.76 ± 0.32 mm/s	0.9
Distance at strike/abort	0.34 ± 0.18 mm	0.77 ± 0.59 mm	0.0123

Distances and times associated with successful and aborted feeding episodes are provided. Pause time is given as a percentage of the total duration of each feeding episode.

zebrafish and prey movements were recorded in the dark. A representative episode is shown in the montages in **Figure 11**, where an *Artemia* (inside white circle) can be seen swimming alongside a juvenile for about 800 ms (**Figure 11A**). Then, the zebrafish abruptly turns and makes several attempts to capture the *Artemia*, beginning about the second frame in **Figure 11B** (pectoral fin movements are indicated by arrows). Two unsuccessful strikes (indicated by jaw protrusions, asterisks) occur at 856 and 900 ms, while a third strike at 968 ms was successful.

The mechanosensory lateral line is a candidate system for mediating prey capture in the dark. To investigate this possibility, feeding rates of late larval ($n = 96$) and juvenile ($n = 68$) zebrafish (that had not been fed for 24 h) were measured under four different sensory conditions: (a) Light with lateral line intact; (b) Light with lateral line lesioned (by neomycin exposure); (c) Dark with lateral line intact; (d) Dark with lateral line lesioned. After housing fish with 30 *Artemia* for 2 h, the remaining *Artemia* were counted (**Table 2**). Both late larvae and juveniles consumed far more *Artemia* in the light, as compared to dark. In the "Light + Neomycin" group, feeding rates were not significantly depressed, but the combination of "Dark + Neomycin" leads to dramatically lower feeding rates, with larvae consuming about 37-fold fewer *Artemia* than during normal feeding in the light.

To further investigate the impact of lateral line lesioning, high-speed recordings were made of normal and neomycin-treated fish. The average value of feeding success (given as the percentage of successful strikes) was lower for all age groups after neomycin exposure (**Figure 12A**). The drop in feeding success in the late larval, 24 dpf group was statistically significant ($p < 0.05$). The median success rate of early (8 dpf) larvae also dropped, from 50% to about 10%, and while this result was

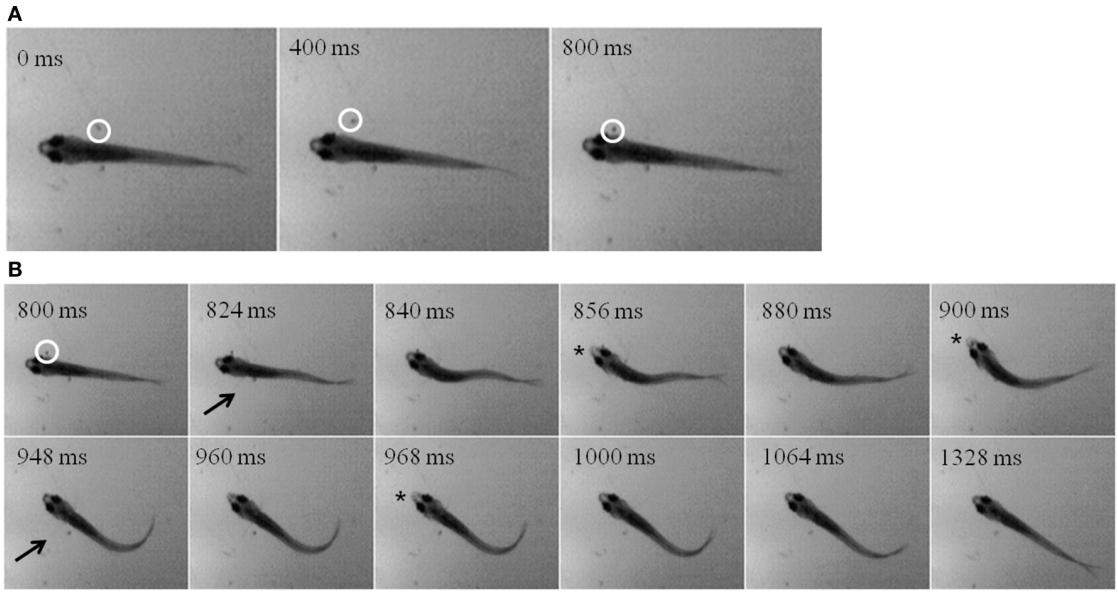

FIGURE 11 | "Dark Feeding" episode of a 39 dpf, juvenile zebrafish. Video was collected at 250 frames per second under IR-illumination and representative frames are shown. **(A)** Three frames, each separated by 400 ms, show the motion of the prey item which occurs before initiation of the feeding episode. Note that the *Artemia* is moving in a caudal to rostral direction as highlighted by the white circle. **(B)** Dark feeding by this juvenile is documented via select frames showing locomotor (fin) movements (arrows) and strike attempts, i.e., jaw protrusions (asterisks), with success occurring on the third attempt. The fins are very thin and light and so difficult to see in still photos, but are more apparent when viewing movie files. Note that the jaw protrusion occurring at 968 ms can be seen as a light, anterior extension of the snout, which is not occurring in the frame just above it (at 840 ms).

Table 2 | Feeding rates of late larval and juvenile zebrafish in the presence and absence of visual and lateral line sensory information.

Treatment	Feeding rate (artemia/2 h)	
	Late larvae ($n = 96$)	Juveniles ($n = 68$)
Light	16.92 ± 9.57	29.96 ± 0.21
Light + Neomycin	12.33 ± 10.26	27.86 ± 3.67
Dark	2.70 ± 5.56	8.88 ± 9.73
Dark + Neomycin	0.45 ± 1.0	3.2 ± 3.11

not statistically significant, some of these larvae captured zero *Artemia*. Early larvae have a more difficult time with *Artemia* (vs. *Paramecia*) because of their size, but the drop-off in success rate with neomycin suggests a role for lateral line in guiding the capture swim, which is potentially mediated by anterior neuromasts, shown stained with DASPEI in **Figure 12B**. The adult fish were most successful with many adults showing 100% success in both the control and neomycin groups.

Strike distances and success rates were compared in light vs. dark conditions, as shown for feeding episodes of nine 39-dpf juvenile zebrafish recorded under IR vs. normal illumination (**Figure 13A**). Of nine feeding events recorded in the dark, five were successful (55%), compared with 9/10 (90%) successful feeding episodes from the same fish in the light. During dark feeding episodes, juveniles initiated feeding at 1.55 ± 1.11 mm from the prey, but launched strikes from 4.29 ± 1.96 mm in the light (p-value $= 0.02$) (**Figure 13B**). This fits with the longer range of vision vs. lateral line, which functions better at short distances. While sustained tracking movements were not apparent in the dark, in agreement with data of Patterson et al. (2013) on larvae, our modest set of recorded dark feeds precludes strong conclusions on juveniles.

DISCUSSION

The transition of zebrafish predation from discrete, simple maneuvers to elegant homing strikes is suggestive of an evolutionary process whereby progressively more sophisticated motor programs emerged from basic motor patterns. The observed ontogenetic progression can be considered from three distinct contexts: improving motor performance, sensory contributions and the underlying neural controls.

LOCOMOTOR PERFORMANCE

The predatory capabilities of early larval zebrafish are limited but presumably sufficient for natural prey items, although ecological details remain sparse (Engeszer et al., 2007a,b; Spence et al., 2007, 2008). Over the next 4 weeks, motor performance improves rapidly and is highlighted by the fusion of discrete early larval maneuvers into seamless homing strikes. This is not a simple "merger" of tracking and capture movements because J-turns and the kinematic features of capture swims disappear. Instead, what emerges is an ability to fuse orientation and propulsion, which allows juveniles to strike prey items over a wide range of angles and distances within the arena (**Figure 8**). This fusion of tracking and capture maneuvers also enables a sharp drop in feeding episode duration (**Figure 5**), while the episode velocity increases

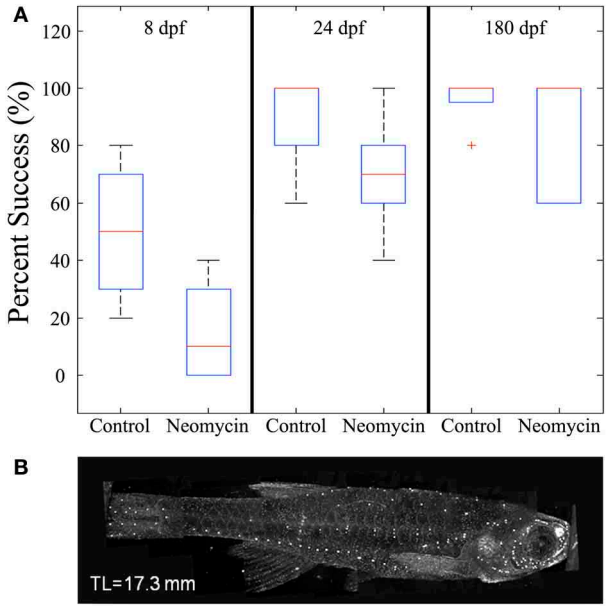

FIGURE 12 | The effect of neomycin exposure on feeding success in zebrafish. (A) While early larvae are able to feed on *Artemia*, at 8 dpf their strikes are successful only about 50% of the time and this success rate is less after neomycin treatment. Both 24 dpf fish and adult zebrafish are quite efficient in capturing *Artemia* in the light. Success rate in 24 dpf fish is significantly degraded by neomycin, although the success rate is still greater than with 8 dpf fish. (8 dpf $n = 4$; 24 dpf $n = 8$, 180 dpf $n = 5$). **(B)** Shows DASPEI labeling of anterior neuromasts on an older juvenile zebrafish. Neomycin treatment eliminates neuromasts (and this labeling) for a day or more (Owens et al., 2009). The red cross represents an outlier data point.

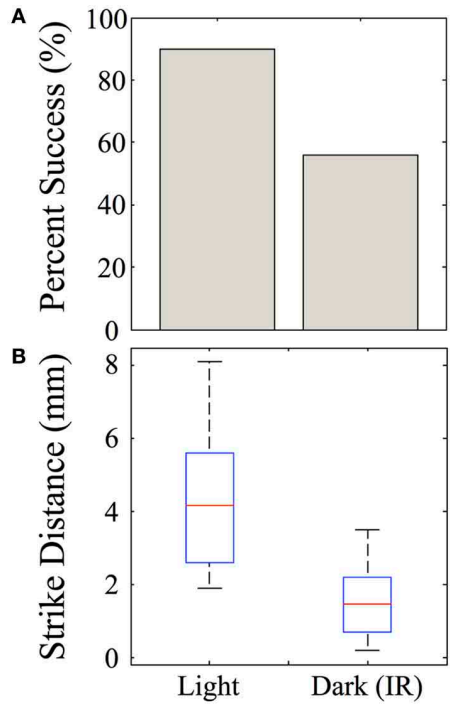

FIGURE 13 | Effect of darkness on juvenile feeding success and strike distance. Juveniles were observed striking at Artemia under IR illumination and this behavior was compared with feeding strikes made in the light. **(A)** The success rate of strikes on *Artemia* are roughly 90% in the light, but substantially lower in the dark for these 39-day-old juveniles. **(B)** Strikes made in the dark are initiated from shorter distances than those in the light *(t-test, p = 0.02)*, which fits with the suggested involvement of lateral line. $n = 9$ fish.

in both normalized and absolute terms (**Figures 6**, **7**). In contrast, early larvae are able to launch their *final strike* only when they are very close and precisely aligned with the prey (**Figure 8**), although *feeding episodes* are initiated from much larger directions and distances.

This is not to discount early larval efforts, which are quite successful from first feedings, but rather reflects changing capabilities as zebrafish grow in size and begin to strike larger and faster prey items. The observed peak feeding velocities of larval and juvenile zebrafish do not change greatly across ontogeny, in absolute terms (**Figure 7**), although they exceed the velocity of our laboratory prey items, *Paramecia* and *Artemia* (**Figure 4**). What seems more important are the shorter overall durations of episodes: faster relative velocities may often be useful in predation, but a more rapid rate of capture should be advantageous in terms of total acquired nutrition and in terms of competition with conspecifics, if resources are limited.

SENSORY CONTRIBUTIONS TO PREY CAPTURE

Many fishes visually hunt prey items (Drost, 1987; Batty et al., 1990; Job and Bellwood, 1996; New et al., 2001; Rice and Westneat, 2005; Fleisch and Neuhauss, 2006) and vision is central to larval zebrafish feeding, based on the role of optic tectum (Gahtan et al., 2005), the lack of tracking movements in the dark (McElligott and O'Malley, 2005; Patterson et al., 2013) and the elicitation of J-turns by artificial visual stimuli (Bianco et al., 2011). Vision remains the predominant sensory modality in older larvae and juveniles, given the large drop in feeding rates seen in the dark (**Table 2**) and the longer strike distance and better accuracy in light vs. dark conditions (**Figure 13**). Feeding continues, however, at a low rate in darkness and juveniles can execute targeted predatory maneuvers (**Figure 11**), suggesting use of another modality for prey detection.

Lateral line contributes to predation in a variety of fishes (Montgomery, 1989; New et al., 2001; Pohlmann et al., 2004). **Table 2** shows that ablation of lateral line sensors with neomycin decreases feeding rate in both late larvae and juveniles, but not to nearly the extent as darkness. Neomycin also decreases strike accuracy in the light, in both early and late larvae (**Figure 12**), but older juveniles fare better, perhaps because visual targeting and/or inertia of the strikes makes the lateral line less necessary. The combination of darkness and neomycin has the most profound effect, reducing feeding to very low levels in late larvae and juveniles (**Table 2**). Early larvae strike (initiate capture swims) from very close range (**Figure 8B**), and anterior neuromasts (visualized in **Figure 12**) may aid this behavior (New et al., 2001; Pohlmann et al., 2004). Our neomycin data, however, are not definitive regarding capture swim modality because these swims remain well formed in the *Light + Neomycin* condition. Contributions to

the control of capture swims by olfactory and gustatory senses (Caprio, 1978; Kanwal and Finger, 1997; Friedrich et al., 2004; Gardiner and Atema, 2007) or tactile interactions (Patterson et al., 2013) remain a possibility.

Optic tectum is the largest visual structure in the teleost brain (Burrill and Easter, 1994; Wullimann et al., 1996), and accumulating evidence suggests a role in zebrafish prey capture (Gahtan et al., 2005; Del Bene et al., 2010; Bianco et al., 2011). The larval optic tectum already has a diversity of cell types (Niell and Smith, 2005; Sumbre et al., 2008; Gabriel et al., 2012) which is potentially greater by the juvenile stage and might contribute to the visual analyses that guide homing strikes. Tectum appears to play a central role in sensorimotor transformations that convert spatial information into motor commands (Ewert, 1987; Scott and Baier, 2009; Ahrens et al., 2012; Grama and Engert, 2012), presumably in conjunction with brainstem circuits and associated descending pathways that include the reticulospinal array and nMLF (Lee and Eaton, 1991; Foreman and Eaton, 1993; O'Malley et al., 1996; Zelenin et al., 2001; Bosch and Roberts, 2001; Gahtan et al., 2002; Gahtan and O'Malley, 2003; Sankrithi and O'Malley, 2010). Details of these transformations are just beginning to be understood (Del Bene et al., 2010; Bianco et al., 2011; Koyama et al., 2011; Fajardo et al., 2013).

UNDERLYING NEURAL CONTROLS

Larval J-turns require neural controls distinct from other larval turns being (1) of much slower angular velocity than escape turns (Eaton et al., 1991; Liu and Fetcho, 1999) and (2) kinematically distinct from spontaneous routine turns (Budick and O'Malley, 2000; Danos and Lauder, 2007) which are also used in optomotor behaviors (Roeser and Baier, 2003; Day et al., 2006; Burgess and Granato, 2007; Orger et al., 2008). J-turns are incremental "turn left" or "turn right" responses (Bianco et al., 2011) that achieve precise orientation in a stepwise fashion. The significant pauses between discrete tracking maneuvers (**Figures 3**, **5**) might allow for visual updating of direction and distance, after which the correct next maneuver can be selected. Recent optogenetic results suggest there are specialized tectal circuits for J-turns and that a winner-take-all mechanism enables a specific behavior (J-turn vs. slow swim) to be selected (Fajardo et al., 2013). While early larvae approach *Paramecia* in an iterative fashion, juveniles strike from comparatively long distances (**Figures 8**, **13**) and with sufficient precision that their trajectories accurately and quickly strike small targets (**Figures 3**, **5**, **9** and **12**).

Larval zebrafish have slow and fast motor systems which manifests as distinct "gaits" for the slow vs. fast/burst swims (Thorsen et al., 2004; Green and Hale, 2012). They depend upon red and white muscle (Buss and Drapeau, 2002) and distinct spinal oscillators or CPGs (Budick and O'Malley, 2000; Buchanan, 2001; Bhatt et al., 2007; McLean et al., 2008). The slow swims used in prey tracking are identical to those used in other larval behaviors (McElligott and O'Malley, 2005) and have been modeled in regards to CPG-frequency modulation (Hill et al., 2005; Kuo and Eliasmith, 2005; Knudsen et al., 2006). The high TBFs seen in early larval strikes are within the range of larval burst swim TBFs (Budick and O'Malley, 2000; Müller and van Leeuwen, 2004; Bhatt et al., 2007; McLean et al., 2008) but gradually decline over the next several weeks (**Figure 6C**). While the descending commands for predatory vs. other behaviors must differ, parsimony suggests conserved use of slow and fast spinal motor systems given the limited number of spinal interneuron classes seen anatomically (Bernhardt et al., 1990; Hale et al., 2001). These spinal networks could potentially be reconfigured to support the generation of a diverse variety of behaviors (Marder and Bucher, 2007; Bargmann, 2012).

The kinematic diversity of homing strikes (**Figure 9**) suggests further organizational capability, namely flexible composition of underlying neural commands in relation to the prey's distance and direction. For example, *Strike #1* is accomplished by a single slow bend (turn), reflecting an asymmetric motor command. *Strike #2* begins with a similarly low-angular velocity turn, but it then transitions into a low TBF forward swim bout, whose controlling neurons remain unknown (but see Green and Hale, 2012). In *Strike #2* slow swimming ceases after ∼ five cycles, just before the moment of capture. The mechanism for halting in zebrafish is unknown, but based on *Xenopus* studies might reflect an explicit "halting" command (Perrins et al., 2002), or the run-down of spinal CPG activity after an initial, excitatory forward swim command (Dale, 1998). Inertia allows the juvenile in *Strike #2* to coast through the *Artemia*'*s* location, with suction jaw movements executed about 1080 ms after onset of the episode.

Juvenile *Strike #3* has some overlap with *Strike #2* in utilizing a command system that produces caudally-propagating bends, but at no time is a conventional slow-swimming pattern seen. *Strike #3* contains only 3 bends in total (vs. the 11 bends in *Strike #2,* and just one bend in *Strike #1)*. Of particular note is the bent posture of the trunk which is held between ∼50 and 250 ms post-initiation of the episode. The kinematics suggests that sustained (i.e., non-oscillating) muscle contraction occurs concurrently with propulsive bends that propagate into the caudal trunk. This diversity of homing strikes rules out the use of rote, generic sensorimotor transformations and instead suggests that specific types of commands and command sequences are selected as a motor package based on the exigencies of each predatory opportunity. Such a process might depend on maturing forebrain structures, including an ancestral basal ganglia found in fishes (Medina and Reiner, 1995; Mueller et al., 2008; Ganz et al., 2012).

MOTOR LEARNING vs. INNATE KNOWLEDGE

The initial prey-tracking and strike maneuvers are not "learned" behaviors, since they are performed with precision on the very first predation attempts of early larvae (Borla et al., 2002; McElligott and O'Malley, 2005; McClenahan et al., 2012), in agreement with observations of other larval fishes (Drost, 1987; Job and Bellwood, 1996). These sensorimotor programs thus constitute a kind of "innate knowledge" of predatory opportunities in that they were learned over evolutionary time, stored in the developmental programs of the zebrafish genome and are expressed through development (Adami et al., 2000; McNamara et al., 2006), aided presumably by ongoing sensory feedback that influences general motor and visual system development. The extent to which transitional behaviors and subsequent homing strikes might be innate is uncertain. We did not observe repetitive efforts to strike at a particular location in the arena. Had such repetition

existed, larvae could in principle have utilized error signals and cerebellar learning mechanisms to improve performance, but the paucity of errors in conjunction with variable strike patterns, does not fit with conventional error-correction learning algorithms (Portugues and Engert, 2011; Ahrens et al., 2012). While zebrafish larvae exhibit cerebellar function and associative learning (Aizenberg and Schuman, 2011; Valente et al., 2012), the vanishing number of misses with age, along with good success at a young age (roughly 90% hits at 24 dpf; **Figure 12**), further suggests that growing zebrafish have either extremely fast sensorimotor learning algorithms or employ a series of innate motor programs that appear sequentially across ontogeny. A hybrid mechanism, whereby innate capabilities amplify larval learning skills, is perhaps most parsimonious.

ACKNOWLEDGMENTS

We would like to thank Maggie Moyer for excellent technical assistance.

REFERENCES

Adami, C., Ofria, C., and Collier, T. C. (2000). Evolution of biological complexity. *Proc. Natl. Acad. Sci. U.S.A.* 97, 4463–4468. doi: 10.1073/pnas.97.9.4463

Ahrens, M. B., Li, J. M., Orger, M. B., Robson, D. N., Schier, A. F., Engert, F., et al. (2012). Brain-wide neuronal dynamics during motor adaptation in zebrafish. *Nature* 485, 471–477. doi: 10.1038/nature11057

Aizenberg, M., and Schuman, E. M. (2011). Cerebellar-dependent learning in larval zebrafish. *J. Neurosci.* 31, 8708–8712. doi: 10.1523/JNEUROSCI.6565-10.2011

Bae, Y. K., Kani, S., Shimizu, T., Tanabe, K., Nojima, H., Kimura, Y., et al. (2009). Anatomy of zebrafish cerebellum and screen for mutations affecting its development. *Dev. Biol.* 330, 406–426. doi: 10.1016/j.ydbio.2009.04.013

Bargmann, C. I. (2012). Beyond the connectome: how neuromodulators shape neural circuits. *Bioessays* 34, 458–465. doi: 10.1002/bies.201100185

Bassett, D. K., Carton, A. G., and Montgomery, J. C. (2007). Saltatory search in a lateral line predator. *J. Fish Biol.* 70, 1148–1160. doi: 10.1111/j.1095-8649.2007.01380.x

Batty, R. S., Blaxter, J. H. S., and Richard, J. M. (1990). Light intensity and the feeding behaviour of herring, *Clupea harengus*. *Mar. Biol.* 107, 383–388.

Bernhardt, R. R., Chitnis, A. B., Lindamer, L., and Kuwada, J. Y. (1990). Identification of spinal neurons in the embryonic and larval zebrafish. *J. Comp. Neurol.* 302, 603–616. doi: 10.1002/cne.903020315

Bhatt, D. H., McLean, D. L., Hale, M. E., and Fetcho, J. R. (2007). Grading movement strength by changes in firing intensity versus recruitment of spinal interneurons. *Neuron* 53, 91–102. doi: 10.1016/j.neuron.2006.11.011

Bianco, I. H., Kampff, A. R., and Engert, F. (2011). Prey capture behavior evoked by simple visual stimuli in larval zebrafish. *Front. Sys. Neurosci.* 5:101. doi: 10.3389/fnsys.2011.00101

Bonaiuto, R. E., Schubert, J., Trautwein, M., and O'Malley, D. M. (2007). Maturation of the zebrafish prey capture behavior: changes in kinematics and sensory control. *Soc. Neurosci. Abst* 2007, #312.5.

Borla, M. A., Palecek, B., Budick, S., and O'Malley, D. (2002). Prey capture by larval zebrafish: evidence for fine axial motor control. *Brain Behav. Evol.* 60, 207–229. doi: 10.1159/000066699

Bosch, T. J., and Roberts, B. L. (2001). The relationships of brain stem systems to their targets in the spinal cord of the eel, *Anguilla anguilla*. *Brain Behav. Evol.* 57, 106–116. doi: 10.1159/000047230

Buchanan, J. T. (2001). Contributions of identifiable neurons and neuron classes to lamprey vertebrate neurobiology. *Prog. Neurobiol.* 63, 441–466. doi: 10.1016/S0301-0082(00)00050-2

Budick, S. A., and O'Malley, D. M. (2000). Locomotor repertoire of the larval zebrafish: swimming, turning, and prey capture. *J. Exp. Biol.* 203, 2565–2579.

Burgess, H. A., and Granato, M. (2007). Modulation of locomotor activity in larval zebrafish during light adaptation. *J. Exp. Biol.* 210, 2526–2539. doi: 10.1242/jeb.003939

Burrill, J. D., and Easter, S. S. (1994). Development of the retinofugal projections in the embryonic and larval zebrafish (*Brachydanio rerio*). *J Comp. Neurol.* 346, 583–600. doi: 10.1002/cne.903460410

Buss, R. R., and Drapeau, P. (2002). Activation of embryonic red and white muscle fibers during fictive swimming in the developing zebrafish. *J. Neurophysiol.* 87, 1244–1251.

Caprio, J. (1978). Olfaction and taste in the channel catfish: an electrophysiological study of the responses to amino acids and derivatives. *J. Comp. Physiol.* 123, 357–371. doi: 10.1007/BF00656970

Dale, N. (1998). Delayed production of adenosine underlies temporal modulation of swimming in frog embryo. *J. Physiol.* 511, 265–272. doi: 10.1111/j.1469-7793.1998.265bi.x

Danos, N., and Lauder, G. V. (2007). The ontogeny of fin function during routine turns in zebrafish Danio rerio. *J. Exp. Biol.* 210, 3374–3386. doi: 10.1242/jeb.007484

Day, L. J., Dhanota, H. A., Severi, K. S., Josephs, T. A., Holmes, T. S., and O'Malley, D. M. (2006). How do we classify the diversity of zebrafish locomotor behaviors? *Soc. Neurosci. Abs.* 32, 448.22.

Del Bene, F., Wyart, C., Robles, E., Tran, A., Looger, L., Scott, E. K., et al. (2010). Filtering of visual information in the tectum by an identified neural circuit. *Science* 330, 669–673. doi: 10.1126/science.1192949

Drost, M. R. (1987). Relation between aiming and catch success in larval fishes. *Can. J. Fish. Aqua. Sci.* 44, 304–315.

Eaton, R. C., DiDomenico, R., and Nissanov, J. (1991). Role of the Mauthner cell in sensorimotor integration by the brainstem escape network. *Brain Behav. Evol.* 37, 272–285.

Engeszer, R. E., Barbiano, L.,A., Ryan, M. J., and Parichy, D. M. (2007a). Timing and plasticity of shoaling behaviour in the zebrafish, *Danio rerio*. *Anim. Behav.* 74, 1269–1275. doi: 10.1016/j.anbehav.2007.01.032

Engeszer, R. E., Patterson, L. B., Roa, A. A., and Parichy, D. M. (2007b). Zebrafish in the wild: a review of natural history and new notes from the field. *Zebrafish* 4, 21–40. doi: 10.1089/zeb.2006.9997

Ewert, J. (1987). Neuroethology of releasing mechanisms: prey-catching in toads. *Behav. Brain Sci.* 10, 337–405.

Fajardo, O., Zhu, P., and Friedrich, R. W. (2013). Control of a specific motor program by a small brain area in zebrafish. *Front. Neural Circuits* 7:67. doi: 10.3389/fncir.2013.00067

Fleisch, V. C., and Neuhauss, S. C. (2006). Visual behavior in zebrafish. *Zebrafish* 3, 191–201. doi: 10.1089/zeb.2006.3.191

Foreman, M. B., and Eaton, R. C. (1993). The direction change concept for reticulospinal control of goldfish escape. *J. Neurosci.* 13, 4101–4113.

Friedrich, R. W., Habermann, C. J., Laurent, G. (2004). Multiplexing using synchrony in the zebrafish olfactory bulb. *Nat. Neurosci.* 8, 862–871. doi: 10.1038/nn1292

Gabriel, J. P., Trivedi, C. A., Maurer, C. M., Ryu, S., and Bollmann, J. H. (2012). Layer-specific targeting of direction-selective neurons in the zebrafish optic tectum. *Neuron* 76, 1147–1160. doi: 10.1016/j.neuron.2012.12.003as

Gahtan, E., and O'Malley, D. M. (2003). Visually guided injection of identified reticulospinal neurons in zebrafish: a survey of spinal arborization patterns. *J. Comp. Neurol.* 459, 186–200. doi: 10.1002/cne.10621

Gahtan, E., Sankrithi, N., Campos, J. B., and O'Malley, D. M. (2002). Evidence for a widespread brain stem escape network in larval zebrafish. *J. Neurophysiol.* 87, 608–614.

Gahtan, E., Tanger, P., and Baier, H. (2005). Visual prey capture in larval zebrafish is controlled by identified reticulospinal neurons downstream of the tectum. *J. Neurosci.* 25, 9294–9303. doi: 10.1523/JNEUROSCI.2678-05.2005

Ganz, J., Kaslin, J., Freudenreich, D., Machate, A., Geffarth, M., and Brand, M. (2012). Subdivisions of the adult zebrafish subpallium by molecular marker analysis. *J. Comp. Neurol.* 520, 633–655. doi: 10.1002/cne.22757

Gardiner, J. M., and Atema, J. (2007). Sharks need lateral line to locate odor sources: rheotaxis and eddy chemotaxis. *J. Exp. Biol.* 210, 1925–1934. doi: 10.1242/jeb.000075

Ghysen, A., and Dambly-Chaudière, C. (2004). Development of the zebrafish lateral line. *Curr.*

Opin. Neurobiol. 14, 67–73. doi: 10.1016/j.conb.2004.01.012

Grama, A., and Engert, F. (2012). Direction selectivity in the larval zebrafish tectum is mediated by asymmetric inhibition. *Front. Neural Circuits* 6:59. doi: 10.3389/fncir.2012.00059

Green, M. H., and Hale, M. E. (2012). Activity of pectoral fin motoneurons during two swimming gaits in the larval zebrafish (*Danio rerio*) and localization of upstream circuit elements. *J. Neurophysiol.* 108, 3393–3402. doi: 10.1152/jn.00623.2012

Hale, M. E., Ritter, D. A., and Fetcho, J. R. (2001). A confocal study of spinal interneurons in living larval zebrafish. *J. Comp. Neurol.* 437, 1–16. doi: 10.1002/cne.1266

Hassan, E. S. (1989). "Hydrodynamic Imaging of the surroundings by the lateral line of blind cavefish *Anoptichthys jordani*," in *The Mechanosensory Lateral Line: Neurobiology and Evolution*, (eds) S. Coombs, P. Gorner, and H. Munz (New York, NY: Springer-Verlag), 217–227.

Hernández, L. P. (2000). Intraspecific scaling of feeding mechanisms in an ontogenetic series of zebrafish, *Danio rerio*. *J. Exp. Biol.* 203, 3033–3043.

Hernández, L. P., Barresi, M. J., and Devoto, S. H. (2002). Functional morphology and developmental biology of zebrafish: reciprocal illumination from an unlikely couple. *Integr. Comp. Biol.* 42, 222–231. doi: 10.1093/icb/42.2.222

Hernández, L. P., Patterson, S. E., and Devoto, S. H. (2005). The development of muscle fiber type identity in zebrafish cranial muscles. *Anat. Embryol. (Berl.)* 209, 323–334. doi: 10.1007/s00429-004-0448-4

Hill, S. A., Liu, X.-P., Borla, M. A., José, J. V., and O'Malley, D. M. (2005). Neurokinematic modeling of complex swimming patterns of the larval zebrafish. *Neurocomputing* 65, 61–68.

Janssen, J., and Corcoran, J. (1993). Lateral line stimuli can override vision to determine sunfish strike trajectory. *J. Exp. Biol.* 176, 299–305.

Job, S. D., and Bellwood, D. R. (1996). Visual acuity and feeding in larval Pemnas biaculaeatus. *J. Fish Biol.* 48, 952–963. doi: 10.1111/j.1095-8649.1996.tb01489.x pp.952-963

Kanwal, J. S., and Finger, T. E. (1997). Parallel medullary gustatospinal pathways in a catfish: possible neural substrates for taste-mediated food search. *J. Neurosci.* 17, 4873–4885.

Kimmel, C. B. (1982). Reticulospinal and vestibulospinal neurons in the young larva of a teleost fish, *Brachydanio rerio*. *Prog. Brain Res.* 57, 1–23. doi: 10.1016/S0079-6123(08)64122-9

Kimmel, C. B., Powell, S. L., and Metcalfe, W. K. (1982). Brain neurons which project to the spinal cord in young larvae of the zebrafish. *J. Comp. Neurol.* 205, 112–127. doi: 10.1002/cne.902050203

Kimmel, C. B., Metcalfe, W. K., and Schabtach, E. (1985). T reticular interneurons: a class of serially repeating cells in the zebrafish hindbrain. *J. Comp. Neurol.* 233, 365–376. doi: 10.1002/cne.902330306

Knudsen, D. P., Arsenault, J. T., Hill, S. A., O'Malley, D. M., and José, J. V. (2006). Locomotive network modeling based on identified neurons in zebrafish. *Neurocomputing* 69, 1169–1174. doi: 10.1016/j.neucom.2005.12.068

Koyama, M., Kinkhabwala, A., Satou, C., Higashijima, S., and Fetcho, J. (2011). Mapping a sensory-motor network onto a structural and functional ground plan in the hindbrain. *Proc. Natl. Acad. Sci. U.S.A.* 108, 1170–1175. doi: 10.1073/pnas.1012189108

Kuo, P. D., and Eliasmith, C. (2005). Integrating behavioral and neural data in a model of zebrafish network interaction. *Biol. Cyber.* 93, 178–187 doi: 10.1007/s00422-005-0576-9

Larson, E. T., O'Malley, D. M., and Melloni, R. H. Jr. (2006). Aggression and vasotocin are associated with dominant-subordinate relationships in zebrafish. *Behav. Brain Res.* 167, 94–102. doi: 10.1016/j.bbr.2005.08.020

Lee, R. K., and Eaton, R. C. (1991). Identifiable reticulospinal neurons of the adult zebrafish, *Brachydanio rerio*. *J. Comp. Neurol.* 304, 34–52. doi: 10.1002/cne.903040104

Liu, K. S., and Fetcho, J. R. (1999). Laser ablations reveal functional relationships of segmental hindbrain neurons in zebrafish. *Neuron* 23, 325–335. doi: 10.1016/S0896-6273(00)80783-7

Marder, E., and Bucher, D. (2007). Understanding circuit dynamics using the stomatogastric nervous system of lobsters and crabs. *Annu. Rev. Physiol.* 69, 291–316. doi: 10.1146/annurev.physiol.69.031905.161516

McClenahan, P., Troup, M., and Scott, E. K. (2012). Fin-tail coordination during escape and predatory behavior in larval zebrafish. *PLoS ONE* 7:e32295. doi: 10.1371/journal.pone.0032295

McElligott, M. B., and O'Malley, D. M. (2005). Prey tracking in larval zebrafish: axial kinematics and visual control. *Brain Behav. Evol.* 66, 177–196. doi: 10.1159/000087158

McHenry, M. J., and Lauder, G. V. (2006). Ontogeny of form and function: locomotor morphology and drag in zebrafish (*Danio rerio*). *J. Morphol.* 267, 1099–1109 doi: 10.1002/jmor.10462

McHenry, M. J., Feitl, K. E., and Van Trump, W. J. (2009). Larval zebrafish rapidly sense the water flow of a predator's strike. *Biology Lett.* 5, 477–479. doi: 10.1098/rsbl.2009.0048

McLean, D. L., Masino, M. A., Koh, I. Y., Lindquist, W. B., and Fetcho, J. R. (2008). Continuous shifts in the active set of spinal interneurons during changes in locomotor speed. *Nat. Neurosci.* 11, 1419–1429. doi: 10.1038/nn.2225

McNamara, J. M., Green, R. F., and Olsson, O. (2006). Bayes' theorem and its applications in animal behaviour. *Oikos* 112, 243–251.

Medina, L., and Reiner, A. (1995). Neurotransmitter organization and connectivity of the basal ganglia in vertebrates: implications for the evolution of basal ganglia. *Brain Behav. Evol.* 46, 235–258.

Metcalfe, W. K., Mendelson, B., and Kimmel, C. B. (1986). Segmental homologies among reticulospinal neurons in the hindbrain of the zebrafish larva. *J. Comp. Neurol.* 251, 147–159. doi: 10.1002/cne.902510202

Montgomery, J. C. (1989). "Lateral line detection of planktonic prey," in *The Mechanosensory Lateral Line. Neurobiology and Evolution*, (eds) S. Coombs, P. Gorner, and H. Munz (New York, NY: Springer-Verlag), 561–574. doi: 10.1007/978-1-4612-3560-6_28

Montgomery, J. C., Baker, C. F., and Carton, A. G. (1997). The lateral line can mediate rheotaxis in fish. *Nature* 389, 960–963. doi: 10.1038/40135

Montgomery, J. C., MacDonald, F., Baker, C. F., and Carton, A. G. (2002). Hydrodynamic contributions to multimodal guidance of prey capture behavior in fish. *Brain Behav. Evol.* 59, 190–198. doi: 10.1159/000064906

Montgomery, J. C., McDonald, F., Baker, C. F., Carton, A. G., Ling, N. (2003). Sensory integration in the hydrodynamic world of rainbow trout. *Proc. Biol. Sci.* 270, S195–S197. doi: 10.1098/rsbl.2003.0052

Mueller, T., Wullimann, M. F., and Guo, S. (2008). Early teleostean basal ganglia development visualized by zebrafish Dlx2a, Lhx6, Lhx7, Tbr2 (eomesa), and GAD67 gene expression. *J. Comp. Neurol.* 507, 1245–1257. doi: 10.1002/cne.21604

Müller, U. K., and van Leeuwen, J. L. (2004). Swimming of larval zebrafish: ontogeny of body waves and implications for locomotor development. *J. Exp. Biol.* 207, 853–868. doi: 10.1242/jeb.00821

Münz, H. (1989). "Functional organisation of the lateral line periphery," in *The Mechanosensory Lateral Line. Neurobiology and Evolution*, (eds) S. Coombs, P. Görner, and H. Münz (New York, NY: Springer-Verlag), 17–78.

New, J. G., Alborg Fukes, L., and Khan, A. N. (2001). Strike feeding behavior in the muskellunge, Esox masquinongy: contributions of the lateral line and visual sensory systems. *J. Exp. Biol.* 204, 1207–1221.

Niell, C. M., and Smith, S. J. (2005). Functional imaging reveals rapid development of visual response properties in the zebrafish tectum. *Neuron* 45, 941–951. doi: 10.1016/j.neuron.2005.01.047

Nüsslein-Volhard, C., and Dahm, R. (2002). *Zebrafish: A Practical Approach*. Oxford, England: Oxford University Press.

Olszewski, J., Haehnel, M., Taguchi, M., and Liao, J. C. (2012). Zebrafish larvae exhibit rheotaxis and can escape a continuous suction source using their lateral line. *PLoS ONE* 7:e36661. doi: 10.1371/journal.pone.0036661

O'Malley, D. M., Kao, Y. H., and Fetcho, J. R. (1996). Imaging the functional organization of zebrafish hindbrain segments during escape behaviors. *Neuron* 17, 1145–1155. doi: 10.1016/S0896-6273(00)80246-9

O'Malley, D. M., Zhou, Q., and Gahtan, E. (2003). Probing neural circuits in the zebrafish: a suite of optical techniques. *Methods* 30, 49–63. doi: 10.1016/S1046-2023(03)00007-0

Orger, M. B., Kampff, A. R., Severi, K. S., Bollmann, J. H., and Engert, F. (2008). Control of visually guided behavior by distinct populations of spinal projection neurons. *Nat. Neurosci.* 11, 327–333. doi: 10.1038/nn2048

Owens, K. N., Coffin, A. B., Hong, L. S., O'Connell Bennett, K., Edwin, W. R., and Raible, D. W. (2009). Response of mechanosensory hair cells of the zebrafish

lateral line to aminoglycosides reveals distinct cell death pathways. *Hear. Res.* 253, 32–41. doi: 10.1016/j.heares.2009.03.001

Parichy, D. M., Elizondo, M. R., Mills, M. G., Gordon, T. N., and Engeszer, R. E. (2009). Normal table of postembryonic zebrafish development: staging by externally visible anatomy of the living fish. *Dev. Dyn.* 238, 2975–3015. doi: 10.1002/dvdy.22113

Patterson, B. W., Abraham, A. O., MacIver, M. A., and McLean, D. L. (2013). Visually guided gradation of prey capture movements in larval zebrafish. *J. Exp. Biol.* doi: 10.1242/jeb.087742. [Epub ahead of print].

Perrins, R., Walford, A., and Roberts, A. (2002). Sensory activation and role of inhibitory reticulospinal neurons that stop swimming in hatchling frog tadpoles. *J. Neurosci.* 22, 4229–4240.

Pohlmann, K., Atema, J., and Breithaupt, T. (2004). The importance of the lateral line in nocturnal predation of piscivorous catfish. *J. Exp. Biol.* 207, 2971–2978. doi: 10.1242/jeb.01129

Portugues, R., and Engert, F. (2011). Adaptive locomotor behavior in larval zebrafish. *Front. Syst. Neurosci.* 5:72. doi: 10.3389/fnsys.2011.00072

Rice, A. N., and Westneat, M. W. (2005). Coordination of feeding, locomotor and visual systems in parrotfishes (Teleostei: Labridae). *J. Exp. Biol.* 208, 3503–3518. doi: 10.1242/jeb.01779

Roeser, T., and Baier, H. (2003). Visuomotor behaviors in larval zebrafish after GFP-guided laser ablation of the optic tectum. *J. Neurosci.* 23, 3726–3734.

Sankrithi, N., and O'Malley, D. M. (2010). Activation of a multisensory, multifunctional nucleus in the zebrafish midbrain during diverse locomotor behaviors. *Neuroscience* 166, 970–993. doi: 10.1016/j.neuroscience.2010.01.003

Scott, E. K., and Baier, H. (2009). The cellular architecture of the larval zebrafish tectum, as revealed by gal4 enhancer trap lines. *Front. Neural Circuits* 3:13. doi: 10.3389/neuro.04.013.2009

Spence, R., Fatema, M. K., Ellis, S., Ahmed, Z. F., and Smith, C. (2007). The diet, growth and recruitment of wild zebrafish (*Danio rerio*) in Bangladesh. *J. Fish Biol.* 71, 304–309. doi: 10.1111/j.1095-8649.2007.01492.x

Spence, R., Gerlach, G., Lawrence, C., and Smith, C. (2008). The behavior and ecology of the zebrafish, *Danio rerio*. *Bio. Rev.* 83, 13–34. doi: 10.1111/j.1469-185X.2007.00030.x

Staab, K. L., and Hernández, L. P. (2010). Development of the cypriniform protrusible jaw complex in *Danio rerio*: constructional insights for evolution. *J. Morphol.* 271, 814–825. doi: 10.1002/jmor.10836

Stewart, W. J., Cardenas, G. S., and McHenry, M. J. (2013). Zebrafish larvae evade predators by sensing water flow. *J. Exp. Biol.* 216, 388–398. doi: 10.1242/jeb.072751

Sumbre, G., Muto, A., Baier, H., and Poo, M. M. (2008). Entrained rhythmic activities of neuronal ensembles as perceptual memory of time interval. *Nature* 456, 102–106. doi: 10.1038/nature07351

Thorsen, D. H., and Hale, M. E. (2005). Development of zebrafish (*Danio rerio*) pectoral fin musculature. *J. Morph.* 266, 241–255. doi: 10.1002/jmor.10374

Thorsen, D. H., and Hale, M. E. (2007). Neural development of the zebrafish (*Danio rerio*) pectoral fin. *J. Comp. Neurol.* 504, 168–184. doi: 10.1002/cne.21425

Thorsen, D. H., Cassidy, J. J., and Hale, M. E. (2004). Swimming of larval zebrafish: fin-axis coordination and implications for functional and neural control. *J. Exp. Biol.* 207, 4175–4183. doi: 10.1242/jeb.01285

Valente, A., Huang, K. H., Portugues, R., and Engert, F. (2012). Ontogeny of classical and operant learning behaviors in zebrafish. *Learn. Mem.* 19, 170–177. doi: 10.1101/lm.025668.112

Webb, J. F., and Shirey, J. E. (2003). Postembryonic development of the cranial lateral line canals and neuromasts in zebrafish. *Dev. Dyn.* 228, 370–385. doi: 10.1002/dvdy.10385

Westphal, R. E., and O'Malley, D. M. (2010). Feeding strategies of the larval zebrafish and the Mexican tetra. *Soc. Neurosci. Abst* 2010, #777.14.

Windsor, S. P., Tan, D., and Montgomery, J. C. (2008). Swimming kinematics and hydrodynamic imaging in the blind Mexican cave fish (*Astyanax fasciatus*). *J. Exp. Biol.* 211, 2950–2959. doi: 10.1242/jeb.020453

Wullimann, M. F., Rupp, B., and Reichert, H. (1996). *Neuroanatomy of the Zebrafish Brain: A Topological Atlas*. Basel: Birkhäuser-Verlag.

Zelenin, P. V., Grillner, S., Orlovsky, G. N., and Deliagina, T. G. (2001). Heterogeneity of the population of command neurons in the lamprey. *J. Neurosci.* 21, 7793–7803.

Conflict of Interest Statement: The authors declare that the research was conducted in the absence of any commercial or financial relationships that could be construed as a potential conflict of interest.

Received: 29 January 2013; paper pending published: 03 March 2013; accepted: 21 May 2013; published online: 07 June 2013.

Citation: Westphal RE and O'Malley DM (2013) Fusion of locomotor maneuvers, and improving sensory capabilities, give rise to the flexible homing strikes of juvenile zebrafish. Front. Neural Circuits 7:108. doi: 10.3389/fncir.2013.00108

frontiers in
NEURAL CIRCUITS

ORIGINAL RESEARCH ARTICLE
published: 10 June 2013
doi: 10.3389/fncir.2013.00109

Quantification of locomotor activity in larval zebrafish: considerations for the design of high-throughput behavioral studies

Justin J. Ingebretson and Mark A. Masino*

Department of Neuroscience, University of Minnesota, Minneapolis, MN, USA

Edited by:
Gonzalo G. De Polavieja, Instituto Cajal. CSIC, Spain

Reviewed by:
Claire Wyart, Brain and Spinal cord Institute (ICM), France
Pertti Panula, University of Helsinki, Finland

***Correspondence:**
Mark A. Masino, Department of Neuroscience, University of Minnesota, 321 Church Street, Minneapolis, MN 55455, USA
e-mail: masino@umn.edu

High-throughput behavioral studies using larval zebrafish often assess locomotor activity to determine the effects of experimental perturbations. However, the results reported by different groups are difficult to compare because there is not a standardized experimental paradigm or measure of locomotor activity. To address this, we investigated the effects that several factors, including the stage of larval development and the physical dimensions (depth and diameter) of the behavioral arena, have on the locomotor activity produced by larval zebrafish. We provide evidence for differences in locomotor activity between larvae at different stages and when recorded in wells of different depths, but not in wells of different diameters. We also show that the variability for most properties of locomotor activity is less for older than younger larvae, which is consistent with previous reports. Finally, we show that conflicting interpretations of activity level can occur when activity is assessed with a single measure of locomotor activity. Thus, we conclude that although a combination of factors should be considered when designing behavioral experiments, the use of older larvae in deep wells will reduce the variability of locomotor activity, and that multiple properties of locomotor activity should be measured to determine activity level.

Keywords: locomotor activity, high-throughput screening assays, larval zebrafish, measurement, model organism, development

INTRODUCTION

The use of larval zebrafish as a model organism in high-throughput behavioral screens is rapidly expanding due, at least in part, to the development and availability of commercial and academic analytical platforms designed to assess locomotor activity in larval zebrafish (Lessman, 2002; Anichtchik et al., 2004; Lockwood et al., 2004; Zon and Peterson, 2005; Giacomini et al., 2006; Prober et al., 2006; Burgess and Granato, 2007; Cahill, 2007; Parng et al., 2007; Winter et al., 2008; Creton, 2009; MacPhail et al., 2009; Sallinen et al., 2009a,b; Irons et al., 2010; Sylvain et al., 2010; Ali et al., 2011; Cario et al., 2011; Chen et al., 2011; Farrell et al., 2011; Padilla et al., 2011; Pelkowski et al., 2011; Cowden et al., 2012; Irons et al., 2013). Several characteristics of zebrafish embryos/larvae make them amenable to high-throughput behavioral screens. A high degree of conservation of the nervous system is present between zebrafish and mammals, so comparative studies are possible (Postlethwait et al., 2000; Higashijima et al., 2004; Kimura et al., 2006; Panula et al., 2010; Eklöf-Ljunggren et al., 2012). The small size of zebrafish larvae (∼4 mm in length) and large number of embryos produced from a single mating permits high-throughput testing of large numbers of animals and experimental conditions simultaneously. Finally, zebrafish larvae are useful for chemical and pharmacological/toxicological screens, as they are permeable to small molecules (Kokel et al., 2010; Rihel et al., 2010; Peterson and Fishman, 2011; Tan and Zon, 2011).

There has not been, however, a systematic characterization of how experimental conditions affect the locomotor activity in larval zebrafish in the context of high-throughput testing. Evaluation of the current methods used for high-throughput studies has led us to propose that several factors, which vary between research groups, could affect locomotor activity or the conclusions drawn from such studies. First, large sample-sizes are necessary due to the recognized high degree of intra-larval variability in the locomotor activity (Colwill and Creton, 2011; Farrell et al., 2011; Lambert et al., 2012). Second, assessing activity by measuring and reporting a single property of locomotor activity (i.e., swim speed or total distance) may lead to an incomplete understanding of activity level. For example, different groups of larvae can produce similar total distances traveled per time by generating different swim durations and/or swim speeds. This strongly suggests that multiple properties of locomotor activity must be examined and integrated to fully depict activity levels. Third, skeletal deformities, such as tail kinks are often observed when zebrafish embryos/larvae are reared in multiwell plates (Selderslaghs et al., 2009; Padilla et al., 2011). Such deformities can affect how larvae locomote and, if these larvae are eliminated from the study, can reduce throughput. Finally, the ratio of larval body length to behavioral well diameter (length-to-diameter) may alter the properties of locomotor activity. For example, when the ratio nears one (length and diameter are nearly equivalent, as in 96-well plates), space constraints may affect the speed and duration of locomotion, but not when the ratio is less than one (length is smaller than well diameter, as in 6, 12, 24, or 48 well plates). Recent reports showed that the locomotor activity was different for larvae in 96 well and 24-well plates (Farrell et al., 2011; Padilla et al., 2011), but did not examine a range of well

dimensions to determine the effect of diameter on locomotor activity.

To date, these factors have not been fully taken into consideration for the experimental design or data interpretation of locomotor activity. Thus, the goal of this study was to determine the effects of these factors in an attempt to identify and standardize the parameters necessary to assess locomotor activity.

MATERIALS AND METHODS

ANIMALS

All experiments were performed on zebrafish (*Danio rerio*) larvae at 4 and 7 days post-fertilization (dpf). Wild-type larvae were obtained from a laboratory stock (Segrest Farms; Gibsonton, FL) of adults at the University of Minnesota. Embryos and larvae were maintained in petri dishes (100 mm dia) filled with embryo water (60 μg/mL Instant Ocean salt mix; Cincinnati, OH) in a 28.5°C incubator under a 14/10 h light/dark cycle until the start of behavioral recordings at 4 or 7 dpf. The density was not greater than 60 embryos or larvae per dish. Larvae hatched spontaneously between 2 and 3 dpf and were not fed until 8 dpf; one day after the final video recording at 7 dpf. Only larvae with inflated air bladders at 4 dpf were selected for these studies. Larvae were kept at room temperature during recording sessions. All procedures were approved by the Institutional Animal Care and Use Committee at the University of Minnesota and were in accordance with National Institutes of Health guidelines.

VIDEO ACQUISITION

To acquire video recordings of free-swimming behavior and to eliminate group interactions, larvae were placed individually in wells (see below) containing embryo media on custom-built plates. The plates were composed of either acetal resin (L × W × D: 165 × 102 × 1.5 mm; Delrin, DuPont) or acrylic plastic (L × W × D: 165 × 102 × 5.5 mm; polymethyl methacrylate, PlexiGlas); both materials were black in color. The plates were secured to a piece of glass (L × W × D: 178 × 114 × 2 mm) with dental cement (polyvinylsiloxane impression material Type I, medium viscosity #3604-14952, Kerr Manufacturing Company). Each plate was comprised of six arenas ("wells") with different combinations of depth [1.5 mm (shallow) or 5.5 mm (deep)] and diameter [10 mm (small), 20 mm (medium), or 30 mm (large)]. The wells were made with a computer-controlled laser-cutter, which left the inner surface of the well with a matte-like finish. All six wells on an individual plate were composed of a single depth and a single diameter. The following volumes of embryo water were used to fill the wells: 150 μL (1.5 mm depth × 10 mm dia.), 600 μL (1.5 mm depth × 20 mm dia.), and 1.8 mL (1.5 mm depth × 30 mm dia.); 500 μL (5.5 mm depth × 10 mm dia.), 2.0 mL (5.5 mm depth × 20 mm dia.), and 4.1 mL (5.5 mm depth × 30 mm dia.). Due to the convex meniscus formed, the depth of the shallow wells was ∼2 mm and the deep wells was ∼6 mm. Depths were chosen to bound the vertical range over which the larvae could access; either to restrict locomotion to two-dimensions (*x* and *y*; shallow) or to allow access to the vertical dimension (*z*; deep) of the well, while diameters were chosen based on commercially available well plates typically used for locomotor assessment (48 well: 10.5 mm; 12 well: 22.1 mm; 6 well: 34.8 mm; Creton, 2009; Sallinen et al., 2009a,b; Selderslaghs et al., 2009; Cario et al., 2011; Chen et al., 2011; Colwill and Creton, 2011; Farrell et al., 2011; Padilla et al., 2011). We did not assess activity in 96 well plates (6.8 mm well diameter), in which the larval body length to behavioral well diameter ratio was near one, because others have previously reported that space constraints affect locomotor activity (Selderslaghs et al., 2009; Farrell et al., 2011; Padilla et al., 2011). The plates were positioned atop a transmitted LED light stage (Metaphase Technologies) and a light meter (Extech Instruments) was used to measure the light intensity at the level of the arena, which was 4 Klx to maximize contrast and facilitate tracking of dark targets on a light background. For all experiments, testing occurred between 9 am and 4 pm using a randomized trial design to eliminate systematic effects due to time of day. The larvae acclimated to the recording arena for 10 min before the start of video acquisition. Subsequently, video of spontaneous free-swimming was recorded for 10 min at 60 frames/s using a digital CMOS camera (Firefly MV; Point Grey Research) with an attached 12 mm lens (Navitar). The camera was mounted to a copystand and videos were acquired and saved without compression, via Fview (Straw and Dickinson, 2009).

TRACKING AND ANALYSIS

The videos generated by Fview were analyzed to obtain independent trajectories of each target within the arena as previously described (Lambert et al., 2012). We used the open-source Fix Errors Matlab Toolbox (FEMT), provided by the creators of Ctrax (Branson et al., 2009), to identify and fix tracking errors, such as loss of target or false target recognition. The total number of errors per 10-min video was 0.06 ± 0.03 ($n = 288$ videos) and all errors were corrected via the FEMT. Scripts from the open-source Behavioral Microarray MATLAB Toolbox (Branson et al., 2009) were used to compute a suite of behavioral parameters for each of the individual targets from the fixed Ctrax trajectories. The speed of the center of rotation was extracted for each target to define and detect swimming event onsets and offsets, as described previously (Lambert et al., 2012), with minor modifications; we used a 2.0 mm/s speed threshold filter and a minimum 10 frame (166.6 ms) inter-event interval (end-to-start). Episodes of swimming were defined as the activity between event onsets and offsets. Identical filters were applied for all videos across all developmental stages and well dimensions. Next, the speed of the center of mass was extracted for each target to determine the instantaneous velocities during swimming episodes. Larvae were considered "motile" when at least one swimming episode was identified during the 10 min recording and "non-motile" when swimming episodes were absent.

The properties of locomotor activity that we measured were: (1) Episode Frequency [number of episodes per sec (Hz)], (2) Episode Duration [duration of time between events onset and offset (ms)], (3) Swim Speed [mean instantaneous velocity per episode (mm/s)], (4) Active Swim Time [sum of the number of frames between events onset and offset divided by the frame rate (s)], and (5) Total Distance [summed instantaneous speeds during swimming episodes divided by frame rate (cm)] and measured for each larva. All measures were then averaged

across larvae within each condition and reported as population means ± SD.

ETHANOL TREATMENT

Ethanol (200 proof, undenatured, Decon Laboratories) was prepared at a 1% concentration (v/v) in embryo media. This ethanol concentration was selected on the basis of pilot studies (data not shown) and previous reports (Lockwood et al., 2004; Gerlai et al., 2009; MacPhail et al., 2009; Irons et al., 2010; Chen et al., 2011; Cowden et al., 2012). The effects of acute ethanol exposure on locomotor activity in larval zebrafish were examined using the experimental paradigm described above (see Video Acquisition). However, we restricted the factors in this analysis to include only 7 dpf larvae in deep wells; all well diameters were used. As described above, the larvae acclimated to the behavioral arena and then a 10 min video of spontaneous free-swimming was acquired. The larvae were then exposed to ethanol (1%) for 30 min followed by a second 10 min video of spontaneous free-swimming; larvae remained in ethanol during video acquisition. Only larvae that were motile in both the control and treatment conditions were used for this analysis.

STATISTICAL ANALYSIS

Statistical analyses were performed with SigmaPlot 12.0 (Systat Software). Motile larvae were analyzed using Fisher's *z*-coefficient to test for significant differences between proportions. The main effects of stage, depth and diameter on locomotor activity were tested for significance using a Three-Way ANOVA. For the ethanol study, a repeated measures ANOVA was used. *Post-hoc* tests were performed using the Holm–Sidak correction for multiple comparisons. Significance was established using an α criterion of $p = 0.05$. To estimate the variability of the measures of locomotor activity the group coefficients of variation (CoVs) were calculated as the group standard deviation (SD) divided by the group mean.

RESULTS

LOCOMOTOR ACTIVITY DIFFERS BETWEEN LARVAE AT DISTINCT DEVELOPMENTAL STAGES

Previous studies showed that larvae at distinct developmental stages produce different locomotor activities (Saint-Amant and Drapeau, 1998, 2000; Budick and O'Malley, 2000; Drapeau et al., 2002; Colwill and Creton, 2011; Lambert et al., 2012; Tong and McDearmid, 2012). We examined locomotor activity produced by larvae at 4 and 7 dpf because larvae at these stages of development produce beat-and-glide swimming (Buss and Drapeau, 2001; Drapeau et al., 2002). Larvae at earlier and later developmental stages were excluded from this study because they produce either burst locomotion at 3 dpf (Saint-Amant and Drapeau, 1998; Budick and O'Malley, 2000; Buss and Drapeau, 2001; Drapeau et al., 2002) or subtle changes to the locomotor activity between 5 and 8 dpf (Müller and van Leeuwen, 2004; Colwill and Creton, 2011; Farrell et al., 2011), respectively. As a first approximation of locomotor activity, we determined the proportions of 4 and 7 dpf larvae ($n = 144$ for both groups) that were motile (see Materials and Methods) across all well depths (deep and shallow) and diameters (small, medium, and large). A significantly higher proportion of larvae were motile at 7 dpf than at 4 dpf (97 and 65%, respectively; Fisher's *z*-coefficient = 6.64, $p < 0.005$; **Figure 1A**), which was consistent with previous results from our lab (Lambert et al., 2012). Next, we determined whether developmental stage affected the locomotor properties of larvae. Larvae at 7 dpf produced significantly greater episode frequency (**Figure 1B**), shorter episode duration, slower swim speed, less active swim time and less total distance than did 4 dpf larvae (**Table 1**). Note that these measures of the properties of locomotor activity are not independent from one another. Finally, to determine whether the variability measured in the locomotor properties was affected by the developmental stage of the larvae, we calculated the coefficient of variation (CoV) for each measure and compared them across developmental stages (4 and 7 dpf). The CoVs of all properties except episode duration were smaller for 7 dpf larvae than for 4 dpf larvae (**Figure 1C**). These results showed that developmental stage affected motility and the properties and the variability of locomotor activity.

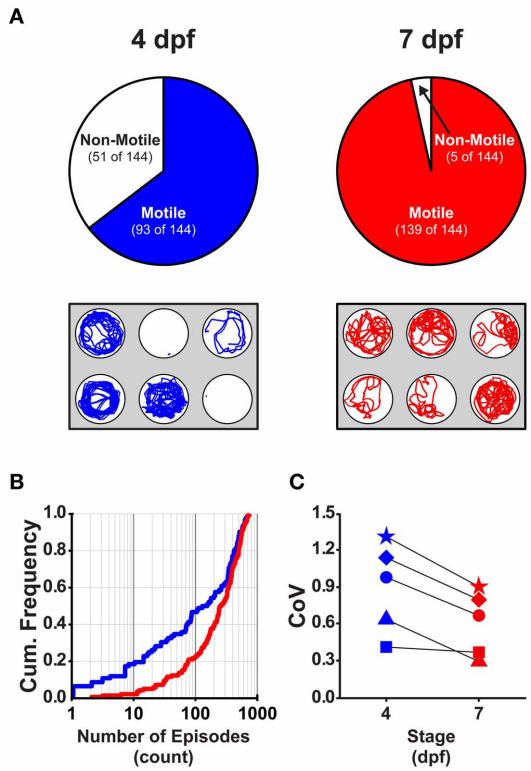

FIGURE 1 | The proportion of motile larvae and the variability among the locomotor properties are different between 4 and 7 dpf larvae. **(A)** *Top Row*, Pie charts depicting the proportions of motile and non-motile larvae at 4 dpf and 7 dpf (blue and red, respectively). *Bottom Row*, Representative trajectory plots for larvae in 6-well behavioral arena plates (30 mm well diameter shown); single larva per well. **(B)** Cumulative frequency plots for the number of swim episodes produced by 4 dpf and 7 dpf larvae (blue and red, respectively). **(C)** Plots of the group coefficients of variation (CoV) for all measured locomotor properties at 4 dpf ($n = 93$) and 7 dpf ($n = 139$) (blue and red, respectively). Symbols are: circle, episode frequency; square, episode duration; triangle, swim speed; diamond, active swim time; star, total distance.

Table 1 | Comparison of the properties of locomotor activity for larvae at 4 and 7 dpf.

Stage	Episode frequency (Hz)	Episode duration (ms)	Swim speed (mm/s)	Active swim time (s)	Total distance (cm)
4 dpf	0.36 ± 0.36	196.5 ± 87.6	8.0 ± 5.2	44.5 ± 50.3	38.8 ± 50.1
7 dpf	0.48 ± 0.34	114.3 ± 46.7	6.7 ± 2.2	32.8 ± 26.5	21.9 ± 20.0
F	8.603	88.643	6.573	4.088	10.793
p	0.004	<0.001	0.011	0.044	0.001

Data expressed as group means ± SD. F, test statistic for Three-Way ANOVA; p, probability.

LOCOMOTOR ACTIVITY DIFFERS BETWEEN LARVAE IN WELLS OF DIFFERENT DEPTHS

Currently, there is a lack of information regarding how the dimensions (depth and diameter) of the behavioral arenas affect locomotor activity in larval zebrafish. We determined the proportions of larvae that were motile (see Materials and Methods) in shallow and deep wells ($n = 144$ for both groups) across all stages (4 and 7 dpf) and well diameters (small, medium, and large). A larger proportion of larvae were motile in deep wells than in shallow wells (85 and 75%, respectively; Fisher's *z*-coefficient = 2.13, $p < 0.05$; **Figure 2A**). Next, we determined whether well depth affected the locomotor properties of larvae. Larvae in deep wells produced significantly greater episode frequency (**Figure 2B**), active swim time and total distance than did larvae in shallow wells (**Table 2**). However, the episode durations and swim speeds were not significantly different (**Table 2**). Finally, to determine whether the variability measured in the locomotor properties was affected by well depth, we calculated the CoV for each measure and compared them across well depths. The CoVs of all properties except active swim time and total distance were smaller for larvae in deep wells than for larvae in shallow wells (**Figure 2C**). These results showed that well depth affected motility and the properties and variability of locomotor activity.

LOCOMOTOR ACTIVITY DIFFERS BETWEEN LARVAE IN WELLS OF DIFFERENT DIAMETERS

To test the effect of well diameter on locomotor activity in larval zebrafish, we determined the proportions of larvae that were motile (see Materials and Methods) in small, medium, and large diameter wells across all stages (4 and 7 dpf) and well depths (shallow and deep). The proportion of larvae that were motile did not vary with diameter; all pairwise comparisons produced Fisher's *z*-coefficients that were ≤ 1.02 and *p*-values that were ≥ 0.05 (**Figure 3A**). Next, we determined whether locomotor properties were different for larvae in behavioral wells of different diameters (small, medium, or large). We found that none of the measured locomotor properties were significantly different between groups (**Table 3**). Finally, to determine whether the variability measured in the locomotor properties was affected by well diameter, we calculated the CoV for each measure and compared them across diameters. The CoVs of all measured properties were smallest for larvae in small diameter wells and largest for larvae in medium diameter wells (**Figure 3C**). These results showed that well diameter did not affect larval motility or the measured properties of locomotor activity, yet the variability of some, but not all, measured properties of locomotor activity differed by well diameter.

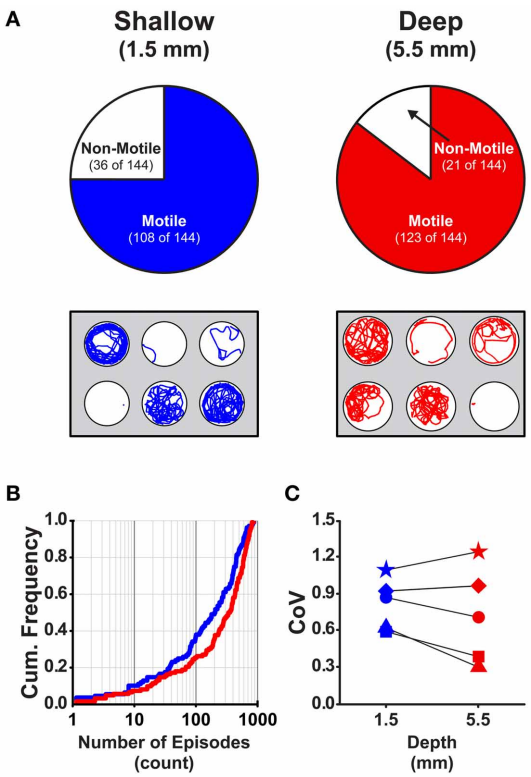

FIGURE 2 | The proportion of motile larvae and the variability among the locomotor properties are different for larvae in shallow and deep behavioral wells. (A) *Top Row*, Pie charts depicting the proportions of motile and non-motile larvae in Shallow and Deep wells (blue and red, respectively). *Bottom Row*, Representative trajectory plots for larvae in 6-well behavioral arena plates (30 mm well diameter shown); single larva per well. **(B)** Cumulative frequency plots for the number of swim episodes produced by larvae in Shallow and Deep wells (blue and red, respectively). **(C)** Plots of the group coefficients of variation (CoV) for all measured locomotor properties in Shallow ($n = 108$) and Deep ($n = 123$) wells (blue and red, respectively). Symbols are: circle, episode frequency; square, episode duration; triangle, swim speed; diamond, active swim time; star, total distance.

LOCOMOTOR ACTIVITY IS AFFECTED BY INTERACTIONS BETWEEN DEVELOPMENTAL STAGE AND WELL DEPTH

In addition to the differences observed for developmental stage (**Figure 1**; **Table 1**) and well depth (**Figure 2**; **Table 2**), the analysis of variance revealed significant interactions between developmental stage and depth for both active swim time ($F = 5.37$,

Table 2 | Comparison of the properties of locomotor activity for larvae in behavioral wells of different depths.

Depth	Episode frequency (Hz)	Episode duration (ms)	Swim speed (mm/s)	Active swim time (s)	Total distance (cm)
Shallow	0.38 ± 0.32	147 ± 90.7	7.5 ± 4.9	28.9 ± 28.2	20.8 ± 22.7
Deep	0.50 ± 0.36	147.4 ± 63.6	6.8 ± 2.4	45.1 ± 43.9	35.6 ± 43.7
F	10.225	0.0214	2.421	13.762	13.112
p	0.002	0.884	0.121	<0.001	<0.001

Data expressed as group means ± SD. F, test statistic for Three-Way ANOVA; p, probability.

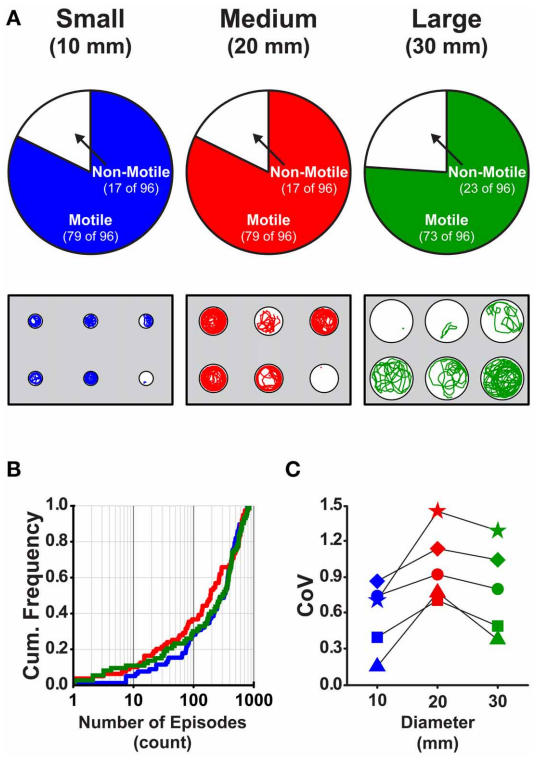

FIGURE 3 | The proportions of motile larvae are not different, but the variability among the locomotor properties is different for larvae in wells of different diameters. (A) *Top Row*, Pie charts depicting the proportions of motile and non-motile larvae in Small, Medium, and Large diameter wells (blue, red, and green, respectively). *Bottom Row*, Representative trajectory plots for larvae in 6-well behavioral arena plates (10, 20, and 30 mm diameter wells shown); single larva per well. **(B)** Cumulative frequency plots for the number of swim episodes produced by larvae in Small, Medium, and Large diameter wells (blue, red, and green, respectively). **(C)** Plots of the group coefficients of variation (CoV) for all measured locomotor properties in Small ($n = 79$), Medium ($n = 79$), and Large ($n = 73$) diameter wells (blue, red, and green, respectively). Symbols are: circle, episode frequency; square, episode duration; triangle, swim speed; diamond, active swim time; star, total distance.

$p = 0.02$) and total distance ($F = 6.31$, $p = 0.01$). *Post-hoc* analyses revealed that larvae at 4 dpf spent more time swimming in deep wells than in shallow wells ($t = 3.9$, $p < 0.001$, $n = 92$; **Figure 4A**, left), while 7 dpf larvae spent similar amounts of time swimming in deep and shallow wells ($t = 1.1$, $p = 0.27$, $n = 138$; **Figure 4A**, left). In deep wells, 4 dpf larvae spent more time swimming than did 7 dpf larvae ($t = 3.2$, $p = 0.002$, $n = 122$; **Figure 4A**, left), while in shallow wells, 4 and 7 dpf larvae spent similar amounts of time swimming ($t = 0.2$, $p = 0.84$, $n = 108$; **Figure 4A**, left). The CoV was smallest for 7 dpf larvae in deep wells, and larger for all other combinations of stage and depth (**Figure 4A**, right). These results showed that, although 4 dpf larvae in deep wells spent the greatest amount of time swimming, 7 dpf larvae in deep wells produced the most reliable measure (lowest CoV) for active swim time.

Post-hoc analyses also revealed that larvae at 4 dpf traveled greater total distances in deep wells than in shallow wells ($t = 3.9$, $p < 0.001$, $n = 92$; **Figure 4B**, left), while 7 dpf larvae traveled similar total distances in deep and shallow wells ($t = 0.9$, $p = 0.38$, $n = 138$; **Figure 4B**, left). In deep wells, 4 dpf larvae traveled greater total distances than did 7 dpf larvae ($t = 4.3$, $p < 0.001$, $n = 122$; **Figure 4B**, left), while in shallow wells, 4 and 7 dpf larvae traveled similar total distances ($t = 0.5$, $p < 0.001$, $n = 108$; **Figure 4B**, left). The CoV was smallest for 7 dpf larvae in deep wells, and larger for all other combinations of stage and depth (**Figure 4B**, right). These results showed that 4 dpf larvae in deep wells traveled the greatest total distance and 7 dpf larvae in deep wells produced the least variation in total distance.

INTERPRETATION OF ACTIVITY LEVEL REQUIRES THE ASSESSMENT OF MULTIPLE PROPERTIES OF LOCOMOTOR ACTIVITY

Previous studies that examined the effects of acute ethanol treatment on locomotor activity in zebrafish larvae report increased (hyper-) activity due to ethanol as assessed by comparing swim speeds or total distance traveled between control and ethanol treated larvae (Lockwood et al., 2004; MacPhail et al., 2009; Irons et al., 2010; Chen et al., 2011). This result was comparable to the effects on locomotor activity observed in mammals in response to acute ethanol exposure (Frye and Breese, 1981; Masur and dos Santos, 1988; Dudek et al., 1991; Phillips et al., 1991, 1992; Shen et al., 1995; Palmer et al., 2002; Addicott et al., 2007). To better understand how ethanol treatment affects locomotor activity in larval zebrafish, we examined all measured properties of locomotor activity (see Materials and Methods). We used larvae at 7 dpf in deep wells because this combination of factors produced the most reliable measures of the locomotor properties (**Figures 1**, **2**, **4**). Further, all well diameters were included because locomotor activity was not affected by diameter (**Figure 3**). A larger proportion of control larvae than ethanol treated larvae were motile (99 and 79%, respectively; Fisher's *z*-coefficient = 2.95, $p < 0.01$; **Figure 5A**). Significantly lower episode frequency (**Figure 5B**) and greater episode duration and faster swim speed were produced by ethanol treated larvae than by

Table 3 | Comparison of the properties of locomotor activity for larvae in behavioral wells of different diameters.

Diameter	Episode frequency (Hz)	Episode duration (ms)	Swim speed (mm/s)	Active swim time (s)	Total distance (cm)
Small	0.45 ± 0.33	137.6 ± 47.5	7.5 ± 2.7	36.4 ± 31	28.5 ± 28
Medium	0.40 ± 0.36	153.2 ± 104.4	7.3 ± 5.5	34.4 ± 39.2	26.5 ± 39
Large	0.46 ± 0.36	150.9 ± 68.3	6.6 ± 2.2	41.9 ± 43.6	31.1 ± 40.5
F	0.662	2.793	1.868	0.780	0.386
p	0.517	0.063	0.157	0.460	0.680

Data expressed as group means ± SD. F, test statistic for Three-Way ANOVA; p, probability.

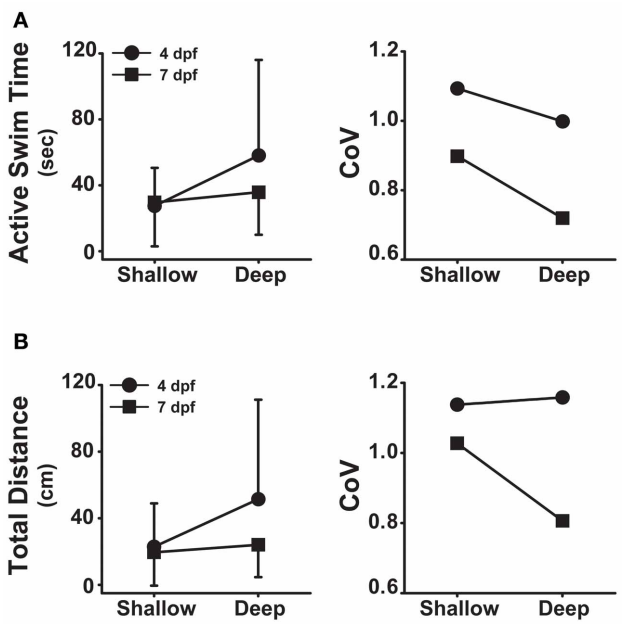

FIGURE 4 | Developmental stage and well depth interact to affect locomotor activity. (A) *Left*, plot of the interaction between stage and depth for active swim time. *Right*, plot of the group coefficients of variation for each interaction condition (4 dpf × Shallow, $n = 41$; 4 dpf × Deep, $n = 51$; 7 dpf × Shallow, $n = 67$; 7 dpf × Deep, $n = 71$). **(B)** *Left*, plot of the interaction between stage and depth for total distance. *Right*, plot of the group coefficients of variation (CoV) for each interaction condition (4 dpf × Shallow, $n = 41$; 4 dpf × Deep, $n = 51$; 7 dpf × Shallow, $n = 67$; 7 dpf × Deep, $n = 71$). Measures of active swim time and total distance are expressed as mean ± SD.

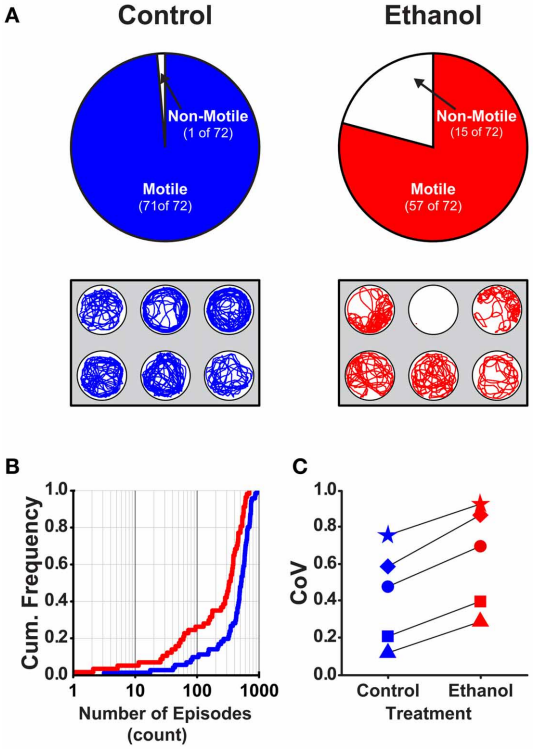

FIGURE 5 | The proportion of motile larvae and the variability among the locomotor properties are different for control and ethanol treated larvae (7 dpf in deep behavioral wells). (A) *Top Row*, Pie charts depicting the proportions of motile and non-motile larvae in Control and Ethanol treated groups (blue and red, respectively). *Bottom Row*, Representative trajectory plots for larvae in 6-well behavioral arena plates (30 mm well diameter shown); single larva per well. **(B)** Cumulative frequency plots for the number of swim episodes produced by Control and Ethanol treated larvae (blue and red, respectively). **(C)** Plots of the group coefficients of variation (CoV) for all measured locomotor properties for Control ($n = 71$) and Ethanol ($n = 57$) treated groups (blue and red, respectively). Symbols are: circle, episode frequency; square, episode duration; triangle, swim speed; diamond, active swim time; star, total distance.

control larvae (**Table 4**). However, active swim time and total distance were not significantly different between groups (**Table 4**). Again, this suggests that the assessment of locomotor activity by any one of these properties alone was not sufficient to fully depict activity level. The CoVs for all properties were smaller for control larvae than for treated larvae (**Figure 5C**). These results indicated that ethanol treated larvae were hypoactive relative to control (non-treated) larvae when activity was assessed based on the episode frequency (**Table 4**). However, these results also indicated that ethanol treated larvae were hyperactive relative to control (non-treated) larvae when activity was assessed based on swim speed or episode duration (**Table 4**). Thus, depending on the locomotor property reported, differing interpretations of the activity level for treated larvae can be made.

DISCUSSION

Previous studies have shown that patterns of locomotor activity change during development (Saint-Amant and Drapeau, 1998,

Table 4 | Comparison of the properties of locomotor activity for larvae in control and ethanol treated groups.

Treatment	Episode frequency (Hz)	Episode duration (ms)	Swim speed (mm/s)	Active swimming (s)	Total distance (cm)
Control	0.80 ± 0.38	115.4 ± 24.8	6.4 ± 1.3	57.2 ± 34.0	39.1 ± 29.9
Ethanol	0.50 ± 0.33	175.5 ± 69.6	7.6 ± 2.2	59.5 ± 51.7	47.8 ± 44.3
F	22.131	36.804	10.903	0.147	2.144
p	<0.001	<0.001	0.002	0.703	0.149

Data expressed as group means ± SD. F, test statistic for Three-Way ANOVA; p, probability.

2000; Budick and O'Malley, 2000; Drapeau et al., 2002; Colwill and Creton, 2011; Lambert et al., 2012; Tong and McDearmid, 2012). Here, we report that most 7 dpf larvae were motile, whereas significantly fewer larvae were motile at 4 dpf (**Figure 1A**). Further, all of the measured locomotor properties were significantly different between larvae at 4 and 7 dpf (**Table 1**), and were less variable for 7 dpf than for 4 dpf larvae (**Figure 1C**), which was consistent with a previous report (Farrell et al., 2011). We propose that the use of larvae at later developmental stages (e.g., 7 dpf) to assess locomotor activity will generate more reliable data as larvae at this stage produced more consistent locomotor activity.

Our data also showed that locomotor activity was sensitive to differences in well depth; most larvae were motile in deep wells, whereas significantly fewer larvae were motile in shallow wells (**Figure 2A**). In addition, significant differences were found for many of the measured locomotor properties produced between larvae in shallow and deep wells (**Table 2**). Finally, most of the measured locomotor properties were less variable for larvae in deep wells than in shallow wells (**Figure 2C**). Thus, we suggest the use of deep wells to assess locomotor activity because larvae in deep wells produced more reliable and consistent locomotor activity (e.g., 5.5 mm well depth reported here).

Locomotor activity was not sensitive, however, to differences in well diameter; ∼80% of all larvae were motile in wells of all diameters examined (**Figure 3A**), and there were no significant differences for any the measured locomotor properties produced between larvae in wells of different diameters (**Table 3**). Most of the locomotor properties were less variable for larvae in small diameter wells than for larvae in either medium or large wells (**Figure 3C**). It was surprising to us that well diameter did not have a significant effect on locomotor activity. However, this result does provide a benefit for experimental design; specifically, for a given field of view set by the camera and lens combination, one can maximize the high-throughput capacity simply by decreasing the diameter of the wells and, therefore, increasing the number of wells per behavioral plate. There is a limit, however, to the reduction of the well diameter. When the length-to-diameter ratio of the embryonic/larval zebrafish to the behavioral well is near one, then the speed and duration of locomotor activity will be affected (Farrell et al., 2011; Padilla et al., 2011), and if the fish are reared in small diameter wells, there is potential for structural and morphological defects to arise, such as tail links (Selderslaghs et al., 2009; Padilla et al., 2011) that will also adversely affect the properties of locomotor activity.

CONSIDERATIONS FOR THE QUANTITATIVE ASSESSMENT OF LOCOMOTOR ACTIVITY

Prior to this study it was shown that larval developmental stage affected locomotor activity, however, the effects of the dimensions of the behavioral arena were less well understood. We hypothesized that locomotor activity would be strongly influenced by several interacting factors, including developmental stage and the dimensions (depth and diameter) of the behavioral arena. Here, we showed that stage and depth not only affected locomotor activity (**Figures 1**, **2**, respectively), but stage and depth also interacted to affect active swim time and total distance (**Figure 4**). In addition, 7 dpf larvae in deep wells produced the most consistent (lowest CoV) measures of active swim time and total distance (**Figure 4**). Together, these results suggest the use of older larvae in deep wells to assess locomotor activity.

For most current experimental paradigms, a single quantitative measure, such as swim speed or total distance, is used to assess locomotor activity in larval zebrafish (Vogl et al., 1999; Lockwood et al., 2004; Giacomini et al., 2006; MacPhail et al., 2009; Sallinen et al., 2009a; Selderslaghs et al., 2009; Padilla et al., 2011; Cowden et al., 2012; Irons et al., 2013). Although more recent studies have included measures of multiple parameters of locomotor activity (Anichtchik et al., 2004; Prober et al., 2006; Burgess and Granato, 2007; Sallinen et al., 2009b; Chou et al., 2010; Chen et al., 2011; Colwill and Creton, 2011; Sundvik et al., 2011), the critical step of integrating these parameters necessary to more fully assess and depict locomotor activity is missing. Our data showed that the reliance on a single measure of locomotor activity was not sufficient to assess global activity levels, but that a more thorough examination of multiple properties of locomotor activity may be necessary (**Tables 1–3**). For example, our results indicate that 7 dpf larvae are hyperactive relative to 4 dpf larvae when activity is assessed based on the episode frequency (**Table 1**). However, our results also indicate that 7 dpf larvae are hypoactive relative to 4 dpf larvae when activity is assessed based on the total distance (**Table 1**). Even comparing within developmental stage, our results indicate that ethanol treated larvae are hypoactive relative to control (non-treated) larvae when activity is assessed based on the episode frequency (**Table 4**). However, our results also indicate that ethanol treated larvae are hyperactive relative to control (non-treated) larvae when activity is assessed based on swim speed or episode duration (**Table 4**). Although these measures are relevant attributes of locomotor activity, we find that no single measure fully depicts the activity level and thus different interpretations of locomotor activity can be made. It is also important to recognize that, although the larvae used for

this study were reared in a group setting, the data reported here are based exclusively on larvae isolated in individual wells. Thus, group interactions are not present in this experimental paradigm and, therefore, these results cannot be extended to paradigms that examine larval zebrafish locomotor activity in various group settings.

We conclude that high-throughput experiments that measure and assess locomotor activity in larval zebrafish benefit from the reduced variability observed when older larvae (7 dpf) in deep (5.5 mm) wells are used. In addition, since we have shown that a single measure of locomotor activity (e.g., swim speed or total distance traveled) is not sufficient to fully describe activity level, we suggest that a more detailed assessment of the effects on activity level requires the evaluation and integration of multiple properties of locomotor activity.

ACKNOWLEDGMENTS

We thank Dr. Henning Schneider, Dr. Jack Peck, Dr. Jacob Montgomery, Dr. Matthew Beckman, Aaron Lambert, and Timothy Wiggin for their helpful discussions and critical comments on the manuscript. This work was supported by National Institutes of Health Grant R01-NS065054 (Mark A. Masino).

REFERENCES

Addicott, M. A., Marsh-Richard, D. M., Mathias, C. W., and Dougherty, D. M. (2007). The biphasic effects of alcohol: comparisons of subjective and objective measures of stimulation, sedation, and physical activity. *Alcohol. Clin. Exp. Res.* 31, 1883–1890. doi: 10.1111/j.1530-0277.2007.00518.x

Ali, S., Champagne, D. L., Alia, A., and Richardson, M. K. (2011). Large-scale analysis of acute ethanol exposure in zebrafish development: a critical time window and resilience. *PLoS ONE* 6:e20037. doi: 10.1371/journal.pone.0020037

Anichtchik, O. V., Kaslin, J., Peitsaro, N., Scheinin, M., and Panula, P. (2004). Neurochemical and behavioural changes in zebrafish *Danio rerio* after systemic administration of 6-hydroxydopamine and 1-methyl-4-phenyl-1, 2, 3, 6-tetrahydropyridine. *J. Neurochem.* 88, 443–453. doi: 10.1111/j.1471-4159.2004.02190.x

Branson, K., Robie, A. A., Bender, J., Perona, P., and Dickinson, M. H. (2009). High-throughput ethomics in large groups of Drosophila. *Nat. Chem. Biol.* 6, 451–457. doi: 10.1038/nmeth.1328

Budick, S. A., and O'Malley, D. M. (2000). Locomotor repertoire of the larval zebrafish: swimming, turning and prey capture. *J. Exp. Biol.* 203, 2565–2579.

Burgess, H. A., and Granato, M. (2007). Modulation of locomotor activity in larval zebrafish during light adaptation. *J. Exp. Biol.* 210, 2526–2539. doi: 10.1242/jeb.003939

Buss, R. R., and Drapeau, P. (2001). Synaptic drive to motoneurons during fictive swimming in the developing zebrafish. *J. Neurophysiol.* 86, 197–210.

Cahill, G. M. (2007). Automated video image analysis of larval zebrafish locomotor rhythms. *Methods Mol. Biol.* 362, 83–94. doi: 10.1007/978-1-59745-257-1_5

Cario, C. L., Farrell, T. C., Milanese, C., and Burton, E. A. (2011). Automated measurement of zebrafish larval movement. *J. Physiol. (Lond.)* 589, 3703–3708. doi: 10.1113/jphysiol.2011.207308

Chen, T.-H., Wang, Y.-H., and Wu, Y.-H. (2011). Developmental exposures to ethanol or dimethylsulfoxide at low concentrations alter locomotor activity in larval zebrafish: implications for behavioral toxicity bioassays. *Aquat. Toxicol.* 102, 162–166. doi: 10.1016/j.aquatox.2011.01.010

Chou, C.-T., Hsiao, Y.-C., Ko, F.-C., Cheng, J.-O., Cheng, Y.-M., and Chen, T.-H. (2010). Chronic exposure of 2, 2′, 4, 4′-tetrabromodiphenyl ether (PBDE-47) alters locomotion behavior in juvenile zebrafish (*Danio rerio*). *Aquat. Toxicol.* 98, 388–395. doi: 10.1016/j.aquatox.2010.03.012

Colwill, R. M., and Creton, R. (2011). Locomotor behaviors in zebrafish (*Danio rerio*) larvae. *Behav. Processes* 86, 222–229. doi: 10.1016/j.beproc.2010.12.003

Cowden, J., Padnos, B., Hunter, D., MacPhail, R., Jensen, K., and Padilla, S. (2012). Developmental exposure to valproate and ethanol alters locomotor activity and retino-tectal projection area in zebrafish embryos. *Reprod. Toxicol.* 33, 165–173. doi: 10.1016/j.reprotox.2011.11.111

Creton, R. (2009). Automated analysis of behavior in zebrafish larvae. *Behav. Brain Res.* 203, 127–136. doi: 10.1016/j.bbr.2009.04.030

Drapeau, P., Saint-Amant, L., Buss, R. R., Chong, M., McDearmid, J. R., and Brustein, E. (2002). Development of the locomotor network in zebrafish. *Prog. Neurobiol.* 68, 85–111. doi: 10.1016/S0301-0082(02)00075-8

Dudek, B. C., Phillips, T. J., and Hahn, M. E. (1991). Genetic analyses of the biphasic nature of the alcohol dose-response curve. *Alcohol. Clin. Exp. Res.* 15, 262–269. doi: 10.1111/j.1530-0277.1991.tb01867.x

Eklöf-Ljunggren, E., Haupt, S., Ausborn, J., Dehnisch, I., Uhlén, P., Higashijima, S.-I., et al. (2012). Origin of excitation underlying locomotion in the spinal circuit of zebrafish. *Proc. Natl. Acad. Sci.* 109, 5511–5516. doi: 10.1073/pnas.1115377109

Farrell, T. C., Cario, C. L., Milanese, C., Vogt, A., Jeong, J.-H., and Burton, E. A. (2011). Evaluation of spontaneous propulsive movement as a screening tool to detect rescue of Parkinsonism phenotypes in zebrafish models. *Neurobiol. Dis.* 44, 9–18. doi: 10.1016/j.nbd.2011.05.016

Frye, G. D., and Breese, G. R. (1981). An evaluation of the locomotor stimulating action of ethanol in rats and mice. *Psychopharmacology* 75, 372–379. doi: 10.1007/BF00435856

Gerlai, R., Chatterjee, D., Pereira, T., Sawashima, T., and Krishnannair, R. (2009). Acute and chronic alcohol dose: population differences in behavior and neurochemistry of zebrafish. *Genes Brain Behav.* 8, 586–599. doi: 10.1111/j.1601-183X.2009.00488.x

Giacomini, N. J., Rose, B., Kobayashi, K., and Guo, S. (2006). Antipsychotics produce locomotor impairment in larval zebrafish. *Neurotoxicol. Teratol.* 28, 245–250. doi: 10.1016/j.ntt.2006.01.013

Higashijima, S.-I., Masino, M. A., Mandel, G., and Fetcho, J. R. (2004). Engrailed-1 expression marks a primitive class of inhibitory spinal interneuron. *J. Neurosci.* 24, 5827–5839. doi: 10.1523/JNEUROSCI.5342-03.2004

Irons, T. D., Kelly, P. E., Hunter, D. L., MacPhail, R. C., and Padilla, S. (2013). Acute administration of dopaminergic drugs has differential effects on locomotion in larval zebrafish. *Pharmacol. Biochem. Behav.* 103, 792–813. doi: 10.1016/j.pbb.2012.12.010

Irons, T. D., MacPhail, R. C., Hunter, D. L., and Padilla, S. (2010). Acute neuroactive drug exposures alter locomotor activity in larval zebrafish. *Neurotoxicol. Teratol.* 32, 84–90. doi: 10.1016/j.ntt.2009.04.066

Kimura, Y., Okamura, Y., and Higashijima, S.-I. (2006). alx, a zebrafish homolog of Chx10, marks ipsilateral descending excitatory interneurons that participate in the regulation of spinal locomotor circuits. *J. Neurosci.* 26, 5684–5697. doi: 10.1523/JNEUROSCI.4993-05.2006

Kokel, D., Bryan, J., Laggner, C., White, R., Cheung, C. Y. J., Mateus, R., et al. (2010). Rapid behavior-based identification of neuroactive small molecules in the zebrafish. *Nat. Chem. Biol.* 6, 231–237. doi: 10.1038/nchembio.307

Lambert, A. M., Bonkowsky, J. L., and Masino, M. A. (2012). The conserved dopaminergic diencephalospinal tract mediates vertebrate locomotor development in zebrafish larvae. *J. Neurosci.* 32, 13488–13500. doi: 10.1523/JNEUROSCI.1638-12.2012

Lessman, C. A. (2002). Use of computer-aided screening for detection of motility mutants in zebrafish embryos. *Real-Time Imaging* 8, 189–201. doi: 10.1006/rtim.2001.0282

Lockwood, B., Bjerke, S., Kobayashi, K., and Guo, S. (2004). Acute effects of alcohol on larval zebrafish: a genetic system for large-scale screening. *Pharmacol. Biochem. Behav.* 77, 647–654. doi: 10.1016/j.pbb.2004.01.003

MacPhail, R. C., Brooks, J., Hunter, D. L., Padnos, B., Irons, T. D., and Padilla, S. (2009). Locomotion in larval zebrafish: Influence of time of day, lighting and ethanol. *Neurotoxicology* 30, 52–58. doi: 10.1016/j.neuro.2008.09.011

Masur, J., and dos Santos, H. M. (1988). Response variability of ethanol-induced locomotor activation in mice. *Psychopharmacology* 96, 547–550. doi: 10.1007/BF02180038

Müller, U. K., and van Leeuwen, J. L. (2004). Swimming of larval zebrafish: ontogeny of body waves and implications for locomotory development. *J. Exp. Biol.* 207, 853–868. doi: 10.1242/jeb.00821

Padilla, S., Hunter, D. L., Padnos, B., Frady, S., and MacPhail, R. C. (2011). Assessing locomotor activity in larval zebrafish: Influence of extrinsic and intrinsic variables. *Neurotoxicol. Teratol.* 33, 624–630. doi: 10.1016/j.ntt.2011.08.005

Palmer, A. A., McKinnon, C. S., Bergstrom, H. C., and Phillips, T. J. (2002). Locomotor activity responses to ethanol, other alcohols and GABA-A acting compounds in forward-and reverse-selected FAST and SLOW mouse lines. *Behav. Neurosci.* 116, 958.

Panula, P., Chen, Y. C., Priyadarshini, M., Kudo, H., Semenova, S., Sundvik, M., et al. (2010). The comparative neuroanatomy and neurochemistry of zebrafish CNS systems of relevance to human neuropsychiatric diseases. *Neurobiol. Dis.* 40, 46–57. doi: 10.1016/j.nbd.2010.05.010

Parng, C., Roy, N. M., Ton, C., Lin, Y., and McGrath, P. (2007). Neurotoxicity assessment using zebrafish. *J. Pharmacol. Toxicol. Methods* 55, 103–112. doi: 10.1016/j.vascn.2006.04.004

Pelkowski, S. D., Kapoor, M., Richendrfer, H. A., Wang, X., Colwill, R. M., and Creton, R. (2011). A novel high-throughput imaging system for automated analyses of avoidance behavior in zebrafish larvae. *Behav. Brain Res.* 223, 135–144. doi: 10.1016/j.bbr.2011.04.033

Peterson, R. T., and Fishman, M. C. (2011). Designing zebrafish chemical screens. *Methods Cell Biol.* 105, 525–541. doi: 10.1016/B978-0-12-381320-6.00023-0

Phillips, T. J., Burkhart-Kasch, S., Gwiazdon, C. C., and Crabbe, J. C. (1992). Acute sensitivity of FAST and SLOW mice to the effects of abused drugs on locomotor activity. *J. Pharmacol. Exp. Ther.* 261, 525–533.

Phillips, T. J., Burkhart-Kasch, S., Terdal, E. S., and Crabbe, J. C. (1991). Response to selection for ethanol-induced locomotor activation: genetic analyses and selection response characterization. *Psychopharmacology* 103, 557–566. doi: 10.1007/BF02244259

Postlethwait, J. H., Woods, I. G., Ngo-Hazelett, P., Yan, Y. L., Kelly, P. D., Chu, F., et al. (2000). Zebrafish comparative genomics and the origins of vertebrate chromosomes. *Genome Res.* 10, 1890–1902. doi: 10.1101/gr.164800

Prober, D. A., Rihel, J., Onah, A. A., Sung, R.-J., and Schier, A. F. (2006). Hypocretin/orexin overexpression induces an insomnia-like phenotype in zebrafish. *J. Neurosci.* 26, 13400–13410. doi: 10.1523/JNEUROSCI.4332-06.2006

Rihel, J., Prober, D. A., Arvanites, A., Lam, K., Zimmerman, S., Jang, S., et al. (2010). Zebrafish behavioral profiling links drugs to biological targets and rest/wake regulation. *Science* 327, 348–351. doi: 10.1126/science.1183090

Saint-Amant, L., and Drapeau, P. (1998). Time course of the development of motor behaviors in the zebrafish embryo. *J. Neurobiol.* 37, 622–632. doi: 10.1002/(SICI)1097-4695(199812)37:4<622::AID-NEU10>3.0.CO;2-S

Saint-Amant, L., and Drapeau, P. (2000). Motoneuron activity patterns related to the earliest behavior of the zebrafish embryo. *J. Neurosci.* 20, 3964–3972.

Sallinen, V., Torkko, V., Sundvik, M., Reenilä, I., Khrustalyov, D., Kaslin, J., et al. (2009a). MPTP and MPP+ target specific aminergic cell populations in larval zebrafish. *J. Neurochem.* 108, 719–731. doi: 10.1111/j.1471-4159.2008.05793.x

Sallinen, V., Sundvik, M., Reenilä, I., Peitsaro, N., Khrustalyov, D., Anichtchik, O., et al. (2009b). Hyperserotonergic phenotype after monoamine oxidase inhibition in larval zebrafish. *J. Neurochem.* 109, 403–415. doi: 10.1111/j.1471-4159.2009.05986.x

Selderslaghs, I. W. T., Van Rompay, A. R., De Coen, W., and Witters, H. E. (2009). Development of a screening assay to identify teratogenic and embryotoxic chemicals using the zebrafish embryo. *Reprod. Toxicol.* 28, 308–320. doi: 10.1016/j.reprotox.2009.05.004

Shen, E. H., Harland, R. D., Crabbe, J. C., and Phillips, T. J. (1995). Bidirectional selective breeding for ethanol effects on locomotor activity: characterization of FAST and SLOW mice through selection generation 35. *Alcohol. Clin. Exp. Res.* 19, 1234–1245. doi: 10.1111/j.1530-0277.1995.tb01606.x

Straw, A. D., and Dickinson, M. H. (2009). Motmot, an open-source toolkit for realtime video acquisition and analysis. *Source Code Biol. Med.* 4, 5. doi: 10.1186/1751-0473-4-5

Sundvik, M., Kudo, H., Toivonen, P., Rozov, S., Chen, Y.-C., and Panula, P. (2011). The histaminergic system regulates wakefulness and orexin/hypocretin neuron development via histamine receptor H1 in zebrafish. *FASEB J.* 25, 4338–4347. doi: 10.1096/fj.11-188268

Sylvain, N. J., Brewster, D. L., and Ali, D. W. (2010). Zebrafish embryos exposed to alcohol undergo abnormal development of motor neurons and muscle fibers. *Neurotoxicol. Teratol.* 32, 472–480. doi: 10.1016/j.ntt.2010.03.001

Tan, J. L., and Zon, L. I. (2011). Chemical screening in zebrafish for novel biological and therapeutic discovery. *Methods Cell Biol.* 105, 493–516. doi: 10.1016/B978-0-12-381320-6.00021-7

Tong, H., and McDearmid, J. R. (2012). Pacemaker and plateau potentials shape output of a developing locomotor network. *Curr. Biol.* 22, 2285–2293. doi: 10.1016/j.cub.2012.10.025

Vogl, C., Grillitsch, B., Wytek, R., Spieser, O. H., and Scholz, W. (1999). Qualification of spontaneous undirected locomotor behavior of fish for sublethal toxicity testing. Part, I. Variability of measurement parameters under general test conditions. *Environ. Toxicol. Chem.* 18, 2736–2742.

Winter, M. J., Redfern, W. S., Hayfield, A. J., Owen, S. F., Valentin, J.-P., and Hutchinson, T. H. (2008). Validation of a larval zebrafish locomotor assay for assessing the seizure liability of early-stage development drugs. *J. Pharmacol. Toxicol. Methods* 57, 176–187. doi: 10.1016/j.vascn.2008.01.004

Zon, L. I., and Peterson, R. T. (2005). *In vivo* drug discovery in the zebrafish. *Nat. Rev. Drug Discov.* 4, 35–44. doi: 10.1038/nrd1606

Conflict of Interest Statement: The authors declare that the research was conducted in the absence of any commercial or financial relationships that could be construed as a potential conflict of interest.

Received: 21 February 2013; accepted: 22 May 2013; published online: 10 June 2013.

Citation: Ingebretson JJ and Masino MA (2013) Quantification of locomotor activity in larval zebrafish: considerations for the design of high-throughput behavioral studies. Front. Neural Circuits 7:109. doi: 10.3389/fncir.2013.00109

frontiers in
NEURAL CIRCUITS

METHODS ARTICLE
published: 12 June 2013
doi: 10.3389/fncir.2013.00107

ZebraZoom: an automated program for high-throughput behavioral analysis and categorization

Olivier Mirat*[1,2], *Jenna R. Sternberg*[1,3], *Kristen E. Severi*[1] and *Claire Wyart*[1]

[1] Centre de Recherche de l'Institut du Cerveau et de la Moelle Épinière, UPMC, Inserm UMR S975, CNRS UMR 7225, Fondation ICM, Campus Hospitalier Pitié Salpétrière, Paris, France
[2] Université Paris Descartes, Paris, France
[3] Université Pierre et Marie Curie, Paris, France

Edited by:
Gonzalo G. De Polavieja, Instituto Cajal. CSIC, Spain

Reviewed by:
Kristin Branson, HHMI Janelia Farm Research Campus, USA
Alfonso Perez-Escudero, Consejo Superior de Investigaciones Cientificas, Spain

***Correspondence:**
Claire Wyart, Centre de Recherche de l'Institut du Cerveau et de la Moelle Épinière, Inserm U975, CNRS UPMC UMR 975, Fondation ICM, Campus Hospitalier Universitaire, Pitié-Salpétrière, 83, Bld de l hôpital, 75013 Paris, France
e-mail: claire.wyart@icm-institute.org

The zebrafish larva stands out as an emergent model organism for translational studies involving gene or drug screening thanks to its size, genetics, and permeability. At the larval stage, locomotion occurs in short episodes punctuated by periods of rest. Although phenotyping behavior is a key component of large-scale screens, it has not yet been automated in this model system. We developed ZebraZoom, a program to automatically track larvae and identify maneuvers for many animals performing discrete movements. Our program detects each episodic movement and extracts large-scale statistics on motor patterns to produce a quantification of the locomotor repertoire. We used ZebraZoom to identify motor defects induced by a glycinergic receptor antagonist. The analysis of the blind mutant *atoh7* revealed small locomotor defects associated with the mutation. Using multiclass supervised machine learning, ZebraZoom categorized all episodes of movement for each larva into one of three possible maneuvers: slow forward swim, routine turn, and escape. ZebraZoom reached 91% accuracy for categorization of stereotypical maneuvers that four independent experimenters unanimously identified. For all maneuvers in the data set, ZebraZoom agreed with four experimenters in 73.2–82.5% of cases. We modeled the series of maneuvers performed by larvae as Markov chains and observed that larvae often repeated the same maneuvers within a group. When analyzing subsequent maneuvers performed by different larvae, we found that larva–larva interactions occurred as series of escapes. Overall, ZebraZoom reached the level of precision found in manual analysis but accomplished tasks in a high-throughput format necessary for large screens.

Keywords: machine learning, tracking, analysis of kinematics, collective behavior, support vector machine classifier, multiclass categorization, locomotion in intact behaving animals

A central question in systems neuroscience is how neural circuit assembly and function relate to animal behavior. Genetic screens in invertebrate models, such as *Drosophila melanogaster* and *Caenorhabditis elegans* have begun to unravel the genetic basis of circuit function and behavior (Chalfie et al., 1985; Moore et al., 1998; Scholz et al., 2000). Automated methods have recently been developed in these species to track the position of individuals alone or in a group (Branson et al., 2009; Swierczek et al., 2011) and to categorize behavior (Dankert et al., 2009; Kabra et al., 2013). The zebrafish has emerged as an important vertebrate model organism for developmental biology, neurobiology, and human disease models, and is now used as a genetic model organism for the study of the mechanisms modulating complex behaviors in vertebrates such as depression and anxiety (Blaser et al., 2010; Lee et al., 2010; Cachat et al., 2011; Vermoesen et al., 2011; Zakhary et al., 2011; Ziv et al., 2013), sleep (Zhdanova et al., 2001; Appelbaum et al., 2009), or addiction (Petzold et al., 2009; Khor et al., 2011). The permeability, small size, genetic tractability, transparency, and low cost of zebrafish make them highly suitable for large-scale genetic and chemical screens (Driever et al., 1996; Granato et al., 1996; Haffter and Nusslein-Volhard, 1996).

Although simple for a vertebrate, the locomotor patterns of the zebrafish larva bring technical challenges to automated analysis. Larvae spontaneously swim in discrete bouts in a manner often described as "beat and glide," which can be classified as individual maneuvers, including slow forward swim, routine turn, or escape. These short movements are characterized by a large range of tail-beat frequencies (15–100 Hz), which require high-speed imaging to capture accurately and can be separated by long resting periods of up to a few seconds. Manual tracking via frame-by-frame analysis has formed the basis of contemporary knowledge and has enabled initial characterization of the larval zebrafish locomotor repertoire (Budick and O'Malley, 2000; Borla et al., 2002; McElligott and O'Malley, 2005). However, manual techniques are both laborious and limited in scope for high-throughput screens (Driever et al., 1996; Granato et al., 1996; Haffter and Nusslein-Volhard, 1996). The currently available automated tools have limitations in either refinement or time-scale. Recent chemical or genetic screens have relied on commercial software that estimates

an index of mobility of the larvae, usually measured as the distance traveled during a recording session or the amount of time spent moving (Rihel et al., 2010; Elbaz et al., 2012; Rihel and Schier, 2012). These approaches for high-throughput screens provide information about average velocity and distance traveled by tracking the animals' center-of-mass over minutes to hours. Previous studies have either focused on analyzing movement duration and speed at low frequency over long periods of time or on fine analysis of kinematics at high frequency but for very short acquisition (typically 1000 ms, Burgess and Granato, 2007; Liu et al., 2012). Accurate categorization of maneuvers for each individual in a group requires novel methods to record behavior with high temporal resolution and over long durations, automatically tracking and categorizing thousands of maneuvers.

Here we developed a new program, ZebraZoom, to track the full body position over a multiple-minute timescale of 56 larvae simultaneously recorded at high frequency and to finely characterize each maneuver. To identify core and tail positions for large datasets, videos were obtained on multiple larvae simultaneously over long periods of time and at high resolution using a high-speed camera run in a streaming-to-disk interface (Methods). Typically 500–1000 movements from seven larvae were recorded per dish in four minutes and eight dishes were monitored in parallel. To simplify tracking, we placed larvae in conditions that reduced overlapping in the z-plane during swimming (Methods; overlaps occurred on average once every 145 s per larva). We developed an offline 2D tracking method for identifying and separating each animal even when in close contact (Methods, **Figure 1**). For each larva several features were identified, a core position that included the head and swim bladder (**Figure 1A**) and ten points along the tail (Methods and **Figure 1B**; **Video S1**). As movements occurred as discrete episodes, ZebraZoom detected movements based on the tail-bending angle over time (Methods and **Figures 1C–D**). To validate the accuracy of movement detection, one trained experimenter manually identified all movements occurring in a subset of videos. In three videos representing a total of 189 events, movements occurred with a false negative rate of 2.7% and a false positive rate of 3.7%.

To quantify movements in a consistent manner, we used the location of the head, the position of the tail, the heading direction and the tail-bending angle to estimate global parameters of locomotion (**Figure 2A**, Methods). We observed that movements for 5–7 dpf wild-type (WT) larvae occurred every 2.22 s on average per larva (at 0.4495 ± 0.0117 Hz). For all movements identified, larvae performed on average 3.19 ± 0.01 oscillations per movement, had a 24.29 ± 0.03 Hz tail-beat frequency (TBF), lasting 189.5 ± 0.0004 ms with a 51.14 ± 0.18° heading direction range, 2.49 ± 0.008 mm traveled distance and 13.35 ± 0.04 mm/s speed per maneuver. We illustrated the use of ZebraZoom for quantifying the effects of a known glycinergic receptor antagonist, and for analyzing a blind genetic mutant. Glycine is responsible for reciprocal inhibition in the spinal cord that permits left-right alternation to sustain oscillations (Dale, 1985; Grillner et al., 1995; Granato et al., 1996; Drapeau et al., 2002; Li et al., 2004). In zebrafish, mutants for glycinergic receptors or transporters have been associated with defects in motor pattern generation

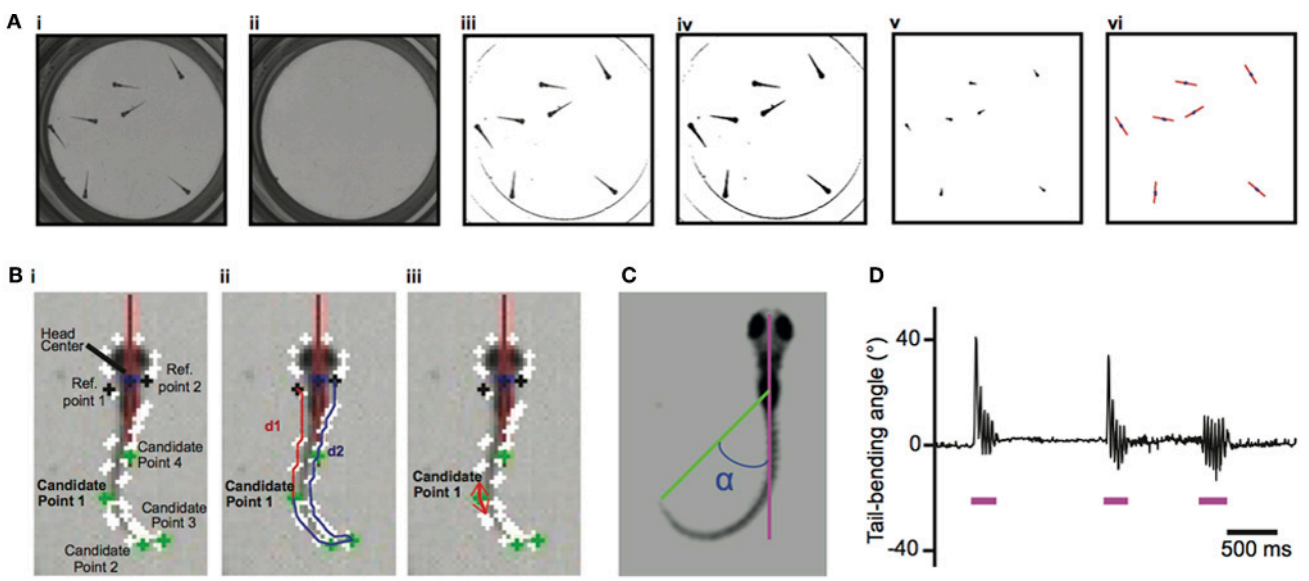

FIGURE 1 | Image processing for tracking of larvae's core positions and larvae's tail and detection of movements based on the tail-bending angle. (A) Tracking of the larvae's core positions. **(Ai)** Initial image. **(Aii)** Background image. **(Aiii)** Image with background subtracted. **(Aiv)** Binary image. **(Av)** Eroded image. **(Avi)** For each larva, identification of the core (blue dot) and heading direction (red axis). **(B)**. Identifying the tip of the tail. **(Bi)** The head center is located at the boundary of the head and trunk. Candidate Point 1–4 along the tail are the four points of the contour with the smallest *x*-value, smallest *y*-value, largest *x*-value, and largest *y*-value caudal to reference points 1 and 2. **(Bii)** The two distances d1 and d2 shown for candidate point 1. **(Biii)** The two vectors used to identify the tail tip defined with the minimal scalar product for candidate point 1. **(C)** Definition of the tail-bending angle (α) separating the body axis (pink) and the line connecting the core and the tip of the tail (green). **(D)** Example of the tail-bending angle over time with detection of movements indicated by the pink line.

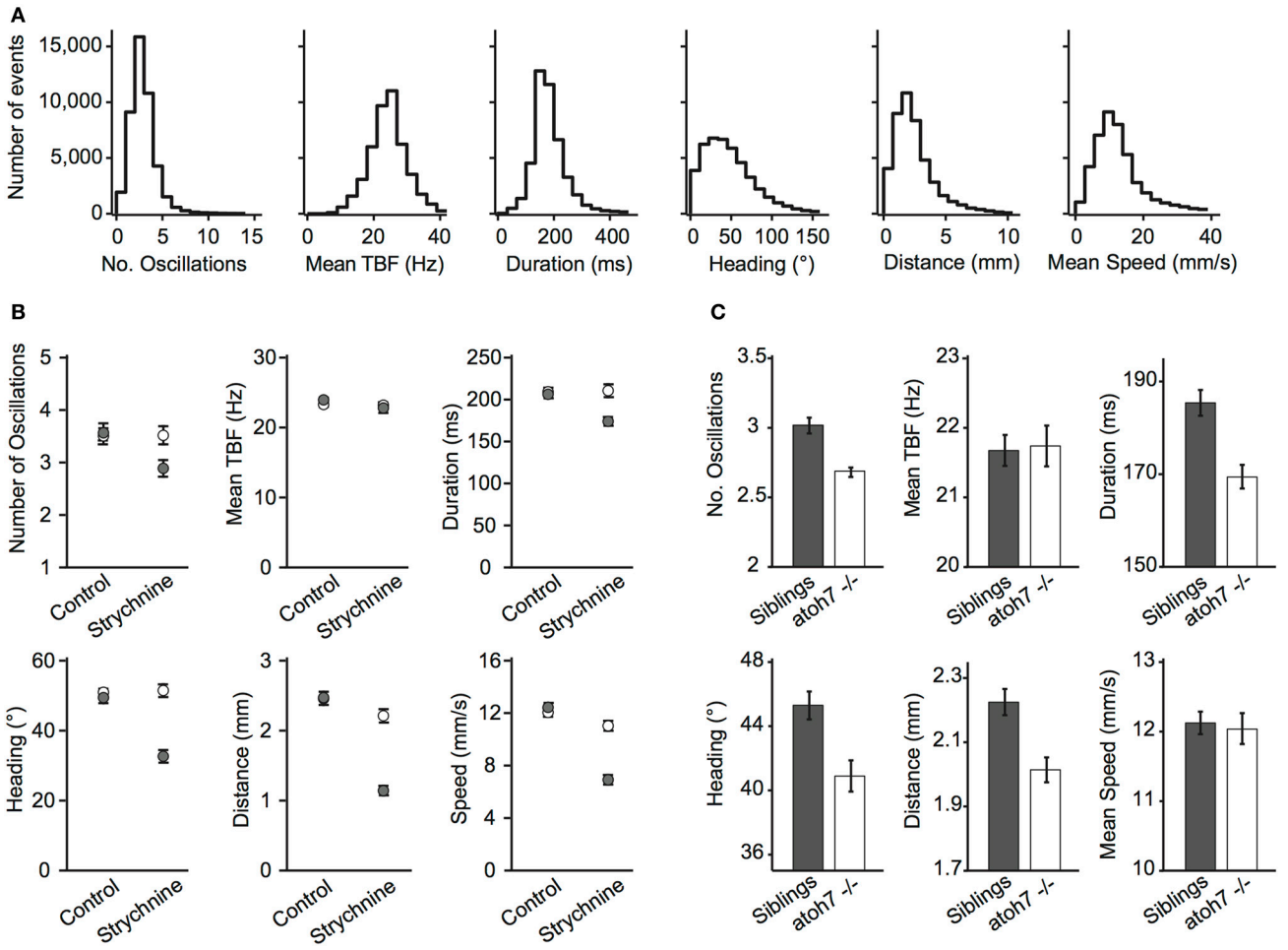

FIGURE 2 | Global parameters describing locomotion in wild-type, mutant, or drug-treated larvae. (A) Distribution of global parameters of movements for 5–7 dpf WT larvae. From left to right: Number of oscillations per movement, TBF in Hz across all movements, duration of each movement in ms, heading direction range in degrees, distance traveled per movement in mm, speed in mm/s during each movement (eight videos, 420 larvae, six clutches, 5–7 dpf, 44,688 movements). All values were calculated per movement. **(B)** Effect of the glycinergic receptor antagonist strychnine on the global parameters of movements. White circles are before application, gray are after application (two videos, 42 larvae for each condition, two clutches, 6–7 dpf, 10,459 movements). **(C)** Effect of the *atoh7* mutation on the global parameters characterizing movements (four videos, 112 mutants *atoh7*$^{-/-}$, and 112 control siblings, four clutches, 6 dpf). For **(B,C)**: error bars are standard errors of the mean and statistics were calculated per larva.

(Granato et al., 1996; Odenthal et al., 1996; Hirata et al., 2005; Masino and Fetcho, 2005). We measured the effect of bath application of 75 μM strychnine on spontaneous locomotor activity in larvae and compared to control siblings that were not exposed to the drug (**Figure 2B**, Methods). For control larvae, we did not observe a significant change in the occurrence of movements over time (0.35 ± 0.05 movements per larva/s before and 0.27 ± 0.03 movements per larva/s after), or on any of the global parameters (**Figure 2B**; all $p > 0.15$). However the locomotor behavior of larvae treated with strychnine was significantly impacted (**Figure 2B**). Overall, movements occurred less frequently (0.30 ± 0.04 Hz before and 0.12 ± 0.02 Hz after, $p < 0.0002$). Although the average TBF during a movement did not change ($p > 0.81$), the number of oscillations decreased (3.52 ± 0.17 before and 2.89 ± 0.16 after; $p < 0.0078$), an effect that was associated with a decrease in movement duration ($p < 0.0001$), distance traveled ($p < 10^{-5}$), and average speed ($p < 10^{-5}$). Strychnine application also resulted in a decrease in the range of heading direction ($p < 10^{-5}$). *atoh7* mutant larva lack retinal ganglion cells, rendering them blind (*atoh7*$^{-/-}$, Kay et al., 2001). Considering the importance of vision for zebrafish larvae, analyzing their locomotor output could reveal corresponding behavioral differences. Overall *atoh7*$^{-/-}$ mutants generated episodic movements less frequently than control siblings (0.33 ± 0.02 Hz vs. 0.51 ± 0.02 Hz, 112 larvae for each condition). Quantitative analysis of global parameters of the blind mutants showed no difference in the average TBF or the average speed per larva (**Figure 2C**; $p > 0.85$ and $p > 0.83$, respectively) but there were small but significant decreases in the number of oscillations, duration, heading direction range, and distance traveled (**Figure 2C**; all $p < 10^{-3}$).

These defects were observed systematically in four clutches. *atoh7*$^{-/-}$ mutants thus display small but substantial differences in basic motor behavior when compared to control siblings.

Zebrafish larvae display a variety of locomotor maneuvers that are often grouped into discrete categories. In these experimental conditions, three types of movement occur in groups of larvae at early stages: slow forward swims (S), routine turns (T, also referred to as slow turns), and escapes (E, including C-turns or burst swims). **Figure 3** shows examples of these movements reported by ZebraZoom. For each maneuver, we superimposed a succession of images (**Figures 3Ai–Ci**), the tail-bending angle over time (**Figures 3Aii–Cii**) and the curvature along the rostro-caudal axis and as a function of time (**Figures 3Aiii–Ciii**). The three types of maneuvers included a series of slow left-right alternation; high values of curvature were confined to the caudal tail (**Figures 3Aiii–Ciii**). While high values of curvature of the tail were confined to the caudal end for slow forward swims (**Figure 3Aiii**), high values of curvature were distributed from head to tail for routine turns and escapes (**Figures 3Biii,Ciii**). Stereotypical routine turns and escapes differed by the frequency of left-right alternation in the tail bend (**Figures 3Biii,Ciii**). As larvae did not always exhibit a canonical slow forward swim, routine turn or escape, some movements were ambiguous. To estimate the percentage of these movements, four experimenters subjectively classified 390 movements distributed over eight videos. Overall about 82% of all movements were classified uniformly by at least three out of four experimenters (Methods) indicating that 18% of movements were difficult to categorize.

Using knowledge of stereotypical locomotor events, we designed a multiclass categorization approach with supervised machine learning to automatically sort each movement into one of the three categories. To implement the multiclass categorization, we used two successive support vector machine (SVM) classifiers: the first classifier sorted S vs. all other maneuvers, and when necessary the second classifier sorted T vs. E. Locomotor events were segregated subjectively in the training set ($n = 201$). This machine learning approach relied on associating dynamic parameters extracted from the tail-bending angle over time with each maneuver type identified in the training set (**Figure 4A** and Methods). To reduce the dimensionality of the data, we

Table 1 | Estimation of ZebraZoom categorizing accuracy based on the different reference experimenters.

	All movements (%)	*S* (%)	*T* (%)	*E* (%)
Experimenter #1	82.5	85	82	79
Experimenter #2	73.2	85	60	53
Experimenter #3	74.3	73	80	58
Experimenter #4	75.4	79	77	47

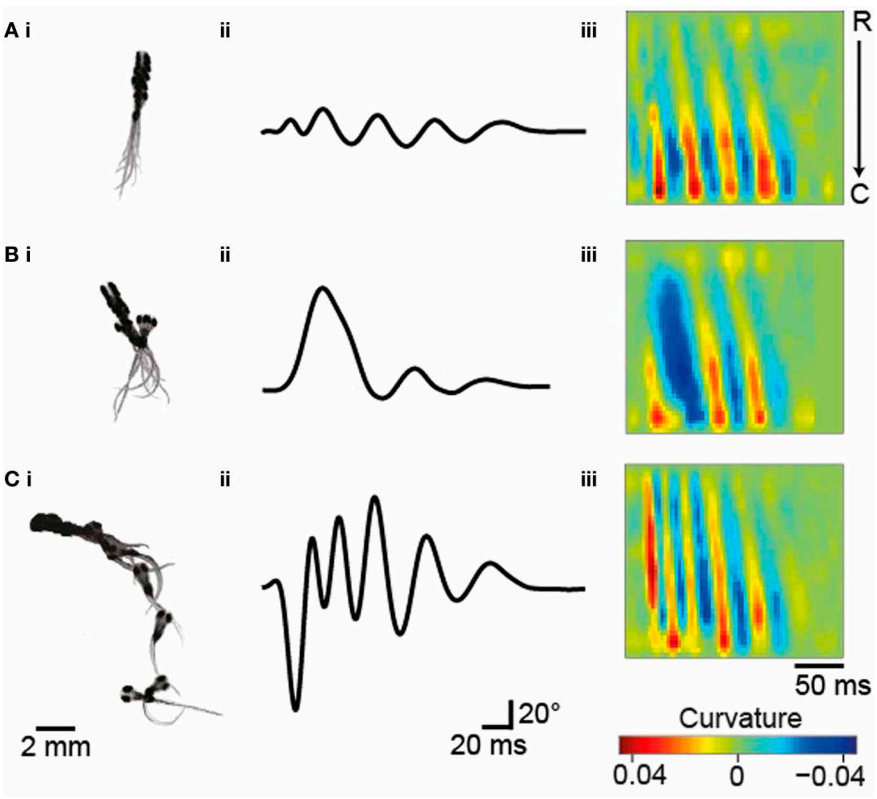

FIGURE 3 | Typical maneuvers occurring in groups of 5–6 dpf larvae. **(A)** Slow forward swim (S). **(B)** Routine turn (T). **(C)** Escape response (E). **(Ai–Ci)** Superimposed images taken every 17 ms. **(Aii–Cii)** The tail-bending angle over time for each maneuver. **(Aiii–Ciii)** Plots of the curvature of the tail as a function of time and position along the rostro-caudal body axis.

performed Principal Component Analysis (PCA). Based on the selection of a trained experimenter on the learning set, we validated the multiclass categorization to sort maneuvers by comparison with the subjective classification performed by a trained experimenter for a recognition set ($n = 189$; **Figures 4B,C**). We observed that ZebraZoom agreed with the trained experimenter 82.5% of the time for the recognition dataset (85% for S, 82% for T, and 79% for E; **Figures 4B,C**; **Table 1** and Methods). When compared to four independent experimenters, ZebraZoom reached 91% accuracy for categorization of stereotypical maneuvers that all experimenters had unanimously identified and 76.4% on average for all maneuvers (73.2–82.5%, **Table 1**). Once validated, we applied the ZebraZoom categorization algorithm on a large dataset of 44,688 movements of WT larvae (**Figure 4D**). We identified 14.911 S (33.36%), 21,432 T (49.96%), and 8,345 E (18.67%). The distribution of global parameters for the three classes of maneuvers were similar in terms of number of oscillations and duration, but they differed in terms of mean TBF, heading direction range, distance traveled and speed (**Figure 4D**).

The investigation of interactions between individuals leading to coordinated motion in animal groups has been a longstanding challenge that is central to elucidating the mechanisms and evolution of collective behavior. Most studies have focused on the analysis of speed or directionality to reflect the interaction between animals (Katz et al., 2011; Gautrais et al., 2012). We availed ourselves of ZebraZoom's features to accurately identify each larva and categorize their maneuvers to study how larvae interacted. In comparison to juvenile and adult zebrafish that swim continuously, larval zebrafish swim episodically with maneuvers that occur in a beat-and-glide manner. Each movement can be regarded as a discrete event, therefore we were motivated to explore how local perturbations of a single individual could impact the group. The program switched identity of larvae once every 109 s (once every 49 movements on average), allowing us to track single larvae. We modeled sequences of maneuvers performed by larvae within a group as Markov chains. Utilizing the classifier, we described larva–larva interactions in a group and intrinsic properties of individuals. We calculated a transition index (I) for each sequence of two maneuvers as the transition probability between first and second maneuvers divided by the probability of random occurrence of the second maneuver (**Figure 5**; **Table 2** and Methods). When the two successive maneuvers were the same, a higher transition index indicated the probability of repetition of this maneuver was greater than chance. The transition index was equal to one when the order of sequential maneuvers was random. Overall I was greater than one for repetition of the same maneuvers (**Table 2**). We sorted the data into interactions between different animals and the repetition within the same animal. We analyzed how the transition index for a given succession of maneuvers depended on the distance between the two larvae's core positions at the onset of the movement and the time between the onset of each movement (**Figure 5** and Methods). Individual larvae often performed the same type of maneuver sequentially (maximal values $I_{S\ max\ (same)} = 1.43$, $I_{T\ max\ (same)} = 1.37$, $I_{E\ (same)} = 2.38$, all $p < 0.002$; **Figure 5A**, **Table 2**, and Methods). Although slow forward swims or routine turns were not frequently repeated between larvae (I close to 1: maximal values $I_{S\ (diff)} = 1.09$ and $I_{T\ (diff)} = 1.01$, $p > 0.05$; **Figures 5Bi,ii**, **Table 2**, and Methods), we found that recurrent escapes were very frequent between different larvae (maximal value $I_{E\ (diff)} = 3.6$, $p < 0.002$; **Figure 5Biii**, **Table 2**, and Methods). Five to seven dpf larvae do not show evidence for social interactions (Buske and Gerlai, 2011). By taking advantage of the algorithm for identifying single larva and categorizing simple maneuvers, we reveal that larva–larva interactions primarily occurred for escape responses. These series of escapes occurred after direct collisions (in one third of the cases) or via long distance interaction (two third of cases). Blind *atoh7*$^{-/-}$ larvae showed a similar profile of interactions for escapes (data *not shown*); these interactions were most likely mechanically triggered.

Large-scale chemical and genetic screens would benefit from a quantitative approach to analyze fine locomotor patterns over long periods of time. Compared to other genetic models, zebrafish locomotion is difficult to analyze because larvae initiate maneuvers intermittently and during these short events, the larvae swim at a high speed with TBFs ranging from 15–100 Hz. The quantitative analysis of motor behavior for large-scale screens requires solving the problem of recording multiple animals simultaneously at high frequency (above 200 Hz) and for long periods of time (minutes). Here we implemented a reliable method for quantifying global parameters of movements based on stream-to-disk recordings acquired at high frequency and over long periods of time, limited only by data storage. Next we developed a robust method for tracking the full body position of zebrafish larvae swimming in groups. We first manually validated that the tracking accurately detected discrete movements, and then used the global parameters obtained to characterize the locomotion of WT larvae. Quantification of the global parameters describing larval movements corroborates previous observations based on fewer samples (Budick and O'Malley, 2000; Danos and Lauder, 2007; Liu et al., 2012). Similar estimates of the duration of movements, distance traveled and speed were obtained from the recent application of C-trax (designed originally for *Drosophila*) to zebrafish larvae [Lambert et al. (2012) based on Branson et al. (2009)]. In these conditions, recordings at low frequency over long periods of time, typically 60 Hz for minutes or hours, revealed the global level of activity over time but no information on fine kinematics during individual maneuvers (Elbaz et al., 2012). When recordings were performed at high frequency to capture the dynamics of motion, they usually lasted 1000 ms (Burgess and Granato, 2007).

We illustrated the benefit of ZebraZoom to quantify global parameters of movements by analyzing the effect of a drug to block glycinergic neurotransmission, which has been known to be involved in motor pattern generation and alternation between the left and right side of the spinal cord across vertebrate species (Grillner, 2003; Korn and Faber, 2005; Nishimaru and Kakizaki, 2009). Most studies relied on ventral nerve root recordings where muscles were dissected out or paralyzed in order to record the activity of motor neurons at the level of a few segments at most. Our automated quantification of locomotor events enabled

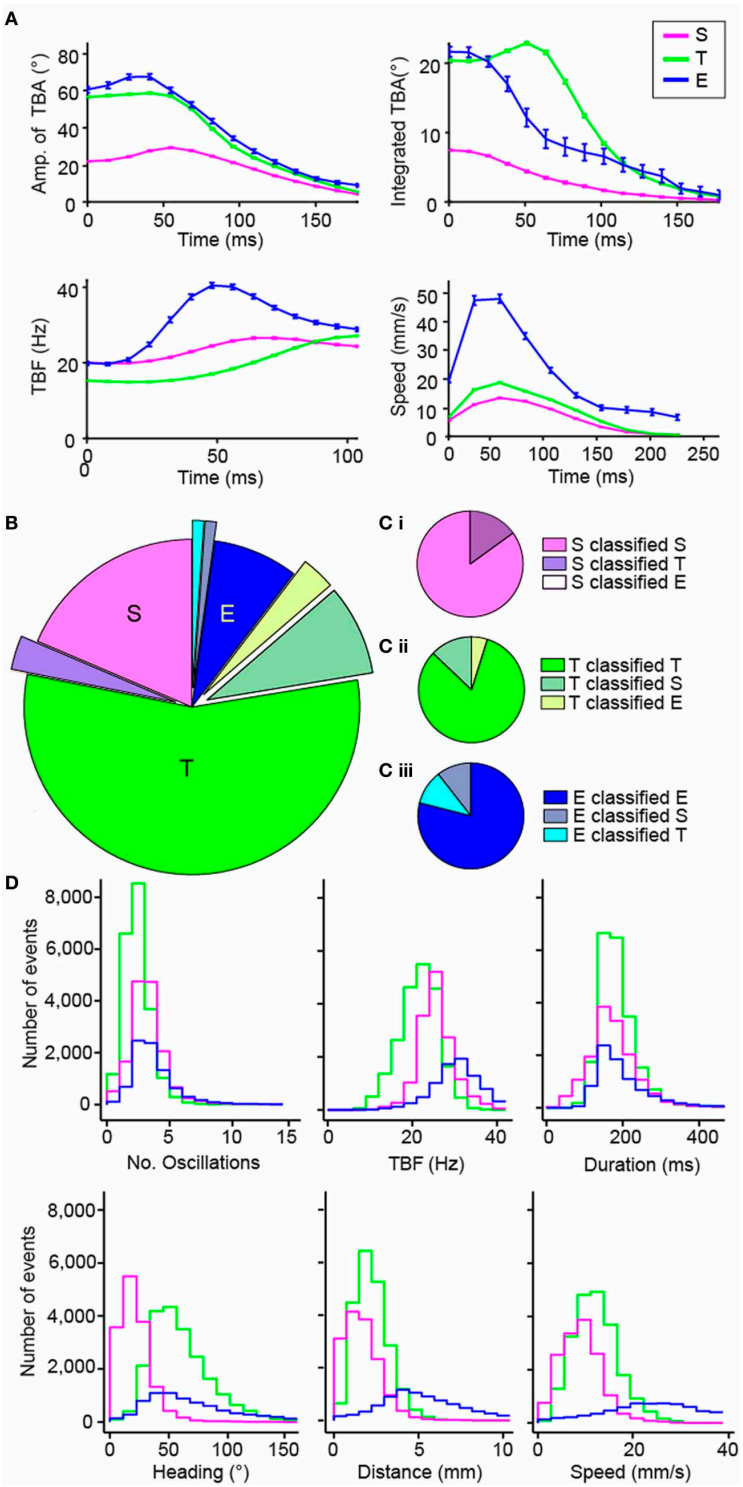

FIGURE 4 | Validation of the automated categorization of maneuvers: slow forward swim (S), routine turn (T) and escape (E). (A) Dynamic parameters used for categorizing the different maneuvers: amplitude of tail-bending angle (TBA) in degrees, integrated TBA in degrees, TBF in Hz, and speed in mm/s. The mean of each parameter for each time bin is shown and error bars are standard error of the mean: S in pink, T in green and E in blue. Time 0 is taken at the peak of the first bend of the movement. **(B,C)** Comparison of the results of the automatic categorization from ZebraZoom with the subjective categorization by a trained experimenter on 189 movements from one video. The comparison of the categorization is shown overall **(B)** and for each maneuver (**C**: **Ci** for S, **Cii** for T, **Ciii** for E). The proportion of movements categorized the same way by both methods is shown in addition to the proportion of movements miscategorized and how they were categorized. **(D)** Distribution of global parameters for each maneuver S, T, and E of WT larvae (same color code as in **A**; 44,688 movements total from eight videos, six clutches).

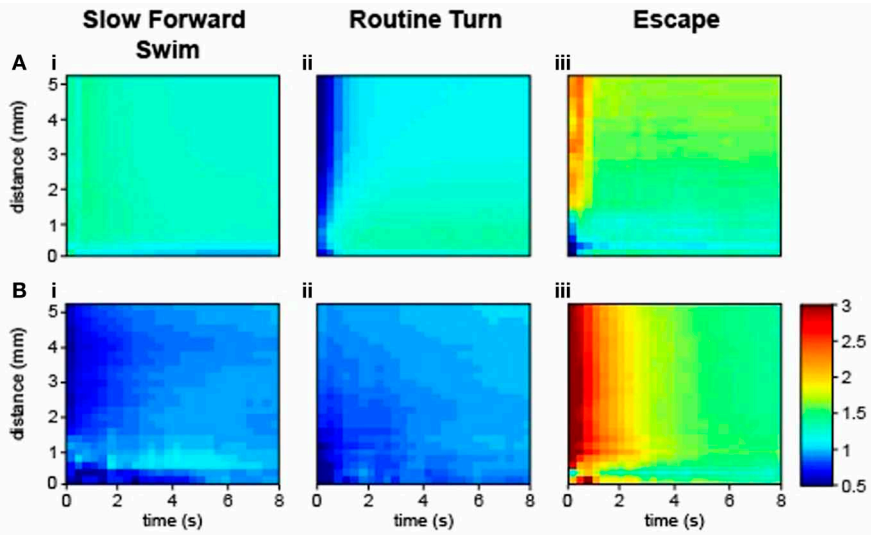

FIGURE 5 | Larva–larva interactions occurred most frequently as sequences of escapes. Transition index for the same larvae **(A)** and for different larvae **(B)**. Time is plotted in seconds from the time of initiation of the first movement. Distance is plotted from the core position of the larva at the beginning of a movement. **(Ai,Bi)** The sequence S–S. **(Aii,Bii)** The sequence T–T. **(Aiii,Biii)** The sequence E–E (36,068 total movements from five videos, 280 WT larvae, four clutches, 5–6 dpf).

Table 2 | Transition index for sequence of two maneuvers estimated as the probability of transition from maneuver 1 to maneuver 2 divided by the occurrence of the maneuver 2.

	S	*T*	*E*
INTERACTIONS BETWEEN DIFFERENT ANIMALS			
S	1.0498	1.0152	0.8481
T	1.0087	1.0413	0.8606
E	0.8549	0.8493	1.7528
REPETITIONS WITHIN THE SAME ANIMAL			
S	1.2162	0.8947	0.8413
T	0.9091	1.1185	0.8499
E	0.8263	0.8887	1.6995

identification of effects induced by bath application of the glycinergic antagonist strychnine on locomotion in intact animals. As predicted, bath application of strychnine dramatically reduced the occurrence of movements and the number of oscillations per movement, that was correlated with a reduction of the duration of movement and of the distance traveled. While mean TBF was not affected, we observed a reduction in the heading direction range and in speed. Our approach pinpointed effects of glycinergic blockade, including a reduction in the number of oscillations per movement, a kinematic feature not estimated in commercially available software. The analysis of the mutant *atoh7* revealed that although TBF and speed were not affected in the blind mutant, there was a small but significant decrease in the number of oscillations, heading direction range, distance, and duration of each bout compared to their control siblings. These effects were systematically observed on four clutches suggesting that visual feedback may impact some global parameters of locomotion. However since the pattern of expression of *atoh7* has not yet been fully characterized, it cannot be excluded that the gene may be expressed in cells other than retinal ganglion cells.

The originality of ZebraZoom lies in categorizing all maneuvers performed by individual larvae in a group. The subjective analysis of maneuvers based on four independent experimenters revealed that locomotor maneuvers were not obvious to categorize. Based on subjective estimates, 18% of all movements corresponded to ambiguous maneuvers. By using a machine-learning paradigm, we trained ZebraZoom to categorize all maneuvers over tens of thousands of movements with 82.5% accuracy, a similar value to the 72% agreement rate of all four experimenters measured over a few hundreds of movements. The approach we developed here could be expanded to include directionality of the turns, sequences of maneuvers such as those occurring during prey tracking, and subcategories of escapes.

This study constitutes an important first step for accurate tracking of multiple larvae in groups over long periods of time and for categorizing maneuvers. Some improvements could be implemented in the future. While our tracking method currently relies on a simple "blob" approach solely based on raw image analysis, a model-based approach may be more reliable in particular when animals are in close contact (Fontaine et al., 2008). We show here that ZebraZoom can achieve an accurate categorization of maneuvers, comparable to experimenters' estimates, based solely on the dynamics of movement of head and tail. An interesting avenue of exploration to address this could be investigation of novel dynamic parameters for the learning and recognition process of the classifier to yield subtler methods for detection of defects. Quantification of motor patterns in *C. elegans* is based on a description of all possible positions of the animal over time (Stephens et al., 2008). In order to fully understand larval zebrafish behavior we need to identify a minimal set of parameters sufficient to describe all motor patterns. All together this

work brings new insight to the complexity of behavior determination in zebrafish larvae and could be applied to investigation of the mechanisms of addiction, arousal, feeding, social interaction and aggression in larvae and juveniles (Gahtan et al., 2005; Bianco et al., 2011; Buske and Gerlai, 2011; Miller and Gerlai, 2012; Ziv et al., 2013). The observation of complex interactions in juveniles raises the hope that it will soon be possible to investigate the neuronal circuits and molecular pathways underlying social interactions. The fact that we can track individual larva and analyze their interactions is a major advance over existing methods. Our approach that systematically quantifies and categorizes thousands of motor patterns was designed to bring efficiency and reliability to drug screening and forward genetic screens. ZebraZoom can detect, quantify, and categorize movements to provide a quantitative description of global parameters as well as a qualitative description of all maneuvers performed by individual larvae.

METHODS

ZEBRAFISH HUSBANDRY

All experiments were performed on *Danio rerio* larvae between 5 and 7 dpf. AB and TL strains of WT larvae were obtained from our laboratory stock of adults. Embryos and larvae were raised in an incubator at 28.5°C under a 14/10 light/dark cycle (lights on, 8:00 A.M.; lights off, 10:00 P.M.) until the start of behavioral recordings. The mutant line for *atoh7* (Kay et al., 2001) was given by Dr. Herwig Baier, MPI Munich. Double recessive *atoh7*$^{-/-}$ mutants were identified at 5 dpf by their dark pigmentation. All procedures were approved by the Institutional Ethics Committee at the Research Center of the Institut du Cerveau et de la Moelle épinière (CRICM).

BEHAVIORAL RECORDINGS

Motor behavior of 56 larvae split into eight dishes (seven larvae per dish, **Figure 1Ai**) on a homogeneous illumination plate (light intensity 0.78 mW/cm^2, Phlox, ref. LEDW-BL-200/200-LLUB-Q-1R24) in egg water (http://zfin.org/zf_info/zfbook/chapt1/1.3.html, methylene blue added at 0.5 ppm). Following acclimation, larvae were recorded for 4 min at 337 Hz with a high-speed camera (VC-2MC-M340E0-C, CMOS chip 2048 × 1088 pixels, Vieworks, South Korea) placed above the setup and coupled to a camera objective (AF Nikkor 50 mm f/1.8D, Nikon, Japan). Pixel size was 66 μm. We developed a direct-to-disk high-speed imaging system designed for long acquisitions of raw images in collaboration with R&D Vision, France. Behavioral recordings were performed between 2:00 and 5:00 P.M. Larvae were acclimated for 60 minutes on the light source at room temperature (21–22°C) and kept at room temperature during all recordings. Larvae were kept in dishes with an inner diameter of 2.2 cm and an outer diameter of 3.5 cm (**Figure 1A**). Water was kept at a low level (2 mm) in order to reduce the occurrence of crossings between larvae. Typically 500–1000 movements were recorded in each 4-min session for each well.

ZEBRAZOOM TRACKING ALGORITHM

The first step is to track the core and then the tail for all larvae over time. Written in C++ using the *openCV* library, the program identified the center position and heading direction of each larva (**Figures 1Ai–vi**). The algorithm used a Hough transform to identify the eight wells. For each well the background was estimated as the maximum pixel value over all frames of the video recording (**Figure 1Aii**) and then subtracted for all frames for that well (**Figure 1Aiii**). The resulting image was converted to binary (**Figure 1Aiv**). An erosion filter was applied twice in a row with a 3 by 3 structuring element (**Figure 1Av**). The "core" of the larva referred to the resulting connected components that had an appropriate area (between 0.0871 and 0.8712 mm^2). The core of the larva included the head and the trunk with swim bladder (**Figure 1Avi**). The algorithm identified the head center position as the center of mass of the putative cores for each larva in a frame. To follow each larva across subsequent frames, ZebraZoom used the information from the previous two frames (core position and speed) to predict the position of the larva and located the closest core out of all the possible cores. The heading direction for each larva was calculated simultaneously using the moments of the eroded body (up to the second order, see red lines in **Figure 1Avi**).

For each larva with an identified core, we determined the "full body" referring to the connected component of the binary image in **Figure 1Aiv**. In order to track the tail, the full body was rotated so that the head axis was parallel to the y-axis, always in the same orientation. To identify the contour of the tail in the coordinate system defined by the head axis, a series of points was extracted from the full body by using the algorithm of Suzuki and Abe (1985), (white dots in **Figures 1Bi–iii**). Reference point A1 was the closest point on the contour line from the head center and reference point A2 was the point symmetrical along the head axis to reference point A1 on the contour. In order to identify the tip of the tail, four candidate points on the contour were selected with minimal and maximal *x*- and *y*-values (**Figures 1Bi–iii**). For the maximal *y*-value the point also had to be above a given distance away from the two reference points [below a 20% threshold for the ratio $|(d_1 - d_2)|/(d_1 + d_2)$, **Figure 1Bii**]. Distances d1 and d2 were calculated from each candidate point to the reference points A1 and A2 along the contour (**Figure 1Bii**). Candidate points with a ratio $|(d_1 - d_2)|/(d_1 + d_2)$ over 0.25 were excluded. The tip of the tail was then identified as the point associated with the smallest scalar product of the tangential vectors pointing in opposite directions (**Figure 1Biii**). The midline of the larva was defined as the line equidistant to the contour line on the left and right side.

ERRORS IN CORE AND TAIL TRACKING

If an error occurred in the core tracking, the larva was missing for that frame and there was no tracking of its tail. If the core of a larva was identified, the algorithm proceeded to the tail tracking. To confirm that the tail tracking was correct, the algorithm checked that the tail length was greater than 1.32 and less than 3.96 mm. If this criterion was invalid, the tail position was set to the previous frame. This happened in 13.46% of frames on average but was compensated by a smoothing spline on the center positions between the left and right contour points of the tail and a median filter applied on the tail-bending angle over time. The tail-bending angle was defined as the angle between the axis formed by the tip of the tail and the center of the head with respect to the larva heading direction (**Figures 1C,D**).

SEPARATING LARVAE DURING CONTACTS

Tracking was optimized to separate larvae in close vicinity to one another or in direct contact. For core tracking, if the trajectories of the two cores merged at a given time point, then the algorithm considered that a collision occurred between the two larvae. When the predicted positions of two larvae based on core position and speed in the two previous frames were closest to the same core, the algorithm considered that a collision between the two larvae occurred at that frame. When a collision was detected, the algorithm applied erosion filters in the region of interest defined by the core until more than one isolated core emerged. In rare cases, the multiple cores were not resolved and the larva could not be tracked for that frame. For the tail tracking, if the area of the larva's full body was greater than 1.9 mm^2, the algorithm considered that two larvae were in direct contact. The distance separating the larvae's cores determined which of two algorithms was used to isolate the tails: if the distance was less than 1.32 mm, a line separation algorithm was applied. A line was created to separate the two larvae by optimizing the area of the resulting tails, calculated by maximizing the sum of the two largest areas containing a head center position. If the distance was greater than 1.32 mm, a pixel intensity separation algorithm was applied instead. The threshold used to convert the image into binary was adjusted until two separate full bodies, each a connected component, emerged and contained the head center position. Larvae crossings occurred once every 145 s on average per larva (0.0069 ± 0.0019 events per second) and the switching of identification between two larvae after a collision was estimated manually to occur every 109 s on average (0.0092 ± 0.0036 events per second per larva based on 720 s of recordings from four videos, and 28 larvae).

DETECTION OF MOVEMENTS

Algorithms for the detection of movements and the behavior analysis were written in MATLAB (The Mathworks, Inc., USA). The detection of movement was based solely on thresholding the tail-bending angle measured over time (**Figures 1C,D**). ZebraZoom detected the start of a movement when the value for the tail-bending angle at a given frame varied over 1.15° from the mean value of the tail-bending angle for the ten surrounding frames, or 29.7 ms. To avoid separating single maneuvers into multiple events, movements that occur within 14.8 ms of each other were merged. To avoid false positives we considered only movements in which the larva core had moved more than 0.099 mm and where the range of tail-bending angle values was above 2.86 degrees. Additionally, only events during which the eroded binary image of the larva had moved more than a set number of pixels between subsequent images were considered based on the parameters used for the erosion. Rarely we have observed two distinct movements occurring without a pause, such as a slow forward swim followed by an escape due to a collision. In these few cases when two movements occurred without a noticeable stabilization in the tail-bending angle over time, the movements were merged into one movement in our analysis.

Our tracking method was robust in these experimental conditions. We cannot probe the impact of a reduction of contrast or spatial resolution. All numerical thresholds used above for tracking were fixed empirically, but they could easily be modified for other users to adapt to other recording conditions.

CALCULATION OF THE CURVATURE

After alignment of the body axis with the y-axis in a consistent orientation, the tail was represented parametrically in Cartesian coordinates as $[x(t), y(t)]$. The midline of the tail was fitted to the $x(t)$, $y(t)$ function with a spline. Curvature was calculated in Cartesian coordinates:

$$c = \frac{\left|x'y'' - y'x''\right|}{\left(x'^2 + y'^2\right)^{\left(\frac{3}{2}\right)}}$$

where the derivatives were all calculated with respect to t, the distance along the tail.

EXTRACTION OF GLOBAL PARAMETERS

For all frames of a video, ZebraZoom outputs variables for each larva in each dish including: the position of its core, head axis, midline position of its tail and tail-bending angle. For each detected movement, a reference number for the larvae was extracted along with the corresponding well number, start and end time of the movement, and global parameters such as the number of oscillations, TBF, movement duration, heading direction range referring to the range of values of the heading axis for one movement with the heading angle reset to zero at the onset of movement, distance traveled, average speed (distance traveled divided by movement duration).

AUTOMATIC MULTICLASS CATEGORIZATION

We automatically attributed each movement detected in the video to either one of the three maneuvers: slow forward swim, routine turn or escape response. Our method relied on a dynamic set of parameters extracted from the bending angle of the tail estimated from the first tail bend over a limited time window (**Figures 1C**, **4A**). We based our categorization on the four following parameters: (1) the amplitude of the tail-bending angle (0–178 ms, bins of 12 ms), (2) the instantaneous frequency (0–104 ms, bins of 7 ms), (3) the cumulative tail-bending angle calculated as the average angle value over time (0–178 ms, bins of 12 ms), and (4) the speed (0–240 ms, bins of 24 ms) (**Figure 4A**). The values of these four dynamic parameters were interpolated with a spline for a given time window during the movement and then used for categorization of every movement. PCA was first performed to reduce noise and dimensionality. Each movement was subsequently represented by the fourteen first principal components of the PCA out of 53 components (representing all together about 93% of the variance), to which the total duration of the movement was added. Multiclass categorization was implemented in two steps: a series of two subsequent SVM classifiers with linear kernel was applied for automatic categorization of movements: the first SVM classifier discriminated slow forward swims vs. turns and escapes, and if necessary a second SVM discriminated between a routine turn and an escape. We used two distinct datasets from WT 5–7 dpf larvae, one for learning the three maneuver types (five videos, $n = 201$ movements) and one for testing their recognition (three videos, $n = 189$ movements).

ESTIMATING THE RECURRENCE OF MANEUVERS

Successions of maneuvers performed by larvae in a given dish were modeled as Markov chains. Out of the nine possible sequences of two maneuvers (S–S, S–T, S–E, T–S, T–T, T–E, E–S, E–T, E–E), we estimated the frequency of occurrence of each sequence. For a given movement classified as S, T, or E occurring at a given time in one dish, we calculated the transition probability for the subsequent movement to be classified as S, T, or E. We calculated a weighted transition index (I) for each sequence of two sequential maneuvers as the ratio of the transition probability from the first maneuver to the second, divided by the probability of occurrence of the second maneuver (**Table 2** for values of all transition indexes). When I is equal to 1, the probability of repeating a maneuver is equal to the probability of random occurrence of the maneuver (probability of random occurrence was 0.35 for S; 0.48 for T and 0.16 for E; **Table 2**). Thus the index of recurrence I was defined as:

$$I(B1, B2) = \frac{p(x_i = B1 | x_{i-1} = B2)}{p(x_i = B1)}$$

with $B1$ and $B2$ as two possible maneuvers (S, T, or E) and x_{i-1} and x_i as two successive movements. WT larvae were used to estimate the transition index (36,068 movements from 280 larvae originating from four clutches and obtained from 40 wells). To investigate the recurrence of maneuvers as a function of time and distance, we calculated I as a function of the distance separating the two head centers of the larvae at the onset of their respective movement and the time as the time interval between the onsets of the first and second movement. I was calculated for many different time and distance windows. In **Figure 5**, we plotted these indexes for the sequences S–S, T–T, and E–E. We first calculated the index for the same larva (**Figures 5Ai–iii**) and across different larvae (**Figures 5Bi–iii**).

STATISTICAL ANALYSIS

The data used for **Figure 2A** were based on eight videos, 420 WT AB larvae from six different clutches between 5 and 7 dpf. All values were given as mean ± standard error of the mean (s.e.m.) calculated per movement. For the pharmacology experiments (**Figure 2B**), strychnine was bath applied at 75 μM and the data were based on two videos of 84 WT larvae coming from two clutches (42 for controls and 42 for strychnine) between 6 and 7 dpf. The data on *atoh7*$^{-/-}$ mutants in **Figure 2C** were generated using four videos, 224 larvae total originating from four clutches (112 *atoh7*$^{-/-}$ and 112 control siblings). All global parameters plotted in **Figures 2B,C** were calculated per larva then averaged across all larvae and means were given ± s.e.m. across all larvae. Since the distributions of global parameters were not normal, a standard non-parametric Wilcoxon rank sum test was used in MATLAB for calculating differences between conditions with vs. without drugs for **Figure 2B** and *atoh7*$^{-/-}$ vs. siblings for **Figure 2C**. The data used for **Figure 4D** were based on 44,688 movements from eight videos, 448 larvae, six clutches and for **Figure 5** from 36,068 movements from five videos, 280 WT AB larvae from four clutches. To test how the maximal values of the transition index were different from random, we calculated I_{max} after randomly permuting maneuvers while keeping track of the larva identity, time, and location the same for 50 iterations. For each comparison, S–S, T–T, E–E across different larvae or within the same larva, we compared the values of I_{max} after randomization to the measured value I_{max} using a two-sample T-test.

DATA AND ALGORITHM SHARING

The software ZebraZoom is documented and available online from Source Forge in the code tab (http://sourceforge.net/p/zebrazoom/wiki/Home/). ZebraZoom requires MATLAB and works reliably on an Ubuntu 11.04 computer with OpenCV installed and MATLAB 7.10.

CONTRIBUTIONS

Claire Wyart and Olivier Mirat designed the project with help from Jenna R. Sternberg. Olivier Mirat wrote all algorithms of the ZebraZoom program. Jenna R. Sternberg and Claire Wyart assembled the experimental setup. Jenna R. Sternberg performed all experiments. Olivier Mirat and Claire Wyart analyzed the data. Kristen E. Severi, Olivier Mirat, and Claire Wyart prepared the figures. All authors tested and validated the program and wrote the paper.

ACKNOWLEDGMENTS

We thank Dr. Stanley Durleman, Dr. Lionel Moisan, Dr. Carlos Pantoja, and Claire Oldfield for critical reading of the manuscript. We thank Dr. Olivier Colliot, and Drs. Stanley Durleman and Lionel Moisan again for advice on machine learning, tracking, and Markov chain analysis. We thank Caroline Vidal, Philippe Domineaux, and Antoine Mongay for data server access. We thank Laura Garnero, Audrey Baradel, Lydia Djenoune, Victor Adenis, Devika Nair, and Maxime Gaudin for technical assistance and fish care. We thank Dr. Herwig Baier for kindly sharing the *atoh7* mutant line. This work received critical support from the Institut du Cerveau et de la Moelle Epinière (ICM/CR), the Ecole des Neurosciences de Paris (ENP), the Fondation Bettencourt Schueller, Mr. Pierre Belle, the City of Paris Emergence program, the ATIP-AVENIR program from INSERM and CNRS, the Fyssen Foundation, the International Reintegration Grant from Marie Curie Actions Framework Program 6, and the European Research Council (ERC) starter grant "OptoLoco." Jenna R. Sternberg is affiliated with the graduate program of the Ecole des Neurosciences de Paris (ENP) associated with the ED3C. Olivier Mirat is funded by a DIGITEO PhD fellowship associated with the Ecole Doctorale Interdisciplinaire Européenne Frontières du vivant ED474 program doctoral Bettencourt.

SUPPLEMENTARY MATERIAL

The Supplementary Material for this article can be found online at: http://www.frontiersin.org/Neural_Circuits/10.3389/fncir.2013.00107/abstract

Video S1 | ZebraZoom tracking of seven larvae in a dish. Acquisition was performed at 300 Hz, and one out of every ten images is displayed (every 33.3 ms).

REFERENCES

Appelbaum, L., Wang, G. X., Maro, G. S., Mori, R., Tovin, A., Marin, W., et al. (2009). Sleep-wake regulation and hypocretin-melatonin interaction in zebrafish. *Proc. Natl. Acad. Sci. U.S.A.* 106, 21942–21947. doi: 10.1073/pnas.906637106

Bianco, I. H., Kampff, A. R., and Engert, F. (2011). Prey capture behavior evoked by simple visual stimuli in larval zebrafish. *Front. Syst. Neurosci.* 5:101. doi: 10.3389/fnsys.2011.00101

Blaser, R. E., Chadwick, L., and McGinnis, G. C. (2010). Behavioral measures of anxiety in zebrafish (*Danio rerio*). *Behav. Brain Res.* 208, 56–62. doi: 10.1016/j.bbr.2009.11.009

Borla, M. A., Palecek, B., Budick, S., and O'Malley, D. M. (2002). Prey capture by larval zebrafish: evidence for fine axial motor control. *Brain Behav. Evol.* 60, 207–229. doi: 10.1159/000066699

Branson, K., Robie, A. A., Bender, J., Perona, P., and Dickinson, M. H. (2009). High-throughput ethomics in large groups of Drosophila. *Nat. Methods* 6, 451–457. doi: 10.1038/nmeth.1328

Budick, S. A., and O'Malley, D. M. (2000). Locomotor repertoire of the larval zebrafish: swimming, turning and prey capture. *J. Exp. Biol.* 203(Pt 17), 2565–2579.

Burgess, H. A., and Granato, M. (2007). Modulation of locomotor activity in larval zebrafish during light adaptation. *J. Exp. Biol.* 210(Pt 14), 2526–2539. doi: 10.1242/jeb.003939

Buske, C., and Gerlai, R. (2011). Shoaling develops with age in Zebrafish (*Danio rerio*). *Prog. Neuropsychopharmacol. Biol. Psychiatry* 35, 409–1415. doi: 10.1016/j.pnpbp.2010.09.003

Cachat, J., Stewart, A., Utterback, E., Hart, P., Gaikwad, S., Wong, K., et al. (2011). Three-dimensional neurophenotyping of adult zebrafish behavior. *PLoS ONE* 6:e17597. doi: 10.1371/journal.pone.0017597

Chalfie, M., Sulston, J. E., White, J. G., Southgate, E., Thomson, J. N., and Brenner, S. (1985). The neural circuit for touch sensitivity in *Caenorhabditis elegans*. *J. Neurosci.* 5, 956–964.

Dale, N. (1985). Reciprocal inhibitory interneurones in the Xenopus embryo spinal cord. *J. Physiol.* 363, 61–70.

Dankert, H., Wang, L., Hoopfer, E. D., Anderson, D. J., and Perona, P. (2009). Automated monitoring and analysis of social behavior in Drosophila. *Nat. Methods* 6, 297–303. doi: 10.1038/nmeth.1310

Danos, N., and Lauder, G. V. (2007). The ontogeny of fin function during routine turns in zebrafish *Danio rerio*. *J. Exp. Biol.* 210(Pt 19), 3374–3386. doi: 10.1242/jeb.007484

Drapeau, P., Saint-Amant, L., Buss, R. R., Chong, M., McDearmid, J. R., and Brustein, E. (2002). Development of the locomotor network in zebrafish. *Prog. Neurobiol.* 68, 85–111. doi: 10.1016/S0301-0082(02)00075-8

Driever, W., Solnica-Krezel, L., Schier, A. F., Neuhauss, S. C., Malicki, J., Stemple, D. L., et al. (1996). A genetic screen for mutations affecting embryogenesis in zebrafish. *Development* 123, 37–46.

Elbaz, I., Yelin-Bekerman, L., Nicenboim, J., Vatine, G., and Appelbaum, L. (2012). Genetic ablation of hypocretin neurons alters behavioral state transitions in zebrafish. *J. Neurosci.* 32, 12961–12972. doi: 10.1523/JNEUROSCI.1284-12.2012

Fontaine, E., Lentink, D., Kranenbarg, S., Müller, U. K., van Leeuwen, J. L., Barr, A. H., et al. (2008). Automated visual tracking for studying the ontogeny of zebrafish swimming. *J. Exp. Biol.* 211(Pt 8), 1305–1316. doi: 10.1242/jeb.010272

Gahtan, E., Tanger, P., and Baier, H. (2005). Visual prey capture in larval zebrafish is controlled by identified reticulospinal neurons downstream of the tectum. *J. Neurosci.* 25, 9294–9303. doi: 10.1523/JNEUROSCI.2678-05.2005

Gautrais, J., Ginelli, F., Fournier, R., Blanco, S., Soria, M., Chaté H., et al. (2012). Deciphering interactions in moving animal groups. *PLoS Comput. Biol.* 8:e1002678. doi: 10.1371/journal.pcbi.1002678

Granato, M., van Eeden, F. J., Schach, U., Trowe, T., Brand, M., Furutani-Seiki, M., et al. (1996). Genes controlling and mediating locomotion behavior of the zebrafish embryo and larva. *Development* 123, 399–413.

Grillner, S. (2003). The motor infrastructure: from ion channels to neuronal networks. *Nat. Rev. Neurosci.* 4, 573–586. doi: 10.1038/nrn1137

Grillner, S., Deliagina, T., Ekeberg, O., el Manira, A., Hill, R. H., Lansner, A., et al. (1995). Neural networks that co-ordinate locomotion and body orientation in lamprey. *Trends Neurosci.* 18, 270–279. doi: 10.1016/0166-2236(95)80008-P

Haffter, P., and Nusslein-Volhard, C. (1996). Large scale genetics in a small vertebrate, the zebrafish. *Int. J. Dev. Biol.* 40, 221–227.

Hirata, H., Saint-Amant, L., Downes, G. B., Cui, W. W., Zhou, W., Granato, M., et al. (2005). Zebrafish bandoneon mutants display behavioral defects due to a mutation in the glycine receptor beta-subunit. *Proc. Natl. Acad. Sci. U.S.A.* 102, 8345–8350. doi: 10.1073/pnas.0500862102

Kabra, M., Robie, A. A., Rivera-Alba, M., Branson, S., and Branson, K. (2013). JAABA: interactive machine learning for automatic annotation of animal behavior. *Nat. Methods* 10, 64–67. doi: 10.1038/nmeth.2281

Katz, Y., Tunstrøm, K., Ioannou, C. C., Huepe, C., and Couzin, I. D. (2011). Inferring the structure and dynamics of interactions in schooling fish. *Proc. Natl. Acad. Sci. U.S.A.* 108, 18720–18725. doi: 10.1073/pnas.1107583108

Kay, J. N., Finger-Baier, K. C., Roeser, T., Staub, W., and Baier, H. (2001). Retinal ganglion cell genesis requires lakritz, a Zebrafish atonal Homolog. *Neuron* 30, 725–736.

Khor, B. S., Jamil, M. F., Adenan, M. I., and Shu-Chien, A. C. (2011). Mitragynine attenuates withdrawal syndrome in morphine-withdrawn zebrafish. *PLoS ONE* 6:e28340. doi: 10.1371/journal.pone.0028340

Korn, H., and Faber, D. S. (2005). The Mauthner cell half a century later: a neurobiological model for decision-making? *Neuron* 47, 13–28. doi: 10.1016/j.neuron.2005.05.019

Lambert, A. M., Bonkowsky, J. L., and Masino, M. A. (2012). The conserved dopaminergic diencephalospinal tract mediates vertebrate locomotor development in zebrafish larvae. *J. Neurosci.* 32, 13488–13500. doi: 10.1523/JNEUROSCI.1638-12.2012

Lee, A., Mathuru, A. S., Teh, C., Kibat, C., Korzh, V., Penney, T. B., et al. (2010). The habenula prevents helpless behavior in larval zebrafish. *Curr. Biol.* 20, 2211–2216. doi: 10.1016/j.cub.2010.11.025

Li, W. C., Higashijima, S., Parry, D. M., Roberts, A., and Soffe, S. R. (2004). Primitive roles for inhibitory interneurons in developing frog spinal cord. *J. Neurosci.* 24, 5840–5848. doi: 10.1523/JNEUROSCI.1633-04.2004

Liu, Y. C., Bailey, I., and Hale, M. E. (2012). Alternative startle motor patterns and behaviors in the larval zebrafish (*Danio rerio*). *J. Comp. Physiol. A Neuroethol. Sens. Neural Behav. Physiol.* 198, 11–24. doi: 10.1007/s00359-011-0682-1

Masino, M. A., and Fetcho, J. R. (2005). Fictive swimming motor patterns in wild type and mutant larval zebrafish. *J. Neurophysiol.* 93, 3177–3188. doi: 10.1152/jn.01248.2004

McElligott, M. B., and O'Malley, D. M. (2005). Prey tracking by larval zebrafish: axial kinematics and visual control. *Brain Behav. Evol.* 66, 177–196. doi: 10.1159/000087158

Miller, N., and Gerlai, R. (2012). From schooling to shoaling: patterns of collective motion in zebrafish (*Danio rerio*). *PLoS ONE* 7:e48865. doi: 10.1371/journal.pone.0048865

Moore, M. S., DeZazzo, J., Luk, A. Y., Tully, T., Singh, C. M., and Heberlein, U. (1998). Ethanol intoxication in Drosophila: genetic and pharmacological evidence for regulation by the cAMP signaling pathway. *Cell* 93, 997–1007. doi: 10.1016/S0092-8674(00)81205-2

Nishimaru, H., and Kakizaki, M. (2009). The role of inhibitory neurotransmission in locomotor circuits of the developing mammalian spinal cord. *Acta Physiol. (Oxf.)* 197, 83–97. doi: 10.1111/j.1748-1716.2009.02020.x

Odenthal, J., Rossnagel, K., Haffter, P., Kelsh, R. N., Vogelsang, E., Brand, M., et al. (1996). Mutations affecting xanthophore pigmentation in the zebrafish, *Danio rerio*. *Development* 123, 391–398.

Petzold, A. M., Balciunas, D., Sivasubbu, S., Clark, K. J., Bedell, V. M., Westcot, S. E., et al. (2009). Nicotine response genetics in the zebrafish. *Proc. Natl. Acad. Sci. U.S.A.* 106, 18662–18667. doi: 10.1073/pnas.0908247106

Rihel, J., Prober, D. A., Arvanites, A., Lam, K., Zimmerman, S., Jang, S., et al. (2010). Zebrafish behavioral profiling links drugs to biological targets and rest/wake regulation. *Science* 327, 348–351. doi: 10.1126/science.1183090

Rihel, J., and Schier, A. F. (2012). Behavioral screening for neuroactive drugs in zebrafish. *Dev. Neurobiol.* 72, 373–385. doi: 10.1002/dneu.20910

Scholz, H., Ramond, J., Singh, C. M., and Heberlein, U. (2000). Functional ethanol tolerance in Drosophila. *Neuron* 28, 261–271.

Stephens, G. J., Johnson-Kerner, B., Bialek, W., and Ryu, W. S. (2008). Dimensionality and dynamics in the behavior of *C. elegans*. *PLoS Comput. Biol.* 4:e1000028. doi: 10.1371/journal.pcbi.1000028

Suzuki, S., and Abe, K. (1985). Topological structural analysis of

digital binary image by border following. *Comput. Vis. Graph. Image Process.* 30, 32–46.

Swierczek, N. A., Giles, A. C., Rankin, C. H., and Kerr, R. A. (2011). High-throughput behavioral analysis in *C. elegans*. *Nat. Methods* 8, 592–598. doi: 10.1038/nmeth.1625

Vermoesen, K., Serruys, A. S., Loyens, E., Afrikanova, T., Massie, A., Schallier, A., et al. (2011). Assessment of the convulsant liability of antidepressants using zebrafish and mouse seizure models. *Epilepsy Behav.* 22, 450–460. doi: 10.1016/j.yebeh.2011.08.016

Zakhary, S. M., Ayubcha, D., Ansari, F., Kamran, K., Karim, M., Leheste, J. R., et al. (2011). A behavioral and molecular analysis of ketamine in zebrafish. *Synapse* 65, 160–167. doi: 10.1002/syn.20830

Zhdanova, I. V., Wang, S. Y., Leclair, O. U., and Danilova, N. P. (2001). Melatonin promotes sleep-like state in zebrafish. *Brain Res.* 903, 263–268. doi: 10.1016/S0006-8993(01)02444-1

Ziv, L., Muto, A., Schoonheim, P. J., Meijsing, S. H., Strasser, D., Ingraham, H. A., et al. (2013). An affective disorder in zebrafish with mutation of the glucocorticoid receptor. *Mol. Psychiatry* 18, 681–691. doi: 10.1038/mp.2012.64

Conflict of Interest Statement: The authors declare that the research was conducted in the absence of any commercial or financial relationships that could be construed as a potential conflict of interest.

Received: 28 February 2013; accepted: 21 May 2013; published online: 12 June 2013.

Citation: Mirat O, Sternberg JR, Severi KE and Wyart C (2013) ZebraZoom: an automated program for high-throughput behavioral analysis and categorization. Front. Neural Circuits **7**:*107. doi: 10.3389/fncir.2013.00107*

frontiers in
NEURAL CIRCUITS

MINI REVIEW ARTICLE
published: 01 February 2013
doi: 10.3389/fncir.2013.00009

Circadian clocks, rhythmic synaptic plasticity and the sleep-wake cycle in zebrafish

Idan Elbaz[1], Nicholas S. Foulkes[2], Yoav Gothilf[3] and Lior Appelbaum[1]*

[1] *The Mina and Everard Goodman Faculty of Life Sciences, The Leslie and Susan Gonda Multidisciplinary Brain Research Center, Bar-Ilan University, Ramat-Gan, Israel*
[2] *Karlsruhe Institute of Technology, Campus North, Institute of Toxicology and Genetics, Eggenstein-Leopoldshafen, Germany*
[3] *Department of Neurobiology, George S. Wise Faculty of Life Sciences, Sagol School of Neurosciences, Tel Aviv University, Tel Aviv, Israel*

Edited by:
German Sumbre, École normale supérieure, France

Reviewed by:
Karl Æ. Karlsson, Reykjavik University, Iceland
Diego A. Golombek, Universidad Nacional de Quilmes, Argentina

***Correspondence:**
Lior Appelbaum, The Mina and Everard Goodman Faculty of Life Sciences, Bar-Ilan University, The Nanotechnology Center, Building 206, Room B-938, Ramat-Gan 52900, Israel.
e-mail: lior.appelbaum@biu.ac.il

The circadian clock and homeostatic processes are fundamental mechanisms that regulate sleep. Surprisingly, despite decades of research, we still do not know why we sleep. Intriguing hypotheses suggest that sleep regulates synaptic plasticity and consequently has a beneficial role in learning and memory. However, direct evidence is still limited and the molecular regulatory mechanisms remain unclear. The zebrafish provides a powerful vertebrate model system that enables simple genetic manipulation, imaging of neuronal circuits and synapses in living animals, and the monitoring of behavioral performance during day and night. Thus, the zebrafish has become an attractive model to study circadian and homeostatic processes that regulate sleep. Zebrafish clock- and sleep-related genes have been cloned, neuronal circuits that exhibit circadian rhythms of activity and synaptic plasticity have been studied, and rhythmic behavioral outputs have been characterized. Integration of this data could lead to a better understanding of sleep regulation. Here, we review the progress of circadian clock and sleep studies in zebrafish with special emphasis on the genetic and neuroendocrine mechanisms that regulate rhythms of melatonin secretion, structural synaptic plasticity, locomotor activity and sleep.

Keywords: zebrafish, circadian rhythms, synaptic plasticity, circadian clock, sleep, hypocretin, orexin, melatonin

INTRODUCTION

All organisms demonstrate a wide variety of physiological, biochemical and behavioral daily rhythms that are driven by a highly conserved endogenous timing mechanism, the circadian clock. The maintenance and synchronization of this clock and the concurrent rhythms constitute an adaptive advantage, and its disruption in humans has been associated with physiological and mental disorders. A well-studied output of the circadian clock is the sleep-wake cycle. Sleep is a highly conserved process (Hartse, 2011) although its function remains one of the biggest mysteries in science (Cirelli and Tononi, 2008; Mignot, 2008). Theories that attempt to explain the role of sleep range from ecological considerations and energy conservation to synaptic plasticity and memory consolidation (Saper et al., 2005; Siegel, 2005; Nishino and Sakurai, 2006; Tononi and Cirelli, 2006; Cirelli, 2009; Sehgal and Mignot, 2011; Wang et al., 2011). The sleep state is associated with cycles of electroencephalograph (EEG) patterns (primarily in mammals), a species-specific sleep posture, a period of reversible quiescence, and decreased levels of sensory awareness to external stimuli. Sleep is regulated both by the circadian clock, which sets the timing of sleep, and by homeostatic mechanisms, as indicated by a compensatory increase in the intensity and duration of sleep after sleep deprivation (SD).

In mammals, including humans, sleep and other circadian rhythms are driven by a master oscillator that resides in the suprachiasmatic nucleus (SCN) of the hypothalamus (Reppert et al., 1981; Granados-Fuentes and Herzog, 2012). Among the many targets that are controlled by the mammalian SCN are hormonal and neuronal circuits that, in turn, feedback on the master oscillator and influence sleep/wake cycles. These include the rhythmic production of melatonin in the pineal gland and rhythmic secretion of neuropeptides and monoamines in the brain (Morris et al., 2012). Melatonin is secreted only during the night in all vertebrates. It affects the activity of the SCN, where the expression of melatonin receptors is enriched, and in diurnal birds and fish, it is a strong sleep-promoting hormone (Zhdanova, 2005). Another sleep/wake regulatory factor is the hypothalamic neuropeptide hypocretin/orexin (HCRT). Loss of HCRT neurons is associated with the sleep disorder narcolepsy, which is characterized by excessive daytime sleepiness, fragmentation of sleep during the night and cataplexy (brief loss of muscle tone triggered by emotional stimuli) (Lin et al., 1999; Nishino and Sakurai, 2006; Adamantidis and De Lecea, 2008).

The zebrafish offers many advantages for studying the circadian clock and the regulation of sleep. It is amenable to high throughput genetic and behavioral experiments, and its early developmental stages are transparent, enabling neuronal imaging *in vivo*. The complex neuro-regulatory mechanisms and sleep regulating nuclei underlying sleep/wake cycles in mammals are conserved, but much simpler in zebrafish. For example, the zebrafish HCRT neuronal circuits are similar in function and anatomy to mammals (Panula, 2010), but are represented by small number of neurons in the zebrafish brain (Faraco et al., 2006). The pineal gland in zebrafish develops remarkably early (Vatine et al.,

2011), is photoreceptive and contains an intrinsic circadian oscillator that directs melatonin rhythms. Thus, the pineal gland is considered a central circadian pacemaker that conveys circadian timing information to physiological and behavioral processes. In this review, we describe the progress of circadian and sleep studies in zebrafish with special emphasis on their neuroendocrine regulation.

THE CIRCADIAN CLOCK SYSTEM IN ZEBRAFISH

One of the most studied outputs of the circadian clock in vertebrates is the melatonin rhythm. The zebrafish pineal gland drives rhythms of melatonin-independent of any neuronal input or other master clock structures (Cahill, 1996; Noche et al., 2011). The aralkylamine-*N*-acetyltransferase (*aanat*) gene encodes the key enzyme of melatonin synthesis. Zebrafish *aanat2* expression and melatonin synthesis begin remarkably early, within 1 day post fertilization (dpf), and exhibit circadian clock-controlled rhythms at 2 dpf (Gothilf et al., 1999; Kazimi and Cahill, 1999). Genetic investigations of the pineal circadian clock mechanisms and its functional development have revealed that light and light-induced genes are required for the onset of the core molecular oscillator in the pineal gland (Ziv et al., 2005; Vuilleumier et al., 2006; Vatine et al., 2011). Extensive studies performed by Zhdanova and co-workers on the role of melatonin in zebrafish indicate that melatonin is a sleep-promoting agent (Zhdanova, 2011). Melatonin was also shown to affect memory acquisition (Rawashdeh et al., 2007), and to schedule the timing of reproduction (Carnevali et al., 2011) and feeding (Piccinetti et al., 2010).

Another important feature of the zebrafish circadian clock system is that light-entrainable circadian oscillators exist in all organs and even in cell cultures (Whitmore et al., 2000; Pando et al., 2001). Zebrafish cell lines have been used to study the role of the different clock genes within the core oscillator (Vallone et al., 2004, 2005) revealing that similar mechanisms constitute the core molecular oscillator in central and peripheral clocks. Current and future studies combining functional analysis of clock genes in living animals and in the light-entrainable, clock-containing zebrafish cell lines will enhance our understanding of the molecular mechanisms underlying the circadian clock and its entrainment (Tamai et al., 2005, 2007; Carr et al., 2006; Vatine et al., 2009).

Monitoring rhythms of locomotor activity is very frequently used to measure circadian clock output. Being a diurnal species, adult zebrafish demonstrate locomotor activity that peaks during the day (Hurd et al., 1998). The larvae start to exhibit a stable diurnal rhythm of locomotor activity at 4 dpf (Hurd and Cahill, 2002). An important hallmark of a circadian clock-driven rhythm is that it persists under constant photic conditions. Indeed, adult zebrafish also exhibit rhythmic activity and increase activity during the subjective day under constant dark (DD) conditions (Cahill et al., 1998; Hurd et al., 1998). Similarly, zebrafish larvae are rhythmic under DD (Hurd and Cahill, 2002) or constant dim light (Appelbaum et al., 2009, 2010; Tovin et al., 2012). It should be noted, however, that zebrafish are directly influenced by the photic conditions, which promote constant activity; i.e., "masking effects." Thus, while robust rhythms of locomotor activity are detected under light/dark cycles (LD), under constant light (LL) most individuals are constantly active, which also leads to a complete loss of their rhythms. Likewise, under DD, locomotor activity is reduced to the point in which rhythms are lost in some individuals, therefore, constant dim light has been used (Tovin et al., 2012). Rhythmic locomotor activity clearly reflects an integration of environmental effects and regulation by intrinsic central and peripheral circadian clocks. As sleep/wake cycles are a key output of the circadian clock, the extent to which rhythmic locomotor activity reflects sleep and wakefulness was studied in larvae and adults.

SLEEP IN ZEBRAFISH

USING BEHAVIORAL CRITERIA TO MEASURE THE SLEEP STATE IN ZEBRAFISH

Sleep has been examined in various fish species either in the natural environment or in laboratory conditions. During sleep, fish exhibit place preference, reduced heart and respiratory rates, typical sleep-postures and reduced sensitivity to external stimuli such as food, electric current or mechanical contact (Tauber et al., 1969; Shapiro and Hepburn, 1976; Campbell and Tobler, 1984; Tobler and Borbely, 1985; Goldshmid et al., 2004). The zebrafish has been established as a promising model for sleep and sleep disorder research (Zhdanova et al., 2001; Prober et al., 2006; Yokogawa et al., 2007; Appelbaum et al., 2009; Rihel et al., 2010; Sigurgeirsson et al., 2011; Elbaz et al., 2012). Since its small size and the water habitat preclude EEG measurements, behavioral criteria are used to distinguish sleep and wake states in zebrafish. Notably, in infant mammals, before the differentiation of EEG (when sleep state-dependent neocortical activity is absent), sleep is reliably characterized by the presence of tonic and phasic muscle tone (Karlsson and Blumberg, 2005; Karlsson et al., 2005). Therefore, as determined for other small non-mammalian species (Hendricks et al., 2000; Raizen et al., 2008), the key behavioral criteria for sleep are: (1) a period of immobility that is associated with a specific posture; (2) quick reversibility to wakefulness (distinguishes sleep from coma or hibernation); (3) increased arousal threshold to external stimuli (indication of low level of sensory awareness); (4) sleep-rebound after SD (indication of homeostatic regulation), and (5) preference for nocturnal or diurnal sleep (indication of circadian regulation) (Zimmerman et al., 2008). These behavioral criteria were used to show that a minimum of 1 min of immobility is associated with elevated arousal threshold and a sleep-like state in 5–7 dpf larvae (Prober et al., 2006; Elbaz et al., 2012). In these studies, arousal was stimulated by pulses of light, a procedure which may not be ideal because retinal responsiveness is reduced at night (Emran et al., 2010). However, responsiveness to changes in light intensity is also mediated by extra-retinal photoreceptors (Fernandes et al., 2012). In adults, an electrical stimulus, rather than light, was used to set the arousal threshold and define sleep as a minimum of 6 sec of immobility (Yokogawa et al., 2007). Thus, as in the fly where 5 min of immobility was defined as a sleep-like state (Hendricks et al., 2000), an array of behavioral experiments was used to define sleep in zebrafish. However, since EEG is not applicable in zebrafish, additional techniques should be applied to differentiate rest from sleep. For example, sleep in zebrafish was also studied using *c-fos* expression (Appelbaum et al., 2010; Elbaz

et al., 2012), a well-established marker for wakefulness (Cirelli and Tononi, 2000). Recently developed techniques for measuring neuron activity via genetically encoded calcium sensors in the whole brain of live larvae (Ahrens et al., 2012) or by rapid bioluminescent signals in genetically specified neurons of free swimming zebrafish (Naumann et al., 2010) promise to provide a causal link between neural activity and the state of sleep or wakefulness.

HOMEOSTATIC AND CIRCADIAN REGULATION OF SLEEP IN ZEBRAFISH

Adult zebrafish sleep mainly during the night under both LD and DD, indicating circadian clock regulation of the sleep/wake cycle. In contrast, under LL, light seems to suppress sleep, and rhythms of sleep/wake behavior disappear, reflecting the masking effect of light. Indeed, in adults kept under LL, sleep-like behavior could be noted only after 1 week (Yokogawa et al., 2007). Similarly, zebrafish larvae also demonstrate a rhythmic sleep/wake cycle, under LD (Elbaz et al., 2012). However, the sleep/wake cycle was not examined in larvae under constant conditions. Here, we show circadian rhythms of sleep/wake cycles under constant dim light, indicating that sleep is regulated by the circadian clock in 6–8 dpf larvae (**Figure 1A**).

The timing of sleep is mainly controlled by the circadian clock, however, in all animals sleep is also regulated by a homeostatic mechanism. SD is followed by sleep-rebound that is independent of the circadian time. This has been revealed in studies of adult zebrafish that were sleep deprived by electrical stimulation during the 6 h of the dark prior to usual light onset, and then released into the subjective day. Under the dark, a sleep-rebound was observed, indicating homeostatic regulation of sleep (Yokogawa et al., 2007). Homeostatic control of sleep in zebrafish larvae was first demonstrated by Zhdanova and colleagues. Six hours of SD, induced by constant vibration, increased sleep time during the following subjective day (Zhdanova et al., 2001). More recently, a similar but more moderate protocol was used to uncovered a subtle behavioral phenotype in a zebrafish model for narcolepsy (Elbaz et al., 2012).

NEURAL NETWORKS THAT REGULATE SLEEP AND WAKEFULNESS IN ZEBRAFISH

Several networks regulate sleep and wakefulness in mammals including aminergic, cholinergic, GABAergic and hypocretinergic systems. The organization and role of these networks is conserved in zebrafish (Panula et al., 2010). Furthermore, the zebrafish offers many advantages for high throughput, whole animal pharmacological screens since compounds can be delivered easily by simply dissolving them into the culture water of individual embryos (Rihel et al., 2010). Thus, the zebrafish larva emerges as a promising model to dissect the neuronal networks that regulate sleep using chemical genetics and to search for putative pharmacological sleep regulators.

The HCRT is an example of a neuronal network that has been a subject of intense studies in zebrafish, primarily because of its association with narcolepsy. Only 16–40 HCRT neurons, located in the lateral hypothalamus, innervate wide areas within the zebrafish brain (Kaslin et al., 2004; Faraco et al., 2006; Prober et al., 2006; Yokogawa et al., 2007; Appelbaum et al., 2009). To understand the role of HCRT in zebrafish, several genetic strategies have been developed including inducible global HCRT overexpression (Prober et al., 2006), mutation of the HCRT receptor, HCRTR (Yokogawa et al., 2007), expression of the Ca^{2+}-sensitive photoprotein GFP-apoAequorin in HCRT neurons (Naumann et al., 2010), and genetic ablation of HCRT neurons (Elbaz et al., 2012). These studies have showed that HCRT neurons regulate both wake and sleep and are most important during sleep/wake transitions (**Table 1**). Interestingly, HCRT neuron-ablated larvae increase sleep during the day and demonstrate fragmented sleep during the night, consistent with the results observed under HCRT overexpression and HCRTR mutation, respectively (**Table 1**). This function may be mediated by a hypothalamic-pineal gland circuit, which regulates HCRT and melatonin secretion (Appelbaum et al., 2009).

CIRCADIAN AND HOMEOSTATIC SLEEP-DEPENDENT CONTROL OF STRUCTURAL SYNAPTIC PLASTICITY

To synchronize physiology and behavior with the daily cycle, the circadian clock acts at different levels, ranging from the control of rhythmic gene expression, protein degradation and transportation, to the modification of the structure of neuronal circuits and synapses. While circadian control of the expression of genes and proteins has been studied extensively (Bass and Takahashi, 2010), data on the circadian regulation of synaptic plasticity and how this, in turn, controls circuit function and rhythmic behavior is limited (Frenkel and Ceriani, 2011). Species with a simple nervous system provide an ideal platform to study rhythmic structural synaptic plasticity that is associated with behavior (Wang et al., 2011). "Structural" synaptic plasticity is defined here as changes in the size, shape, orientation, and number of inhibitory or excitatory synapses. In *Drosophila*, several studies have demonstrated that the circadian clock controls daily changes in neuronal and synaptic structure (Mehnert et al., 2007; Fernandez et al., 2008; Pyza and Gorska-Andrzejak, 2008; Damulewicz and Pyza, 2011). It is imperative that findings in the fruit fly are extended to assess the regulation and role of rhythmic structural synaptic plasticity in vertebrate models where it is possible to monitor multiple excitatory and inhibitory neuronal circuits in live animals. The genetic and live imaging tools available for the zebrafish make this model particularly attractive for this task. Indeed, using synaptic fluorescence markers (Niell et al., 2004; Meyer and Smith, 2006) and time-lapse two photon imaging, rhythmic synaptic plasticity was monitored in live larvae. Visualizing synapses in transgenic lines that express the pre-synaptic protein, synaptophysin (SYP), fused to EGFP, revealed that the number of synapses along HCRT axons follow a diurnal rhythm under both LD and DD conditions (Appelbaum et al., 2010). This data suggest that the circadian clock regulate structural synaptic plasticity, a hypothesis that can be directly tested in zebrafish mutants for clock genes.

Although the data above indicate circadian control of structural synaptic plasticity, homeostatic sleep-dependent process should also be considered as regulators of rhythmic neuronal plasticity. In flies, brain-wide quantification of proteins that are associated with synaptic potentiation and circuit-specific imaging of synaptic terminals showed that the levels of synaptic components are high during wakefulness and low during

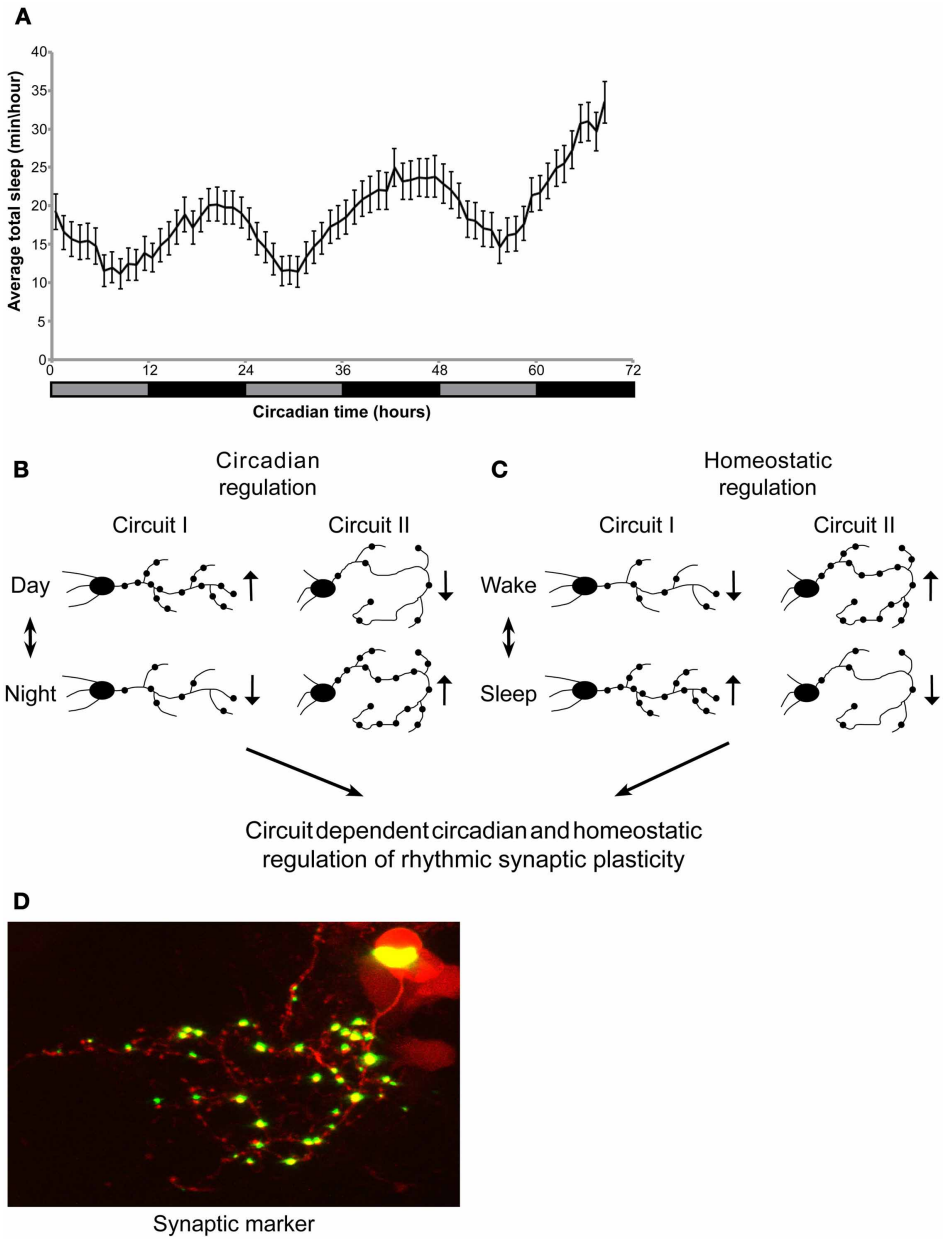

FIGURE 1 | Circadian regulation of sleep in larvae. Circadian and homeostatic (sleep-dependent) regulation of circuit-dependent rhythmic structural synaptic plasticity. (A) Zebrafish larvae were kept under LD for 6 days. At 6-8 dpf, sleep was monitored under constant dim light for three consecutive days (gray and black bar represent subjective day and night, respectively). Sleep was defined and monitored as previously described (Elbaz et al., 2012). Sleep time was rhythmic and peaked during the night ($n = 55$). **(B,C)** A proposed model demonstrating circadian and sleep/wake regulation of structural synaptic plasticity in the brain. Rhythmicity of synapse number, size and location is affected by: **(B)** the circadian clock **(C)** homeostatic process (sleep and wake). **(B)** While the number of synapses in a given circuit I increase during the day, the circadian clock could drive, at the same time, a reduction in synapse number in circuit II. **(C)** In parallel, homeostatic process controls the number of synapses in both circuits I and II. These two processes may be opposed or additive. Thus, the identity and role of a specific circuit determines its relative regulation by the circadian and homeostatic processes. **(D)** Imaging of synaptic fluorescence marker in live zebrafish larvae. This technique enables monitoring of structural synaptic plasticity in specific circuit during day and night, sleep and wakefulness.

sleep (Donlea et al., 2009; Gilestro et al., 2009). In zebrafish, two-photon imaging of fluorescent synaptic markers revealed that rhythms of structural synaptic plasticity in HCRT axons are mainly regulated by the circadian clock. Nevertheless, a minor, yet significant effect of SD on synapse number was also demonstrated, indicating a homeostatic control of synaptic density (Appelbaum et al., 2010). To further understand the effect of sleep on brain plasticity, time-lapse imaging of several circuits under sleep-promoting drugs or in genetically manipulated sleep mutants, such as the HCRT neuron-ablated larvae

Table 1 | HCRT neurons control behavioral sleep-wake transitions.

Genetic manipulation	Developmental stage	Circadian time	Sleep time	Sleep/Wake transitions	References
HCRT mRNA over-expression	Larvae	Day	⮟	⮟	Prober et al., 2006
		Night	⮟	⮟	
HCRT receptor mutant	Adult	Day	n.e.	n.e.	Yokogawa et al., 2007
		Night	⮟	⮝	
HCRT neuron-ablation	Larvae	Day	⮝	⮝	Elbaz et al., 2012
		Night	n.e.	⮝	

HCRT over-expression in larvae reduced sleep time and sleep-wake transitions both during the day and night (Prober et al., 2006). In the adult HCRT receptor mutant (HCRTR$^{-/-}$; Yokogawa et al., 2007), sleep time was reduced and fragmented during the night. However, during the day no effect (n.e.) on sleep was observed. In both cases, genetic manipulation of the HCRT system altered sleep/wake transitions, and the apparent contradictory effect on sleep time may reflect larval vs. adult behavior. In agreement with these observations, ablation of HCRT neurons increased sleep during the day, and increase sleep/wake transitions during day and night (Elbaz et al., 2012). Thus, the most profound and consistent behavioral role of HCRT neurons is the regulation of behavioral sleep/wake state transitions. Indeed, HCRT neurons are most active during the transition in locomotor activity (Naumann et al., 2010).

(that demonstrate fragmented sleep, Elbaz et al., 2012), could provide significant data that link the sleep/wake cycle with circuit modifications. Based on the current limited data, we proposed a model for combined circadian and homeostatic regulation of rhythmic structural synaptic plasticity. The balance between these processes is expected to vary significantly among circuits and may be opposed or additive, depending on the role of the specific circuit. For example, brain regions, such as the hypothalamus, that regulate fundamental behavioral rhythms (such as feeding, sleep, and wake activity) would exhibit mainly clock-controlled synaptic plasticity with minor homeostatic effect (as for the HCRT axons, Appelbaum et al., 2010). In contrast, brain regions that mediate experience-dependent behavior (such as learning and memory) would demonstrate mainly sleep-dependent structural synaptic plasticity (**Figures 1B–D**). Thus, the brain undergoes significant circuit and synaptic changes during the circadian cycle as well as during sleep and wake episodes.

FUTURE DIRECTIONS AND CONCLUDING REMARKS

Clearly advances in genetic and imaging tools will play a key role in the future application of zebrafish to study sleep and clock regulation within the nervous system. Genetic bipartite methods for refined neuronal gene targeting, such as the UAS/Gal4 system, are routinely used in zebrafish (Scott et al., 2007; Asakawa and Kawakami, 2008; Vatine et al., 2013). Application of this technique to image synapses in many brain circuits will provide a powerful future approach. Real-time imaging of synaptic markers in a specific circuit in the zebrafish brain during day and night and after SD will shed light on how circadian and homeostatic processes regulate synaptic plasticity. A limitation of this approach is that anatomical changes of fluorescence synaptic markers do not necessarily represent synaptic transmission and neuronal activity. Monitoring structural synaptic plasticity in correlation with behavior in the same individual fish can partially overcome this limitation. Moreover, imaging of genetically modified calcium indicators fused to synaptic markers (Dreosti et al., 2009) that can identify locations and activity of synapses, simultaneously, in the living animal, could provide a complete solution.

What is so important about sleep that warrants the risk of being at a reduced state of awareness? To answer this fundamental question, a critical challenge is to visualize circadian- and sleep-related circuits in the living brain, which contains an incomprehensible, dense population of sleep and wake regulatory neurons and their processes. The zebrafish is a vertebrate model, which provides a unique opportunity to look into a relatively simple nervous system, which retains the fundamental sleep- and clock-regulating circuits.

ACKNOWLEDGMENTS

Lior Appelbaum is supported by Grant 366/11 from the Israel Science Foundation, by Grant 398/11 from the Legacy Heritage biomedical program of the Israel Science Foundation, by Grant 2011335 from the US-Israel Binational Science Foundation, and by the Marie Curie Actions-International Reintegration grants FP7-PEOPLE-2010-RG 274333. Yoav Gothilf is supported by Grant 1084/12 from the Israel Science Foundation, Jerusalem, and by Grant 2009290 from the US-Israel Binational Science Foundation. Nicholas S. Foulkes is funded by the BioInterfaces Programme of the Helmholtz association. We thank Dr. Adi Tovin for technical assistance.

REFERENCES

Adamantidis, A., and De Lecea, L. (2008). Sleep and metabolism: shared circuits, new connections. *Trends Endocrinol. Metab.* 19, 362–370.

Ahrens, M. B., Li, J. M., Orger, M. B., Robson, D. N., Schier, A. F., Engert, F., et al. (2012). Brain-wide neuronal dynamics during motor adaptation in zebrafish. *Nature* 485, 471–477.

Appelbaum, L., Wang, G., Yokogawa, T., Skariah, G. M., Smith, S. J., Mourrain, P., et al. (2010). Circadian and homeostatic regulation of structural synaptic plasticity in hypocretin neurons. *Neuron* 68, 87–98.

Appelbaum, L., Wang, G. X., Maro, G. S., Mori, R., Tovin, A., Marin, W., et al. (2009). Sleep-wake regulation and hypocretin-melatonin interaction in zebrafish. *Proc. Natl. Acad. Sci. U.S.A.* 106, 21942–21947.

Asakawa, K., and Kawakami, K. (2008). Targeted gene expression by the Gal4-UAS system in zebrafish. *Dev. Growth Differ.* 50, 391–399.

Bass, J., and Takahashi, J. S. (2010). Circadian integration of metabolism and energetics. *Science* 330, 1349–1354.

Cahill, G. M. (1996). Circadian regulation of melatonin production in cultured zebrafish pineal and retina. *Brain Res.* 708, 177–181.

Cahill, G. M., Hurd, M. W., and Batchelor, M. M. (1998). Circadian

rhythmicity in the locomotor activity of larval zebrafish. *Neuroreport* 9, 3445–3449.

Campbell, S. S., and Tobler, I. (1984). Animal sleep: a review of sleep duration across phylogeny. *Neurosci. Biobehav. Rev.* 8, 269–300.

Carnevali, O., Gioacchini, G., Maradonna, F., Olivotto, I., and Migliarini, B. (2011). Melatonin induces follicle maturation in Danio rerio. *PLoS ONE* 6:e19978. doi: 10.1371/journal.pone.0019978

Carr, A. J., Tamai, T. K., Young, L. C., Ferrer, V., Dekens, M. P., and Whitmore, D. (2006). Light reaches the very heart of the zebrafish clock. *Chronobiol. Int.* 23, 91–100.

Cirelli, C. (2009). The genetic and molecular regulation of sleep: from fruit flies to humans. *Nat. Rev. Neurosci.* 10, 549–560.

Cirelli, C., and Tononi, G. (2000). On the functional significance of c-fos induction during the sleep-waking cycle. *Sleep* 23, 453–469.

Cirelli, C., and Tononi, G. (2008). Is sleep essential? *PLoS Biol.* 6:e216. doi: 10.1371/journal.pbio.0060216

Damulewicz, M., and Pyza, E. (2011). The clock input to the first optic neuropil of Drosophila melanogaster expressing neuronal circadian plasticity. *PLoS ONE* 6:e21258. doi: 10.1371/journal.pone.0021258

Donlea, J. M., Ramanan, N., and Shaw, P. J. (2009). Use-dependent plasticity in clock neurons regulates sleep need in Drosophila. *Science* 324, 105–108.

Dreosti, E., Odermatt, B., Dorostkar, M. M., and Lagnado, L. (2009). A genetically encoded reporter of synaptic activity *in vivo*. *Nat. Methods* 6, 883–889.

Elbaz, I., Yelin-Bekerman, L., Nicenboim, J., Vatine, G., and Appelbaum, L. (2012). Genetic ablation of hypocretin neurons alters behavioral state transitions in zebrafish. *J. Neurosci.* 32, 12961–12972.

Emran, F., Rihel, J., Adolph, A. R., and Dowling, J. E. (2010). Zebrafish larvae lose vision at night. *Proc. Natl. Acad. Sci. U.S.A.* 107, 6034–6039.

Faraco, J. H., Appelbaum, L., Marin, W., Gaus, S. E., Mourrain, P., and Mignot, E. (2006). Regulation of hypocretin (orexin) expression in embryonic zebrafish. *J. Biol. Chem.* 281, 29753–29761.

Fernandes, A. M., Fero, K., Arrenberg, A. B., Bergeron, S. A., Driever, W., and Burgess, H. A. (2012). Deep brain photoreceptors control light-seeking behavior in zebrafish larvae. *Curr. Biol.* 22, 2042–2047.

Fernandez, M. P., Berni, J., and Ceriani, M. F. (2008). Circadian remodeling of neuronal circuits involved in rhythmic behavior. *PLoS Biol.* 6:e69. doi: 10.1371/journal.pbio.0060069

Frenkel, L., and Ceriani, M. F. (2011). Circadian plasticity: from structure to behavior. *Int. Rev. Neurobiol.* 99, 107–138.

Gilestro, G. F., Tononi, G., and Cirelli, C. (2009). Widespread changes in synaptic markers as a function of sleep and wakefulness in Drosophila. *Science* 324, 109–112.

Goldshmid, R., Holzman, R., Weihs, D., and Genin, A. (2004). Aeration of corals by sleep-swimming fish. *Limnol. Oceanogr.* 49, 1832–1839.

Gothilf, Y., Coon, S. L., Toyama, R., Chitnis, A., Namboodiri, M. A., and Klein, D. C. (1999). Zebrafish serotonin N-acetyltransferase-2: marker for development of pineal photoreceptors and circadian clock function. *Endocrinology* 140, 4895–4903.

Granados-Fuentes, D., and Herzog, E. D. (2012). The clock shop: coupled circadian oscillators. *Exp. Neurol.* doi: 10.1016/j.expneurol.2012.10.011. [Epub ahead of print].

Hartse, K. M. (2011). The phylogeny of sleep. *Handb. Clin. Neurol.* 98, 97–109.

Hendricks, J. C., Finn, S. M., Panckeri, K. A., Chavkin, J., Williams, J. A., Sehgal, A., et al. (2000). Rest in Drosophila is a sleep-like state. *Neuron* 25, 129–138.

Hurd, M. W., and Cahill, G. M. (2002). Entraining signals initiate behavioral circadian rhythmicity in larval zebrafish. *J. Biol. Rhythms* 17, 307–314.

Hurd, M. W., Debruyne, J., Straume, M., and Cahill, G. M. (1998). Circadian rhythms of locomotor activity in zebrafish. *Physiol. Behav.* 65, 465–472.

Karlsson, K. A., and Blumberg, M. S. (2005). Active medullary control of atonia in week-old rats. *Neuroscience* 130, 275–283.

Karlsson, K. A., Gall, A. J., Mohns, E. J., Seelke, A. M., and Blumberg, M. S. (2005). The neural substrates of infant sleep in rats. *PLoS Biol.* 3:e143. doi: 10.1371/journal.pbio.0030143

Kaslin, J., Nystedt, J. M., Ostergard, M., Peitsaro, N., and Panula, P. (2004). The orexin/hypocretin system in zebrafish is connected to the aminergic and cholinergic systems. *J. Neurosci.* 24, 2678–2689.

Kazimi, N., and Cahill, G. M. (1999). Development of a circadian melatonin rhythm in embryonic zebrafish. *Brain Res. Dev. Brain Res.* 117, 47–52.

Lin, L., Faraco, J., Li, R., Kadotani, H., Rogers, W., Lin, X., et al. (1999). The sleep disorder canine narcolepsy is caused by a mutation in the hypocretin (orexin) receptor 2 gene. *Cell* 98, 365–376.

Mehnert, K. I., Beramendi, A., Elghazali, F., Negro, P., Kyriacou, C. P., and Cantera, R. (2007). Circadian changes in Drosophila motor terminals. *Dev. Neurobiol.* 67, 415–421.

Meyer, M. P., and Smith, S. J. (2006). Evidence from *in vivo* imaging that synaptogenesis guides the growth and branching of axonal arbors by two distinct mechanisms. *J. Neurosci.* 26, 3604–3614.

Mignot, E. (2008). Why we sleep: the temporal organization of recovery. *PLoS Biol.* 6:e106. doi: 10.1371/journal.pbio.0060106

Morris, C. J., Aeschbach, D., and Scheer, F. A. (2012). Circadian system, sleep and endocrinology. *Mol. Cell. Endocrinol.* 349, 91–104.

Naumann, E. A., Kampff, A. R., Prober, D. A., Schier, A. F., and Engert, F. (2010). Monitoring neural activity with bioluminescence during natural behavior. *Nat. Neurosci.* 13, 513–520.

Niell, C. M., Meyer, M. P., and Smith, S. J. (2004). *In vivo* imaging of synapse formation on a growing dendritic arbor. *Nat. Neurosci.* 7, 254–260.

Nishino, S., and Sakurai, T. (2006). *The Orexin/Hypocretin System: Physiology and Pathophysiology*. Towota, NJ: Humana Press.

Noche, R. R., Lu, P. N., Goldstein-Kral, L., Glasgow, E., and Liang, J. O. (2011). Circadian rhythms in the pineal organ persist in zebrafish larvae that lack ventral brain. *BMC Neurosci.* 12:7. doi: 10.1186/1471-2202-12-7.

Pando, M. P., Pinchak, A. B., Cermakian, N., and Sassone-Corsi, P. (2001). A cell-based system that recapitulates the dynamic light-dependent regulation of the vertebrate clock. *Proc. Natl. Acad. Sci. U.S.A.* 98, 10178–10183.

Panula, P. (2010). Hypocretin/orexin in fish physiology with emphasis on zebrafish. *Acta Physiol. (Oxf.)* 198, 381–386.

Panula, P., Chen, Y. C., Priyadarshini, M., Kudo, H., Semenova, S., Sundvik, M., et al. (2010). The comparative neuroanatomy and neurochemistry of zebrafish CNS systems of relevance to human neuropsychiatric diseases. *Neurobiol. Dis.* 40, 46–57.

Piccinetti, C. C., Migliarini, B., Olivotto, I., Coletti, G., Amici, A., and Carnevali, O. (2010). Appetite regulation: the central role of melatonin in Danio rerio. *Horm. Behav.* 58, 780–785.

Prober, D. A., Rihel, J., Onah, A. A., Sung, R. J., and Schier, A. F. (2006). Hypocretin/orexin overexpression induces an insomnia-like phenotype in zebrafish. *J. Neurosci.* 26, 13400–13410.

Pyza, E., and Gorska-Andrzejak, J. (2008). External and internal inputs affecting plasticity of dendrites and axons of the fly's neurons. *Acta Neurobiol. Exp. (Wars)* 68, 322–333.

Raizen, D. M., Zimmerman, J. E., Maycock, M. H., Ta, U. D., You, Y. J., Sundaram, M. V., et al. (2008). Lethargus is a Caenorhabditis elegans sleep-like state. *Nature* 451, 569–572.

Rawashdeh, O., De Borsetti, N. H., Roman, G., and Cahill, G. M. (2007). Melatonin suppresses nighttime memory formation in zebrafish. *Science* 318, 1144–1146.

Reppert, S. M., Perlow, M. J., Ungerleider, L. G., Mishkin, M., Tamarkin, L., Orloff, D. G., et al. (1981). Effects of damage to the suprachiasmatic area of the anterior hypothalamus on the daily melatonin and cortisol rhythms in the rhesus monkey. *J. Neurosci.* 1, 1414–1425.

Rihel, J., Prober, D. A., Arvanites, A., Lam, K., Zimmerman, S., Jang, S., et al. (2010). Zebrafish behavioral profiling links drugs to biological targets and rest/wake regulation. *Science* 327, 348–351.

Saper, C. B., Scammell, T. E., and Lu, J. (2005). Hypothalamic regulation of sleep and circadian rhythms. *Nature* 437, 1257–1263.

Scott, E. K., Mason, L., Arrenberg, A. B., Ziv, L., Gosse, N. J., Xiao, T., et al. (2007). Targeting neural circuitry in zebrafish using GAL4 enhancer trapping. *Nat. Methods* 4, 323–326.

Sehgal, A., and Mignot, E. (2011). Genetics of sleep and sleep disorders. *Cell* 146, 194–207.

Shapiro, C. M., and Hepburn, H. R. (1976). Sleep in a schooling fish, Tilapia mossambica. *Physiol. Behav.* 16, 613–615.

Siegel, J. M. (2005). Clues to the functions of mammalian sleep. *Nature* 437, 1264–1271.

Sigurgeirsson, B., Thornorsteinsson, H., Arnardottir, H., Johannesdottir, I. T., and Karlsson, K. A. (2011). Effects of modafinil on sleep-wake cycles in larval zebrafish. *Zebrafish* 8, 133–140.

Tamai, T. K., Carr, A. J., and Whitmore, D. (2005). Zebrafish circadian clocks: cells that see light. *Biochem. Soc. Trans.* 33, 962–966.

Tamai, T. K., Young, L. C., and Whitmore, D. (2007). Light signaling to the zebrafish circadian clock by Cryptochrome 1a. *Proc. Natl. Acad. Sci. U.S.A.* 104, 14712–14717.

Tauber, E., Weitzman, E., and Korey, S. (1969). Eye movements during behavioral inactivity in certain Bermuda reef fish. *Commun. Behav. Biol.* 3, 131–135.

Tobler, I., and Borbely, A. A. (1985). Effect of rest deprivation on motor activity of fish. *J. Comp. Physiol. A* 157, 817–822.

Tononi, G., and Cirelli, C. (2006). Sleep function and synaptic homeostasis. *Sleep Med. Rev.* 10, 49–62.

Tovin, A., Alon, S., Ben-Moshe, Z., Mracek, P., Vatine, G., Foulkes, N. S., et al. (2012). Systematic identification of rhythmic genes reveals *camk1gb* as a new element in the circadian clockwork. *PLoS Genet.* 8:e1003116. doi: 10.1371/journal.pgen.1003116

Vallone, D., Gondi, S. B., Whitmore, D., and Foulkes, N. S. (2004). E-box function in a period gene repressed by light. *Proc. Natl. Acad. Sci. U.S.A.* 101, 4106–4111.

Vallone, D., Lahiri, K., Dickmeis, T., and Foulkes, N. S. (2005). Zebrafish cell clocks feel the heat and see the light! *Zebrafish* 2, 171–187.

Vatine, G., Vallone, D., Appelbaum, L., Mracek, P., Ben-Moshe, Z., Lahiri, K., et al. (2009). Light directs zebrafish period2 expression via conserved D and E boxes. *PLoS Biol.* 7:e1000223. doi: 10.1371/journal.pbio.1000223

Vatine, G., Vallone, D., Gothilf, Y., and Foulkes, N. S. (2011). It's time to swim! Zebrafish and the circadian clock. *FEBS Lett.* 585, 1485–1494.

Vatine, G. D., Zada, D., Lerer-Goldshtein, T., Tovin, A., Malkinson, G., Yaniv, K., et al. (2013). Zebrafish as a model for monocarboxyl transporter 8-deficiency. *J. Biol. Chem.* 288, 169–180.

Vuilleumier, R., Besseau, L., Boeuf, G., Piparelli, A., Gothilf, Y., Gehring, W. G., et al. (2006). Starting the zebrafish pineal circadian clock with a single photic transition. *Endocrinology* 147, 2273–2279.

Wang, G., Grone, B., Colas, D., Appelbaum, L., and Mourrain, P. (2011). Synaptic plasticity in sleep: learning, homeostasis and disease. *Trends Neurosci.* 34, 452–463.

Whitmore, D., Foulkes, N. S., and Sassone-Corsi, P. (2000). Light acts directly on organs and cells in culture to set the vertebrate circadian clock. *Nature* 404, 87–91.

Yokogawa, T., Marin, W., Faraco, J., Pezeron, G., Appelbaum, L., Zhang, J., et al. (2007). Characterization of sleep in zebrafish and insomnia in hypocretin receptor mutants. *PLoS Biol.* 5:e277. doi: 10.1371/journal.pbio.0050277

Zhdanova, I. V. (2005). Melatonin as a hypnotic: pro. *Sleep Med. Rev.* 9, 51–65.

Zhdanova, I. V. (2011). Sleep and its regulation in zebrafish. *Rev. Neurosci.* 22, 27–36.

Zhdanova, I. V., Wang, S. Y., Leclair, O. U., and Danilova, N. P. (2001). Melatonin promotes sleep-like state in zebrafish. *Brain Res.* 903, 263–268.

Zimmerman, J. E., Naidoo, N., Raizen, D. M., and Pack, A. I. (2008). Conservation of sleep: insights from non-mammalian model systems. *Trends Neurosci.* 31, 371–376.

Ziv, L., Levkovitz, S., Toyama, R., Falcon, J., and Gothilf, Y. (2005). Functional development of the zebrafish pineal gland: light-induced expression of period2 is required for onset of the circadian clock. *J. Neuroendocrinol.* 17, 314–320.

Conflict of Interest Statement: The authors declare that the research was conducted in the absence of any commercial or financial relationships that could be construed as a potential conflict of interest.

Received: 30 November 2012; paper pending published: 15 December 2012; accepted: 15 January 2013; published online: 01 February 2013.

Citation: Elbaz I, Foulkes NS, Gothilf Y and Appelbaum L (2013) Circadian clocks, rhythmic synaptic plasticity and the sleep-wake cycle in zebrafish. Front. Neural Circuits 7:9. doi: 10.3389/fncir.2013.00009

frontiers in
NEURAL CIRCUITS

HYPOTHESIS AND THEORY ARTICLE
published: 24 April 2013
doi: 10.3389/fncir.2013.00076

Imaging zebrafish neural circuitry from whole brain to synapse

Louis C. Leung*, Gordon X. Wang and Philippe Mourrain*

Department of Psychiatry and Behavioral Sciences, Center for Sleep Sciences, Beckman Center, Stanford University, Palo Alto, CA, USA

Edited by:
German Sumbre, École Normale Supérieure, France

Reviewed by:
Ruben Portugues, Harvard University, USA
Lior Appelbaum, Bar Ilan University, Israel
Limor Ziv, Sheba Medical Center, Israel

****Correspondence:***
Louis C. Leung and Philippe Mourrain, Department of Psychiatry and Behavioral Sciences, Center for Sleep Sciences, Beckman Center, Stanford University, 279 Campus Drive, Room B201, Stanford, CA 94305, USA.
e-mail: llcy@stanford.edu; mourrain@stanford.edu

Recent advances in imaging tools are inspiring zebrafish researchers to tackle ever more ambitious questions in the neurosciences. Behaviorally fundamental conserved neural networks can now be potentially studied using zebrafish from a brain-wide scale to molecular resolution. In this perspective, we offer a roadmap by which a zebrafish researcher can navigate the course from collecting neural activities across the brain associated with a behavior, to unraveling molecular identities and testing the functional relevance of active neurons. In doing so, important insights will be gained as to how neural networks generate behaviors and assimilate changes in synaptic connectivity.

Keywords: zebrafish, clinical neuroscience, psychiatry, calcium imaging, synapse imaging, array tomography, whole brain imaging

INTRODUCTION

One of the major goals of neuroscience is to understand how the nervous system, as a dynamic assembly of cells and connections, generates behaviors as a suite of motor outputs. Impressive progress has been made in recent times in understanding how the nervous system develops and functions. However, with the current set of animal models, neuroscience is approaching a problem of how one can simultaneously work and integrate data across the different scales and modalities at which one can interrogate brain function. To understand a neural process across the scales–from molecules, synapses, neurons, networks to whole brain–is a *bona fide* frontier in the neurosciences today.

Advances in functional neuroimaging are allowing us to identify with increasing precision which brain regions are correlated with a particular behavioral output. However, brain-wide visualization, permitted by electroencephalography (EEG) and functional magnetic resonance imaging (fMRI), does not reliably approach the cellular and/or synaptic spatial resolution of brain processing (Thai et al., 2009; Lenkov et al., 2012). Conversely, electrophysiological or high-resolution imaging methods to record neural activity are difficult to extend beyond discrete brain regions. To understand the neural basis of behavior, a challenging goal in basic and clinical neuroscience will be to bridge the gap between these distant levels–i.e., to be able to record and analyze the entire brain with single neuron, if not, single synapse accuracy. Here, we suggest that the recent developments in live whole brain Ca^{2+} imaging and super resolution array tomography (AT) can, when applied to a suitably compact brain (**Figure 1**), reveal and correlate whole brain activity maps down to circuit function and changes in the synaptic landscape. Already an established vertebrate model for developmental biology, the zebrafish's genetic toolbox and unique physical characteristics can now be exploited for the neurosciences.

THE ZEBRAFISH CAN BE A KEY BRIDGING MODEL FROM CIRCUIT TO MOLECULAR NEUROSCIENCE

As with other animal models, the zebrafish will never fully recapitulate the complex psyche and behaviors of humans. However, the fundamental computational units of brain processing are likely to be conserved and are thus well-studied outside the human brain in model organisms (Sengupta and Samuel, 2009; Bellen et al., 2010; Friedrich et al., 2010; Rinkwitz et al., 2011; Wang et al., 2011).The most common mammalian model used in neuroscience is the mouse, which offers a great variety of complex behaviors, powerful genetics and excellent *ex vivo* brain slice electrophysiological techniques (Kullander, 2005; Van Meer and Raber, 2005; Ward et al., 2011; Kim et al., 2013). However, attempting whole brain modeling with a mouse is a formidable challenge despite being three orders of magnitude smaller than an adult human brain, which has an estimated 10^{11} neurons each making around 10^4 connections (**Figure 1**). At this time, a genetic model with fewer neurons and a smaller, more accessible brain would be a more feasible option.

Zebrafish, sharing conserved neurochemistry and broad brain organization with their mammalian counterparts, may help to bridge this gap and give the first insights of circuit dynamics from whole brain down to molecular changes during conserved behaviors. Five key advantages of studying the zebrafish brain are its (i) compact size, (ii) conservation of the neuropeptide pool (in contrast to invertebrates), (iii) linear organization of brain regions, (iv) structural accessibility of internal nuclei (no overlaying neocortex), and (v) optical clarity (Akanji et al., 1990; Charonis et al.,

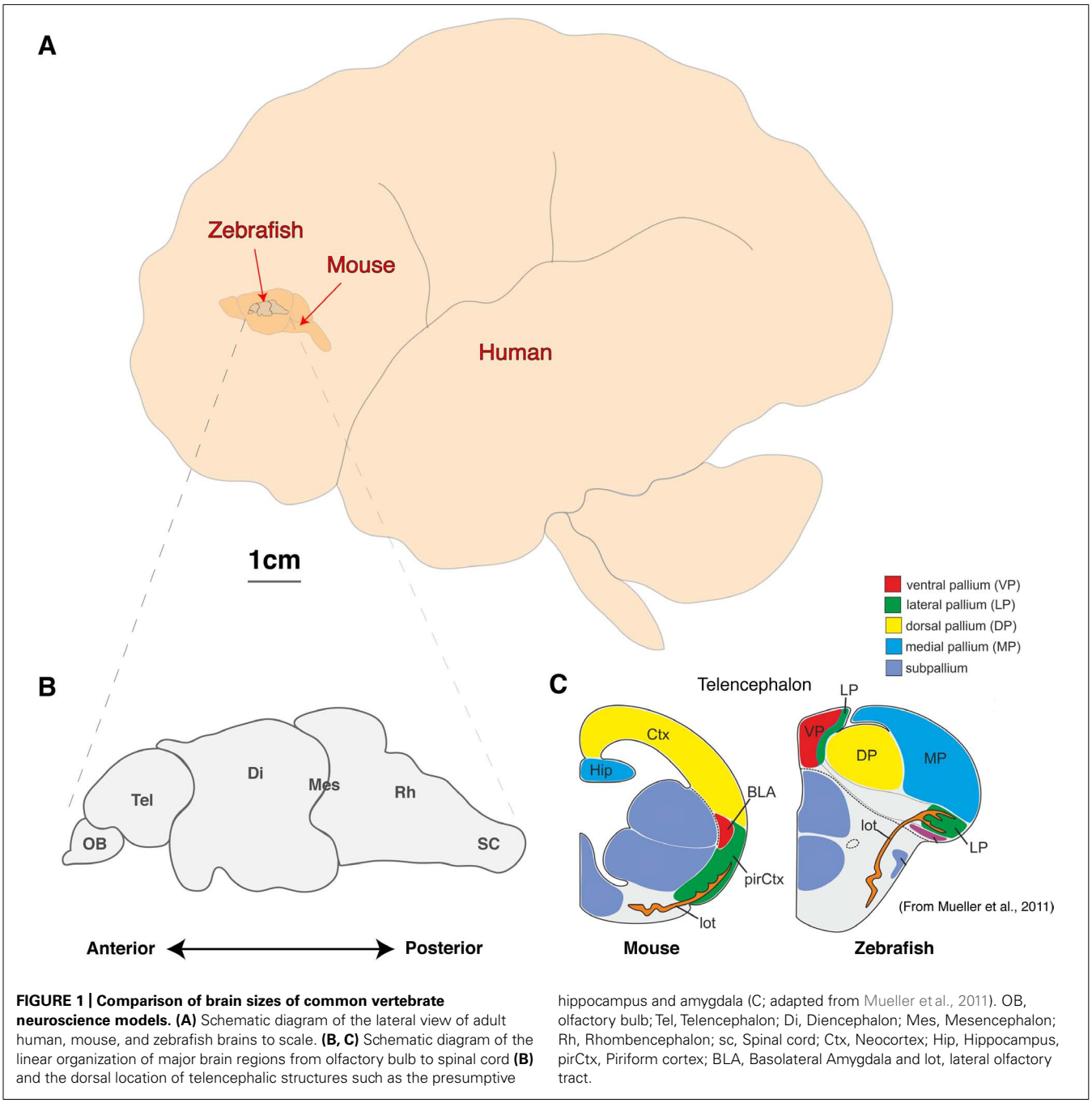

FIGURE 1 | Comparison of brain sizes of common vertebrate neuroscience models. (A) Schematic diagram of the lateral view of adult human, mouse, and zebrafish brains to scale. **(B, C)** Schematic diagram of the linear organization of major brain regions from olfactory bulb to spinal cord **(B)** and the dorsal location of telencephalic structures such as the presumptive hippocampus and amygdala (C; adapted from Mueller et al., 2011). OB, olfactory bulb; Tel, Telencephalon; Di, Diencephalon; Mes, Mesencephalon; Rh, Rhombencephalon; sc, Spinal cord; Ctx, Neocortex; Hip, Hippocampus, pirCtx, Piriform cortex; BLA, Basolateral Amygdala and lot, lateral olfactory tract.

1990; Appelbaum et al., 2009; Berman et al., 2009; Friedrich et al., 2010; Engert and Wilson, 2012). Particularly with respect to imaging dynamic processes, the zebrafish model uniquely excels as its brain is translucent and small enough that the entire volume can be captured at single cell resolution by standard microscopy magnifications. Even at 6 days old, this represents a formidable 100,000 neurons (Naumann et al., 2010), but the linear organization of the major brain regions from olfactory bulbs to spinal cord tip further facilitates brain-wide imaging (**Figure 1B**). In addition, while the amygdala, hippocampus and habenula are difficult regions to scan in mammals due to their deep location beneath the neocortex, their position is inverted in zebrafish. While the anterior neural tube of mammals undergoes invagination during development, leading to their deep location beneath the neocortex, the eversion process in the development offish telencephalic makes these behaviorally important structures the most dorsal nuclei of the telencephalon (**Figure 1C**; Northcutt, 2008; Mueller et al., 2011). Further, the ease of transgenesis, pharmacological studies, and conservation of behaviors (fear, anxiety, learning and memory, feeding/preying, social and sexual behavior, sleep and diurnality, etc.), altogether makes zebrafish a powerful complement to other models used to study neural processing fundamentals likely to be

conserved in humans. As we set out a roadmap below (**Figure 2**), we contend approaches using zebrafish could yield insights to coordinated brain activity and function that underpin the normal healthy brain and what goes awry in pathological contexts.

WHOLE BRAIN IMAGING OF NEURAL ACTIVITY

The ability to image dynamic cellular and subcellular processes during development has revolutionized the field of developmental biology, ever moving from analyzing fixed samples to dynamic processes in living animals (Huisken and Stainier, 2009; Leung et al., 2011; Randlett et al., 2011; Leung and Holt, 2012). Similarly, the central nervous system is also a highly dynamic entity and adopting methods to interrogate the neural activity of cells and networks at brain-wide, single cell resolution in the context of a behaving animal will be a turning point in systems neuroscience. To characterize the activity landscape of a brain at rest or engaged in a defined behavior on these scales, we suggest the minimum requirements are a neural marker of activity that can be used across the brain without *a priori* hypotheses and an appropriate method to record this activity over time in a specific animal. Following that, an ability to identify these active neurons molecularly is crucial for subsequent progress.

A popular method to mark active neurons involves sacrificing an animal while (or just after) it performs a behavior/process and post-stain for a genetic marker of neural activity-the immediate early genes [IEGs such as cFos and early growth response protein 1 (EGR-1)] – in whole or specific brain regions of interest.

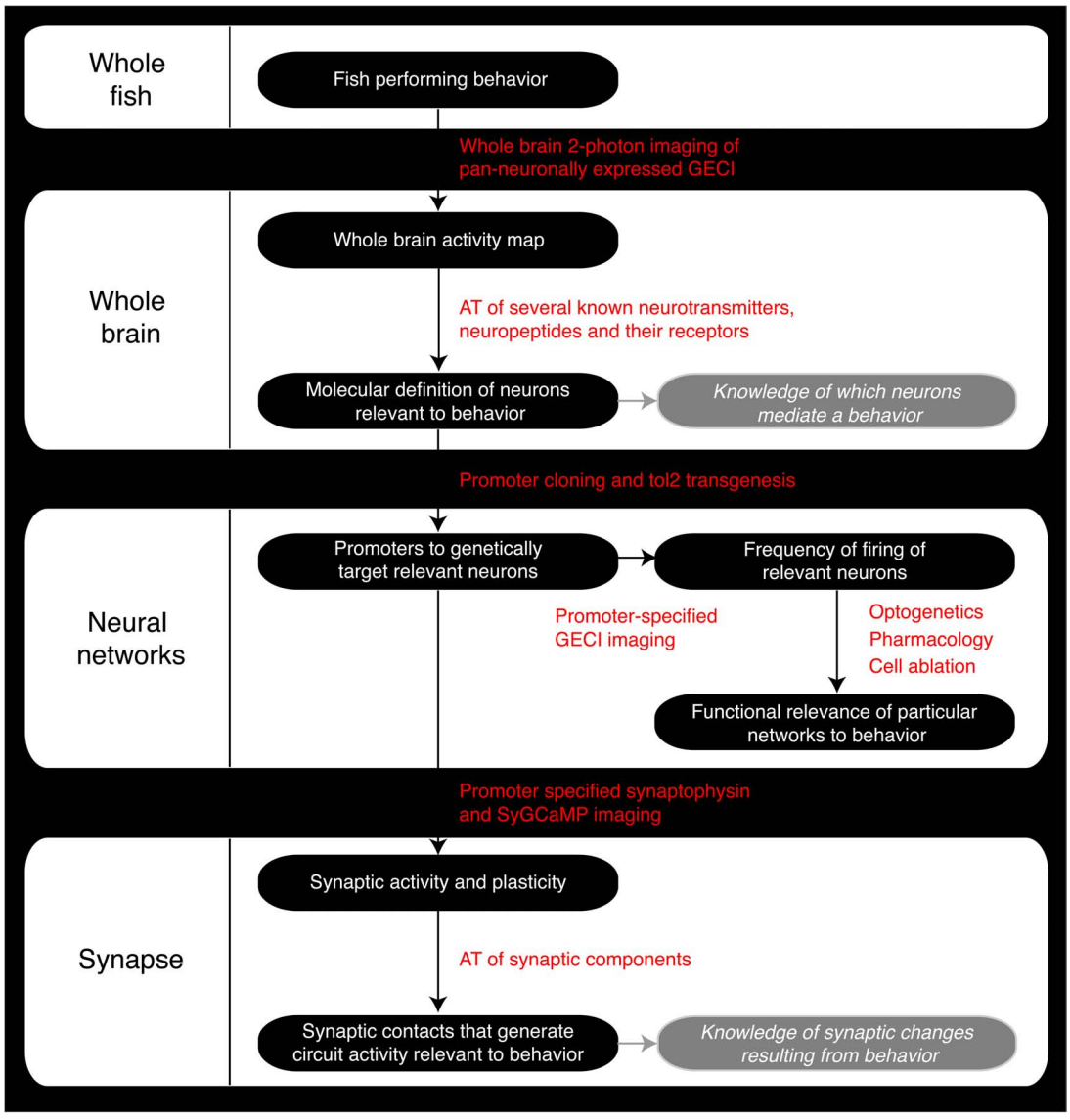

FIGURE 2 | Roadmap of the steps a zebrafish neuroscience researcher can take to integrate the various levels of analysis within the same model organism. GECI, Genetically encoded calcium indicator; AT, Array Tomography; tol2, Tol2 transposase; SyGCaMP, Synaptophysin-specific GCaMP sensor.

This has led to the identification of several nuclei involved in behavioral processes (Hoffman et al., 1993; Sherin et al., 1996; Murphy et al., 2004), but despite good correspondence with neural activity, methods using IEGs have their limitations. Firstly, it is possible that IEGs are only induced when neurons are highly/over activated. Indeed, it is likely that tonic or low firing neurons, which may also be important for a particular computation, may have little or no IEGs induced. Therefore, until further demonstrations of the degree of activation required to induce IEG expression are made, caution should be exercised in concluding that they mark the entire firing population involved in a process. Secondly, a single IEG like cFos is not pan neuronally expressed so it is unlikely to be the sole gene used by *all* the neurons active during a given behavior. Thirdly, there is important computational information encoded when neurons cease firing as opposed to when they become active, and no IEG currently reports the end of a period of activity. Finally, the fixation for IEG staining precludes dynamic information about activity and firing patterns which could provide a crucial handle on the processing and functions carried out by active neurons.

The development of genetically encoded Ca^{2+} indicators (GECIs) sets to solve many of these limitations and zebrafish is particularly suited to the use of GECIs with the ease of genetics/transgenesis and a translucent central nervous system. GECIs, such as GCaMP (Nakai et al., 2001; Muto et al., 2011, 2013) respond with changes in fluorescence intensity proportional to subcellular Ca^{2+} changes. In fact, the latest generation of GCaMPs have the ability to reliably indicate single action potential (AP) events and a whole library of versions exist to suit various potential uses (Akerboom et al., 2012; Ohkura et al., 2012) as well as Ca^{2+} sensors that operate at UV and red-shifted excitation wavelengths (Zhao et al., 2011; Akerboom et al., 2013). A further advantage of GECIs as compared to traditional electrophysiological recordings is their minimal invasiveness. A multi-electrode array that can discriminate spiking activity from a dozen neurons is prohibitively large for a zebrafish brain, while GECI imaging is completely non-invasive and can acquire spiking activity from hundreds of neurons from one image plane. Combined with pan-neuronal promoters and two-photon excitation microscopy, the monitoring of brain-wide neural activity during brain computations holds great potential (**Figure 3B**). By focusing excitation to small precise volumes in a tissue, two-photon imaging greatly reduces phototoxicity resulting from illumination of tissues above regions of interest typical of epifluorescent and confocal microscopy (Carvalho and Heisenberg, 2009). This permits longer term imaging of living samples than previously possible. An important advantage of operating in the infrared range is that the imaging also does not interfere with light-sensitive behaviors such as circadian and sleep rhythms (Appelbaum et al., 2010). Such excitation also confers benefits to the depth of tissue penetration and thus the imaging of deeper structures in the brain. To give an idea of scale, an entire 1 month juvenile fish brain has a thickness of ∼1 mm, which can be fully covered in depth with two-photon scanning. Indeed, the entire brain of a 7 dpf larva can be covered with few imaging frames, as has already been attempted with remarkable success even with the modestly sensitive GCaMP2 (Ahrens et al., 2012). Here, the larva's computations during changes in motor gain during fictive swimming were located without *a priori* assumptions to specific brain regions such as the inferior olivary complexes. With advanced microscopy, the possibility of whole brain imaging at single cell resolution at physiological frequencies is within reach to zebrafish researchers (Ahrens and Keller, 2013).The recent developments in imaging Ca^{2+} sensitive emitters of bioluminescence, such as green fluorescent protein (GFP)-aequorin, in freely behaving zebrafish offers further exciting avenues to complement GCaMP data of stabilized/paralyzed animals (Naumann et al., 2010). After gaining such volumes of information, the upcoming challenge with brain-wide "activity screens" will be to accurately define the neuronal populations of interest. Without accurate knowledge of the neuroanatomical location or access to specified circuits, this remains a challenging hurdle to a true understanding of circuit function.

IDENTIFYING MOLECULAR MARKERS WITH ARRAY TOMOGRAPHY

So how do we progress from locating the active nuclei correlated with particular behaviors and knowing their molecular identity? What method can provide this missing link? We propose the use of AT to take the same zebrafish that are used in Ca^{2+} imaging studies and perform a powerful spatial proteomic approach to gain the molecular identity of the neurons that are active in a given process (**Figure 3C**). AT is an imaging technique that uses nanometer-thin physical sectioning of a fixed tissue sample to facilitate the multiplexed imaging of dozens of protein markers with exquisite spatial resolution and large volumetric tissue coverage (Micheva and Smith, 2007; Wang and Smith, 2012).To date, AT has been broadly used to characterized genetically targeted neurons in zebrafish (Robles et al., 2011), assess the synapse deficits caused by Tau accumulation in mouse and humans (Kopeikina et al., 2011), quantify the three-dimensional microstructural changes of mouse aortic tissue after aneurysm (Saatchi et al., 2012), and measure synapse density changes due to astrocytic glypican release (Allen et al., 2012) and thalamic network stimulation (Lacey et al., 2012).

Conjugated live imaging of neuronal activity and subcellular-level AT will allow the quantitative analysis of cell physiology on a circuit level. AT analysis of cell-type specific antigens will provide single neuron differentiation of cell classes based on transmitter expression, e.g., glutamate, GABA, acetylcholine, etc., (**Figure 3**). Moreover, these transmitter-determined neuron types can be further classified by the expression of neuropeptides or transcription factors. By properly aligning Ca^{2+} and AT data, single neuron activity profiles can be mapped from Ca^{2+} imaging experiments to molecularly identified neurons. This *post hoc* identification of the molecular physiology of measured circuit members in conjunction with the temporal data from live imaging should allow a more robust classification of functional relevance in terms of understanding how inhibition, excitation and global modulation affect the discrete calculations made by a specific circuit. Further, since the sectioned sample can be kept indefinitely (Micheva and Smith, 2007), when new markers for neuron identity become available, previously unidentified nuclei that displayed interesting activities can be marked and leads to a model that becomes more accurate with time.

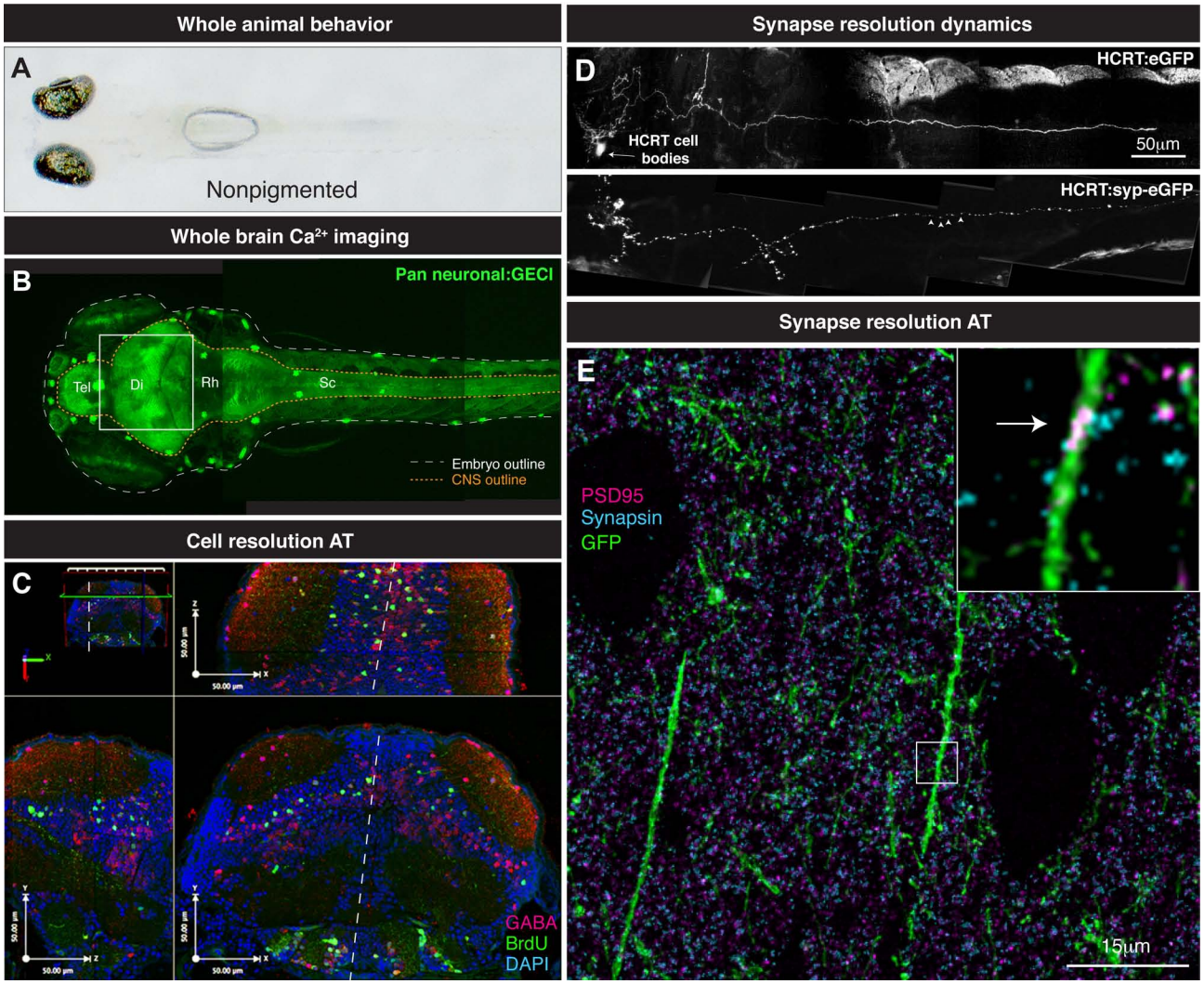

FIGURE 3 | From whole brain to single synapse. (A) Behavioral processes can be studied in non-pigmented (Nacre; mitfa mutant) species of zebrafish. **(B)** Two-photon volume image of 5 dpf zebrafish expressing GCaMP pan-neuronally, note the linear organization of the brain along the rostrocaudal axis from telencephalon (tel) to spinal cord (sc). **(C)** Various maximal projections (from area indicated in B by white box) of the 5 dpf zebrafish midbrain reconstructed after array tomography against GABA (magenta), BrdU (green) and DAPI (cyan) markers. White dashed line depicts midline. **(D)** Genetically specified circuit analysis. Synaptophysin-eGFP (syp-eGFP) allows imaging of structural plasticity of synapses (white arrowheads) in hypocretin (HCRT) neurons. **(E)** Single synapse resolution projection of array tomography sections stained for GFP (green), PSD95 (magenta) and Synapsin (cyan). Inset, magnification of a single shaft synapse (white arrow).

The combination of Ca^{2+} imaging and AT means we will be able to map functionally relevant brain regions or nuclei in terms of their temporal activity patterns and their molecular topology. When correlated to behavior, the temporal structure could also provide us with a map of how sensory inputs change the active connections of a defined neural circuit. Obtained under both baseline and challenged conditions, firing patterns could also be examined to gain insights to the nature of the disruptions involved in brain disorders and neural degeneration (see Future directions). On top of this functional structure we will then be able to overlay a relevant molecular topology that will reveal the identity of the nodes, whether inhibitory or excitatory, being connected in the functional activity structure. At its simplest, the temporal correlation of inhibitory and excitatory inputs into a circuit will be the basis of the computation performed by that group of neurons, and once both the identity and the activity structures stereotypic to a specific set of inputs and outputs are known, it will then be possible to reconstruct the actual algorithm performed by the circuit in relation to the set of inputs. Moreover, with the wealth of molecular information we can obtain from AT, we will be able to look at how patterns of activity might affect global modulation of the brain through the induction of various categories of neurotransmitters from monoamines to peptides.

Distinguishing the molecular identity of each brain nucleus – if not neuron - is crucial so that we can exploit the use of transgenesis to genetically capture these circuits in order to

further study their functions. As with other model organisms, genetic tagging of circuits will be critical since there is significant interindividual variation in the spatial location of neurons that prevents ease of comparison by the activity map alone. With promoter driven transgenic lines at hand, specific neural populations can be imaged in more detail for their firing rates [GCaMP, aequorin and genetically-encoded voltage indicators (GEVIs)] to begin to understand the relative contributions of subgroups or individual neurons to a behavioral output. Further, once relevant firing circuits or nuclei are established, pharmacological treatment, ablations, and optogenetic techniques (for review, Portugues et al., 2013) can be used more accurately to dissect the necessity and sufficiency for those regions (or even single cells) in normal behavioral processes and put us in a position to model brain disorders.

SYNAPSE IMAGING WITH TWO-PHOTON OR ARRAY TOMOGRAPHY

An ideal understanding of brain computation and function will also require insights at the synaptic level. Perturbations at this level as seen with Schizophrenia, Fragile X syndrome, and Rett syndrome highlight the need to understand what constitutes normal brain connectivity (Chahrour and Zoghbi, 2007; Lauriat and Mcinnes, 2007; Featherstone, 2010; Toro et al., 2010; Auerbach et al., 2011; Grant, 2012). Zebrafish allow a large shift in scale, from whole brain to neural network down to subsynaptic components. For example, zebrafish permit both longitudinal studies of synapses and whole brain coverage of the synaptic landscape. Thanks to the accessibility of the zebrafish brain, live two-photon imaging of genetically specified synaptic populations offers an important glimpse into the dynamics of synapse formation and disassembly related to the function of networks. For example, a longitudinal study of zebrafish hypocretin synapses on axons innervating the pineal gland at larval stages demonstrated rhythmicity of synaptic connections made by this circuit over time (Appelbaum et al., 2010). The reduction in phototoxicity allowed the imaging of the same genetically defined neuronal process in a live vertebrate over 24 h (live zebrafish can be safely imaged in agarose during a full sleep/wake cycle; Appelbaum et al., 2010). Such insights are not possible using fixed samples of several individuals and no other animal model currently offers opportunities to study such phenomenon on a brain-wide scale over time. Ca^{2+} dynamics can also be investigated at the synaptic level across the brain or a genetically defined circuit to demonstrate functionality. GCaMP indicators fused to synaptic markers (e.g., SyGCaMP and SyRGECO) have allowed the deciphering of the neural coding involved in the transfer of information between cells in the zebrafish retina (Dreosti et al., 2011) and tectum (Nikolaou et al., 2012; Walker et al., 2013), showing the exciting potential of understanding synaptic firing at specific connections. Such a gain in resolution – access to the firing pattern of individual synapses – bears tremendous potential for revealing the potential disruptions in brain diseases.

As discussed above for circuit dynamics, it is useful to know the molecular identity of an activity profile – and AT again affords this opportunity at the level of the synapse. Such information identifies the nature of these synapses, whether they are excitatory or inhibitory and if they are undergoing plasticity changes such as those for long-term potentiation/long-term depression (LTP/LTD) induction. The sub-diffraction resolution (Wang and Smith, 2012) and the proteomic coverage (Micheva and Smith, 2007) of AT is ideal for the analysis and classification of synapses in a large tissue volume. The combination of live two-photon structural analysis with AT will allow the identification of proteins involved in the structural dynamics of synapses in the brain (**Figure 3D**). A straightforward longitudinal analysis of synapse dynamics (Niell et al., 2004; Appelbaum et al., 2010) followed by *post hoc* AT analysis of the stable or newly formed synapses can give insight into the molecular mechanism by which synapses are stabilized or generated (**Figure 3E**). This further combined with measured activity of those synapses could open the door to finding the molecular and synaptic mechanisms underpinning behavioral control.

In this new regime, perturbations that affect synaptic plasticity, e.g., disease or behavioral challenges, can be characterized during longitudinal analysis, and the affected synapses will be targeted for *post hoc* proteomic dissection to reveal potential molecular changes. Then the candidate molecules can be labeled and modified and put back into a living system and then reanalyzed in terms of their effects on synaptic plasticity and dynamics. In this manner, deep molecular knowledge about the workings and deficits of nervous systems can be gleamed by this iterative process of longitudinal, quantitative observation and conjugate molecular dissection.

FUTURE DIRECTION AND APPLICATIONS FOR HUMAN DISORDERS

Zebrafish as a genetic model system has driven change in developmental biology and we expect a similar impact in the neurosciences with the advent of whole brain and synapse imaging techniques. While the zebrafish, as with all other animal models, can never accurately recapitulate the behavioral output of a human, we contend that at the level of the synapse and neuron, invaluable insights can be made, with techniques that leverage the unique properties of this vertebrate model, in understanding the basic conserved principles of how neuronal networks coordinate and function.

Knowledge of normal vertebrate brain function will have a huge impact understanding normal brain health and psychiatry. Importantly, there is an increasing realization that some psychiatric/brain diseases are predominantly genetic, developmental and neuronal/synaptic disorders. Indeed, insights to brain health and psychiatry require a whole brain perspective at single synapse resolution. Such a situation may appear to be an unreachable goal today, but zebrafish comes very close to bridging these scales of neural circuit investigation. Psychiatry as a field is now becoming a more integrated field benefiting of neuroscience and genetic studies. The introduction of novel uses of established animal models such as zebrafish in psychiatry and clinical neurosciences should allow new perspective and strategies. With development of psychiatric therapies in decline, advances in our understanding of the molecular basis of synaptic changes in normal and diseased brains should offer new targets for the pharmacological industry. Mental health disorders are the

leading cause of disability according to most medical sources. For most mental illnesses, the etiology is unknown, detection and prevention are poor, and current medication is not consistently effective. We hope whole brain studies with synapse resolution in the vertebrate zebrafish will soon allow breakthrough advances in our understanding of complex brain disorders.

ACKNOWLEDGMENTS

Our work is supported by the National Institutes of Health (NS062798, DK090065, MH099647). We thank Dr. Brian Grone for critical reading of the manuscript, Dr. Thomas Mueller for providing images for **Figure 1C** and Dr. Estuardo Robles for the panels in **Figure 3C**.

REFERENCES

Ahrens, M. B., and Keller, P. J. (2013). Whole-brain functional imaging at cellular resolution using light-sheet microscopy. *Nat. Methods* doi: 10.1038/nmeth.2434 [Epub ahead of print].

Ahrens, M. B., Li, J. M., Orger, M. B., Robson, D. N., Schier, A. F., Engert, F., et al. (2012). Brain-wide neuronal dynamics during motor adaptation in zebrafish. *Nature* 485, 471–477.

Akanji, A. O., George, A. O., Olasode, B. J., and Osotimehin, B. O. (1990). Fasting hypoglycaemia due to insulinoma in pregnancy. *Postgrad. Med. J.* 66, 156.

Akerboom, J., Carreras Calderon, N., Tian, L., Wabnig, S., Prigge, M., Tolo, J., et al. (2013). Genetically encoded calcium indicators for multi-color neural activity imaging and combination with optogenetics. *Front. Mol. Neurosci.* 6:2. doi: 10.3389/fnmol.2013.00002

Akerboom, J., Chen, T. W., Wardill, T. J., Tian, L., Marvin, J. S., Mutlu, S., et al. (2012). Optimization of a GCaMP calcium indicator for neural activity imaging. *J. Neurosci.* 32, 13819–13840.

Allen, N. J., Bennett, M. L., Foo, L. C., Wang, G. X., Chakraborty, C., Smith, S. J., et al. (2012). Astrocyte glypicans 4 and 6 promote formation of excitatory synapses via GluA1 AMPA receptors. *Nature* 486, 410–414.

Appelbaum, L., Wang, G., Yokogawa, T., Skariah, G. M., Smith, S. J., Mourrain, P., et al. (2010). Circadian and homeostatic regulation of structural synaptic plasticity in hypocretin neurons. *Neuron* 68, 87–98.

Appelbaum, L., Wang, G. X., Maro, G. S., Mori, R., Tovin, A., Marin, W., et al. (2009). Sleep-wake regulation and hypocretin-melatonin interaction in zebrafish. *Proc. Natl. Acad. Sci. U.S.A.* 106, 21942–21947.

Auerbach, B. D., Osterweil, E. K., and Bear, M. F. (2011). Mutations causing syndromic autism define an axis of synaptic pathophysiology. *Nature* 480, 63–68.

Bellen, H. J., Tong, C., and Tsuda, H. (2010). 100 years of *Drosophila* research and its impact on vertebrate neuroscience: a history lesson for the future. *Nat. Rev. Neurosci.* 11, 514–522.

Berman, J. R., Skariah, G., Maro, G. S., Mignot, E., and Mourrain, P. (2009). Characterization of two melanin-concentrating hormone genes in zebrafish reveals evolutionary and physiological links with the mammalian MCH system. *J. Comp. Neurol.* 517, 695–710.

Carvalho, L., and Heisenberg, C. P. (2009). Imaging zebrafish embryos by two-photon excitation time-lapse microscopy. *Methods Mol. Biol.* 546, 273–287.

Chahrour, M., and Zoghbi, H. Y. (2007). The story of Rett syndrome: from clinic to neurobiology. *Neuron* 56, 422–437.

Charonis, A. S., Reger, L. A., Dege, J. E., Kouzi-Koliakos, K., Furcht, L. T., Wohlhueter, R. M., et al. (1990). Laminin alterations after in vitro nonenzymatic glycosylation. *Diabetes* 39, 807–814.

Dreosti, E., Esposti, F., Baden, T., and Lagnado, L. (2011). In vivo evidence that retinal bipolar cells generate spikes modulated by light. *Nat. Neurosci.* 14, 951–952.

Engert, F., and Wilson, S. W. (2012). Zebrafish neurobiology: from development to circuit function and behaviour. *Dev. Neurobiol.* 72, 215–217.

Featherstone, D. E. (2010). Intercellular glutamate signaling in the nervous system and beyond. *ACS Chem. Neurosci.* 1, 4–12.

Friedrich, R. W., Jacobson, G. A., and Zhu, P. (2010). Circuit neuroscience in zebrafish. *Curr. Biol.* 20, R371–R381.

Grant, S. G. (2012). Synaptopathies: diseases of the synaptome. *Curr. Opin. Neurobiol.* 22, 522–529.

Hoffman, G. E., Smith, M. S., and Verbalis, J. G. (1993). c-Fos and related immediate early gene products as markers of activity in neuroendocrine systems. *Front. Neuroendocrinol.* 14, 173–213.

Huisken, J., and Stainier, D. Y. (2009). Selective plane illumination microscopy techniques in developmental biology. *Development* 136, 1963–1975.

Kim, H., Kim, E., Park, M., Lee, E., and Namkoong, K. (2013). Organotypic hippocampal slice culture from the adult mouse brain: a versatile tool for translational neuropsychopharmacology. *Prog. Neuropsychopharmacol. Biol. Psychiatry* 41, 36–43.

Kopeikina, K. J., Carlson, G. A., Pitstick, R., Ludvigson, A. E., Peters, A., Luebke, J. I., et al. (2011). Tau accumulation causes mitochondrial distribution deficits in neurons in a mouse model of tauopathy and in human Alzheimer's disease brain. *Am. J. Pathol.* 179, 2071–2082.

Kullander, K. (2005). Genetics moving to neuronal networks. *Trends Neurosci.* 28, 239–247.

Lacey, C. J., Bryant, A., Brill, J., and Huguenard, J. R. (2012). Enhanced NMDA receptor-dependent thalamic excitation and network oscillations in stargazer mice. *J. Neurosci.* 32, 11067–11081.

Lauriat, T. L., and Mcinnes, L. A. (2007). EAAT2 regulation and splicing: relevance to psychiatric and neurological disorders. *Mol. Psychiatry* 12, 1065–1078.

Lenkov, D. N., Volnova, A. B., Pope, A. R., and Tsytsarev, V. (2012). Advantages and limitations of brain imaging methods in the research of absence epilepsy in humans and animal models. *J. Neurosci. Methods* 212, 195–202.

Leung, L., and Holt, C. E. (2012). Imaging axon pathfinding in zebrafish in vivo. *Cold Spring Harb. Protoc.* 2012, 992–997.

Leung, L., Klopper, A. V., Grill, S. W., Harris, W. A., and Norden, C. (2011). Apical migration of nuclei during G2 is a prerequisite for all nuclear motion in zebrafish neuroepithelia. *Development* 138, 5003–5013.

Micheva, K. D., and Smith, S. J. (2007). Array tomography: a new tool for imaging the molecular architecture and ultrastructure of neural circuits. *Neuron* 55, 25–36.

Mueller, T., Dong, Z., Berberoglu, M. A., and Guo, S. (2011). The dorsal pallium in zebrafish, *Danio rerio* (Cyprinidae, Teleostei). *Brain Res.* 1381, 95–105.

Murphy, M., Greferath, U., Nag, N., Nithianantharajah, J., and Wilson, Y. M. (2004). Tracing functional circuits using c-Fos regulated expression of marker genes targeted to neuronal projections. *Front. Biosci.* 9, 40–47.

Muto, A., Ohkura, M., Abe, G., Nakai, J., and Kawakami, K. (2013). Real-time visualization of neuronal activity during perception. *Curr. Biol.* 23, 307–311.

Muto, A., Ohkura, M., Kotani, T., Higashijima, S., Nakai, J., and Kawakami, K. (2011). Genetic visualization with an improved GCaMP calcium indicator reveals spatiotemporal activation of the spinal motor neurons in zebrafish. *Proc. Natl. Acad. Sci. U.S.A.* 108, 5425–5430.

Nakai, J., Ohkura, M., and Imoto, K. (2001). A high signal-to-noise Ca(2+) probe composed of a single green fluorescent protein. *Nat. Biotechnol.* 19, 137–141.

Naumann, E. A., Kampff, A. R., Prober, D. A., Schier, A. F., and Engert, F. (2010). Monitoring neural activity with bioluminescence during natural behavior. *Nat. Neurosci.* 13, 513–520.

Niell, C. M., Meyer, M. P., and Smith, S. J. (2004). In vivo imaging of synapse formation on a growing dendritic arbor. *Nat. Neurosci.* 7, 254–260.

Nikolaou, N., Lowe, A. S., Walker, A. S., Abbas, F., Hunter, P. R., Thompson, I. D., et al. (2012). Parametric functional maps of visual inputs to the tectum. *Neuron* 76, 317–324.

Northcutt, R. G. (2008). Forebrain evolution in bony fishes. *Brain Res. Bull.* 75, 191–205.

Ohkura, M., Sasaki, T., Sadakari, J., Gengyo-Ando, K., Kagawa-Nagamura, Y., Kobayashi, C., et al. (2012). Genetically encoded green fluorescent ca(2+) indicators with improved detectability for neuronal ca(2+) signals. *PLoS ONE* 7:e51286. doi: 10.1371/journal.pone.0051286

Portugues, R., Severi, K. E., Wyart, C., and Ahrens, M. B. (2013). Optogenetics in a transparent animal: circuit function in the larval zebrafish. *Curr. Opin. Neurobiol.* 23, 119–126.

Randlett, O., Poggi, L., Zolessi, F. R., and Harris, W. A. (2011). The oriented emergence of axons from retinal ganglion cells is directed by laminin contact in vivo. *Neuron* 70, 266–280.

Rinkwitz, S., Mourrain, P., and Becker, T. S. (2011). Zebrafish: an integrative system for neurogenomics and neurosciences. *Prog. Neurobiol.* 93, 231–243.

Robles, E., Smith, S. J., and Baier, H. (2011). Characterization of genetically targeted neuron types in the zebrafish optic tectum. *Front. Neural Circuits* 5:1. doi: 10.3389/fncir.2011.00001

Saatchi, S., Azuma, J., Wanchoo, N., Smith, S. J., Yock, P. G., Taylor, C. A., et al. (2012). Three-dimensional microstructural changes in murine abdominal aortic aneurysms quantified using immunofluorescent array tomography. *J. Histochem. Cytochem.* 60, 97–109.

Sengupta, P., and Samuel, A. D. (2009). Caenorhabditis elegans: a model system for systems neuroscience. *Curr. Opin. Neurobiol.* 19, 637–643.

Sherin, J. E., Shiromani, P. J., Mccarley, R. W., and Saper, C. B. (1996). Activation of ventrolateral preoptic neurons during sleep. *Science* 271, 216–219.

Thai, N. J., Longe, O., and Rippon, G. (2009). Disconnected brains: what is the role of fMRI in connectivity research? *Int. J. Psychophysiol.* 73, 27–32.

Toro, R., Konyukh, M., Delorme, R., Leblond, C., Chaste, P., Fauchereau, F., et al. (2010). Key role for gene dosage and synaptic homeostasis in autism spectrum disorders. *Trends Genet.* 26, 363–372.

Van Meer, P., and Raber, J. (2005). Mouse behavioural analysis in systems biology. *Biochem. J.* 389, 593–610.

Walker, A. S., Burrone, J., and Meyer, M. P. (2013). Functional imaging in the zebrafish retinotectal system using RGECO. *Front. in Neural Circuits* 7:34. doi: 10.3389/fncir.2013.00034

Wang, G., Grone, B., Colas, D., Appelbaum, L., and Mourrain, P. (2011). Synaptic plasticity in sleep: learning, homeostasis and disease. *Trends Neurosci.* 34, 452–463.

Wang, G., and Smith, S. J. (2012). Sub-diffraction limit localization of proteins in volumetric space using Bayesian restoration of fluorescence images from ultrathin specimens. *PLoS Comput. Biol.* 8:e1002671. doi: 10.1371/journal.pcbi.1002671

Ward, R. D., Simpson, E. H., Kandel, E. R., and Balsam, P. D. (2011). Modeling motivational deficits in mouse models of schizophrenia: behavior analysis as a guide for neuroscience. *Behav. Processes* 87, 149–156.

Zhao, Y., Araki, S., Wu, J., Teramoto, T., Chang, Y. F., Nakano, M., et al. (2011). An expanded palette of genetically encoded Ca(2+) indicators. *Science* 333, 1888–1891.

Conflict of Interest Statement: The authors declare that the research was conducted in the absence of any commercial or financial relationships that could be construed as a potential conflict of interest.

Received: 31 January 2013; paper pending published: 18 February 2013; accepted: 03 April 2013; published online: 24 April 2013.

*Citation: Leung LC, Wang GX and Mourrain P (2013) Imaging zebrafish neural circuitry from whole brain to synapse. Front. Neural Circuits **7**:76. doi: 10.3389/fncir.2013.00076*

frontiers in
NEURAL CIRCUITS

REVIEW ARTICLE
published: 09 April 2013
doi: 10.3389/fncir.2013.00058

Regulation of zebrafish sleep and arousal states: current and prospective approaches

Cindy N. Chiu and David A. Prober*

Division of Biology, California Institute of Technology, Pasadena, CA, USA

Edited by:
Gonzalo G. De Polavieja, Consejo Superior de Investigaciones Científicas, Spain

Reviewed by:
Karl Æ Karlsson, Reykjavik University, Iceland
Caroline H. Brennan, Queen Mary University of London, UK

***Correspondence:**
David A. Prober, Division of Biology, California Institute of Technology, 1200 E. California Blvd., Pasadena, CA 91125, USA.
e-mail: dprober@caltech.edu

Every day, we shift among various states of sleep and arousal to meet the many demands of our bodies and environment. A central puzzle in neurobiology is how the brain controls these behavioral states, which are essential to an animal's well-being and survival. Mammalian models have predominated sleep and arousal research, although in the past decade, invertebrate models have made significant contributions to our understanding of the genetic underpinnings of behavioral states. More recently, the zebrafish has emerged as a promising model system for sleep and arousal research. Here we review experimental evidence that the zebrafish, a diurnal vertebrate, exhibits fundamental behavioral and neurochemical characteristics of mammalian sleep and arousal. We also propose how specific advantages of the zebrafish can be harnessed to advance the field. These include tractable genetics to identify and manipulate molecular and cellular regulators of behavioral states, optical transparency to facilitate *in vivo* observation of neural structure and function, and amenability to high-throughput drug screens to discover novel therapies for neurological disorders.

Keywords: zebrafish, sleep, arousal, hypocretin, orexin, neuromodulator

INTRODUCTION

Animals engage in diverse activities that require adaptive changes in behavior. A fundamental goal in neuroscience is to understand how the brain enables animals to make dynamic changes in behavioral state in response to changing internal or environmental demands. A particularly striking example of such a change in behavioral state is the switch between sleep and wakefulness. Once awake, animals must further modulate arousal levels—for example, transitioning between inattentive and attentive states—as required for the task at hand. Underscoring the significance of these behavioral states, sleep and arousal states are conserved across the animal kingdom, from worms and flies to fish and humans (Allada and Siegel, 2008; Cirelli and Tononi, 2008). Despite the severe consequences and prevalence of sleep and arousal disorders (Mahowald and Schenck, 2005), the mechanisms that regulate behavioral states and transitions between states remain mysterious.

Theories to account for the regulation of sleep and arousal states span the hierarchy of biological organization, from organismal physiology, behavior, and cognition to neurons and neural ensembles, and more recently to genetic and molecular mechanisms (Hobson and Pace-Schott, 2002; Pace-Schott and Hobson, 2002). The zebrafish, which offers experimental advantages at many levels, is well-suited to contribute to our understanding of these states. These advantages include a simplified yet conserved vertebrate brain, facile genetics, an increasingly well-characterized behavioral repertoire, amenability to pharmacological and high-throughput assays, and optical transparency for *in vivo* visualization of the brain (Lieschke and Currie, 2007). The zebrafish is also gaining traction as a useful system for circuit neuroscience (Friedrich et al., 2010; McLean and Fetcho, 2011; Portugues et al., 2013).

In this review we will survey key concepts and open questions in the field of sleep and arousal regulation and then examine current approaches to identifying these behavioral states in zebrafish. To exemplify these concepts and the issues that arise when using zebrafish to study neuromodulation of sleep and arousal, we will focus our discussion on studies that explore the role of hypocretin, an important mammalian neuromodulator of sleep and arousal, in regulating zebrafish behavioral state. Finally, we will highlight recent innovations in the zebrafish toolkit that have the potential to open new avenues of discovery in sleep and arousal research.

REGULATION OF SLEEP AND AROUSAL: KEY CONCEPTS AND PROBLEMS

In the early twentieth century, the neurologist Constantin von Economo examined encephalitis patients suffering from profound sleep disorders. He discovered that excessive sleepiness was associated with a specific pattern of brain lesions located at the junction of the brainstem and forebrain, whereas insomnia was associated with lesions in a nearby, more anterior region (von Economo, 1930). Subsequently, Moruzzi, Magoun, and others found that sleep or arousal could be induced by lesion or electrical activation along a subcortical pathway ascending from the brainstem (Moruzzi and Magoun, 1949). These findings advanced the idea that sleep and arousal states are actively generated and maintained by the brain. The main subcortical regions identified by von Economo and others (brainstem, posterior hypothalamus, basal forebrain) are now known to contain distinct aminergic and

peptidergic cell populations (Saper et al., 2005). These systems promote arousal via ascending projections that increase forebrain excitation as well as descending brainstem and spinal cord projections that increase muscle tone and sensorimotor function (Jones, 2003).

Neuromodulatory systems that promote arousal include (refer to **Figure 1A**):

- Noradrenergic neurons of the locus coeruleus, located in the pontine brainstem;
- Serotonergic neurons of the raphe nuclei, located in the midbrain;
- Dopaminergic neurons, particularly those of the ventral periaqueductal gray (vPAG) and ventral tegmental area (VTA) of the midbrain, and also the A11 dopaminergic cell cluster, located in the hypothalamus;
- Histaminergic neurons of the tuberomammillary nucleus, located in the posterior hypothalamus;
- Hypocretin (Hcrt) neurons located in the lateral hypothalamus;
- Cholinergic neurons located in the basal forebrain and also in the pedunculopontine and laterodorsal tegmental nuclei, located in the pontine brainstem.

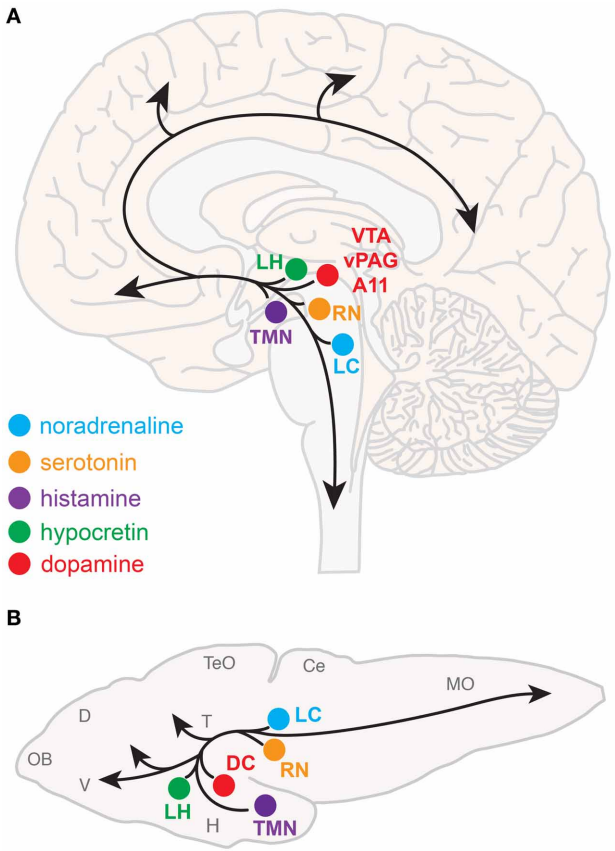

FIGURE 1 | Neuromodulatory systems that promote arousal in vertebrates. The approximate locations of key neuromodulatory regions are shown for human **(A)** and larval zebrafish **(B)** brains. Arrows indicate ascending projections that increase forebrain excitation and descending projections that increase muscle tone and sensorimotor function. Abbreviations of neuromodulatory regions: LC, locus coeruleus; RN, raphe nuclei; VTA, ventral tegmental area; vPAG, ventral periaqueductal gray; A11, mammalian dopamine cell group A11; DC, dopaminergic diencephalic cluster; TMN, tuberomammillary nucleus; LH, lateral hypothalamus. Abbreviations of larval zebrafish brain anatomy: OB, olfactory bulb; D, dorsal telencephalon; V, ventral telencephalon; TeO, optic tectum; H, hypothalamus; T, thalamus; Ce, cerebellum; MO, medulla oblongata. Note human and larval zebrafish brains are not depicted to scale.

In contrast to the many known arousal-promoting systems, attempts to identify distinct sleep-promoting cell populations have been less fruitful. One exception is the ventrolateral preoptic area (VLPO), which was identified as a cluster of cells in the basal forebrain which provides inputs to systems in the hypothalamus and brainstem that promote arousal (Saper et al., 2005). These neurons are likely the site of lesion in von Economo's insomnia patients, and subsequent work in animal models showed that VLPO lesions reduce sleep by more than half (Lu et al., 2000). VLPO neurons contain the inhibitory transmitters GABA and galanin, and they are likely to promote sleep by inhibiting arousal systems. The VLPO, in turn, is directly and indirectly inhibited by arousal systems (Saper et al., 2005).

A crucial question is how these neural populations operate together to regulate distinct states and the transitions between them. The bistable flip-flop switch, adopted from electronics theory, is one appealing circuit-level model that can explain the rapid transition between distinct behavioral states such as sleep and waking (Saper et al., 2001). The flip-flop circuit derives its features from two reciprocally inhibitory components; this could be implemented in the brain by mutual inhibition between the VLPO and arousal systems. Because the flip-flop switch is inherently unstable, the circuit model might be supplemented by additional elements (i.e., neuromodulatory systems) that serve to stabilize and sustain a wake or sleep state. For example, in mammals, the neuromodulator Hcrt might serve to stabilize sleep-wake states by promoting arousal. Indeed, loss of Hcrt signaling is a hallmark of narcolepsy, a disorder characterized by fragmented sleep-wake states.

A more phenomenological but influential model proposes that sleep is regulated by two main drives: homeostatic drive (also known as "Process S") that is regulated by internal cues and circadian drive ("Process C") that is regulated by environmental cues (Borbély et al., 1989). Genetic approaches have made remarkable contributions toward a molecular-level understanding of Process C. The core mechanism of the circadian clock is conserved across species and consists of a network of positive and negative molecular feedback loops that can cell-autonomously maintain a 24-h periodic rhythm (Zhang and Kay, 2010; Mohawk et al., 2012). In many animals, neurons of the hypothalamic suprachiasmatic nucleus (SCN) function as a "master clock" that orchestrates organismal circadian physiology and behavior. Despite our mechanistic understanding of the circadian clock, it remains unclear how the circadian system regulates behaviors associated with sleep and wakefulness, although secreted peptides such as prokineticin 2 and transforming growth factor alpha/epidermal growth factor appear to play key roles (Kramer et al., 2001; Cheng et al., 2002; Foltenyi et al., 2007; Van Buskirk

and Sternberg, 2007; Gilbert and Davis, 2009). Our understanding of mechanisms that underlie Process S are more limited. One hypothesis is that adenosine, which accumulates as ATP energy stores are depleted during wakefulness, might serve as a signal for sleep need (Porkka-Heiskanen and Kalinchuk, 2011). Indeed, extracellular adenosine levels rise in specific regions of the mammalian brain during prolonged wakefulness and decline during sleep (Porkka-Heiskanen et al., 1997), and pharmacological activation of adenosine signaling promotes sleep (Benington et al., 1995; Hendricks et al., 2000; Thakkar et al., 2001; Rihel and Schier, 2012) and activates the VLPO (Scammell et al., 2001; Gallopin et al., 2005). However, the role of adenosine in sleep remains controversial because adenosine receptor mutants exhibit relatively normal sleep/wake behaviors (Stenberg et al., 2003; Urade et al., 2003; Huang et al., 2005; Bjorness et al., 2009; Wu et al., 2009).

A common theme that has emerged from studies of sleep and arousal regulatory mechanisms is that they play multiple roles in animal behavior and physiology. For example, many of the key players in sleep and circadian function are linked to metabolic regulation (Adamantidis and de Lecea, 2009; Bass, 2012). In fact, at the same time that Hcrt's link to narcolepsy was discovered (Chemelli et al., 1999; Lin et al., 1999), this peptide was also given the name orexin because intracerebroventricular injection of the peptide induced voracious feeding in rodents (Sakurai et al., 1998). Also, there are well-documented links between obesity and abnormal circadian behaviors, including voluntary behaviors such as shift-work (Antunes et al., 2010). This has led to the hypothesis that the circadian clock coordinates various physiological and behavioral functions in addition to sleep, such as liver function and feeding. Additionally, a number of sleep regulators have known interactions and/or overlap with regulators of immune function (Krueger, 2008) and learning and memory (Harris and Aston-Jones, 2006). Similarly, memory, attention, anxiety, and depression are among the many behavioral processes linked to arousal regulation and dysregulation (Johnson et al., 2012), and several neurological disorders, including autism and schizophrenia, are associated with sleep and arousal defects (Glickman, 2010; Pritchett et al., 2012).

Understanding how sleep and arousal are regulated might lead to new treatments for neurological diseases as well as explain normal individual variations in sleep and arousal. Going forward, a few of the many outstanding questions regarding how behavioral states are regulated include:

- What are the undiscovered genetic and neural substrates of sleep and arousal states?
- Do conserved or diverse neural and genetic mechanisms regulate sleep and arousal throughout the animal kingdom?
- What are the downstream effectors of "Process S" and "Process C"? For example, what are the neural and genetic pathways that link circadian input signals to a circadian behavioral output?
- How are circadian, homeostatic, and other behaviorally-relevant drives integrated at the circuit level?
- Are dynamic changes in neuromodulatory influences responsible for the transitions between different behavioral states?
- Which properties are unique and which are shared among neuromodulator systems that regulate sleep and arousal?
- Are there anatomical and functional subdivisions within each arousal-promoting neuromodulator system?
- Can we develop or discover effective remedies for sleep and arousal-related disorders? In particular, can we learn enough about mechanism to treat specific pathologies without grossly affecting other brain functions?

Despite their tremendous contributions to sleep and arousal research, prevalent animal model systems have limitations in addressing some of these questions. For example, drawbacks of rodent model systems include the relative complexity of their nervous systems, the difficulty of monitoring the activity of genetically identified neurons during behavior, and a nocturnal sleep/wake pattern, which differs from diurnal humans. Also, the long generation time, small litter size, and expense makes the rodent an unwieldy model for large-scale behavioral screening. On the other hand, the fruit fly and the worm are particularly amenable to genetic screens, but their nervous systems lack structures and some neuromodulators analogous to mammals. In this light, the zebrafish, a diurnal vertebrate with cutting-edge genetic and *in vivo* neuroimaging capabilities and a successful track-record in high-throughput behavioral screens, is an excellent system to complement the advances made using mammalian and invertebrate model systems.

ANALYSIS OF ZEBRAFISH BEHAVIORAL STATES

After only a few days of development, larval zebrafish begin to swim around in their environment, typically in brief, phasic locomotor episodes. High-speed infrared video capture combined with computational image analyses have been used to quantitatively describe specific locomotor behaviors in larval zebrafish. For example, by measuring values for indicator variables, such as those characterizing an animal's posture (tail bend location and amplitude, turning angle, yaw) and timing (tail-beat frequency, swimming speed), it is possible to objectively define and differentiate basic locomotor modules such as scoots, burst swims, routine-turns, and escape-turns (Budick and O'Malley, 2000).

Similarly, an animal's behavioral state can be defined as a *"recurring, temporally enduring constellation of values of a set of indicator variables of the organism"* (Steriade and McCarley, 2005). Sleep and waking states are typically defined in this manner. In humans and other mammals, these states can be distinguished by obvious differences in behavior, but they are more conveniently identified by objective electrophysiological measures that correlate with behavioral state, such as the electroencephalogram (EEG), which measures cerebral electrical activity (Berger, 1929). In fact, the EEG and similar measures of global brain activity reveal physiological subdivisions within sleep and waking, suggesting that they are not unitary states (Lin and Gervasoni, 2008). The use of physiological criteria is a practical and standardizable approach to defining behavioral states (Rechtschaffen and Kales, 1968; Datta and Hobson, 2000), although it is associated with the hazards of inferring cause from inappropriate or indirect measures (Hobson and Steriade, 1986). Indeed, when studying mammalian sleep early in ontogeny before adult EEG signatures

are established, one must rely on mostly behavioral criteria (Blumberg et al., 2005). With this in mind, behavioral measures are more appropriate for describing behavioral states, whereas physiological measures of sleep and arousal, while experimentally convenient in some animals, should be carefully regarded as correlative.

There are also important methodological issues to address when measuring behavioral states in non-human animals including zebrafish. First, tracking of individual rather than groups of animals is ideal for resolving the temporal structure of sleep and arousal states. Second, the impact of genetic variations (Valatx et al., 1972) and prior experiences (Ganguly-Fitzgerald et al., 2006) on sleep and arousal must be carefully controlled for reproducible measurements. Fortunately, with care, these issues can be reasonably addressed using zebrafish (**Figure 2A**). Large clutches of embryos allow for experimental comparisons of siblings that are raised and tested together in identical conditions. Because they can survive on their yolk sac for the first week of development, the confounding effects of variable feeding behavior are avoided. Most importantly, the small size of larval zebrafish (~4 mm in length) allows for simultaneous behavioral tracking of individually-housed animals in a 96-well-plate.

ZEBRAFISH SLEEP STATES

In non-mammalian and non-avian animal model systems, sleep is defined according to several behavioral criteria (Campbell and Tobler, 1984): (1) quiescent state regulated by a circadian rhythm, (2) reduced sensory responsiveness, and (3) homeostatic regulation. Based on these criteria, behavioral sleep states have been demonstrated in flies and worms (Hendricks et al., 2000; Shaw et al., 2000; Van Buskirk and Sternberg, 2007; Raizen et al., 2008), and indeed, a number of studies have documented at least the first criterion for behavioral sleep in many fish species (Reebs, 1992). Recently, larval and adult zebrafish have been reported to exhibit all three behavioral criteria for sleep (Zhdanova et al., 2001; Prober et al., 2006; Yokogawa et al., 2007).

Criterion No. 1: quiescent state regulated by circadian rhythm

Starting around 4 days post fertilization (dpf), zebrafish raised on a 24-h alternating light: dark cycle (e.g., 14 h light:10 h dark) exhibit daily fluctuations in locomotor activity (Hurd and Cahill, 2002; Prober et al., 2006). Like humans, zebrafish are diurnal and thus exhibit peak activity during the light phase and increased quiescence during the dark phase (**Figure 2B**). Particularly at night, zebrafish spend bouts of several minutes or longer in a state of inactivity (**Figure 2C**).

As has been observed in many other animals, larval and adult zebrafish that have been entrained on a light: dark cycle maintain circadian oscillations in locomotor activity even after external circadian cues are removed (Hurd et al., 1998; Hurd and Cahill, 2002). The core molecular machinery of the mammalian circadian clock is well-conserved in zebrafish [reviewed in Vatine et al. (2011)], although zebrafish possess two paralogs of some mammalian genes (Postlethwait et al., 1998). A notable difference between zebrafish and mammals is that zebrafish peripheral circadian clocks are directly entrainable by light (Whitmore et al., 2000; Pando et al., 2001), a function that may have evolved in zebrafish due to their relative transparency. This innovation suggests that zebrafish may not require a "master clock" analogous to the mammalian SCN to orchestrate circadian rhythms throughout the body. We also note that some widely-used inbred strains of laboratory mice lack enzymes required to synthesize melatonin

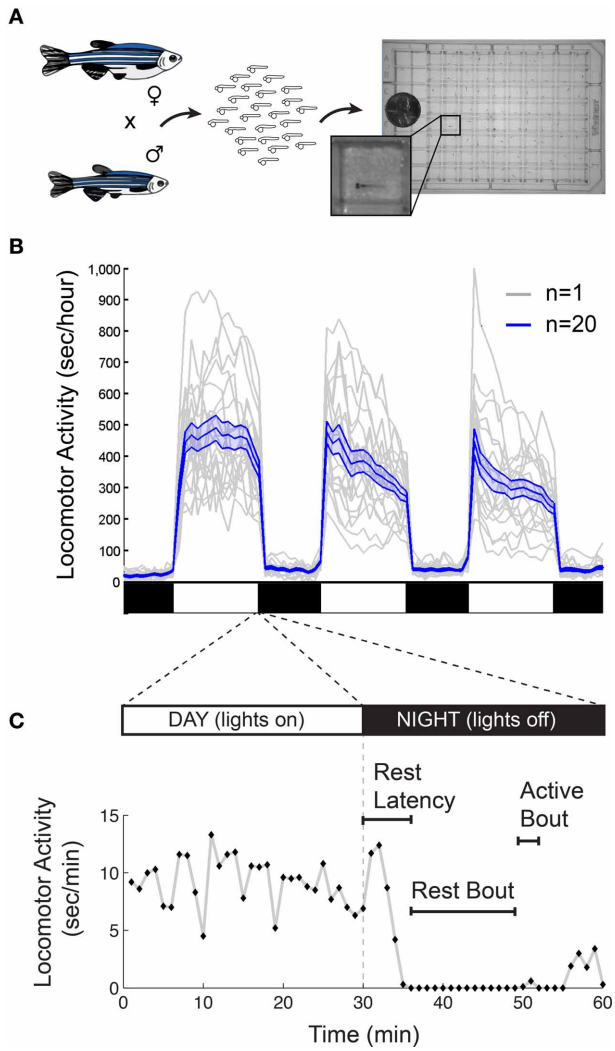

FIGURE 2 | Monitoring larval zebrafish sleep and wake behaviors. (A) Zebrafish larval locomotor activity assay. Individual zebrafish larva are placed in each well of a 96-well-plate on the 5th day of development. The plate is placed in a temperature-controlled chamber that is illuminated by white lights during the day and is continuously illuminated by infrared lights. The larvae are monitored by an infrared camera and the locomotor activity of each larva is recorded by a computer. **(B)** Representative locomotor activity data for each of 20 individual wild-type larvae (gray traces) and their mean locomotor activity (blue trace, ±standard error of the mean) is shown. Black and white bars indicate day and night, respectively. Larvae are more active during the day than at night, although there is considerable variability among individuals. **(C)** An example of typical larval zebrafish behavior at the end of the day is shown. A rest bout is defined as a period of at least 1 min of inactivity, which is associated with an increase in arousal threshold (Prober et al., 2006). Rest latency indicates the time between lights off at night and initiation of the first rest bout. Figure modified from Prober et al. (2006).

(Ebihara et al., 1986; Goto et al., 2007), a hormone produced in the pineal gland that is thought to play a key role in transmitting circadian cues in humans and zebrafish. Thus, the role of the pineal gland and melatonin might be underestimated in mammalian research using these laboratory mouse strains. This fact, together with the diurnal sleep/wake pattern of zebrafish, suggests that zebrafish have some important advantages over rodents for modeling the circadian regulation of human sleep.

Criterion No. 2: reduced sensory responsiveness

Sleeping animals exhibit reduced responsiveness to sensory stimuli, which distinguishes sleep from quiet wakefulness. During quiescent periods, larval zebrafish show reduced responsiveness to mechanical stimuli (Zhdanova et al., 2001) and delayed responses to sudden changes in light intensity (Prober et al., 2006), and quiescent adult zebrafish are less responsive to electrical stimuli (Yokogawa et al., 2007). Because larval zebrafish exhibit reduced responsiveness after at least 1 min of inactivity, sleep in larval zebrafish has been operationally defined as a quiescent bout lasting at least 1 min. A similar approach has been used to define sleep in adult zebrafish as a minimum 6-s inactive bout (Yokogawa et al., 2007). Presently, it is unclear whether differences between adult and larval zebrafish sleep reflect true differences in biological phenomena or merely differences in methodology across different studies; further experiments using standardized approaches across different zebrafish developmental stages should clarify this issue. Nonetheless, this approach to defining sleep states has been useful for identifying evolutionarily conserved sleep regulators in zebrafish (see next section). However, additional work may further refine the definition of zebrafish sleep by using detailed assays of physiology and arousal across various sensory modalities during quiescence. For example, one report indicates that quiescence during day and night are not equivalent based on the observation that nighttime quiescence is associated with reduced respiration and postural changes compared to daytime quiescence (Zhdanova, 2006).

Criterion No. 3: homeostatic regulation

A common approach to assaying homeostatic regulation of sleep is to test whether compensatory sleep occurs following a period of deprivation. Indeed, both larval and adult zebrafish exhibit this so-called "sleep rebound" behavior. In a study of larval zebrafish (Zhdanova et al., 2001), a vibration stimulus applied during the last 6 h of the night resulted in sleep rebound the following day. The reduced locomotor activity during sleep rebound was accompanied by a significantly decreased sensitivity to a mechanical stimulus as compared to siblings not subjected to sleep deprivation. In a study of adult zebrafish (Yokogawa et al., 2007), electroshock or light stimuli applied for 6 h at night reduced locomotor activity the following day, although arousal threshold was not assessed. Notably, sleep rebound in zebrafish has only been observed in dark testing conditions (Yokogawa et al., 2007).

Although these data are suggestive of rebound sleep, further advances in both technique and knowledge are needed to firmly establish homeostatic control of sleep in zebrafish. One important consideration in the design of sleep deprivation studies is the possibility of off-target effects of the deprivation protocol. For example, while light is a profoundly arousing stimulus for zebrafish, its utility as a specific sleep deprivation stimulus is limited because light also affects the circadian clock. Another confounding effect of sleep deprivation that can vary with different deprivation protocols is stimulus-induced stress, which may be caused by the prolonged and high-amplitude stimulus application needed to overcome behavioral habituation and sleep. The use of yoked test subjects that are stimulated randomly relative to sleep bouts is an important control for stress effects. However, data using this methodology have thus far only yielded modest effects of sleep deprivation on sleep rebound (Yokogawa et al., 2007).

Technical issues aside, an important, unresolved scientific issue is whether the amount of sleep rebound is proportionate to the amount of sleep deprivation in zebrafish. Additionally, better-refined definitions of zebrafish sleep and more sophisticated methods of monitoring and quantifying sleep states will provide new possibilities to study whether sleep deprivation affects sleep quality. For example, it would be interesting to test the hypothesis that sleep deprivation increases the depth in addition to the duration of sleep rebound in zebrafish.

ZEBRAFISH AROUSAL STATES

Whereas sleep and waking are relatively easy to define with objective behavioral criteria, specific arousal states are more difficult to characterize. An animal's arousal state can be characterized by: (1) changes in frequency or intensity of voluntary locomotor activity and (2) altered responsiveness to sensory or emotional stimuli (Pfaff et al., 2008). In addition to these general characteristics, arousal can be characterized by the specific behavioral outputs that it motivates, such as reward-seeking and sexual or courtship behaviors.

Arousal-associated changes in locomotor activity can be triggered by intense stimuli. For example, in response to sudden changes in light intensity (e.g., light to darkness over 10 ms), larval zebrafish exhibit a biphasic response that begins with a transient, high-amplitude movement followed by a sustained, low-amplitude increase in locomotor activity that persists for at least several minutes (Prober et al., 2006; Emran et al., 2010). In addition to external stimuli, arousal states are also triggered by physiological drives such as hunger, sex, and pain. For example, adult zebrafish respond to caloric restriction with the same biphasic behavioral response resulting from mammalian hunger; starved fish are initially hyperactive, but become lethargic after prolonged caloric restriction (Novak et al., 2005). Arousal states can also be manifested as goal-seeking behaviors that change the structure of spontaneous locomotor activity. Food-seeking behavior is readily measured in larval zebrafish, which begin to hunt for food almost as soon as they can swim. This behavior can be quantitatively described by a temporal sequence that begins with ocular angle convergence followed by a series of orienting "J-turns" and forward swimming toward the target (Borla et al., 2002; Gahtan et al., 2005; McElligott and O'Malley, 2005; Bianco et al., 2011). These eye and tail movements are distinct from routine, spontaneous movements, enabling the objective identification of a food-seeking arousal state in both free-swimming and partially restrained preparations.

Zebrafish exhibiting heightened locomotor activity can also exhibit enhanced sensory responsiveness, consistent with the behavioral criteria for arousal. For example, zebrafish exposed to a sudden change in water flow rate become hyperactive and respond more quickly to a repeat application of the flow stimulus (Yokogawa et al., 2012). Zebrafish also exhibit similarly enhanced responses to a whole-field visual motion stimulus, which is thought to be a crucial sensory cue underlying the behavioral response to water flow. Notably, flow-induced arousal did not affect responses to electroshock and touch stimuli, which is suggestive of distinct arousal states. Although this study provides evidence of sensory modality-specific arousal states, the timecourses and behavioral readouts of the other stimuli were substantially different from the flow-related stimuli, leaving open the interesting question of what determines the specificity of an arousal state.

SLEEP/AROUSAL NEUROMODULATORY SYSTEMS IN ZEBRAFISH

The neuroanatomical and neurochemical systems that regulate sleep and arousal in mammals are largely conserved in zebrafish (**Figure 1B**). One notable difference is that zebrafish lack midbrain dopaminergic neurons analogous to the mammalian vPAG and VTA (Holzschuh et al., 2001; Kaslin and Panula, 2001; Rink and Wullimann, 2002; McLean and Fetcho, 2004), although the less-studied mammalian dopaminergic A11 group, which is noted for its roles in sensorimotor function and the human sleep disorder restless legs syndrome (Mignot et al., 2002), has a likely homolog in zebrafish ventral diencephalic dopamine clusters (Ryu et al., 2007; Tay et al., 2011). Also, zebrafish do not have a layered cortex, a principal target of mammalian ascending arousal systems, although homology between mammalian cortical areas and zones in the zebrafish dorsal telencephalon have been proposed based on common molecular developmental patterns (Wullimann and Mueller, 2004). Basal forebrain and brainstem cholinergic neurons have not been clearly described in zebrafish larvae.

Importantly, the neuropharmacology of mammalian behavior is well-conserved in zebrafish (Rihel and Schier, 2012), and drugs or bioactive agents that affect sleep and/or arousal in mammals produce comparable effects in zebrafish. Zebrafish exhibit a dose-dependent decrease in locomotor activity when treated with known hypnotics and sedatives, including melatonin, GABA receptor agonists (e.g., benzodiazepines, barbiturates, diazepam), histamine H1 receptor antagonists, and α2 adrenergic receptor agonists (Zhdanova et al., 2001; Ruuskanen et al., 2005; Renier et al., 2007; Sundvik et al., 2011), and modafinil, a wakefulness-promoting drug that is used to treat human sleep disorders, increases wakefulness in zebrafish (Sigurgeirsson et al., 2011). More recently, an unbiased screen of nearly 4000 small molecules corroborated the roles of arousal and sleep modulators, including noradrenaline, serotonin, dopamine, GABA, glutamate, histamine, adenosine, and melatonin, in regulating zebrafish sleep/wake behavior (Rihel et al., 2010). Studies examining more specialized aspects of arousal such as sensorimotor responses have also confirmed the role of key monoaminergic systems, including dopamine and serotonin, in regulating arousal states in zebrafish (Burgess and Granato, 2007; Mu et al., 2012; Yokogawa et al., 2012).

HYPOCRETIN

The Hcrt neuromodulatory system is the best-characterized regulator of sleep and arousal in zebrafish, and we focus on these studies to illustrate the current discoveries, concepts and issues that arise when studying neuromodulators of zebrafish sleep and arousal.

The zebrafish *hcrt* gene encodes two structurally-related peptides homologous to mammalian Hcrt1 and Hcrt2 (Kaslin et al., 2004; Faraco et al., 2006). Among vertebrates including zebrafish, there is particularly high sequence homology near the C-terminus of each Hcrt peptide, which is the critical region for biological activity and receptor selectivity (Asahi et al., 1999; Darker et al., 2001; Lang et al., 2004). The zebrafish genome contains a single *hcrt receptor* ortholog (*hcrtr2*; previously named *hcrtr*), a G-protein coupled receptor (GPCR) that is structurally similar to the two mammalian *hcrt receptor* paralogs (Prober et al., 2006; Yokogawa et al., 2007).

At 5 dpf, when larval zebrafish sleep/wake behaviors are first observed, *hcrt* is specifically expressed in a bilateral nucleus in the posterior hypothalamus that encompasses ∼10 neurons per hemisphere, as determined by *in situ* hybridization (ISH) and immunohistochemistry using a Hcrt1-specific antibody (Faraco et al., 2006; Prober et al., 2006). Furthermore, enhanced green fluorescent protein (EGFP) expression driven by various *hcrt* upstream promotor sequences faithfully recapitulates the endogenous *hcrt* expression pattern (Faraco et al., 2006; Prober et al., 2006) (**Figure 3A**). This cluster expands to approximately 40 neurons in the adult zebrafish hypothalamus (Kaslin et al., 2004; Appelbaum et al., 2009, 2010). While the zebrafish *hcrt* expression pattern is consistent with mammals, the number of *hcrt* neurons is on the order of 10^2 fewer in zebrafish (de Lecea et al., 1998; Sakurai et al., 1998; Lin et al., 1999; Peyron et al., 2000; Prober et al., 2006). Two molecular markers of mammalian *hcrt* neurons, *vesicular glutamate transporter* and *neuronal pentraxin2*, also colocalize with *hcrt* in zebrafish (Appelbaum et al., 2009, 2010). Thus, the zebrafish provides a simple vertebrate system to study the development and function of Hcrt neurons.

Zebrafish *hcrt* neurons send widespread ascending and descending projections to brain areas associated with arousal (**Figure 3B**), as they do in mammals (Peyron et al., 1998; Taheri et al., 1999). Using a transgenic *hcrt*-EGFP line, Hcrt projections in larval zebrafish were found in close apposition to noradrenergic cells of the locus coeruleus and processes of diencephalic dopaminergic cells in larval zebrafish (Prober et al., 2006). By adulthood, Hcrt-immunoreactive fibers contact these targets and also densely innervate the serotonergic raphe and possibly histaminergic and cholinergic populations (Kaslin et al., 2004).

Consistent with widespread Hcrt neuron projections and with mammalian *hcrtr* expression, zebrafish *hcrtr2* expression is considerably more extensive than *hcrt* and is detected in widespread areas of the zebrafish brain. In larval zebrafish, one study used a high-resolution double fluorescent ISH method and found that *hcrtr2* colocalizes with *dopamine beta hydroxylase* in noradrenergic cells of the locus coeruleus and *dopamine transporter*

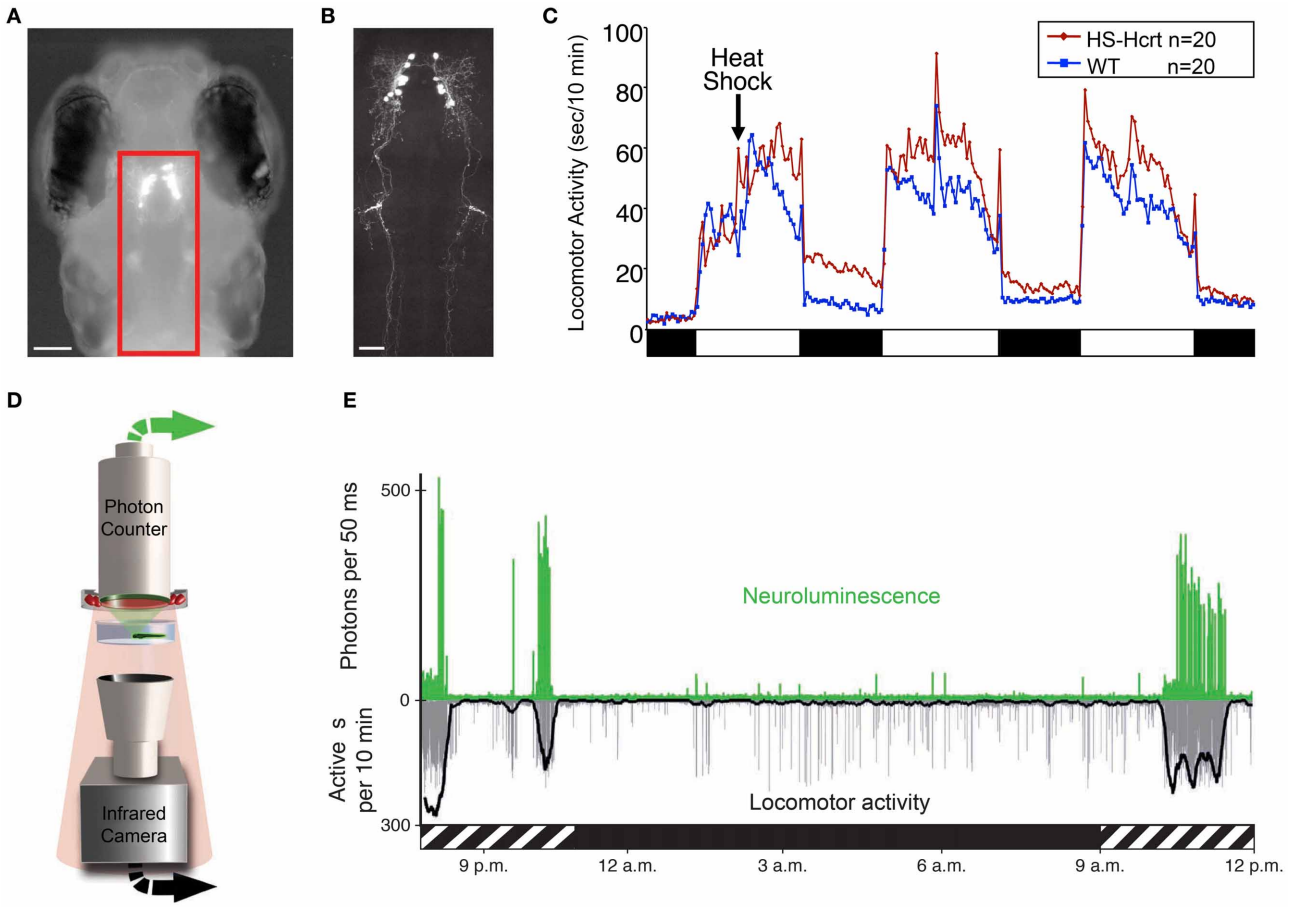

FIGURE 3 | Zebrafish hypocretin is associated with arousal. (A) Dorsal view of a 4 dpf zebrafish larva that expresses GFP-Aequorin (GA) specifically in Hcrt neurons. **(B)** Two-photon z-projection image of the boxed area in **(A)**. Scale bars represent 100 μm **(A)** and 50 μm **(B)**. **(C)** Overexpression of Hcrt using a heat shock-inducible promoter (HS-Hcrt) increases locomotor activity. The mean locomotor activity of 20 HS-Hcrt larvae and 20 of their wild-type siblings is shown. The spike in activity during the afternoon of the 2nd and 3rd days of the experiment resulted from the addition of water to offset evaporation. **(D)** The GA assay. A large-area photon-counting photomultiplier tube is placed above a transparent behavior chamber in which a zebrafish larva that expresses GA in specific neurons is allowed to freely swim. The larva is imaged using infrared (IR) lights and an IR camera that is placed below the recording chamber. Spectral separation between GA neuroluminescence and the IR illumination allows the simultaneous recording of GA neuroluminescence and larval behavior. **(E)** Activity of Hcrt neurons during natural behavior. Data for a representative 4 dpf larva is shown. The larva exhibited periods of increased spontaneous locomotor activity (lower trace, thick line indicates 10 min running average) during the subjective day (hatched bar below graph) and little activity during the subjective night (black bar below graph). Most neuroluminescence signals produced by Hcrt neurons (upper trace) coincide with periods of robust locomotor activity during the subjective day, suggesting that Hcrt neuron activity is associated with arousal. Figure modified from Prober et al. (2006), Naumann et al. (2010).

in diencephalic dopaminergic cells (Prober et al., 2006), as in mammals (Trivedi et al., 1998; Marcus et al., 2001). However, another study concluded that there is no *hcrtr2* coexpression with these monoaminergic populations in 2 dpf or adult zebrafish, and instead reported that *hcrtr2* is expressed in GABAergic, adrenergic, cholinergic, and glycinergic systems (Yokogawa et al., 2007). The discrepancies reported in these studies may stem from differences in detection method, probe sensitivity and specificity, and possibly the developmental stages studied. For example, the latter study made extensive use of a two-color chromogenic ISH procedure, which cannot reliably report colocalization because the differently colored stains can mask each other, the colors cannot be spectrally separated into distinct channels, and high resolution imaging methods such as confocal microscopy cannot be used to resolve samples in three dimensions (Jowett and Yan, 1996; Vize et al., 2009; Lauter et al., 2011). Neither study observed expression of *hcrtr2* in histaminergic or serotonergic cells. However, the methods used in both studies, especially fluorescent ISH, often are not sensitive enough to detect low-abundance transcripts such as those encoding GPCRs, so negative data obtained using this method should be interpreted with caution. Indeed, a close examination of data obtained by the latter study suggests coexpression of faintly stained *hcrtr2* in some monoaminergic nuclei, consistent with the former study.

Several studies have also explored the functional role of the *hcrt* system in zebrafish. One study of larval zebrafish found that

heat shock inducible overexpression of a *hcrt* transgene promotes wakefulness by consolidating active states, increasing arousal, and reducing sleep (Prober et al., 2006). Thus, the zebrafish Hcrt gain of-function (GOF) phenotype (**Figure 3C**) is comparable to the effects of intracerebroventricular injection of Hcrt peptide in rodents (España et al., 2001; Thakkar et al., 2001) and goldfish (Nakamachi et al., 2006). Conversely, sleep fragmentation is observed in adult zebrafish containing a null mutation in the *hcrtr2* gene (Yokogawa et al., 2007). This loss-of-function (LOF) result is strikingly similar to the sleep/wake fragmentation observed in rodents, canines and humans that lack Hcrt signaling (Sutcliffe and de Lecea, 2002). However, this study also made a controversial proposal that the zebrafish Hcrt system may be functionally divergent from the mammalian Hcrt system based on the observation that the *hcrtr2* mutant displayed a mild decrease in sleep, whereas Hcrt peptide injection caused a mild decrease in locomotor activity. However, the decreased sleep in *hcrtr2* mutants was only significant compared to unrelated, non-mutagenized animals, and the decreased locomotor activity following Hcrt peptide injection may have resulted from the relatively high doses of peptide used (280–2800 pmol/g body weight in adult zebrafish vs. 2.8–28 pmol/g body weight that increased locomotor activity in adult goldfish). Indeed, a subsequent study using the same *hcrtr2* mutant did not report a decreased sleep phenotype (Appelbaum et al., 2009). More recently, this debate seems to have been resolved by a report that inducible ablation of *hcrt* neurons using a genetically targeted toxin increased sleep and sleep/wake transitions in larval zebrafish (Elbaz et al., 2012). Thus, in non-invasive, inducible zebrafish systems, Hcrt GOF consolidates sleep/wake states and reduces sleep, whereas Hcrt LOF fragments sleep/wake states and increases sleep.

Taken together, the neuroanatomical and functional data from different research groups indicate that the zebrafish Hcrt system is interconnected with major neuromodulatory arousal systems and regulates sleep/wake transitions by promoting arousal. Thus, the zebrafish provides a simple model of the vertebrate Hcrt system. The zebrafish system is poised to tackle unanswered questions about how Hcrt regulates sleep and arousal states. For example, although the zebrafish data point to a role for Hcrt in arousal state regulation, its specific role in different forms of arousal is unknown. Zebrafish can also be used to characterize the neural mechanisms through which Hcrt affects sleep and arousal using GOF and LOF genetic tools such as heat shock inducible Hcrt transgenic zebrafish and the *hcrtr2* mutant in combination with mutant and transgenic zebrafish that lack other neuromodulatory systems. The relatively small number of Hcrt neurons should also facilitate studies of their development and connectivity, as well as analysis of their activity during different behaviors. Finally, small molecule screens in zebrafish can be used to identify therapeutic pathways for the treatment of narcolepsy.

UP-AND-COMING APPROACHES TO STUDYING SLEEP AND AROUSAL IN ZEBRAFISH

Still in its infancy, zebrafish research on sleep and arousal has focused on establishing behavioral assays and identifying known regulators of behavioral states. Now that the zebrafish has been established as a useful model of vertebrate sleep and arousal, it is well-suited among commonly used model organisms to address two long-standing yet fundamental questions in sleep research. First, what are the genetic mechanisms that regulate sleep and arousal behaviors? Second, what are the neural mechanisms that underlie these behaviors?

DISCOVERY GENETICS AND SCREENS TO IDENTIFY SLEEP AND AROUSAL REGULATORS

Progress in understanding mechanisms that regulate mammalian sleep has been limited by the challenge of performing unbiased screens in mammals. This limitation is underscored by recent progress in understanding genetic and neuronal mechanisms that regulate *Drosophila* sleep through the use of screens (Cirelli et al., 2005; Koh et al., 2008; Stavropoulos and Young, 2011; Pfeiffenberger and Allada, 2012; Rogulja and Young, 2012). In contrast to mammals, zebrafish are uniquely well-suited among vertebrate model systems for large-scale and unbiased screens. Indeed, two large-scale forward genetic screens for developmental and simple behavioral phenotypes stimulated the widespread adoption of zebrafish as a model system (Driever et al., 1996; Haffter et al., 1996). These screens used chemical mutagenesis to induce point mutations, and embryos and larvae were then screened for recessive phenotypes. The identification of a large number of developmental and behavioral mutants established zebrafish as the only vertebrate model system in which such screens are practical, and many labs have subsequently performed screens for a wide range of phenotypes.

However, there are several limitations in using forward genetics to identify genes that affect complex and quantitative behaviors such as sleep. First, as in mammals, sleep varies considerably among individual zebrafish, making it difficult to identify a population of individuals that exhibit a recessive phenotype. Second, mapping genes responsible for recessive phenotypes requires a significant amount of time and labor, and it can be challenging for variable and quantitative phenotypes. Recent advances in deep sequencing technologies can accelerate this process (Obholzer et al., 2012; Miller et al., 2013), but they do not reduce the challenge of mapping a variable quantitative trait such as sleep. These two factors likely underlie the relative paucity of genes that have been identified by *Drosophila* forward genetic screens despite large-scale efforts in several labs. Third, chemical mutagens typically induce thousands of mutations in each animal, and this high background mutational load may affect behavior. These problems can be avoided by performing insertional mutagenesis using retroviruses and transposons (Golling et al., 2002; Varshney et al., 2013), but these mutagens are much less efficient at inducing mutant phenotypes. This limitation is particularly problematic for screens that use relatively low-throughput assays, such as those required to identify sleep defects.

Two approaches have been developed that overcome some of the limitations of forward genetic screens. First, gene trap approaches use a modified transposon that creates a fluorescent fusion protein when it inserts within a gene (Clark et al., 2011; Maddison et al., 2011; Trinh et al., 2011). In some methods (Maddison et al., 2011; Trinh et al., 2011), the transposon can be induced to undergo genetic recombination, which creates a premature stop codon in the trapped gene. This approach

is particularly useful when laborious screening assays are necessary because it allows for pre-selection of lines that are considered likely to be involved in the process of interest. For example, lines that exhibit fluorescence in specific neural populations, but not those that fluoresce in skin or muscle, can be selected for behavioral analysis. Because recombination within the transposon is inducible, the targeted gene can be mutated in specific cells and at specific times. This feature is useful for genes that have different functions in different cell types or are required for development. However, this technique often fails to create null mutants, and preselecting genes based on their expression pattern introduces a bias into the screen.

A second discovery approach that has recently been applied to zebrafish is the use of small molecule libraries to screen for behavioral phenotypes. Zebrafish larvae readily take up small molecules that are added to the water (Peterson and Fishman, 2004) and lack a mature blood brain barrier (Jeong et al., 2008). In addition, the small size of zebrafish larvae allows screening in 96 or 384 well-plates, and thousands of embryos can be routinely collected, which allows large numbers of compounds to be tested quickly. Taken together, zebrafish larvae allow physiologically relevant whole-animal assays combined with high-throughput, low-cost drug screening, making them perhaps the most suitable multicellular model organism for small molecule screens. This approach has led to the discovery of mechanisms that regulate development (North et al., 2007; Yu et al., 2008) and behavior (Kokel et al., 2010; Rihel et al., 2010; Wolman et al., 2011), and to the development of clinically relevant compounds (North et al., 2007). A significant challenge of small molecule screens is that it can be difficult to identify the targets of poorly annotated compounds. However, this problem will become less acute with the growth of databases that compile the effects of small molecules in a wide range of biological assays (Lamb et al., 2006; Tolopko et al., 2010) and the development of chemical bioinformatic approaches (Laggner et al., 2012).

As an alternative to forward genetic and chemical approaches, reverse genetic techniques have undergone rapid growth over the last few years and promise to transform the use of zebrafish in the genetic analysis of behavior. One method, known as TILLING (Kettleborough et al., 2011), uses chemical mutagenesis to create thousands of mutant zebrafish, each of which is then screened for mutations in a gene of interest using deep sequencing. This approach is expected to identify null mutations in most zebrafish genes within the next few years, although it will likely fail to identify mutations in many small genes. A second approach uses zinc finger nuclease (ZFN) and TAL-effector nuclease (TALEN) technologies (Bogdanove and Voytas, 2011). These nucleases can be designed to create double-stranded DNA breaks at specific sites in the genome, which are repaired by an error-prone process that often generates short insertions or deletions. TALENs are emerging as the superior technology because they are easy to generate, can target essentially any DNA sequence and are generally more mutagenic than ZFNs (Huang et al., 2011; Cade et al., 2012; Dahlem et al., 2012; Moore et al., 2012; Chen et al., 2013). Additionally, high-throughput methods (Briggs et al., 2012; Reyon et al., 2012; Wang et al., 2012) should allow the synthesis of TALEN libraries that target every zebrafish gene. Through a combination of these reverse genetic approaches, it is likely that a knock-out mutant will be available for essentially all zebrafish genes within the next few years. Large collections of these mutants can then be screened for behavioral phenotypes. Finally, TALENs can also be used to insert exogenous sequences into the zebrafish genome (Bedell et al., 2012). This technology should eventually allow the insertion of recombination sites, epitope tags and reporter genes at precise sites in the genome, which will enable sophisticated genetic approaches that are currently limited to more established genetic models such as mice, flies, and worms. A disadvantage of these approaches is that they preclude behavioral analysis of genes that are required for development. An alternative reverse genetic technique that can overcome this problem uses short hairpin RNAs (shRNAs) to target specific mRNAs for degradation. shRNA expression can be controlled in a spatial and temporal manner through the use of appropriate expression systems, thus avoiding complications for genes whose function is required during development or for different functions in different cell types. While this technology is not yet fully developed in zebrafish (De Rienzo et al., 2012), it is encouraging that it has been successfully used to identify genes that regulate sleep in flies (Rogulja and Young, 2012) and we expect that shRNA libraries that target all zebrafish genes will soon be developed.

CHARACTERIZATION OF NEURAL CIRCUIT STRUCTURE AND FUNCTION

The complexity of mammalian neural circuits and the difficulty of manipulating these circuits present major challenges in deciphering the neural mechanisms that regulate mammalian sleep and arousal. In contrast, the optical transparency and conserved yet relatively simple nervous system of zebrafish larvae present an opportunity to characterize the basic neural mechanisms that regulate vertebrate sleep. Zebrafish larvae are commonly used to monitor the development of particular neurons during development through the genetic targeting of fluorescent proteins. While useful, this approach is generally limited to visualizing individual neurons using transient plasmid injections, or all neurons of a genetically defined circuit using stable transgenic animals. However, it is difficult to simultaneously monitor the development of each neuron of a genetically specified neural population using a single fluorescent protein. A new transgenic tool, referred to as Brainbow, promises to overcome this limitation. Brainbow uses Cre/Lox recombination to generate the expression of random combinations of green, red and blue fluorescent proteins (Livet et al., 2007). The presence of multiple copies of the Brainbow transgene generates a large palette of colors that allows the axonal and dendritic projections of up to 100 neurons to be distinguished from their neighbors. While initially developed for the mouse, the poor accessibility of mouse brains for imaging limits the use of Brainbow in living mice, but zebrafish larvae are well-suited for this approach (Pan et al., 2011). The original Brainbow transgene is limited by use of the relatively dim cerulean fluorescent protein and the cytoplasmic localization of all three fluorescent proteins. However, we expect that use of membrane-targeted, brighter and more photostable fluorescent proteins will allow the axonal and dendritic projections of individual neurons among genetically specified neural populations to be characterized at the single cell level in developing zebrafish larvae.

A variety of transgenic tools have recently been developed that allow the stimulation or inhibition of genetically defined neural populations. So-called "optogenetic" tools allow genetically specified neurons to be stimulated or inhibited by specific wavelengths of light (Mattis et al., 2012). In principle, zebrafish larvae are well-suited for this technology due to their optical transparency, which is a significant advantage over non-transparent organisms such as rodents, which typically require the use of fiber optics to deliver light to specific brain regions. Indeed, this technology has been used to functionally characterize the roles of specific neurons in sensory and motor control in restrained zebrafish larvae (Douglass et al., 2008; Arrenberg et al., 2009; Wyart et al., 2009). However, zebrafish larvae exhibit robust behavioral responses to the light stimulus, which can be problematic for experiments using freely behaving larvae (Zhu et al., 2009). Alternative approaches using transgenes that modulate neural activity in the presence of specific small molecules (Szobota et al., 2007; Arenkiel et al., 2008; Alexander et al., 2009; Magnus et al., 2011) or at specific temperatures (Pulver et al., 2009) provide alternative approaches that avoid the confounding effects of light, but have yet to be tested in zebrafish.

NEUROPHYSIOLOGICAL CORRELATES OF SLEEP AND AROUSAL

Electrophysiology is often used to record neural activity during mammalian sleep/wake behaviors, but the available techniques are invasive and it is difficult to target specific neuron types for recording. While it is not feasible to perform electrophysiological neural recordings on freely behaving zebrafish larvae due to their small size, two alternative approaches may be used. First, fluorescent genetically encoded calcium indicators (GECIs) such as GCaMP report cellular calcium levels, which can be used as a proxy for neural activity (Akerboom et al., 2012). An important advantage of using GECIs is that cell-type specific promoters can be used to target their expression to specific neuron types for recording. Alternatively, GECIs can be broadly expressed in many neurons, and the activities of individual neurons can be spatially resolved in the context of anatomical or molecular markers. Because zebrafish larvae are transparent, changes in GECI fluorescence can be monitored in essentially any neuron in intact larvae, and many neurons can be monitored simultaneously (Ahrens et al., 2012). A disadvantage of this technique is that animals must be restrained to maintain a stable image of neural activity, although a closed-loop virtual reality system recently developed for head-restrained larvae augments the behavioral repertoire that can be recorded simultaneously with neural activity (Portugues and Engert, 2011; Ahrens et al., 2012). However, using GECIs to monitor neural activity during sleep/wake behaviors is particularly problematic because the light that is required to excite GECI fluorescence will affect behavior.

An alternative approach that was recently developed for zebrafish larvae and avoids some limitations of GECIs uses a GFP-Aequorin (GA) reporter (Naumann et al., 2010). This technique is non-invasive, does not require excitation light and allows an animal to freely behave while the activities of genetically specified neurons are monitored. In the presence of a cofactor and the increased levels of cytoplasmic calcium that accompany neural activity, neuronally-expressed, luminescent GA emits photons (neuroluminescence) that can be detected from a recording chamber by a large-area photon counter (**Figure 3D**). Simultaneously, behavior is monitored using an infrared camera. The utility of this technique was validated using transgenic zebrafish expressing GA specifically in Hcrt neurons (**Figures 3A,B**). Strikingly, Hcrt neuron neuroluminescence corresponds to peak periods of locomotor activity that occur during the subjective daytime (**Figure 3E**), suggesting that Hcrt neuron activity is correlated with arousal. These results are similar to the limited *in vivo* data obtained from identified Hcrt neurons in restrained and behaving rats (Lee et al., 2005; Mileykovskiy et al., 2005). A limitation to the non-imaging GA approach is that it does not provide spatial information about the neurons that are producing bioluminescent signals. It is therefore necessary to restrict GA expression to the neurons of interest, which is currently only possible for a small number of neural populations where a cell type-specific promotor has been identified. Particularly troublesome is the observation that promoters used to drive gene expression in neurons often also drive gene expression in muscle, although inclusion of a neuron-restrictive silencing element (NRSE) adjacent to the promoter sequence can significantly reduce non-neural gene expression (Bergeron et al., 2012). Another limitation to this technique is that it is limited to monitoring individual larvae, although it may be possible to scale up the assay using multiwell plates and PMT arrays or an electron-multiplying CCD camera. Thus, while this technique is still in development, it has the potential to transform studies of neural circuit activity, function and behavior in transparent and genetically tractable model organisms such as zebrafish.

CONCLUDING REMARKS

These are still early days for using zebrafish as a model to study sleep and arousal states, but it is already clear that zebrafish can provide new and important insights into genetic and neural mechanisms that regulate behavior. High-throughput screens have revealed new mechanisms that regulate arousal (Kokel et al., 2010; Rihel et al., 2010), and tools that exploit advantageous features of zebrafish have provided new insights into the neural regulation of sleep and arousal (Naumann et al., 2010; Yokogawa et al., 2012). The development of new tools to monitor and manipulate neural activity, as well as technologies that allow precise genome editing, are rapidly increasing the scope of experiments that can be performed with zebrafish. We expect that these developments will lead to the discovery of new mechanisms that regulate sleep and arousal states that would be difficult to obtain using other vertebrate model organisms. Finally, the utility of zebrafish for performing high-throughput whole animal small molecule screens may lead to new therapies for sleep and arousal disorders.

ACKNOWLEDGMENTS

This work was supported by grants from the National Institutes of Health (R00 NS060996, R01 NS070911 and R01 DA031367), and the Edward Mallinckrodt Jr., Rita Allen and Brain and Behavior Research Foundations.

REFERENCES

Adamantidis, A., and de Lecea, L. (2009). The hypocretins as sensors for metabolism and arousal. *J. Physiol.* 587, 33–40.

Ahrens, M. B., Li, J. M., Orger, M. B., Robson, D. N., Schier, A. F., Engert, F., et al. (2012). Brain-wide neuronal dynamics during motor adaptation in zebrafish. *Nature* 485, 471–477.

Akerboom, J., Chen, T.-W., Wardill, T. J., Tian, L., Marvin, J. S., Mutlu, S., et al. (2012). Optimization of a GCaMP calcium indicator for neural activity imaging. *J. Neurosci.* 32, 13819–13840.

Alexander, G. M., Rogan, S. C., Abbas, A. I., Armbruster, B. N., Pei, Y., Allen, J. A., et al. (2009). Remote control of neuronal activity in transgenic mice expressing evolved G protein-coupled receptors. *Neuron* 63, 27–39.

Allada, R., and Siegel, J. M. (2008). Unearthing the phylogenetic roots of sleep. *Curr. Biol.* 18, R670–R679.

Antunes, L. C., Levandovski, R., Dantas, G., Caumo, W., and Hidalgo, M. P. (2010). Obesity and shift work: chronobiological aspects. *Nutr. Res. Rev.* 23, 155–168.

Appelbaum, L., Wang, G. X., Maro, G. S., Mori, R., Tovin, A., Marin, W., et al. (2009). Sleep-wake regulation and hypocretin-melatonin interaction in zebrafish. *Proc. Natl. Acad. Sci. U.S.A.* 106, 21942–21947.

Appelbaum, L., Wang, G., Yokogawa, T., Skariah, G. M., Smith, S. J., Mourrain, P., et al. (2010). Circadian and homeostatic regulation of structural synaptic plasticity in hypocretin neurons. *Neuron* 68, 87–98.

Arenkiel, B. R., Klein, M. E., Davison, I. G., Katz, L. C., and Ehlers, M. D. (2008). Genetic control of neuronal activity in mice conditionally expressing TRPV1. *Nat. Methods* 5, 299–302.

Arrenberg, A. B., Del Bene, F., and Baier, H. (2009). Optical control of zebrafish behavior with halorhodopsin. *Proc. Natl. Acad. Sci. U.S.A.* 106, 17968–17973.

Asahi, S., Egashira, S.-I., Matsuda, M., Iwaasa, H., Kanatani, A., Ohkubo, M., et al. (1999). "Structure-activity relationship studies on the novel neuropeptide orexin," in *Peptides Science*, ed N. Fujii (Tokyo: The Japanese Peptide Society), 37–40.

Bass, J. (2012). Circadian topology of metabolism. *Nature* 491, 348–356.

Bedell, V. M., Wang, Y., Campbell, J. M., Poshusta, T. L., Starker, C. G., Krug, R. G., et al. (2012). *In vivo* genome editing using a high-efficiency TALEN system. *Nature* 491, 114–118.

Benington, J. H., Kodali, S. K., and Heller, H. C. (1995). Stimulation of A1 adenosine receptors mimics the electroencephalographic effects of sleep deprivation. *Brain Res.* 692, 79–85.

Berger, H. (1929). Über daselektrenkephalogramm des menschen. *Naturwissenschaften* 87, 527–570.

Bergeron, S. A., Hannan, M. C., Codore, H., Fero, K., Li, G. H., Moak, Z., et al. (2012). Brain selective transgene expression in zebrafish using an NRSE derived motif. *Front. Neural Circuits* 6:110. doi: 10.3389/fncir.2012.00110

Bianco, I. H., Kampff, A. R., and Engert, F. (2011). Prey capture behavior evoked by simple visual stimuli in larval zebrafish. *Front. Syst. Neurosci.* 5:101. doi: 10.3389/fnsys.2011.00101

Bjorness, T. E., Kelly, C. L., Gao, T., Poffenberger, V., and Greene, R. W. (2009). Control and function of the homeostatic sleep response by adenosine A1 receptors. *J. Neurosci.* 29, 1267–1276.

Blumberg, M. S., Karlsson, K. A. E., Seelke, A. M. H., and Mohns, E. J. (2005). The ontogeny of mammalian sleep: a response to Frank and Heller (2003). *J. Sleep Res.* 14, 91–98.

Bogdanove, A. J., and Voytas, D. F. (2011). TAL effectors: customizable proteins for DNA targeting. *Science* 333, 1843–1846.

Borbély, A. A., Achermann, P., Trachsel, L., and Tobler, I. (1989). Sleep initiation and initial sleep intensity: interactions of homeostatic and circadian mechanisms. *J. Biol. Rhythms* 4, 149–160.

Borla, M. A., Palecek, B., Budick, S., and O'Malley, D. M. (2002). Prey capture by larval zebrafish: evidence for fine axial motor control. *Brain. Behav. Evol.* 60, 207–229.

Briggs, A. W., Rios, X., Chari, R., Yang, L., Zhang, F., Mali, P., et al. (2012). Iterative capped assembly: rapid and scalable synthesis of repeat-module DNA such as TAL effectors from individual monomers. *Nucleic Acids Res.* 40, e117.

Budick, S. A., and O'Malley, D. M. (2000). Locomotor repertoire of the larval zebrafish: swimming, turning and prey capture. *J. Exp. Biol.* 203, 2565–2579.

Burgess, H. A., and Granato, M. (2007). Sensorimotor gating in larval zebrafish. *J. Neurosci.* 27, 4984–4994.

Cade, L., Reyon, D., Hwang, W. Y., Tsai, S. Q., Patel, S., Khayter, C., et al. (2012). Highly efficient generation of heritable zebrafish gene mutations using homo- and heterodimeric TALENs. *Nucleic Acids Res.* 40, 8001–8010.

Campbell, S. S., and Tobler, I. (1984). Animal sleep: a review of sleep duration across phylogeny. *Neurosci. Biobehav. Rev.* 8, 269–300.

Chemelli, R. M., Willie, J. T., Sinton, C. M., Elmquist, J. K., Scammell, T., Lee, C., et al. (1999). Narcolepsy in orexin knockout mice: molecular genetics of sleep regulation. *Cell* 98, 437–451.

Chen, S., Oikonomou, G., Chiu, C. N., Niles, B. J., Liu, J., Lee, D. A., et al. (2013). A large-scale *in vivo* analysis reveals that TALENs are significantly more mutagenic than ZFNs generated using context-dependent assembly. *Nucleic Acids Res.* 41, 2769–2778.

Cheng, M. Y., Bullock, C. M., Li, C., Lee, A. G., Bermak, J. C., Belluzzi, J., et al. (2002). Prokineticin 2 transmits the behavioural circadian rhythm of the suprachiasmatic nucleus. *Nature* 417, 405–410.

Cirelli, C., Bushey, D., Hill, S., Huber, R., Kreber, R., Ganetzky, B., et al. (2005). Reduced sleep in Drosophila Shaker mutants. *Nature* 434, 1087–1092.

Cirelli, C., and Tononi, G. (2008). Is sleep essential? *PLoS Biol.* 6:e216. doi: 10.1371/journal.pbio.0060216

Clark, K. J., Balciunas, D., Pogoda, H.-M., Ding, Y., Westcot, S. E., Bedell, V. M., et al. (2011). *In vivo* protein trapping produces a functional expression codex of the vertebrate proteome. *Nat. Methods* 8, 506–515.

Dahlem, T. J., Hoshijima, K., Jurynec, M. J., Gunther, D., Starker, C. G., Locke, A. S., et al. (2012). Simple methods for generating and detecting locus-specific mutations induced with TALENs in the zebrafish genome. *PLoS Genet.* 8:e1002861. doi: 10.1371/journal.pgen.1002861

Darker, J. G., Porter, R. A., Eggleston, D. S., Smart, D., Brough, S. J., Sabido-David, C., et al. (2001). Structure-activity analysis of truncated orexin-A analogues at the orexin-1 receptor. *Bioorg. Med. Chem. Lett.* 11, 737–740.

Datta, S., and Hobson, J. A. (2000). The rat as an experimental model for sleep neurophysiology. *Behav. Neurosci.* 114, 1239–1244.

de Lecea, L., Kilduff, T. S., Peyron, C., Gao, X., Foye, P. E., Danielson, P. E., et al. (1998). The hypocretins: hypothalamus-specific peptides with neuroexcitatory activity. *Proc. Natl. Acad. Sci. U.S.A.* 95, 322–327.

De Rienzo, G., Gutzman, J. H., and Sive, H. (2012). Efficient shRNA-mediated inhibition of gene expression in zebrafish. *Zebrafish* 9, 97–107.

Douglass, A. D., Kraves, S., Deisseroth, K., Schier, A. F., and Engert, F. (2008). Escape behavior elicited by single, channelrhodopsin-2-evoked spikes in zebrafish somatosensory neurons. *Curr. Biol.* 18, 1133–1137.

Driever, W., Solnica-Krezel, L., Schier, A. F., Neuhauss, S. C., Malicki, J., Stemple, D. L., et al. (1996). A genetic screen for mutations affecting embryogenesis in zebrafish. *Development* 123, 37–46.

Ebihara, S., Marks, T., Hudson, D. J., and Menaker, M. (1986). Genetic control of melatonin synthesis in the pineal gland of the mouse. *Science* 231, 491–493.

Elbaz, I., Yelin-Bekerman, L., Nicenboim, J., Vatine, G., and Appelbaum, L. (2012). Genetic ablation of hypocretin neurons alters behavioral state transitions in zebrafish. *J. Neurosci.* 32, 12961–12972.

Emran, F., Rihel, J., Adolph, A. R., and Dowling, J. E. (2010). Zebrafish larvae lose vision at night. *Proc. Natl. Acad. Sci. U.S.A.* 107, 6034–6039.

España, R. A., Baldo, B. A., Kelley, A. E., and Berridge, C. W. (2001). Wake-promoting and sleep-suppressing actions of hypocretin (orexin): basal forebrain sites of action. *Neuroscience* 106, 699–715.

Faraco, J. H., Appelbaum, L., Marin, W., Gaus, S. E., Mourrain, P., and Mignot, E. (2006). Regulation of hypocretin (orexin) expression in embryonic zebrafish. *J. Biol. Chem.* 281, 29753–29761.

Foltenyi, K., Greenspan, R. J., and Newport, J. W. (2007). Activation of EGFR and ERK by rhomboid signaling regulates the consolidation and maintenance of sleep in Drosophila. *Nat. Neurosci.* 10, 1160–1167.

Friedrich, R. W., Jacobson, G. A., and Zhu, P. (2010). Circuit neuroscience in zebrafish. *Curr. Biol.* 20, 371–381.

Gahtan, E., Tanger, P., and Baier, H. (2005). Visual prey capture in larval zebrafish is controlled by identified reticulospinal neurons downstream of the tectum. *J. Neurosci.* 25, 9294–9303.

Gallopin, T., Luppi, P.-H., Cauli, B., Urade, Y., Rossier, J., Hayaishi, O., et al. (2005). The endogenous somnogen adenosine excites a subset of sleep-promoting neurons via A2A receptors in the ventrolateral preoptic nucleus. *Neuroscience* 134, 1377–1390.

Ganguly-Fitzgerald, I., Donlea, J., and Shaw, P. J. (2006). Waking experience affects sleep need in Drosophila. *Science* 313, 1775–1781.

Gilbert, J., and Davis, F. C. (2009). Behavioral effects of systemic transforming growth factor-alpha in Syrian hamsters. *Behav. Brain Res.* 198, 440–448.

Glickman, G. (2010). Circadian rhythms and sleep in children with autism. *Neurosci. Biobehav. Rev.* 34, 755–768.

Golling, G., Amsterdam, A., Sun, Z., Antonelli, M., Maldonado, E., Chen, W., et al. (2002). Insertional mutagenesis in zebrafish rapidly identifies genes essential for early vertebrate development. *Nat. Genet.* 31, 135–140.

Goto, M., Oshima, I., Tomita, T., and Ebihara, S. (2007). Melatonin content of the pineal gland in different mouse strains. *J. Pineal Res.* 7, 195–204.

Haffter, P., Granato, M., Brand, M., Mullins, M. C., Hammerschmidt, M., Kane, D. A., et al. (1996). The identification of genes with unique and essential functions in the development of the zebrafish, Danio rerio. *Development* 123, 1–36.

Harris, G. C., and Aston-Jones, G. (2006). Arousal and reward: a dichotomy in orexin function. *Trends Neurosci.* 29, 571–577.

Hendricks, J. C., Finn, S. M., Panckeri, K. A., Chavkin, J., Williams, J. A., Sehgal, A., et al. (2000). Rest in Drosophila is a sleep-like state. *Neuron* 25, 129–138.

Hobson, J. A., and Pace-Schott, E. F. (2002). The cognitive neuroscience of sleep: neuronal systems, consciousness and learning. *Nat. Rev. Neurosci.* 3, 679–693.

Hobson, J. A., and Steriade, M. (1986). "Neuronal basis of behavioral state control," *Handbook of Physiology, Vol. 4*, eds V. B. Mountcastle and F. E. Bloom (Bethesda, MD: American Physiological Society), 701–823.

Holzschuh, J., Ryu, S., Aberger, F., and Driever, W. (2001). Dopamine transporter expression distinguishes dopaminergic neurons from other catecholaminergic neurons in the developing zebrafish embryo. *Mech. Dev.* 101, 237–243.

Huang, P., Xiao, A., Zhou, M., Zhu, Z., Lin, S., and Zhang, B. (2011). Heritable gene targeting in zebrafish using customized TALENs. *Nat. Biotechnol.* 29, 699–700.

Huang, Z.-L., Qu, W.-M., Eguchi, N., Chen, J.-F., Schwarzschild, M. A., Fredholm, B. B., et al. (2005). Adenosine A2A, but not A1, receptors mediate the arousal effect of caffeine. *Nat. Neurosci.* 8, 858–859.

Hurd, M. W., and Cahill, G. M. (2002). Entraining signals initiate behavioral circadian rhythmicity in larval zebrafish. *J. Biol. Rhythms* 17, 307–314.

Hurd, M. W., Debruyne, J., Straume, M., and Cahill, G. M. (1998). Circadian rhythms of locomotor activity in zebrafish. *Physiol. Behav.* 65, 465–472.

Jeong, J.-Y., Kwon, H.-B., Ahn, J.-C., Kang, D., Kwon, S.-H., Park, J. A., et al. (2008). Functional and developmental analysis of the blood–brain barrier in zebrafish. *FEBS Lett.* 75, 619–628.

Johnson, P. L., Molosh, A., Fitz, S. D., Truitt, W. A., and Shekhar, A. (2012). Orexin, stress, and anxiety/panic states. *Prog. Brain Res.* 198, 133–161.

Jones, B. E. (2003). Arousal systems. *Front. Biosci.* 8, s438–s451.

Jowett, T., and Yan, Y. L. (1996). Double fluorescent *in situ* hybridization to zebrafish embryos. *Trends Genet.* 12, 387–389.

Kaslin, J., Nystedt, J. M., Ostergård, M., Peitsaro, N., and Panula, P. (2004). The orexin/hypocretin system in zebrafish is connected to the aminergic and cholinergic systems. *J. Neurosci.* 24, 2678–2689.

Kaslin, J., and Panula, P. (2001). Comparative anatomy of the histaminergic and other aminergic systems in zebrafish (Danio rerio). *J. Comp. Neurol.* 440, 342–377.

Kettleborough, R. N. W., Bruijn, E., de Eeden, F. V., Cuppen, E., and Stemple, D. L. (2011). High-throughput target-selected gene inactivation in zebrafish. *Methods Cell Biol.* 104, 121–127.

Koh, K., Joiner, W. J., Wu, M. N., Yue, Z., Smith, C. J., and Sehgal, A. (2008). Identification of SLEEPLESS, a sleep-promoting factor. *Science* 321, 372–376.

Kokel, D., Bryan, J., Laggner, C., White, R., Cheung, C. Y. J., Mateus, R., et al. (2010). Rapid behavior-based identification of neuroactive small molecules in the zebrafish. *Nat. Chem. Biol.* 6, 231–237.

Kramer, A., Yang, F. C., Snodgrass, P., Li, X., Scammell, T. E., Davis, F. C. et al. (2001). Regulation of daily locomotor activity and sleep by hypothalamic EGF receptor signaling. *Science* 294, 2511–2515.

Krueger, J. M. (2008). The role of cytokines in sleep regulation. *Curr. Pharm. Des.* 14, 3408.

Laggner, C., Kokel, D., Setola, V., Tolia, A., Lin, H., Irwin, J. J., et al. (2012). Chemical informatics and target identification in a zebrafish phenotypic screen. *Nat. Chem. Biol.* 8, 144–146.

Lamb, J., Crawford, E. D., Peck, D., Modell, J. W., Blat, I. C., Wrobel, M. J., et al. (2006). The Connectivity Map: using gene-expression signatures to connect small molecules, genes, and disease. *Science* 313, 1929–1935.

Lang, M., Söll, R. M., Dürrenberger, F., Dautzenberg, F. M., and Beck-Sickinger, A. G. (2004). Structure-activity studies of orexin a and orexin B at the human orexin 1 and orexin 2 receptors led to orexin 2 receptor selective and orexin 1 receptor preferring ligands. *J. Med. Chem.* 47, 1153–1160.

Lauter, G., Söll, I., and Hauptmann, G. (2011). Multicolor fluorescent *in situ* hybridization to define abutting and overlapping gene expression in the embryonic zebrafish brain. *Neural Dev.* 6:10. doi: 10.1186/1749-8104-6-10

Lee, M. G., Hassani, O. K., and Jones, B. E. (2005). Discharge of identified orexin/hypocretin neurons across the sleep-waking cycle. *J. Neurosci.* 25, 6716–6720.

Lieschke, G. J., and Currie, P. D. (2007). Animal models of human disease: zebrafish swim into view. *Nat. Rev. Genet.* 8, 353–367.

Lin, L., Faraco, J., Li, R., Kadotani, H., Rogers, W., Lin, X., et al. (1999). The sleep disorder canine narcolepsy is caused by a mutation in the hypocretin (orexin) receptor 2 gene. *Cell* 98, 365–376.

Lin, S.-C., and Gervasoni, D. (2008). "Defining global brain states using multielectrode field potential recordings," in *Methods for Neural Ensemble Recordings, 2nd Edn.*, ed M. A. L. Nicolelis (Boca Raton, FL: CRC Press), 145–165.

Livet, J., Weissman, T. A., Kang, H., Draft, R. W., Lu, J., Bennis, R. A., et al. (2007). Transgenic strategies for combinatorial expression of fluorescent proteins in the nervous system. *Nature* 450, 56–62.

Lu, J., Greco, M. A., Shiromani, P., and Saper, C. B. (2000). Effect of lesions of the ventrolateral preoptic nucleus on NREM and REM sleep. *J. Neurosci.* 20, 3830–3842.

Maddison, L. A., Lu, J., and Chen, W. (2011). Generating conditional mutations in zebrafish using gene-trap mutagenesis. *Methods Cell Biol.* 104, 1–22.

Magnus, C. J., Lee, P. H., Atasoy, D., Su, H. H., Looger, L. L., and Sternson, S. M. (2011). Chemical and genetic engineering of selective ion channel-ligand interactions. *Science* 333, 1292–1296.

Mahowald, M. W., and Schenck, C. H. (2005). Insights from studying human sleep disorders. *Nature* 437, 1279–1285.

Marcus, J. N., Aschkenasi, C. J., Lee, C. E., Chemelli, R. M., Saper, C. B., Yanagisawa, M., et al. (2001). Differential expression of orexin receptors 1 and 2 in the rat brain. *J. Comp. Neurol.* 435, 6–25.

Mattis, J., Tye, K. M., Ferenczi, E. A., Ramakrishnan, C., O'Shea, D. J., Prakash, R., et al. (2012). Principles for applying optogenetic tools derived from direct comparative analysis of microbial opsins. *Nat. Methods* 9, 159–172.

McElligott, M. B., and O'Malley, D. M. (2005). Prey tracking by larval zebrafish: axial kinematics and visual control. *Brain. Behav. Evol.* 66, 177–196.

McLean, D. L., and Fetcho, J. R. (2004). Relationship of tyrosine hydroxylase and serotonin immunoreactivity to sensorimotor circuitry in larval zebrafish. *J. Comp. Neurol.* 480, 57–71.

McLean, D. L., and Fetcho, J. R. (2011). Movement, technology and discovery in the zebrafish. *Curr. Opin. Neurobiol.* 21, 110–115.

Mignot, E., Taheri, S., and Nishino, S. (2002). Sleeping with the hypothalamus: emerging therapeutic targets for sleep disorders. *Nat. Neurosci.* 5(Suppl.), 1071–1075.

Mileykovskiy, B. Y., Kiyashchenko, L. I., and Siegel, J. M. (2005). Behavioral correlates of activity in identified hypocretin/orexin neurons. *Neuron* 46, 787–798.

Miller, A. C., Obholzer, N. D., Shah, A. N., Megason, S. G., and Moens, C. B. (2013). RNA-seq based mapping and candidate identification of mutations from forward genetic screens. *Genome Res.* doi: 10.1101/gr.147322.112. [Epub ahead of print].

Mohawk, J. A., Green, C. B., and Takahashi, J. S. (2012). Central and peripheral circadian clocks in mammals. *Annu. Rev. Neurosci.* 35, 445–462.

Moore, F. E., Reyon, D., Sander, J. D., Martinez, S. A., Blackburn, J. S., Khayter, C., et al. (2012). Improved somatic mutagenesis in zebrafish using transcription activator-like effector nucleases (TALENs). *PLoS ONE* 7:e37877. doi: 10.1371/journal.pone.0037877

Moruzzi, G., and Magoun, H. W. (1949). Brain stem reticular formation and activation of the

EEG. *Electroencephalogr. Clin. Neurophysiol.* 1, 455–473.

Mu, Y., Li, X.-Q., Zhang, B., and Du, J.-L. (2012). Visual input modulates audiomotor function via hypothalamic dopaminergic neurons through a cooperative mechanism. *Neuron* 75, 688–699.

Nakamachi, T., Matsuda, K., Maruyama, K., Miura, T., Uchiyama, M., Funahashi, H., et al. (2006). Regulation by orexin of feeding behaviour and locomotor activity in the goldfish. *J. Neuroendocrinol.* 18, 290–297.

Naumann, E. A., Kampff, A. R., Prober, D. A., Schier, A. F., and Engert, F. (2010). Monitoring neural activity with bioluminescence during natural behavior. *Nat. Neurosci.* 13, 513–520.

North, T. E., Goessling, W., Walkley, C. R., Lengerke, C., Kopani, K. R., Lord, A. M., et al. (2007). Prostaglandin E2 regulates vertebrate haematopoietic stem cell homeostasis. *Nature* 447, 1007–1011.

Novak, C. M., Jiang, X., Wang, C., Teske, J. A., Kotz, C. M., and Levine, J. A. (2005). Caloric restriction and physical activity in zebrafish (Danio rerio). *Neurosci. Lett.* 383, 99–104.

Obholzer, N., Swinburne, I. A., Schwab, E., Nechiporuk, A. V., Nicolson, T., and Megason, S. G. (2012). Rapid positional cloning of zebrafish mutations by linkage and homozygosity mapping using whole-genome sequencing. *Development* 139, 4280–4290.

Pace-Schott, E. F., and Hobson, J. A. (2002). The neurobiology of sleep: genetics, cellular physiology and subcortical networks. *Nat. Rev. Neurosci.* 3, 591–605.

Pan, Y. A., Zhu, P., Livet, J., Narita, Y., Sanes, J. R., Bundschuh, S. T., et al. (2011). Multicolor brainbow imaging in zebrafish. *Cold Spring Harbor Protocols* 2011:pdb.prot5546. doi: 10.1101/pdb.prot5546

Pando, M. P., Pinchak, A. B., Cermakian, N., and Sassone-Corsi, P. (2001). A cell-based system that recapitulates the dynamic light-dependent regulation of the vertebrate clock. *Proc. Natl. Acad. Sci. U.S.A.* 98, 10178–10183.

Peterson, R. T., and Fishman, M. C. (2004). Discovery and use of small molecules for probing biological processes in zebrafish. *Methods Cell Biol.* 76, 569–591.

Peyron, C., Faraco, J., Rogers, W., Ripley, B., Overeem, S., Charnay, Y., et al. (2000). A mutation in a case of early onset narcolepsy and a generalized absence of hypocretin peptides in human narcoleptic brains. *Nat. Med.* 6, 991–997.

Peyron, C., Tighe, D. K., van den Pol, A. N., de Lecea, L., Heller, H. C., Sutcliffe, J. G., et al. (1998). Neurons containing hypocretin (orexin) project to multiple neuronal systems. *J. Neurosci.* 18, 9996–10015.

Pfaff, D., Ribeiro, A., Matthews, J., and Kow, L.-M. (2008). Concepts and mechanisms of generalized central nervous system arousal. *Ann. N.Y. Acad. Sci.* 1129, 11–25.

Pfeiffenberger, C., and Allada, R. (2012). Cul3 and the BTB adaptor insomniac are key regulators of sleep homeostasis and a dopamine arousal pathway in Drosophila. *PLoS Genet.* 8:e1003003. doi: 10.1371/journal.pgen.1003003

Porkka-Heiskanen, T., and Kalinchuk, A. V. (2011). Adenosine, energy metabolism and sleep homeostasis. *Sleep Med. Rev.* 15, 123–135.

Porkka-Heiskanen, T., Strecker, R. E., Thakkar, M., Bjørkum, A. A., Greene, R. W., and McCarley, R. W. (1997). Adenosine: a mediator of the sleep-inducing effects of prolonged wakefulness. *Science* 276, 1265–1268.

Portugues, R., and Engert, F. (2011). Adaptive locomotor behavior in larval zebrafish. *Front. Syst. Neurosci.* 5:72. doi: 10.3389/fnsys.2011.00072

Portugues, R., Severi, K. E., Wyart, C., and Ahrens, M. B. (2013). Optogenetics in a transparent animal: circuit function in the larval zebrafish. *Curr. Opin. Neurobiol.* 23, 119–126.

Postlethwait, J. H., Yan, Y. L., Gates, M. A., Horne, S., Amores, A., Brownlie, A., et al. (1998). Vertebrate genome evolution and the zebrafish gene map. *Nat. Genet.* 18, 345–349.

Pritchett, D., Wulff, K., Oliver, P. L., Bannerman, D. M., Davies, K. E., Harrison, P. J., et al. (2012). Evaluating the links between schizophrenia and sleep and circadian rhythm disruption. *J. Neural Transm.* 119, 1061–1075.

Prober, D. A., Rihel, J., Onah, A. A., Sung, R.-J., and Schier, A. F. (2006). Hypocretin/orexin overexpression induces an insomnia-like phenotype in zebrafish. *J. Neurosci.* 26, 13400–13410.

Pulver, S. R., Pashkovski, S. L., Hornstein, N. J., Garrity, P. A., and Griffith, L. C. (2009). Temporal dynamics of neuronal activation by Channelrhodopsin-2 and TRPA1 determine behavioral output in Drosophila larvae. *J. Neurophysiol.* 101, 3075–3088.

Raizen, D. M., Zimmerman, J. E., Maycock, M. H., Ta, U. D., You, Y.-J., Sundaram, M. V., et al. (2008). Lethargus is a Caenorhabditis elegans sleep-like state. *Nature* 451, 569–572.

Rechtschaffen, A., and Kales, A. (1968). *A Manual of Standardized Terminology, Techniques and Scoring System for Sleep Stages of Human Subjects.* Washington, DC: US Department of Health, Education and Welfare.

Reebs, S. (1992). "Sleep, inactivity, and circadian rhythms in fish," in *Rhythms in Fishes,* ed M. A. Ali (New York, NY: Springer), 127–136.

Renier, C., Faraco, J. H., Bourgin, P., Motley, T., Bonaventure, P., Rosa, F., et al. (2007). Genomic and functional conservation of sedative-hypnotic targets in the zebrafish. *Pharmacogenet. Genomics* 17, 237–253.

Reyon, D., Tsai, S. Q., Khayter, C., Foden, J. A., Sander, J. D., and Joung, J. K. (2012). FLASH assembly of TALENs for high-throughput genome editing. *Nat. Biotechnol.* 30, 460–465.

Rihel, J., Prober, D. A., Arvanites, A., Lam, K., Zimmerman, S., Jang, S., et al. (2010). Zebrafish behavioral profiling links drugs to biological targets and rest/wake regulation. *Science* 327, 348–351.

Rihel, J., and Schier, A. F. (2012). Behavioral screening for neuroactive drugs in zebrafish. *Dev. Neurobiol* 72, 373–385.

Rink, E., and Wullimann, M. F. (2002). Development of the catecholaminergic system in the early zebrafish brain: an immunohistochemical study. *Dev. Brain Res.* 137, 89–100.

Rogulja, D., and Young, M. W. (2012). Control of sleep by cyclin A and its regulator. *Science* 335, 1617–1621.

Ruuskanen, J. O., Peitsaro, N., Kaslin, J. V. M., Panula, P., and Scheinin, M. (2005). Expression and function of alpha-adrenoceptors in zebrafish: drug effects, mRNA and receptor distributions. *J. Neurochem.* 94, 1559–1569.

Ryu, S., Mahler, J., Acampora, D., Holzschuh, J., Erhardt, S., Omodei, D., et al. (2007). Orthopedia homeodomain protein is essential for diencephalic dopaminergic neuron development. *Curr. Biol.* 17, 873–880.

Sakurai, T., Amemiya, A., Ishii, M., Matsuzaki, I., Chemelli, R. M., Tanaka, H., et al. (1998). Orexins and orexin receptors: a family of hypothalamic neuropeptides and G protein-coupled receptors that regulate feeding behavior. *Cell* 92, 573–585.

Saper, C. B., Chou, T. C., and Scammell, T. E. (2001). The sleep switch: hypothalamic control of sleep and wakefulness. *Trends Neurosci.* 24, 726–731.

Saper, C. B., Scammell, T. E., and Lu, J. (2005). Hypothalamic regulation of sleep and circadian rhythms. *Nature* 437, 1257–1263.

Scammell, T. E., Gerashchenko, D. Y., Mochizuki, T., McCarthy, M. T., Estabrooke, I. V., Sears, C. A., et al. (2001). An adenosine A2a agonist increases sleep and induces Fos in ventrolateral preoptic neurons. *Neuroscience* 107, 653–663.

Shaw, P. J., Cirelli, C., Greenspan, R. J., and Tononi, G. (2000). Correlates of sleep and waking in *Drosophila melanogaster*. *Science* 287, 1834–1837.

Sigurgeirsson, B., Thorsteinsson, H., Arnardóttir, H., Jóhannesdóttir, I. T., and Karlsson, K. A. (2011). Effects of modafinil on sleep-wake cycles in larval zebrafish. *Zebrafish* 8, 133–140.

Stavropoulos, N., and Young, M. W. (2011). Insomniac and Cullin-3 regulate sleep and wakefulness in Drosophila. *Neuron* 72, 964–976.

Stenberg, D., Litonius, E., Halldner, L., Johansson, B., Fredholm, B. B., and Porkka-Heiskanen, T. (2003). Sleep and its homeostatic regulation in mice lacking the adenosine A1 receptor. *J. Sleep Res.* 12, 283–290.

Steriade, M., and McCarley, R. W. (2005). *Brain Control of Wakefulness and Sleep*. 2nd ed. New York, NY: Kluwer Academic/Plenum Publishers.

Sundvik, M., Kudo, H., Toivonen, P., Rozov, S., Chen, Y.-C., and Panula, P. (2011). The histaminergic system regulates wakefulness and orexin/hypocretin neuron development via histamine receptor H1 in zebrafish. *FASEB J.* 25, 4338–4347.

Sutcliffe, J. G., and de Lecea, L. (2002). The hypocretins: setting the arousal threshold. *Nat. Rev. Neurosci.* 3, 339–349.

Szobota, S., Gorostiza, P., Del Bene, F., Wyart, C., Fortin, D. L., Kolstad, K. D., et al. (2007). Remote control of neuronal activity with a light-gated glutamate receptor. *Neuron* 54, 535–545.

Taheri, S., Mahmoodi, M., Opacka-Juffry, J., Ghatei, M. A., and Bloom, S. R. (1999). Distribution and quantification of immunoreactive orexin A in rat tissues. *FEBS Lett.* 457, 157–161.

Tay, T. L., Ronneberger, O., Ryu, S., Nitschke, R., and Driever,

W. (2011). Comprehensive catecholaminergic projectome analysis reveals single-neuron integration of zebrafish ascending and descending dopaminergic systems. *Nat. Commun.* 2:171. doi: 10.1038/ncomms1171

Thakkar, M. M., Ramesh, V., Strecker, R. E., and McCarley, R. W. (2001). Microdialysis perfusion of orexin-A in the basal forebrain increases wakefulness in freely behaving rats. *Arch. Ital. Biol.* 139, 313–328.

Tolopko, A. N., Sullivan, J. P., Erickson, S. D., Wrobel, D., Chiang, S. L., Rudnicki, K., et al. (2010). Screensaver: an open source lab information management system (LIMS) for high throughput screening facilities. *BMC Bioinformatics* 11:260. doi: 10.1186/1471-2105-11-260

Trinh, L. A., Hochgreb, T., Graham, M., Wu, D., Ruf-Zamojski, F., Jayasena, C. S., et al. (2011). A versatile gene trap to visualize and interrogate the function of the vertebrate proteome. *Genes Dev.* 25, 2306–2320.

Trivedi, P., Yu, H., MacNeil, D. J., Van der Ploeg, L. H., and Guan, X. M. (1998). Distribution of orexin receptor mRNA in the rat brain. *FEBS Lett.* 438, 71–75.

Urade, Y., Eguchi, N., Qu, W.-M., Sakata, M., Huang, Z.-L., Chen, J.-F., et al. (2003). Sleep regulation in adenosine A2A receptor-deficient mice. *Neurology* 61, S94–S96.

Valatx, J. L., Bugat, R., and Jouvet, M. (1972). Genetic studies of sleep in mice. *Nature* 238, 226–227.

Van Buskirk, C., and Sternberg, P. W. (2007). Epidermal growth factor signaling induces behavioral quiescence in *Caenorhabditis elegans*. *Nat. Neurosci.* 10, 1300–1307.

Varshney, G. K., Huang, H., Zhang, S., Lu, J., Gildea, D. E., Yang, Z., et al. (2013). The Zebrafish Insertion Collection (ZInC): a web based, searchable collection of zebrafish mutations generated by DNA insertion. *Nucleic Acids Res.* 41, D861–D864.

Vatine, G., Vallone, D., Gothilf, Y., and Foulkes, N. S. (2011). It's time to swim! Zebrafish and the circadian clock. *FEBS Lett.* 585, 1485–1494.

Vize, P. D., McCoy, K. E., and Zhou, X. (2009). Multichannel wholemount fluorescent and fluorescent/chromogenic *in situ* hybridization in Xenopus embryos. *Nat. Protoc.* 4, 975–983.

von Economo, C. (1930). Sleep as a problem of localization. *J. Nerv. Ment. Dis.* 71, 249–259.

Wang, Z., Li, J., Huang, H., Wang, G., Jiang, M., Yin, S., et al. (2012). An integrated chip for the high-throughput synthesis of transcription activator-like effectors. *Angew. Chem. Int. Ed. Engl.* 124, 8633–8636.

Whitmore, D., Foulkes, N. S., and Sassone-Corsi, P. (2000). Light acts directly on organs and cells in culture to set the vertebrate circadian clock. *Nature* 404, 87–91.

Wolman, M. A., Jain, R. A., Liss, L., and Granato, M. (2011). Chemical modulation of memory formation in larval zebrafish. *Proc. Natl. Acad. Sci. U.S.A.* 108, 15468–15473.

Wu, M. N., Ho, K., Crocker, A., Yue, Z., Koh, K., and Sehgal, A. (2009). The effects of caffeine on sleep in Drosophila require PKA activity, but not the adenosine receptor. *J. Neurosci.* 29, 11029–11037.

Wullimann, M. F., and Mueller, T. (2004). Teleostean and mammalian forebrains contrasted: evidence from genes to behavior. *J. Comp. Neurol.* 475, 143–162.

Wyart, C., Del Bene, F., Warp, E., Scott, E. K., Trauner, D., Baier, H., et al. (2009). Optogenetic dissection of a behavioural module in the vertebrate spinal cord. *Nature* 461, 407–410.

Yokogawa, T., Hannan, M. C., and Burgess, H. A. (2012). The dorsal raphe modulates sensory responsiveness during arousal in zebrafish. *J. Neurosci.* 32, 15205–15215.

Yokogawa, T., Marin, W., Faraco, J., Pézeron, G., Appelbaum, L., Zhang, J., et al. (2007). Characterization of sleep in zebrafish and insomnia in hypocretin receptor mutants. *PLoS Biol* 5:e277. doi: 10.1371/journal.pbio.0050277

Yu, P. B., Hong, C. C., Sachidanandan, C., Babitt, J. L., Deng, D. Y., Hoyng, S. A., et al. (2008). Dorsomorphin inhibits BMP signals required for embryogenesis and iron metabolism. *Nat. Chem. Biol.* 4, 33–41.

Zhang, E. E., and Kay, S. A. (2010). Clocks not winding down: unravelling circadian networks. *Nat. Rev. Mol. Cell Biol.* 11, 764–776.

Zhdanova, I. V. (2006). Sleep in zebrafish. *Zebrafish* 3, 215–226.

Zhdanova, I. V., Wang, S. Y., Leclair, O. U., and Danilova, N. P. (2001). Melatonin promotes sleep-like state in zebrafish. *Brain Res.* 903, 263–268.

Zhu, P., Narita, Y., Bundschuh, S. T., Fajardo, O., Schärer, Y.-P. Z., Chattopadhyaya, B., et al. (2009). Optogenetic dissection of neuronal circuits in zebrafish using viral gene transfer and the tet system. *Front. Neural Circuits* 3:21. doi: 10.3389/neuro.04.021.2009

Conflict of Interest Statement: The authors declare that the research was conducted in the absence of any commercial or financial relationships that could be construed as a potential conflict of interest.

Received: 07 February 2013; paper pending published: 03 March 2013; accepted: 14 March 2013; published online: 09 April 2013.

Citation: Chiu CN and Prober DA (2013) Regulation of zebrafish sleep and arousal states: current and prospective approaches. Front. Neural Circuits 7:58. doi: 10.3389/fncir.2013.00058

frontiers in
NEURAL CIRCUITS

ORIGINAL RESEARCH ARTICLE
published: 13 November 2013
doi: 10.3389/fncir.2013.00178

The ontogeny of sleep–wake cycles in zebrafish: a comparison to humans

Amanda Sorribes[1], Haraldur Þorsteinsson[2,3], Hrönn Arnardóttir[2], Ingibjörg Þ. Jóhannesdóttir[2], Benjamín Sigurgeirsson[2], Gonzalo G. de Polavieja[1] and Karl Æ. Karlsson[2,3]*

[1] *Instituto Cajal, Consejo Superior de Investigaciones Científicas, Madrid, Spain*
[2] *Biomedical Engineering, School of Science and Engineering, Reykjavik University, Reykjavik, Iceland*
[3] *3Z Pharmaceuticals, Reykjavik, Iceland*

Edited by:
German Sumbre, Ecole Normale Superieure, France

Reviewed by:
Lior Appelbaum, Bar-Ilan University, Israel
Philippe Mourrain, Stanford University, USA

****Correspondence:***
Karl Æ. Karlsson, Biomedical Engineering, School of Science and Engineering, Reykjavik University, 101 Reykjavik, Iceland
e-mail: karlsson@ru.is

Zebrafish (*Danio rerio*) are used extensively in sleep research; both to further understanding of sleep in general and also as a model of human sleep. To date, sleep studies have been performed in larval and adult zebrafish but no efforts have been made to document the ontogeny of zebrafish sleep–wake cycles. Because sleep differs across phylogeny and ontogeny it is important to validate the use of zebrafish in elucidating the neural substrates of sleep. Here we describe the development of sleep and wake across the zebrafish lifespan and how it compares to humans. We find power-law distributions to best fit wake bout data but demonstrate that exponential distributions, previously used to describe sleep bout distributions, fail to adequately account for the data in either species. Regardless, the data reveal remarkable similarities in the ontogeny of sleep cycles in zebrafish and humans. Moreover, as seen in other organisms, zebrafish sleep levels are highest early in ontogeny and sleep and wake bouts gradually consolidate to form the adult sleep pattern. Finally, sleep percentage, bout duration, bout number, and sleep fragmentation are shown to allow for meaningful comparisons between zebrafish and human sleep.

Keywords: sleep, wakefulness, *Danio rerio*, humans, ontogeny, bout structure

INTRODUCTION

In all species studied so far, sleep levels are highest and sleep bouts are shortest early in ontogeny (Kleitman and Engelman, 1951; Roffwarg et al., 1966; Jouvet-Mounier et al., 1970; Blumberg et al., 2005; Jenni et al., 2006). Cetaceans, however, represent an exception from this rule (Lyamin et al., 2005). For example, human infants spend about two-thirds of the day (i.e., 24-h) asleep whereas adults sleep for only one-third of the day (Roffwarg et al., 1966). This reduction in sleep levels across ontogeny has been reported in many other species (Jouvet-Mounier et al., 1970; Hoppenbrouwers and Sterman, 1975; McGinty et al., 1977). Another seemingly universal feature of sleep development is the gradual consolidation of sleep and wake bouts (Blumberg et al., 2005; Arnardóttir et al., 2010; Karlsson et al., 2011). For example, the average length of a sleep bout in 2-day-old rats is less than 25 s, over the next 14 days this average length increases to about 100 s (Blumberg et al., 2005) and the same trend has been demonstrated in other rodent species and humans; in flies sleep is more abundant in young rather than old flies (Shaw et al., 2000; Jenni et al., 2006; Todd et al., 2012). Even though sleep has been studied in larvae and adults, no such description of sleep–wake ontogeny exists for zebrafish (*Danio rerio*), a recent, promising model for sleep research (Zhdanova, 2006; Zhdanova et al., 2006; Yokogawa et al., 2007; Rihel et al., 2010a,b; Sigurgeirsson et al., 2011).

Zebrafish are a highly regarded model in developmental biology because of their fecundity, larval-stage transparency, short time to hatching, and ease in handling (Eisen, 1996); furthermore, they are well characterized in terms of development, neurobiology, and genetics (Westerfield, 2000). Sleep in zebrafish (adults as well as larvae) is measured in behavioral assays where it has been shown to exhibit the hallmarks of mammalian sleep, that is, (1) the absence of voluntary movement; (2) reversibility; (3) spontaneous occurrence with a circadian rhythm; (4) increased arousal thresholds; and (5) homeostatic regulation (Prober et al., 2006; Zhdanova, 2006; Zhdanova et al., 2006; Yokogawa et al., 2007). Moreover, zebrafish utilize all neurotransmitters currently known to be important for the regulation of sleep and wakefulness (Panula et al., 2010), and respond similarly to mammals when exposed to pharmacological agents that promote either sleep or wakefulness (Rihel et al., 2010a; Sigurgeirsson et al., 2011). In addition, there are many experimental tools (e.g., morpholino-oligonucleotide knock-downs, optical imaging techniques, large forward genetic screens), not easily applied in mammalian models, that can be readily applied to zebrafish (McLean and Fetcho, 2008; Appelbaum et al., 2010; Friedrich et al., 2010; Naumann et al., 2010; Bedell et al., 2012). Neural circuits driving sleep–wake cycles have only just begun to be delineated in zebrafish.

Many attempts have been made to provide a mathematical description of sleep (Achermann and Borbely, 1990, 1994, 2003; Borbely and Achermann, 1999; Best et al., 2007; Rempe et al., 2010) as well as provide a description of the sleep–wake bout dynamics (Lo et al., 2002, 2004; Blumberg et al., 2005, 2007a; Bianchi et al., 2010; Chu-Shore et al., 2010). These efforts have mostly been confined to mammalian data and our knowledge this has not been attempted for fish or invertebrates. Briefly, in adult mammals, sleep bouts have been shown to fit exponential distributions

whereas wake bouts have been shown to fit power-law distributions (Lo et al., 2002, 2004; Blumberg et al., 2005; Arnardóttir et al., 2010; Karlsson et al., 2011). Quantification of sleep architecture in terms of bout duration and state transitions has important applications; e.g., state transition data has been used to monitor sleep quality in obstructive sleep apnea (Bianchi et al., 2010) and it has been used to gage developmental milestones in sleep development (Blumberg et al., 2005, 2007b). Since transitions between sleep states [i.e., rapid eye movement (REM)/non-REM (NREM) alternations] and events within a sleep state (e.g., micro-arousals, K-complexes, and apneas) are ignored, state transition analysis can be performed identically in different animals making sleep states comparable across ontogeny and phylogeny. In mammals, the waking state is largely believed to be represented by high tonic activity of brainstem neurons releasing noradrenaline, histamine, and serotonin (Pace-Schott and Hobson, 2002; McCarley, 2007). Acetylcholine is released both at the level of basal forebrain and brainstem and hypothalamic hypocretin is released in concert with arousal peaks (McCarley, 2007; Blouin et al., 2013); even though in the absence of hypocretin function both sleep and wake are de-stabilized (Saper et al., 2001). All of these wake-active neurons form a circuit that maintains arousal (including cortical arousal in mammals) and, during REM, dis-facilitate motor neurons via activation of GABA-ergic interneurons (Siegel, 2000). Hypothalamic melatonin and neural peptides are highly conserved in zebrafish (Appelbaum et al., 2009; Berman et al., 2009). The transition to sleep may depend on the activation of GABA-ergic neurons in the ventrolateral preoptic area which inhibit all the wake-active monoamine-ergic and hypocretin cells (Saper et al., 2001). These state transition dynamics likely reflect differences in the neural substrates governing sleep–wake cycles.

To substantiate the use of zebrafish in sleep research; as a model of human sleep and sleep disorders and their use in screening pharmacological sleep aids (Zon and Peterson, 2005; Rihel and Schier, 2012), we present data on the development of sleep and sleep–wake bout architecture across the zebrafish lifespan. First, we describe sleep across ontogeny in humans and zebrafish and describe its development. Next, we contrast sleep development between zebrafish and humans. We show that sleep–wake dynamics and bout structure follow similar developmental trajectories in humans and zebrafish.

MATERIALS AND METHODS

HUMANS

Participants

Fifty participants, from 2- to 74-year-olds, participated in the study. The data collection has previously been presented in detail (Arnardóttir et al., 2010) but in the current study the data are re-analyzed using different methods and age groups. Briefly, data were sampled cross-sectionally from multiple ages representative of the human lifespan. The groups were as follows: Children (ages 2–8, $n = 15$), Preteen and teens (ages 11–16, $n = 9$), Adults (ages 23–43, $n = 15$), and Adults (ages 49–74, $n = 11$), from here on referred to as "Adults 50+." The study was approved by the Icelandic National Bioethics Committee (permit VSNb2007100011/03-15).

Recruitment

Participants were drawn from a randomized sample of 1000 inhabitants from the Reykjavik area, taken from the national registry of Iceland. Participants (or their legal guardians) were contacted by phone and offered to take part in the study. Of over 250 potential participants contacted, 78 accepted to take part and were pre-screened for health status over the phone; subsequently 21 participants (9 female, 12 male; age range 13–66 years) were dropped from the study before undergoing the polysomnography (PSG) due to at least one of the following conditions that may alter sleep patterns: obesity, depression, insomnia, snoring, alcohol and/or substance abuse, recent hospitalization, or the use of sleep altering medications. One participant underwent PSG but was dropped due to suspected hypothyroidism and six PSGs were unusable for technical reasons.

Questionnaire

Before the study, each participant (or their legal guardians) completed a 38-item questionnaire on sleep habits, adapted from the National University Hospital of Iceland and the Epworth sleepiness scale (ESS; Johns, 1991). The questionnaire included: five items about smoking and alcohol use, open ended questions on medical conditions, hospitalizations, and use of prescription medicines; 23 items on sleep quality; four items aimed at identifying complaints of restless leg syndrome, and six items aimed at identifying complaints of respiratory disturbances. None of the participants that provided data for the present study suffered from any condition that could have altered sleep patterns.

Procedure

Each participant underwent an unattended ambulatory PSG with a digital recording system (Medcare Inc., Iceland). The experimenter prepared the recording at the participant's house after 21:00 and instructed the participant to follow his normal daily sleep routine as closely as possible. All recordings were made between 22:00 and 08:00. The PSG included a four-channel (C3-A2; C4-A1; O3-A2; O4-A1) electroencephalogram (EEG), electrooculogram (EOG), chin electromyogram (EMG), and electrocardiogram (ECG). Airflow was recorded via nasal cannula. Thoracic and abdominal respiratory movements were recorded with plethysmography. Arterial oxygen saturation was measured continuously via an infrared finger probe and a piezo-electric sensor was used to monitor postural changes.

Data preprocessing

Sleep–wake cycles were scored by an accredited sleep technologist. All sleep parameters were scored in accordance to the Rechtschaffen and Kales criteria (Rechtschaffen and Kales, 1968). In all groups sleep was scored in 30-s epochs according to conventional methods (Rechtschaffen and Kales, 1968) using the Neuroscore software (DSI). After conventional sleep–wake scoring and analysis, all bouts of SWS 1–4 and REM were merged, since subsequent analyses do not require information on alternations within sleep states (or other parameters such as respiratory indexes, micro-arousals, etc.).

ZEBRAFISH

Fish

Stock fish of the Tübingen strain were provided by the University of Oregon Zebrafish International Resource Center. Fish were fed twice a day on a diet of TetraMin flakes (Tetra Holding GmbH) and kept in a 14:10 light:dark cycle (lights-on at 07:00) in either a 3- or 10-L multi-tank constant flow system tanks (Aquatic Habitats). Water temperature was held at a constant 28.5°C, and water was replaced at a rate of 10% per day. Zebrafish eggs were harvested between 08:00 and 10:00 and placed in a separate tank (with methylene blue) until hatching. All procedures were in compliance with the regulations of the National Bioethics Committee of Iceland; permit issued to Karl Æ. Karlsson, May 19, 2008 (no number).

Procedure

Sixty-one zebrafish were assigned to one of four age groups: 6–10 days post-fertilization (dpf; $n = 16$); 4–6 weeks ($n = 16$); 4–6 months ($n = 14$); over 12 months ($n = 15$). These age groups roughly represent larval, juvenile, adult, and senior zebrafish, respectively. It is important to note that while there are four age groups assigned for both fish and humans, there is no experimental data available that allows them to be fully equated. Regardless, analysis of sleep behavior for groups 1–2 occurred in 24- and 12-well plates, respectively, while groups 3–4 were studied in 75-L aquarium (at 28.5°C), with a black divider setup keeping fish isolated within an environment of 10 cm across, 6.5 cm deep, and 13 cm tall. All data were collected using Ethovision XT 7.0 behavioral tracking system (Noldus Information Technology) under white and IR lights for 48 h. All groups were recorded under the same temperature (28.5°C) and 14–10 light cycle with lights-on at 07:00, lights off at 21:00. The recording commenced at 12:00; data following 24-h acclimation period was used for analysis. During recording and acclimation larvae and adult fish were fed daily at 12:00, zebrafish larval food (Zeigler Bros) and TetraMin flakes (Tetra Holding GmbH), respectively. Feeding was done at 12:00 noon. No recording was made over the seconds that took to dispense the food. Each recording was 24 h; reset at 12:00 (the food items are too small to be tracked; minimal tracking size was set at 25 pixels). No special care was taken to avoid monitoring the movements following feeding.

Larval and young zebrafish (two youngest groups) were placed individually into wells and plates were then placed in a custom-built transparent Plexiglas holder with circulating water; the holder was placed in the activity monitoring system, which was blocked from daylight and illuminated from below with white (255 lx; light-phase) or infrared light (0 lx; dark-phase). The velocity of each fish was tracked in two dimensions, at 8.33 Hz using a Sony XC-E150 infrared camera (Sony Inc.) with a 50-mm CCTV Pentax lens (Pentax, GMBH).

Young adult and adult zebrafish (two oldest groups) were placed in the recording tank at 12:00. The aquarium was illuminated with two infrared lights (0 lx; dark-phase) and a fluorescent light (255 lx; light-phase), all of which was housed in an opaque black plexiglas box with an ambient lighting of 0 lx. All data tracking and recording is identical to what is described for larvae.

Data preprocessing

Behavioral states were dichotomized into 1-s bins of movement/non-movement. Prior, in-depth frame-by-frame video analysis by three independent raters resulted in the adoption of the speed of 0.5 cm/s as the threshold for movement for larval zebrafish (Sigurgeirsson et al., 2011). All activity that was slower than that threshold was described as non-movement. Due to the changes in the size of the fish the threshold for movement had to be adjusted for age. A comparison between a threshold determined by mathematical scaling with body size and a threshold obtained by visual video analysis did not suggest a significant difference between these two approaches. The thresholds for groups 2–4 were set as follows: group 2: 0.75 cm/s; group 3: 1.0 cm/s; group 4: 1.5 cm/s. Following previously established criteria in adult zebrafish (Yokogawa et al., 2007; Zhdanova et al., 2008; Singh et al., 2013) after six or more consecutive 1-s bins of non-movement, the seventh second and above were classified as sleep; all other bouts were classified as wake. In prior work we applied the same criteria to larval fish (Sigurgeirsson et al., 2011). We validated this approach by calculating the response time to a 60-s light stimulus (550 lx) in 252 additional 6-dpf larvae as a function of immobile time during night. Three categories of immobile time were compared: 0–6 s, 6–11 s, and 11 and above. Mean response times were 2.28, 6.66, and 6.67 s, respectively. 0–6 s group differed from 6–11 s group ($t = -2.256$, $\mathrm{df} = 25.57$, $p = 0.033$) and from 11+ group ($t = 2.33$, $\mathrm{df} = 15.74$, $p = 0.41$). The 6–11 and 11+ group did not differ ($t = 0.002$, $\mathrm{df} = 34$, $p = 0.998$).

DATA ANALYSIS

Statistical analysis

All sleep–wake bout data were imported into Matlab 2010a (The MathWorks Inc.) for subsequent data analysis. For each individual, mean durations of sleep and wake bouts were calculated and fragmentation indexes were calculated as the number of sleep (wake) bouts divided by the total sleep (wake) time, in minutes. Analysis of variance (ANOVA) was used to test for the influence of age on percent sleep/wake, mean durations, number of bouts and fragmentation indexes, while Holm–Bonferroni corrected multiple two-tailed t-tests were used to test the specific differences between the age groups, with the family-wise type I error rate (alpha) set to 0.05. One of three different implementations of the t-test was applied for each comparison, depending on the characteristics of the two test samples. If both sets were normally distributed (or rather, failed to be rejected as coming from a normal distribution by the Lilliefors test of normality) and the variances were not unequal (i.e., "equal," as determined by a two-sample F-test for equal variances) the standard parametric Student's t-test was used. If the variances were unequal, the Welch's t-test was used. Finally, if at least one of the two samples were not normally distributed the p-value was instead estimated by first bootstrapping the t-statistic, with a resampling of $n = 10{,}000$ and then calculating the probability of finding a result at least as extreme as the test t-statistic.

Group results are presented as mean ± standard error of the mean. In the box plots, the whiskers extend to the lowest and highest values within the 1.5 interquartile range (IQR). This corresponds to approximately $\pm 2.7\sigma$ and 99.3% coverage if the data

are normally distributed. Values outside the 1.5 IQR are considered outliers.

Bout distributions

The sleep and wake bout duration distributions were tested against four models: (i) exponential distribution, $f(x;\ \tau) = 1/\tau\ \exp(-x/\tau)$, (ii) stretched exponential distribution, $f(x;\ k,\ \lambda) = (k/\lambda)(x/\lambda)^{k-1}\ \exp[-(x/\lambda)^{k}]$, (iii) power-law distribution $f(x;\ \alpha,\ x_{low}) = (\alpha - 1)x_{low}{}^{\alpha-1}x^{\alpha}$, and (iv) lognormal distribution $f(x;\ \mu,\ \sigma) = (1/x)(\sigma^2 2\pi)^{-1/2}\ \exp[-(\ln\ x - \pi)^2/2\sigma^2]$. For all the distributions $x = t - t_{min}$, where t_{min} is the shortest bout duration for each behavioral state as determined by the experimental procedure (30 s for human sleep and wake bouts, 6 and 1 s, respectively for zebrafish sleep and wake). The exponential distribution, power-law and lognormal distribution parameters were estimated using maximum likelihood estimators (MLE). To find the power-law best fit estimates for the exponent α and lower cut-off x_{low} the method described in Clauset et al. (2009) was used. To estimate the best fit parameters for the stretched exponential distribution the linear fit between $\log(x)$ and $\log[-\log(y)]$, where y is the survival distribution was used, as it has previously been shown to robustly estimate the stretched exponential parameters for small sample sizes (Sorribes et al., 2011).

RESULTS

HUMAN SLEEP RATIO DECREASES WITH AGE

In humans, a reduction in sleep ratio (percentage of sleep across the night) was found across age [$F(3,46) = 11{,}69$, $p < 0.0001$]. The Adults 50+ age group had a lower sleep ratio compared to Children ($p < 0.01$), Preteens and teens ($p < 0.01$), and Adults ($p < 0.01$; **Figure 1A**; **Table 1**). No changes were found in the average length of sleep bouts, number of sleep bouts or sleep fragmentation across age (**Figures 1B–D**; **Table 1**).

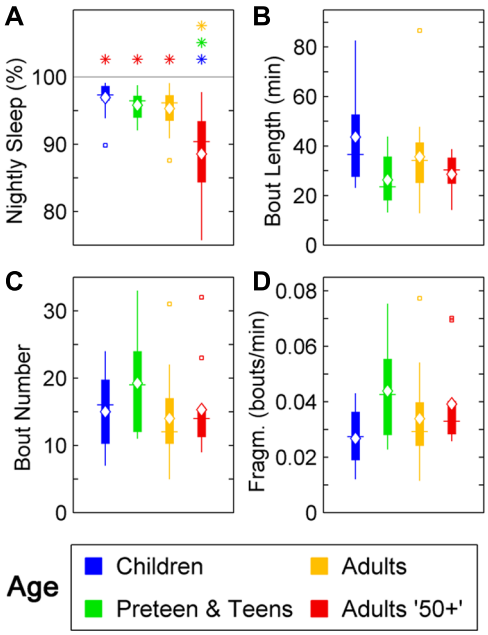

FIGURE 1 | Sleep parameters during the night in humans across age groups: Children (blue), Preteens and teens (green), Adults (orange), and Adults 50+ (red). Colored asterisks above bars indicate a statistically significant difference between the bar group and the group with the corresponding color of the asterisk. **(A)** Percentage sleep time. The mean percentage of sleep is significantly lower in Adults older than 50 than in all other age groups. **(B)** Mean sleep bout length. There is no difference between age groups in the mean duration of the sleep bouts. **(C)** The number of sleep bouts during nightly sleep do not change across the age groups. **(D)** Sleep bout fragmentation (bouts/min). There are no significant changes of the sleep fragmentation with age. Diamond, white line, and squares indicate mean, median, and outlier values, respectively.

HUMAN AWAKENINGS AT NIGHT LENGTHEN WITH AGE

Changes were seen in wake ratio (percentage of time spent awake during night) [$F(3,46) = 11.69$, $p < 0.0001$]. Wake percentage increased significantly after the age of 50 compared to Children ($p < 0.01$), Preteens and teens ($p < 0.01$), and Adults ($p < 0.01$; **Figure 2A**; **Table 1**). Average wake bout length also increased with age [$F(3,46) = 9.08$, $p < 0.0001$]. Wake bouts were longer in the age group Adults 50+ compared to Children ($p < 0.0001$) and Preteens and teens ($p < 0.0001$; **Figure 2B**; **Table 1**). However, wake bout number was unchanged across age (**Figure 2C**; **Table 1**). Wake fragmentation, defined as the number of awakenings divided by the total time awake, decreased after the age of 50 [$F(3,46) = 6.94$, $p < 0.001$; **Figure 2D**; **Table 1**], that is, the Adults 50+ age group showed reduced wake fragmentation (i.e., when awake, the wake bout is longer) compared to Children ($p < 0.0001$), Preteens and teens ($p < 0.001$), and Adults ($p < 0.0001$).

ZEBRAFISH SLEEP RATIO DECREASES WITH AGE AND SLEEP BOUTS CONSOLIDATE

In zebrafish, sleep ratio at night decreased with age [percentage of time spent asleep during night; $F(3,57) = 6.87$, $p < 0.001$] as well as the full 24 h sleep ratio (**Figure 3**; **Table 1**). Four- to six-month-olds showed significantly decreased sleep ratio compared to the 6- to 10-day-olds ($p < 0.001$) and 4- to 6-week-olds ($p < 0.01$). The 12 month+ group also had decreased sleep ratio compared to the 6- to 10-day-old group ($p < 0.01$) and 4- to 6-week-old group ($p < 0.05$). Furthermore, in zebrafish the sleep bout number during night decreased with age [$F(3,57) = 17.25$, $p < 0.0001$]. The 4- to 6-month-old group showed significantly less number of sleep bouts compared to 6–10 days ($p < 0.001$) and 4–6 weeks old ($p < 0.0001$; **Figures 4A–C**; **Table 1**). Also the 12+ month group had fewer sleep bouts compared to 6- to 10-day-olds ($p < 0.0001$) and 4- to 6-week-old fish ($p < 0.0001$). No changes were seen across age in sleep bout length or sleep fragmentation in zebrafish (**Figures 4B–D**; **Table 1**).

ZEBRAFISH WAKE RATIO INCREASES AND AWAKENINGS AT NIGHT LENGTHEN WITH AGE

Wake behavior during night in zebrafish showed a clear change with age. The wake ratio increased significantly [$F(3,57) = 6.87$, $p < 0.001$], from 6- to 10-day-olds to the 12+ month old group. Specifically, 12+ month olds showed increased wake ratio compared to 6- to 10-day ($p < 0.01$) and 4- to 6-week-olds ($p < 0.05$), and the 4- to 6-month-old group had a higher wake ratio than 6- to 10-day ($p < 0.001$) and 4- to 6-week-old fish ($p < 0.01$; **Figure 5A**; **Table 1**). Wake bout length also increased with age

Table 1 | Sleep and wake parameters across ontogeny in humans and zebrafish.

	Age group	Percent time of night (%)		Bout length (min)		Total number of bouts		Fragmentation (bouts/min)		Number of different bout lengths		Favored model	Model shape parameter
		Mean	SE	Mean	SE	Mean	SE	Mean	SE	Mean	SE		Mean ± SE
Human sleep	Children	96.96	0.63	43.64	4.89	15.00	1.46	0.03	0.00	13.60	1.14	Stretched exponential	$\kappa = 0.84 \pm 0.06$
	Preteen and teens	95.82	0.71	26.33	3.48	19.22	2.71	0.04	0.01	16.56	2.01	Stretched exponential	$\kappa = 0.84 \pm 0.05$
	Adults	95.32	0.80	35.62	4.44	14.00	1.67	0.03	0.00	12.47	1.20	Stretched exponential	$\kappa = 0.79 \pm 0.07$
	Adults '50+'	88.54	1.93	28.62	2.58	15.27	2.01	0.04	0.00	13.64	1.34	Power-law	$\alpha = 2.63 \pm 0.48$
Zebrafish sleep	6–10 days	58.17	4.25	0.44	0.15	1315.69	135.74	4.49	0.59	94.69	8.10	Stretched exponential	$\kappa = 0.69 \pm 0.03$
	4–6 weeks	54.25	5.02	0.32	0.05	1144.44	63.22	4.52	0.75	94.31	8.72	Stretched exponential	$\kappa = 0.77 \pm 0.03$
	4–6 months	33.37	4.40	0.30	0.04	674.86	62.11	4.37	0.85	81.93	7.20	Stretched exponential	$\kappa = 0.71 \pm 0.02$
	12 months+	33.06	6.44	0.41	0.11	506.40	79.13	5.43	1.29	75.60	11.20	Power-law	$\alpha = 2.80 \pm 0.17$
Human wake	Children	3.04	0.63	1.21	0.21	14.07	1.43	1.03	0.10	3.93	0.36	Power-law	$\alpha = 1.78 \pm 0.04$
	Preteen and teens	4.18	0.71	1.16	0.30	18.22	2.71	1.09	0.13	4.22	0.40	Power-law	$\alpha = 1.90 \pm 0.04$
	Adults	4.68	0.80	1.61	0.22	13.00	1.67	0.81	0.12	4.53	0.48	Power-law	$\alpha = 1.71 \pm 0.03$
	Adults '50+'	11.46	1.93	4.01	0.85	14.36	1.98	0.40	0.09	6.36	0.74	Power-law	$\alpha = 1.83 \pm 0.13$
Zebrafish wake	6–10 days	41.83	4.25	0.19	0.01	1315.63	135.68	5.56	0.26	42.81	4.07	Power-law	$\alpha = 4.09 \pm 0.44$
	4–6 weeks	45.75	5.02	0.23	0.02	1144.44	63.22	4.64	0.30	51.75	5.35	Power-law	$\alpha = 3.96 \pm 0.11$
	4–6 months	66.63	4.40	0.77	0.18	674.00	62.11	1.94	0.27	85.93	5.55	Power-law	$\alpha = 2.57 \pm 0.11$
	12 months+	66.94	6.44	1.52	0.54	505.67	79.17	1.65	0.31	85.27	7.91	Power-law	$\alpha = 2.45 \pm 0.13$

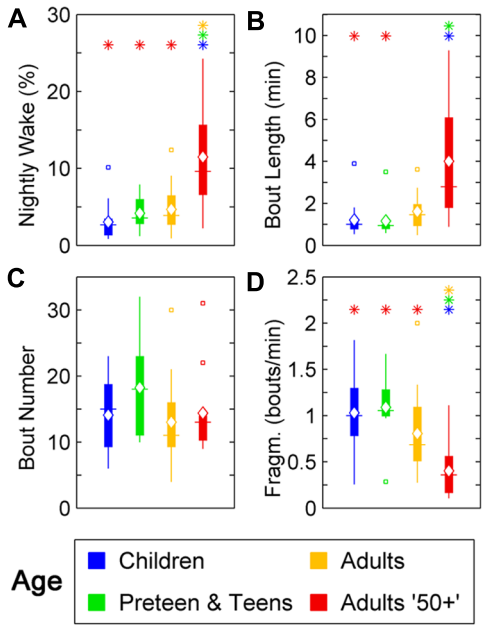

FIGURE 2 | Wake parameters of nightly sleep in humans across age groups: Children (blue), Preteens and teens (green), Adults (orange), and Adults 50+ (red). Colored asterisks above bars indicate a statistically significant difference between the bar group and the group with the corresponding color of the asterisk. **(A)** Percentage wake time. The mean percentage of time awake is significantly lower for Adults over 50 than for all other age groups. **(B)** Mean wake bout duration. Adults over 50 have significantly longer wake bouts during the night than Children and Preteens and teens. **(C)** The number of wake bouts do not change with age. **(D)** Wake bout fragmentation (bouts/min). Adults over 50 show significantly less fragmented wake than the younger age groups. Diamond, white line, and squares indicate mean, median, and outlier values, respectively.

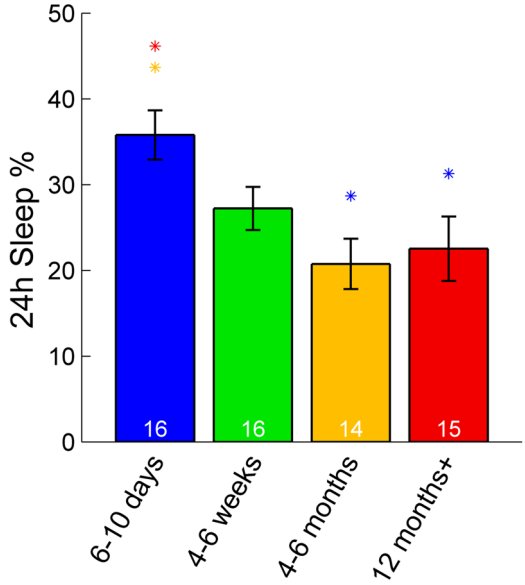

FIGURE 3 | Sleep percentage across 24 h in zebrafish. The youngest group (6–10 days post-fertilization) sleep significantly more over a full 24-h time period than adult fish (4–6 and 12+ months). Colored asterisks above bars indicate a statistically significant difference between the bar group and the group with the corresponding color of the asterisk. White numbers on the bars indicate the number of zebrafish in each age group.

[$F(3,57) = 5.05$, $p < 0.01$], i.e., the 12+ month old group showed increased wake bout length compared to 6- to 10-day ($p < 0.0001$) and 4- to 6-week-old group ($p < 0.0001$), and the 4–6 months group had longer wake bouts than 6–10 days ($p < 0.0001$) and 4–6 weeks old ($p < 0.0001$). Furthermore, wake bout number showed a decrease with age [$F(3,57) = 17.29$, $p < 0.0001$], i.e., the 12+ month old group had less wake bouts than 6–10 days ($p < 0.0001$) and 4–6 weeks old ($p < 0.0001$), and the 4–6 months group had fewer wake bouts than 6–10 days ($p < 0.001$) and 4- to 6-week group ($p < 0.0001$). Finally wake fragmentation decreased with age [$F(3,57) = 45.8$, $p < 0.0001$], i.e., the 12+ months group showed less fragmentation compared to 6- to 10-day ($p < 0.0001$) and 4- to 6-week-old fish ($p < 0.0001$), and the 4- to 6-month group exhibited less fragmentation compared to 6–10 days ($p < 0.0001$) and 4- to 6-week-old ($p < 0.0001$; see **Figures 5B–D**; **Table 1**).

SLEEP BOUTS EXHIBIT A STRETCHED EXPONENTIAL BEHAVIOR AND WAKE BOUTS POWER-LAW BEHAVIOR IN BOTH HUMANS AND ZEBRAFISH

Sleep and wake bout length distributions were tested against the exponential and power-law distributions, since these have previously been found to describe human sleep–wake behavior (Lo et al., 2002, 2004; Arnardóttir et al., 2010; Bianchi et al., 2010). In addition, the stretched exponential (Weibull) distribution was included as it has been shown to describe wake dynamics in fruit flies (Sorribes et al., 2011) and the lognormal distribution as another possible full range alternative to the power-law. These distributions represent four different basic generating mechanisms commonly found throughout nature, and in particular, the observation of an exponential survival distribution implies that the state transitions are random events while a power-law or a lognormal distribution are indicative of bursty dynamics. The stretched exponential distribution, on the other hand, allows for a sliding measure between random dynamics and bursts, quantified by the shape parameter k, where $k = 1$ in the case of random dynamics and $k < 1$ when the state transitions appear in bursts.

The model selection procedure was followed from Clauset et al. (2009), which, for each model, briefly consisted of (i) find the best fit to the data and its corresponding Kolmogorov–Smirnov (KS) distance, (ii) draw a large number ($N_{rep} = 10{,}000$) of random samples from the model distribution using the estimated parameters from the data, where each random sample is the same size as the data, and (iii) perform a "plausibility" or consistency test by comparing the empirical KS distance to the ones from the randomly sampled data, yielding a p-value. Lastly, the Akaike Information Criterion with a correction for finite sample sizes (AICc) and the Bayesian Information Criterion (BIC) are used to select between the different plausible models.

In humans, however, sleep is characterized by relatively few sleep–wake transitions. To accurately assess the possible functional forms of the distributions of sleep and wake bouts, the numbers

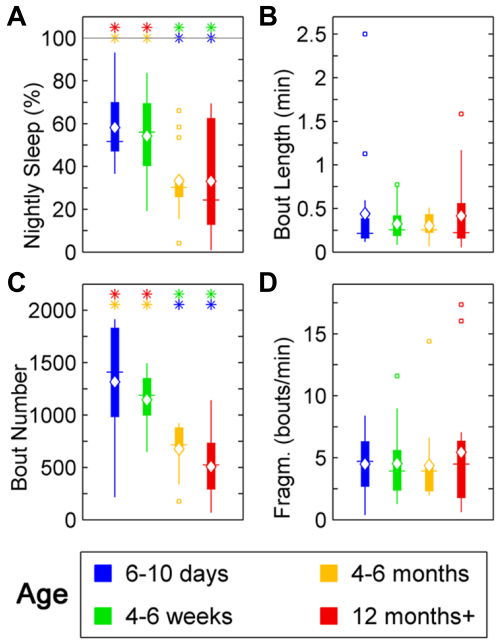

FIGURE 4 | Sleep parameters for zebrafish during the night for age groups: 4–6 days post-fertilization (group 1, blue), 4–6 weeks (group 2, green), 4–6 months (group 3, orange), and 12 months + (group 4, red). Colored asterisks above bars indicate a statistically significant difference between the bar group and the group with the corresponding color of the asterisk. **(A)** Percentage sleep time. Larvae (groups 1 and 2) sleep significantly more than adult fish (groups 3 and 4) during the dark-phase. **(B)** There is no significant change in the mean sleep bout duration between the age groups. **(C)** Number of sleep bouts. Larvae (groups 1 and 2) show significantly more sleep–wake transitions than adult fish (groups 3 and 4). **(D)** Sleep bout fragmentation (bouts/min). No changes of the fragmentation of sleep are observed across the age groups. Diamond, white line, and squares indicate mean, median, and outlier values, respectively.

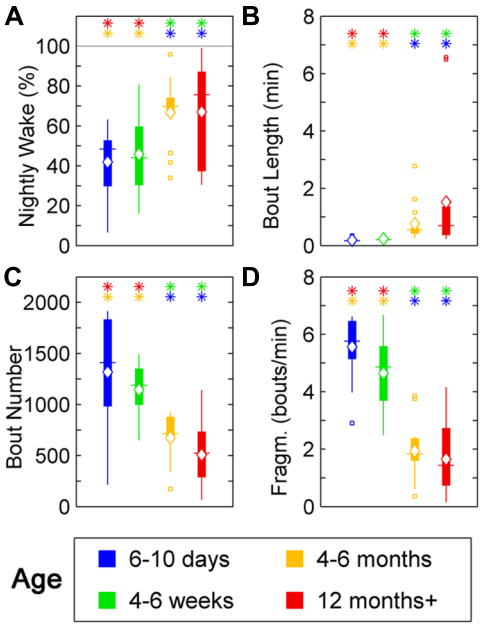

FIGURE 5 | Wake parameters for zebrafish during the night for age groups: 4–6 days post-fertilization (group 1, blue), 4–6 weeks (group 2, green), 4–6 months (group 3, orange), and 12 months + (group 4, red). Colored asterisks above bars indicate a statistically significant difference between the bar group and the group with the corresponding color of the asterisk. **(A)** Percentage wake time. Larvae (groups 1 and 2) spend less time awake during the night than adult fish (groups 3 and 4). **(B)** Mean wake bout duration. The wake bout lengths in larvae (groups 1 and 2) are significantly shorter than in adult fish (groups 3 and 4). **(C)** Number of sleep bouts for groups 1–4. Larvae (groups 1 and 2) show significantly more sleep–wake transitions than adult fish (groups 3 and 4). **(D)** Sleep bout fragmentation (bouts/min). The wake time of larvae (groups 1 and 2) is significantly more fragmented than for adult zebrafish (groups 3 and 4). Diamond, white line, and squares indicate mean, median, and outlier values, respectively.

of unique bout durations become important, as these determine the number of points in the survival distributions. The number of different sleep bout lengths (which determines the survival distribution) were on average 13.6 (range 7–21) for Children, 16.6 (range 10–28) for Preteens and teens, 12.5 (range 5–21) for Adults, and 13.6 (range 9–25) for Adults 50+. The number of unique wake bouts lengths were even lower since most awakenings are short (and thus fall in the 30- or 60-s bins, see Materials and Methods, Human Data Preprocessing), with an average of 3.9 (range 2–7) for Children, 4.2 (range 2–6) for Preteens and teens, 4.5 (range 1–8) for Adults, and 6.4 (range 3–11) for the Adults 50+ group. Fits were performed on an individual basis, however, a minimum number of five unique bouts were considered necessary for obtaining meaningful fits. This left only five Children, four Preteens and teens, eight Adults, and eight Adults 50+, so pooled values for each group were analyzed as well for model selection.

Pooled sleep bout distributions were found to be consistent with a stretched exponential distribution for Children ($k = 0.79$, $\lambda = 31.6$ min), Preteens and teens ($k = 0.78$, $\lambda = 19.6$ min), and the Adults group ($k = 0.76$, $\lambda = 23.0$ min), **Figures 6A,B**, whereas a power-law distribution was favored for sleep of Adults 50+ group ($\alpha = 2.2$, $x_{\text{low}} = 2.5$ min). From the fits to each individual survival distribution we obtained $k = 0.84 \pm 0.06$ for Children, $k = 0.84 \pm 0.05$ for Preteens and teens, and $k = 0.79 \pm 0.07$ for Adults (**Figure 6A**; **Table 1**). The pooled wake bout distributions were found to be well fit by a power-law for all age groups, with the exponent for Children estimated at $\alpha = 2.4$ ($x_{\text{low}} = 2.5$ min), Preteens and teens $\alpha = 2.7$ ($x_{\text{low}} = 1$ min), Adults $\alpha = 2.2$ ($x_{\text{low}} = 1.5$ min), and Adults 50+ $\alpha = 2.2$ ($x_{\text{low}} = 2.5$ min), **Figures 6C,D**. The group mean exponents were $\alpha = 1.78 \pm 0.04$ for Children, $\alpha = 1.90 \pm 0.04$ for Preteen and teens, $\alpha = 1.71 \pm 0.03$ for Adults, and $\alpha = 1.83 \pm 0.13$ for Adults 50+ (**Figure 6D**; **Table 1**). No statistically significant differences were found for neither sleep nor wake distribution parameters between age groups.

Zebrafish sleep–wake dynamics are characterized by many more transitions during the dark-phase as compared to human nocturnal sleep dynamics, on the order of 10–100 times as often (cf. **Figures 1D** and **4D**). The average number of discrete sleep bouts were for the 6–10 days group 94.7 (range 58–164), 4- to 6-week group 94.3 (range 27–154), 4–6 months group 81.9 (range 22–131), and 12+ months group 75.6 (range 11–134). Similarly

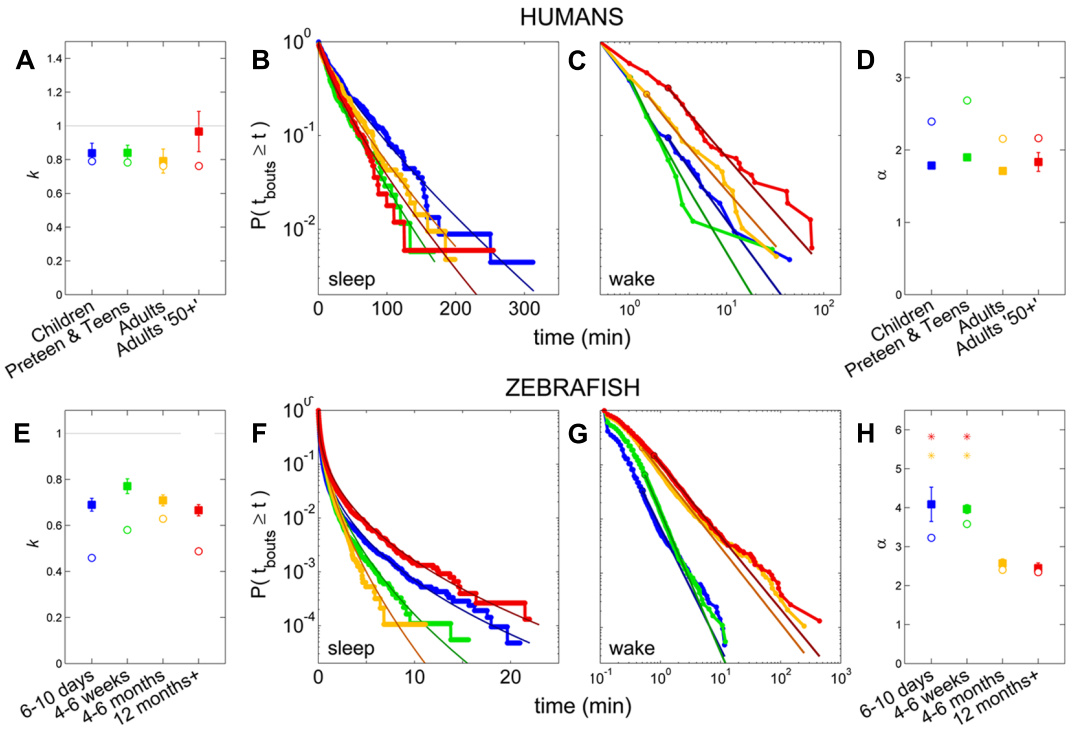

FIGURE 6 | Survivor plots of sleep and wake bouts in humans and zebrafish. (A–D) Sleep and wake bout distributions and fits in humans, with Children (blue), Preteens and teens (green), Adults (orange), and Adults 50+ (red). **(E–H)** Sleep and wake bout distributions and fits in zebrafish, with 4–6 days (blue), 4–6 weeks (green), 4–6 months (orange), and 12 months + (red). **(B,F)** Sleep bout distribution of pooled values for each group, with overlain stretched exponential fits in darker shades, shown on a log-lin scale. A straight diagonal line on these axes would indicate an exponential distribution. **(A,E)** Open circles indicate the value of the shape parameter k of the stretched exponential fit to the pooled distributions, while filled squares show the mean of the k's from fits to each individual and error bars show the standard error of the mean. The gray horizontal line marks $k = 1$, which corresponds to the special case where the stretched exponential "collapses" and becomes equal to the standard exponential distribution. No statistically significant differences between the age groups are present in either humans or zebrafish. **(C,G)** Wake bout distribution of pooled values for each group, with overlain power-law fits in darker shades, shown on a log–log scale. **(D,H)** Open circles indicate the value of the power-law exponent α from the fits to the pooled distributions, while filled squares show the mean of the α's from the individual fits and the error bars show the standard error. For humans, no significant change is seen on the α across age. In zebrafish, the larval stages (blue, green) have statistically significantly larger power-law exponents than the adult fish (orange, red).

to human sleep–wake dynamics, we observed fewer numbers of unique wake bout durations with averages of 42.8 (range 23–88) for the 6- to 10-day-olds, 51.8 (range 23–98) for the 4–6 weeks group, 85.9 (range 56–128) for the 4–6 months and 85.3 (range 39–130) for the fish older than 12 months.

For each zebrafish, the exponential, stretched exponential, power-law and lognormal distributions were fit to the sleep and wake bout length distributions. The fitting procedure was performed as described above in steps i–iii, culminating in a p-value for each model that measures how consistent, or plausible, the model is given the data. Ideally, several models would pass as plausible for each distribution, and the AICc or BIC is then used to determine the best model. Since we are interested in assessing the effect of age on the sleep and wake distributions, we would then determine which model is most frequently found to be a good fit for the individuals of each age, and so compare the age groups. For the empirical sleep bout data, however, only 54% (33 of 61) of the fits were found to be consistent with one of the models, and of these, 79% were only consistent with a single model. For the wake bout distributions we found a similar situation, with 36% consistent with one or more models, of which 91% were consistent with only one. Since AIC and BIC should be used to compare between plausible models and in the vast majority of cases there was only one in question, we instead quantified the most probable model out of the four for each age group. These results may seem like low "hit rates" and one may be tempted to try fitting more distributions with more complicated expressions, but the downside to that approach is that the introduction of more parameters makes it difficult to interpret the distribution parameters and what they say about the sleep–wake dynamics. Another reason for not delving into a large number of test models is that many of the individual distributions are noisy, and are therefore very unlikely to ever be consistent with the still reasonably simple model distributions that we would likely test. This is probably most easily seen visually (see **Figure 7**) where we see that the fits seem quite good, despite the noisy data and often failed plausibility tests. It is important to note here, that a failed plausibility test only indicates that the data does not purely follow the exact functional form of the model, and does not rule out that the model could still be useful as a tool for measuring

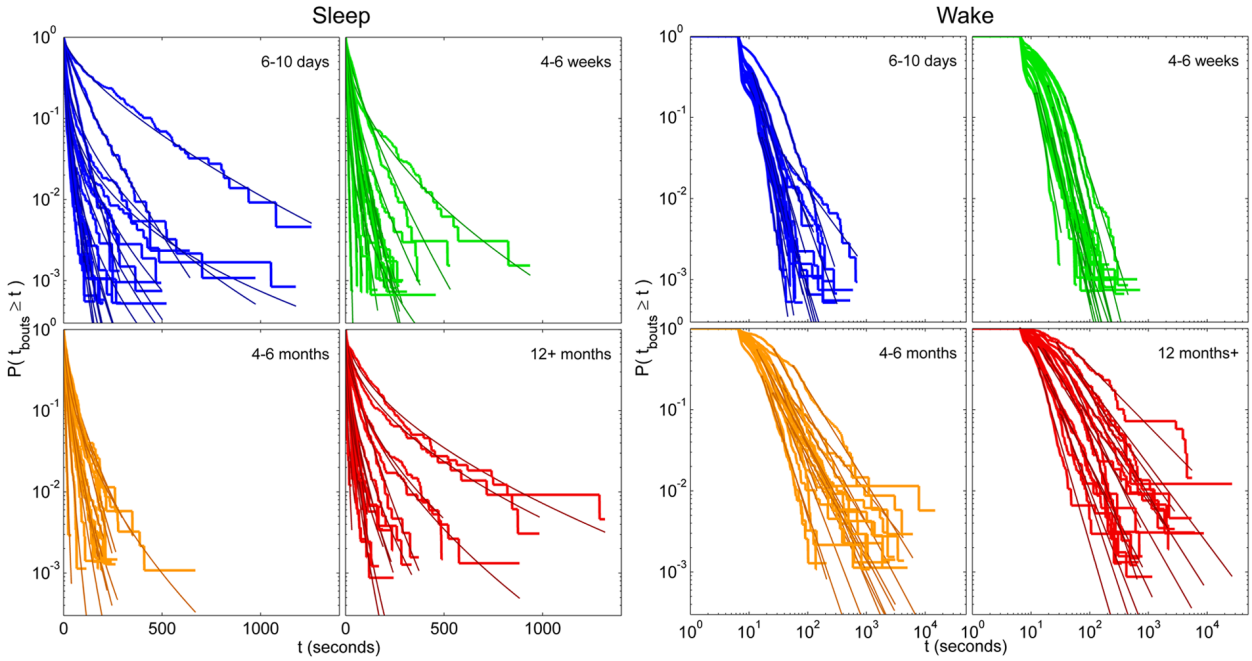

FIGURE 7 | Individual survival distributions of zebrafish sleep and wake bout lengths with corresponding stretched exponential and power-law fits. Survivor plots of (left panel) sleep and (right panel) wake bouts in zebrafish for age groups 6–10 days (blue), 4–6 weeks (green), 4–6 months (orange), and 12 months+ (red). Each trace encompasses data from a single fish. On the left panel the axes are shown using semi-log coordinates and stretched exponential fits are overlain each individual distribution in a darker shade. Straight diagonal lines on these plots indicate an exponential distribution of bout lengths. On the right the axes are shown in log–log coordinates and power-law fits are overlain each individual distribution in a darker shade. Straight diagonal lines on these plots indicate a power-law distribution.

and comparing different distributions that show a reasonable, but noisy, fit.

Following the above reasoning, thus, we found that the stretched exponential distribution most often fitted the sleep bout duration distributions of the 6–10 days olds ($k = 0.69 \pm 0.03$, $\lambda = 20 \pm 7$ s), 4–6 weeks ($k = 0.77 \pm 0.03$, $\lambda = 16 \pm 2$ s), and 4–6 months ($k = 0.71 \pm 0.02$, $\lambda = 14 \pm 2$ s). No statistically significant difference on the mean values was found between the shapes k of the different age groups (**Figure 6E**) or of the scales λ. **Figures 6F,G** depict sleep bout and wake bout distributions, respectively. For the 12+ month old group the power-law and the lognormal distributions tied with equal number of consistent cases, however, applying AICc on the two cases where both models were plausible tipped the scale in favor of the power-law distribution ($\alpha = 2.8 \pm 0.2$). For all age groups we thus observe a sleep distribution indicative of bursty dynamics, where longer sleep bouts occur more often than in the random (exponential distribution) case. For the wake bout distributions the power-law was favored at all ages, with $\alpha = 4.1 \pm 0.4$ for 6- to 10-day-olds, $\alpha = 4.0 \pm 0.1$ for the 4- to 6-week group, $\alpha = 2.6 \pm 0.1$ for the 4–6 months, and $\alpha = 2.4 \pm 0.1$ for the zebrafish older than 12 months of age and a decrease of the power-law exponent α was seen with age [$F(3,57) = 12.1$, $p < 0.0001$]. This is indicative of a strongly bursty dynamics where once an awakening has occurred, the probability of falling back to sleep again shortly, decreases with age. The wake bout distributions of adult fish (4–6 months and 12+ months) had significantly lower exponents than the wake bout distributions of the larval stages (6–10 days and 4–6 weeks), $p < 0.0001$, **Figure 6H**. In concordance with previous study by Prober et al. (2006) sleep and wake bouts in larval zebrafish were further analyzed using a 60-s immobility threshold for sleep onset. As expected, sleep percentage decreases whereas wake percentage increases using this criteria (20.3 and 79.7%, respectively). Full list of sleep parameters using a 60-s threshold are depicted in **Table 2**. Sleep and wake bouts, however, maintain their respective distributions: we found that the stretched exponential distribution most often fitted the sleep bout duration distributions ($k = 0.928 \pm 0.049$, $\lambda = 73.234$) and the power-law most often fitted the wake bouts ($\alpha = 2.651 \pm 0.234$).

DISCUSSION

We characterize the ontogeny of sleep–wake cycles in zebrafish and by defining sleep architecture in terms of state transitions, we demonstrate that sleep–wake cycles in zebrafish develop in a trajectory that can be meaningfully compared to humans (Kleitman and Engelman, 1951; Roffwarg et al., 1966; Jenni et al., 2006). By showing that sleep architecture in humans and zebrafish can be directly contrasted using multiple measures, zebrafish are further validated as a highly useful sleep model (Rihel et al., 2010b).The similarities demonstrated between zebrafish (order: Cyprinidae) and humans is consistent with the notion of evolutionarily conserved neural substrates controlling the sleep states.

In the present study, we replicate and extend previous findings on human sleep development. We show that sleep percentage overnight decreases with age whereas sleep bout length, sleep bout

Table 2 | Sleep and wake parameters in larval zebrafish using a 60 immobility threshold.

	Threshold (s)	Percent time of night (%)		Bout length (min)		Total number of bouts		Fragmentation (bouts/min)		Number of different bout lengths	
		Mean	SE	Mean	SE	Mean	SE	Mean	SE	Mean	SE
Sleep	60	20.3	6.6	1.3	0.3	73.0	15.7	1.18	0.166	47.2	8.8
Wake	60	79.7	6.6	12.1	2.6	72.8	15.7	0.23	0.067	42.1	7.1

number and sleep fragmentation do not change with age. Since the recordings are done during night only, analyzing the wake bouts (the interruption of sleep) is rich with information on sleep quality. We show that wake time increases with age and so does average wake bout length. There is no change in the wake bout number but wake fragmentation does decrease with age. In short, sleep percentage decreases with age and the decrease is explained by longer wake bouts and not by an increase in the number of wake bouts during night. It should be stressed that these data reflect only nighttime recordings and the youngest participant was 2 years old. Generally, across a full 24-h period, sleep fragmentation decreases rapidly over the first year in humans (Kleitman and Engelman, 1951; Jenni et al., 2006).

Second, in zebrafish we show that sleep percentage also decreases with age. Similar to humans, average sleep bout length and sleep fragmentation did not change with age, however, in contrast to humans, sleep bout number also decreased. The drop in sleep percentage in zebrafish with age is due to fewer but not shorter sleep bouts. We show that, similar to humans, wake percentage increases, the average wake bouts increase in length and wake fragmentation decreases (i.e., once awake the probability of falling asleep again decreases) with age. In contrast to humans, wake bout number decreases with age in zebrafish. Thus, in terms of these four parameters, percentage, bout length, bout number and fragmentation, zebrafish and humans follow a highly similar developmental trajectory. They differ only in the change of the number of sleep–wake transitions with age (no change in humans but a decrease in zebrafish).

Third, consistent with recent findings (Chu-Shore et al., 2010) we reveal that sleep–wake bout length distributions are more complex than suggested by previous work. Previously it has been shown that wake bouts exhibit a scale-free power-law distribution with an exponent that remains constant across adult humans, cats, rats, and mice (Lo et al., 2002, 2004). In contrast, it was also shown that sleep bout durations follow an exponential distribution with a characteristic time scale whose main determinants are body size and metabolic rate (Lo et al., 2002, 2004). Turning to development, it was shown in neonatal rats and mice that both sleep and wake bouts exhibit an exponential distribution immediately after birth, with a power-law behavior of wake bouts emerging only after the second postnatal week (Blumberg et al., 2005, 2007a,b). A similar developmental trajectory of sleep–wake dynamics has been reported in sheep (Karlsson et al., 2011). The data from all these species, therefore, indicated that the power-law exponent, α, is constant across multiple adult species; in contrast, the sleep-related time constant τ varies across species and age (Lo et al., 2002, 2004). Previous studies have, however, reported age-restricted exponential behavior of sleep bout distributions (Arnardóttir et al., 2010). Regardless, the conformity of the data from adult cats, rats, mice and humans (Lo et al., 2002, 2004) as well as from developing rats and mice (Blumberg et al., 2005, 2007a), supported the notion that these trends in sleep–wake bout distribution represent universal mammalian phenomena. It is tempting to speculate that similar bout distributions can be measured in invertebrates such as *Drosophila*. Presently we show that of the models tested, sleep bouts are most consistent with a stretched exponential in humans – except for in the 50+ group were they exhibit a better fit to a power-law. Wake bouts were shown to have a better fit to a power-law at all ages. Humans under the age of two might exhibit different distributions, even though wake bouts in prematurely born humans do not show a better fit to either a power-law or an exponential distribution (Arnardóttir et al., 2010). Similarly, in zebrafish sleep bout distributions most often fitted with a stretched exponential but in the 12+ month old group the power-law distribution showed better fits. Also, we demonstrate that α decreases with age in zebrafish; α is thus not a stable species characteristic in zebrafish, but the adult values compare well to those of mammals.

Brief awakenings during night are not random disruptions of sleep but a regulated process that may reveal the underlying mechanisms of behavioral state control (Lo et al., 2002, 2004; Bianchi et al., 2010; Chu-Shore et al., 2010). Previous rodent work has shown that the consolidation of wake bouts, and the concurrent emergence of a power-law wake bout distribution, across development, depends on intact hypothalamic-to-brainstem connections (Karlsson et al., 2004). This developmental trend may depend on hypocretin neurons, whose caudal connections develop in concert with the emergence of the power-law; since both hypocretin knock-out or locus coeruleus lesions (containing the highest density of hypocretin receptors) reverse the trend (Blumberg et al., 2007a; Gall et al., 2009). It is parsimonious to assume that the same underlying neural circuitry explains the bout length distributions in zebrafish as in mammals. Gall et al. (2009) stress that scale-free networks are more robust and resistant to failure than are random networks (Albert et al., 2000) and suggest that this organization evolved to protect the waking state from random neural damage. At face value this idea seems plausible since an organism partly awake cannot forage, mate, etc. Moreover, it follows that since the sleep state is organized in a less robust manner it should be more prone to failures – and sleep disorders are among the most common disorders

(Partinen and Hublin, 2005). This notion does no account for the stretched exponential and the emergence of a power-law behavior of sleep bouts in either older zebrafish or humans, however, which implies that the sleep state has more structure than was previously thought. Regardless, the fact that both species exhibit similar organization in sleep architecture, i.e., both species exhibit transition from stretched exponential to power-law behavior of the sleep bouts at the oldest age tested, is consistent with the notion that there are conserved evolutionary constraints on the structure of neural circuits governing sleep and wake.

Even though we have the utmost confidence in our data and analysis methods, some potential drawbacks of our study should be discussed. The first is the choice of age groups. Immense efforts have been made to generate tools to meaningfully compare different model species across development (see http://translatingtime.org/public/index; Clancy et al., 2001). Unfortunately, no such efforts have been for made for zebrafish making the choice of age groups difficult. The choice of age groups, both for humans and zebrafish, is meant to capture general trends in sleep development across the lifespan. Judging from the rapid fall in sleep percentages between 6–10 days and 4–6 weeks it seems likely that the largest differences in sleep development are to be found over the first weeks post-fertilization in zebrafish. In mammals, the largest changes also take place at a very early age (Jouvet-Mounier et al., 1970; Blumberg et al., 2005; Jenni et al., 2006). A detailed comparison of sleep–wake cycle development in zebrafish with dense group sampling over the first weeks post-fertilization may be warranted. This is also a period of synaptogenesis and pruning of neural circuits and also the age in which the fish are, conveniently, highly amenable to many of the molecular and neurophysiological tools available (Fetcho, 2005, 2007; McLean and Fetcho, 2008; Appelbaum et al., 2010; Friedrich et al., 2010; Vargas et al., 2012). We suggest that in terms of delineating the neural circuits of sleep, focusing on mapping behavioral to neural changes over this period in early ontogeny will be fruitful. Another valid critique is our choice of temperature. Total sleep time varies with basal metabolic rate (Zepelin and Rechtschaffen, 1974) which in turn is affected by temperature (Clarke and Johnston, 1999). It is conceivable that different values for total sleep time, or other sleep parameters, would be attained when recording at different temperature. In the current experiment we restricted ourselves to temperatures used by other authors (Zhdanova et al., 2006; Yokogawa et al., 2007; Appelbaum et al., 2009; Rihel et al., 2010b). Lastly, we use 6 s of immobility as our threshold for sleep onset for all our age groups. This was the immobility-to-sleep threshold measured by Yokogawa et al. (2007) in adult zebrafish. In that study the authors used mild electric shock to first find a threshold for arousal. Next, they applied the same stimulus to zebrafish, at different time points after the onset of immobility, determining that this arousal threshold rose after 6 s. That is, after 6 s, on average, larger stimulus was needed to generate a response. While choosing to use the low value (6 s) for all the age groups we do not feel that the 60-s threshold is inadequate; larval fish, however, exhibit shorter average wake (i.e., mobility) bouts than older fish, while average sleep bout lengths remain constant across age. This is evidence of a more rapid average sleep onset in larvae and is consistent with the use of the same immobility time threshold for sleep in young and old fish. Analyzing the bout distribution data using a 60-s immobility threshold for sleep onset reveals that sleep parameters are altered. Sleep percentage and number of bouts are reduced whereas the basic structure of bout distributions is conserved. For direct comparison between zebrafish sleep studies all parameters, e.g., movements and time thresholds need to be standardized and made fully comparable. To this end, more studies are needed.

The method of classifying sleep–wake states used here only requires knowledge on the duration of sleep and wake bouts, as opposed to the detailed knowledge of REM–NREM alternations, micro-arousals, or other phenomena required for traditional analysis methods in mammals (Rechtschaffen and Kales, 1968). We have shown that this method is highly sensitive to developmental changes and therefore could be used for gaging developmental milestones. Since electrographic criteria are not necessary for the analysis, data from a large group of animals that have only recently begun to be used in sleep research, such as fruit flies, zebrafish, and even nematodes (Hendricks et al., 2000; Shaw et al., 2000; Zhdanova, 2006; Zhdanova et al., 2006; Raizen et al., 2008), can be analyzed in a manner directly and meaningfully comparable to humans. These findings argue for evolutionary conserved neural substrates controlling sleep and further solidify zebrafish as a valuable model in sleep research.

ACKNOWLEDGMENTS

We thank Dr. G. Sokoloff for a careful reading of an earlier version of the manuscript and Ó. Arason and M. Ó. Sigurgunnarsdóttir for technical assistance. This work was supported by European Research Council Marie Curie grant no 0044932 (to Karl Æ. Karlsson), Icelandic Centre for Research grant no 080441022 (to Karl Æ. Karlsson), Spanish Plan Nacional MICINN BFU2012-33448 (to Gonzalo G. de Polavieja), the ERASysBio+ initiative supported under the European Union European Research Area Networks Plus scheme in Framework Program 7 (to Gonzalo G. de Polavieja) and a CAM fellowship (to Amanda Sorribes).

REFERENCES

Achermann, P., and Borbely, A. A. (1990). Simulation of human sleep: ultradian dynamics of electroencephalographic slow-wave activity. *J. Biol. Rhythms* 5, 141–157.

Achermann, P., and Borbely, A. A. (1994). Simulation of daytime vigilance by the additive interaction of a homeostatic and a circadian process. *Biol. Cybern.* 71, 115–121. doi: 10.1007/BF00197314

Achermann, P., and Borbely, A. A. (2003). Mathematical models of sleep regulation. *Front. Biosci.* 8:s683–s693. doi: 10.2741/1064

Albert, R., Jeong, H., and Barabasi, A. L. (2000). Error and attack tolerance of complex networks. *Nature* 406, 378–382. doi: 10.1038/35019019

Appelbaum, L., Wang, G., Yokogawa, T., Skariah, G. M., Smith, S. J., Mourrain, P., et al. (2010). Circadian and homeostatic regulation of structural synaptic plasticity in hypocretin neurons. *Neuron* 68, 87–98. doi: 10.1016/j.neuron.2010.09.006

Appelbaum, L., Wang, G. X., Maro, G. S., Mori, R., Tovin, A., Marin, W., et al. (2009). Sleep–wake regulation and hypocretin–melatonin interaction in zebrafish. *Proc. Natl. Acad. Sci. U.S.A.* 106, 21942–21947. doi: 10.1073/pnas.906637106

Arnardóttir, H., Porsteinsson, H., and Karlsson, K. Æ. (2010). Dynamics of sleep–wake cyclicity at night across the human lifespan. *Front. Neurol.* 1:156. doi: 10.3389/fneur.201000156

Bedell, V. M., Wang, Y., Campbell, J. M., Poshusta, T. L., Starker, C. G., Krug, R. G. II, et al. (2012). In vivo genome editing using a high-efficiency TALEN system. *Nature* 491, 114–118. doi: 10.1038/nature11537

Berman, J. R., Skariah, G., Maro, G. S., Mignot, E., and Mourrain, P. (2009). Characterization of two melanin-concentrating hormone genes in zebrafish reveals evolutionary and physiological links with the mammalian MCH system. *J. Comp. Neurol.* 517, 695–710. doi: 10.1002/cne.22171

Best, J., Diniz Behn, C., Poe, G. R., and Booth, V. (2007). Neuronal models for sleep–wake regulation and synaptic reorganization in the sleeping hippocampus. *J. Biol. Rhythms* 22, 220–232. doi: 10.1177/0748730407301239

Bianchi, M. T., Cash, S. S., Mietus, J., Peng, C. K., and Thomas, R. (2010). Obstructive sleep apnea alters sleep stage transition dynamics. *PLoS ONE* 5:e11356. doi: 10.1371/journal.pone.0011356

Blouin, A., Fried, I., Wilson, C. L., Staba, R. J., Behnke, E. J., Lam, H. A., et al. (2013). Human hypocretin and melanin-concentrating hormone levels are linked to emotion and social interaction. *Nat. Commun.* 4, 1547. doi: 10.1038/ncomms2461

Blumberg, M. S., Coleman, C. M., Johnson, E. D., and Shaw, C. (2007a). Developmental divergence of sleep–wake patterns in orexin knockout and wild-type mice. *Eur. J. Neurosci.* 25, 512–518. doi: 10.1111/j.1460-9568.2006.05292.x

Blumberg, M. S., Karlsson, K. A., and Seelke, A. M. (2007b). Sleep, development, and human health. *Sleep* 30, 549–550.

Blumberg, M. S., Seelke, A. M., Lowen, S. B., and Karlsson, K. A. (2005). Dynamics of sleep–wake cyclicity in developing rats. *Proc. Natl. Acad. Sci. U.S.A.* 102, 14860–14864. doi: 10.1073/pnas.0506340102

Borbely, A. A., and Achermann, P. (1999). Sleep homeostasis and models of sleep regulation. *J. Biol. Rhythms* 14, 557–568. doi: 10.1177/074873099129000894

Chu-Shore, J., Westover, M. B., and Bianchi, M. T. (2010). Power law versus exponential state transition dynamics: application to sleep–wake architecture. *PLoS ONE* 5:e14204. doi: 10.1371/journal.pone.0014204

Clancy, B., Darlington, R. B., and Finlay, B. L. (2001). Translating developmental time across mammalian species. *Neuroscience* 105, 7–17. doi: 10.1016/S0306-4522(01)00171-3

Clarke, A., and Johnston, N. M. (1999). Scaling of metabolic rate with body mass and temperature in teleost fish. *J. Anim. Ecol.* 68, 893–905. doi: 10.1046/j.1365-2656.1999.00337.x

Clauset, A., Shalizi, C. R., and Newman, E. J. (2009). Power-law distributions in empirical data. *SIAM Rev.* 51, 661–703. doi: 10.1137/070710111

Eisen, J. S. (1996). Zebrafish make a big splash. *Cell* 87, 969–977. doi: 10.1016/S0092-8674(00)81792-4

Fetcho, J. R. (2005). "Imaging neuronal activity with calcium indicators in larval zebrafish," in *Imaging in Neuroscience and Development: A Laboratory Manual*, eds R. Yuste and K. Konnerth (New York: Cold Spring Harbor Laboratory Press), 707–710.

Fetcho, J. R. (2007). The utility of zebrafish for studies of the comparative biology of motor systems. *J. Exp. Zool. B Mol. Dev. Evol.* 308, 550–562. doi: 10.1002/jez.b.21127

Friedrich, R. W., Jacobson, G. A., and Zhu, P. (2010). Circuit neuroscience in zebrafish. *Curr. Biol.* 20, R371–R381. doi: 10.1016/j.cub.2010.02.039

Gall, A. J., Joshi, B., Best, J., Florang, V. R., Doorn, J. A., and Blumberg, M. S. (2009). Developmental emergence of power–law wake behavior depends upon the functional integrity of the locus coeruleus. *Sleep* 32, 920–926.

Hendricks, J. C., Sehgal, A., and Pack, A. I. (2000). The need for a simple model to understand sleep. *Prog. Neurobiol.* 61, 339–351. doi: 10.1016/S0301-0082(99)00048-9

Hoppenbrouwers, T., and Sterman, M. B. (1975). Development of sleep state patterns in the kitten. *Exp. Neurol.* 49, 822–838. doi: 10.1016/0014-4886(75)90062-X

Jenni, O. G., Deboer, T., and Achermann, P. (2006). Development of the 24-h rest-activity pattern in human infants. *Infant Behav. Dev.* 29, 143–152. doi: 10.1016/j.infbeh.2005.11.001

Johns, M. W. (1991). A new method for measuring sleep daytime sleepiness: the Epworth sleepiness scale. *Sleep* 14, 540–545.

Jouvet-Mounier, D., Astic, L., and Lacote, D. (1970). Ontogenesis of the states of sleep in rat, cat, and guinea pig during the first postnatal month. *Dev. Psychobiol.* 2, 216–239. doi: 10.1002/dev.420020407

Karlsson, K. A., Arnardottir, H., Robinson, S. R., and Blumberg, M. S. (2011). Dynamics of sleep–wake cyclicity across the fetal period in sheep (*Ovis aries*). *Dev. Psychobiol.* 53, 89–95. doi: 10.1002/dev.20495

Karlsson, K. Æ., Kreider, J. C., and Blumberg, M. S. (2004). Hypothalamic contributions to sleep–wake cycle development. *Neuroscience* 123, 575–582. doi: 10.1016/j.neuroscience.2003.09.025

Kleitman, N., and Engelman, T. G. (1951). Sleep characteristics in infants. *J. Appl. Physiol.* 6, 269–282.

Lo, C. C., Amaral, L. A. N., Havlin, S., Ivanov, P., Penzel, T., Peter, J. H., et al. (2002). Dynamics of sleep–wake transitions during sleep. *Europhys. Lett.* 57, 625–631. doi: 10.1209/epl/i2002-00508-7

Lo, C. C., Chou, T., Penzel, T., Scammell, T. E., Strecker, R. E., Stanley, H. E., et al. (2004). Common scale-invariant patterns of sleep–wake transitions across mammalian species. *Proc. Natl. Acad. Sci. U.S.A.* 101, 17545–17548. doi: 10.1073/pnas.0408242101

Lyamin, O., Pryaslova, J., Lance, V., and Siegel, J. (2005). Animal behaviour: continuous activity in cetaceans after birth. *Nature* 435, 1177. doi: 10.1038/4351177a

McCarley, R. W. (2007). Neurobiology of REM and NREM sleep. *Sleep Med.* 8, 302–330. doi: 10.1016/j.sleep.2007.03.005

McGinty, D. J., Stevenson, M., Hoppenbrouwers, T., Harper, R. M., Sterman, M. B., and Hodgman, J. (1977). Polygraphic studies of kitten development: sleep state patterns. *Dev. Psychobiol.* 10, 455–469. doi: 10.1002/dev.420100506

McLean, D. L., and Fetcho, J. R. (2008). Using imaging and genetics in zebrafish to study developing spinal circuits in vivo. *Dev. Neurobiol.* 68, 817–834. doi: 10.1002/dneu.20617

Naumann, E. A., Kampff, A. R., Prober, D. A., Schier, A. F., and Engert, F. (2010). Monitoring neural activity with bioluminescence during natural behavior. *Nat. Neurosci.* 13, 513–520. doi: 10.1038/nn.2518

Pace-Schott, E. F., and Hobson, J. A. (2002). The neurobiology of sleep: genetics, cellular physiology and subcortical networks. *Nat. Rev. Neurosci.* 3, 591–605.

Panula, P., Chen, Y. C., Priyadarshini, M., Kudo, H., Semenova, S., Sundvik, M., et al. (2010). The comparative neuroanatomy and neurochemistry of zebrafish CNS systems of relevance to human neuropsychiatric diseases. *Neurobiol. Dis.* 40, 46–57. doi: 10.1016/j.nbd.2010.05.010

Partinen, M., and Hublin, C. (2005). "Epidemiology of sleep disorders," in *Principles and Practice of Sleep Medicine*, M. H. Kryger, G. Roth, and W. C. Dement (Philadelphia: Saunders), 626–647.

Prober, D. A., Rihel, J., Onah, A. A., Sung, R. J., and Schier, A. F. (2006). Hypocretin/orexin overexpression induces an insomnia-like phenotype in zebrafish. *J. Neurosci.* 26, 13400–13410. doi: 10.1523/JNEUROSCI.4332-06.2006

Raizen, D. M., Zimmerman, J. E., Maycock, M. H., Ta, U. D., You, Y. J., Sundaram, M. V., et al. (2008). Lethargus is a *Caenorhabditis elegans* sleep-like state. *Nature* 451, 569–572. doi: 10.1038/nature06535

Rechtschaffen, A., and Kales, A. (1968). *A Manual of Standardized Terminology, Techniques and Scoring System for Sleep Stages of Human Subjects*. Washington, DC: Public Health Service, US Government Printing Office.

Rempe, M. J., Best, J., and Terman, D. (2010). A mathematical model of the sleep/wake cycle. *J. Math. Biol.* 60, 615–644. doi: 10.1007/s00285-009-0276-5

Rihel, J., Prober, D. A., Arvanites, A., Lam, K., Zimmerman, S., Jang, S., et al. (2010a). Zebrafish behavioral profiling links drugs to biological targets and rest/wake regulation. *Science* 327, 348–351. doi: 10.1126/science.1183090

Rihel, J., Prober, D. A., and Schier, A. F. (2010b). Monitoring sleep and arousal in zebrafish. *Methods Cell Biol.* 100, 281–294. doi: 10.1016/B978-0-12-384892-5.00011-6

Rihel, J., and Schier, A. F. (2012). Behavioral screening for neuroactive drugs in zebrafish. *Dev. Neurobiol.* 72, 373–385. doi: 10.1002/dneu.20910

Roffwarg, H. P., Muzio, J. N., and Dement, W. C. (1966). Ontogenetic development of the human sleep-dream cycle. *Science* 152, 604–619. doi: 10.1126/science.152.3722.604

Saper, C. B., Chou, T. C., and Scammell, T. E. (2001). The sleep switch: hypothalamic control of sleep and wakefulness. *Trends Neurosci.* 24, 726–731. doi: 10.1016/S0166-2236(00)02002-6

Shaw, P. J., Cirelli, C., Greenspan, R. J., and Tononi, G. (2000). Correlates of sleep and waking in *Drosophila melanogaster*. *Science* 287, 1834–1837. doi: 10.1126/science.287.5459.1834

Siegel, J. M. (2000). "Brain mechanisms generating REM sleep," in *Principles and Practice of Sleep Medicine*, 2n Edn, eds M. K. Kryger, T. Roth, and W. C. Dement (New York: Saunders). 112–133.

Sigurgeirsson, B., Thornorsteinsson, H., Arnardottir, H., Johannesdottir, I. T., and Karlsson, K. A. (2011). Effects of modafinil on sleep–wake cycles in larval zebrafish. *Zebrafish* 8, 133–140. doi: 10.1089/zeb.2011.0708

Singh, A., Subhashini, N., Sharma, S., and Mallick, B. N. (2013). Involvement of the alpha1-adrenoceptor in sleep–waking and sleep loss-induced anxiety behavior in zebrafish. *Neuroscience* 245, 136–147. doi: 10.1016/j.neuroscience.2013.04.026

Sorribes, A., Armendariz, B. G., Lopez-Pigozzi, D., Murga, C., and de Polavieja, G. G. (2011). The origin of behavioral bursts in decision-making circuitry. *PLoS Comput. Biol.* 7:e1002075. doi: 10.1371/journal.pcbi.1002075

Todd, W. D., Gall, A. J., Weiner, J. A., and Blumberg, M. S. (2012). Distinct retinohypothalamic innervation patterns predict the developmental emergence of species-typical circadian phase preference in nocturnal Norway rats and diurnal nile grass rats. *J. Comp. Neurol.* 520, 3277–3292. doi: 10.1002/cne.23098

Vargas, R., Thornorsteinsson, H., and Karlsson, K. (2012). Spontaneous neural activity of the anterodorsal lobe and entopeduncular nucleus in adult zebrafish: a putative homologue of hippocampal sharp waves. *Behav. Brain Res.* 229, 10–20. doi: 10.1016/j.bbr.2011.12.025

Westerfield, M. (2000). *The Zebrafish Book: A Guide for the Laboratory Use of Zebrafish (Danio rerio)*. Eugene: University of Oregon Press.

Yokogawa, T., Marin, W., Faraco, J., Pezeron, G., Appelbaum, L., Zhang, J., et al. (2007). Characterization of sleep in zebrafish and insomnia in hypocretin receptor mutants. *PLoS Biol.* 5:e277. doi: 10.1371/journal.pbio.0050277

Zepelin, H., and Rechtschaffen, A. (1974). Mammalian sleep, longevity, and energy metabolism. *Brain Behav. Evol.* 10, 425–470. doi: 10.1159/000124330

Zhdanova, I. V. (2006). Sleep in zebrafish. *Zebrafish* 3, 215–226. doi: 10.1089/zeb.2006.3.215

Zhdanova, I. V., Wang, S. Y., Leclair, O. U., and Danilova, N. P. (2006). Melatonin promotes sleep-like state in zebrafish. *Brain Res.* 903, 263–268. doi: 10.1016/S0006-8993(01)02444-1

Zhdanova, I. V., Yu, L., Lopez-Patino, M., Shang, E., Kishi, S., and Guelin, E. (2008). Aging of the circadian system in zebrafish and the effects of melatonin on sleep and cognitive performance. *Brain Res. Bull.* 75, 433–441. doi: 10.1016/j.brainresbull.2007.10.053

Zon, L. I., and Peterson, R. T. (2005). In vivo drug discovery in the zebrafish. *Nat. Rev. Drug Discov.* 4, 35–44. doi: 10.1038/nrd1606

Conflict of Interest Statement: The authors declare that the research was conducted in the absence of any commercial or financial relationships that could be construed as a potential conflict of interest.

Received: 14 March 2013; paper pending published: 29 March 2013; accepted: 19 October 2013; published online: 13 November 2013.

Citation: Sorribes A, Þorsteinsson H, Arnardóttir H, Jóhannesdóttir IP, Sigurgeirsson B, de Polavieja GG and Karlsson KÆ (2013) The ontogeny of sleep–wake cycles in zebrafish: a comparison to humans. Front. Neural Circuits **7**:*178. doi: 10.3389/fncir.2013.00178*

This article was submitted to the journal Frontiers in Neural Circuits.

frontiers in
NEURAL CIRCUITS

REVIEW ARTICLE
published: 02 August 2013
doi: 10.3389/fncir.2013.00126

Learning and memory in zebrafish larvae

Adam C. Roberts[1], Brent R. Bill[2,3] and David L. Glanzman[1,4,5]*

[1] *Department of Integrative Biology and Physiology, University of California at Los Angeles, Los Angeles, CA, USA*
[2] *Center for Autism Research and Program in Neurobehavioral Genetics, David Geffen School of Medicine, Semel Institute for Neuroscience and Human Behavior, University of California at Los Angeles, Los Angeles, CA, USA*
[3] *Department of Psychiatry, David Geffen School of Medicine, University of California at Los Angeles, Los Angeles, CA, USA*
[4] *Department of Neurobiology, David Geffen School of Medicine, University of California at Los Angeles, Los Angeles, CA, USA*
[5] *Integrative Center for Learning and Memory, David Geffen School of Medicine, Brain Research Institute, University of California at Los Angeles, Los Angeles, CA, USA*

Edited by:
German Sumbre, Ecole Normale Supérieure, France

Reviewed by:
Gonzalo G. De Polavieja, Instituto Cajal. CSIC, Spain
Misha B. Ahrens, Howard Hughes Medical Institute, USA

***Correspondence:**
David L. Glanzman, Integrative Biology and Physiology, and Neurobiology, University of California, Los Angeles, 695 Charles E. Young Drive South, Los Angeles, CA 90035, USA
e-mail: dglanzman@physci.ucla.edu

Larval zebrafish possess several experimental advantages for investigating the molecular and neural bases of learning and memory. Despite this, neuroscientists have only recently begun to use these animals to study memory. However, in a relatively short period of time a number of forms of learning have been described in zebrafish larvae, and significant progress has been made toward their understanding. Here we provide a comprehensive review of this progress; we also describe several promising new experimental technologies currently being used in larval zebrafish that are likely to contribute major insights into the processes that underlie learning and memory.

Keywords: zebrafish, learning, memory, habituation, NMDA receptor

INTRODUCTION

Even relatively simple instances of learning in vertebrates can involve complex interactions of hundreds of molecules, each with distinct spatial and temporal kinetics, as well as neural circuits containing hundreds to thousands of neurons, and thousands to tens of thousands of synapses, which must first be identified and then monitored over time. A proven strategy for reducing this daunting complexity to a manageable level has been to study forms of learning and memory that involve restricted neural circuits. The efficacy of such a reductionist approach has been convincingly demonstrated by investigators of invertebrate learning and memory during the past several decades (Byrne and Kandel, 1996; Dubnau and Tully, 1998; Rankin, 2002; Roberts and Glanzman, 2003; Menzel, 2012). Reductionist neurobiological approaches toward understanding learning in vertebrates have been generally impeded by the enormous size and complexity of the vertebrate brain, especially the mammalian brain. One vertebrate that possesses a nervous system that may be better suited to reductionist analyses of behavior, however, is the zebrafish, *Danio rerio*. Zebrafish display a rich repertoire of behaviors, including associative learning (Norton and Bally-Cuif, 2010; Sison and Gerlai, 2010; Aizenberg and Schuman, 2011; Valente et al., 2012), social learning (Zala and Määttänen, 2013), and shoaling, a type of group behavior (Engeszer et al., 2007). Importantly, they also exhibit simple behaviors that appear to be mediated by relatively simply neural circuits (Kimmel et al., 1974; O'Malley et al., 1996; Easter and Nicola, 1997; Liu and Fetcho, 1999; Eaton et al., 2001; Roeser and Baier, 2003; Gahtan et al., 2005; Burgess and Granato, 2007b; Orger et al., 2008). Furthermore, zebrafish have other qualities that facilitate biological analyses of behavior. For example, because they readily absorb chemicals from water, drugs can be rapidly applied to zebrafish simply by immersing the fish in drug-containing water, which greatly simplifies pharmacological manipulation (Goldsmith, 2004). Undoubtedly one of the most attractive properties of the zebrafish as a model vertebrate organism for the study of behavior, however, is its ease of genetic manipulability. Indeed, the zebrafish approaches such invertebrate models as *Drosophila* and *C. elegans* with respect to the number of forward (Gaiano et al., 1996; Haffter et al., 1996; Schier et al., 1996; Kotani et al., 2006; Sivasubbu et al., 2006) and reverse genetic approaches to which it is amenable (Nasevicius and Ekker, 2000; Wienholds et al., 2003; Guo, 2004; Doyon et al., 2008; Meng et al., 2008; Dong et al., 2009; Bedell et al., 2012; Cade et al., 2012; Dahlem et al., 2012; Hwang et al., 2013). A major advance in genetic manipulation in zebrafish has been the recent development of an effective GAL4/Upstream Activating Sequence (GAL4/UAS) system for use in zebrafish (Asakawa and Kawakami, 2008; Halpern et al., 2008). This system, described in more detail below, enables researchers to target the expression of genes to specific cells. In particular, the GAL4/UAS system has been used to express the genes, such as green fluorescent protein (GFP), as well as of optical probes, such as channelrhodopsin and halorhodopsin, in specific groups of neurons in the zebrafish CNS (Scott et al., 2007; Scott, 2009; Wyart et al., 2009; Warp et al., 2012). These innovations allow neuroscientists to visually identify behaviorally relevant neural circuits in the zebrafish brain and spinal cord, and to optically monitor the functional activity of these circuits. The technical challenges posed by such studies are greatly reduced in the zebrafish by a remarkable feature of its larval form, namely that it is translucent; this feature permits optical investigations of neuronal structure and activity in the intact, and in some instances, behaving animal.

Identified neurons can be photoactivated or inhibited in the intact zebrafish larva, and the effect of this optical manipulation of neuronal activity on behavior examined (see Baier and Scott, 2009; Friedrich et al., 2010). Optical manipulation of neural activity is also presently feasible in mammals (e.g., Yizhar et al., 2011) of course; but the specificity of the resulting pattern of activity, as well as its behavioral consequences, is significantly less restricted, and therefore less mechanistically informative, than in the larval zebrafish.

The readiness with which zebrafish larvae lend themselves to optogenetics and other molecular tools (each with its own distinct efficacy across development), together with the general experimental advantages of zebrafish for reductionist analyses of behavior possessing different ontogenies (**Figure 1**), might be expected to excite interest among neuroscientists focused on learning and memory. However, to date the cognitive capabilities of larval zebrafish have been relatively unexplored. Here, we will review the various forms of learning and memory shown in these animals. We will also discuss what is currently known regarding the cellular and molecular mechanisms that underlie these forms of learning and memory. Finally, we will discuss potential future directions in learning and memory research in zebrafish larvae.

TYPES OF LEARNING AND MEMORY IN LARVAL ZEBRAFISH

HABITUATION

Habituation is a non-associative form of learning during which the response of an animal to repeated presentations of a stimulus of fixed intensity or strength gradually declines; furthermore, this decline is not due to sensory adaptation, motor fati, or injury (Thompson and Spencer, 1966; Rankin et al., 2009). Despite habituation's simplicity and apparent ubiquity, at present we lack a comprehensive neurobiological understanding of this form of learning (Glanzman, 2009).

Teleost fish, including zebrafish, exhibit a simple startle response, the C-start, that is controlled by a bilateral pair of large command neurons, the Mauthner cells, in the fish's hindbrain (Eaton et al., 2001) (**Figure 2**). The C-start is triggered by an abrupt sensory (auditory, visual, or tactile) stimulus (Eaton et al., 1984; Weiss et al., 2006); it first appears in zebrafish larvae in response to an auditory stimulus at 4 days postfertilization (dpf), and the response begins to exhibit habituation to a repetitious sensory stimulus at about the same time (Eaton et al., 1977). The onset latency of the C-start is rapid (~6 ms) and the resulting behavior of the fish—the bending of the fish into a C shape, from which the response gets its name—is highly stereotyped (Burgess and Granato, 2007b; Issa et al., 2011); its function is to rapidly propel the fish away from potential predators. Zebrafish larvae also exhibit a related escape behavior that has a longer onset latency (~30 ms), is less stereotyped than the C-start, and is mediated by the activity of non-Mauthner cell circuits rather than by the Mauthner cells (Burgess and Granato, 2007b; Issa et al., 2011) (but see Liu and Fetcho, 1999).

Three forms of habituation of the C-start have been described. These forms are induced by different training protocols and

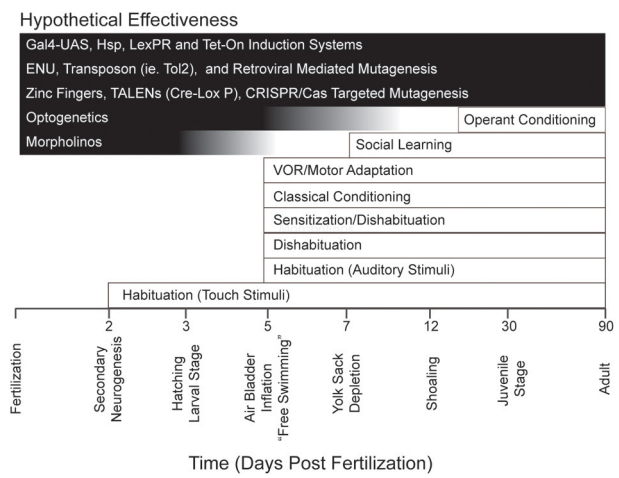

FIGURE 1 | Repertoire of behavior and learning exhibited by zebrafish during development together with major experimental techniques and their effective age of use. The timeline at the bottom of the figure indicates important developmental milestones in zebrafish. Note that several forms of learning have been identified as early as 5 dpf, an age at which such powerful experimental techniques as optogenetics are still effective. Note, also, that there are many molecular tools (for example, the GAL4-UAS system; see Halpern et al., 2008) that are effective at all developmental stages in zebrafish.

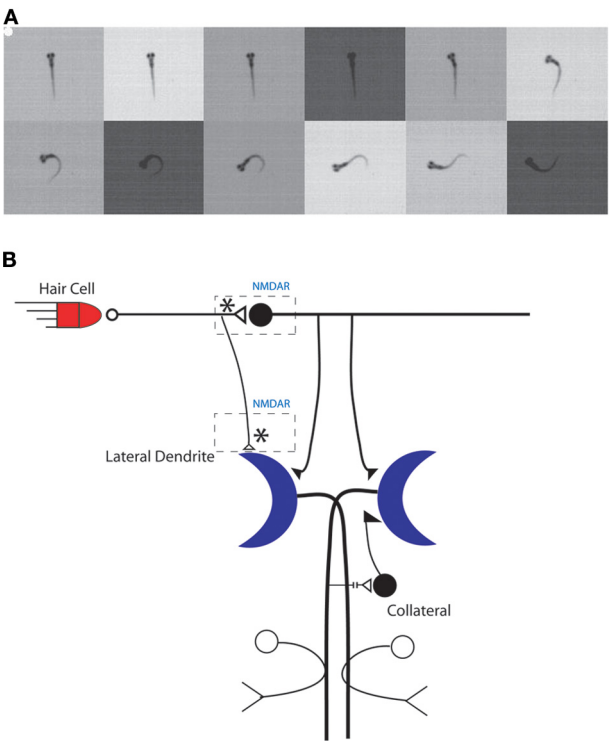

FIGURE 2 | The C-start reflex in larval zebrafish is mediated by the Mauthner neuron-mediated circuit. (A) An example of a larval zebrafish C-start reflex in response to an auditory/vibrational stimulus. The initiation of the C-start reflex is marked by a white dot and images were recorded every 1 ms. Frames are shown every 2 ms for illustration purposes. **(B)** Model of the Mauthner neuron circuitry. Potential sites of NMDAR-dependent plasticity are indicated by asterisks. Adapted with permission from Roberts et al. (2011).

are mechanistically distinct. There are two forms of relatively short-lived habituation that we have termed "rapid" and "short-term" (Roberts et al., 2011). Rapid habituation can be induced by massed presentation of 50–120 brief auditory pulses (1 ms in duration, 200 Hz ramp wave, 109 dB), or "pips," at 1 Hz (**Figure 3**); the consequent habituation is significant at 1 min after training but the response returns to its initial strength within 3–15 min post-training (Roberts et al., 2011; Wolman et al., 2011). Short-term habituation (STH), which persists for up to 1 h after training, is induced by spaced training, specifically, by 10 blocks of 900 pips (1 Hz) with a 5 min interblock interval (Roberts et al., 2011). Roberts et al. (2011) found that STH of the C-start requires *N*-methyl-d-aspartate receptor (NMDAR) activity, whereas rapid habituation does not. Wolman et al. (2011), however, reported that NMDAR activity was required for rapid habituation as well. (The source of this discrepancy may be the specific NMDAR antagonist used by the two groups; Roberts and colleagues observed that MK801, a non-competitive NMDAR antagonist, used by Wolman and colleagues, did disrupt rapid habituation, whereas DL-2-amino-5-phosphonopentanoic acid (APV), a competitive NMDAR antagonist used in the experiments of Roberts et al., did not alter rapid habituation). Recently, we (Pearce et al., 2012) have shown that the C-start can also undergo long-term habituation (LTH) in larval zebrafish. Here, the fish were stimulated with six spaced blocks of auditory pips; each block comprised spaced 8 trains of pips (120 pips at 1 Hz per train). The spaced training produced significant habituation of the C-start in the larvae that persisted for at least 18 h. Like STH, the induction of LTH depended on the activity of NMDARs; unlike STH, however, LTH depended on macromolecular synthesis, because its induction was disrupted by cold shock, and gene transcription—bathing the fish in the transcriptional inhibitor 5,6-dichlorobenzimidazole 1-β-D-ribofuranoside (DRB) during training blocked LTH. LTH of the C-start in larval zebrafish exhibits a striking mechanistic similarity to LTH of the gill- and siphon-withdrawal reflex in the marine snail *Aplysia* in its requirement for NMDAR activity, translation, and transcription (Ezzeddine and Glanzman, 2003; Esdin et al., 2010).

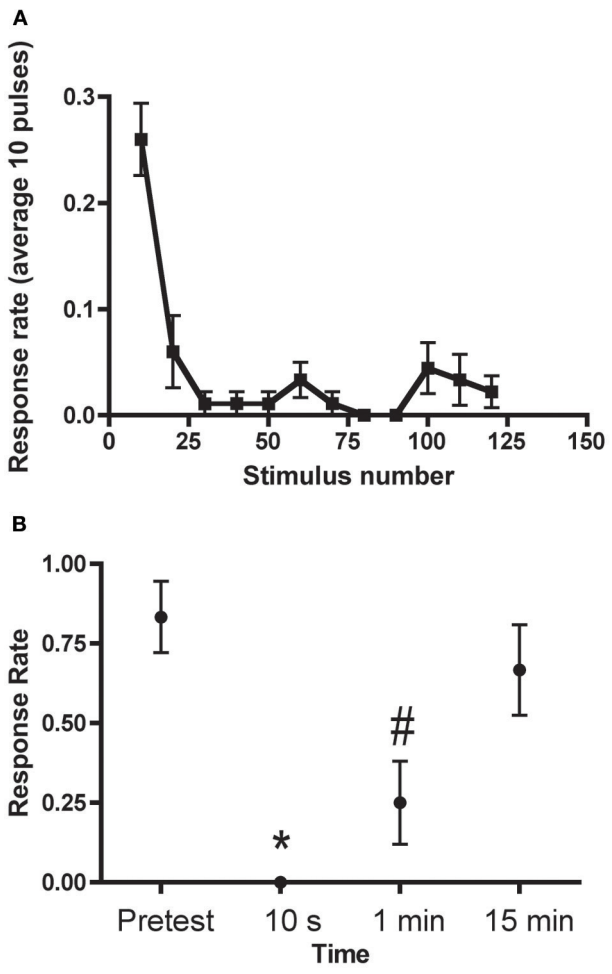

FIGURE 3 | Rapid Habituation of the C-start (A) C-start responses to 120 pulses delivered at 1 Hz (binned into groups of 10). (B) Persistence of rapid habituation. The training protocol resulted in short-lived habituation of the C-start, which returned to its original (pretraining) level of responsiveness within 15 min. The asterisk indicates that the 10 s test is significantly different from the pretest and 15 min test; the pound sign indicates that the 1 min test is significantly different from the pretest and the 15 min test. Adapted with permission from Roberts et al. (2011).

In response to the sudden extinction of light ("dark flash") larval zebrafish show another form of escape behavior that differs from the C-start; this response, the O-bend, is characterized by a significantly larger amplitude bend of the fish's body than occurs during the C-start (Burgess and Granato, 2007a). Unlike the C-start, the O-bend is not mediated by the Mauthner cells. Like the C-start, however, the O-bend can undergo LTH as a result of spaced training (120 min of exposure to dark flashes using an interstimulus interval of 15–60 s) (Wolman et al., 2011). LTH of the O-bend persists for up to 24 h and requires protein synthesis, as indicated by its blockage when training is performed in cyclohexamide, a translational inhibitor.

The experiments documenting LTH of escape behaviors in larval zebrafish represent a major advance because they demonstrate, for the first time to our knowledge, that immature zebrafish possess the capacity for long-term memory. Similar to long-term memory for a wide variety of learning tasks in a broad range of organisms, long-term memory in zebrafish larvae is more readily induced by spaced than by massed training (Ebbinghaus, 1964), training, and depends on protein synthesis and gene transcription (Davis and Squire, 1984; Goelet et al., 1986; Yin et al., 1994, 1995; Alberini, 2009; Ardiel and Rankin, 2010).

DISHABITUATION AND SENSITIZATION

Sensitization is a form of non-associative learning in which exposure to an arousing stimulus, commonly one that is painful or noxious, causes response enhancement (Groves and Thompson, 1970). The same stimulus that induces sensitization can typically be used to enhance a habituated response, a phenomenon known as dishabituation. Despite their phenomenological (Thompson and Spencer, 1966; Hawkins et al., 1998) and mechanistic (Antonov et al., 1999) similarities, sensitization and dishabituation are now recognized to be distinct forms of learning (Hawkins et al., 2006; Antonov et al., 2010).

Dishabituation of the rapid escape response in zebrafish larvae (5–7 dpf) has been observed by three laboratories. After habituating the escape response in larvae to auditory pips, Best et al. (2008) produced dishabituation by delivering a brief stimulus of a different sensory modality (a pulse of light) to the fish. Similarly, Wolman et al. (2011) first habituated the C-start in larvae to acoustic stimuli, and then dishabituated it by applying a brief tactile stimulus to the larval head. Using similar methods we have recently succeeded in dishabituating the C-start following LTH of this response.

A short-lived form of cross-modal modulation of the C-start that resembles sensitization (the enhancement of a non-habituated response) has also recently been shown in larval zebrafish. Mu et al. (2012) used auditory pips to evoke the C-start in 5–6 dpf zebrafish. When the sound stimulus was preceded by about 500 ms by a brief (15 ms) pulse of white light (a "flash"), the probability of a C-start being evoked by the subsequent sound stimulus was facilitated; by itself, the flash did not evoke the escape response. Through whole-cell electrophysiological recordings from the Mauthner cell in paralyzed fish embedded in agar, the investigators found that the preceding visual stimulus significantly enhanced the compound synaptic current (CSC) evoked in the Mauthner cell by the auditory pips; the flash alone, however, evoked only a very small CSC. Furthermore, a preceding flash enhanced the biphasic excitatory postsynaptic current (EPSC) evoked in the Mauthner cell by extracellular stimulation of the VIIIth cranial nerve, which transmits auditory information to the brain. The biphasic EPSC contains an early electrical component and a later chemical component; the chemical component is mediated by α-amino-3-hydroxy-5-methyl-4-isoxazolepropionic acid receptors (AMPARs) and NMDARs; both the electrical and chemical components of the EPSC were enhanced by the preceding flash. Mu et al. showed that the enhancement of VIIIth nerve-Mauthner cell synaptic transmission produced by a preceding visual stimulus was mimicked by exogenous application of dopamine and was blocked by antagonists of the D1 dopamine receptor. In support of the idea that the flash causes release of dopamine within the C-start circuit, laser ablation of the GFP-expressing dopaminergic neurons in the brains of the larval fish, as well as down-regulation of dopamine synthesis in hypothalamic dopaminergic neurons by knocking down tyrosine hydroxylase (the enzyme that converts L-tyrosine to L-DOPA) or two transcription factors required for the development of dopaminergic neurons with morpholino oligonucleotides (Mu et al., 2012) reduced the modulation of the auditory-evoked C-start by the preceding flash. Finally, the investigators determined that the visual flash induced bursting activity in dopaminergic neurons in the hypothalamus. It is interesting that the basis of cross-modal enhancement of the auditory-evoked C-start in larval zebrafish is modulatory neuronal actions caused by the release of dopamine within the fish's brain. This scheme is broadly consistent with that for sensitization of the defensive withdrawal reflex in *Aplysia*, which results from modulatory actions on sensorimotor pathways within the snail of another monoamine, serotonin; serotonin's release, in turn, is triggered by noxious stimulation (Brunelli et al., 1976; Castellucci and Kandel, 1976; Kandel and Schwartz, 1982).

The enhancing action of the flash on the sound-elicited C-start in zebrafish larvae appears to be quite brief. It remains to be determined whether more persistent enhancement could be induced in the larvae. Possibly, the briefness of the flash-induced modulation of the escape response may reflects the developmental immaturity of monoaminergic neurotransmission within the CNS of larval fish. In support of this idea, Buske and Gerlai (2012) report that levels of dopamine and serotonin increase dramatically in zebrafish around 10–12 dpf (see below).

Drug-induced sensitization of locomotor activity has been shown in both larval (Petzold et al., 2009) and adult (Blaser et al., 2010) zebrafish. Petzold et al. (2009) observed that the locomotor activity of larval (5–6 dpf, but not 4 dpf) zebrafish was enhanced by nicotine and that re-exposure to the drug sensitized the nicotine response. Interestingly, administration of APV together with nicotine blocked the sensitization. Therefore, NMDAR activity appears to mediate at least some forms of habituation and sensitization. Blaser et al. (2010) examined the effects of repeated exposure to ethanol on locomotor activity in adult zebrafish. They observed sensitization of ethanol-induced hyperactivity in the fish; furthermore, the sensitization was context-specific: fish given a second exposure to ethanol in the same context in which they received their first exposure exhibited enhanced locomotor hyperactivity, whereas fish re-exposed to ethanol in a different context did not show sensitization. (Note that the fish did not classically condition to the context, because their locomotor activity did not increase when they were re-exposed to the original context in the absence of ethanol.) Context specificity of drug-induced sensitization of locomotor activity remains to be shown in larval zebrafish.

CLASSICAL CONDITIONING

Classical conditioning, first described by Pavlov (1927), is the ability of an animal to associate a neutral stimulus (the conditioned stimulus or CS) with a reinforcing stimulus (the unconditioned stimulus or US). As the result of the paired delivery of a CS and a US, the CS acquires the ability to predict the occurrence of the US and, consequently, the animal's response to the CS (the conditioned response or CR) comes to resemble its response to the US (the unconditioned response or UCR). Classical conditioning is the most basic form of associative learning; consequently, understanding its biological basis is a major goal of behavioral neuroscientists.

Adult teleost fish classically condition readily (Agranoff and Davis, 1968; Flood et al., 1976; Amiro and Bitterman, 1980; Mattioli et al., 1998; Eisenberg et al., 2003; Salas et al., 2006; Yoshida and Kondo, 2012), and there have been several published reports of classical conditioning in adult zebrafish (Braubach et al., 2009; Agetsuma et al., 2010; Karnik and Gerlai, 2012; Aoki et al., 2013). To date, there have been just two reports of successful classical conditioning in larval to juvenile zebrafish. In one successful study, Aizenberg and Schuman (2011) trained 6-to-8-day-old larval zebrafish to associate a moving spot of light (the CS) with a touch to the side of the body (the US). The fish were partially restrained in agarose during the experiments such that their tails were free to move. The CR was enhanced movement of the tail in response to the CS. Aizenberg and Schuman

also measured changes in intracellular Ca^{2+} in cerebellar neurons in the restrained fish during the experiments. They observed that prior to training the CS and the US activated partially distinct populations of cerebellar neurons prior to conditioning; as a consequence of learning, the number of CS-activated neurons in the cerebellum was increased. Laser-ablation of the cerebellum immediately after the first training trial prevented conditioning, whereas cerebellar ablation after the last training trial impaired extinction of the CR. Interestingly, ablating the cerebellum after training, although it altered extinction, did not affect memory retention, which suggests that the memory for the CR is stored outside the cerebellum.

In the second demonstration of classical conditioning Valente et al. (2012) trained fish to associate a visual pattern projected onto an LCD screen below half of the tank of water in which the fish freely swam (the CS), to a whole-tank electric shock (the US). The experimenters measured the turns away from the side of the tank to which the CS was delivered as the CR. The zebrafish did not exhibit significant evidence of learning on this task until 4 weeks of age (∼late larval stage or early juvenile stage), after which their learning steadily improved, reaching an adult level at 6 weeks of age. Valente and colleagues also used a modification of this learning task to attempt to train larval zebrafish. In this modification the CS was a visual stimulus projected from below the fish, which were restrained in agarose, and the US was either an electric shock applied to the head of the fish, or a tap delivered to the fish's ear. However, the training did not produce evidence of learning in 7-day-old larvae.

MOTOR LEARNING

A type of vertebrate motor learning that has both formal and mechanistic similarities to classical conditioning is the vestibulo-ocular reflex (VOR) (Lac et al., 1995; Cohen et al., 2004). The VOR is a reflexive eye movement in which vestibular signals are used to generate compensatory eye movements in the opposite direction from head movements; its function is to stabilize retinal images. Calibration of the VOR requires motor learning; when head movements are consistently paired with the undesirable motion of the retinal image, learning occurs and the gain of the reflex is changed to reduce the image motion. Learning in the VOR depends on the cerebellum; furthermore, the cellular mechanisms that mediate this form of learning resemble those that mediate classical conditioning of the eyeblink response (Lac et al., 1995). Adult teleost fish, including adult zebrafish, exhibit a robust VOR (Graf and Baker, 1983; Pastor et al., 1994; Marsh and Baker, 1997). Initially, it was reported that larval zebrafish exhibit angular VORs (VORs evoked by stimulation of the semicircular canals) by 96 h postfertilization (hpf) (Easter and Nicola, 1997; Moorman et al., 2002); however, a later study did not find angular VORs in zebrafish until 35 dpf (Beck et al., 2004). Mo et al. (2010) reexamined this issue, and found evidence for an angular VOR in zebrafish as early as 72 hpf; furthermore, this group showed that several lines of mutant fish with defects of the vestibular system exhibited either a loss of VOR or reduced VOR. Mo and colleagues attributed the earlier failure to recognize the VOR in larval zebrafish (Beck et al., 2004) to mistaken attribution of vestibularly mediated eye movements to visually mediated movements. More recently, Bianco et al. (2012) also reported that larval zebrafish possess a VOR.

A recent study used motor learning in paralyzed zebrafish larvae, together with whole brain imaging of activity-dependent changes in intracellular calcium in individual neurons, to show the promise of larval zebrafish as model organisms for cellular investigations of learning (Ahrens et al., 2012). Ahrens and colleagues examined a type of motor adaptation (the optomotor response) related to the VOR. Here, paralyzed, restrained zebrafish larvae were exposed to a moving whole-field visual stimulus that simulated the visual effect in freely swimming fish of being swept backwards by the water flow. In response, the fish initiated motor commands ("fictive swims") that would have—were they not paralyzed—moved them forward; the purpose of these fictive swims was to stabilize the virtual location of the fish. The motor commands were recorded electrophysiologically from motor neurons in the fish, and these electrical signals were then translated into visual feedback that mimicked the optic flow produced in freely swimming fish by forward movement. The fish used in this study were transgenics that expressed the calcium sensor GCaMP2 (Akerboom et al., 2012) in almost all neurons. By means of two-photon microscopy the investigators were able to optically record neural activity throughout the brain at single-neuron resolution while the fish "behaved" in the virtual reality setup. They observed many neurons in the inferior olive and cerebellum whose firing correlated with motor adaptation by the fish to the visual stimulation. That the activity of these neurons was somehow causally related to the fish's behavior was indicated by the fact that lesioning the inferior olive post-training eliminated the motor adaptation. Although this study was unable to specify the actual cellular mechanism of motor learning, it nonetheless represents an impressive demonstration of the analytic power of the combination of transgenic manipulation and optical recording in the living, intact brain that zebrafish larvae enable.

OPERANT CONDITIONING

Operant conditioning, another major form of associative learning, differs from classical conditioning in that the consequences (outcomes) of an animal's voluntary response to a reinforcing stimulus alters the future probability of the animal's responses or behavior; in classical conditioning the animal's (involuntary) responses to the training stimuli are not altered by the behavior's outcomes (Gluck et al., 2014). One operant conditioning paradigm that has been used successfully with fish is avoidance conditioning. In a protocol originally developed for use with the goldfish over 40 years ago (Agranoff and Davis, 1968; Agranoff, 1971), fish must learn to swim to the other side of a shuttle box at the onset of a light to avoid an electric shock. Adult zebrafish condition readily in this protocol (Pradel et al., 1999, 2000; Xu et al., 2007) moreover, the learning depends on NMDARs (Blank et al., 2009). Two studies have used variants of the original shuttle box training protocol to show avoidance conditioning in larval to juvenile zebrafish. Lee et al. (2010) trained three-to-five-week-old fish to avoid the side of a shuttle box illuminated with a red light. They showed that the learning required the habenula—a diencephalic structure involved in the regulation

of dopaminergic and serotonergic pathways, and which mediates avoidance learning in mammals (Shumake et al., 2010)—by using genetic technologies to disrupt habenular circuits. Lee and colleagues used a mutant line that expresses the phototoxic fluorescent protein, KillerRed, in forebrain afferents to the habenula; photobleaching KillerRed-expressing neurons by illuminating the larvae with green light damaged the afferents and, when performed prior to behavioral training, prevented acquisition of conditioned avoidance. Interestingly, photobleaching habenular afferents after training did not impair expression of the learning. Lee et al. also used the GAL4/UAS system to express tetanus toxin specifically in habenular neurons. (This toxin prevents neurons from releasing transmitter by cleaving synaptobrevin.) Larvae with habenular expression of tetanus showed deficits in avoidance conditioning, particularly in the later training trails. The study of Lee and colleagues nicely illustrates the potential of zebrafish for investigations of learning and memory involving modern genetic tools. Valente et al. (2012) also used a shuttle box-type protocol to measure the ontogeny of operant conditioning in zebrafish. The zebrafish did not exhibit significant conditioning until 3 weeks of age (∼late larval stage), reaching a maximal (adult) level by week 6.

SOCIAL LEARNING

A shoal is a group of fish, typically of the same species and age, that swim together for social reasons. (Shoaling is distinguished from schooling in which fish swim together in tight, synchronized fashion.) It is believed that this social behavior serves, in part, as a protection against predation through increasing the detection of predators and decreasing the probability of individual capture (Peichel, 2004). As first shown by McCann et al. (1971), shoaling preferences in zebrafish have been shown to be at least partly learned. More recently, Engeszer et al. (2004) examined preferences of zebrafish who had been raised from hatching either in isolation, with siblings of the same phenotype, or with siblings of a different phenotype (cross-rearing). The fish in the study were either wild-type (normally striped) or mutant fish lacking melanophore stripes (*nacre* mutants). The fish were tested for social preference when they reached adulthood ($\geq$90 dpf). Social isolates exhibited no preference for either the wild-type or *nacre* phenotypes. However, fish in the other groups preferred the phenotypes they had been raised with, e.g., wild-type fish raised with *nacre* fish from hatching preferred to shoal with *nacre* fish as adults. These results suggest that shoaling preferences are determined, at least partly, by early experience. In a later study (Engeszer et al., 2007) Engeszer and colleagues ascertained the onset of conspecific preferences in zebrafish; they found that zebrafish begin to show conspecific preferences at approximately the post-flexion stage (∼12 dpf), and that zebrafish first exhibit significant shoaling preferences as juveniles. Furthermore, shoaling preferences were not plastic; as adults zebrafish preferred to shoal with the phenotypes they were reared with, even if given prolonged (30 days) exposure to the other phenotypes in adulthood. In addition to visual features, olfactory cues have also been shown to be a significant factor in determining shoaling preferences in zebrafish (Gerlach and Lysiak, 2006; Gerlach et al., 2007).

Two papers by Gerlai and colleagues provide some additional support for the notion that shoaling is a learned social behavior in zebrafish. Al-Imari and Gerlai (2008) raised zebrafish singly to adulthood (the experimental fish). Then the experimental fish were given 10 training trials in which they were placed in a four-arm aquatic maze. Beside each arm of the maze was a small tank—the contents of which were visible from the maze arm—one of which contained seven stimulus fish; a red plastic cue card was placed at the end of the maze arm next to the tank containing the stimulus fish. (The location within the maze of the stimulus fish and red cue card was changed from trial to trial.) Another group of fish (unpaired group) was given ten training trails in the maze, but the red cue card and the stimulus fish were placed separately in different arms. (The locations of the cue card and the stimulus fish were also moved from trial to trial.) Following the training the fish were presented with the red cue card alone, and the amount of time the fish spent in proximity to the card was measured. Fish in the paired group spent significantly more time near the red cue card than would be predicted by chance alone, whereas fish in the unpaired group preformed at chance level, i.e., the amount of time the unpaired fish spent in proximity to the card was no more than would predicted by chance given the total area of the maze. This result demonstrates that the zebrafish found the presence of a shoal mate rewarding. A second paper from this laboratory, that of Buske and Gerlai (2012), used high-pressure liquid chromatographic (HPLC) analyses of whole-brain extracts and behavioral measurements of the tendency to shoal to gain insights into potential neurobiological processes underlying the ontogenesis of shoaling in zebrafish. These investigators found, as had others (Engeszer et al., 2007; Buske and Gerlai, 2011), that shoaling-related behavior increased gradually in zebrafish from 10 to 75 dpf. At the approximately the same time there were also significant increases in the brain levels of both dopamine (DA) and serotonin (5-HT). Although this correlation does not prove that the increase in the brain levels of the monoamines underlay the increase in shoaling behavior, it is nonetheless suggestive; dopaminergic and serotonergic processes are known to play prominent roles in many forms of vertebrate and invertebrate learning and memory (e.g., Kandel, 2001; Wise, 2004; Riemensperger et al., 2005; Sitaraman et al., 2008; Hart et al., 2011; Johnson et al., 2011; Wood et al., 2011; Roberts and Hedlund, 2012).

FUTURE DIRECTIONS

As the above review indicates, zebrafish larvae possess a surprisingly rich repertoire of learning abilities, including not only non-associative, but also associative and even social learning. Given that at present neurobiologists lack a comprehensive understanding of any form of learning in any organism (discussed in Glanzman, 2009), we should not underestimate the formidable analytic challenge posed by the types of learning and memory that zebrafish larvae are known to exhibit. Moreover, the future is likely to bring an increased appreciation of the cognitive capabilities of these animals, which are almost certainly underrated at present.

In addition to the development of new learning and memory assays in larval zebrafish, one can anticipate that the genetic

tools available for use in zebrafish will steadily improve (see **Figure 1**). At present the most widely used method of altering gene function in larval zebrafish is gene knockdown by morpholinos (Mullins et al., 1994) This method has been widely employed in standard studies of the zebrafish developmental biology, but has had only partial success in behavioral studies due to the temporally restricted nature of the mRNA knockdown (Bill et al., 2009). Many behavioral assays (see, e.g., Valente et al., 2012) require fish to be 5 dpf or older, at which time the efficacy of morpholino gene knockdown is questionable; this method is therefore of limited value in learning and memory research. A relatively new method that should ultimately prove more useful than morpholinos for molecular analyses of behavior is Targeting Induced Local Lesions IN Genomes, (TILLING); here, zebrafish mutants are initially produced by exposure of embryos to the mutagen *N*-ethyl-*N*-nitrosourea (ENU), and then the DNA of these fish is screened and sequenced to identify mutations within specific genes (Wienholds et al., 2003). Currently, the Sanger Institute and the Zebrafish TILLING Project have available a large number of mutant fish with predicted mutations that should code for nonfunctional proteins (http://www.sanger.ac.uk/Projects/D_rerio/zmp/ and http://webapps.fhcrc.org/science/tilling/index.php). This resource should lead to the identification of novel molecular pathways involved in learning and memory. In addition, newer techniques, such as zinc finger nucleases, CRISPR, and TALENS, allow for site-directed mutagenesis of zebrafish genes (Doyon et al., 2008; Meng et al., 2008; Bedell et al., 2012; Dahlem et al., 2012; Moore et al., 2012; Hwang et al., 2013). This ability, available in mice for decades through homologous recombination (Capecchi, 1989), has facilitated the identification of many of the molecules important for learning and memory (Grant et al., 1992; Silva et al., 1992a,b). Site-directed mutagenesis promises to be equally useful in molecular analyses of zebrafish learning and memory. Finally, a powerful genetic tool, the GAL4/UAS system (Scott, 2009, and above), has only just begun to be used in memory research in larval zebrafish (Lee et al.), but is likely to become increasingly popular. Scott et al. (2007) have developed several GAL4 combined enhancer trap zebrafish lines; these will permit UAS-linked transgenes to be targeted to specific regions or, in some instances, specific cell types of the larval brain. The GAL4/UAS system has been used to great effect in mechanistic studies of *Drosophila* memory (Joiner and Griffith, 1999; Zars et al., 2000a,b; Akalal et al., 2006; Kasuya et al., 2009; Berry et al., 2012), and is likely to prove equally valuable in the analysis of memory in larval zebrafish.

Investigators have long taken advantage of the transparency of larvae to image optical activity in the brain of intact zebrafish using calcium indicator dyes (Fetcho and O'Malley, 1995, 1997; Ritter et al., 2001; Higashijima et al., 2003). However, new improvements in imaging techniques, combined with genetic manipulation, has made this basic methodology increasingly powerful. Rather than having to inject calcium indicator dyes into single neurons, investigators can now express genetically encoded calcium indicators, such as GCamPs (Del Bene et al., 2010), in the zebrafish brain. The indicators may be expressed throughout the brain (Ahrens et al., 2012), or expressed in restricted regions of the brain (Del Bene et al., 2010; Muto et al., 2011). Furthermore, increasingly powerful genetically encoded calcium indicators are being developed (Akerboom et al., 2012) and this, together with improvements in optical techniques, such as two-photon microscopy and, more recently, light-sheet microscopy (Ahrens et al., 2013), make it now feasible to record the activity of more than 80% of the neurons in the larval zebrafish brain at the same time with single-cell resolution (Ahrens et al., 2012). This is a remarkable advance, one that could revolutionize our understanding of the brain circuits generate behaviors and encode learned experiences. Moreover, zebrafish larvae are uniquely suited to take advantage of this new technology.

Another new optical method to which zebrafish larvae are highly amenable is optogenetics. Through the use of light-gated glutamate receptors (Szobota et al., 2007), channelrhodopsin (Douglass et al., 2008; Bundschuh et al., 2012; Fajardo et al., 2013) and halorhodopsin (Arrenberg et al., 2009) one can either excite or inhibit neurons in the intact, behaving fish. Also, the specificity of optical manipulation of neuronal activity can be further refined by means of genetic tools. This technology has already been used for mechanistic studies of behavior in zebrafish larvae, although not yet for studies of learning and memory. However, optogenetic investigations of learning and memory have recently been carried out in mice (Alonso et al., 2012; Liu et al., 2012), and one can anticipate similar studies in zebrafish larvae in the near future.

Mention should also be made of other new methods for manipulating or monitoring neural function in the intact larval zebrafish's brain. For example, GAL4-UAS technology can be used to target the expression of tetanus toxin, which blocks neurotransmitter release, to specific neurons and thereby eliminate their contribution to behavior-related brain activity (Asakawa et al., 2008; Wyart et al., 2009). Furthermore, Schuman and colleagues (Hinz et al., 2011) have recently developed methods for identifying and visualizing newly synthesized proteins in the brain of the intact larval zebrafish. As they point out, this methodology should prove useful for determining the molecules that are important for long-term memory.

CONCLUSIONS

Zebrafish larvae are uniquely adapted to new genetic and optical technologies for studies of behavior. For this reason, it is gratifying that these relatively simple animals possess significant capabilities for learning. In particular, as we have discussed in this review, zebrafish larvae exhibit not only short-term, but also long-term memory, as well as associative and social learning. As neurobiologists increasingly recognize the advantages of zebrafish larvae for investigations of learning and memory, our knowledge of the mnemonic repertoire of these animals will undoubtedly expand. Possibly, studies of this tiny, immature, deceptively humble creature will one day unlock some of the most profound secrets about how brains acquire and store memories.

REFERENCES

Agetsuma, M., Aizawa, H., Aoki, T., Nakayama, R., Takahoko, M., Goto, M., et al. (2010). The habenula is crucial for experience-dependent modification of fear responses in zebrafish. *Nat. Neurosci.* 13, 1354–1356. doi: 10.1038/nn.2654

Agranoff, B. W. (1971). "Effect of antibiotics on long-term memory formation in the goldfish," in *Animal Memory*, eds W. K. Honig and P. H. R. James (New York, NY: Academic Press), 243–258.

Agranoff, B. W., and Davis, R. E. (1968). "The use of fishes in studies of memory formation," in *The Central Nervous System and Fish Behavior*, ed D. Ingle (Chicago, IL: University of Chicago Press), 193–201.

Ahrens, M. B., Li, J. M., Orger, M. B., Robson, D. N., Schier, A. F., Engert, F., et al. (2012). Brain-wide neuronal dynamics during motor adaptation in zebrafish. *Nature* 485, 471–477.

Ahrens, M. B., Orger, M. B., Robson, D. N., Li, J. M., and Keller, P. J. (2013). Whole-brain functional imaging at cellular resolution using light-sheet microscopy. *Nat. Methods* 10, 413–420. doi: 10.1038/nmeth.2434

Aizenberg, M., and Schuman, E. M. (2011). Cerebellar-dependent learning in larval zebrafish. *J. Neurosci.* 31, 8708–8712. doi: 10.1523/JNEUROSCI.6565-10.2011

Akalal, D.-B. G., Wilson, C. F., Zong, L., Tanaka, N. K., Ito, K., and Davis, R. L. (2006). Roles for Drosophila mushroom body neurons in olfactory learning and memory. *Learn. Mem.* 13, 659–668. doi: 10.1101/lm.221206

Akerboom, J., Chen, T.-W., Wardill, T. J., Tian, L., Marvin, J. S., Mutlu, S., et al. (2012). Optimization of a GCaMP calcium indicator for neural activity imaging. *J. Neurosci.* 32, 13819–13840. doi: 10.1523/JNEUROSCI.2601-12.2012

Alberini, C. M. (2009). Transcription factors in long-term memory and synaptic plasticity. *Physiol. Rev.* 89, 121–145. doi: 10.1152/physrev.00017.2008

Al-Imari, L., and Gerlai, R. (2008). Sight of conspecifics as reward in associative learning in zebrafish (*Danio rerio*). *Behav. Brain Res.* 189, 216–219. doi: 10.1016/j.bbr.2007.12.007

Alonso, M., Lepousez, G., Wagner, S., Bardy, C., Gabellec, M.-M., Torquet, N., et al. (2012). Activation of adult-born neurons facilitates learning and memory. *Nat. Neurosci.* 15, 897–904. doi: 10.1038/nn.3108

Amiro, T. W., and Bitterman, M. E. (1980). Second-order appetitive conditioning in goldfish. *J. Exp. Psychol. Anim. Behav. Process.* 6, 41–48. doi: 10.1037/0097-7403.6.1.41

Antonov, I., Kandel, E. R., and Hawkins, R. D. (1999). The contribution of facilitation of monosynaptic PSPs to dishabituation and sensitization of the Aplysia siphon withdrawal reflex. *J. Neurosci.* 19, 10438–10450.

Antonov, I., Kandel, E. R., and Hawkins, R. D. (2010). Presynaptic and postsynaptic mechanisms of synaptic plasticity and metaplasticity during intermediate-term memory formation in Aplysia. *J. Neurosci.* 30, 5781–5791. doi: 10.1523/JNEUROSCI.4947-09.2010

Aoki, T., Kinoshita, M., Aoki, R., Agetsuma, M., Aizawa, H., Yamazaki, M., et al. (2013). Imaging of neural ensemble for the retrieval of a learned behavioral program. *Neuron* 78, 881–894. doi: 10.1016/j.neuron.2013.04.009

Ardiel, E. L., and Rankin, C. H. (2010). An elegant mind: learning and memory in *Caenorhabditis elegans*. *Learn. Mem.* 17, 191–201. doi: 10.1101/lm.960510

Arrenberg, A. B., Del Bene, F., and Baier, H. (2009). Optical control of zebrafish behavior with halorhodopsin. *Proc. Natl. Acad. Sci. U.S.A.* 106, 17968–17973. doi: 10.1073/pnas.0906252106

Asakawa, K., and Kawakami, K. (2008). Targeted gene expression by the Gal4-UAS system in zebrafish. *Dev. Growth Diff.* 50, 391–399. doi: 10.1111/j.1440-169X.2008.01044.x

Asakawa, K., Suster, M. L., Mizusawa, K., Nagayoshi, S., Kotani, T., Urasaki, A., et al. (2008). Genetic dissection of neural circuits by Tol2 transposon-mediated Gal4 gene and enhancer trapping in zebrafish. *Proc. Natl. Acad. Sci. U.S.A.* 105, 1255–1260. doi: 10.1073/pnas.0704963105

Baier, H., and Scott, E. K. (2009). Genetic and optical targeting of neural circuits and behavior–zebrafish in the spotlight. *Curr. Opin. Neurobiol.* 19, 553–560. doi: 10.1016/j.conb.2009.08.001

Beck, J. C., Gilland, E., Tank, D. W., and Baker, R. (2004). Quantifying the ontogeny of optokinetic and vestibuloocular behaviors in zebrafish, medaka, and goldfish. *J. Neurophysiol.* 92, 3546–3561. doi: 10.1152/jn.00311.2004

Bedell, V. M., Wang, Y., Campbell, J. M., Poshusta, T. L., Starker, C. G., Krug, R. G., et al. (2012). *In vivo* genome editing using a high-efficiency TALEN system. *Nature* 491, 114–118. doi: 10.1038/nature11537

Berry, J. A., Cervantes-Sandoval, I., Nicholas, E. P., and Davis, R. L. (2012). Dopamine is required for learning and forgetting in Drosophila. *Neuron* 74, 530–542.

Best, J. D., Berghmans, S., Hunt, J. J., Clarke, S. C., Fleming, A., Goldsmith, P., et al. (2008). Non-associative learning in larval zebrafish. *Neuropsychopharmacology* 33, 1206–1215. doi: 10.1038/sj.npp.1301489

Bianco, I. H., Ma, L. H., Schoppik, D., Robson, D. N., Orger, M. B., Beck, J. C., et al. (2012). The tangential nucleus controls a gravito-inertial vestibulo-ocular reflex. *Curr. Biol.* 22, 1285–1295. doi: 10.1016/j.cub.2012.05.026

Bill, B. R., Petzold, A. M., Clark, K. J., Schimmenti, L. A., and Ekker, S. C. (2009). A primer for morpholino use in zebrafish. *Zebrafish* 6, 69–77. doi: 10.1089/zeb.2008.0555

Blank, M., Guerim, L. D., Cordeiro, R. F., and Vianna, M. R. M. (2009). A one-trial inhibitory avoidance task to zebrafish: rapid acquisition of an NMDA-dependent long-term memory. *Neurobiol. Learn. Mem.* 92, 529–534. doi: 10.1016/j.nlm.2009.07.001

Blaser, R. E., Koid, A., and Poliner, R. M. (2010). Context-dependent sensitization to ethanol in zebrafish (*Danio rerio*). *Pharmacol. Biochem. Behav.* 95, 278–284. doi: 10.1016/j.pbb.2010.02.002

Braubach, O. R., Wood, H.-D., Gadbois, S., Fine, A., and Croll, R. P. (2009). Olfactory conditioning in the zebrafish (*Danio rerio*). *Behav. Brain Res.* 198, 190–198. doi: 10.1016/j.bbr.2008.10.044

Brunelli, M., Castellucci, V., and Kandel, E. R. (1976). Synaptic facilitation and behavioral sensitization in Aplysia: possible role of serotonin and cyclic AMP. *Science* 194, 1178–1181. doi: 10.1126/science.186870

Bundschuh, S. T., Zhu, P., Schärer, Y.-P. Z., and Friedrich, R. W. (2012). Dopaminergic modulation of mitral cells and odor responses in the zebrafish olfactory bulb. *J. Neurosci.* 32, 6830–6840. doi: 10.1523/JNEUROSCI.6026-11.2012

Burgess, H. A., and Granato, M. (2007a). Modulation of locomotor activity in larval zebrafish during light adaptation. *J. Exp. Biol.* 210, 2526–2539. doi: 10.1242/jeb.003939

Burgess, H. A., and Granato, M. (2007b). Sensorimotor gating in larval zebrafish. *J. Neurosci.* 27, 4984–4994. doi: 10.1523/JNEUROSCI.0615-07.2007

Buske, C., and Gerlai, R. (2011). Shoaling develops with age in zebrafish (*Danio rerio*). *Prog. Neuropsychopharmacol. Biol. Psychiatry* 35, 1409–1415. doi: 10.1016/j.pnpbp.2010.09.003

Buske, C., and Gerlai, R. (2012). Maturation of shoaling behavior is accompanied by changes in the dopaminergic and serotoninergic systems in zebrafish. *Dev. Psychobiol.* 54, 28–35. doi: 10.1002/dev.20571

Byrne, J. H., and Kandel, E. R. (1996). Presynaptic facilitation revisited: state and time dependence. *J. Neurosci.* 16, 425–435.

Cade, L., Reyon, D., Hwang, W. Y., Tsai, S. Q., Patel, S., Khayter, C., et al. (2012). Highly efficient generation of heritable zebrafish gene mutations using homo- and heterodimeric TALENs. *Nucleic Acids Res.* 40, 8001–8010. doi: 10.1093/nar/gks518

Capecchi, M. R. (1989). Altering the genome by homologous recombination. *Science* 244, 1288–1292. doi: 10.1126/science.2660260

Castellucci, V., and Kandel, E. R. (1976). Presynaptic facilitation as a mechanism for behavioral sensitization in Aplysia. *Science* 194, 1176–1178. doi: 10.1126/science.11560

Cohen, M. R., Meissner, G. W., Schafer, R. J., and Raymond, J. L. (2004). Reversal of motor learning in the vestibulo-ocular reflex in the absence of visual input. *Learn. Mem.* 11, 559–565. doi: 10.1101/lm.82304

Dahlem, T. J., Hoshijima, K., Jurynec, M. J., Gunther, D., Starker, C. G., Locke, A. S., et al. (2012). Simple methods for generating and detecting locus-specific mutations induced with TALENs in the zebrafish genome. *PLoS Genet.* 8:e1002861. doi: 10.1371/journal.pgen.1002861

Davis, H. P., and Squire, L. R. (1984). Protein synthesis and memory: a review. *Psychol. Bull.* 96, 518–559. doi: 10.1037/0033-2909.96.3.518

Del Bene, F., Wyart, C., Robles, E., Tran, A., Looger, L., Scott, E. K., et al. (2010). Filtering of visual information in the tectum by an identified neural circuit. *Science* 330, 669–673. doi: 10.1126/science.1192949

Dong, M., Fu, Y. F., Du, T. T., Jing, C. B., Fu, C. T., Chen, Y., et al. (2009). Heritable and lineage-specific gene knockdown in zebrafish

embryo. *PLoS ONE* 4:e6125. doi: 10.1371/journal.pone.0006125

Douglass, A. D., Kraves, S., Deisseroth, K., Schier, A. F., and Engert, F. (2008). Escape behavior elicited by single, channelrhodopsin-2-evoked spikes in zebrafish somatosensory neurons. *Curr. Biol.* 18, 1133–1137. doi: 10.1016/j.cub.2008.06.077

Doyon, Y., McCammon, J. M., Miller, J. C., Faraji, F., Ngo, C., Katibah, G. E., et al. (2008). Heritable targeted gene disruption in zebrafish using designed zinc-finger nucleases. *Nat. Biotechnol.* 26, 702–708. doi: 10.1038/nbt1409

Dubnau, J., and Tully, T. (1998). Gene discovery in Drosophila: new insights for learning and memory. *Annu. Rev. Neurosci.* 21, 407–444. doi: 10.1146/annurev.neuro.21.1.407

Easter, S. S. Jr., and Nicola, G. N. (1997). The development of eye movements in the zebrafish (*Danio rerio*). *Dev. Psychobiol.* 31, 267–276.

Eaton, R., Nissanov, J., and Wieland, C. (1984). Differential activation of Mauthner and non-Mauthner startle circuits in the zebrafish: implications for functional substitution. *J. Comp. Physiol. A* 155, 813–820. doi: 10.1007/BF00611598

Eaton, R. C., Farley, R. D., Kimmel, C. B., and Schabtach, E. (1977). Functional development in the Mauthner cell system of embryos and larvae of the zebra fish. *J. Neurobiol.* 8, 151–172. doi: 10.1002/neu.480080207

Eaton, R. C., Lee, R. K. K., and Foreman, M. B. (2001). The Mauthner cell and other identified neurons of the brainstem escape network of fish. *Prog. Neurobiol.* 63, 467–485. doi: 10.1016/S0301-008200047-2

Ebbinghaus, H. (1964). *Memory: a Contribution to Experimental Psychology*. New York, NY: Dover.

Eisenberg, M., Kobilo, T., Berman, D. E., and Dudai, Y. (2003). Stability of retrieved memory: inverse correlation with trace dominance. *Science* 301, 1102–1104. doi: 10.1126/science.1086881

Engeszer, R. E., Da Barbiano, L. A., Ryan, M. J., and Parichy, D. M. (2007). Timing and plasticity of shoaling behaviour in the zebrafish, *Danio rerio*. *Anim. Behav.* 74, 1269–1275. doi: 10.1016/j.anbehav.2007.01.032

Engeszer, R. E., Ryan, M. J., and Parichy, D. M. (2004). Learned social preference in zebrafish. *Curr. Biol.* 14, 881–884. doi: 10.1016/j.cub.2004.04.042

Esdin, J., Pearce, K., and Glanzman, D. L. (2010). Long-term habituation of the gill-withdrawal reflex in Aplysia requires gene transcription, calcineurin and L-type voltage-gated calcium channels. *Front. Behav. Neurosci.* 4:181. doi: 10.3389/fnbeh.2010.00181

Ezzeddine, Y., and Glanzman, D. L. (2003). Prolonged habituation of the gill-withdrawal reflex in Aplysia depends on protein synthesis, protein phosphatase activity, and postsynaptic glutamate receptors. *J. Neurosci.* 23, 9585–9594.

Fajardo, O., Zhu, P., and Friedrich, R. W. (2013). Control of a specific motor program by a small brain area in zebrafish. *Front. Neural Circuits* 7:67. doi: 10.3389/fncir.2013.00067

Fetcho, J. R., and O'Malley, D. M. (1995). Visualization of active neural circuitry in the spinal cord of intact zebrafish. *J. Neurophysiol.* 73, 399–406.

Fetcho, J. R., and O'Malley, D. M. (1997). Imaging neuronal networks in behaving animals. *Curr. Opin. Neurobiol.* 7, 832–838. doi: 10.1016/S0959-438880143-2

Flood, N. C., Overmier, J. B., and Savage, G. E. (1976). Teleost telencephalon and learning: an interpretive review of data and hypotheses. *Physiol. Behav.* 16, 783–798. doi: 10.1016/0031-938490251-1

Friedrich, R. W., Jacobson, G. A., and Zhu, P. (2010). Circuit neuroscience in zebrafish. *Curr. Biol.* 20, R371–R381. doi: 10.1016/j.cub.2010.02.039

Gahtan, E., Tanger, P., and Baier, H. (2005). Visual prey capture in larval zebrafish is controlled by identified reticulospinal neurons downstream of the tectum. *J. Neurosci.* 25, 9294–9303. doi: 10.1523/JNEUROSCI.2678-05.2005

Gaiano, N., Amsterdam, A., Kawakami, K., Allende, M., Becker, T., and Hopkins, N. (1996). Insertional mutagenesis and rapid cloning of essential genes in zebrafish. *Nature* 383, 829–832. doi: 10.1038/383829a0

Gerlach, G., Hodgins-Davis, A., MacDonald, B., and Hannah, R. C. (2007). Benefits of kin association: related and familiar zebrafish larvae (*Danio rerio*) show improved growth. *Behav. Ecol. Sociobiol.* 61, 1765–1770. doi: 10.1007/s00265-007-0409-z

Gerlach, G., and Lysiak, N. (2006). Kin recognition and inbreeding avoidance in zebrafish, *Danio rerio*, is based on phenotype matching. *Anim. Behav.* 71, 1371–1377. doi: 10.1016/j.anbehav.2005.10.010

Glanzman, D. L. (2009). Habituation in Aplysia: the cheshire cat of neurobiology. *Neurobiol. Learn. Mem.* 92, 147–154. doi: 10.1016/j.nlm.2009.03.005

Gluck, M. A., Mercado, E., and Myers, C. E. (2014). *Learning and Memory: from Brain to Behavior, 2nd Edn.* New York, NY: Worth.

Goelet, P., Castellucci, V. F., Schacher, S., and Kandel, E. R. (1986). The long and the short of long-term memory—a molecular framework. *Nature* 322, 419–422. doi: 10.1038/322419a0

Goldsmith, P. (2004). Zebrafish as a pharmacological tool: the how, why and when. *Curr. Opin. Pharmacol.* 4, 504–512. doi: 10.1016/j.coph.2004.04.005

Graf, W., and Baker, R. (1983). Adaptive changes of the vestibulo-ocular reflex in flatfish are achieved by reorganization of central nervous pathways. *Science* 221, 777–779. doi: 10.1126/science.6603656

Grant, S. G., O'Dell, T. J., Karl, K. A., Stein, P. L., Soriano, P., and Kandel, E. R. (1992). Impaired long-term potentiation, spatial learning, and hippocampal development in fyn mutant mice. *Science* 258, 1903–1910. doi: 10.1126/science.1361685

Groves, P. M., and Thompson, R. F. (1970). Habituation: a dual-process theory. *Psychol. Rev.* 77, 419–450. doi: 10.1037/h0029810

Guo, S. (2004). Linking genes to brain, behavior and neurological diseases: what can we learn from zebrafish. *Genes Brain Behav.* 3, 63–74. doi: 10.1046/j.1601-183X.2003.00053.x

Haffter, P., Granato, M., Brand, M., Mullins, M. C., Hammerschmidt, M., Kane, D. A., et al. (1996). The identification of genes with unique and essential functions in the development of the zebrafish, *Danio rerio*. *Development* 123, 1–36.

Halpern, M. E., Rhee, J., Goll, M. G., Akitake, C. M., Parsons, M., and Leach, S. D. (2008). Gal4/UAS transgenic tools and their application to zebrafish. *Zebrafish* 5, 97–110. doi: 10.1089/zeb.2008.0530

Hart, A. K., Fioravante, D., Liu, R.-Y., Phares, G. A., Cleary, L. J., and Byrne, J. H. (2011). Serotonin-mediated synapsin expression is necessary for long-term facilitation of the aplysia sensorimotor synapse. *J. Neurosci.* 31, 18401–18411. doi: 10.1523/JNEUROSCI.2816-11.2011

Hawkins, R. D., Cohen, T. E., Greene, W., and Kandel, E. R. (1998). Relationships between dishabituation, sensitization, and inhibition of the gill- and siphon-withdrawal reflex in Aplysia californica: effects of response measure, test time, and training stimulus. *Behav. Neurosci.* 112, 24–38. doi: 10.1037/0735-7044.112.1.24

Hawkins, R. D., Cohen, T. E., and Kandel, E. R. (2006). Dishabituation in Aplysia can involve either reversal of habituation or superimposed sensitization. *Learn. Mem.* 13, 397–403. doi: 10.1101/lm.49706

Higashijima, S., Masino, M. A., Mandel, G., and Fetcho, J. R. (2003). Imaging neuronal activity during zebrafish behavior with a genetically encoded calcium indicator. *J. Neurophysiol.* 90, 3986–3997. doi: 10.1152/jn.00576.2003

Hinz, F. I., Dieterich, D. C., Tirrell, D. A., and Schuman, E. M. (2011). Noncanonical amino acid labeling *in vivo* to visualize and affinity purify newly synthesized proteins in larval zebrafish. *ACS Chem. Neurosci.* 3, 40–49. doi: 10.1021/cn2000876

Hwang, W. Y., Fu, Y., Reyon, D., Maeder, M. L., Tsai, S. Q., Sander, J. D., et al. (2013). Efficient genome editing in zebrafish using a CRISPR-Cas system. *Nat. Biotechnol.* 31, 227–229. doi: 10.1038/nbt.2501

Issa, F. A., O'Brien, G., Kettunen, P., Sagasti, A., Glanzman, D. L., and Papazian, D. M. (2011). Neural circuit activity in freely behaving zebrafish (*Danio rerio*). *J. Exp. Biol.* 214, 1028–1038. doi: 10.1242/jeb.048876

Johnson, O., Becnel, J., and Nichols, C. D. (2011). Serotonin receptor activity is necessary for olfactory learning and memory in *Drosophila melanogaster*. *Neuroscience* 192, 372–381. doi: 10.1016/j.neuroscience.2011.06.058

Joiner, M. A., and Griffith, L. C. (1999). Mapping of the anatomical circuit of CaM Kinase-dependent courtship conditioning in Drosophila. *Learn. Mem.* 6, 177–192.

Kandel, E. R. (2001). The molecular biology of memory storage: a dialogue between genes and synapses. *Science* 294, 1030–1038. doi: 10.1126/science.1067020

Kandel, E. R., and Schwartz, J. H. (1982). Molecular biology of learning: modulation of transmitter release. *Science* 218, 433–443. doi: 10.1126/science.6289442

Karnik, I., and Gerlai, R. (2012). Can zebrafish learn spatial tasks. An empirical analysis of place and single CS–US associative learning.

Behav. Brain Res. 233, 415–421. doi: 10.1016/j.bbr.2012.05.024

Kasuya, J., Ishimoto, H., and Kitamoto, T. (2009). Neuronal mechanisms of learning and memory revealed by spatial and temporal suppression of neurotransmission using shibirets1, a temperature-sensitive dynamin mutant gene in *Drosophila melanogaster*. *Front. Mol. Neurosci.* 2:11. doi: 10.3389/neuro.02.011.2009

Kimmel, C. B., Patterson, J., and Kimmel, R. O. (1974). The development and behavioral characteristics of the startle response in the zebra fish. *Dev. Psychobiol.* 7, 47–60. doi: 10.1002/dev.420070109

Kotani, T., Nagayoshi, S., Urasaki, A., and Kawakami, K. (2006). Transposon-mediated gene trapping in zebrafish. *Methods* 39, 199–206. doi: 10.1016/j.ymeth.2005.12.006

Lac, S., Raymond, J. L., Sejnowski, T. J., and Lisberger, S. G. (1995). Learning and memory in the vestibulo-ocular reflex. *Annu. Rev. Neurosci.* 18, 409–441. doi: 10.1146/annurev.ne.18.030195.002205

Lee, A., Mathuru, A. S., Teh, C., Kibat, C., Korzh, V., Penney, T. B., et al. (2010). The habenula prevents helpless behavior in larval zebrafish. *Curr. Biol.* 20, 2211–2216. doi: 10.1016/j.cub.2010.11.025

Liu, K. S., and Fetcho, J. R. (1999). Laser ablations reveal functional relationships of segmental hindbrain neurons in zebrafish. *Neuron* 23, 325–335. doi: 10.1016/S0896-627380783-7

Liu, X., Ramirez, S., Pang, P. T., Puryear, C. B., Govindarajan, A., Deisseroth, K., et al. (2012). Optogenetic stimulation of a hippocampal engram activates fear memory recall. *Nature* 484, 381–385.

Marsh, E., and Baker, R. (1997). Normal and adapted visuooculomotor reflexes in goldfish. *J. Neurophysiol.* 77, 1099–1118.

Mattioli, R., Nelson, C. A., Huston, J. P., and Spieler, R. E. (1998). Conditioned place-preference analysis in the goldfish with the H1 histamine antagonist chlorpheniramine. *Brain Res. Bull.* 45, 41–44. doi: 10.1016/S0361-923000287-6

McCann, L. I., Koehn, D. J., and Kline, N. J. (1971). The effects of body size and body markings on nonpolarized schooling behavior of zebra fish (*Brachydanio rerio*). *J. Psychol.* 79, 71–75. doi: 10.1080/00223980.1971.9923769

Meng, X., Noyes, M. B., Zhu, L. J., Lawson, N. D., and Wolfe, S. A. (2008). Targeted gene inactivation in zebrafish using engineered zinc-finger nucleases. *Nat. Biotechnol.* 26, 695–701. doi: 10.1038/nbt1398

Menzel, R. (2012). The honeybee as a model for understanding the basis of cognition. *Nat. Rev. Neurosci.* 13, 758–768. doi: 10.1038/nrn3357

Mo, W., Chen, F., Nechiporuk, A., and Nicolson, T. (2010). Quantification of vestibular-induced eye movements in zebrafish larvae. *BMC Neurosci.* 11:110. doi: 10.1186/1471–2202-11-110.

Moore, F. E., Reyon, D., Sander, J. D., Martinez, S. A., Blackburn, J. S., Khayter, C., et al. (2012). Improved somatic mutagenesis in zebrafish using transcription activator-like effector nucleases (TALENs). *PLoS ONE* 7:e37877. doi: 10.1371/journal.pone.0037877

Moorman, S. J., Cordova, R., and Davies, S. A. (2002). A critical period for functional vestibular development in zebrafish. *Dev. Dyn.* 223, 285–291. doi: 10.1002/dvdy.10052

Mu, Y., Li, X.-Q., Zhang, B., and Du, J.-l. (2012). Visual input modulates audiomotor function via hypothalamic dopaminergic neurons through a cooperative mechanism. *Neuron* 75, 688–699. doi: 10.1016/j.neuron.2012.05.035

Mullins, M. C., Hammerschmidt, M., Haffter, P., and Nüsslein-Volhard, C. (1994). Large-scale mutagenesis in the zebrafish: in search of genes controlling development in a vertebrate. *Curr. Biol.* 4, 189–202. doi: 10.1016/S0960-982200048-8

Muto, A., Ohkura, M., Kotani, T., Higashijima, S.-I., Nakai, J., and Kawakami, K. (2011). Genetic visualization with an improved GCaMP calcium indicator reveals spatiotemporal activation of the spinal motor neurons in zebrafish. *Proc. Natl. Acad. Sci. U.S.A.* 108, 5425–5430. doi: 10.1073/pnas.1000887108

Nasevicius, A., and Ekker, S. C. (2000). Effective targeted gene "knockdown" in zebrafish. *Nat. Genet.* 26, 216–220. doi: 10.1038/79951

Norton, W., and Bally-Cuif, L. (2010). Adult zebrafish as a model organism for behavioral genetics. *BMC Neurosci.* 11:90. doi: 10.1186/1471–2202-11-90

O'Malley, D. M., Kao, Y. H., and Fetcho, J. R. (1996). Imaging the functional organization of zebrafish hindbrain segments during escape behaviors. *Neuron* 17, 1145–1155. doi: 10.1016/S0896-627380246-9

Orger, M. B., Kampff, A. R., Severi, K. E., Bollmann, J. H., and Engert, F. (2008). Control of visually guided behavior by distinct populations of spinal projection neurons. *Nat. Neurosci.* 11, 327–333. doi: 10.1038/nn2048

Pastor, A. M., de la Cruz, R. R., and Baker, R. (1994). Cerebellar role in adaptation of the goldfish vestibuloocular reflex. *J. Neurophysiol.* 72, 1383–1394.

Pavlov, I. P. (1927). *Conditioned Reflexes: an Investigation of the Physiological Activity of the Cerebral Cortex*. London: Oxford University Press.

Pearce, K., Roberts, A. C., Yeung, A. K., Bill, B. R., Geng, M., Chen, S., et al. (2012). Long-term habituation of the startle response in the larval zebrafish, *Danio rerio*. *Soc. Neurosci. Abstr.* 38, 703.08.

Peichel, C. L. (2004). Social behavior: how do fish find their shoal mate. *Curr. Biol.* 14, R503–R504. doi: 10.1016/j.cub.2004.06.037.

Petzold, A. M., Balciunas, D., Sivasubbu, S., Clark, K. J., Bedell, V. M., Westcot, S. E., et al. (2009). Nicotine response genetics in the zebrafish. *Proc. Natl. Acad. Sci. U.S.A.* 106, 18662–18667. doi: 10.1073/pnas.0908247106

Pradel, G., Schachner, M., and Schmidt, R. (1999). Inhibition of memory consolidation by antibodies against cell adhesion molecules after active avoidance conditioning in zebrafish. *J. Neurobiol.* 39, 197–206.

Pradel, G., Schmidt, R., and Schachner, M. (2000). Involvement of L1.1 in memory consolidation after active avoidance conditioning in zebrafish. *J. Neurobiol.* 43, 389–403.

Rankin, C. H. (2002). From gene to identified neuron to behaviour in *Caenorhabditis elegans*. *Nat. Rev. Genet.* 3, 622–630.

Rankin, C. H., Abrams, T., Barry, R. J., Bhatnagar, S., Clayton, D. F., Colombo, J., et al. (2009). Habituation revisited: an updated and revised description of the behavioral characteristics of habituation. *Neurobiol. Learn. Mem.* 92, 135–138. doi: 10.1016/j.nlm.2008.09.012

Riemensperger, T., Völler, T., Stock, P., Buchner, E., and Fiala, A. (2005). Punishment prediction by dopaminergic neurons in Drosophila. *Curr. Biol.* 15, 1953–1960. doi: 10.1016/j.cub.2005.09.042

Ritter, D. A., Bhatt, D. H., and Fetcho, J. R. (2001). *In vivo* imaging of zebrafish reveals differences in the spinal networks for escape and swimming movements. *J. Neurosci.* 21, 8956–8965.

Roberts, A. C., and Glanzman, D. L. (2003). Learning in Aplysia: looking at synaptic plasticity from both sides. *Trends Neurosci.* 26, 662–670. doi: 10.1016/j.tins.2003.09.014

Roberts, A. C., Reichl, J., Song, M. Y., Dearinger, A. D., Moridzadeh, N., Lu, E. D., et al. (2011). Habituation of the C-start response in larval zebrafish exhibits several distinct phases and sensitivity to NMDA receptor blockade. *PLoS ONE* 6:e29132. doi: 10.1371/journal.pone.0029132

Roberts, A. J., and Hedlund, P. B. (2012). The 5-HT7 receptor in learning and memory. *Hippocampus* 22, 762–771. doi: 10.1002/hipo.20938

Roeser, T., and Baier, H. (2003). Visuomotor behaviors in larval zebrafish after GFP-guided laser ablation of the optic tectum. *J. Neurosci.* 23, 3726–3734.

Salas, C., Broglio, C., Durán, E., Gómez, A., Ocaña, F. M., Jiménez-Moya, F., et al. (2006). Neuropsychology of learning and memory in teleost fish. *Zebrafish* 3, 157–171.

Schier, A. F., Neuhauss, S. C., Harvey, M., Malicki, J., Solnica-Krezel, L., Stainier, D. Y., et al. (1996). Mutations affecting the development of the embryonic zebrafish brain. *Development* 123, 165–178.

Scott, E. K. (2009). The Gal4/UAS toolbox in zebrafish: new approaches for defining behavioral circuits. *J. Neurochem.* 110, 441–456. doi: 10.1111/j.1471-4159.2009.06161.x

Scott, E. K., Mason, L., Arrenberg, A. B., Ziv, L., Gosse, N. J., Xiao, T., et al. (2007). Targeting neural circuitry in zebrafish using GAL4 enhancer trapping. *Nat. Methods* 4, 323–326.

Shumake, J., Ilango, A., Scheich, H., Wetzel, W., and Ohl, F. W. (2010). Differential neuromodulation of acquisition and retrieval of avoidance learning by the lateral habenula and ventral tegmental area. *J. Neurosci.* 30, 5876–5883. doi: 10.1523/JNEUROSCI.3604-09.2010

Silva, A. J., Paylor, R., Wehner, J. M., and Tonegawa, S. (1992a). Impaired spatial learning in a-calcium-calmodulin kinase II mutant mice. *Science* 257, 206–211. doi: 10.1126/science.1321493

Silva, A. J., Stevens, C. F., Tonegawa, S., and Wang, Y. (1992b). Deficient hippocampal long-term-potentiation in a-calcium-calmodulin kinase II mutant mice. *Science* 257, 201–206. doi: 10.1126/science.1378648

Sison, M., and Gerlai, R. (2010). Associative learning in zebrafish (*Danio rerio*) in the plus maze.

Behav. Brain Res. 207, 99–104. doi: 10.1016/j.bbr.2009.09.043

Sitaraman, D., Zars, M., LaFerriere, H., Chen, Y.-C., Sable-Smith, A., Kitamoto, T., et al. (2008). Serotonin is necessary for place memory in *Drosophila*. *Proc. Natl. Acad. Sci. U.S.A.* 105, 5579–5584. doi: 10.1073/pnas.0710168105

Sivasubbu, S., Balciunas, D., Davidson, A. E., Pickart, M. A., Hermanson, S. B., Wangensteen, K. J., et al. (2006). Gene-breaking transposon mutagenesis reveals an essential role for histone H2afza in zebrafish larval development. *Mech. Dev.* 123, 513–529. doi: 10.1016/j.mod.2006.06.002

Szobota, S., Gorostiza, P., Del Bene, F., Wyart, C., Fortin, D. L., Kolstad, K. D., et al. (2007). Remote control of neuronal activity with a light-gated glutamate receptor. *Neuron* 54, 535–545. doi: 10.1016/j.neuron.2007.05.010

Thompson, R. F., and Spencer, W. A. (1966). Habituation: a model phenomenon for the study of neuronal substrates of behavior. *Psychol. Rev.* 73, 16–43. doi: 10.1037/h0022681

Valente, A., Huang, K. H., Portugues, R., and Engert, F. (2012). Ontogeny of classical and operant learning behaviors in zebrafish. *Learn. Mem.* 19, 170–177. doi: 10.1101/lm.025668.112

Warp, E., Agarwal, G., Wyart, C., Friedmann, D., Oldfield, Claire, S., et al. (2012). Emergence of patterned activity in the developing zebrafish spinal cord. *Curr. Biol.* 22, 93–102.

Weiss, S. A., Zottoli, S. J., Do, S. C., Faber, D. S., and Preuss, T. (2006). Correlation of C-start behaviors with neural activity recorded from the hindbrain in free-swimming goldfish (*Carassius auratus*). *J. Exp. Biol.* 209, 4788–4801. doi: 10.1242/jeb.02582

Wienholds, E., van Eeden, F., Kosters, M., Mudde, J., Plasterk, R. H. A., and Cuppen, E. (2003). Efficient target-selected mutagenesis in zebrafish. *Genome Res.* 13, 2700–2707. doi: 10.1101/gr.1725103

Wise, R. A. (2004). Dopamine, learning and motivation. *Nat. Rev. Neurosci.* 5, 483–494. doi: 10.1038/nrn1406

Wolman, M. A., Jain, R. A., Liss, L., and Granato, M. (2011). Chemical modulation of memory formation in larval zebrafish. *Proc. Natl. Acad. Sci. U.S.A.* 108, 15468–15473. doi: 10.1073/pnas.1107156108

Wood, W. E., Lovell, P. V., Mello, C. V., and Perkel, D. J. (2011). Serotonin, via HTR2 receptors, excites neurons in a cortical-like premotor nucleus necessary for song learning and production. *J. Neurosci.* 31, 13808–13815. doi: 10.1523/JNEUROSCI.2281-11.2011

Wyart, C., Bene, F. D., Warp, E., Scott, E. K., Trauner, D., Baier, H., et al. (2009). Optogenetic dissection of a behavioural module in the vertebrate spinal cord. *Nature* 461, 407–410. doi: 10.1038/nature08323

Xu, X., Scott-Scheiern, T., Kempker, L., and Simons, K. (2007). Active avoidance conditioning in zebrafish (*Danio rerio*). *Neurobiol. Learn. Mem.* 87, 72–77. doi: 10.1016/j.nlm.2006.06.002

Yin, J. C., Del Vecchio, M., Zhou, H., and Tully, T. (1995). CREB as a memory modulator: induced expression of a dCREB2 activator isoform enhances long-term memory in Drosophila. *Cell* 81, 107–115. doi: 10.1016/0092-867490375-5

Yin, J. C., Wallach, J. S., Del Vecchio, M., Wilder, E. L., Zhou, H., Quinn, W. G., et al. (1994). Induction of a dominant negative CREB transgene specifically blocks long-term memory in Drosophila. *Cell* 79, 49–58. doi: 10.1016/0092-867490399-9

Yizhar, O., Fenno, L. E., Prigge, M., Schneider, F., Davidson, T. J., O'Shea, D. J., et al. (2011). Neocortical excitation/inhibition balance in information processing and social dysfunction. *Nature* 477, 171–178. doi: 10.1038/nature10360

Yoshida, M., and Kondo, H. (2012). Fear conditioning-related changes in cerebellar Purkinje cell activities in goldfish. *Behav. Brain Funct.* 8:52. doi: 10.1186/1744–9081-8-52

Zala, S., and Määttänen, I. (2013). Social learning of an associative foraging task in zebrafish. *Naturwissenschaften* 100, 469–472. doi: 10.1007/s00114-013-1017-6

Zars, T., Fischer, M., Schulz, R., and Heisenberg, M. (2000a). Localization of a short-term memory in *Drosophila*. *Science* 288, 672–675. doi: 10.1126/science.288.5466.672

Zars, T., Wolf, R., Davis, R., and Heisenberg, M. (2000b). Tissue-specific expression of a type I adenylyl cyclase rescues the rutabaga mutant memory defect: in search of the engram. *Learn. Mem.* 7, 18–31. doi: 10.1101/lm.7.1.18

Conflict of Interest Statement: The authors declare that the research was conducted in the absence of any commercial or financial relationships that could be construed as a potential conflict of interest.

Received: 16 May 2013; accepted: 11 July 2013; published online: 02 August 2013.
Citation: Roberts AC, Bill BR and Glanzman DL (2013) Learning and memory in zebrafish larvae. Front. Neural Circuits 7:126. doi: 10.3389/fncir.2013.00126

frontiers in
NEURAL CIRCUITS

REVIEW ARTICLE
published: 08 August 2013
doi: 10.3389/fncir.2013.00131

Mind the fish: zebrafish as a model in cognitive social neuroscience

Rui F. Oliveira [1,2] *

[1] *Unidade de Investigação em Eco-Etologia, ISPA – Instituto Universitário, Lisboa, Portugal*
[2] *Champalimaud Neuroscience Programme, Instituto Gulbenkian de Ciência, Oeiras, Portugal*

Edited by:
Gonzalo G. De Polavieja, Instituto Cajal, Consejo Superior de Investigaciones Científicas, Spain

Reviewed by:
Hitoshi Okamoto, RIKEN Brain Science Institute, Japan
Robert Gerlai, University of Toronto, Canada
Peter Neri, University of Aberdeen, UK

***Correspondence:**
Rui F. Oliveira, Unidade de Investigação em Eco-Etologia, ISPA – Instituto Universitário, Rua Jardim do Tabaco 34, 1149-041 Lisboa, Portugal
e-mail: ruiol@ispa.pt

Understanding how the brain implements social behavior on one hand, and how social processes feedback on the brain to promote fine-tuning of behavioral output according to changes in the social environment is a major challenge in contemporary neuroscience. A critical step to take this challenge successfully is finding the appropriate level of analysis when relating social to biological phenomena. Given the enormous complexity of both the neural networks of the brain and social systems, the use of a cognitive level of analysis (in an information processing perspective) is proposed here as an explanatory interface between brain and behavior. A conceptual framework for a cognitive approach to comparative social neuroscience is proposed, consisting of the following steps to be taken across different species with varying social systems: (1) identification of the functional building blocks of social skills; (2) identification of the cognitive mechanisms underlying the previously identified social skills; and (3) mapping these information processing mechanisms onto the brain. Teleost fish are presented here as a group of choice to develop this approach, given the diversity of social systems present in closely related species that allows for planned phylogenetic comparisons, and the availability of neurogenetic tools that allows the visualization and manipulation of selected neural circuits in model species such as the zebrafish. Finally, the state-of-the art of zebrafish social cognition and of the tools available to map social cognitive abilities to neural circuits in zebrafish are reviewed.

Keywords: social neuroscience, zebrafish, social cognition, cognitive modules, social behavior, social brain

INTRODUCTION: A COGNITIVE APPROACH TO COMPARATIVE SOCIAL NEUROSCIENCE

In social species animals interact frequently with their conspecifics and have to adjust the expression of their social behavior according to previous social experience and to social context. This behavioral flexibility in the social domain (aka social competence; Taborsky and Oliveira, 2012) allows the animal to navigate daily changes in the social environment and should be viewed as an adaptive performance trait that impacts the Darwinian fitness of the animal, for example by allowing it to avoid getting involved in costly social interactions or being ejected from its social group (Oliveira, 2009, 2012). Understanding social competence at the proximate level is a major challenge in contemporary neuroscience. The new field of social neuroscience has emerged in the past two decades in an attempt to understand how biological systems in general, and the brain in particular, implement social behavior on one hand, and how social processes feedback on biological mechanisms and the brain, on the other (Cacioppo and Decety, 2011). One major challenge in this new field is finding the appropriate level of analysis when relating social to biological phenomena. Given the enormous complexity of both the neural networks of the brain and social systems, mapping adaptive social behaviors in the real world onto putative underlying neural circuits in the brain is a daunting task (Adolphs, 2010). One promising approach to this challenge is to use the cognitive level of analysis as an interface level of explanation between brain and behavior, which enables the development of manageable theories of social behavior that can generate testable predictions of observable behavior. Cognition is used here in an information processing perspective, that is as a set of neuronal processes concerned with the acquisition, retention, and use of information, that enables the animal to integrate input information with stored information, when making ecologically relevant decisions (Shettleworth, 2001; Dukas, 2004). These encompass a wide array of cognitive processes such as: perception, learning, memory, attention, and decision making. It should be stressed that the use of the term cognition as proposed here is neither in opposition to association learning explanations of animal behavior in the associative vs. cognitive debate (e.g., Byrne and Bates, 2006; Heyes, 2012a), nor does it equate with intelligence, intentionality or consciousness, as sometimes suggested in anthropomorphic accounts of animal behavior (e.g., Ristau, 1991).

Arguably, it has been proposed that the mechanisms controlling the organism interactions with other behavioral agents (i.e., social interactions) differ from those involved in the interactions of the organism with its physical environment, and therefore the term social cognition has been created to refer specifically to cognitive processes involved in social interactions (e.g., Zuberbuhler and Byrne, 2006). Social phenomena that have been examined under the label of social cognition include recognition of individuals or social categories, social partner preferences, development and management of social relationships (attachment, reconciliation,

alliances), triadic relationships (requesting transitive inference), learning new skills from conspecifics (social learning), social coordination, manipulation, and deception, and theory of mind among many others (Jensen et al., 2011). Most research on comparative social cognition has focused mainly on declarative human-like cognitive abilities apparently needed to navigate highly complex social systems such as those of primates (e.g., "theory of mind," Premack and Woodruff, 1978; Penn and Povinelli, 2007; "Machiavellian intelligence," Whiten and Byrne, 1988, 1997), and not so much on the basic information processing mechanisms that make up the building blocks of the behavioral control systems involved in social behavior irrespective of its complexity (Barrett et al., 2007). This approach is limiting since highly complex social systems do not necessarily request highly complex individual cognitive abilities, as can be illustrated by insect societies or by elaborated mutualistic relationships in cleaner fish (Chittka and Niven, 2009; Bshary, 2011), and as a consequence most "simple-minded" species have not been considered in comparative studies of social cognition. Moreover, functionally similar social phenomena may rely on different underlying mechanisms in different species (e.g., different cognitive mechanisms underlying transitive inference, see below for details). Therefore, a more productive approach to comparative social cognition would be the adoption of a rationale that can be applied universally across species with varying degrees of complexity of their social structures and that takes into account the underlying mechanisms.

In this paper, I propose a conceptual framework for comparative social neuroscience based on: (1) the identification of the functional building blocks of social behavior and the underlying cognitive mechanisms across different species with varying social systems, and (2) how these information processing mechanisms are inbuilt in the brain, which is viewed as an information processing organ. Following Krogh's principle, that "for many problems there is an animal on which it can be most conveniently studied" (Krebs, 1975), teleost fish are presented here as a golden model to develop this approach given the diversity of social systems present in closely related species that allows for planned phylogenetic comparisons of cognitive abilities (e.g., MacLean et al., 2012), and the availability of genetic tools that allows the visualization and manipulation of selected neural circuits in model species such as the zebrafish (e.g., Muto and Kawakami, 2011).

COGNITIVE MODULES OF SOCIAL COMPETENCE

The first step of the conceptual framework proposed here is to identify the information processing problems posed by the social domain of the environment in order to identify the cognitive abilities underlying social skills. For instance, what are the mechanisms required for an individual to tolerate the presence of conspecifics, to recognized different classes of conspecifics and assess their behavior, to use public information available in social environments and to choose the appropriate responses from the available behavioral repertoire? Once we identify these building blocks of social competence we can investigate their phylogenetic distribution and how they map onto neural networks underlying behavior. The putative building blocks of social competence are identified and discussed below (see **Table 1** and **Figure 1** for summary and selected examples in teleost fish, respectively).

SOCIAL VALUE AND SOCIAL PREFERENCES

Approach/ avoidance is a basic behavioral mechanism present in all animals. Given that an a priori condition for social groups to form is that individuals show a predisposition to approach conspecifics and tolerate their presence, this prosocial tendency has to overcome the one for social withdrawal. At the cognitive level prosocial behavior relies on a value system that attributes valence (on a negative–positive continuum) and salience (on a low to high continuum) to social agents (Paul et al., 2005), such that conspecifics tend to have reward value (i.e., high salience, positive valence; Thiel et al., 2008) hence eliciting approach responses. However, different conspecifics may pose different challenges/opportunities, hence not all group members are expected to have the same social value. Some might be competitors, others potential partners or mates. These differences in reward value of different conspecifics lead to social preferences (e.g., mate choice preferences; Ryan et al., 2007), which in turn may lead to social bonding, when individuals establish long-lasting relationships.

COGNITIVE APPRAISAL

Given the wide array of social signals conveyed in multiple sensory modalities it is postulated that a general appraisal mechanism that assesses the valence and salience of social stimuli across different sensory modalities and functional domains must operate. According to this view the evaluation of valence and salience of social information is not just a result of direct effects of perceptual information (e.g., image of conspecific elicits approach), but rather a function of what that perceptual information means to the organism at that moment in time (e.g., image of conspecific is appraised and its valence elicits appropriate response, such as: if dominant avoid; Paul et al., 2005; Mendl et al., 2010). This subjective value of social stimuli is assessed through a set of stimulus evaluation checks which include intrinsic valence of the stimuli, novelty (as defined by suddenness, familiarity, and predictability), prediction error and controllability (Paul et al., 2005; Mendl et al., 2010). Despite the fact that some of these checks have been described in animals (e.g., predictability in fish; Galhardo et al., 2011), a systematic study of stimulus evaluation checks in animals is still lacking. Cognitive appraisal classifies social stimuli in terms of their valence, salience and the organism capacity for control, therefore decoupling stimulus and response and allowing the animal to give a flexible response.

SOCIAL RECOGNITION AND MEMORY

For the expression of both prosocial behavior and social preferences individuals need to discriminate between classes of social agents, namely conspecifics from heterospecifics and between conspecifics with different social valences. Different forms of social recognition might occur, from individual recognition, where individuals are recognized by unique cues (Tibbetts and Dale, 2007), to the recognition of social classes of individuals, such as kin (Hepper, 1986) or social rank conveyed by status badges (Johnstone and Norris, 1993). Individual recognition is expected to evolve in semi-permanent groups where individuals engage

Table 1 | Social skills, their putative underlying cognitive mechanisms and selected examples of their occurrence in teleost fish.

Social skill	Cognitive mechanisms*	Species	Reference
Prosociality			
social reward	Innate response; Selective attention	Zebrafish, *Danio rerio*	Al-Imari and Gerlai (2008)
Social preferences			
Shoal mate preference	discrimination learning	Zebrafish, *Danio rerio*	Engeszer et al. (2007)
Mate choice	discrimination learning	Peacock blenny, *Salaria pavo*	Fagundes et al. (2007)
Pair bond	recognition learning and social memory	African cichlid, *Tropheus moorii*	Egger et al. (2006)
Cognitive appraisal			
Predictability	S-S learning	Mozambique tilapia, *Oreochromis mossambicus*	Galhardo et al. (2011)
Social recognition and memory			
Individual recognition	Single stimulus learning + long-term memory	Cleaner wrasse, *Labroides dimidiatus*	Tebbich et al. (2002)
Kin recognition		Zebrafish, *Danio rerio*	Gerlach and Lysiak (2006)
Social status		Mozambique tilapia, *Oreochromis mossambicus*	Barata et al. (2007)
Familiarity			
Social inference			
Social eavesdropping	Selective attention, S–R learning	Siamese fighting fish, *Betta splendens*	Oliveira et al. (1998)
Transitive inference	Associative strength, ordinal representation	African cichlid, *Astatotilapia burtoni*	Grosenick et al. (2007)
Audience effects	Selective attention, S–R learning	Siamese fighting fish, *Betta splendens*	Doutrelant et al. (2001)
Deception	Selective attention, S–R learning	Cleaner wrasse, *Labroides dimidiatus*	Pinto et al. (2011)
Social learning			
Stimulus enhancement	Single stimulus learning	Zebrafish, *Danio rerio*	Lindeyer and Reader (2010)
Observational conditioning	S–S learning	Zebrafish, *Danio rerio*	Suboski et al. (1990)
Copying	S–R learning	Sailfin molly, *Poecilia latipinna*	Witte and Ryan (2002)
Intertemporal choice			
Spatial discounting	Reversal learning	Guppies, *Poecilia reticulata*	Muhlhoff et al. (2011)

**Following the terminology used by Shettleworth (2010)*

in repeated interactions, since it reduces the costs associated with agonistic interactions and it stabilizes dominance hierarchies (Barnard and Burk, 1979; Pagel and Dawkins, 1997). Any kind of social recognition requires memory for conspecifics so that the acquired discrimination of different individuals or classes of individuals is carried forward in time in a computational way that is accessible for retrieval by the animal at a future time. There is some evidence that social memory is independent of asocial memory. For example, AVP V1b receptor knockout mice have impaired memory for social odors, despite having normal olfactory ability and other memory functions (e.g., spatial memory; Wersinger et al., 2004).

SOCIAL INFERENCE

In a social group, individuals may gain information by observing social interactions between third parties, thus avoiding the potential costs involved in direct agonistic interactions (McGregor and Peake, 2000). Bystanders may use the information about interacting partners in order to adjust their future behavior in subsequent interactions with the observed individuals (social eavesdropping; Peake, 2005). Similarly, the presence of bystanders may influence current behavior of interacting individuals that will try to manipulate the information available to bystanders (audience effects; Matos and Schlupp, 2005). In social groups information obtained from observing relationships between third parties (e.g., A > B and B > C) can be used to infer unknown relationships among group members (e.g., A > C; Paz-Y-Miño et al., 2004; Grosenick et al., 2007). Therefore, together with individual recognition, transitive inference can stabilize hierarchies in groups with repeated interactions among individuals, since the relative dominance of unfamiliar individuals can be estimated from observing these interacting with familiar ones. Thus, transitive inference (i.e., if A > B and B > C then A > C) is a skill that is expected to develop with increasing social complexity. Indeed, in two independent comparative studies of transitive inference abilities in closely related species differing in sociality, it was found in both cases that the more highly social of the two species performed better in the transitive inference task (corvids: Bond et al., 2003; prosimian primates: MacLean et al., 2008). It should be pointed out that transitive inference can be achieved using different cognitive mechanisms (transfer of associative strength, i.e., value transfer vs. representation of ordinal list), hence it does not necessarily require high-order reasoning abilities (Von Fersen et al., 1991; Allen, 2006); see also (De Lillo et al., 2001) for a description of neural network that solves a transitive inference task using a simple error-correcting rule.

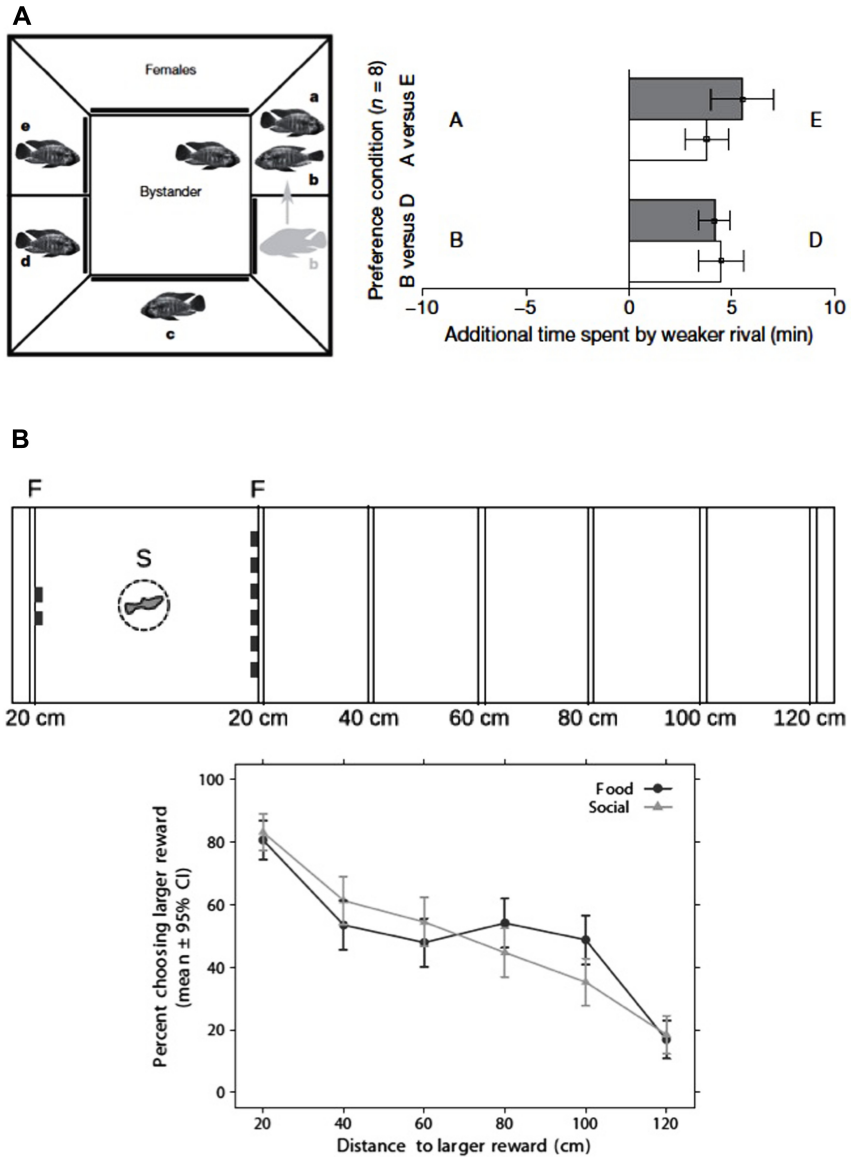

FIGURE 1 | Examples of two complex social abilities in teleost fish. **(A)** Transitive inference in a cichlid fish (*Astatotilapia burtoni*; left panel) experimental set-up for transitive inference training; the bystander male is placed in the middle compartment and allowed to observe a sequence of paired fights among neighboring conspecifics; in each fight the scheduled loser male is placed in the territory of the scheduled winner (e.g., A wins over B), so that the following sequence of fights is produced: A > B, B > C, C > D, D > E; in order to test for transitive inference of social dominance focal males were given a preference test between the pairs AE and BD (where A > E and B > D; right panel) focal males prefer to associate with the lower ranking male from each dyad both in familiar (filled bars) and in novel contexts (open bars), suggesting tha males are able to infer the relative rankings (i.e., A > E and B > D) from the observed dominance hierarchy A > B > C > D > E (reproduced with permission from Grosenick et al., 2007). **(B)** Spatial discounting in guppies (*Poecilia reticulata*; upper panel) experimental set-up for the study of spatial discounting; subjects were given a choice between two vs. six items (food items in the food-reward condition and conspecifics in the social-reward condition); the six items (food or conspecifics) were placed at increasing distances (20, 40, 60, 80, 100, 120cm), whereas the two items were always located at 20 cm from the starting place; (lower panel) in choice tests subjects show a preference for the larger reward that decreases with the distance to the larger reward (reproduced with permission from Muhlhoff et al., 2011).

SOCIAL LEARNING

Public information is readily available in social networks, which allows individuals to acquire adaptive information produced by others without paying the costs typically associated with exploring the environment to learn about its contingencies (e.g., Burns et al., 2011; Mery, 2013). Extracting potentially useful information from observing or interacting with other behavioral agents or their products (aka social learning; Heyes, 1994; Galef and Laland, 2005) has been considered to rely on social-domain specific cognitive modules and in learning mechanisms that are distinct from those used in individual learning by trial and error. However, recent research challenges these assumptions and it has

been proposed that asocial and social learning share the same basic learning mechanisms, namely single stimulus learning (e.g., habituation and sensitization vs. local/stimulus enhancement), stimulus–stimulus learning (Pavlovian conditioning vs. observational conditioning), or stimulus–response learning (instrumental learning vs. copying/ imitation; Heyes, 2012b). For example, it has been pointed out that prediction error (i.e., the difference between predicted and obtained outcomes), that is considered to be the learning signal asocial associative learning, is not directly experienced in social learning. However, a new form of observational prediction error has been proposed recently that acts as a learning signal based on externally observed information (e.g., Burke et al., 2010). Social learning is usually use strategically by animals depending on who and when rules, so that they optimize the trade-off between the accuracy and the costs of personal vs. social information (Kendal et al., 2009).

INTERTEMPORAL CHOICE

In order to maintain social relationships individuals have sometimes to choose a smaller immediate reward to guarantee larger future benefits. This trade-off between two or more pay-offs at different points in time is called temporal discounting. For example, in the cleaning mutualism between the cleaner wrasse (*Labroides dimidiatus*) and its reef fish clients, cleaners feed against their preference (ectoparasites instead clients' mucus) in order to secure the possibility for numerous future interactions (Grutter and Bshary, 2003), hence exhibiting temporal discounting.

TRAFFIC RULES

Group-living animals need to synchronize and coordinate their behavior in order to maintain the functionality of the social group (e.g., in collective motion a group member needs to move with the group in order to keep the benefits of group membership such as predator avoidance). This behavioral synchronization and coordination of individuals within social groups has lead to the emergence of collective patterns that can be impressive, such as the aerial movements of bird flocks, or the spatial behavior of insect swarms, fish schools, ungulate herds, and even human crowds. In most of these cases complex collective patterns can be explained by individual decision-making rules and by the way information flows between group members (Sumpter, 2006; Couzin, 2009). For example, fish schools can be modeled using individual-based models that follow as few as three rules: avoid individuals that are too close, align with individuals at intermediate distance, and move toward those further away (Parrish and Turchin, 1997; Parrish and Viscido, 2005). Therefore, simple heuristics at the level of the individual may explain the emergence of self-organized social patterns without the need of complex cognitive abilities. This does not mean, however, that the cognitive abilities mentioned above are not needed for optimized social behavior in varying social environments.

More complex social systems are predicted to impose a higher cognitive demand, hence recruiting quantitatively more resources of the abovementioned social skills or promoting qualitative progress of new social skills (e.g., "theory of mind" in humans and questionably in non-human primates; Byrne and Bates, 2010). Evidence supporting this view came from comparative work in primates that established an association between brain size (in particular neocortex), social complexity (as measured by social group size or by occurrence of long-term relationships), and social skills (as a proxy of cognitive complexity), which has been interpreted as evidence for positive selection on executive brain size driven by social complexity (aka "Social brain hypothesis;" Dunbar, 1998; Reader and Laland, 2002; Byrne and Corp, 2004; Dunbar and Shultz, 2007). Although originally developed in primates (Dunbar, 1992; Barton, 1996), the social brain hypothesis has been extended to other taxa, including non-primate mammals (e.g., Perez-Barberia et al., 2007), birds (e.g., Burish et al., 2004; Emery et al., 2007), fish (e.g., Pollen et al., 2007; Gonzalez-Voyer et al., 2009) and insects, on which the relationship between sociality and a brain area size was first described (see review in Lihoreau et al., 2012). However, it has been pointed out that apparently complex social skills may require little information-processing capabilities (Chittka and Niven, 2009) and that even qualitative enhancements in information-processing behind behavioral innovations may be achieved with minor changes in the connectivity of neural networks (see below). Therefore, future research on the co-evolution of brain and social cognition/behavior should move beyond comparative analyses of brain size and focus on unraveling the neural circuitry underlying specific social cognitive abilities.

FUNCTIONAL ARCHITECTURE OF THE SOCIAL BRAIN

The second step of the proposed conceptual framework is to map the cognitive processes involved in social competence onto the brain. There is ample evidence indicating that complex cognitive functions are associated with distributed brain networks, rather than with single brain regions, such that their behavioral manifestations are better reflected by the overall pattern of activation across the different loci of the network than by the activity of any of the single nodes (McIntosh, 2000; Sporns, 2010). These networks are also dynamic so that each node (i.e., brain region) may participate in multiple cognitive functions by rapid functional connectivity reconfigurations (Sporns, 2010). The combination of functional specialization in domain-specific modules with the integration at the neural network level provides coherence to mental states and to behavioral (motor) decision making, allowing for the expression of complex and flexible behavior. Each functional network may exhibit a variety of states, as defined by the configuration of activated nodes, each of which expressing the network encoded knowledge regarding a specific input. The existence of social domain-specific modules within these networks has been demonstrated both at the sensory and central levels as can be illustrated by the parallel stream of social odor processing by the mammalian vomeronasal system relative to asocial odors processed by the main olfactory system (Døving and Trotier, 1998), or by the specialized face recognition areas in the brains of humans, macaques (*Macaca mulatta*) and sheep (Kendrick and Baldwin, 1987; Kanwisher and Yovel, 2006; Tsao et al., 2006, 2008).

Recently, the occurrence of an evolutionary conserved social decision-making network in vertebrates has been proposed, based on conserved patterns of expression of developmental genes and

neurochemical systems in the telencephalon (O'Connell and Hofmann, 2011, 2012). This vertebrate social decision-making network would be composed of two interconnected sister networks: the basal forebrain reward system and the social behavior network (*sensu*; Goodson, 2005). The reward system would provide value information to other domain-specific modules in the network so that the valence and salience of social stimuli can be integrated in social decision-making, allowing for the reinforcement of adaptive behaviors through natural rewards (Kelley and Berridge, 2002). The social behavior network would be involved in the regulation of multiple forms of social behavior and includes the extended medial amygdala, the lateral septum, the preoptic area, the anterior hypothalamus, the ventromedial hypothalamus, and the periaqueductal gray in mammals and their homologs in non-mammals (Newman, 1999; Goodson, 2005; Goodson and Kabelik, 2009; O'Connell and Hofmann, 2011; see **Figure 2**). Functional evidence for the presence of the social behavior network is difficult to obtain since it requires the simultaneous recording of neural activity in multiple brain regions. Given the difficulty of obtaining large-scale electrophysiological recordings indirect measures of neural activity, such as the expression of immediate early genes (e.g., *c-fos, egr-1*) or the activity of cytochrome oxidase, in relation to the expression of different social behaviors, have been used to test this hypothesis. In recent years this type of studies has been accumulating evidence in favor of the social brain network hypothesis. In the African cichlid *Astatotilapia burtoni* subordinate males given the opportunity to rise in social rank show higher expression of immediate early genes in all nodes of the social behavior network when compared either to stable subordinate or dominant males (Maruska et al., 2013). In the green anole lizard (*Anolis carolinensis*) repeated exposure to video-playbacks of aggressive displays of conspecific males induced changes in functional connectivity within the network (Yang and Wilczynski, 2007). And in estrildid finches, different nodes of the network are differentially activated in response to the presence of a conspecific, in a way that is related to inter-specific differences in sociality (Goodson et al., 2005). Despite this evidence for the association of this brain network with social behavior, a systematic approach to the study of the relationship between specific social phenomena (e.g., individual recognition, social inference, etc.) and network state, that would potentially allow the identification of specific social cognitive modules and their integration, is still missing. So far the study of these processes in relation to large-scale brain activity has been mainly restricted to humans and other primates for which functional brain imaging techniques (e.g., MRI, PET) are available (e.g., Sallet et al., 2011; Kumaran et al., 2012). However, given the unique role of the neocortex in human and non-human primate social cognition the relevance of this type of data for testing the wider social brain network hypothesis outlined above has been limited (Adolphs, 2009).

At the evolutionary level the combination of functional segregation and integration in neural networks also provides a simple explanation for qualitative enhancements in information-processing leading to behavioral innovations with gains in flexibility, that may coexist with ancestral stereotyped responses. For example, in honeybees vertical functional modules, such as those specialized in processing conspecific odors, provide rapid and stereotyped responses, while central integration across multiple interconnected domain-specific modules provides novel and adaptive solutions (Menzel and Giurfa, 2001).

Finally, it must be stressed that evidence supporting the occurrence of this putative social behavior network does not mean that that the nodes of this network are exclusively involved in social decision-making. On the contrary, it is expected each node to be shared by multiple brain networks (e.g., stress and social behavior networks).

TELEOSTS AS MODELS FOR COMPARATIVE SOCIAL COGNITION

A successful comparative research program in cognitive social neuroscience has two key requirements: (1) the possibility for cladistic research on the evolution of social behavior and cognition aiming to uncover how pre-existing cognitive modules may evolve quantitatively (e.g., increase in memory storage capacity) and how networks may be reconfigured leading to the emergence of qualitatively new solutions to adaptive problems; and (2) the possibility for reductionist research on the mapping of cognitive function into neural networks, which requires model organisms with appropriate social behavior and with an available "tool box" for the analysis of neural circuits. Therefore, the combination of comparative behavioral work on selected species in naturalistic settings covering the expected diversity in cognitive abilities with neuroethological research on a phylogenetically related model organism is a promising approach. Teleost fish fulfill both requirements and therefore they offer an excellent opportunity to fulfill such a research program on comparative cognitive social neuroscience.

First, they offer a unique possibility for planned phylogenetic comparisons on social skills and underlying cognitive modules. With over 29,000 species described so far, teleost fish are the most diverse of the vertebrate taxa, and this diversity also translates into a wide variation within closely related groups of species in modes of social organization (e.g., variation in mating systems and parental care type in African cichlids, Machado et al., 2009). Fish also excel in social plasticity, as can be illustrated by the profound behavioral and phenotypic changes induced by the social environment, which ranges from fish of different social status displaying different neurobehavioral profiles to socially driven sex-change (Godwin, 2010; Fernald, 2012). Complex social behavior is also present among teleost fish, as is the case of transitive inference shown by cichlid fish (Grosenick et al., 2007), or strategic behavior, including deception, punishment, reconciliation, partner choice, manipulation, and social prestige, displayed by the obligatory cleaning wrasse (*Labroides dimidiatus*) on the context of cleaning mutualism (Bshary, 2011). So complex forms of social behavior are present in fish and they offer ample opportunity for comparative work both at the inter- and intra-specific levels.

Second, a number of model organisms have been developed among teleost fish (e.g., zebrafish, medaka) for which neurobiological and genetic tools are becoming increasingly available. Among the current teleost model organisms zebrafish offers the best conditions for research in social neuroscience due to a combination of relevant social behavior with availability of relevant tools for studying brain function in relation to behavior.

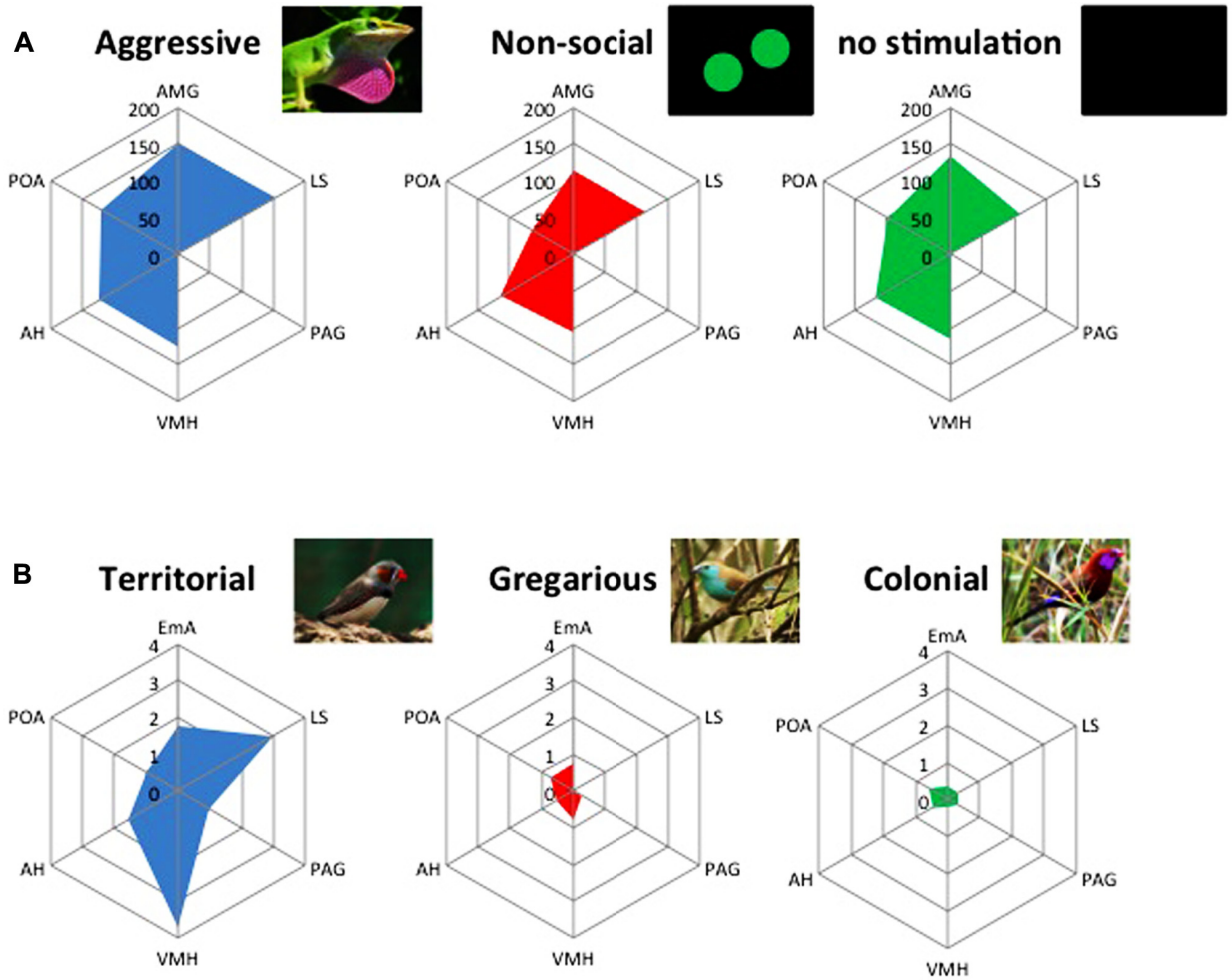

FIGURE 2 | The brain social behavior network (BSBN) presents different activation states associated with the expression of different social behaviors both at the intra- (A) and interspecific level (B). (A) Pattern of activation of the BSBN in the green anole lizard (*Anolis carolinensis*), as measured by the activity of cytochrome oxidase (μmol/min/g tissue), elicited by the exposure to videoplaybacks of an aggressive display, a non-social stimulus (moving balls) or no stimulation (adapted from Yang and Wilczynski, 2007). **(B)** Divergent patterns of activation of the BSBN, as measured by the expression of the immediate early gene c-fos (arbitrary units), elicited by the exposure to a conspecific in closely related songbird species with divergent social systems: territorial (violet-eared waxbill, *Uraeginthus granatina*), gregarious (Angolan blue waxbill, *Uraeginthus angolensis*), highly colonial species (zebra finch, *Taeniopygia guttata*). Note the higher activation of EmA, AH, VMH, and LS in the territorial species (adapted from Goodson et al., 2005). EmA, extended medial amygdala; LS, lateral septum; PAG, periaqueductal gray; VMH, ventromedial hypothalamus; AH, anterior hypothalamus; POA, pre-optic area.

SOCIAL ZEBRAFISH

Zebrafish are highly social animals that live in groups with structured social relationships including shoaling, dominance hierarchies, and territoriality (Spence et al., 2008; Spence, 2011). Furthermore, social behavior in zebrafish shows considerable flexibility as recently shown by the occurrence of acute winner and loser effects (i.e., winner/loser effects; Oliveira et al., 2011), where short-term social interactions are effective in inducing changes in social behavior that are paralleled by massive changes in the profile of gene expression in the brain (Oliveira et al., unpublished data). This richness and flexibility of social behavior predicts that at least some of the social cognitive modules discussed above must be present in zebrafish. Below the available evidence for the occurrence of some of these modules in zebrafish will be discussed.

SOCIAL VALUE IN ZEBRAFISH

The sight of conspecifics has rewarding value in zebrafish and can be used as a reinforcer in an associative learning task (Al-Imari and Gerlai, 2008). Given the rewarding value of conspecifics it is not surprising that zebrafish form aggregations (shoals) from early in development and that shoaling behavior, as measured by the cohesion of the social aggregation (i.e., distance between each pair of shoal members), increases with age (Engeszer et al., 2007; Buske and Gerlai, 2011). Shoal cohesion varies with social context, increasing in the presence of a predator and decreasing during feeding, which is coherent with the function of shoals in reducing predation risk and enhancing foraging efficiency (Miller and Gerlai, 2007). The maturation of shoaling during development is paralleled by an increase in whole brain dopaminergic

and serotonergic activity (Buske and Gerlai, 2012). However, the exposure to conspecific images only induces an increase in brain dopamine, but not in serotonin levels, suggesting a specific involvement of the dopaminergic system in social reward in zebrafish (Saif et al., 2013). This result is in agreement with the well established role of dopamine in the reward circuitry of mammals (Schultz, 2010). However, in anamniotes a midbrain dopaminergic population similar to the ventral tegmental area (VTA), that plays a key role in the mammalian mesolimbic reward system, is missing (Smeets et al., 2000), and the identification of a homologous dopamine reward circuit in fish has remained elusive for many years. The identification of dopaminergic cell groups in the ventral diencephalon projecting to the subpallium (Rink and Wullimann, 2001, 2002), raised the hypothesis that this ascending dopaminergic pathway could be homologous to the mammalian mesostriatal pathway. However, recent data on the expression of developmental factors in larval zebrafish made clear that the ventral diencephalic dopaminergic neurons, that have ascending projections to the telencephalon (i.e., dopaminergic groups DC2 and DC4), are homologous to the A11 mammalian diencephalic dopaminergic cell group (Lohr et al., 2009), rather than to the midbrain mammalian dopaminergic group (i.e., A10). Morever, a detailed projectome of the dopaminergic circuitry in zebrafish showed that most subpallial dopaminergic inputs originate in a local subpallial system that also connects to the ventral telencephalon (Tay et al., 2011). In summary, a the ventral diencephalic-subpallial dopamine system has been characterize in zebrafish that is a good candidate for the dopamine reward system in fish. However, it cannot be seen as homologous to the mammalian dopaminergic mesolimbic pathway, which apparently emerged later in the evolution of dopaminergic modulatory systems (Yamamoto and Vernier, 2011).

SOCIAL PREFERENCES IN ZEBRAFISH

Although conspecifics act as social rewards zebrafish are not equally attracted to all conspecifics, exhibiting shoaling preferences that emerge during the juvenile phase (Engeszer et al., 2007). These shoaling preferences are visually mediated, so that when given a choice between shoal mates with different coloration patterns, individuals prefer to shoal with those sharing the same coloration pattern as the fish with whom they were raised (Engeszer et al., 2007). Once established shoaling preference remains stable and it is not reversed by changing their social environment (Engeszer et al., 2007). In accordance to this finding, once adults wild type zebrafish do not exhibit a shoaling preference based on visual cues for different phenotypic variants (e.g., leopard danios; Spence and Smith, 2007); transgenic red fluorescent Glofish (Snekser et al., 2006). Other characteristics of the shoal than the phenotype of shoal mates are also relevant for the expression of shoaling preferences in zebrafish, that tend to prefer larger and more active shoals (Pritchard et al., 2001; Ruhl and McRobert, 2005). In mammals social preferences and social bonding are known to be moderated by oxytocin and arginine-vasopressin (Donaldson and Young, 2008). Interestingly, it has been shown that their homologs in fish, isotocin and arginine-vasotocin, respectively, also regulate social preference in zebrafish (Braida et al., 2012), suggesting a conserved mechanism for prosocial behavior involving these two neuropeptides. Social preferences can also be expressed in the sexual context, as mate choice preferences according to which individuals do not mate randomly but prefer males with specific characteristics (Spence and Smith, 2006). Female mating preferences for larger males have been described in zebrafish (Pyron, 2003). Given that fin size can increase perceived body size the preference of female zebrafish for longer fins as also been tested but yielded negative results (Kitevski and Pyron, 2003; Gumm et al., 2009).

SOCIAL RECOGNITION IN ZEBRAFISH

As mentioned before a prerequisite for individuals to express social preferences is the ability to recognize individuals or classes of individuals. Zebrafish use both visual and olfactory cues in social recognition. Studies on zebrafish reared in social isolation and on cross-reared intra-specific phenotypes showed that visually mediated species recognition is based on a mechanism of phenotype matching against a learned template early in life (McCann and Matthews, 1974; McCann and Carlson, 1982; Engeszer et al., 2004). Olfaction also plays a role in species recognition as well as in kin recognition in zebrafish, again through a process of phenotype matching (Gerlach and Lysiak, 2006). Olfactory kin recognition is based on imprinting with a 24 h critical period on day 6 post-fertilization during which exposure to kin necessary and sufficient (Gerlach et al., 2008). Neither exposure to own chemical cues nor exposure to non-kin in the critical period results in imprinting. Although individual recognition has not been investigated yet in zebrafish, the occurrence of dominance hierarchies in both sexes (Grant and Kramer, 1992; Delaney et al., 2002; Spence and Smith, 2005; Paull et al., 2010), suggests that it may be present.

COGNITIVE APPRAISAL IN ZEBRAFISH

Cognitive appraisal and cognitive bias are recent research areas that only now are starting to be explored in zebrafish. In our lab we have collected preliminary evidence suggesting that in dyadic agonistic interactions it is the perception that the individual has of the event rather than its objective structure that triggers the physiological and genomic responses differentially observed in winners and losers (Oliveira et al., unpublished data). These results are in accordance with previous work on cichlid fish that showed that ambiguous agonistic interactions between fish and their own image on a mirror (i.e., where the expression of aggressive behavior is decoupled from the experience of gaining or losing social status) failed to elicit the physiological responses observed in winners and losers of real opponent fights (Oliveira et al., 2005).

SOCIAL LEARNING IN ZEBRAFISH

So far the use of public information in zebrafish has been documented mainly in the context of response to aversive stimuli. A first suggestion of social learning in zebrafish comes from data showing that groups of zebrafish learn an avoidance response to an electric shock faster than single individuals (Gleason et al., 1977). However, the better performance while in a social group may be explained by other mechanism, including motivational factors related to the stress of being in isolation. In another set of studies social facilitation of fear response to a predator cue was established (Suboski et al., 1990; Hall and Suboski, 1995). Like

many other ostariophysian fishes zebrafish release an alarm substance to the water when injured which causes a fright response in other fish (Waldman, 1982; Speedie and Gerlai, 2008). This innate fear response can be conditioned by pairing a conditioned stimulus (CS; e.g., innocuous odor or red light) with the exposure to the alarm substance unconditioned stimulus (US; Suboski et al., 1990; Hall and Suboski, 1995). Conditioned individuals can be subsequently used as demonstrators to naïve fish in trained-naïve mixed groups in the presence of the CS alone (i.e., red light in the absence of the alarm substance). In these conditions all fish of the mixed groups exhibited the alarm response indicating social transmission of the conditioned response from the demonstrators to the naïve fish. Moreover, when sorted out from the mixed groups, naïve individuals kept the response to the CS, indicating the acquisition of the response to the predator cue by observational conditioning in naïve individuals (Suboski et al., 1990; Hall and Suboski, 1995). More recently, it has been shown that zebrafish can learn escape routes from trained demonstrators, and that the presence of demonstrators in groups of naïve individuals increased the escape response (i.e., escaped faster) from an approaching trawl. Moreover, observers successfully became demonstrators for further groups of naïve fish and escape responses were experimentally propagated across three generations of social learning (Lindeyer and Reader, 2010). Interestingly, route traditions (i.e., preference for a particular escape route) were not kept along the chain of social transmission, suggesting a mechanism of social facilitation that increases escape response without learning the specific route followed by the demonstrator. Social learning in zebrafish may also be impacted by attributes of the demonstrator. Zebrafish shoals are structured social networks with different individuals having a differential involvement in social interactions (Vital and Martins, 2011), so that central individuals in the network (aka Keystone individuals; Sih et al., 2009) can be recognized. Such keystone individuals play important roles in social groups, acting as learning models and as leaders in group movement (King and Cowlishaw, 2009; Bode et al., 2011). In a recent study keystone and non-key (i.e., less central in the social network) individuals in zebrafish shoals were identified, individually trained in an aversive response task and returned to their shoal. Shoals with trained keystone individuals escaped aversive stimuli more rapidly than those with trained non-key individuals, supporting the hypothesis that social roles play a critical role in social learning also in zebrafish. Apart from the social learning abilities described above, zebrafish also exhibit a wide range of asocial learning abilities in different ecological domains (e.g., Gerlai, 2011; Karnik and Gerlai, 2012), therefore offering the possibility for contrasting the mechanisms underlying learning in the social and physical domains.

INTERTEMPORAL CHOICE IN ZEBRAFISH

Temporal discounting has not been studied in fish so far. However, spatial discounting (i.e., when animals choose between smaller and closer vs. larger and distant rewards) for social rewards has been recently demonstrated in guppies (Muhlhoff et al., 2011). Both types of discounting require impulse control which is usually tested using reversal learning paradigms. A recent study established the occurrence of reversal learning in zebrafish, hence opening the possibility for the occurrence of intertemporal choices in this species (Parker et al., 2012).

TRAFFIC RULES IN ZEBRAFISH

Fish groups can be classified either as "shoals" or as "schools", depending on the degree of synchronization and polarization among group members. Thus, shoals are aggregations of individuals [with four body lengths (BLs) commonly used as a criterion for shoal membership in cyprinid species; Pitcher et al., 1983], whereas schools are highly synchronized and coordinated shoals with polarized orientation of individuals (Pitcher and Parrish, 1993). Both types of groups are present in zebrafish, with schools being faster and less dense than zebrafish shoals, and occurring at lower densities (Miller and Gerlai, 2012). Zebrafish groups may vary in size and are characterized by a high degree of changes in individual relative position within the group and by motion pathways with a high rate of changes in direction (Miller and Gerlai, 2007, 2008, 2011; see also Viscido et al., 2004 for data on the giant danio, *Danio aequipinnatus*). The average distance among zebrafish shoal mates is approximately of 20 cm, and it responds to environmental factors, increasing in the presence of food and predators to over 30 cm (Miller and Gerlai, 2007). Considering that adult zebrafish BL varies between 3 and 4 cm, the average distance between any shoal mates corresponds to 5–6.6 BLs, which is above the proposed threshold of four BLs for shoal membership. However, this distance to the nearest neighbor is stable over time suggesting temporal shoal cohesion in zebrafish (Miller and Gerlai, 2007, 2008, 2011). Although many traffic rules have been developed to explain schooling and shoaling behavior in fish (e.g., Parrish and Turchin, 1997; Parrish and Viscido, 2005), only recently one of these models have been tested in zebrafish. This model showed that zebrafish follows a simple rule in social decision-making based on Bayesian estimation that uses the behaviors of other individuals to improve the estimation (Arganda et al., 2012), therefore confirming the idea that simple heuristics may explain apparently complex collective behavior also in zebrafish.

TOOLS FOR STUDYING BRAIN FUNCTION IN ADULT ZEBRAFISH

A significant number of genetic and neuroanatomy tools and resources are becoming available for zebrafish, making it a tractable species to study brain behavior relationships. Detailed brain atlases are now available for adult zebrafish (Wullimann et al., 1996), and homologies, based on topological and functional data, between zebrafish and mammalian brain areas have been established (Wullimann and Mueller, 2004). More recently, magnetic resonance imaging (MRI) techniques were developed for zebrafish and a detailed MRI three-dimensional atlas is now available for adult zebrafish (Ullmann et al., 2010c,d). The use of MRI will potentially allow non-invasive acquisition of brain morphological data and provides more precise estimates of brain area size than those obtained by classical histological methods, which are prone to tissue deformations due to dissection or histological processing (Ullmann et al., 2010b). This technique has a high potential not only for intra-specific studies with a model organism like the zebrafish, but also for

inter-specific comparative studies of brain volumes in relation to social behavior (Pollen et al., 2007). As an example of the rapid development of the field recently 3D MRI atlases became available for two more fish species (i.e., Tilapia, *Oreochromis mossambicus*: Simões et al., 2012; and barramundi, *Lates calcarifer*: Ullmann et al., 2010a).

The functional study of neural circuits in zebrafish has benefited from the development of optogenetic and transgenic techniques that together allow the close monitoring of activity in neural networks and experimental gain and loss of function manipulations to assess causal relationships between specific neural patterns and specific behaviors (Baier and Scott, 2009; Portugues et al., 2013). Imaging of neural activity in the brain of both larvae and adults (explants in the later case) has been achieved using genetically encoded calcium indicators, of which successive versions of GCaMP have been the more widely used (Baier and Scott, 2009; Portugues et al., 2013). The use of these fluorescent reporters requires the restrain of the animal during image acquisition which limits the behavioral tasks that can be investigated. In order to overcome this limitation a virtual reality system has been recently developed for zebrafish larvae, in which the larvae is stationary but the putative motor output is recorded from the motor neuron axons in the tail and is used in real time to drive movement in the virtual environment (Ahrens et al., 2012). Gain and loss of function studies at the level of cell type or small groups of neurons have used opsin photoswitchable probes, such as channelrhodopsin (ChR2) and halorhodopsin (NpHR), that activate neurons in a reversible way in response to light pulses of specific wave-lengths (e.g., Douglass et al., 2008; Arrenberg et al., 2009). Loss of function studies have also used chemical or photo inducible probes (e.g., Tetanus toxin, nitroreductase, Killer red) to selectively silence specific neurons in neural circuits (e.g., Koide et al., 2009). Viral transfection and transgenesis have been used as two alternative ways to restrict the expression of the abovementioned reporters and manipulators of neural activity to specific components of the neural networks (Zhu et al., 2009). In particular the Gal-UAS binary transgenic system has been used successfully to specify genetically targeted cell populations and to relate them to specific behaviors, even in adults (e.g., Agetsuma et al., 2010; Okamoto et al., 2012; Muto et al., 2013).

In contrast to the optogenetics toolbox available to study brain function in larval zebrafish, the available tools for adults are far more limited. With the ossification of the skull during development the efficacy of optogenetic techniques decreases and at most they can still be used *in vivo* in the juvenile phase. On the other hand, the repertoire of social behavior is very limited in larvae, whose ethogram is limited to locomotor action patterns involved in swimming and in prey capture (Budick and O'Malley, 2000). Thus, a major challenge for future research on zebrafish social neuroscience is to try to match in development the efficient use of optogenetic tools with the availability of relevant behavior. For doing this the period during which optogenetic tools can be efficiently used will have to be moved forward in development on one hand, and on the other a detailed characterization of the ontogeny of the cognitive abilities underlying social skills is needed in order to identify how early different cognitive abilities can be successfully studied in zebrafish. Whenever the use of the zebrafish optogenetic toolbox becomes available to the study of social abilities, it will offer an unprecedented opportunity to characterize the neural networks underlying social cognitive modules, and to experimentally manipulate particular nodes of the network and infer their potential role on domain-specific modules on a vertebrate model. Until then mapping of the neural activity that underlies cognitive processes in adult zebrafish is still recurring to the expression of immediate early genes as markers of neural activity (e.g., Lau et al., 2011).

PROSPECTS

The field of social neuroscience has emerged in the past two decades as a vibrant and very successful branch of twenty-first century neuroscience, and understanding the relationship between social cognition and the social brain became a hot topic. However, different research traditions coexist within the field with parallel research programs. Researchers from a more Biomedical or Human Psychology background have been mainly focused on human social behavior and on translational research (e.g., Cole et al., 2007; Norman et al., 2012). Primatologists and comparative psychologists have focused on testing the occurrence of "uniquely human" cognitive abilities (e.g., theory of mind, deception, cooperation) in a small subset of "cognitively complex" animals such as primates, dolphins, and more recently corvids and elephants (Connor, 2007; Byrne and Bates, 2009, 2010; Bugnyar, 2011). Finally, behavioral ecologists and neuroethologists focus their research on understanding the functional value and the underlying neural mechanisms of social cognitive skills in a wide range of "simple-minded" animals (e.g., insects, fish), that are seen as adaptive traits that help survival and successful breeding (Bshary et al., 2002; Chittka and Niven, 2009; Bshary, 2011; Chittka and Skorupski, 2011; Taborsky and Oliveira, 2012). In recent years significant efforts to integrate these different research streams have been made, namely through the organization of thematic discussions and meetings. Although challenging due to the multitude of concepts, methodologies, and conflicting points of view (e.g., associative vs. cognitive explanations of animal behavior), an integration of these traditions would be a major breakthrough for the understanding of the basic proximate and ultimate mechanisms of social cognition and behavior. The present paper was written in that spirit and would finish by identifying some outstanding questions and future challenges in the field that would benefit from an integrated approach and that the adoption of the conceptual framework proposed here will hopefully help to address:

(1) The creation of a common cognitive lexicon and taxonomy so that clear concepts are shared – the occurrence of complex social behaviors does not necessarily request complex cognitive abilities; therefore functionally similar cognitive abilities that rely on different underlying mechanisms should be recognized (e.g., transitive inference and transitive inference-like abilities).

(2) The modularity of social cognition – experimental approaches are needed to clarify the conflicting results between intra- and inter-specific analyses of social cognitive modularity. Group living species whose social behavior can be easily recreated in captivity, with relatively short inter-generation times (when compared to the 6 weeks of the mice that is the standard model

for behavioral genetics) and easy to breed in the lab, can be successfully used in the future to address this question using experimental evolution paradigms, as suggested by a recent study on artificial selection for larger brains in guppies (*Poecilia reticulata*) that had an impact on cognitive skills within two generations (Kotrschal et al., 2013).

(3) The distributed nature of information processing in neural networks should be taken into account when trying to map cognitive processes onto brain activity; therefore comparative analyses should move beyond the comparison of brain sizes and focus on inter-specific convergence/divergence in functional connectivity in the social decision making neural network.

In answering all these questions I foresee a relevant role for species that offer the possibility to integrate imaging of brain activity with relevant behavioral tasks, as is the case of zebrafish.

ACKNOWLEDGMENTS

The writing of this paper was supported by the research grant PTDC/PSI-PCO/118776/2010 from Fundação para a Ciência e a Tecnologia (FCT, Portugal) and by the European Union Framework Program 7 project COPEWELL (# 265957). Rui F. Oliveira is a member of the FCT Eco-Ethology R&D Unit (PEst-OE/MAR/UI0331/2011). I thank Jim Goodson for giving permission to use the songbird pictures presented in **Figure 2** (photo credits: violet-eared waxbill by D. Swanepoel, Angolan waxbill by C. Sekercioglu, and zebra finch by J. Ownby).

REFERENCES

Adolphs, R. (2009). The social brain: neural basis of social knowledge. *Annu. Rev. Psychol.* 60, 693–716. doi: 10.1146/annurev.psych.60.110707.163514

Adolphs, R. (2010). Conceptual challenges and directions for social neuroscience. *Neuron* 65, 752–767. doi: 10.1016/j.neuron.2010.03.006

Agetsuma, M., Aizawa, H., Aoki, T., Nakayama, R., Takahoko, M., Goto, M., et al. (2010). The habenula is crucial for experience-dependent modification of fear responses in zebrafish. *Nat. Neurosci.* 13, 1354–1356. doi: 10.1038/nn.2654

Ahrens, M. B., Li, J. M., Orger, M. B., Robson, D. N., Schier, A. F., Engert, F., et al. (2012). Brain-wide neuronal dynamics during motor adaptation in zebrafish. *Nature* 485, 471–477. doi: 10.1038/nature11057

Al-Imari, L., and Gerlai, R. (2008). Sight of conspecifics as reward in associative learning in zebrafish (*Danio rerio*). *Behav. Brain Res.* 189, 216–219. doi: 10.1016/j.bbr.2007.12.007

Allen, C. (2006). "Transitive inference in animals: reasoning or conditioned associations," in *Rational Animals*, eds S. Hurley and M. Nudds (Oxford: Oxford University Press), 175–185.

Arganda, S., Perez-Escudero, A., and de Polavieja, G. G. (2012). A common rule for decision-making in animal collectives across species. *Proc. Natl. Acad. Sci. U.S.A.* 109, 20508–20513. doi: 10.1073/pnas.1210664109

Arrenberg, A. B., Del Bene, F., and Baier, H. (2009). Optical control of zebrafish behavior with halorhodopsin. *Proc. Natl. Acad. Sci. U.S.A.* 106, 17968–17973. doi: 10.1073/pnas.0906252106

Baier, H., and Scott, E. K. (2009). Genetic and optical targeting of neural circuits and behavior – zebrafish in the spotlight. *Curr. Opin. Neurobiol.* 19, 553–560. doi: 10.1016/j.conb.2009.08.001

Barata, E. N., Hubbard, P. C., Almeida, O. G., Miranda, A., and Canário, A. V. M. (2007). Male urine signals social rank in the Mozambique tilapia (*Oreochromis mossambicus*). *BMC Biol.* 5:54. doi: 10.1186/1741-7007-5-54

Barnard, C., and Burk, T. (1979). Dominance hierarchies and the evolution of "individual recognition". *J. Theor. Biol.* 81, 65–73. doi: 10.1016/0022-5193(79)90081-X

Barrett, L., Henzi, P., and Rendall, D. (2007). Social brains, simple minds: does social complexity really require cognitive complexity? *Philos. Trans. R. Soc. Lond. B* 362, 561–575. doi: 10.1098/rstb.2006.1995

Barton, R. A. (1996). Neocortex size and behavioural ecology in primates. *Proc. R. Soc. B* 263, 173–177. doi: 10.1098/rspb.1996.0028

Bode, N. W., Wood, A. J., and Franks, D. W. (2011). Social networks and models for collective motion in animals. *Behav. Ecol. Sociobiol.* 65, 117–130. doi: 10.1007/s00265-010-1111-0

Bond, A. B., Kamil, A. C., and Balda, R. P. (2003). Social complexity and transitive inference in corvids. *Anim. Behav.* 65, 479–487. doi: 10.1006/anbe.2003.2101

Braida, D., Donzelli, A., Martucci, R., Capurro, V., Busnelli, M., Chini, B., et al. (2012). Neurohypophyseal hormones manipulation modulate social and anxiety-related behavior in zebrafish. *Psychopharmacology (Berl.)* 220, 319–330. doi: 10.1007/s00213-011-2482-2

Bshary, R. (2011). "Machiavellian intelligence in fishes," in *Fish Cognition and Behavior*, eds C. Brown, K. Laland, and J. Krause (Oxford: Blackwell), 277–297.

Bshary, R., Wickler, W., and Fricke, H. (2002). Fish cognition: a primate's eye view. *Anim. Cogn.* 5, 1–13. doi: 10.1007/s10071-001-0116-5

Budick, S. A., and O'Malley, D. M. (2000). Locomotor repertoire of the larval zebrafish: swimming, turning and prey capture. *J. Exp. Biol.* 203, 2565–2579.

Bugnyar, T. (2011). Knower–guesser differentiation in ravens: others' viewpoints matter. *Proc. R. Soc. B* 278, 634–640. doi: 10.1098/rspb.2010.1514

Burish, M. J., Kueh, H. Y., and Wang, S. S. (2004). Brain architecture and social complexity in modern and ancient birds. *Brain Behav. Evol.* 63, 107–124. doi: 10.1159/000075674

Burke, C. J., Tobler, P. N., Baddeley, M., and Schultz, W. (2010). Neural mechanisms of observational learning. *Proc. Natl. Acad. Sci. U.S.A.* 107, 14431–14436. doi: 10.1073/pnas.1003111107

Burns, J. G., Foucaud, J., and Mery, F. (2011). Costs of memory: lessons from 'mini' brains. *Proc. R. Soc. B* 278, 923–929. doi: 10.1098/rspb.2010.2488

Buske, C., and Gerlai, R. (2011). Shoaling develops with age in zebrafish (*Danio rerio*). *Prog. Neuropsychopharmacol. Biol. Psychiatry* 35, 1409–1415. doi: 10.1016/j.pnpbp.2010.09.003

Buske, C., and Gerlai, R. (2012). Maturation of shoaling behavior is accompanied by changes in the dopaminergic and serotoninergic systems in zebrafish. *Dev. Psychobiol.* 54, 28–35. doi: 10.1002/dev.20571

Byrne, R. W., and Bates, L. A. (2006). Why are animals cognitive? *Curr. Biol.* 16, R445–R448. doi: 10.1016/j.cub.2006.05.040

Byrne, R. W., and Bates, L. A. (2009). Elephant cognition in primate perspective. *Comp. Cog. Behav. Rev.* 4, 1–15. doi: 10.3819/ccbr.2009.40009

Byrne, R. W., and Bates, L. A. (2010). Primate social cognition: uniquely primate, uniquely social, or just unique? *Neuron* 65, 815–830. doi: 10.1016/j.neuron.2010.03.010

Byrne, R. W., and Corp, N. (2004). Neocortex size predicts deception rate in primates. *Proc. R. Soc. B* 271, 1693–1699. doi: 10.1098/rspb.2004.2780

Cacioppo, J. T., and Decety, J. (2011). Social neuroscience: challenges and opportunities in the study of complex behavior. *Ann. N. Y. Acad. Sci.* 1224, 162–173. doi: 10.1111/j.1749-6632.2010.05858.x

Chittka, L., and Niven, J. (2009). Are bigger brains better? *Curr. Biol.* 19, R995–R1008. doi: 10.1016/j.cub.2009.08.023

Chittka, L., and Skorupski, P. (2011). Information processing in miniature brains. *Proc R. Soc. B* 278, 885–888. doi: 10.1098/rspb.2010.2699

Cole, S. W., Hawkley, L. C., Arevalo, J. M., Sung, C. Y., Rose, R. M., and Cacioppo, J. T. (2007). Social regulation of gene expression in human leukocytes. *Genome Biol.* 8, R189. doi: 10.1186/gb-2007-8-9-r189

Connor, R. C. (2007). Dolphin social intelligence: complex alliance relationships in bottlenose dolphins and a consideration of selective environments for extreme brain size evolution in mammals. *Philos. Trans. R. Soc. Lond. B* 362, 587–602. doi: 10.1098/rstb.2006.1997

Couzin, I. D. (2009). Collective cognition in animal groups. *Trends Cogn. Sci.* 13, 36–43. doi: 10.1016/j.tics.2008.10.002

Delaney, M., Follet, C., Ryan, N., Hanney, N., Lusk-Yablick, J., and Gerlach, G. (2002). Social interaction and distribution of female zebrafish (*Danio rerio*) in a large aquarium. *Biol.*

Bull. 203, 240–241. doi: 10.2307/1543418

De Lillo, C., Floreano, D., and Antinucci, F. (2001). Transitive choices by a simple, fully connected, backpropagation neural network: implications for the comparative study of transitive inference. *Anim. Cogn.* 4, 61–68. doi: 10.1007/s100710100092

Donaldson, Z. R., and Young, L. J. (2008). Oxytocin, vasopressin, and the neurogenetics of sociality. *Science* 322, 900–904. doi: 10.1126/science.1158668

Douglass, A. D., Kraves, S., Deisseroth, K., Schier, A. F., and Engert, F. (2008). Escape behavior elicited by single, channelrhodopsin-2-evoked spikes in zebrafish somatosensory neurons. *Curr. Biol.* 18, 1133–1137. doi: 10.1016/j.cub.2008.06.077

Doutrelant, C., Mcgregor, P. K., and Oliveira, R. F. (2001). The effect of an audience on intrasexual communication in male Siamese fighting fish, *Betta splendens*. *Behav. Ecol.* 12, 283–286. doi: 10.1093/beheco/12.3.283

Døving, K. B., and Trotier, D. (1998). Structure and function of the vomeronasal organ. *J. Exp. Biol.* 201, 2913–2925.

Dukas, R. (2004). Evolutionary biology of animal cognition. *Ann. Rev. Ecol. Evol. Syst.* 35, 347–374. doi: 10.1146/annurev.ecolsys.35.112202.130152

Dunbar, R. I., and Shultz, S. (2007). Evolution in the social brain. *Science* 317, 1344–1347. doi: 10.1126/science.1145463

Dunbar, R. I. M. (1992). Neocortex size as a constraint on group size in primates. *J. Hum. Evol.* 22, 469–493. doi: 10.1016/0047-2484(92)90081-J

Dunbar, R. I. M. (1998). The social brain hypothesis. *Evol. Anthropol.* 6, 178–190. doi: 10.1002/(SICI)1520-6505(1998)6:5

Egger, B., Obermuller, B., Phiri, H., Sturmbauer, C., and Sefc, K. M. (2006). Monogamy in the maternally mouthbrooding Lake Tanganyika cichlid fish *Tropheus moorii*. *Proc. R. Soc. B* 273, 1797–1802. doi: 10.1098/rspb.2006.3504

Emery, N. J., Seed, A. M., Von Bayern, A. M., and Clayton, N. S. (2007). Cognitive adaptations of social bonding in birds. *Philos. Trans. R. Soc. Lond. B* 362, 489–505. doi: 10.1098/rstb.2006.1991

Engeszer, R. E., Barbiano, L. A., Ryan, M. J., and Parichy, D. M. (2007). Timing and plasticity of shoaling behaviour in the zebrafish, *Danio rerio*. *Anim. Behav.* 74, 1269–1275. doi: 10.1016/j.anbehav.2007.01.032

Engeszer, R. E., Ryan, M. J., and Parichy, D. M. (2004). Learned social preference in zebrafish. *Curr. Biol.* 14, 881–884. doi: 10.1016/j.cub.2004.04.042

Fagundes, T., Goncalves, D. M., and Oliveira, R. F. (2007). Female mate choice and mate search tactics in a sex role reversed population of the peacock blenny *Salaria pavo* (Risso, 1810). *J. Fish Biol.* 71, 77–89. doi: 10.1111/j.1095-8649.2007.01466.x

Fernald, R. D. (2012). Social control of the brain. *Annu. Rev. Neurosci.* 35, 133–151. doi: 10.1146/annurev-neuro-062111-150520

Galef, B. G., and Laland, K. N. (2005). Social learning in animals: empirical studies and theoretical models. *Bioscience* 55, 489–499. doi: 10.1641/0006-3568(2005)055[0489:SLIAES]2.0.CO;2

Galhardo, L., Vital, J., and Oliveira, R. F. (2011). The role of predictability in the stress response of a cichlid fish. *Physiol. Behav.* 102, 367–372. doi: 10.1016/j.physbeh.2010.11.035

Gerlach, G., Hodgins-Davis, A., Avolio, C., and Schunter, C. (2008). Kin recognition in zebrafish: a 24-hour window for olfactory imprinting. *Proc. R. Soc. B* 275, 2165–2170. doi: 10.1098/rspb.2008.0647

Gerlach, G., and Lysiak, N. (2006). Kin recognition and inbreeding avoidance in zebrafish, *Danio rerio*, is based on phenotype matching. *Anim. Behav.* 71, 1371–1377. doi: 10.1016/j.anbehav.2005.10.010

Gerlai, R. (2011). "Chapter 12 – Associative learning in zebrafish (*Danio rerio*)," in *Methods Cell Biology*, eds M. W. H. William Detrich and I. Z. Leonard (USA: Academic Press), 249–270.

Gleason, P. E., Weber, P. G., and Weber, S. P. (1977). Effect of group size on avoidance learning in zebra fish, *Brachydanio rerio* (Pisces: Cyprinidae). *Anim. Learn. Behav.* 5, 213–216. doi: 10.3758/BF03214081

Godwin, J. (2010). Neuroendocrinology of sexual plasticity in teleost fishes. *Front. Neuroendocrinol.* 31:203–216. doi: 10.1016/j.yfrne.2010.02.002

Gonzalez-Voyer, A., Winberg, S., and Kolm, N. (2009). Social fishes and single mothers: brain evolution in African cichlids. *Proc. R. Soc. B* 276, 161–167. doi: 10.1098/rspb.2008.0979

Goodson, J. L. (2005). The vertebrate social behavior network: evolutionary themes and variations. *Horm. Behav.* 48, 11–22. doi: 10.1016/j.yhbeh.2005.02.003

Goodson, J. L., Evans, A. K., Lindberg, L., and Allen, C. D. (2005). Neuroevolutionary patterning of sociality. *Proc. R. Soc. B* 272, 227–235. doi: 10.1098/rspb.2004.2892

Goodson, J. L., and Kabelik, D. (2009). Dynamic limbic networks and social diversity in vertebrates: from neural context to neuromodulatory patterning. *Front. Neuroendocrinol.* 30:429–441. doi: 10.1016/j.yfrne.2009.05.007

Grant, J. W. A., and Kramer, D. L. (1992). Temporal clumping of food arrival reduces its monopolization and defence by zebrafish, Brachydanio rerio. *Anim. Behav.* 44, 101–110. doi: 10.1016/S0003-3472(05)80759-6

Grosenick, L., Clement, T. S., and Fernald, R. D. (2007). Fish can infer social rank by observation alone. *Nature* 445, 429–432. doi: 10.1038/nature05511

Grutter, A. S., and Bshary, R. (2003). Cleaner wrasse prefer client mucus: support for partner control mechanisms in cleaning interactions. *Proc. Biol. Sci.* 270(Suppl. 2), S242–S244. doi: 10.1098/rsbl.2003.0077

Gumm, J. M., Snekser, J. L., and Iovine, M. K. (2009). Fin-mutant female zebrafish (*Danio rerio*) exhibit differences in association preferences for male fin length. *Behav. Processes* 80, 35–38. doi: 10.1016/j.beproc.2008.09.004

Hall, D., and Suboski, M. D. (1995). Visual and olfactory stimuli in learned release of alarm reactions by zebra danio fish (Brachydanio rerio). *Neurobiol. Learn. Mem.* 63, 229–240. doi: 10.1006/nlme.1995.1027

Hepper, P. G. (1986). Kin recognition: functions and mechanisms. A review. *Biol. Rev.* 61, 63–93. doi: 10.1111/j.1469-185X.1986.tb00427.x

Heyes, C. (1994). Social learning in animals: categories and mechanisms. *Biol. Rev.* 69, 207–231. doi: 10.1111/j.1469-185X.1994.tb01506.x

Heyes, C. (2012a). Simple minds: a qualified defence of associative learning. *Philos. Trans. R. Soc. Lond. B* 367, 2695–2703. doi: 10.1098/rstb.2012.0217

Heyes, C. (2012b). What's social about social learning? *J. Comp. Psychol.* 126, 193–202. doi: 10.1037/a0025180

Jensen, K., Silk, J. B., Andrews, K., Bshary, R., Cheney, D. L., Emery, N., et al. (2011). "Social knowledge," in *Animal Thinking: Contemporary Issues in Comparative Cognition*, eds R. Menzel and J. Fischer (Cambridge, MA: MIT Press), 267–291.

Johnstone, R. A., and Norris, K. (1993). Badges of status and the cost of aggression. *Behav. Ecol. Sociobiol.* 32, 127–134. doi: 10.1007/BF00164045

Kanwisher, N., and Yovel, G. (2006). The fusiform face area: a cortical region specialized for the perception of faces. *Philos. Trans. R. Soc. Lond. B* 361, 2109–2128. doi: 10.1098/rstb.2006.1934

Karnik, I., and Gerlai, R. (2012). Can zebrafish learn spatial tasks? An empirical analysis of place and single CS-US associative learning. *Behav. Brain Res.* 233, 415–421. doi: 10.1016/j.bbr.2012.05.024

Kelley, A. E., and Berridge, K. C. (2002). The neuroscience of natural rewards: relevance to addictive drugs. *J. Neurosci.* 22, 3306–3311.

Kendal, R. L., Coolen, I., and Laland, K. N. (2009). "Adaptive trade-offs in the use of social and personal information," in *Cognitive Ecology II* eds R. Dukas and J.M. Ratcliffe (Chicago: University of Chicago Press), 249–271.

Kendrick, K., and Baldwin, B. (1987). Cells in temporal cortex of conscious sheep can respond preferentially to the sight of faces. *Science* 236, 448. doi: 10.1126/science.3563521

King, A. J., and Cowlishaw, G. (2009). Leaders, followers and group decision-making. *Commun. Integr. Biol.* 2, 147–150.

Kitevski, B., and Pyron, M. (2003). Female zebrafish (*Danio rerio*) do not prefer mutant longfin males. *J. Freshw. Ecol.* 18, 501–502. doi: 10.1080/02705060.2003.9663988

Koide, T., Miyasaka, N., Morimoto, K., Asakawa, K., Urasaki, A., Kawakami, K., et al. (2009). Olfactory neural circuitry for attraction to amino acids revealed by transposon-mediated gene trap approach in zebrafish. *Proc. Natl. Acad. Sci. U.S.A.* 106, 9884–9889. doi: 10.1073/pnas.0900470106

Kotrschal, A., Rogell, B., Bundsen, A., Svensson, B., Zajitschek, S., Brännström, I., et al. (2013). Artificial selection on relative brain size in the guppy reveals costs and benefits of evolving a larger brain. *Curr. Biol.* 23, 168–171. doi: 10.1016/j.cub.2012.11.058

Krebs, H. A. (1975). The august Krogh principle:"for many problems there is an animal on which it can be most conveniently studied". *J. Exp. Zool.* 194, 221–226. doi: 10.1002/jez.1401940115

Kumaran, D., Melo, H. L., and Duzel, E. (2012). The emergence

and representation of knowledge about social and nonsocial hierarchies. *Neuron* 76, 653–666. doi: 10.1016/j.neuron.2012.09.035

Lau, B. Y., Mathur, P., Gould, G. G., and Guo, S. (2011). Identification of a brain center whose activity discriminates a choice behavior in zebrafish. *Proc. Natl. Acad. Sci. U.S.A.* 108, 2581–2586. doi: 10.1073/pnas.1018275108

Lihoreau, M., Latty, T., and Chittka, L. (2012). An exploration of the social brain hypothesis in insects. *Front. Physiol.* 3:442. doi: 10.3389/fphys.2012.00442

Lindeyer, C. M., and Reader, S. M. (2010). Social learning of escape routes in zebrafish and the stability of behavioural traditions. *Anim. Behav.* 79, 827–834. doi: 10.1016/j.anbehav.2009.12.024

Lohr, H., Ryu, S., and Driever, W. (2009). Zebrafish diencephalic A11-related dopaminergic neurons share a conserved transcriptional network with neuroendocrine cell lineages. *Development* 136, 1007–1017. doi: 10.1242/dev.033878

Machado, H. E., Pollen, A. A., Hofmann, H. A., and Renn, S. C. (2009). Interspecific profiling of gene expression informed by comparative genomic hybridization: a review and a novel approach in African cichlid fishes. *Integr. Comp. Biol.* 49, 644–659. doi: 10.1093/icb/icp080

MacLean, E. L., Matthews, L. J., Hare, B. A., Nunn, C. L., Anderson, R. C., Aureli, F., et al. (2012). How does cognition evolve? Phylogenetic comparative psychology. *Anim. Cogn.* 15, 223–238. doi: 10.1007/s10071-011-0448-8

MacLean, E. L., Merritt, D. J., and Brannon, E. M. (2008). Social complexity predicts transitive reasoning in prosimian primates. *Anim. Behav.* 76, 479–486. doi: 10.1016/j.anbehav.2008.01.025

Maruska, K. P., Zhang, A., Neboori, A., and Fernald, R. D. (2013). Social opportunity causes rapid transcriptional changes in the social behaviour network of the brain in an African cichlid fish. *J. Neuroendocrinol.* 25, 145–157. doi: 10.1111/j.1365-2826.2012.02382.x

Matos, R. J., and Schlupp, I. (2005). "Performing in front of an audience: signalers and the social environment," in *Animal Communication Networks*, ed. P. K. McGregor (Cambridge: Cambrige University Press), 63–83.

McCann, L. I., and Carlson, C. C. (1982). Effect of cross-rearing on species identification in zebra fish and pearl danios. *Dev. Psychobiol.* 15, 71–74. doi: 10.1002/dev.420150110

McCann, L. I., and Matthews, J. J. (1974). The effects of lifelong isolation on species identification in zebra fish (Brachydanio rerio). *Dev. Psychobiol.* 7, 159–163. doi: 10.1002/dev.420070209

McGregor, P. K., and Peake, T. M. (2000). Communication networks: social environments for receiving and signalling behaviour. *Acta Ethol.* 2, 71–81. doi: 10.1007/s10211000015

McIntosh, A. (2000). Towards a network theory of cognition. *Neural Netw.* 13, 861–870. doi: 10.1016/S0893-6080(00)00059-9

Mendl, M., Burman, O. H., and Paul, E. S. (2010). An integrative and functional framework for the study of animal emotion and mood. *Proc. R. Soc. B* 277, 2895–2904. doi: 10.1098/rspb.2010.0303

Menzel, R., and Giurfa, M. (2001). Cognitive architecture of a mini-brain: the honeybee. *Trends Cogn. Sci.* 5, 62–71. doi: 10.1016/S1364-6613(00)01601-6

Mery, F. (2013). Natural variation in learning and memory. *Curr. Opin. Neurobiol.* 23, 52–56. doi: 10.1016/j.conb.2012.09.001

Miller, N., and Gerlai, R. (2007). Quantification of shoaling behaviour in zebrafish (*Danio rerio*). *Behav. Brain Res.* 184, 157–166. doi: 10.1016/j.bbr.2007.07.007

Miller, N., and Gerlai, R. (2008). Oscillations in shoal cohesion in zebrafish (*Danio rerio*). *Behav. Brain Res.* 193, 148–151. doi: 10.1016/j.bbr.2008.05.004

Miller, N., and Gerlai, R. (2011). Shoaling in zebrafish: what we don't know. *Rev. Neurosci.* 22, 17–25. doi: 10.1515/RNS.2011.004

Miller, N., and Gerlai, R. (2012). From schooling to shoaling: patterns of collective motion in zebrafish (*Danio rerio*). *PLoS ONE* 7:e48865. doi: 10.1371/journal.pone.0048865

Muhlhoff, N., Stevens, J. R., and Reader, S. M. (2011). Spatial discounting of food and social rewards in guppies (*Poecilia reticulata*). *Front. Psychol.* 2:68. doi: 10.3389/fpsyg.2011.00068

Muto, A., and Kawakami, K. (2011). Imaging functional neural circuits in zebrafish with a new GCaMP and the Gal4FF-UAS system. *Commun. Integr. Biol.* 4, 566–568. doi: 10.4161/cib.4.5.15848

Muto, A., Ohkura, M., Abe, G., Nakai, J., and Kawakami, K. (2013). Real-time visualization of neuronal activity during perception. *Curr. Biol.* doi: 10.1016/j.cub.2012.12.040 [Epub ahead of print].

Newman, S. W. (1999). The medial extended amygdala in male reproductive behavior a node in the mammalian social behavior network. *Ann. N. Y. Acad. Sci.* 877, 242–257. doi: 10.1111/j.1749-6632.1999.tb09271.x

Norman, G. J., Hawkley, L. C., Cole, S. W., Berntson, G. G., and Cacioppo, J. T. (2012). Social neuroscience: the social brain, oxytocin, and health. *Soc. Neurosci.* 7, 18–29. doi: 10.1080/17470919.2011.568702

O'Connell, L. A., and Hofmann, H. A. (2011). The vertebrate mesolimbic reward system and social behavior network: a comparative synthesis. *J. Comp. Neurol.* 519, 3599–3639. doi: 10.1002/cne.22735

O'Connell, L. A., and Hofmann, H. A. (2012). Evolution of a vertebrate social decision-making network. *Science* 336, 1154–1157. doi: 10.1126/science.1218889

Okamoto, H., Agetsuma, M., and Aizawa, H. (2012). Genetic dissection of the zebrafish habenula, a possible switching board for selection of behavioral strategy to cope with fear and anxiety. *Dev. Neurobiol.* 72, 386–394. doi: 10.1002/dneu.20913

Oliveira, R. F. (2009). Social behavior in context: hormonal modulation of behavioral plasticity and social competence. *Integr. Comp. Biol.* 49, 423–440. doi: 10.1093/icb/icp055

Oliveira, R. F. (2012). Social plasticity in fish: integrating mechanisms and function. *J. Fish Biol.* 81, 2127–2150. doi: 10.1111/j.1095-8649.2012.03477.x

Oliveira, R. F., Carneiro, L. A., and Canario, A. V. (2005). No hormonal response in tied fights. *Nature* 437, 207–208. doi: 10.1038/437207a

Oliveira, R. F., Mcgregor, P. K., and Latruffe, C. (1998). Know thine enemy: fighting fish gather information from observing conspecific interactions. *Proc. R. Soc. B* 265, 1045–1049. doi: 10.1098/rspb.1998.0397

Oliveira, R. F., Silva, J. F., and Simoes, J. M. (2011). Fighting zebrafish: characterization of aggressive behavior and winner-loser effects. *Zebrafish* 8, 73–81. doi: 10.1089/zeb.2011.0690

Pagel, M., and Dawkins, M. (1997). Peck orders and group size in laying hens: futures contracts' for non-aggression. *Behav. Processes* 40, 13–25. doi: 10.1016/S0376-6357(96)00761-9

Parker, M. O., Gaviria, J., Haigh, A., Millington, M. E., Brown, V. J., Combe, F. J., et al. (2012). Discrimination reversal and attentional sets in zebrafish (*Danio rerio*). *Behav. Brain Res.* 232, 264–268. doi: 10.1016/j.bbr.2012.04.035

Parrish, J. K., and Turchin, P. (1997). "Individual decisions, traffic rules, and emergent pattern in schooling fish," in *Animal Groups in Three Dimensions*, eds J. K. Parrish and W. M. Hamner (Cambridge: Cambridge University Press), 126–142.

Parrish, J. K., and Viscido, S. V. (2005). "Traffic rules of fish schools: a review of agent-based approaches," in *Self-Organisation and the Evolution of Social Behaviour*, eds C. K. Hemelrijk (Cambridge, UK: Cambridge University Press), 81–107.

Paul, E. S., Harding, E. J., and Mendl, M. (2005). Measuring emotional processes in animals: the utility of a cognitive approach. *Neurosci. Biobehav. Rev.* 29, 469–491. doi: 10.1016/j.neubiorev.2005.01.002

Paull, G. C., Filby, A. L., Giddins, H. G., Coe, T. S., Hamilton, P. B., and Tyler, C. R. (2010). Dominance hierarchies in zebrafish (*Danio rerio*) and their relationship with reproductive success. *Zebrafish* 7, 109–117. doi: 10.1089/zeb.2009.0618

Paz-Y-Miño, C. G., Bond, A. B., Kamil, A. C., and Balda, R. P. (2004). Pinyon jays use transitive inference to predict social dominance. *Nature* 430, 778–781. doi: 10.1038/nature02723

Peake, T. M. (2005). "Eavesdropping in communication networks. Animal communication networks," in *Animal Communication Networks*, ed. P. K. McGregor (Cambridge: Cambrige University Press), 13–37.

Penn, D. C., and Povinelli, D. J. (2007). On the lack of evidence that non-human animals possess anything remotely resembling a 'theory of mind'. *Philos. Trans. R. Soc. Lond. B* 362, 731–744. doi: 10.1098/rstb.2006.2023

Perez-Barberia, F. J., Shultz, S., and Dunbar, R. I. (2007). Evidence for coevolution of sociality and relative brain size in three orders of mammals. *Evolution* 61,

2811–2821. doi: 10.1111/j.1558-5646.2007.00229.x

Pinto, A., Oates, J., Grutter, A., and Bshary, R. (2011). Cleaner wrasses *Labroides dimidiatus* are more cooperative in the presence of an audience. *Curr. Biol.* 21, 1140–1144. doi: 10.1016/j.cub.2011.05.021

Pitcher, T. J., Magurran, A. E., and Allen, J. R. (1983). Shifts of behaviour with shoal size in cyprinids. *Proc. Br. Freshw. Fish Conf.* 3, 220–228. doi: 10.1371/journal.pone.0032411

Pitcher, T. J., and Parrish, J. K. (1993). "Functions of shoaling behavior in teleosts," in *Behaviour of Teleost Fishes*, ed. T. J. Pitcher (New York: Chapman & Hall), 363–440. doi: 10.1007/978-94-011-1578-0_12

Pollen, A. A., Dobberfuhl, A. P., Scace, J., Igulu, M. M., Renn, S. C., Shumway, C. A., et al. (2007). Environmental complexity and social organization sculpt the brain in Lake Tanganyikan cichlid fish. *Brain Behav. Evol.* 70, 21–39. doi: 10.1159/000101067

Portugues, R., Severi, K. E., Wyart, C., and Ahrens, M. B. (2013). Optogenetics in a transparent animal: circuit function in the larval zebrafish. *Curr. Opin. Neurobiol.* 23, 119–126. doi: 10.1016/j.conb.2012.11.001

Premack, D., and Woodruff, G. (1978). Does the chimpanzee have a theory of mind? *Behav. Brain Sci.* 1, 515–526. doi: 10.1017/S0140525X00076512

Pritchard, V. L., Lawrence, J., Butlin, R. K., and Krause, J. (2001). Shoal choice in zebrafish, *Danio rerio*: the influence of shoal size and activity. *Anim. Behav.* 62, 1085–1088. doi: 10.1006/anbe.2001.1858

Pyron, M. (2003). Female preferences and male male interactions in zebrafish (*Danio rerio*). *Can. J. Zool.* 81, 122–125. doi: 10.1139/z02-229

Reader, S. M., and Laland, K. N. (2002). Social intelligence, innovation, and enhanced brain size in primates. *Proc. Natl. Acad. Sci. U.S.A.* 99, 4436–4441. doi: 10.1073/pnas.062041299

Rink, E., and Wullimann, M. F. (2001). The teleostean (zebrafish) dopaminergic system ascending to the subpallium (striatum) is located in the basal diencephalon (posterior tuberculum). *Brain Res.* 889, 316–330. doi: 10.1016/S0006-8993(00)03174-7

Rink, E., and Wullimann, M. F. (2002). Connections of the ventral telencephalon and tyrosine hydroxylase distribution in the zebrafish brain (*Danio rerio*) lead to identification of an ascending dopaminergic system in a teleost. *Brain Res. Bull.* 57, 385–387. doi: 10.1016/S0361-9230(01)00696-7

Ristau, C. A. (1991). *Cognitive Ethology: The Minds of Other Animals: Essays in Honor of Donald R. Griffin.* Hillsdale, NJ: Lawrence Erlbaum Associates.

Ruhl, N., and McRobert, S. (2005). The effect of sex and shoal size on shoaling behaviour in *Danio rerio*. *J. Fish Biol.* 67, 1318–1326. doi: 10.1111/j.0022-1112.2005.00826.x

Ryan, M. J., Akre, K. L., and Kirkpatrick, M. (2007). Mate choice. *Curr. Biol.* 17, R313–316. doi: 10.1016/j.cub.2007.02.002

Saif, M., Chatterjee, D., Buske, C., and Gerlai, R. (2013). Sight of conspecific images induces changes in neurochemistry in zebrafish. *Behav. Brain Res.* doi: 10.1016/j.bbr.2013.01.020 [Epub ahead of print].

Sallet, J., Mars, R. B., Noonan, M. P., Andersson, J. L., O'Reilly, J. X., Jbabdi, S., et al. (2011). Social network size affects neural circuits in macaques. *Science* 334, 697–700. doi: 10.1126/science.1210027

Schultz, W. (2010). Review Dopamine signals for reward value and risk: basic and recent data. *Behav. Brain Funct.* 6, 24. doi: 10.1186/1744-9081-6-24

Shettleworth, S. J. (2001). Animal cognition and animal behaviour. *Anim. Behav.* 61, 277–286. doi: 10.1006/anbe.2000.1606

Shettleworth, S. J. (2010). *Cognition, Evolution and Behavior,* 2nd Edn. New York: Oxford University Press.

Sih, A., Hanser, S. F., and Mchugh, K. A. (2009). Social network theory: new insights and issues for behavioral ecologists. *Behav. Ecol. Sociobiol.* 63, 975–988. doi: 10.1007/s00265-009-0725-6

Simões, J. M., Teles, M. C., Oliveira, R. F., Van Der Linden, A., and Verhoye, M. (2012). A three-dimensional stereotaxic MRI brain atlas of the cichlid fish *Oreochromis mossambicus*. *PLoS ONE* 7:e44086. doi: 10.1371/journal.pone.0044086

Smeets, W. J. A. J., Marin, O., and Gonzalez, A. (2000). Evolution of the basal ganglia: new perspectives through a comparative approach. *J. Anat.* 196, 501–517. doi: 10.1046/j.1469-7580.2000.19640501.x

Snekser, J. L., Mcrobert, S. P., Murphy, C. E., and Clotfelter, E. D. (2006). Aggregation behavior in wildtype and transgenic zebrafish. *Ethology* 112, 181–187. doi: 10.1111/j.1439-0310.2006.01139.x

Speedie, N., and Gerlai, R. (2008). Alarm substance induced behavioral responses in zebrafish (*Danio rerio*). *Behav. Brain Res.* 188, 168–177. doi: 10.1016/j.bbr.2007.10.031

Spence, R. (2011). "Zebrafish ecology and behaviour," in *Zebrafish Models in Neurobehavioral Research*, eds A.V. Kalueff and J. M. Cachat (Berlin: Springer Verlag), 1–46. doi: 10.1007/978-1-60761-922-2_1

Spence, R., Gerlach, G., Lawrence, C., and Smith, C. (2008). The behaviour and ecology of the zebrafish, *Danio rerio*. *Biol. Rev.* 83, 13–34. doi: 10.1111/j.1469-185X.2007.00030.x

Spence, R., and Smith, C. (2005). Male territoriality mediates density and sex ratio effects on oviposition in the zebrafish, *Danio rerio*. *Anim. Behav.* 69, 1317–1323. doi: 10.1016/j.anbehav.2004.10.010

Spence, R., and Smith, C. (2006). Mating preference of female zebrafish, *Danio rerio*, in relation to male dominance. *Behav. Ecol.* 17, 779–783. doi: 10.1093/beheco/arl016

Spence, R., and Smith, C. (2007). The role of early learning in determining shoaling preferences based on visual cues in the zebrafish, *Danio rerio*. *Ethology* 113, 62–67. doi: 10.1111/j.1439-0310.2006.01295.x

Sporns, O. (2010). Networks of the brain. Cambridge, MA: MIT Press.

Suboski, M. D., Bain, S., Carty, A. E., Mcquoid, L. M., Seelen, M. I., and Seifert, M. (1990). Alarm reaction in acquisition and social transmission of simulated-predator recognition by zebra danio fish (Brachydanio rerio). *J. Comp. Psychol.* 104, 101–112. doi: 10.1037/0735-7036.104.1.101

Sumpter, D. J. T. (2006). The principles of collective animal behaviour. *Philos. Trans. R. Soc. B* 361, 5–22. doi: 10.1098/rstb.2005.1733

Taborsky, B., and Oliveira, R. F. (2012). Social competence: an evolutionary approach. *Trends Ecol. Evol.* 27, 679–688. doi: 10.1016/j.tree.2012.09.003

Tay, T. L., Ronneberger, O., Ryu, S., Nitschke, R., and Driever, W. (2011). Comprehensive catecholaminergic projectome analysis reveals single-neuron integration of zebrafish ascending and descending dopaminergic systems. *Nat. Commun.* 2, 171. doi: 10.1038/ncomms1171

Tebbich, S., Bshary, R., and Grutter, A. S. (2002). Cleaner fish *Labroides dimidiatus* recognise familiar clients. *Anim. Cogn.* 5, 139–145. doi: 10.1007/s10071-002-0141-z

Thiel, K. J., Okun, A. C., and Neisewander, J. L. (2008). Social reward-conditioned place preference: a model revealing an interaction between cocaine and social context rewards in rats. *Drug Alcohol Depend* 96, 202–212. doi: 10.1016/j.drugalcdep.2008.02.013

Tibbetts, E. A., and Dale, J. (2007). Individual recognition: it is good to be different. *Trends Ecol. Evol.* 22, 529–537. doi: 10.1016/j.tree.2007.09.001

Tsao, D. Y., Freiwald, W. A., Tootell, R. B., and Livingstone, M. S. (2006). A cortical region consisting entirely of face-selective cells. *Science* 311, 670–674. doi: 10.1126/science.1119983

Tsao, D. Y., Schweers, N., Moeller, S., and Freiwald, W. A. (2008). Patches of face-selective cortex in the macaque frontal lobe. *Nat. Neurosci.* 11, 877–879. doi: 10.1038/nn.2158

Ullmann, J. F., Cowin, G., and Collin, S. P. (2010a). Magnetic resonance microscopy of the barramundi (*Lates calcarifer*) brain. *J. Morphol.* 271, 1446–1456. doi: 10.1002/jmor.10887

Ullmann, J. F., Cowin, G., and Collin, S. P. (2010b). Quantitative assessment of brain volumes in fish: comparison of methodologies. *Brain Behav. Evol.* 76, 261–270. doi: 10.1159/000321467

Ullmann, J. F., Cowin, G., Kurniawan, N. D., and Collin, S. P. (2010c). Magnetic resonance histology of the adult zebrafish brain: optimization of fixation and gadolinium contrast enhancement. *NMR Biomed.* 23, 341–346. doi: 10.1002/nbm.1465

Ullmann, J. F., Cowin, G., Kurniawan, N. D., and Collin, S. P. (2010d). A three-dimensional digital atlas of the zebrafish brain. *Neuroimage* 51, 76–82. doi: 10.1016/j.neuroimage.2010.01.086

Viscido, S. V., Parrish, J. K., and Grünbaum, D. (2004). Individual behavior and emergent properties of fish schools: a comparison of observation and theory. *Mar. Ecol. Prog. Ser.* 273, 239–249. doi: 10.3354/meps273239

Vital, C., and Martins, E. P. (2011). Strain differences in zebrafish (*Danio rerio*) social roles and their impact on group task performance. *J. Comp. Psychol.* 125, 278–285. doi: 10.1037/a0023906

Von Fersen, L., Wynne, C., Delius, J. D., and Staddon, J. (1991). Transitive inference formation in pigeons. *J. Exp. Psychol. Anim. Behav. Process* 17, 334–341. doi: 10.1037/0097-7403.17.3.334

Waldman, B. (1982). Quantitative and developmental analysis of the alarm reaction in the zebra Danio Brachydanio rerio. *Copeia* 1982, 1–9.

Wersinger, S. R., Kelliher, K. R., Zufall, F., Lolait, S. J., O'Carroll, A.-M., and Young, W. S. (2004). Social motivation is reduced in vasopressin 1b receptor null mice despite normal performance in an olfactory discrimination task. *Horm. Behav.* 46, 638–645. doi: 10.1016/j.yhbeh.2004.07.004

Whiten, A., and Byrne, R. W. (1988). "The Machiavellian intelligence hypothesis," in *Machiavellian Intelligence*, eds R. W. Byrne and A. Whiten (Oxford: Oxford University Press), 1–9.

Whiten, A., and Byrne, R. W. (1997). *Machiavellian Intelligence II: Extensions and Evaluations.* Cambridge: Cambridge University Press.

Witte, K., and Ryan, M. J. (2002). Mate choice copying in the sailfin molly, *Poecilia latipinna*, in the wild. *Anim. Behav.* 63, 943–949. doi: 10.1006/anbe.2001.1982

Wullimann, M. F., and Mueller, T. (2004). Teleostean and mammalian forebrains contrasted: evidence from genes to behavior. *J. Comp. Neurol.* 478, 427–428.

Wullimann, M. F., Rupp, B., and Reichert, H. (1996). Neuroanatomy of the zebrafish brain: a topological atlas. Basel: Birkhäuser.

Yamamoto, K., and Vernier, P. (2011). The evolution of dopamine systems in chordates. *Front. Neuroanat.* 5:21. doi: 10.3389/fnana.2011.00021

Yang, E. J., and Wilczynski, W. (2007). Social experience organizes parallel networks in sensory and limbic forebrain. *Dev. Neurobiol.* 67, 285–303. doi: 10.1002/dneu.20347

Zhu, P., Narita, Y., Bundschuh, S. T., Fajardo, O., Scharer, Y. P., Chattopadhyaya, B., et al. (2009). Optogenetic dissection of neuronal circuits in zebrafish using viral gene transfer and the tet system. *Front. Neural Circuits* 3:21. doi: 10.3389/neuro.04.021.2009

Zuberbuhler, K., and Byrne, R. W. (2006). Social cognition. *Curr. Biol.* 16, R786–R790. doi: 10.1016/j.cub.2006.08.046

Conflict of Interest Statement: The author declares that the research was conducted in the absence of any commercial or financial relationships that could be construed as a potential conflict of interest.

Received: 22 February 2013; accepted: 22 July 2013; published online: 08 August 2013.

Citation: Oliveira RF (2013) Mind the fish: zebrafish as a model in cognitive social neuroscience. Front. Neural Circuits ***7****:131. doi: 10.3389/fncir.2013.00131*

frontiers in
NEURAL CIRCUITS

HYPOTHESIS AND THEORY ARTICLE
published: 23 April 2013
doi: 10.3389/fncir.2013.00074

Integrating anatomy and function for zebrafish circuit analysis

Aristides B. Arrenberg* and Wolfgang Driever*

Developmental Biology, Institute of Biology I, Faculty of Biology, BIOSS - Centre for Biological Signalling Studies, Albert-Ludwigs-University Freiburg, Freiburg, Germany

Edited by:
Gonzalo G. De Polavieja, Instituto Cajal, Spain

Reviewed by:
Claire Wyart, Brain and Spinal cord Institute, France
Akira Muto, National Institute of Genetics, Japan
Misha B. Ahrens, Howard Hughes Medical Institute, USA

****Correspondence:***
Aristides B. Arrenberg and Wolfgang Driever, Developmental Biology, Institute of Biology 1, Faculty of Biology, BIOSS - Centre for Biological Signalling Studies, Albert-Ludwigs-University Freiburg, Hauptstrasse 1, D-79104 Freiburg, Germany.
e-mail: aristides.arrenberg@biologie.uni-freiburg.de; driever@biologie.uni-freiburg.de

Due to its transparency, virtually every brain structure of the larval zebrafish is accessible to light-based interrogation of circuit function. Advanced stimulation techniques allow the activation of optogenetic actuators at different resolution levels, and genetically encoded calcium indicators report the activity of a large proportion of neurons in the CNS. Large datasets result and need to be analyzed to identify cells that have specific properties—e.g., activity correlation to sensory stimulation or behavior. Advances in three-dimensional (3D) functional mapping in zebrafish are promising; however, the mere coordinates of implicated neurons are not sufficient. To comprehensively understand circuit function, these functional maps need to be placed into the proper context of morphological features and projection patterns, neurotransmitter phenotypes, and key anatomical landmarks. We discuss the prospect of merging functional and anatomical data in an integrated atlas from the perspective of our work on long-range dopaminergic neuromodulation and the oculomotor system. We propose that such a resource would help researchers to surpass current hurdles in circuit analysis to achieve an integrated understanding of anatomy and function.

Keywords: zebrafish model system, optogenetics, neural circuits, calcium imaging, brain anatomy, neuronal types

THE ZEBRAFISH AS A GENETIC MODEL FOR NEURAL SYSTEM AND BEHAVIORAL ANALYSIS

About 30 years after George Streisinger introduced zebrafish as a model system (Streisinger et al., 1981), zebrafish continues to be an attractive animal model. Initially, investigators were fascinated by this small vertebrate because the external development of zebrafish embryos and the favorable husbandry were advantageous for developmental and genetic studies. Over the past two decades, researchers started to increasingly use zebrafish as a model for understanding how neuronal circuits generate behavior, a fundamental goal in neuroscience. Mutagenesis screens revealed genes that are important for proper brain development or required for sensory processing (Brockerhoff et al., 1995; Neuhauss et al., 1999; Muto et al., 2005) or locomotion (Granato et al., 1996). Many of these mutants only affect the sensory or motor periphery and provided little insight into central brain processing. Since gene functions often affect multiple neuronal groups when mutated, mutational dissection of individual contributions to defined circuits is impeded (as discussed in Gahtan and Baier, 2004; McLean and Fetcho, 2008). Therefore, new tools were needed that enable to probe brain function locally after normal development has taken place. Optogenetic tools perfectly fit this purpose and are providing another boost to this already much appreciated animal model.

OPTOGENETIC ACTUATORS

The discovery of light-activated channels and transporters in single-cell organisms (Schobert and Lanyi, 1982; Kalaidzidis et al., 1998; Nagel, 2002, 2003) and their subsequent incorporation into neurons (Zhang et al., 2007; Fenno et al., 2011) established a highly-versatile optogenetic toolbox for conditionally and reversibly manipulating brain activity in zebrafish (Szobota et al., 2007; Douglass et al., 2008; Arrenberg et al., 2009; Wyart et al., 2009; Zhu et al., 2009; reviewed in Baier and Scott, 2009; McLean and Fetcho, 2011). These actuators enable unprecedented spatial and temporal resolution of activity perturbation. For example, Warp et al. (2012) investigated the development of the spinal central pattern generator using these tools. Initially, the cells of the future central pattern generator are sporadically and seemingly randomly active. They then develop into ipsilaterally correlated clusters and eventually form a single ipsilateral network on each side producing the alternating left-right excitation needed during swimming. The authors used brief local halorhodopsin stimulations and concurrent calcium imaging to reveal the development of coupling between the targeted cell and neighboring cells during the period from 18 to 21 h post fertilization. Using chronic halorhodopsin stimulations, the authors furthermore showed that the development of coupled, synchronous activity is dependent on activity. This study exemplifies the power of targeted optogenetic manipulations for answering questions regarding the activity-dependent development of networks.

Apart from genetic targeting of selected cell types, the specificity obtained with optogenetic expression can be improved by limiting the illumination volume in the brain. Several optical stimulation techniques are available and can be chosen

based on the required spatial resolution. Fiber-optic stimulations (Arrenberg et al., 2009) provide a method for low resolution localizing circuit function. Digital micromirror devices (DMDs)—a technology used in video projectors—are an attractive option, because they allow the simultaneous stimulation in any combination of pixels of the photostimulation mask and provide focal stimulation when mounted on a microscope (Wyart et al., 2009; Arrenberg et al., 2010; Blumhagen et al., 2011; Zhu et al., 2012). Such a DMD device can be used to map functions in the focal plane of interest (**Figure 1**). However, a one-photon optical focus generates considerable light excitation in out-of-focus planes, especially when the effective numerical aperture of the objective is small. Ideally, the expression can be genetically restricted to the cells of interest, thus evading problems regarding off-target stimulation. While the local activation of small groups of genetically defined neurons will be sufficient in many experiments, other experiments will require the stimulation of single cells. To accomplish single cell stimulation, more sophisticated photostimulation techniques are likely needed, such as holographic stimulation (Lutz et al., 2008), two-photon stimulation using temporally focused beams (Andrasfalvy et al., 2010; Papagiakoumou et al., 2010; Oron et al., 2012), or quick scanning of the membrane surface of the cell (Rickgauer and Tank, 2009; Zhu et al., 2009).

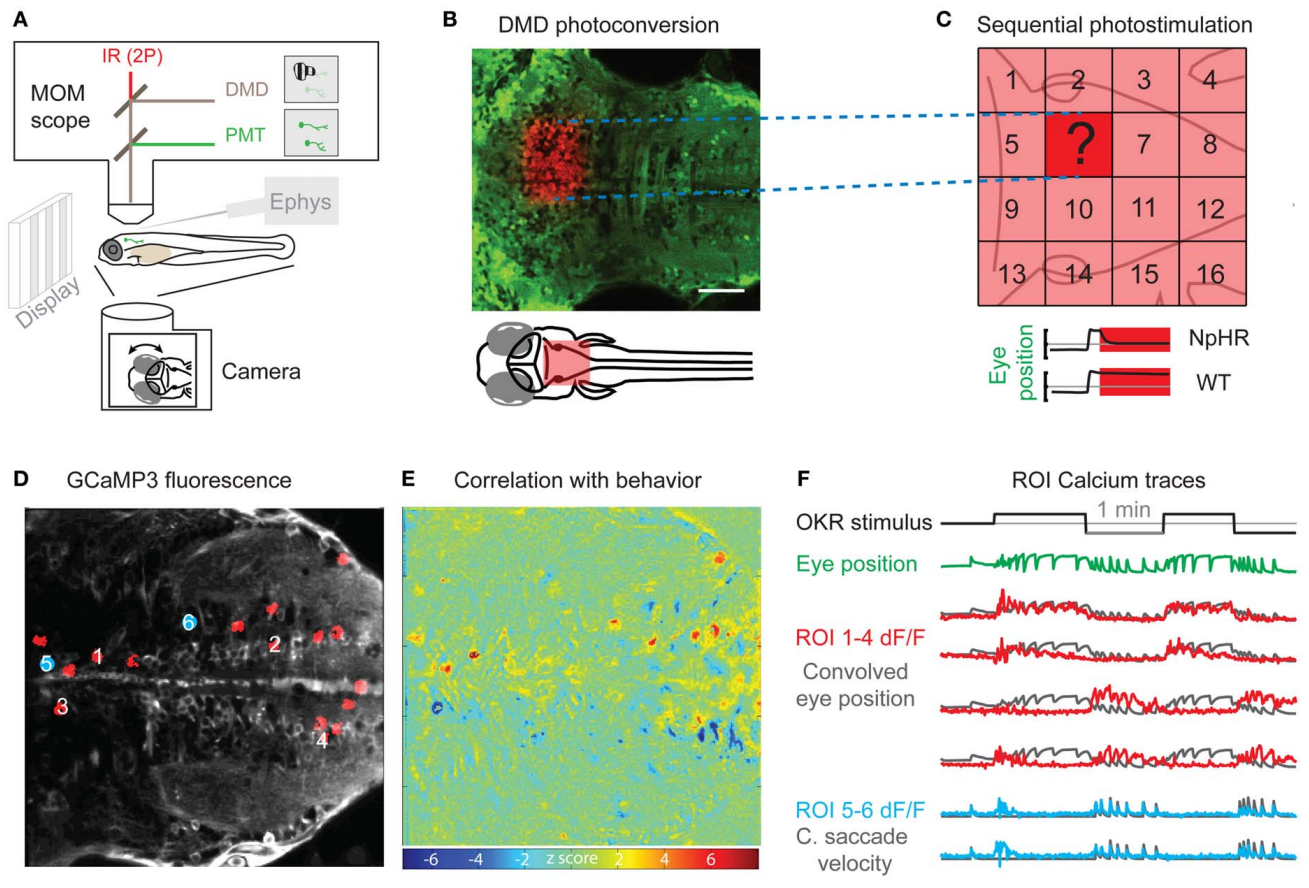

FIGURE 1 | Perturbation and Measurement of brain activity via optogenetics. (A) Scheme of a moveable objective microscope (MOM) that allows two photon (2P) calcium imaging (PMT, photomultiplier tubes) and photostimulation via a digital micro mirror device (DMD). At the same time, the animal can be visually stimulated and eye or tail movements are recorded with a camera. **(B)** A rectangular region of interest was photoconverted with the DMD device in an *Et(E1b:Gal4)s1101t; Tg(UAS:Kaede)s1999t* transgenic animal. **(C)** Schematic for the systematic mapping of circuit function by measuring behavioral performance (e.g., eye position stability) during sequential photostimulation (16 regions shown here) in animals transgenic for optogenetic actuators (e.g., halorhodopsin, NpHR). The question mark illustrates an individual tested region as shown in **(B)**. **(D)** Averaged frame of a calcium imaging time series during visual optokinetic response (OKR) stimulation in an *Et(E1b:Gal4)s1101t; Tg(UAS:GCaMP3)* transgenic 5-day-old animal. Red regions of interest (ROIs) correspond to highly correlated pixels in **(E)**. Blue regions of interest are correlated with quick eye movements. **(E)** A heat map of Z-scores identifies pixels correlated with average eye position. The algorithm is based on Miri et al. (2011b) and provides an unbiased, quick way of correlating pixel time series with any time-varying regressor of interest. The Z-score heat map for correlation with saccadic eye movements [blue positions in **(D)**] is not shown. **(F)** The black line indicates the velocity of the visual stimulus (vertical stripes) and the green line shows the average eye position. The calcium fluorescence $\Delta F/F$ signal of the ROIs 1–4 in **(D)** (red) is plotted over eye position regressor traces (black). ROIs 1 and 2 have a positive correlation with the eye position regressor and ROIs 3 and 4 are anti-correlated with the eye position regressor. The lower two calcium signal traces (blue) correspond to the blue positions in **(D)** and are correlated with the occurrence of quick eye movements (saccades). The black traces show the high-pass filtered eye velocity regressor. Note that all six black regressors were convolved to account for the slow calcium indicator kinetics. Scale bar: 50 μm.

HOLISTIC CALCIUM IMAGING

While optogenetic activation and inhibition experiments directly test the causal link between circuit modules and behavior, these experiments typically require sequential point-by-point testing of brain tissues. In contrast, activity probes such as calcium indicators are complementary tools and enable simultaneous read-out of brain activity from a large number of neurons, thereby accumulating correlative evidence. To optically record neural activity, zebrafish scientists have mainly relied on local injections of synthetic calcium indicator dyes in the past, which - among others - advanced our knowledge about reticulospinal cells (O'Malley et al., 1996; Liu and Fetcho, 1999; Gahtan et al., 2002; Orger et al., 2008), visual circuitry (Niell and Smith, 2005; Sumbre et al., 2008), olfaction (Friedrich and Korsching, 1997), and motor circuitry (Fetcho and O'Malley, 1995). With synthetic organic calcium indicators, only the fraction of cells that took up the injected calcium indicator can be imaged. In contrast, genetically encoded calcium indicators (Grienberger and Konnerth, 2012; Knöpfel, 2012) enable genetic targeting of neurons. When combined with (almost) pan-neuronal promoters, homogeneous expression of genetically encoded calcium indicators throughout the CNS can be achieved and used to study function of whole brain areas in a non-biased way (Niell and Smith, 2005; Aizenberg and Schuman, 2011; Tao et al., 2011; Ahrens et al., 2012). The calcium signal of hundreds of cells can be imaged concurrently and automated algorithms can be applied to calculate the correlation of each pixel in the calcium imaging fluorescence time series with any aspect of the time-varying behaviors or sensory stimuli. Efficient algorithms have been developed (Miri et al., 2011b) and allow for quick identification of correlated pixels (and then neurons) by regressing pixel time series with any regressor of choice (e.g., eye position in **Figure 1**). Since a large number of cells can be imaged concurrently, the small size of the larval brain [roughly $500 \times 500 \times 1000\,\mu m$, 100,000 neurons (Hill et al., 2003)] opens the prospect to sequentially record the activity of all cells in a single animal (here, we refer to this whole brain approach as "holistic"). Using light sheet microscopy with a sCMOS camera, Ahrens and Keller (2013) achieved 1.3 s temporal resolution for recording calcium imaging stacks covering about 90 percent of the 5-day-old larval brain volume at single cell resolution. This work demonstrated that whole brain functional imaging at cellular resolution is well feasible in zebrafish larva.

Whole brain calcium imaging at cellular resolution requires sensitive genetically encoded calcium indicators and homogeneous expression in order to allow activity recording in all neurons of the animal. In a pioneering study, Ahrens et al. (2012) reported on brain-wide activity at cellular resolution during a motor learning paradigm. The authors identified activity that was correlated with a visual stimulus, fictive swimming behavior, or with altered motor performance. This study, which elegantly illustrated the power of holistic calcium recording, also revealed some of its limitations. Due to the relatively low sensitivity of the genetically encoded calcium indicator used, GCaMP2 (Tallini et al., 2006), much of the brain activity was likely missed, and the authors accordingly report that activity could only be detected in about 1% of the cells during the experiments. More recent calcium indicators, like GCaMP5G (Akerboom et al., 2012) already allow to observe activity in a much larger fraction of neurons. In the study by Akerboom et al., GCaMP5G, GCaMP3, and the synthetic indicator OGB-1-AM were compared side by side in a test of visual responsiveness in mouse cortex. While GCaMP5G was twice as good as GCaMP3 (20 vs. 10% of the expressing cells were visually responsive), it still lagged the performance of the synthetic dye OGB-1-AM, for which almost 40% of the cells responded. A low calcium indicator sensitivity also biases toward detection of large calcium events, while low firing rates of responsive cells are likely missed. In the above mentioned light sheet microscopy study, Ahrens and Keller (2013) already used a recent genetically encoded calcium indicator, GCaMP5G, for whole brain imaging, which should allow improved activity detection compared to the previous study with GCaMP2 (Ahrens et al., 2012). However, the fraction of responsive cells was not reported. Genetically encoded activity probes with improved sensitivities and linear dynamic ranges are in demand and will likely be developed in the near future (Akemann et al., 2012; Chen et al., 2012; Muto et al., 2013). In addition, suitable promoters for the homogeneous pan-neuronal expression need to be identified to avoid differences in expression levels (e.g., the HuC/elavl3 promoter induces only very low levels of expression in the diencephalon at 5 dpf). Furthermore, the cytosolic expression of genetically encoded calcium indicators (and their exclusion from the nucleus) results in strong neurite signals, and complicates the analysis of cellular signals. Alternative expression strategies, e.g. using nuclear localization sequences, could facilitate the differentiation between somatic and neurite signals.

While there is still room for improvement of technology, zebrafish larva now provide the opportunity to look at the brain's response in a holistic fashion at cellular resolution, which has not been possible in any vertebrate model organism before. Correlations of activity in distant brain regions could be revealed, that would be very hard to show by electrophysiology or in bigger animals. For example, regarding the dopaminergic system, the long-range neuromodulatory A11 dopaminergic system could be imaged to study the integration of dopaminergic modulation from the telencephalon to the spinal cord (Tay et al., 2011).

BEHAVIOR DURING HOLISTIC IMAGING

While the sensitivity of calcium indicators is limiting on the activity detection side, the behavioral paradigms that can be elicited in an immobilized preparation are crucially limiting the extent to which functional analyses can be performed during whole brain calcium imaging. For circuit neuroscience, the usefulness of zebrafish holistic imaging scales with the number and quality of applicable behavioral or sensory stimulation paradigms. Good candidates for the rapid generation of functional data are neurons that process sensory information, since their activity likely does not rely on proper behavioral performance, and neurons mediating robust reflex behaviors, e.g., the escape response, the optokinetic response, and the optomotor response. Other behaviors might require appropriate sensory feedback during unrestrained swimming, or lengthy experimental protocols. Such behaviors are therefore more difficult to analyze in immobilized fish under a microscope, e.g., prey capture (Bianco et al., 2011),

the diving response during dark photokinesis (Fernandes et al., 2012), or learning paradigms (Aizenberg and Schuman, 2011; Wolman et al., 2011; Valente et al., 2012). Improvements in animal mounting, monitoring, and feedback methods, including closed-loop fictive swimming paradigms (Ahrens et al., 2012), will likely facilitate the development of behavioral paradigms in immobilized preparations.

ANATOMICAL ANNOTATION IN LARVAL ZEBRAFISH

Calcium imaging in larval zebrafish enables the generation of three-dimensional (3D) maps of whole brain activity, similar in anatomical scale to data obtained from functional magnetic resonance imaging (fMRI) in larger animals. However, whole brain calcium imaging in zebrafish has the benefits of direct activity measurement and high (sub-cellular) spatial and temporal resolution. To reveal the cellular identities of the imaged brain volumes, a correct anatomical framework needs to be available. Anatomical atlases and gene expression databases already exist for zebrafish and are listed in **Table 1**, including links and references for the resources mentioned in the following text. Some resources include anatomical annotations in the absence of expression markers (ZFIN anatomy resources, PSU Zebrafish Atlas). Furthermore, detailed anatomical ontologies are curated (ZFIN anatomical ontologies), but their application to larval stages is handicapped by the fact that the ontologies rely on morphologically identifiable structures, which are scarce in the larval zebrafish brain. Therefore, the larval brain is somewhat "under-annotated," which will only improve once gene expression data are integrated with morphology data to define larval brain structures. Other atlas initiatives include expression analysis [ZFIN database; Zebrafish Brain Atlas; hardcopy atlas by Mueller and Wullimann (2005)]. However, the precise anatomical annotation is a current hurdle in zebrafish circuit neuroscience.

Work in rodents allows stereotactic targeting of identified brain nuclei [e.g., hard copy-atlas from Franklin and Paxinos (2012)]. While the transparency of larval zebrafish should facilitate identification of stereotactic landmarks, the small size of larval zebrafish, the non-rigid consistency of the larva, and potential inter-larval shape-differences complicate the development of stereotactic methods. If larval zebrafish had very stereotypic, rigid shapes, three landmarks should suffice to calculate the rotation and translation of the animal and its neural structures with respect to a reference animal. However, such straightforward registration approaches are not precise enough to reliably identify small cell groups. For example, Ahrens et al. (2012) report on a precision of only 25 μm when registering microscopical optical slices to a reference brain using rigid translation.

Table 1 | Selected anatomical resources for the larval and adult zebrafish brain.

Name of resource	Internet address	Developmental stages	Available information	Authors
ZFIN	http://zfin.org/action/anatomy/anatomy-search; http://www.berkeleybop.org/ontologies/zfa.obo	Any	Detailed anatomical ontologies	Zebrafish Anatomical Dictionary Workgroup http://zfin.org/zf_info/anatomy/dict/mem.html
	http://zfin.org/cgi-bin/webdriver?MIval=aa-xpatselect.apg	Any	Expression database linking to gene expression publications	Bradford et al., 2011
	http://zfin.org/zf_info/anatomy/dict/sum.html	1, 2, 3, 5 dpf	Annotated anatomical sections	Workgroup see: http://zfin.org/zf_info/anatomy.html
Zebrafish Atlas	http://zfatlas.psu.edu	2, 3, 4, 5, 6, 7–13, 14–20, 21–29 dpf, and up to 12 months	Annotated anatomical sections; coronal, sagittal, and transversal	Cheng and Copper, 2012 (Jake Gittlen Cancer Research Foundation)
Zebrafish Brain Atlas	http://www.zebrafishbrain.org/	Several	Chapters on different brain regions and systems, making use of transgenic lines	Wilson et al., 2012
Atlas of Early Zebrafish Brain Development	Hardcopy atlas	2, 3, 4, 5 dpf	Neuroanatomical expression atlas	Mueller and Wullimann, 2005
Neuroanatomy of the Zebrafish Brain	Hardcopy atlas	Adult	Neuroanatomical structures	Wullimann et al., 1996
Virtual Brain Explorer for Zebrafish (ViBE-Z)	http://vibez.informatik.uni-freiburg.de	2, 3, 4 dpf	Tool to register 3D datasets to reference brain, small database with aligned gene expression patterns	Ronneberger et al., 2012

Transgenic zebrafish lines expressing fluorescent proteins under the control of specific promoters are frequently used to identify specific neuronal groups or provide additional landmarks. However, only a small number of markers can be used in parallel in any given experiment. In addition, the unavailability of suitable promoters frequently necessitates identification by other means, e.g., based on activity or projection patterns. Therefore, a serial strategy would be beneficial, where gene expression and functional information from different locations in the brain, different times, and different laboratories can be placed and registered to a reference, allowing the community to build a multidimensional brain map. While many functional neuronal entities form tight spatial clusters—e.g., cranial nuclei (Higashijima et al., 2000) and dopaminergic cell groups (Filippi et al., 2010)—other neuronal entities might be less clustered and intermingle with cells having non-related functions—e.g., cells of the neural integrator for horizontal eye movements do not appear to be tightly clustered (Miri et al., 2011a). For larval zebrafish, therefore, the combination of activity imaging data from several specimens will not suffice to identify anatomically distinct nuclei, but generate likelihood clouds positioning circuit activity components in an anatomical framework. Linking such likelihood cloud data to molecular markers from gene expression analysis of transgenic lines may then enable to identify the neuronal populations involved, and also to relate them to late juvenile and adult brain structures.

VIRTUAL THREE-DIMENSIONAL ANATOMICAL FRAMEWORKS

For several animal models, 3D databases have been developed to begin to integrate morphological, gene expression, and functional data. In *C. elegans*, the defined cell lineage provides a framework for such databases. For *Drosophila*, cellular resolution has been achieved for registration of different brains (BrainAligner, Peng et al., 2011), while for mouse and human such databases operate at a more coarse anatomical level (Allen Brain Atlas, http://www.brain-map.org and MGI Mouse Genome Informatics Jackson, http://www.informatics.jax.org, Finger et al., 2011). However, for zebrafish, none of the databases listed in the last paragraph offers a framework in which scientists could use their own expression data and align it to already existing data in a digital atlas.

To address this deficit, our group recently developed the Virtual Brain Explorer for Zebrafish (ViBE-Z), a microscopy and computational framework to align expression pattern data to a reference brain (Ronneberger et al., 2012; "http://vibez.informatik.uni-freiburg.de"). ViBE-Z detects characteristic landmarks in the fish embryo and early larva based on fluorescent stain of all cell nuclei. Landmarks and subsequent fine elastic registration are used to register experimental data to a reference brain, thereby accounting for inter-fish differences resulting from variations in brain morphology or staining artifacts. The atlas has a precision of about 2 μm, so that expression comparisons can be performed at near-cellular resolution (**Figure 2**). ViBE-Z facilitates the characterization of neuronal identities and subtypes, and also helps to postulate potential regulatory mechanisms based on genetic intersectional strategies. Although ViBE-Z can serve as a tool to define likelihood clouds for expression domains, it cannot predict expression in individual neurons across different brains since the positions of individual defined neurons are variable. It also does not—as of yet—provide a means to integrate *in vivo* functional data, and thus contribute to understand the circuits that certain brain volumes are involved in. Furthermore, Vibe-Z only includes the positions of somata and does not take into account the position and targets of neuronal processes.

INTEGRATION OF DIVERSE DATA TYPES IN A VIRTUAL FRAMEWORK

We propose that a framework like the ViBE-Z atlas could be used to include maps of projection patterns, neurotransmitter identities, as well as maps of functional data. The mapping of reticulospinal connections (Kimmel et al., 1982) has been a good example of how the establishment of projection information can serve as a seeding point for scientific discovery. The reticulospinal cells are relatively few in number and therefore provide a bottleneck in relaying swim commands to the spinal cord. Identified sets of reticulospinal neurons control escape responses (O'Malley et al., 1996; Liu and Fetcho, 1999), aspects of prey capture (Gahtan et al., 2005), and swim turns (Orger et al., 2008). Regarding other "projectomes" (Kasthuri and Lichtman, 2007), for zebrafish the complete projection patterns of dopaminergic and noradrenergic neurons have been established (Tay et al., 2011), revealing that generation of such data is possible for long-range projection systems in zebrafish. The projectome of Otp-dependent diencephalic dopaminergic cell clusters of the A11 type revealed both ascending projections to the telencephalon and long-range projections into the hindbrain and spinal cord, providing a new framework to study A11 dopamine neurons in vertebrates. In the cases of reticulospinal cells and dopaminergic cells, projection patterns have been established based on projection target and neurotransmitter identity, respectively. In the future, the application of serial block face electron microscopy and other methods like trans-synaptic viral tracing or the use of photoactivatable/-convertible fluorophores offer the potential to contribute to the generation of rich projectome information (Denk et al., 2012).

In order to fully exploit the potential of whole brain calcium imaging we need to know the identities of the recorded cells. A particularly meaningful marker in many circuits is the type of neurotransmitter the cells are using. For example, in the case of the neural integrator for horizontal eye movements, the precise connectivity of the integrator network is not known, although electrophysiological data (Aksay et al., 2000, 2003) suggests that glutamatergic cells of the integrator are auto-excitatory to the ipsilateral side, whereas inhibitory integrator cells are likely GABAergic and inhibit the contralateral side. Recent work on the arrangement of hindbrain cell types (Kinkhabwala et al., 2011) revealed that hindbrain circuitry is made up of stripes of cells with specific wiring properties. The neurotransmitter type and mediolateral positioning in the hindbrain together thus affect whether the cells have ascending, descending, ipsilateral or contralateral projections or a combination of different projection types. Therefore, the knowledge of neurotransmitter type will - together

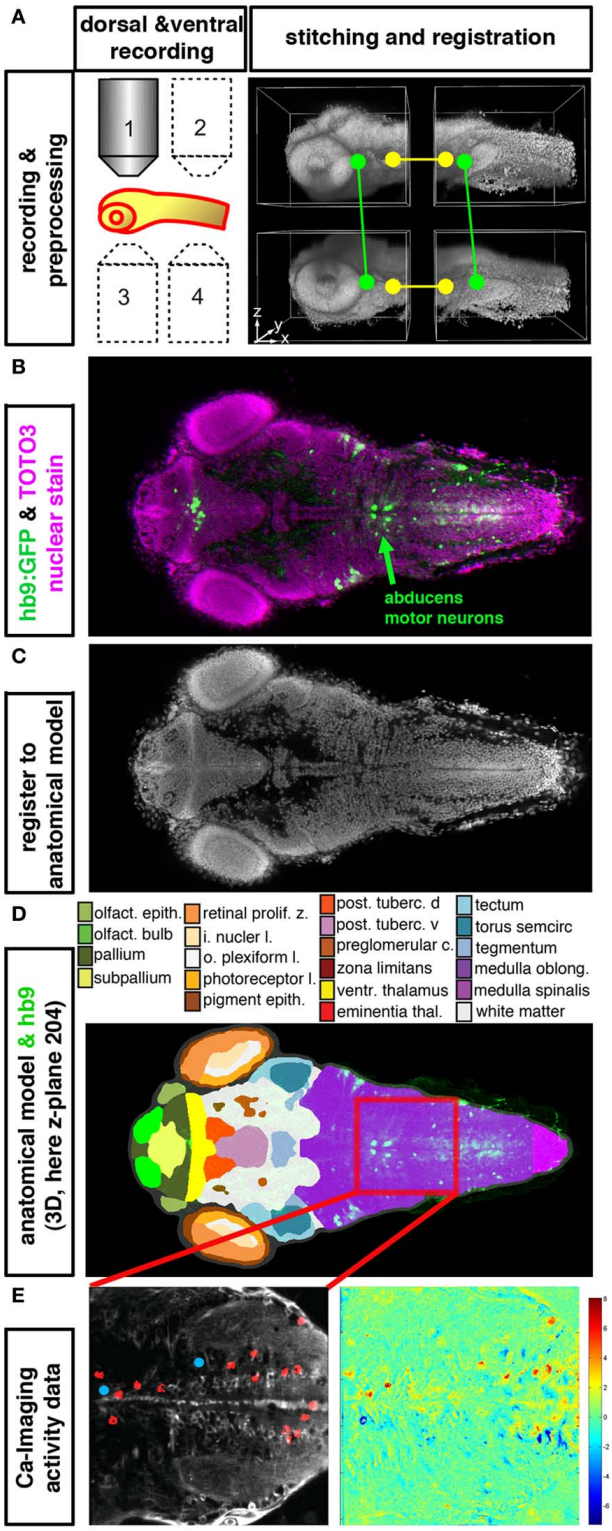

FIGURE 2 | Integration of anatomical, gene expression, and functional information in 3D. (A–E) High resolution datasets generated using an anatomical reference stain for each developmental stage may serve to establish an anatomical reference to register different data types into an anatomical and functional atlas of the nervous system. The Virtual Brain

(Continued)

FIGURE 2 | Continued

Explorer for Zebrafish (ViBE-Z) provides a framework for generation of high resolution 3D image stacks and for registration into an anatomical model (Ronneberger et al., 2012). **(A)** For single cell resolution documentation of the whole zebrafish brain, image stacks of rostral and caudal parts of the brain are recorded from ventral and dorsal sides using standard single photon confocal microscopes. Fluorescent stain of all cell nuclei is used to obtain anatomical information, and also to correct for loss of signal in deep tissues, assuming that all nuclei contain the same amount of DNA and have similar stain intensities. ViBE-Z stitches the individual stacks into one high resolution 3D data volume and performs correction of optical attenuation (light absorption and scattering in tissue). **(B)** Example of a ViBE-Z processed dataset of a 3-day-old larva showing GFP expression from *Tg(hb9:GFP)* (Flanagan-Steet et al., 2005) and TOTO3 fluorescent nuclear stain. **(C)** The fluorescent stain of cell nuclei is used by ViBE-Z to extract landmark information and register the experimental datasets in 3D to a reference larva. **(D)** The anatomical model of the reference embryo may now be combined with the experimental data set. Here, a dorsal view at focal plane z_204 of the reference larva is shown. The experimental *Tg(hb9:GFP)* expression provides neuronal information even in the medulla oblongata hindbrain region, which has only few anatomical annotations in reference databases (www.ZFIN.org). **(E)** In the future, as soon as anatomical references may be recorded also in live larva, the anatomical and gene expression information in ViBE-Z may be used to identify neurons which have defined recorded activity patterns. In this case, neurons with activity patterns correlating with oculomotor activity have been detected (see **Figure 1**), and ViBE-Z may be used to determine whether some of these active neurons may correspond to abducens motor neurons, which are labeled in the *Tg(hb9:GFP)* transgenic line.

with the precisely annotated position of the cells - greatly facilitate the understanding of the functions of oculomotor system cells' calcium signals.

The generation of 3D activity maps will help to identify neuronal groups correlated with behavioral functions. To test the function of these neurons causally, perturbation maps in which brain volumes are systematically activated or silenced during behavior (see **Figure 1C**), could be generated at different levels of resolution. In bigger animals, electrical stimulation has been used to identify topographic maps of behavioral function. For example, in the superior colliculus of monkeys, cats and goldfish, saccades can be elicited by electrical stimulation and the location of stimulation affects the magnitude and direction of the saccades in a topographic manner (Robinson, 1972; Guitton et al., 1980; Angeles Luque et al., 2005). Similar perturbation maps could be generated for larval zebrafish making use of optogenetics and high-resolution photostimulation. Inclusion of projectomes and functional data in a potential digital atlas of the future will facilitate pathway mapping and advance our understanding of brain functions.

To be most useful, a digital reference atlas should allow researchers to add their own functional and anatomical data to the atlas. In the current ViBE-Z implementation, this is facilitated by using a simple fluorescent stain of cell nuclei as anatomical reference stain. However, in the future one would also like to implement data from live brain recordings. Therefore, a widely available reference fish line would be useful that may fluorescently label a sufficient number of structures to enable landmark detection and fine elastic registration. While some promoters might be broadly used in laboratories performing calcium imaging (e.g., HuC/elavl3), *in vivo* nuclear staining dyes could provide a

simple reference. Several cell-permeable DNA-binding dyes are available and are potentially applicable, but protocols need to be developed for live zebrafish larva. Alternatively, it could be explored whether autofluorescence, differential interference contrast, or IR-scanning gradient contrast imaging (Dodt et al., 1999; Wimmer et al., 2004) provide enough information to serve as a reference. An additional limitation is that the high spatial resolution of ViBE-Z currently comes at the cost of a large effort to record the high quality confocal data stacks. Therefore, algorithms suitable for lower quality data need to be developed in order to save microscope recording time. In parallel, the development and application of faster imaging techniques like selective plane illumination microscopy (SPIM; Huisken and Stainier, 2009) will also speed up and thus facilitate generation of *in vivo* data for integration into a reference atlas.

OUTLOOK

The integration of functional and anatomical data will advance our knowledge and facilitate interpretation of experimental results. Moreover, it should also improve the experimental design in the future. If one imagines a functional-anatomical atlas of the future, scientists could use the contained stereotactical information to guide their experiments in a hypothesis-driven fashion. For example, it could be attempted to only stimulate excitatory or inhibitory cells within a certain circuit module or to test different stimulation patterns that are chosen based on the expected connectivity in local circuits. In combination with advanced optical methods, the temporal and spatial photostimulation patterns could evolve to be as physiological as possible and test the combinatorial effects of multiplexed photostimulations in networks of neurons. These perturbation experiments, together with the projection patterns and expression markers in a zebrafish atlas of the future should open up new avenues of circuit analysis. It seems that zebrafish circuit neuroscience has a bright future in which advanced genetic, optogenetic, optical and computational methods will enable circuit analysis in three dimensions, at cellular resolution in the whole brain.

ACKNOWLEDGMENTS

We are grateful to Claire Wyart for sharing her *Tg(UAS:GCaMP3)* zebrafish line. We thank Emre Aksay for advice on an early version of the manuscript and A. Miguel Fernandes for feedback. The authors are supported by the Excellence Initiative of the German Federal and State Governments (Centre for Biological Signalling Studies EXC 294, Wolfgang Driever) and the German Research Foundation (DFG-SFB780, Wolfgang Driever).

REFERENCES

Ahrens, M. B., and Keller, P. J. (2013). Whole-brain functional imaging at cellular resolution using light-sheet microscopy. *Nat. Methods*. doi: 10.1038/nmeth.2434. [Epub ahead of print].

Ahrens, M. B., Li, J. M., Orger, M. B., Robson, D. N., Schier, A. F., Engert, F., et al. (2012). Brain-wide neuronal dynamics during motor adaptation in zebrafish. *Nature* 485, 471–477.

Aizenberg, M., and Schuman, E. M. (2011). Cerebellar-dependent learning in larval zebrafish. *J. Neurosci.* 31, 8708–8712.

Akemann, W., Mutoh, H., Perron, A., Park, Y. K., Iwamoto, Y., and Knopfel, T. (2012). Imaging neural circuit dynamics with a voltage-sensitive fluorescent protein. *J. Neurophysiol.* 108, 2323–2337.

Akerboom, J., Chen, T.-W., Wardill, T. J., Tian, L., Marvin, J. S., Mutlu, S., et al. (2012). Optimization of a GCaMP calcium indicator for neural activity imaging. *J. Neurosci.* 32, 13819–13840.

Aksay, E., Baker, R., Seung, H. S., and Tank, D. W. (2000). Anatomy and discharge properties of pre-motor neurons in the goldfish medulla that have eye-position signals during fixations. *J. Neurophysiol.* 84, 1035–1049.

Aksay, E., Baker, R., Seung, H. S., and Tank, D. W. (2003). Correlated discharge among cell pairs within the oculomotor horizontal velocity-to-position integrator. *J. Neurosci.* 23, 10852–10858.

Andrasfalvy, B. K., Zemelman, B. V., Tang, J., and Vaziri, A. (2010). Two-photon single-cell optogenetic control of neuronal activity by sculpted light. *Proc. Natl. Acad. Sci. U.S.A.* 107, 11981–11986.

Angeles Luque, M., Pilar Pérez-Pérez, M., Herrero, L., and Torres, B. (2005). Involvement of the optic tectum and mesencephalic reticular formation in the generation of saccadic eye movements in goldfish. *Brain Res. Brain Res. Rev.* 49, 388–397.

Arrenberg, A. B., Del Bene, F., and Baier, H. (2009). Optical control of zebrafish behavior with halorhodopsin. *Proc. Natl. Acad. Sci. U.S.A.* 106, 17968–17973.

Arrenberg, A. B., Stainier, D. Y. R., Baier, H., and Huisken, J. (2010). Optogenetic control of cardiac function. *Science* 330, 971–974.

Baier, H., and Scott, E. K. (2009). Genetic and optical targeting of neural circuits and behavior—zebrafish in the spotlight. *Curr. Opin. Neurobiol.* 19, 553–560.

Bianco, I. H., Kampff, A. R., and Engert, F. (2011). Prey capture behavior evoked by simple visual stimuli in Larval Zebrafish. *Front. Syst. Neurosci.* 5:101. doi: 10.3389/fnsys.2011.00101

Blumhagen, F., Zhu, P., Shum, J., Schärer, Y.-P. Z., Yaksi, E., Deisseroth, K., et al. (2011). Neuronal filtering of multiplexed odour representations. *Nature* 479, 493–498.

Bradford, Y., Conlin, T., Dunn, N., Fashena, D., Frazer, K., Howe, D. G., et al. (2011). ZFIN: enhancements and updates to the Zebrafish Model Organism Database. *Nucleic Acids Res.* 39, D822–D829. (Database issue).

Brockerhoff, S. E., Hurley, J. B., Janssen-Bienhold, U., Neuhauss, S. C., Driever, W., and Dowling, J. E. (1995). A behavioral screen for isolating zebrafish mutants with visual system defects. *Proc. Natl. Acad. Sci. U.S.A.* 92, 10545–10549.

Chen, T.-W., Wardill, T. J., Hasseman, J. P., Tsegaye, G., Fosque, B. F., Schreiter, E. R., et al. (2012). Engineering next generation GCaMP calcium indicators using neuron-based screening. *Soc. Neuroci.* 207.14/DDD38. Available online at: http://www.abstractsonline.com

Cheng, K., and Copper, J. (2012). *Zebrafish Atlas. Jake Gittlen Cancer Research Foundation*. Available online at: http://zfatlas.psu.edu/

Denk, W., Briggman, K. L., and Helmstaedter, M. (2012). Structural neurobiology: missing link to a mechanistic understanding of neural computation. *Nat. Rev. Neurosci*. 13, 351–358.

Dodt, H., Eder, M., Frick, A., and Zieglgansberger, W. (1999). Precisely localized LTD in the neocortex revealed by infrared-guided laser stimulation. *Science* 286, 110–113.

Douglass, A. D., Kraves, S., Deisseroth, K., Schier, A. F., and Engert, F. (2008). Escape behavior elicited by single, channelrhodopsin-2-evoked spikes in zebrafish somatosensory neurons. *Curr. Biol.* 18, 1133–1137.

Fenno, L., Yizhar, O., and Deisseroth, K. (2011). The development and application of optogenetics. *Annu. Rev. Neurosci.* 34, 389–412.

Fernandes, A. M., Fero, K., Arrenberg, A. B., Bergeron, S. A., Driever, W., and Burgess, H. A. (2012). Deep brain photoreceptors control light-seeking behavior in zebrafish larva. *Curr. Biol.* 22, 2042–2047.

Fetcho, J. R., and O'Malley, D. M. (1995). Visualization of active neural circuitry in the spinal cord of intact zebrafish. *J. Neurophysiol.* 73, 399–406.

Filippi, A., Mahler, J., Schweitzer, J., and Driever, W. (2010). Expression of the paralogous tyrosine hydroxylase encoding genes th1 and th2 reveals the full complement of dopaminergic and noradrenergic neurons in zebrafish larval and juvenile brain. *J. Comp. Neurol.* 518, 423–438.

Finger, J. H., Smith, C. M., Hayamizu, T. F., McCright, I. J., Eppig, J. T., Kadin, J. A., et al. (2011). The mouse Gene Expression Database (GXD): 2011 update. *Nucleic Acids Res.* 39, D835–D841. (Database issue).

Flanagan-Steet, H., Fox, M. A., Meyer, D., and Sanes, J. R. (2005). Neuromuscular synapses can form *in vivo* by incorporation of initially aneural postsynaptic specializations. *Development* 132, 4471–4481.

Franklin, K. B. J., and Paxinos, G. (2012). *The Mouse Brain in Stereotaxic Coordinates.* 4th Edn. Amsterdam [u.a.]: Elsevier.

Friedrich, R. W., and Korsching, S. I. (1997). Combinatorial and chemotopic odorant coding in the zebrafish olfactory bulb visualized by optical imaging. *Neuron* 18, 737–752.

Gahtan, E., and Baier, H. (2004). Of lasers, mutants, and see-through brains: functional neuroanatomy in zebrafish. *J. Neurobiol.* 59, 147–161.

Gahtan, E., Sankrithi, N., Campos, J. B., and O'Malley, D. M. (2002). Evidence for a widespread brain stem escape network in larval zebrafish. *J. Neurophysiol.* 87, 608–614.

Gahtan, E., Tanger, P., and Baier, H. (2005). Visual prey capture in larval zebrafish is controlled by identified reticulospinal neurons downstream of the tectum. *J. Neurosci.* 25, 9294–9303.

Granato, M., van Eeden, F. J., Schach, U., Trowe, T., Brand, M., Furutani-Seiki, M., et al. (1996). Genes controlling and mediating locomotion behavior of the zebrafish embryo and larva. *Development* 123, 399–413.

Grienberger, C., and Konnerth, A. (2012). Imaging calcium in neurons. *Neuron* 73, 862–885.

Guitton, D., Crommelinck, M., and Roucoux, A. (1980). Stimulation of the superior colliculus in the alert cat. I. Eye movements and neck EMG activity evoked when the head is restrained. *Exp. Brain Res.* 39, 63–73.

Higashijima, S., Hotta, Y., and Okamoto, H. (2000). Visualization of cranial motor neurons in live transgenic zebrafish expressing green fluorescent protein under the control of the islet-1 promoter/enhancer. *J. Neurosci.* 20, 206–218.

Hill, A., Howard, C. V., Strahle, U., and Cossins, A. (2003). Neurodevelopmental defects in zebrafish (*Danio rerio*) at environmentally relevant dioxin (TCDD) concentrations. *Toxicol. Sci.* 76, 392–399.

Huisken, J., and Stainier, D. Y. R. (2009). Selective plane illumination microscopy techniques in developmental biology. *Development* 136, 1963–1975.

Kalaidzidis, I. V., Kalaidzidis, Y. L., and Kaulen, A. D. (1998). Flash-induced voltage changes in halorhodopsin from Natronobacterium pharaonis. *FEBS Lett.* 427, 59–63.

Kasthuri, N., and Lichtman, J. W. (2007). The rise of the 'projectome'. *Nat. Methods* 4, 307–308.

Kimmel, C. B., Powell, S. L., and Metcalfe, W. K. (1982). Brain neurons which project to the spinal cord in young larva of the zebrafish. *J. Comp. Neurol.* 205, 112–127.

Kinkhabwala, A., Riley, M., Koyama, M., Monen, J., Satou, C., Kimura, Y., et al. (2011). A structural and functional ground plan for neurons in the hindbrain of zebrafish. *Proc. Natl. Acad. Sci. U.S.A.* 108, 1164–1169.

Knöpfel, T. (2012). Genetically encoded optical indicators for the analysis of neuronal circuits. *Nat. Rev. Neurosci.* 10, 687–700.

Liu, K. S., and Fetcho, J. R. (1999). Laser ablations reveal functional relationships of segmental hindbrain neurons in zebrafish. *Neuron* 23, 325–335.

Lutz, C., Otis, T. S., DeSars, V., Charpak, S., DiGregorio, D. A., and Emiliani, V. (2008). Holographic photolysis of caged neurotransmitters. *Nat. Methods* 5, 821–827.

McLean, D. L., and Fetcho, J. R. (2008). Using imaging and genetics in zebrafish to study developing spinal circuits *in vivo*. *Dev. Neurobiol.* 68, 817–834.

McLean, D. L., and Fetcho, J. R. (2011). Movement, technology and discovery in the zebrafish. *Curr. Opin. Neurobiol.* 21, 110–115.

Miri, A., Daie, K., Arrenberg, A. B., Baier, H., Aksay, E., and Tank, D. W. (2011a). Spatial gradients and multidimensional dynamics in a neural integrator circuit. *Nat. Neurosci.* 14, 1150–1159.

Miri, A., Daie, K., Burdine, R. D., Aksay, E., and Tank, D. W. (2011b). Regression-based identification of behavior-encoding neurons during large-scale optical imaging of neural activity at cellular resolution. *J. Neurophysiol.* 105, 964–980.

Mueller, T., and Wullimann, M. F. (2005). *Atlas of Early Zebrafish Brain Development.* Amsterdam; Boston: Elsevier.

Muto, A., Ohkura, M., Abe, G., Nakai, J., and Kawakami, K. (2013). Real-time visualization of neuronal activity during perception. *Curr. Biol.* 23, 307–311.

Muto, A., Orger, M. B., Wehman, A. M., Smear, M. C., Kay, J. N., Page-McCaw, P. S., et al. (2005). Forward genetic analysis of visual behavior in zebrafish. *PLoS Genet.* 1:e66. doi: 10.1371/journal.pgen.0010066

Nagel, G. (2002). Channelrhodopsin-1: a light-gated proton channel in green algae. *Science* 296, 2395–2398.

Nagel, G. (2003). Channelrhodopsin-2, a directly light-gated cation-selective membrane channel. *Proc. Natl. Acad. Sci. U.S.A.* 100, 13940–13945.

Neuhauss, S. C., Biehlmaier, O., Seeliger, M. W., Das, T., Kohler, K., Harris, W. A., et al. (1999). Genetic disorders of vision revealed by a behavioral screen of 400 essential loci in zebrafish. *J. Neurosci.* 19, 8603–8615.

Niell, C. M., and Smith, S. J. (2005). Functional imaging reveals rapid development of visual response properties in the zebrafish tectum. *Neuron* 45, 941–951.

O'Malley, D. M., Kao, Y. H., and Fetcho, J. R. (1996). Imaging the functional organization of zebrafish hindbrain segments during escape behaviors. *Neuron* 17, 1145–1155.

Orger, M. B., Kampff, A. R., Severi, K. E., Bollmann, J. H., and Engert, F. (2008). Control of visually guided behavior by distinct populations of spinal projection neurons. *Nat. Neurosci.* 11, 327–333.

Oron, D., Papagiakoumou, E., Anselmi, F., and Emiliani, V. (2012). Two-photon optogenetics. *Prog. Brain Res.* 196, 119–143.

Papagiakoumou, E., Anselmi, F., Begue, A., de Sars, V., Gluckstad, J., Isacoff, E. Y., et al. (2010). Scanless two-photon excitation of channelrhodopsin-2. *Nat. Methods* 7, 848–854.

Peng, H., Chung, P., Long, F., Qu, L., Jenett, A., Seeds, A. M., et al. (2011). BrainAligner: 3D registration atlases of Drosophila brains. *Nat. Methods* 8, 493–500.

Rickgauer, J. P., and Tank, D. W. (2009). Two-photon excitation of channelrhodopsin-2 at saturation. *Proc. Natl. Acad. Sci. U.S.A.* 106, 15025–15030.

Robinson, D. A. (1972). Eye movements evoked by collicular stimulation in the alert monkey. *Vision Res.* 12, 1795–1808.

Ronneberger, O., Liu, K., Rath, M., Rueβ, D., Mueller, T., Skibbe, H., et al. (2012). ViBE-Z: a framework for 3D virtual colocalization analysis in zebrafish larval brains. *Nat. Methods* 9, 735–742.

Schobert, B., and Lanyi, J. K. (1982). Halorhodopsin is a light-driven chloride pump. *J. Biol. Chem.* 257, 10306–10313.

Streisinger, G., Walker, C., Dower, N., Knauber, D., and Singer, F. (1981). Production of clones of homozygous diploid zebra fish (*Brachydanio rerio*). *Nature* 291, 293–296.

Sumbre, G., Muto, A., Baier, H., and Poo, M.-M. (2008). Entrained rhythmic activities of neuronal ensembles as perceptual memory of time interval. *Nature* 456, 102–106.

Szobota, S., Gorostiza, P., Del Bene, F., Wyart, C., Fortin, D. L., Kolstad, K. D., et al. (2007). Remote control of neuronal activity with a light-gated glutamate receptor. *Neuron* 54, 535–545.

Tallini, Y. N., Ohkura, M., Choi, B.-R., Ji, G., Imoto, K., Doran, R., et al. (2006). Imaging cellular signals in the heart *in vivo*: cardiac expression of the high-signal Ca2+ indicator GCaMP2. *Proc. Natl. Acad. Sci. U.S.A.* 103, 4753–4758.

Tao, L., Lauderdale, J. D., and Sornborger, A. T. (2011). Mapping functional connectivity between neuronal ensembles with larval zebrafish transgenic for a ratiometric calcium indicator. *Front. Neural Circuits* 5:2. doi: 10.3389/fncir.2011.00002

Tay, T. L., Ronneberger, O., Ryu, S., Nitschke, R., and Driever, W. (2011). Comprehensive catecholaminergic projectome analysis reveals single-neuron integration of zebrafish ascending and descending dopaminergic systems. *Nat. Commun.* 2, 171.

Valente, A., Huang, K.-H., Portugues, R., and Engert, F. (2012). Ontogeny of classical and operant learning behaviors in zebrafish. *Learn. Mem.* 19, 170–177.

Warp, E., Agarwal, G., Wyart, C., Friedmann, D., Oldfield, C. S., Conner, A., et al. (2012). Emergence of patterned activity in the developing zebrafish spinal cord. *Curr. Biol.* 22, 93–102.

Wilson, S., Symonds, A., Bianco, I., Turner, K., Folgueira, M., O'Connor, S., et al. (2012). *Zebrafish Brain Atlas*. University College London, King's College London. Available online at: www.zebrafishbrain.org

Wimmer, V. C., Nevian, T., and Kuner, T. (2004). Targeted *in vivo*

expression of proteins in the calyx of Held. *Pflugers Arch.* 449, 319–333.

Wolman, M. A., Jain, R. A., Liss, L., and Granato, M. (2011). Chemical modulation of memory formation in larval zebrafish. *Proc. Natl. Acad. Sci. U.S.A.* 108, 15468–15473.

Wullimann, M. F., Rupp, B., and Reichert, H. (1996). *Neuroanatomy of the Zebrafish Brain*. Basel; Boston: Birkhäuser Verlag.

Wyart, C., Bene, F. D., Warp, E., Scott, E. K., Trauner, D., Baier, H., et al. (2009). Optogenetic dissection of a behavioural module in the vertebrate spinal cord. *Nature* 461, 407–410.

Zhang, F., Wang, L.-P., Brauner, M., Liewald, J. F., Kay, K., Watzke, N., et al. (2007). Multimodal fast optical interrogation of neural circuitry. *Nature* 446, 633–639.

Zhu, P., Fajardo, O., Shum, J., Zhang Schärer, Y.-P., and Friedrich, R. W. (2012). High-resolution optical control of spatiotemporal neuronal activity patterns in zebrafish using a digital micromirror device. *Nat. Protoc.* 7, 1410–1425.

Zhu, P., Narita, Y., Bundschuh, S. T., Fajardo, O., Zhang Schärer, Y.-P., Chattopadhyaya, B., et al. (2009). Optogenetic dissection of neuronal circuits in zebrafish using viral gene transfer and the Tet system. *Front. Neural Circuits* 3:21. doi: 10.3389/neuro.04.021.2009

Conflict of Interest Statement: The authors declare that the research was conducted in the absence of any commercial or financial relationships that could be construed as a potential *conflict of interest*.

Received: 31 January 2013; paper pending published: 06 March 2013; accepted: 03 April 2013; published online: 23 April 2013.

Citation: Arrenberg AB and Driever W (2013) Integrating anatomy and function for zebrafish circuit analysis. Front. Neural Circuits 7:74. doi: 10.3389/fncir.2013.00074

frontiers in
NEURAL CIRCUITS

ORIGINAL RESEARCH ARTICLE
published: 01 April 2013
doi: 10.3389/fncir.2013.00053

Cerebellar output in zebrafish: an analysis of spatial patterns and topography in eurydendroid cell projections

Lucy A. Heap[1], Chi Ching Goh[1†], Karin S. Kassahn[2] and Ethan K. Scott[1,3]*

[1] School of Biomedical Sciences, The University of Queensland, Brisbane, QLD, Australia
[2] Institute for Molecular Bioscience, The University of Queensland, Brisbane, QLD, Australia
[3] Queensland Brain Institute, The University of Queensland, Brisbane, QLD, Australia

Edited by:
German Sumbre, Ecole Normale Superieure, France

Reviewed by:
Gilad A. Jacobson, Friedrich Miescher Institute, Switzerland
Naoyuki Yamamoto, Nagoya University, Japan

***Correspondence:**
Ethan K. Scott, School of Biomedical Sciences, The University of Queensland, Brisbane, QLD 4072, Australia.
e-mail: ethan.scott@uq.edu.au

[†]***Present address:***
Chi Ching Goh, Department of Microbiology, Yong Loo Lin School of Medicine, National University of Singapore, 117456 Singapore.

The cerebellum is a brain region responsible for motor coordination and for refining motor programs. While a great deal is known about the structure and connectivity of the mammalian cerebellum, fundamental questions regarding its function in behavior remain unanswered. Recently, the zebrafish has emerged as a useful model organism for cerebellar studies, owing in part to the similarity in cerebellar circuits between zebrafish and mammals. While the cell types composing their cerebellar cortical circuits are generally conserved with mammals, zebrafish lack deep cerebellar nuclei, and instead a majority of cerebellar output comes from a single type of neuron: the eurydendroid cell. To describe spatial patterns of cerebellar output in zebrafish, we have used genetic techniques to label and trace eurydendroid cells individually and *en masse*. We have found that cerebellar output targets the thalamus and optic tectum, and have confirmed the presence of presynaptic terminals from eurydendroid cells in these structures using a synaptically targeted GFP. By observing individual eurydendroid cells, we have shown that different medial-lateral regions of the cerebellum have eurydendroid cells projecting to different targets. Finally, we found topographic organization in the connectivity between the cerebellum and the optic tectum, where more medial eurydendroid cells project to the rostral tectum while lateral cells project to the caudal tectum. These findings indicate that there is spatial logic underpinning cerebellar output in zebrafish with likely implications for cerebellar function.

Keywords: zebrafish, cerebellum, eurydendroid, optic tectum, thalamus, topography, Gal4

INTRODUCTION

Coordinated smooth movements and motor learning require the cerebellum, a structure located in the hindbrain of all vertebrates (Glickstein et al., 2011). Cerebellar processing is believed to be based on comparisons between the intended outcomes of motor programs and sensory information reflecting the actual outcomes (Miall et al., 1993; Blakemore et al., 1998; Tseng et al., 2007). Mismatches are indicative of failures of motor programs, and the nature of the mismatches provide information with which the cerebellum can calibrate the associated motor programs (Miall et al., 1993; Tseng et al., 2007).

The cerebellar cortex is composed of a highly ordered, repeating structure made up of the granule cell, Purkinje cell (PC), and molecular layers (Dow and Moruzzi, 1958). PCs are the points of convergence for two pathways of information: the climbing fibers from the inferior olive, and the mossy fibers principally from the pontine nuclei (via granule cell parallel fibers). As such, they are believed to have a role in identifying discrepancies between intended and actual outcomes from motor programs (Albus, 1971). The PCs send their inhibitory signals out of the cerebellar cortex and into the deep cerebellar nuclei (DCN), which provide cerebellar output (Eccles, 1971). The DCN are also a point of convergence for the climbing and mossy fibers, and may themselves have important roles in detecting motor errors (Miles and Lisberger, 1981). Indeed, the relative importance of plasticity in PCs versus DCN plasticity is still the topic of intense debate (reviewed by Carey, 2011).

Anatomically, DCN outputs have been shown to send both excitatory and inhibitory information to areas involved in sensory integration such as the superior colliculus, sensory nuclei of the thalamus (Andrezik et al., 1984; Aumann et al., 1994; Sultan et al., 2012), and motor areas such as the inferior olive and premotor regions of the thalamus (Andrezik et al., 1984). The patterns of output activity generated by the DCN have been studied electrophysiologically in both primates and rodents (Thach, 1968; Hepp et al., 1982; Hoebeek et al., 2010), but the ways in which these patterns subserve motor learning are less well understood. These limitations are partially due to the complexity of the DCN themselves. As a result, research in a simpler and more experimentally accessible model may be beneficial for describing cerebellar output and the ways in which the output guides motor learning.

Zebrafish are proving to be a particularly advantageous model system for behavioral and functional circuit analysis, largely owing to their optical transparency and external development (Scott and Baier, 2009; Friedrich et al., 2010; Simmich et al., 2012). These characteristics, in combination with the quickly developing field of optogenetics, permit the observation and manipulation of neural activity *in vivo*, and may therefore aid in describing patterns of cerebellar activity and output that subserve motor learning. Therefore, it is important to develop a detailed and comprehensive

anatomical description of cerebellar circuits in zebrafish that can serve as a scaffold for future functional mapping. The zebrafish cerebellum is composed of three lobes, which are, from rostral to caudal, the valvula cerebelli, corpus cerebelli, and vestibulolateral lobe (Finger, 1983; Bae et al., 2009). As in the mammalian cerebellum, the valvula and corpus cerebelli contain the granule cell, PC, and molecular layers. Reports differ on the structures of layers within the vestibulolateral lobe, which may vary among teleost species (Bass, 1982; Murakami and Morita, 1987; Zhang et al., 2008; Bae et al., 2009). Development of the zebrafish cerebellum starts at 2 days post fertilization (dpf), with complete and functioning circuits by 6 dpf (Aizenberg and Schuman, 2011; Hibi and Shimizu, 2012). As in mammals, the glutamatergic neurons (granule and eurydendroid cells) are derived from the upper rhombic lip while GABAergic neurons (Golgi and PCs) come from the ventricular zone (Kani et al., 2010).

Although there are broad similarities in the structure, connectivity, and development of the zebrafish and mammalian cerebella, a significant difference lies in their output structures. In contrast to mammals, teleosts do not have DCN that are spatially segregated from the cerebellar cortex. Instead, they have a single type of neuron within the cerebellar cortex, the eurydendroid cell, that provides cerebellar output (Finger, 1983; McFarland et al., 2008; Bae et al., 2009). These cells are post-synaptic to PCs, receive input from parallel fibers and possibly climbing fibers, and extend axons beyond the cerebellum (Bae et al., 2009; Hibi and Shimizu, 2012), indicating that they occupy the same circuit position as do the DCN in mammals. Previously, multiple subtypes of eurydendroid cells have been described in both scorpion fish and goldfish, differing in appearance, distribution, and target structures (Murakami and Morita, 1987). These descriptions have shown that type A eurydendroid cells are in the caudal lobe of the cerebellum and project largely to the oculomotor complex, whereas type B eurydendroid cells are located in the valvula and corpus cerebelli and project to a much broader range of structures, including the brainstem, the nucleus ventromedialis thalami, and the nucleus ruber (Murakami and Morita, 1987). Dye-tracing experiments in goldfish have shown that eurydendroid cell subtypes with different morphologies target specific regions including the optic tectum, thalamus (Ikenaga et al., 2006), inferior olive, and hindbrain reticular formation (Finger, 1983). In mormyrid fish, different lobes of the corpus cerebelli target different structures. The first lobe of the corpus cerebelli targets structures including the nucleus of the fasciculus longitudinalis medialis, the trigeminal motor nucleus, and the tectum whereas the third lobe targets the midbrain tegmentum, the torus longitudinalis, and the nucleus reticularis superior (Meek et al., 1986a,b).

It is not clear, however, whether there are multiple eurydendroid cell subtypes in larval zebrafish, whether different parts of the zebrafish cerebellum target different brain regions, or whether topography exists between the cerebellum and its targets in teleosts.

Transgenesis, the process of delivering exogenous genes into a model system's genome, is an effective approach for labeling neural structures for anatomical description (Feng et al., 2000; Kawakami, 2004; reviewed by Luo et al., 2008). The Gal4-UAS system (Brand and Perrimon, 1993; Scheer and Campos-Ortega, 1999), which allows separate control over the location of expression and the marker being expressed, has brought particular utility to the labeling of circuits for anatomical analysis (Scott, 2009). This has been especially true in the zebrafish model system, since fluorescently labeled neurons can be imaged in live, intact animals. As a result of several enhancer trap screens using Gal4 (Davison et al., 2007; Scott et al., 2007; Asakawa et al., 2008; Distel et al., 2009; Scott and Baier, 2009), hundreds of lines of zebrafish exist with Gal4 expression in specific parts of the nervous system.

While these Gal4 lines exhibit their overall expression patterns when crossed to any line carrying a UAS:fluorophore transgene, this overall expression is often insufficient for judging the connectivity or cellular composition of the population of Gal4-positive cells. To improve upon this, past studies have expressed fluorophores that are targeted specifically to pre- or post-synaptic terminals, thus revealing the neurons' dendrites or axonal terminals specifically (Niell et al., 2004; Meyer and Smith, 2006). The individual neurons composing an expression pattern can be visualized by driving highly variegated expression, either through injection of a plasmid containing the gene for a UAS-linked fluorophore (Scheer and Campos-Ortega, 1999), or through the use of a highly variegated UAS:GFP (Xiao et al., 2005; Scott et al., 2007; Scott and Baier, 2009; Wyart et al., 2009; Simpson et al., 2013). Since these approaches allow for single neurons to be seen in the context of the expression pattern as a whole, they provide a powerful tool for generating a catalog of a brain region's cell types, each in anatomical detail and spatial registration.

In this study, we describe a Gal4 ET line (*Gal4^{s1168t}*) with expression in the cerebellum, and we use this line to map the projections of eurydendroid cells in larval zebrafish. Using overall expression, a pre-synaptic marker, and imaging of individual eurydendroid cells, we describe the anatomy of cerebellar projections to the tectum and thalamus, thus revealing the spatial and topographic properties of these projections.

MATERIALS AND METHODS

GENERATION OF ANIMALS

All procedures were performed with approval from the University of Queensland Animal Ethics Committee (in accordance with approvals QBI/811/07 and SBMS/362/10/NHMRC). Adult fish were maintained, fed, and mated as previously described (Westerfield, 2000). The wild-type strain Tupfel long fin (TL) and the pigment free *nacre* mutant (Lister et al., 1999) were used throughout the experiments. The transgenic lines *Gal4^{s1168t}* (Scott and Baier, 2009) *pou4f3: GAL4,UAS:GAP-GFP* (*BGUG*) (Scott et al., 2007), and *UAS:Kaede* (Scott et al., 2007) have previously been described. To make the *UAS:mCherry* line, monomeric Cherry with a K-ras membrane localization signal was subcloned into the pT2KXIGΔ in vector (Kotani et al., 2006) using *Eco*RI and *Not*I, downstream of a 14X UAS element. Similarly, the *UAS:synaptophysin-GFP* (*UAS:syn-GFP*) construct was made by subcloning *synaptophysin-GFP* (Meyer and Smith, 2006) into the pT2KXIGΔ in vector (Kotani et al., 2006) using *Eco*RI and *Not*I, downstream of a 14X UAS element. Embryos were injected at single cell stage with a solution containing 25 ng/μL plasmid DNA, 50 ng/μL transposase mRNA, and 0.04% Phenol Red.

To create variegated expression of a plasmid, eggs were injected with a *UAS:Brainbow2.1* construct (Livet et al., 2007) flanked by Tol2 transposon elements (Kawakami, 2004). This construct was generated by inserting *Brainbow2.1*, in reversed orientation, into the pME-MCS vector (Kwan et al., 2007) using *Xho*I and *Xba*I. *UAS:Brainbow2.1* was then generated in the Tol2kit (Kwan et al., 2007). Injection mix consisted of 100 ng/μL transposase, 75 ng/μL *UAS:Brainbow2.1*, and 50 ng/μL *Cre* recombinase, diluted in water, and phenol red was added to allow visualization during injections. *Gal4^{s1168t}; UAS:mCherry* embryos were collected within 20 min of fertilization, and were injected under a dissecting light microscope at the single or two cell stage. At 24 and 48 h post fertilization, embryos were sorted for transient Brainbow expression, indicated by yellow and green fluorescent protein (YFP and GFP), and YFP-positive cells in these animals were imaged at 6 dpf. Images from a total of 21 larvae generated the data for the single cell analyses in this study, with an additional 9 larvae providing data from pairs or small clusters of cells.

IDENTIFICATION OF GENOMIC INSERTION SEQUENCES

The insertion site for *Gal4^{s1168t}* was mapped as described by Kotani et al. (2006) and Laplante et al. (2006), using *Mbol* and linker mediated PCR. The following modifications were made to the primer sequences used by Kotani et al. (2006): Ap1: 5′GGATTTGCTGGTGCAGTACAG3′, Ap2: 5′AGTACAGGCCTTAAGAGGGA3′, L100-Out: 5′AGATTCTAGC CAGATACT3′, R100-Out: 5′GTATTGATTTTTAATTGTA3′, L150-Out: 5′GAGTAAAAAGTACTTTTTTTTCT3′, R150-Out: 5′TAATA CTCAAGTACAATTTTA3′, L175-Out: 5′CTTTTTGACTGTAAATA AAATTG3′, R175-Out: 5′TCTTTCTTGCTTTTACTTTTACTTC3′.

MOUNTING AND MICROSCOPY

At 1 dpf, 25 μL of 7.5% phenylthiourea (PTU) in solution with dimethyl sulfoxide was added to 100 ml E3 media. This media was used to suppress the formation of skin pigmentation that interferes with imaging. Embryos were observed for fluorescence at 48 h post fertilization, and imaging was carried out at 6 or 7 dpf. Larvae with the genotype *Gal4^{s1168t}; UAS:mCherry, UAS:Brainbow* or *Gal4^{s1168t}; UAS:mCherry, BGUG* were mounted dorsal side up in 2% low melt agarose (Progen Biosciences, Murarrie, QLD, Australia). In some cases, photoconverted red Kaede was used in the place of mCherry as described (Scott et al., 2007). Imaging was carried out on the Zeiss-LSM 510 upright confocal microscope using a 543 nm laser and 560 nm long pass filter for mCherry and 488 nm laser and 505–530 nm band pass filter for YFP and GFP. Images were taken using 10, 20, and 63× objectives.

IMAGE ANALYSIS

Images were viewed on ImageJ version 1.45s (U.S. National Institutes of Health, Bethesda, MD, USA), and the plugin "Neurite tracer" (Longair et al., 2011) was used to trace axon projections from the cell body to termination. The medial-lateral, rostral-caudal, and dorsal-ventral positions of the cell body within the cerebellum were measured, and were converted to percentage values.

Separate red and green channels were used on Imaris version 7.4 (Bitplane, Zürich, Switzerland) to create three-dimensional tracings of individual cells. Cells imaged over multiple stacks were stitched together using the freeware XUV stitch program (Emmenlauer et al., 2009). Using the Neurite Wizard function on Imaris version 7, the cell body and axon termination of each neuron were identified and joined using the manual trace function.

To determine the coordinates of a cell termination in the tectal neuropil, the three-dimensional Imaris image was rotated so that the rostral-caudal axis of the tectum was vertical in the viewing panel.

STATISTICAL ANALYSIS

The position of the cell body in the cerebellum and its termination in the tectal neuropil were compared against each other in all axes to see whether correlations were present, using Graph Pad Prism version 6 for Windows (GraphPad Software Inc., La Jolla, CA, USA) and R freeware (R Core Team, Vienna, Austria, http://www.R-project.org). A Schapiro-Wilk test for normality was performed, and all datasets across tectal and cerebellar axes were found to be normally distributed. A Pearson's correlation test was used to test for correlations within the data. A Holm test was used to adjust p values for multiple comparisons. Significance was accepted as $p \leq 0.05$.

RESULTS

THE *GAL4^{s1168t}* INSERTION IS LOCATED BETWEEN TWO GENES WITH CEREBELLAR EXPRESSION

The transgenic zebrafish line *Gal4^{s1168t}*, with Gal4 expression in the cerebellum and trunk muscles, was identified in an enhancer trap screen performed by Scott et al. (2007), and further characterized by Kani et al. (2010) as having expression in atoh1a-positive cells within the cerebellum. The insertion site of *Gal4* in this line is in an intergenic region on chromosome nine, 7.8 kb downstream of the *insig2* gene and 11.8 kb upstream of *eng1a*. These genes are homologous, respectively, to the genes Insig2 and EN1 in humans and mice, and the expression levels in multiple mammalian tissues have been identified. The gene Insig2 is highly expressed in the human nervous system, and expression is highest in the cerebellum and thalamus (Becanovic et al., 2010), as well as skeletal muscle (Thierry-Mieg and Thierry-Mieg, 2006). In mouse, high expression of EN1 has been shown in the cerebellum (Donarum et al., 2006), superior colliculus, and brain stem (Zapala et al., 2005). Given the highly overlapping expression patterns of these two genes, it is difficult to judge whether the expression of Gal4 in the cerebellum and trunk muscles of *Gal4^{s1168t}* larvae results from enhancers belonging to one, the other, or both genes.

CEREBELLAR EXPRESSION IN THE *GAL4^{S1168T}* ENHANCER TRAP LINE

Our initial characterization of the *Gal4^{s1168t}* line involved imaging *Gal4^{s1168t}; UAS:Kaede* larvae at 6 dpf. Observations of these animals were in keeping with preliminary descriptions for this line from the original screen (Scott and Baier, 2009). We found expression to be strongest in trunk muscles and in the cerebellum (**Figure 1A**), and noted the presence of neurites exiting the cerebellum (**Figures 1B–E**). Structures sharing projections with the cerebellum included the crista cerebellaris (CC) in the hindbrain (**Figure 1C**), the optic tectum in the midbrain (**Figure 1D**), and the thalamus in the forebrain (**Figure 1E**). Few neurons outside of

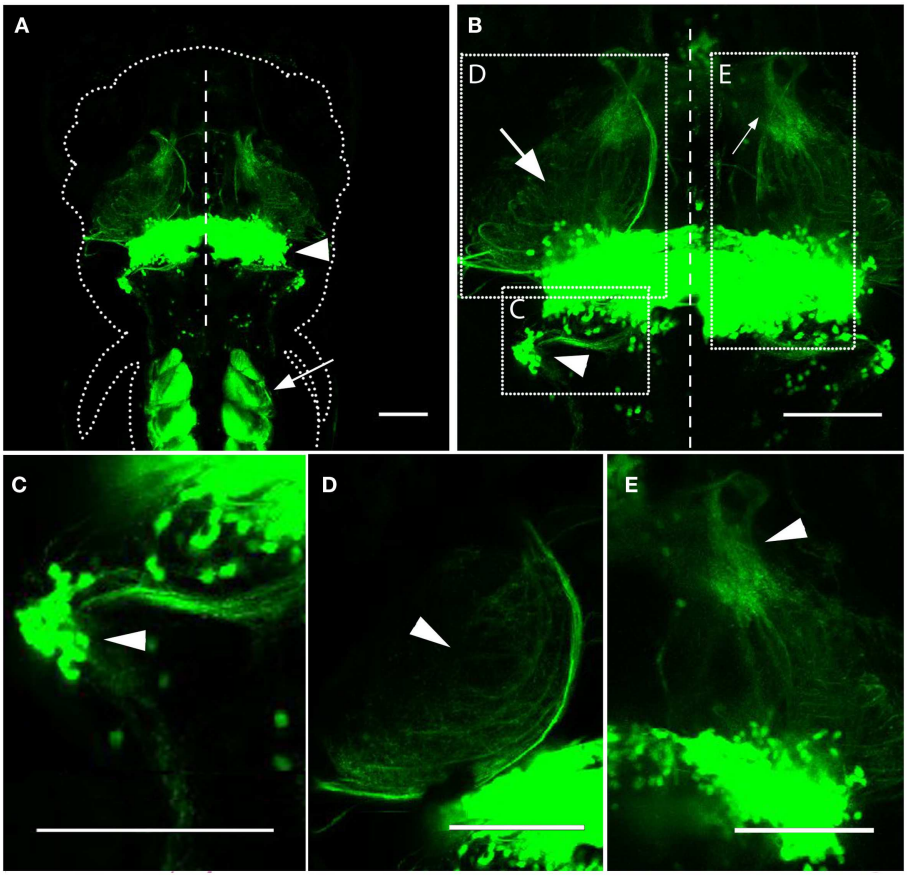

FIGURE 1 | Expression in the *Gal4*^{s1168t} line. (A) Dorsal image of a 6 dpf *Gal4*^{s1168t}*; UAS: Kaede* larva, anterior at the top. The approximate boundary of the animal is shown with a dotted line, and the midline of the animal is indicated by a dashed line. Expression is strongest in the cerebellum (arrowhead) and trunk muscles (arrow). **(B)** A higher-magnification image of the same animal in **(A)**. Neurites between the cerebellum and the CC (arrowhead), tectum (arrow), and thalamus (small arrow) are evident. The regions shown in **(C–E)** are indicated with dashed boxes, and the midline is depicted by a dashed line. **(C)** Neurites are evident between the cerebellum and the CC (arrowhead), where some Gal4-positive cell bodies also reside. **(D)** Cerebellar neurites also project to the tectal neuropil (arrowhead). **(E)** More sparse neurites from the cerebellum are found in the thalamus (arrowhead). Scale bars represent 100 μm. A *z*-series of **(B)** can be viewed in Movie S1 in Supplementary Material.

the cerebellum were seen to be Gal4-positive. Movie S1 in Supplementary Material shows a *z*-series through the structures shown in **Figure 1B**.

A majority of these neurites exit the cerebellum and proceed toward the optic tectum and thalamus. These include two groups of neurites, with the first exiting the ventral lateral part of the corpus cerebelli, extending ventrally and rostrally, and then traveling dorsally to pass through the deep layers of the tectal neuropil (**Figure 1B**; Movie S1 in Supplementary Material). The second group includes neurites that extend rostrally from the ventral cerebellum throughout its medial-lateral range, and project more directly into the deep tectal neuropil (Movie S1 in Supplementary Material). Combined, these neurites blanket the deepest layers of the tectal neuropil, making it impossible to determine the structures of the individual neurites. A subset of the neurites in the tectal neuropil extend further into the dorsal thalamus, but viewing these neurites *en masse*, we are not able to judge whether they have any other distinguishing characteristics that could be used to classify them as a subtype of cerebellar projection neuron. We also observed axon tracts exiting the cerebellum to other regions of the midbrain and forebrain (Movie S1 in Supplementary Material), but these were inconsistent, and were not confirmed in the more detailed analyses presented below.

Axons from the caudal cerebellum were seen targeting the CC (**Figure 1C**). These axons traveled laterally to reach the CC at depths of between 10 and 30 μm below the dorsal surface of the animal. Since Gal4-positive cell bodies are present in the CC (**Figure 1C**), the possibility also exists that these projections run in the opposite direction, from the CC to the cerebellum. That said, axon tracts from Purkinje and granule cells originating in the valvula cerebellum have been reported to project to the CC (Miyamura and Nakayasu, 2001). Therefore axons traveling between the CC and the cerebellum are likely to have originated from cells in this area.

In order to identify the Gal4-positive cells within the cerebellum, we observed variegated expression of GFP provided by the

BGUG transgenic line (Scott et al., 2007). For reasons that are unclear, expression from *UAS:GFP* in this construct is extremely sparse, and this permits GFP-positive neurons to be visualized individually (Scott, 2009). We found two cell types that were regularly labeled using this technique in the *Gal4*^{s1168t} line: PCs (**Figures 2A–A″**) and eurydendroid cells (**Figures 2B–B″**). The latter have previously been described as the output neuron of the teleost cerebellum (Finger, 1983; Meek et al., 1986a,b; Murakami and Morita, 1987; Ikenaga et al., 2006; Bae et al., 2009; Kani et al., 2010), and can be seen contributing projections beyond the cerebellum in our *BGUG* analyses (arrowheads, **Figures 2B′,B″**). From this, we suggest that the neurites observed in this ET line are efferent axons from cerebellar eurydendroid cells.

BRAIN STRUCTURES TARGETED BY CEREBELLAR OUTPUT

We next crossed *Gal4*^{s1168t} to a transgenic line for *UAS:syn-GFP*, leading to the expression of GFP at axonal terminals (Meyer and Smith, 2006; Li et al., 2010). This was intended to confirm that the neurites that we have observed are, in fact, output axons, and to judge how well the above-described cerebellar projections register against this more direct readout of output. *Gal4*^{s1168t}*; UAS:Kaede; UAS:syn-GFP* larvae (**Figure 3A**), with photoconverted red Kaede (Ando et al., 2002) predominantly in cell bodies and GFP in axonal terminals, show cerebellar output to the deep tectal neuropil (**Figure 3C**), the thalamus (**Figure 3D**), and the CC (**Figure 3E**). In the case of the CC, we also observe cell bodies (red, **Figure 3E**), raising the possibility that the syn-GFP signal in the CC is actually due to local circuitry, rather than cerebellar output. In addition to this remote labeling, there are robust GFP signals within the cerebellum itself (**Figures 3A,B**), likely belonging to the axons of PCs, and in the trunk muscles (**Figure 3A**).

This corresponds well to the above description of the tracts exiting the cerebellum in this line. It confirms that the tracts comprise axons, and that the axons form synapses in the structures in which they terminate or pass through. This means, for example, that the tectum receives output from eurydendroid cells, rather than simply being a conduit for axons terminating in the thalamus. It is not clear from this analysis, however, whether there are distinct populations of eurydendroid cells targeting the tectum, the thalamus, or both.

SPATIAL MAPPING OF INDIVIDUAL EURYDENDROID CELLS

To resolve ambiguities like those just described, and to determine whether there is topographic organization of cerebellar outputs, we next undertook a systematic description of eurydendroid cells in terms of their cell body positions, target areas, and points of axon termination. We employed two methods: sparse expression from the *BGUG* transgene (Scott et al., 2007; Scott and Baier, 2009) and variegated expression resulting from injections of *UAS:Brainbow* DNA (Livet et al., 2007). In both cases, rates of labeling were low. In the case of *Gal4*^{s1168t}*; UAS:mCherry, BGUG* and *Gal4*^{s1168t}*; UAS:Kaede, BGUG* triple transgenic larvae, a small percentage (approximately 0.4%) expressed mGFP in resolvable cells within the cerebellum ($n = 9$ larvae, each with an individually resolvable eurydendroid cell). *UAS:Brainbow* injections into *Gal4*^{s1168t}*; UAS:mCherry* embryos resulted in single cell labeling within the cerebellum 1.9% of the time ($n = 12$, with 16 resolvable cells). In a few cases, two or more cells were

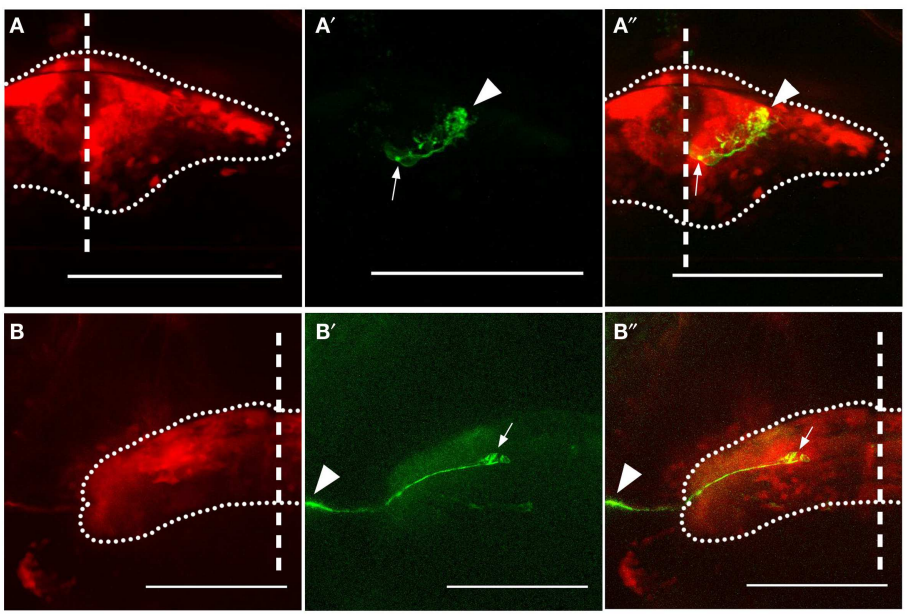

FIGURE 2 | Expression in Purkinje and eurydendroid cells. Expression of GFP in a Purkinje cell **(A–A″)** and eurydendroid cell **(B–B″)** in *Gal4*^{s1168t}*; UAS:Kaede; BGUG* transgenic larvae are shown. For each cell, the overall expression pattern is visible as red Kaede **(A,B)**, and the approximate bounds of the cerebellum are indicated with a dotted line. The Purkinje cell has its soma [arrow in **(A′,A″)**] located ventrally in the cerebellum, with dendrites (arrowhead) elaborating in the dorsal region, presumed to be the molecular layer. The eurydendroid cell [arrow in **(B′,B″)**] extends a neurite laterally and beyond the cerebellum (arrowheads). This neurite is temporarily lost from the image as it plunges ventrally before resurfacing. Scale bars represent 100 μm, and the midline is indicated with a vertical dashed line.

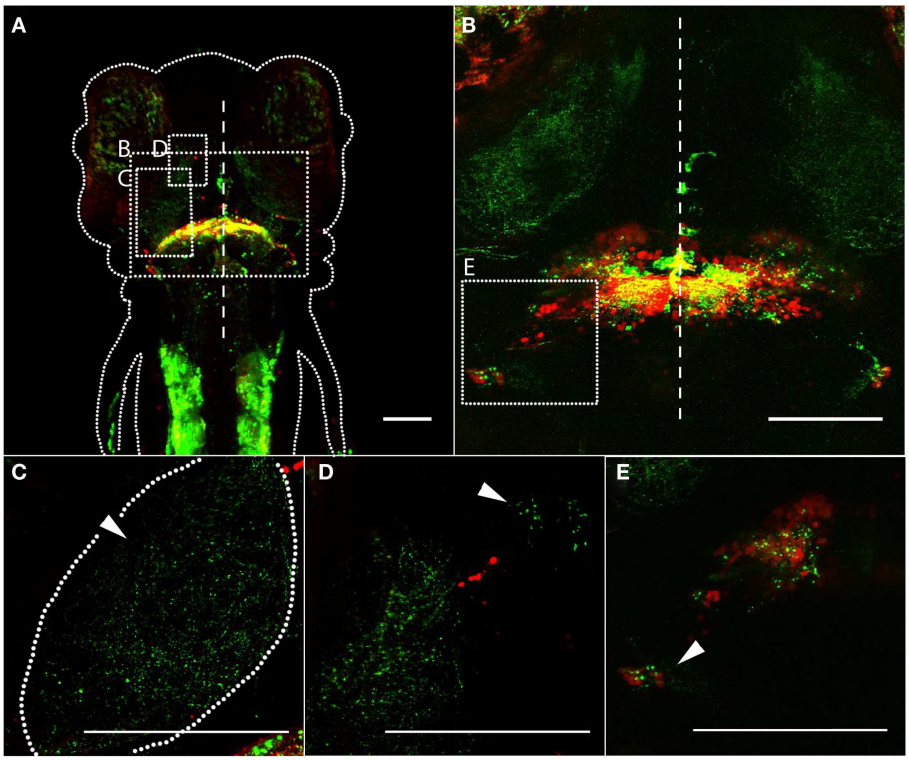

FIGURE 3 | Synaptic targets of the cerebellum, revealed by a pre-synaptic marker. In *Gal4*^{s1168t}*; UAS:Kaede; UAS:syn-GFP* transgenic larvae, photoconverted Kaede is shown in red, and syn-GFP is shown in green. **(A)** Dorsal image of a 6 dpf larva, anterior at the top. The approximate boundary of the animal is depicted by a dotted line, and the midline of the animal is shown by the dashed line. The approximate locations of **(B–D)** are shown with dashed boxes. **(B)** A higher-magnification dorsal image of a 6 dpf larva, with the midline indicated by a dashed line. The greatest concentration of pre-synaptic terminals is in the cerebellum itself, but regions outside of the cerebellum **(C–E)** also show GFP. The approximate location shown in **(E)** is indicated with a dashed box. **(C)** Cerebellar synaptic output in the tectal neuropil (arrowhead) is shown. The approximate boundaries of the neuropil are indicated with a dashed line. **(D)** A high-magnification image showing cerebellar synaptic output in the thalamus. The presence of a smaller cluster of GFP puncta (arrowhead) indicates that multiple distinct parts of the thalamus may be targeted. **(E)** Synapses are apparent in the CC, shown with an arrowhead. Scale bars represent 100 μm. A *z*-series of **(B)** can be viewed in Movie S2 in Supplementary Material.

labeled in the same animal, but could be unambiguously traced as individuals.

The optic tectum was seen to receive output from the cerebellum at a single cell level ($n = 21$ animals), and several pairs or small clusters of eurydendroid cells were seen targeting the dorsal thalamus ($n = 9$ animals). Although they appear to receive axon tracts from the cerebellum, the CC and hindbrain were not targeted by the individual cells that we observed. This could be a function of relatively sparse innervation to these structures combined with a limited number of observed cells, or could be due to possible unintended biases in the labeling methods.

SUBTYPES OF EURYDENDROID CELLS TARGETING THE TECTUM AND THALAMUS

To determine whether spatial organization exists in cerebellar output, we compared the locations of eurydendroid cells' somata with the termination points of their axons. Cell body locations were quantified as a percentage value within a given axis of the cerebellum. We found eurydendroid cells to be distributed broadly throughout the cerebellum, from 7 to 97% along the medial-lateral axis, 7–95% of the rostral-caudal axis, and 21–83% of the dorsal-ventral axis.

We observed cerebellar output to the thalamus from eurydendroid cells whose cell bodies were in the most medial part of the cerebellum (approximately the most medial 20% of the medial-lateral axis) (**Figures 4A–A″**). These cells typically appeared in pairs (see **Figure 4**) or small clusters ($n = 9$ animals). The axons of these medial cells exit the lateral corpus cerebelli, requiring them to project laterally through the cerebellum before exiting (**Figures 4A″,C,C′**). After exiting the cerebellum, their axons project ventrolaterally before turning dorsally to the medial edge of the tectal neuropil. They then follow the medial/ventral edge of the tectal neuropil before exiting the rostral tectum, and projecting ventrally to the thalamus. These cells were often seen extending small neurites (<10 μm) radially into the tectal neuropil as they passed through. Although it is not proven by these observations, these seem likely points for *en passant* synapses in the deep tectal neuropil.

We observed output to the optic tectum, without further extensions to the thalamus, in 25 individually labeled eurydendroid cells ($n = 21$ larvae). These cells (**Figures 4B–B″,D,D′**) were located

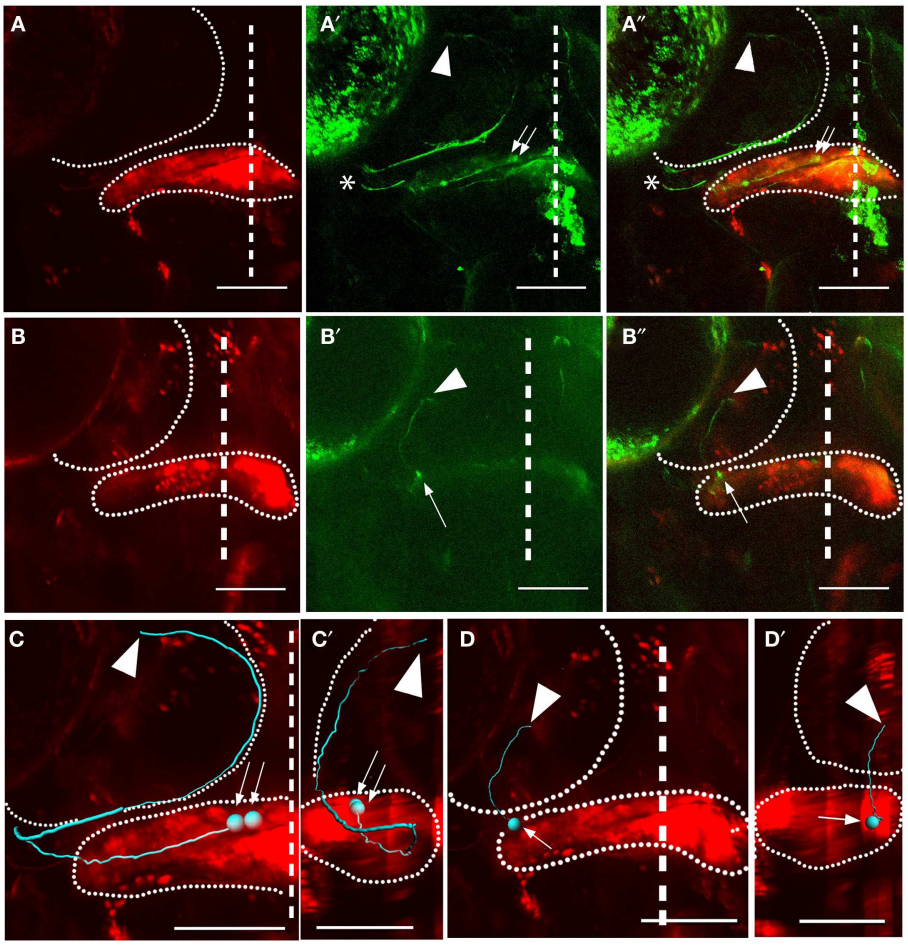

FIGURE 4 | Subtypes of eurydendroid cells. Red shows Kaede and green shows GFP (expressed from the *BGUG* transgene). **(A)** A dorsal *z*-projection of a pair of cells from the medial cerebellum targeting the thalamus. **(A)** Shows the red channel (photoconverted Kaede), and **(A′)** shows the green channel (GFP), with an arrow indicating the cell bodies and arrowhead indicating the corresponding termination points. **(A″)** Shows a merged image of **(A,A′)**. Imaging of this projection is weak when the neurites are in deep ventral positions, and overlying neurites from other neurons [asterisks in **(A′,A″)**] can obscure these *z*-projections, so these cells are best viewed as *z*-series (Movies S3 and S4 in Supplementary Material). **(B)** A dorsal *z*-projection of a cell from the intermediate cerebellum targeting the tectum. The positions of the cell body (arrow) and axon terminal (arrowhead) are indicated. **(C,D)** show dorsal Imaris tracings of cells shown in **(A′,A″)** and **(B′,B″)**, respectively, with cell bodies indicated by arrows and terminations indicated with arrowheads. Both the cerebellum and tectum are indicated with dotted lines. **(C′–D′)** show sagittal views of tracings in **(A′,A″)** and **(B′,B″)**, dorsal to the left, with the cerebellum and tectum indicated with dotted lines. The cell in **(A′,A″)** can be seen to extend to deep ventral positions before extending to the tectum and thalamus, while cell in **(B′,B″)** has a relatively flat sagittal profile. Scale bars represent 100 μm. For *z*-series of the cells shown in **(A,B)**, see Movies S3 and S4 in Supplementary Material, where the paths of the axons are clearer than in the two-dimensional shown here.

throughout most of the cerebellum's medial-lateral axis (roughly the lateral 80%). Axons from these cells project ventrally within the cerebellum before exiting at ventral-rostral points along the cerebellum's medial-lateral axis. They then enter the tectal neuropil on its ventral side, and travel dorsally until reaching their termination points within the deep layers of the tectal neuropil. In contrast to the medial eurydendroid cells that project to the tectum and thalamus, these more numerous eurydendroid cells do not form thick fascicles, and rather extend their axons individually to the tectum.

In addition to these two types of eurydendroid cell, we observed one example of a projection neuron with its cell body in the tegmentum, adjacent to the cerebellum, and with long projections to the hypothalamus (not shown). This type of neuron, which is not a eurydendroid cell, has previously been described in the *Gal4*^{s1168t} line by Kani et al. (2010).

TOPOGRAPHY IN CEREBELLO-TECTAL PROJECTIONS

Since the optic tectum is a topographically organized structure (Sajovic and Levinthal, 1982; Collin and Pettigrew, 1988; Stuermer, 1988), we investigated whether topography exists between the cerebellum and the tectum. We did this by comparing the position of individual eurydendroid cells' bodies in the cerebellum with the termination points of their axons within the tectal neuropil (**Figure 5**). We found significant topography between the cell body position along the medial-lateral axis of the cerebellum

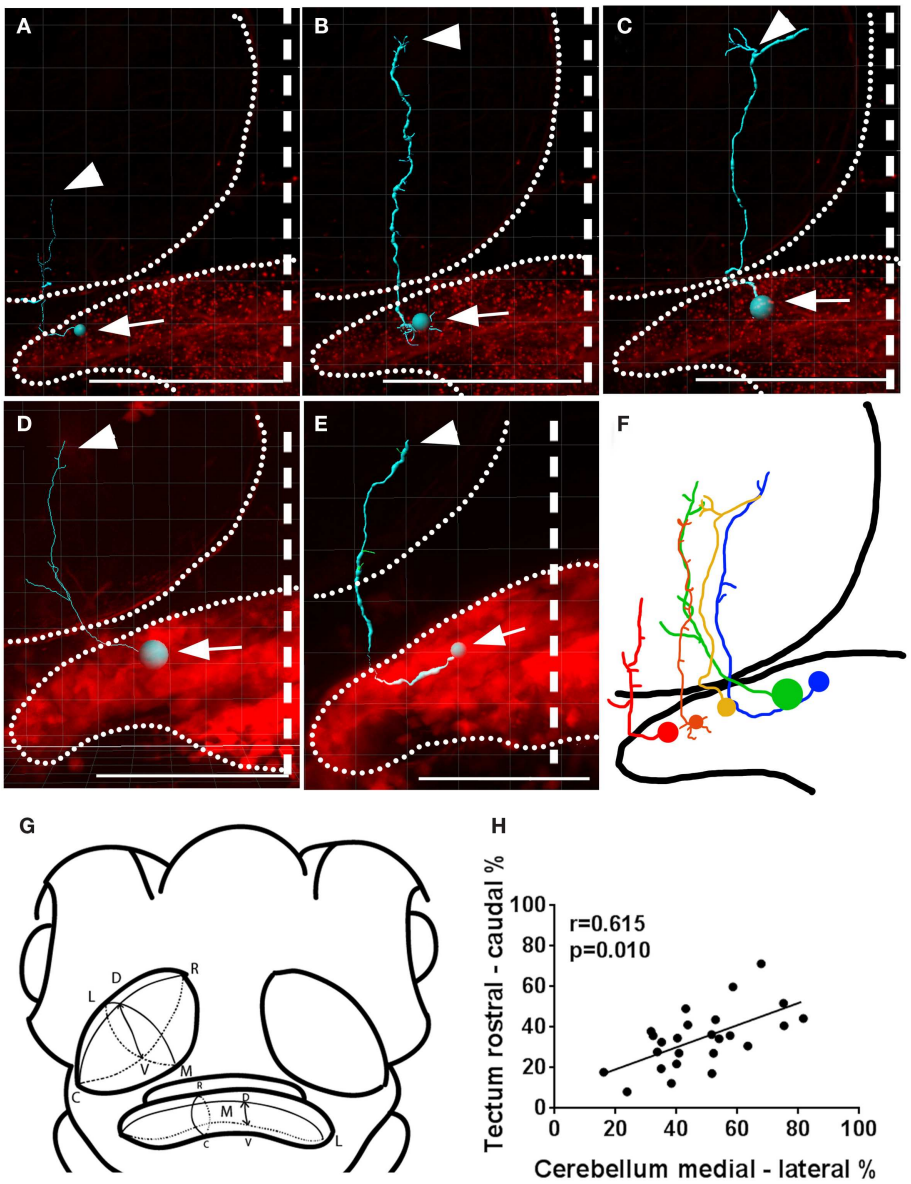

FIGURE 5 | Topography between the cerebellar medial-lateral and the tectal rostral-caudal axes. (A–E) Imaris tracings of individual eurydendroid cells with the cell bodies (arrows) and axonal terminals (arrowheads) indicated. The expression pattern as a whole is shown in red and the boundaries of the tectal neuropil and cerebellum are indicated with dotted lines. **(F)** A representation of cells in **(A–E)**, registered against one another spatially, both in the cerebellum and the tectal neuropil. **(G)** Shows the orientations in which the axes were measured in a way that compensates for the tectal neuropil's slanted orientation (R, rostral; C, caudal; M, medial; L, lateral; D, dorsal; V, ventral). **(H)** A correlation was found between the cell body position within the medial-lateral axis of the cerebellum and the rostral-caudal position of termination points within the tectal neuropil, as shown by a Pearson's product moment correlation, $r = 0.645$, $p = 0.010$. Larvae are 6 dpf with genotypes *Gal4^{s1168t}; UAS:mCherry, UAS:Brainbow* **(A–C)** or *Gal4^{s1168t}; UAS:Kaede:UAS; BGUG* **(D,E)**. Scale bars indicate 100 μm, and the midline is shown with a dashed line.

and the axon termination point along the rostral-caudal axis of the tectal neuropil (Pearson's correlation, $r = 0.615$, $p = 0.010$). Among the eurydendroid cells projecting exclusively to the tectum, the more medial ones project to the rostral parts of the optic tectum, and the more lateral ones project to caudal areas of the tectal neuropil (25 individual cells, $n = 21$ larvae, regression shown in **Figure 5H**). This topography was overlaid on a trend toward axon terminations in the rostral tectal neuropil, as a majority of all eurydendroid cells observed extended into the rostral half of the tectum (**Figure 5H**).

We continued this analysis to look for trends between all pairs of axes in the cerebellum and tectum, and (with the exception of the correlation described above) these showed little or no evidence for further topography (**Figure 6**). It should be noted that a significant correlation was found to exist between the medial-lateral axis of the cerebellum and the dorsal-ventral axis of the optic

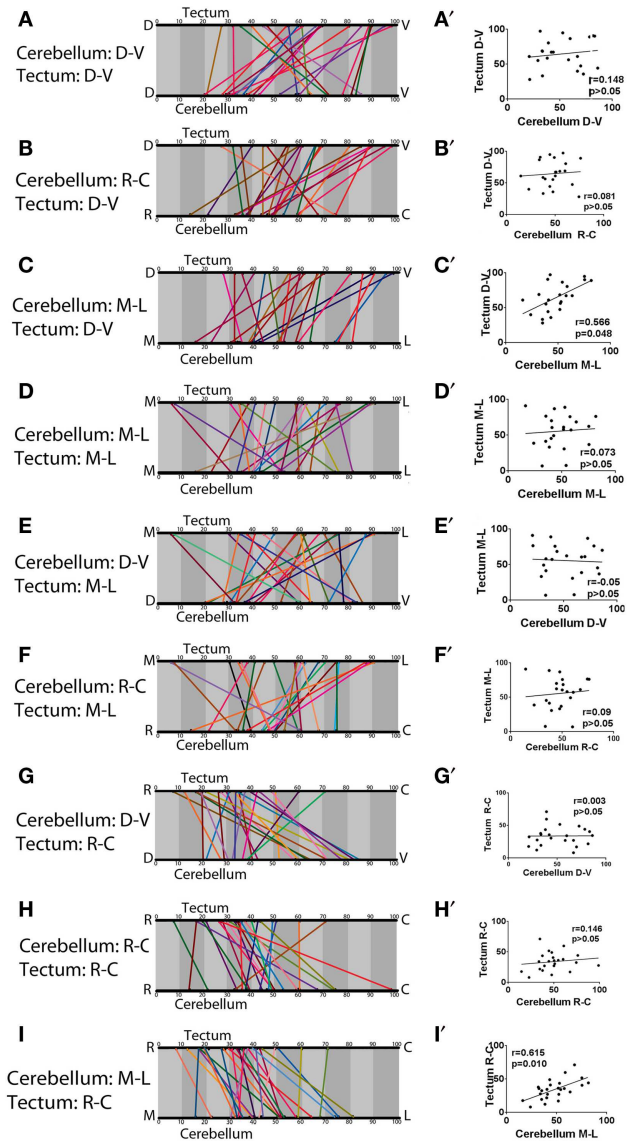

FIGURE 6 | A test for topography across all cerebellar and tectal axes. All pairs of axes between the cerebellum and tectum were compared to determine whether topography exists. The majority of comparisons showed no significant correlation. The exceptions are between the medial-lateral axis of the cerebellum and the dorsal-ventral axis of the tectum **(C)** (Pearson's r coefficient = 0.566, $p = 0.048$), and the medial-lateral axis of the cerebellum and rostral-caudal axis of the optic tectum **(I)**, also shown in **Figure 5**. (Pearson's $r = 0.615$, $p = 0.010$). **(A–I)** show linear representations of the cell body position and corresponding axon terminal position of each cell, represented as percentages along the indicated axes. **(A′–I′)** show scatter plots with each eurydendroid cell as a single point and a line of best fit.

tectum (**Figure 6C**) (Pearson's correlation, $r = 0.566$, $p = 0.048$). This, however, is likely a combined product of our measurement technique and the tectal neuropil's lens-shaped structure, rather than a biologically interesting pattern of connectivity. Since the tectal neuropil is thinner at its edges than its center, and since a majority of eurydendroid terminals are in the rostral neuropil, our more rostral terminals would show a higher percentage value on the dorsal-ventral axis, even if they are a set distance from the floor of the neuropil. Given the topography between the medial-lateral axis of the cerebellum and the rostral-caudal axis of the tectum, this introduces a bias that makes the medial eurydendroid cells, which terminate rostrally, appear to be in more dorsal layers of the neuropil. Direct measurements of the terminals' distances from the floor of the neuropil do not show a significant correlation with corresponding cell body positions in the medial-lateral axis of the cerebellum (Pearson's correlation, $r = -0.467$, $p = 0.263$), indicating that there is no important targeting between spatially distinct eurydendroid cells and different dorsal-ventral layers of the tectal neuropil.

DISCUSSION

TARGETS AND SPATIAL ORGANIZATION OF CEREBELLAR OUTPUT

In this study, we report the structural characteristics of eurydendroid cells, *en masse* and individually, in zebrafish larvae (**Figure 7**). We find that these neurons project principally to the tectal neuropil and the thalamus, and report a spatial logic in which the most medially positioned eurydendroid cells project axons through the tectal neuropil to the thalamus, while cells located throughout the remainder of the medial-lateral axis project exclusively to the tectal neuropil. Among these tectally projecting eurydendroid cells, we observe topography in which more medial eurydendroid cells extend axons to the rostral tectal neuropil while more lateral cells project to the caudal tectal neuropil. Eurydendroid axon terminals in the tectum are restricted to the deep layers of the neuropil, and since thalamus-bound eurydendroid axons also appear to synapse while passing through the tectal neuropil, these deep tectal targets receive a bulk of cerebellar output, at least among the cells represented in this study. Evidence supporting the existence of cerebellar output to the tectum has been previously observed in other teleost species including the scorpion fish (Murakami and Morita, 1987), long nose garfish (Northcutt, 1982), and catfish (Finger, 1983), although other studies have not observed these connections (Fiebig et al., 1983; Finger, 1983; Ikenaga et al., 2006). As well as the direct cerebello-tectal projections in teleost species, it has been shown that an indirect pathway between the valvula cerebellum and the optic tectum (via the torus semicircularis) exists (Folgueira et al., 2006, 2007). At a broad structural level, we did observe axons exiting the valvula cerebellum and terminating in the vicinity of the torus longitudinalis (Movie S1 in Supplementary Material), but these cells were not apparent in our single cell analysis, preventing us from comparing them to the ones described by Folgueira et al. (2006, 2007).

Surprisingly, projections to the hindbrain are faint in the *Gal4*^{s1168t} expression pattern as a whole, and are not represented in our single cell analysis. Since this output has been described previously in mammals (Armstrong and Harvey, 1966; Sedgwick and Williams, 1967), and teleosts (Szabo, 1983; Murakami and Morita, 1987; Wullimann and Northcutt, 1988; Bae et al., 2009) we believe that their absence from this analysis results from proportionally small numbers, the possibility that they fail to express Gal4 in the *Gal4*^{s1168t} line, or perhaps non-random labeling of cells using *BGUG* and variegated Brainbow. With this in mind, the results of this study should be viewed as a description of thalamic- and

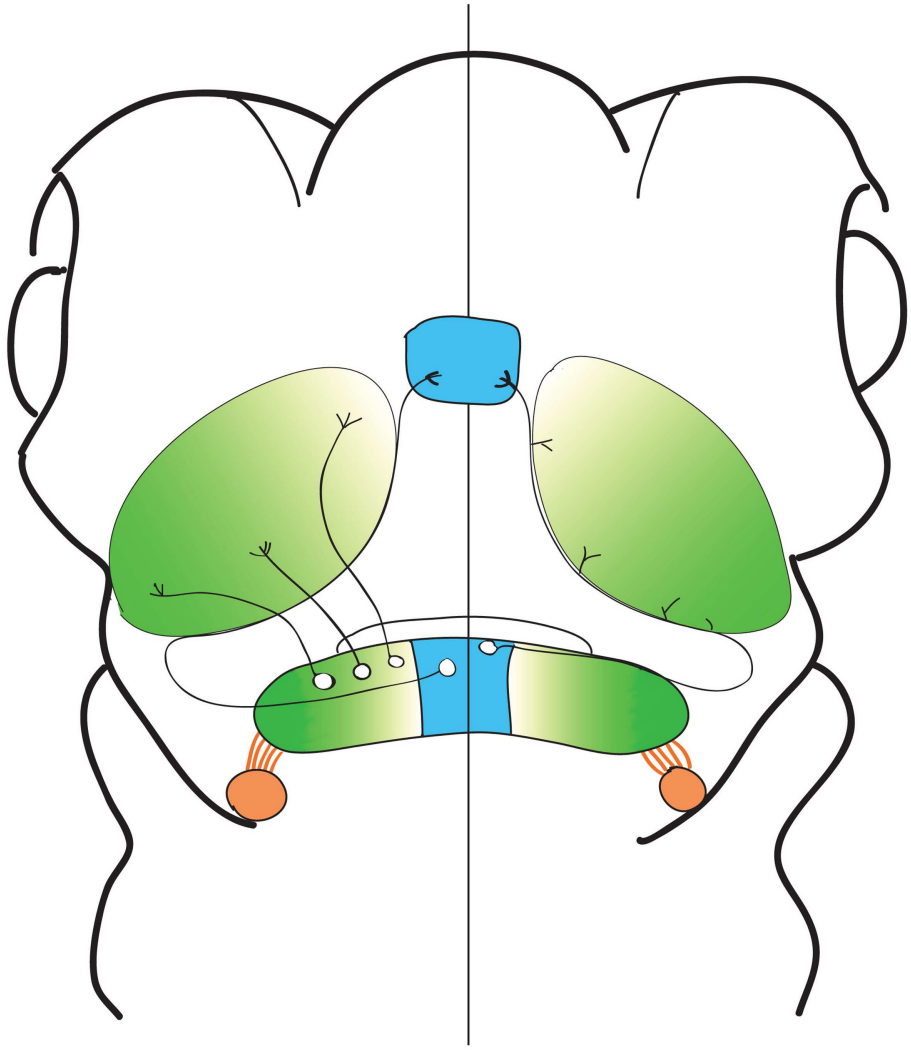

FIGURE 7 | Spatial patterns of eurydendroid projections. A cartoon representation of the observed spatial organization of cerebellar output. Areas sending output to the thalamus, represented in blue, were confined to the most medial portions of the cerebellum, and areas sending output exclusively to the tectal neuropil were spread across the remainder of the medial-lateral axis. Topography was seen in the output to the optic tectum, with more medial cells projecting to rostral areas of the tectum, and more lateral areas projecting to the caudal areas of the cerebellum, represented by green shading. Axon tracts were visualized connecting the eminentia granularis to the CC (orange shading), but this was not observed at a single cell level.

tectal-projecting eurydendroid cells rather than a comprehensive catalog of all cerebellar output in zebrafish larvae.

In adults of other teleost species, it has been shown that projections from the cerebellum are both contralateral and ipsilateral, with the majority being contralateral (Murakami and Morita, 1987; Ikenaga et al., 2006). In one case, the use of young adult fish indicated that the majority of eurydendroid cells projected ipsilaterally (Folgueira et al., 2006), and whether this is maintained in later-stage fish is uncertain. In contrast to this, all single cells that we have described project ipsilaterally. This raises the possibility that there is a gradual transition from ipsilateral cerebellar output early in development to predominantly contralateral output in adults. Other possibilities include sampling bias in our single cell labeling like that proposed above, or inter-species differences in the levels of midline crossing of cerebellar output axons.

EURYDENDROID DIVERSITY AND REGIONAL SPECIALIZATION IN THE CEREBELLUM

As described above, eurydendroid cells fill the same role in teleosts that the DCN do in mammals. Given the complexity of the DCN in terms of cell type diversity and connectivity, it is surprising that a single cell type could be sufficient for this role. In Japanese scorpion fish and goldfish, both teleosts, two subtypes of eurydendroid cells have been identified in adults that differ in terms of morphology, with either monopolar or multipolar morphologies (Murakami and Morita, 1987; Ikenaga et al., 2002). Efferent axons from monopolar eurydendroid cells are thought to project into the vicinity of the oculomotor complex, whereas multipolar cells project to all cerebellar targets (Murakami and Morita, 1987). Likewise, two categories of eurydendroid cells have been reported in zebrafish (Bae et al., 2009) and mormyrid fish (Meek et al.,

1986a,b), based on the presence or absence of *calretinin* expression, although the anatomical and functional correlates of this expression are unclear.

Here, we show that there are at least two subtypes of eurydendroid cell in the larval zebrafish cerebellum, and it is likely that additional subtypes, projecting to the hindbrain and elsewhere, are missed by the current analysis. One subtype projects to the tectum only, consistently terminates in the very deepest layers of the tectal neuropil, and forms a topographic map between the cerebellum and the tectum. The other projects to the thalamus, crossing the tectal neuropil *en route*. Within the tectal neuropil, these axons course through the ventral and medial margin, extending short processes axially into the neuropil. Assuming that the tips of these processes contain pre-synaptic terminals, it appears likely that they innervate a slightly more superficial layer than the tectum-only eurydendroid cells do (data not shown), although the small number of cells that we have described in this category precludes a quantitative confirmation of this observation. Previously, it has been shown that cerebellar output to the thalamus passes through the medial longitudinal fascicle in adult goldfish (Ikenaga et al., 2002). In contrast to this, we see monosynaptic cerebellar outputs to the thalamus passing along the medial edge of the optic tectum. These differences may be due either to the differences in age, suggesting a remodeling between larval and adult fish, or to a difference between zebrafish and goldfish.

The two subtypes' distinct targeting suggests that they may be playing different circuit roles, and therefore may be receiving distinct types of input. This possibility is supported by the spatial observation that medial eurydendroid cells project to the tectum and the thalamus while the remainder project only to the tectum. Characterization of the eurydendroid cell markers *calb2b* and *olig2* in the cerebellum has shown that they are expressed in a region specific manner, with medial (dorsal) eurydendroid cells expressing *olig2* and lateral (ventral) eurydendroid cells expressing *calb2b* (McFarland et al., 2008). This alignment of spatial characteristics between prior gene expression studies and our current anatomical work raises the possibility that our medial thalamic-projecting eurydendroid cells are the *olig2*-positive population and our more lateral tectal-projecting cells express *calb2b*. This suggests that regions of functional specialization across the cerebellar medial-lateral axis exist as is seen in mammals, where the DCN have distinct gene expression, physiology, connectivity, and behavioral relevance. A better understanding of these specialized regions in teleosts will await more detailed descriptions both of the inputs to different medial-lateral positions within the cerebellum and of the tectal and thalamic circuits into which these two types of eurydendroid cells synapse.

FUNCTIONAL IMPLICATIONS OF EURYDENDROID ANATOMY

Projections from the cerebellum to the thalamus have been described in numerous systems, including goldfish (Ikenaga et al., 2002), rainbow trout (Folgueira et al., 2006), and mammals including rats, humans, and dogs (Person et al., 1986; Aumann et al., 1994; Gallay et al., 2008). Indeed, in mammals, the thalamus is one of the primary targets of the DCN, and the cerebello-thalamo-cortical pathway is critical to cerebellar function as a whole. It is perhaps surprising that a minority of our mapped eurydendroid cells project to the thalamus, and that these appear also to innervate the optic tectum. We cannot judge whether this results from a sampling bias in our experiments or a relative de-emphasis of cerebello-thalamic signaling in zebrafish. The latter, however, is plausible, given dramatic differences in connectivity between the thalamus and the telencephalon in teleosts versus mammals (reviewed by Mueller, 2012). Teleosts have telencephalic structures broadly homologous to the mammalian cerebral cortex (Northcutt, 2006), but the degree to which they possess structures homologous to the neocortex is debated (Wullimann and Mueller, 2004; Ito and Yamamoto, 2009). Because of the differences between the forebrain structures in mammals and teleosts, it is likely that the storage and tuning of motor programs in the two are carried out differently, with correspondingly different demands on communication among the cerebellum, thalamus, and telencephalon. It is also possible that thalamic output in mammals is proportionally heavier as a result of the mammalian expansion of the cerebellar hemispheres, which provide output to the cerebral cortex via the thalamus.

The optic tectum, in contrast, receives the exclusive output of a majority of the eurydendroid cells that we have observed, and may be post-synaptic even to those fibers that continue on to the thalamus. The robustness of this connection between the cerebellum and the tectum may speak to a major role for the tectum in relaying cerebellar output in teleosts. Within the tectal neuropil, eurydendroid terminals are seen exclusively in the deep layers. This is not surprising, since the superficial layers are primarily retinorecipient (Stuermer, 1988). Deep layers receive processed visual information from superficial tectal layers (Del Bene et al., 2010), mechanosensory information from the lateral line, as well as auditory and somatosensory inputs (Nederstigt and Schellart, 1986; Kinoshita et al., 2006), and they also generate the tectum's output (Scott and Baier, 2009). These deep layers can therefore be viewed as a point of integration for several types of input, and as a result have the potential to produce output informed by a range of sensory and motor information (reviewed by Nevin et al., 2010). In larval zebrafish, output from the deep tectal layers goes to the superior raphe nucleus, the hindbrain reticular formation, the medulla oblongata, and possibly other targets (Sato et al., 2007; Scott and Baier, 2009). This puts the tectum in a position to blend sensory information with feedback from the cerebellum, and to relay this information to motor centers in the hindbrain.

The retino-tectal map is a textbook example of topography, where a retinal ganglion cell's position in the retina determines its axon's termination point in the tectum. The result is a spatial representation of the visual world in the tectum (or superior colliculus) that is conserved among vertebrates. In mammals, deep layers of the superior colliculus also have a topographic auditory map (Palmer and King, 1982), and these signals (along with visual signals from the retino-tectal map) contribute to the control of saccadic eye movements (Jay and Sparks, 1987a,b; Sparks and Hartwich-Young, 1989). Here, we report an additional topographic input to the tectum: that of the cerebellar eurydendroid cells. The implications of these overlaid topographic maps are not immediately obvious because the spatial underpinnings of tectal function are poorly understood in zebrafish (aside from retinal inputs). Since several of the modalities (auditory, visual,

somatosensory, and proprioceptive) involved in motor calibration have a spatial component, it is possible that the tectum serves as a location for registering these modalities against one another spatially. Further detailed descriptions of tectal inputs will be necessary to see whether this is indeed the case.

LIMITATIONS OF THIS STUDY, AND SUGGESTIONS FOR FURTHER RESEARCH

As is always the case with purely anatomical studies, our results merely provide clues as to how these circuits function. Describing a circuit in terms of its cell type diversity, spatial arrangement, and connectivity is a prerequisite for understanding how activity through that circuit can drive behavior, but it is only a start. In the case of the teleost cerebellum, it will be interesting to identify the upstream and downstream neurons and circuits, and to see how output from the cerebellum is integrated with sensory and motor information from throughout the body. It will also be important to link these anatomical descriptions to function. This will be best approached by observing patterns of eurydendroid activity during behaviors that depend on the cerebellum, and by testing the impacts of eurydendroid silencing on the performance of these behaviors. Ever-improving optical tools for studying connectivity, and for observing and manipulating neural activity, dovetail with the transparency of zebrafish larvae. The concurrent development of new behavioral readouts for motor coordination (McClenahan et al., 2012) and learning (Aizenberg and Schuman, 2011; Ahrens et al., 2012) in zebrafish make this an appealing avenue for future research into the structure and function of cerebellar circuits.

ACKNOWLEDGMENTS

The authors thank Andrew Thompson, Fahad Sultan, and Masahiko Hibi for providing suggestions that improved this manuscript. Filippo Del Bene generously provided the *UAS:mCherry* transgenic line, and technical support was provided by Andrew Thompson and Rebecca Dunning. This work was supported by an Australian Research Council Future Fellowship (FT110100887) and Discovery Project Grant (DP110103612) to Ethan K. Scott.

SUPPLEMENTARY MATERIAL

The Supplementary Material for this article can be found online at http://www.frontiersin.org/Neural_Circuits/10.3389/fncir.2013.00053/abstract

Movie S1 | A *z*-series of the Gal4s1168t; UAS:kaede line, in a 6 dpf larva. Image is dorsal side up, with the anterior to the top of the image. Interval between slices is 3.94 μm. Scale bar represents 100 μm.

Movie S2 | A *z*-series of the Gal4s1168t; UAS:kaede, UAS: syn-GFP line, 6 dpf, with photoconverted Kaede shown in red and synaptically targeted GFP shown as green. Image is dorsal side up, with the anterior to the top of the image. Interval between slices is 1.60 μm. Scale bar represents 100 μm.

Movies S3 and S4 | A *z*-series of a 6 dpf Gal4s1168t; UAS:kaede, UAS:BGUG larva with a pair of eurydendroid cells located in the medial cerebellum and projecting to the thalamus, and an intermediate eurydendroid cell projecting to the optic tectum. Supplementary Movie 3: A *z*-series of the green channel (GFP) shown in **Figures 4A′,B′**. Supplementary Movie 4: A *z*-series of the merged green and red channels (GFP and photoconverted Kaede) shown in **Figures 4A″,4B″**. Interval between slices is 1.60 μm. Scale bar represents 100 μm.

REFERENCES

Ahrens, B., Li, J. M., Orger, B., Robson, N., Schier, A. F., Engert, F., et al. (2012). Brain-wide neuronal dynamics during motor adaptation in zebrafish. *Nature* 485, 471–477.

Aizenberg, M., and Schuman, E. M. (2011). Cerebellar-dependent learning in larval zebrafish. *J. Neurosci.* 31, 8708–8712.

Albus, J. S. (1971). A theory of cerebellar function. *Math. Biosci.* 10, 25–61.

Ando, R., Hama, H., Yamamoto-Hino, M., Mizuno, H., and Miyawaki, A. (2002). An optical marker based on the UV-induced green-to-red photoconversion of a fluorescent protein. *Proc. Natl. Acad. Sci. U.S.A.* 99, 12651–12656.

Andrezik, J. A., Dormer, K. J., Foreman, R. D., and Person, R. J. (1984). Fastigial nucleus projections to the brain stem in beagles: pathways for autonomic regulation. *Neuroscience* 11, 497–507.

Armstrong, B. D., and Harvey, R. J. (1966). Responses in the inferior olive to stimulation of the cerebellar and cerebral cortices in the cat. *J. Physiol. (Lond.)* 187, 553–574.

Asakawa, K., Suster, M. L., Mizusawa, K., Nagayoshi, S., Kotani, T., Urasaki, A., et al. (2008). Genetic dissection of neural circuits by Tol2 transposon-mediated Gal4 gene and enhancer trapping in zebrafish. *Proc. Natl. Acad. Sci. U.S.A.* 105, 1255–1260.

Aumann, T. D., Rawson, J. A., Finkelstein, D. I., and Horne, M. K. (1994). Projections from the lateral and interposed cerebellar nuclei to the thalamus of the rat: a light and electron microscopic study using single and double anterograde labelling. *J. Comp. Neurol.* 349, 165–181.

Bae, Y. K., Kani, S., Shimizu, T., Tanabe, K., Nojima, H., Kimura, Y., et al. (2009). Anatomy of zebrafish cerebellum and screen for mutations affecting its development. *Dev. Biol.* 330, 406–426.

Bass, A. H. (1982). Evolution of the vestibulolateral lobe of the cerebellum in electroreceptive and nonelectroreceptive teleosts. *J. Morphol.* 174, 335–348.

Becanovic, K., Pouladi, M. A., Lim, R. S., Kuhn, A., Pavlidis, P., Luthi-Carter, R., et al. (2010). Transcriptional changes in Huntington disease identified using genome-wide expression profiling and cross-platform analysis. *Hum. Mol. Genet.* 19, 1438–1452.

Blakemore, S. J., Wolpert, D. M., and Frith, C. D. (1998). Central cancellation of self-produced tickle sensation. *Nat. Neurosci.* 1, 635–640.

Brand, A. H., and Perrimon, N. (1993). Targeted gene expression as a means of altering cell fates and generating dominant phenotypes. *Development* 118, 401–415.

Carey, M. R. (2011). Synaptic mechanisms of sensorimotor learning in the cerebellum. *Curr. Opin. Neurobiol.* 21, 609–615.

Collin, S. P., and Pettigrew, J. D. (1988). Retinal topography in reef teleosts. I. Some species with well-developed areae but poorly-developed streaks. *Brain Behav. Evol.* 31, 269–282.

Davison, J. M., Akitake, C. M., Goll, M. G., Rhee, J. M., Gosse, N., Baier, H., et al. (2007). Transactivation from Gal4-VP16 transgenic insertions for tissue-specific cell labeling and ablation in zebrafish. *Dev. Biol.* 304, 811–824.

Del Bene, F., Wyart, C., Robles, E., Tran, A., Looger, L., Scott, E. K., et al. (2010). Filtering of visual information in the tectum by an identified neural circuit. *Science* 330, 669–673.

Distel, M., Wullimann, M. F., and Koster, R. W. (2009). Optimized Gal4 genetics for permanent gene expression mapping in zebrafish. *Proc. Natl. Acad. Sci. U.S.A.* 106, 13365–13370.

Donarum, E. A., Stephan, D. A., Larkin, K., Murphy, E. J., Gupta, M., Senephansiri, H., et al. (2006). Expression profiling reveals multiple myelin alterations in murine succinate semialdehyde dehydrogenase deficiency. *J. Inherit. Metab. Dis.* 29, 143–156.

Dow, R. S., and Moruzzi, G. (1958). *The Physiology and Pathology of the Cerebellum*. Minneapolis: The University of Minnesota Press.

Eccles, J. D. (1971). Functional significance of arrangement of neurones in cell assemblies. *Arch. Psychiatr. Nevenkr.* 215, 92–106.

Emmenlauer, M., Ronneberger, O., Ponti, A., Schwarb, P., Griffa, A., Filippi, A., et al. (2009). XuvTools: free, fast and reliable stitching of large 3D datasets. *J. Microsc.* 233, 42–60.

Feng, G., Mellor, R. H., Bernstein, M., Keller-Peck, C., Nguyen, Q. T., Wallace, M., et al. (2000). Imaging neuronal subsets in transgenic mice expressing multiple spectral variants of GFP. *Neuron* 28, 41–51.

Fiebig, E., Ebbesson, S. O. E., and Meyerm, D. L. (1983). Afferent connections of the optic tectum in the piranha (*Serrasalmus nattereri*). *Cell Tissue Res.* 231, 55–72.

Finger, T. E. (1983). Organization of the teleost cerebellum. *Fish Neurobiol.* 1, 261–284.

Folgueira, M., Anadon, R., and Yanez, J. (2006). Afferent and efferent connections of the cerebellum of a salmonid, the rainbow trout (*Oncorhynchus mykiss*): a tract-tracing study. *J. Comp. Neurol.* 497, 542–565.

Folgueira, M., Sueiro, C., Rodriguez-Moldes, I., Yanez, J., and Anadon, R. (2007). Organization of the torus longitudinalis in the rainbow trout (*Oncorhynchus mykiss*): an immunohistochemical study of the GABAergic system and a DiI tract-tracing study. *J. Comp. Neurol.* 503, 348–370.

Friedrich, R. W., Jacobson, G. A., and Zhu, P. (2010). Circuit neuroscience in zebrafish. *Curr. Biol.* 20, R371–R381.

Gallay, M. N., Jeanmonod, D., Liu, J., and Morel, A. (2008). Human pallidothalamic and cerebellothalamic tracts: anatomical basis for functional stereotactic neurosurgery. *Brain Struct. Funct.* 212, 443–463.

Glickstein, M., Sultan, F., and Voogd, J. (2011). Functional localization in the cerebellum. *Cortex* 47, 59–80.

Hepp, K., Henn, V., and Jaeger, J. (1982). Eye movement related neurons in the cerebellar nuclei of the alert monkey. *Exp. Brain Res.* 45, 253–264.

Hibi, M., and Shimizu, T. (2012). Development of the cerebellum and cerebellar neural circuits. *Dev. Neurobiol.* 72, 282–301.

Hoebeek, F. E., Witter, L., Ruigrok, T. J., and De Zeeuw, C. I. (2010). Differential olivo-cerebellar cortical control of rebound activity in the cerebellar nuclei. *Proc. Natl. Acad. Sci. U.S.A.* 107, 8410–8415.

Ikenaga, T., Yoshida, M., and Uematsu, K. (2002). Efferent connections of the cerebellum of the goldfish, *Carassius auratus*. *Brain Behav. Evol.* 60, 36–51.

Ikenaga, T., Yoshida, M., and Uematsu, K. (2006). Cerebellar efferent neurons in teleost fish. *Cerebellum* 5, 268–274.

Ito, H., and Yamamoto, N. (2009). Nonlaminar cerebral cortex in teleost fishes? *Biol. Lett.* 5, 117–121.

Jay, M. F., and Sparks, D. L. (1987a). Sensorimotor integration in the primate superior colliculus. I. Motor convergence. *J. Neurophysiol.* 57, 22–34.

Jay, M. F., and Sparks, D. L. (1987b). Sensorimotor integration in the primate superior colliculus. II. Coordinates of auditory signals. *J. Neurophysiol.* 57, 35–55.

Kani, S., Bae, Y. K., Shimizu, T., Tanabe, K., Satou, C., Parsons, M. J., et al. (2010). Proneural gene-linked neurogenesis in zebrafish cerebellum. *Dev. Biol.* 343, 1–17.

Kawakami, K. (2004). Transgenesis and gene trap methods in zebrafish by using the Tol2 transposable element. *Methods Cell Biol.* 77, 201–222.

Kinoshita, M., Ito, E., Urano, A., Ito, H., and Yamamoto, N. (2006). Periventricular efferent neurons in the optic tectum of rainbow trout. *J. Comp. Neurol.* 499, 546–564.

Kotani, T., Nagayoshi, S., Urasaki, A., and Kawakami, K. (2006). Transposon-mediated gene trapping in zebrafish. *Methods* 39, 199–206.

Kwan, K. M., Fujimoto, E., Grabher, C., Mangum, B. D., Hardy, M. E., Campbell, D. S., et al. (2007). The Tol2kit: a multisite gateway-based construction kit for Tol2 transposon transgenesis constructs. *Dev. Dyn.* 236, 3088–3099.

Laplante, M., Kikuta, H., König, M., and Becker, T. S. (2006). Enhancer detection in the zebrafish using pseudotyped murine retroviruses. *Methods* 39, 189–198.

Li, L., Tasic, B., Micheva, K. D., Ivanov, V. M., Spletter, M. L., Smith, S. J., et al. (2010). Visualizing the distribution of synapses from individual neurons in the mouse brain. *PLoS ONE* 5:e11503. doi:10.1371/journal.pone.0011503

Lister, J. A., Robertson, C. P., Lepage, T., Johnson, S. L., and Raible, D. W. (1999). Nacre encodes a zebrafish microphthalmia-related protein that regulates neural-crest-derived pigment cell fate. *Development* 126, 3757–3767.

Livet, J., Weissman, T. A., Kang, H., Draft, R. W., Lu, J., Bennis, R. A., et al. (2007). Transgenic strategies for combinatorial expression of fluorescent proteins in the nervous system. *Nature* 450, 56–62.

Longair, M. H., Baker, D. A., and Armstrong, J. D. (2011). Simple neurite tracer: open source software for reconstruction, visualization and analysis of neuronal processes. *Bioinformatics* 27, 2453–2454.

Luo, L., Callaway, E. M., and Svoboda, K. (2008). Genetic dissection of neural circuits. *Neuron* 57, 634–660.

McClenahan, P., Troup, M., and Scott, E. K. (2012). Fin-tail coordination during escape and predatory behavior in larval zebrafish. *PLoS ONE* 7:e32295. doi:10.1371/journal.pone.0032295

McFarland, K. A., Topczewska, J. M., Weidinger, G., Dorsky, R. I., and Appel, B. (2008). Hh and Wnt signaling regulate formation of olig2+ neurons in the zebrafish cerebellum. *Dev. Biol.* 318, 162–171.

Meek, J., Nieuwenhuys, R., and Elsavier, D. (1986a). Afferent and efferent connections of cerebellar lobe C_1 of the mormyrid fish *Gnathonemus petersi*: an HRP study. *J. Comp. Neurol.* 245, 319–341.

Meek, J., Nieuwenhuys, R., and Elsevier, D. (1986b). Afferent and efferent connections of cerebellar lobe C3 of the mormyrid fish *Gnathonemus petersi*: an HRP study. *J. Comp. Neurol.* 245, 342–358.

Meyer, M. P., and Smith, S. J. (2006). Evidence from in vivo imaging that synaptogenesis guides the growth and branching of axonal arbors by two distinct mechanisms. *J. Neurosci.* 26, 3604–3614.

Miall, R. C., Weir, D. J., Wolpert, D. M., and Stein, J. F. (1993). Is the cerebellum a smith predictor? *J. Mot. Behav.* 25, 203–216.

Miles, F. A., and Lisberger, S. G. (1981). Plasticity in the vestibulo-ocular reflex: a new hypothesis. *Annu. Rev. Neurosci.* 4, 273–299.

Miyamura, Y., and Nakayasu, H. (2001). Zonal distribution of Purkinje cells in the zebrafish cerebellum: analysis by means of a specific monoclonal antibody. *Cell Tissue Res.* 305, 299–305.

Mueller, T. (2012). What is the thalamus in zebrafish? *Front. Neurosci.* 6:64. doi:10.3389/fnins.2012.00064

Murakami, T., and Morita, Y. (1987). Morphology and distribution of the projection neurons in the cerebellum in a teleost, *Sebastiscus marmoratus*. *J. Comp. Neurol.* 256, 607–623.

Nederstigt, L. J., and Schellart, N. A. (1986). Acousticolateral processing in the torus semicircularis of the trout *Salmo gairdneri*. *Pflugers Arch.* 406, 151–157.

Nevin, L. M., Robles, E., Baier, H., and Scott, E. K. (2010). Focusing on optic tectum circuitry through the lens of genetics. *BMC Biol.* 8:126. doi:10.1186/1741-7007-8-126

Niell, C. M., Meyer, M. P., and Smith, S. J. (2004). In vivo imaging of synapse formation on a growing dendritic arbor. *Nat. Neurosci.* 7, 254–260.

Northcutt, R. G. (1982). Localization of neurons afferent to the optic tectum in longnose gars. *J. Comp. Neurol.* 204, 325–335.

Northcutt, R. G. (2006). Connections of the lateral and medial divisions of the goldfish telencephalic pallium. *J. Comp. Neurol.* 494, 903–943.

Palmer, A. R., and King, A. J. (1982). The representation of auditory space in the mammalian superior colliculus. *Nature* 299, 248–249.

Person, R. J., Andrezik, J. A., Dormer, K. J., and Foreman, R. D. (1986). Fastigial nucleus projections in the midbrain and thalamus in dogs. *Neuroscience* 18, 105–120.

Sajovic, P., and Levinthal, C. (1982). Visual cells of zebrafish optic tectum: mapping with small spots. *Neuroscience* 7, 2407–2426.

Sato, T., Hamaoka, T., Aizawa, H., Hosoya, T., and Okamoto, H. (2007). Genetic single-cell mosaic analysis implicates ephrinB2 reverse signaling in projections from the posterior tectum to the hindbrain in zebrafish. *J. Neurosci.* 27, 5271–5279.

Scheer, N., and Campos-Ortega, J. A. (1999). Use of the Gal4-UAS technique for targeted gene expression in the zebrafish. *Mech. Dev.* 80, 153–158.

Scott, E. K. (2009). The Gal4/UAS toolbox in zebrafish: new approaches for defining behavioral circuits. *J. Neurochem.* 110, 441–456.

Scott, E. K., and Baier, H. (2009). The cellular architecture of the larval zebrafish tectum, as revealed by gal4 enhancer trap lines. *Front. Neural Circuits* 3:13. doi:10.3389/neuro.04.013.2009

Scott, E. K., Mason, L., Arrenberg, A. B., Ziv, L., Gosse, N. J., Xiao, T., et al. (2007). Targeting neural circuitry in zebrafish using GAL4 enhancer trapping. *Nat. Methods* 4, 323–326.

Sedgwick, E. M., and Williams, T. D. (1967). Responses of single units in the inferior olive to stimulation of the limb nerves, peripheral skin receptors, cerebellum, caudate nucleus and motor cortex. *J. Physiol. (Lond.)* 189, 261–279.

Simmich, J., Staykov, E., and Scott, E. (2012). Zebrafish as an appealing model for optogenetic studies. *Prog. Brain Res.* 196, 145–162.

Simpson, H. D., Kita, E. M., Scott, E. K., and Goodhill, G. J. (2013). A quantitative analysis of branching, growth cone turning and directed growth in zebrafish retinotectal axon guidance. *J. Comp. Neurol.* 521, 1409–1429.

Sparks, D. L., and Hartwich-Young, R. (1989). The deep layers of the superior colliculus. *Rev. Oculomot. Res.* 3, 213–255.

Stuermer, C. A. (1988). Retinotopic organization of the developing retinotectal projection in the

zebrafish embryo. *J. Neurosci.* 8, 4513–4530.

Sultan, F., Augath, M., Hamodeh, S., Murayama, Y., Oeltermann, A., Rauch, A., et al. (2012). Unravelling cerebellar pathways with high temporal precision targeting motor and extensive sensory and parietal networks. *Nat. Commun.* 3, 924.

Szabo, T. (1983). Cerebellar pathways in the brain of the mormyrid teleost fish. *Acta Morphol. Hung.* 31, 219–234.

Thach, W. T. (1968). Discharge of Purkinje and cerebellar nuclear neurons during rapidly alternating arm movements in the monkey. *J. Neurophysiol.* 31, 785–797.

Thierry-Mieg, D., and Thierry-Mieg, J. (2006). AceView: a comprehensive cDNA-supported gene and transcripts annotation. *Genome Biol.* 7(Suppl. 1–12), 1–14.

Tseng, Y. W., Diedrichsen, J., Krakauer, J. W., Shadmehr, R., and Bastian, A. J. (2007). Sensory prediction errors drive cerebellum-dependent adaptation of reaching. *J. Neurophysiol.* 98, 54–62.

Westerfield, M. (2000). *The Zebrafish Book. A Guide for the Laboratory Use of Zebrafish (Danio rerio)*, 4th Edn. Eugene: University of Oregon Press.

Wullimann, M. F., and Mueller, T. (2004). Teleostean and mammalian forebrains contrasted: evidence from genes to behavior. *J. Comp. Neurol.* 475, 143–162.

Wullimann, M. F., and Northcutt, R. G. (1988). Connections of the corpus cerebelli in the green sunfish and the common goldfish: a comparison of perciform and cypriniform teleosts. *Brain Behav. Evol.* 32, 293–316.

Wyart, C., Del Bene, F., Warp, E., Scott, E. K., Trauner, D., Baier, H., et al. (2009). Optogenetic dissection of a behavioural module in the vertebrate spinal cord. *Nature* 461, 407–410.

Xiao, T., Roeser, T., Staub, W., and Baier, H. (2005). A GFP-based genetic screen reveals mutations that disrupt the architecture of the zebrafish retinotectal projection. *Development* 132, 2955–2967.

Zapala, M. A., Hovatta, I., Ellison, J. A., Wodicka, L., Del Rio, J. A., Tennant, R., et al. (2005). Adult mouse brain gene expression patterns bear an embryologic imprint. *Proc. Natl. Acad. Sci. U.S.A.* 102, 10357–10362.

Zhang, Y., Magnus, G., and Han, V. Z. (2008). Local circuitry in the anterior lateral caudal lobe of the mormyrid cerebellum: a study of intracellular recording and labelling. *J. Comp. Neurol.* 509, 1–22.

Conflict of Interest Statement: The authors declare that the research was conducted in the absence of any commercial or financial relationships that could be construed as a potential conflict of interest.

Received: 30 January 2013; paper pending published: 14 February 2013; accepted: 09 March 2013; published online: 01 April 2013.

Citation: Heap LA, Goh CC, Kassahn KS and Scott EK (2013) Cerebellar output in zebrafish: an analysis of spatial patterns and topography in eurydendroid cell projections. Front. Neural Circuits ***7****:53. doi: 10.3389/fncir.2013.00053*

frontiers in
NEURAL CIRCUITS

REVIEW ARTICLE
published: 26 March 2013
doi: 10.3389/fncir.2013.00047

Developmental and architectural principles of the lateral-line neural map

Jesús Pujol-Martí and Hernán López-Schier*

Research Unit of Sensory Biology and Organogenesis, Helmholtz Zentrum München, Neuherberg, Munich, Germany

Edited by:
Gonzalo G. De Polavieja, Instituto Cajal - Consejo Superior de Investigaciones Científicas, Spain

Reviewed by:
Vivek Jayaraman, Janelia Farm Research Campus, Howard Hughes Medical Institute, USA
Claire Wyart, Brain and Spinal Cord Institute, Paris, France

****Correspondence:***
Hernán López-Schier, Research Unit of Sensory Biology and Organogenesis, Helmholtz Zentrum München, Ingolstädter Landstrasse 1, 85764 Neuherberg, Munich, Germany.
e-mail: hernan.lopez-schier@helmholtz-muenchen.de

The transmission and central representation of sensory cues through the accurate construction of neural maps is essential for animals to react to environmental stimuli. Structural diversity of sensorineural maps along a continuum between discrete- and continuous-map architectures can influence behavior. The mechanosensory lateral line of fishes and amphibians, for example, detects complex hydrodynamics occurring around the animal body. It triggers innate fast escape reactions but also modulates complex navigation behaviors that require constant knowledge about the environment. The aim of this article is to summarize recent work in the zebrafish that has shed light on the development and structure of the lateralis neural map, which is helping to understand how individual sensory modalities generate appropriate behavioral responses to the sensory context.

Keywords: lateral line, Mauthner, behavior, neural circuit, hair cells, auditory, somatotopy

INTRODUCTION

The sensation of external stimuli is essential for all life forms to react appropriately to environmental cues. Even the simplest animals are endowed with sensory systems. For example, changes in light intensity directly affect the activity of cilia in the photoreceptor cells of sponge larvae, which influences local motor responses (Leys and Degnan, 2001). It is the higher probability of a biased individual action of ciliary movement that directs swimming along the luminosity gradient. In more complex animals, the evolution of neurons and a centralized nervous system allows sensory organs to control the activity of motor centers in a coordinated manner, thereby improving the speed and accuracy of sensory-motor transformations (Moroz, 2009; Jékély, 2011; Arber, 2012; Northcutt, 2012). The meaningful use of dynamic sensory stimuli is a complex computational problem. Sensory systems can optimize a solution by combining the acquisition and processing of the quality, quantity and spatial distribution of the stimuli (Chaudhari and Roper, 2010; DeMaria and Ngai, 2010; Lumpkin et al., 2010; Schwander et al., 2010; Sung and Chuang, 2010; Chacron et al., 2011). This can be achieved via two architectural properties of the sensory systems: the structure of the peripheral receptors, which is important for information acquisition and filtering, and the neural representation of the information, which is essential for consistent sensory processing.

High-order processing of sensory information largely relies on the accurate construction of spatially arranged neuronal projections, known as neural maps (Gardner and Martin, 2000; Luo and Flanagan, 2007; Feldheim and O'Leary, 2010; Imai et al., 2010). Neural maps appear to be a universal solution to this problem because they are present in phylogenetically distant animals and in diverse sensory systems (Knudsen et al., 1987; Kaas, 1997; Weinberg, 1997). For example, the visual system of invertebrates and vertebrates exhibits a neural projection structure known as retinotopic map, in which nearby positions in the sensory region project afferent neurons onto nearby regions of the brain (Lemke and Reber, 2005; Feldheim and O'Leary, 2010). Neural maps showing this arrangement encode positional information and are called continuous or topographic. Other sensory systems show qualitatively different map architecture, known as discrete, whereby discrete information such as stimulus identity is separately represented in the brain (Luo and Flanagan, 2007). This is the case of the olfactory systems in which each odor is encoded by a unique ensemble of neurons without any spatial arrangement in relation to the olfactory area (Imai et al., 2010). Some sensory modalities, however, construct neural maps that fall between the discrete and the continuous (topographic; Scheich, 1991).

The superficial mechanosensory lateral line in fishes and amphibians combines some structural and physiological characteristics of the mammalian vestibulo-auditory and somatosensory systems. It comprises the three basic elements of a vertebrate sensory system: peripheral receptors, intermediate afferent transmission elements, and central processing units (Winklbauer, 1989; Ghysen and Dambly-Chaudière, 2007; Bleckmann and Zelick, 2009). The peripheral organs are a group of mechanoreceptive neuromasts, which locally acquire mechanical signals using their sensory elements called hair cells. The spatial sensitivity of the lateral line is about one body length from the surface of the animal, for which it also receives the name of "sense of distant touch" (Engelmann et al., 2000; Coombs, 2001). Hair cells transform mechanical stimuli into chemical signals that are further converted into electrical impulses that lateralis afferent neurons transport to the brain (Hudspeth, 1989; Chagnaud et al., 2007; Bleckmann and Zelick, 2009; Schwander et al., 2010). This first-order neuronal population projects central axons to contact second-order output

neurons located in the medial octavolateralis nucleus (MON) of the hindbrain. From this first relay center, most lateral-line information is transmitted to the torus semicircularis (TS) in the midbrain (Bleckmann, 2008). The TS is equivalent to the mammalian inferior colliculus, which is a major target of auditory information (Barrett, 1973; Wubbels and Schellart, 1997).

The lateral line is able to localize fast-changing mechanical signals in three dimensions around the animal's body and provides essential sensory information for centrally controlled complex motor behaviors such as navigation, schooling, rheotaxis, and prey tracking (Montgomery et al., 1997, 2000; Coombs et al., 1998; Bleckmann, 2008; Goulet et al., 2008; Bleckmann and Zelick, 2009; Chaudhari and Roper, 2010). It also mediates fast reflex reactions mediated by a large reticulospinal neuron called Mauthner cell (Zottoli and Van Horne, 1983; Metcalfe et al., 1985). The lateral line, therefore, is a prime example of a sensory system that commands contrasting behaviors in response to a unique sensory cue: mechanical fluctuations of the surrounding fluid (Engelmann et al., 2000; Chagnaud et al., 2007). How does the architecture of the lateralis neural map allow for a robust and accurate information flow from the sensory receptors to brain areas underlying the different behaviors? In this review we will discuss this question using recent studies in the zebrafish that provide important insights about lateral-line neural map development and architecture. We will also use the current knowledge and technological state-of-the-art to anticipate research directions of this important problem in neurobiology.

BACKGROUND

DEVELOPMENT AND ORGANIZATION OF THE LATERAL-LINE SENSORY RECEPTORS

Most of what we know about the development and organization of the zebrafish lateral line comes from studies on the posterior aspect of the system, which comprises all the elements associated to the neuromasts on the trunk of the animal. The posterior lateral line develops early during embryogenesis from bilateral cephalic placodes. At around 18 hpf (hours post-fertilization) a first placode appears just caudal to the ear and gives rise to neuroblast precursors of the lateralis afferent neurons, and to a moving group of cells known as first primordium (primI; **Figure 1A**). At around 20 hpf the primI begins to migrate toward the tail along the horizontal myoseptum. During a journey lasting about 20 h it deposits an average of eight cellular rosettes that will eventually differentiate into neuromasts (Ghysen and Dambly-Chaudière, 2007). Few hours after primI, a second placode arises at the same place of origin of primI. This placode splits into several groups of cells. One group directly differentiates on location as the so-called D1 neuromast, which together with primI-derived neuromasts form the primary posterior lateral line. The two other groups of cells form the migratory second and dorsal primordia (primII and primD). PrimII deposits two or three neuromasts along the trail of primI. PrimD follows an upward path to produce two neuromasts on the dorsum of the fry. These later-born neuromasts form the secondary posterior lateral line (**Figure 1A**; Ghysen and Dambly-Chaudière, 2007).

A mature neuromast consists of a core of 20–30 mechanosensory hair cells surrounded by a similar number of non-sensory supporting cells (**Figure 1B**). Hair cells derive their name from the hair bundle, a mechanosensing organelle that protrudes from the cell's apical surface. In the neuromast, hair bundles are contained within a gelatinous cupula that projects into the surrounding water. The hair bundle is formed by an array of stereocilia arranged in rows of increasing length, like a staircase, and a kinocilium eccentrically located adjacent to the tallest stereocilia. In this way, each hair bundle and thus, each hair cell, is polarized within the plane of the neuromast epithelium (Duvall et al., 1966; Ghysen and Dambly-Chaudière, 2007). A mechanical deflection of the stereocilia toward the kinocilium depolarizes the cell, whereas a deflection away from the kinocilium hyperpolarizes it (Hudspeth, 1989). Therefore, the polarity of hair bundle endows hair cells with vectorial excitability. Each neuromast contains two intermingled populations of hair cells, equal in number, whose stereocilia are oriented along a single axis but in opposite directions (**Figures 1B** and **C**; Rouse and Pickles, 1991; López-Schier et al., 2004). Thus, each neuromast is mechanically bidirectional sensitive. Furthermore, two types of neuromasts have been described according to the planar polarization of their hair cells. Parallel neuromasts are oriented along the animal's anteroposterior body axis, whereas perpendicular neuromasts orient orthogonally (**Figure 1C**; López-Schier et al., 2004). Parallel and perpendicular neuromasts originate from different primordia. While all primI-derived neuromasts and the D1 neuromast are parallel, primII-derived neuromasts and those deposited by primD are perpendicular. Consequently, the posterior lateral line from the one-week old zebrafish larva consists of about 14 neuromasts that occupy stereotypical positions covering the dorsal and lateral aspects of the fish's trunk and that are able to locally detect bidirectional mechanical signals at orthogonal axes (**Figure 1A**).

DEVELOPMENT OF THE LATERALIS AFFERENT NEURONS

Pioneering studies on the development of the lateral line in the zebrafish have shown that the first placode, which gives rise to primI, also generates lateralis afferent neurons. Lateralis afferents begin to project central and peripheral axons concurrently as soon as they differentiate. Growing central axons extend toward the hindbrain whereas peripheral axons project growth cones that follow the migrating primI and eventually innervate each deposited neuromasts (**Figure 2A**; Gompel et al., 2001; Ghysen and Dambly-Chaudière, 2007). The use of newly developed tools for cellular birth dating has shown that lateralis neurogenesis during embryonic development occurs in two discrete waves (Sarrazín et al., 2010). The earliest differentiating neurons extend their peripheral axons to the adjacent primI, which expresses the glial-derived neurotrophic factor (GDNF) that likely acts as a short-range attractive cue for the axons (Schuster et al., 2010). High local levels of GDNF tow these early axons along as the primI migrates all the way to the tail of the fish. Following neurons begin to extend their axons after primI has migrated some distance. These axons arrest elongation earlier and innervate more anterior neuromasts. Increasingly younger neurons first project their axons as the primI is further away. They arrest elongation even earlier to innervate the most anterior primary neuromasts (Pujol-Martí et al., 2010). The second wave of neurogenesis occurs coincidentally with the formation of the primII and primD primordial (Sarrazín et al., 2010). The

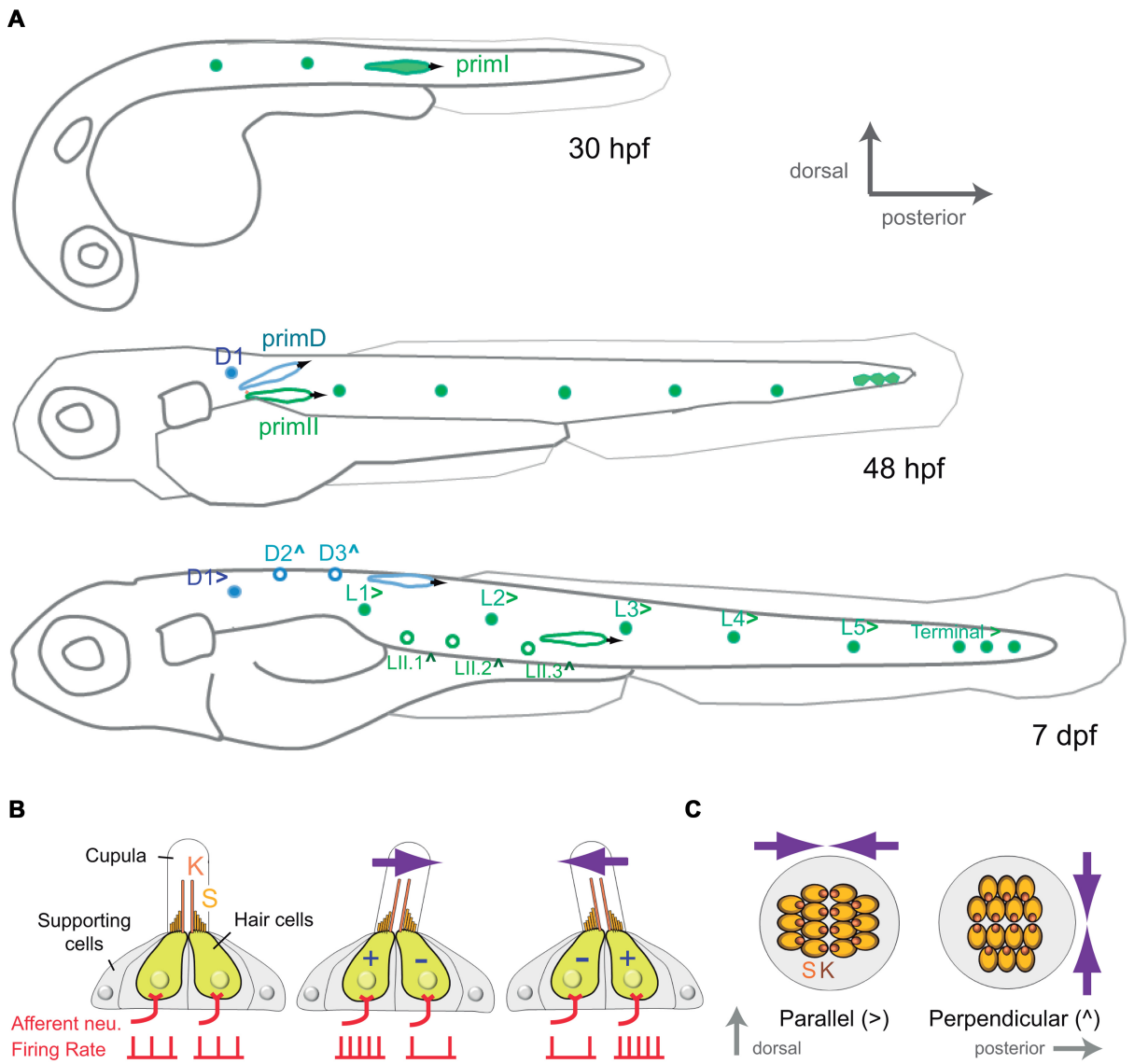

FIGURE 1 | Development and organization of the posterior lateral-line sensory receptors. (A) Lateral view of a developing zebrafish at around 30, 48 hpf and 7 dpf (days post-fertilization) showing the development of the mechanoreceptive neuromasts that form the posterior lateral line. primI, first primordium; primII, second primordium; primD, dorsal primordium. (>) and (^) indicate parallel and perpendicular neuromasts, respectively. **(B)** Lateral view of a neuromast. The hair-bundle comprises the kinocilium (K) and the stereocilia (S), and is contained within a gelatinous cupula. A neuromast contains two populations of hair cells of opposing hair-bundle polarities. Thus, a water movement (blue arrow) bending the cupula in a given direction depolarizes (+) one population of hair cells, whereas hyperpolarizes (–) the other one. This is translated into an increase or a decrease of the firing rate of the afferent neuron associated to each hair-cell population. **(C)** Top view of a parallel and a perpendicular neuromast, which are sensitive to water movements across orthogonal axes.

axons of these new neurons follow these primordia and innervate their neuromasts. Some younger neurons also innervate primary neuromasts. At the end of the process, primary (older) neuromasts are innervated by first- and second-wave neurons, whereas secondary (younger) neuromasts are only innervated by neurons from the second wave (**Figure 2A**; Pujol-Martí et al., 2012).

ORGANIZATION OF THE LATERALIS AFFERENT NEURONS

Pioneering neuroanatomical studies have shown that neurons that innervate anterior neuromasts project central axons to ventrolateral locations in the hindbrain, whereas neurons innervating more posterior neuromasts project dorsomedially (Alexandre and Ghysen, 1999). Therefore, it appears that the lateral line builds a continuous neural map by which the position of the lateralis afferents' central axons along the dorsoventral projection column in the hindbrain reflects the spatial distribution of the neuromasts in the periphery (**Figure 2A**; Alexandre and Ghysen, 1999; Gompel et al., 2001; Luo and Flanagan, 2007). This type of neural-map organization receives the name of somatotopic. Of note, although some authors rightly point out that the lateralis neural

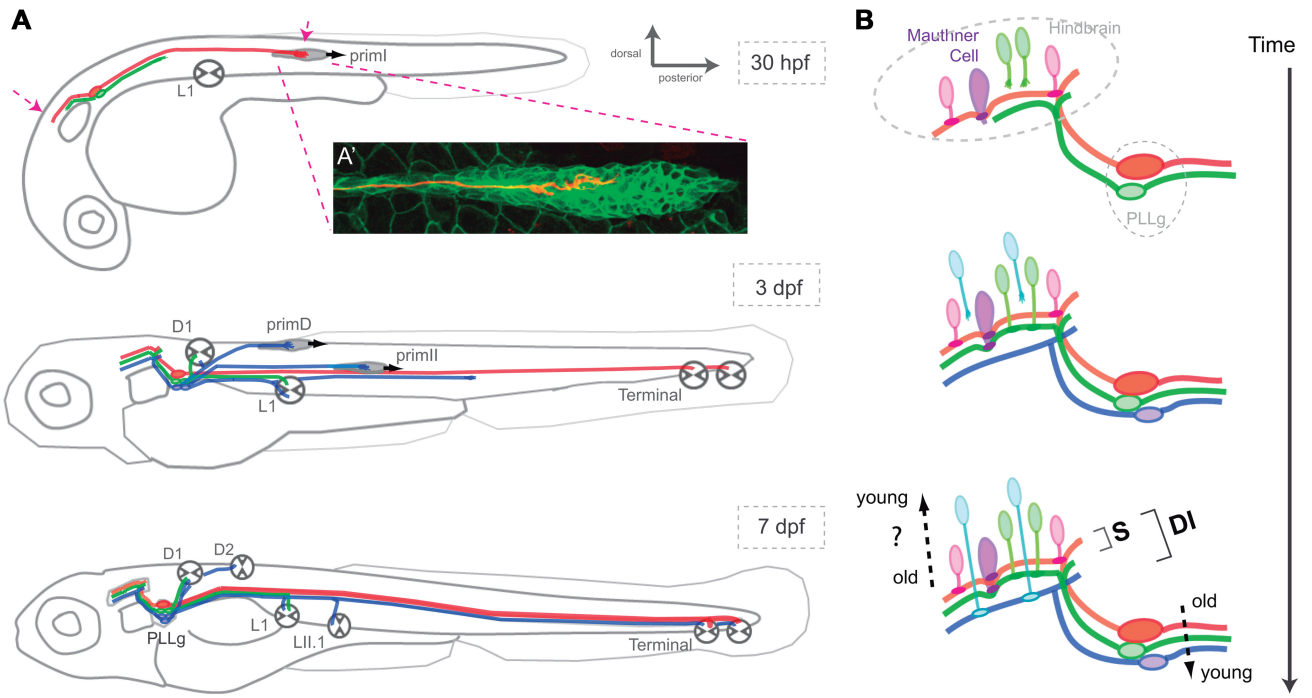

FIGURE 2 | Assembly of the posterior lateral-line neural map. (A) Lateral view of a developing zebrafish at around 30 hpf, 3 and 7 dpf showing the coincident progressive development of the lateralis afferents and their peripheral targets. Arrows at 30 hpf indicate growing lateralis afferent's central and peripheral axons. PLLg: posterior lateralis ganglion formed by the lateralis afferent's cell bodies. **(A')** A single lateralis afferent neuron is labeled in red in a transgenic zebrafish embryo expressing GFP in primI. The peripheral axonal growth cone can be observed within the migrating primordium. **(B)** Lateral view of the developing hindbrain and lateralis afferent's central axons at around 30 hpf, 3 and 7 dpf depicting an hypothetical temporal code that matches lateralis afferents with second-order neurons that are born at similar times. Both in **(A)** and **(B)**, red and green lateralis afferents belong to the first neuronal subclass which projects dorsal axons that contact the Mauthner cell. Red and green neurons innervate posterior and anterior primary neuromasts, respectively. Blue lateralis afferents belong to the second neuronal subclass which projects ventrolateral axons that do not contact the Mauthner cell. The two neuronal subclasses form a dimorphic neural map (DI) whereas only the neurons of the first subclass shape the somatotopic map (S). Neurons in red are the first-born neurons whereas neurons in blue are the latest-born neurons. primI, first primordium; primD, dorsal primordium; primII, second primordium. L1, Terminal and D1 neuromasts are primary and parallel (>). LII.1 and D2 neuromasts are secondary and perpendicular (^).

map should be called "neurotopic," we shall continue to (mis)-call it somatotopic because this definition appears in the bulk of the literature (Gompel et al., 2001). Live videomicroscopy combined with sparse fluorescent labeling of lateralis afferents showed early morphological and behavioral heterogeneities within the neuronal population, which correlate with their final central-projection patterns (Gompel et al., 2001). This result suggests that each neuron is pre-specified to occupy a particular position along the somatotopic axis. Importantly, cellular birth dating showed that neuronal morphology, behavior and projection pattern correlate with the time of neurogenesis (Liao, 2010; Pujol-Martí et al., 2010; Liao and Haehnel, 2012). During the first wave of neurogenesis, early differentiating lateralis afferents project dorsal central axons and innervate posterior neuromasts, whereas late-differentiating neurons project central axons more ventrally and innervate anterior neuromasts (**Figure 2**). These results suggest that neurogenic timing defines lateralis somatotopy (Pujol-Martí et al., 2010). Very recent observations have shown a more complex ordering of the lateralis central and peripheral axons (Pujol-Martí et al., 2012). Axons from second-wave neurons always occupy more ventral positions in the central-projection column than axons from first-wave neurons. To maintain somatotopy, second-wave neurons must project peripheral axons exclusively to anterior neuromasts. However, these neurons invariably innervate anterior as well as posterior neuromasts. Therefore, somatotopy is evident among neurons derived from the first wave of neurogenesis. When the whole population of lateralis afferents is examined simultaneously, the simple somatotopic ordering is lost (**Figure 2**).

ARCHITECTURE OF THE LATERAL-LINE NEURAL MAP

The distribution and structure of the neuromasts enable the lateral line to decompose a complex hydrodynamic stimulus into its basic components: location, direction, and velocity. First, each neuromast responds to mechanical stimuli in its proximity by capturing sensory information from a discrete location along the animal's body (**Figure 1**). Second, parallel and perpendicular neuromasts are sensitive to water movements along two perpendicular axes. Third, hair cells of each planar polarity class maximally detect water motions occurring along a single vector. Fourth, the collection of neuromasts along the animal body captures time-resolved stimuli, which represents water flow velocity. Once all components of the mechanical stimuli have been extracted by the receptors, they must be accurately conveyed to the central nervous system (Bleckmann, 2008). One possible mechanism to achieve

this feat involves that signal location, direction, and polarity are segregated in the population of first-order lateralis afferents neurons, to be relayed through separate channels, and subsequently encoded by the spatial arrangement of neuronal projections in the brain.

THE LATERAL-LINE NEURAL MAP IS HETEROGENEOUS

Very recent neuroanatomical work has re-explored the projection patterns of the lateralis afferent neurons in the zebrafish larva, putting emphasis on their connectivity (Faucherre et al., 2010; Liao, 2010; Haehnel et al., 2012; Liao and Haehnel, 2012; Pujol-Martí et al., 2012). These studies have revealed two classes of lateralis afferents in the posterior lateral line (Liao and Haehnel, 2012; Pujol-Martí et al., 2012). The first neuronal sub-class projects central axons to contact the lateral dendrite of the Mauthner cell, a *bona fide* output neuron of the lateral line (**Figure 2B**; Pujol-Martí et al., 2012). These neurons always project dorsally along the central-projection column. A second sub-class is characterized by central axons that do not contact the Mauthner cell, and that occupy more ventrolateral positions within the central-projection column. Recent data also demonstrated that birth-order correlates with lateralis map dimorphism (Liao and Haehnel, 2012; Pujol-Martí et al., 2012). Early born, dorsal projecting neurons that solely innervate primary neuromasts converge on the Mauthner cell, whereas later-born neurons innervating primary and secondary neuromasts do not converge on the Mauthner cell. Therefore, whereas every neuromast is somatotopically represented in the hindbrain, the lateral line also appears to directly input to the Mauthner cell in a putatively non-somatotopic fashion for it to broaden the receptive field of this reticulospinal command neuron (Pujol-Martí et al., 2012). Although such signal input to the Mauthner cell would decrease spatial discrimination, it may be essential to effectively evoke fast escape responses. Thus, the existence of two neuronal projection patterns indicates that the lateralis neural map is dimorphic, combining structural attributes of both the continuous and discrete maps (Luo and Flanagan, 2007; Pujol-Martí et al., 2012). Collectively, these studies provide solid evidence for a key twofold contribution of progressive neurogenesis to the patterning of lateral-line neural map (Pujol-Martí et al., 2010; Pujol-Martí et al., 2012). First, it arranges somatotopy by representing the spatial distribution of the mechanosensory stimuli that is likely to be essential for the complex neuronal computations used for navigation. Second, it delineates a dimorphic map architecture, which might represent independent channels of sensory-information transfer used for navigation and reflexive escape responses. Altogether, these data are helping formulate a simplifying principle that posits time as a key determinant of neural-map development.

THE LATERAL-LINE NEURONAL POPULATION IS HETEROGENEOUS

Recent anatomical and genetic studies have shown further dimorphism among posterior lateralis afferents neurons in the zebrafish larva. A "large" sub-class of lateralis afferents has bigger somata and larger-diameter peripheral axons than the "small" sub-class (Liao and Haehnel, 2012; Pujol-Martí et al., 2012). Both neuronal subclasses are myelinated (Lyons et al., 2005). Because the conduction velocity of myelinated axons in vertebrates increases linearly with their diameter, the large neuronal class is likely to conduct signals faster than the small (Goldman and Albus, 1968). Electrophysiological recordings have shown that the largest lateralis afferent neurons are less excitable and have a lower spontaneous firing rate (Liao and Haehnel, 2012). Although these recording were performed at the level of the neuronal cell body and, therefore, do not probe directly the actual excitability at the site of initiation of the action potentials, the collective evidence strongly suggests that the posterior lateral line of the zebrafish larva contains neurons that display heterogeneous anatomical and physiological properties. The large sub-class of neurons has "low excitability and high conduction velocity," whereas the small sub-class has "high excitability and low conduction velocity." What is truly interesting is that this anatomical-functional sub-division correlates with the neuronal classification that defines lateralis neural-map dimorphism. This is because large neurons project central axons dorsally and directly contact the Mauthner cell, whereas small, ventrolateral-projecting neurons do not contact the Mauthner (Haehnel et al., 2012; Pujol-Martí et al., 2012). This further divergence could explain how mechanical stimuli elicit either behavior governed by the lateral line. Rheotaxis, shoaling, and prey tracking would rely on a divergent sub-map in which each "high excitability/low conduction velocity" lateralis afferent synapses with up to 60 output targets in the hindbrain. Innate reflex escape responses, by contrast, would be based on a convergent sub-map in which "low excitability/high conduction velocity" neurons directly contact the lateral dendrite of the Mauthner cell to send strong depolarizing inputs with very short latencies. Thus, the activation of the large sub-class might suffice to trigger an escape reaction. However, because some small lateralis afferent also converge on the Mauthner cell, the escape response may be triggered by the coincident input on the Mauthner cell by small and large neurons. This neural-map architecture would safeguard animals from startling upon stimuli that would depolarize one neuronal sub-class but not the other, and is reminiscent of the escape strategy of crayfish, in which mechanosensory stimuli activate parallel neuronal pathways with different reaction times to trigger the startle reaction only when arriving coincidently to an output command neuron (Mellon and Christison-Lagay, 2008).

NEURONAL ENCODING AND CENTRAL REPRESENTATION OF STIMULUS LOCATION

Anatomical studies have shown that each lateralis afferent neuron innervates a single neuromast in the zebrafish embryo and larva (Nagiel et al., 2008; Faucherre et al., 2009). During these early stages, multiple innervations are infrequent, but when they occur it is among adjacent neuromasts (Nagiel et al., 2008; Faucherre et al., 2009; Feldheim and O'Leary, 2010). For example, a single neuron can innervate all the terminal neuromasts. Therefore, the receptive field of an individual afferent neuron is generally defined by the neuromasts it innervates. Therefore, somatotopy in the afferent pathway likely forms a neuroanatomical code of the external hydrodynamic field. However, no physiological studies have so far been conducted in the central nervous system of the zebrafish, and studies in other fish species have failed to find space-selective neurons in the MON or the TS (Kunzel et al., 2011; Voges and Bleckmann, 2011; Mogdans and Bleckmann, 2012). These

results, if confirmed by more exhaustive studies, would call into question the relevance of somatotopy for upper-level encoding of the dynamics of the hydromechanic scene (Kaas, 1997; Weinberg, 1997). One alternative mechanism is that stimulus location might be encoded by signal patterns in spatially non-segregated central neuronal population.

NEURONAL ENCODING AND CENTRAL REPRESENTATION OF STIMULUS DIRECTION

Recent anatomical and physiological analyses in the zebrafish larva have shown that each neuromast is innervated by at least two lateralis afferents, each making synapses with hair cells of identical orientation, effectively dividing the neuromast epithelium in synaptic compartments of planar polarity (Nagiel et al., 2008; Faucherre et al., 2009; Feldheim and O'Leary, 2010). This holds true even in the case of neurons innervating multiple neuromasts (Nagiel et al., 2008; Faucherre et al., 2009). By doing so the input from each hair-cell polarity group may be conveyed by separate channels to the central nervous system. Physiological studies in other fish species have shown evidence for MON and TS neurons that are sensitive to the direction of water flow. This may occur if vector-sensitive central neurons existed and received input exclusively from a single hair-cells polarity group (Bleckmann, 2008). Alternatively, the direction of a water flow might be encoded in the brain exclusively by relying on somatotopy (see previous section). For instance, central neurons receiving inputs from different neuromasts might perform spatiotemporal cross-correlations to determine the direction of water flow (Chagnaud et al., 2008).

OUTLOOK

The optical transparency of the zebrafish, coupled with its external and fast development, its diverse genetic toolkit, and the simplicity of the lateral-line mechanosensory system provide a powerful paradigm to study the development and homeostasis of sensorineural maps, and how they underlie the generation of appropriate behaviors to the environmental context (Friedrich et al., 2010). We now outline several interesting and central questions in neurobiology that could be answered using this model system.

Does the timing of neurogenesis contribute to the architecture of a neural map? If so, would time play a permissive or an instructive role? Recent investigations in the zebrafish started to reveal some of the mechanisms underlying the establishment of the lateral-line neural map during development (Pujol-Martí et al., 2012). Several findings strongly suggest that neurogenic timing is contributing to this process, supporting what it has already been found in other sensory systems (Jefferis et al., 2001; Pearson and Doe, 2003; Petrovic and Hummel, 2008; Tripodi et al., 2011). One emergent possibility is that neurons acquire different properties on the basis of their birth- or differentiation-dates. In the case of the lateral line, each afferent neuron could have an intrinsic date-of-birth-given identity that determines its final projection patterns. For instance, lateralis neurons born at different times could express different combinations of proteins (molecular codes) that might account for connectivity specificity in the context of a Sperry-type chemoaffinity mechanism (Sperry, 1963). This would be analogous to molecular heterogeneities within the retina and the tectum that govern retinotopic map formation (Lemke and Reber, 2005). Alternatively, differential expression of guidance receptors and ligands might occur in neurons born at different times, which could account for axonal segregation before neurons reach their peripheral and central targets (Imai et al., 2009).

Neuronal diversity may indicate that the projection pattern is an intrinsic property of the neuron. However, progressive neurogenesis might instruct map formation without necessarily diversifying neurons. Topographic mapping in the visual system of arthropods appears to occur in this way (Flaster and Macagno, 1984). In the case of the lateral line, progressive neurogenesis could be permissive and simply give rise to identical neurons that differ in their final projection patterns because they extend axons at different times to encounter environments that change as a consequence of the continuous growth of the brain. Thus, the final projection patterns of each neuron might exclusively reflect the interaction between the status of the surrounding tissue at axon growth. In such a case, the position of each neuron within the map would be circumstantial, rather than given by intrinsic properties of the neuron. Regardless, a temporal code might help match lateralis afferents with second-order neurons by first-born lateralis afferents reaching the target area first and associate with the earliest-born second-order neurons, whereas lateralis and second-order neurons that are born subsequently would synapse progressively, repeating the process (**Figure 2B**). To test this possibility directly, it will be essential to generate transgenic animals to identify and visualize second-order neurons in the hindbrain, and to examine their connectivity. Experimentally, it will be interesting to pause transiently the extension of the central axons. If neural map topology shows no differences after this manipulation, one could argue that factors other than timing of neurogenesis or axonogenesis play a role in neural map formation. Of course, it is also possible that the temporal factor plays no essential role in neural map formation in the lateral line.

Retinotopic map formation, for example, relies on a combinatorial action of molecular gradients, neural activity, and axonal competition (Triplett et al., 2011). Recent observations indicate that neither evoked activity nor inter-class axonal competition is a major force behind the ordering of the lateralis central axons along the hindbrain central-projection column (Faucherre et al., 2010; Pujol-Martí et al., 2012). However, the impact of these processes in connectivity or map refinement remains unknown. The assembly of a sensory neural map represents a remarkable developmental challenge. However, how neural maps are remodeled with the growth of the animal, are maintained during adulthood, or repaired after damage are equally important questions for which we currently lack an answer.

Does neural map dimorphism reflect the existence of functionally distinct neurons, which may subtract different aspects of a complex stimulus to convey them to separate groups of second-order neurons in the brain? If this were the case, it would be analogous to the central representation of sub-modalities observed in other sensory systems. For instance, the mammalian vestibular system, which is morphologically and physiologically analogous to the lateral line, also contains two afferent channels, characterized

by complementary physiological properties, which are suited for driving distinct vestibular-related behaviors (Eatock and Songer, 2011). Are there molecular heterogeneities among the lateralis afferent neurons, which could play a role in neural map assembly? Recent work has revealed that some morphological and behavioral differences within the lateralis peripheral axons correlate with the expression levels of a transcription factor involved in neurogenesis called NeuroD (Sato and Takeda, 2013). The authors of this study suggest that different levels of NeuroD could switch-on different genes to create neuronal heterogeneities with an ultimate impact on their projection pattern. However, the observed different levels of NeuroD could simply reflect different stages of neuronal differentiation. Testing these hypotheses would require functional studies by genetic loss- and gain-of-function approaches in a spatiotemporally regulated manner (Asakawa et al., 2008; Abe et al., 2011; Faucherre and López-Schier, 2011; Lawson and Wolfe, 2011). Reverse genetic approaches using gain- and loss-of-function of candidate genes that are known to drive the development of other neural maps may answer this question. In addition, specific mutagenic and gene-trap screens will provide an unbiased entry point to this problem (Scott and Baier, 2009; Abe et al., 2011).

Fish should not startle by non-threatening stimuli. Also, behaviors such as navigation, rheotaxis, and schooling necessitate continuous input. It transpires that these contrasting behaviors would have different activating thresholds. Large neurons with low excitability and high conduction velocity that project from terminal neuromasts are well suited to produce the first and fastest lateral-line stimulus to the Mauthner cell, suggesting that terminal neuromasts have a disproportionate relevance in the escape behavior. Unlike neurons from other parts of the lateral line, each large neuron innervates up to three terminal neuromasts, which may increase their depolarization probability. Are terminal neuromasts enough to trigger the escape response in the zebrafish larva? If so, it may present clear survival advantages because terminal neuromasts would suffice to trigger an escape reaction by sending strong depolarizing inputs to the Mauthner cell with very short latencies. At least for the goldfish, afferent neurons with different excitability and conduction velocities have been found in the posterior lateral line. It would be interesting to explore these questions by combining laser-mediated neuronal ablation on transgenic animals, electrophysiological recordings to measure conduction velocities and patterns of neuronal excitability, and behavioral tests (Gahtan and Baier, 2004; Burgess and Granato, 2007; McLean and Fetcho, 2011).

One fascinating question is whether there are other sub-maps embedded into the lateral line. For instance, the second sub-class of lateralis afferents might assemble a second independent somatotopic map. Such a degree of complexity would not be unique to the lateral line. The visual cortex, for instance, contains a topographic representation of the retina and embedded in this map are multiple, superimposed maps of different stimulus attributes, such as eye dominance or motion direction preference (Swindale, 2001; Luo and Flanagan, 2007). A recent study on the organization of cutaneous low-threshold mechanoreceptors (LTMRs) in mice has shown that each hair-follicle type is innervated by a unique combination of LTMRs subtypes characterized by distinct physiological properties (Li et al., 2011). Although the neural map of the mammalian somatosensory system is somatotopic, the central projections of the distinct LTMRs subtypes terminate in different, yet partially overlapping laminae of the spinal cord dorsal horn, forming a discrete neural map in which neuronal subtypes are represented. The authors propose that such a neural map would allow for the integration of the individual mechanical properties of a tactile stimulus that takes place at a particular skin region. The structural similarity of their neural maps suggests that the mammalian LTMRs and the lateral-line sensory systems similarly integrate and process mechanical inputs.

What is the behavioral relevance of neural-map dimorphism? We have argued that the lateral line assembles a convergent/discrete sub-map for reaction speed, and a divergent/continuous sub-map for motor accuracy. This model could be tested using transgenic technology, cell biological and embryological manipulations. For example, laser nanosurgery on transgenic fish to ablate specific populations of neurons, and optogenetic actuators and sensors to excite or silence neurons, may be combined to probe their individual contribution of distinct subsets of lateralis neurons to a specific behavior. A detailed dissection of the connectivity patterns between the lateralis afferents and their central targets at the single-cell or whole-circuit levels will be essential to answer this question.

Another outstanding issue is the functional significance of the planar polarization of hair cells (López-Schier et al., 2004; Nagiel et al., 2008; Faucherre et al., 2009; Mogdans and Bleckmann, 2012). The existence of hair cells of two opposite polarities in the neuromast, and the somatotopic representation of the neuromasts in the brain, indicate that the lateral line may be able to localize mechanical signals along the animal's body and discriminate the signals' vectorial component (Faucherre et al., 2009; Faucherre et al., 2010; Mogdans and Bleckmann, 2012). Although to date there is no evidence supporting the idea that lateralis neurons collecting information from hair cells of opposite polarities establish connections with separate groups of second-order neurons in the brain, sensory information from signal location, direction and orientation may still be transmitted through different channels. If so, are these specific features of the sensory scene represented in maps or in clusters of similarly tuned high-order neurons? Where and how are they integrated? A combination of cell biology, genetics, electrophysiology, and optogenetics could help to unravel the functional role played by planar cell polarity in a sensory system.

CONCLUSION

The zebrafish lateral line is emerging as a powerful model system to investigate how environmental cues are used to generate appropriate behavioral reactions to the sensory context. Future studies should combine physical and computational approaches to quantify the sensory landscape, genetic and optogenetic manipulations to dissect how the peripheral receptors extract and fractionate hydromechanical stimuli, and electrophysiological recordings to measure how the peripheral nervous system encodes and the central nervous system decodes stimuli. Such multidisciplinary approach will help to uncover and understand the mechanisms by which a sensory modality initiates and mediates contrasting behavioral programs.

ACKNOWLEDGMENTS

We would like to thank A. Ghysen, B. Chagnaud, F. Pinto-Teixeira, and members of our group for constructive comments on the manuscript. The work from our group reviewed in this article was supported by funds provided by the AGAUR (2009-SGR-305), by the Ministerio de Ciencia e Innovación of Spain, and by the European Research Council (ERC-2007-StG SENSORINEURAL).

REFERENCES

Abe, G., Suster, M. L., and Kawakami, K. (2011). Tol2-mediated transgenesis, gene trapping, enhancer trapping, and the Gal4-UAS system. *Methods Cell Biol.* 104, 23–49.

Alexandre, D., and Ghysen, A. (1999). Somatotopy of the lateral line projection in larval zebrafish. *Proc. Natl. Acad. Sci. U.S.A.* 96, 7558–7562.

Arber, S. (2012). Motor circuits in action: specification, connectivity, and function. *Neuron* 74, 975–989.

Asakawa, K., Suster, M. L., Mizusawa, K., Nagayoshi, S., Kotani, T., Urasaki, A., et al. (2008). Genetic dissection of neural circuits by Tol2 transposon-mediated Gal4 gene and enhancer trapping in zebrafish. *Proc. Natl. Acad. Sci. U.S.A.* 105, 1255–1260.

Barrett, T. W. (1973). Information processing in the inferior colliculus of cat using high frequency acoustical stimulation and direct electrical stimulation of the osseous spiral laminae. *Behav. Biol.* 9, 189–219.

Bleckmann, H. (2008). Peripheral and central processing of lateral line information. *J. Comp. Physiol. A Neuroethol. Sens. Neural. Behav. Physiol.* 194, 145–158.

Bleckmann, H., and Zelick, R. (2009). Lateral line system of fish. *Integr. Zool.* 4, 13–25.

Burgess, H. A., and Granato, M. (2007). Modulation of locomotor activity in larval zebrafish during light adaptation. *J. Exp. Biol.* 210, 2526–2539.

Chacron, M. J., Longtin, A., and Maler, L. (2011). Efficient computation via sparse coding in electrosensory neural networks. *Curr. Opin. Neurobiol.* 21, 752–760.

Chagnaud, B. P., Brucker, C., Hofmann, M. H., and Bleckmann, H. (2008). Measuring flow velocity and flow direction by spatial and temporal analysis of flow fluctuations. *J. Neurosci.* 28, 4479–4487.

Chagnaud, B. P., Hofmann, M. H., and Mogdans, J. (2007). Responses to dipole stimuli of anterior lateral line nerve fibres in goldfish, *Carassius auratus*, under still and running water conditions. *J. Comp. Physiol. A Neuroethol. Sens. Neural. Behav. Physiol.* 193, 249–263.

Chaudhari, N., and Roper, S. D. (2010). The cell biology of taste. *J. Cell Biol.* 190, 285–296.

Coombs, S. (2001). Smart Skins: information processing by the lateral line system. *Auton. Robots* 11, 255–261.

Coombs, S., Mogdans, J., Halstead, M., and Montgomery, J. (1998). Transformation of peripheral inputs by the first-order lateral line brainstem nucleus. *J. comp. physiol. A* 182 606–626.

DeMaria, S., and Ngai, J. (2010). The cell biology of smell. *J. Cell Biol.* 191, 443–452.

Duvall, A. J. III, Flock, A., and Wersall, J. (1966). The ultrastructure of the sensory hairs and associated organelles of the cochlear inner hair cell, with reference to directional sensitivity. *J. Cell Biol.* 29, 497–505.

Eatock, R. A., and Songer, J. E. (2011). Vestibular hair cells and afferents: two channels for head motion signals. *Annu. Rev. Neurosci.* 34, 501–534.

Engelmann, J., Hanke, W., Mogdans, J., and Bleckmann, H. (2000). Hydrodynamic stimuli and the fish lateral line. *Nature* 408, 51–52.

Faucherre, A., Baudoin, J. P., Pujol-Martí, J., and López-Schier, H. (2010). Multispectral four-dimensional imaging reveals that evoked activity modulates peripheral arborization and the selection of plane-polarized targets by sensory neurons. *Development* 137, 1635–1643.

Faucherre, A., and López-Schier, H. (2011). Delaying Gal4-driven gene expression in the zebrafish with morpholinos and Gal80. *PloS ONE* 6:e16587. doi: 10.1371/journal.pone.0016587

Faucherre, A., Pujol-Martí, J., Kawakami, K., and López-Schier, H. (2009). Afferent neurons of the zebrafish lateral line are strict selectors of hair-cell orientation. *PloS ONE* 4:e4477. doi: 10.1371/journal.pone.0004477

Feldheim, D. A., and O'Leary, D. D. (2010). Visual map development: bidirectional signaling, bifunctional guidance molecules, and competition. *Cold Spring Harb. Perspect. Biol.* 2 a001768.

Flaster, M. S., and Macagno, E. R. (1984). Cellular interactions and pattern formation in the visual system of the branchiopod crustacean, *Daphnia magna*. III. The relationship between cell birthdates and cell fates in the optic lamina. *J. Neurosci.* 4, 1486–1498.

Friedrich, R. W., Jacobson, G. A., and Zhu, P. (2010). Circuit neuroscience in zebrafish. *Curr. Biol.* 20, R371–R381.

Gahtan, E., and Baier, H. (2004). Of lasers, mutants, and see-through brains: functional neuroanatomy in zebrafish. *J. Neurobiol.* 59, 147–161.

Gardner, E. P., and Martin, J. H. (2000). "Coding of sensory information," in *Principles of Neural Science*, E. R. Kandel, J. Schwartz, and T. M. Jessell (New York: McGraw-Hill), 411–428.

Ghysen, A., and Dambly-Chaudière, C. (2007). The lateral line microcosmos. *Genes Dev.* 21, 2118–2130.

Goldman, L., and Albus, J. S. (1968). Computation of impulse conduction in myelinated fibers; theoretical basis of the velocity-diameter relation. *Biophys. J.* 8, 596–607.

Gompel, N., Dambly-Chaudière, C., and Ghysen, A. (2001). Neuronal differences prefigure somatotopy in the zebrafish lateral line. *Development* 128, 387–393.

Goulet, J., Engelmann, J., Chagnaud, B. P., Franosch, J. M., Suttner, M. D., and van Hemmen, J. L. (2008). Object localization through the lateral line system of fish: theory and experiment. *J. Comp. Physiol. A Neuroethol. Sens. Neural. Behav. Physiol.* 194, 1–17.

Haehnel, M., Taguchi, M., and Liao, J. C. (2012). Heterogeneity and dynamics of lateral line afferent innervation during development in zebrafish (Danio rerio). *J. Comp. Neurol.* 520, 1376–1386.

Hudspeth, A. J. (1989). How the ear's works work. *Nature* 341, 397–404.

Imai, T., Sakano, H., and Vosshall, L. B. (2010). Topographic mapping-the olfactory system. *Cold Spring Harb. Perspect. Biol.* 2, a001776.

Imai, T., Yamazaki, T., Kobayakawa, R., Kobayakawa, K., Abe, T., Suzuki, M., et al. (2009). Pre-target axon sorting establishes the neural map topography. *Science* 325, 585–590.

Jefferis, G. S., Marin, E. C., Stocker, R. F., and Luo, L. (2001). Target neuron prespecification in the olfactory map of *Drosophila*. *Nature* 414, 204–208.

Jékély, G. (2011). Origin and early evolution of neural circuits for the control of ciliary locomotion. *Proc. Biol. Sci.* 278, 914–922.

Kaas, J. H. (1997). Topographic maps are fundamental to sensory processing. *Brain Res. Bull.* 44, 107–112.

Knudsen, E. I., du Lac, S., and Esterly, S. D. (1987). Computational maps in the brain. *Annu. Rev. Neurosci.* 10, 41–65.

Kunzel, S., Bleckmann, H., and Mogdans, J. (2011). Responses of brainstem lateral line units to different stimulus source locations and vibration directions. *J. Comp. physiol. A Neuroethol. Sens. Neural. Behav. Physiol.* 197, 773–787.

Lawson, N. D., and Wolfe, S. A. (2011). Forward and reverse genetic approaches for the analysis of vertebrate development in the zebrafish. *Dev. Cell* 21, 48–64.

Lemke, G., and Reber, M. (2005). Retinotectal mapping: new insights from molecular genetics. *Annu. Rev. Cell Dev. Biol.* 21, 551–580.

Leys, S. P., and Degnan, B. M. (2001). Cytological basis of photoresponsive behavior in a sponge larva. *Biol. Bull.* 201, 323–338.

Li, L., Rutlin, M., Abraira, V. E., Cassidy, C., Kus, L., Gong, S., et al. (2011). The functional organization of cutaneous low-threshold mechanosensory neurons. *Cell* 147, 1615–1627.

Liao, J. C. (2010). Organization and physiology of posterior lateral line afferent neurons in larval zebrafish. *Biol. Lett.* 6, 402–405.

Liao, J. C., and Haehnel, M. (2012). Physiology of afferent neurons in larval zebrafish provides a functional framework for lateral line somatotopy. *J. Neurophysiol.* 107, 2615–2623.

López-Schier, H., Starr, C. J., Kappler, J. A., Kollmar, R., and Hudspeth, A. J. (2004). Directional cell migration establishes the axes of planar polarity in the posterior lateral-line organ of the zebrafish. *Dev. Cell* 7, 401–412.

Lumpkin, E. A., Marshall, K. L., and Nelson, A. M. (2010). The cell biology of touch. *J. Cell Biol.* 191, 237–248.

Luo, L., and Flanagan, J. G. (2007). Development of continuous and discrete neural maps. *Neuron* 56, 284–300.

Lyons, D. A., Pogoda, H. M., Voas, M. G., Woods, I. G., Diamond, B., Nix, R., et al. (2005). erbb3 and erbb2 are essential for schwann cell migration and myelination in zebrafish. *Curr. Biol.* 15, 513–524.

McLean, D. L., and Fetcho, J. R. (2011). Movement, technology and discovery in the zebrafish. *Curr. Opin. Neurobiol.* 21, 110–115.

Mellon, D. Jr., and Christison-Lagay, K. (2008). A mechanism for neuronal

coincidence revealed in the crayfish antennule. *Proc. Natl. Acad. Sci. U.S.A.* 105, 14626–14631.

Metcalfe, W. K., Kimmel, C. B., and Schabtach, E. (1985). Anatomy of the posterior lateral line system in young larvae of the zebrafish. *J. Comp. Neurol.* 233, 377–389.

Mogdans, J., and Bleckmann, H. (2012). Coping with flow: behavior, neurophysiology and modeling of the fish lateral line system. *Biol. Cybern.* 106, 627–642.

Montgomery, J., Baker, C., Carton, A. G. (1997). The lateral line can mediate rheotaxis in fish. *Nature* 389, 960–963.

Montgomery, J., Carton, G., Voigt, R., Baker, C., and Diebel, C. (2000). Sensory processing of water currents by fishes. *Philos. Trans. R. Soc. Lond. B Biol. Sci.* 355, 1325–1327.

Moroz, L. L. (2009). On the independent origins of complex brains and neurons. *Brain Behav. Evol.* 74, 177–190.

Nagiel, A., Andor-Ardó, D., and Hudspeth, A. J. (2008). Specificity of afferent synapses onto plane-polarized hair cells in the posterior lateral line of the zebrafish. *J. Neurosci.* 28, 8442–8453.

Northcutt, R. G. (2012). Evolution of centralized nervous systems: two schools of evolutionary thought. *Proc. Natl. Acad. Sci. U.S.A.* 109(Suppl 1), 10626–10633.

Pearson, B. J., and Doe, C. Q. (2003). Regulation of neuroblast competence in *Drosophila. Nature* 425, 624–628.

Petrovic, M., and Hummel, T. (2008). Temporal identity in axonal target layer recognition. *Nature* 456, 800–803.

Pujol-Martí, J., Baudoin, J. P., Faucherre, A., Kawakami, K., and López-Schier, H. (2010). Progressive neurogenesis defines lateralis somatotopy. *Dev. Dyn.* 239, 1919–1930.

Pujol-Martí, J., Zecca, A., Baudoin, J. P., Faucherre, A., Asakawa, K., Kawakami, K., et al. (2012). Neuronal birth order identifies a dimorphic sensorineural map. *J. Neurosci.* 32, 2976–2987.

Rouse, G. W., and Pickles, J. O. (1991). Paired development of hair cells in neuromasts of the teleost lateral line. *Proc. Biol. Sci.* 246, 123–128.

Sarrazín, A. F., Nunez, V. A., Sapede, D., Tassin, V., Dambly-Chaudière, C., and Ghysen, A. (2010). Origin and early development of the posterior lateral line system of zebrafish. *J. Neurosci.* 30, 8234–8244.

Sato, A., and Takeda, H. (2013). Neuronal subtypes are specified by the level of neurod expression in the zebrafish lateral line. The *J. Neurosci.* 33, 556–562.

Scheich, H. (1991). Auditory cortex: comparative aspects of maps and plasticity. *Curr. Opin. Neurobiol.* 1, 236–247.

Schuster, K., Dambly-Chaudière, C., and Ghysen, A. (2010). Glial cell line-derived neurotrophic factor defines the path of developing and regenerating axons in the lateral line system of zebrafish. *Proc. Natl. Acad. Sci. U.S.A.* 107, 19531–19536.

Schwander, M., Kachar, B., and Muller, U. (2010). The cell biology of hearing. *J. Cell Biol.* 190, 9–20.

Scott, E. K., and Baier, H. (2009). The cellular architecture of the larval zebrafish tectum, as revealed by gal4 enhancer trap lines. *Front. Neural Circuits* 3:13. doi: 10.3389/neuro.04.013.2009

Sperry, R. W. (1963). Chemoaffinity in the orderly growth of nerve fiber patterns and connections. *Proc. Natl. Acad. Sci. U.S.A.* 50, 703–710.

Sung, C. H., and Chuang, J. Z. (2010). The cell biology of vision. *J. Cell Biol.* 190, 953–963.

Swindale, N. (2001). Cortical cartography: what's in a map? *Curr. Biol.* 11, R764–R767.

Triplett, J. W., Pfeiffenberger, C., Yamada, J., Stafford, B. K., Sweeney, N. T., Litke, A. M., et al. (2011). Competition is a driving force in topographic mapping. *Proc. Natl. Acad. Sci. U.S.A.* 108, 19060–19065.

Tripodi, M., Stepien, A. E., and Arber, S. (2011). Motor antagonism exposed by spatial segregation and timing of neurogenesis. *Nature* 479, 61–66.

Voges, K., and Bleckmann, H. (2011). Two-dimensional receptive fields of midbrain lateral line units in the goldfish, *Carassius auratus. J. Comp. Physiol. A Neuroethol. Sens. Neural. Behav. Physiol.* 197, 827–837.

Weinberg, R. J. (1997). Are topographic maps fundamental to sensory processing? *Brain Res. Bull.* 44, 113–116.

Winklbauer, R. (1989). Development of the lateral line system in *Xenopus. Prog. Neurobiol.* 32, 181–206.

Wubbels, R. J., and Schellart, N. A. (1997). Neuronal encoding of sound direction in the auditory midbrain of the rainbow trout. *J. Neurophysiol.* 77, 3060–3074.

Zottoli, S. J., and Van Horne, C. (1983). Posterior lateral line afferent and efferent pathways within the central nervous system of the goldfish with special reference to the Mauthner cell. *J. Comp. Neurol.* 219, 100–111.

Conflict of Interest Statement: The authors declare that the research was conducted in the absence of any commercial or financial relationships that could be construed as a potential conflict of interest.

Received: 16 January 2013; paper pending published: 26 February 2013; accepted: 06 March 2013; published online: 26 March 2013.

Citation: Pujol-Martí J and López-Schier H (2013) Developmental and architectural principles of the lateral-line neural map. Front. Neural Circuits 7:47. doi: 10.3389/fncir.2013.00047

frontiers in
NEURAL CIRCUITS

ORIGINAL RESEARCH ARTICLE
published: 28 May 2013
doi: 10.3389/fncir.2013.00100

Cellular dissection of the spinal cord motor column by BAC transgenesis and gene trapping in zebrafish

Kazuhide Asakawa*[1,2]*, *Gembu Abe*[1] *and Koichi Kawakami*[1,2]

[1] *Department of Developmental Genetics, Division of Molecular and Developmental Biology, National Institute of Genetics, Mishima, Shizuoka, Japan*
[2] *Department of Genetics, Graduate University for Advanced Studies (SOKENDAI), Mishima, Shizuoka, Japan*

Edited by:
German Sumbre, Ecole Normale Superieure, France

Reviewed by:
Joseph Fetcho, Cornell University, USA
Herwig Baier, Max Planck Institute of Neurobiology, Germany
Claire Wyart, Brain and Spinal cord Institute (ICM), France

***Correspondence:**
Kazuhide Asakawa and Koichi Kawakami, Division of Molecular and Developmental Biology, National Institute of Genetics, 1111 Yata, Mishima, Shizuoka, 411-8540, Japan.
e-mail: kasakawa@nig.ac.jp; kokakawa@nig.ac.jp

Bacterial artificial chromosome (BAC) transgenesis and gene/enhancer trapping are effective approaches for identification of genetically defined neuronal populations in the central nervous system (CNS). Here, we applied these techniques to zebrafish (*Danio rerio*) in order to obtain insights into the cellular architecture of the axial motor column in vertebrates. First, by using the BAC for the Mnx class homeodomain protein gene *mnr2b*/*mnx2b*, we established the mnGFF7 transgenic line expressing the Gal4FF transcriptional activator in a large part of the motor column. Single cell labeling of Gal4FF-expressing cells in the mnGFF7 line enabled a detailed investigation of the morphological characteristics of individual spinal motoneurons, as well as the overall organization of the motor column in a spinal segment. Secondly, from a large-scale gene trap screen, we identified transgenic lines that marked discrete subpopulations of spinal motoneurons with Gal4FF. Molecular characterization of these lines led to the identification of the ADAMTS3 gene, which encodes an evolutionarily conserved ADAMTS family of peptidases and is dynamically expressed in the ventral spinal cord. The transgenic fish established here, along with the identified gene, should facilitate an understanding of the cellular and molecular architecture of the spinal cord motor column and its connection to muscles in vertebrates.

Keywords: motor column, zebrafish, Gal4, Mnx, ADAMTS3, gene trapping, BAC

INTRODUCTION

A comprehensive understanding of how the nervous system generates behavior depends in large part on knowing how the system is organized. With an ever-increasing number of genetic techniques available for visualizing the cellular structures of the nervous system in a wide variety of organisms, our knowledge of the individual neuronal types and their connectivity has been expanding. Among the major challenges which remain is the identification of the functional neural circuits that produce measureable behavioral outputs from the diverse anatomical data and also the genetic programs that assemble these circuits. To achieve this end, it is essential to develop methods for visualizing and manipulating functional neuronal circuits as well as analyzing the gene functions that allow neuronal circuits to operate (Luo et al., 2008; Fenno et al., 2011).

The Gal4-UAS system has been shown to be a useful tool for visualizing and manipulating neural circuits in *Drosophila* (Brand and Perrimon, 1993; Jones, 2009). In this binary gene expression system, the yeast transcriptional activator Gal4 binds to its specific recognition sequence UAS (for upstream activating sequence) and activates the transcription of the target genes downstream of UAS. In zebrafish (*Danio rerio*), targeted expression of Gal4 in specific neuronal populations has been demonstrated using the transgenic technologies based on a meganuclease and transposons (Kawakami et al., 2000; Thermes et al., 2002; Davidson et al., 2003). Of these, the *Tol2* transposon has been extensively applied to gene/enhancer trapping to generate transgenic lines expressing Gal4 in specific neural tissues due to its high transgenesis efficiency (Davison et al., 2007; Scott et al., 2007; Asakawa and Kawakami, 2008; Asakawa et al., 2008). In zebrafish, several different Gal4 derivatives have been tested for stronger and more stable transcriptional activation (Koster and Fraser, 2001; Inbal et al., 2006; Asakawa et al., 2008; Distel et al., 2009; Ogura et al., 2009). In addition, methods of manipulating Gal4 activity using the Gal4 repressor Gal80 (Faucherre and Lopez-Schier, 2011; Fujimoto et al., 2011), morpholino antisense oligonucleotides against Gal4 (Faucherre and Lopez-Schier, 2011; Tallafuss et al., 2012), and the Cre/lox system (Sato et al., 2007) have also been reported. Further, *Tol2*-mediated bacterial artificial chromosome (BAC) transgenesis has been applied to the generation of transgenic fish expressing Gal4 in specific neuronal types (Suster et al., 2009a,b; Bussmann and Schulte-Merker, 2011). With all of these technological advancements and optimizations, the Gal4-UAS system has been applied to a detailed visualization of neuronal morphology with a variety of fluorophores (Sagasti et al., 2005; Aramaki and Hatta, 2006; Hatta et al., 2006; Scott et al., 2007; Arrenberg et al., 2009), monitoring neural activity with fluorescent probes (Dreosti et al., 2009; Del Bene et al., 2010; Muto et al., 2011; Marvin et al., 2013) and manipulating neuronal function with neurotoxin, cytotoxin, and optogenetic probes (Szobota et al., 2007; Asakawa et al., 2008; Douglass et al., 2008; Arrenberg et al., 2009; Del Bene et al., 2010; Janovjak et al., 2010; Yokogawa et al., 2012).

The zebrafish has been a valuable vertebrate model to study neural networks for locomotor behaviors (Saint-Amant and Drapeau, 1998; Budick and O'Malley, 2000; Grillner and Jessell, 2009; McLean and Fetcho, 2011). During locomotion, the motor column of the spinal cord performs the final neural computation prior to the sequential activation of muscles that generates body movement. In zebrafish, the motor column consists of a segmentally iterated set of motoneurons and each segment contains two distinct motoneuron classes: primary motoneurons that are large in size and located dorsally, and smaller secondary motoneurons that are located ventrally (Myers, 1985; Myers et al., 1986; Westerfield et al., 1986). The topographic organization of the motor column has been demonstrated to match the developmental timing of motoneurons and their recruitment pattern during swimming at different speeds (Liu and Westerfield, 1988; McLean et al., 2007, 2008; Gabriel et al., 2011; Menelaou and McLean, 2012).

The development of spinal motoneurons and their connection to the target muscle domains are both under the control of a complex combinatorial network of transcription factors from a variety of different gene families (Jessell, 2000; Shirasaki and Pfaff, 2002; Lewis and Eisen, 2003; Bonanomi and Pfaff, 2010). In zebrafish, the primary motoneurons are produced from a progenitor domain marked by the basic helix-loop-helix (bHLH) olig2 transcription factor in the ventral spinal cord, which is called the pMN domain (Park et al., 2004). Then, the hierarchical interplay between transcription factors from the LIM-homeodomain, as well as the Nkx6 and Mnx homeodomain families, determines the identity of the primary motoneurons (Appel et al., 1995; Tokumoto et al., 1995; Cheesman et al., 2004; Hutchinson and Eisen, 2006; Hutchinson et al., 2007; Seredick et al., 2012). The roles of the transcription factors in the axonal outgrowth of the primary motoneurons have also been reported (Segawa et al., 2001; Liu et al., 2012). On the other hand, the regulatory mechanisms for secondary motoneuron development have largely remained elusive, although several genes, including the LIM-homeodomain protein genes, are known to affect it, when they are mutated or knocked down (Beattie et al., 1997; Cheesman et al., 2004; Pineda et al., 2006; Hutchinson et al., 2007). The availability of transgenic markers for visualizing specific subsets of the secondary motoneurons has also been limited thus far (Meng et al., 1997; Higashijima et al., 2000; Balciunas et al., 2004). Since secondary motoneurons comprise the major cell-type of the motor column, delineating the regulatory mechanisms for secondary motoneuron development, as well as those for primary motoneuron development, is crucial for understanding the motor column organization. Further, since the primary motoneurons have only been described in the anamniote vertebrates to date, cellular and molecular descriptions of the secondary motoneuron should be important to understand the evolution of the motoneurons innervating the axial musculature (Fetcho, 1987, 1992; Tsuchida et al., 1994; Sharma et al., 1998; Agalliu et al., 2009).

Here, we applied BAC transgenesis and gene/enhancer trapping to the dissection of the spinal cord motor column. First, we modified a BAC containing the Mnx-class homeodomain protein gene *mnr2b*/*mnx2b* to establish a transgenic line expressing Gal4FF in a large number of spinal motoneurons. Single cell labeling allowed us to identify diverse types of the spinal motoneurons and to describe both their morphological characteristics and distribution in a spinal segment. Second, we dissected the motor column by means of gene trapping and identified transgenic lines in which specific subpopulations of spinal motoneurons were labeled with Gal4FF. Molecular characterization of one of these lines led to the identification of the ADAMTS3 gene, which encodes an evolutionarily conserved ADAMTS family of peptidases and is dynamically expressed in the ventral spinal cord. The transgenic fish established here, along with the identified gene, provides insights into the cellular and molecular architecture of the motor column and its connection to muscles in vertebrates.

RESULTS

GENERATION OF A Gal4FF DRIVER LINE FOR THE SPINAL MOTONEURONS USING THE BAC DNA FOR *mnr2b/mnx2b*

We previously established the mnr2b-GFP transgenic line, which labels the spinal motoneurons with GFP by the enhancer trap insertion located upstream of the Mnx-class homeodomain transcription factor gene *mnr2b/mnx2b* (hereafter, *mnr2b*) (**Figure 1A**) (Asakawa et al., 2012). We found that *mnr2b* was broadly expressed in the ventral spinal cord at 48 hours post-fertilization (hpf) (**Figure 1B**), consistent with the GFP reporter expression in mnr2b-GFP animals (**Figure 2E**). Therefore, to establish a Gal4 driver line for the spinal motoneurons, we used a BAC containing the *mnr2b* locus (CH211-172N16), which contains the full coding sequence of *mnr2b* as well as its 55 kb upstream and 78 kb downstream genomic regions. By homologous recombination, we introduced the Gal4FF gene encoding a variant of the yeast Gal4 (Asakawa et al., 2008) immediately downstream of the *mnr2b* 5′UTR (**Figure 1C**). The resulting BAC construct was named mnGFF. A stable transgenic line carrying mnGFF was established by *Tol2*-mediated BAC transgenesis (Suster et al., 2009b) and designated mnGFF7. We found that the expression pattern of Gal4FF in mnGFF7 line was consistent with that of GFP in the *mnr2b*-GFP line (**Figure 1G**). Indeed, in the spinal cord of mnGFF7;UAS:RFP;mnr2b-GFP triple transgenic embryos, 97% of the RFP-labeled Gal4FF-expressing cells were also marked by GFP fluorescence at 48 hpf (**Figures 1D–F**, 116 out of 120 RFP-positive cells from four embryos), suggesting that the mnGFF construct contains most of the *cis*-elements required for *mnr2b* expression in the spinal cord. In mnGFF7;UAS:GFP animals, the GFP signal was also detected in the endodermal and mesodermal tissues, where *mnr2b* is known to be expressed (Wendik et al., 2004), as well as in the abducens and pectoral fin motoneurons (**Figure 1H**).

THE SINGLE CELLS LABELLING IDENTIFIED THE SPINAL MOTONEURONS AND AN INTERNEURON IN mnGFF7

In mnGFF7;UAS:GFP larvae at 76–78 hpf, we identified approximately 63 GFP-labeled cells per spinal hemi-segment (62.9 ± 3.2; $n = 8$ hemi-segments at the segment levels 11–13 from three different larvae), which were located within the ventral two-thirds of the spinal cord. The number of the GFP-labeled cells per hemi-segment was significantly higher than the lower limit of the number of axial motoneuron estimated in a previous study

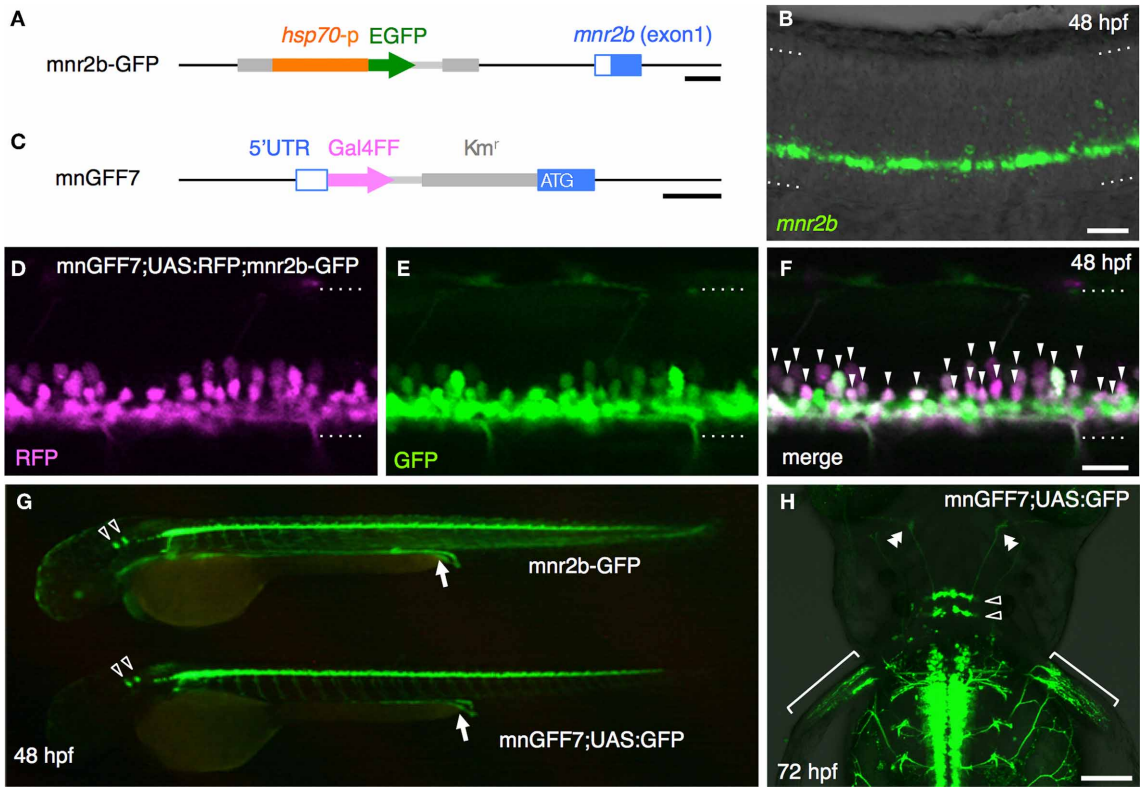

FIGURE 1 | Construction and characterization of the BAC transgenic line, mnGFF7. (A) The *mnr2b* genomic locus in the mnr2b-GFP enhancer trap line. The hsp70p-EGFP enhancer trap construct was integrated 1.9 kb upstream of the *mnr2b* gene. **(B)** Expression of *mnr2b* at 48 hpf detected by fluorescent *in situ* hybridization. A confocal section of the spinal cord above the yolk extension in a wild type embryo is shown. The rostral is to the left. **(C)** The *mnr2b* locus on the mnGFF BAC DNA. The PCR-amplified Gal4FF-polyA-Km^r cassette is inserted downstream of the 5′UTR of the *mnr2b* (open blue box) by homologous recombination. The coding sequence of exon1 of *mnr2b* (filled blue box) is left intact after the recombination. **(D–F)** The lateral view of the spinal cord of the mnGFF7;UAS:RFP; mnr2b-GFP triple transgenic embryo at 48 hpf. The images shown are the RFP (left), GFP (middle), and merged (right) images of a single confocal slice. The RFP-positive cells whose somata are identifiable are indicated by the arrowheads in **(F)**. The dotted lines demarcate the dorsal and ventral limit of the spinal cord. The rostral is to the left. **(G)** GFP expression in mnr2b-GFP (top) and mnGFF7;UAS:GFP (bottom) embryos at 48 hpf. The arrows indicate the GFP expression in the gut. The open arrowheads indicate the abducens motoneurons. **(H)** The dorsal view of the mnGFF7;UAS:GFP larvae at 72 hpf. GFP is expressed in the abducens and pectoral fin motoneurons. The open and double arrowheads indicate the soma positions and the axon terminals of the abducens motoneurons, respectively. The brackets indicate the axon terminals of the pectoral fin motoneurons. The rostral is to the top. The dotted lines demarcate the dorsal (top) and ventral limit of the spinal cord in **(B,D–F)**. The bars indicate 500 base-pair (bp) in **(A)** and **(C)**, 20 μm in **(B,D,F)**, and 100 μm in **(H)**.

(approximately 40 per hemi-segment during day 4–5) (Menelaou and McLean, 2012). These observations prompted us to examine in more detail the GFP-labeled cells in the spinal cord of the mnGFF7;UAS:GFP larvae.

To investigate the cellular characteristics of individual GFP-labeled cells in the spinal cord of mnGFF7 larvae, we performed a single-cell labeling experiment. The plasmid DNA carrying the UAS:GFP construct was injected into a blastomere of the mnGFF7 embryo at the 4–8 cell stage. To rigorously judge the morphology, individual GFP-positive cells that were uniquely labeled in a hemi-segment were investigated at 72–100 hpf. In total, we observed 103 GFP-labeled single cells (**Table 1**, $N = 68$ larvae). Of these, 102 cells possessed an axon that exited the spinal cord, indicating that these cells are spinal motoneurons. We found that one out of the 103 cells possessed the soma situated ventrally at segment level 1 and extended its axon ipsilaterally to segment level 18 (**Figure A1**), suggesting that a small population of descending interneurons is also labeled in mnGFF7 fish.

THE mnGFF7 LINE LABELS THE PRIMARY AND DIVERSE TYPES OF SECONDARY MOTONEURONS

The 102 single GFP-labeled motoneurons were found in various positions in a spinal hemi-segment and displayed a typical topographic distribution along the dorso-ventral (DV) axis according to soma size, as determined by their cross-sectional area (**Figures 2A,B**). Of these, 87% (89 cells) exhibited a main axon innervating axial muscles (**Figures 2C–G**). The remaining 13% (13 cells) possessed a main axon projecting to the ventral and medial side of the body. The axon terminals and collaterals of this cell type were observed in the vicinity of the axial blood vessels or pronephric ducts (**Figures 2J,K**). We tentatively named this cell-type "vmS," for "ventromedial secondary," because the target tissue(s) of vmS remained to be determined.

Table 1 | Summary of the cell types identified in the spinal cord of mnGFF7 larvae.

Motoneuron	Target	Type	Characteristics	Name	Cell number (103 cells in total)
	Axial muscle	Primary	Extensive axonal arborization in the medial muscle. Large, dorsally positioned soma	CaP*, MiP*, RoP* dRoP**, vRoP**	9
		Secondary	Extensive axonal arborization in the medial muscle. Specific muscle innervation territory	dS**, vS**	15
		Secondary	A bifurcating main axon innervating both the dorsal and ventral musculature	dvS**	10
		Secondary	Innervating the superficial intermyotomal region	iS**	50
		Secondary	No arborization or superficial innervation		5
	Ventromedial area	Secondary	Axon extended toward the ventromedial area close to the axial blood vessels or pronephric duct	vmS***	13
Interneuron			Ventrally positioned soma with an ipsilateral descending axon		1

*Myers et al., 1986, **Menelaou and McLean, 2012, ***This study.

The 89 cells innervating the axial muscles were categorized into five distinct classes based on their axon trajectories and pattern of muscle innervation. The first class was composed of the cells that displayed a highly extensive axonal arborization that covered a specific territory of the dorsal, lateral, or ventral musculature (10%, 9/89 cells, **Figures 2C–E**). Based on their larger soma size, dorsal soma positioning and extensive branching of the axon terminal in the medial muscles, these cells likely correspond to the primary motoneurons MiP, RoP, and CaP. The laterally projecting cells were further categorized into the dorsolaterally (dRoP) and ventrolaterally (vRoP) projecting types based on their innervation territory (**Figure 2E**) (Menelaou and McLean, 2012). The second class was composed of the cells that also innervated the medial muscles, but displayed less branching and had both a smaller soma size and innervation territory, compared to the primary motoneurons (**Figure 2F**, 17%, 15/89). Some of these correspond to vS (ventrally projecting secondary) and dS (dorsally projecting secondary) (Menelaou and McLean, 2012). The third class was made up of the cells that innervated most of the myotome along the DV axis through a bifurcating main axon (11%, 10/89 cells, **Figures 2C,Fc**). These cells correspond to the dorsoventrally projecting secondary dvS (Menelaou and McLean, 2012). The fourth class included the secondary motoneurons that possess a main axon extending superficially along the intermyotomal boundary (66%, 50/89 cells, **Figures 2C,Ga–e**). Of these, the laterally projecting cells could further be classified based on their ventrolateral (32%), horizontal (41%), or dorsolateral (27%) innervation (**Figures 2Gb–d**). Based on these innervation patterns, these cell types correspond to intermyotomal secondary (iS)-type neurons (Menelaou and McLean, 2012). While the main axons of the class II cells did not cross the myoseptum, their short axon collaterals contacted the myotome structures on both sides (**Figures 2H,I**), implying that a single iS neuron is able to innervate both of the myotomes that form a myoseptal boundary. The fifth class was composed of the cells that possessed the motor axon but did not exhibit either axonal arborization or superficial innervation, presumably because they were undergoing development (6% 5/89 cells, data not shown). Taken together, these observations demonstrate that the mnGFF7 line is a pan-motoneuronal Gal4 driver that marks the primary motoneurons and diverse types of secondary motoneurons. Interestingly, we noticed that the somas of the dorsally projecting neurons were situated predominantly (84%, 28/33 cells) in the dorsal half of the motor column and clustered within 21 μm of the exit point of the ventral root along the RC axis, mostly on the rostral side, while the ventrally and laterally projecting cells did not display such a bias (**Figures 2B**, **A2A**). These observations imply a topographic connection between the GFP-labeled dorsally projecting cells and the dorsal musculature (see Discussion).

A *Tol2* TRANSPOSON-MEDIATED GENE TRAP SCREEN FOR GENES EXPRESSED IN SPINAL MOTONEURONS

Having identified the various subtypes of spinal motoneurons, we next attempted to identify genetically-defined subpopulations by means of gene trapping. We have been screening transgenic lines expressing Gal4FF in various tissues and cell-types using *Tol2* transposon-based gene/enhancer trap constructs. In these screens (**Figure 3A**), the wild type fish at the single-cell stage were injected with a plasmid carrying the Gal4FF trap constructs and

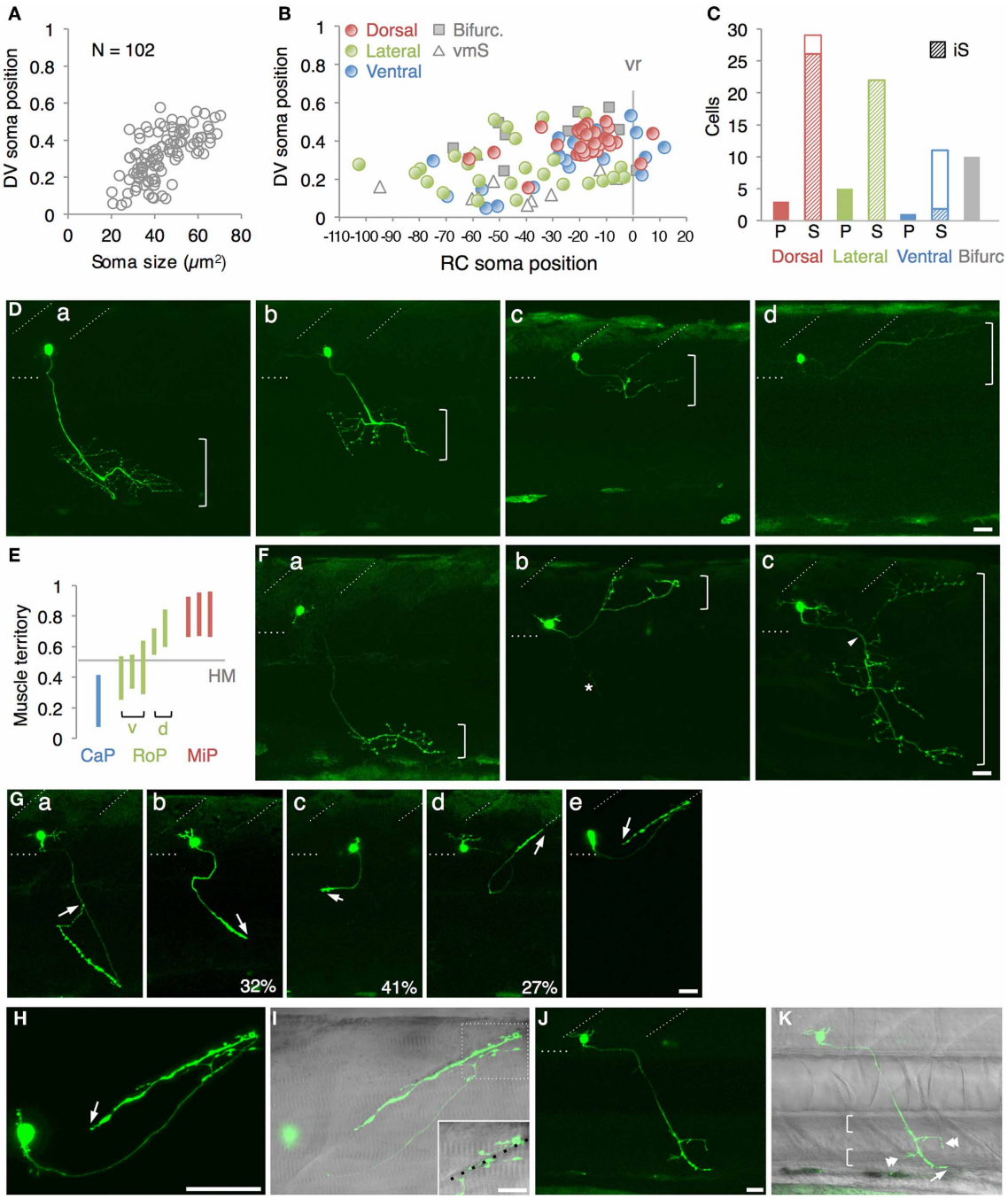

FIGURE 2 | Single cell labeling of Gal4FF expressing cells in mnGFF7. **(A)** The plot of the single GFP-labeled motoneurons (open gray circles) with respect to the soma size on the horizontal axis and to the position of the soma along with the DV axis on the vertical axis. The DV soma position is normalized to the dorsal ($y = 1$) and the ventral ($y = 0$) edge of the spinal cord. **(B)** Distribution of the GFP-labeled cells plotted with respect to the soma position along the RC axis on the horizontal axis and to the DV soma position on the vertical axis. The exit point of the ventral root from the spinal cord is indicated on the RC axis by the gray vertical line marked as vr ($x = 0$). The dorsally, laterally and ventrally projecting cells are shown as red, green, and blue circles, respectively. The cells with bifurcating main axon and the vmS motoneurons are shown as gray squares and open triangles, respectively. **(C)** Cell counts of the neurons innervating the axial muscles based on the axon trajectory and muscle innervation pattern. P and S indicate primary and secondary motoneurons, respectively. Diagonally-striped bars indicate iS-type neurons. "Bifurc" indicates the motoneurons with a bifurcating main axon. **(D)** Primary motoneurons innervating ventrally **(a)**, ventrolaterally **(b)**, dorsolaterally **(c)**, or dorsally **(d)**. **(E)** Muscle innervation territory of the primary motoneurons. The position of the horizontal myoseptum ($y = 0.5$) is indicated as a gray horizontal bar. **(F)** Secondary motoneurons innervating ventrally (**a**, vS), dorsally (**b**, dS), or dorsoventrally (**c**, dvS). The arrowhead in **(c)** indicates the bifurcation in the main axon. The asterisk in **(b)** is the axon of another motoneuron in the opposite hemi-segment. **(G)** The secondary motoneuron innervating the ventral **(a)**, ventrolateral **(b)**, horizontal **(c)**, dorsolateral **(d)**, or dorsal **(e)**

(Continued)

FIGURE 2 | Continued
myoseptal region. The arrows indicate the axon terminals and roughly indicate their direction of extension. The percentiles show the ratio among the laterally projecting cells. **(H)** A cell innervating the dorsal myotseptum. The arrow indicates the axon terminal. This cell is identical to the one shown in **(Ge)** and the image was taken 6 h after the image **(Ge)** was taken. Note that the morphology of the soma changed dramatically in 6 h. **(I)** The superficial myoseptal region of **(H)** merged with the DIC image. The inset shows a stack of a few confocal sections indicated in the dotted square in **(I)**. The axon collaterals cross the myoseptal boundary marked by the black dotted line. **(J,K)** A vmS-type neuron. The arrow and arrowheads indicate the axon terminal and the collaterals extending along the blood vessels, respectively. All images in **(D–I)** were taken during 72–100 hpf and the rostral is to the left. In **(D,F,G,J)**, the oblique and horizontal dotted lines demarcate the myoseptal boundaries and the ventral edge of the spinal cord, respectively. The brackets roughly indicate the innervation territory along the dorsoventral axis in **(D,F)**, and the axial blood vessels in **(K)**. The bars indicate 20 μm, except in **(I)**, where the bars indicate 10 μm.

then raised to adulthood. The injected fish were crossed with homozygous UAS:GFP reporter fish and, for each injected fish, more than 20 F1 embryos were examined for GFP expression at 1 day and 5 days post fertilization. In the ongoing screening with this trap construct, we identified an F1 expressing GFP in the spinal cord approximately every 50 injected fish. These included lines that marked the primary motoneuron selectively (**Figure 3B**, left), as well as ones that labeled a larger number of spinal motoneurons including the secondary motoneurons (**Figure 3B**, right).

THE M602A INSERT PREDOMINANTLY LABELS THE SPINAL MOTONEURON WITH EXTENSIVE AXON ARBORIZATION

From the GFP-expressing F1 progeny, we identified gSAIzGFFM602A (hereafter, M602A) fish showing GFP expression in a relatively large number of cells in the ventral spinal cord and motor nerves (**Figures 4A–C**). In M602A;UAS:GFP embryos, GFP expression was clearly detectable in the ventral spinal cord at 20 hpf (**Figures 4A,B**), and persisted during the embryonic and larval stages (**Figure 4C**). GFP expression was also detected in the rostral-most and caudal hindbrain (**Figures 4A,C**) and very weakly in the dorsal spinal cord. We noticed that the dorsal motor nerve was only weakly stained with GFP in M602A;UAS:GFP animals, while the GFP signal in the lateral and ventral motor nerves were clearly visible (**Figure 4C**). Consistent with this observation, the dorsally projecting motoneurons innervating the myoseptal region were scarcely labeled with M602A, as judged by *mnr2b*-GFP used as a marker (**Figures 4D–F**), suggesting that M602A visualizes a subpopulation of the spinal motoneurons.

In order to identify the types of the spinal motoneuron labeled by the M602 insertion, we performed a single cell labeling experiment by injecting the UAS:GFP plasmid and observed individual GFP-labeled cells at 72–96 hpf, as described above. In total, we observed 40 single GFP-labeled cells that possessed an axon that exited the spinal cord ($N = 31$ larvae). The rate of identifying the single GFP-labeled cells was substantially lower in M602A than mnGFF7, most likely due to the early Gal4FF expression in the progenitor cells in M602A. Not surprisingly, we identified other cell types as a single GFP-labeled cell as well, including spinal interneurons and floorplate cells, in M602A larvae.

The 40 single GFP-labeled cells exhibited a topographic distribution pattern along the DV axis according to soma size (**Figure 4G**). Of these, 35 cells (88%) possessed a main axon innervating axial muscles (**Figures 4H,I**). The remaining five cells (12%) innervated the ventromedial region of the body, suggesting that they are vmS-type motoneurons (see **Figures 2J,K**). Interestingly, we found that the neurons innervating axial muscles

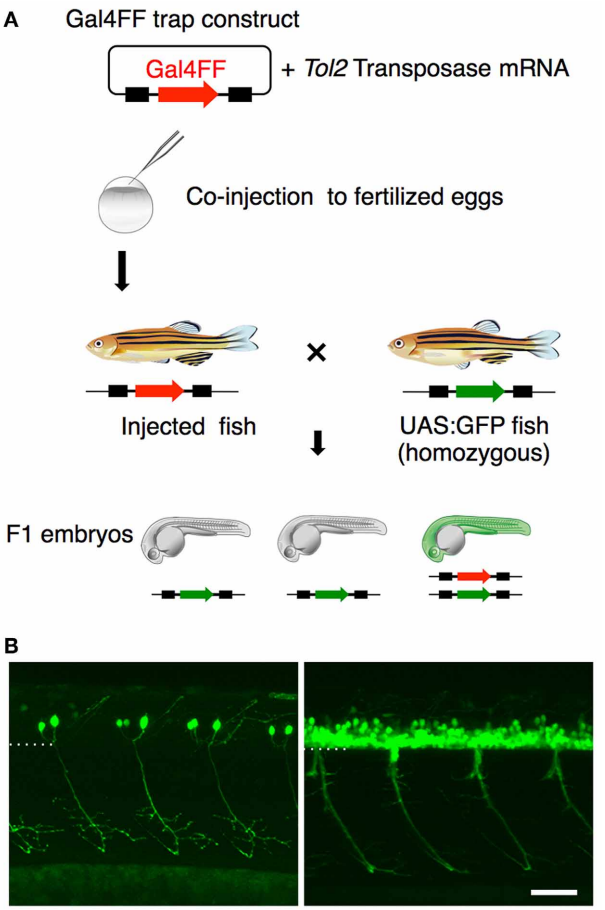

FIGURE 3 | Gene trapping using the Gal4FF-UAS system. (A) Scheme for the Gal4FF gene trapping. A plasmid DNA containing a Gal4FF construct and the transposase mRNA were co-injected into fertilized eggs. The injected fish were raised and mated with the reporter fish homozygous for the UAS:GFP insertion. The resulting F1 embryos were analyzed with a fluorescence stereomicroscope. F1 embryos expressing GFP were collected and raised for further studies. **(B)** Examples of GFP expression in the spinal cord and the motor nerve in F1 embryos at 48 hpf. In the left, the primary motoneurons are exclusively labeled. In the right, a large number of GFP labeled cells are observed in the ventral spinal cord. The dotted line demarcates the ventral limit of the spinal cord. The rostral is to the left. The bar indicates 50 μm.

to be larger in soma size in the M602 larvae (54.5 ± 15 μm^2, $p < 0.002$) than the mnGFF7 larvae (44.6 ± 12 μm^2). In addition, the GFP-labeled motoneurons were located in a slightly but still significantly more dorsal side of the spinal cord in the

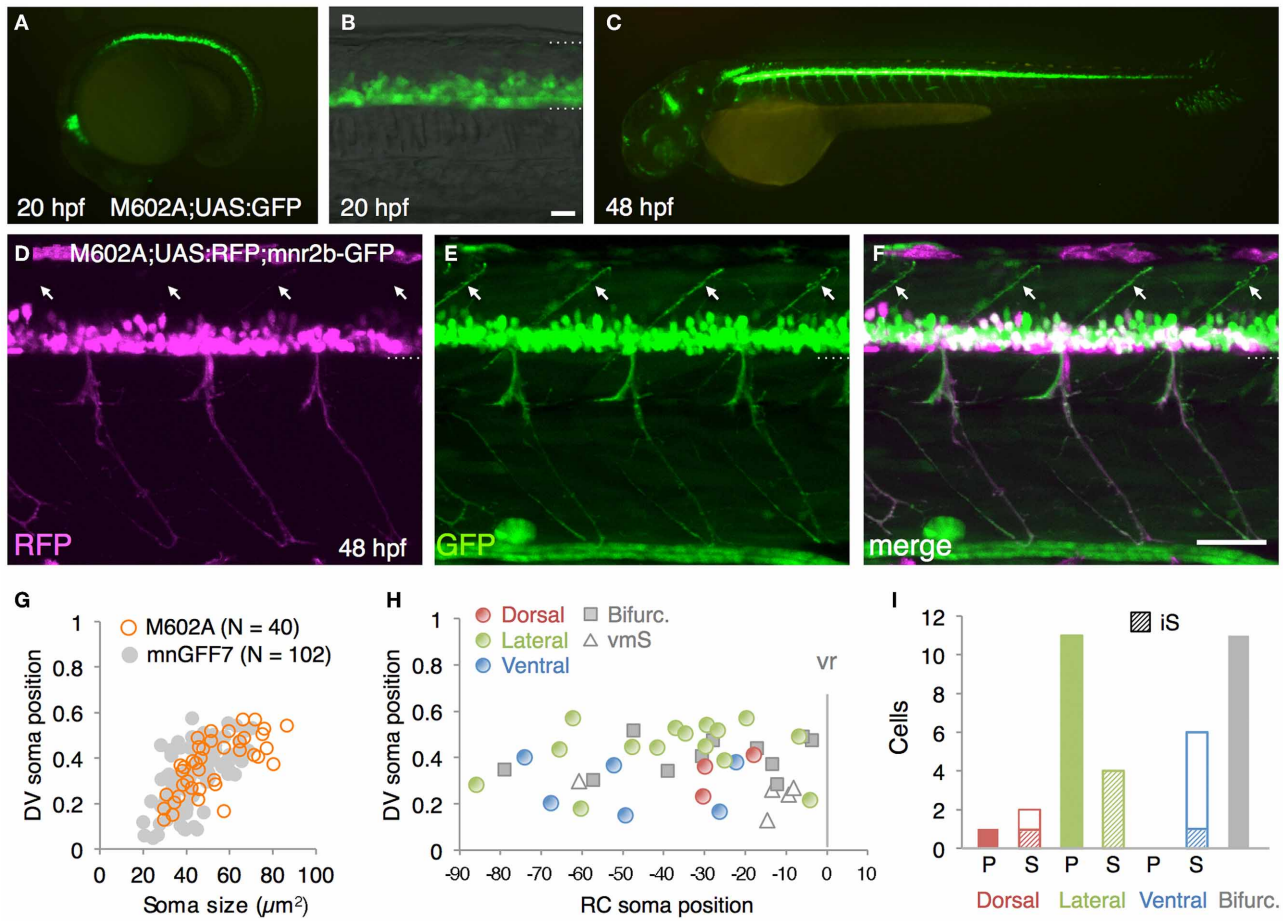

FIGURE 4 | The spinal motoneurons marked by the M602 insertions. **(A–C)** Lateral views of the M602A; UAS:GFP animals. At 20 hpf, GFP expression was detected in the ventral spinal cord and the rostral hindbrain **(A,B)**. The dotted lines demarcate the dorsal and ventral limit of the spinal cord in **(B)**. At 48 hpf, GFP is strongly detected in the ventral spinal cord and the rostral and caudal hindbrain, as well as weakly in other tissues. **(D–F)** Lateral view of the M602A;UAS:RFP; mnr2b-GFP triple transgenic animal at 48 hpf. Arrows indicate the myoseptal region in the dorsal musculature. **(G)** The plot of single GFP-labeled cells (open orange circles, $N = 40$ cells). For reference, the results from the experiment with mnGFF7 in **Figure 2A** are superimposed as gray circles. **(H)** Distribution of the GFP-labeled cells plotted with respect to the soma position along the RC axis on the horizontal axis and to the DV soma position on the vertical axis. The exit point of the ventral root from the spinal cord is indicated on the RC axis by the gray vertical line marked as vr ($x = 0$). The dorsally, laterally, and ventrally projecting cells are shown as red, green, and blue circles, respectively. The cells with bifurcating main axon and the vmS motoneurons are shown as gray squares and open triangles, respectively. **(I)** Cell counts of the neurons innervating the axial muscles based on the axon trajectory and muscle innervation pattern. P and S indicate primary and secondary motoneurons, respectively. Diagonally-striped bars indicate iS type neurons. "Bifurc" indicates the motoneurons with a bifurcating main axon. The bars indicate 20 μm in **(B)**, and 50 μm in **(F)**.

M602A larvae (0.39 ± 0.12, $p = 0.024$) than mnGFF7 larvae (0.34 ± 0.12). Consistent with these observations, the majority of the GFP-labeled cells (83%, 29/35 cells) were primary and secondary motoneurons innervating medial muscles with an extensively arborized main axon in the M602A;UAS:GFP animals (**Figure 4I**). Among these, cells possessing a laterally projecting axon ($N = 11/29$) and a bifurcating axon ($N = 10/29$) were predominant. The laterally projecting cells innervated a ventral (5/11 cells), lateral (1/11 cells), or dorsal (5/11 cells) subregion of the lateral musculature (**Figure 2B**). Collectively, these observations suggest that the M602A insertion predominantly labels the motoneurons that are located dorsally in the motor column and have a highly extensive axonal arborization.

M602A INSERTION TRAPPED ADAMTS3

In order to identify the gene responsible for the GFP expression in the M602A;UAS:GFP animals, we set out to determine the integration site of the M602A insertion. We cloned the genomic sequences flanking the M602A insertion by adaptor-ligation PCR and found that the insertion was located in a putative gene encoding a protein homologous to the ADAMTS3 protein (a disintegrin and metalloproteinase with thrombospondin motifs3, **Figure 5A**). The 5′RACE and RT-PCR analysis revealed that the putative gene encoded a 1164 amino-acid protein with multiple functional domains, which was 77% identical to the human ADAMTS3 ortholog (**Figure 5A**). To analyze the expression pattern of ADAMTS3 in zebrafish, we performed mRNA *in situ*

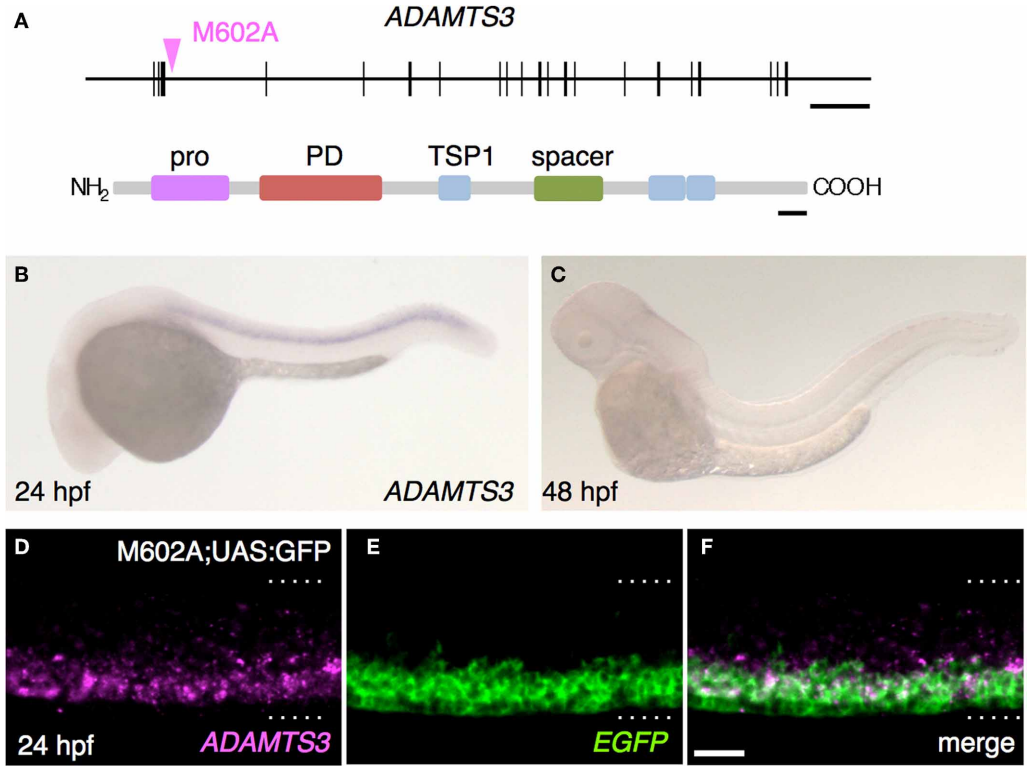

FIGURE 5 | The M602A insertion traps ADAMTS3. (A) Structure of the ADAMTS3 locus and the integration site of M602A. M602A is inserted in the 3rd intron of ADAMTS3. The long horizontal bar and vertical bars denote the genomic DNA and the exons of ADAMTS3, respectively. ADAMTS3 consists of multiple functional domains: pro, pro domain; PD, metalloprotease domain; TSP1, thrombospondin type 1 motif; spacer, spacer region [according to Porter et al. (2005)]. **(B,C)** Expression of ADAMTS3 at 24 hpf **(B)** and 48 hpf **(C)**, detected by *in situ* hybridization. **(D–F)** Expression of ADAMTS3 and EGFP detected by double fluorescent *in situ* hybridization. A confocal section of the spinal cord of the M602A;UAS:GFP embryo at 24 hpf was shown. The dotted lines demarcate the dorsal and ventral limit of the spinal cord. The scale bars indicate 20 kbp (top) and 50 amino acids (bottom) in **(A)**, and 20 μm in **(F)**.

hybridization experiments. The expression of ADAMTS3 was detected in the spinal cord at 24 hpf (**Figure 5B**). At 48 hpf, the ADAMTS3 expression in the spinal cord was reduced to below a detectable level (**Figure 5C**), suggesting that ADAMTS3 is dynamically expressed in the ventral spinal cord. The double fluorescent *in situ* hybridization showed that, in M602A;UAS:GFP embryos, the ADAMTS3 and EGFP transcripts were substantially overlapped in the ventral spinal cord (**Figures 5D–F**). Taken together, these results suggest that the M602A insertion traps the ADAMTS3 gene.

DISCUSSION

CELLULAR ORGANISATION OF THE SPINAL CORD MOTOR COLUMN IN YOUNG ZEBRAFISH AS VIEWED THROUGH mnGFF7

In the present study, we established the mnGFF7 line, a Gal4FF driver for spinal motoneurons using a BAC DNA containing the *mnr2b* locus sequence. The characterization of the mnGFF7 line disclosed at least three characteristics of the target tissue innervation by the spinal motoneuron that have previously been unreported. First, we found that the dorsally projecting neurons innervating the superficial slow muscle in the myoseptal regions were preferentially identified in the caudal portion of a spinal segment and in the dorsal half of the motor column in mnGFF7 animals. Interestingly, it has been reported that the dorsally projecting neurons with extensive axonal arborization in fast skeletal muscle (dS-type) are typically found in the rostral portion of the spinal segment (Menelaou and McLean, 2012). These two lines of evidence together predict that dorsally projecting secondary motoneurons are topographically positioned along the RC axis and thereby linked to the muscle types they innervate. From the currently available data (**Figures 2B**, **A2A**, **A2B**) (Menelaou and McLean, 2012), such a topographic configuration is not readily apparent for the ventrally or laterally projecting secondary motoneurons. Second, we found that the axon collaterals of single secondary motoneurons innervating the myoseptal regions often crossed the myoseptum, implying that these cell types can make contact with and activate the muscles on both sides of the myoseptum. Similarly, it has been reported that the axons of some secondary motoneurons cross the myoseptum and terminate in the adjacent segment in the adult stage (Westerfield et al., 1986). Such cross-myoseptal innervation would help achieve a near synchronous and unilateral activation of body wall muscles so as to generate coordinated axial movements during the larval, as well as in the adult stage. Finally, in the mnGFF7 larvae, we identified vmS-type motoneurons, which have been only poorly characterized thus far. The observation that axon

terminals and collaterals of this cell type were often observable in the vicinity of blood vessels and pronephric ducts raises the possibility that the vmS neurons serve as a part of the autonomic nervous system by directly innervating these tissues or indirectly innervating them via ganglia. These ideas need to be validated in the future by identifying the synaptic targets of vmS neurons.

The establishment of the mnGFF7 line also provided a unique tool to for obtaining insights into the overall organization of the motor column in young zebrafish. In mnGFF7;UAS:GFP larvae, we identified 63 GFP-labeled cells in a spinal hemi-segment on average. Intriguingly, it has been reported that zebrafish on average possesses 65 spinal motoneurons per spinal hemisegment at the late larval and adult stage (Van Raamsdonk et al., 1983). Therefore, our results raise a possibility that the zebrafish generates spinal motoneurons that are nearly comparable to that in the adult stage, in terms of the total number, over the first 4 days of development. The following two observations, however, suggest that the identity of a fraction of the GFP-labeled cells remains to be determined, and thus precluded an estimation of the number of GFP-labeled spinal motoneuron in mnGFF7;UAS:GFP larvae. First, we identified an interneuron among the 103 GFP-labeled single cells, suggesting that mnGFF7 labels a small population of interneurons. Secondly, the single cell labeling method rarely identified the cells at the two ends of a spinal segment along the RC axis, while we did not observe any such "gap regions" in stable mnGFF7;UAS:GFP or mnGFF7;UAS:RFP double transgenic larvae (see **Figure 1D**). This is most likely because the transient expression of GFP from the UAS:GFP plasmid tends to label cells with stronger Gal4FF activity, which results in a biased staining compared to the rather uniform labeling achieved with the stable UAS:GFP reporter transgene. In the future, the number of the spinal motoneurons expressing Gal4FF in mnGFF7 fish will be estimated more accurately by retrograde labeling using the photoconversion of the Kaede protein at the ventral root in mnGFF7;UAS:Kaede double transgenic larvae (Kazuhide Asakawa, Koichi Kawakami unpublished observation).

The 102 motoneurons that were analyzed in the single cell labeling experiment displayed a variety of dendritic morphologies: some displayed elaborate branches while others displayed only very tiny ones. The relationship between the dendritic morphologies and the cellular properties we have reported remains a subject for future investigation.

GENETIC DISSECTION OF THE MOTOR COLUMN WITH BAC TRANSGENESIS AND GENE TRAPPING

Mnx transcription factors are involved in motoneuron differentiation (Tanabe et al., 1998; Seredick et al., 2012). Recently, the zebrafish Mnx genes, *mnx1*, *mnr2a*/*mnx2a,* and *mnr2b*, were shown to be necessary for the specification of the MiP primary motoneuron (Seredick et al., 2012). Our observation that *mnr2b* is expressed rather broadly in the ventral spinal cord at 48 hpf suggests that *mnr2b* is also expressed in the secondary motoneurons and plays a role in their differentiation. An intriguing observation is that *mnr2b* is first expressed transiently in all of the primary motoneurons, and then the expression becomes restricted to the dorsally projecting subtype, MiP (Seredick et al., 2012). Therefore, it would be interesting to determine whether *mnr2b* is expressed in the secondary motoneurons in a similar manner; i.e., *mnr2b* is first expressed in a number of secondary motoneurons and then is restricted to a dorsally projecting subtype. Our observation that the dorsally projecting neurons were the most frequently identified type in the single cell labeling experiment at 72–100 hpf is consistent with this idea. In addition to the motoneuron types labeled in mnGFF7 animals, characterization of those that are labeled with *mnx1* (Wyart et al., 2009; Zelenchuk and Bruses, 2011; Seredick et al., 2012) and *mnr2a cis*-elements will ultimately provide a more comprehensive view of the connections between the axial motoneurons and their target axial muscles established by the Mnx transcriptional program.

We have demonstrated that gene trapping is an effective approach both for identifying genes expressed in a specific population of neurons and analyzing the detailed morphologies of these genetically tagged neurons. We analyzed the gene trap insertion M602A, and identified ADAMTS3 as being expressed in the ventral spinal cord. ADAMTS proteases are known to be evolutionarily conserved non-membrane-bound enzymes that interact with components of the extracellular matrix (ECM) so as to induce degradation (Porter et al., 2005; Salter et al., 2010). It has been demonstrated that ADAMTS3 can process procollagen I and II in cultured cells (Fernandes et al., 2001; Le Goff et al., 2006). Because the M602A insertion primarily labels the motoneurons that have extensive arborization (83%, 29/35 cells), one possible role of ADAMTS3 might be to the promotion the arborization of motor axons through a processing of the ECM. The exact physiological role(s) of ADAMTS3 should be determined by manipulating its function *in vivo*. In the mouse, ADAMTS3 is reported to be expressed in the hindbrain, developing cerebral cortex and dorsal root ganglia, as well as musculoskeletal tissues, but its expression in the spinal cord has not been previously shown (Le Goff et al., 2006). Whether ADAMTS3 function in the spinal cord is evolutionarily conserved also remains elusive at present.

TOWARD A FUNCTIONAL ANALYSIS OF THE SPINAL CORD MOTOR COLUMN WITH THE Gal4-UAS SYSTEM

Obviously, the Gal4FF driver lines established in the study will be applicable to ectopic expression of various genes and their mutant forms in motoneurons via the Gal4FF-UAS system, and thus should prove to be valuable in the study of motoneuron development, function and disease. Additionally, genetically-encoded functional probes for neurobiology research such as neurotoxins, light-gated ion channels for optogenetics and fluorescent sensors for monitoring neuronal activity can also be delivered to the Gal4FF-expressing motoneurons. Among these approaches, *in vivo* calcium imaging of spinal motoneurons appears promising for motoneuron functional analysis, allowing for the simultaneous visualization of the activity of groups of neurons distributed in the motor column (McLean et al., 2007; Muto et al., 2011, 2013; Warp et al., 2012). We found that when the UAS-regulated calcium indicator GCaMP7a (Muto et al., 2013) was expressed in the spinal motoneurons in mnGFF7

and M602A, the change in fluorescent intensity of the GCaMP associated with body movements was detectable in the cell bodies as well as the axons of spinal motoneurons in larvae. Moreover, the change in fluorescent intensity of the GCaMP was also detectable in pectoral and abducens motoneurons (Kazuhide Asakawa, Koichi Kawakami unpublished observation). Therefore, the mnGFF7 and M602A lines should be applied not only to a functional analysis of axial motoneurons, but also to that of the abducens and limb motoneurons in the near future.

MATERIALS AND METHODS

FISH

This study was carried out in accordance with the Guide for the Care and Use of Laboratory Animals of the Institutional Animal Care and Use Committee (IACUC, approval identification number 24-2) of the National Institute of Genetics (NIG, Japan), which has an Animal Welfare Assurance on file (assurance number A5561-01) at the Office of Laboratory Animal Welfare of the National Institutes of Health (NIH, USA).

BAC ENGINEERING AND TRANSGENESIS

For BAC manipulation, the purified mnr2b-BAC DNA (CH211-172N16, BACPAC Resources Center) was introduced into SW102 *E coli* cells (Warming et al., 2005). Transformation through electroporation was performed as described in (Suster et al., 2009b). For *Tol2* transposon-mediated BAC transgenesis, the iTol2-amp cassette (Suster et al., 2009b) was introduced into the backbone (pBeloBAC11, U51113) of the mnr2b-BAC. The iTol2-amp cassette was amplified by PCR with the primer pair iTol2A-f (5′-gcg cgc caa tag tca tgc ccc gcg ccc acc gga agg agc tga ctg ggt tgC CCT GCT CGA GCC GGG CCC-3′) and iTol2A-r (5′-agc aat ata gtc cta caa tgt caa gct cga ccg atg ccc ttg aga gcc ttA TTA TGA TCC TCT AGA TCA GAT CT-3′), where the lower and upper cases indicate the pBeloBAC11 sequences for homologous recombination and the iTol2-amp annealing sequences, respectively. Two hundred ng of the PCR product (1∼2 μl) were used against 25 μl of cell pellet for transformation by electroporation using a Gene Pulser cuvette (0.1 cm, Bio-Rad) and a MicroPulser (Bio-Rad). For introducing the Gal4FF gene into the *mnr2b* locus in the resulting mnr2b-iTol2-amp-BAC, the Gal4FF-polyA-Km^r cassette was amplified by PCR using the pKZGFFKm plasmid as the template with the primer pair mnr2b-Gal4FF-f (5′-tat cag cgc aat tac ctg caa ctc taa aca caa caa aag tgt tgc aAT GAA GCT ACT GTC TTC TAT CGA A-3′) and Km-r (5′-ggt tct tca gct aaa agg gcg tcg atc ctg aag ttc ttt gac ttt tcc atC AAT TCA GAA GAA CTC GTC AAG AA-3′), where the lower and upper cases indicate the *mnr2b* sequences for homologous recombination and the pKZGFFKm-annealing sequences, respectively. For BAC transgensis, BAC DNAs were purified with Nucleobond® BAC100 (MACHEREY-NAGEL). A wild-type embryo at the one-cell stage was injected with 45 pg of the purified BAC DNA and 45 pg of *Tol2* transposase mRNA. Germline transmission was confirmed by crossing the injected fish with the homozygous UAS:GFP fish. By crossing sixteen injected fish with the UAS:GFP reporter fish, we identified three founder fish that gave rise to the GFP-positive F1 offspring (germline transmission rate 19%). We chose one of these F1s, named mnGFF7, for further analysis, because it displayed the strongest GFP signal when combined with UAS:GFP at 24 hpf, while the overall GFP reporter expression patterns were indistinguishable among these F1s.

SINGLE CELL LABELLING

For single cell labeling of Gal4FF-expressing cells in mnGFF7 and M602A larvae, 18pg of pT2KUASGFP plasmid (Asakawa et al., 2008) were injected into a blastomere at the 4- or 8-cell stage. The injected embryos were raised in embryonic buffer containing 0.003% (w/v) *N*-Phenylthiourea (SIGMA, P7629) to inhibit melanogenesis. The cells uniquely labeled with GFP or clearly identifiable as isolated single cells in a hemi-segment were analyzed by confocal microscopy. The GFP-labeled motoneurons at the segment levels 4–20 were analyzed. Soma size, which was defined by measuring the largest cross sectional area of the soma, and location (center of mass) were determined by ImageJ software. Dorsal and ventral limits of the spinal cord were determined based on a DIC image taken with a GFP image. Statistical analyses were performed using Mann–Whitney U tests.

GENE TRAPPING

Wild type fish were injected with the pT2GgSAIzGFFM plasmid, containing a *Tol2*-based gene trap construct with a splice acceptor from the zebrafish gata6 gene and the codon-optimized Gal4FF gene, and the synthesized mRNA encoding codon-optimized Tol2 transposase (Abe et al., 2011) at one-cell stage, raised and crossed with the UAS:GFP reporter line. Details of pT2GgSAIzGFFM will be described elsewhere (Abe et al. unpublished results).

LINKER-MEDIATED PCR, 5′RACE AND RT-PCR

Adaptor ligation-mediated PCR was carried out as described previously (Asakawa and Kawakami, 2009). For RT-PCR and 5′RACE, the total RNA was prepared from 147 wild-type embryos at 48 hpf by homogenizing the embryos in 1 ml of Trizol Reagent (Life Technologies). Five μg of the total RNA were used for cDNA synthesis along with a primer in the ADAMTS3 coding sequence adamts3-ex4r (5′- GAT TGG CTG GTA ATC CAA AGA G-3′) and the 5′RACE System for Rapid Amplification of cDNA Ends version 2.0 (Invitrogen). By using the cDNA as a template, 35 cycles of a first round PCR (94°C for 30 s; 55°C for 30 s; 72°C for 2min) was carried out using the primers adamts3-ex3r1 (5′-TGC AGT CTG TTT TTA GCA ACT CTC-3′) and Abridged Anchor Primer (AAP: 5′-GGC CAC GCG TCG ACT AGT ACG GGI IGG GII GGG IIG-3′) followed by a second round of PCR using adamts3-ex3r2 (5′-CTT GTG ATT GGC TGA TAG AAA ATG-3′) and Abridged Universal Amplification Primer (AUAP: 5′-GGC CAC GCG TCG ACT AGT AC-3′). The 5′RACE products were cloned with a TA cloning kit (Invitrogen) and sequenced. For RT-PCR analysis of the ADAMTS3 gene, the primer pair adamts3-f1 (5′-AGG CCT ACC ATG GTT GTC CTG TCA CTT AGG TTA-3′), and adamts3-r1 (5′-CTC GAG TCA TCT CTC CAC CTC AGA AGA TGT-3′) were used based on the nucleotide sequence for the putative ADAMTS3 (XM_692142). The cDNA obtained from wild type embryos at 48 hpf was used as the PCR template. The cDNA of ADAMTS3

were cloned with a TA cloning kit (Invitrogen) and sequenced (KC894955).

WHOLE-MOUNT *in situ* HYBRIDISATION

In situ hybridization experiments for *mnr2b* and ADAMTS3 were performed against wild-type embryos as described in (Nagayoshi et al., 2008). Antisense probes for *mnr2b* and ADAMTS3 were synthesized with a DIG RNA labeling kit (Roche) using the open reading frame (ORF) of *mnr2b* and the ORF of ADAMTS3 cloned from the RT-PCR analysis as templates, respectively. The ORF of *mnr2b* was cloned by PCR with the primers mnr2b-f1 (5′-ATG GAA AAG TCA AAG AAC TTC AGG-3′) and mnr2b-963r (5′-TCA TAA CCC TGC CCG GAT CTT CCT-3′). The DIG-labeled *mnr2b* and ADAMTS3 antisense probes were detected with a TSA Kit#16 AlexaFluor647 tyramide (T20926, Molecular Probes) and BM Purple AP Substrate (Roche), respectively. The double fluorescent *in situ* hybridization for ADAMTS3 and EGFP was performed against M602A;UAS:GFP embryos as described in (Brend and Holley, 2009). Antisense probes for ADAMTS3 and EGFP were synthesized with DIG RNA labeling kit (Roche) and Fluorescenin RNA labeling kit (Roche), respectively. The DIG-labeled ADAMTS3 and Fluorescein-labeled EGFP were detected with a TSA Kit#16 AlexaFluor647 tyramide and TSA Plus Fluorescein system (NEL74100KT, PerkinElmer), respectively.

MICROSCOPIC ANALYSIS

A fluorescence stereomicroscope (MZ16FA, Leica) equipped with a CCD camera (DFC300FX, Leica) was used to observe and take images of GFP-expressing embryos. A live embryo or larva was embedded in 1% low-melting agarose (NuSieve® GTG® Agarose, Lonza) on a Glass Base dish (IWAKI, 3010-035) and subjected to confocal microscopy using an Olympus FV-1000D laser confocal microscope. Images of live embryos and larvae were acquired as serial sections along the *z*-axis and processed with an Olympus Fluoview Ver2.1b Viewer and Adobe Photoshop CS6.

ACKNOWLEDGMENTS

We would like to thank Drs. R. Fukuda, A. Muto, N. Mochizuki, and S. Isogai for the plasmids and discussions, and A. Ito, M. Suzuki, M. Mizushina, N. Mouri, and Y. Kanebako for fish maintenance. This work was supported by JSPS KAKENHI Grant numbers 23241063 (Koichi Kawakami), 22700349 (Kazuhide Asakawa), MEXT KAKENHI Grant number 23115720 (Kazuhide Asakawa), The Uehara Memorial Foundation (Kazuhide Asakawa), The Kao Foundation for Arts and Sciences (Kazuhide Asakawa), Mitsubishi Foundation (Kazuhide Asakawa), Daiichi-Sankyo Foundation of Life Science (Kazuhide Asakawa) and the National BioResource Project from the Ministry of education, Culture, Sports, Science, and Technology of Japan (Koichi Kawakami).

REFERENCES

Abe, G., Suster, M. L., and Kawakami, K. (2011). Tol2-mediated transgenesis, gene trapping, enhancer trapping, and the Gal4-UAS system. *Methods Cell Biol.* 104, 23–49.

Agalliu, D., Takada, S., Agalliu, I., McMahon, A. P., and Jessell, T. M. (2009). Motor neurons with axial muscle projections specified by Wnt4/5 signaling. *Neuron* 61, 708–720.

Appel, B., Korzh, V., Glasgow, E., Thor, S., Edlund, T., Dawid, I. B., et al. (1995). Motoneuron fate specification revealed by patterned LIM homeobox gene expression in embryonic zebrafish. *Development* 121, 4117–4125.

Aramaki, S., and Hatta, K. (2006). Visualizing neurons one-by-one *in vivo*: optical dissection and reconstruction of neural networks with reversible fluorescent proteins. *Dev. Dyn.* 235, 2192–2199.

Arrenberg, A. B., Del Bene, F., and Baier, H. (2009). Optical control of zebrafish behavior with halorhodopsin. *Proc. Natl. Acad. Sci. U.S.A.* 106, 17968–17973.

Asakawa, K., Higashijima, S., and Kawakami, K. (2012). An mnr2b/hlxb9lb enhancer trap line that labels spinal and abducens motor neurons in zebrafish. *Dev. Dyn.* 241, 327–332.

Asakawa, K., and Kawakami, K. (2008). Targeted gene expression by the Gal4-UAS system in zebrafish. *Dev. Growth Differ.* 50, 391–399.

Asakawa, K., and Kawakami, K. (2009). The Tol2-mediated Gal4-UAS method for gene and enhancer trapping in zebrafish. *Methods* 49, 275–281.

Asakawa, K., Suster, M. L., Mizusawa, K., Nagayoshi, S., Kotani, T., Urasaki, A., et al. (2008). Genetic dissection of neural circuits by Tol2 transposon-mediated Gal4 gene and enhancer trapping in zebrafish. *Proc. Natl. Acad. Sci. U.S.A.* 105, 1255–1260.

Balciunas, D., Davidson, A. E., Sivasubbu, S., Hermanson, S. B., Welle, Z., and Ekker, S. C. (2004). Enhancer trapping in zebrafish using the Sleeping Beauty transposon. *BMC Genomics* 5:62. doi: 10.1186/1471-2164-5-62

Beattie, C. E., Hatta, K., Halpern, M. E., Liu, H., Eisen, J. S., and Kimmel, C. B. (1997). Temporal separation in the specification of primary and secondary motoneurons in zebrafish. *Dev. Biol.* 187, 171–182.

Bonanomi, D., and Pfaff, S. L. (2010). Motor axon pathfinding. *Cold Spring Harb. Perspect. Biol.* 2, a001735.

Brand, A. H., and Perrimon, N. (1993). Targeted gene expression as a means of altering cell fates and generating dominant phenotypes. *Development* 118, 401–415.

Brend, T., and Holley, S. A. (2009). Zebrafish whole mount high-resolution double fluorescent *in situ* hybridization. *J. Vis. Exp.* 25:e1229. doi: 10.3791/1229

Budick, S. A., and O'Malley, D. M. (2000). Locomotor repertoire of the larval zebrafish: swimming, turning and prey capture. *J. Exp. Biol.* 203, 2565–2579.

Bussmann, J., and Schulte-Merker, S. (2011). Rapid BAC selection for tol2-mediated transgenesis in zebrafish. *Development* 138, 4327–4332.

Cheesman, S. E., Layden, M. J., Von Ohlen, T., Doe, C. Q., and Eisen, J. S. (2004). Zebrafish and fly Nkx6 proteins have similar CNS expression patterns and regulate motoneuron formation. *Development* 131, 5221–5232.

Davidson, A. E., Balciunas, D., Mohn, D., Shaffer, J., Hermanson, S., Sivasubbu, S., et al. (2003). Efficient gene delivery and gene expression in zebrafish using the Sleeping Beauty transposon. *Dev. Biol.* 263, 191–202.

Davison, J. M., Akitake, C. M., Goll, M. G., Rhee, J. M., Gosse, N., Baier, H., et al. (2007). Transactivation from Gal4-VP16 transgenic insertions for tissue-specific cell labeling and ablation in zebrafish. *Dev. Biol.* 304, 811–824.

Del Bene, F., Wyart, C., Robles, E., Tran, A., Looger, L., Scott, E. K., et al. (2010). Filtering of visual information in the tectum by an identified neural circuit. *Science* 330, 669–673.

Distel, M., Wullimann, M. F., and Koster, R. W. (2009). Optimized Gal4 genetics for permanent gene expression mapping in zebrafish. *Proc. Natl. Acad. Sci. U.S.A.* 106, 13365–13370.

Douglass, A. D., Kraves, S., Deisseroth, K., Schier, A. F., and Engert, F. (2008). Escape behavior elicited by single, channelrhodopsin-2-evoked spikes in zebrafish somatosensory neurons. *Curr. Biol.* 18, 1133–1137.

Dreosti, E., Odermatt, B., Dorostkar, M. M., and Lagnado, L. (2009). A genetically encoded reporter of synaptic activity *in vivo*. *Nat. Methods* 6, 883–889.

Faucherre, A., and Lopez-Schier, H. (2011). Delaying Gal4-driven gene expression in the zebrafish with morpholinos and Gal80. *PLoS ONE* 6:e16587. doi: 10.1371/journal.pone.0016587

Fenno, L., Yizhar, O., and Deisseroth, K. (2011). The development and application of optogenetics. *Annu. Rev. Neurosci.* 34, 389–412.

Fernandes, R. J., Hirohata, S., Engle, J. M., Colige, A., Cohn, D. H., Eyre, D. R., et al. (2001). Procollagen II amino propeptide processing by ADAMTS-3. Insights on dermatosparaxis. *J. Biol. Chem.* 276, 31502–31509.

Fetcho, J. R. (1987). A review of the organization and evolution of motoneurons innervating the axial musculature of vertebrates. *Brain Res.* 434, 243–280.

Fetcho, J. R. (1992). The spinal motor system in early vertebrates and some of its evolutionary changes. *Brain Behav. Evol.* 40, 82–97.

Fujimoto, E., Gaynes, B., Brimley, C. J., Chien, C. B., and Bonkowsky, J. L. (2011). Gal80 intersectional regulation of cell-type specific expression in vertebrates. *Dev. Dyn.* 240, 2324–2334.

Gabriel, J. P., Ausborn, J., Ampatzis, K., Mahmood, R., Eklof-Ljunggren, E., and El Manira, A. (2011). Principles governing recruitment of motoneurons during swimming in zebrafish. *Nat. Neurosci.* 14, 93–99.

Grillner, S., and Jessell, T. M. (2009). Measured motion: searching for simplicity in spinal locomotor networks. *Curr. Opin. Neurobiol.* 19, 572–586.

Hatta, K., Tsujii, H., and Omura, T. (2006). Cell tracking using a photoconvertible fluorescent protein. *Nat. Protoc.* 1, 960–967.

Higashijima, S., Hotta, Y., and Okamoto, H. (2000). Visualization of cranial motor neurons in live transgenic zebrafish expressing green fluorescent protein under the control of the islet-1 promoter/enhancer. *J. Neurosci.* 20, 206–218.

Hutchinson, S. A., Cheesman, S. E., Hale, L. A., Boone, J. Q., and Eisen, J. S. (2007). Nkx6 proteins specify one zebrafish primary motoneuron subtype by regulating late islet1 expression. *Development* 134, 1671–1677.

Hutchinson, S. A., and Eisen, J. S. (2006). Islet1 and Islet2 have equivalent abilities to promote motoneuron formation and to specify motoneuron subtype identity. *Development* 133, 2137–2147.

Inbal, A., Topczewski, J., and Solnica-Krezel, L. (2006). Targeted gene expression in the zebrafish prechordal plate. *Genesis* 44, 584–588.

Janovjak, H., Szobota, S., Wyart, C., Trauner, D., and Isacoff, E. Y. (2010). A light-gated, potassium-selective glutamate receptor for the optical inhibition of neuronal firing. *Nat. Neurosci.* 13, 1027–1032.

Jessell, T. M. (2000). Neuronal specification in the spinal cord: inductive signals and transcriptional codes. *Nat. Rev. Genet.* 1, 20–29.

Jones, W. D. (2009). The expanding reach of the GAL4/UAS system into the behavioral neurobiology of Drosophila. *BMB Rep.* 42, 705–712.

Kawakami, K., Shima, A., and Kawakami, N. (2000). Identification of a functional transposase of the Tol2 element, an Ac-like element from the Japanese medaka fish, and its transposition in the zebrafish germ lineage. *Proc. Natl. Acad. Sci. U.S.A.* 97, 11403–11408.

Koster, R. W., and Fraser, S. E. (2001). Tracing transgene expression in living zebrafish embryos. *Dev. Biol.* 233, 329–346.

Le Goff, C., Somerville, R. P., Kesteloot, F., Powell, K., Birk, D. E., Colige, A. C., et al. (2006). Regulation of procollagen amino-propeptide processing during mouse embryogenesis by specialization of homologous ADAMTS proteases: insights on collagen biosynthesis and dermatosparaxis. *Development* 133, 1587–1596.

Lewis, K. E., and Eisen, J. S. (2003). From cells to circuits: development of the zebrafish spinal cord. *Prog. Neurobiol.* 69, 419–449.

Liu, C., Ma, W., Su, W., and Zhang, J. (2012). Prdm14 acts upstream of islet2 transcription to regulate axon growth of primary motoneurons in zebrafish. *Development* 139, 4591–4600.

Liu, D. W., and Westerfield, M. (1988). Function of identified motoneurones and co-ordination of primary and secondary motor systems during zebra fish swimming. *J. Physiol.* 403, 73–89.

Luo, L., Callaway, E. M., and Svoboda, K. (2008). Genetic dissection of neural circuits. *Neuron* 57, 634–660.

Marvin, J. S., Borghuis, B. G., Tian, L., Cichon, J., Harnett, M. T., Akerboom, J., et al. (2013). An optimized fluorescent probe for visualizing glutamate neurotransmission. *Nat. Methods* 10, 162–170.

McLean, D. L., Fan, J., Higashijima, S., Hale, M. E., and Fetcho, J. R. (2007). A topographic map of recruitment in spinal cord. *Nature* 446, 71–75.

McLean, D. L., and Fetcho, J. R. (2011). Movement, technology and discovery in the zebrafish. *Curr. Opin. Neurobiol.* 21, 110–115.

McLean, D. L., Masino, M. A., Koh, I. Y., Lindquist, W. B., and Fetcho, J. R. (2008). Continuous shifts in the active set of spinal interneurons during changes in locomotor speed. *Nat. Neurosci.* 11, 1419–1429.

Menelaou, E., and McLean, D. L. (2012). A gradient in endogenous rhythmicity and oscillatory drive matches recruitment order in an axial motor pool. *J. Neurosci.* 32, 10925–10939.

Meng, A., Tang, H., Ong, B. A., Farrell, M. J., and Lin, S. (1997). Promoter analysis in living zebrafish embryos identifies a cis-acting motif required for neuronal expression of GATA-2. *Proc. Natl. Acad. Sci. U.S.A.* 94, 6267–6272.

Muto, A., Ohkura, M., Abe, G., Nakai, J., and Kawakami, K. (2013). Real-time visualization of neuronal activity during perception. *Curr. Biol.* 23, 307–311.

Muto, A., Ohkura, M., Kotani, T., Higashijima, S., Nakai, J., and Kawakami, K. (2011). Genetic visualization with an improved GCaMP calcium indicator reveals spatiotemporal activation of the spinal motor neurons in zebrafish. *Proc. Natl. Acad. Sci. U.S.A.* 108, 5425–5430.

Myers, P. Z. (1985). Spinal motoneurons of the larval zebrafish. *J. Comp. Neurol.* 236, 555–561.

Myers, P. Z., Eisen, J. S., and Westerfield, M. (1986). Development and axonal outgrowth of identified motoneurons in the zebrafish. *J. Neurosci.* 6, 2278–2289.

Nagayoshi, S., Hayashi, E., Abe, G., Osato, N., Asakawa, K., Urasaki, A., et al. (2008). Insertional mutagenesis by the Tol2 transposon-mediated enhancer trap approach generated mutations in two developmental genes: tcf7 and synembryn-like. *Development* 135, 159–169.

Ogura, E., Okuda, Y., Kondoh, H., and Kamachi, Y. (2009). Adaptation of GAL4 activators for GAL4 enhancer trapping in zebrafish. *Dev. Dyn.* 238, 641–655.

Park, H. C., Shin, J., and Appel, B. (2004). Spatial and temporal regulation of ventral spinal cord precursor specification by Hedgehog signaling. *Development* 131, 5959–5969.

Pineda, R. H., Svoboda, K. R., Wright, M. A., Taylor, A. D., Novak, A. E., Gamse, J. T., et al. (2006). Knockdown of Nav1.6a Na+ channels affects zebrafish motoneuron development. *Development* 133, 3827–3836.

Porter, S., Clark, I. M., Kevorkian, L., and Edwards, D. R. (2005). The ADAMTS metalloproteinases. *Biochem. J.* 386, 15–27.

Sagasti, A., Guido, M. R., Raible, D. W., and Schier, A. F. (2005). Repulsive interactions shape the morphologies and functional arrangement of zebrafish peripheral sensory arbors. *Curr. Biol.* 15, 804–814.

Saint-Amant, L., and Drapeau, P. (1998). Time course of the development of motor behaviors in the zebrafish embryo. *J. Neurobiol.* 37, 622–632.

Salter, R. C., Ashlin, T. G., Kwan, A. P., and Ramji, D. P. (2010). ADAMTS proteases: key roles in atherosclerosis? *J. Mol. Med.* 88, 1203–1211.

Sato, T., Hamaoka, T., Aizawa, H., Hosoya, T., and Okamoto, H. (2007). Genetic single-cell mosaic analysis implicates ephrinB2 reverse signaling in projections from the posterior tectum to the hindbrain in zebrafish. *J. Neurosci.* 27, 5271–5279.

Scott, E. K., Mason, L., Arrenberg, A. B., Ziv, L., Gosse, N. J., Xiao, T., et al. (2007). Targeting neural circuitry in zebrafish using GAL4 enhancer trapping. *Nat. Methods* 4, 323–326.

Segawa, H., Miyashita, T., Hirate, Y., Higashijima, S., Chino, N., Uyemura, K., et al. (2001). Functional repression of Islet-2 by disruption of complex with Ldb impairs peripheral axonal outgrowth in embryonic zebrafish. *Neuron* 30, 423–436.

Seredick, S., Ryswyk, L., Hutchinson, S. A., and Eisen, J. S. (2012). Zebrafish Mnx proteins specify one motoneuron subtype and suppress acquisition of interneuron characteristics. *Neural Dev.* 7, 35.

Sharma, K., Sheng, H. Z., Lettieri, K., Li, H., Karavanov, A., Potter, S., et al. (1998). LIM homeodomain factors Lhx3 and Lhx4 assign subtype identities for motor neurons. *Cell* 95, 817–828.

Shirasaki, R., and Pfaff, S. L. (2002). Transcriptional codes and the control of neuronal identity. *Annu. Rev. Neurosci.* 25, 251–281.

Suster, M. L., Kania, A., Liao, M., Asakawa, K., Charron, F., Kawakami, K., et al. (2009a). A novel conserved evx1 enhancer links spinal interneuron morphology and cis-regulation from fish to mammals. *Dev. Biol.* 325, 422–433.

Suster, M. L., Sumiyama, K., and Kawakami, K. (2009b). Transposon-mediated BAC transgenesis in zebrafish and mice. *BMC Genomics* 10:477. doi: 10.1186/1471-2164-10-477

Szobota, S., Gorostiza, P., Del Bene, F., Wyart, C., Fortin, D. L., Kolstad, K. D., et al. (2007). Remote control of neuronal activity with a light-gated glutamate receptor. *Neuron* 54, 535–545.

Tallafuss, A., Gibson, D., Morcos, P., Li, Y., Seredick, S., Eisen, J., et al. (2012). Turning gene function ON and OFF using sense and antisense photo-morpholinos in zebrafish. *Development* 139, 1691–1699.

Tanabe, Y., William, C., and Jessell, T. M. (1998). Specification of motor neuron identity by the MNR2 homeodomain protein. *Cell* 95, 67–80.

Thermes, V., Grabher, C., Ristoratore, F., Bourrat, F., Choulika, A., Wittbrodt, J., et al. (2002). I-SceI meganuclease mediates highly efficient transgenesis in fish. *Mech. Dev.* 118, 91–98.

Tokumoto, M., Gong, Z., Tsubokawa, T., Hew, C. L., Uyemura, K., Hotta, Y., et al. (1995). Molecular heterogeneity among primary motoneurons and within myotomes revealed by the differential mRNA expression of novel islet-1 homologs in embryonic zebrafish. *Dev. Biol.* 171, 578–589.

Tsuchida, T., Ensini, M., Morton, S. B., Baldassare, M., Edlund, T., Jessell, T. M., et al. (1994). Topographic organization of embryonic motor neurons defined by expression of LIM homeobox genes. *Cell* 79, 957–970.

Van Raamsdonk, W., Mos, W., Smit-Onel, M. J., Van Der Laarse, W. J., and Fehres, R. (1983). The development of the spinal motor column in relation to the myotomal muscle fibers in the zebrafish (Brachydanio rerio). I. Posthatching development. *Anat. Embryol.* 167, 125–139.

Warming, S., Costantino, N., Court, D. L., Jenkins, N. A., and Copeland, N. G. (2005). Simple and highly efficient BAC recombineering using galK selection. *Nucleic Acids Res.* 33, e36.

Warp, E., Agarwal, G., Wyart, C., Friedmann, D., Oldfield, C. S., Conner, A., et al. (2012). Emergence of patterned activity in the developing zebrafish spinal cord. *Curr. Biol.* 22, 93–102.

Wendik, B., Maier, E., and Meyer, D. (2004). Zebrafish mnx genes in endocrine and exocrine pancreas formation. *Dev. Biol.* 268, 372–383.

Westerfield, M., McMurray, J. V., and Eisen, J. S. (1986). Identified motoneurons and their innervation of axial muscles in the zebrafish. *J. Neurosci.* 6, 2267–2277.

Wyart, C., Del Bene, F., Warp, E., Scott, E. K., Trauner, D., Baier, H., et al. (2009). Optogenetic dissection of a behavioural module in the vertebrate spinal cord. *Nature* 461, 407–410.

Yokogawa, T., Hannan, M. C., and Burgess, H. A. (2012). The dorsal raphe modulates sensory responsiveness during arousal in zebrafish. *J. Neurosci.* 32, 15205–15215.

Zelenchuk, T. A., and Bruses, J. L. (2011). *In vivo* labeling of zebrafish motor neurons using an *mnx1* enhancer and Gal4/UAS. *Genesis* 49, 546–554.

Conflict of Interest Statement: The authors declare that the research was conducted in the absence of any commercial or financial relationships that could be construed as a potential conflict of interest.

Received: 02 February 2013; paper pending published: 08 March 2013; accepted: 04 May 2013; published online: 28 May 2013.

Citation: Asakawa K, Abe G and Kawakami K (2013) Cellular dissection of the spinal cord motor column by BAC transgenesis and gene trapping in zebrafish. Front. Neural Circuits ***7****:100. doi: 10.3389/fncir.2013.00100*

APPENDIX

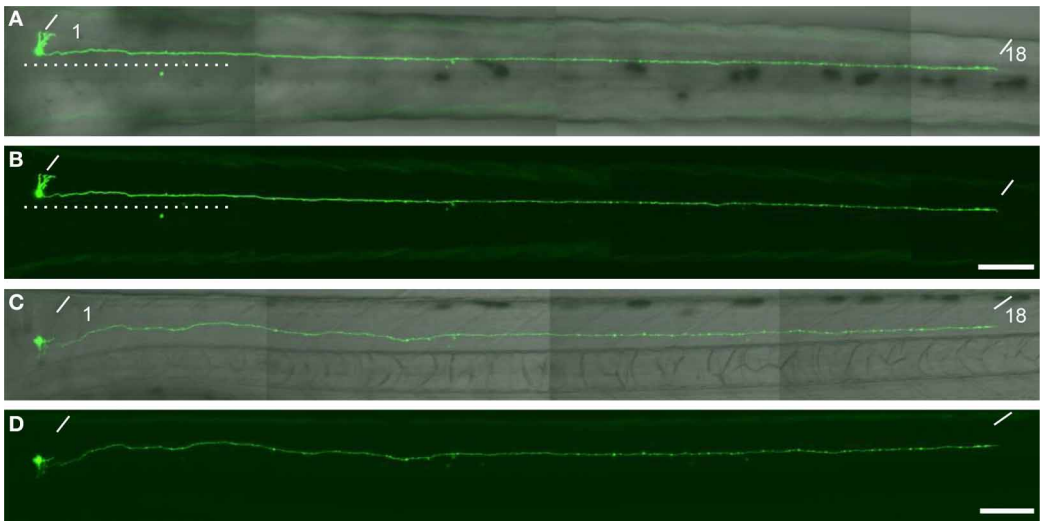

FIGURE A1 | A descending interneuron identified in the single cell labelling experiment. (A,B) The dorsal view of a larvae at 76 hpf. The soma of the GFP-labelled cell located at the level of the anterior boundary of somite 1. The axon descended ipsilaterally to the level of somite 18. The dotted lines indicate the position of the midline. (**C** and **D**) The lateral view of the same larva. The oblique lines indicate the anterior boundary of somite 1 and 18. In **(A)** and **(C)**, the DIC image was superimposed onto the GFP image. The scale bars indicate 100 μm in **(B)** and **(D)**.

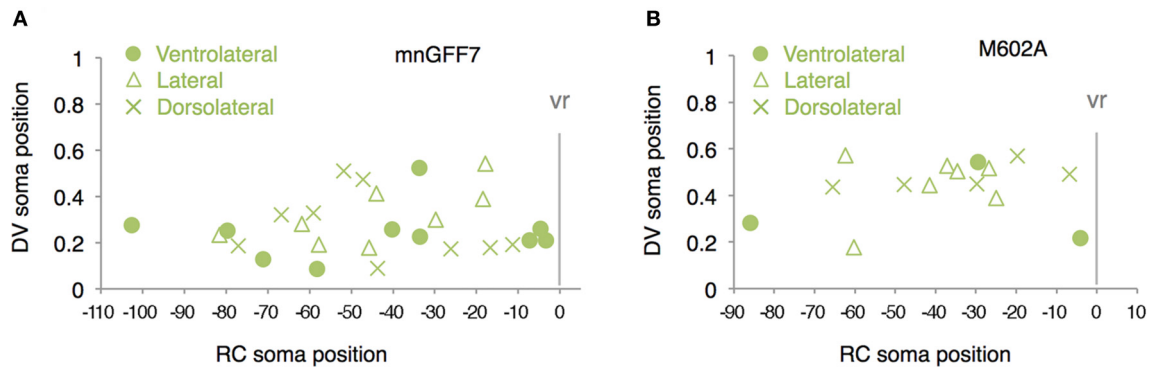

FIGURE A2 | Distribution of the laterally projecting cells in mnGFF7 (A) and M602A (B) plotted with respect to the soma position along the RC axis on the horizontal axis and to the DV soma position on the vertical axis. The exit point of the ventral root from the spinal cord is indicated on the RC axis by the gray vertical line marked as vr ($x = 0$). The ventrolaterally, laterally and dorsolaterally projecting cells are shown as circles, triangles, and crosses, respectively.

frontiers in
NEURAL CIRCUITS

ORIGINAL RESEARCH ARTICLE
published: 14 May 2013
doi: 10.3389/fncir.2013.00091

Distribution of the gap junction protein connexin 35 in the central nervous system of developing zebrafish larvae

Shaista Jabeen and Vatsala Thirumalai*

National Centre for Biological Sciences, NCBS-TIFR, Bangalore, India

Edited by:
German Sumbre, Ecole Normale Superieure, France

Reviewed by:
German Sumbre, Ecole Normale Superieure, France
Deborah Baro, Georgia State University, USA
Filippo Del Bene, Institut Curie, France

***Correspondence:**
Vatsala Thirumalai, National Centre for Biological Sciences, NCBS-TIFR, GKVK Campus, Bellary Road, Bangalore 560065, Karnataka, India.
e-mail: vatsala@ncbs.res.in

Gap junctions are membrane specializations that allow the passage of ions and small molecules from one cell to another. In vertebrates, connexins are the protein subunits that assemble to form gap junctional plaques. Connexin-35 (Cx35) is the fish ortholog of mammalian Cx36, which is enriched in the retina and the brain and has been shown to form neuronal gap junctions. As a first step toward understanding the role of neuronal gap junctions in central nervous system (CNS) development, we describe here the distribution of Cx35 in the CNS during zebrafish development. Cx35 expression is first seen at 1 day post fertilization (dpf) along cell boundaries throughout the nervous system. At 2 dpf, Cx35 immunoreactivity appears in commissures and fiber tracts throughout the CNS and along the edges of the tectal neuropil. In the rhombencephalon, the Mauthner neurons and fiber tracts show strong Cx35 immunoreactivity. As the larva develops, the commissures and fiber tracts continue to be immunoreactive for Cx35. In addition, the area of the tectal neuropil stained increases vastly and tectal commissures are visible. Furthermore, at 4–5 dpf, Cx35 is seen in the habenulae, cerebellum and in radial glia lining the rhombencephalic ventricle. This pattern of Cx35 immunoreactivity is stable at least until 15 dpf. To test whether the Cx35 immunoreactivity seen corresponds to functional gap junctional coupling, we documented the number of dye-coupled neurons in the hindbrain. We found several dye-coupled neurons within the reticulospinal network indicating functional gap junctional connectivity in the developing zebrafish brain.

Keywords: whole mount immunohistochemistry, confocal microscopy, dye-coupling, optic tectum, electrical synapse, electrotonic coupling, cerebellum

INTRODUCTION

Ever since electrical synapses were first described (Furshpan and Potter, 1957), their role in the formation and function of neural circuits has been the focus of intense study. Electrical synapses or neuronal gap junctions are formed by associations of protein subunits that form a functional hemi-channel on each partner neuron membrane. The coming together of two hemi-channels forms a continuous pore between the partner neurons through which ions and small molecules can be exchanged (Söhl et al., 2005). Gap junctions are formed by innexin subunits in invertebrates and connexin subunits in vertebrates. Connexin and innexin protein families are unrelated, while the vertebrate homolog of innexins, the pannexins, are thought to be not involved in gap junction assembly (Sosinsky et al., 2011; Abascal and Zardoya, 2013).

Gap junctions are present on neurons as well as in glia, vascular smooth muscle, inner ear hair cells, pancreatic epithelial cells and in multiple cell types in the retina (Kar et al., 2012). However, gap junctions in these diverse tissues are assembled from distinct connexin subunits. Twenty connexin genes have been identified in the mouse genome, 21 in the human and the same number of innexin genes is present in the medicinal leech, *Hirudo verbana* (Kandarian et al., 2012). Connexin genes and their protein products are named by the molecular weight of the protein—Cx43 stands for a connexin subunit of 43 kDa. Among these connexin family proteins, (Connexin-35) Cx35/Cx36, Cx40, Cx45, and Cx57 have been shown to form neuronal gap junctions (Söhl et al., 2005). Cx36 is widely expressed in the central nervous system (CNS) of mammals, notably in the dendrites of inferior olivary neurons, and in interneurons of the hippocampus, cerebellum, and cerebral cortex (Condorelli et al., 2000; Söhl et al., 2005). Although the functional significance of Cx36-mediated electrical synapses in the CNS is not yet completely understood, there is some evidence that it may be involved in increasing synchrony among oscillating neurons (Connors and Long, 2004). During development, neuronal gap junctions are transiently increased ahead of chemical synaptogenesis. This has led to the notion that gap junctions may prefigure chemical synapses, an idea that has gained support from gap junction perturbation experiments in the leech (Todd et al., 2010). However, mice lacking Cx36 [$Cx36^{(-/-)}$] did not exhibit major deficits in physiology or behavior (Connors and Long, 2004; Söhl et al., 2005). Because null mutants may compensate for the loss of one

Abbreviations: AC, Anterior commissure; CCe, Corpus cerebelli; Chab, Habenular Commissure; Ctec, Tectal commissure; Di, Diencephalon; Hab, Habenula; Hb, Hindbrain; Hy, Hypothalamus; M, Mauthner neuron; ML, Molecular layer; OB, Olfactory bulb; OT, Optic Tectum; P, Pineal; Pd, Dorsal pallium; POC, Post-optic commissure; Pv, Ventral pallium; RG, Radial glia; RV, Rhombencephalic ventricle; SOT, Supra optic tract; TPOC, Tract of the post-optic commissure; TelV, Telencephalic ventricle.

isoform of connexin with another, or use alternate mechanisms of development, the function of Cx35/36 during development needs to be better-addressed using techniques that allow greater spatial and temporal specificity in knocking down gene expression. Toward this end, we have started to study gap junctions in the small tropical teleost, *Danio rerio*, where such experiments are elegantly possible.

Although there are four orthologs in zebrafish for the mammalian Cx36, Cx35 is the only ortholog that shows high similarity (∼90%) to Cx36 and has been shown to be expressed and enriched in the CNS. It has been previously demonstrated to be present in gap junctions formed by the Mauthner neuron in goldfish and zebrafish (Pereda et al., 2003; Satou et al., 2009). Cx35 is present on mixed synapses formed by auditory nerve afferents on the Mauthner neuron lateral dendrite where Cx35 is in close association with NMDA receptors (Rash et al., 2004). Cx35 is a 962 base pair gene with two exons located on chromosome 20 and encodes a 304 amino-acid protein. The zebrafish Cx35 shares a 99% similarity with perch Cx35 and a 90% similarity with mouse and human Cx36. Cx35 protein was detected in punctate form in the photoreceptors and the inner plexiform layer of the retina in larval zebrafish (McLachlan et al., 2003; Li et al., 2009). However, the distribution and ontogeny of Cx35 within the CNS of zebrafish have not yet been studied. Here, using whole-mount immunohistochemistry, we describe the distribution of Cx35-like immunoreactivity in zebrafish larvae from 1 day post fertilization (dpf) to 15 dpf in different regions of the brain. We also show that neurons in the hindbrain of larval zebrafish are extensively dye-coupled, suggesting that the Cx35 immunoreactive puncta that we observe assemble into functional gap junctions.

MATERIALS AND METHODS

Adult wild type zebrafish *(Danio rerio)* were obtained from a commercial supplier, housed in a recirculating water system (Tecniplast, Italy) and used for generating embryos. All procedures were approved by the Institutional Animal Ethics Committee, National Centre for Biological Sciences.

WHOLE-MOUNT IMMUNOHISTOCHEMISTRY

Zebrafish larvae were staged based on external morphological features (Kimmel et al., 1995). Larvae from 1 to 6 dpf, 10 and 15 dpf were anaesthetized in ethyl 3-aminobenzoate methane sulfonate (MS-222; 0.01% w/v) and then were fixed in 4% paraformaldehyde (PFA) for 12–14 h at 4°C. Fixed larvae were washed with 0.1 M phosphate-buffered saline (PBS). Larvae were pinned down using 0.001″ diameter Tungsten wire (California Fine Wire Company, Grover Beach, CA) on a petri dish lined with Sylgard (Dow Corning, Midland, MI). Skin from the top of the head was gently peeled off and the yolk sac, eyes, jaws, and palate were removed carefully leaving only the brain and the tail region containing the spinal cord. Dissected larvae were then blocked overnight in 3 mg/ml normal donkey serum (Jackson Immuno Research, West Grove, PA) in 0.1 M PBS and 0.5% Triton X-100 (PBST) followed by incubation for 48 h at 4°C with mouse anti-Cx35 antibody (MAB3045, EMD Millipore, Billerica, MA) at 1:200 dilution. After washing larvae in PBST several times, they were incubated with donkey anti-mouse IgG-coupled with Dylight 649 (Jackson Immuno Research) or Alexa Fluor 488 (Invitrogen, Whitefield, Bangalore) at 1:500 dilution for 12 h at 4°C. Larvae were then washed several times with cold 0.1 M PBS and mounted with Prolong Gold Anti-Fade reagent (Invitrogen) between two cover slips for imaging. Stacks of images were taken using a Zeiss LSM 510 meta NLO confocal microscope under optimal intensity conditions. Images were taken using 40X oil immersion objective with z-spacing set at 0.44 μm. The numbers of animals used in each stage is given in **Table 1**.

RETROGRADE LABELING

Larvae were anaesthetized in ethyl 3-amino benzoate methane sulfonate (MS-222; 0.01% w/v). A mixture of 25% w/v Neurobiotin (Vector Laboratories; 287Da) and 25% w/v tetra methyl rhodamine-dextran (Invitrogen; 3 kDa), dissolved in autoclaved, filtered and deionized water was pressure injected into the spinal cord of the anaesthetized larvae using a Pico-spritzer III (Parker Hannifin Corp, Pine Brook, NJ). In some larvae, only tetra-methyl rhodamine dextran was injected and these larvae were subsequently processed for whole-mount immunostaining as described above. Larvae were allowed to recover for 24 h in Hank's solution (137 mM NaCl, 5.4 mM KCl, 0.25 mM Na_2HPO_4, 0.44 mM KH_2PO_4, 1.3 mm$CaCl_2$, 1.0 mM $MgSO_4$, 4.2 mM $NaHCO_3$). After recovery larvae were examined under the Olympus SZX16 epifluorescence stereo-microscope for dye labeling in the hindbrain. Larvae having dye-filled neurons were euthanized in cold MS-222 followed by fixation in 4% w/v PFA for 12–14 h. Brain and spinal cord were then dissected out as described above and processed further with 5μg/ml Streptavidin-Alexafluor-488. Larvae were then imaged under a Zeiss LSM 510 meta NLO confocal microscope using the appropriate excitation wavelengths and filters.

FIGURE PRODUCTION AND ANALYSIS

Images were viewed offline using Fiji (http://fiji.sc/) and figures were produced using Adobe Photoshop. The neurobiotin-filled cells were counted using plug-ins in Fiji and results were tabulated in Microsoft Excel.

RESULTS

We used a monoclonal antibody raised against perch Cx35 to study the distribution of Cx35 in whole-mount larval zebrafish from 1 to 15 dpf. This antibody has been previously shown to bind specifically to perch and zebrafish Cx35. Western blots on brain lysates showed no cross-reactivity with other connexin isoforms (Pereda et al., 2003; Satou et al., 2009). Therefore, we proceeded to perform whole-mount immunohistochemistry using this antibody and found reliable staining from identifiable anatomical structures. The Cx35 immunoreactivity was punctate and was seen in both neuropil and membranes of cell bodies, as would be expected of Cx35. Further, no staining was seen when the primary

Table 1 | Numbers of larvae imaged at each stage.

Age	1 dpf	2 dpf	3 dpf	4 dpf	5 dpf	6 dpf	10 dpf	15 dpf
Animals (n)	5	7	5	5	11	11	3	7

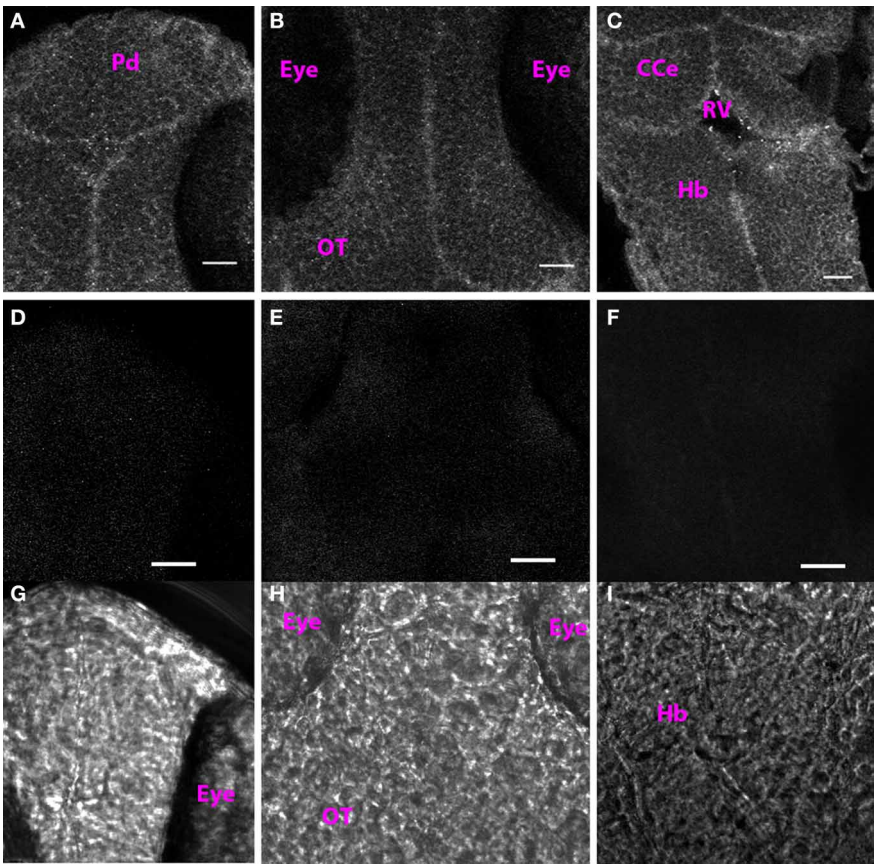

FIGURE 1 | Cx35 staining pattern in 1 dpf larva. (A) Single optical section of the dorsal pallium (Pd). **(B)** Optic tectum (OT). **(C)** Hindbrain (Hb). The cerebellum (CCe), and the rhombencephalic ventricle (RV) can be also be seen. Anterior is at the top and posterior is at the bottom. Larva is in dorsoventral position. **(D–F)** Single optical sections from control larvae in which the primary antibody was not included in the incubation mixture. **(D)** Dorsal telencephalon. **(E)** Optic tectum. **(F)** Hindbrain. **(G–I)** Transmitted light images of the regions imaged in **(D–F)**. Scale bar for all panels: 20 μm.

or the secondary antibodies were omitted from the incubation mixture. In all preparations except in 1 dpf larvae, the eye was dissected out and therefore we do not discuss the retinal staining pattern, which can be found elsewhere (McLachlan et al., 2003; Li et al., 2009). Here we describe the development of Cx35 immunoreactivity in the CNS of zebrafish from 1 dpf through 15 dpf.

1 dpf

At 1 dpf, we found punctate Cx35 labeling along cell membranes throughout the rostrocaudal extent of the CNS (**Figures 1A–C**). This staining was specific because omission of the primary antibody from the incubation mixture abolished all signal (**Figures 1D–F**: fluorescence image; **Figures 1G–I** show the respective transmitted light images). No defined structures such as nuclei, commissures or tracts were visible at this stage.

2 dpf

At 2 dpf, the anterior and the post-optic commissures, the tract of the post optic commissure and the supra-optic tract were labeled in the ventral forebrain (**Figure 2A**). Cx35-positive ellipsoid cells were found in the dorsal pallium (**Figure 2B**). Thick fiber tracts were present in the ventral diencephalon and the posterior commissure was prominently labeled in the dorsal aspect (**Figure 2B**, arrowhead). The rim of the optic tectal neuropil was Cx35 positive but no other fiber tracts or cells were labeled in the mesencephalon (**Figure 2C**). In the rhombencephalon, large rounded cells were seen lining the rhombencephalic ventricle. No processes were visible on these cells (**Figure 2D**). The hindbrain displayed intense staining in the ventral aspect, with fiber tracts labeling strongly with the anti-Cx35 antibody. Prominently, fiber tracts in the lateral longitudinal fascicle were labeled and a ladder-like pattern was visible (**Figure 2E**). A little more dorsally, the Mauthner neurons were clearly labeled with the antibody (**Figure 2F**). Many other cells were also faintly stained in the vicinity of the Mauthner neurons.

3 dpf

The Cx35 staining pattern at 3 dpf was very largely similar to that seen at 2 dpf. As at 2 dpf, the anterior and post-optic commissures along with the tract of the post-optic commissure were labeled (**Figures 3A** and **C**). Dorsally, cells in the pallium were intensely labeled as was the posterior commissure (**Figure 3B**). The tectal neuropil area stained was larger as would be expected with the

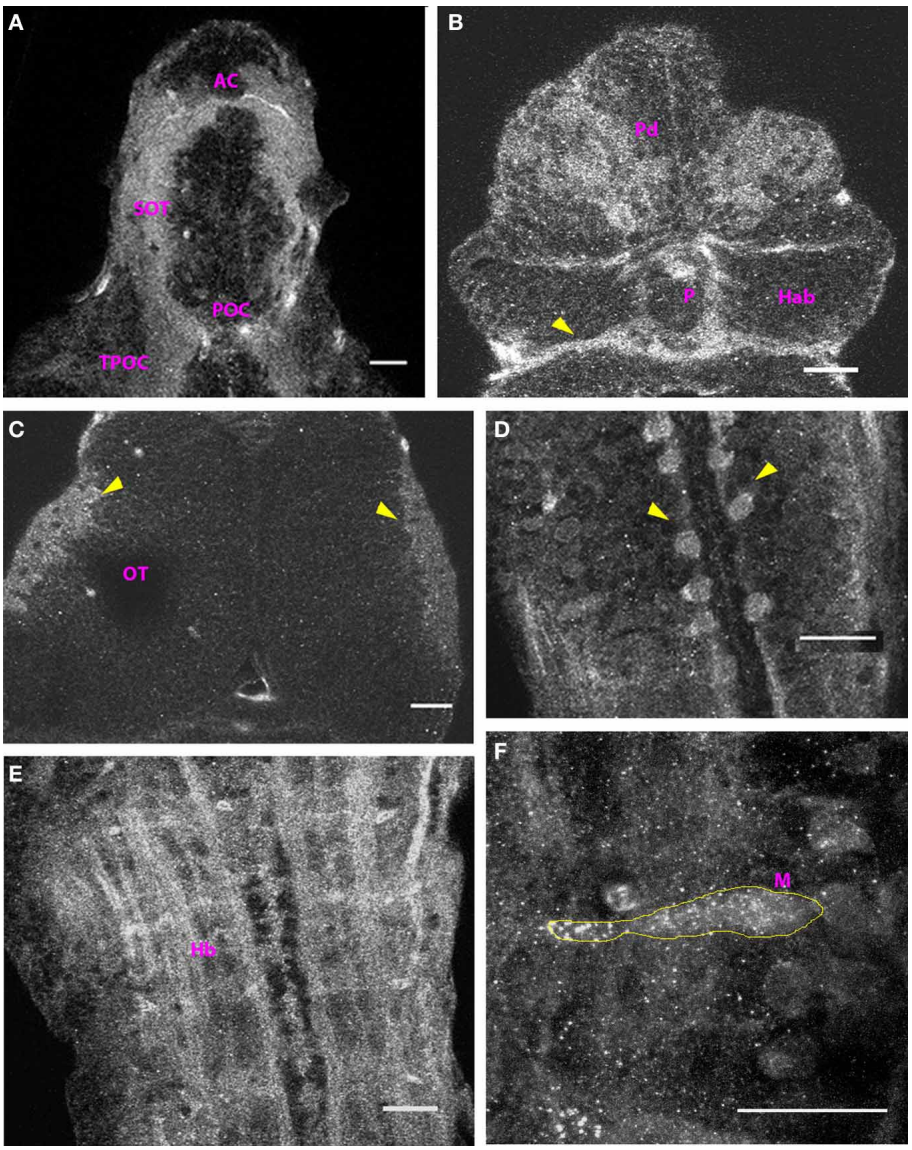

FIGURE 2 | Cx35 distribution in the CNS of 2 dpf larvae. Larvae are dorso-ventrally placed with anterior on top in all panels. All panels except **(F)** show single optical sections taken at a z-resolution of 0.44 μm. **(A)** Ventral telencephalon showing the anterior commissure (AC), supra-optic tract (SOT), and the post-optic commissure (POC). **(B)** Dorsal view of forebrain showing Cx35 positive cells in the dorsal pallium (Pd). The posterior commissure can be seen (arrowhead) while the habenulae (Hab) and the pineal body (P) lack Cx35 immunoreactivity. **(C)** Dorsal view of the optic tectum (OT). A single optical section showing Cx35 immunoreactivity in the developing neuropil region (arrowheads). **(D)** Cell bodies (arrowheads) in hindbrain lining the rhombencephalic ventricle. **(E)** Ventral hindbrain (Hb) showing intense Cx35 immunoreactivity in fibers coursing through it. **(F)** Zoomed image of a Mauthner neuron (M, yellow outline) showing punctate Cx35 immunoreactivity. The image is a maximum intensity projection of optical slices collected from a 16 μm thick tissue slice encompassing the Mauthner neuron. Scale bar for all panels: 20 μm.

ingrowth of retinal ganglion cell axons and tectal axons into this region. No other fiber tracts or cells were stained in the mesencephalon at this stage (**Figure 3D**). In the rhombencephalon, the ladder-like pattern of fiber tracts (**Figure 3E**), the Mauthner neurons and several hindbrain cell bodies in its vicinity could be seen labeled. The Mauthner neuron showed sharp intense puncta of Cx35 staining across its cell body (**Figure 3F**). However, we failed to observe any cells lining the rhombencephalic ventricle at this stage.

4 dpf–15 dpf

By 4 dpf, the distribution of Cx35-immunoreactivity was almost fully mature and the structures labeled at 4 dpf continued to be Cx35-positive at least until 15 dpf, the oldest stage examined by us. In the telencephalon, cell bodies in the dorsal pallium could be clearly seen (**Figure 4A**). In addition, at 4 dpf, the habenulae were brightly labeled and the habenular commissure was also visible (**Figure 4A**). Ventrally, the supra-optic tract and the anterior and post-optic commissures continued to be labeled

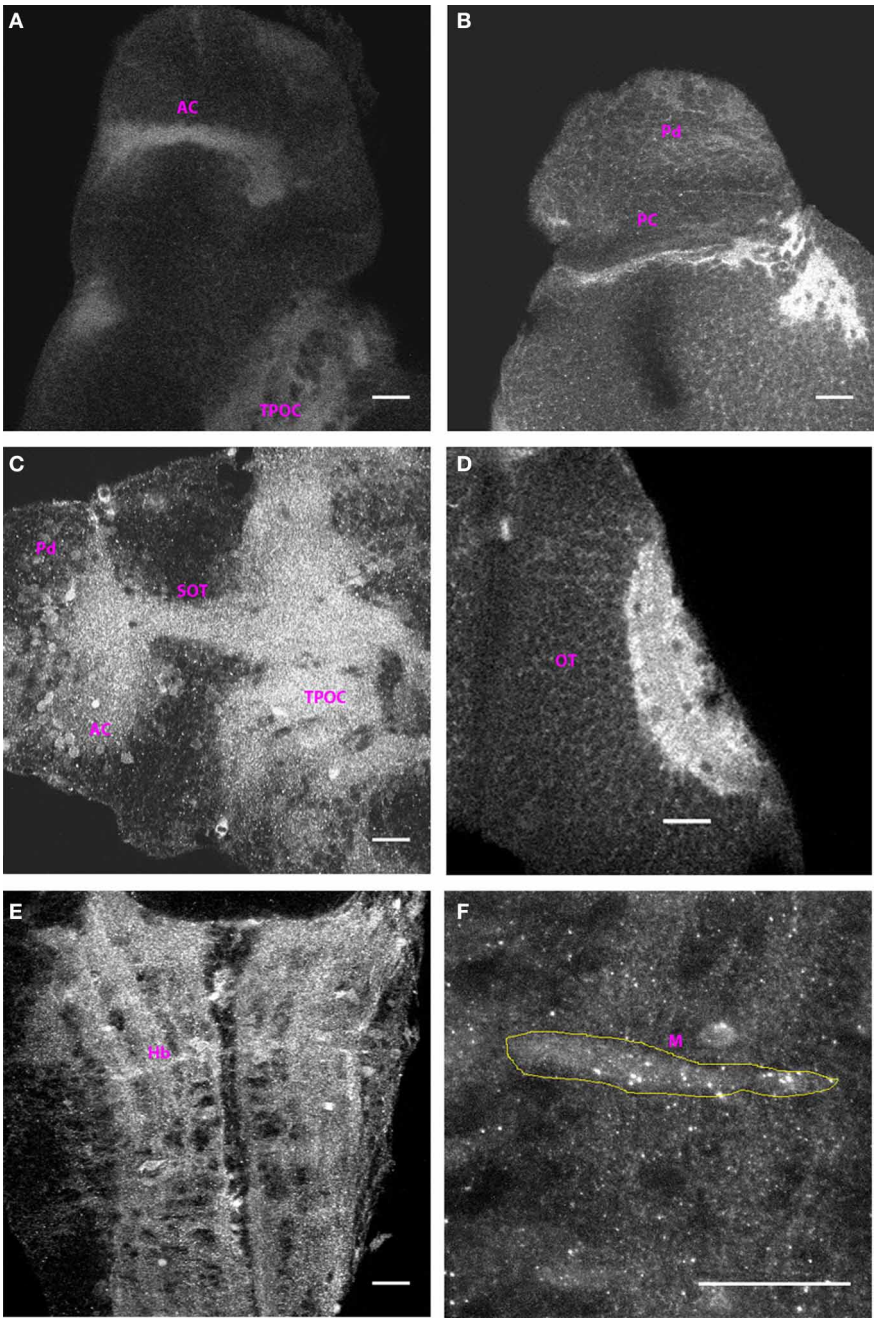

FIGURE 3 | Distribution of Cx35 immunoreactivity in 3 dpf larvae. All panels except **(C)** show dorso-ventrally placed larvae, with the anterior end of the animal at the top of the panel. All panels are single optical sections taken at a z-resolution of 0.44 μm. **(A)** Ventral forebrain showing immunoreactivity in the anterior commissure (AC) and in the tract of the post-optic commissure (TPOC). **(B)** Dorsal telencephalon and rostral mesencephalon. Staining in cells of the dorsal pallium (Pd) and in the posterior commissure (PC) can be seen. **(C)** Lateral view of forebrain. Dorsal is on top and anterior to the left. Cx35 immunoreactivity is seen in the anterior commissure, in the supra-optic tract and in thick fiber tracts in ventral diencephalon. Numerous cell bodies can also be seen in the vicinity of the anterior commissure. **(D)** Intense Cx35 immunoreactivity in the optic tectal (OT) neuropil. **(E)** Ventral hindbrain (Hb) showing fiber tracts criss-crossing the hindbrain. **(F)** Zoomed image of a single Mauthner neuron (M) showing intense Cx35 immunoreactive puncta. The approximate boundary of the Mauthner neuron as seen in DIC is shown in yellow. Scale bar for all panels: 20 μm.

strongly (**Figure 4B**). In addition, cell bodies in the olfactory bulb showed intense labeling. Staining was also seen in the glomerular region (**Figure 4B**). Ventrally, thick fiber tracts continuing from the tract of the post-optic commissure could be seen in the diencephalon (**Figure 4C**). In the mesencephalon, the neuropil of the tectum was the most brightly-labeled structure in the entire CNS (**Figure 4D**). Puncta dotted the outlines of cell bodies in the tectal lobes and tectal commissures were seen to

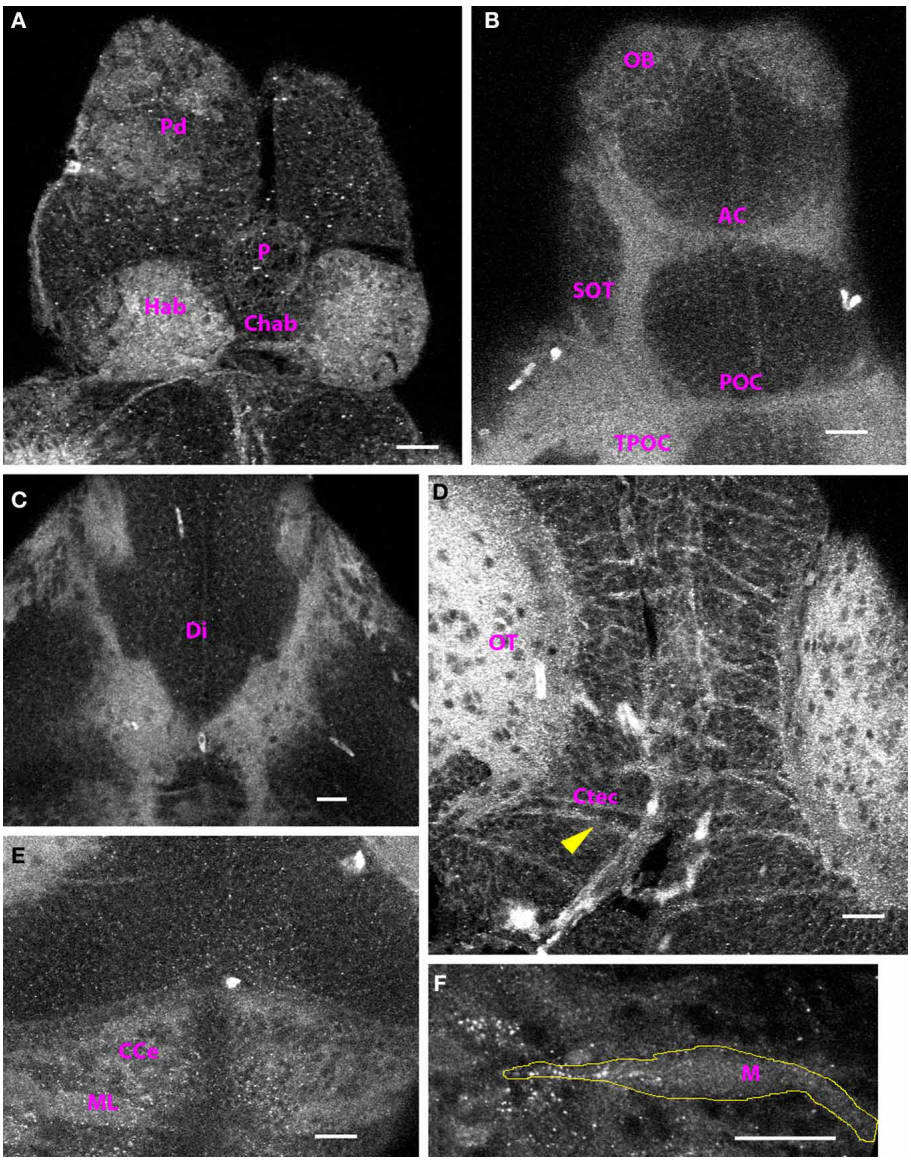

FIGURE 4 | Cx35 immunostaining in 4 dpf larvae. Larvae are dorso-ventrally placed with anterior on top in all panels. All panels show single optical sections taken at a z-resolution of 0.44 μm. **(A)** Dorsal forebrain showing Cx35 staining in the paired habenulae (Hab) and in the habenular commissure (Chab). Cell bodies in dorsal pallium (Pd) continue to stain positive. No staining is seen in the pineal body (P). **(B)** Ventral telencephalon showing Cx35 immunoreactivity in the olfactory bulb (OB), anterior commissure (AC), supra-optic tract (SOT), post-optic commissure (POC), and the tract of the post-optic commissure (TPOC). **(C)** Cx35 immunoreactivity in fiber tracts in the ventral diencephalon (Di). **(D)** Intense Cx35 immunoreactivity in the optic tectal neuropil (OT) and in the intertectal commissures (Ctec; arrowhead) in the mesencephalon. Tectal cell bodies are also weakly labeled. **(E)** Weak staining is seen in the cerebellum within the molecular layer (ML) and in the corpus cerebelli (CCe). **(F)** Zoomed image of a single Mauthner neuron (M) showing intense Cx35 immunoreactive puncta. The approximate boundary of the Mauthner neuron as seen in DIC is shown in yellow. Scale bar for all panels: 20 μm.

run across the lobes. Paired longitudinal tracts were also seen medially in dorsal tectum. Beginning at 4 dpf, Cx35 immunoreactivity could be seen in the cerebellum. The molecular layer was prominent and staining was seen in the climbing fibers as well as in the corpus cerebelli (**Figure 4E**). Similarly, the hindbrain was also brightly stained with the ladder-like fiber tracts. Intense puncta were visible on the Mauthner neuron somata (**Figure 4F**).

Subsequently, at 5 dpf and 6 dpf, the distribution of Cx35 immunoreactivity was similar to what was seen at 4 dpf (**Figure 5**). In ventral telencephalon, the anterior commissure and the olfactory bulb were labeled (**Figure 5A**). In dorsal telencephalon, cell bodies in the Pallium and the habenulae could be clearly seen. The posterior cimmissure was also labeled (**Figure 5B**). In the mesencephalon, the much larger tectal neuropil was strongly stained (**Figures 5C,D**) and the

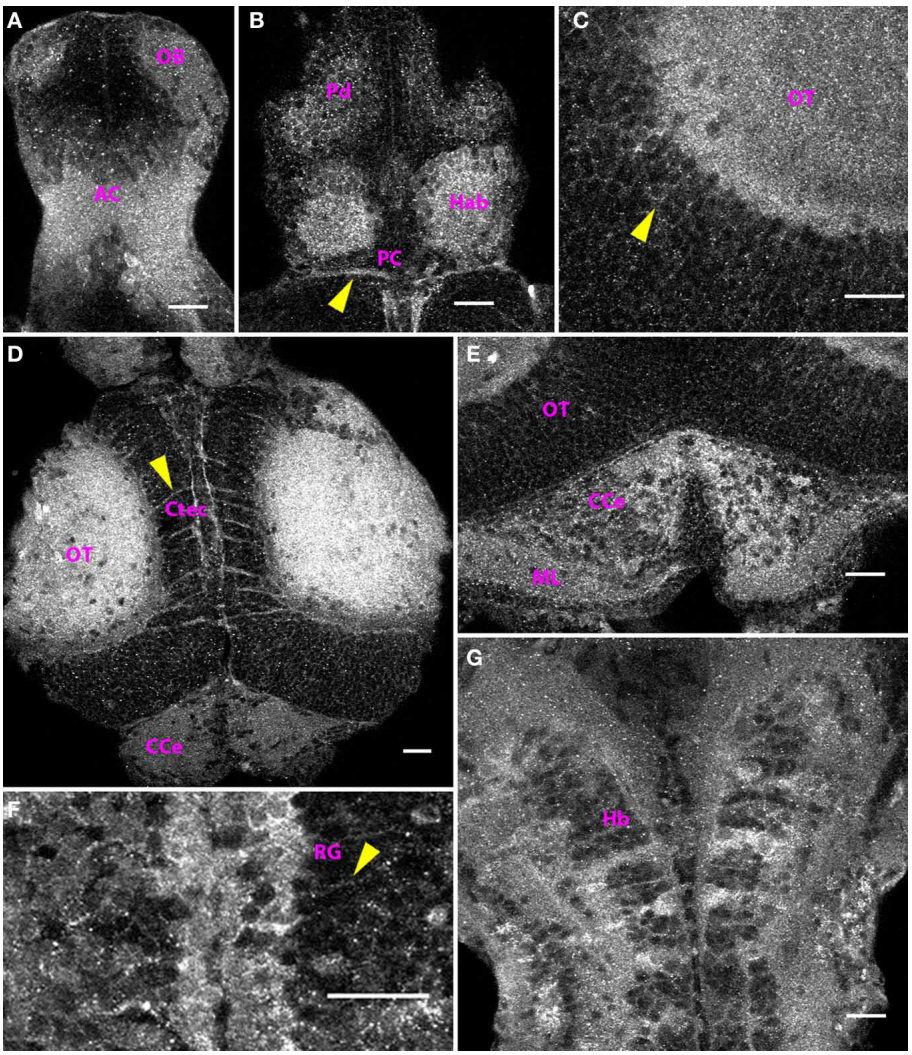

FIGURE 5 | Distribution of Cx35 immunoreactivity in the CNS of 6 dpf larvae. Larvae are dorso-ventrally placed with anterior on top in all panels. All panels show single optical sections taken at a z-resolution of 0.44 μm. **(A)** Ventral telencephalon showing staining in anterior commissure (AC) and the olfactory bulb (OB). A few faintly stained cell bodies can be seen in the vicinity of the anterior commissure. **(B)** Dorsal forebrain showing Cx35 staining in the habenulae (Hab), dorsal pallium (Pd), and the posterior commissure (PC; arrowhead). **(C)** Magnified dorsal view of the optic tectum (OT) showing intense staining in the neuropil area. Faint labeling in cell bodies is also seen (arrowhead). **(D)** Cx35 staining in the mesencephalon showing intense staining in the optic tectal lobes in the neuropil area as well as in intertectal commissures (Ctec; arrowhead). The corpus cerebelli (CCe) can also be seen. **(E)** Cerebellar staining showing punctate pattern within the corpus cerebelli (CCe) and the molecular layer (ML). **(F)** Strong staining present in radial glia (RG) lining the rhombencephalic ventricle. Arrowhead marks the process from one glial cell coursing laterally. **(G)** Ladder-like staining pattern in ventral hindbrain (Hb). Scale bar for all panels: 20 μm.

outlines of tectal cell bodies were marked by Cx35-positive puncta (**Figure 5C**). Intertectal commissures and paired longitudinal tracts running in medial tectum were clearly visible (**Figure 5D**). As in the 4 dpf larvae, the cerebellum was also strongly Cx35-immunoreactive (**Figure 5E**). Additionally, beginning at 5 dpf, radial glia lining the rhombencephalic ventricle were seen to express Cx35 and their straight processes were seen to traverse the hindbrain from the medial to the lateral margins (**Figure 5F**). Strong Cx35 staining was also seen in ventral hindbrain, in a pattern similar to that seen at 4 dpf.

In 5–6 dpf larvae, we could see bright puncta of Cx35 immunoreactivity in the Mauthner neurons. To study the placement of these puncta on the Mauthner neuron, we retrogradely labeled the Mauthner neuron with tetra methyl rhodamine dextran and then processed the larvae for Cx35 immunoreactivity. We found puncta lining the axon in the axon-cap region of the Mauthner neuron (**Figure 6A**), on the lateral dendrite at club-endings (**Figure 6B**) and on the soma (**Figure 6C**).

At 10 dpf (data not shown) and 15 dpf, the distribution pattern of Cx35 immunoreactivity was similar to that seen at

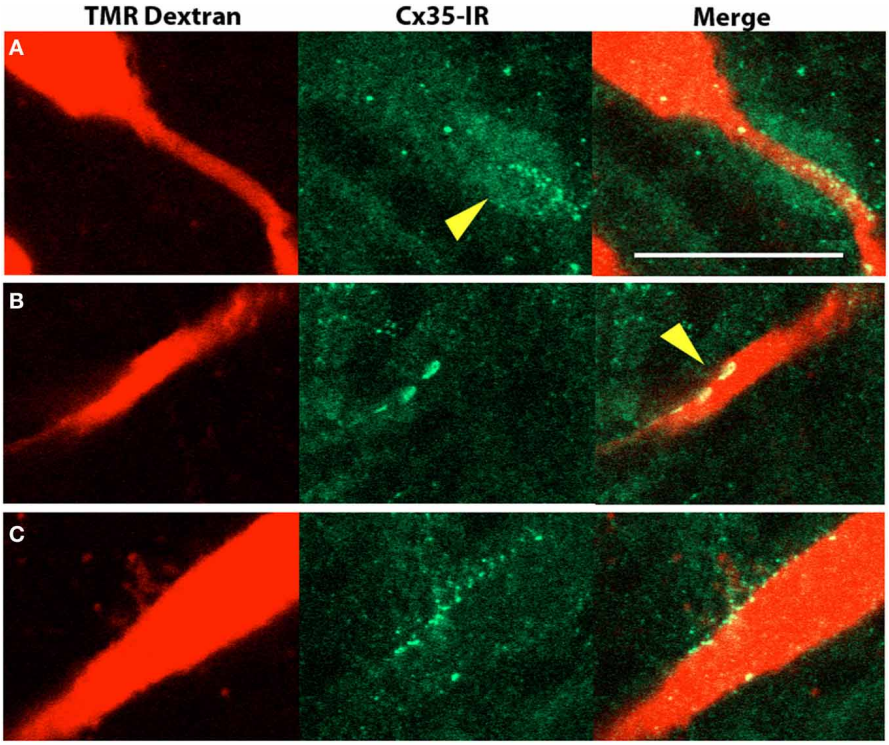

FIGURE 6 | Cx35 immunoreactivity in Mauthner neurons of 6 dpf larvae. The left panels show retrograde labeling of a Mauthner neuron with tetra-methyl rhodamine dextran (TMR dextran, red). The middle panels show Cx35 immunoreactivity in green and the right panels show merge of the two channels. All images are single optical sections taken at a z-spacing of 0.44 μm. **(A)** Cx35-immunoreactive puncta line the Mauthner axon and form a dense cloud in the axon-cap region (arrowhead). **(B)** Club endings on the lateral dendrite are large bouton-like structures (arrowhead) that are intensely Cx35 immunoreactive. **(C)** Cx35 puncta are also seen to line the Mauthner soma. Scale bar for all panels: 20 μm.

6 dpf. The regions that stained positive at 6 dpf, continued to stain positive through 15 dpf and no new regions were seen (**Figure 7**).

DYE-COUPLING IN RETICULOSPINAL NEURONS

We sought to determine if the high intensity of Cx35 immunoreactivity in the hindbrain of zebrafish larvae indicates a high level of gap junction connectivity between hindbrain neurons. We retrogradely labeled reticulospinal neurons by pressure injecting a 50:50 mixture of neurobiotin and tetra-methyl rhodamine dextran into the spinal cord. These dyes are retrogradely transported by the spinal axons to their respective somata in the hindbrain. While tetra methyl rhodamine dextran stays within the same cell, neurobiotin can cross any gap junctions due to its small mass (287 Da). When the neurobiotin is visualized using fluorophore-coupled streptavidin, while the cells directly labeled retrogradely colocalize both neurobiotin and the higher molecular weight dextran, the dye-coupled cells are only positive for neurobiotin (**Figure 8**). We counted the number of neurons labeled with neurobiotin only and normalized it to the number of retrogradely labeled neurons (containing both neurobiotin and tetra-methyl rhodamine dextran). This yields a dye-coupling ratio, which indicates the number of neurons with which a single reticulospinal neuron may share gap junctions. Between 4 dpf and 6 dpf, we found a dye-coupling ratio of 2.5 ± 0.7 (Mean ± SD, $n = 6$), indicating a high degree of gap junctional coupling between reticulospinal neurons and other hindbrain neurons.

DISCUSSION

We have followed the appearance of Cx35 immunoreactivity in the CNS of embryonic and larval zebrafish from 1 dpf through 15 dpf. We find that while some structures such as the Mauthner neurons and the commissures acquire Cx35 immunoreactivity relatively early (2 dpf), other structures such as the habenulae and the cerebellum begin to express Cx35 only by 4 dpf. However, on the whole, the Cx35 distribution pattern seems to mature in the early larval stage and remains stable into late larval stages (**Figure 9**).

We used a monoclonal antibody raised against perch Cx35, which shows specificity for Cx35 in perch, zebrafish and gold fish (Pereda et al., 2003; Satou et al., 2009). As noted earlier, perch Cx35 and zebrafish Cx35 share a 96% identity and 99% similarity at the amino acid level, therefore it is not surprising that this antibody specifically recognizes the zebrafish Cx35 protein. Earlier this antibody was shown to detect gap junctional contacts between the Mauthner axon and a spinal inhibitory interneuron in zebrafish larvae (Satou et al., 2009). Furthermore, this antibody also specifically detects Cx35-mediated gap junctional plaques in the Mauthner neuron of goldfish (Pereda et al., 2003). There are four known orthologs of mammalian Cx36 in zebrafish—Cx35

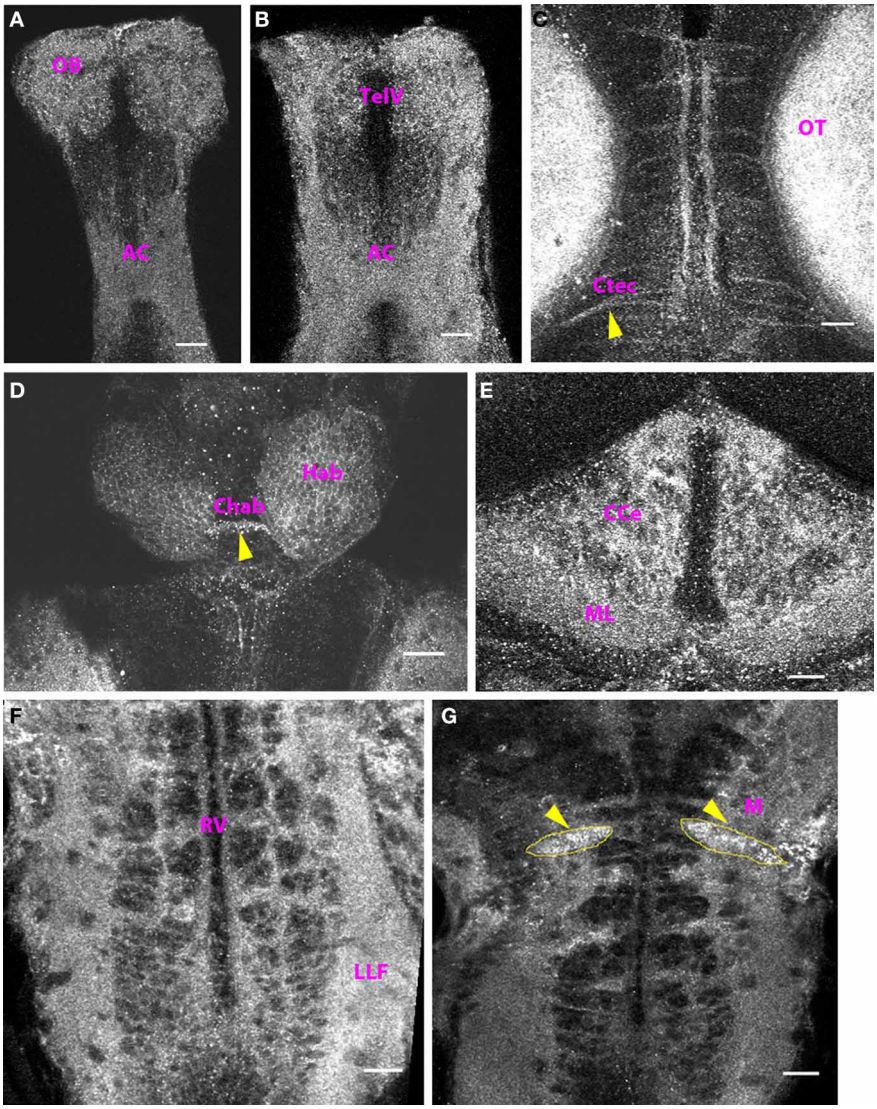

FIGURE 7 | Cx35 staining pattern in the CNS of 15 dpf zebrafish. Larvae are dorso-ventrally placed with anterior on top in all panels. All panels show single optical sections taken at a z-resolution of 0.44 μm. **(A)** Ventral telencephalon showing punctate Cx35 immunoreactivity in the anterior commissure (AC) and the olfactory bulb (OB). **(B)** Telencephalon 50 μm from the ventral surface showing staining in the anterior commissure (AC) and in the olfactory bulb (OB). The telencephalic ventricle (TelV) can be seen. **(C)** Mesencephalon, dorsal view showing staining in the optic tectal (OT) neuropil and in intertectal commissures (Ctec, arrowhead). **(D)** Habenulae (Hab) and the habenular commissure (Chab; arrowhead). Polygonal cell bodies can be seen in the habenulae **(E)** Cerebellum showing intense Cx35 immunoreactivity in the corpus cerebelli (CCe) and the molecular layer (ML) **(F)** Ventral Hindbrain (Hb) showing a ladder-like pattern that includes Cx35 staining in the lateral longitudinal fasciculus (LLF) and hindbrain commissures. The rhombencephalic ventricle (RV) can be seen. **(G)** Intense punctate Cx35 immunoreactivity in the Mauthner neurons (M; arrowheads). The approximate boundaries of the Mauthner neurons is drawn in yellow. Scale bar for all panels: 20 μm.

on chromosome 20 and three other genes on chromosomes 5, 7, and 17. While there is currently no evidence that the ortholog on chromosome 17 is expressed, the other two isoforms have very low similarity to the intracellular loop of the perch Cx35, the antigen against which the antibody was raised. Furthermore, western blots show no cross-reactivity with other connexin isoforms (Pereda et al., 2003). Therefore, our results indicate true Cx35 distribution within the CNS of developing zebrafish larvae.

We found that Cx35 distribution in the zebrafish CNS recapitulates Cx36 distribution in the mammalian CNS to a large extent. For example, Cx36 is known to be present in the retina, olfactory bulb, cerebellum, habenula, inferior olive and other brain stem nuclei in the adult rodent brain (Condorelli et al., 2000; Söhl et al., 2005). Earlier studies have demonstrated Cx35 presence in the retina of zebrafish between photoreceptors and in the inner plexiform layer (McLachlan et al., 2003; Li et al., 2009). Our studies now show that Cx35 is present in many regions of the CNS including the olfactory bulb, cerebellum, habenulae, and the hindbrain. Together, these results suggest that Cx35 and Cx36 are not only homologous

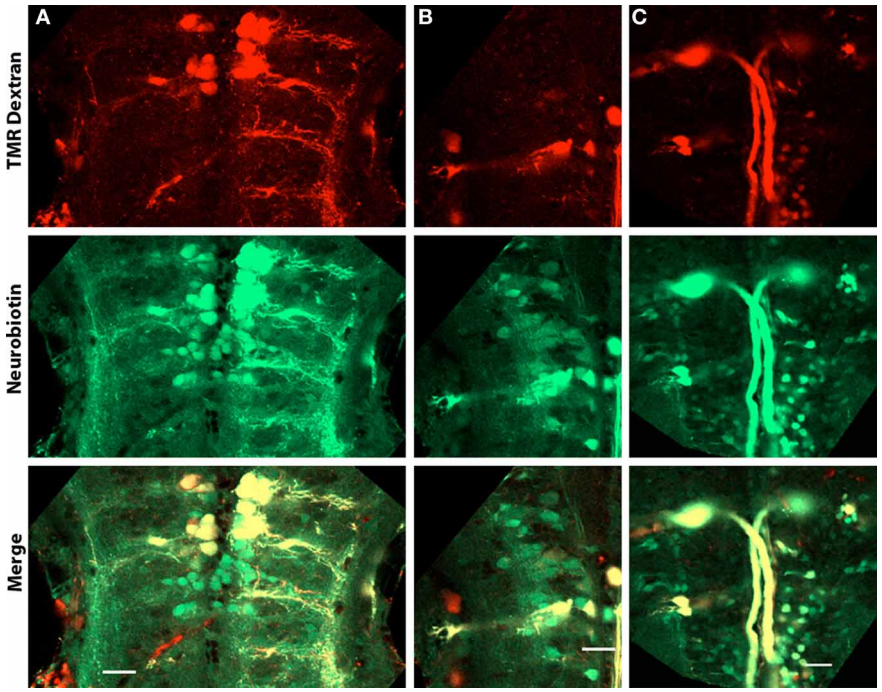

FIGURE 8 | Dye-coupled cells in the hindbrain of 4 dpf larvae. Larvae are dorso-ventrally placed with anterior on top in all panels. All panels show single optical sections taken at a z-resolution of 0.44 μm. **(A–C)** Images at depths of 20, 30, and 43 μm from the ventral surface showing reticulospinal neurons retrogradely labeled with neurobiotin (green) and tetramethyl rhodamine dextran (red). Cells electrically coupled to the labeled neurons but not projecting into the spinal cord are green in color, while the neurons that project into the spinal cord are yellow because of the presence of both neurobiotin and tetra methyl rhodamine dextran. Scale bar for all panels: 20 μm.

with respect to their sequence but might serve similar functions in homologous areas of the teleost and mammalian brains.

While an earlier study indicated that Cx35 is not present at 1 dpf (McLachlan et al., 2003), our immunostaining results show that a low level of Cx35 is present throughout the rostrocaudal extent of the larval CNS. These results are also supported by recent preliminary experiments from another group (Martin and Ribera, 2012). Beginning at 2 dpf, we observed that the anterior, post-optic and posterior commissures exhibit Cx35 immunoreactivity. Additionally, fiber tracts in ventral diencephalon and in ventral hindbrain were labeled. This suggests gap-junctional contacts between axons, especially since axons are not myelinated at 2 dpf (Brösamle and Halpern, 2002; Jung et al., 2010). The mammalian ortholog of Cx35, Cx36 is indeed found along hippocampal mossy fibers where pairs of mossy fibers were found to be electrically coupled via Cx36 containing plaques (Hamzei-Sichani et al., 2007). Such axo-axonic electrical coupling may serve to spread action potentials from one axon to another and synchronize populations of neurons, resulting in oscillations. We found Cx35 immunoreactivity along many commissures and fiber tracts throughout the rostro-caudal extent of the zebrafish CNS. The functional relevance of such extensive electrical coupling remains to be evaluated.

The optic tectal neuropil showed intense Cx35 immunoreactivity. The extent of staining seen increased with development as the neuropil grew (see **Figures 2C**, **3D**, **4D**, **5D**, and **7C**). We see Cx35 immunoreactivity begin to appear within the growing tectal neuropil as early as 2 dpf, a stage when retinal axons have not yet innervated their target region within the tectum (Stuermer, 1988). This suggests that Cx35-mediated gap junctions might be present in contacts between tectal neurons as they grow their neurites into the tectal neuropil. We also found Cx35 puncta dotting the boundaries of tectal cell bodies (for e.g., **Figure 5C**) suggesting gap junctional connectivity between somata in the tectum. Physiological validation of such electrical coupling and its function in visual processing remain to be investigated.

In contrast to the optic tectum, Cx35 immunoreactivity in the habenulae and the cerebellum developed later, starting at 4 dpf. Although the habenulae and the habenular commissure can be distinguished by 2 dpf (Hendricks and Jesuthasan, 2007), we did not see Cx35 immunoreactivity in them until 4 dpf. We saw intense labeling in habenular neurons and in the commissure indicating gap junctional connectivity among habenular neurons from 4 dpf onwards. Cerebellar glutamatergic and GABAergic neurons are first detected at 3 dpf and a layered structure is first seen at 5 dpf. By 5 dpf, vGlut1-positive presynaptic terminals contact dendrites from Purkinje neurons and a rapid rate of synapse formation continues at least until 15 dpf (Bae et al., 2009). We find it significant that Cx35 immunoreactivity is seen immediately prior to the start of synaptogenesis in the cerebellum. In many systems, electrical synapses have been shown to be upregulated before the period of chemical synaptogenesis and recently, knocking down gap junctions was shown to interfere with chemical

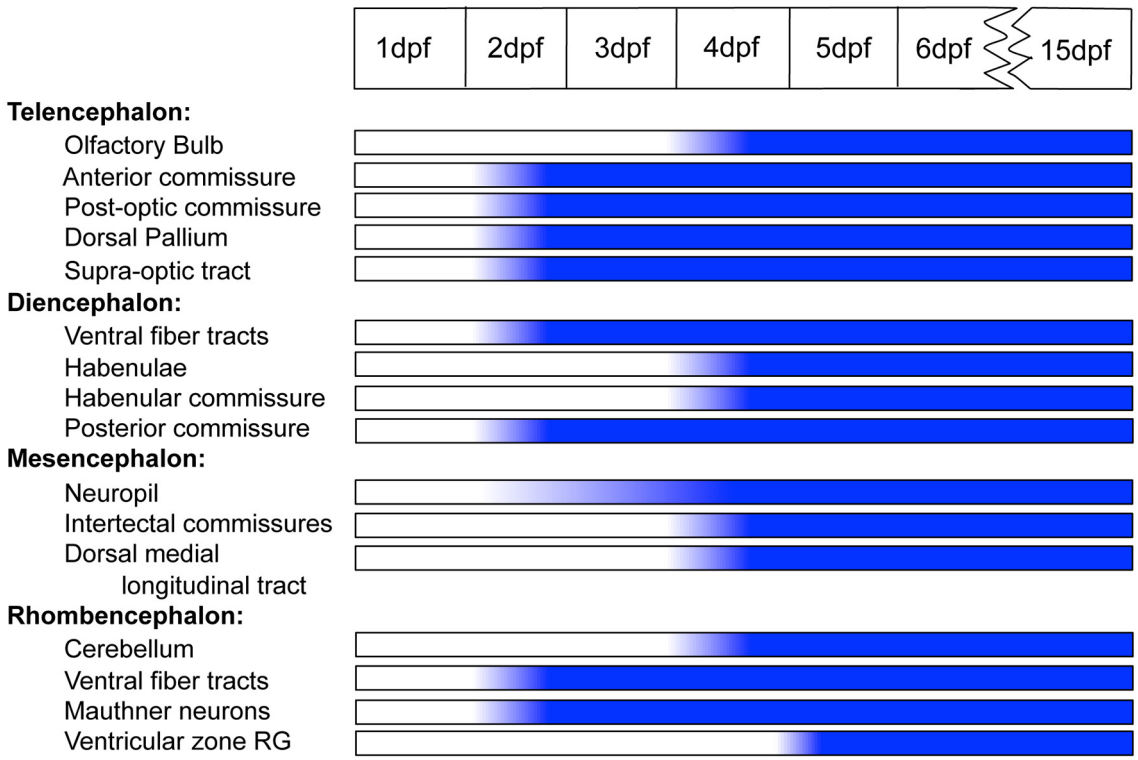

FIGURE 9 | Timeline showing the ontogeny of Cx35 immunoreactivity in the CNS of zebrafish from 1 dpf through 15 dpf. Abbreviations are as given in the text.

synapse formation (Todd et al., 2010). It is likely that in the cerebellum, Cx35-mediated gap junctions provide instructional cues for the formation of appropriate chemical synaptic connections.

The Mauthner neurons are large neurons in rhombomere 4 that are critical for escape behavior. Electrical synapses on the Mauthner neurons are numerous: they are present in mixed synapses formed by the eighth cranial nerve club endings and in spiral fiber endings on the axon cap. These gap junctions are known to be present by 2 dpf (Kimmel et al., 1981) and the gap junctions at club endings are known to be mediated by Cx35 in goldfish (Pereda et al., 2003). Consistent with these data, we found intense Cx35 immunoreactivity in Mauthner neuron somata beginning at 2 dpf and at least until 15 dpf, suggesting the presence of Cx35-mediated gap junctions. Club endings are known to be located on the lateral dendrite of the Mauthner neuron, whereas spiral fiber endings are on the axon cap (Kimmel et al., 1981). Consistent with this, we see bright and intense puncta in these locations (**Figure 6**). Notably, we see large button-like puncta whose shape is characteristic of the club endings formed by the eighth cranial nerve (**Figure 6B**). We also see several dimly stained cell bodies in the hindbrain. Since their morphology could not be traced with the antibody staining or with retrograde labeling, it is not clear whether these are neurons or glia.

Cx35/36 is a neuronal connexin—it is enriched in the retina and in neurons and is not found in non-neuronal tissues (O'Brien et al., 1998; Söhl et al., 1998). Cx36 has been shown to preferentially localize in neural–neural gap junctions and is absent in astrocytes and oligodendrocytes (Rash et al., 2001). Surprisingly, here we found Cx35 in radial glia lining the rhombencephalic ventricle beginning at 5 dpf. Though we found cell bodies in the same region at 2 dpf, these could not be unequivocally identified as radial glia at 2 dpf. Nevertheless, Cx35 has been previously shown to be present in cell lines derived from teleostian radial glia (Wen et al., 2010) and in clusters of cells lining the ventricular zone in mice (Lo Turco and Kriegstein, 1991; Bittman et al., 1997). We propose that Cx35-containing gap junctions might be involved in the exchange of signaling factors during proliferation, migration and differentiation of neurons. It has been previously observed that neurons of similar age acquire the same neurotransmitter phenotype and have similar morphological properties (Kinkhabwala et al., 2011). Neuronal lineage has been shown to govern early transient electrical coupling and subsequent excitatory synaptic connectivity in neocortex (Yu et al., 2012). Early Cx35-mediated gap junctional coupling of neural precursors along the ventricular wall might be important for specifying uniform properties across populations of newly-born neurons.

ACKNOWLEDGMENTS

This work was supported by NCBS and a Wellcome Trust DBT India Alliance Intermediate Fellowship to Vatsala Thirumalai.

REFERENCES

Abascal, F., and Zardoya, R. (2013). Evolutionary analyses of gap junction protein families. *Biochim. Biophys. Acta* 1828, 4–14.

Bae, Y.-K., Kani, S., Shimizu, T., Tanabe, K., Nojima, H., Kimura, Y., et al. (2009). Anatomy of zebrafish cerebellum and screen for mutations affecting its development. *Dev. Biol.* 330, 406–426.

Bittman, K., Owens, D. F., Kriegstein, A. R., and Lo Turco, J. J. (1997). Cell coupling and uncoupling in the ventricular zone of developing neocortex. *J. Neurosci.* 17, 7037–7044.

Brösamle, C., and Halpern, M. E. (2002). Characterization of myelination in the developing zebrafish. *Glia* 39, 47–57.

Condorelli, D. F., Belluardo, N., Trovato-Salinaro, A., and Mudò, G. (2000). Expression of Cx36 in mammalian neurons. *Brain Res. Rev.* 32, 72–85.

Connors, B. W., and Long, M. A. (2004). Electrical synapses in the mammalian brain. *Annu. Rev. Neurosci.* 27, 393–418.

Furshpan, E. J., and Potter, D. D. (1957). Mechanism of nerve-impulse transmission at a crayfish synapse. *Nature* 180, 342–343.

Hamzei-Sichani, F., Kamasawa, N., Janssen, W. G. M., Yasumura, T., Davidson, K. G. V., Hof, P. R., et al. (2007). Gap junctions on hippocampal mossy fiber axons demonstrated by thin-section electron microscopy and freeze fracture replica immunogold labeling. *Proc. Natl. Acad. Sci. U.S.A.* 104, 12548–12553.

Hendricks, M., and Jesuthasan, S. (2007). Asymmetric innervation of the habenula in zebrafish. *J. Comp. Neurol.* 502, 611–619.

Jung, S.-H., Kim, S., Chung, A.-Y., Kim, H.-T., So, J.-H., Ryu, J., et al. (2010). Visualization of myelination in GFP-transgenic zebrafish. *Dev. Dyn.* 239, 592–597.

Kandarian, B., Sethi, J., Wu, A., Baker, M., Yazdani, N., Kym, E., et al. (2012). The medicinal leech genome encodes 21 innexin genes: different combinations are expressed by identified central neurons. *Dev. Genes Evol.* 222, 29–44.

Kar, R., Batra, N., Riquelme, M. A., and Jiang, J. X. (2012). Biological role of connexin intercellular channels and hemichannels. *Arch. Biochem. Biophys.* 524, 2–15.

Kimmel, C. B., Ballard, W. W., Kimmel, S. R., Ullmann, B., and Schilling, T. F. (1995). Stages of embryonic development of the zebrafish. *Dev. Dyn.* 203, 253–310.

Kimmel, C. B., Sessions, S. K., and Kimmel, R. J. (1981). Morphogenesis and synaptogenesis of the zebrafish Mauthner neuron. *J. Comp. Neurol.* 198, 101–120.

Kinkhabwala, A., Riley, M., Koyama, M., Monen, J., Satou, C., Kimura, Y., et al. (2011). A structural and functional ground plan for neurons in the hindbrain of zebrafish. *Proc. Natl. Acad. Sci. U.S.A.* 108, 1164–1169.

Li, H., Chuang, A. Z., and O'Brien, J. (2009). Photoreceptor coupling is controlled by connexin 35 phosphorylation in zebrafish retina. *J. Neurosci.* 29, 15178–15186.

Lo Turco, J. J., and Kriegstein, A. R. (1991). Clusters of coupled neuroblasts in embryonic neocortex. *Science* 252, 563–566.

Martin, T., and Ribera, A. (2012). "Connexin 35 in zebrafish spinal cord development. Program No. 31.21. 2012," in *Neuroscience Meeting Planner* (New Orleans, LA: Society for Neuroscience), [Online].

McLachlan, E., White, T. W., Ugonabo, C., Olson, C., Nagy, J. I., and Valdimarsson, G. (2003). Zebrafish Cx35: cloning and characterization of a gap junction gene highly expressed in the retina. *J. Neurosci. Res.* 73, 753–764.

O'Brien, J., Bruzzone, R., White, T. W., Al-Ubaidi, M. R., and Ripps, H. (1998). Cloning and expression of two related connexins from the perch retina define a distinct subgroup of the connexin family. *J. Neurosci.* 18, 7625–7637.

Pereda, A., O'Brien, J., Nagy, J. I., Bukauskas, F., Davidson, K. G. V., Kamasawa, N., et al. (2003). Connexin35 mediates electrical transmission at mixed synapses on mauthner cells. *J. Neurosci.* 23, 7489–7503.

Rash, J. E., Pereda, A., Kamasawa, N., Furman, C. S., Yasumura, T., Davidson, K. G. V., et al. (2004). High-resolution proteomic mapping in the vertebrate central nervous system: close proximity of connexin35 to NMDA glutamate receptor clusters and co-localization of connexin36 with immunoreactivity for zonula occludens protein-1 (ZO-1). *J. Neurocytol.* 33, 131–151.

Rash, J. E., Yasumura, T., Dudek, F. E., and Nagy, J. I. (2001). Cell-specific expression of connexins and evidence of restricted gap junctional coupling between glial cells and between neurons. *J. Neurosci.* 21, 1983–2000.

Satou, C., Kimura, Y., Kohashi, T., Horikawa, K., Takeda, H., Oda, Y., et al. (2009). Functional role of a specialized class of spinal commissural inhibitory neurons during fast escapes in zebrafish. *J. Neurosci.* 29, 6780–6793.

Söhl, G., Degen, J., Teubner, B., and Willecke, K. (1998). The murine gap junction gene connexin36 is highly expressed in mouse retina and regulated during brain development. *FEBS Lett.* 428, 27–31.

Söhl, G., Maxeiner, S., and Willecke, K. (2005). Expression and functions of neuronal gap junctions. *Nat. Rev. Neurosci.* 6, 191–200.

Sosinsky, G. E., Boassa, D., Dermietzel, R., Duffy, H. S., Laird, D. W., MacVicar, B., et al. (2011). Pannexin channels are not gap junction hemichannels. *Channels (Austin).* 5, 193–197.

Stuermer, C. A. (1988). Retinotopic organization of the developing retinotectal projection in the zebrafish embryo. *J. Neurosci.* 8, 4513–4530.

Todd, K. L., Kristan, W. B. Jr., and French, K. A. (2010). Gap junction expression is required for normal chemical synapse formation. *J. Neurosci.* 30, 15277–15285.

Wen, C.-M., Wang, C.-S., Chin, T.-C., Cheng, S.-T., and Nan, F.-H. (2010). Immunochemical and molecular characterization of a novel cell line derived from the brain of *Trachinotus blochii* (Teleostei, Perciformes): a fish cell line with oligodendrocyte progenitor cell and tanycyte characteristics. *Comp. Biochem. Physiol. A Mol. Integr. Physiol.* 156, 224–231.

Yu, Y.-C., He, S., Chen, S., Fu, Y., Brown, K. N., Yao, X.-H., et al. (2012). Preferential electrical coupling regulates neocortical lineage-dependent microcircuit assembly. *Nature* 486, 113–117.

Conflict of Interest Statement: The authors declare that the research was conducted in the absence of any commercial or financial relationships that could be construed as a potential conflict of interest.

Received: 05 March 2013; paper pending published: 22 March 2013; accepted: 23 April 2013; published online: 14 May 2013.

Citation: Jabeen S and Thirumalai V (2013) Distribution of the gap junction protein connexin 35 in the central nervous system of developing zebrafish larvae. Front. Neural Circuits 7:91. doi: 10.3389/fncir.2013.00091

frontiers in
NEURAL CIRCUITS

REVIEW ARTICLE
published: 26 April 2013
doi: 10.3389/fncir.2013.00079

Toward developmental models of psychiatric disorders in zebrafish

William H. J. Norton*

Department of Biology, College of Medicine, Biological Sciences and Psychiatry, University of Leicester, Leicester, UK

Edited by:
Gonzalo G. De Polavieja, Instituto Cajal, Consejo Superior de Investigaciones Científicas, Spain

Reviewed by:
Hitoshi Okamoto, RIKEN Brain Science Institute, Japan
David Parker, Cambridge University, UK

Correspondence:
William H. J. Norton, Department of Biology, College of Medicine, Biological Sciences and Psychiatry, University of Leicester, University Road, Leicester LE1 7RH, UK.
e-mail: whjn1@le.ac.uk

Psychiatric disorders are a diverse set of diseases that affect all aspects of mental function including social interaction, thinking, feeling, and mood. Although psychiatric disorders place a large economic burden on society, the drugs available to treat them are often palliative with variable efficacy and intolerable side-effects. The development of novel drugs has been hindered by a lack of knowledge about the etiology of these diseases. It is thus necessary to further investigate psychiatric disorders using a combination of human molecular genetics, gene-by-environment studies, *in vitro* pharmacological and biochemistry experiments, animal models, and investigation of the non-biological basis of these diseases, such as environmental effects. Many psychiatric disorders, including autism spectrum disorder, attention-deficit/hyperactivity disorder, mental retardation, and schizophrenia can be triggered by alterations to neural development. The zebrafish is a popular model for developmental biology that is increasingly used to study human disease. Recent work has extended this approach to examine psychiatric disorders as well. However, since psychiatric disorders affect complex mental functions that might be human specific, it is not possible to fully model them in fish. In this review, I will propose that the suitability of zebrafish for developmental studies, and the genetic tools available to manipulate them, provide a powerful model to study the roles of genes that are linked to psychiatric disorders during neural development. The relative speed and ease of conducting experiments in zebrafish can be used to address two areas of future research: the contribution of environmental factors to disease onset, and screening for novel therapeutic compounds.

Keywords: zebrafish, psychiatric disorders, development, attention-deficit/hyperactivity disorder, autism spectrum disorder, schizophrenia, mental retardation

INTRODUCTION

Psychiatric disorders are a diverse group of diseases that can affect all aspects of mental function including thinking, feeling, mood, and sociability. Psychiatric disorders place a massive strain on society. They are the leading cause of disability in Europe and North America (Eaton, 2008) and rank second in the burden of diseases in established market economies (World Health Organisation [WHO], 2008). However, the drug therapies available to treat psychiatric diseases are often only palliative and have variable efficacy and side-effects. Many of the compounds used to treat psychiatric disorders were discovered serendipitously more than 50 years ago and have not been significantly improved since (WHO, 2008). Furthermore, the high costs associated with developing new treatments, estimated at roughly $1.8 billion per drug, has prompted several major pharmaceutical companies to reduce or cancel their central nervous system research programs (Paul et al., 2010). One of the factors that have hindered the discovery of novel drugs is a lack of knowledge regarding the genetics and neurobiology of these diseases. Further research into the etiology of psychiatric disorders, driven by a combination of human genetic studies and animal models, and taking into account environmental influences, is needed in order to improve drug treatments and develop early prodomic interventions (before disease symptoms are visible) that could prevent or delay disease onset.

THE ENVIRONMENTAL AND GENETIC BASIS OF PSYCHIATRIC DISORDERS

Psychiatric disorders are caused by interaction of multiple factors that has been described by Gottesman and Gould (2003) as a "ballet that is choreographed over time between the action of multiple genes, environment and epigenetic factors." Initially, psychiatric disorders were thought to be triggered by the environment with only a limited influence of genes (Cooper, 2001). However, since the advent of genome-wide association studies (GWAS), there has been an increase in the amount of work that focuses on the genetic basis of psychiatric disorders. In parallel, data from twin family and adoption studies have uncovered heritability estimates for diseases such as schizophrenia (81%), attention-deficit/hyperactivity disorder (ADHD, 80%), and autism spectrum disorder (ASD, 70–80%) suggesting a critical role for genetic lesions in these disorders (Sullivan et al., 2003; Bailey et al., 2005; Rosenberg et al., 2009; Banaschewski et al., 2010). Since it is difficult to study psychosocial interactions in animal models, this review will concentrate on the genetics of psychiatric disorders with a focus on alterations to early neural development.

The genetics of psychiatric disorders are often complicated, with a non-Mendelian inheritance pattern and a continuous variation in phenotype suggesting that they might be caused by the action of multiple genes. This observation led to the common disease-common variant (CDCV) hypothesis: inheritance of one variant alone is not enough to cause a disease, but when combined with others a theoretical threshold will be passed and the disease triggered (Mitchell, 2011). As a result of the CDCV hypothesis, GWAS have been used to identify many genes associated with psychiatric disorders. GWAS are based upon the principle that multiple disease-causing variants (such as single nucleotide polymorphisms, SNPs) will be maintained in linkage-disequilibrium and so can be detected in an unbiased manner (Frazer et al., 2009). However, it is often unclear whether a loss or gain of gene function leads to expression of a psychiatric disorder. Following GWAS, mechanistic studies are then needed to show that identified variants participate in the disease being studied. Despite their promise, the contribution of GWAS to the understanding of psychiatric disorders has not been very impressive (Gottesman and Gould, 2003). Genes identified by GWAS still only account for a small percentage of the heritability of complex traits (Frazer et al., 2009) with poor correspondence of data across studies (Mitchell and Porteus, 2011). This is due to a combination of the modest effect of causative mutations on disease susceptibility, under-powered studies with small sample sizes, and the need to take environmental influences into account when studying genetic lesions.

Recent research has provided evidence that some psychiatric disorders, including schizophrenia, ADHD, autism, and mental retardation can also be triggered by mutations in single genes [sometimes referred to as the common disease rare variant (CDRV) hypothesis; Sebat, 2007; Walsh et al., 2008; Elia et al., 2009; Girirajan and Eichler, 2010; Williams et al., 2010; Geschwind, 2011; Lesch et al., 2011; Lionel et al., 2011; Veltman and Brunner, 2012]. Studies of families that suffer from psychiatric disorders often reveal *de novo* (or private) mutations which are unique to a given population or family. In fact, current estimates suggest that on average up to 74 novel mutations may occur per genome per generation in the non-disease population (Veltman and Brunner, 2012), with psychiatric disease families showing even higher than normal rates (Girard et al., 2011). These mutations are rare (comprising less than 1% of the minor allele frequency) and can either represent SNPs or be contained within copy number variations (CNVs) – deletions or duplications that can affect one or more genes at the same time (Sebat et al., 2009). CNVs occur quite frequently and have a mutation rate that is three to four times higher than other genomic areas, accounting for more genetic variation than other types of polymorphism (Cook and Scherer, 2008). Mutations can alter gene function in several ways, each of which can potentially lead to a psychiatric phenotype: they can activate proteins, create abnormal biochemical functions, or abrogate gene activity (Walsh, 1999; Walsh and Engle, 2010). Furthermore, a single gene can sometimes be mutated in multiple positions, each of which can trigger a different disease; whilst psychiatric disorders may be caused by a large number of different mutations, they might paradoxically only be linked to a small number of genes. For example, mutations in *Disrupted in Schizophrenia 1* (*Disc1*) can lead to schizophrenia, bipolar disorder, major depressive disorder, and autism (Porteous et al., 2011). Similarly, a microdeletion at human chromosome locus 22q11 is associated with a range of diseases including schizophrenia and velocardiofacial syndrome, anxiety, depression, ADHD, obsessive-compulsive disorder, and ASDs (Gothelf et al., 2004). Thus, seemingly diverse diseases may share a common genetic basis, making it possible to identify disease-causing variants in known – rather than novel genes in some cases.

The relative contribution of rare or common mutations to disease susceptibility is not known. Psychiatric disorders could be caused by a combination of several types of genetic lesion rather than a single mutation alone (Veltman and Brunner, 2012). Single mutations might predispose patients to mental illness, while other SNP polymorphisms in the genetic background (or mutations in a second critical gene) could alter disease penetrance (Girirajan and Eichler, 2010; Mitchell and Porteus, 2011). Therefore, a single mutation may be necessary but not sufficient to trigger the disorder. Such a combined model would explain the large heterogeneity of symptoms and the low penetrance that is sometimes observed. The potential interaction between rare and common mutations in the etiology of mental disease is reminiscent of the genetics of cancer. According to Knudson's two-hit hypothesis, cancer can be triggered by the combination of two or more mutations (Knudson, 1971). A recessive germline mutated allele is inherited from one parent, followed by a novel somatic mutation in the same gene (Guidry and Kent, 1999). The combination of common variants and rare mutations associated with psychiatric disorders raises the possibility that psychiatric disorders may also be caused by loss of heterozygosity or by the inheritance of two "hits" in separate genes (Girirajan and Eichler, 2010; Toro et al., 2010). The considerable number of brain areas and processes affected by psychiatric disorders provide a large pool of mutable genes which could lead to expression of a disease (Xu et al., 2008). As an example of this, CNVs in both *NRXN1* and *CNTNAP2* have been linked to Pitt–Hopkins-like syndrome, a familial disease that includes autistic symptoms (Zweier et al., 2009). Patients with Pitt–Hopkins-like syndrome have been found to have lost one copy of *NRXN1* or *CNTNAP2* coupled to a deleterious point mutation in the second allele of the same gene (Toro et al., 2010).

Interestingly, phylogenetic analysis of disease-causing mutations suggests that our current classification of psychiatric disorders may be based upon culturally acceptable behavioral norms. For example, in the case of the ADHD-linked gene *LATROPHILIN3*, the disease-causing variant is ancestral with protective variants arising over time (Arcos-Burgos et al., 2010; Domene et al., 2011). Thus some of the symptoms of ADHD – including hyperactivity and impulsivity – were either advantageous or at least not selected against during evolution. Similar results have been found for *Calretinin* polymorphisms linked to schizophrenia (Farokhashtiani et al., 2011), with disease-causing variants found in other distantly related vertebrate species.

The interaction of genes with environmental factors (including infection, drugs, malnutrition, psychosocial adversity, or obstetric complications) is likely to play a significant role in the risk of suffering from a psychiatric disorder. Genes may predispose

people to suffer from a disease, which is triggered when an adverse environment is encountered. Thus the severity of a disease might be determined by the interaction of a single gene with different environmental factors. These environmental factors may also be under genetic control. For example, the genetic variants that cause maternal ADHD also increase the propensity of mothers to drink or smoke (Castellanos et al., 1996; Laucht et al., 2007; Thapar et al., 2009). Furthermore, the number of germline mutations in sperm increases with age, exacerbating the likelihood of suffering from psychiatric disorders such as autism (Veltman and Brunner, 2012). In some cases, environmental influences may ultimately reflect the interaction of the parent's and child's genomes in expression of mental illness (Castellanos et al., 1996; Laucht et al., 2007). The gene-by-environment (G × E) interactions that lead to psychiatric disorders are poorly understood. However, a recent study of the human ADHD-risk gene *LATROPHILIN3* suggests that G × E interactions may not have a linear impact upon disease susceptibility (Choudhry et al., 2012). In impoverished environments (such as maternal stress during pregnancy), mutation of *LPHN3* has little contribution to disease onset with environmental factors playing a major role. However, in adequate or enriched environments, polymorphisms in *LPHN3* have a greater chance to trigger the disorder (Choudhry et al., 2012).

ALTERATIONS TO EMBRYONIC DEVELOPMENT CAN LEAD TO PSYCHIATRIC DISORDERS

Many of the rare mutations linked to psychiatric disorders are found in genes that are active during embryonic development. Subtle disruptions to the homeostasis of normal development can have far-reaching consequences that lead to permanent alterations in the function of the mature brain (Mitchell, 2011). Psychiatric disorders can thus be conceptualized as deviations in the normal trajectory of embryonic development within acceptable noise levels resulting in non-lethal modifications of behavior (West-Eberhard, 2005). Genetic variation and developmental plasticity (including chance events) are a fundamental property of all living organisms and provide the raw material upon which evolution can act. Development thus constitutes a series of branching pathways in which developmental decisions switch between different potential endpoints (West-Eberhard, 2005). For example, dopaminergic neurons show a surprisingly stochastic wiring pattern in larval zebrafish, even though they are thought to be genetically homogenous (Tay et al., 2011). Extreme alterations to embryonic development are likely to be lethal. However, if a mutation coincides with a chance event, a subtle change to embryonic development that leads to a psychiatric disorder may occur. Alterations to neural development can act at the cellular or circuit level. In some cases mutations may cause specific phenotypes linked to neurological disorders, such as the control of cell division, migration, differentiation, and survival, or changes to neurite outgrowth, axon pathfinding, and dendritic architecture (Thornton and Woods, 2009; Valiente and Marin, 2010). Alternatively, mutations may cause more diffuse and variable alterations to brain function: miswiring of neural circuits, disinhibition of local interneurons, or adjustment of normal brain homeostasis leading to pathophysiology (Lisman et al., 2008), a process which has been called "developmental disconnection" in relation to ASDs (Geschwind and Levitt, 2007). Diffuse changes to brain function seem particularly likely to lead to psychiatric diseases when considering that genes do not directly control behavior, but rather act via the formation, connection, and function of neural circuits.

TRANSLATIONAL MODELS OF PSYCHIATRIC DISORDERS IN ZEBRAFISH

Although recent studies have uncovered many genes linked to psychiatric disorders, only few of them have been experimentally validated. Therefore, mechanistic studies are required in order to investigate whether a loss− or gain−of-function contributes to disease pathology in each case. The complex genetic basis of psychiatric disorders makes it difficult to fully recreate them in animal models. Thus, the challenge of studying these diseases consists of integrating basic molecular data from animals with information about complex human mental functions at the circuit level (Geschwind, 2008). One way to simplify this problem is to measure endophenotypes, neuropsychological or biological markers that correlate to a disease-gene's activity (Gottesman and Gould, 2003; Kendler and Neale, 2010). An ideal endophenotype should be controlled by a single gene, be associated with expression of the disease in the population and be both heritable and state independent (meaning that it is expressed even when the illness is not active; Rommelse, 2008). Although in animal models endophenotypes have rarely fulfilled all of these criteria, their use may simplify the translation of information to human patients. Furthermore, the division of psychiatric disorders according to endophenotypes may help refine their diagnosis; diseases could thus be reclassified on the basis of their molecular pathology instead of behavioral or psychological symptoms, providing an explanation for comorbidity with other disorders (Gottesman and Gould, 2003).

Despite the difficulty of modeling psychiatric disorders, animal studies still have the potential to give insights into the etiology of mental illness. The advent of tools to manipulate genes has now allowed the creation of animal models that are firmly based upon the genetic pathways underlying a disease. A perfect animal model should have three main attributes: construct validity (meaning that it conforms to the underlying rationale of the disease), face validity (mimicking some of the characteristics of the disease), and predictive validity (the ability to accurately predict outcomes or symptoms in humans; Sarter et al., 1992; Einat et al., 2003; Arime et al., 2011). The animal model should also combine genetic tractability, tools to visualize and manipulate neurons *in vivo*, and the ability to translate findings to patients based upon conserved neurobiology.

Zebrafish have already been established as a powerful model for developmental biology and neuroscience. Zebrafish develop rapidly outside of the mother making it easy to collect and manipulate embryos. By 6 days, larval fish swim continuously, search for food, and are able to escape from predators thus demonstrating a range of behaviors. Zebrafish are transparent until larval stages allowing the study and manipulation of neural circuits at the cellular level in the intact brain (Fetcho and Liu, 1998). Furthermore, a large number of identified mutant lines, genetic tools such as TALENs (transcription activator-like effector nucleases) and zinc-finger nucleases to knock-out genes; Amacher,

2008; Huang et al., 2011; Sander et al., 2011), genetic ablation (Curado et al., 2007), optogenetics (Nagel et al., 2003; Zhang et al., 2007), and techniques to monitor neural activity (including calcium indicators and electrophysiology; Higashijima et al., 2003) have already been established. Although the formation, position, and function of neurotransmitter signaling pathways sometimes differ between zebrafish and other vertebrates, comparative studies are beginning to precisely map these differences, allowing the transfer of information gained in zebrafish to other species (Tropepe and Sive, 2003). Furthermore, a battery of tests for behavioral analysis of both larval and adult zebrafish has already been developed (Fero et al., 2011; Norton and Bally-Cuif, 2010; Norton et al., 2011). Although tools to study neuroscience are already available in other genetically tractable vertebrates such as mouse, the ease of generating large numbers of zebrafish and their transparency make them ideal for high-throughput analyses and imaging studies. As a model for behavioral neuroscience, the zebrafish is particularly useful for optogenetic dissection of the behavior, time-lapse analysis of neurotransmitter pathway formation during development and screening for novel therapeutic treatments. For example, the compensatory changes to neurotransmitter signaling pathways that occur following genetic manipulation can be examined in zebrafish. Abrogation of a single gene will most likely lead to the modification of multiple neurotransmitters. These fluctuations could be examined in two ways. The levels of neurotransmitters in the brain could be measured directly by either high pressure liquid chromatography (HPLC) or an enzyme-linked immunosorbent assay (ELISA). Alternatively, the alterations to neural circuits in the brain could be uncovered using calcium indicators driven by neurotransmitter-specific promoters [such as otpb. A for dopamine (DA; Fujimoto et al., 2011) or pet1 for serotonin (5-HT; Lillesaar et al., 2009)]. Neural activity (detected as flashes of calcium signaling) could be measured in fish lacking a functional copy of an ADHD-linked gene. This information might provide clues about the signaling pathways and brain areas underlying a phenotype and so provide avenues for future research.

The power of zebrafish to study developmental biology suggests that it may make important contributions to the study of genes associated with psychiatric disorders. The zebrafish homologs of genes linked to psychiatric disorders can be identified, and their basic function during neural development (related to neural circuit formation or behavior for example) analyzed following manipulation. For example, a zebrafish line could be created which harbors a mutation mimicking the situation in human patients. This could include replacing the wild-type zebrafish transcript with a humanized form of the gene or knocking the gene down by TALEN or morpholino injection. The developmental and behavioral phenotype of the manipulated fish could then be characterized. Environmental interactions with these models could be studied by applying standardized environmental manipulations – for example, by stressing the fish before testing behavior (Amir-Zilberstein et al., 2012), growing embryos in a hypoxic environment (Marks et al., 2005) or treating with alcohol or nicotine (see below). The data generated by this approach could then be verified in rodents and if similar results are obtained then clinical trials would be initiated. Apparent behavioral similarities between animals (which are often used to develop models of human diseases) may not ensure that the same underlying process is being measured, since each behavior might not serve the same purpose in all species. In contrast to this, developmental models of psychiatric disorders may have improved construct validity if the model is based upon the same underlying changes to development which lead to expression of the disease.

In the following section, I will briefly summarize zebrafish models of ADHD, schizophrenia, ASDs, and X-linked mental retardation (XLMR).

ZEBRAFISH MODELS OF ADHD

Attention-deficit/hyperactivity disorder is a common neuropsychiatric disorder that is characterized by developmentally inappropriate inattention, hyperactivity, and impulsivity. It affects around 3–5% of children worldwide regardless of nationality or cultural setting (Swanson et al., 1998; Polanczyk et al., 2007). The symptoms of ADHD persist into adulthood in about 50% of cases and can lead to a reduction in the quality of the sufferer's life including impairment of academic, behavioral, and social performance (Barkley et al., 2006; Schmidt and Petermann, 2009). ADHD patients are also more likely to suffer from other psychiatric disorders, including depression, anxiety, and substance use disorder (Molina and Pelham, 2003; Lesch et al., 2008; Sharp et al., 2009). Data from drug treatments and genetic analyses have suggested that alterations in DA and noradrenaline (NA; and to a lesser extent 5-HT and glutamate) signaling most likely underlie the symptoms of ADHD. For example, methylphenidate (MPH), an amphetamine like compound that increases both DA and NA levels in the prefrontal cortex (Berridge et al., 2006) can be used to manage ADHD and so has orientated research toward monoaminergic signaling. ADHD patients are thought to have a reduction of dopaminergic signaling in the prefrontal cortex. Other brain areas which have been connected to ADHD include the striatum (caudate nucleus and putamen) the parietal cortex and both the vermis and the inferior lobes of the cerebellum (Berquin et al., 1998; Arnsten, 2007; Bush, 2010; Rubia, 2011).

Multiple DA pathway-related genes have been linked to ADHD. Association with polymorphisms in the gene encoding the DA D4 receptor (*DRD4*; Ebstein et al., 1996; LaHoste et al., 1996), the DA D5 receptor (*DRD5*; Hawi et al., 2002), and the DA transporter gene (*DAT*/*SLC6A3*; Cook et al., 1995) have been reported. Most studies of *DAT* have focused on a 40 base-pair variable number tandem repeat (VNTR) found in the 3′ untranslated region (UTR) of the gene (Vandenbergh et al., 1992; Curran et al., 2001; Purper-Ouakil et al., 2005). There is also some evidence associating the DA synthesis enzyme *Dopamine-beta hydroxylase* (*DBH*) and the disease (Comings et al., 1996). In the 5-HT pathway, the 5-HT synthesis enzymes *TPH1* and *TPH2* (Walitza et al., 2005; Li et al., 2007) and the 5-HT transporter gene (*SERT/SLC6A4*; Gizer et al., 2009) have all been linked to ADHD formation. Recent GWAS and candidate gene studies have also identified polymorphisms in genes that are involved in cell adhesion (including *ASTN2* and *CDH13*) and synaptogenesis (*SNAP25*, *CTNNA2*, and *KLRN*; Faraone et al., 2005; Lesch et al., 2011). Thus, as well as being caused by direct modification of neurotransmitter signaling, ADHD may be triggered by more general alterations in

brain formation, including cell-signaling, morphogenesis, and migration during development.

There is currently only one study that has reported the use of fish to directly study an ADHD-linked gene (Lange et al., 2012). Lange et al. (2012) have studied *latrophilin3.1*, a zebrafish homolog of the human ADHD-susceptibility gene *LATROPHILIN3*. *LPHN3* was identified by linkage analysis of a genetically isolated European population in Columbia, followed by fine-mapping of several North American and European populations (Arcos-Burgos et al., 2010). Recent research has identified two families of endogenous ligands for Latrophilin3, the Teneurins and the FLRTs (Fibronectin Leucine-rich repeat transmembrane proteins; Silva et al., 2011; O'Sullivan et al., 2012). *latrophilin3.1* is one of two zebrafish homologs of human *LPHN3*, both of which are expressed in differentiated neurons throughout the brain up to 6 days post fertilization. *lphn3.1* morphants show an increase in the distance swum at 6 days, a hyperactive phenotype. This hyperactivity is also maintained during the night suggesting a permanent increase in locomotion compared to animals injected with a control morpholino. Furthermore, *lphn3.1* morphants also show an increase in the number of bursts of acceleration while swimming indicative of motor impulsivity. Both hyperactivity and motor impulsivity can be rescued by applying the ADHD treatment drugs MPH and atomoxetine. Acute treatment of either drug had no effect on control-injected larval behavior at the doses used (10 μM MPH or 1 μM atomoxetine for 1 h), but rescued morphant behavior bringing locomotion back to control levels. *lphn3.1* morphants also display a parallel reduction of dopaminergic cells in the posterior tuberculum (PT), a prominent group of dopaminergic neurons in the ventral diencephalon that controls larval locomotion (Bretaud et al., 2004; Sallinen et al., 2009; Tay et al., 2011). Recent analysis of the molecular signature and projection pattern of zebrafish PT neurons suggests they are similar to mammalian hypothalamic A11 DA neurons (Tay et al., 2011). Similar to A11, individual PT DA neurons project both anteriorly and posteriorly with the majority of projections (80%) going to the spinal cord (Ryu et al., 2007; Tay et al., 2011). Lesion of A11 DA neurons in rat causes a restless legs syndrome (RLS)-like hyperactivity phenotype and comorbidity between RLS and ADHD has been observed (Cortese et al., 2005). Thus common genes and neural circuits might underlie both diseases in mammals. Regardless of the homology of the zebrafish PT with other species, *lphn3.1* appears have a critical role in controlling the development of dopaminergic neurons (Lange et al., 2012), a finding which has recently been confirmed in mice (Wallis et al., 2012).

ZEBRAFISH MODELS OF SCHIZOPHRENIA

Schizophrenia is a severe psychiatric disorder whose symptoms include mood changes (such as delusions and hallucinations), disorganization of thought, agitated body movements, anhedonia, depression, speech problems, and a lack of motivation. Although schizophrenia is thought to be caused by defects in early brain development (Weinberger, 1995), disease symptoms often do not appear until the second or third decade of life (typically between 16 and 30 years of age). Schizophrenia affects around 1% of the adult population in the USA according to the National Institute of Mental Health. Twin studies give a heritability estimate of about 81% for schizophrenia, and an environmental effect (including variables such as diet, parenting style, and exposure to toxins or teratogens) of around 11% (Sullivan et al., 2003). A large number of schizophrenia cases are sporadic, appearing for the first time in a family with no previous history of the disease (Xu et al., 2008). Rare *de novo* CNVs are one mechanism that can account for sporadic cases. In agreement with this, schizophrenia patients carry more CNVs than the general population and also have a higher than normal *de novo* mutation rate (Girard et al., 2011, 2012).

Neurobiological studies have identified defects in the frontal and temporal lobes of schizophrenia patients. Many schizophrenics also have enlarged cerebral ventricles linked to a 5–10% reduction in gray matter volume in the absence of gliosis, suggesting that loss of tissue is not caused by degeneration (Mueser and McGurk, 2004). Both dopaminergic and glutamatergic neurotransmission has been linked to the disease. For example, a reduction of blood flow in the prefrontal cortex related to DA activity has been documented in schizophrenia patients (Mueser and McGurk, 2004). Many genes have been connected to the susceptibility to suffer from schizophrenia. For example, genes with particularly strong linkage to the disease include *DISRUPTED IN SCHIZOPHRENIA1* (*DISC1*), *NEUREGULIN1*, *DYSTROBREVIN BINDING PROTEIN1* (*DTNBP1*), *KIF1*, *KIF17*, *SHANK3*, and *NOTCH4* (Tarabeux et al., 2010; Girard et al., 2012). Developmental processes which might be affected include genes which affect neural proliferation, differentiation, and migration during development or abnormal myelination in the schizophrenic brain (Flynn et al., 2003).

Although it is not possible to study the positive symptoms of schizophrenia such as disordered thought, delusions, and hallucinations in zebrafish, the basic developmental function of genes linked to this disease can still be studied. For example, schizophrenia candidate genes may be important for neurogenesis, neuronal migration, and cell fate determination (Morris, 2009). Burgess and Granato (2007) have developed a schizophrenia endophenotype in zebrafish: prepulse inhibition (PPI). PPI is a type of sensorimotor gaiting (a reduction of startle response that occurs when preceded by a weak non-startling stimulus) that is impaired in schizophrenic patients (Braff et al., 2007). Zebrafish PPI is modified by both apomorphine and ketamine [which affect DA and *N*-methyl-*D*-aspartate (NMDA) signaling respectively] and thus appears to be mediated by similar neurotransmitters as in other animals. Five novel mutant lines with abnormal PPI responses were also identified in the same study. Characterization of these mutants might give novel insights into the genes and brain areas that control behaviors linked to schizophrenia.

One of the most intensely studied schizophrenia-related genes is *DISC1*, which was first identified in a Scottish pedigree displaying high incidence of depression, schizophrenia, and bipolar disorder (Millar et al., 2000). *DISC1* has subsequently been shown to be involved in neurogenesis, neural migration, axon growth, synaptogenesis and function, dopaminergic neuron function, and cell–cell adhesion. Studies of *disc1* in zebrafish have provided novel information about the function of this gene. De Rienzo et al. (2011) have shown that *disc1* has a critical role in both the canonical (β-catenin-mediated) and non-canonical Wnt signaling

pathways during embryonic development. Furthermore, different humanized forms of *disc1* have been shown to activate different signaling pathways in zebrafish. For example, Ala38Val, Arg264Gln, and Leu607Phe *disc1* variants interact with canonical Wnt signaling, whereas a Ser704Cys variant modifies neuronal migration via the cytoskeletal genes *nde1* and *dixdc1* (Singh et al., 2011). *disc1* has also been shown to control oligodendrocyte proliferation, a phenotype that can also be generated by inhibiting the schizophrenia-susceptibility genes *neuregulin1* and its receptor *erbb4* (Wood et al., 2009).

There have been several studies that have characterized schizophrenia-related genes in zebrafish. For example, the connection between Akt signaling, dopaminergic neurotransmission, and schizophrenia has been investigated. Cheng et al. (2013) have used zebrafish to study *rgs4*, a regulator of G-protein signaling family that is expressed in the developing nervous system. Loss of gene function causes both neurite outgrowth defects in the hindbrain and spinal cord and a reduction of motility. Activation of Akt signaling can rescue the outgrowth phenotype in the spinal cord but not hindbrain, indicating that Akt signaling is required for some *rgs4*-mediated axon formation (Cheng et al., 2013). Souza et al. (2011) have further examined the connection between Akt signaling and dopaminergic neurotransmission in the developing brain. Since alterations in Akt signaling have also been linked to schizophrenia, this strengthens the suggestion that altered dopaminergic signaling during development might underlie the disease. Other human disease-causing genes have been studied as well. Knock-down of the synaptically expressed schizophrenia-susceptibility gene *kinesin17* (*kif17*) causes a severe phenotype in zebrafish embryos including stunted development and a curly tail phenotype suggesting that *kif17* is active during embryonic development (Tarabeux et al., 2010). Finally, treatment of zebrafish with the NMDA receptor antagonist MK-801 causes several behavioral alterations including changes to social interaction, hyperactivity, and amnesia, which have been interpreted as being schizophreniform (schizophrenia-like; Chen et al., 2010; Seibt et al., 2010, 2011; Echevarria et al., 2011) and are similar to the behavioral changes elicited by these psychotics in rodents.

In summary, although it is not possible to model some of the more complex psychological symptoms of schizophrenia in fish, several recent studies have given insights into some of the basic processes underlying this disease.

ZEBRAFISH MODELS OF AUTISM SPECTRUM DISORDER

Autism spectrum disorder encompasses a range of psychiatric diseases including autism (the severest form of ASD), Rett's syndrome, and Asperger's syndrome. The symptoms of ASD are highly variable between patients making it difficult uncover the genetic and neurobiological changes that underlie these disorders. Broadly speaking, the main symptoms of ASD include alterations in social behavior, repetitive behavior, and language development that appear before 3 years of age (Lord et al., 2000). There is a heritability estimate of between 70 and 80% for ASD (Bailey et al., 2005; Rosenberg et al., 2009). However, the number of people thought to suffer from ASD is increasing over time which might be due to a shift in the diagnostic criteria used (Lord, 2010). Although it is not possible to study complex behaviors such as language development in fish, a few recent studies have provided information about the function of ASD-linked genes during neural development.

Both common and rare (*de novo*) genetic variants, acting in combination with environmental influences, are associated with ASD. ASD-linked polymorphisms are predominantly found in genes that regulate synapse development, cell proliferation, neural migration, and neural projection. Rare mutations seem to account for around 10% of cases of ASD (Geschwind, 2008). It has been suggested that there may be a different genetic basis for simplex families (where only one child is affected and rare mutations are common) and multiplex families (where multiple genetic variants lead to ASD expression in several family members; Geschwind, 2008). For example, there is a higher frequency of CNVs in ASD families with only one affected child compared to those with two or more ASD children (Toro et al., 2010). Interestingly, there is also some data suggesting that rare and common variants interact to trigger ASD symptoms (Ben-David and Shifman, 2012). Genes which have been linked to ASD include the Fragile X gene *FRAGILE X MENTAL RETARDATION 1* (*FMR1*), the $GABA_A$ β 3 subunit gene *GABRB3* as well as SHANK3, *TSC1*, *NEUROLIGIN3* and *NEUROLIGIN4*, *PTEN* and *CNTNAP2* (Cook and Scherer, 2008; Geschwind, 2008, 2011; Lord, 2010) amongst others. The neurobiology of ASD is not well understood, but most likely includes brain areas which are needed for the control of social behavior and language. For example, altered connections between the frontal lobe (the orbitofrontal cortex) and temporal lobe (including the superior temporal gyrus and temporal polar cortex) may mediate some symptoms of the disease (Geschwind, 2011). Other important brain areas include the cerebellum, brainstem, and limbic areas including the hippocampus, amygdala, septal nuclei, and the anterior cingulate cortex (Lord et al., 2000). Finally, autism has also been related to megalencephaly, an overall increase in brain size in some patients.

Since the symptoms of ASD first occur during neural development it is possible to study the early function of ASD-related genes in this species (Tropepe and Sive, 2003). There are only a few research articles reporting the use of zebrafish in this type of research. In humans, a CNV at 16p11.2 has been associated with susceptibility to suffer from several disorders, including ASD, epilepsy, autism, and schizophrenia. The 16p11.2 CNV has been studied in zebrafish by two groups (Blaker-Lee et al., 2012; Golzio et al., 2012). In a landmark study, Golzio et al. (2012) analyzed 24 of the genes contained within this CNV and identified one, *KCDT13*, as most likely being causative for the disease. Overexpression of *kcdt13* (by mRNA injection) led to microcephaly, whereas gene-specific morpholino knock-down caused an increase in head size, likely due to alteration of the cell cycle in both cases. This study provides a neat demonstration of the use of zebrafish to identify disease-causing variants within large genomic regions. Gauthier et al. (2010) have used morpholinos to knock-down *SHANK3*, a gene linked to schizophrenia and ASD in human patients. *shank3* morphant zebrafish show decreased swimming after being touched, a phenotype which can be rescued with a wild-type (but not a mutant) version of the corresponding rat gene. Therefore, this study validated alterations to *shank3* as being

important in the control of behavior, with potential implications for both schizophrenia and ASD.

ZEBRAFISH MODELS OF MENTAL RETARDATION

Mental retardation constitutes a significant impairment of cognitive function that can be symptomatic of a number of underlying neural defects. In this review, I have chosen to focus on XLMR (also called Fragile X syndrome, FXS) a common inherited form of mental retardation which affects around 1 in 4000 people. However, zebrafish have also been used to examine other types of mental retardation (for recent studies, refer to Komoike et al., 2010; Song et al., 2010; Brockschmidt et al., 2011; Friedrich et al., 2012; Veleri et al., 2012; Aspatwar et al., 2013). The symptoms of FXS include mental retardation, epilepsy, autistic-like behavior, attention deficits, macroorchidism, and mild craniofacial defects which have been linked to the maturation of dendritic spines during development.

Similar to schizophrenia and ASD, it is likely to be impossible to model the cognitive symptoms of mental retardation in fish. However, several zebrafish groups have analyzed XLMR-linked genes and provided information about their role during development. For example, XLMR is most often caused by mutations in the *FMR1* gene, which contains a variable CGG trinucleotide repeat sequence in its 5′ UTR (Verkerk et al., 1991). Once this repeat passes 200 copies, the gene becomes hypermethylated and loss of function occurs. Interestingly, this methylation appears to be mediated by a microRNA which is present in the 3′ UTR of *FMR1*, an observation which has been experimentally confirmed in zebrafish (Lin et al., 2006). Injection of a construct targeting the anti-fmr1 miRNA causes abnormal neural morphology and an increase in the size of the head (Lin et al., 2006).

Studies of the zebrafish homolog of the *FMR1* gene have given equivocal results. Intriguingly, different phenotypes were observed when comparing morpholino-mediated knock-down and a stable *fmr1* mutant line. Morphant larvae show craniofacial defects, hydrocephaly, and pericardial edema as well as abnormal branching of the trigeminal ganglion and lateral longitudinal fasciculus (Tucker et al., 2006). However, in contrast to this, *fmr1* mutant larvae are adult viable and show no detectable morphological differences (Den Broeder et al., 2009). Thus, it is clear that further studies are needed in order to fully understand the function of this gene during development. Qi et al. (2010) studied the XLMR gene *phf8* during zebrafish development. *phf8* is a mono-methyl histone H4 lysine 20 demethylase that is expressed in the developing head and jaw of zebrafish at 1 day. Loss of gene function causes severe disruption to development of these structures, most likely caused by increases in apoptosis (Qi et al., 2010). Histone methylation has also been linked to XLMR in a study of the *smcx/jarid1c* gene, a H3K4 demethylase (Iwase et al., 2007). Loss of *smcx* function during development leads to increased cell death and a smaller brain as well as a reduced number of dendrites. Together, both of these studies suggest that epigenetic events might play an important role in the etiology of XLMR. Another XLMR-linked gene, *rbmx*, shows strong expression in the anterior developing embryo including the brain (Tsend-Ayush et al., 2005). Knock-down of *rmbx* leads to a reduction in body size, pericardial edema, hydrocephaly, and reduced motility (Tsend-Ayush et al., 2005). Finally, the non-syndromic mental retardation genes *il1rapl1a*, *il1rapl1b*, and *il1rapl2* (zebrafish homologs of human *IL1RAPL*, which is located on the X chromosome) are widely expressed throughout the brain. Knock-down of one of the homologs, *ilrapl1b*, inhibits presynaptic differentiation during development (Yoshida and Mishina, 2008).

There are several learning and choice discrimination tests that have been developed for adult zebrafish which could be used to test possible cognitive functions of mental retardation-associated genes. For example, Brennan and colleagues have developed a 3-choice serial reaction time task (3CSRTT) that can be used to measure impulsivity (Parker et al., 2012). The 3CSRTT is measured in a tank that has a green light-emitting diode (LED) on one side and three yellow LEDs in separate compartments on the other. Following illumination of the green LED, adult zebrafish are taught to only enter the compartment where the yellow LED is switched on. The correct execution of this behavior is reinforced with a food reward. Following a training period in which the fish learns to associate the yellow light with a reward the 3CSRTT can begin. The green stimulus LED is first activated and is then followed by a 10-s intertrial interval (ITI). Following this pause, one of the yellow LEDs is lit and the fish is rewarded with food upon entering the correct compartment. However, entry into any compartment before the end of the ITI, perhaps indicative of impulsivity, will result in a punishment (a 10-s time-out with no food). Entry into an incorrect compartment on the other side (i.e., one in which the yellow LED is not illuminated) will also trigger the punishment. Other tests of learning and memory, including associative-, avoidance-, and spatial memory have also been established (reviewed in Norton and Bally-Cuif, 2010). Although these tests appear to be promising in to study zebrafish cognition, they have mostly only been tested on wild-type fish and so need further validation (for example, in fish lacking the function of a disease-linked gene) before they can be proposed as retardation-linked phenotypes.

FUTURE DIRECTIONS FOR RESEARCH INTO PSYCHIATRIC DISORDERS USING ZEBRAFISH

The functions of genes linked to psychiatric disorders are still relatively understudied in zebrafish. However, the power of zebrafish as a model organism to study neural development and behavior suggest that there are several areas in which the zebrafish has the potential to provide more information related to these diseases, as discussed below.

ENVIRONMENTAL CONTRIBUTIONS TO DISEASE ONSET

Since zebrafish embryos develop outside of their mother, it is easy to manipulate their environment and so carry out G × E studies. Although it is not possible to model adverse psychosocial environments (such as parenting styles) in fish, other environmental factors including exposure to alcohol or nicotine could easily be studied. Ethanol exposure during development causes a range of phenotypes depending on the timing and concentration used, making it difficult to get an overview of the mechanism underlying the action of this drug, or how it might relate to alcohol-related changes to behavior in humans. At concentrations greater than 2%, ethanol causes gross body abnormalities including cardiac edema,

cyclopia, and dysmorphia (Blader and Strahle, 1998; Sylvain et al., 2010). Lower concentrations trigger behavioral alterations in the absence of obvious morphological changes. For example, transient exposure to ethanol can lead to either locomotor hyperactivity (Tal et al., 2012), a reduction of swimming coupled to defects in secondary motorneuron development and synaptogenesis (Sylvain et al., 2010, 2011) or reduced shoaling in adult fish (Fernandes and Gerlai, 2009; Buske and Gerlai, 2011). Embryos which are treated with nicotine during development tend to be smaller, with a permanent delay and disruption of secondary motorneuron development (Svoboda et al., 2002; Menelaou and Svoboda, 2009). Nicotine also causes a transient increase in swimming speed, followed by a long-lasting reduction in both startle response and swimming speed, a phenotype which is most likely mediated via activation of nAChRs (Svoboda et al., 2002; Eddins et al., 2010).

One of the difficulties of designing G × E studies, highlighted by the examples related to ethanol and nicotine, will be to mimic the situation in nature as closely as possible. Although environmental alterations may modify the severity of an obvious pre-existing phenotype, in some cases environmental influences would be expected to trigger disease-related symptoms in a genotype that initially looks normal. One way to address this issue would be to develop a zebrafish transgenic line that contains a humanized form of the disease-risk gene and then subject embryos to different environmental conditions (such as varying concentrations of ethanol or nicotine exposure) before measuring behavior. Although such an approach is not more technically difficult than starting with a measurable behavioral change, it would require researchers to have more confidence when developing the assay.

SCREENING FOR NOVEL DRUGS

Zebrafish are a good model system for pharmacological studies, since compounds can be diluted in the embryo medium, and larvae are transparent meaning that internal organs can be visualized throughout development (Peterson et al., 2000). Furthermore, larvae are small, easy to generate in large numbers and easy to manipulate making them ideal for high-throughput work. However, since screens that use behavior as a read-out are difficult to design and implement efficiently (particularly if focusing on complex behaviors other than locomotion), it might be easier to carry out an initial pre-screen of a disease endophenotype. For example, zebrafish lacking the function of the ADHD-linked gene *lphn3.1* show a reduction and displacement of dopaminergic neurons in the PT of the diencephalon (Lange et al., 2012). Pre-screening libraries for compounds which can rescue this phenotype might speed up the screening process, with a subset of promising drugs then being re-tested to assess their behavioral function.

Two studies have combined analysis of underlying chemical structure and high-throughput screening of chemical libraries to look for alterations to the photomotor response, an embryonic motor response to a series of light flashes (Kokel et al., 2010; Laggner et al., 2012). This assay can be performed in a 96-well plate, and can be scaled up to analyze around 5000 novel chemicals every day. Rihel et al. (2010) uncovered the effect of drugs on locomotor activity across different sleep/wake cycles, providing novel information about neuroactive drugs which can affect behavior. In this study, chemicals were categorized according to their "behavioral fingerprint," a combination of their chemical structure and their ability to modify aspects of behavior, thus permitting prediction of the function of novel chemicals.

A screen for novel anti-epileptic drugs was conducted in 2-day-old zebrafish embryos by Baxendale et al. (2012). Although not a developmental psychiatric disorder, this work further demonstrates the utility of zebrafish for drug identification. Exposure of embryos to the convulsant pentylenetetrazole (PTZ) upregulates expression of the immediate-early gene *fos* in the brain. The level of *fos* expression (assayed by *in situ* hybridization) was then used to screen a bioactive small-molecule library with a hit rate of 2.3% for anti-convulsive drugs (Baxendale et al., 2012). Using a similar approach, Baraban (2007) screened for novel zebrafish mutant lines which are resistant to the seizure-inducing properties of PTZ at 7 days post fertilization. Six novel mutant lines were identified, raising the possibility of uncovering novel genes with a seizure-protective function. The effects of the stimulants ethanol, amphetamine, and cocaine on larval swimming behavior have also been reported (Irons et al., 2010). Whilst not high-throughput, this study demonstrates the ease of screening motor behavior in 96-well plates, meaning that this paradigm could potentially be used to look at hyperactivity or startle, endophenotypes related to psychiatric disorders.

Although zebrafish constitute a power model system for drug screens, further experiments will be required before data can be translated to human patients. In a first step, the results will need to be verified in a second animal model – most likely a knockout mouse harboring a similar genetic lesion. Analysis of further disease models with and without drug treatment will provide information about selectivity of the chemical compound for one or more signaling pathways. A drug with a similar profile in both fish and mouse will represent a very promising target for clinical trials as long as no toxic effects are detected.

CONCLUSION

A full understanding of the basis of psychiatric disorders requires the characterization of complex behaviors such as thought, feeling, and emotion, most likely through translational experiments in a combination of model organisms such as zebrafish and rodents. However, the suitability of zebrafish for developmental studies, and the genetic tools which are available to manipulate them suggest that the early development function of psychiatric disorder-linked genes can be studied in this model organism. Studies of genes linked to ADHD, schizophrenia, ASD, and mental retardation that have been performed in zebrafish have already demonstrated the validity of this approach. I look forward to future developments in this exciting field.

ACKNOWLEDGMENTS

I am grateful to Marion Coolen, Merlin Lange, and Mike Jay for critically reading an earlier version of this manuscript. Many of the ideas and concepts presented in this review were formed during discussions with Laure Bally-Cuif and colleagues in Gif-sur-Yvette. I am indebted to these people for their input and support.

REFERENCES

Amacher, S. L. (2008). Emerging gene knockout technology in zebrafish: zinc-finger nucleases. *Brief. Funct. Genomics Proteomics* 7, 460–464.

Amir-Zilberstein, L., Blechman, J., Sztainberg, Y., Norton, W., Reuveny, A., Borodovsky, N., et al. (2012). Homeodomain protein Otp and activity-dependent splicing modulate neuronal adaptation to stress. *Neuron* 73, 279–291.

Arcos-Burgos, M., Jain, M., Acosta, M. T., Shively, S., Stanescu, H., Wallis, D., et al. (2010). A common variant of the latrophilin 3 gene, LPHN3, confers susceptibility to ADHD and predicts effectiveness of stimulant medication. *Mol. Psychiatry* 15, 1053–1066.

Arime, Y., Kubo, Y., and Sora, I. (2011). Animal models of attention-deficit/hyperactivity disorder. *Biol. Pharm. Bull.* 34, 1373–1376.

Arnsten, A. F. (2007). Catecholamine and second messenger influences on prefrontal cortical networks of "representational knowledge": a rational bridge between genetics and the symptoms of mental illness. *Cereb. Cortex* 17(Suppl. 1), i6–i15.

Aspatwar, A., Tolvanen, M. E., Jokitalo, E., Parikka, M., Ortutay, C., Harjula, S. K., et al. (2013). Abnormal cerebellar development and ataxia in CARP VIII morphant zebrafish. *Hum. Mol. Genet.* 22, 417–432.

Bailey, A. J., Braeutigam, S., Jousmaki, V., and Swithenby, S. J. (2005). Abnormal activation of face processing systems at early and intermediate latency in individuals with autism spectrum disorder: a magnetoencephalographic study. *Eur. J. Neurosci.* 21, 2575–2585.

Banaschewski, T., Becker, K., Scherag, S., Franke, B., and Coghill, D. (2010). Molecular genetics of attention-deficit/hyperactivity disorder: an overview. *Eur. Child Adolesc. Psychiatry* 19, 237–257.

Baraban, S. C. (2007). Emerging epilepsy models: insights from mice, flies, worms and fish. *Curr. Opin. Neurol.* 20, 164–168.

Barkley, R. A., Fischer, M., Smallish, L., and Fletcher, K. (2006). Young adult outcome of hyperactive children: adaptive functioning in major life activities. *J. Am. Acad. Child Adolesc. Psychiatry* 45, 192–202.

Baxendale, S., Holdsworth, C. J., Meza Santoscoy, P. L., Harrison, M. R., Fox, J., Parkin, C. A., et al. (2012). Identification of compounds with anticonvulsant properties in a zebrafish model of epileptic seizures. *Dis. Models Mech.* 5, 773–784.

Ben-David, E., and Shifman, S. (2012). Networks of neuronal genes affected by common and rare variants in autism spectrum disorders. *PLoS Genet.* 8:e1002556. doi: 10.1371/journal.pgen.1002556

Berquin, P. C., Giedd, J. N., Jacobsen, L. K., Hamburger, S. D., Krain, A. L., Rapoport, J. L., et al. (1998). Cerebellum in attention-deficit hyperactivity disorder: a morphometric MRI study. *Neurology* 50, 1087–1093.

Berridge, C. W., Devilbiss, D. M., Andrzejewski, M. E., Arnsten, A. F., Kelley, A. E., Schmeichel, B., et al. (2006). Methylphenidate preferentially increases catecholamine neurotransmission within the prefrontal cortex at low doses that enhance cognitive function. *Biol. Psychiatry* 60, 1111–1120.

Blader, P., and Strahle, U. (1998). Ethanol impairs migration of the prechordal plate in the zebrafish embryo. *Dev. Biol.* 201, 185–201.

Blaker-Lee, A., Gupta, S., McCammon, J. M., De Rienzo, G., and Sive, H. (2012). Zebrafish homologs of genes within 16p11.2, a genomic region associated with brain disorders, are active during brain development, and include two deletion dosage sensor genes. *Dis. Models Mech.* 5, 834–851.

Braff, D., Schork, N. J., and Gottesman, I. (2007). Endophenotyping schizophrenia. *Am. J. Psychiatry* 164, 705–707.

Bretaud, S., Lee, S., and Guo, S. (2004). Sensitivity of zebrafish to environmental toxins implicated in Parkinson's disease. *Neurotoxicol. Teratol.* 26, 857–864.

Brockschmidt, A., Filippi, A., Charbel Issa, P., Nelles, M., Urbach, H., Eter, N., et al. (2011). Neurologic and ocular phenotype in Pitt–Hopkins syndrome and a zebrafish model. *Hum. Genet.* 130, 645–655.

Burgess, H. A., and Granato, M. (2007). Modulation of locomotor activity in larval zebrafish during light adaptation. *J. Exp. Biol.* 210, 2526–2539.

Bush, G. (2010). Attention-deficit /hyperactivity disorder and attention networks. *Neuropsychopharmacology* 35, 278–300.

Buske, C., and Gerlai, R. (2011). Early embryonic ethanol exposure impairs shoaling and the dopaminergic and serotoninergic systems in adult zebrafish. *Neurotoxicol. Teratol.* 33, 698–707.

Castellanos, F. X., Giedd, J. N., Marsh, W. L., Hamburger, S. D., Vaituzis, A. C., Dickstein, D. P., et al. (1996). Quantitative brain magnetic resonance imaging in attention-deficit hyperactivity disorder. *Arch. Gen. Psychiatry* 53, 607–616.

Chen, J., Patel, R., Friedman, T. C., and Jones, K. S. (2010). The behavioral and pharmacological actions of NMDA receptor antagonism are conserved in zebrafish larvae. *Int. J. Comp. Psychol.* 23, 82–90.

Cheng, Y. C., Scotting, P. J., Hsu, L. S., Lin, S. J., Shih, H. Y., Hsieh, F. Y., et al. (2013). Zebrafish rgs4 is essential for motility and axonogenesis mediated by Akt signaling. *Cell. Mol. Life Sci.* 70, 935–950.

Choudhry, Z., Sengupta, S. M., Grizenko, N., Fortier, M. E., Thakur, G. A., Bellingham, J., et al. (2012). LPHN3 and attention-deficit/hyperactivity disorder: interaction with maternal stress during pregnancy. *J. Child Psychol. Psychiatry* 53, 892–902.

Comings, D. E., Wu, S., Chiu, C., Ring, R. H., Gade, R., Ahn, C., et al. (1996). Polygenic inheritance of Tourette syndrome, stuttering, attention deficit hyperactivity, conduct, and oppositional defiant disorder: the additive and subtractive effect of the three dopaminergic genes – DRD2, D beta H, and DAT1. *Am. J. Med. Genet.* 67, 264–288.

Cook, E. H., and Scherer, S. W. (2008). Copy-number variations associated with neuropsychiatric conditions. *Nature* 455, 919–923.

Cook, E. H., Stein, M. A., Krasowski, M. D., Cox, N. J., Olkon, D. M., Kieffer, J. E., et al. (1995). Association of attention-deficit disorder and the dopamine transporter gene. *Am. J. Hum. Genet.* 56, 993–998.

Cooper, B. (2001). Nature, nurture and mental disorder: old concepts in the new millennium. *Br. J. Psychiatry Suppl.* 178, s91–s101.

Cortese, S., Konofal, E., Lecendreux, M., Arnulf, I., Mouren, M.-C., Darra, F., et al. (2005). Restless legs syndrome and attention-deficit/hyperactivity disorder: a review of the literature. *Sleep* 28, 1007–1013.

Curado, S., Anderson, R. M., Jungblut, B., Mumm, J., Schroeter, E., and Stainier, D. Y. (2007). Conditional targeted cell ablation in zebrafish: a new tool for regeneration studies. *Dev. Dyn.* 236, 1025–1035.

Curran, S., Mill, J., Tahir, E., Kent, L., Richards, S., Gould, A., et al. (2001). Association study of a dopamine transporter polymorphism and attention deficit hyperactivity disorder in UK and Turkish samples. *Mol. Psychiatry* 6, 425–428.

Den Broeder, M. J., Van der Linde, H., Brouwer, J. R., Oostra, B. A., Willemsen, R., and Ketting, R. F. (2009). Generation and characterization of FMR1 knockout zebrafish. *PLoS ONE* 4:e7910. doi: 10.1371/journal.pone.0007910

De Rienzo, G., Bishop, J. A., Mao, Y., Pan, L., Ma, T. P., Moens, C. B., et al. (2011). Disc1 regulates both β-catenin-mediated and noncanonical Wnt signaling during vertebrate embryogenesis. *FASEB J.* 25, 4184–4197.

Domene, S., Stanescu, H., Wallis, D., Tinloy, B., Pineda, D. E., Kleta, R., et al. (2011). Screening of human LPHN3 for variants with a potential impact on ADHD susceptibility. *Am. J. Med. Genet. B Neuropsychiatr. Genet.* 156B, 11–18.

Eaton, L. (2008). Healthcare Commission's standards of psychiatric care. *Ment. Health Today* 5.

Ebstein, R. P., Novick, O., Umansky, R., Priel, B., Osher, Y., Blaine, D., et al. (1996). Dopamine D4 receptor (D4DR) exon III polymorphism associated with the human personality trait of Novelty Seeking. *Nat. Genet.* 12, 78–80.

Echevarria, D. J., Jouandot, D. J., and Toms, C. N. (2011). Assessing attention in the zebrafish: are we there yet? *Prog. Neuropsychopharmacol. Biol. Psychiatry* 35, 1416–1420.

Eddins, D., Cerutti, D., Williams, P., Linney, E., and Levin, E. D. (2010). Zebrafish provide a sensitive model of persisting neurobehavioral effects of developmental chlorpyrifos exposure: comparison with nicotine and pilocarpine effects and relationship to dopamine deficits. *Neurotoxicol. Teratol.* 32, 99–108.

Einat, H., Manji, H. K., and Belmaker, R. H. (2003). New approaches to modeling bipolar disorder. *Psychopharmacol. Bull.* 37, 47–63.

Elia, J., Gai, X., Xie, H. M., Perin, J. C., Geiger, E., Glessner, J. T., et al. (2009). Rare structural variants found in attention-deficit hyperactivity disorder are preferentially associated with neurodevelopmental genes. *Mol. Psychiatry* 15, 637–646.

Faraone, S. V., Perlis, R. H., Doyle, A. E., Smoller, J. W., Goralnick, J. J., Holmgren, M. A., et al. (2005). Molecular genetics of attention-deficit/hyperactivity disorder. *Biol. Psychiatry* 57, 1313–1323.

Farokhashtiani, T., Mirabzadeh, A., Olad Nabi, M., Magham, Z. G., Khorshid, H. R., Najmabadi, H., et al. (2011). Reversion of the human calreticulin gene promoter to the ancestral type as a result of a novel psychosis-associated mutation. *Prog. Neuropsychopharmacol. Biol. Psychiatry* 35, 541–544.

Fernandes, Y., and Gerlai, R. (2009). Long-term behavioral changes in response to early developmental exposure to ethanol in zebrafish. *Alcohol. Clin. Exp. Res.* 33, 601–609.

Fero, K., Yokogawa, T., and Burgess, H. A. (2011). "The behavioral repertoire of larval zebrafish," in *Zebrafish Models in Neurobehavioral Research*, eds A. V. Kalueff and J. M. Cachat (New York: Springer), 249–291.

Fetcho, J. R., and Liu, K. S. (1998). Zebrafish as a model system for studying neuronal circuits and behavior. *Ann. N. Y. Acad. Sci.* 860, 333–345.

Flynn, S. W., Lang, D. J., Mackay, A. L., Goghari, V., Vavasour, I. M., Whittall, K. P., et al. (2003). Abnormalities of myelination in schizophrenia detected in vivo with MRI, and post-mortem with analysis of oligodendrocyte proteins. *Mol. Psychiatry* 8, 811–820.

Frazer, K. A., Murray, S. S., Schork, N. J., and Topol, E. J. (2009). Human genetic variation and its contribution to complex traits. *Nat. Rev.* 10, 241–251.

Friedrich, T., Lambert, A. M., Masino, M. A., and Downes, G. B. (2012). Mutation of zebrafish dihydrolipoamide branched-chain transacylase E2 results in motor dysfunction and models maple syrup urine disease. *Dis. Models Mech.* 5, 248–258.

Fujimoto, E., Stevenson, T. J., Chien, C. B., and Bonkowsky, J. L. (2011). Identification of a dopaminergic enhancer indicates complexity in vertebrate dopamine neuron phenotype specification. *Dev. Biol.* 352, 393–404.

Gauthier, J., Champagne, N., Lafreniere, R. G., Xiong, L., Spiegelman, D., Brustein, E., et al. (2010). De novo mutations in the gene encoding the synaptic scaffolding protein SHANK3 in patients ascertained for schizophrenia. *Proc. Natl. Acad. Sci. U.S.A.* 107, 7863–7868.

Geschwind, D. H. (2008). Autism: many genes, common pathways? *Cell* 135, 391–395.

Geschwind, D. H. (2011). Genetics of autism spectrum disorders. *Trends Cogn. Sci.* 15, 409–416.

Geschwind, D. H., and Levitt, P. (2007). Autism spectrum disorders: developmental disconnection syndromes. *Curr. Opin. Neurobiol.* 17, 103–111.

Girard, S. L., Dion, P. A., and Rouleau, G. A. (2012). Schizophrenia genetics: putting all the pieces together. *Curr. Neurol. Neurosci. Rep.* 12, 261–266.

Girard, S. L., Gauthier, J., Noreau, A., Xiong, L., Zhou, S., Jouan, L., et al. (2011). Increased exonic de novo mutation rate in individuals with schizophrenia. *Nat. Genet.* 43, 860–863.

Girirajan, S., and Eichler, E. E. (2010). Phenotypic variability and genetic susceptibility to genomic disorders. *Hum. Mol. Genet.* 19, R176–R187.

Gizer, I. R., Ficks, C., and Waldman, I. D. (2009). Candidate gene studies of ADHD: a meta-analytic review. *Hum. Genet.* 126, 51–90.

Golzio, C., Willer, J., Talkowski, M. E., Oh, E. C., Taniguchi, Y., Jacquemont, S., et al. (2012). KCTD13 is a major driver of mirrored neuroanatomical phenotypes of the 16p11.2 copy number variant. *Nature* 485, 363–367.

Gothelf, D., Presburger, G., Levy, D., Nahmani, A., Burg, M., Berant, M., et al. (2004). Genetic, developmental, and physical factors associated with attention deficit hyperactivity disorder in patients with velocardiofacial syndrome. *Am. J. Med. Genet. B Neuropsychiatr. Genet.* 126B, 116–121.

Gottesman, I., and Gould, T. D. (2003). The endophenotype concept in psychiatry: etymology and strategic intentions. *Am. J. Psychiatry* 160, 636–645.

Guidry, J., and Kent, T. A. (1999). New genetic hypothesis of schizophrenia. *Med. Hypotheses* 52, 69–75.

Hawi, Z., Dring, M., Kirley, A., Foley, D., Kent, L., Craddock, N., et al. (2002). Serotonergic system and attention deficit hyperactivity disorder (ADHD): a potential susceptibility locus at the 5-HT(1B) receptor gene in 273 nuclear families from a multi-centre sample. *Mol. Psychiatry* 7, 718–725.

Higashijima, S., Masino, M. A., Mandel, G., and Fetcho, J. R. (2003). Imaging neuronal activity during zebrafish behavior with a genetically encoded calcium indicator. *J. Neurophysiol.* 90, 3986–3997.

Huang, P., Xiao, A., Zhou, M., Zhu, Z., Lin, S., and Zhang, B. (2011). Heritable gene targeting in zebrafish using customized TALENs. *Nat. Biotechnol.* 29, 699–700.

Irons, T. D., MacPhail, R. C., Hunter, D. L., and Padilla, S. (2010). Acute neuroactive drug exposures alter locomotor activity in larval zebrafish. *Neurotoxicol. Teratol.* 32, 84–90.

Iwase, S., Lan, F., Bayliss, P., De la Torre-Ubieta, L., Huarte, M., Qi, H. H., et al. (2007). The X-linked mental retardation gene SMCX/JARID1C defines a family of histone H3 lysine 4 demethylases. *Cell* 128, 1077–1088.

Kendler, K. S., and Neale, M. C. (2010). Endophenotype: a conceptual analysis. *Mol. Psychiatry* 15, 789–797.

Knudson, A. G. (1971). Mutation and cancer: statistical study of retinoblastoma. *Proc. Natl. Acad. Sci. U.S.A.* 68, 820–823.

Kokel, D., Bryan, J., Laggner, C., White, R., Cheung, C. Y., Mateus, R., et al. (2010). Rapid behavior-based identification of neuroactive small molecules in the zebrafish. *Nat. Chem. Biol.* 6, 231–237.

Komoike, Y., Shimojima, K., Liang, J. S., Fujii, H., Maegaki, Y., Osawa, M., et al. (2010). A functional analysis of GABARAP on 17p13.1 by knockdown zebrafish. *J. Hum. Genet.* 55, 155–162.

Laggner, C., Kokel, D., Setola, V., Tolia, A., Lin, H., Irwin, J. J., et al. (2012). Chemical informatics and target identification in a zebrafish phenotypic screen. *Nat. Chem. Biol.* 8, 144–146.

LaHoste, G. J., Swanson, J. M., Wigal, S. B., Glabe, C., Wigal, T., King, N., et al. (1996). Dopamine D4 receptor gene polymorphism is associated with attention deficit hyperactivity disorder. *Mol. Psychiatry* 1, 121–124.

Lange, M., Norton, W., Coolen, M., Chaminade, M., Merker, S., Proft, F., et al. (2012). The ADHD-susceptibility gene lphn3.1 modulates dopaminergic neuron formation and locomotor activity during zebrafish development. *Mol. Psychiatry* 17, 946–954.

Laucht, M., Skowronek, M. H., Becker, K., Schmidt, M. H., Esser, G., Schulze, T. G., et al. (2007). Interacting effects of the dopamine transporter gene and psychosocial adversity on attention-deficit/hyperactivity disorder symptoms among 15-year-olds from a high-risk community sample. *Arch. Gen. Psychiatry* 64, 585–590.

Lesch, K. P., Selch, S., Renner, T. J., Jacob, C., Nguyen, T. T., Hahn, T., et al. (2011). Genome-wide copy number variation analysis in attention-deficit/hyperactivity disorder: association with neuropeptide Y gene dosage in an extended pedigree. *Mol. Psychiatry* 16, 491–503.

Lesch, K. P., Timmesfeld, N., Renner, T. J., Halperin, R., Roser, C., Nguyen, T. T., et al. (2008). Molecular genetics of adult ADHD: converging evidence from genome-wide association and extended pedigree linkage studies. *J. Neural. Transm.* 115, 1573–1585.

Li, J., Wang, Y., Zhou, R., Zhang, H., Yang, L., Wang, B., et al. (2007). Association between polymorphisms in serotonin transporter gene and attention deficit hyperactivity disorder in Chinese Han subjects. *Am. J. Med. Genet. B Neuropsychiatr. Genet.* 144B, 14–19.

Lillesaar, C., Stigloher, C., Tannhauser, B., Wullimann, M. F., and Bally-Cuif, L. (2009). Axonal projections originating from raphe serotonergic neurons in the developing and adult zebrafish, *Danio rerio*, using transgenics to visualize raphe-specific pet1 expression. *J. Comp. Neurol.* 512, 158–182.

Lin, S. L., Chang, S. J., and Ying, S. Y. (2006). First in vivo evidence of microRNA-induced fragile X mental retardation syndrome. *Mol. Psychiatry* 11, 616–617.

Lionel, A. C., Crosbie, J., Barbosa, N., Goodale, T., Thiruvahindrapuram, B., Rickaby, J., et al. (2011). Rare copy number variation discovery and cross-disorder comparisons identify risk genes for ADHD. *Sci. Transl. Med.* 3, 95ra75.

Lisman, J. E., Coyle, J. T., Green, R. W., Javitt, D. C., Benes, F. M., Heckers, S., et al. (2008). Circuit-based framework for understanding neurotransmitter and risk gene interactions in schizophrenia. *Trends Neurosci.* 31, 234–242.

Lord, C., Cook, E. H., Leventhal, B. L., and Amaral, D. G. (2000). Autism spectrum disorders. *Neuron* 28, 355–363.

Lord, C. E. (2010). Autism: from research to practice. *Am. Psychol.* 65, 815–826.

Marks, C., West, T. N., Bagatto, B., and Moore, F. B.-G. (2005). Developmental environment alters conditional aggression in zebrafish. *Copeia* 4, 901–908.

Menelaou, E., and Svoboda, K. R. (2009). Secondary motoneurons in juvenile and adult zebrafish: axonal pathfinding errors caused by embryonic nicotine exposure. *J. Comp. Neurol.* 512, 305–322.

Millar, J. K., Christie, S., Semple, C. A., and Porteous, D. J. (2000). Chromosomal location and genomic structure of the human translin-associated factor X gene (TRAX; TSNAX) revealed by intergenic splicing to DISC1, a gene disrupted by a translocation segregating with schizophrenia. *Genomics* 67, 69–77.

Mitchell, K. (2011). The miswired brain: making connections from neurodevelopment to psychopathology. *BMC Biol.* 9:23. doi: 10.1186/1741-7007-9-23

Mitchell, K., and Porteus, D. J. (2011). Rethinking the genetic architecture of schizophrenia. *Psychol. Med.* 41, 19–32.

Molina, B. S., and Pelham, W. E. (2003). Childhood predictors of adolescent substance use in a longitudinal study

of children with ADHD. *J. Abnorm. Psychol.* 112, 497–507.

Morris, J. A. (2009). Zebrafish: a model system to examine the neurodevelopmental basis of schizophrenia. *Prog. Brain Res.* 179, 97–106.

Mueser, K. T., and McGurk, S. R. (2004). Schizophrenia. *Lancet* 363, 2063–2072.

Nagel, G., Szellas, T., Huhn, W., Kateriya, S., Adeishvili, N., Berthold, P., et al. (2003). Channelrhodopsin-2, a directly light-gated cation-selective membrane channel. *Proc. Natl. Acad. Sci. U.S.A.* 100, 13940–13945.

Norton, W., and Bally-Cuif, L. (2010). Adult zebrafish as a model organism for behavioural genetics. *BMC Neurosci.* 11:90. doi: 10.1186/1471-2202-11-90

Norton, W. H., Stumpenhorst, K., Faus-Kessler, T., Folchert, A., Rohner, N., Harris, M. P., et al. (2011). Modulation of Fgfr1a signaling in zebrafish reveals a genetic basis for the aggression-boldness syndrome. *J. Neurosci.* 31, 13796–13807.

O'Sullivan, M. L., De Wit, J., Savas, J. N., Comoletti, D., Otto-Hitt, S., Yates, J. R., et al. (2012). FLRT proteins are endogenous latrophilin ligands and regulate excitatory synapse development. *Neuron* 73, 903–910.

Parker, M. O., Millington, M. E., Combe, F. J., and Brennan, C. H. (2012). Development and implementation of a three-choice serial reaction time task for zebrafish (*Danio rerio*). *Behav. Brain Res.* 227, 73–80.

Paul, S. M., Mytelka, D. S., Dunwiddie, C. T., Persinger, C. C., Munos, B. H., Lindborg, S. R., et al. (2010). How to improve R&D productivity: the pharmaceutical industry's grand challenge. *Nat. Rev. Drug Discov.* 9, 203–214.

Peterson, R. T., Link, B. A., Dowling, J. E., and Schreiber, S. L. (2000). Small molecule developmental screens reveal the logic and timing of vertebrate development. *Proc. Natl. Acad. Sci. U.S.A.* 97, 12965–12969.

Polanczyk, G., De Lima, M. S., Horta, B. L., Biederman, J., and Rohde, L. A. (2007). The worldwide prevalence of ADHD: a systematic review and metaregression analysis. *Am. J. Psychiatry* 164, 942–948.

Porteous, D. J., Millar, J. K., Brandon, N. J., and Sawa, A. (2011). DISC1 at 10: connecting psychiatric genetics and neuroscience. *Trends Mol. Med.* 17, 699–706.

Purper-Ouakil, D., Wohl, M., Mouren, M. C., Verpillat, P., Ades, J., and Gorwood, P. (2005). Meta-analysis of family-based association studies between the dopamine transporter gene and attention deficit hyperactivity disorder. *Psychiatr. Genet.* 15, 53–59.

Qi, H. H., Sarkissian, M., Hu, G. Q., Wang, Z., Bhattacharjee, A., Gordon, D. B., et al. (2010). Histone H4K20/H3K9 demethylase PHF8 regulates zebrafish brain and craniofacial development. *Nature* 466, 503–507.

Rihel, J., Prober, D. A., Arvanites, A., Lam, K., Zimmerman, S., Jang, S., et al. (2010). Zebrafish behavioral profiling links drugs to biological targets and rest/wake regulation. *Science* 327, 348–351.

Rommelse, N. N. (2008). Endophenotypes in the genetic research of ADHD over the last decade: have they lived up to their expectations? *Expert Rev. Neurother.* 8, 1425–1429.

Rosenberg, R. E., Daniels, A. M., Law, J. K., Law, P. A., and Kaufmann, W. E. (2009). Trends in autism spectrum disorder diagnoses: 1994–2007. *J. Autism. Dev. Disord.* 39, 1099–1111.

Rubia, K. (2011). "Cool" inferior frontostriatal dysfunction in attention-deficit/hyperactivity disorder versus "hot" ventromedial orbitofrontal-limbic dysfunction in conduct disorder: a review. *Biol. Psychiatry* 69, e69–e87.

Ryu, S., Mahler, J., Acampora, D., Holzschuh, J., Erhardt, S., Omodei, D., et al. (2007). Orthopedia homeodomain protein is essential for diencephalic dopaminergic neuron development. *Curr. Biol.* 17, 873–880.

Sallinen, V., Sundvik, M., Reenila, I., Peitsaro, N., Khrustalyov, D., Anichtchik, O., et al. (2009). Hyperserotonergic phenotype after monoamine oxidase inhibition in larval zebrafish. *J. Neurochem.* 109, 403–415.

Sander, J. D., Cade, L., Khayter, C., Reyon, D., Peterson, R. T., Joung, J. K., et al. (2011). Targeted gene disruption in somatic zebrafish cells using engineered TALENs. *Nat. Biotechnol.* 29, 697–698.

Sarter, M., Hagan, J., and Dudchenko, P. (1992). Behavioral screening for cognition enhancers: from indiscriminate to valid testing: part I. *Psychopharmacology* 107, 144–159.

Schmidt, S., and Petermann, F. (2009). Developmental psychopathology: attention deficit hyperactivity disorder (ADHD). *BMC Psychiatry* 9:58. doi: 10.1186/1471-244X-9-58

Sebat, J. (2007). Major changes in our DNA lead to major changes in our thinking. *Nat. Genet.* 39, S3–S5.

Sebat, J., Levy, D. L., and McCarthy, S. E. (2009). Rare structural variants in schizophrenia: one disorder, multiple mutations; one mutation, multiple disorders. *Trends Genet.* 25, 528–535.

Seibt, K. J., Oliveira Rda, L., Zimmermann, F. F., Capiotti, K. M., Bogo, M. R., Ghisleni, G., et al. (2010). Antipsychotic drugs prevent the motor hyperactivity induced by psychotomimetic MK-801 in zebrafish (*Danio rerio*). *Behav. Brain Res.* 214, 417–422.

Seibt, K. J., Piato, A. L., Da Luz Oliveira, R., Capiotti, K. M., Vianna, M. R., and Bonan, C. D. (2011). Antipsychotic drugs reverse MK-801-induced cognitive and social interaction deficits in zebrafish (*Danio rerio*). *Behav. Brain Res.* 224, 135–139.

Sharp, S. I., McQuillin, A., and Gurling, H. M. (2009). Genetics of attention-deficit hyperactivity disorder (ADHD). *Neuropharmacology* 57, 590–600.

Silva, J. P., Lelianova, V. G., Ermolyuk, Y. S., Vysokov, N., Hitchen, P. G., Berninghausen, O., et al. (2011). Latrophilin 1 and its endogenous ligand Lasso/teneurin-2 form a high-affinity transsynaptic receptor pair with signaling capabilities. *Proc. Natl. Acad. Sci. U.S.A.* 108, 12113–12118.

Singh, K. K., De Rienzo, G., Drane, L., Mao, Y., Flood, Z., Madison, J., et al. (2011). Common DISC1 polymorphisms disrupt Wnt/GSK3beta signaling and brain development. *Neuron* 72, 545–558.

Song, Y., Willer, J. R., Scherer, P. C., Panzer, J. A., Kugath, A., Skordalakes, E., et al. (2010). Neural and synaptic defects in slytherin, a zebrafish model for human congenital disorders of glycosylation. *PLoS ONE* 5:e13743. doi: 10.1371/journal.pone.0013743

Souza, B. R., Romano-Silva, M. A., and Tropepe, V. (2011). Dopamine D2 receptor activity modulates Akt signaling and alters GABAergic neuron development and motor behavior in zebrafish larvae. *J. Neurosci.* 31, 5512–5525.

Sullivan, P. F., Kendler, K. S., and Neale, M. C. (2003). Schizophrenia as a complex trait: evidence from a meta-analysis of twin studies. *Arch. Gen. Psychiatry* 60, 1187–1192.

Svoboda, K. R., Vijayaraghavan, S., and Tanguay, R. L. (2002). Nicotinic receptors mediate changes in spinal motoneuron development and axonal pathfinding in embryonic zebrafish exposed to nicotine. *J. Neurosci.* 22, 10731–10741.

Swanson, J., Castellanos, F. X., Murias, M., LaHoste, G., and Kennedy, J. (1998). Cognitive neuroscience of attention deficit hyperactivity disorder and hyperkinetic disorder. *Curr. Opin. Neurobiol* 8, 263–271.

Sylvain, N. J., Brewster, D. L., and Ali, D. W. (2010). Zebrafish embryos exposed to alcohol undergo abnormal development of motor neurons and muscle fibers. *Neurotoxicol. Teratol.* 32, 472–480.

Sylvain, N. J., Brewster, D. L., and Ali, D. W. (2011). Embryonic ethanol exposure alters synaptic properties at zebrafish neuromuscular junctions. *Neurotoxicol. Teratol.* 33, 313–321.

Tal, T. L., Franzosa, J. A., Tilton, S. C., Philbrick, K. A., Iwaniec, U. T., Turner, R. T., et al. (2012). MicroRNAs control neurobehavioral development and function in zebrafish. *FASEB J.* 26, 1452–1461.

Tarabeux, J., Champagne, N., Brustein, E., Hamdan, F. F., Gauthier, J., Lapointe, M., et al. (2010). De novo truncating mutation in Kinesin 17 associated with schizophrenia. *Biol. Psychiatry* 68, 649–656.

Tay, T. L., Ronneberger, O., Ryu, S., Nitschke, R., and Driever, W. (2011). Comprehensive catecholaminergic projectome analysis reveals single-neuron integration of zebrafish ascending and descending dopaminergic systems. *Nat. Commun.* 2, 171.

Thapar, A., Rice, F., Hay, D., Boivin, J., Langley, K., Van den Bree, M., et al. (2009). Prenatal smoking might not cause attention-deficit/hyperactivity disorder: evidence from a novel design. *Biol. Psychiatry* 66, 722–727.

Thornton, G. K., and Woods, C. G. (2009). Primary microcephaly: do all roads lead to Rome? *Trends Genet.* 25, 501–510.

Toro, R., Konyukh, M., Delorme, R., Leblond, C., Chaste, P., Fauchereau, F., et al. (2010). Key role for gene dosage and synaptic homeostasis in autism spectrum disorders. *Trends Genet.* 26, 363–372.

Tropepe, V., and Sive, H. L. (2003). Can zebrafish be used as a model to study the neurodevelopmental causes of autism? *Genes Brain Behav.* 2, 268–281.

Tsend-Ayush, E., O'Sullivan, L. A., Grutzner, F. S., Onnebo, S. M., Lewis, R. S., Delbridge, M. L., et al. (2005). RBMX gene is essential for brain development in zebrafish. *Dev. Dyn.* 234, 682–688.

Tucker, B., Richards, R. I., and Lardelli, M. (2006). Contribution of mGluR and Fmr1 functional pathways to neurite morphogenesis, craniofacial development and fragile X syndrome. *Hum. Mol. Genet.* 15, 3446–3458.

Valiente, M., and Marin, O. (2010). Neuronal migration mechanisms in development and disease. *Curr. Opin. Neurobiol.* 20, 68–78.

Vandenbergh, D. J., Persico, A. M., Hawkins, A. L., Griffin, C. A., Li, X., Jabs, E. W., et al. (1992). Human dopamine transporter gene (DAT1) maps to chromosome 5p15.3 and displays a VNTR. *Genomics* 14, 1104–1106.

Veleri, S., Bishop, K., Dalle Nogare, D. E., English, M. A., Foskett, T. J., Chitnis, A., et al. (2012). Knockdown of Bardet–Biedl syndrome gene BBS9/PTHB1 leads to cilia defects. *PLoS ONE* 7:e34389. doi: 10.1371/journal.pone.0034389

Veltman, J. A., and Brunner, H. G. (2012). De novo mutations in human genetic disease. *Nat. Rev. Genet.* 13, 565–575.

Verkerk, A. J., Pieretti, M., Sutcliffe, J. S., Fu, Y. H., Kuhl, D. P., Pizzuti, A., et al. (1991). Identification of a gene (FMR-1) containing a CGG repeat coincident with a breakpoint cluster region exhibiting length variation in fragile X syndrome. *Cell* 65, 905–914.

Walitza, S., Renner, T. J., Dempfle, A., Konrad, K., Wewetzer, C., Halbach, A., et al. (2005). Transmission disequilibrium of polymorphic variants in the tryptophan hydroxylase-2 gene in attention-deficit/hyperactivity disorder. *Mol. Psychiatry* 10, 1126–1132.

Wallis, D., Hill, D. S., Mendez, I. A., Abbott, L. C., Finnell, R. H., Wellman, P. J., et al. (2012). Initial characterization of mice null for Lphn3, a gene implicated in ADHD and addiction. *Brain Res.* 1463, 85–92.

Walsh, C. A. (1999). Genetic malformations of the human cerebral cortex. *Neuron* 23, 19–29.

Walsh, C. A., and Engle, E. C. (2010). Allelic diversity in human developmental neurogenetics: insights into biology and disease. *Neuron* 68, 245–253.

Walsh, T., McClellan, J. M., McCarthy, S. E., Addington, A. M., Pierce, S. B., Cooper, G. M., et al. (2008). Rare structural variants disrupt multiple genes in neurodevelopmental pathways in schizophrenia. *Science* 320, 539–543.

Weinberger, D. R. (1995). From neuropathology to neurodevelopment. *Lancet* 346, 552–557.

West-Eberhard, M. J. (2005). Developmental plasticity and the origin of species differences. *Proc. Natl. Acad. Sci. U.S.A.* 102(Suppl. 1), 6543–6549.

Williams, N. M., Zaharieva, I., Martin, A., Langley, K., Mantripragada, K., Fossdal, R., et al. (2010). Rare chromosomal deletions and duplications in attention-deficit hyperactivity disorder: a genome-wide analysis. *Lancet* 376, 1401–1408.

Wood, A. C., Rijsdijk, F., Asherson, P., and Kuntsi, J. (2009). Hyperactive-impulsive symptom scores and oppositional behaviours reflect alternate manifestations of a single liability. *Behav. Genet.* 39, 447–460.

World Health Organisation (WHO). (2008). *The Global Burden of Disease. 2004 Update*. Geneva: WHO.

Xu, B., Roos, J. L., Levy, S., Van Rensburg, E. J., Gogos, J. A., and Karayiorgou, M. (2008). Strong association of de novo copy number mutations with sporadic schizophrenia. *Nat. Genet.* 40, 880–885.

Yoshida, T., and Mishina, M. (2008). Zebrafish orthologue of mental retardation protein IL1RAPL1 regulates presynaptic differentiation. *Mol. Cell. Neurosci.* 39, 218–228.

Zhang, F., Wang, L. P., Brauner, M., Liewald, J. F., Kay, K., Watzke, N., et al. (2007). Multimodal fast optical interrogation of neural circuitry. *Nature* 446, 633–639.

Zweier, C., De Jong, E. K., Zweier, M., Orrico, A., Ousager, L. B., Collins, A. L., et al. (2009). CNTNAP2 and NRXN1 are mutated in autosomal-recessive Pitt–Hopkins-like mental retardation and determine the level of a common synaptic protein in *Drosophila*. *Am. J. Hum. Genet.* 85, 655–666.

Conflict of Interest Statement: The author declares that the research was conducted in the absence of any commercial or financial relationships that could be construed as a potential conflict of interest.

Received: 24 January 2013; accepted: 09 April 2013; published online: 26 April 2013.

Citation: Norton WHJ (2013) Toward developmental models of psychiatric disorders in zebrafish. Front. Neural Circuits 7:79. doi: 10.3389/fncir.2013.00079

frontiers in
NEURAL CIRCUITS

REVIEW ARTICLE
published: 08 April 2013
doi: 10.3389/fncir.2013.00063

The role of zebrafish (*Danio rerio*) in dissecting the genetics and neural circuits of executive function

Matthew O. Parker, Alistair J. Brock, Robert T. Walton and Caroline H. Brennan*

School of Biological and Chemical Sciences, Queen Mary University of London, London, UK

Edited by:
Gonzalo G. De Polavieja, Instituto Cajal - Consejo Superior de Investigaciones Científicas, Spain

Reviewed by:
David Parker, Cambridge University, UK
Akira Muto, National Institute of Genetics, Japan

***Correspondence:**
Caroline H. Brennan, School of Biological and Chemical Sciences, Queen Mary University of London, Mile End, London E1 4NS, UK.
e-mail: c.h.brennan@qmul.ac.uk

Zebrafish have great potential to contribute to our understanding of behavioral genetics and thus to contribute to our understanding of the etiology of psychiatric disease. However, progress is dependent upon the rate at which behavioral assays addressing complex behavioral phenotypes are designed, reported and validated. Here we critically review existing behavioral assays with particular focus on the use of adult zebrafish to explore executive processes and phenotypes associated with human psychiatric disease. We outline the case for using zebrafish as models to study impulse control and attention, discussing the validity of applying extant rodent assays to zebrafish and evidence for the conservation of relevant neural circuits.

Keywords: zebrafish, attention, impulsivity, behavioral flexibility, psychiatric disorder, neural circuits

INTRODUCTION

Gaining a better understanding of the etiology and pathogenesis of psychiatric disease is currently a priority area of research (Campbell, 2010). Advances in human neuroimaging and genetics are giving insight into the cellular regions and processes involved. However, partly because studies in humans must deal with genetic, diagnostic and etiological heterogeneity as well as environmental (cultural, societal) factors, and it is not possible to undertake molecular studies *in vivo*, progress remains slow (Burmeister et al., 2008). In order to address some of these concerns animal, primarily rodent, models targeting symptoms consistent with DSM-IV (APA, 2000) diagnoses of psychiatric disorder have been developed (Gould and Gottesman, 2006). Recently, with the establishment of zebrafish as a developmental genetic model with unparalleled utility for neural imaging, the potential of this genetically tractable vertebrate as a model in behavioral neuroscience has started to be realized (Levin and Cerutti, 2009; Norton and Bally-Cuif, 2010; Levin, 2011; Gerlai, 2012; Parker and Brennan, 2012).

In this paper, we review the current position with regards to the development and validation of zebrafish behavioral assays pertinent to human psychiatric disorder. We present an overview of neural pathways underlying key behaviors in rodents and the evidence for their conservation in fish. Finally we discuss prospects for the future: in particular, ways in which zebrafish can contribute to our understanding of cellular and molecular processes underlying psychiatric disease. Despite the numerous benefits of larval models and the progress that has been made in recent years (see Ahmad et al., 2012 for recent review), the utility of larvae to measure some of the subtle endophenotypes pertinent to vulnerability to psychiatric disorders may be limited. For example, although analysis of unconditioned or reflexive behaviors is clearly possible, it is unlikely that studying endophenotypes relative to cognitive or executive processes would be suitable owing to the immaturity of the larval neural systems. Thus here, we focus on adult behavioral phenotypes.

THE BENEFITS OF DEVELOPING ZEBRAFISH MODELS OF BEHAVIORAL PHENOTYPES ASSOCIATED WITH PSYCHIATRIC DISEASE

There are a great many practical benefits of using zebrafish as a model organism, e.g., their small size and low housing costs, their transparent, rapidly developing, ex-utero embryos, and their unsurpassed genetic tractability. However, in the age of technological advances in *in vivo* methodologies, such as optogenetics, enabling modulation of cell physiology and activity at the single cell level, their utility may soon be even greater. In this section, we discuss the potential for using zebrafish for behavioral assays pertinent to psychiatric disease.

There are inherent difficulties in comparing behaviors observed in non-primate species – particularly those associated with psychiatric disease – with those seen in humans (Brown and Bowman, 2002). One key issue is the lack of an expanded telencephalon and prefrontal cortex (PFC), the primary areas controlling executive functions commonly disrupted in psychiatric disease. There did exist a central dogma in neuroscience that cognitive processes have evolved in concert with the expansion of the telencephalon and lamination of the cortex, and therefore, animals without this expansion cannot perform these behaviors. However, there is now increasing evidence that smaller-brained vertebrates, which lack expanded telencephali, are capable of cognitive processing and even complex decision-making. For example, non-mammalian brains that do not have a laminar structure, such as nucleated bird brains, (a) show complex cognition, (b) have similar neural and neurochemical systems (especially dopamine(DA) and (c) display executive functions like mammals which are controlled by homologous brain structures (nidopallium instead of PFC; Jarvis et al., 2005). Thus it seems that several species may have faced

niche-specific selection pressures leading to evolution of comparable executive processes. This suggestion raises two questions regarding the use of zebrafish to explore molecular and cellular processes contributing to psychiatric disease: first, *do* fish show comparable behaviors? Second, if fish *can* perform executive tasks, have different regions or systems within their brains evolved to perform the tasks; or alternatively, have simple circuits (present in rudimentary form in common ancestors) evolved, albeit with topographical differences and different degrees of sophistication, to perform the same tasks, i.e., are the behavioral processes analogous or homologous? If the behaviors in fish, birds, and mammals share neurochemical pathways and show similar connectivity, it would suggest a common root and that the processes are homologous. In this event studies in fish, that do not model primate PFC executive function *per se,* can allow the extrapolation of common cell:cell interactions and physiological processes to give insight into molecules involved (in the human condition) despite differences in topography.

As the zebrafish is a uniquely tractable vertebrate genetic model species, assays of endophenotypes associated with psychiatric disease have been established and work to determine the neural pathways involved is underway. However, in the light of differences in structures, and possible differences in connectivity, there is a need for careful validation of the behavioral assays in zebrafish to establish their relevance to the human condition.

A good model of a human disease phenotype needs to demonstrate face-validity (the model *looks like* it is measuring the disease in question), construct validity (whether it *actually measures* what it claims to measure) and predictive power (Gould and Gottesman, 2006). As rodent models fulfill these criteria in many cases, zebrafish researchers have modified extant rodent assays, taking into account the specific behavioral system of the species. An example of this would be the novel tank test (Levin et al., 2007; Parker et al., 2012c). The novel tank test is an adaptation of the rodent open-field test of anxiety, developed with high face validity as it was designed with the zebrafish's natural tendency to dive to the bottom of a new environment in mind. Construct validity has been demonstrated using anxiolytic drugs; buspirone; and diazepam reduce the amount of time spent in the bottom of the tank in a dose-dependent manner (Bencan et al., 2009). For other behaviors, rapid progress is being made and in many instances construct validity has been similarly established by the use of pharmacological manipulation and genetic loss-of-function lines. In this section, we will briefly describe some assays used in rodent models of psychiatric disease, and how these have been adapted for, and validated in, zebrafish. Although a number of different behavioral phenotypes can be linked to psychiatric disease, such as anxiety, in this review we will concentrate on disorders relating to executive functioning rather than affective state, which has been reviewed extensively elsewhere (e.g., see Maximino et al., 2010).

BEHAVIORAL FLEXIBILITY

Deficits in cognitive or behavioral flexibility are commonly reported in patients with a variety of psychiatric diagnoses, such as somatoform disorders (anorexia nervosa, bulimia nervosa: Button et al., 2007; Cardona et al., 2011), bipolar disorder (Balleine and Dickinson, 1998), schizophrenia (Fernandez-Ruiz et al., 2001), substance abuse disorders (Collins et al., 2011) and obsessive compulsive disorder (OCD; Brembs, 2009). Behavioral flexibility is operationally defined as the ability to shift or adapt response strategy in the face of changing environmental contingencies (Ragozzino et al., 1999).

In animal models, behavioral flexibility may be measured by serial reversal of contingencies in two-choice discriminations, or by intra- and extra-dimensional (ED) set-shift tasks (see **Figure 1**; Ragozzino et al., 1999). Convergence of evidence from pharmacological (Saus et al., 2010), lesion (Hoopes, 1999) and genetic knockout (White et al., 2008) studies suggest a high degree of construct validity when compared with human task performance on tests of behavioral flexibility. Typically, the assay involves the

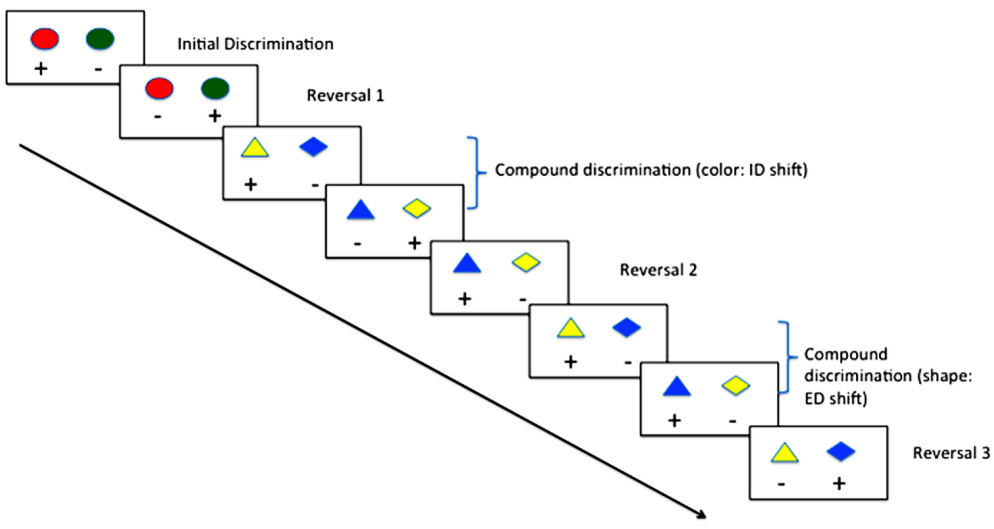

FIGURE 1 | Typical procedure for reversal learning with intra- (ID) and extra-dimensional (ED) set shifting using color and shape.

animal being trained to discriminate two stimuli (e.g., blue vs. green light), where in the first instance responses to the blue light are reinforced, and those to the green non-reinforced. Once the animal reaches a set criterion, the contingency is reversed, such that responses to the green light are now reinforced, and responses to the blue light non-reinforced. Subsequently, the colors can be changed (intra-dimensional [ID] shift) and reversed, or a third dimension can be introduced (e.g., shape; ED shift) and subsequently reversed. Many studies have demonstrated that rodents (Hoopes, 1999), primates (Doyle et al., 2006) and birds (Wilens et al., 2005) show a gradual improvement in their trials-to-criteria in this context.

Zebrafish are capable of reversal learning (Colwill et al., 2005), and recently they have been shown to follow a similar pattern of improvement over multiple reversals and ID shift as mammals. Parker et al. (2012a) trained adult zebrafish first on a simple color discrimination, once the fish had reached criterion (6 consecutive correct trials for 2 consecutive training sessions) the contingencies were reversed. Once the fish had reached criterion on the reversal condition, they were subjected to an ID shift, and subsequently contingency reversal. As has been shown in mammals, trials-to-criterion reduced during the course of the four training phases suggesting that the fish had formed an attentional-set, and could demonstrate flexibility in their learning with a changing environment. These findings were of particular interest, as they were the first to suggest that zebrafish were capable of behavioral flexibility in this context, complementing previous work in other fish species (e.g., goldfish; Woodward et al., 1971). Other, more ethological approaches to studying behavioral flexibility have also been used. Oliveira (2009), for example, observed that zebrafish adapt their social behavior dependent on outcomes of conflicts between conspecifics. These data raise the possibility of examining the cellular and molecular processes governing the operation of neural circuits involved in behavioral flexibility using zebrafish.

ATTENTION

Attention can be described as *selective*, operationally defined as the ability to pick a target from an array of distracters (Desimone and Duncan, 1995), or *sustained*, operationally defined as the ability to detect the presence of a stimulus presented at various intervals over a prolonged period (Sarter et al., 2001). Deficits in sustained and selective attention are common features of a number of psychiatric disorders such as attention-deficit hyperactivity disorder (ADHD; Barkley, 1997), schizophrenia (Meshorer and Soreq, 2006), OCD (Kume et al., 2005), and substance abuse disorders (Tsutsui-Kimura et al., 2010). Both selective and sustained attention can be measured in a number of ways using animal models, and again, construct validity has been established using pharmacological, lesion and genetic models.

In a widely used assay of selective attention (see **Figure 2**), an animal is initially trained to respond when a target cue is present. The target cue can then be presented among an array of distracter stimuli, and depending on the number of shared features with the target, the animal will either use serial search (i.e., scan every item in the array in order to locate the target) or parallel search (the entire scene is processed in parallel, and the target stimulus appears to "pop-out" of the array; Treisman and Gelade, 1980).

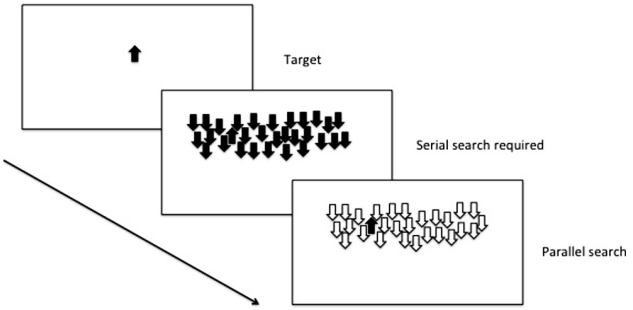

FIGURE 2 | Selective attention: parallel and serial search mechanisms are both used depending on the number of shared features with the distracters.

Selective attention can be inferred in zebrafish from their performance forming attentional sets in the reversal learning and ID-shift procedure described earlier (Parker et al., 2012a), but there is also promise to develop assays to examine more complex tasks examining serial and parallel processing in visual discrimination tasks. Zebrafish are effective at discriminating two stimuli in a variety of different conditions, under control of both aversive and appetitive contingencies (Levin and Chen, 2004; Colwill et al., 2005). In addition, further work that requires explicitly either top-down or bottom-up processing (Proulx and Serences, 2006) will provide an opportunity to explore the use of these attentional mechanisms in the zebrafish model.

Sustained attention can be assayed in humans using a continuous performance task (CPT; Rosvold et al., 1956). In animals, a variety of tests have been used (e.g., stop-signal task (Logan et al., 1997); go no-go task (Finn et al., 1999), but arguably the most useful has been the 5-choice serial reaction time task (5-CSRTT; Carli et al., 1983; Robbins, 2002), owing to the rich variety of parameters measurable in this assay. The 5-CSRTT (see **Figure 3**) tests the ability of animals to detect the presence of a briefly presented stimulus in one of five randomly ordered spatial locations following an inter-trial interval (ITI). Responses in the correct location during a limited time following the stimulus presentation (limited hold; LH) are conditionally reinforced with illumination of the magazine light, and subsequently food reinforcement, at the opposite end of the apparatus. Incorrect responses (errors of commission), anticipatory/premature responses during the ITI or failure to respond during the LH (errors of omission) are punished with a brief time-out. Subsequent trials are initiated with a nose-poke in the magazine. The 5-CSRTT can also be used to measure selective attention, as auditory or visual distracters can be added to the test environment during training or test sessions (Bari et al., 2008).

Sustained attention has been successfully demonstrated in zebrafish in two tasks (**Figure 4**). Initially, Bilotta et al. (2005) designed a task whereby fish were required to swim into one of three apertures. A light was illuminated in one of the chambers (see **Figure 4A**), and the barrier was lifted to allow the fish access to the choice area. The fish was reinforced for swimming into the

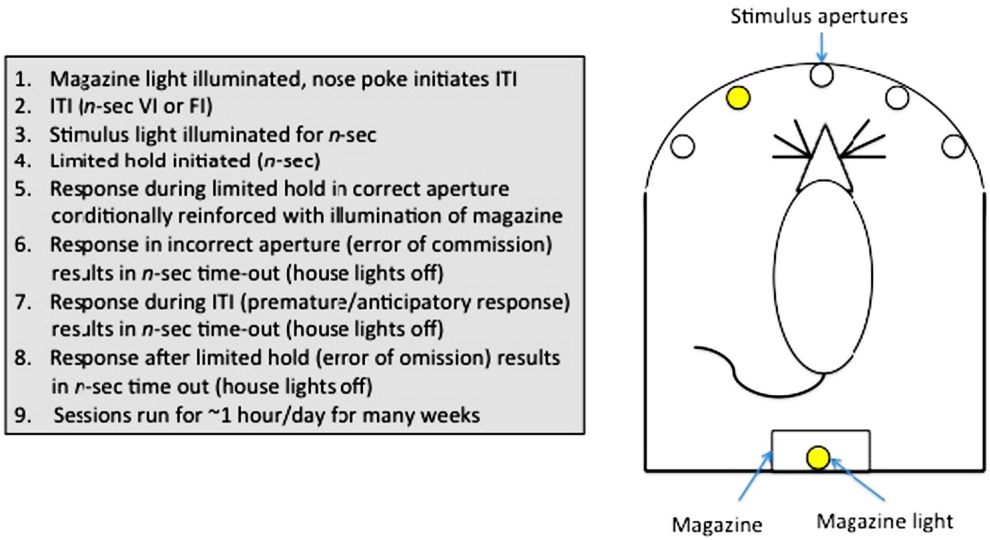

FIGURE 3 | Measurement of sustained attention and impulse control in rodents: The 5-choice serial reaction time task.

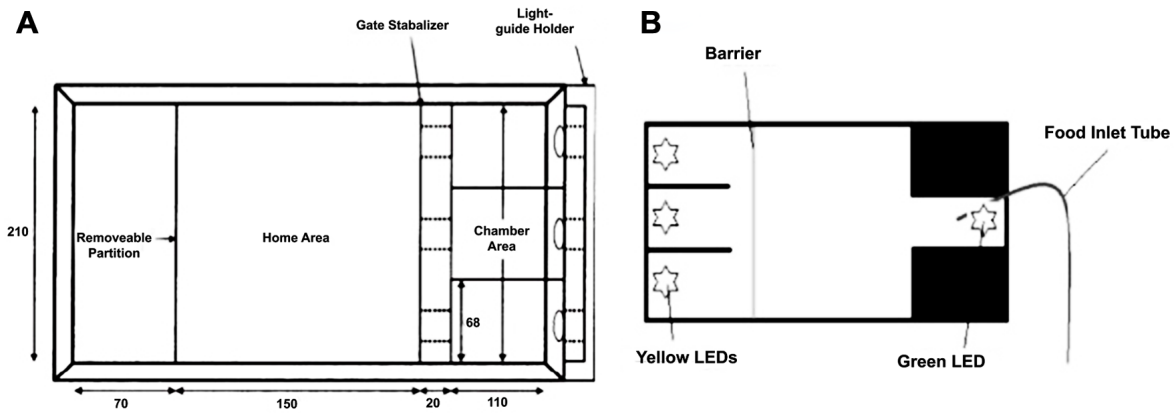

FIGURE 4 | Two different environments for assaying three-choice discriminations in zebrafish to measure sustained visual attention. (A) adapted from Bilotta et al. (2005); **(B)** adapted from Parker et al. (2012b).

correct chamber. Incorrect choices were punished by confining the fish to the incorrect chamber for 30-sec with no food. Fish were found to perform well on this task, quickly reaching 80% correct choices with repeated testing.

Another version of the task increased the complexity by: (1) requiring the zebrafish to maintain attention of the three stimulus apertures prior to making a response, and (2) by requiring the fish to return to the opposite end of the tank to receive their reinforcer (**Figure 5B**; Parker et al., 2012b). Both tasks have the ability to examine aspects of sustained attention, such as increasing attentional load by varying the duration or intensity of the stimuli, and hold great promise in terms of assessing attentional processes in zebrafish. In addition, it will be possible to adapt either of these tasks to include visual or auditory distracters to attempt to produce a parametric assessment of selective attention in zebrafish.

IMPULSE CONTROL

Impulsive behaviors can be broadly divided into two categories: those resulting from deficits in the ability to withhold responding (impulsive action) and those that result from deficits in decision-making (impulsive choice). Impulsive action can be operationally defined in terms of anticipatory responding on assays such as the 5-CSRTT (Robbins, 2002), the go/no-go task (Finn et al., 1999), or the stop-signal reaction time task (Logan et al., 1997); impulsive choice is exemplified by the choice of a small, immediate reward over a delayed, more substantial reward (delay-discounting; Winstanley et al., 2006; Dalley et al., 2008; Diergaarde et al., 2008). Both categories of impulsive behavior are reported in a number of psychiatric conditions such as ADHD (Barkley, 1997), substance abuse disorder (Belin et al., 2008), pathological gambling (Alessi and Petry, 2003), schizophrenia (Winstanley et al., 2003) and OCD (Brembs, 2009). Animal (e.g., rodent) models of impulse control

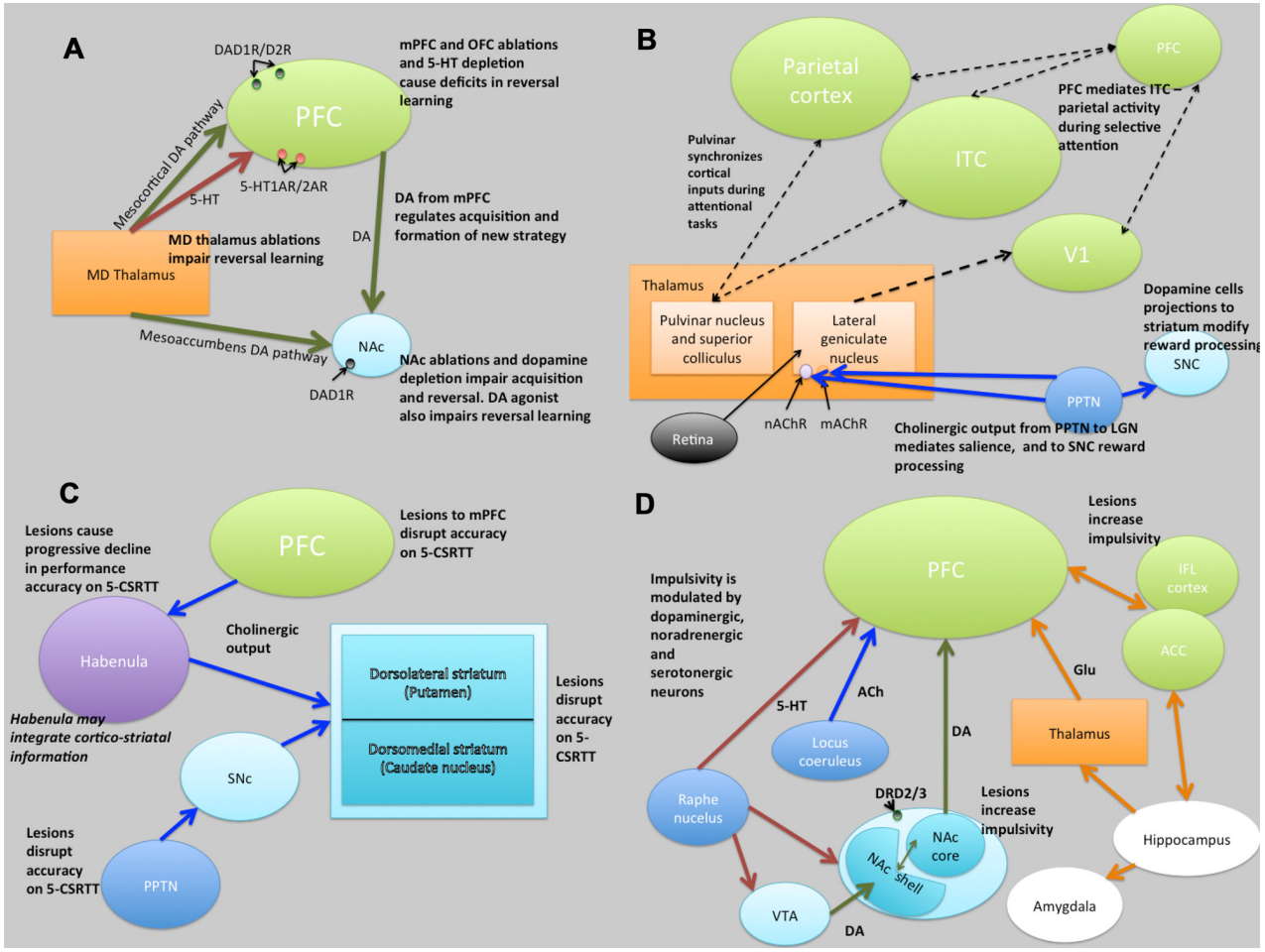

FIGURE 5 | Schematic illustrations of putative neural circuits of behavioral flexibility (A), selective attention (B), sustained attention (C), and impulse control (D). For detailed explanations see text. PFC, prefrontal cortices; MD Thalamus, medial dorsal thalamus; NAc, nucleus accumbens; DA, dopamine; 5-HT, 5-hydroxytryptamine (serotonin); ITC, infero-temporal cortex; V1, primary visual cortex (striate cortex); PPTN, pedunculopontine tegmental nucleus; SNc, substantia nigra pars compacta; nAChR, nicotinic acetylcholine receptor; mAChR, muscarinic acetylcholine receptor; LGN, lateral geniculate nucleus; PN, pulvinar nucleus; SC, superior colliculus; 5-CSRTT, 5-choice serial reaction time task; Ach, acetylcholine VTA, ventral tegmental area; ACC, anterior cingulate cortex; IFL cortex, infralimbic cortex; Glu, glutamate. Key: green lines, dopamine; orange lines, gluatamate; blue lines, acetylcholine; red lines, 5-HT; black dashed lines, multiple neurotransmitter pathways. Light green structures, cortical regions; orange structures, thalamic regions; light blue, basal ganglia/striatal (ventral and dorsal structures) regions; dark blue, brainstem structures; white, limbic structures; purple, other.

have been shown to have a good degree of construct validity, again using a combination of pharmacological, lesion and knockout studies.

Our lab has recently reported data pertaining to the performance of zebrafish in a three-choice version of the 5-CSRTT. Our version of the task is different from the rodent version, in that: 1) we use longer stimulus intervals (rodents = ~0.5-sec, fish = 5–10-sec), 2) we initiate the start of each trial by lifting the barrier to expose the stimulus apertures, while in rodents trials are initiated by nose-poking the magazine. Using this procedure, we demonstrated not only that zebrafish show similar rates of basal anticipatory responding on the task as rodents, but also that a low dose (0.025 mg/Kg i.p.) of amphetamine significantly reduced anticipatory responding during long ITI probe trials (low doses of psychostimulants reduce impulsivity in other animal models, and in humans; Robbins, 2002) whereas a saline injection had no effect (Parker et al., 2012b). In order to validate the procedure as a measure of impulse control, these findings need to be replicated with further pharmacological manipulations, and potentially with existing mutant lines. These preliminary findings are very encouraging, however, and we are in the process of automating the procedure to facilitate validation studies and future screening programs. Measures of impulsive choice, as measured in rodents by delayed reinforcement procedures, are currently lacking in zebrafish.

NEURAL CIRCUITS MEDIATING BEHAVIORAL PHENOTYPES

In this section we outline what is currently known about the neural circuits that underlie the behaviors described above and their conservation in zebrafish.

BEHAVIORAL FLEXIBILITY

Evidence from lesion studies suggests that regions of the PFC (medial pre-frontal cortex [mPFC]; orbitofrontal cortex [OFC]; lateral PFC), striatum (specifically the nucleus accumbens [NAc] and the dorsal-medial striatum [DMS]) and thalamic nuclei are involved with various aspects of behavioral flexibility (Ragozzino et al., 1999; Brown and Bowman, 2002; Ragozzino, 2007). Collectively, these data have suggested that reversal learning in mammals is mediated by cortical- striatal-thalamo-cortical loops (**Figure 5**). There is also much evidence to suggest that reversal learning is modulated by both DA and serotonin (5-HT). For example, impairments of reversal learning can be induced by DA depletion in the NAc (6-OHDA lesions of NAc: Taghzouti et al., 1985), by inhibition of DA reuptake with amphetamine (Ridley et al., 1981) or by 5-HT depletion in the PFC (Clarke et al., 2004). **Figure 5A** summarizes the putative circuits of behavioral flexibility in mammalian systems.

The topography of the zebrafish brain differs from the mammalian brain, but homologues for the different brain regions have been identified. For example, both the mammalian and the zebrafish thalamic nuclei are located in the diencephalon (**Figure 6**), and homologues of midbrain regions such as the VTA (posterior tuberal nucleus; PTN) and NAc (ventral [Vv] and dorsal [Vd] telencephalic nuclei; Rink and Wullimann, 2002; Panula et al., 2010) have been determined. Recently, Mueller et al. (2011) have also identified the central region of the dorsal pallium (area Dc in **Figure 6**) as a potential homologue of the isocortex, that in mammals encompasses the above-mentioned cortical regions. There are a number of neurochemical pathways relevant to behavioral flexibility that have a good degree of homology. For example, the ascending midbrain DA pathways have been well characterized using tyrosine hydroxylase (TH) immunohistochemistry (Rink and Wullimann, 2001, 2002; Filippi et al., 2010), with a number of putative functional homologues being identified owing to their neuronal connections and projections (**Figure 6**). Much of the evidence pertaining to the cholinergic, DAergic and 5-HTergic neural clusters in the zebrafish brain has been generated from extensive immuno-staining of relevant cell bodies. There is little evidence of how the systems functionally interact, and no direct evidence for a homologous circuit for the cortico-striatal-thalamo-cortical loops. Specifically, whether or not the neural clusters are reciprocally connected remains to be seen.

SELECTIVE ATTENTION

Figure 5B summarizes the putative neural circuits of selective attention in mammalian systems. The cholinergic system plays a central role in selective attention (Robbins, 1997). Cholinergic neurons project widely to such basal forebrain structures as the habenula (Claudio Cuello et al., 1978) and the striatum (Woolf and Butcher, 1986), releasing ACh at various synaptic terminals across all layers of the cortex via activation of cholinergic receptor sub-types (Sarter and Bruno, 1997). ACh binds to two distinct categories of cholinergic receptors: G-protein coupled metabotropic muscarinic receptors (mAChR) and ligand-gated ionotrophic nicotinic receptors (nAChR), both of which are implicated in attention (Noudoost and Moore, 2011). In addition, the pedunculopontine tegmental nucleus (PPTN) may play a dual role in selective attention pertaining to the processing of saliency and reward-cues. Specifically, cholinergic outputs from the PPTN synapsing on lateral geniculate nucleus (LGN) cells expressing nAChRs and mAChRs regulate saliency, and those synapsing on substantia nigra pars compacta (SNc) DAergic cells regulate reward processing (Kobayashi and Isa, 2002).

The role of the DA system in attention is also well established (Nieoullon, 2002). For example, people with Parkinson's disease (characterized by a loss of nigrostriatal DA neurons; Owen et al., 1993) and ADHD (characterized by reductions in PFC DA; Barkley, 1997) both show deficits in selective attention, as do people with schizophrenia (characterized by increases in D2-like receptors in the striatum; Seeman et al., 1993). Although not universally accepted, there is some evidence that ACh modulation may relate more to aspects of saliency (Asadollahi et al., 2010; Knudsen, 2011), and DA more to motivated search. As such, it may be that the roles of ACh and DA are, respectively, related to bottom-up and top-down processing in a dissociated, or at least partially dissociated manner (Noudoost and Moore, 2011).

In terms of homologous brain regions involved in cholinergic signalling, the cortical regions thought to be involved with selective attention are relatively well conserved in zebrafish, although the topography is, again, somewhat different (**Figure 6**). Thus, the cholinergic projections from the PPTN to the brainstem, habenula and thalamic (e.g., LGN) regions in rodents are mirrored by projections from the superior reticular nucleus (SRN) to the brainstem, habenula and subpallium in fish. As discussed above, the neurotransmitter systems thought to modulate selective attention (DA, ACh) are well conserved in zebrafish (see **Figure 6**). For example, the mAChRs and nAChRs have been identified in zebrafish and their binding characteristics and expression patterns described (Zirger et al., 2003). Similarly, the DA system has been characterized and the homologues of key components of the reward pathway identified as discussed above (Filippi et al., 2010). In the light of this, neuromodulatory influences may be conserved between the species.

SUSTAINED ATTENTION

The frontal cortices (frontal executive system) are thought to mediate sustained attention (Barkley, 1997). Indeed, some theories of ADHD (which is characterized, in part, by difficulties in sustained attention) suggest that the symptoms may be caused by delayed cortical maturation (Loo and Barkley, 2005). Although the circuits underlying sustained attention are less clearly defined, lesions studies have indicated brain regions involved (see **Figure 5C**). Notably, the PPTN has outputs via the SNc to striatum and to PFC suggesting a role of the nigrostriatal DA pathway in some aspects of sustained attention, perhaps relating to motor control during tasks requiring sustained attention. In addition to the frontal cortices, the striatum appears to be crucially linked to aspects of sustained attention (Barkley, 1997).

The cholinergic system, including cholinergic neuronal projections and cholinergic receptors (mAChR and nAChR), plays a crucial role in sustained attention. Cortical ACh is released during tasks requiring sustained attention (Arnold et al., 2002), and as the task increases in difficulty, the release of ACh increases (Himmelheber et al., 2000). The DAergic system has also been

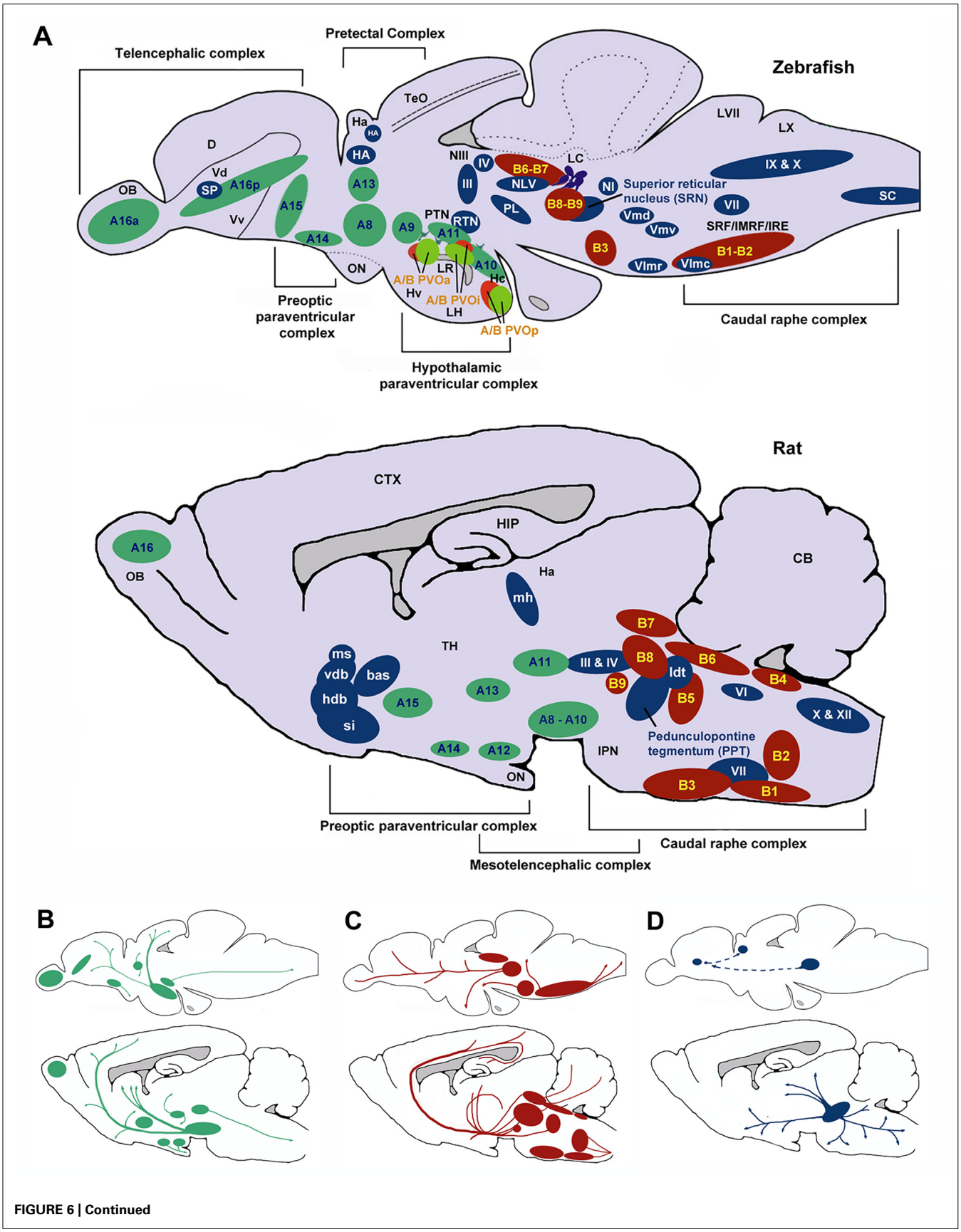

FIGURE 6 | Continued

FIGURE 6 | Continued
Schematic sagittal view comparing dopaminergic (green), serotonergic (red), and cholinergic (blue) neuronal populations in zebrafish (upper) and rat (lower) brains. Nomenclature for serotonergic and dopaminergic populations were based on their rostrocaudal distribution in the adult rat and zebrafish brain previously described (Schweitzer and Driever, 2009; Panula et al., 2010) allowing comparison between cell body distribution in adult brains. **(A)** Cell body distribution (adapted from Manger et al., 2002; Butcher and Woolf, 2003; Mueller et al., 2004; Schweitzer and Driever, 2009; Panula et al., 2010). Corresponding **(A,B)** nomenclature for dopaminergic and Serotonergic cell bodies derived from Panula et al. (2010) and Schweitzer and Driever (2009). Dopaminergic populations (zebrafish): A8: parvocellular preoptic nucleus, posterior part (PPp); A9: periventricular nucleus of posterior tuberculum (TPp); A10: periventricular hypothalamus and posterior tuberculum (PTN); A11: posterior tuberculum (PTN); A13: anterior, intermediate, ventrolateral, and ventromedial thalami nuclei (A, I, VM, and VL); A14: parvocellular preoptic nucleus, anterior part (PPa); A15: parvocellular preoptic nucleus, anterior part (PPa); A16p: ventral telencephalic nuclei (Vv, Vd and Vs); A16a: olfactory bulb (Ob). Dopaminergic populations (rat): A8: midbrain reticular formation (MRF); A9: ventrolateral midbrain (VLM); A10: ventral midbrain tegmentum (VTAe); A11: posterior periventricular nucleus and intermediate periventricular nucleus (PVNP and PVNI); A12: hypothalamic arcuate nucleus (ARH); A13: mammillothalamic tract (MTT); A14: anteroventral periventricular nucleus (AVPV); A15: Anteroventral periventricular nucleus (AVPV); A16: olfactory bulb (OB). Serotonergic populations (zebrafish): B1-B2: caudal raphe complex; B3-B9: rostral raphe complex; BPVOa: paraventricularorgan, anterior part (PVOa); BPVOi: paraventricular organ, intermediate part (PVOi); BPVOp paraventricularorgan posterior part (PVOp). Serotonergic populations (Rodent): B1: raphe pallidus (RPa); B2: raphe obscurus (NRO); B3: raphe magnus (NRM); B4: vestibular nucleus (VN); B5: pontine raphe nucleus (PRN); B6: medial longitudinal fasciculus (MLF); B7: dorsal raphe nucleus (DRN); B8: median raphe nucleus (MRN); B9: median raphe nucleus (MRN). Cholinergic populations (zebrafish): IX: glossopharyngeal nerve motor nucleus; X: vagal nerve motor nucleus; SC: spinal cord motoneurons; NI: nucleus isthmi; HA: Habenula; NLV: nucleus lateralis valvulae; III: oculomotor nerve nucleus; IV: trochlear nerve motor nucleus; RTN: rostral tegmental nucleus; PL: perimeniscal nucleus; Vmd: dorsal trigeminal nerve motor nucleus; Vmv: ventral trigeminal nerve motor nucleus; VII: facial nerve motor nucleus; VImr: rostral abducens nerve motor nucleus; VImc: caudal abducens nerve motor nucleus. Cholinergic populations (rat): ldt: lateral dorsal tegmental nucleus; si: substantia innominate; hdb: horizontal diagonal band nucleus; vdb: vertical diagonal band nucleus; bas: nucleus basalis; ms: medial septal nucleus (MS); md: medial habenula (MH); III: oculomotor nucleus (IIIn); IV: trochlear nucleus (IVn); VII: facial nucleus (VIIn); X: dorsal motor vagus nucleus (Xn); XII: hypoglossal nucleus (Xn). SP: Subpalium (Sp). **(B)** Schematic drawing illustrating the location of dopaminergic projections in adult zebrafish and rat brains (sagittal view; adapted from Schweitzer and Driever, 2009). **(C)** Schematic drawing illustrating the location of serotoninergic projections in adult zebrafish (adapted from Gaspar and Lillesaar, 2012) and rat brains (adapted from Di Giovanni et al., 2008; sagittal view). **(D)** Schematic drawing illustrating the location of cholinergic neuron projections from PPT in adult rats (adapted from (Manger et al., 2002)) and predicted projections from zebrafish SRN to subpallium and habenula. D, dorsal telencephalic area; Dc, caudal dorsal telencephalic area; CTX, cerebral cortex CB, cerebellum; Ha, habenula; Hc, caudal zone of periventricular hypothalamus; HIP, hippocampus; Hv, ventral zone of periventricular hypothalamus; IMRF, intermediate reticular formation; IPN, interpeduncular nucleus; IRF, inferior reticular formation; LC, locus coeruleus; LH, lateral hypothalamic nucleus; LR, lateral recesses of the diencephalic ventricle; LVII, facial lobe; LX, vagal lobe; NIII, oculomotor nucleus; OB, olfactory bulb; ON, optic nerve; OBN, olfactory bulboptic nerve; PTN, posterior tuberculum; PVO, paraventricular organ, anterior part; PVOi, paraventricular organ, intermediate part; BPVOp, paraventricular organ posterior part; SRF, superior reticular formation; Vd, dorsal telencephalic area; Vv, ventral telencephalic area; TeO, optic tectum; TH, thamalus.

strongly linked to sustained attention, in particular relating to the dissociable roles of D1 and D2 receptors in the mPFC. **Figure 5C** summarizes the putative neural circuits of sustained attention.

As mentioned above, homologous regions exist and the midbrain DAergic system has been well characterized in zebrafish. In addition to this, the cholinergic system in zebrafish has been characterized with choline acetyltransferase (ChAT) immunohistochemistry (Mueller et al., 2004; **Figure 6**). Cholinergic cell bodies are found in the caudal raphe complex of both mammals and zebrafish (**Figure 6**). Of particular note here, zebrafish have an ascending SRN cholinergic system which is a putative homologue for the mammalian PPTN, lesions of which are known to impair sustained attention in rats (Kozak et al., 2005).

IMPULSE CONTROL

Impulse control and motivational circuits are inextricably linked. Motivational circuits have been extensively characterized (Dalley et al., 2008; **Figure 5D**). As is the case with behavioral flexibility, lesions to the medial dorsal, but not anterior, thalamic nucleus, cause increases in premature responding (Chudasama and Muir, 2001). The data strongly suggest that impulsivity, at least that form of impulsivity measured by the 5-CSRTT, is mediated by DAergic and 5-HTergic cortico-striatal-thalamo-cortical loops (Robbins, 2002). Clearly this suggests a role for catecholaminergic systems in impulsivity, and indeed high doses of systemic amphetamine administration increases premature responding, an effect that is reversed by 6-OHDA lesions of the NAc (Cole and Robbins, 1989). In addition, systemic atomoxetine, a noradrenergic reuptake inhibitor, reduces impulsivity (Robinson et al., 2008). Finally, rats characterized as "high-impulsive" on the 5-CSRTT have reduced DA D2/3 receptors in the NAc (Dalley et al., 2007). **Figure 5D** summarizes the putative circuits of impulse control in mammalian systems.

The neural circuits currently hypothesized to modulate impulse control (e.g., ascending midbrain DA pathways and raphe complex 5-HT pathways; **Figure 6B**) are present in zebrafish, or at least, putative functional homologues exist (**Figure 6**). For example, the caudal raphe complex is well conserved between species, as are the 5-HT projections from this region to prefrontal regions in rats and dorsal pallial regions in the zebrafish. In addition, homologues for the VTA (PTN), NAc (Vv and Vd; Rink and Wullimann, 2002; Panula et al., 2010) and area Dc (Mueller et al., 2011) have been identified and DA projections in these regions are similar. In the zebrafish brain DAergic and 5-HTergic projections from the pallium to the thalamic nuclei, in addition to DAergic projections from the telencephalic nuclei to the pallium (see **Figure 6**), suggest similar patterns of connectivity to mammalian brains.

FUTURE PROSPECTS: HOW CAN ZEBRAFISH CONTRIBUTE TO THE UNDERSTANDING OF EXECUTIVE FUNCTION AND THE ETIOLOGY OF PSYCHIATRIC DISEASE?

To date researchers interested in using zebrafish to study executive function have focused on the development of appropriate behavioral paradigms. Now that many assays have been established zebrafish are well placed to address key questions relating to the control of these behaviors, particularly in the areas of impulse control and attention, and the etiology of disease: (1) Which neural circuits are involved and how do they develop? (2) What are the genetic factors that influence impulse control and attention?

(3) What are the cell biological processes by which genetic factors act to influence these behaviors and contribute to behavioral disease? The primary advantages zebrafish have in the search for knowledge in these areas are their transparency, which facilitates *in vivo* analysis of the development and functioning of neural circuits controlling behavior, and the ability to perform large scale pharmacological and genetic screens.

DISSECTION OF THE NEURAL CONTROL OF BEHAVIOR

The information regarding brain regions and pathways involved in the rodent behaviors described above were in large part obtained using lesion studies and pharmacological manipulations. These approaches are relatively crude as manipulations often affect surrounding cell types and processes or have slow reversibility (Mei and Zhang, 2012). In contrast, the use of optogenetic techniques that combine the use of light-controlled reporters and manipulators of neuronal activity with genetic targeting, allows more precise dissection of the neural control of behavior. A number of different optogenetic constructs for manipulating neuronal activity are available for use in fish as in other species. For example, channelrhodopsin cation channels can activate neurons by depolarising the membrane potential upon activation by light, whereas halorhodopsin and bateriorhodopsin channels act as light sensitive chloride and proton pumps capable of hyperpolarizing the membrane thus inhibiting action potentials. Although utilized in many model organisms, zebrafish are particularly well suited to the application of optogenetic techniques. In transparent larval and, to lesser extent, adult *casper* (White et al., 2008) forms, we have the ability to drive expression in specific cell types using GAL4:UAS constructs (Davison et al., 2007; Scott et al., 2007; Asakawa and Kawakami, 2008; Asakawa et al., 2008) or transposon technologies (Petzold et al., 2009). This provides an almost entirely non-invasive method for visualizing and modulating neuronal activity at even the single cell level and examining the effect on behavior. By comparison, in other animal systems, such as murine or primate models, holes must be drilled into the skull and fiber optic cables inserted to have access to the brain and control behavior *in vivo* with light optics (Cao et al., 2010). As the application of optogenetic techniques to address development and functioning of neural circuits in zebrafish have been extensively discussed elsewhere (Schoonheim et al., 2010; Del Bene and Wyart, 2012; Portugues et al., 2012; Umeda et al., 2012), in the section below we summarize more recent advances in technologies to visualize developing neuronal circuits.

Recent technological advances based on the use of genetically encoded GFP variants allow individual projections (*Brainbow*; Pan et al., 2011) and synaptic contacts GFP reconstituted across synaptic partners (GRASP) to be resolved, and activity within neuronal circuits (GCaMP) to be followed using fluorescence microscopy. *Brainbow* relies on combinatorial expression of several fluorophores (XFPs) to label individual neurons and their projections. Using Cre-lox recombination technology under the control of neuron specific promoters, each individual neuron expresses a random combination of each of up to four different XFPs to generate a specific fluorescence signal. As each neuron expresses the four XFPs at different levels, up to 100 different spectra can be obtained. Using this technology it is possible to trace the neuronal projections and formation of neuronal circuits in developing embryos and larvae. Pan et al. (2011) used this approach to map the zebrafish trigeminal projections.

"GFP reconstituted across synaptic partners" technology developed in *c. elegans* (Feinberg et al., 2008) can be used to trace the formation of synaptic contacts at high resolution *in vivo*. GRASP involves the expression of complementary fragments of GFP tethered to extracellular domains of transmembrane carrier proteins on pre- and post-synaptic membranes. The individual fragments of GFP are not fluorescent, but the formation of a synapse brings the two fragments into close proximity allowing reconstitution of the fluorescent molecule. Although application of this technique to zebrafish circuits has yet to be published, it has been used to map neuronal connections in *c. elegans*, *Drosophila* and mice (Feinberg et al., 2008; Arenkiel and Ehlers, 2009; Kim et al., 2011) and has the potential to trace synapse formation *in vivo* in wild-type and behaviorally mutant zebrafish.

In addition to tracing neuronal projections and synapse formation, fluorescence, including GFP technologies, have been used to monitor activity within neuronal populations in living behaving larval zebrafish. For example, the group of Rainer Friedrich (Li et al., 2005) has used whole brain calcium imaging to track activity within neuronal olfactory circuits as larval fish respond to changes in olfactory cues. Herwig Baier's group (Del Bene et al., 2010) used GCaMP reporter constructs under the control of neuron specific promoters to identify neural circuits involved in processing visual information. Using a similar approach, Koichi Kawakami's group (Muto and Kawakami, 2011; Muto et al., 2011, 2013) have identified circuits involved in spontaneous motor behavior and perception in embryonic zebrafish. When coupled with optogenetic approaches to manipulate activity in specific cells, these techniques provide a powerful means of dissecting neuronal circuits controlling behavior. Another particularly elegant larval assay that could be used to address the neurobiology of selective attention was recently described. Bianco et al. (2011) tracked the eye convergence and body position in 7dpf larvae, partially restrained in agarose, in response to different sized virtual stimuli. They found that the larvae tracked small moving spots, adopted a J-bend of their tail (the body shape that precedes prey capture; McElligott and O'Malley, 2005) and showed eye convergence on the target. This initial evidence of oculomotor processing of prey provides some evidence of a basic form of saliency-based selective attention, which may hold great promise for the development of tests of executive function in zebrafish in the future. As discussed by Bianco et al. (2011), by combining the assay with functional imaging of genetically encoded calcium indicators (Higashijima et al., 2003), techniques to manipulate circuits (Douglass et al., 2008; Janovjak et al., 2010; Schoonheim et al., 2010), and targeted laser-ablations (McLean et al., 2007; Satou et al., 2009; Burgess et al., 2010) it will be possible to identify the neuronal circuits controlling this, and similar, behavior.

Although the majority of these fluorescence techniques have to date only been applied to larval fish, advances in multiphoton confocal technology and computer processing raises the possibility of performing similar studies in juvenile and adult fish in the

future. These imaging approaches coupled with the large-scale mutagenesis analysis possible in zebrafish have unprecedented potential to extend understanding of the cellular and molecular bases of behavior

FORWARD GENETIC SCREENING

The ability to perform forward genetic screens for behavioral phenotypes also has great potential to advance understanding of the neurobiology of behavior. Forward genetic mutagenesis screens in zebrafish have been widely used to identify mutant alleles affecting developmental phenotypes. The classic three-generation mutagenesis screen for recessive alleles looks for families in which 25% of the F3 offspring show a given phenotype. This approach works well for recessive (or dominant) alleles of major effect but has, thus far, proved less effective for complex behavioral phenotypes likely to be governed by multi-allelic variations, each of minor effect and variable penetrance. Nonetheless, forward genetic screens for behavioral phenotypes have been undertaken. Darland and Dowling (2001) and Ninkovic et al. (2006) performed screens for cocaine and amphetamine-induced place preference, respectively. Both isolated lines of fish with differential drug seeking behavior, but neither have successfully isolated the causal mutations, possibly due to difficulties in unambiguously identifying the mutant carrier; the performance of control individuals often falls within the range of affected individuals and vice versa (Jain et al., 2011) making linkage analysis difficult.

Population based breeding and selection, or GFP insertion techniques can be used to address this problem. For example, Jain et al. (2011) used a "phenotyping by segregation" approach, based on commonly used breeding and selection strategies, to map the hypersensitive zebrafish *houdini* mutant. This strategy is attractive as it allows for fine mapping of subtle phenotypes that may have variable penetrance in the general population. An alternative approach taken by Petzold et al. (2009) used fluorescently tagged gene breaking transposons to mutagenize zebrafish. These transposons permit visual sorting of carriers from non-carriers (fluorescent vs. non-fluorescent larvae) and have the advantage of allowing rapid cloning of the mutagenized gene. Petzold et al. (2009) successfully used this insertional mutagenesis approach to identify two genes involved in the behavioral response of larval fish to nicotine.

Application of such breeding and selection-based and insertional mutagenesis screening approaches to the adult behavioral assays outlined above may lead to the identification of novel genes contributing to complex behavioral phenotypes. Such studies will make a valuable contribution to complement genome wide association studies (Sullivan, 2010) and analyses of copy number variants (Cook and Scherer, 2008) aimed at understanding the genetics of psychiatric disease.

IDENTIFYING CELL BIOLOGICAL PROCESSES AFFECTING COMPLEX BEHAVIORS

Genome-wide association studies in humans are excellent tools for identifying genetic variations associated with psychiatric disorder phenotypes (Mitchell and Porteous, 2009; Ersland et al., 2012). In some instances these studies are even being able to identify endophenotypes associated with multiple psychiatric disorders (Hall and Smoller, 2010; Consortium, 2013). However, while being able to identify genetic markers associated with a particular disorder, they are not able to establish which variations are of causal effect. The ability in zebrafish to generate targeted knockouts of candidate genes using TALEN technology (Sander et al., 2011) offers a cost effective and convenient means of investigating which of the candidate alleles identified in human GWAS studies are causally linked to behaviors. Further, once an allele of effect is identified, zebrafish provide an ideal model system in which to investigate the neurodevelopmental and cellular processes affected.

CONCLUSION

In this review, we have discussed the potential for using zebrafish to uncover some of the molecular and cellular processes related to psychiatric disorder, in particular relating to disorders of executive function. These are exciting times for zebrafish researchers. New assays of subtle behavioral phenotypes are fast being developed and replicated in different laboratories, and validation of these phenotypes is underway and progressing well. Given the huge repertoire of genetic tools available and the ever-expanding mutant resource, zebrafish will soon become one of the leading animal models in behavioral neuroscience. Even in the event that there are significant differences in anatomy or connectivity, many of the behaviors we have discussed are extensions of evolutionarily ancient reward and impulse control processes that appear to have conserved neurochemical pathways. In this regard, understanding the molecular mechanisms regulating these processes in fish will still give insight into regulation in mammals. As a final thought, there still remains much debate over how best to describe even simple neural circuits, and at this point no vertebrate system, regardless of technological advances, can come close to dealing with this issue (Yuste, 2008). Even in the age of the Human Connectome Project, the complexities of characterizing functional neural circuits should not be underestimated (Koch, 2012).

REFERENCES

Ahmad, F., Noldus, L. P. J. J., Tegelenbosch, R. A. J., and Richardson, M. K. (2012). Zebrafish embryos and larvae in behavioural assays. *Behaviour* 149, 10–12.

Alessi, S., and Petry, N. (2003). Pathological gambling severity is associated with impulsivity in a delay discounting procedure. *Behav. Processes* 64, 345–354.

APA. (2000). *Diagnostic and Statistical Manual of Mental Disorders: DSM-IV-TR*. Arlington: American Psychiatric Publishing, Inc.

Arenkiel, B. R., and Ehlers, M. D. (2009). Molecular genetics and imaging technologies for circuit-based neuroanatomy. *Nature* 461, 900–907.

Arnold, H., Burk, J., Hodgson, E., Sarter, M., and Bruno, J. (2002). Differential cortical acetylcholine release in rats performing a sustained attention task versus behavioral control tasks that do not explicitly tax attention. *Neuroscience* 114, 451–460.

Asadollahi, A., Mysore, S. P., and Knudsen, E. I. (2010). Stimulus-driven competition in a cholinergic midbrain nucleus. *Nat. Neurosci.* 13, 889–895.

Asakawa, K., and Kawakami, K. (2008). Targeted gene expression by the Gal4-UAS system in zebrafish. *Dev. Growth Differ.* 50, 391–399.

Asakawa, K., Suster, M. L., Mizusawa, K., Nagayoshi, S., Kotani, T., Urasaki, A., et al. (2008). Genetic dissection of neural circuits by Tol2 transposon-mediated Gal4 gene and enhancer trapping in zebrafish. *Proc. Natl. Acad. Sci. U.S.A.* 105, 1255–1260.

Balleine, B. W., and Dickinson, A. (1998). Goal-directed instrumental

action: contingency and incentive learning and their cortical substrates. *Neuropharmacology* 37, 407–419.

Bari, A., Dalley, J. W., and Robbins, T. W. (2008). The application of the 5-choice serial reaction time task for the assessment of visual attentional processes and impulse control in rats. *Nat. Protoc.* 3, 759–767.

Barkley, R. A. (1997). Behavioral inhibition, sustained attention, and executive functions: constructing a unifying theory of ADHD. *Psychol. Bull.* 121, 65.

Belin, D., Mar, A. C., Dalley, J. W., Robbins, T. W., and Everitt, B. J. (2008). High impulsivity predicts the switch to compulsive cocaine-taking. *Science* 320, 1352–1355.

Bencan, Z., Sledge, D., and Levin, E. D. (2009). Buspirone, chlordiazepoxide and diazepam effects in a zebrafish model of anxiety. *Pharmacol. Biochem. Behav.* 94, 75–80.

Bianco, I. H., Kampff, A. R., and Engert, F. (2011). Prey capture behavior evoked by simple visual stimuli in larval zebrafish. *Front. Syst. Neurosci.* 5:101. doi: 10.3389/fnsys.2011.00101

Bilotta, J., Risner, M. L., Davis, E. C., and Haggbloom, S. J. (2005). Assessing appetitive choice discrimination learning in zebrafish. *Zebrafish* 2, 259–268.

Brembs, B. (2009). Mushroom bodies regulate habit formation in *Drosophila*. *Curr. Biol.* 19, 1351–1355.

Brown, V. J., and Bowman, E. M. (2002). Rodent models of prefrontal cortical function. *Trends Neurosci.* 25, 340–343.

Burgess, H. A., Schoch, H., and Granato, M. (2010). Distinct retinal pathways drive spatial orientation behaviors in zebrafish navigation. *Curr. Biol.* 20, 381–386.

Burmeister, M., Mcinnis, M. G., and Zöllner, S. (2008). Psychiatric genetics: progress amid controversy. *Nat. Rev. Genet.* 9, 527–540.

Butcher, L. L., and Woolf, N. J. (2003). "Cholinergic neurons and networks revisited," *The Rat Nervous System*, ed. Paxions (Amsterdam: Elsevier), 1257–1268.

Button, T. M. M., Maughan, B., and Mcguffin, P. (2007). The relationship of maternal smoking to psychological problems in the offspring. *Early Hum. Dev.* 83, 727.

Campbell, P. (2010). A decade for psychiatric disorders. *Nature* 463, 9.

Cao, J. L., Covington, H. E., Friedman, A. K., Wilkinson, M. B., Walsh, J. J., Cooper, D. C., et al. (2010). Mesolimbic dopamine neurons in the brain reward circuit mediate susceptibility to social defeat and antidepressant action. *J. Neurosci.* 30, 16453–16458.

Cardona, D., López-Crespo, G., Sánchez-Amate, M., Flores, P., and Sánchez-Santed, F. (2011). Impulsivity as long-term sequelae after chlorpyrifos intoxication: time course and individual differences. *Neurotox. Res.* 19, 128–137.

Carli, M., Robbins, T., Evenden, J., and Everitt, B. (1983). Effects of lesions to ascending noradrenergic neurones on performance of a 5-choice serial reaction task in rats; implications for theories of dorsal noradrenergic bundle function based on selective attention and arousal. *Behav. Brain Res.* 9, 361–380.

Chudasama, Y., and Muir, J. L. (2001). Visual attention in the rat: A role for the prelimbic cortex and thalamic nuclei? *Behav. Neurosci.* 115, 417–428.

Clarke, H., Dalley, J., Crofts, H., Robbins, T., and Roberts, A. (2004). Cognitive inflexibility after prefrontal serotonin depletion. *Science* 304, 878–880.

Claudio Cuello, A., Emson, P. C., Paxinos, G., and Jessell, T. (1978). Substance P containing and cholinergic projections from the habenula. *Brain Res.* 149, 413–429.

Cole, B. J., and Robbins, T. W. (1989). Effects of 6-hydroxydopamine lesions of the nucleus accumbens septi on performance of a 5-choice serial reaction time task in rats: implications for theories of selective attention and arousal. *Behav. Brain Res.* 33, 165–179.

Collins, L. M., Asher, L., Pfeiffer, D. U., Browne, W. J., and Nicol, C. J. (2011). Clustering and synchrony in laying hens: The effect of environmental resources on social dynamics. *Appl. Anim. Behav. Sci.* 129, 43–53.

Colwill, R. M., Raymond, M. P., Ferreira, L., and Escudero, H. (2005). Visual discrimination learning in zebrafish (*Danio rerio*). *Behav. Processes* 70, 19–31.

Consortium, C.-D. G. O. T. P. G. (2013). Identification of risk loci with shared effects on five major psychiatric disorders: a genome-wide analysis. *Lancet* doi: 10.1016/S0140-6736(12)62129-1

Cook, E. H. Jr., and Scherer, S. W. (2008). Copy-number variations associated with neuropsychiatric conditions. *Nature* 455, 919–923.

Dalley, J. W., Fryer, T. D., Brichard, L., Robinson, E. S., Theobald, D. E., Laane, K., et al. (2007). Nucleus accumbens D2/3 receptors predict trait impulsivity and cocaine reinforcement. *Science* 315, 1267–1270.

Dalley, J. W., Mar, A. C., Economidou, D., and Robbins, T. W. (2008). Neurobehavioral mechanisms of impulsivity: fronto-striatal systems and functional neurochemistry. *Pharmacol. Biochem. Behav.* 90, 250–260.

Darland, T., and Dowling, J. E. (2001). Behavioral screening for cocaine sensitivity in mutagenized zebrafish. *Proc. Natl. Acad. Sci. U.S.A.* 98, 11691–11696.

Davison, J. M., Akitake, C. M., Goll, M. G., Rhee, J. M., Gosse, N., Baier, H., et al. (2007). Transactivation from Gal4-VP16 transgenic insertions for tissue-specific cell labeling and ablation in zebrafish. *Dev. Biol.* 304, 811–824.

Del Bene, F., and Wyart, C. (2012). Optogenetics: a new enlightenment age for zebrafish neurobiology. *Dev. Neurobiol.* 72, 404–414.

Del Bene, F., Wyart, C., Robles, E., Tran, A., Looger, L., Scott, E. K., et al. (2010). Filtering of visual information in the tectum by an identified neural circuit. *Science* 330, 669–673.

Desimone, R., and Duncan, J. (1995). Neural mechanisms of selective visual attention. *Annu. Rev. Neurosci.* 18, 193–222.

Diergaarde, L., Pattij, T., Poortvliet, I., Hogenboom, F., De Vries, W., Schoffelmeer, A. N., et al. (2008). Impulsive choice and impulsive action predict vulnerability to distinct stages of nicotine seeking in rats. *Biol. Psychiatry* 63, 301–308.

Di Giovanni, G., Di Matteo, V., Pierucci, M., and Esposito, E. (2008). Serotonin-dopamine interaction: electrophysiological evidence. *Prog. Brain Res.* 172, 45–71.

Douglass, A. D., Kraves, S., Deisseroth, K., Schier, A. F., and Engert, F. (2008). Escape behavior elicited by single, channelrhodopsin-2-evoked spikes in zebrafish somatosensory neurons. *Curr. Biol.* 18, 1133–1137.

Doyle, R. L., Frazier, J., Spencer, T. J., Geller, D., Biederman, J., and Wilens, T. (2006). Donepezil in the treatment of ADHD-Like symptoms in youths with pervasive developmental disorder a case series. *J. Atten. Disord.* 9, 543–549.

Ersland, K. M., Christoforou, A., Stansberg, C., Espeseth, T., Mattheisen, M., Mattingsdal, M., et al. (2012). Gene-based analysis of regionally enriched cortical genes in GWAS data sets of cognitive traits and psychiatric disorders. *PLoS ONE* 7:e31687. doi: 10.1371/journal.pone.0031687

Feinberg, E. H., Vanhoven, M. K., Bendesky, A., Wang, G., Fetter, R. D., Shen, K., et al. (2008). GFP reconstitution across synaptic partners (GRASP) defines cell contacts and synapses in living nervous systems. *Neuron* 57, 353–363.

Fernandez-Ruiz, J., Wang, J., Aigner, T. G., and Mishkin, M. (2001). Visual habit formation in monkeys with neurotoxic lesions of the ventrocaudal neostriatum. *Proc. Natl. Acad. Sci. U.S.A.* 98, 4196–4201.

Filippi, A., Mahler, J., Schweitzer, J., and Driever, W. (2010). Expression of the paralogous tyrosine hydroxylase encoding genes th1 and th2 reveals the full complement of dopaminergic and noradrenergic neurons in zebrafish larval and juvenile brain. *J. Comp. Neurol.* 518, 423–438.

Finn, P. R., Justus, A., Mazas, C., and Steinmetz, J. E. (1999). Working memory, executive processes and the effects of alcohol on Go/No-Go learning: testing a model of behavioral regulation and impulsivity. *Psychopharmacology* 146, 465–472.

Gaspar, P., and Lillesaar, C. (2012). Probing the diversity of serotonin neurons. *Philos. Trans. R. Soc. Lond. B Biol. Sci.* 367, 2382–2394.

Gerlai, R. (2012). Using zebrafish to unravel the genetics of complex brain disorders. *Curr. Top. Behav. Neurosci.* 12, 3–24.

Gould, T., and Gottesman, I. (2006). Psychiatric endophenotypes and the development of valid animal models. *Genes Brain Behav.* 5, 113–119.

Hall, M. H., and Smoller, J. W. (2010). A new role for endophenotypes in the GWAS era: functional characterization of risk variants. *Harv. Rev. Psychiatry* 18, 67–74.

Higashijima, S., Masino, M. A., Mandel, G., and Fetcho, J. R. (2003). Imaging neuronal activity during zebrafish behavior with a genetically encoded calcium indicator. *J. Neurophysiol.* 90, 3986–3997.

Himmelheber, A. M., Sarter, M., and Bruno, J. P. (2000). Increases in cortical acetylcholine release during sustained attention performance in rats. *Cog. Brain Res.* 9, 313–325.

Hoopes, S. P. (1999). Donepezil for Tourette's disorder and ADHD. *J. Clin. Psychopharmacol.* 19, 381–382.

Jain, R. A., Wolman, M. A., Schmidt, L. A., Burgess, H. A., and Granato, M. (2011). Molecular-Genetic mapping of zebrafish mutants with variable phenotypic penetrance. *PLoS ONE* 6:e26510. doi: 10.1371/journal.pone.0026510

Janovjak, H., Szobota, S., Wyart, C., Trauner, D., and Isacoff, E. Y. (2010). A light-gated, potassium-selective glutamate receptor for the

optical inhibition of neuronal firing. *Nat. Neurosci.* 13, 1027–1032.

Jarvis, E. D., Güntürkün, O., Bruce, L., Csillag, A., Karten, H., Kuenzel, W., et al. (2005). Avian brains and a new understanding of vertebrate brain evolution. *Nat. Rev. Neurosci.* 6, 151–159.

Kim, J., Zhao, T., Petralia, R. S., Yu, Y., Peng, H., Myers, E., et al. (2011). mGRASP enables mapping mammalian synaptic connectivity with light microscopy. *Nat. Methods* 9, 96–102.

Knudsen, E. I. (2011). Control from below: the role of a midbrain network in spatial attention. *Eur. J. Neurosci.* 33, 1961–1972.

Kobayashi, Y., and Isa, T. (2002). Sensory-motor gating and cognitive control by the brainstem cholinergic system. *Neural Netw.* 15, 731–741.

Koch, C. (2012). Modular biological complexity. *Science* 337, 531–532.

Kozak, R., Bowman, E. M., Latimer, M. P., Rostron, C. L., and Winn, P. (2005). Excitotoxic lesions of the pedunculopontine tegmental nucleus in rats impair performance on a test of sustained attention. *Exp. Brain Res.* 162, 257–264.

Kume, T., Sugimoto, M., Takada, Y., Yamaguchi, T., Yonezawa, A., Katsuki, H., et al. (2005). Up-regulation of nicotinic acetylcholine receptors by central-type acetylcholinesterase inhibitors in rat cortical neurons. *Eur. J. Pharmacol* 527, 77–85.

Levin, E. D. (2011). Zebrafish assessment of cognitive improvement and anxiolysis: filling the gap between in vitro and rodent models for drug development. *Rev. Neurosci.* 22, 75–84.

Levin, E. D., Bencan, Z., and Cerutti, D. T. (2007). Anxiolytic effects of nicotine in zebrafish. *Physiol. Behav.* 90, 54–58.

Levin, E. D., and Cerutti, D. T. (2009). "Behavioral neuroscience of zebrafish," in *Methods of Behavior Analysis in Neuroscience*, ed. J. J. Buccafusco 2nd Edn. Boca Raton (FL): CRC Press.

Levin, E. D., and Chen, E. (2004). Nicotinic involvement in memory function in zebrafish. *Neurotoxicol. Teratol.* 26, 731–735.

Li, J., Mack, J. A., Souren, M., Yaksi, E., Higashijima, S.-I., Mione, M., et al. (2005). Early development of functional spatial maps in the zebrafish olfactory bulb. *J. Neurosci.* 25, 5784–5795.

Logan, G. D., Schachar, R. J., and Tannock, R. (1997). Impulsivity and inhibitory control. *Psychol. Sci.* 8, 60–64.

Loo, S. K., and Barkley, R. A. (2005). Clinical utility of EEG in attention deficit hyperactivity disorder. *Appl. Neuropsychol.* 12, 64–76.

Manger, P. R., Fahringer, H. M., Pettigrew, J. D., and Siegel, J. M. (2002). The distribution and morphological characteristics of cholinergic cells in the brain of monotremes as revealed by ChAT immunohistochemistry. *Brain Behav. Evol.* 60, 275–297.

Maximino, C., De Brito, T. M., Da Silva Batista, A. W., Herculano, A. M., Morato, S., and Gouveia, A. Jr. (2010). Measuring anxiety in zebrafish: a critical review. *Behav. Brain Res.* 214, 157–171.

McElligott, M. B., and O'Malley, D. M. (2005). Prey tracking by larval zebrafish: axial kinematics and visual control. *Brain Behav. Evol.* 66, 177–196.

McLean, D. L., Fan, J., Higashijima, S., Hale, M. E., and Fetcho, J. R. (2007). A topographic map of recruitment in spinal cord. *Nature* 446, 71–75.

Mei, Y., and Zhang, F. (2012). Molecular tools and approaches for optogenetics. *Biol. Psychiatry* 71, 1033–1038.

Meshorer, E., and Soreq, H. (2006). Virtues and woes of AChE alternative splicing in stress-related neuropathologies. *Trends Neurosci.* 29, 216–224.

Mitchell, K. J., and Porteous, D. J. (2009). GWAS for psychiatric disease: is the framework built on a solid foundation? *Mol. Psychiatry* 14, 740–741.

Mueller, T., Dong, Z., Berberoglu, M. A., and Guo, S. (2011). The dorsal pallium in zebrafish, *Danio rerio* (Cyprinidae, Teleostei). *Brain Res.* 1381, 95–105.

Mueller, T., Vernier, P., and Wullimann, M. F. (2004). The adult central nervous cholinergic system of a neurogenetic model animal, the zebrafish *Danio rerio*. *Brain Res.* 1011, 156–169.

Muto, A., and Kawakami, K. (2011). Imaging functional neural circuits in zebrafish with a new GCaMP and the Gal4FF-UAS system. *Commun. Integr. Biol.* 4, 566–568.

Muto, A., Ohkura, M., Abe, G., Nakai, J., and Kawakami, K. (2013). Real-Time visualization of neuronal activity during perception. *Curr. Biol.* 23, 307–311.

Muto, A., Ohkura, M., Kotani, T., Higashijima, S.-I., Nakai, J., and Kawakami, K. (2011). Genetic visualization with an improved GCaMP calcium indicator reveals spatiotemporal activation of the spinal motor neurons in zebrafish. *Proc. Natl. Acad. Sci. U.S.A.* 108, 5425–5430.

Nieoullon, A. (2002). Dopamine and the regulation of cognition and attention. *Prog. Neurobiol.* 67, 53–83.

Ninkovic, J., Folchert, A., Makhankov, Y. V., Neuhauss, S. C., Sillaber, I., Straehle, U., et al. (2006). Genetic identification of AChE as a positive modulator of addiction to the psychostimulant D-amphetamine in zebrafish. *J. Neurobiol.* 66, 463–475.

Norton, W., and Bally-Cuif, L. (2010). Adult zebrafish as a model organism for behavioural genetics. *BMC Neurosci.* 11:90. doi: 10.1186/1471-2202-11-90

Noudoost, B., and Moore, T. (2011). The role of neuromodulators in selective attention. *Trends Cogn. Sci.* 15, 585–591.

Oliveira, R. F. (2009). Social behavior in context: hormonal modulation of behavioral plasticity and social competence. *Integr. Comp. Biol.* 49, 423–440.

Owen, A. M., Roberts, A. C., Hodges, J. R., and Robbins, T. W. (1993). Contrasting mechanisms of impaired attentional set-shifting in patients with frontal lobe damage or Parkinson's disease. *Brain* 116, 1159–1175.

Pan, Y. A., Livet, J., Sanes, J. R., Lichtman, J. W., and Schier, A. F. (2011). Multicolor brainbow imaging in zebrafish. *Cold Spring Harb. Protoc.* 2011, pdb. prot5546.

Panula, P., Chen, Y. C., Priyadarshini, M., Kudo, H., Semenova, S., Sundvik, M., et al. (2010). The comparative neuroanatomy and neurochemistry of zebrafish CNS systems of relevance to human neuropsychiatric diseases. *Neurobiol. Dis.* 40, 46–57.

Parker, M. O., and Brennan, C. H. (2012). Zebrafish (*Danio rerio*) models of substance abuse: Harnessing the capabilities. *Behaviour* 149, 10–12.

Parker, M. O., Gaviria, J., Haigh, A., Millington, M. E., Brown, V. J., Combe, F. J., et al. (2012a). Discrimination reversal and attentional sets in zebrafish (*Danio rerio*). *Behav. Brain Res.* 232, 264–268.

Parker, M. O., Millington, M. E., Combe, F. J., and Brennan, C. H. (2012b). Development and implementation of a three-choice serial reaction time task for zebrafish (*Danio rerio*). *Behav. Brain Res.* 227, 73–80.

Parker, M. O., Millington, M. E., Combe, F. J., and Brennan, C. H. (2012c). Housing conditions affect physiological and behavioural responses of zebrafish to the novel tank diving test. *PLoS ONE* 7:e34992. doi: 10.1371/journal.pone.0034992

Petzold, A. M., Balciunas, D., Sivasubbu, S., Clark, K. J., Bedell, V. M., Westcot, S. E., et al. (2009). Nicotine response genetics in the zebrafish. *Proc. Natl. Acad. Sci. U.S.A.* 106, 18662–18667.

Portugues, R., Severi, K. E., Wyart, C., and Ahrens, M. B. (2012). Optogenetics in a transparent animal: circuit function in the larval zebrafish. *Curr. Opin. Neurobiol.* 23, 119–126.

Proulx, M. J., and Serences, J. T. (2006). Searching for an oddball: Neural correlates of singleton detection mode in parietal cortex. *J. Neurosci.* 26, 12631–12632.

Ragozzino, M. E. (2007). The contribution of the medial prefrontal cortex, orbitofrontal cortex, and dorsomedial striatum to behavioral flexibility. *Ann. N. Y. Acad. Sci.* 1121, 355–375.

Ragozzino, M. E., Detrick, S., and Kesner, R. P. (1999). Involvement of the prelimbic–infralimbic areas of the rodent prefrontal cortex in behavioral flexibility for place and response learning. *J. Neurosci.* 19, 4585–4594.

Ridley, R., Haystead, T., and Baker, H. (1981). An analysis of visual object reversal learning in the marmoset after amphetamine and haloperidol. *Pharmacol. Biochem. Behav.* 14, 345–351.

Rink, E., and Wullimann, M. F. (2001). The teleostean (zebrafish) dopaminergic system ascending to the subpallium (striatum) is located in the basal diencephalon (posterior tuberculum). *Brain Res.* 889, 316–330.

Rink, E., and Wullimann, M. F. (2002). Development of the catecholaminergic system in the early zebrafish brain: an immunohistochemical study. *Dev. Brain Res.* 137, 89–100.

Robbins, T. (2002). The 5-choice serial reaction time task: behavioural pharmacology and functional neurochemistry. *Psychopharmacology (Berl.)* 163, 362–380.

Robbins, T. W. (1997). Arousal systems and attentional processes. *Biol. Psychol.* 45, 57–71.

Robinson, E. S., Eagle, D. M., Mar, A. C., Bari, A., Banerjee, G., Jiang, X., et al. (2008). Similar effects of the selective noradrenaline reuptake inhibitor atomoxetine on three distinct forms of impulsivity in the rat. *Neuropsychopharmacology* 33, 1028–1037.

Rosvold, H. E., Mirsky, A. F., Sarason, I., Bransome E. D. Jr., and Beck, L. H. (1956). A continuous performance test of brain damage. *J. Consul. Psychol.* 20, 343–350.

Sander, J. D., Cade, L., Khayter, C., Reyon, D., Peterson, R. T., Joung, J. K., et al. (2011). Targeted gene disruption in somatic zebrafish cells using

engineered TALENs. *Nat. Biotechnol.* 29, 697.
Sarter, M., and Bruno, J. P. (1997). Cognitive functions of cortical acetylcholine: toward a unifying hypothesis. *Brain Res. Rev.* 23, 28–46.
Sarter, M., Givens, B., and Bruno, J. P. (2001). The cognitive neuroscience of sustained attention: where top-down meets bottom-up. *Brain Res. Rev.* 35, 146–160.
Satou, C., Kimura, Y., Kohashi, T., Horikawa, K., Takeda, H., Oda, Y., et al. (2009). Functional role of a specialized class of spinal commissural inhibitory neurons during fast escapes in zebrafish. *J. Neurosci.* 29, 6780–6793.
Saus, E., Brunet, A., Armengol, L., Alonso, P., Crespo, J. M., Fernández-Aranda, F., et al. (2010). Comprehensive copy number variant (CNV) analysis of neuronal pathways genes in psychiatric disorders identifies rare variants within patients. *J. Psychiatr. Res.* 44, 971–978.
Schoonheim, P. J., Arrenberg, A. B., Del Bene, F., and Baier, H. (2010). Optogenetic localization and genetic perturbation of saccade-generating neurons in zebrafish. *J. Neurosci.* 30, 7111–7120.
Schweitzer, J., and Driever, W. (2009). Development of the dopamine systems in zebrafish. *Adv. Exp. Med. Biol.* 651, 1–14.
Scott, E. K., Mason, L., Arrenberg, A. B., Ziv, L., Gosse, N. J., Xiao, T., et al. (2007). Targeting neural circuitry in zebrafish using GAL4 enhancer trapping. *Nat. Methods* 4, 323–326.
Seeman, P., Guan, H. C., and Van Tol, H. H. M. (1993). Dopamine D4 receptors elevated in schizophrenia. *Nature* 365, 441–445.
Sullivan, P. F. (2010). The psychiatric GWAS consortium: big science comes to psychiatry. *Neuron* 68, 182–186.
Taghzouti, K., Louilot, A., Herman, J., Le Moal, M., and Simon, H. (1985). Alternation behavior, spatial discrimination, and reversal disturbances following 6-hydroxydopamine lesions in the nucleus accumbens of the rat. *Behav. Neural Biol.* 44, 354–363.
Treisman, A. M., and Gelade, G. (1980). A feature-integration theory of attention. *Cognit. Psychol.* 12, 97–136.
Tsutsui-Kimura, I., Ohmura, Y., Izumi, T., Yamaguchi, T., Yoshida, T., and Yoshioka, M. (2010). Endogenous acetylcholine modulates impulsive action via α4β2 nicotinic acetylcholine receptors in rats. *Eur. J. Pharmacol.* 641, 148–153.
Umeda, K., Shoji, W., Sakai, S., Muto, A., Kawakami, K., Ishizuka, T., et al. (2012). Targeted expression of a chimeric channelrhodopsin in zebrafish under regulation of Gal4-UAS system. *Neurosci. Res.* 75, 69–75.
White, R. M., Sessa, A., Burke, C., Bowman, T., Leblanc, J., Ceol, C., et al. (2008). Transparent adult zebrafish as a tool for in vivo transplantation analysis. *Cell Stem Cell* 2, 183–189.
Wilens, T. E., Waxmonsky, J., Scott, M., Swezey, A., Kwon, A., Spencer, T. J., et al. (2005). An open trial of adjunctive donepezil in attention-deficit/hyperactivity disorder. *J. Child Adolesc. Psychopharmacol.* 15, 947–955.
Winstanley, C. A., Chudasama, Y., Dalley, J. W., Theobald, D. E., Glennon, J. C., and Robbins, T. W. (2003). Intra-prefrontal 8-OH-DPAT and M100907 improve visuospatial attention and decrease impulsivity on the five-choice serial reaction time task in rats. *Psychopharmacology (Berl)* 167, 304–314.
Winstanley, C. A., Eagle, D. M., and Robbins, T. W. (2006). Behavioral models of impulsivity in relation to ADHD: translation between clinical and preclinical studies. *Clin. Psychol. Rev.* 26, 379–395.
Woodward, W. T., Schoel, W. M., and Bitterman, M. E. (1971). Reversal learning with singly presented stimuli in pigeons and goldfish. *J. Comp. Physiol. Psychol.* 76, 460–467.
Woolf, N. J., and Butcher, L. L. (1986). Cholinergic systems in the rat brain: III. Projections from the pontomesencephalic tegmentum to the thalamus, tectum, basal ganglia, and basal forebrain. *Brain Res. Bull.* 16, 603–637.
Yuste, R. (2008). Circuit neuroscience: the road ahead. *Front Neurosci.* 2, 6–9.
Zirger, J. M., Beattie, C. E., Mckay, D. B., and Thomas Boyd, R. (2003). Cloning and expression of zebrafish neuronal nicotinic acetylcholine receptors. *Gene Expr. Patterns* 3, 747–754.

Conflict of Interest Statement: The authors declare that the research was conducted in the absence of any commercial or financial relationships that could be construed as a potential conflict of interest.

Received: 08 January 2013; accepted: 19 March 2013; published online: 08 April 2013.
*Citation: Parker MO, Brock AJ, Walton RT and Brennan CH (2013) The role of zebrafish (Danio rerio) in dissecting the genetics and neural circuits of executive function. Front. Neural Circuits **7**:63. doi: 10.3389/fncir.2013.00063*

frontiers in
NEURAL CIRCUITS

ORIGINAL RESEARCH ARTICLE
published: 16 July 2013
doi: 10.3389/fncir.2013.00118

The first mecp2-null zebrafish model shows altered motor behaviors

Thomas Pietri[1,2,3]*, Angel-Carlos Roman[4†], Nicolas Guyon[1,2,3†], Sebastián A. Romano[1,2,3], Philip Washbourne[5], Cecilia B. Moens[6], Gonzalo G. de Polavieja[4] and Germán Sumbre[1,2,3]

[1] Ecole Normale Supérieure, Institut de Biologie de l'ENS, Paris, France
[2] Inserm, U1024, Paris, France
[3] CNRS, UMR 8197, Paris, France
[4] Instituto Cajal, Consejo Superior de Investigaciones Científicas, Madrid, Spain
[5] Institute of Neuroscience, University of Oregon, Eugene, OR, USA
[6] Division of Basic Sciences, Fred Hutchinson Cancer Research Center, Seattle, WA, USA

Edited by:
Rainer W. Friedrich, Friedrich Miescher Institute for Biomedical Research, Switzerland

Reviewed by:
Emre Yaksi, VIB, Belgium
Caroline H. Brennan, Queen Mary University of London, UK

***Correspondence:**
Thomas Pietri, Ecole Normale Supérieure, Institut de Biologie de l'ENS, 46 rue d'Ulm, 75005 Paris, France
e-mail: pietri@biologie.ens.fr
† These authors have contributed equally to this work.

Rett syndrome (RTT) is an X-linked neurodevelopmental disorder and one of the most common causes of mental retardation in affected girls. Other symptoms include a rapid regression of motor and cognitive skills after an apparently early normal development. Sporadic mutations in the transcription factor MECP2 has been shown to be present in more than 90% of the patients and several models of MeCP2-deficient mice have been created to understand the role of this gene. These models have pointed toward alterations in the maintenance of the central nervous system rather than its development, in line with the late onset of the disease in humans. However, the exact functions of MeCP2 remain difficult to delineate and the animal models have yielded contradictory results. Here, we present the first *mecp2*-null allele mutation zebrafish model. Surprisingly and in contrast to MeCP2-null mouse models, *mecp2*-null zebrafish are viable and fertile. They present nonetheless clear behavioral alterations during their early development, including spontaneous and sensory-evoked motor anomalies, as well as defective thigmotaxis.

Keywords: zebrafish, motor behavior, Rett syndrome, mecp2, early development, thigmotaxis

INTRODUCTION

Epigenetic regulations of gene expression play a crucial role in brain development and maturation. Accordingly, alterations of factors involved in epigenetic regulation at the level of gene transcription lead to critical defects in brain function. Methyl-CpG-binding protein 2 (MECP2), a basic transcription factor, is a major epigenetic regulator. It was first described as a global repressor of transcription (Lewis et al., 1992). More recently, apart from its well documented repressor activity, MECP2 seems to act as a gene expression activator (Yasui et al., 2007; Chahrour et al., 2008), to modulate gene expression by long range chromatin remodeling (Skene et al., 2010) and to regulate RNA splicing (Young et al., 2005).

MeCP2, present in all vertebrate species, appears to be an innovation of this phylum. It shows a high level of conservation among mammals with, for instance, more than 95% protein sequence identity between human and mouse, and to a lesser extent, between humans and zebrafish (48%). In mammals, like in zebrafish, MeCP2 appears to be expressed throughout the body in multiple organs, and particularly enriched in the nervous system. Its expression in the nervous system is first detected during early embryonic development and it is highly expressed in post-mitotic neurons (Shahbazian et al., 2002a; Curado et al., 2007). The structure and expression patterns of MeCP2 in zebrafish and mammals are similar (Coverdale et al., 2004), suggesting strong evolutionary pressure and therefore probable conserved functions.

Alterations of MECP2 functions have been shown to be causative of several neurodevelopmental diseases associated with autism spectrum disorders. In particular, sporadic mutations of MECP2 have been uncovered in more than 90% of patients diagnosed with Rett syndrome (RTT, Amir et al., 1999). At the clinical level, patients with RTT are asymptomatic during the first 6 to 18 months of life, appearing to develop normally. Subsequently, a period of stagnation precedes a net regression of the acquired skills. It is during this period that mental retardation appears and psychomotor skills degrade. Some patients also display seizures, abnormal cardiac, or breathing cycles (Matsuishi et al., 2011).

Various mouse models of RTT have been created, ranging from null-MeCP2 mutations to specific point ones mimicking those in humans. These models closely phenocopy several motor and cognitive dysfunctions described in RTT patients (Chen et al., 2001; Guy et al., 2001; Shahbazian et al., 2002b; Moretti et al., 2005, 2006; Picker et al., 2006; Santos et al., 2007). These different models point toward alterations of synaptic and neural circuits maturation and maintenance, in particular an imbalance between excitation and inhibition (Dani et al., 2005). Interestingly, this imbalance could affect various brain regions and at different stages of development (Blue et al., 2011; Kron et al., 2012). In addition to the effect on neurons, it has been recently shown that MeCP2 dysfunction may also perturb glial cells (Ballas et al., 2009; Lioy et al., 2011). Overall, these findings suggest that MeCP2 functions appear to be cell type and developmental stage dependent, thus impeding the delineation of the entire spectrum of

MeCP2 functions and the association of a particular functional alteration to a specific phenotype.

Zebrafish has recently gained much attention as a vertebrate model for human neurodevelopmental and neurodegenerative diseases (Panula et al., 2006; Beattie et al., 2007; Morris, 2009; Brennan, 2011; Kabashi et al., 2011; Steenbergen et al., 2011; Xi et al., 2011). Importantly, zebrafish produce a large number of progeny, with fast and external embryonic and larval development. They have a large repertoire of well-studied motor behaviors (for recent review, see Saint-Amant, 2010). Molecular manipulations of its genome can be achieved through forward genetic screening of mutagenized fish (Draper et al., 2004) or genome editing methods (Huang et al., 2011). Overall, these features have established zebrafish as a powerful and complementary vertebrate model for behavioral and genetic analysis, and more recently as an invaluable human disease model.

Here, we introduce the first zebrafish model of RTT, in which mecp2 function was abolished. A kinematic analysis of motor activity in embryos and young larvae reveals alterations of spontaneous, sensory-evoked and thigmotaxic behaviors.

MATERIALS AND METHODS

ANIMALS

AB adult, larva, and embryo zebrafish, from the University of Oregon Zebrafish Facility, were maintained at 28.5°C on a 14–10 h on/off light cycles at the Institut de Biologie de l'Ecole Normale Supérieure zebrafish facility. Embryos and larvae were grown accordingly to Westerfield (2000). All experimental procedures were performed at room temperature (21–23°C). Zebrafish *mecp2*^{Q63*} mutation was generated through *N*-ethyl-*N*-nitrosourea (ENU)-mutagenesis and selected by TILLING as previously described (Draper et al., 2004). As ENU-mutagenesis generates random mutations throughout the genome, heterozygote *mecp2* mutant fish were outcrossed several times in the AB background to remove off-target mutations. Mutant fish were identified by PCR using DNA extracted from fin clip (the primers 5′-AAAGGAAAGGCATGATGTGG-3′ and 5′-GTATCGCCAACCTTTTGGAA-3′ flank the position of the mutation), followed by sequencing. To keep the closest genetic background between different genotypes in the experiments, heterozygote *mecp2* mutant embryos and larvae were generated by outcrossing homozygote *mecp2* mutants with AB wild-type fish. Wild-type, heterozygote and homozygote *mecp2* mutant fish are, respectively, labeled WT, Het, and Mut in the figures. Morphological assessment of aged-matched wild-type, homozygote and heterozygote mecp2 mutant embryos and larvae did not reveal any difference, indicating that the rate of development is similar in the three groups of embryos and larvae. Accordingly, we used hours post fertilization (hpf) and days post fertilization (dpf) to stage embryos and larvae, respectively.

All procedures were carried out in compliance with the guidelines of the University of Oregon and Le Comite d'Ethique pour l'Experimentation Animale Charles Darwin.

SYNTENY MAPPING

Synteny mapping was performed by comparing the organization of the human genomic region bearing the MECP2 gene, with the zebrafish genome. To carry out this analysis, BLASTp searches were implemented using human proteins, inferred from genes present in this region, against the zebrafish database. Each first hit in the searches where then confirmed by a reciprocal BLASTp search. Only the reciprocal best hits of BLASTp searches were considered.

WESTERN BLOTTING

Adult brain was homogenized in 1× RIPA extraction buffer (Cell Signaling) complemented with protease inhibitor cocktail tablets (Roche) and incubated on ice for 45 min, then centrifuged at 14,000 g for 5 min. The supernatant was collected and the protein concentration was measured with the BCA Protein Assay Kit (Pierce). Samples were then boiled in Laemmli buffer, separated on SDS-PAGE gel, transferred to nitrocellulose membrane and successively probed with a chicken anti-human MeCP2 C-terminal antibody (gift from Dr. LaSalle) at a dilution of 1 μg/ml and visualized with a goat anti-chicken IgY HRP-coupled antibody (Jackson Laboratories) at a dilution of 0.1 μg/ml.

KINEMATIC ANALYSIS OF MOTOR BEHAVIORS

Experiments were performed on 25 hpf, 51 hpf embryos, and 6 dpf larvae. The 25 hpf embryos were dechorionated at least one hour before the experiments. All embryos and larvae were acclimatized to room temperature for at least 20 min before the beginning of the experiments. To estimate the rate of spontaneous contractions, the freely moving 25 hpf embryos were recorded under a stereo-microscope (Leica LZMFIII) using a monochrome digital camera (PixeLINK PL-A741) at 20 Hz. over a period of 5 min. Fifty one hpf larvae were subjected to light mechanical stimulation using an eyelash either on the side of the trunk or on the head of the larvae. Stimulations were applied 5–7 times separated by at least 1 s. Larva motor responses were recorded at 100 Hz. The startle responses induced by the stimulations were analyzed with ImageJ software. Only the duration of complete coilings were measured. These were defined as the period between the first deviation of the trunk from its resting state until its return to its initial position. In case of multiple contractions after a stimulation, only the first coiling period was taken into account. To monitor the spontaneous swimming activity, 6 dpf wild-type and mecp2-mutant larvae were randomly placed in a custom-made Plexiglas 35-well plate (15 mm diameter × 0.5 mm height) filled-in with 500 μl embryo medium at room temperature and let to habituate for 20 min before the experiment. Homogeneous illumination was provided by an electroluminescent panel (MiniNeon, France). Spontaneous motor behavior was monitored with a ImagingSource DMK 21BF04 camera at 30 Hz for 15 min. Custom Matlab scripts (MathWorks) were developed to compute the trajectories, activity, velocities, and the thigmotactic behavior. All Matlab scripts are available upon request. Larva activity was defined as the percentage of time in which movement was detected. Activity bouts and resting times were calculated as the periods of movement and between consecutive movements, respectively. Both were fitted to a power law of the $Y = aX^{-k}$ form. Thigmotactic behavior analysis described the relative position of the larvae within the well over time. For this purpose, we divided the wells in two zones: an

inner zone at the center of the well covering 36% of the total area, and an outer ring region covering the remaining 64% (see **Figure 3B**). To take into account potential alterations of motor functions in mecp2-null larvae, we analyzed the kinematics of a subset of swimming periods. Criteria for the selection of these subsets of trajectories are detailed in the results section.

STATISTICS

Results are presented by classical box-and-whisker diagrams with the median as the central red mark, the first quartile (q1) and third quartile (q3) for the edge of the box, and the extreme data points represented by the whiskers in the range of q1–1.5*(q3–q1) to q3 + 1.5*(q3–q1). Statistical significance was assessed using the Kolmogorov–Smirnov test.

RESULTS

ZEBRAFISH mecp2 IS AN ORTHOLOG OF HUMAN MECP2

Tetrapod vertebrates possess one copy of the *mecp2* gene located on the X chromosome. However, during evolution, teleost fish underwent an additional round of full genome duplication, leading to the possibility that in zebrafish two copies of the *mecp2* gene are present. Synteny analysis was therefore carried out to compare the genomic region of the human chromosome X flanking the MECP2 gene to the zebrafish genome. After reciprocal BLASTp searches with the sequences of the human proteins inferred from the genes flanking human MECP2, we found two syntenic regions in chromosome 8 and chromosome 11 (**Figure 1A**), in which zebrafish genes orthologous to the human genes flanking MECP2 were detected. Moreover, several paralog genes were present in these two zebrafish genomic regions, covering 2.07 megabases (Mb) in chromosome 8 and 0.07 Mb in chromosome 11 (only the cxxc1 and hcfc1 paralog group has been indicated for clarity) and flank the *mecp2* gene in chromosome 8. The comparison of the genomic organization of these two regions enabled us to conclude that the zebrafish genome has retained only one copy of the *mecp2* gene which is the ortholog of the human MECP2.

CHARACTERIZATION OF THE *mecp2*^{Q63*} MUTATION

Screening of the two last exons of *mecp2* in ENU-mutagenized zebrafish sperm allowed us to recover by TILLING a C to T transition near the 5′ part of the *mecp2* coding sequence, at position 187, causing a non-sense mutation and putatively truncating the protein at position 63. The mutant allele would then encode a form of the protein lacking both the crucial methyl-CpG binding (MBD) and the transcription repressor (TRD) functional domains (**Figure 1B**) most probably engendering a full loss of function of mecp2. C to T transition in homozygote mutants was confirmed by sequencing *mecp2* PCR-amplified genomic DNA fragments, showing the creation of a non-sense amber codon in place of a glutamine codon in position 187/189 (**Figure 1C**). F1 generation was outcrossed in the AB background to remove potential mutations carried along with the *mecp*^{Q63*} allele, heterozygotes (*mecp*$^{Q63*/+}$) were outcrossed for at least 3 generations before to be incrossed to produce homozygote mutants (*mecp*$^{Q63*/Q63*}$). Surprisingly, the homozygote *mecp2* mutant fish appears to develop normally, with no obvious morphological defects, they reach adulthood and reproduce. As maternally expressed *mecp2* mRNA has been detected in large amounts (Coverdale et al., 2004), *mecp*$^{Q63*/Q63*}$ fish were incrossed to remove any potential maternal contribution toward a milder phenotype. Similarly to the *mecp*$^{Q63*/Q63*}$ from *mecp*$^{Q63*/+}$ parents, the progeny of *mecp*$^{Q63*/Q63*}$ fish develop

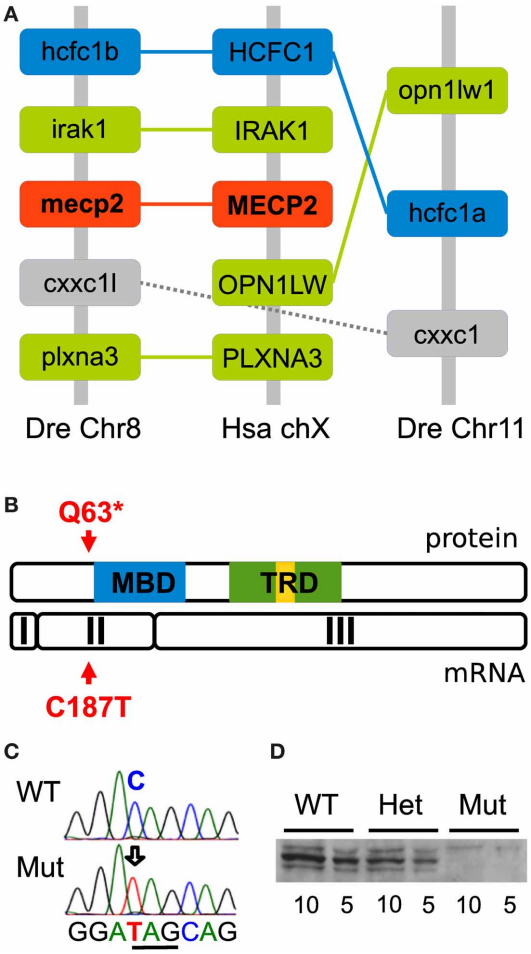

FIGURE 1 | Conserved synteny and generation of the zebrafish mecp2^{Q63*} mutation. (A) Synteny analysis between zebrafish chromosome 8 and 11 and human chromosome X. The diagram shows regions of 2.07 Mb and 0.07 Mb, respectively, in zebrafish chromosome 8 and 11 and 0.5 Mb in human chromosome X. The paralog hcfc1 group and ortholog to HCFC1 is indicated in blue, others in green. In addition, the second indicated paralog group is depicted in gray and mecp2 in red. The structure of these genomic regions shows that mecp2 is unique in the zebrafish genome and an ortholog of the human MECP2. **(B)** TILLING of ENU-mutagenized fish sperm after screening of exon 2 has allowed for the recovery of a C187T transition, creating a non-sense mutation. This mutation is upstream of the MBD and TRD functionnal domains, causing putatively a null mutation. **(C)** Sequence of mecp2 PCR from genomic DNA confirmed the C to T transition and the creation of a stop codon (underlined). **(D)** Western blot analysis of wild-type, mecp$^{Q63*/+}$ and mecp$^{Q63*/Q63*}$ adult zebrafish brain tissue. Two quantities of proteins (10 and 5 μg of total lysate) were loaded for each genotype. A major band around 75 kD reveals the presence of mecp2 in wild-type and mecp$^{Q63*/+}$, but not in mecp$^{Q63*/Q63*}$ adult zebrafish brain (minor bands might represent alternative post-translational mecp2 forms).

apparently normally and are viable. Thus, maternal *mecp2* mRNA does not play a role in the moderation of the phenotype. However, albeit not quantified, in comparison to wild-type or *mecp*$^{Q463*/+}$ fish, *mecp*$^{Q63*/Q63*}$ fish appear to have a slightly shorter lifespan. This lighter-than-expected phenotype in comparison to the mecp2-null mouse models could be explained by the fact that the mutation does not produce a null allele. Therefore, to assess how the mutation affects the protein level in the homozygote *mecp2* mutant, 5 and 10 μg of adult brain proteins from wild-type, *mecp*$^{Q63*/+}$ and *mecp*$^{Q63*/Q63*}$ fish were loaded on gels and subjected to Western blotting, with an antibody recognizing the C-terminus of the protein. In contrast to wild-type and heterozygote mutant fish, mecp2 protein could not be detected in *mecp*$^{Q63*/Q63*}$ fish (**Figure 1D**), indicating that the C187T transition is very likely to produce a null allele.

EARLY MOTOR BEHAVIOR

Spontaneous contractions were monitored in 25 hpf dechorionated embryos at 21–22°C. Wild-type embryos mainly showed unique side coiling of the trunk separated by a period of rest of several seconds. However, in some occasions, the contraction events led to several successive coilings without noticeable delay between each movement. Isolated, as well as multiple contraction movements were considered as single spontaneous motor activity events. The spontaneous motor activity of wild-type, heterozygote, and homozygote *mecp2* mutant embryos was then quantified. In line with a previous report (Pietri et al., 2009), wild-type embryos presented a median frequency of coiling of 5.12 events/min ($n = 71$) at 25 hpf (**Figure 2A**), not significantly different from *mecp2*$^{Q63*/+}$ or *mecp2*$^{Q63*/Q63*}$ embryos, with 5.66 events/min ($n = 33$) and 3.70 events/min ($n = 33$), respectively. Interestingly, the *mecp2*$^{Q63*/Q63*}$ embryos showed higher activity in comparison to the others, with a larger number of contractions per event in contrast to the wild-type and *mecp2*$^{Q63*/+}$ embryos. During the recording period, 80.6% of the *mecp2*$^{Q63*/Q63*}$ embryos exhibit at least one event with more than one contraction, in contrast to 24.3% of the other embryos. Overall, a significant median increase was observed in *mecp2*$^{Q63*/Q63*}$ embryos, where 30.55% of the events were composed of multiple coilings, in comparison to wild-type embryos (0%, $p < 10^{-8}$, **Figure 2B**).

To further study the early development of motor behavior of the *mecp2*$^{Q63*/Q63*}$ fish, we characterized the escape response to tactile stimuli of 51 hpf embryos. In contrast to spontaneous activity or stimulus-evoked response in earlier embryos, where only the local circuit within the spinal cord is necessary and sufficient to produce motor behaviors (Pietri et al., 2009), escape-induced stimuli in 51 hpf embryos involves hindbrain structures, in particular the reticulospinal neurons (O'Malley et al., 1996; Liu and Fetcho, 1999). These cells notably receive inputs from the spinal sensory Rohon-Beard cells (Fetcho and Faber, 1988), and the multi-sensory recipient trigeminal ganglia afferents innervating the skin of the head (Kimmel et al., 1990). To test both pathways, we mechanically stimulated the trunk or the head of the embryos (see **Figure 2C** as an example of response to head tactile stimulation). Both types of stimulus produced an escape-like behavior, with embryos turning away from the stimulus in a characteristic C-bend followed by a burst of swim bouts. **Figure 1C** shows an example of a 51 hpf *mecp2*$^{Q63*/Q63*}$ embryo where tactile stimulation of the head (0 ms) induced a C-bend (coiling period: 10–70 ms), and a swim bout (from 80 ms onward). In wild-type embryos, head and tail tactile stimulations produced behavioral responses with significantly different median C-bend durations [head (h, $n = 11$): 50 ms and tail (t, $n = 20$): 30 ms, $p < 10^{-5}$, **Figure 2D**]. The same trend is observed between tail and head tactile stimulation responses in *mecp2*$^{Q63*/Q63*}$ embryos [h ($n = 16$): 65 ms and t ($n = 11$): 40 ms, $p = 0.0017$], indicating that the principles governing both responses are conserved. Comparison of wild-type and *mecp2*$^{Q63*/Q63*}$ embryos for head or tail tactile stimulation

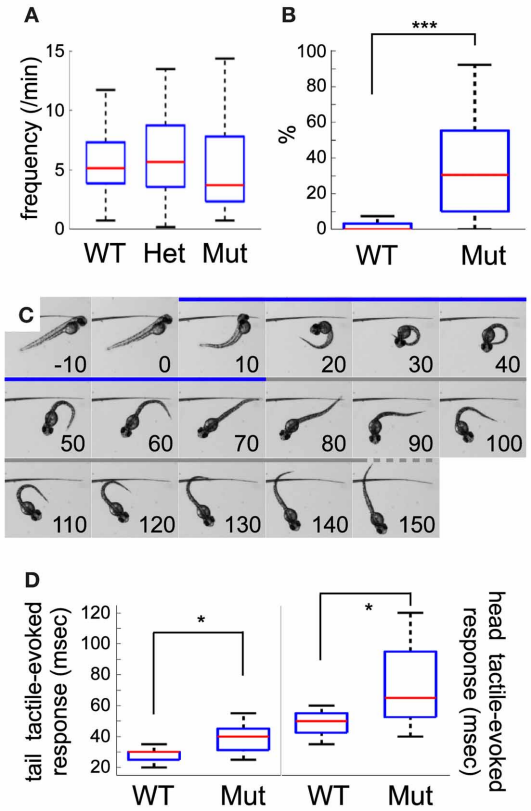

FIGURE 2 | Comparison between wild-type and mecp2-mutant embryo motor behavior. (A) Frequency of coiling in wild-type, mecp$^{Q63*/+}$ and mecp$^{Q63*/Q63*}$ 25 hpf embryos. No statistical difference was detected between the three groups of embryos. **(B)** mecp$^{Q63*/Q63*}$ 25 hpf embryos showed a significant larger number of multiple contractions per event than wild-type embryos. **(C)** Selected frames from high-speed video sequences showing a head-tactile-evoked response of a mecp$^{Q63*/Q63*}$ 51 hpf embryo. The coiling and swim bout periods are depicted in blue and gray, respectively. After the stimulation, the embryo performs an escape-like response, moving away from the stimulus, through a classical C-bend flexion. Time, in msec, is indicated in each panel. **(D)** Kinematic quantification of tail and head tactile stimulation in wild-type and mecp$^{Q63*/Q63*}$ 51 hpf embryos. Duration of the C-bend response to tail stimulation is shorter than head stimulation. A significant statistical difference between the two groups of embryos was observed for the duration of tail as well as head-evoked coilings. Significant statistical differences are indicated by * for $p < 0.05$ and *** for $p < 0.001$.

revealed however, for both types of stimuli, a longer duration of the C-bend for the *mecp2*$^{Q63*/Q63*}$ embryos (h: 65 ms vs. 50 ms, $p = 0.0113$; and t: 40 ms vs. 30 ms, $p = 0.0151$).

SPONTANEOUS SWIMMING ACTIVITY

Differences between wild-type and *mecp2* mutant fish were also assessed by monitoring their spontaneous motor behavior at 6 dpf. We found that the thigmotactic responses of *mecp2*$^{Q63*/Q63*}$ larvae were different from their wild-type counterparts (**Figures 3**, **4**). Wild-type animals preferred to swim along the walls of the arena, while *mecp2*$^{Q63*/Q63*}$ larvae showed much less preference for the borders of the well, covering homogeneously most of its surface (**Figure 3A** for a single animal and for an average of $n = 80$, for both groups of larvae). We performed a quantitative analysis of the preferred swimming regions according to an inner region of radius 4.5 mm and an outer ring to the limit of the circular arena of radius 7.5 mm (**Figure 3B**). Wild-type animals spent 88.5 % of the time in the outer ring while *mecp2*$^{Q63*/Q63*}$ larvae 73 % ($p = 0.001$, **Figure 3C**), closer to the random case of 64% (dashed green line, **Figure 3C**). To discriminate whether this difference had a motor origin or was due to the different interactions with the wall, we analyzed their trajectories to and from the walls. In addition, we found that the distribution of the resting times of wild-type and *mecp2*$^{Q63*/Q63*}$ larvae could be fitted to the same power law $Y = aX^{-k}$, by adjusting the constant k accordingly. In comparison to wild-type, *mecp2*$^{Q63*/Q63*}$ larvae showed a significantly lower median k constant (0.0525 vs. 0.2399 for wild-type larvae, $p = 0.0007$). In a reciprocal way, active time bouts had a larger k-value in *mecp2*$^{Q63*/Q63*}$ larvae (2.79 vs. 1.92 for wild-type larvae, $p = 0.0051$). These altered values of k are coherent with the lower total motor activity (26.4 % vs. 56.0 % $p < 10^{-6}$, **Figure 3D**), and lower bout velocities (13.0 mm/sec vs 18.9 mm/sec, $p < 10^{-7}$, **Figure 3E**) for *mecp2*$^{Q63*/Q63*}$ in comparison to wild-type larvae. These results would then predict that *mecp2*$^{Q63*/Q63*}$ larvae already at the outer ring would stay longer at this location, but we observed the opposite (**Figures 4A,B**). Analysis of the portion of the trajectories starting when the larvae reached the wall edge showed that most *mecp2*$^{Q63*/Q63*}$ larvae had a lower probability to stay in this region than their wild-type counterparts (**Figures 4A,B**). Interestingly, for the first 2 s, *mecp2*$^{Q63*/Q63*}$ larvae had a higher probability of staying at the wall, consistent with the lower activity and velocities, but this quickly decreased afterwards to values below those of wild-type larvae, with significant differences after 5 s, reaching $p < 10^{-10}$ at 30 s. We also analyzed the portion of trajectories moving from the center toward the wall (using the inner/outer separation as $t = 0$) and found that *mecp2*$^{Q63*/Q63*}$ larvae showed a significant lower probability in reaching the wall (after 30 s: $p < 10^{-9}$, **Figure 4C**). To test if the latter is a consequence of the lower activity and velocity, we computed the length of the path from the center (within an area of less than 5% of the well) to the wall; a parameter completely independent of activity and velocity. *mecp2*$^{Q63*/Q63*}$ larvae showed significantly longer paths than wild-type larvae (19.9 mm vs 12 mm, $p < 10^{-13}$, **Figure 4D**). Overall, these results suggest that *mecp2*$^{Q63*/Q63*}$ larvae have impaired locomotion and decreased thigmotaxis.

DISCUSSION

In this study, we introduce the first mecp2-null RTT zebrafish model. In comparison to other mecp2-deficient animal models, this mutant shows a weaker phenotype as they are viable and

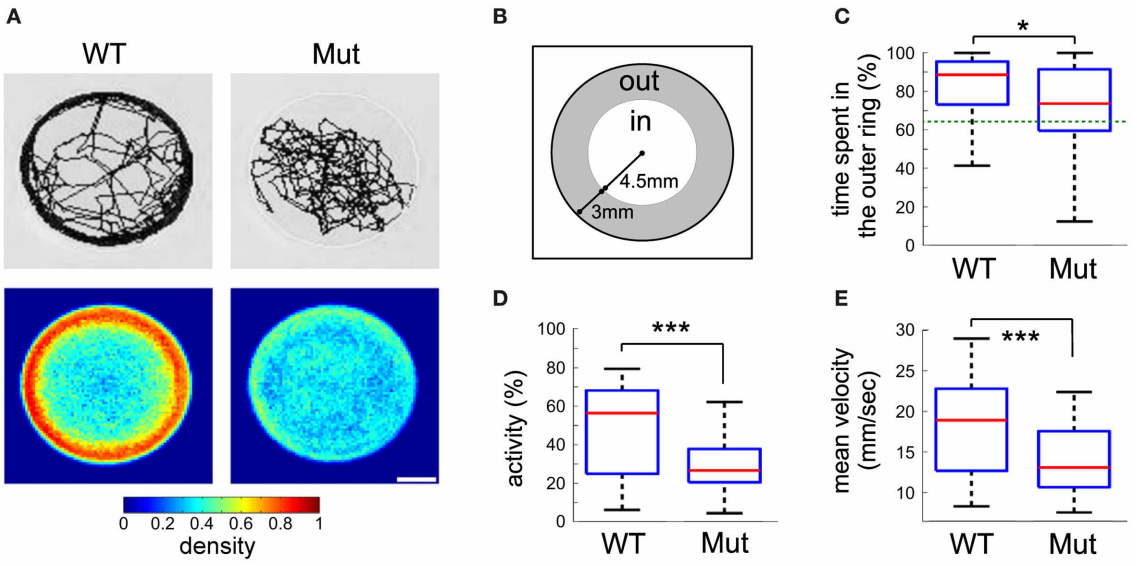

FIGURE 3 | Kinematic analysis of free swimming wild-type and mecp$^{Q63*/Q63*}$ 6 dpf larvae. (A) Example of traces for wild-type and mecp$^{Q63*/Q63*}$ larvae, obtained from a recording session of 15 min (top), and density maps representing the proportion of larvae at each position in the well (bottom, $n = 80$ for both groups of larvae). **(B)** The arena-surface division into inner and outer regions as used for data analysis. **(C)** Quantification of the time spent in the inner and outer regions of **(B)**. Dotted green line is the random case. **(D)** Percentage of time when the larvae were active. **(E)** Mean velocity during activity. Significant statistical differences are indicated by * for $p < 0.05$ and *** for $p < 0.001$.

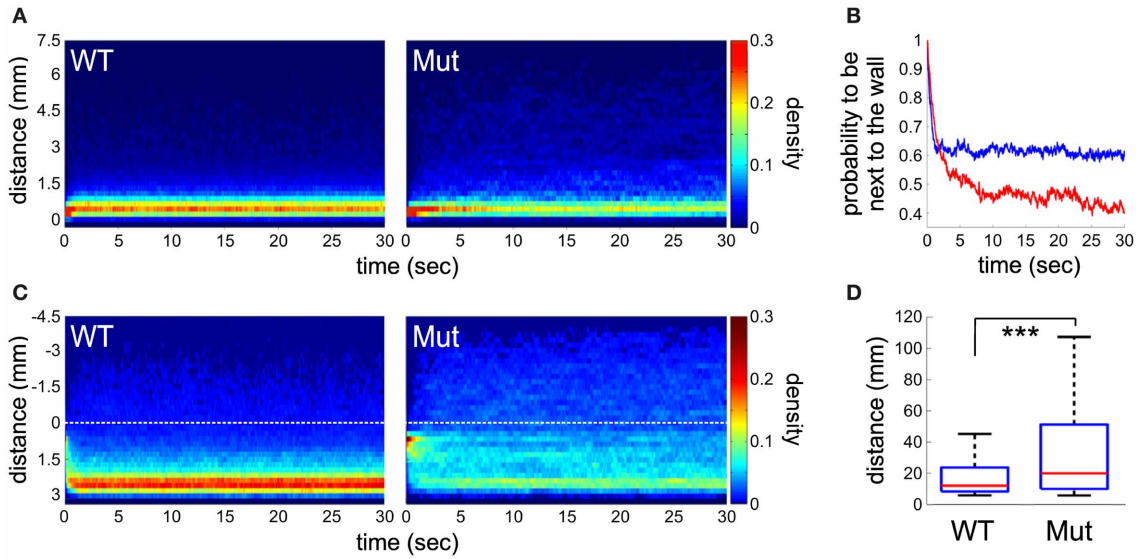

FIGURE 4 | Analysis of trajectories and thigmotaxis. (A) Place preference of the larvae after they reached the edge of the wall (< 0.5 mm) during a period of 30 s. Density plot representing, for each time point, the proportion of larvae at a given distance from the well's edge ($n = 80$ for both groups of larvae). **(B)** The probability of larvae to remain next to the wall edge (< 1 mm) along time. Statistical difference is observed after 5 s ($p < 0.001$), between mecp$^{Q63*/Q63*}$ (in red) and wild-type (in blue) larvae. **(C)** Trajectory analysis of the larvae after crossing from the inner to outer region (color coded as in **A**). The dotted lines indicate the boundary between the two regions. **(D)** The length of the paths from the center (a disc representing 5% of the total area) to the well's edge. Significant statistical differences are indicated by *** for $p < 0.001$.

fertile with a seemingly shorter lifespan. However, it shows clear behavioral impairments.

KNOCK-OUT OF mecp2 IN ZEBRAFISH PRODUCES AN UNEXPECTEDLY MILD PHENOTYPE

In this model, suppression of the mecp2 functions was achieved by TILLING selection of a non-sense mutation upstream of the structural MBD domain. The position of the mutation within the gene predicted to be a null mutation. This prediction was supported by protein expression analysis that confirmed the complete loss of mecp2 in *mecp2*$^{Q63*/Q63*}$ zebrafish. In mouse, null mutations of MeCP2 induce phenotypes reminiscent of RTT (Chen et al., 2001; Guy et al., 2001). In particular, the lifespan of mutant mice is drastically reduced to 6 to 8 weeks after birth. To our surprise *mecp2*$^{Q63*/Q63*}$ zebrafish are viable and reproduce normally (in presence or absence of unaltered mecp2 maternal contribution). We noticed however, a tendency of this mutant fish to have a relatively shorter lifespan than wild-type zebrafish. This modest phenotype with respect to mice may indicate functional compensatory mechanisms, for instance, by the presence of a *mecp2* paralog gene. Synteny mapping, comparing human and zebrafish *mecp2* loci and extensive genome database mining of zebrafish and other teleost fish [in which the whole-genome duplication occurred before the radiation of these species (not shown; Postlethwait et al., 2004)] excludes the existence of *mecp2* paralog groups in the various fish species tested, indicating that the loss of the duplicated *mecp2* gene occurred probably early after the whole teleost genome duplication, and so in zebrafish. Partial functional compensation may also exist through the action of close MeCP2 protein family members, such as MBD2 that, like MeCP2 bears MBD and TRD domains. MBD2 is able to bind to methylated CpG dinucleotides and modulates the level of gene expression (Ng et al., 1999). This hypothesis has been raised to point out the lack of phenotype in null-MeCP2 mutant mouse in non-neural tissues, where MeCP2 is also expressed (Guy et al., 2001); this possibility has however not been thoroughly tested yet. In addition, due to the duplication of many genes in the zebrafish genome, compensatory mechanisms can take place at the level of the *mecp2* target genes. For instance, MeCP2-deficient mice present various alterations of NMDA receptor expressions that are region and age specific (Blue et al., 2011). In zebrafish, all five NMDA receptors present in mammals are duplicated (Cox et al., 2005), raising the possibility that *mecp2*-induced alterations of the expression of one of the genes in a paralog group is compensated by expression of the second one. Moreover, these receptors are heteromeric, and if compensation within a paralog group cannot be achieved, alternative forms of the receptors could, at least partially, be used. Finally, the difference in the phenotypes between mouse and zebrafish might be explained by the far greater regenerative abilities of the zebrafish brain than those of the mammalian ones. In contrast to mammals, zebrafish neurogenesis occurs throughout life in many brain regions (Zupanc, 2008). While new-born neurons integrate into already established networks, "old" neurons are eliminated by apoptosis. The late onset of the neural phenotype of the MeCP2-deficient mouse (Chen et al., 2001; Guy et al., 2001) and postnatal neural restoration of MeCP2 expression in MeCP2-null mouse were shown to be sufficient to largely rescue the RTT phenotypes (Guy et al., 2007), thus, suggesting that alteration of MeCP2 functions perturbs the maintenance of the nervous system rather than its initial

development. It is conceivable that the constant addition of new neurons in zebrafish neural circuits could prevent the appearance of the lethal phenotype seen in MeCP2-null mouse models. These various compensatory mechanisms that are for some of them uniquely present in zebrafish, may explain its high resilience to the loss of *mecp2*. On the other hand, the ENU-mutagenesis used in the TILLING procedure produces a large number of mutations. Some may be carried along with the mutation of interest, even after several generations. We thus cannot completely exclude the presence of a second genetically-linked mutation to *mecp2*^{Q63*}. Our mecp2-null model presents a milder-than-expected phenotype. Thus, if indeed zebrafish and mammals mecp2 functions are conserved, a second genetic alteration would have to be a suppressor of the effect of the *mecp2*^{Q63*} mutation. The probability of such mutation in this context is very low. In-depth sequencing or s*ingle nucleotide polymorphisms* analysis of the mecp2 region could be used to rule out this concern.

SPONTANEOUS AND EVOKED EARLY MOTOR ALTERATIONS SUGGEST AN EXCITATION/INHIBITION UNBALANCE

By 24 hpf, spontaneous motor activity seems to be triggered by an intraspinal premotor circuit (Saint-Amant and Drapeau, 1998; Pietri et al., 2009). At this developmental stage, the excitatory components rely on electrical coupling via gap junctions, reinforced by nascent glutamatergic synapses (Saint-Amant and Drapeau, 1998; Pietri et al., 2009). On the other hand, inhibition appears to be driven only by glycinergic inputs, as evidence of GABAergic participation in the early spontaneous activity could not be detected (Saint-Amant and Drapeau, 2000, 2001). The similarity in the frequency of spontaneous muscular contractions between wild-type and mutant mecp2 embryos suggests that excitation in the spinal cord may remain intact in *mecp2*$^{Q63*/Q63*}$ embryos, while the sustained spontaneous motor activity events in these embryos would argue for a decrease in inhibition efficacy, likely through perturbation of the glycinergic system. A less parsimonious hypothesis would be that both excitation and inhibition are depressed in 25 hpf *mecp2*$^{Q63*/Q63*}$ embryos, but with a stronger alteration of the glycinergic inhibitory component. This hypothesis is supported by the observed tendency for a lower rate of spontaneous activity events in 25 hpf *mecp2*$^{Q63*/Q63*}$ embryos. In contradiction with these hypothesis, one study on the medulla of MeCP2-null mouse at postnatal day 7 has shown that glycinergic transmission is unaltered, while GABAergic transmission is strongly depressed (Medrihan et al., 2008). However, modulation of the defects of particular neurotransmitters appears to be region and age specific (Blue et al., 2011). It is therefore plausible that alteration of glycinergic transmission is either transient or only effective in the spinal cord of *mecp2*$^{Q63*/Q63*}$ fish.

One of the symptoms observed in autistic patients, including RTT patients, is their hyper-responsiveness to sensory stimuli (Belmonte et al., 2004). To investigate sensorimotor behavior in zebrafish early development, light mechanical stimuli were thus applied on the trunk or the head of the embryos to induce a startle/escape behavior. By 2 dpf, head and tail sensory stimuli are integrated through hindbrain reticulospinal neurons to produce a motor response. These sets of neurons receive inputs from the sensory trigeminal and Rohon-Beard neurons innervating respectively the head and body skin (Kimmel et al., 1990; Kuwada et al., 1990). While they appear similar at 21 hpf (Saint-Amant and Drapeau, 1998), responses to head and tail tactile stimulations showed different kinematics in 4–5 dpf larvae (Liu and Fetcho, 1999; Liu et al., 2012), reflecting the involvement of different reticulospinal neurons in mediating the escape response (Gahtan et al., 2002). In 51 hpf embryos, tail tactile stimulations induced coiling responses of shorter durations than those evoked by head stimulations, similar to what was found at 5 dpf, and thus suggesting that t different sets of reticulospinal neurons are already required at an early stage of development. *Mecp2*$^{Q63*/Q63*}$ embryos responded to tactile stimulations showing a similar difference between the duration of head and tail-induced responses seen in wild-type embryos. This suggests that the structure of the network necessary for both sensory-evoked motor responses is not altered. However, careful examinations of the mouse models, previously believed to be asymptomatic in their early development, have uncovered alterations of their sensory reflexes and sensory-motor gating development (Picker et al., 2006; Santos et al., 2007). Similarly, at 51 hpf, *mecp2*$^{Q63*/Q63*}$ embryos showed alterations of sensory-evoked motor responses characterized by a lengthening of the coiling duration. Both trigeminal and Rohon-Beard sensory neurons implicated in the transmission of the mechanical stimulation as well as the Mauthner neurons are glutamatergic neurons (Higashijima et al., 2004). At this age, glycinergic neurotransmition appears to remain the main inhibitory system in the spinal cord (Saint-Amant, 2010). Similar alteration of the coiling responses of both sensory stimulations in *mecp2*$^{Q63*/Q63*}$ embryos may imply that only the premotor network (downstream of the reticulospinal neurons) is affected and like in earlier stage embryos, the perturbation of the glycinergic system is responsible for the observed phenotype. Alternatively, glutamatergic neurotransmission may be altered in a similar way in both types of sensory neurons. This hypothesis can not be ruled out, as our experiments did not allow for the quantification of the delay of the response to a tactile stimulation, which would be indicative of such perturbation. It is therefore possible that defects in glutamatergic excitation are combined with alterations of the inhibitory neurotransmission, as seen in the mouse model of RTT (Chao et al., 2007, 2010; Medrihan et al., 2008; Blue et al., 2011).

Mecp2-MUTANT LARVAE SHOWED REDUCTION IN ACTIVITY AND A DECREASE IN ANXIETY-LIKE BEHAVIOR

Patients with RTT suffer from pronounced alterations of their motor systems. These defects have been phenocopied in RTT mouse models. We therefore tested our zebrafish model for motor dysfunctions in 6 dpf larvae in the open-field paradigm. As seen in mouse models, alteration of *mecp2* functions in zebrafish larvae induced a sharp decrease of the activity level, notably characterized by an increase of the resting times between swimming bouts. Interestingly, both resting times in wild-type and *mecp2*$^{Q63*/Q63*}$ larvae followed the same power-law distribution. The fact that a power law can describe the kinematics of both *mecp2*$^{Q63*/Q63*}$ and wild-type larvae suggests that the mutation modulates wild-type neural networks rather than generating major muscular or/and morphological abnormalities that could

indirectly affect motor behavior. (Harnos et al., 2000; Faure et al., 2003). In mecp2-null mouse models, the different aminergic systems have been shown to be specifically defective (Panayotis et al., 2011). In particular, defects in the dopaminergic system have been shown to be responsible for the movement abnormalities (Samaco et al., 2009; Gantz et al., 2011). In zebrafish, dopaminergic systems regulate the development of locomotor circuits, putatively by regulating synaptogenesis or influencing other neuromodulatory pathways (Thirumalai and Cline, 2008). It is thus possible that suppression of *mecp2* functions in zebrafish larvae induces a perturbation of neuromodulation of the motor network development that would then underlie the motor phenotype.

The dopaminergic, among other neuromodulatory systems, is also implicated in the control of anxiety-related behaviors (Wood and Toth, 2001). Thus, we tested for thigmotaxis in 6 dpf larvae, a behavioral test commonly used to evaluate the level of anxiety in humans and other animals. In zebrafish, this test has been particularly used in adults (Peitsaro et al., 2003; Anichtchik et al., 2004), but recently validated in larvae as young as 5 dpf (Colwill and Creton, 2011; Schnorr et al., 2012). In larvae, as well as in adults, thigmotaxis has been interpreted as a defensive strategy to avoid detection by predators and is reduced in familiar environments (Colwill and Creton, 2011) or after exposure to anxiolytic drugs (Schnorr et al., 2012). Studies of anxiety in mouse models of RTT have brought so far inconsistent results on the presence of elevated or reduced anxiety-like behaviors. The complexity of this behavior involving several brain structures, neurotransmitter systems and hormonal neuromodulation makes the interpretation of the various tests difficult and may thus explain such discrepancy. However, place preference analysis in an open-field arena, which would be the equivalent of wells for zebrafish, have shown an increase in anxiety levels in 3 and 5 month old $MeCP2^{308}$ mice (Shahbazian et al., 2002b) and in 8-week old mecp2-null mice (Stearns et al., 2007). This is in contradiction with our results showing that $mecp2^{Q63*/Q63*}$ larvae spent less time close to the well's edge than wild-type larvae. However, motor dysfunction present in the mutant larvae may lead to false interpretation of the place-preference results. Thus, a subset of trajectories were chosen to test for attraction toward edges and maintenance of edge preference during the active phases of swimming. $mecp2^{Q63*/Q63*}$ larvae showed a clear reduction in both parameters, strongly suggesting a decreased level of thigmotaxis in comparison to wild-type age-matched larvae. Moreover, the mutant larvae covered more distance in the inner region of the well than their wild-type counterparts in their periods of activity, a variable that has also been shown to be indicative of the level of anxiety in mice in the open-field paradigm (Paylor et al., 1998). Overall, these results suggest that $mecp^{Q63*/Q63*}$ larvae are less anxious than their wild-type counterparts.

Several autistic features have also been explained as a possible dysfunction of the reward system (Scott-Van Zeeland et al., 2010; Dichter et al., 2012). Interestingly, the dopaminergic system is also a core component of the reward circuits (Dichter et al., 2012). The decrease in locomotor activity of $mecp^{Q63*/Q63*}$ larvae could thus be explained as a reduction of interest in environment exploration. The decreased thigmotaxis could be the result of avoiding tactile stimulation from the wall, as expected from hyper-responsive autistic patients (Belmonte et al., 2004).

CONCLUSION

While rodents have been the historical model of choice to study the genetic alterations present in neurodevelopmental and neurodegenerative human diseases, zebrafish is currently becoming an important complementary model for translational neuroscience research, as it is the only suitable vertebrate model for high throughput drug screening. Analysis of *mecp2*-deficient zebrafish during early development has uncovered motor defects compatible with motor phenotypes observed in MeCP2-null mouse models and RTT patients. The zebrafish RTT model, in contrast to other vertebrate ones, will enable monitoring brain dynamics, neural morphology and behaviors, through the entire normal lifespan of the organism. Furthermore, the non-lethality of this model will enable the study of the natural genetic compensatory mechanisms. Deciphering these mechanisms would potentially lead to alternative directions in the understanding of the pathophysiology of RTT and open the way for the discovery of novel treatments.

ACKNOWLEDGMENTS

The authors thank our respective teams for their support during the elaboration of this work, in particular Adrien Jouary and Morgane Nouvian for fruitful discussions, the animal facility staff of the University of Oregon and the Institut de Biologie de l'Ecole Normale Supérieure for the constant care of the zebrafish and Dr. J. LaSalle for the anti-MECP2 antibody. This research was supported by fellowships from Autism Speak and the Fondation pour la Recherche Medicale to Thomas Pietri, and Juan de la Cierva (Spain) to Angel-Carlos Roman, grants from NINDS R01 NS065795 to Philip Washbourne, NIH R01 HD076585 to Cecilia B. Moens, Ministerio de Economia as Plan Nacional (Spain), EraSysBio+ ZeBrain to Gonzalo G. de Polavieja and Germán Sumbre and ERC stg 243106 to Germán Sumbre.

REFERENCES

Amir, R. E., Van den Veyver, I. B., Wan, M., Tran, C. Q., Francke, U., and Zoghbi, H. Y. (1999). Rett syndrome is caused by mutations in X-linked MeCP2, encoding methyl-CpG-binding protein 2. *Nat. Genet.* 23, 185–188. doi: 10.1038/13810

Anichtchik, O. V., Kaslin, J., Peitsaro, N., Scheinin, M., and Panula, P. (2004). Neurochemical and behavioural changes in zebrafish *Danio rerio* after systemic administration of 6-hydroxydopamine and 1-methyl-4-phenyl-1,2,3,6-tetrahydropyridine. *J. Neurochem.* 88, 443–453. doi: 10.1111/j.1471-4159.2004.02190.x

Ballas, N., Lioy, D. T., Grunseich, C., and Mandel, G. (2009). Non-cell autonomous influence of MeCP2-deficient glia on neuronal dendritic morphology. *Nat. Neurosci.* 12, 311–317. doi: 10.1038/nn.2275

Beattie, C. E., Carrel, T. L., and McWhorter, M. L. (2007). Fishing for a mechanism: using zebrafish to understand spinal muscular atrophy. *J. Child Neurol.* 22, 995–1003. doi: 10.1177/0883073807305671

Belmonte, M. K., Cook, E. H. Jr., Anderson, G. M., Rubenstein, J. L., Greenough, W. T., Beckel-Mitchener, A., et al. (2004). Autism as a disorder of neural information processing: directions for research and targets for therapy. *Mol. Psychiatry* 9, 646–663.

Blue, M. E., Kaufmann, W. E., Bressler, J., Eyring, C., O'Driscoll, C., Naidu, S., et al. (2011). Temporal and regional alterations in NMDA receptor expression in MeCP2-null

mice. *Anat. Rec. (Hoboken)* 294, 1624–1634. doi: 10.1002/ar.21380

Brennan, C. H. (2011). Zebrafish behavioural assays of translational relevance for the study of psychiatric disease. *Rev. Neurosci*. 22, 37–48. doi: 10.1515/rns.2011.006

Chahrour, M., Jung, S. Y., Shaw, C., Zhou, X., Wong, S. T. C., Qin, J., et al. (2008). MeCP2, a key contributor to neurological disease, activates and represses transcription. *Science* 320, 1224–1229. doi: 10.1126/science.1153252

Chao, H., Zoghbi, H. Y., and Rosenmund, C. (2007). MeCP2 controls excitatory synaptic strength by regulating glutamatergic synapse number. *Neuron* 56, 58–65. doi: 10.1016/j.neuron.2007.08.018

Chao, H., Chen, H., Samaco, R. C., Xue, M., Chahrour, M., Yoo, J., et al. (2010). Dysfunction in GABA signaling mediates autism-like stereotypies and Rett syndrome phenotypes. *Nature* 468, 263–269. doi: 10.1038/nature09582

Chen, R. Z., Akbarian, S., Tudor, M., and Jaenisch, R. (2001). Deficiency of methyl-CpC binding protein-2 in CNS neurons results in a Rett-like phenotype in mice. *Nat. Genet*. 27, 327–331. doi: 10.1038/85906

Colwill, R. M., and Creton, R. (2011) Locomotor behaviors in zebrafish (*Danio rerio*) larvae. *Behav. Processes.* 86, 222–229. doi: 10.1016/j.beproc.2010.12.003

Coverdale, L. E., Martyniuk,C. J., Trudeau, V. L., and Martin, C. C. (2004). Differential expression of the methyl-cytosine binding protein 2 gene in embryonic and adult brain of zebrafish. *Brain Res. Dev. Brain Res*. 153, 281–287. doi: 10.1016/j.devbrainres.2004.08.009

Cox, J. A., Kucenas, S., and Voigt, M. M. (2005) Molecular characterization and embryonic expression of the family of N-methyl-D-aspartate receptor subunit genes in the zebrafish. *Dev. Dyn*. 234, 756–766. doi: 10.1002/dvdy.20532

Curado, S., Anderson, R. M., Jungblut, B., Mumm, J., Schroeter, E., and Stainier, D. Y. R. (2007). Conditional targeted cell ablation in zebrafish: a new tool for regeneration studies. *Dev. Dyn*. 236, 1025–1035. doi: 10.1002/dvdy.21100

Dani, V. S., Chang, Q., Maffei, A., Turrigiano, G. G., Jaenisch, R., and Nelson, S. B. (2005). Reduced cortical activity due to a shift in the balance between excitation and inhibition in a mouse model of Rett syndrome. *Proc. Natl. Acad. Sci. U.S.A*. 102, 12560–12565. doi: 10.1073/pnas.0506071102

Dichter, G. S., Damiano, C. A., and Allen, J. A. (2012). Reward circuitry dysfunction in psychiatric and neurodevelopmental disorders and genetic syndromes: animal models and clinical findings. *J. Neurodev. Disord*. 4:19. doi: 10.1186/1866-1955-4-19

Draper, B. W., McCallum, C. M., Stout, J. L., Slade, A. J., and Moens, C. B. (2004). A high-throughput method for identifying N-ethyl-N-nitrosourea (ENU)-induced point mutations in zebrafish. *Methods Cell Biol*. 77, 91–112. doi: 10.1016/S0091-679X(04)77005-3

Faure, P., Neumeister, H., Faber, D. S., and Korn, H. (2003). Symbolic analysis of swimming trajectories reveals scale invariance and provides a model for fish locomotion. *Fractals* 11, 233–243. doi: 10.1142/S0218348X03002166

Fetcho, J. R., and Faber, D. S. (1988). Identification of motoneurons and interneurons in the spinal network for escapes initiated by the mauthner cell in goldfish. *J. Neurosci.* 8, 4192–4213.

Gahtan, E., Sankrithi, N., Campos, J. B., and O'Malley, D. M. (2002). Evidence for a widespread brain stem escape network in larval zebrafish. *J. Neurophysiol*. 87, 608–614.

Gantz, S. C., Ford, C. P., Neve, K. A., and Williams, J. T. (2011). Loss of MeCP2 in substantia nigra dopamine neurons compromises the nigrostriatal pathway. *J. Neurosci*. 31, 12629–12637. doi: 10.1523/JNEUROSCI.0684-11.2011

Guy, J., Gan, J., Selfridge, J., Cobb, S., and Bird, A. (2007). Reversal of neurological defects in a mouse model of Rett syndrome. *Science* 315, 1143–1147. doi: 10.1126/science.1138389

Guy, J., Hendrich, B., Holmes, M., Martin, J. E., and Bird, A. (2001). A mouse MeCP2-null mutation causes neurological symptoms that mimic Rett syndrome. *Nat. Genet*. 27, 322–326. doi: 10.1038/85899

Harnos, A., Horvath, G., Lawrence, A. B., and Vattay, G. (2000). Scaling and intermittency in animal behavior. *Physica A* 286, 312–320. doi: 10.1016/S0378-4371(00)00332-0

Higashijima, S., Mandel, G., and Fetcho, J. (2004). Distribution of prospective glutamatergic, glycinergic, and GABAergic neurons in embryonic and larval zebrafish. *J. Comp. Neurol*. 480, 1–18. doi: 10.1002/cne.20278

Huang, P., Xiao, A., Zhou, M., Zhu, Z., Lin, S., and Zhang, B. (2011). Heritable gene targeting in zebrafish using customized TALENS. *Nat. Biotechnol*. 29, 699–700. doi: 10.1038/nbt.1939

Kabashi, E., Brustein, E., Champagne, N., and Drapeau, P. (2011). Zebrafish models for the functional genomics of neurogenetic disorders. *Biochim. Biophys. Acta* 1812, 335–345. doi: 10.1016/j.bbadis.2010.09.011

Kimmel, C. B., Hatta, K., and Metcalfe, W. K. (1990). Early axonal contacts during development of an identified dendrite in the brain of the zebrafish. *Neuron* 4, 535–545. doi: 10.1016/0896-6273(90)90111-R

Kron, M., Howell, C. J., Adams, I. T., Ransbottom, M., Christian, D., Ogier, M., et al. (2012). Brain activity mapping in MeCP2 mutant mice reveals functional deficits in forebrain circuits, including key nodes in the default mode network, that are reversed with ketamine treatment. *J. Neurosci*. 32, 13860–13872. doi: 10.1523/JNEUROSCI.2159-12.2012

Kuwada, J. Y., Bernhardt, R. R., and Nguyen, N. (1990). Development of spinal neurons and tracts in the zebrafish embryo. *J. Comp. Neurol*. 302, 617–628. doi: 10.1002/cne.903020316

Lewis, J. D., Meehan, R. R., Henzel, W. J., Maurer-Fogy, I., Jeppesen, P., Klein, F., et al. (1992). Purification, sequence, and cellular localization of a novel chromosomal protein that binds to methylated DNA. *Cell* 69, 905–914. doi: 10.1016/0092-8674(92)90610-O

Lioy, D. T., Garg, S. K., Monaghan, C. E., Raber, J., Foust, K. D., Kaspar, B. K., et al. (2011). A role for glia in the progression of Rett's syndrome. *Nature* 475, 497–500. doi: 10.1038/nature10214

Liu, K. S., and Fetcho, J. R. (1999). Laser ablations reveal functional relationships of segmental hindbrain neurons in zebrafish. *Neuron* 23, 325–335. doi: 10.1016/S0896-6273(00)80783-7

Liu, Y., Bailey, I., and Hale, M. E. (2012). Alternative startle motor patterns and behaviors in the larval zebrafish (*Danio rerio*). *J. Comp. Physiol. A Neuroethol. Sens. Neural. Behav. Physiol*. 198, 11–24. doi: 10.1007/s00359-011-0682-1

Matsuishi, T., Yamashita, Y., Takahashi, T., and Nagamitsu, S. (2011). Rett syndrome: the state of clinical and basic research, and future perspectives. *Brain Dev*. 33, 627–631. doi: 10.1016/j.braindev.2010.12.007

Medrihan, L., Tantalaki, E., Aramuni, G., Sargsyan, V., Dudanova, I., Missler, M., et al. (2008). Early defects of GABAergic synapses in the brain stem of a MeCP2 mouse model of Rett syndrome. *J. Neurophysiol*. 99, 112–121. doi: 10.1152/jn.00826.2007

Moretti, P., Bouwknecht, J. A., Teague, R., Paylor, R., and Zoghbi, H. Y. (2005). Abnormalities of social interactions and home-cage behavior in a mouse model of Rett syndrome. *Hum. Mol. Genet*. 14, 205–220. doi: 10.1093/hmg/ddi016

Moretti, P., Levenson, J. M., Battaglia, F., Atkinson, R., Teague, R., Antalffy, B., et al. (2006). Learning and memory and synaptic plasticity are impaired in a mouse model of Rett syndrome. *J. Neurosci*. 26, 319–327. doi: 10.1523/JNEUROSCI.2623-05.2006

Morris, J. A. (2009). Zebrafish: a model system to examine the neurodevelopmental basis of schizophrenia. *Prog. Brain Res*. 179, 97–106. doi: 10.1016/S0079-6123(09)17911-6

Ng, H. H., Zhang, Y., Hendrich, B., Johnson, C. A., Turner, B. M., Erdjument-Bromage, H., et al. (1999). MBD2 is a transcriptional repressor belonging to the MeCP1 histone deacetylase complex. *Nat. Genet*. 23, 58–61. doi: 10.1038/12659

O'Malley, D. M., Kao, Y.-H, and Fetcho, J. R. (1996). Imaging the functional organization of zebrafish hindbrain segments during escape behaviors. *Neuron* 17, 1145–1155. doi: 10.1016/S0896-6273(00)80246-9

Panayotis, N., Ghata, A., Villard, L., and Roux, J. C. (2011). Biogenic amines and their metabolites are differentially affected in the MeCP2-deficient mouse brain. *BMC Neurosci*. 12:47. doi: 10.1186/1471-2202-12-47

Panula, P., Sallinen, V., Sundvik, M., Kolehmainen, J., Torkko, V., Tiittula, A., et al. (2006). Modulatory neurotransmitter systems and behavior: towards zebrafish models of neurodegenerative diseases. *Zebrafish* 3, 235–247. doi: 10.1089/zeb.2006.3.235

Paylor, R., Nguyen, M., Crawley, J. N., Patrick, J., Beaudet, A., and Orr-Urtreger, A. (1998). Alpha7 nicotinic receptor subunits are not necessary for hippocampal-dependent learning or sensorimotor gating: a behavioral characterization of Acra7-deficient mice. *Learn Mem.* 5, 302–316.

Picker, J. D., Yang, R., Ricceri, L., and Berger-Sweeney, J. (2006). An altered neonatal behavioral phenotype in mecp2 mutant mice. *Neuroreport* 17, 541–544. doi: 10.1097/01.wnr.0000208995.38695.2f

Pietri, T., Manalo, E., Ryan, J., Saint-Amant, L., and Washbourne, P. (2009). Glutamate drives the touch response through a rostral loop in the spinal cord of zebrafish embryos. *Dev. Neurobiol.* 69, 780–795. doi: 10.1002/dneu.20741

Peitsaro, N., Kaslin, J., Anichtchik, O. V., and Panula, P. (2003). Modulation of the histaminergic system and behaviour by alpha-fluoromethylhistidine in zebrafish. *J. Neurochem.* 86, 432–441. doi: 10.1046/j.1471-4159.2003.01850.x

Postlethwait, J., Amores, A., Cresko, W., Singer, A., and Yan, Y. L. (2004). Subfunction partitioning, the teleost radiation and the annotation of the human genome. *Trends Genet.* 20, 481–490. doi: 10.1016/j.tig.2004.08.001

Saint-Amant, L. (2010). Development of motor rhythms in zebrafish embryos.. *Prog. Brain Res.* 187, 47–61. doi: 10.1016/B978-0-444-53613-6.00004-6

Saint-Amant, L., and Drapeau, P. (1998). Time course of the development of motor behaviors in the zebrafish embryo. *J. Neurobiol.* 37, 622–632.

Saint-Amant, L., and Drapeau, P. (2000). Motoneuron activity patterns related to the earliest behavior of the zebrafish embryo. *J. Neurosci.* 20, 3964–3972.

Saint-Amant, L., and Drapeau, P. (2001). Synchronization of an embryonic network of identified spinal interneurons solely by electrical coupling. *Neuron* 31, 1035–1046. doi: 10.1016/S0896-6273(01)00416-0

Samaco, R. C., Mandel-Brehm, C., Chao, H. T., Ward, C. S., Fyffe-Maricich, S. L., Ren, J., et al. (2009). Loss of MeCP2 in aminergic neurons causes cell-autonomous defects in neurotransmitter synthesis and specific behavioral abnormalities. *Proc. Natl. Acad. Sci. U.S.A.* 106, 21966–21971. doi: 10.1073/pnas.0912257106

Santos, M., Silva-Fernandes, A., Oliveira, P., Sousa, N., and Maciel, P. (2007). Evidence for abnormal early development in a mouse model of Rett syndrome. *Genes Brain Behav.* 6, 277–286. doi: 10.1111/j.1601-183X.2006.00258.x

Scott-Van Zeeland, A. A., Dapretto, M., Ghahremani, D. G., Poldrack, R. A., and Bookheimer, S. Y. (2010). Reward processing in autism. *Autism Res.* 3, 53–67.

Shahbazian, M. D., Antalffy, B., Armstrong, D. L., and Zoghbi, H. Y. (2002a). Insight into Rett syndrome: MeCP2 levels display tissue- and cell-specific differences and correlate with neuronal maturation. *Hum. Mol. Genet.* 11, 115–124. doi: 10.1093/hmg/11.2.115

Shahbazian, M. D., Young, J., Yuva-Paylor, L., Spencer, C., Antalffy, B., Noebels, J., et al. (2002b). Mice with truncated MeCP2 recapitulate many Rett syndrome features and display hyperacetylation of histone H3. *Neuron* 35, 243–254. doi: 10.1016/S0896-6273(02)00768-7

Skene, P. J., Illingworth, R. S., Webb, S., Kerr, A. R. W., James, K. D., Turner, D. J., et al. (2010). Neuronal MeCP2 is expressed at near histone-octamer levels and globally alters the chromatin state. *Mol. Cell* 37, 457–468. doi: 10.1016/j.molcel.2010.01.030

Schnorr, S. J., Steenbergen, P. J., Richardson, M. K., and Champagne, D. L. (2012). Measuring thigmotaxis in larval zebrafish. *Behav. Brain Res.* 228, 367–374. doi: 10.1016/j.bbr.2011.12.016

Stearns, N. A., Schaevitz, L. R., Bowling, H., Nag, N., Berger, U. V., and Berger-Sweeney, J. (2007). Behavioral and anatomical abnormalities in mecp2 mutant mice: a model for Rett syndrome. *Neuroscience* 146, 907–921. doi: 10.1016/j.neuroscience.2007.02.009

Steenbergen, P. J., Richardson, M. K., and Champagne, D. L. (2011). The use of the zebrafish model in stress research. *Prog. Neuropsychopharmacol. Biol. Psychiatry* 35, 1432–1451. doi: 10.1016/j.pnpbp.2010.10.010

Thirumalai, V., and Cline, H. T. (2008). Endogenous dopamine suppresses initiation of swimming in prefeeding zebrafish larvae. *J. Neurophysiol.* 100, 1635–1648. doi: 10.1152/jn.90568.2008

Westerfield, M. (2000). *The Zebrafish Book a Guide for the Laboratory Use of Zebrafish Danio (Brachydanio) rerio*. 4th edn. Eugene, OR: University of Oregon Press.

Wood, S. J., and Toth, M. (2001). Molecular pathways of anxiety revealed by knockout mice. *Mol. Neurobiol.* 2, 101–119.

Xi, Y., Noble, S., and Ekker, M. (2011). Modeling neurodegeneration in zebrafish. *Curr. Neurol. Neurosci. Rep.* 11, 274–282. doi: 10.1007/s11910-011-0182-2

Yasui, D. H., Peddada, S., Bieda, M. C., Vallero, R. O., Hogart, A., Nagarajan, R. P., et al. (2007). Integrated epigenomic analyses of neuronal MeCP2 reveal a role for long-range interaction with active genes. *Proc. Natl. Acad. Sci. U.S.A.* 104, 19416–19421. doi: 10.1073/pnas.0707442104

Young, J. I., Hong, E. P., Castle, J. C., Crespo-Barreto, J., Bowman, A. B., Rose, M. F., et al. (2005). Regulation of RNA splicing by the methylation-dependent transcriptional repressor methyl-CpG binding protein 2. *Proc. Natl. Acad. Sci. U.S.A.* 102, 17551–17558. doi: 10.1073/pnas.0507856102

Zupanc, G. K. H. (2008). Adult neurogenesis and neuronal regeneration in the brain of teleost fish. *J. Physiol. Paris* 102, 357–373. doi: 10.1016/j.jphysparis.2008.10.007

Conflict of Interest Statement: The authors declare that the research was conducted in the absence of any commercial or financial relationships that could be construed as a potential conflict of interest.

Received: 12 April 2013; accepted: 21 June 2013; published online: 16 July 2013.

Citation: Pietri T, Roman A-C, Guyon N, Romano SA, Washbourne P, Moens CB, de Polavieja GG and Sumbre G (2013) The first mecp2-null zebrafish model shows altered motor behaviors. Front. Neural Circuits 7:118. doi: 10.3389/fncir.2013.00118

frontiers in
NEURAL CIRCUITS

OPINION ARTICLE
published: 27 May 2013
doi: 10.3389/fncir.2013.00099

The medial habenula as a regulator of anxiety in adult zebrafish

Ajay S. Mathuru [1] ***and Suresh Jesuthasan*** [1,2,3]*

[1] *Neural Circuitry and Behavior Laboratory, Institute of Molecular and Cell Biology, Singapore, Singapore*
[2] *Neuroscience and Behavioral Disorders Program, Duke-NUS Graduate Medical School, Singapore, Singapore*
[3] *Department of Physiology, Yong Loo Lin School of Medicine, National University of Singapore, Singapore, Singapore*
**Correspondence: sureshjj@imcb.a-star.edu.sg*

Edited by:
Gonzalo G. De Polavieja, Instituto Cajal. CSIC, Spain

Reviewed by:
Hitoshi Okamoto, RIKEN Brain Science Institute, Japan

The habenula consists of a set of nuclei located in the epithalamus. It regulates the release of multiple neuromodulators including serotonin and dopamine, and consists of two major subdivisions—medial and lateral. In all vertebrates, the medial habenula projects to the interpeduncular nucleus (IPN), a midline structure with poorly defined functions (Morley, 1986). Both the medial habenula and the IPN are rich in nicotinic receptors (nAChR). Activity in this pathway, triggered by opioids and nicotine, leads to a rise in dopamine in the nucleus accumbens (Glick et al., 2006; McCallum et al., 2012) and thus underlies the rewarding aspect of substance abuse. Strong activation of nicotinic receptors in the medial habenula or IPN, however, is sufficient to mediate the aversion to high concentration of nicotine (Fowler et al., 2011; Frahm et al., 2011). In contrast, absence of activity in this pathway is critical for the effects of withdrawal (Salas et al., 2009; Baldwin et al., 2011). Hence, depending on the level of activity, the medial habenula-IPN pathway can trigger reward, aversion or the physical and emotional changes that are characteristic of withdrawal.

The medial habenula regulates the expression of fear in zebrafish. Following silencing with tetanus toxin or lesioning with nitroreductase (Agetsuma et al., 2010; Lee et al., 2010), enhanced freezing was seen in aversive conditioning paradigms in both adult and larvae. The freezing response in habenula-lesioned fish was experience-dependent. In the case of adults, both control and lesioned fish froze when first exposed to an electric shock paired with a red light (the conditioning stimulus, CS) in a Pavlovian conditioning paradigm. As more shocks were delivered, freezing decreased in control fish, but not in habenula-lesioned fish (Agetsuma et al., 2010). The experiment with larval fish involved instrumental conditioning: fish had to swim away from the side of the tank containing a red light, which had been paired with a mild electric shock. In this case, freezing appeared gradually in lesioned fish in the later half of the conditioning session, but never in control fish (Lee et al., 2010).

One interpretation that has been suggested for these observations is that silencing the medial habenula biases fish to a passive coping strategy of freezing, due to modulation in the activity of the downstream griseum centrale [homologous to periaqueductal gray (PAG) in mammals] and nucleus incertus (Okamoto et al., 2012). As different regions of the PAG have been implicated in selection of different actions for coping against stress, a role for the medial habenula in such selection via PAG is a distinct possibility. An additional possibility is that medial habenula silencing increases anxiety in animals.

A consequence of elevated generalized anxiety in an animal is predisposition toward larger fear responses (Davis et al., 2010). The swimming behavior of an isolated fish when introduced into a novel tank can be used as a measure of baseline generalized anxiety (Levin et al., 2007): anxious fish spend more time near the bottom in a novel tank. Therefore, by using this assay, it is possible to quantify if adult fish where the medial habenula has been silenced display a similar, a lower, or a higher level of baseline anxiety when compared to control fish. We compared the behavior of adult fish that express the light chain of tetanus toxin (TeTXlc) in the medial habenula (Lee et al., 2010), under the control of the GAL4^{s1019t} driver (Scott et al., 2007), with fish that did not express this transgene. TeTXlc expressing fish spent more time in the bottom half of the tank compared to controls (**Figures 1A**,**B**), consistent with the possibility that these fish may indeed have a higher baseline generalized anxiety.

Mild stressors can elicit disproportionate reactions in anxious animals. In rats, for example, strong illumination, which is anxiogenic, causes an abnormally large startle to a tone (Walker and Davis, 1997). We examined the response of TeTXlc-expressing fish to naturalistic stimuli that are expected to be mildly stressful. Low concentration of the alarm substance (Jesuthasan and Mathuru, 2008) normally triggers a response that naïve, control fish recover from within seconds (0.1 unit; Mathuru et al., 2012). We followed this with an overhead shadow, which is thought to mimic the threat of a predator (Luca and Gerlai, 2012). These stimuli provide an opportunity to examine the role of medial habenula when the subject is challenged with stimuli that mimic complex natural stressors as opposed to its role in conditioning experiments that use unnatural repetitive stimuli. In such conditions, control fish displayed behavior indicative of mild fear—marginal increase in episodes of darting [Wilcoxon Signed Rank Test ($n = 7$), $p = 0.1$; **Figure 1F**], while other measures remained unchanged. TeTxlc-expressing fish, in contrast, spent more time spent in the bottom quarter of the tank (Mann–Whitney U-test, n1, n2, 7, 9, $U = 7, p = 0.005$; **Figure 1C**), displayed

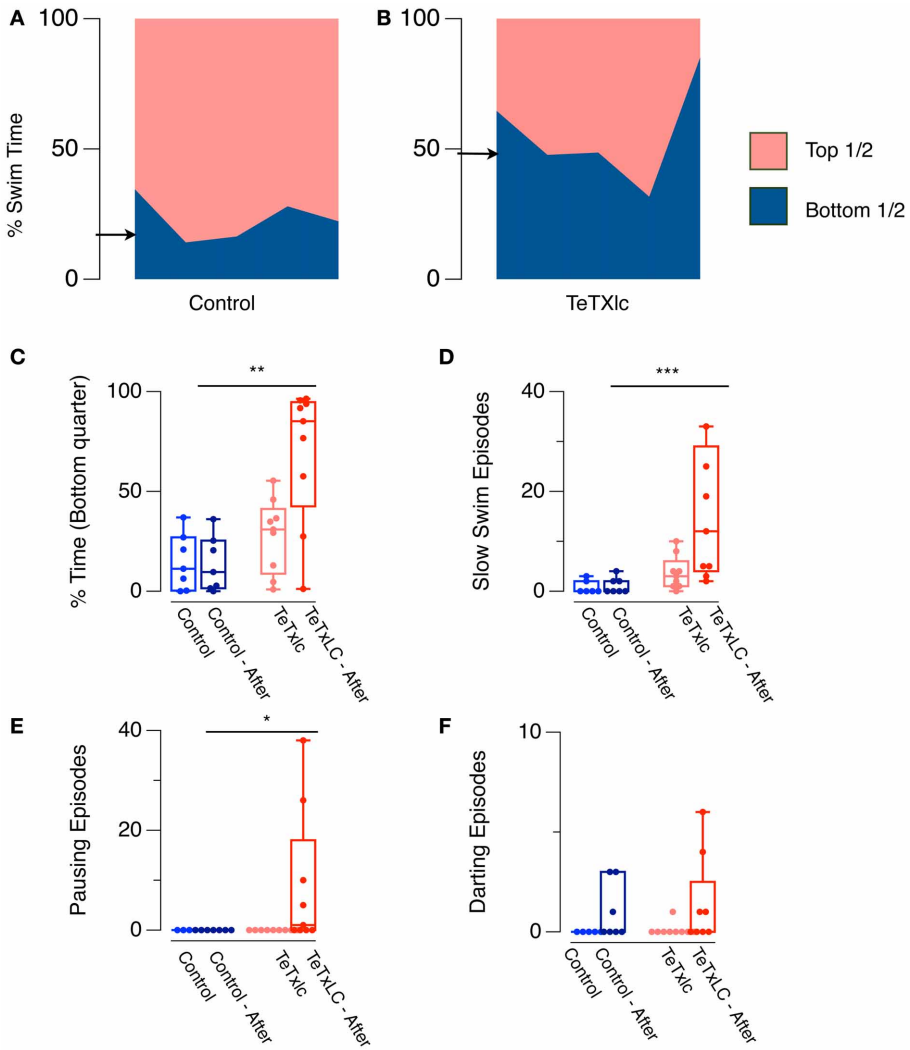

FIGURE 1 | (A,B) Novel tank assay. Area in each color shows percentage time spent in either half of a novel tank in one minute by five Control fish and five TeTXlc expressing fish. Arrows indicate median swim time in the bottom half for controls (20.4 ± 3.7%) and TeTXlc fish (48.6 ± 9%). **(C–F)** Response to dilute alarm substance and an overhead shadow. **(C)** Time spent in the bottom quarter of a tank, and median number of **(D)** slow swimming, **(E)** pauses, and **(F)** darts. Non-parametric, Mann–Whitney *U*-test was used to compare behavior of control and TeTXlc fish following exposure to the stimuli. (Mann–Whitney *U*-test, $^{*}p < 0.05$, $^{**}p < 0.01$, $^{***}p < 0.001$). Zebrafish expressing TeTXlc-CFP in the habenula were generated by crossing GAL4^{s1019t} with UAS:TeTXlc-CFP, and selected on the basis of CFP fluorescence in the brain. For the novel tank assay, fish were transferred into a glass tank measuring 20 × 12 × 5 cm—L × H × W containing 1 L of water and observed for 1 min. Digital videos were recorded as described before (Mathuru et al., 2012). Fish position in the tank was tracked and analyzed automatically using "track objects" algorithm in MetaMorph. 6.3 and custom written macros for Excel. Alarm substance was prepared as described before (Mathuru et al., 2012). This was introduced into the tank and a shadow, created by passing a hand under the overhead light, was presented after 2 min. Darting was defined as episodes during which the swimming speed exceeded baseline speed by more than 8 SD, slow swim episodes were defined as episodes greater than one second in duration during which the swim speed never exceeded half the mean baseline speed, while one second of immobility (speed less than 3 mm/s) was considered as a pause episode.

more episodes of slow swimming (Mann–Whitney *U*-test, n1, n2, 7, 9, $U = 3$, $p = 0.001$; **Figure 1D**) and pauses (Mann–Whitney *U*-test, n1, n2, 7, 9, $U = 14$, $p = 0.021$; **Figure 1E**). Darting episodes were comparable to controls (MW n1, n2, 7, 9, $U = 17.5$, $p = 0.435$; **Figure 1F**). The response of TeTxlc-expressing fish resembled that of naïve fish that exhibit intense innate fear upon exposure to a high concentration of the alarm substance (1 unit; Mathuru et al., 2012). In other words, TeTxlc-expressing fish show a disproportionate response when presented with multiple mildly stressful stimuli. Notably, TeTxlc-expressing fish display both active and passive responses, suggesting that there is an increase in the intensity of fear expression rather than a bias toward a particular type of action.

By examining responses to a novel environment, as well as to the alarm substance along with an overhead shadow, i.e., conditions where experience is absent, the behavioral responses of fish with dysfunctional medial habenula appear to be consistent with that of animals in a state

of elevated baseline anxiety. Behavioral deficits are manifest primarily in the presence of stressors, similar to the effects of nicotine withdrawal in rats (Jonkman et al., 2008).

The mechanism by which the habenula regulates a response to stress, both experience dependent and independent is likely to be complex, given the multiplicity of targets and modulators in the medial habenula-IPN pathway, which include somatostatin (Morley et al., 1985), met-Enkephalin, and substance P (Hamill et al., 1984). It is possible that regulation of serotonergic neurons in the raphe by the IPN also plays a role in modulating the response to aversive stimuli. Another intriguing hypothesis that has been suggested recently is that the absence of nicotine in addicts causes an increase in activity in the lateral habenula, which then leads to a decrease in dopamine release from the ventral tegmental area (VTA), thereby causing symptoms associated with withdrawal that include increased anxiety (Baldwin et al., 2011).

Is it possible then that silencing the medial habenula has a similar outcome, i.e., leads to an increase of activity in the lateral habenula? Consistent with the notion that the medial habenula can regulate lateral habenula outputs, projections from the medial to the lateral habenula have been detected in the rat (Kim and Chang, 2005), although it is not known if these projections are inhibitory. As the lateral habenula is able to use errors in prediction (based on experience) to trigger a change of state (Matsumoto and Hikosaka, 2007; Hong and Hikosaka, 2008), this region may also be involved in mediating the experience-dependent deficits of silencing the medial habenula. If activity in an inhibitory pathway from the medial habenula to the lateral habenula is reduced, the overall inhibitory tone on lateral habenula will also be reduced. In this scenario, transmission via the lateral habenula would be increased, and the outcome would be similar to that seen in rats where such an increase is associated with a predisposition for helpless behavior (Li et al., 2011), which includes increased freezing.

Thus, one step to understand both nicotine withdrawal and anxiety will be to characterize signaling between medial and lateral subnuclei of the habenula, in addition to examining downstream circuits. These subnuclei have remained in close proximity throughout vertebrate evolution, and it is possible that intra-habenula signaling modulates output, eventually effecting anxiety and motivated behaviors in animals.

REFERENCES

Agetsuma, M., Aizawa, H., Aoki, T., Nakayama, R., Takahoko, M., Goto, M., et al. (2010). The habenula is crucial for experience-dependent modification of fear responses in zebrafish. *Nat. Neurosci.* 13, 1354–1356.

Baldwin, P. R., Alanis, R., and Salas, R. (2011). The role of the habenula in nicotine addiction. *J. Addict. Res. Ther.* S1:002. doi: 10.4172/2155-6105.S1-002

Davis, M., Walker, D. L., Miles, L., and Grillon, C. (2010). Phasic vs sustained fear in rats and humans: role of the extended amygdala in fear vs anxiety. *Neuropsychopharmacology* 35, 105–135.

Fowler, C. D., Lu, Q., Johnson, P. M., Marks, M. J., and Kenny, P. J. (2011). Habenular α5 nicotinic receptor subunit signalling controls nicotine intake. *Nature* 471, 597–601.

Frahm, S., Slimak, M. A., Ferrarese, L., Santos-Torres, J., Antolin-Fontes, B., Auer, S., et al.. (2011). Aversion to nicotine is regulated by the balanced activity of β4 and α5 nicotinic receptor subunits in the medial habenula. *Neuron* 70, 522–535.

Glick, S. D., Ramirez, R. L., Livi, J. M., and Maisonneuve, I. M. (2006). 18-Methoxycoronaridine acts in the medial habenula and/or interpeduncular nucleus to decrease morphine self-administration in rats. *Eur. J. Pharmacol.* 537, 94–98.

Hamill, G. S., Olschowka, J. A., Lenn, N. J., and Jacobowitz, D. M. (1984). The subnuclear distribution of substance P, cholecystokinin, vasoactive intestinal peptide, somatostatin, leu-enkephalin, dopamine-beta-hydroxylase, and serotonin in the rat interpeduncular nucleus. *J. Comp. Neurol.* 226, 580–596.

Hong, S., and Hikosaka, O. (2008). The globus pallidus sends reward-related signals to the lateral habenula. *Neuron* 60, 720–729.

Jesuthasan, S. J., and Mathuru, A. S. (2008). The alarm response in zebrafish: innate fear in a vertebrate genetic model. *J. Neurogenet.* 22, 211–228.

Jonkman, S., Risbrough, V. B., Geyer, M. A., and Markou, A. (2008). Spontaneous nicotine withdrawal potentiates the effects of stress in rats. *Neuropsychopharmacology* 33, 2131–2138.

Kim, U., and Chang, S.-Y. (2005). Dendritic morphology, local circuitry, and intrinsic electrophysiology of neurons in the rat medial and lateral habenular nuclei of the epithalamus. *J. Comp. Neurol.* 483, 236–250.

Lee, A., Mathuru, A. S., Teh, C., Kibat, C., Korzh, V., Penney, T. B., et al. (2010). The habenula prevents helpless behavior in larval zebrafish. *Curr. Biol.* 20, 2211–2216.

Levin, E. D., Bencan, Z., and Cerutti, D. T. (2007). Anxiolytic effects of nicotine in zebrafish. *Physiol. Behav.* 90, 54–58.

Li, B., Piriz, J., Mirrione, M., Chung, C., Proulx, C. D., Schulz, D., et al. (2011). Synaptic potentiation onto habenula neurons in the learned helplessness model of depression. *Nature* 470, 535–539.

Luca, R. M., and Gerlai, R. (2012). In search of optimal fear inducing stimuli: Differential behavioral responses to computer animated images in zebrafish. *Behav. Brain Res.* 226, 66–76.

Mathuru, A. S., Kibat, C., Cheong, W. F., Shui, G., Wenk, M. R., Friedrich, R. W., et al. (2012). Chondroitin fragments are odorants that trigger fear behavior in fish. *Curr. Biol.* 22, 538–544.

Matsumoto, M., and Hikosaka, O. (2007). Lateral habenula as a source of negative reward signals in dopamine neurons. *Nature* 447, 1111–1115.

McCallum, S. E., Cowe, M. A., Lewis, S. W., and Glick, S. D. (2012). α3β4 nicotinic acetylcholine receptors in the medial habenula modulate the mesolimbic dopaminergic response to acute nicotine *in vivo*. *Neuropharmacology* 63, 434–440.

Morley, B. J. (1986). The interpeduncular nucleus. *Int. Rev. Neurobiol.* 28, 157–182.

Morley, B. J., Spangler, K. M., and Javel, E. (1985). The development of somatostatin immunoreactivity in the interpeduncular nucleus of the cat. *Brain Res.* 352, 241–248.

Okamoto, H., Agetsuma, M., and Aizawa, H. (2012). Genetic dissection of the zebrafish habenula, a possible switching board for selection of behavioral strategy to cope with fear and anxiety. *Dev. Neurobiol.* 72, 386–394.

Salas, R., Sturm, R., Boulter, J., and De Biasi, M. (2009). Nicotinic receptors in the habenulo-interpeduncular system are necessary for nicotine withdrawal in mice. *J. Neurosci.* 29, 3014–3018.

Scott, E. K., Mason, L., Arrenberg, A. B., Ziv, L., Gosse, N. J., Xiao, T., et al. (2007). Targeting neural circuitry in zebrafish using GAL4 enhancer trapping. *Nat. Methods* 4, 323–326.

Walker, D. L., and Davis, M. (1997). Anxiogenic effects of high illumination levels assessed with the acoustic startle response in rats. *Biol. Psychiatry* 42, 461–471.

Received: 27 February 2013; accepted: 03 May 2013; published online: 27 May 2013.

Citation: Mathuru AS and Jesuthasan S (2013) The medial habenula as a regulator of anxiety in adult zebrafish. Front. Neural Circuits 7:99. doi: 10.3389/fncir.2013.00099

frontiers in
NEURAL CIRCUITS

ORIGINAL RESEARCH ARTICLE
published: 31 May 2013
doi: 10.3389/fncir.2013.00102

Acute ethanol treatment upregulates *th1*, *th2*, and *hdc* in larval zebrafish in stable networks

Henri A. J. Puttonen, Maria Sundvik, Stanislav Rozov, Yu-Chia Chen and Pertti Panula*

Neuroscience Center and Institute of Biomedicine/Anatomy, University of Helsinki, Helsinki, Finland

Edited by:
Gonzalo G. De Polavieja, Instituto Cajal, CSIC, Spain

Reviewed by:
Gonzalo G. De Polavieja, Instituto Cajal, CSIC, Spain
Caroline H. Brennan, Queen Mary University of London, UK

Correspondence:
Pertti Panula, Neuroscience Center and Institute of Biomedicum, University of Helsinki, PO Box 63, Haartmaninkatu 8, FIN-00014 Helsinki, Finland
e-mail: pertti.panula@helsinki.fi

Earlier studies in zebrafish have revealed that acutely given ethanol has a stimulatory effect on locomotion in fish larvae but the mechanism of this effect has not been revealed. We studied the effects of ethanol concentrations between 0.75 and 3.00% on 7-day-old larval zebrafish (*Danio rerio*) of the Turku strain. At 0.75-3% concentrations ethanol increased swimming speed during the first minute. At 3% the swimming speed decreased rapidly after the first minute, whereas at 0.75 and 1.5% a prolonged increase in swimming speed was seen. At the highest ethanol concentration dopamine levels decreased significantly after a 10-min treatment. We found that ethanol upregulates key genes involved in the biosynthesis of histamine (*hdc*) and dopamine (*th1* and *th2*) following a short 10-min ethanol treatment, measured by qPCR. Using *in situ* hybridization and immunohistochemistry, we further discovered that the morphology of the histaminergic and dopaminergic neurons and networks in the larval zebrafish brain was unaffected by both the 10-min and a longer 30-min treatment. The results suggest that acute ethanol rapidly decreases dopamine levels, and activates both forms or *th* to replenish the dopamine stores within 30 min. The dynamic changes in histaminergic and dopaminergic system enzymes occurred in the same cells which normally express the transcripts. As both dopamine and histamine are known to be involved in the behavioral effects of ethanol and locomotor stimulation, these results suggest that rapid adaptations of these networks are associated with altered locomotor activity.

Keywords: zebrafish, ethanol, tyrosine hydroxylase, histidine decarboxylase, behavior

INTRODUCTION

Ethanol is the most widely used recreational drug. Ethanol abuse has been associated with many diseases of the brain and hazardous behavior, and due to its increasing prevalence, it is crucial to understand the effects of ethanol on the brain in detail. The dopaminergic system is one of the many targets of ethanol, and it has been widely studied in several models. Earlier studies have shown that the dopaminergic neurons in the VTA in rats are activated by ethanol administration (Gessa et al., 1985). Furthermore, studies have shown that the extracellular dopamine concentration in target areas of these neurons, mainly the nucleus accumbens, increases after ethanol exposure both in rats (Di Chiara and Imperato, 1986; Yoshimoto et al., 1992) and in mice (Tang et al., 2003). The activation of this mesolimbic dopamine pathway has been linked to mechanisms of substance addiction and reinforcement (Di Chiara and Imperato, 1988) and the increase in locomotor activity observed upon administration of ethanol in rodents (Cohen et al., 1997). Although the changes in dopamine levels are well known, the acute effect of ethanol on the expression of tyrosine hydroxylase (TH), the rate-limiting enzyme in dopamine synthesis, is not well-understood, with some evidence reporting an increase in *th* mRNA levels (Oliva et al., 2008). A chronic treatment with ethanol has been shown to increase *th* mRNA levels in the rat brain (Lee et al., 2005; Navarrete et al., 2013), but there is also evidence suggesting that TH protein levels decrease after chronic ethanol treatment (Kashem et al., 2012).

In mammals, the forebrain nucleus accumbens has been considered a critical region for transforming motivational and cognitive inputs to action since the initial concept was presented (Mogenson et al., 1980). Dopamine release in this region is needed for the locomotor activation induced by stimulatory drugs in mammals (Kelly et al., 1975; Farrar et al., 2010). The related functional neural circuits have not been analyzed in zebrafish, although both low concentrations of alcohol and d-amphetamine in swimming water significantly increase locomotor activity in larval zebrafish (Irons et al., 2010). Since the zebrafish do not possess dopaminergic neurons in the mesencephalon, significant efforts have been devoted to identifying the origin of subpallial dopaminergic inputs which might correspond to the mammalian striatonigral dopaminergic system necessary for initiation of voluntary movements. Both in adult zebrafish (Kaslin and Panula, 2001) and early larval zebrafish (McLean and Fetcho, 2004), local TH immunoreactive cells give rise to local projections. The TH-immunoreactive neurons in the posterior tuberculum also give rise to ascending projections toward the subpallium (Kaslin and Panula, 2001; Rink and Wullimann, 2001). A detailed analysis of individual neurons of all dopaminergic clusters using th:rasEGFP transgenic fish suggests that at an early stage (4 dpf) only very few dopaminergic neurons in the posterior tuberculum

send ascending projections, whereas most of the fibers are of intrinsic subpallial origin (Tay et al., 2011). The current concept is that both intrinsic and ascending projections contribute to the dopaminergic inputs to subpallium. Many diencephalic dopaminergic cell clusters give rise to extensive descending projections to the rhombencephalon and spinal cord in both larval and adult zebrafish (Kaslin and Panula, 2001; McLean and Fetcho, 2004; Tay et al., 2011). Thus, dopamine can potentially regulate movement on all levels from telencephalon to spinal cord, where dopaminergic fibers are concentrated in the ventral horn (McLean and Fetcho, 2004).

Although less studied, the histaminergic system is known to be affected by ethanol. Acutely administered ethanol increases histamine content in rodents (Subramanian et al., 1978; Rawat, 1980), with one study reporting a decrease with higher ethanol doses (Papanicolaou and Fennessy, 1980). Histamine has also been associated with ethanol tolerance in rats, with ethanol sensitive alcohol non-tolerant rats showing lower levels of brain histamine than ethanol insensitive alcohol tolerant rats and decreased ethanol tolerance in alcohol tolerant rats upon pharmacological inhibition of histamine synthesis (Lintunen et al., 2002). Recent studies have also shown that knocking out the histamine synthesizing enzyme histidine decarboxylase (HDC) in mice inhibits the increase of locomotor activity caused by ethanol (Nuutinen et al., 2010), and mice treated with histamine H3 receptor antagonists or those lacking H3 receptor do not show ethanol-induced conditioned place preference (Nuutinen et al., 2011). In the light of these new discoveries, the histaminergic system can be considered a major area of interest in ethanol research.

A vast majority of reported ethanol studies have utilized different rodent models. Lately, the zebrafish has been established as an alternative model to study the effects of ethanol. Behavioral analysis methods suitable for ethanol research have been established both for adult (Gerlai et al., 2000; Kily et al., 2008; Mathur et al., 2011) and larval zebrafish (Lockwood et al., 2004). There are also several advantages to using zebrafish, including the possibility to visualize whole neurotransmitter networks *in vivo* in larval stages of the fish, as has been shown in several earlier studies (Chen et al., 2009; Sallinen et al., 2009b). An acute exposure of adult zebrafish to ethanol increases brain dopamine levels in a dose-dependent manner (Chatterjee and Gerlai, 2009), but the kinetics of these changes which potentially modify the functions of important circuits are not known. Furthermore, the regulation of the rate-limiting dopamine synthesizing enzyme TH has not been studied. We hypothesized that the increased dopamine levels should be associated with essential changes in synthesizing enzymes TH, and aimed at identifying which of the two TH forms is activated. We also hypothesized that synthesis of histamine, another amine involved in increased vigilance and motor activity, could undergo essential changes following ethanol exposure. In this study, we used 7-day-old larval zebrafish to study the effect of several acute short-term ethanol treatments on swimming behavior. In addition, we associated the changes observed to possible functional or anatomical alterations in key markers of the histaminergic and dopaminergic circuits using confocal analysis on whole neuronal networks and *in situ* hybridization.

MATERIALS AND METHODS

EXPERIMENTAL ANIMALS

Larval zebrafish of a wild-type Turku strain were used in all experiments. This strain has been maintained in the laboratory for more than a decade, and has been used in several earlier publications (Chen et al., 2009; Sallinen et al., 2009a). Fish were bred and maintained according to Westerfield (Westerfield, 2000). A permit for the experiments was obtained from the Office of the Regional Government of Southern Finland. All batches of embryos were obtained from several parent fish in order to minimize the chance of a rare genotype affecting the results.

ETHANOL TREATMENT FOR HISTOLOGIC AND QUANTITATIVE METHODS

Ten to twenty 7dpf (days post-fertilization) larval zebrafish were transferred to a six-well plate in 1 × E3 (zebrafish embryonic medium; 5.00 mM NaCl, 0.44 mM $CaCl_2$, 0.33 mM $MgSO_4$ and 0.17 mM KCl). The 1 × E3 was then replaced with 1 × E3 containing ethanol. Four different ethanol concentrations were used: 0.00% (control), 0.75, 1.50, and 3.00% (v/v). These concentrations were chosen based on previous studies with zebrafish and ethanol (Lockwood et al., 2004; Chatterjee and Gerlai, 2009). The treatment durations used were 10 and 30 min. Following the ethanol treatment, the larvae were quickly collected into 1.5 ml microcentrifuge tubes and sacrificed on ice.

BEHAVIORAL ANALYSIS

The locomotor activity of 7dpf larvae after ethanol exposure was observed during a 10-min time period. Forty eight larvae were tracked at a time on a 48-well plate, as described previously (Peitsaro et al., 2007). The larvae were divided into four treatment groups of 12 larvae. Ethanol solutions used were the same as those described above. The solution was administered carefully into the wells immediately prior to the tracking in order to assess the acute locomotor effect of ethanol exposure. When analysing total distance moved, fish that did not swim at all during the trial were considered outliers and excluded from the analysis. The amount of larvae excluded from each of the groups due to zero movement was as follows: control: 1 out of 48, 0.75%: 5 out of 61, 1.50%: 7 out of 68 and 3.00%: 2 out of 55. The values were transformed using $\log_{10}$ transformation, after which the values conformed better to a normal distribution and were analysed using 1-way ANOVA followed by Tukey's *post-hoc* test. Other variables were analysed without the use of any transformations using the same statistical tests. Additionally, total distance moved was also analysed with 1-min intervals, with statistical analysis done using Two-Way repeated measures (RM) ANOVA followed by Bonferroni's post hoc test after performing a $\log_{10}$ transformation as described above. Fish that did not move at all during one or more intervals were assigned the value 10^{-4} for total swimming distance during those time points to enable use of a $\log_{10}$ transformation.

QUANTITATIVE PCR

Groups of 15 larvae were treated with ethanol for 10 min as described above. Total RNA was isolated using the RNeasy Mini Kit (Qiagen, Hilden, Germany), followed by cDNA synthesis

using the SuperScriptIII kit (Invitrogen). The SmartCyclerII® cycling platform was used for qPCR. The reaction mix consisted of SYBR Green premix (Takara, Madison, WI, USA), primers and cDNA template. The primer sequences have been described earlier (Sallinen et al., 2010; Pavlidis et al., 2011). Quantification was done by Ct value comparison, using the Ct value of β-actin as an internal standard (Livak and Schmittgen, 2001). Statistical analysis was done using One-Way ANOVA followed by Tukey's *post-hoc* test.

TYROSINE HYDROXYLASE 1 AND 2, AND HISTIDINE DECARBOXYLASE WHOLE-MOUNT *in situ* HYBRIDIZATION

Antisense digoxigenin (DIG)-labeled RNA probes were synthesized using the DIG RNA labeling kit (Roche Diagnostics, Germany). The clones used have been described previously (Chen et al., 2009; Sundvik et al., 2011). Larvae samples for whole-mount *in situ* hybridization (WISH) were collected after ethanol treatment and fixed in 4% PFA (paraformaldehyde) in PBS overnight. *WISH* was carried out according to the Thisse lab protocol with minor modifications (Thisse and Thisse, 2008). The heads were dissected after fixation in order to expose the brain. All hybridization steps were done at 67°C. The probes were detected using NBT (nitro blue tetrazolium, Roche diagnostics GmBH, Mannheim, Germany)/BCIP (5-bromo 4-chloro 3-indolyl phosphate, Roche diagnostics GmBH, Mannheim, Germany).

TYROSINE HYDROXYLASE AND HISTAMINE IMMUNOHISTOCHEMISTRY

Larvae were collected after ethanol treatment and fixed overnight in 4% EDAC (1-ethyl-3,3(dimethyl-aminopropyl) carbodiimide) and 0.1% PFA in PBS for tyrosine hydroxylase (TH1) and histamine double staining. Samples used only for TH1 staining were fixed in 4% PFA in PBS. The detailed protocol for immunohistochemistry has been described earlier (Sallinen et al., 2009b). For primary antibodies, monoclonal mouse anti-TH1 antibody (Diasorin/Immunostar, lot no. 22941) diluted 1:1000 and polyclonal rabbit anti-Histamine serum [rabbit anti-histamine 19C (Panula et al., 1990)] diluted 1:10000 were used. For detection, the samples were incubated with Alexa-conjugated antibodies (Alexa Anti-Mouse 488 lot no. 898230 and Alexa Anti-Rabbit 568 lot no. 757102, Invitrogen) diluted 1:1000. It should be noted that the TH antibody used only detects TH1 in the zebrafish (Chen et al., 2009).

MICROSCOPY AND IMAGING

In situ hybridization samples were observed under a Leica DM IRB inverted microscope with an attached Leica DFC490 camera. Multifocus images were taken using Leica application suite version 2.7.0 software (Leica Microsystems CMS GmbH, Switzerland).

Immunofluorescent samples were visualized using a Leica SP2 AOBS confocal microscope (Leica Microsystems GmbH, Mannheim, Germany). The images were acquired using a HC PL APO 20×/0.70 CS objective. For detection of the fluorophores, a 488 nm argon laser and a 568 nm diode laser were used. The emission was collected at 500–550 nm for the 488 nm laser and at 600–700 nm for the 568 nm laser. The distance between stack planes was set at approximately 1 μm. The image stacks were imported to Fiji [open source imaging software (Schindelin et al., 2012)] for cell number quantification. Statistical analysis of cell numbers was done using One-Way ANOVA.

NEUROTRANSMITTER MEASUREMENT BY HIGH-PERFORMANCE LIQUID CHROMATOGRAPHY

For analysis of catecholamine levels 15–20 whole larvae were sonicated in 10 volumes of 2% perchloric acid, centrifuged for 30 min at 15,000 g after which 10 μL of filtered supernatant was injected into high-performance liquid chromatography (HPLC) system equipped with a Waters Concorde electrochemical detector set to a potential +0.80 V, column oven and a column Gemini C18 5 μm 150 × 4.60 mm (Phenomenex, Torrance, CA, USA). The mobile phase consisted of purified water with 8% methanol, 50 mM citric acid, 1.5 mM 1-octanesulfonic acid, 0.05 mM EDTA, and 50 mM phosphoric acid. The column temperature was set at 37°C and the flow rate at 1 ml/min. System control, data acquisition and analysis were performed using Waters Empower software (Waters, Milford, MA). Concentrations of the catecholamines and metabolites were calculated from standard curves which were linear from 10 nM to 1 μM. The protocol for histamine measurement has been described earlier (Eriksson et al., 1998). In order to normalize the data, sample protein concentration was measured using the Pierce© BCA Protein Assay Kit (Thermo Fisher Scientific INC., Rockford, IL, USA). The measured concentration was normalized per protein, and the data is reported as percent of the average of the control group. Statistical analysis was done using One-Way ANOVA followed by Tukey's *post hoc* test.

RESULTS

THE EFFECT OF ETHANOL ON SWIMMING BEHAVIOR

We measured the total swimming distance and the mean values for meander, turn angle and angular velocity during the 10-min treatment period (**Figure 1**). The 1.50% ethanol concentration increased the total swimming distance significantly ($p < 0.05$). A 3.00% concentration did not have any effect on the total distance moved. We also observed that the group treated with 1.50% ethanol showed a significant increase in mean angular velocity ($p < 0.001$), while the other treatment concentrations did not have any effect on this parameter. Mean meander and turn angle remained unchanged across all groups, except for a significant yet small change in turn angle observed between the 1.50 and 3.00% groups that was inconsistently observed between trials. We therefore do not find it to be of any relevance (**Figures 1B,D**).

In order to further understand the effect on the total distance moved, we analysed the parameter in 1-min intervals (**Figure 1E**). This revealed that the 3.00% concentration actually had a strong stimulatory effect on locomotion during the first few minutes of the treatment, but this effect subsided quickly and locomotor activity clearly diminished in the group for the remaining duration of the trial [time effect, $F_{(9,\ 1791)} = 75.20$, $p < 0.0001$]. This sedative effect explained why there was no apparent effect on the total distance moved throughout the trial. This sedative effect was not observed for the 0.75 and 1.50% groups. The magnitude of the initial increase in locomotor activity appeared

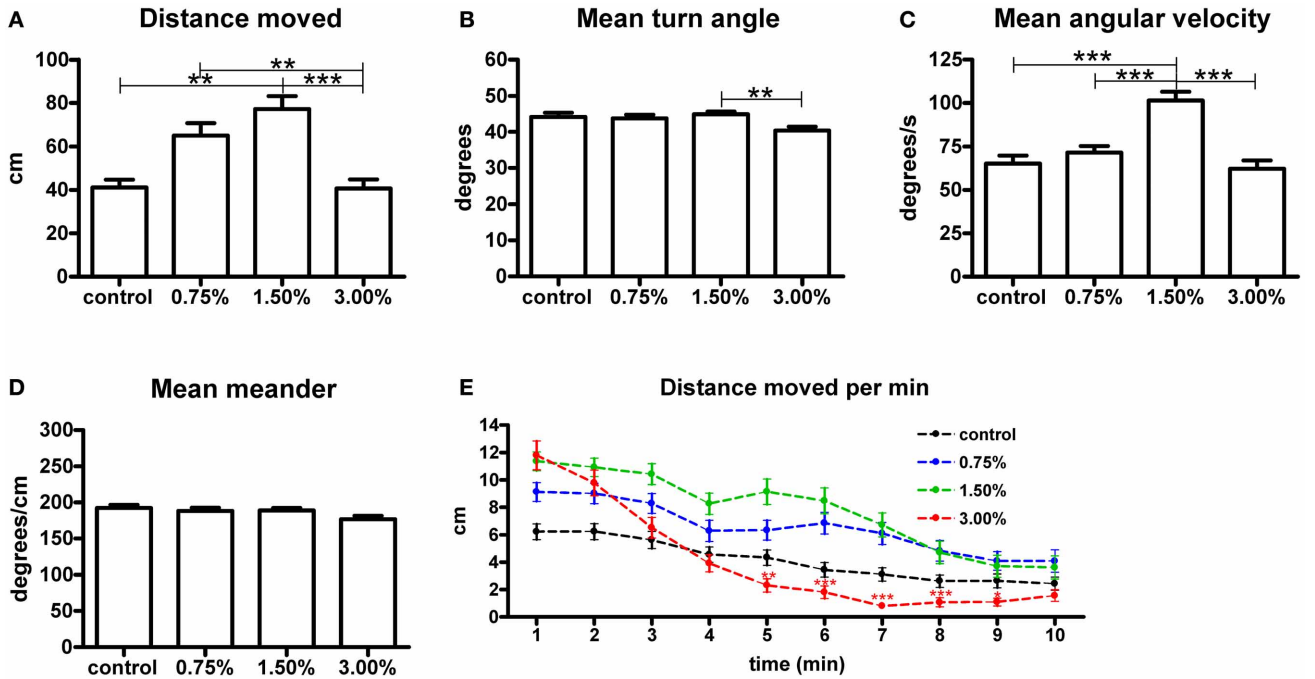

FIGURE 1 | The effect of 0.75%, 1.50% and 3.00% ethanol concentration on locomotion in larval zebrafish during the first 10 minutes after exposure. A significant increase can be seen in the total distance moved **(A)** up to a 1.50% concentration, with a 3.00% concentration having no apparent change on total distance moved [$F_{(3,\ 213)} = 8.304$, $p < 0.0001$]. The angular velocity **(C)** is also significantly altered in the 1.50% group [$F_{(3,\ 213)} = 16.18$, $p < 0.0001$]. We could also see a significant difference in turn angle **(B)** between the 1.50% and 3.00% groups, but this observation was inconsistent across repeats and therefore unlikely to be of any relevance [$F_{(3,\ 213)} = 4.046$, $p = 0.0080$]. No differences are seen in meander **(D)** [$F_{(3,\ 213)} = 2.331$, $p = 0.0753$]. Statistics were done using 1-way ANOVA followed by Tukey's *post-hoc* test, $^{*}p < 0.05$, $^{**}p < 0.01$, $^{***}p < 0.001$. When plotting the data as total distance moved per minute **(E)**, the initial stimulatory effect of the 3.00% concentration can clearly be seen. Both time [$F_{(9,\ 1917)} = 89.02$, $p < 0.0001$] and treatment concentration [$F_{(3,\ 213)} = 5.865$, $p = 0.0007$] had extremely significant effects on the total distance moved. There was also significant interaction between the time and treatment concentration [$F_{(27,\ 1917)} = 4.396$, $p < 0.0001$], but this is mostly attributable to the strong biphasic effect observed for the 3.00% group. Statistics were done using 2-way repeated measures ANOVA followed by Bonferroni's *post-hoc* test. The numbers of larvae in each group were as follows: control: $N = 47$, 0.75%: $N = 56$, 1.50%: $N = 61$, 3.00%: $N = 53$.

to be dose-dependent [treatment effect, $F_{(3,\ 1791)} = 8.21$, $p < 0.0001$].

CHANGES IN TYROSINE HYDROXYLASE 1, TYROSINE HYDROXYLASE 2, AND HISTIDINE DECARBOXYLASE TRANSCRIPT LEVELS

The amount of mRNA for each of the three rate-limiting enzymes in the biosynthesis of dopamine and histamine showed a clear dose-dependent increase trend following exposure to ethanol (**Figure 2**). The zebrafish has two tyrosine hydroxylase isoforms, TH1 and TH2 (Chen et al., 2009). Both *th1* and *th2* mRNA levels were significantly increased by the 3.00% ethanol treatment ($p < 0.05$ for *th1*, $p < 0.01$ for *th2*). The increase in *hdc* mRNA was also significant ($p < 0.01$). These results indicate that ethanol directly or indirectly activates synthesis of the enzymes regulating the synthesis of dopamine and histamine in zebrafish almost immediately following exposure.

IMMUNOHISTOCHEMISTRY AND *in situ* HYBRIDIZATION

We observed no change in the expression pattern of *th1*, *th2*, and *hdc* by *in situ* hybridization in any of the groups after a 10-min treatment (data not shown). These results were supported by immunohistochemistry, which also showed no changes in distribution patterns of TH1- and histamine-immunoreactive cells and fibers (**Figure 3**, data not shown for TH1). This was verified by counting the number of histamine- and TH-immunoreactive cells in the hypothalamus and preoptic group [groups 3 and 4 as defined by Sallinen et al. (2009b)], respectively. No change in cell numbers was seen ($p > 0.05$, **Figure 4**).

In order to determine if a prolonged treatment would alter the morphology of the histaminergic and dopaminergic systems, we repeated the *in situ* hybridization using a 30-min ethanol treatment. For this experiment, only the 1.50% ethanol dose was used, based on the acquired behavioral data. The longer treatment period did not show any difference in the expression patterns of *hdc*, *th1*, and *th2* between the 1.50% group and the control (**Figure 5**, data not shown for *hdc*). Immunohistochemistry also showed that the number and distribution of TH1immunoreactive cells remained unchanged in the preoptic group after the extended ethanol treatment ($p > 0.05$, **Figures 4**, **6**).

CHANGES IN DOPAMINE AND HISTAMINE LEVELS OBSERVED BY HPLC

The higher ethanol concentrations resulted in significantly decreased dopamine levels after a 10-min treatment ($p < 0.05$,

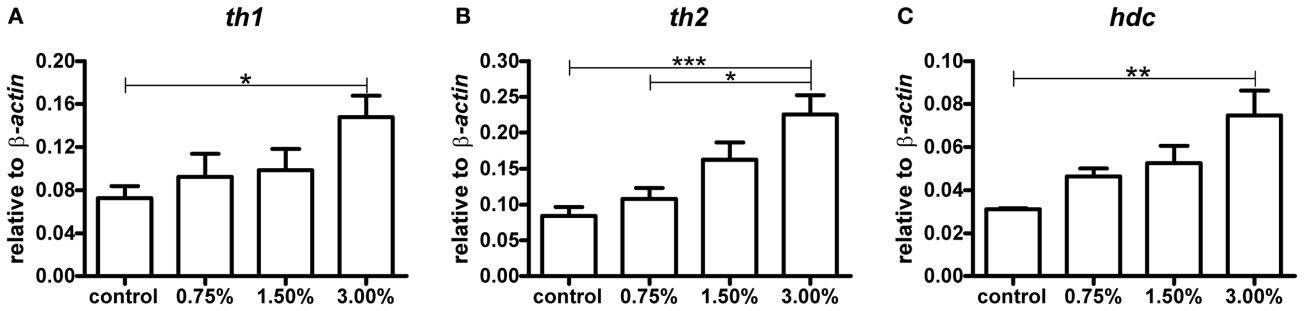

FIGURE 2 | The levels of *th1, th2,* and *hdc* mRNA after a 10-min ethanol treatment. A clear dose-dependent trend can be seen for all mRNA species analysed. Statistical significance was analysed using One-Way ANOVA followed by Tukey's *post-hoc* test. **(A)** $F_{(3,\ 17)} = 3.439$, $P = 0.0405$; **(B)** $F_{(3,\ 17)} = 8.489$, $P = 0.0011$; **(C)** $F_{(3,\ 17)} = 5.515$, $P = 0.0079$, $^{*}p < 0.05$, $^{**}p < 0.01$, $^{***}p < 0.001$ according to the *post-hoc* test. $N = 6$ except for the 0.75% group, for which $N = 3$.

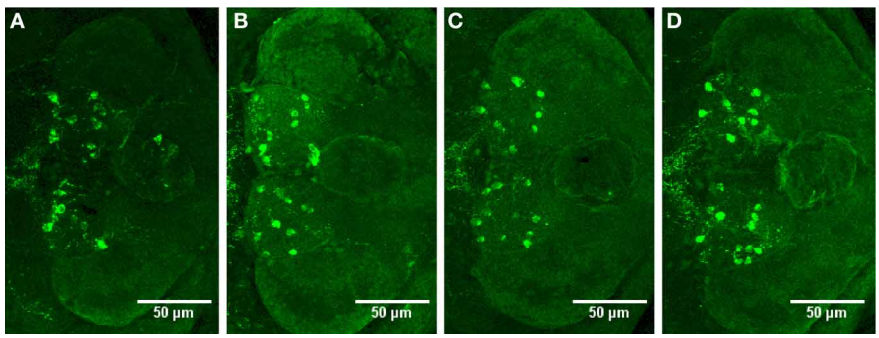

FIGURE 3 | Distribution of histamine-immunoreactive cells after a 10-min ethanol treatment. (A) Control, **(B)** 0.75% ethanol, **(C)** 1.50% ethanol, **(D)** 3.00% ethanol. No changes are seen between the groups, which are further confirmed by cell counting statistics in **Figure 4**. $N = 13$–15 larvae per treatment group.

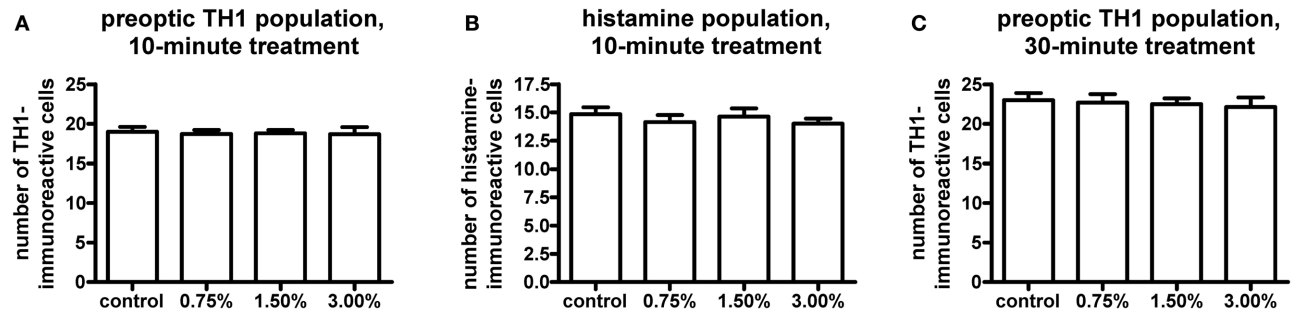

FIGURE 4 | Cell numbers in the histaminergic and preoptic dopaminergic populations after the ethanol treatment. A 10-min ethanol treatment had no effect on either population. In order to see if any change was occurring after a longer treatment, the preoptic dopaminergic population was further analysed after a 30-min treatment. The longer treatment also did not show any changes in cell numbers. Statistical analysis was done using One-Way ANOVA. **(A)** $F_{(3,\ 52)} = 0.05260$, $p = 0.9839$; **(B)** $F_{(3,\ 52)} = 0.4550$, $p = 0.7149$; **(C)** $F_{(3,\ 33)} = 0.1273$, $p = 0.9432$. $N = 13$–15 for the 10-min treatment, $N = 8$–10 for the 30-min treatment.

Figure 7A). Curiously, the 0.75% group did not show a decrease in dopamine. None of the dopamine metabolites analysed [3,4-dihydroxyphenylacetic acid (DOPAC) and homovanillic acid (HVA)] showed any significant changes (**Figures 7B,C**). For the metabolic pathways of dopamine, please refer to **Figure 8**. HVA levels showed a slight dose-dependent decreasing trend, but this observation did not reach statistical significance ($p > 0.05$). The levels of other metabolites remained consistent across all groups. In order to see if the upregulation of *th1* and *th2* observed after a 10-min treatment would counteract the decrease in dopamine observed, we measured the dopamine levels again after a 30-min treatment (**Figure 7F**). At this point, the difference in dopamine

levels observed between the groups was smaller and statistically not significant, indicating that the dopamine loss might indeed be compensated.

Out of other neurotransmitters, histamine, and noradrenaline were measured. Noradrenaline levels were unaffected by the treatment (**Figure 7D**). Only a non-significant decreasing trend in histamine levels ($p > 0.05$) was seen (**Figure 7E**).

DISCUSSION

Our results showed that ethanol concentrations of 0.75 and 1.50% have an acute stimulatory effect on locomotion in larval zebrafish, while a 3.00% concentration resulted in a brief increase in activity, quickly followed by a strong decrease of locomotion. This corresponds well with results obtained from earlier studies (Lockwood et al., 2004; Macphail et al., 2009; De Esch et al., 2012), and shows that the fish strain used here displays a concentration-dependent increase in locomotor activity following exposure to ethanol. Out of these earlier studies, only Lockwood et al. (2004) have analysed the movement activity immediately after administration of ethanol, showing a large difference in the magnitude of the ethanol-induced stimulation between the AB and WIK wild-type strains of zebrafish (Lockwood et al., 2004). Our Turku strain reacted similar to the WIK strain, showing a rather modest increase in locomotor activity. The initial stimulatory effect we observed for the 3.00% treatment could be explained by a similar biphasic effect that was observed in a study with mice (Crabbe et al., 1982), where ethanol doses cause a similar effect for C57BL/6N mice. Another possibility is that the initial response to ethanol would be caused by the presence of an irritating substance. This was, however, also investigated by Lockwood et al. (2004), who showed that a 1.50% methanol treatment had no effect on locomotion (Lockwood et al., 2004). We therefore find it reasonable to interpret the observed stimulation as an effect attributable to the pharmacological properties of ethanol and not as an unspecific reaction to a noxious substance. Our data also suggests that ethanol changes the swimming pattern of larval zebrafish, as shown by the increase in mean angular velocity for the 1.50% group. This might indicate an impairment of motor coordination after a 1.50% ethanol treatment, which is a well-known effect of ethanol (Carta et al., 2004).

The main focus of our study was to characterize the dynamic changes in in key neurotransmitters associated with locomotor activation following ethanol exposure. The stimulatory effect of ethanol is known to be linked to the activation of mesolimbic dopaminergic pathways in mice (Meyer et al., 2009). TH is the rate-limiting enzyme of dopamine synthesis. Zebrafish have two isoforms of TH called TH1 and TH2. The distribution of *th1* and *th2* cells in the zebrafish brain show a complementary pattern, with *th1* being the dominant isoform in the brain (Chen

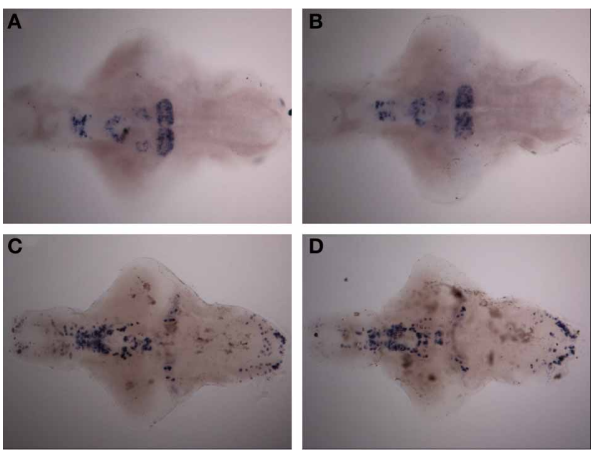

FIGURE 5 | Expression pattern of *th1* and *th2* after a 30-min ethanol treatment. (A) *th2* expression pattern after 30-min of 1.50% ethanol. **(B)** *th2* expression in the control group. **(C)** *th1* expression pattern after 30-min of 1.50% ethanol. **(D)** *th1* expression in the control group. No differences can be seen between the groups. $N = 10$ larvae per treatment group.

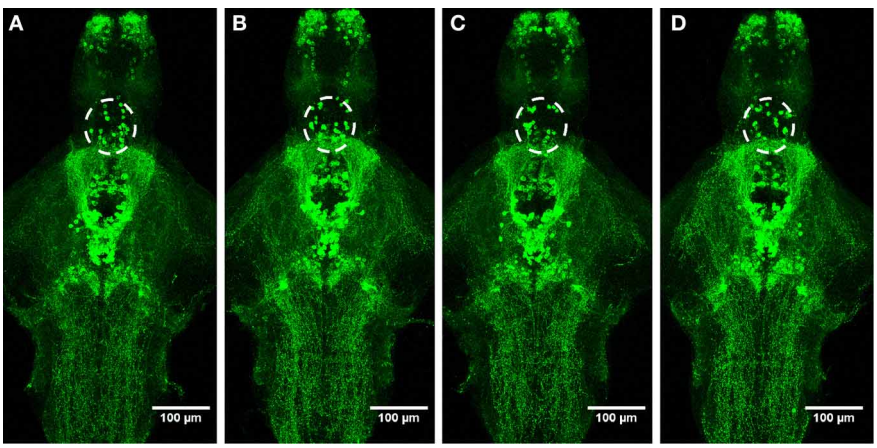

FIGURE 6 | Distribution of TH1-immunoreactive cells and fibers after a 30-min ethanol treatment. (A) Control, **(B)** 0.75% ethanol, **(C)** 1.50% ethanol, **(D)** 3.00% ethanol. No changes are seen between the groups. $N = 8$–10 larvae per treatment group.

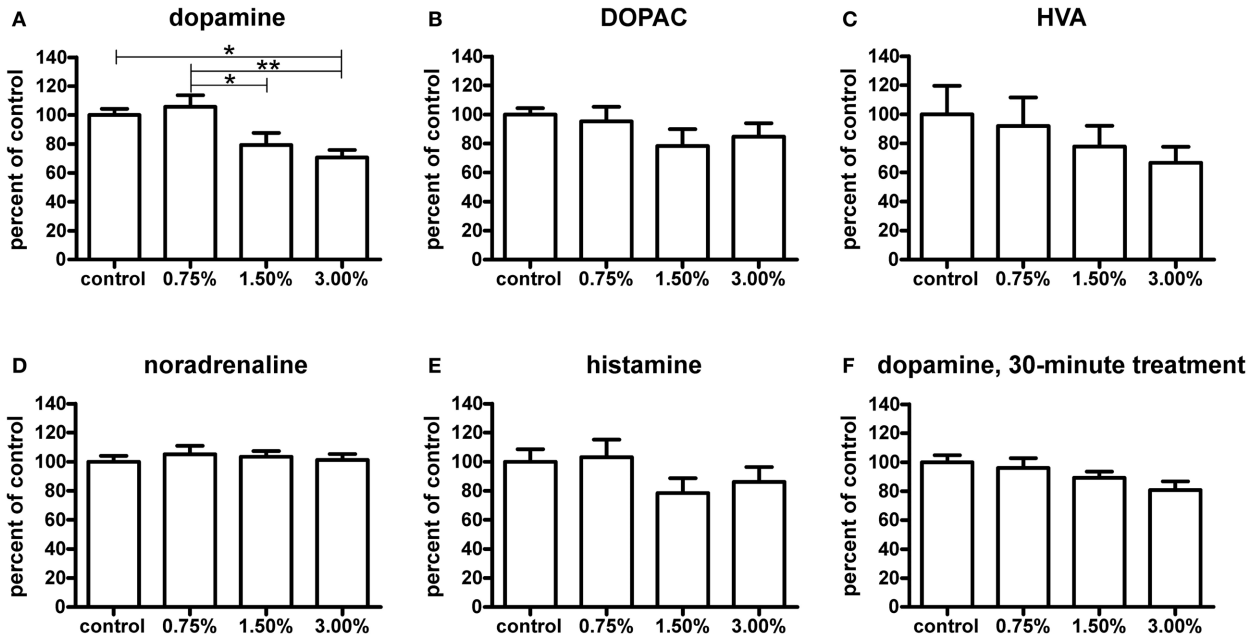

FIGURE 7 | Neurotransmitter levels relative to control group measured by HPLC after a 10-minute ethanol treatment. The dopamine **(A)** levels were significantly decreased with a 1.50% and 3.00% treatment, whereas a 0.75% does not have any visible effect [$F_{(3,\ 24)} = 6.174$, $p = 0.0029$]. The levels of HVA **(C)** show a slight non-significant decreasing trend across treatment groups [$F_{(3,\ 22)} = 0.7453$, $p = 0.5366$], while DOPAC **(B)** levels are unchanged [$F_{(3,\ 24)} = 1.140$, $p = 0.3531$]. Noradrenaline **(D)** and histamine **(E)** levels were not significantly affected [noradrenaline: $F_{(3,\ 24)} = 0.2692$, $p = 0.8470$; histamine: $F_{(3,\ 24)} = 1.246$, $p = 0.3149$], but a slight decrease trend of the histamine levels can be seen in the 1.50% and 3.00% groups. After a 30-minute treatment **(F)**, the observed decrease in dopamine levels was smaller and not significant [$F_{(3,\ 25)} = 2.417$, $p = 0.0901$]. Statistical analysis was done using 1-way ANOVA followed by Tukey's *post-hoc* test. $^{*}p < 0.05$, $^{**}p < 0.01$, according to the *post-hoc* test. $N = 7$, except for the control group and 3.00% group in the HVA data where $N = 6$.

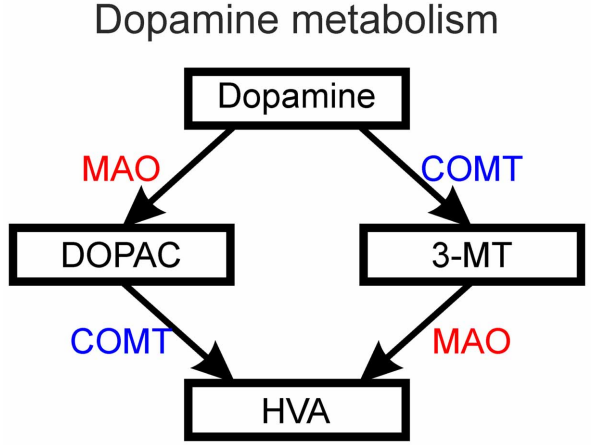

FIGURE 8 | The metabolism of dopamine into DOPAC (3,4-dihydroxyphenylacetic acid) and 3-MT (3-methoxytyramine) followed by metabolism of these intermediate products into HVA (homovanillic acid) by the action of MAO (monoamine oxidase) and COMT (catechol-O-methyltransferase).

et al., 2009). Since an increase in *th2* has been shown to be affected by different states of behavior (Pavlidis et al., 2011), we hypothesized that ethanol might affect either enzyme only. This was, however, not the case, as we saw an increase in transcript numbers of both *th* genes. It would therefore seem that ethanol has a general stimulatory effect on dopamine synthesis in the zebrafish, since these TH forms are expressed in different neuron populations with different projections (Chen et al., 2009). This is also supported by our data obtained by *in situ* hybridization, which showed that the patterns of *th1* and *th2* expression in the brain remained unchanged, and immunohistochemistry, which showed that the number and pattern of TH1-immunoreactive cells remained unaffected.

As different populations of dopaminergic neurons project widely to key areas involved in motor regulation, for instance the subpallium (Rink and Wullimann, 2001; Tay et al., 2011), the nucleus of the medial longitudinal fascicle (McLean and Fetcho, 2004) and even the spinal motor neurons themselves (McLean and Fetcho, 2004), it is of key interest to know if the stimulatory effect of ethanol is mediated by one or several of these systems, or through a diffuse activation of the dopaminergic network. In mammalian models, the activation of locomotion has been strongly linked to effects on the VTA dopaminergic neurons, demonstrating, for instance, increased activation of VTA neurons (Gessa et al., 1985) increased *th* mRNA levels in the VTA (Oliva et al., 2008) and increased dopamine release in VTA target areas (Di Chiara and Imperato, 1986). We were unable to measure the release of dopamine in different brain areas due to the small size of the zebrafish brain, but our data obtained by qPCR, immunohistochemistry and *in situ* hybridization supports the

theory of a diffuse activation of the dopaminergic network, as discussed in the previous section. It should, however, be noted that our analysis on the role of TH2 in this process is incomplete, as we did not have access to a working characterized TH2 antibody during this study. Also, although the activation of the dopaminergic system might be general, this does not directly imply that all possible pathways participating in the stimulation of locomotion are activated. Our results give reason for future studies further investigating this effect. *In situ* hybridization and immunocytochemistry showed that there was no change in cell numbers expressing the *th* transcripts following ethanol. The activation thus occurred in cells which also under control conditions express *th1* or *th2*.

The higher ethanol concentrations seemed to have a decreasing effect on dopamine levels in the zebrafish after a 10-min treatment. The increase in *th1* and *th2* transcription might be a part of a mechanism to increase synthesis of TH and therefore the synthesis of dopamine, which is supported by our data showing no significant differences between treatment groups after a 30-min treatment. A decrease in dopamine also implies that ethanol is stimulating dopamine release, which is a well-known phenomenon in rodents (Di Chiara and Imperato, 1986, 1988). The increase in dopamine release would explain the stimulating effect on locomotion. We were, however, unable to directly demonstrate an increase in dopamine release, as microdialysis is not feasible in larval zebrafish. Although earlier studies with zebrafish have demonstrated an increase in dopamine following an acute ethanol dose (Chatterjee and Gerlai, 2009; Gerlai et al., 2009), these results were obtained using adult zebrafish and lower ethanol treatment doses. Since the pharmacokinetic differences between larval and adult zebrafish have yet to be elucidated, it is difficult to compare our results and results obtained in adult fish. In our study, only the 1.50 and 3.00% ethanol concentrations resulted in a decrease in dopamine levels, while a 0.75% concentration had no significant effect. It is therefore entirely possible that only higher ethanol doses cause dopamine levels to actually decrease, while the increased synthesis implicated by increased *th1* and *th2* transcription compensates the decrease at lower doses. Curiously, we did not see an increase of any of the dopamine metabolites, which would be expected if dopamine levels were decreased due to increased release and metabolism. Instead, we saw that HVA levels actually decreased slightly in a dose-dependent manner. The kinetics of the metabolism of catecholamines in zebrafish is not known, and more research will be necessary in order to explain this change. One might argue that the decrease in dopamine would indicate some kind of acute toxic effect on dopaminergic neurons. We find this to be unlikely, however, as we could not see any change in the expression pattern of *th1* and *th2* or TH1-immunoreactive neurons even after a longer, 30-min ethanol treatment.

Although ethanol treatments of similar concentration have proven to be teratogenic in younger zebrafish (Reimers et al., 2004; Arenzana et al., 2006), there is evidence of changes in the expression of alcohol dehydrogenase 3 (ADH3) during fish development, which implicates possible age-dependent differences in the metabolism and toxicity of ethanol on zebrafish (Dasmahapatra et al., 2001). Internal ethanol concentrations in the 0.75–3.00% range are likely to be lethal in mammals. It was shown by Lockwood et al. that a 20-min treatment of 7-day-old larval zebrafish resulted in internal ethanol concentrations of 25 mM (0.12%) and 71 mM (0.33%) after treatment with 1.5 and 3.0% ethanol solutions, respectively (Lockwood et al., 2004). Internal concentrations around this range have been reported in studies with mice (Nuutinen et al., 2011), and the use of similar ethanol concentrations in other studies with zebrafish (Lockwood et al., 2004; Macphail et al., 2009) further justifies the use of high ethanol concentrations in the treatment solutions.

A novel discovery in our study was that ethanol increased the transcription of HDC, the rate-limiting enzyme of histamine synthesis. Recent studies in mice have demonstrated that histamine indeed is essential in ethanol-induced locomotor activation and also in the associated reward-mechanism (Nuutinen et al., 2010, 2011). Again, the morphology and number of the histaminergic system was unaffected, as verified by *in situ* hybridization and immunohistochemistry, which would support the assumption that the increase is due to an upregulation of the *hdc* gene in cells which express hdc under normal conditions. In zebrafish, the histaminergic neurons show life-long plasticity and there numbers are regulated by presenilin 1 through Notch1 (Sundvik et al., 2013). They are essential in regulation of e.g., dark flash swimming response (Sundvik et al., 2011) and histamine regulates vigilance or anxiety-like behaviors (Peitsaro et al., 2003). Also in rodents activity of histaminergic neurons is linked to increased vigilance and cognitive capacity (Haas and Panula, 2003; Anaclet et al., 2009). Further studies are necessary in order to elucidate the purpose and effects of the increase in *hdc*.

In conclusion, this study shows evidence that an acute ethanol treatment increases locomotor activity with moderate doses of ethanol in larval zebrafish. At high concentration, an acute increase in locomotor activity is associated with a decline in dopamine levels and induction of *th1*, *th2*, and *hdc* without any change in the anatomy of the dopaminergic and histaminergic systems, indicating that ethanol might have a diffuse stimulatory effect on these systems in zebrafish. In addition, this study provides evidence that a 1.50% ethanol concentration causes impairment of motor control in larval zebrafish, as seen by the increase in fish angular velocity. The decline in dopamine levels after a 10-min treatment might result from strongly increased dopamine release followed by upregulation of both *th* forms, resulting in partially normalized dopamine levels after a 30-min treatment. This provides a basis for further study, in order to fully understand the effect of ethanol on the dopaminergic and histaminergic systems in zebrafish.

ACKNOWLEDGMENTS

We thank Henri Koivula, B.Sc., and Susanna Norrbacka, B.Sc., for fish management and expert technical assistance. Supported by the Academy of Finland and Sigrid Juselius Foundation.

REFERENCES

Anaclet, C., Parmentier, R., Ouk, K., Guidon, G., Buda, C., Sastre, J. P., et al. (2009). Orexin/hypocretin and histamine: distinct roles in the control of wakefulness demonstrated using knock-out mouse models. *J. Neurosci.* 29, 14423–14438. doi: 10.1523/JNEUROSCI.2604-09.2009

Arenzana, F. J., Carvan, M. J. 3rd, Aijon, J., Sanchez-Gonzalez, R., Arevalo, R., and Porteros, A. (2006). Teratogenic effects of ethanol exposure on zebrafish visual system development. *Neurotoxicol. Teratol.* 28, 342–348. doi: 10.1016/j.ntt.2006.02.001

Carta, M., Mameli, M., and Valenzuela, C. F. (2004). Alcohol enhances GABAergic transmission to cerebellar granule cells via an increase in Golgi cell excitability. *J. Neurosci.* 24, 3746–3751. doi: 10.1523/JNEUROSCI.0067-04.2004

Chatterjee, D., and Gerlai, R. (2009). High precision liquid chromatography analysis of dopaminergic and serotoninergic responses to acute alcohol exposure in zebrafish. *Behav. Brain Res.* 200, 208–213. doi: 10.1016/j.bbr.2009.01.016

Chen, Y. C., Priyadarshini, M., and Panula, P. (2009). Complementary developmental expression of the two tyrosine hydroxylase transcripts in zebrafish. *Histochem. Cell Biol.* 132, 375–381. doi: 10.1007/s00418-009-0619-8

Cohen, C., Perrault, G., and Sanger, D. J. (1997). Evidence for the involvement of dopamine receptors in ethanol-induced hyperactivity in mice. *Neuropharmacology* 36, 1099–1108. doi: 10.1016/s0028-3908(97)00100-7

Crabbe, J. C. Jr., Johnson, N. A., Gray, D. K., Kosobud, A., and Young, E. R. (1982). Biphasic effects of ethanol on open-field activity: sensitivity and tolerance in C57BL/6N and DBA/2N mice. *J. Comp. Physiol. Psychol.* 96, 440–451. doi: 10.1037/h0077898

Dasmahapatra, A. K., Doucet, H. L., Bhattacharyya, C., and Carvan, M. J. 3rd. (2001). Developmental expression of alcohol dehydrogenase (ADH3) in zebrafish (Danio rerio). *Biochem. Biophys. Res. Commun.* 286, 1082–1086. doi: 10.1006/bbrc.2001.5511

De Esch, C., Van Der Linde, H., Slieker, R., Willemsen, R., Wolterbeek, A., Woutersen, R., et al. (2012). Locomotor activity assay in zebrafish larvae: influence of age, strain and ethanol. *Neurotoxicol. Teratol.* 34, 425–433. doi: 10.1016/j.ntt.2012.03.002

Di Chiara, G., and Imperato, A. (1986). Preferential stimulation of dopamine release in the nucleus accumbens by opiates, alcohol, and barbiturates: studies with transcerebral dialysis in freely moving rats. *Ann. N.Y. Acad. Sci.* 473, 367–381. doi: 10.1111/j.1749-6632.1986.tb23629.x

Di Chiara, G., and Imperato, A. (1988). Drugs abused by humans preferentially increase synaptic dopamine concentrations in the mesolimbic system of freely moving rats. *Proc. Natl. Acad. Sci. U.S.A.* 85, 5274–5278. doi: 10.1073/pnas.85.14.5274

Eriksson, K. S., Peitsaro, N., Karlstedt, K., Kaslin, J., and Panula, P. (1998). Development of the histaminergic neurons and expression of histidine decarboxylase mRNA in the zebrafish brain in the absence of all peripheral histaminergic systems. *Eur. J. Neurosci.* 10, 3799–3812. doi: 10.1046/j.1460-9568.1998.00394.x

Farrar, A. M., Segovia, K. N., Randall, P. A., Nunes, E. J., Collins, L. E., Stopper, C. M., et al. (2010). Nucleus accumbens and effort-related functions: behavioral and neural markers of the interactions between adenosine A2A and dopamine D2 receptors. *Neuroscience* 166, 1056–1067. doi: 10.1016/j.neuroscience.2009.12.056

Gerlai, R., Chatterjee, D., Pereira, T., Sawashima, T., and Krishnannair, R. (2009). Acute and chronic alcohol dose: population differences in behavior and neurochemistry of zebrafish. *Genes Brain Behav.* 8, 586–599. doi: 10.1111/j.1601-183X.2009.00488.x

Gerlai, R., Lahav, M., Guo, S., and Rosenthal, A. (2000). Drinks like a fish: zebra fish (*Danio rerio*) as a behavior genetic model to study alcohol effects. *Pharmacol. Biochem. Behav.* 67, 773–782. doi: 10.1016/S0091-3057(00)00422-6

Gessa, G. L., Muntoni, F., Collu, M., Vargiu, L., and Mereu, G. (1985). Low doses of ethanol activate dopaminergic neurons in the ventral tegmental area. *Brain Res.* 348, 201–203. doi: 10.1016/0006-8993(85)90381-6

Haas, H., and Panula, P. (2003). The role of histamine and the tuberomamillary nucleus in the nervous system. *Nat. Rev. Neurosci.* 4, 121–130. doi: 10.1038/nrn1034

Irons, T. D., Macphail, R. C., Hunter, D. L., and Padilla, S. (2010). Acute neuroactive drug exposures alter locomotor activity in larval zebrafish. *Neurotoxicol. Teratol.* 32, 84–90. doi: 10.1016/j.ntt.2009.04.066

Kashem, M. A., Ahmed, S., Sarker, R., Ahmed, E. U., Hargreaves, G. A., and McGregor, I. S. (2012). Long-term daily access to alcohol alters dopamine-related synthesis and signaling proteins in the rat striatum. *Neurochem. Int.* 61, 1280–1288. doi: 10.1016/j.neuint.2012.08.013

Kaslin, J., and Panula, P. (2001). Comparative anatomy of the histaminergic and other aminergic systems in zebrafish (*Danio rerio*). *J. Comp. Neurol.* 440, 342–377. doi: 10.1002/cne.1390

Kelly, P. H., Seviour, P. W., and Iversen, S. D. (1975). Amphetamine and apomorphine responses in the rat following 6-OHDA lesions of the nucleus accumbens septi and corpus striatum. *Brain Res.* 94, 507–522. doi: 10.1016/0006-8993(75)90233-4

Kily, L. J., Cowe, Y. C., Hussain, O., Patel, S., McElwaine, S., Cotter, F. E., et al. (2008). Gene expression changes in a zebrafish model of drug dependency suggest conservation of neuro-adaptation pathways. *J. Exp. Biol.* 211, 1623–1634. doi: 10.1242/jeb.014399

Lee, Y. K., Park, S. W., Kim, Y. K., Kim, D. J., Jeong, J., Myrick, H., et al. (2005). Effects of naltrexone on the ethanol-induced changes in the rat central dopaminergic system. *Alcohol Alcohol.* 40, 297–301. doi: 10.1093/alcalc/agh163

Lintunen, M., Raatesalmi, K., Sallmen, T., Anichtchik, O., Karlstedt, K., Kaslin, J., et al. (2002). Low brain histamine content affects ethanol-induced motor impairment. *Neurobiol. Dis.* 9, 94–105. doi: 10.1006/nbdi.2001.0453

Livak, K. J., and Schmittgen, T. D. (2001). Analysis of relative gene expression data using real-time quantitative PCR and the 2(-Delta Delta C(T)) Method. *Methods* 25, 402–408. doi: 10.1006/meth.2001.1262

Lockwood, B., Bjerke, S., Kobayashi, K., and Guo, S. (2004). Acute effects of alcohol on larval zebrafish: a genetic system for large-scale screening. *Pharmacol. Biochem. Behav.* 77, 647–654. doi: 10.1016/j.pbb.2004.01.003

Macphail, R. C., Brooks, J., Hunter, D. L., Padnos, B., Irons, T. D., and Padilla, S. (2009). Locomotion in larval zebrafish: influence of time of day, lighting and ethanol. *Neurotoxicology* 30, 52–58. doi: 10.1016/j.neuro.2008.09.011

Mathur, P., Berberoglu, M. A., and Guo, S. (2011). Preference for ethanol in zebrafish following a single exposure. *Behav. Brain Res.* 217, 128–133. doi: 10.1016/j.bbr.2010.10.015

McLean, D. L., and Fetcho, J. R. (2004). Relationship of tyrosine hydroxylase and serotonin immunoreactivity to sensorimotor circuitry in larval zebrafish. *J. Comp. Neurol.* 480, 57–71. doi: 10.1002/cne.20281

Meyer, P. J., Meshul, C. K., and Phillips, T. J. (2009). Ethanol- and cocaine-induced locomotion are genetically related to increases in accumbal dopamine. *Genes Brain Behav.* 8, 346–355. doi: 10.1111/j.1601-183X.2009.00481.x

Mogenson, G. J., Jones, D. L., and Yim, C. Y. (1980). From motivation to action: functional interface between the limbic system and the motor system. *Prog. Neurobiol.* 14, 69–97. doi: 10.1016/0301-0082(80)90018-0

Navarrete, F., Rubio, G., and Manzanares, J. (2013). Effects of naltrexone plus topiramate on ethanol self-administration and tyrosine hydroxylase gene expression changes. *Addict. Biol.* doi: 10.1111/adb.12058. [Epub ahead of print].

Nuutinen, S., Karlstedt, K., Aitta-Aho, T., Korpi, E. R., and Panula, P. (2010). Histamine and H3 receptor-dependent mechanisms regulate ethanol stimulation and conditioned place preference in mice. *Psychopharmacology* 208, 75–86. doi: 10.1007/s00213-009-1710-5

Nuutinen, S., Lintunen, M., Vanhanen, J., Ojala, T., Rozov, S., and Panula, P. (2011). Evidence for the role of histamine H3 receptor in alcohol consumption and alcohol reward in mice. *Neuropsychopharmacology* 36, 2030–2040. doi: 10.1038/npp.2011.90

Oliva, J. M., Ortiz, S., Perez-Rial, S., and Manzanares, J. (2008). Time dependent alterations on tyrosine hydroxylase, opioid and cannabinoid CB1 receptor gene expressions after acute ethanol administration in the rat brain. *Eur. Neuropsychopharmacol.* 18, 373–382. doi: 10.1016/j.euroneuro.2007.09.001

Panula, P., Airaksinen, M. S., Pirvola, U., and Kotilainen, E. (1990). A histamine-containing neuronal system in human brain. *Neuroscience* 34, 127–132. doi: 10.1016/0306-4522(90)90307-P

Papanicolaou, J., and Fennessy, M. R. (1980). The acute effect of ethanol on behaviour, body temperature, and brain histamine in mice. *Psychopharmacology* 72, 73–77. doi: 10.1007/BF00433809

Pavlidis, M., Sundvik, M., Chen, Y. C., and Panula, P. (2011).

Adaptive changes in zebrafish brain in dominant-subordinate behavioral context. *Behav. Brain Res.* 225, 529–537. doi: 10.1016/j.bbr.2011.08.022

Peitsaro, N., Kaslin, J., Anichtchik, O. V., and Panula, P. (2003). Modulation of the histaminergic system and behaviour by alpha-fluoromethylhistidine in zebrafish. *J. Neurochem.* 86, 432–441. doi: 10.1046/j.1471-4159.2003.01850.x

Peitsaro, N., Sundvik, M., Anichtchik, O. V., Kaslin, J., and Panula, P. (2007). Identification of zebrafish histamine H1, H2 and H3 receptors and effects of histaminergic ligands on behavior. *Biochem. Pharmacol.* 73, 1205–1214. doi: 10.1016/j.bcp.2007.01.014

Rawat, A. K. (1980). Development of histaminergic pathways in brain as influenced by maternal alcoholism. *Res. Commun. Chem. Pathol. Pharmacol.* 27, 91–103.

Reimers, M. J., Flockton, A. R., and Tanguay, R. L. (2004). Ethanol- and acetaldehyde-mediated developmental toxicity in zebrafish. *Neurotoxicol. Teratol.* 26, 769–781. doi: 10.1016/j.ntt.2004.06.012

Rink, E., and Wullimann, M. F. (2001). The teleostean (zebrafish) dopaminergic system ascending to the subpallium (striatum) is located in the basal diencephalon (posterior tuberculum). *Brain Res.* 889, 316–330. doi: 10.1016/S0006-8993(00)03174-7

Sallinen, V., Kolehmainen, J., Priyadarshini, M., Toleikyte, G., Chen, Y. C., and Panula, P. (2010). Dopaminergic cell damage and vulnerability to MPTP in Pink1 knockdown zebrafish. *Neurobiol. Dis.* 40, 93–101. doi: 10.1016/j.nbd.2010.06.001

Sallinen, V., Sundvik, M., Reenila, I., Peitsaro, N., Khrustalyov, D., Anichtchik, O., et al. (2009a). Hyperserotonergic phenotype after monoamine oxidase inhibition in larval zebrafish. *J. Neurochem.* 109, 403–415. doi: 10.1111/j.1471-4159.2009.05986.x

Sallinen, V., Torkko, V., Sundvik, M., Reenila, I., Khrustalyov, D., Kaslin, J., et al. (2009b). MPTP and MPP+ target specific aminergic cell populations in larval zebrafish. *J. Neurochem.* 108, 719–731. doi: 10.1111/j.1471-4159.2008.05793.x

Schindelin, J., Arganda-Carreras, I., Frise, E., Kaynig, V., Longair, M., Pietzsch, T., et al. (2012). Fiji: an open-source platform for biological-image analysis. *Nat. Methods* 9, 676–682. doi: 10.1038/nmeth.2019

Subramanian, N., Mitznegg, P., and Estler, C. J. (1978). Ethanol-induced alterations in histamine content and release in the rat hypothalamus. *Naunyn Schmiedebergs Arch. Pharmacol.* 302, 119–121. doi: 10.1007/BF00586607

Sundvik, M., Chen, Y. C., and Panula, P. (2013). Presenilin1 regulates histamine neuron development and behavior in zebrafish, danio rerio. *J. Neurosci.* 33, 1589–1597. doi: 10.1523/JNEUROSCI.1802-12.2013

Sundvik, M., Kudo, H., Toivonen, P., Rozov, S., Chen, Y. C., and Panula, P. (2011). The histaminergic system regulates wakefulness and orexin/hypocretin neuron development via histamine receptor H1 in zebrafish. *FASEB J.* 25, 4338–4347. doi: 10.1096/fj.11-188268

Tang, A., George, M. A., Randall, J. A., and Gonzales, R. A. (2003). Ethanol increases extracellular dopamine concentration in the ventral striatum in C57BL/6 mice. *Alcohol Clin. Exp. Res.* 27, 1083–1089. doi: 10.1097/01.ALC.0000075825.14331.65

Tay, T. L., Ronneberger, O., Ryu, S., Nitschke, R., and Driever, W. (2011). Comprehensive catecholaminergic projectome analysis reveals single-neuron integration of zebrafish ascending and descending dopaminergic systems. *Nat. Commun.* 2, 171. doi: 10.1038/ncomms1171

Thisse, C., and Thisse, B. (2008). High-resolution *in situ* hybridization to whole-mount zebrafish embryos. *Nat. Protoc.* 3, 59–69. doi: 10.1038/nprot.2007.514

Westerfield, M. (2000). "The zebrafish book," in *A Guide for the Laboratory Use of Zebrafish (Danio rerio)*. Eugene, OR: University of Oregon Press. Available online at: http://zfin.org/zf_info/zfbook/zfbk.html

Yoshimoto, K., McBride, W. J., Lumeng, L., and Li, T. K. (1992). Alcohol stimulates the release of dopamine and serotonin in the nucleus accumbens. *Alcohol* 9, 17–22. doi: 10.1016/0741-8329(92)90004-T

Conflict of Interest Statement: The authors declare that the research was conducted in the absence of any commercial or financial relationships that could be construed as a potential conflict of interest.

Received: 13 February 2013; accepted: 10 May 2013; published online: 31 May 2013.

Citation: Puttonen HAJ, Sundvik M, Rozov S, Chen Y-C and Panula P (2013) Acute ethanol treatment upregulates th1, th2, and hdc in larval zebrafish in stable networks. Front. Neural Circuits 7:102. doi: 10.3389/fncir.2013.00102

frontiers in
NEURAL CIRCUITS

METHODS ARTICLE
published: 06 May 2013
doi: 10.3389/fncir.2013.00082

Optogenetic elevation of endogenous glucocorticoid level in larval zebrafish

Rodrigo J. De Marco*, Antonia H. Groneberg, Chen-Min Yeh, Luis A. Castillo Ramírez and Soojin Ryu*

Developmental Genetics of the Nervous System, Max Planck Institute for Medical Research, Heidelberg, Germany

Edited by:
German Sumbre, Ecole Normale Superieure, France

Reviewed by:
Herwig Baier, Max Planck Institute of Neurobiology, Germany
German Sumbre, Ecole Normale Superieure, France
Akira Muto, National Institute of Genetics, Japan

****Correspondence:***
Rodrigo J. De Marco and Soojin Ryu, Developmental Genetics of the Nervous System, Max Planck Institute for Medical Research, Jahnstrasse 29, Heidelberg 69120, Germany.
e-mail: rodrigo.de.marco@mpimf-heidelberg.mpg.de; soojin.ryu@mpimf-heidelberg.mpg.de

The stress response is a suite of physiological and behavioral processes that help to maintain or reestablish homeostasis. Central to the stress response is the hypothalamic-pituitary-adrenal (HPA) axis, as it releases crucial hormones in response to stress. Glucocorticoids (GCs) are the final effector hormones of the HPA axis, and exert a variety of actions under both basal and stress conditions. Despite their far-reaching importance for health, specific GC effects have been difficult to pin-down due to a lack of methods for selectively manipulating endogenous GC levels. Hence, in order to study stress-induced GC effects, we developed a novel optogenetic approach to selectively manipulate the rise of GCs triggered by stress. Using this approach, we could induce both transient hypercortisolic states and persistent forms of hypercortisolaemia in freely behaving larval zebrafish. Our results also established that transient hypercortisolism leads to enhanced locomotion shortly after stressor exposure. Altogether, we present a highly specific method for manipulating the gain of the stress axis with high temporal accuracy, altering endocrine and behavioral responses to stress as well as basal GC levels. Our study offers a powerful tool for the analysis of rapid (non-genomic) and delayed (genomic) GC effects on brain function and behavior, feedbacks within the stress axis and developmental programming by GCs.

Keywords: glucocorticoids, stress response, HPA axis, optogenetics, larval zebrafish

INTRODUCTION

Living organisms respond to stress by activating a complex repertoire of tightly regulated processes. These processes aim to preserve homeostasis and are collectively referred to as the stress response (Selye, 1956; Chrousos, 1998). Evolving adaptive responses to stress is essential for survival. However, dysfunctional stress responses can have devastating consequences for health and have been associated with a number of disorders, ranging from heart and vascular problems to depression, schizophrenia, and affective disorders (Holsboer et al., 1984; Nemeroff et al., 1984; Raber, 1998; De Kloet et al., 2005; McEwen, 2008; Yehuda, 2009). Despite their significance, the development of appropriate stress responsiveness and the mechanisms underlying stress response dysfunction remain largely unknown.

The stress response is mediated by the sympathetic nervous system and the hypothalamic-pituitary-adrenal (HPA) axis. While the sympathetic nervous system is responsible for the so called immediate "fight-or-flight" reactions, the HPA axis regulates both rapid and long-term stress effects (Charmandari et al., 2005). At the core of the HPA axis are corticotropin-releasing-hormone (CRH) and arginine vasopressin (AVP)-expressing neurons in the paraventricular nucleus (PVN) of the rostral hypothalamus, which respond to stress by triggering the release of adrenocorticotrophin hormone (ACTH) from the anterior pituitary. ACTH then stimulates glucocorticoid secretion from the adrenal glands. Glucocorticoids (GCs) are thus the final effectors of the HPA axis, with numerous targets both in the central nervous system and the periphery (Sapolsky et al., 2000).

GCs are known to influence brain function through genomic mechanisms via binding to two ligand-driven transcription factors, the high affinity mineralocorticoid receptor (MR) and the low affinity glucocorticoid receptor (GR), which contribute to delayed GC effects by regulating gene expression (De Kloet et al., 1998). Non-genomic GC effects on neuronal responses and behavior have also been reported, although the mechanisms underlying these rapid effects remain largely unknown (Dallman, 2005; Evanson et al., 2010; Groeneweg et al., 2011). It also remains unknown how non-genomic and genomic GC actions interact with each other to coordinate the activation and inhibition of different processes in multiple brain areas.

The analysis of GC effects under stress, particularly the rapid, non-genomic GC actions, has been hampered by the fact that GC release is tightly couple to that of other hormones. Also, GCs regulate vital functions under non-stress conditions, such as cell proliferation (Dickmeis and Foulkes, 2011). Therefore, elevating GC level is not sufficient to address the role of GCs under stress. It becomes necessary to specifically alter GCs levels under stressful situations triggered by stimuli of known intensity and endocrine effects. Current methods for altering GC levels entail either exposure to stressors or infusions of exogenous GCs. These methods are limited, however. Stressor exposure fails to selectively alter the rate of GC change, as it increases GC levels only via the stimulation of other stress hormones. GC infusion is not straightforward

and can be stressful in itself, making it difficult to assess the impact of the treatment. To advance the analysis of stress correlates in the brain, it is paramount to examine GC actions as a function of time with increased specificity and temporal accuracy.

Because the stress response is conserved across phyla, zebrafish, *Danio rerio*, can aid in dissecting the complexity of GC actions. The zebrafish hypothalamic-pituitary-interrenal (HPI) axis shares key similarities with the HPA axis, with cortisol being the main circulating glucocorticoid in both humans and teleosts (Wendelaar Bonga, 1997; Flik et al., 2006). The preoptic nucleus in teleosts is considered a structure homologous to the mammalian PVN (Peter, 1977; Forlano and Cone, 2007). Adult zebrafish show increased cortisol levels and behavioral stress reactions upon stressor exposure (Ramsay et al., 2006, 2009; Speedie and Gerlai, 2008; Egan et al., 2009; Cachat et al., 2010; Steenbergen et al., 2011). Larval zebrafish also respond to stressors with increased cortisol levels (Alsop and Vijayan, 2008; Alderman and Bernier, 2009; Fuzzen et al., 2010; Clark et al., 2011; Steenbergen et al., 2011). Further, both their basal cortisol levels and expression levels of genes involved in corticosteroid synthesis and signaling increase drastically around the time of hatching, uncovering a stress response system that matures early in development (Alsop and Vijayan, 2008; Alderman and Bernier, 2009). Also importantly, interactions of GRs and serotonin signaling are conserved in zebrafish (Griffiths et al., 2012; Ziv et al., 2012).

In this report, we present a novel protocol for studying stress-induced GC effects. We used larval zebrafish to develop an optogenetic approach aimed at increasing the gain of the stress axis, so as to achieve different levels of endogenous GCs in response to a similarly stressful event. To this end, we expressed photoactivated adenylyl cyclase (bPAC) (Ryu et al., 2010; Stierl et al., 2011) specifically in pituitary cells, which govern GC secretion via ACTH release. Using light as a stressor as well as a source of stimulation for optogenetic control, we could induce both transient and persistent states of hypercortisolaemia in a highly controlled fashion. Importantly, optogenetically elevated GCs also enhanced locomotion shortly after stressor exposure, in line with the fact that stress mobilizes energy via GC signaling (Sapolsky et al., 2000). Our work established a powerful approach to modify the gain of the stress axis, making it possible to examine stress-dependent GC effects with high specificity and temporal accuracy. It provides a valuable tool for the analysis of rapid and delayed GC actions, interactions within the stress axis and feedbacks regulating endocrine and behavioral responses to stress.

MATERIALS AND METHODS

GENERATION OF TRANSGENIC ZEBRAFISH

cDNA encoding myc-tagged bPAC from the soil bacterium *Beggiatoa* bPAC (Stierl et al., 2011) was PCR amplified with a mutated stop-codon and cloned into a vector containing a viral 2A sequence (Tang et al., 2009) and a fluorescent tdTomato marker flanked by I-SceI and Tol2 transposon recognition sites in the pBR322 backbone. This construct was combined with a fragment of the Pomc promoter, which was PCR amplified from a Pomc-GFP construct (Liu et al., 2003). The Pomc:bPAC-2A-tdTomato plasmid was incubated with 100 ng Tol2 transposase RNA for 10 min and injected in the presence of 0.05% phenol red into wild-type embryos (cross of AB and TL strains) in the one-cell stage. For further propagation of the transgenic line, we selected one founder, *Tg(Pomc:bPAC-2A-tdTomato)hd10*, with specific tdTomato expression in the pituitary and no ectopic expression.

ZEBRAFISH HUSBANDRY

Zebrafish breeding and maintenance was performed under standard conditions (Westerfield, 2000). Embryos were collected in the morning and raised on a 12:12 light/dark cycle in E2 medium (Westerfield, 2000). *Tg(Pomc:bPAC-2A-tdTomato)hd10* were crossed with wild-type fish and their progenies selected for the presence of tdTomato expression in the pituitary at 4 or 5 days post fertilization (dpf) using a fluorescent dissecting microscope. To avoid unspecific activation of bPAC prior to the experiments, transgenic embryos were raised in custom-made reflective containers covered by 550 nm long-pass filters (Thorlabs). Zebrafish experimental procedures were performed according to the guidelines of the German animal welfare law and approved by the local government.

cAMP MEASURE

50 pg capped *bPAC* RNA was prepared using a commercial mRNA kit (mMessage T7 Ultra Kit, Ambion) and injected into one-cell-stage wild-type embryos. Embryos were maintained under filtered light (see above) and subjected to blue-light stimulation at 1 dpf using the stimulation protocol described below (light power: 2.8 $mW*cm^{-2}$). Groups of 27 embryos were collected immediately after the light-offset and homogenized in 0.1 M HCl on ice. After centrifugation, the supernatant was stored at −20°C. cAMP level was measured following the acetylation protocol from a cAMP ELISA kit (Enzo Life Sciences). Samples from light-stimulated *bPAC*-injected embryos were diluted 15 times in order to obtain values within the standard range.

IMMUNOHISTOCHEMISTRY

6 dpf larvae were fixed overnight at 4°C in 4% paraformaldehyde (PFA) in phosphate-buffered saline (PBS). Immunohistochemistry was performed as previously described (Ryu et al., 2007), using either polyclonal antibody against human ACTH (National Hormone and Peptide Program, National Institute of Diabetes and Digestive and Kidney Diseases, 1:500) or rabbit polyclonal antibody against Myc-Tag (Cell Signaling Technology, 1:500) as primary antibodies, and Alexa Fluor 488 anti-rabbit (Invitrogen, 1:1000) as a secondary antibody. Detection of residual tdTomato fluorescence after the fixation did not require immunohistochemistry. Larvae were imaged in 80% glycerol using a Nikon 20x glycerol objective and a Leica SP5 CLSM. Confocal image stacks were subsequently evaluated using Amira 5.4 (Visualization Sciences Group) to create maximum intensity projections.

CORTISOL ELISA

For cortisol detection, groups of 30 larvae (6 dpf) were immobilized in ice water, frozen in ethanol/dry ice bath, and

stored at −20°C. Cortisol from homogenized samples was extracted with ethyl acetate. We employed a home-made cortisol ELISA protocol (C. M. Yeh, M. Glöck, R. J. De Marco, S. Ryu, unpublished data), using cortisol mouse antibody (EastCoast Bio), cortisol standards (Hydrocortisone, Sigma-Aldrich) and cortisol-HRP (EastCoast Bio). The reactions were stopped using 1M sulfuric acid and read at 450 nm in an ELISA reader (Multiskan Ascent, Thermo Scientific). The data were corrected for dilution factor, extraction efficiency, and recovery function. In all experiments, cortisol samples were taken 2 min after the offset of light, unless otherwise stated.

MIFEPRISTONE INCUBATION

6 dpf larvae were incubated for 2 h in 1 μM Mifepristone (RU-486, Sigma-Aldrich) dissolved in E2-Medium with 0.1% DMSO. This concentration has been shown to abolish a genomic GC response signal (Weger et al., 2012). During light stimulation, larvae were maintained in the Mifepristone solution to avoid further handling.

LIGHT STIMULATION

A custom-made LED ring was placed at a fixed distance above a mutiwell plate (for behavioral testing) or a single container (for cortisol extraction). The incident angle of the LEDs allowed for homogeneous illumination of the samples. We used custom-made drivers, pulse generators and a TTL control box (USB-IO box, Noldus) to control the LEDs. Larvae were exposed for 18 s or 180 s to either blue- or yellow-light of varying power, using single or multiple stimulation protocols. Each light pulse consisted of 100 ms flashes delivered at 5 Hz. Light power was measured using a hand-held light power meter (Newport). For the multiple stimulation protocol, we used three light pulses delivered with an inter-trial interval of 30 min.

EARLY LIGHT STIMULATION

To facilitate light stimulation with a higher throughput, we arranged LEDs so as to homogeneously illuminate a six well plate with a light power of 0.6 mW^*cm^{-2}. At 4 dpf, we exposed the bPAC-positive ($bPAC^+$) larvae and their negative siblings ($bPAC^-$) to the above described multiple stimulation protocol. Next, the larvae were placed back in the incubator and kept in E2 medium inside the reflective containers covered by the 550 nm long-pass filters. We repeated this procedure 24 h later. At the end of 5 dpf, we screened the larvae for tdTomato expression in the pituitary. At 6 dpf, both the $bPAC^+$ and $bPAC^-$ larvae subjected to the above protocol were either directly collected for measuring basal cortisol levels or first stimulated with a single 180 s squared pulse of blue-light (0.6 mW^*cm^{-2}) and then collected for measuring light-induced cortisol change. Control animals for each group were handled in the same fashion, but omitting the light stimulation at 4 and 5 dpf. Stimulations were performed within a fixed 3 h window during the larvae's day time.

BEHAVIORAL TESTING

Behavioral tests were performed using wild-type, $bPAC^+$ and $bPAC^-$ 6 dpf larvae. Experiments were conducted under infrared (IR) light, delivered through an array of IR-LEDs mounted inside a custom-made light-proof enclosure placed on a vibration-free platform (Newport). We used an infrared-sensitive camera (ICD-49E B/W, Ikegami Tsushinki) to image the movements of the swimming larvae at 25 frames s^{-1}. The lens of the camera (TV Lens, Computer VARI FOCAL H3Z4512 CS-IR, CBC) was surrounded by a custom-made LED ring and positioned above a multiwell plate (Greiner-Bio One). We used EthoVision XT software (Noldus Information Technology) to simultaneously track the movements of 30 larvae swimming individually inside the wells in 50 μL of E2 medium. In all experiments, the larvae were allowed to adjust to the test conditions for 15 min prior to the recordings. Experiments were conducted at room temperature. We continuously monitored the temperature inside a reference well using a thermocouple (npi electronics) connected to a temperature control system (PTC 20, npi electronics; Exos-2 V2 liquid cooling system, Koolance). All the experiments were performed in a blind fashion using unscreened larvae to avoid effects of pre-handling and exposure to unfiltered light. Tests were conducted between 9:00 and 18:00 and the different experimental groups intermixed throughout the day.

STATISTICAL ANALYSIS

All data are shown as mean and standard error of the mean (S.E.M.). To facilitate comparison, locomotor activity is expressed either as distance swam per unit of time (**Figures 2A–C**) or as percentual motion relative to pre-stimulation baseline levels (**Figures 5A–C**), as these levels did not differ between $bPAC^+$ and $bPAC^-$ larvae (Mann–Whitney test, $p = 0.11$). We used Student's *t*-tests (two-tailed) for two-group comparisons, or Mann–Whitney *U*-tests if the data did not fulfill the assumptions of the *t*-test. ANOVAs were used for multiple group comparisons, followed by Bonferroni's *post-hoc* tests, or their non-parametric equivalents. We also used repeated-measures linear regression analysis (Fitzmaurice et al., 2004). Analyzes were carried out using MS-Excel, Matlab 2009b (MathWorks), Prism 5, (Graphpad Software), Sigma Plot (Systat), R and Virtual Dub (Freeware).

RESULTS

A BRIEF LIGHT EXPOSURE IS STRESSFUL FOR DARK-ADAPTED LARVAE

The small transparent bodies of larval zebrafish make them suitable for non-invasive manipulation of neuronal activity using light. Yet, larval zebrafish are highly sensitive to photic stimuli (Burgess and Granato, 2007). While swimming in darkness, for example, they display stable rates of discontinuous motion (**Figure 1A**) and react to a brief exposure to light with stereotyped changes in locomotor activity (Macphail et al., 2009). First, they show a drastic reduction of locomotion after the light onset, followed by increased locomotion after the light-offset. Afterward, locomotion decreases gradually until it reaches steady-state levels several minutes later. A drastic reduction of locomotion in response to external stimulation is generally thought of as a fear-related response. Many species secrete cortisol in threatening situations associated with greater fear. Hence, as a prerequisite to develop optogenetic approaches for stress research, we set up to examine the effect of illumination change on locomotion and cortisol level. Since optogenetic photo-actuators work upon absorption of a wide range of light wavelengths, we first tested whether the larval stereotyped reactions to illumination change could be

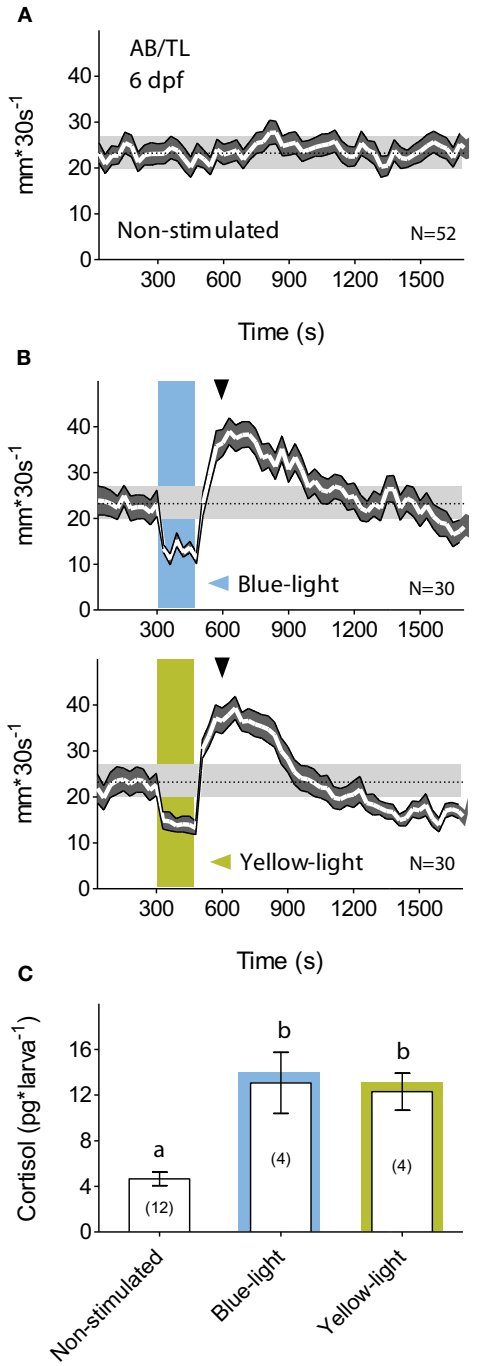

FIGURE 1 | A brief exposure to light is stressful for dark-adapted larvae. (A) Wild-type 6 dpf larval zebrafish display regular motion levels while swimming in darkness (overall mean ± S.E.M. shown as dotted line and gray background, respectively). **(B)** When dark-adapted for 15 min, 6 dpf larvae react to a 180 s squared pulse of either blue- (top) or yellow-light (bottom) with reduced locomotion after the light-onset followed by increased locomotion after the light-offset. Afterward, locomotion decreases gradually until it reaches steady-state levels tens of minutes later (light-power: 2.8 mW*cm^{-2}; gray arrowheads indicate cortisol extraction times). **(C)** Such a brief exposure to either blue- or yellow-light increases whole-body cortisol level (lowercase letters indicate statistical differences among groups; sample size in parenthesis).

similarly evoked by a squared pulse of either blue- or yellow-light. We observed that both light wavelengths elicited similar motion patterns (**Figure 1B**). Next, we examined the extent to which such a brief exposure to light could act as a stressful event, and observed that 6 dpf larvae reacted to a 180 s squared pulse of either blue- or yellow-light with increased cortisol levels (**Figure 1C**; Mann–Whitney test, blue-light: $p < 0.01$, yellow-light: $p = 0.03$), thereby specifying that a squared pulse of light can act as a stressful input signal. This effect of a fast transition from darkness to light could not be accounted for by "wakefulness" variations as reflected in motion. Larvae kept for such a brief period of time either under constant white illumination or in complete darkness displayed similar levels of locomotor activity [t-test, $t_{(24)} = 0.4$, $p = 0.72$].

INCREASING THE GAIN OF THE STRESS AXIS

Since light in itself can stimulate stress networks, we reasoned that the presence of photo-actuators within the HPI axis would allow us to meaningfully alter its light-triggered activation. In particular, we aimed to manipulate the increase of cortisol triggered by light so as to induce greater and controllable rates of cortisol rise in response to otherwise similarly stressful events. Technically speaking, this means that we aimed to increase the gain of the stress axis by amplifying the output (cortisol) of a constant input signal (light). To this end, we chose to target the expression of *Beggiatoa* bPAC (Ryu et al., 2010; Stierl et al., 2011) specifically to ACTH-producing pituitary corticotroph cells. Stress activates complex intracellular CRH signaling cascades in multiple cell types (Arzt and Holsboer, 2006). In pituitary cells, an increase in cAMP downstream of CRH receptor activation causes ACTH release. We therefore hypothesized that blue-light stimulation of bPAC will lead to increased cAMP levels in pituitary corticotrophs and, consequently, also to enhanced ACTH release (**Figure 2A**). Enhanced levels of circulating ACTH will then be expected to co-vary with whole-body cortisol (**Figure 2B**), as the melanocortin receptor type 2 (MC2R) is predominantly expressed in the interrenal gland and not in the zebrafish brain (Agulleiro et al., 2010). We first demonstrated that bPAC is functional in zebrafish larvae. Injecting *bPAC* mRNA into embryos in the one-cell stage led to a blue-light dependent elevation of whole-body cAMP at 1 dpf (**Figure 2C**; Mann–Whitney test, $p = 0.19$ for non-stimulated control vs. bPAC-injected; $p = 0.02$ for light-stimulated control vs. *bPAC*-injected). To target bPAC specifically to pituitary corticotrophs, we used a fragment of the proopiomelanocortin (POMC) promoter whose expression pattern is restricted to corticotroph cells (Liu et al., 2003). To aid in visualization of the expression of the construct, the bPAC protein sequence was fused to myc-tag and a fluorescent reporter, tdTomato, via the viral 2A peptide. The transgenic line expressed bPAC specifically in pituitary corticotrophs, as revealed by the co-localization of ACTH with myc and tdTomato signal (**Figure 2D**).

OPTOGENETIC ELEVATION OF STRESS-INDUCED CORTISOL LEVEL

Consistent with our observations in wild-type larvae (**Figures 1A–C**), a 180 s squared pulse of blue-light led to increased cortisol levels in both bPAC-positive (bPAC^{+}) and

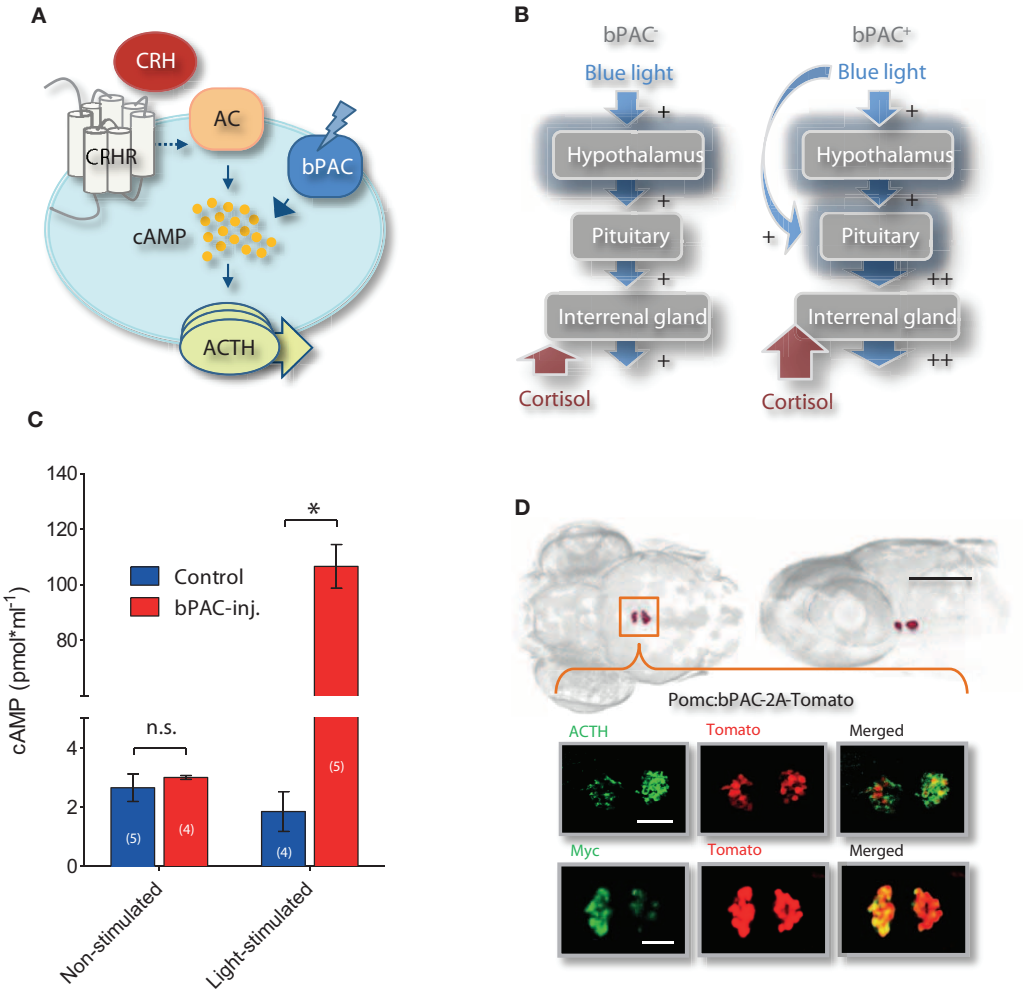

FIGURE 2 | Optogenetic increase of the gain of the stress axis. (A) In pituitary corticotrophs, *Beggiatoa* photoactivated adenylyl cyclase (bPAC) is expected to amplify CRH signaling and ACTH release; CRHR, CRH receptor; AC, adenylyl cyclase. **(B)** We aimed to modify the gain of the HPI axis by targeting bPAC to pituitary corticotrophs. Based on this rationale, blue-light stimulation of bPAC is expected to enhance the increase in cAMP that is central to CRH signaling in corticotroph cells, thereby amplifying ACTH and subsequent cortisol release while preserving analogous levels of hypothalamus activation. According to this scheme, stress-induced over-elevation of cortisol would be varied by modifying the light-power and/or duration of the squared pulse of blue-light. **(C)** Blue-light dependent rise in whole-body cAMP level in 1 dpf larvae using bPAC RNA (asterisks indicate statistical difference between groups at $p < 0.05$). **(D)** Dorsal and lateral views of bPAC expression in two cell clusters in the pituitary of 6 day post fertilization (dpf) larvae (scale bar: 500 μm), as detected by fused tdTomato fluorescence; co-expression of ACTH and fluorescent tdTomato signal (top), and of myc-tag and tdTomato signal (bottom); scale bars: 50 μm.

bPAC-negative (bPAC$^-$) larvae. However, the former showed substantially higher cortisol levels (**Figure 3A**; Two-Way ANOVA, light power: $F_{(3,\ 82)} = 29.48$, $p < 0.0001$; genotype: $F_{(1,\ 82)} = 23.09$, $p < 0.0001$; light power X genotype: $F_{(3,\ 82)} = 1.77$, $p = 0.16$; followed by Bonferroni post-tests for within light-power pair comparisons). Yellow-light failed to enhance the rise of cortisol in the bPAC$^+$ larvae (**Figure 3A**; One-Way ANOVA, $F_{(3,\ 36)} = 10.73$, $p < 0.0001$; followed by Bonferroni post-tests for $bPAC^+_{blue}$ vs. $bPAC^-_{blue}$, $bPAC^+_{yellow}$ or $bPAC^-_{yellow}$, and for $bPAC^+_{yellow}$ vs. either $bPAC^-_{blue}$ or $bPAC^-_{yellow}$), in line with the fact that bPAC activation is blue-light specific due to its BLUF (blue-light receptor using FAD) type light-sensor domain (Ryu et al., 2010; Stierl et al., 2011). Further, already the lowest light-power caused maximum differences between the cortisol levels of the bPAC$^+$ and bPAC$^-$ larvae (**Figure 3A**). This latter result led us to examine the effects of a shorter light stimulation. We then observed that the bPAC$^+$ larvae showed enhanced cortisol levels in response to a ten times shorter stimulation, i.e., a light pulse lasting less than 20 s (**Figure 3B**; Two-Way ANOVA, left, length: $F_{(1,\ 40)} = 33.85$, $p < 0.0001$; genotype: $F_{(1,\ 40)} = 19.56$, $p < 0.0001$; length X genotype: $F_{(1,\ 40)} = 0.47$, $p = 0.50$; right, length: $F_{(1,\ 40)} = 10.85$, $p = 0.002$; genotype: $F_{(1,\ 40)} = 20.37$, $p < 0.0001$; length X genotype: $F_{(1,\ 40)} = 1.13$, $p = 0.29$; followed by Bonferroni post-test for pair comparisons), demonstrating that our approach allows for GC alterations with high temporal resolution.

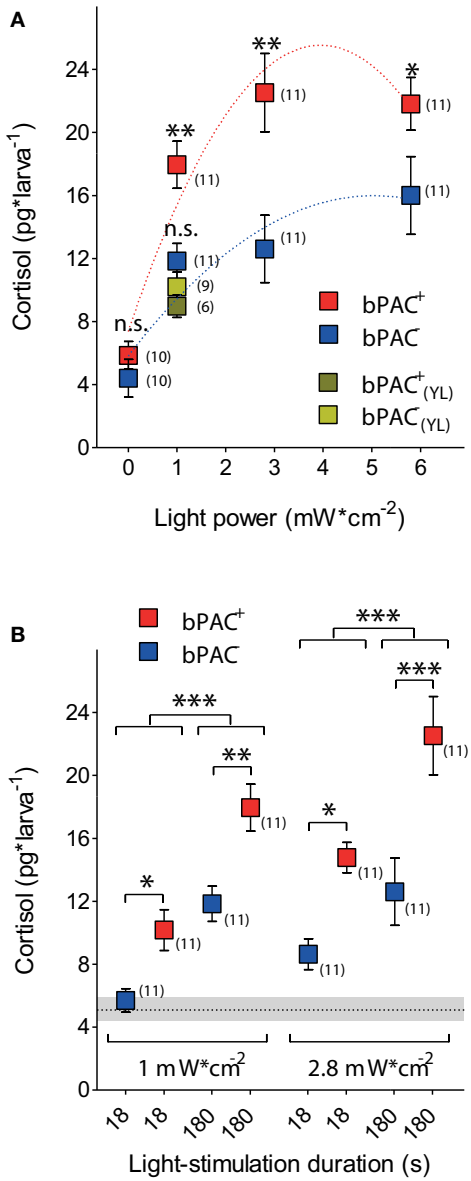

FIGURE 3 | Optogenetic elevation of stress-induced cortisol level. **(A)** A 180 s squared pulse of blue-light leads to higher cortisol levels in bPAC-positive larvae (bPAC$^+$) as compared to their negative siblings (bPAC$^-$) (asterisks indicate statistical differences between groups at $p < 0.05$ or $p < 0.01$; sample size in parenthesis; the red and blue dashed lines depict significant non-linear regressions of cortisol vs. light-power for bPAC$^+$ and bPAC$^-$larvae, respectively). Note that yellow-light fails to differentially enhance cortisol level in bPAC$^+$ larvae. **(B)** Cortisol level in bPAC$^+$ and bPAC$^-$ larvae as a function of exposure time and light-power (asterisks indicate statistical differences between groups at $p < 0.05$, $p < 0.01$, or $p < 0.001$; sample size in parenthesis; Mean ± S.E.M. basal levels shown as dotted line and gray background, respectively).

MULTIPLE LIGHT STIMULATIONS LEAD TO TRANSIENT HYPERCORTISOLIC STATES IN bPAC$^+$ LARVAE

GCs regulate their own production by decreasing CRH and ACTH outputs from the hypothalamus and pituitary, respectively (Dallman and Yates, 1969; Dallman et al., 1994). We then asked whether optogenetic elevation of endogenous GCs could lead to transient hypercortisolic states repeatedly. After the differential rise of cortisol triggered by blue-light, both the bPAC$^+$ and bPAC$^-$ larvae had similar and significantly reduced cortisol levels 20 min after the light offset (**Figure 4A**; bPAC$^+$, $F_{(2,\ 27)} = 38.74, p < 0.0001$; bPAC$^-$, $F_{(2,\ 24)} = 17.70, p < 0.0001$; t-test for pair comparisons within time points), indicating that cortisol-mediated negative feedback is fully functional in zebrafish larvae. Next, we repeatedly exposed groups of bPAC$^+$ and bPAC$^-$ larvae to a sequence of three 180 s squared pulses of blue-light. In order to compare cortisol values resulting from the most recent light pulse and not from previously elevated levels, we used a time interval of 30 min in-between light pulses, which assured similarly low levels in both groups at the time of the second and third pulses (**Figure 4A**). Using this multiple light stimulation protocol, we observed that the bPAC$^+$ larvae responded to each of the light pulses with increased cortisol levels, whereas the bPAC$^-$ larvae failed to do so after the first pulse (**Figure 4B**; Two-Way ANOVA, repeated exposure: $F_{(2,\ 50)} = 12.44$, $p < 0.0001$; genotype: $F_{(1,\ 50)} = 18.55, p < 0.0001$; repeated exposure X genotype: $F_{(2,\ 50)} = 0.13$, $p = 0.88$; one sample t-tests for comparisons against basal level). These results demonstrated that multiple light stimulations can repeatedly lead to hypercortisolic states in bPAC$^+$ larvae, even if the HPI axis has been down-regulated by previously elevated GC levels. To verify the role of the cortisol-mediated negative feedback in this phenomenon, we applied the same stimulation protocol to bPAC$^+$ and bPAC$^-$ larvae that had been incubated with mifepristone (Mif), an antagonist for the GC-receptor (GR) that is effective in larval zebrafish (Weger et al., 2012). Under these circumstances, both the bPAC$^+$ and bPAC$^-$ larvae responded to each of the several light pulses with increased cortisol levels. These stress-induced levels were much higher than those from the non-incubated larvae, verifying that our multiple stimulation protocol leads to down-regulated HPI axis activity. Yet, the bPAC$^+$ larvae still showed substantially higher cortisol levels than the bPAC$^-$ larvae (**Figure 4C**; Two-Way ANOVA, repeated exposure: $F_{(2,\ 41)} = 16.30$, $p < 0.0001$; genotype: $F_{(1,\ 41)} = 21.88, p < 0.0001$; repeated exposure X genotype: $F_{(2,\ 41)} = 0.72$, $p = 0.49$; one sample t-tests for comparisons against basal level). Also, the basal cortisol levels of both groups of larvae were higher in the Mif-incubated larvae as compared to the non-incubated larvae (**Figures 4B,C**; Mann–Whitney test, $p = 0.004$). Taken together, these results show that our approach can be used to induce hypercortisolic states repeatedly, making it possible to examine the effect of repeated GC over-exposure on stress axis development and function.

OPTOGENETICALLY ELEVATED CORTISOL LEVEL LEADS TO ENHANCED LOCOMOTION AFTER STRESSOR EXPOSURE

We noticed that blue-light led to higher post-stimulation locomotion in the bPAC$^+$ larvae, as compared to their negative siblings (**Figure 5A**). Hence, we compared the steady-state post-stimulation motion levels of the bPAC$^+$ and bPAC$^-$ larvae 20 min after a single pulse of either blue- or yellow-light. We then observed that blue- but not yellow-light enhanced locomotion in the bPAC$^+$ larvae, whereas neither blue- nor yellow-light enhanced locomotion in the bPAC$^-$ larvae (**Figure 5B**;

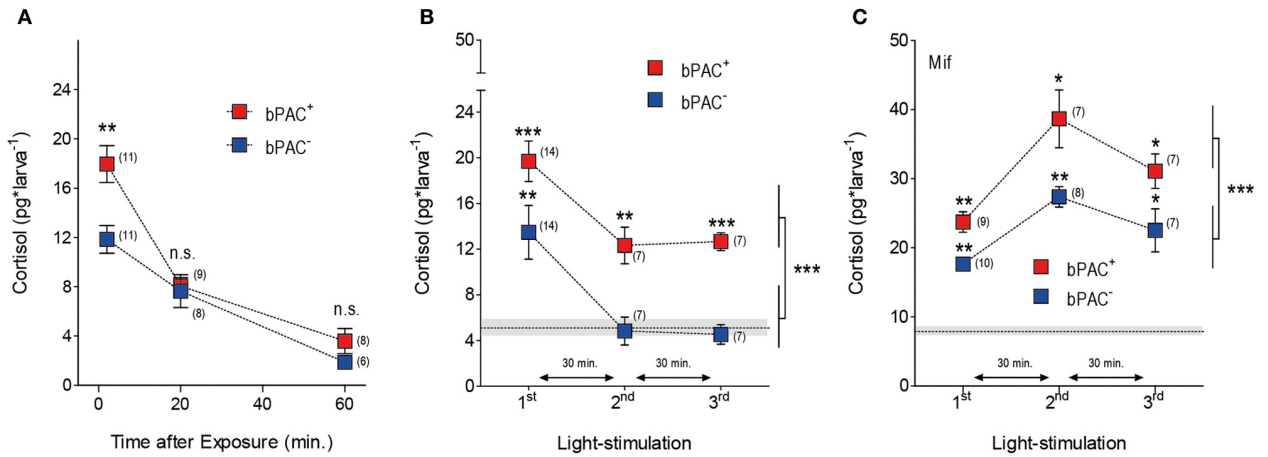

FIGURE 4 | Multiple light stimulations lead to hypercortisolic states in bPAC$^+$ larvae. (A) Light-induced cortisol level decreases as a function of time in both bPAC$^+$ and bPAC$^-$ larvae (asterisks indicate statistical differences between groups at $p < 0.001$; light-power: 1 mW*cm^{-2}, exposure time: 180 s). **(B)** bPAC$^+$ but not bPAC$^-$ larvae respond to a sequence of three 180 s squared pulses of blue-light with increased cortisol levels (asterisks indicate statistical differences between groups at $p < 0.01$ or $p < 0.001$; light-power: 2.8 mW*cm^{-2}; inter-trial interval: 30 min). **(C)** In the presence of the GR antagonist mifepristone (Mif), both bPAC$^+$ and bPAC$^-$ larvae respond to multiple light stimulations with increased cortisol levels, which are, on average, substantially higher than those from non-incubated larvae (asterisks indicate statistical differences between groups at $p < 0.05$ or $p < 0.01$; light-power: 2.8 mW*cm^{-2}; inter-trial interval: 30 min). **(B,C)** Mean basal cortisol level ± S.E.M. shown as a dotted line and gray background, respectively; note that basal cortisol levels are comparatively higher in the Mif-incubated larvae.

Mann–Whitney tests, blue-light: $p < 0.04$, yellow-light: $p = 0.68$). We also compared the post-stimulation motion levels of both groups using data from the multiple light stimulation protocol (**Figure 4B**). Once again, locomotion was higher in the bPAC$^+$ than in the bPAC$^-$ larvae (**Figure 5C**; Two-Way ANOVA, repeated exposure: $F_{(2,\ 306)} = 3.0$, $p = 0.0513$; genotype: $F_{(1,\ 306)} = 8.26$, $p = 0.0043$; repeated exposure X genotype: $F_{(2,\ 306)} = 0.19$, $p = 0.83$). Noticiably, the motion values from both groups of larvae plotted against the corresponding cortisol levels could be linearly approximated (**Figure 5D**; repeated-measures linear regression analysis, $p < 0.001$). These results indicated that a brief exposure to blue-light can cause not only hypercortisolic states in dark-adapted bPAC$^+$ larvae, but also tightly correlated deviations from nominal locomotion.

EARLY BLUE-LIGHT STIMULATION CAUSES LONG-TERM HYPERCORTISOLAEMIA IN bPAC$^+$ LARVAE

Early GC overexposure can lead to persistent alterations of HPA axis function (Kapoor et al., 2006; Seckl and Holmes, 2007; Seckl, 2008). We asked whether multiple light stimulations at early stages of development could lead to long-term forms of hypercortisolaemia in bPAC$^+$ larvae. To answer this question, we applied the multiple light stimulation protocol (**Figure 4**) to the bPAC$^+$ and bPAC$^-$ larvae at 4 and 5 dpf. Later, at 6 dpf, we measured the basal and stress-induced cortisol levels of the larvae following a single 180 s squared pulse of blue-light (**Figure 6**). We then observed that the bPAC$^+$ larvae had increased basal cortisol at 6 dpf (**Figure 6A**; Wilcoxon signed rank test, bPAC$^+$: $p = 0.03$, bPAC$^-$: $p = 0.84$), whereas the basal cortisol levels of the bPAC$^+$ and bPAC$^-$ larvae that had not been exposed to early blue-light stimulation did not differ from each other [t-test, $t_{(23)} = 1.1$, $p = 0.31$]. Also, the bPAC$^+$ larvae responded to a light pulse with higher cortisol level, as compared to either the non-exposed bPAC$^+$ larvae or the exposed and non-exposed bPAC$^-$ larvae (**Figure 6B**; Two-Way ANOVA, early stimulation: $F_{(1,\ 21)} = 9.8$, $p < 0.01$; genotype: $F_{(1,\ 21)} = 11.9$, $p < 0.01$; early stimulation X genotype: $F_{(1,\ 21)} = 1.0$, $p = 0.3$, followed by Bonferroni post-tests for within genotype pair comparisons). These results demonstrated that early blue-light stimulation causes long-term hypercortisolaemia in bPAC$^+$ larvae.

DISCUSSION

Here we provide evidence for optogenetic modification of the gain of stress axis in larval zebrafish. Expressing *Beggiatoa* bPAC (Ryu et al., 2010; Stierl et al., 2011) specifically in ACTH-producing pituitary corticotroph cells enhances the rise of endogenous cortisol triggered by stress. Using cell-specific optogenetic manipulation of cAMP levels *in vivo*, a home-made cortisol ELISA, and behavioral tracking, our experiments determined that blue-light can activate the stress axis and enhance the ensuing cortisol rise in bPAC$^+$ larvae, also causing tightly correlated changes in locomotor activity. Additionally, our data demonstrated that early blue-light stimulation can lead to persistent forms of hypercortisolaemia in bPAC$^+$ larvae. Altogether, we developed a tool suitable for the analysis of rapid and delayed effects of stress-associated glucocorticoid levels.

Our tests were specifically designed to amplify the activity of the stress axis non-invasively, maintaining cortisol levels within their physiological range. Upon absorption of blue-light, *bPAC* mRNA injected into embryos in the one-cell stage elevated whole-body cAMP at 1 dpf, verifying that bPAC is functional in zebrafish larvae (**Figure 2C**). The expression of bPAC was restricted to pituitary corticotroph cells, as we used a specific promoter and the fluorescence of the fused tdTomato marker was detected nowhere

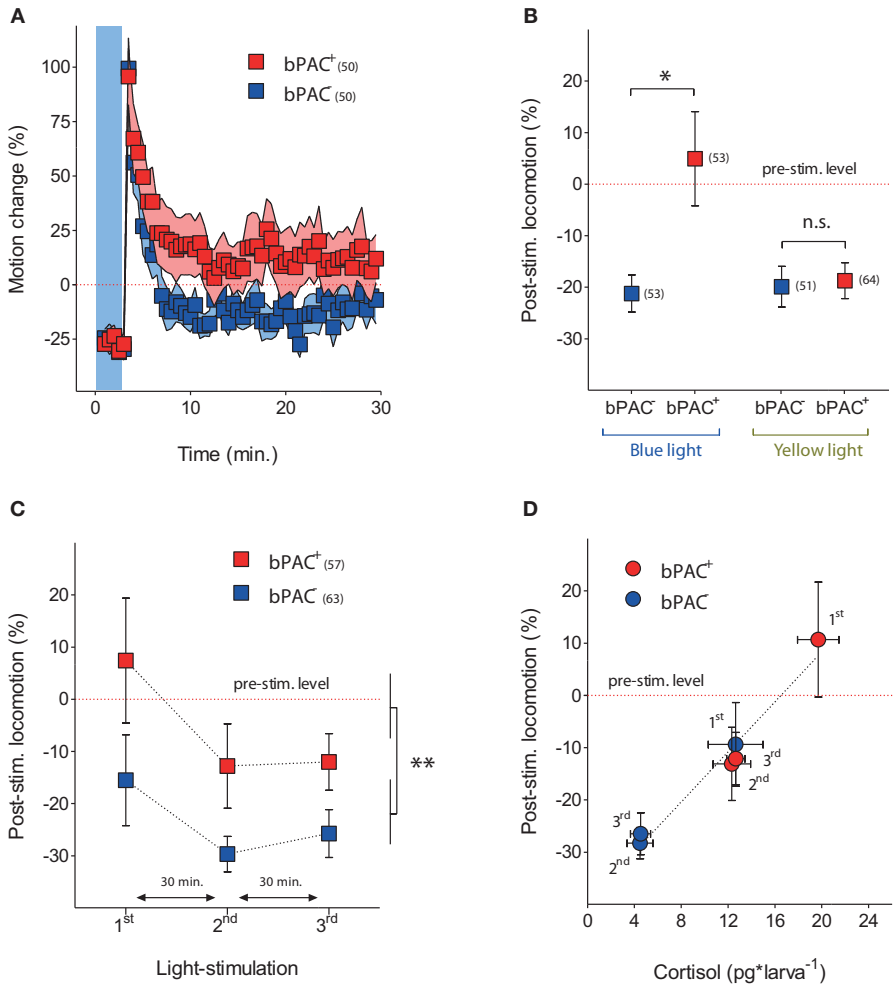

FIGURE 5 | Optogenetically elevated cortisol level leads to enhanced locomotion after stressor exposure. (A) Locomotor activity in bPAC$^+$ (red squares) and bPAC$^-$ larvae (blue squares) during and after a 180 s squared pulse of blue-light (shown as blue background) (light-power: 2.8 mW*cm^{-2}; sample size in parenthesis). **(B)** In bPAC$^+$ larvae, a 180 s squared pulse of blue-light, but not of yellow-light, leads to enhanced locomotion (measured over a 10 min period) after the light offset. In bPAC$^-$ larvae, by contrast, neither blue- nor yellow-light influences locomotion after the light-offset (asterisks indicate statistical difference between groups at $p < 0.05$; light-power: 1 mW*cm^{-2}; sample size in parenthesis; see Materials and Methods for details on motion calculations). **(C)** Over multiple light exposures, post-stimulation locomotion is higher in the bPAC$^+$ larvae than in the bPAC$^-$ larvae (asterisks indicate statistical difference between the groups at $p < 0.01$; light-power: 2.8 mW*cm^{-2}; sample size in parenthesis). **(D)** Locomotion levels from bPAC$^+$ and bPAC$^-$ larvae plotted against corresponding cortisol levels; note how post-stimulation locomotion shows linear dependence of past cortisol levels.

else in the transgenic embryo (**Figure 2D**). *Beggiatoa* PAC has the advantage of having a lower dark activity, as compared to previously reported versions of the enzyme (Schroder-Lang et al., 2007; Ryu et al., 2010; Stierl et al., 2011). Nevertheless, to prevent unspecific activation of bPAC by white light, transgenic embryos were raised under 550 nm long-pass filters. In line with this, both the basal cortisol levels and locomotion estimates of the bPAC$^+$ larvae were similar to those of their negative siblings prior to the tests (**Figure 3A**). The blind design of the motion recordings prevented potential biases caused by any possible differential handling of the larvae. In addition, we randomly distributed groups and treatments throughout the day to avoid biased variability due to circadian cortisol variations (Dickmeis et al., 2007).

Stress causes glucocorticoid secretion via the coupled release of CRH and ACTH. Whereas ACTH primarily stimulates GC secretion, CRH and GCs have widely distributed receptors. Both CRH and GCs have been implicated in a variety of stress correlates, making it difficult to study their specific contributions to the stress response. GCs exert fast and delayed actions in multiple brain areas (Dallman, 2005; Evanson et al., 2010; Groeneweg et al., 2011). For instance, they act rapidly on neurons in the hippocampus (Komatsuzaki et al., 2005), amygdala (Karst et al., 2010), thalamus and caudate nucleus (Strelzyk et al., 2012), among other brain areas. GCs also feedback onto PVN neurons through genomic GR-mediated and non-genomic membrane-initiated mechanisms (Jones et al., 1976; De Kloet et al., 1998; Dallman, 2005; Malcher-Lopes et al., 2006; Di and Tasker, 2008;

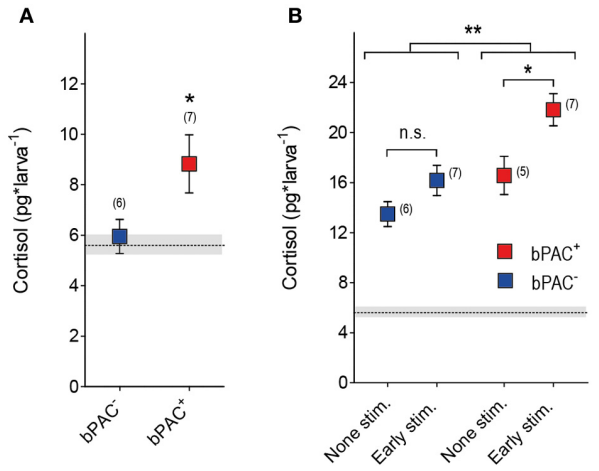

FIGURE 6 | Early blue-light stimulation causes long-term hypercortisolaemia in bPAC$^+$ larvae. (A) bPAC$^+$ (red squares) but not bPAC$^-$ larvae (blue squares) show increased basal cortisol levels after having being exposed to multiple light stimulations over 2 consecutive days (asterisks indicate statistical difference between groups at $p < 0.05$; light-power: 0.6 mW*cm^{-2}; sample size in parenthesis). **(B)** At 6 dpf, bPAC$^+$ larvae (red squares) exposed to light stimulation at 4 and 5 dpf (early stim.) respond to a squared pulse of blue-light with higher cortisol levels as compared to either none-exposed bPAC$^+$ (non-stim.) or exposed and non-exposed bPAC$^-$ larvae (asterisks indicate statistical differences between groups at $p < 0.05$ or $p < 0.01$; light-power: 0.6 mW*cm^{-2}; sample size in parenthesis). **(A,B)** Mean basal cortisol level ± S.E.M. of both bPAC$^+$ and bPAC$^-$ larvae shown as a dotted line and gray background, respectively.

Evanson et al., 2010). Moreover, it has also been reported that inhibition of ACTH release from the anterior pituitary occurs via genomic as well as non-genomic GC actions (Jones et al., 1972; Kaneko and Hiroshige, 1978; Widmaier and Dallman, 1984). In order to specify mechanisms underlying rapid and delayed GC effects under stress, it is necessary to control the rate of variation of endogenous GCs without modifying the activity of upstream hypothalamic networks. However, to date no effective method has been available to selectively modify the rate at which endogenous GC levels vary in response to stress.

Our experiments established a 270% increase of whole-body cortisol level within the first 5 min after the onset of a 180 s squared pulse of either blue- or yellow-light in dark-adapted wild-type larvae (**Figure 1C**). This indicated that a brief exposure to light can be stressful for larval zebrafish. We replicated these experiments using bPAC$^+$ and bPAC$^-$ larvae as well as blue-light of increasing light-power. These experiments determined an average 405% (min.: 350%, max.: 439%) and 263% (min.: 230%, max.: 312%) increase of whole-body cortisol level for the bPAC$^+$ and bPAC$^-$ larvae, respectively. Importantly, yellow-light did not enhance cortisol rise in bPAC$^+$ larvae (**Figure 3A**). Thus, in comparison to their negative siblings, the bPAC$^+$ larvae showed a greater cortisol increase in response to blue-light. This happened while the input signal that triggered the rise of cortisol in the first place remained the same for both groups of larvae. Importantly, a 10 times shorter blue-light pulse also caused a light power-dependent enhancement of stress-induced cortisol rise, demonstrating that our protocol can be used to induce fast changes in endogenous GC level (**Figure 3B**).

Once the stress axis has been activated, GCs feedback onto the brain to limit the release of stress hormones (Dallman and Yates, 1969; Dallman et al., 1994). This feedback is crucial for health, as an excess of GCs is considered a risk factor in humans (Wolkowitz et al., 2009). Studies in humans and other species have shown that prenatal treatment with GCs reduces birth weight and leads to an offspring with altered HPA axis activity and increased risk of cardio-metabolic and psychiatric diseases (Kapoor et al., 2006; Seckl and Holmes, 2007; Seckl, 2008). Moreover, alterations in several brain areas have been reported as a consequence of prenatal stress or injection of synthetic GCs (Cratty et al., 1995; Weaver et al., 2004; Szyf et al., 2005; Kapoor et al., 2006; Murmu et al., 2006). However, since GCs exert pleiotropic developmental effects, it is difficult to distinguish between primary (direct) and secondary effects of GC overexposure. Such a distinction requires suitable model systems and appropriate methods for controlling hypercortisolic states during early development.

Our tests with repeated light stimulation determined that the bPAC$^+$ larvae responded to each pulse of blue-light with increased cortisol levels, whereas the bPAC$^-$ larvae failed to do so after the first pulse (**Figure 4B**). These results demonstrated that multiple light stimulations can repeatedly cause hypercortisolic states in bPAC$^+$ larvae, even if the HPI axis has already been down-regulated by previously elevated cortisol levels. Moreover, when incubated with the antagonist for the GC-receptor Mifepristone, both groups of larvae responded to each of the several light pulses with increased cortisol, but the bPAC$^+$ larvae still showed greater cortisol levels (**Figure 4C**). These results established that multiple light stimulations cause HPI axis down-regulation and verified that the gain of the stress axis is increased in bPAC$^+$ larvae. Our approach thus allows for temporally precise induction of transient hypercortisolaemia, allowing analyses of early GC overexposure on stress response regulation. Strikingly, it can also be used to induce persistent forms hypercortisolaemia in bPAC$^+$ larvae if repeatedly applied during earlier stages of the larval development.

GCs are known to mobilize energy (Sapolsky et al., 2000), which is necessary to cope with the high kinetic energy demands frequently associated with stress. Interestingly, our experiments determined that optogenetically elevated cortisol levels led to enhanced locomotion shortly after stressor exposure (**Figures 5A–D**). Substantial evidence shows that stress and GCs exert significant effects on behavior. But because stressors exert their effects through the closely linked actions of various hormones, not only of GCs, specific GC effects on behavior have been difficult to test. Larval zebrafish offer an excellent opportunity for studying the relationship between stress and behavior, although suitable behavioral endpoints need to be developed. Our protocol can be used alongside novel behavioral tests in order to examine GC effects on stress reactions and coping capacities. It could also be combined with *in vivo* small-molecule behavioral screens (Rihel and Schier, 2012) to find novel modulators of behavioral GC effects.

Optogenetic tools provide hitherto unparalleled means for non-invasive manipulation of neuronal activity. So far, optogenetic applications have been used extensively to modify neuronal activity via light-gated channels. There are comparatively fewer examples of photo-actuators used to manipulate intracellular signaling. Our results demonstrate the feasibility of selectively increasing stress-induced cortisol levels by optogenetic manipulation of cAMP level. The larval zebrafish is highly suitable for non-invasive optogenetics due to its genetic amenability and transparent body (Gahtan and Baier, 2004; Portugues et al., 2013). We showed that the gain of the stress axis can be optogenetically increased in freely behaving larval zebrafish, modifying endocrine and behavioral outputs. So far, bPAC had not been used to modify neuroendocrine and behavioral adjustments in vertebrates. We provide a first demonstration for the feasibility of using it in larval zebrafish to enhance cAMP levels, hormone release and behavioral alteration. Given the availability of a large number of tissue-specific promoters, our protocol could be extended to other cell-types to alter physiological processes *in vivo* using bPAC. Moreover, it could be combined with imaging and bioluminescence techniques for detailed examinations of GC effects on the activity of hypothalamic and pituitary cells.

In summary, our study introduces a powerful tool for the analysis of rapid and delayed GC effects on brain function and behavior, feedbacks within the stress axis and developmental programming by GCs. Follow up work involves analyses of stress circuit development and stress behavior against backgrounds of nominal and increased gain of the HPI axis.

AUTHOR CONTRIBUTIONS

Conception and design of the experiments: Soojin Ryu and Rodrigo J. De Marco. Acquisition of data: Antonia H. Groneberg, Rodrigo J. De Marco, Chen-Min Yeh, Soojin Ryu, Luis A. Castillo Ramírez. Analysis and interpretation of data: Rodrigo J. De Marco, Soojin Ryu, Antonia H. Groneberg, Chen-Min Yeh, Luis A. Castillo Ramírez. Drafting the article: Rodrigo J. De Marco, Soojin Ryu, and Antonia H. Groneberg.

ACKNOWLEDGMENTS

We thank P. Hegemann and G. Nagel for sharing the bPAC plasmid and information about bPAC before publication. We thank U. Herget for assistance with the experiments, C. Maurer and A. Schäfer for helpful comments on the earlier versions of this manuscript, and K. Schmidt, R. Rödel, M. Lukat, and N. Neef for logistic support. We thank G. Shoeman, R. Singer and A. Schoell for expert fish care. This work was supported by DFG-FOR1279, the Max Planck Society and Behrens-Weise Foundation.

REFERENCES

Agulleiro, M. J., Roy, S., Sanchez, E., Puchol, S., Gallo-Payet, N., and Cerda-Reverter, J. M. (2010). Role of melanocortin receptor accessory proteins in the function of zebrafish melanocortin receptor type 2. *Mol. Cell. Endocrinol.* 320, 145–152.

Alderman, S. L., and Bernier, N. J. (2009). Ontogeny of the corticotropin-releasing factor system in zebrafish. *Gen. Comp. Endocrinol.* 164, 61–69.

Alsop, D., and Vijayan, M. M. (2008). Development of the corticosteroid stress axis and receptor expression in zebrafish. *Am. J. Physiol. Regul. Integr. Comp. Physiol.* 294, R711–R719.

Arzt, E., and Holsboer, F. (2006). CRF signaling: molecular specificity for drug targeting in the CNS. *Trends Pharmacol. Sci.* 27, 531–538.

Burgess, H. A., and Granato, M. (2007). Modulation of locomotor activity in larval zebrafish during light adaptation. *J. Exp. Biol.* 210, 2526–2539.

Cachat, J., Stewart, A., Grossman, L., Gaikwad, S., Kadri, F., Chung, K. M., et al. (2010). Measuring behavioral and endocrine responses to novelty stress in adult zebrafish. *Nat. Protoc.* 5, 1786–1799.

Charmandari, E., Tsigos, C., and Chrousos, G. (2005). Endocrinology of the stress response. *Annu. Rev. Physiol.* 67, 259–284.

Chrousos, G. P. (1998). Stressors, stress, and neuroendocrine integration of the adaptive response. The 1997 Hans Selye Memorial Lecture. *Ann. N.Y. Acad. Sci.* 851, 311–335.

Clark, K. J., Boczek, N. J., and Ekker, S. C. (2011). Stressing zebrafish for behavioral genetics. *Rev. Neurosci.* 22, 49–62.

Cratty, M. S., Ward, H. E., Johnson, E. A., Azzaro, A. J., and Birkle, D. L. (1995). Prenatal stress increases corticotropin-releasing factor (CRF) content and release in rat amygdala minces. *Brain Res.* 675, 297–302.

Dallman, M. F. (2005). Fast glucocorticoid actions on brain: back to the future. *Front. Neuroendocrinol.* 26, 103–108.

Dallman, M. F., Akana, S. F., Levin, N., Walker, C. D., Bradbury, M. J., Suemaru, S., et al. (1994). Corticosteroids and the control of function in the hypothalamo-pituitary-adrenal (HPA) axis. *Ann. N.Y. Acad. Sci.* 746, 22–31, discussion: 31–32, 64–27.

Dallman, M. F., and Yates, F. E. (1969). Dynamic asymmetries in the corticosteroid feedback path and distribution-metabolism-binding elements of the adrenocortical system. *Ann. N.Y. Acad. Sci.* 156, 696–721.

De Kloet, E. R., Joels, M., and Holsboer, F. (2005). Stress and the brain: from adaptation to disease. *Nat. Rev. Neurosci.* 6, 463–475.

De Kloet, E. R., Vreugdenhil, E., Oitzl, M. S., and Joels, M. (1998). Brain corticosteroid receptor balance in health and disease. *Endocr. Rev.* 19, 269–301.

Di, S., and Tasker, J. G. (2008). Rapid synapse-specific regulation of hypothalamic magnocellular neurons by glucocorticoids. *Prog. Brain Res.* 170, 379–388.

Dickmeis, T., and Foulkes, N. S. (2011). Glucocorticoids and circadian clock control of cell proliferation: at the interface between three dynamic systems. *Mol. Cell. Endocrinol.* 331, 11–22.

Dickmeis, T., Lahiri, K., Nica, G., Vallone, D., Santoriello, C., Neumann, C. J., et al. (2007). Glucocorticoids play a key role in circadian cell cycle rhythms. *PLoS Biol.* 5:e78. doi: 10.1371/journal.pbio.0050078

Egan, R. J., Bergner, C. L., Hart, P. C., Cachat, J. M., Canavello, P. R., Elegante, M. F., et al. (2009). Understanding behavioral and physiological phenotypes of stress and anxiety in zebrafish. *Behav. Brain Res.* 205, 38–44.

Evanson, N. K., Tasker, J. G., Hill, M. N., Hillard, C. J., and Herman, J. P. (2010). Fast feedback inhibition of the HPA axis by glucocorticoids is mediated by endocannabinoid signaling. *Endocrinology* 151, 4811–4819.

Fitzmaurice, G. M., Laird, N. M., and Ware, J. H. (2004). *Applied Longitudinal Analysis.* Hoboken, NJ: John Wiley and Sons.

Flik, G., Klaren, P. H., Van Den Burg, E. H., Metz, J. R., and Huising, M. O. (2006). CRF and stress in fish. *Gen. Comp. Endocrinol.* 146, 36–44.

Forlano, P. M., and Cone, R. D. (2007). Conserved neurochemical pathways involved in hypothalamic control of energy homeostasis. *J. Comp. Neurol.* 505, 235–248.

Fuzzen, M. L., Van Der Kraak, G., and Bernier, N. J. (2010). Stirring up new ideas about the regulation of the hypothalamic-pituitary-interrenal axis in zebrafish (*Danio rerio*). *Zebrafish* 7, 349–358.

Gahtan, E., and Baier, H. (2004). Of lasers, mutants, and see-through brains: functional neuroanatomy in zebrafish. *J. Neurobiol.* 59, 147–161.

Griffiths, B. B., Schoonheim, P. J., Ziv, L., Voelker, L., Baier, H., and Gahtan, E. (2012). A zebrafish model of glucocorticoid resistance shows serotonergic modulation of the stress response. *Front. Behav. Neurosci.* 6:68. doi: 10.3389/fnbeh.2012.00068

Groeneweg, F. L., Karst, H., De Kloet, E. R., and Joels, M. (2011). Rapid

non-genomic effects of corticosteroids and their role in the central stress response. *J. Endocrinol.* 209, 153–167.

Holsboer, F., Von Bardeleben, U., Gerken, A., Stalla, G. K., and Müller, O. A. (1984). Blunted corticotropin and normal cortisol response to human corticotropin-releasing factor in depression. *N. Engl. J. Med.* 311:1127. doi: 10.1056/NEJM198410253111718

Jones, M. T., Brush, F. R., and Neame, R. L. (1972). Characteristics of fast feedback control of corticotrophin release by corticosteroids. *J. Endocrinol.* 55, 489–497.

Jones, M. T., Hillhouse, E. W., and Burden, J. (1976). Proceedings: mechanism of action of fast and delayed corticosteroid feedback at the hypothalamus. *J. Endocrinol.* 69, 34P–35P.

Kaneko, M., and Hiroshige, T. (1978). Fast, rate-sensitive corticosteroid negative feedback during stress. *Am. J. Physiol.* 234, R39–R45.

Kapoor, A., Dunn, E., Kostaki, A., Andrews, M. H., and Matthews, S. G. (2006). Fetal programming of hypothalamo-pituitary-adrenal function: prenatal stress and glucocorticoids. *J. Physiol.* 572, 31–44.

Karst, H., Berger, S., Erdmann, G., Schütz, G., and Joëls, M. (2010). Metaplasticity of amygdalar responses to the stress hormone corticosterone. *Proc. Natl. Acad. Sci. U.S.A.* 107, 14449–14454.

Komatsuzaki, Y., Murakami, G., Tsurugizawa, T., Mukai, H., Tanabe, N., Mitsuhashi, K., et al. (2005). Rapid spinogenesis of pyramidal neurons induced by activation of glucocorticoid receptors in adult male rat hippocampus. *Biochem. Biophys. Res. Commun.* 335, 1002–1007.

Liu, N. A., Huang, H., Yang, Z., Herzog, W., Hammerschmidt, M., Lin, S., et al. (2003). Pituitary corticotroph ontogeny and regulation in transgenic zebrafish. *Mol. Endocrinol.* 17, 959–966.

Macphail, R. C., Brooks, J., Hunter, D. L., Padnos, B., Irons, T. D., and Padilla, S. (2009). Locomotion in larval zebrafish: influence of time of day, lighting and ethanol. *Neurotoxicology* 30, 52–58.

Malcher-Lopes, R., Di, S., Marcheselli, V. S., Weng, F. J., Stuart, C. T., Bazan, N. G., et al. (2006). Opposing crosstalk between leptin and glucocorticoids rapidly modulates synaptic excitation via endocannabinoid release. *J. Neurosci.* 26, 6643–6650.

McEwen, B. S. (2008). Central effects of stress hormones in health and disease: Understanding the protective and damaging effects of stress and stress mediators. *Eur. J. Pharmacol.* 583, 174–185.

Murmu, M. S., Salomon, S., Biala, Y., Weinstock, M., Braun, K., and Bock, J. (2006). Changes of spine density and dendritic complexity in the prefrontal cortex in offspring of mothers exposed to stress during pregnancy. *Eur. J. Neurosci.* 24, 1477–1487.

Nemeroff, C., Widerlöv, E., Bissette, G., Walléus, H., Karlsson, I., Eklund, K., et al. (1984). Elevated concentrations of CSF corticotropin-releasing factor-like immunoreactivity in depressed patients. *Science* 226, 1342–1344.

Peter, R. E. (1977). The preoptic nucleus in fishes: a comparative discussion of function-activity relationships. *Amer. Zool.* 17, 775–785.

Portugues, R., Severi, K. E., Wyart, C., and Ahrens, M. B. (2013). Optogenetics in a transparent animal: circuit function in the larval zebrafish. *Curr. Opin. Neurobiol.* 23, 119–126.

Raber, J. (1998). Detrimental effects of chronic hypothalamic-pituitary-adrenal axis activation. From obesity to memory deficits. *Mol. Neurobiol.* 18, 1–22.

Ramsay, J., Feist, G., Varga, Z., Westerfield, M., Kent, M., and Schreck, C. (2006). Whole-body cortisol is an indicator of crowding stress in adult zebrafish, *Danio rerio*. *Aquaculture* 258, 565–574.

Ramsay, J. M., Feist, G. W., Varga, Z. M., Westerfield, M., Kent, M. L., and Schreck, C. B. (2009). Whole-body cortisol response of zebrafish to acute net handling stress. *Aquaculture* 297, 157–162.

Rihel, J., and Schier, A. F. (2012). Behavioral screening for neuroactive drugs in zebrafish. *Dev. Neurobiol.* 72, 373–385.

Ryu, M. H., Moskvin, O. V., Siltberg-Liberles, J., and Gomelsky, M. (2010). Natural and engineered photoactivated nucleotidyl cyclases for optogenetic applications. *J. Biol. Chem.* 285, 41501–41508.

Ryu, S., Mahler, J., Acampora, D., Holzschuh, J., Erhardt, S., Omodei, D., et al. (2007). Orthopedia homeodomain protein is essential for diencephalic dopaminergic neuron development. *Curr. Biol.* 17, 873–880.

Sapolsky, R. M., Romero, L. M., and Munck, A. U. (2000). How do glucocorticoids influence stress responses? Integrating permissive, suppressive, stimulatory, and preparative actions. *Endocr. Rev.* 21, 55–89.

Schroder-Lang, S., Schwarzel, M., Seifert, R., Strunker, T., Kateriya, S., Looser, J., et al. (2007). Fast manipulation of cellular cAMP level by light *in vivo*. *Nat. Methods* 4, 39–42.

Seckl, J. R. (2008). Glucocorticoids, developmental 'programming' and the risk of affective dysfunction. *Prog. Brain Res.* 167, 17–34.

Seckl, J. R., and Holmes, M. C. (2007). Mechanisms of disease: glucocorticoids, their placental metabolism and fetal 'programming' of adult pathophysiology. *Nat. Clin. Pract. Endocrinol. Metab.* 3, 479–488.

Selye, H. (1956). *The Stress of Life.* New York, NY: McGraw-Hill.

Speedie, N., and Gerlai, R. (2008). Alarm substance induced behavioral responses in zebrafish (*Danio rerio*). *Behav. Brain Res.* 188, 168–177.

Steenbergen, P. J., Richardson, M. K., and Champagne, D. L. (2011). The use of the zebrafish model in stress research. *Prog. Neuropsychopharmacol. Biol. Psychiatry* 35, 1432–1451.

Stierl, M., Stumpf, P., Udwari, D., Gueta, R., Hagedorn, R., Losi, A., et al. (2011). Light modulation of cellular cAMP by a small bacterial photoactivated adenylyl cyclase, bPAC, of the soil bacterium Beggiatoa. *J. Biol. Chem.* 286, 1181–1188.

Strelzyk, F., Hermes, M., Naumann, E., Oitzl, M., Walter, C., Busch, H. P., et al. (2012). Tune it down to live it up? Rapid, nongenomic effects of cortisol on the human brain. *J. Neurosci.* 32, 616–625.

Szyf, M., Weaver, I. C., Champagne, F. A., Diorio, J., and Meaney, M. J. (2005). Maternal programming of steroid receptor expression and phenotype through DNA methylation in the rat. *Front. Neuroendocrinol.* 26, 139–162.

Tang, W., Ehrlich, I., Wolff, S. B., Michalski, A. M., Wolfl, S., Hasan, M. T., et al. (2009). Faithful expression of multiple proteins via 2A-peptide self-processing: a versatile and reliable method for manipulating brain circuits. *J. Neurosci.* 29, 8621–8629.

Weaver, I. C., Cervoni, N., Champagne, F. A., D'Alessio, A. C., Sharma, S., Seckl, J. R., et al. (2004). Epigenetic programming by maternal behavior. *Nat. Neurosci.* 7, 847–854.

Weger, B. D., Weger, M., Nusser, M., Brenner-Weiss, G., and Dickmeis, T. (2012). A chemical screening system for glucocorticoid stress hormone signaling in an intact vertebrate. *ACS Chem. Biol.* 7, 1178–1183.

Wendelaar Bonga, S. E. (1997). The stress response in fish. *Physiol. Rev.* 77, 591–625.

Westerfield, M. (2000). *The Zebrafish Book. A Guide for the Laboratory Use of Zebrafish (Danio rerio)*, 4th Edn. Eugene: University of Oregon Press.

Widmaier, E. P., and Dallman, M. F. (1984). The effects of corticotropin-releasing factor on adrenocorticotropin secretion from perifused pituitaries *in vitro*: rapid inhibition by glucocorticoids. *Endocrinology* 115, 2368–2374.

Wolkowitz, O. M., Burke, H., Epel, E. S., and Reus, V. I. (2009). Glucocorticoids. Mood, memory, and mechanisms. *Ann. N.Y. Acad. Sci.* 1179, 19–40.

Yehuda, R. (2009). Status of glucocorticoid alterations in post-traumatic stress disorder. *Ann. N.Y. Acad. Sci.* 1179, 56–69.

Ziv, L., Muto, A., Schoonheim, P. J., Meijsing, S. H., Strasser, D., Ingraham, H. A., et al. (2012). An affective disorder in zebrafish with mutation of the glucocorticoid receptor. *Mol. Psychiatry* doi: 10.1038/mp.2012.64. [Epub ahead of print].

Conflict of Interest Statement: Soojin Ryu and Rodrigo J. De Marco have submitted a patent application for the use of optogenetic transgenic zebrafish lines to find novel regulators of stress response.

Received: 14 February 2013; paper pending published: 06 March 2013; accepted: 11 April 2013; published online: 06 May 2013.

Citation: De Marco RJ, Groneberg AH, Yeh C-M, Castillo Ramírez LA and Ryu S (2013) Optogenetic elevation of endogenous glucocorticoid level in larval zebrafish. Front. Neural Circuits 7:82. doi: 10.3389/fncir.2013.00082